



Contract Report 2009-07

Kane County Water Resources Investigations: **Simulation of Groundwater Flow** in Kane County and Northeastern Illinois

Scott C. Meyer, P.G., George S. Roadcap, P.G., Yu-Feng Lin, Douglas D. Walker

Illinois State Water Survey
Institute of Natural Resource Sustainability
University of Illinois at Urbana-Champaign



Kane County Water Resources Investigations: Simulation of Groundwater Flow in Kane County and Northeastern Illinois

Scott C. Meyer, P.G.
George S. Roadcap, Ph.D., P.G.
Yu-Feng Lin, Ph.D.
Douglas D. Walker, Ph.D.

Contract Report 2009-07
Executive Summary

Illinois State Water Survey
A division of the Institute of Natural Resource Sustainability
Champaign, Illinois



Cover photo courtesy PDPhoto.org

Published May 2009

Any opinions, findings, and conclusions or recommendations expressed in this publication are those of the author(s) and do not necessarily reflect the views of the Illinois State Water Survey.

Illinois State Water Survey
2204 Griffith Drive, Champaign, Illinois 61820
www.isws.illinois.edu

© 2009 University of Illinois Board of Trustees. All rights reserved.
For permissions, contact the Illinois State Water Survey.

Printed with soybean ink on recycled paper

Contents

Page

1. Introduction.....	1
2. Sources of Water to Kane County.....	2
3. Groundwater Flow Models	6
4. How Much Groundwater is Available in Kane County?	13
5. Model Analysis	15
5.1. <i>General Flow Patterns.....</i>	<i>15</i>
5.2. <i>Modeling of Historical Conditions</i>	<i>16</i>
5.2.1. Head Change in Deep Aquifers	16
5.2.2. Head Change in Shallow Aquifers.....	25
5.2.3. Changes in Streamflow	29
5.3. <i>Modeling of Future Conditions.....</i>	<i>34</i>
5.3.1. Scenarios	34
5.3.2. Head Change in Deep Aquifers	36
5.3.3. Head Change in Shallow Aquifers.....	46
5.3.4. Changes in Streamflow	51
6. Summary.....	58
7. Future Work.....	59
7.1. <i>Modeling Studies.....</i>	<i>59</i>
7.2. <i>Monitoring</i>	<i>60</i>
7.3. <i>Database Expansion and Improvement</i>	<i>60</i>
8. References.....	61

List of Figures

	Page
Figure 1. Water withdrawals by public water systems, irrigators, and self-supplied commercial and industrial facilities in Kane County from 1964 to 2003.....	2
Figure 2. Major aquifers of the Kane County area.	4
Figure 3. Groundwater withdrawals by public water systems, irrigators, and self-supplied commercial and industrial facilities in Kane County from 1964 through 2003.	5
Figure 4. Areal extent of groundwater flow models.	7
Figure 5. Layer scheme of regional-scale model.	8
Figure 6. Detail of northeastern Illinois showing regional model grid and regional model nearfield.	9
Figure 7. Local-scale model domain.....	11
Figure 8. Layer scheme of local-scale model.	12
Figure 9. Historic and projected groundwater withdrawals in the regional model nearfield of northeastern Illinois (Figure 6).	14
Figure 10. Simulated drawdown due to pumping in the Ancell Unit in the Kane County area in 2002.....	17
Figure 11. Simulated head in feet above mean sea level (ft above MSL) in the Ancell Unit in the Kane County area in 2002.	18
Figure 12. Simulated head from 1864 to 2002 in the Ancell Unit at St. Charles and Maple Park.	19
Figure 13. Simulated head from 1864 to 2002 in the Ironton-Galesville Unit at St. Charles and Maple Park.	20
Figure 14. Change in simulated head in the Ancell Unit in the Kane County area, 1979-2002.....	23
Figure 15. Available simulated head above the top of the Ancell Unit in 2002.....	24
Figure 16. Simulated 2003 drawdown in the Shallow Bedrock Aquifer in the Kane County vicinity, with areas of significant drawdown mentioned in the text identified....	26
Figure 17. Simulated 2003 drawdown in the Shallow Bedrock Aquifer in northeastern Kane County and southeastern McHenry County.	27
Figure 18. Simulated 2003 drawdown in the Shallow Bedrock Aquifer in east-central Kane County and west-central DuPage County.....	28
Figure 19. Total simulated natural groundwater discharge in local model domain.....	30
Figure 20. Change in natural groundwater discharge caused by pumping by stream reach in the Kane County area in 2003, with reaches discussed in text identified (see Table 1 for identification of all reaches).	31
Figure 21. Simulated natural groundwater discharge to Mill Creek upstream of Batavia (reach 512).	32
Figure 22. Change in simulated head between the end of 2002 and end of 2049 in Ancell Unit, scenario HC.....	37
Figure 23. Change in simulated head between the end of 2002 and end of 2049 in Ancell Unit, scenario LC.	38
Figure 24. Simulated head in Ancell Unit at the end of 2002.....	39
Figure 25. Simulated head in Ancell Unit at the end of 2049, scenario HC.....	40
Figure 26. Simulated head in Ancell Unit at the end of 2049, scenario LC.	41

List of Figures (concluded)

	Page
Figure 27. Simulated head from end of 1970 to end of 2049 in Ancell (top) and Ironton-Galesville Units (bottom) at St. Charles. See Figure 10 and Figure 11 for location.	42
Figure 28. Simulated head from end of 1970 to end of 2049 in Ancell (top) and Ironton-Galesville Units (bottom) at Maple Park. See Figure 10 and Figure 11 for location.	43
Figure 29. Available simulated head above the top of the Ancell Unit at the end of 2049, scenerio HC	44
Figure 30. Available simulated head above the top of the Ancell Unit at the end of 2049, scenario LC.	45
Figure 31. Simulated drawdown in the Shallow Bedrock Aquifer at the end of 2049, scenario HL, with areas of significant drawdown mentioned in the text identified.	47
Figure 32. Simulated drawdown in the Shallow Bedrock Aquifer at the end of 2049, scenario HC, with areas of significant drawdown mentioned in the text identified.	48
Figure 33. Simulated drawdown in the Shallow Bedrock Aquifer at the end of 2049, scenario LC, with areas of significant drawdown mentioned in the text identified.	49
Figure 34. Simulated drawdown in the Shallow Bedrock Aquifer at the end of 2049, scenario LH, with areas of significant drawdown mentioned in the text identified.	50
Figure 35. Total natural groundwater discharge to streams in the local-scale model domain.....	52
Figure 36. Change in simulated natural groundwater discharge since predevelopment by stream reach in the Kane County area at the end of 2049, scenario HL, with reaches discussed in text identified (see Table 1 for identification of all reaches).....	53
Figure 37. Change in simulated natural groundwater discharge since predevelopment by stream reach in the Kane County area at the end of 2049, scenario HC, with reaches discussed in text identified (see Table 1 for identification of all reaches).....	54
Figure 38. Change in simulated natural groundwater discharge since predevelopment by stream reach in the Kane County area at the end of 2049, scenario LC, with reaches discussed in text identified (see Table 1 for identification of all reaches).....	55
Figure 39. Change in simulated natural groundwater discharge since predevelopment by stream reach in the Kane County area at the end of 2049, scenario LH, with reaches discussed in text identified (see Table 1 for identification of all reaches).....	56

List of Tables

	Page
Table 1. Principal Streams Included in Reaches.....	33
Table 2. Transient Simulations to 2050	35
Table 3. Estimated Total Change in Natural Groundwater Discharge at end of 2024 and 2049, by Stream Reach	57

1. Introduction

This report discusses an assessment of groundwater resources supplying water to Kane County, Illinois, a rapidly growing county on the west side of the greater Chicago metropolitan area. This study assimilates the available data into a set of computer models of groundwater flow in regional and local aquifers, quantifying the components of the hydrologic cycle and assessing the impact of historical and projected pumping. The modeling study is part of a comprehensive project assessing surface water, geology, and groundwater in Kane County.

The water resources assessment project was motivated by a combination of factors and trends. The population of Kane County is projected to increase more than 70 percent from the 2000 population to over 718,000 by 2030. Although this population increase likely will be accompanied by greatly increased water demand, Lake Michigan, the source of water upon which the northeastern Illinois region has historically relied, may not be available due to legal constraints and the significant expense of conveying water from the lake to Kane County. These limitations have prompted planners and decision-makers to look to water resources within Kane County to meet projected demands. Studies conducted prior to the initiation of the present investigation in 2002 offered only a regional, qualitative understanding of the geology and hydrology, scattered sets of sporadic observations, and isolated studies of local issues. Although these legacy studies are inadequate for fostering detailed water-resources planning, they suggested the possibility of water shortages in Kane County by 2025 (Northeastern Illinois Planning Commission, 2002).

In response to these factors, the Kane County Development Department commissioned the Illinois State Water Survey and Illinois State Geological Survey to assess groundwater and surface water resources to support county water-supply planning efforts. This assessment includes the present study, whose goal is to ascertain the current and future status of groundwater resources in Kane County, Illinois. To achieve this goal, this study develops and applies computer models of groundwater flow to clarify the relationships between aquifers and streams and to quantify the effects of current and future groundwater usage. The study assembles the data collected in the field, retrieved from archives and synthesized during 2002 to 2006, and assimilates them into computer models that simulate groundwater flow.

This executive summary briefly describes the development, application, and results of computer modeling conducted for the study. The more extensive main report discusses the hydrologic characteristics of geological materials in the Kane County area and documents the data review and inference of parameters, the development and calibration of the groundwater models, and their detailed results. Readers should consult the main report for these details, as well as an overview of hydrogeologic concepts, the regional setting, and model development. Readers interested in basic concepts of hydrology may find the introduction by Alley et al. (1999) to be useful. Anderson and Woessner (2002) provide extensive guidance on the practice of developing groundwater flow models.

2. Sources of Water to Kane County

Significant local sources of water to Kane County include the Fox River—already utilized by the Cities of Elgin and Aurora—and groundwater. Total water withdrawals by public water systems, irrigators, and self-supplied commercial and industrial facilities in the county have increased from about 25 to 61 million gallons per day (Mgd) from 1964 to 2003 (Figure 1). Kane County has always relied entirely on its locally available water sources and has never received water from Lake Michigan.

Since the late 1980s, surface water used in the county has been obtained almost entirely from the Fox River by the Elgin and Aurora public water systems. Elgin began withdrawing water from the Fox River in 1983, and Aurora began in 1992. Prior to 1979, surface withdrawal data in the county are not available, but withdrawals were probably near zero during this time period. Questions pertaining to the availability of water from the Fox River in Kane County are beyond the scope of the present report, but the topic is discussed in a related report on the surface waters of Kane County by Knapp et al. (2007).

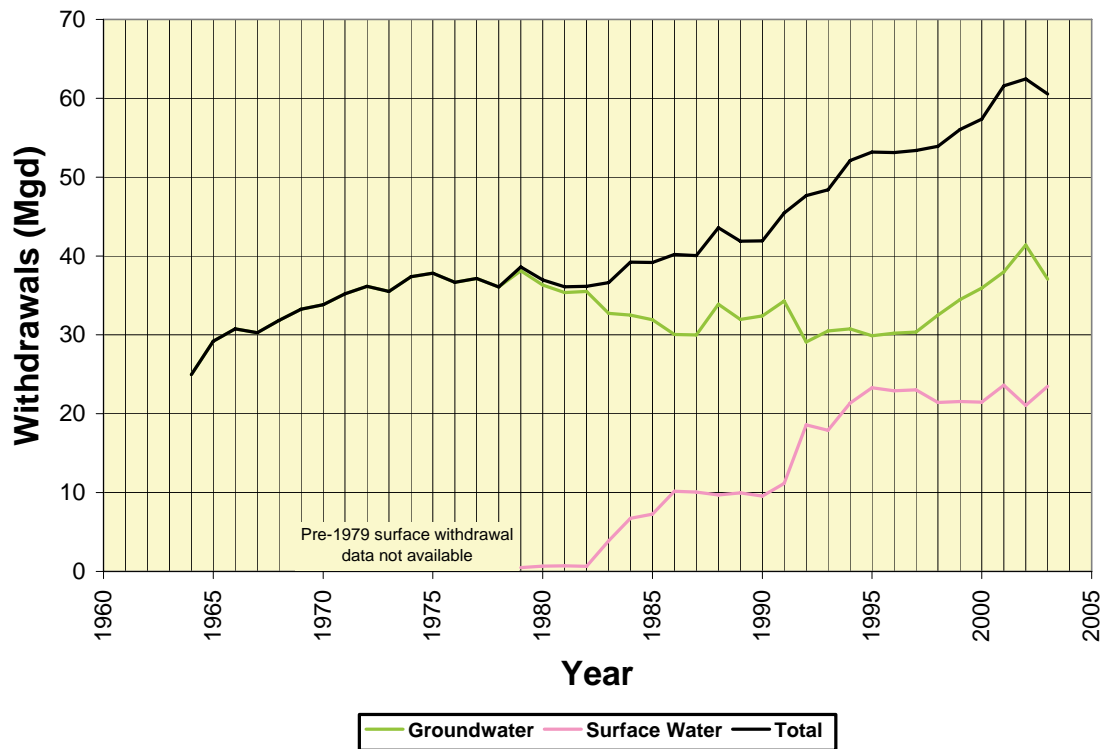


Figure 1. Water withdrawals by public water systems, irrigators, and self-supplied commercial and industrial facilities in Kane County from 1964 to 2003.

Groundwater sources available to Kane County include deep and shallow aquifers (Figure 2). The deep aquifers are layers consisting principally of sandstone, and for purposes of this study are referred to as the Ancell Unit, Ironton-Galesville Unit, and Mt. Simon Unit. In Kane County and the rest of northeastern Illinois, the Ancell Unit consists predominantly of the well-known St. Peter Sandstone, a productive aquifer that is a common target of deep wells in the region. The Mt. Simon Unit is used far less than the Ancell and Ironton-Galesville Units because of the expense of drilling to it and because its lower portions contain water that is too salty for most uses. In other parts of the regional model domain, the rocks included in the Ancell, Ironton-Galesville, and Mt. Simon Units are not aquifers, so the generic term *Unit* is employed to refer to these materials.

Shallow aquifers include the Shallow Bedrock Aquifer (a layer of weathered rocks encompassing the uppermost 50 to 100 feet of bedrock) and several discontinuous layers of unconsolidated sand and gravel contained in the glacial drift overlying the aquifer. In Kane County, the Shallow Bedrock Aquifer consists principally of dolomite and shale of Silurian and Ordovician age. Although the Shallow Bedrock Aquifer is defined by the porosity associated with weathering at the bedrock surface and is therefore present throughout Kane County, it is most productive in the eastern part of the county, where the uppermost bedrock consists of the dolomite of Silurian age. The comparatively pure, thinly bedded Silurian dolomite facilitates weathering and consequent development of porosity and permeability. These factors increase aquifer productivity.

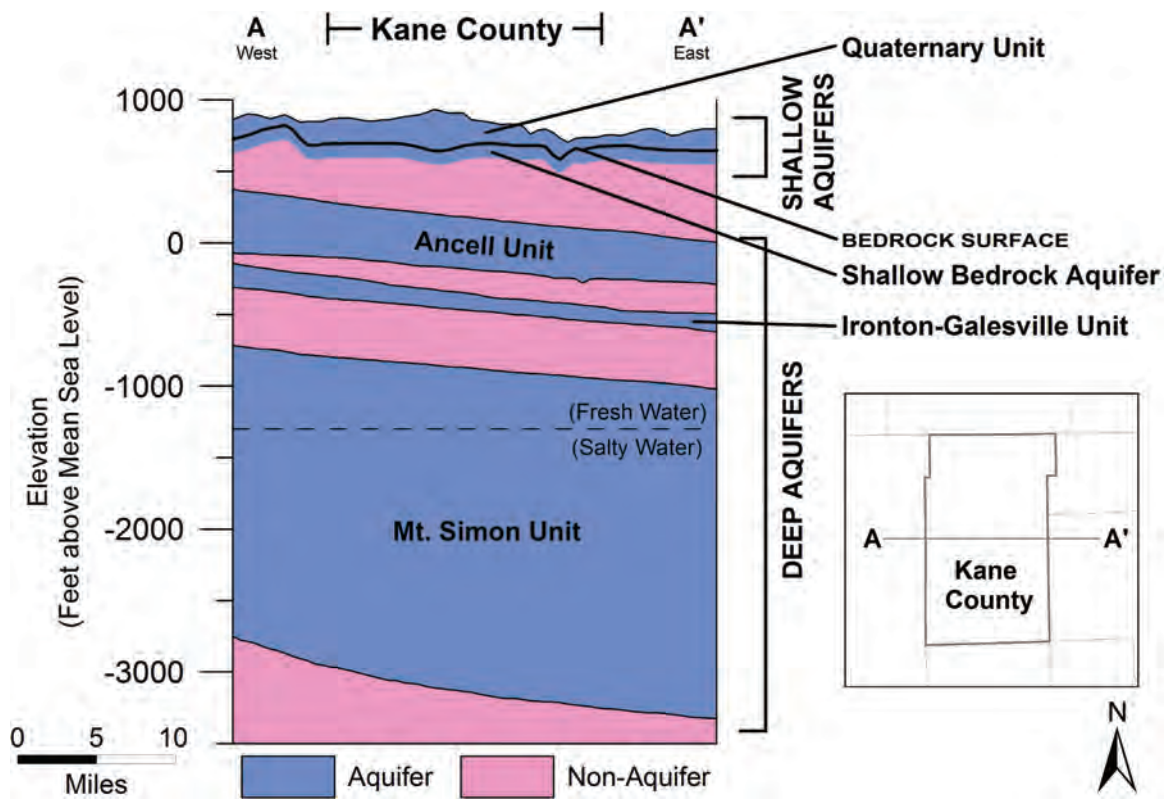


Figure 2. Major aquifers of the Kane County area.

Groundwater withdrawals generally have increased from about 25 Mgd in 1964 to 40 Mgd in 2003 (Figure 3). The exception to this increasing trend was the late 1970s through the early 1990s, when withdrawals declined as the large Elgin and Aurora public water systems shifted from the deep aquifers to the Fox River. Since the early 1990s, groundwater withdrawals have increased significantly, from about 30 to 40 Mgd, to accommodate water demand increases associated with population growth. Since the late 1990s, Kane County groundwater withdrawals have been divided about equally between the deep and shallow aquifers.

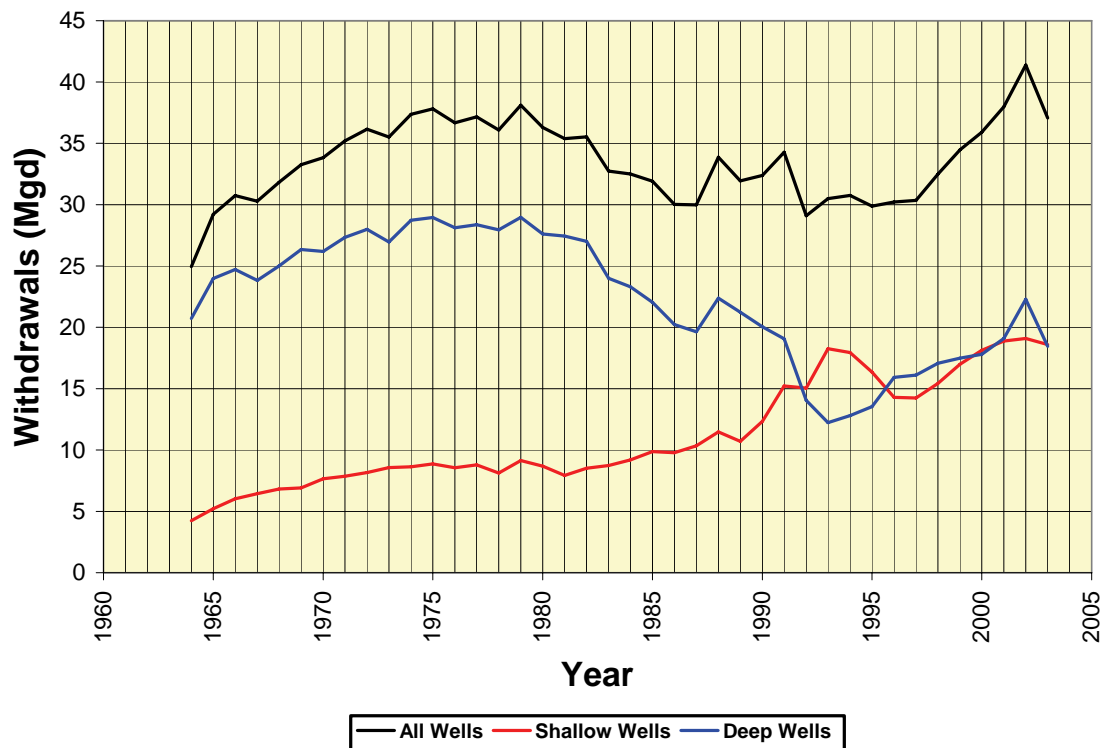


Figure 3. Groundwater withdrawals by public water systems, irrigators, and self-supplied commercial and industrial facilities in Kane County from 1964 through 2003.

3. Groundwater Flow Models

Understanding the relationships between these water resources and their response to withdrawals requires a quantitative approach that assimilates the available observations and knowledge, computes flow rates and water levels, and projects these into the future for alternative water-use scenarios. For the present study, these requirements are met using a computer groundwater flow model, which is a set of interrelated mathematical equations that represent water flow in aquifers and streams, solved using a computer program. Computer modeling of groundwater flow involves reviewing available data and information, developing a conceptual model of the aquifers and the stresses on them, choosing a computer program that solves mathematical equations describing flow, inferring input parameters for the computer program, calibrating and verifying the model against flow and water level observations to ensure realism and accuracy, and simulating various combinations of stresses of interest (Anderson and Woessner, 2002). Models developed for this study use the computer program MODFLOW (Harbaugh et al., 2000; McDonald and Harbaugh, 1988) to simulate groundwater flow processes of the conceptual model. MODFLOW is a thoroughly documented and widely used program developed by the United States Geological Society (USGS) that uses the finite-difference method, a mathematical technique which divides the aquifer into a grid of blocks to solve equations representing groundwater flow through porous media.

Two groundwater models have been developed for this study (Figure 4), the first of which is a *regional-scale model* that provides an analysis of the deep aquifers and the overall groundwater flow patterns. The regional model consists of 20 layers that simulate groundwater flow in all geological materials from the land surface down to the deep underground crystalline rocks that are effectively impervious (Figure 5). It includes both the shallow and deep aquifers in a large portion of Illinois, Indiana, Michigan, Wisconsin, and Lake Michigan. The regional model employs a variable resolution, with its highest resolution in a rectangular *nearfield* area covering all of northeastern Illinois, where cells have horizontal dimensions of 2,500 feet (ft) (Figure 6). The regional-scale model quantifies groundwater flow in the deep aquifers of the model nearfield area and evaluates regional flow patterns in shallow aquifers. Nested inside the regional-scale model is a second, local-scale model of much greater detail that quantifies groundwater flow within the shallow aquifers of Kane County and surrounding townships. The effects of regional-scale groundwater flow are transferred to the local model by assigning flow rates simulated by the regional model to the boundaries of the local model. Because the flow across the local boundaries changes little with time, this process of nesting the models, or Telescopic Mesh Refinement, need only be done once for the local-scale model.

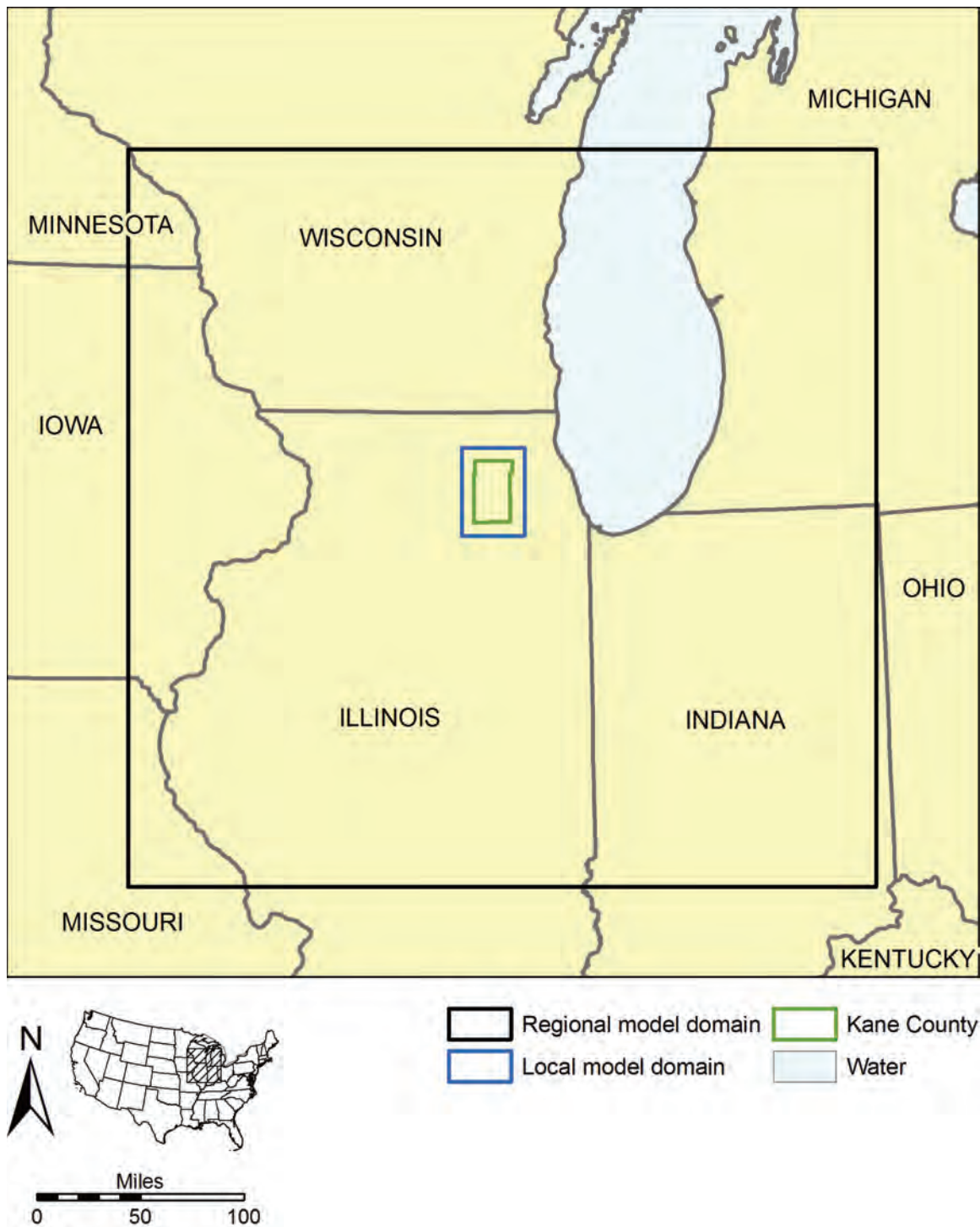


Figure 4. Areal extent of groundwater flow models.

HYDROSTRATIGRAPHIC UNIT	MODEL LAYER
Quaternary Unit (QT)	1
	2
	3
Upper Bedrock Unit (UB)	4
Silurian-Devonian Carbonate Unit (SD)	5
	6
	7
Maquoketa Unit (MQ)	8
	9
Galena-Platteville Unit (GP)	10
	11
Ancell Unit (AN)	12
Prairie du Chien-Eminence Unit (PE)	13
Potosi-Franconia Unit (PF)	14
Ironton-Galesville Unit (IG)	15
Eau Claire Unit (EC)	16
Mt Simon Unit (MS)	17
	18
	19
	20

Figure 5. Layer scheme of regional-scale model.

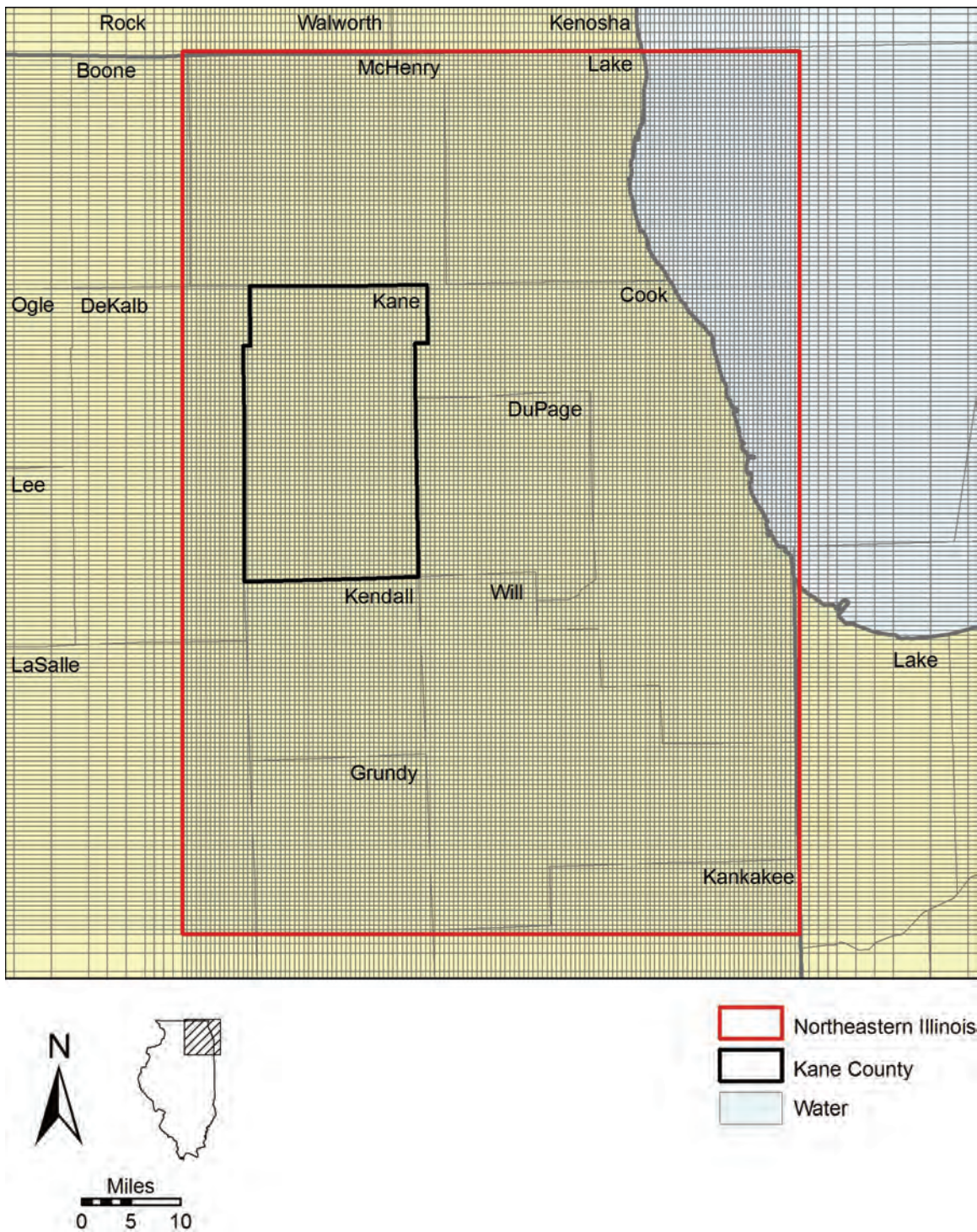


Figure 6. Detail of northeastern Illinois showing regional model grid and regional model nearfield.

The local-scale model is more highly resolved, using 15 layers and a horizontal grid spacing of 660 ft to simulate flow in a domain including only the shallow units in Kane County and the surrounding areas out to a distance of about 6 miles from the county boundaries (Figure 7, Figure 8). The local model provides detailed analysis of groundwater flow in Kane County shallow aquifers and interactions between groundwater and surface water. The purposes of the local model are to quantify groundwater flow, estimate wellfield capture zones, and evaluate groundwater-surface water interaction in the shallow aquifers of Kane County and the immediately adjacent areas. The lowermost interval represented in the local-scale model is the Shallow Bedrock Aquifer (local-scale model layer 15). In terms of the hydrostratigraphic units represented in the regional-scale model (Figure 5), the Shallow Bedrock Aquifer of the local-scale model is equivalent to portions of the Silurian-Devonian Carbonate Unit, Maquoketa Unit, and Galena-Platteville Unit within 50 to 100 ft of the bedrock surface. The Upper Bedrock Unit of the regional-scale model is not present in the Kane County area and is not represented in the local-scale model. The 14 layers of the local-scale model overlying the Shallow Bedrock Aquifer represent the same materials represented in the regional-scale model as the Quaternary Unit; in the regional-scale model, the Quaternary Unit is represented with three model layers.

To ensure that the models accurately represent hydrogeological conditions within their domains, data employed for characterization of layer elevations, parameters, and boundary conditions in both are based to the extent possible on a wide range of published and unpublished observations. Parameters such as hydraulic conductivity and recharge rates are specified on a zoned basis. The models have been calibrated so that they reproduce observed estimates of head and base flow within the uncertainty of these observations. The models facilitate analysis of predevelopment conditions and the impacts of historical and future scenarios of groundwater development, and they readily permit insight into cause-and-effect relationships pertaining to groundwater flow.

Groundwater flow models developed for this project are available to the public to simulate groundwater flow in Kane County and northeastern Illinois and to provide a framework for more detailed, site-specific studies. The models represent a synthesis of data and information available to the authors during the period from 2002 to 2008, and they were developed using procedures and computer software widely accepted during that time. Model users should understand that the models, and the analyses based on them, are works in progress reflecting currently available technologies, modeling approaches, and data. Both models and analyses should be updated periodically to reflect newly available data, information, and analysis, as well as new approaches to data synthesis and analysis, modeling techniques, and computer software.

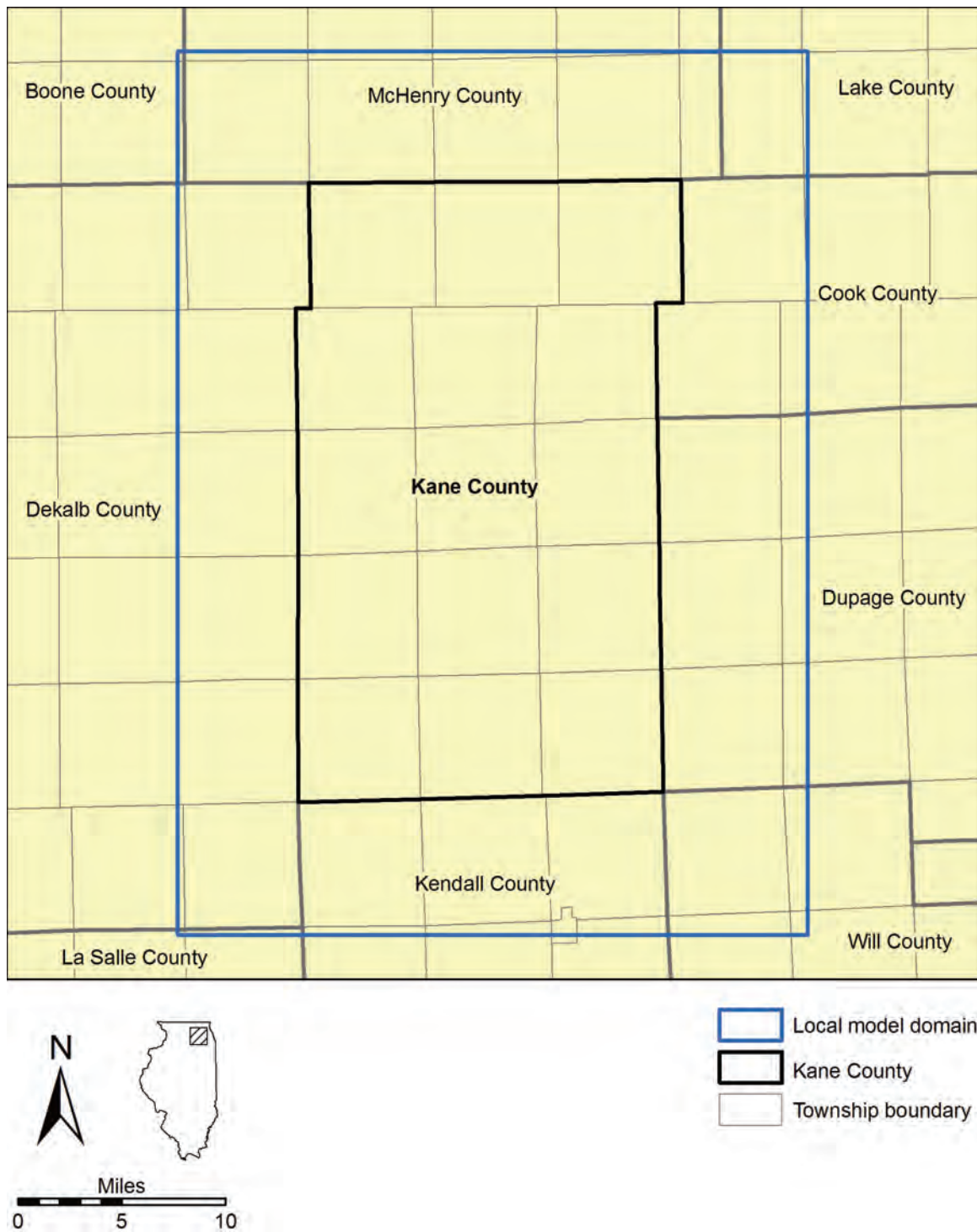


Figure 7. Local-scale model domain.

HYDROSTRATIGRAPHIC UNIT		MODEL LAYER
Equality Unit		1*
Surficial Henry Unit		
Wadsworth Diamicton Unit		2
Wadsworth Sand Unit		
Haeger Diamicton Unit		
Beverly Unit		3
Yorkville Diamicton Unit		4
Yorkville Sand Unit		5
Batestown Diamicton Unit		6
Batestown Sand Unit		7
Tiskilwa Unit		8
Ashmore Unit		9
Glasford Unit	Upper Glasford Diamicton Unit	10
	Upper Glasford Sand Unit	11
	Middle Glasford Diamicton Unit	12
	Lower Glasford Sand Unit	13
	Lower Glasford Diamicton Unit	14
Shallow Bedrock Aquifer		15

*Layer 1 includes the uppermost 10 ft of material. Where the aggregate thickness of the Equality Unit and Surficial Henry Unit is less than 10 ft, layer 1 includes enough of the underlying unit so that total thickness is 10 ft.

Figure 8. Layer scheme of local-scale model.

4. How Much Groundwater is Available in Kane County?

This question cannot be answered without making so many qualifying assumptions that the answer is unusable as a management guideline. Collective withdrawals from a network of wells, such as those in Kane County, cause the water elevation in wells (*head*) that are open to the source aquifers to decline. These head declines (*drawdowns*) can lead to increased pumping expenses and decreased well yields; decreased groundwater discharge to streams, causing reduced streamflow; reduced water levels in lakes and wetlands; and changes in the vegetation. In some settings, reduced heads also can result in decreased groundwater quality, requiring expensive treatment. Therefore, the question of how much water can be pumped from wells sustainably depends on how wells affect the environment and what the public considers to be acceptable environmental impacts (Alley et al., 1999; Bredehoeft, 2002; Bredehoeft et al., 1982; Devlin and Sophocleus, 2005). Moreover, the impacts of groundwater withdrawals constantly change as recharge rates adjust to climate change, new wells are drilled, old wells are abandoned, and pumping rates at individual wells rise and fall both inside and outside of Kane County. Lastly, the availability of groundwater is very much related to the price the public is willing to pay for groundwater treatment. For example, if the public is willing to pay for desalination of deep groundwater or if technological advances decrease the cost of desalination, then more groundwater will be available.

In this study, then, instead of generating single-value estimates of groundwater availability, plausible future pumping and recharge scenarios were simulated using groundwater flow models that quantify the impacts of these scenarios. If these impacts are considered by local water managers to be unacceptable, they may choose to adapt policy and target monitoring and water-management efforts to track and mitigate impacts countywide or in affected areas. Groundwater flow models developed for this project also may be used for future analysis of other scenarios to test effects of alternative management strategies.

For this project, both historic pumping and estimates of future pumping are simulated. Two future *pumping conditions*, which are referred to as low-pumping conditions and high-pumping conditions, are simulated (Figure 9), through the end of 2049. These pumping conditions are simulated for “normal” (i.e., historic) recharge rates and for reduced and elevated recharge rates to demonstrate possible effects of climate change. Historic pumping rates simulated on the models cover the period 1864 through 2003, and are based on databases maintained by university and state authorities in Illinois and Indiana and on data compiled for previous groundwater flow modeling projected in Illinois and Wisconsin. Post-2003 pumping data were not available when the groundwater flow models for this project were developed. Estimates of future pumping through 2050 were developed from forecasts assembled by Dziegielewski et al. (2004, 2005). Under low-pumping conditions, withdrawals in Kane County are assumed to increase from about 37 to 52 Mgd from 2003 to 2050; under high-pumping conditions, Kane County withdrawals are assumed to increase from 37 to 71 Mgd from 2003 to 2050. The project timeline required the authors to estimate pumping rates for both low- and high-pumping conditions in 2005, yet at the time of printing, the 2005 pumping rates are historic fact. Actual pumping in Kane County in 2005 (44 Mgd) exceeded estimated 2005 pumping under both low- and high-pumping conditions (40 Mgd in both cases). Assumed

reduced and elevated recharge rates differ from place to place in the model domains, but in Kane County they are specified at about 12 percent lower and higher than the “normal” historic rate.

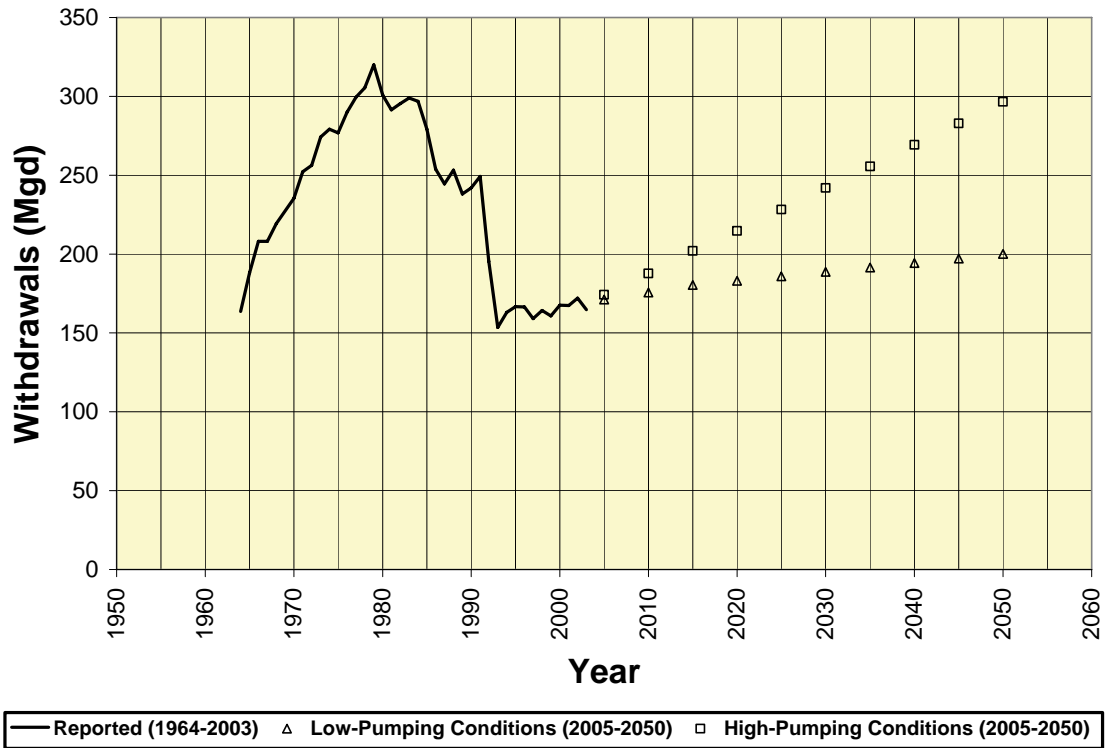


Figure 9. Historic and projected groundwater withdrawals in the regional model nearfield of northeastern Illinois (Figure 6).

5. Model Analysis

5.1. General Flow Patterns

To understand the consequences of present-day withdrawals and to evaluate projected pumping scenarios, this study first assesses *predevelopment conditions* with the models. Predevelopment conditions (i.e., in the late 1800s, prior to the growth in groundwater pumping) are inferred from sparse historical data and modern streamflow statistics. This assumed predevelopment state is a typical assumption of hydrogeologic studies in the Midwest and is justified by the small trend in baseflow reported by Meyer (2005) for urbanization. However, predevelopment conditions are poorly known and remain a research topic that lies outside the scope of the present study. The initial analysis includes model calibration, where input parameters are adjusted within their plausible ranges until model simulations of heads and flows are similar to the observed heads and flows. In general, the regional model is most accurate within the Ancell aquifer of northeastern Illinois, and the local model is most accurate within Kane County. The simulated heads and flows are within the error of the available observations, and the degree of accuracy is similar to comparable models of Midwestern hydrogeology.

Model analysis shows that groundwater in shallow aquifers of Kane County flows from upland recharge areas and discharges to nearby wells or surface waters. Under predevelopment conditions, shallow groundwater discharged exclusively to surface waters and wetlands, but under present-day conditions, a proportion of discharge occurs through wells. This change has the effect of reducing groundwater discharge to wetlands and surface water, although a portion of the withdrawals will ultimately be returned to surface waters as effluent from wastewater treatment plants and runoff. In most of northeastern Illinois, including all but the southwesternmost corner of Kane County, relatively impermeable rocks overlie the deep aquifers, greatly reducing exchange of water between the shallow and deep aquifers. Groundwater flow within the deep aquifers occurs on a regional scale, with most recharge into the aquifers occurring in north-central Illinois, west of Kane County, where the impermeable rocks overlying the deep aquifers are absent. Under predevelopment conditions, groundwater in the deep aquifers underlying northeastern Illinois slowly discharged upward into the shallow units, and ultimately to surface waters—primarily the upper Illinois River and lower Fox River—with limited diffuse upward leakage to Lake Michigan. Presently, the deep groundwater flow is dominated by discharge to wells in Cook, DuPage, Kane, and Will Counties in Illinois and to wells in Milwaukee and Waukesha County, Wisconsin. The greatest drawdowns in the Chicago area correspond to areas of greatest historical pumping, and include Joliet, Aurora, and an area corresponding to the Cook-DuPage county line. Model results indicate that locations and magnitudes of drawdown and streamflow reduction are caused by pumping from both deep and shallow aquifers.

Simulated heads in shallow aquifers mimic surface topography, with a pattern of high heads in northwestern Kane County that decline toward the south and east to lows along the Fox River. This pattern becomes more muted with depth, so small topographic features reflected in the hydraulic heads of the shallowest aquifers are less apparent in the heads of the more deeply-buried aquifers. Drawdown is limited by capture of streamflow, so the impact of wells is not as widespread as in the deep aquifers. Model simulations

suggest that the capture of streamflow by shallow wells can significantly reduce natural groundwater discharge to streams in some areas.

5.2. Modeling of Historical Conditions

Simulations of historical withdrawals (from 1864 to 2002 with the regional-scale model and from 1964 to 2003 with the local-scale model) verified that simulated heads and flows accurately represent observed heads and flows. Regional model simulations were conducted to characterize drawdown in the principal deep aquifers of northeastern Illinois—the Ancell and Ironton-Galesville Units. Simulations with the local-scale model were employed mainly to characterize drawdown in the shallow aquifers in the Kane County area and to quantify reductions in streamflow in Kane County streams.

In general, model simulations show that drawdown in the deep aquifers is much greater than in the shallow aquifers, this difference reflecting the availability of *replacement water* to the aquifers (i.e., water entering the aquifers to replace groundwater withdrawn through wells). In northeastern Illinois, impermeable confining units greatly limit leakage into the deep aquifers from above, so replacement water for these aquifers is derived principally by slow, lateral movement from north-central Illinois where impermeable cover is absent. In contrast, impermeable materials are discontinuous in the Quaternary materials and therefore do not greatly limit entry of replacement water into the shallow aquifers. Thus, drawdown in these aquifers is offset by comparatively high rates of leakage into the aquifers. Some of this replacement water originates as captured streamflow, which is a consequence of (1) diversion of recharge into shallow wells that would otherwise discharge to a stream and (2) leakage of water from stream channels in response to pumping. Although streamflow capture tends to reduce drawdown in shallow aquifers, this can result in reduced groundwater discharge to streams. Pumping from the deep aquifers in southeastern Wisconsin contributes to drawdown in northeastern Illinois, but pumping in northwestern Indiana, which is almost entirely limited to the shallow aquifers, has little effect on heads in northeastern Illinois.

5.2.1. Head Change in Deep Aquifers

Simulation with the regional model for 2002 suggests that drawdown since the start of pumping in the Aurora area—the location of greatest drawdown in Kane County—exceeded 500 ft in the Ancell Unit (Figure 10) and 1100 ft in the Ironton-Galesville Unit, the most important deep aquifers in the region. A steep west-to-east gradient has become established in both aquifers across Kane County, a result of the county's location between the heavily pumped Chicago area to the east and the recharge area to the west. This places the county between the large drawdowns of the Chicago cone of depression and small drawdowns where the impermeable cover is absent and leakage from shallow aquifers is greater (Figure 11). Thus, simulated drawdown in eastern Kane County (e.g., St. Charles, as shown in Figure 12 and Figure 13) is greater than to the west (see Maple Park in Figure 12 and Figure 13) because the eastern area is more affected by heavy pumping and is less affected by leakage from shallow aquifers to the west. This pattern causes water levels in deep wells to decline, requiring increasingly greater expense to lift groundwater from deep wells. In addition, head declines in these units in the Chicago area have the potential to induce migration of salty water from deeper units and from areas south of the metropolitan area, reducing water quality.

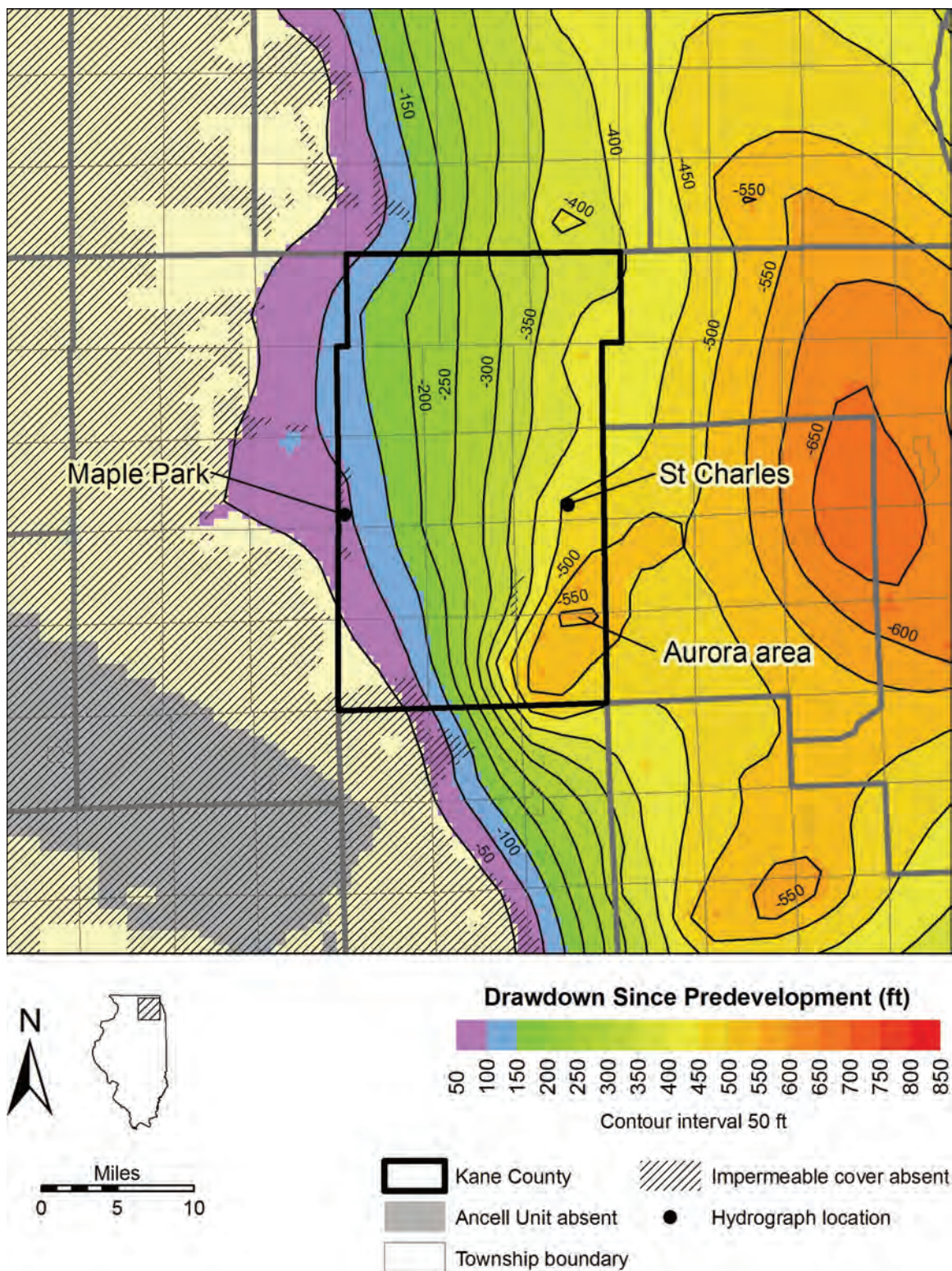


Figure 10. Simulated drawdown due to pumping in the Ancell Unit in the Kane County area in 2002.

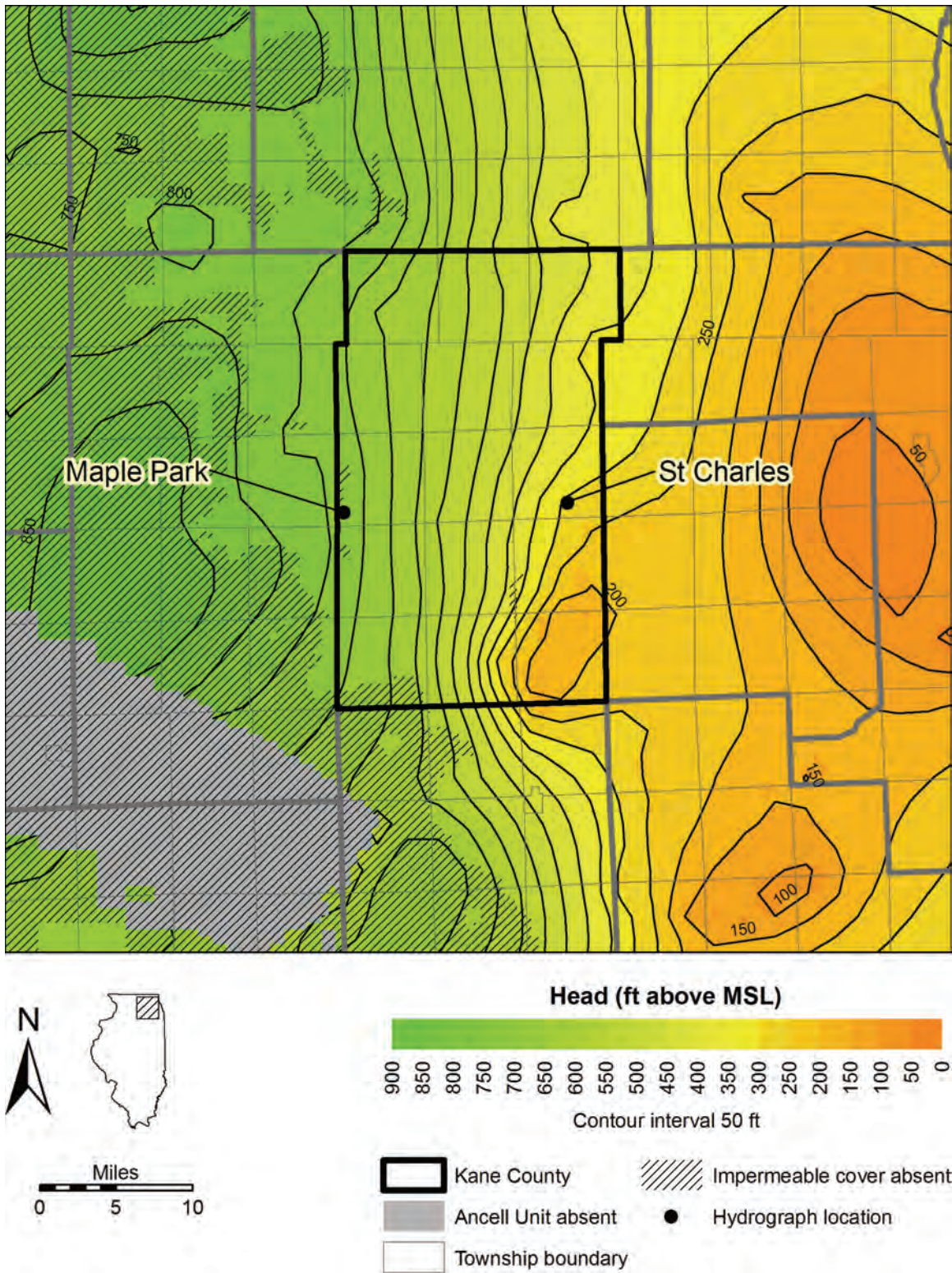


Figure 11. Simulated head in feet above mean sea level (ft above MSL) in the Ancell Unit in the Kane County area in 2002.

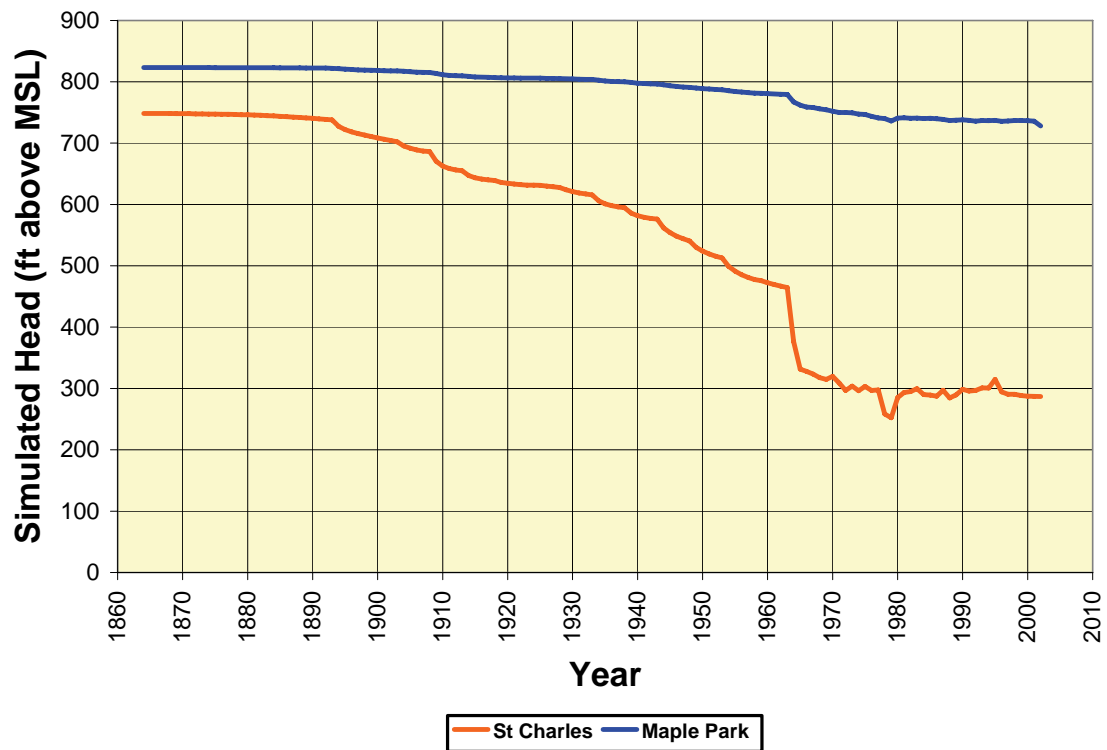


Figure 12. Simulated head from 1864 to 2002 in the Ansell Unit at St. Charles and Maple Park.

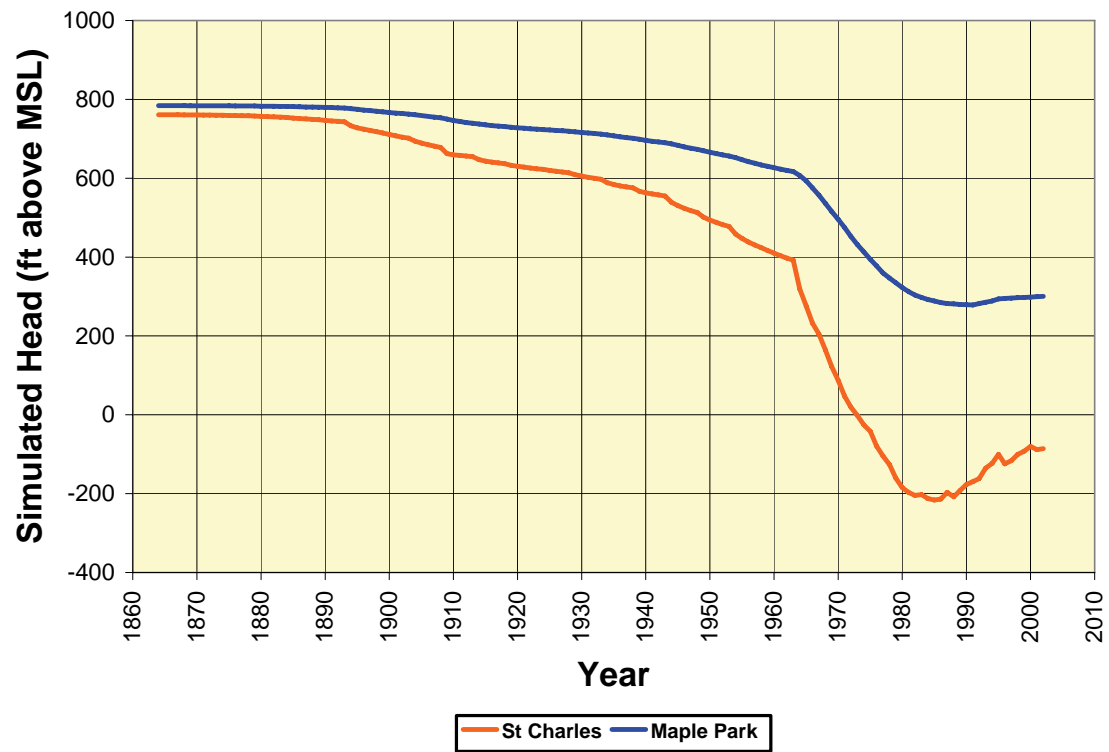


Figure 13. Simulated head from 1864 to 2002 in the Ironton-Galesville Unit at St. Charles and Maple Park.

In parts of northeastern Illinois east of Kane County, simulated heads in the deep aquifers recover after 1979, when numerous deep wells in those areas began to be abandoned as water suppliers converted to a Lake Michigan source (note the overall decline in withdrawals from 1979 to 1993 in Figure 9) (Figure 14). During the same period, public water systems at Elgin (1983) and Aurora (1992) began withdrawing water from the Fox River, greatly reducing their withdrawals from the deep aquifers. Model simulation suggests that the latter conversion, together with communities further east converting to water supplied from Lake Michigan, caused some recovery of heads in Kane County. In Figure 14, this recovery is evident in the Elgin area of northeastern Kane County, where the figure shows an increase in head (recovery) of over 50 ft since 1979. Recovery is not evident in the Aurora area in Figure 14 because the conversion to Fox River water began there in 1992, and heads in 2002 at Aurora were still well below those in 1979. With the exception of Elgin and Aurora, the effect of the water-source conversions on simulated Ancell heads in Kane County has been more to slow the decline in heads than to cause actual recovery.

There are potential problems associated with the decline of Ancell Unit heads near and below the top of the Ancell Unit:

- Studies of the Ancell in the Green Bay area of Wisconsin (Schreiber et al., 2000) suggest that exposure to oxygen of a thin interval at the top of the Ancell Unit containing sulfide minerals including small amounts of arsenic—as could happen where Ancell heads decline to within 100 ft of the top of the unit—could cause an increase in arsenic concentrations in groundwater withdrawn from deep wells to levels exceeding the United States Environmental Protection Agency (USEPA) drinking water standard of 10 micrograms per liter. Studies by the Illinois State Geological Survey suggest that sulfide minerals are present at the top of the Ancell Unit in northeastern Illinois, but it is not understood whether these minerals contain the arsenic that is present in Wisconsin.
- Since many deep wells in northeastern Illinois are open to both the Ancell Unit and the Ironton-Galesville Unit, desaturation of the Ancell Unit could increase the proportion of Ironton-Galesville groundwater withdrawn from these wells. This increased proportion of Ironton-Galesville groundwater may reduce water quality, because the Ironton-Galesville groundwater is believed to be poorer in quality than the Ancell Unit groundwater, containing, most notably, high concentrations of dissolved radium and barium (Gilkeson et al., 1983). Concentrations of barium and radium in the Ironton-Galesville often exceed the USEPA drinking water standards of 1 milligram per liter and 5 picocuries per liter, respectively.
- Since drawdown in the deep aquifers causes water levels in the wells to decline, it can cause deep well productivity to decline and pumping expenses to increase. These problems are exacerbated with desaturation of the Ancell Unit.

Because of these potential difficulties, maps have been developed for this study showing the *available head* above the top of the Ancell. Available head is the difference between Ancell Unit head and the top of the Ancell. These maps do not show areas where available head remains above 100 ft, but areas with less than 100 ft of available head might be considered for monitoring or as priorities for planning. Simulated Ancell Unit head remains above the top of the Ancell Unit in 2002, but pumping from deep wells has caused Ancell head to decline to within 100 ft of the top of the unit in the Aurora area (Figure 15). Model simulations suggest that the areas of low available head southwest of Kane County, adjacent to the area where the Ancell is absent, existed during predevelopment. Maps of future simulated available head are included in Section 5.3.2.

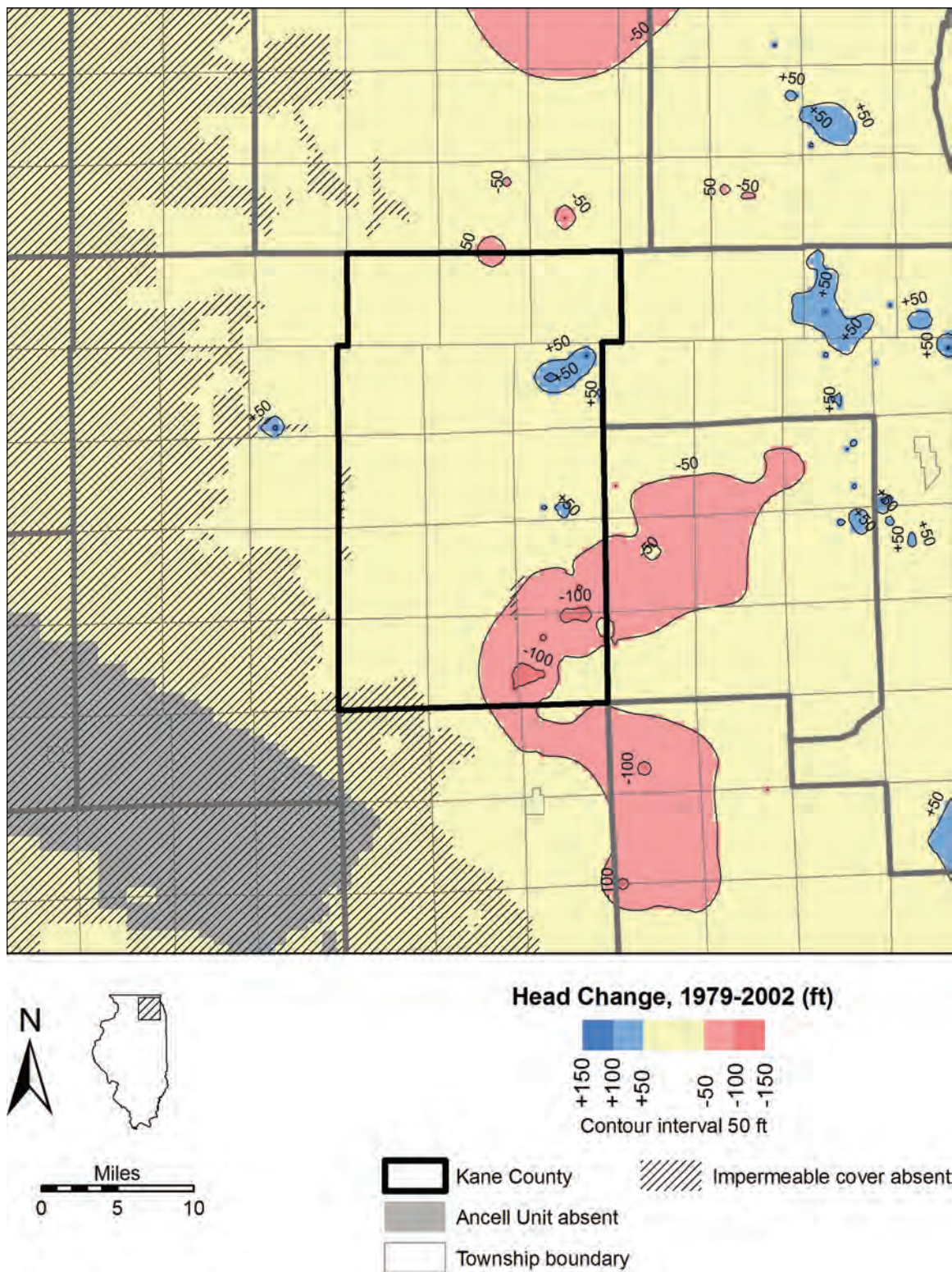


Figure 14. Change in simulated head in the Ancell Unit in the Kane County area, 1979-2002.

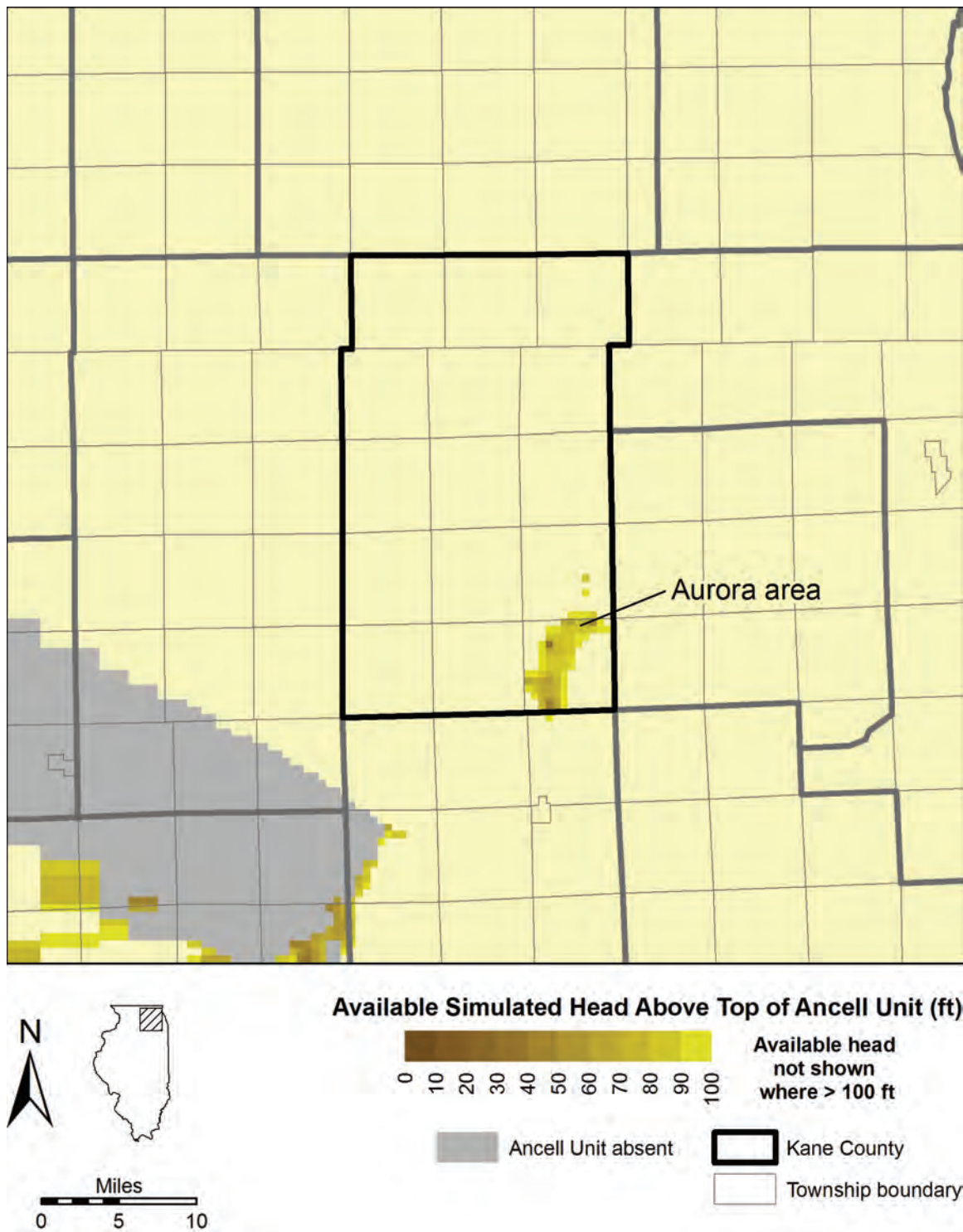


Figure 15. Available simulated head above the top of the Ancell Unit in 2002.

5.2.2. *Head Change in Shallow Aquifers*

Drawdown in the shallow aquifers is much less than in the deep aquifers because withdrawn groundwater is replaced at much higher rates. Two large areas of significant shallow aquifer drawdown (here defined as drawdown greater than or equal to 20 ft) affected the Kane County area in 2003, both crossing the borders of Kane County. A map of simulated drawdown in the Shallow Bedrock Aquifer, the deepest of the shallow aquifers, is representative of drawdown in all overlying aquifers (Figure 16). Drawdown in these areas is partially attributable to pumping outside of the county and is compounded by large withdrawals, low hydraulic conductivities, and hydrogeological settings that reduce streamflow capture. The significant drawdowns observed in northeastern Kane and southeastern McHenry Counties are the consequence of wells operated by the Villages of Algonquin, Carpentersville, East Dundee, Lake in the Hills, and the City of Crystal Lake (Figure 17). The drawdown in this area exceeds 60 ft in Kane County near the McHenry County border, in the area of Algonquin wells 7, 8, 9, and 11. Pumping by the City of West Chicago and Village of Warrenville in DuPage County causes a second area of significant drawdown that crosses into Kane County and impacts the Cities of Batavia and Geneva (Figure 18).

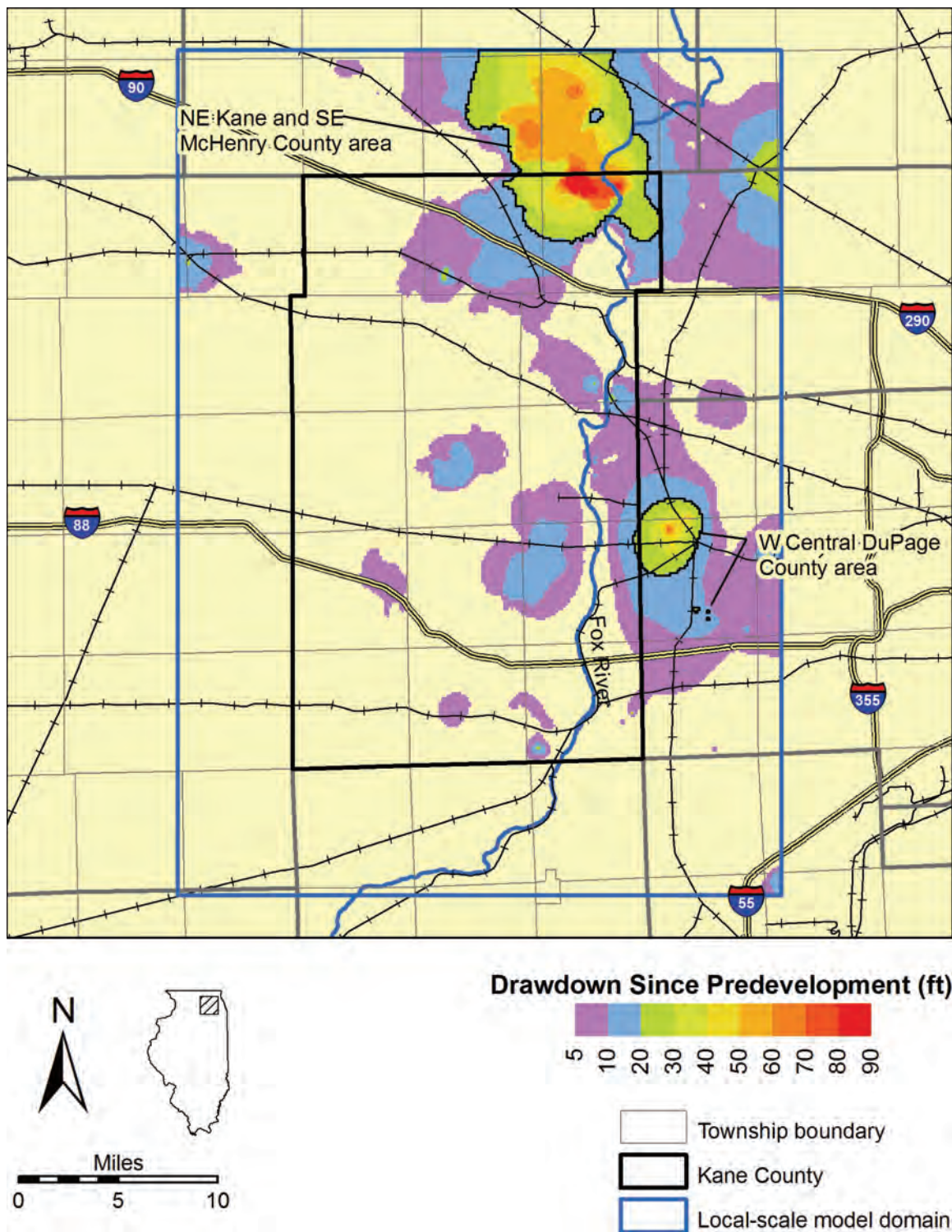


Figure 16. Simulated 2003 drawdown in the Shallow Bedrock Aquifer in the Kane County vicinity, with areas of significant drawdown mentioned in the text identified.

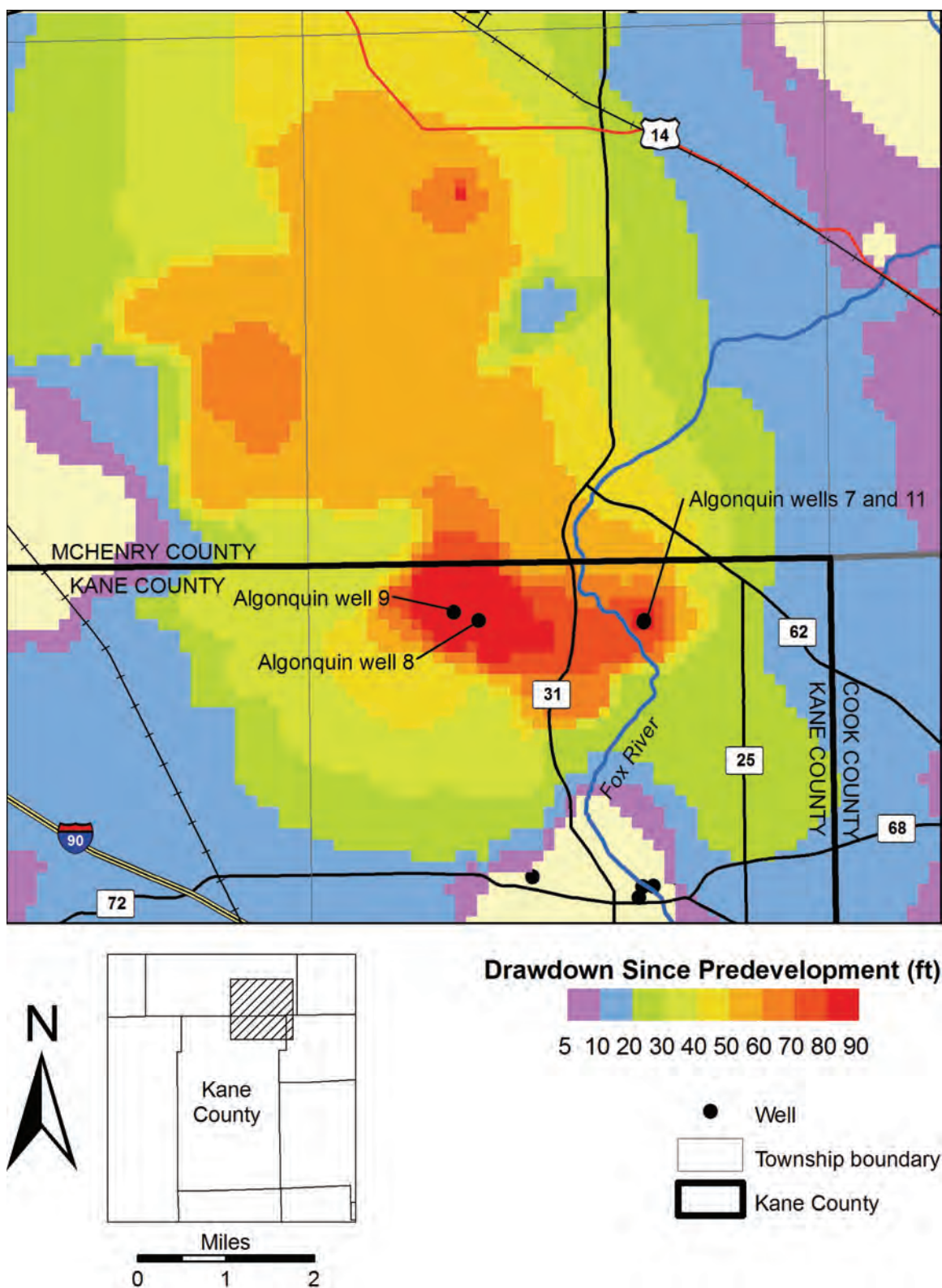


Figure 17. Simulated 2003 drawdown in the Shallow Bedrock Aquifer in northeastern Kane County and southeastern McHenry County.

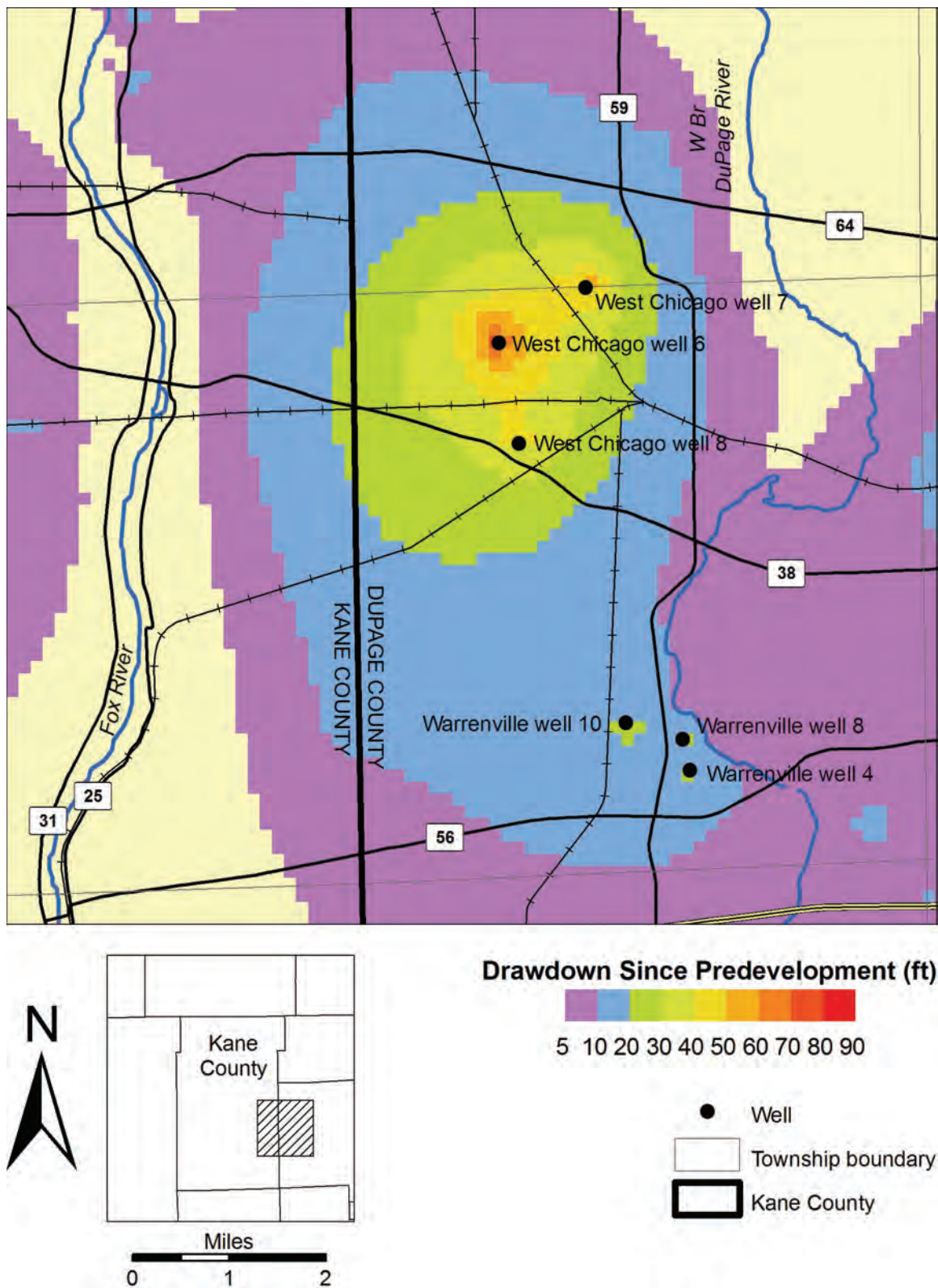


Figure 18. Simulated 2003 drawdown in the Shallow Bedrock Aquifer in east-central Kane County and west-central DuPage County.

5.2.3. *Changes in Streamflow*

As discussed in Section 5.1, a proportion of the water withdrawn from shallow wells originated as captured streamflow, meaning that the pumped water is either groundwater diverted to wells that otherwise would discharge to streams or that it is water induced to leak from stream channels by pumping wells. The local-scale model suggests that, as of 2003, streamflow capture by groundwater pumping had reduced natural groundwater discharge to streams in and near Kane County by about 17 percent (Figure 19). This capture of streamflow by wells would be observable as a reduction in base flow in streams (that part of streamflow originating as groundwater discharge), although it is likely that discharge of effluent compensates for the base flow reduction in some stream reaches downstream of wastewater treatment plant outfalls (Knapp et al., 2007). This reduction of natural groundwater discharge is irregularly distributed and is greatest in streams in the eastern part of the county where shallow pumping is greatest (Figure 20, Table 1). Model simulations suggest that the greatest reduction in natural groundwater discharge by 2003 occurred in Mill Creek upstream of Batavia (reach 512 in Figure 20). In this area, public supply wells operated by the Cities of Batavia and Geneva have reduced groundwater discharge by 68 percent relative to nonpumping conditions (Figure 21).

Other stream reaches receiving substantially less natural groundwater discharge in 2003 as a consequence of pumping include the West Branch of the DuPage River upstream of Warrenville (reach 520 in Figure 20, 52 percent reduction) and the Fox River upstream of Algonquin (reach 503 in Figure 20, 46 percent reduction). Both of these streams lie largely outside Kane County, however, and therefore outside the area of greatest model accuracy.

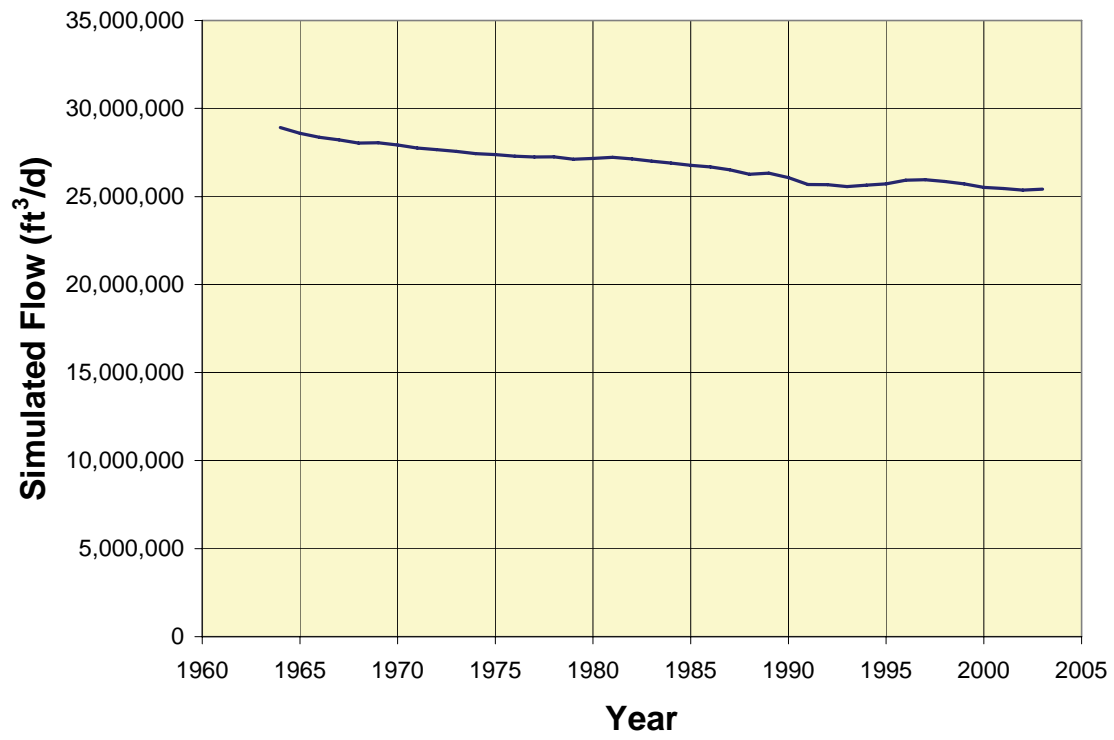


Figure 19. Total simulated natural groundwater discharge in local model domain.

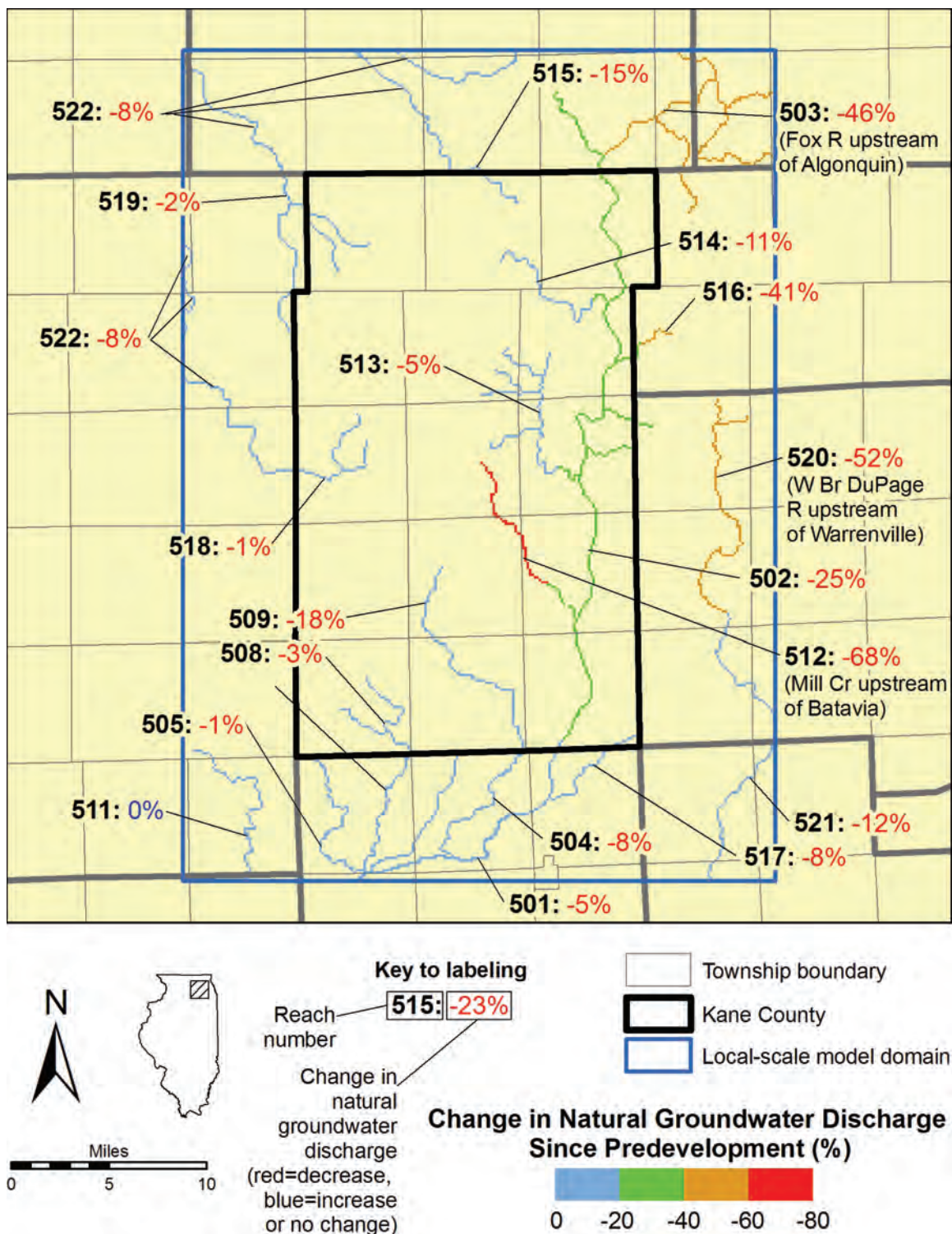


Figure 20. Change in natural groundwater discharge caused by pumping by stream reach in the Kane County area in 2003, with reaches discussed in text identified (see Table 1 for identification of all reaches).

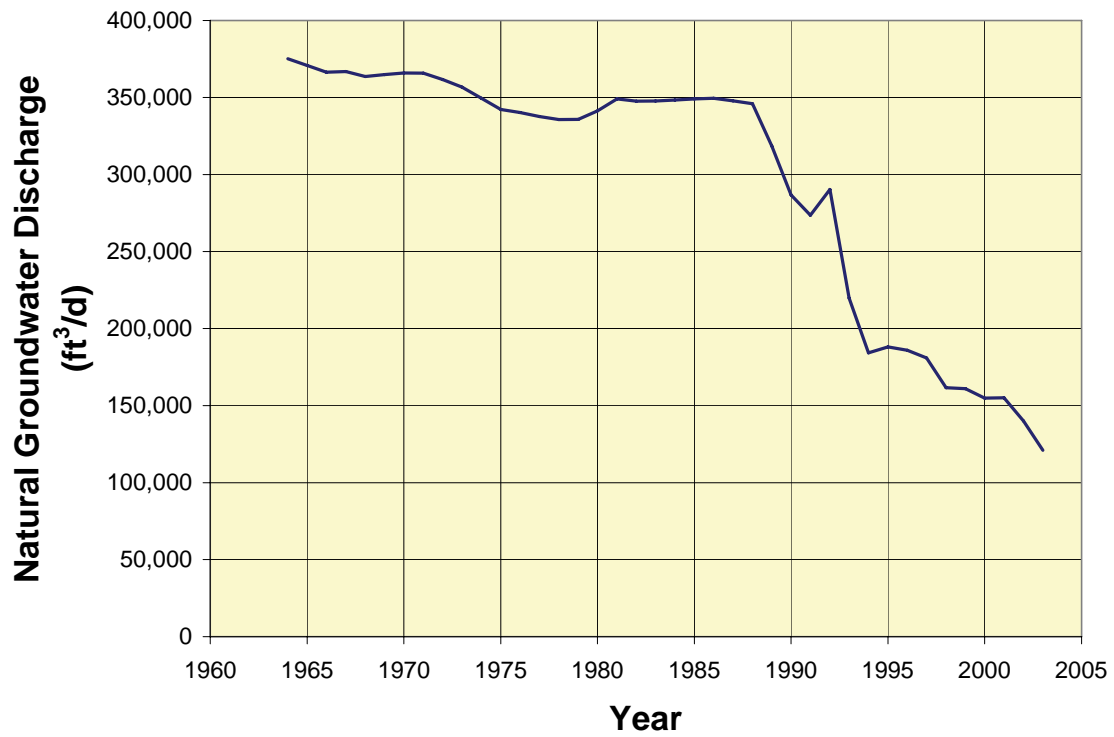


Figure 21. Simulated natural groundwater discharge to Mill Creek upstream of Batavia (reach 512).

**Table 1. Principal Streams Included in Reaches
Shown in Figure 20 and Change in Natural Groundwater Discharge Due to
Pumping in 2003 (%)**

<i>Reach Number</i>	<i>Principal Streams</i>	<i>Change in Natural Groundwater Discharge Due to Pumping (%)</i>
501	Fox River downstream of Montgomery; Big Rock Cr downstream of Kane County boundary	-5
502	Fox River from Algonquin to Montgomery; Norton Cr; Brewster Cr; Crystal Cr; lower portions of Mill Cr, Ferson Cr, Poplar Cr, and Tyler Cr	-25
503	Fox River upstream of Algonquin; Spring Cr; Flint Cr	-46
504	Blackberry Cr from Montgomery to Yorkville	-8
505	Little Rock Cr downstream of Kane County boundary	-1
507	Big Rock Cr downstream of Kane County boundary	-11
508	Big Rock Cr upstream of Kane County boundary; Welch Cr	-3
509	Blackberry Cr from Elburn to Montgomery	-18
511	Somonauk Cr	0
512	Mill Cr upstream of Batavia	-68
513	Ferson Cr upstream of St Charles; Otter Cr; Stony Cr; Fitchie Cr	-5
514	Tyler Cr	-11
515	S Br Kishwaukee River upstream of Huntley	-15
516	Poplar Cr	-41
517	Waubonsie Cr	-8
518	Union Ditch No 3; Virgil Ditch No 3; Union-Virgil Ditch No 2	-1
519	Upper Coon Cr	-2
520	W Br DuPage River upstream of Warrenville	-52
521	DuPage River; W Br DuPage River downstream of Warrenville	-12
522	Aggregated tributaries of S Br Kishwaukee River outside Kane County	-8

5.3. Modeling of Future Conditions

5.3.1. Scenarios

After calibration, the models were used to simulate possible future scenarios of groundwater pumping and changes in recharge rates that might result from climate variability. A total of four scenarios were simulated for the period 2005 to 2050 (Table 2), including two scenarios that assume no change in recharge (i.e., no impact of climate variability) for two different trends in the growth of groundwater pumping (previously discussed as *low-* and *high-pumping conditions* in Section 4). A third scenario, the most resource-intensive of the four, assumes the high-pumping trend and reduced recharge rates. The last scenario, the least resource-intensive, assumes the low-pumping trend and elevated recharge rates. Although this study examines only these four scenarios, the model and its supporting databases have been structured to permit a knowledgeable user to simulate a wide range of future scenarios.

The four scenarios simulated for the investigation were chosen to represent plausible well configurations and pumping rates in addition to a plausible range of recharge rates. Pumping rates are based on county-level forecasts of water withdrawals reported by Dziegielewski et al. (2004, 2005). Low-pumping conditions were characterized based on estimates of Dziegielewski et al. (2005) that assume continued improvements in water conservation by public water systems and self-supplied commercial and industrial facilities. High-pumping conditions are based on estimates of Dziegielewski et al. (2005) that assume improvements in water conservation by such water systems made before 2001 do not continue. Well locations and source aquifers are assumed to be the same as those for wells in operation during the period 2000-2003. The range of recharge rates is intended to simulate the effect that climate variability might have on groundwater recharge in the Kane County area. The simulated range of recharge rates is based on reported plausible ranges of recharge rates in the region for the historic period (Arnold et al., 2000; Bloyd, 1974; Cherkauer, 2001; Holtschlag, 1997). For brevity, the four modeled scenarios are referred to as *HL* (high pumping, low recharge), *HC* (high pumping, calibrated recharge), *LC* (low pumping, calibrated recharge), and *LH* (low pumping, high recharge).

For each scenario, we report change in head in significant aquifers and change in natural groundwater discharge, because these two effects, if large enough, might be considered unacceptable to residents of Kane County. For example, drawdown (reduction in head), affects water levels in wells, and therefore may cause reduced yields and increased pumping expenses. Reduction in natural groundwater discharge reduces stream base flow and consequently may affect the availability of streamflow for water supply, maintenance of riparian habitats, and recreation.

Table 2. Transient Simulations to 2050

<i>Abbreviation</i>	<i>Pumping Conditions</i>	<i>Recharge Conditions</i>	<i>Intensity of Resource Use</i>	<i>Figures Showing Results</i>
HL	High	Low	Most	Figure 31, Figure 35, Figure 36
HC	High	Calibrated	Intermediate	Figure 22, Figure 25, Figure 27, Figure 28, Figure 29, Figure 32, Figure 35, Figure 37
LC	Low			Figure 23, Figure 26, Figure 27, Figure 28, Figure 30, Figure 33, Figure 35, Figure 38
LH	Low	High	Least	Figure 34, Figure 35, Figure 39

5.3.2. *Head Change in Deep Aquifers*

Simulations of these future scenarios using the regional-scale model suggest that recharge variations due to climate variability will have a negligible effect on heads in the deep aquifers of the region before 2050. That is, model simulations of the HL and HC scenarios are nearly identical, as are simulations of the LC and LH scenarios. The results are so similar that this discussion is restricted to the results of regional modeling the HC and LC scenarios.

Model simulations suggest that head in the Ancell Unit will continue to decline through 2049 in all of Kane County, and declines after 2002 will exceed 50 ft in much of the county given both high- and low-pumping conditions. The greatest declines in Ancell Unit head in northeastern Illinois are projected to occur in the vicinity of Joliet and Aurora. In limited parts of these areas, simulated heads decline more than 150 ft between 2002 and 2050 under both high- and low-pumping conditions (Figure 22, Figure 23). The simulations suggest heads will continue to recover to a limited degree in eastern parts of northeastern Illinois, where many water systems abandoned deep wells in the 1980s and 1990s. The combination of continued head declines in the Joliet-Aurora area and continued head recovery in Cook and DuPage Counties shifts the deepest parts of the Chicago area cone of depression west-southwest to the Joliet-Aurora area (compare Figure 24 with Figure 25 and Figure 26). In most of Kane County, model simulations suggest that the recovery of Ironton-Galesville heads, which began in the 1980s, will continue at decreasing rates, followed by a renewed decline (Figure 27, Figure 28).

The modeling suggests that the Ancell Unit may become partially desaturated (i.e., the pore spaces may drain) by 2049 (Figure 29, Figure 30). These areas are surrounded by regions where available Ancell Unit simulated head is less than 100 ft. As discussed in Section 5.2.1, deep wells in the areas where Ancell Unit is near to the top of the Ancell, and where the Ancell Unit is partially desaturated, may be vulnerable to increases in arsenic, barium, and radium concentrations that, left untreated, may be harmful to human health. Partial desaturation of the Ancell Unit could also lead to declines in well yield and increased pumping expenses.

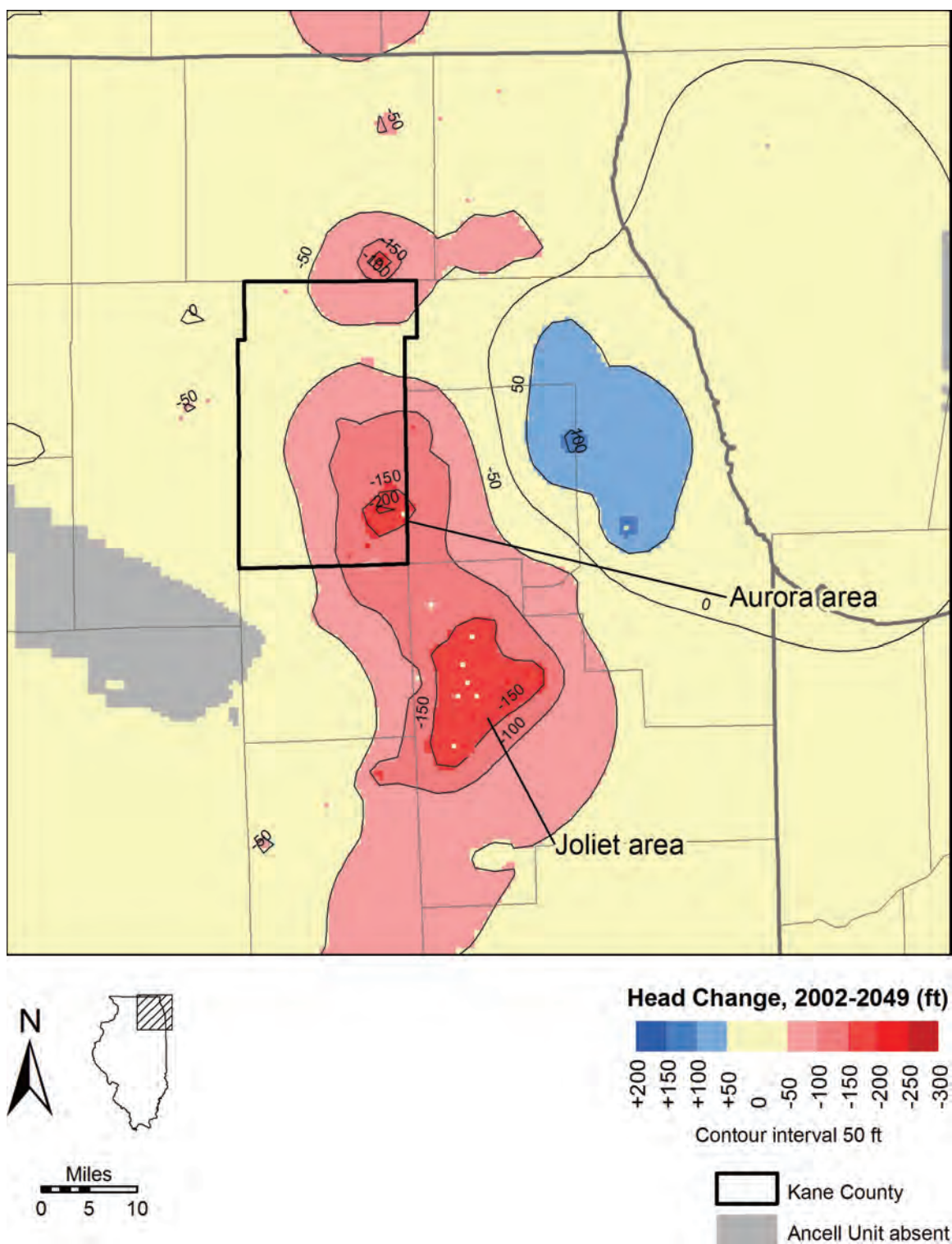


Figure 22. Change in simulated head between the end of 2002 and end of 2049 in Ancell Unit, scenario HC.

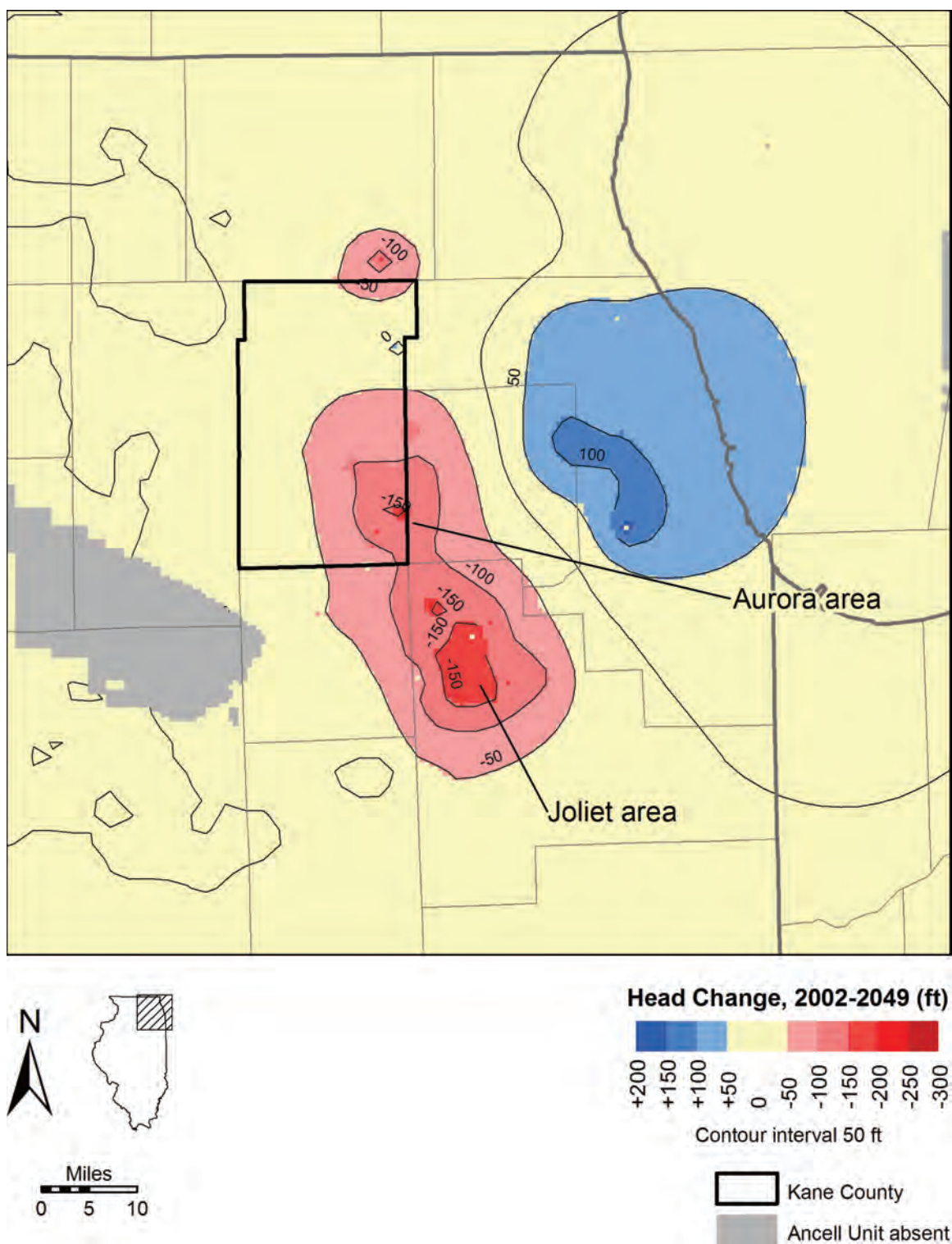


Figure 23. Change in simulated head between the end of 2002 and end of 2049 in Ancell Unit, scenario LC.

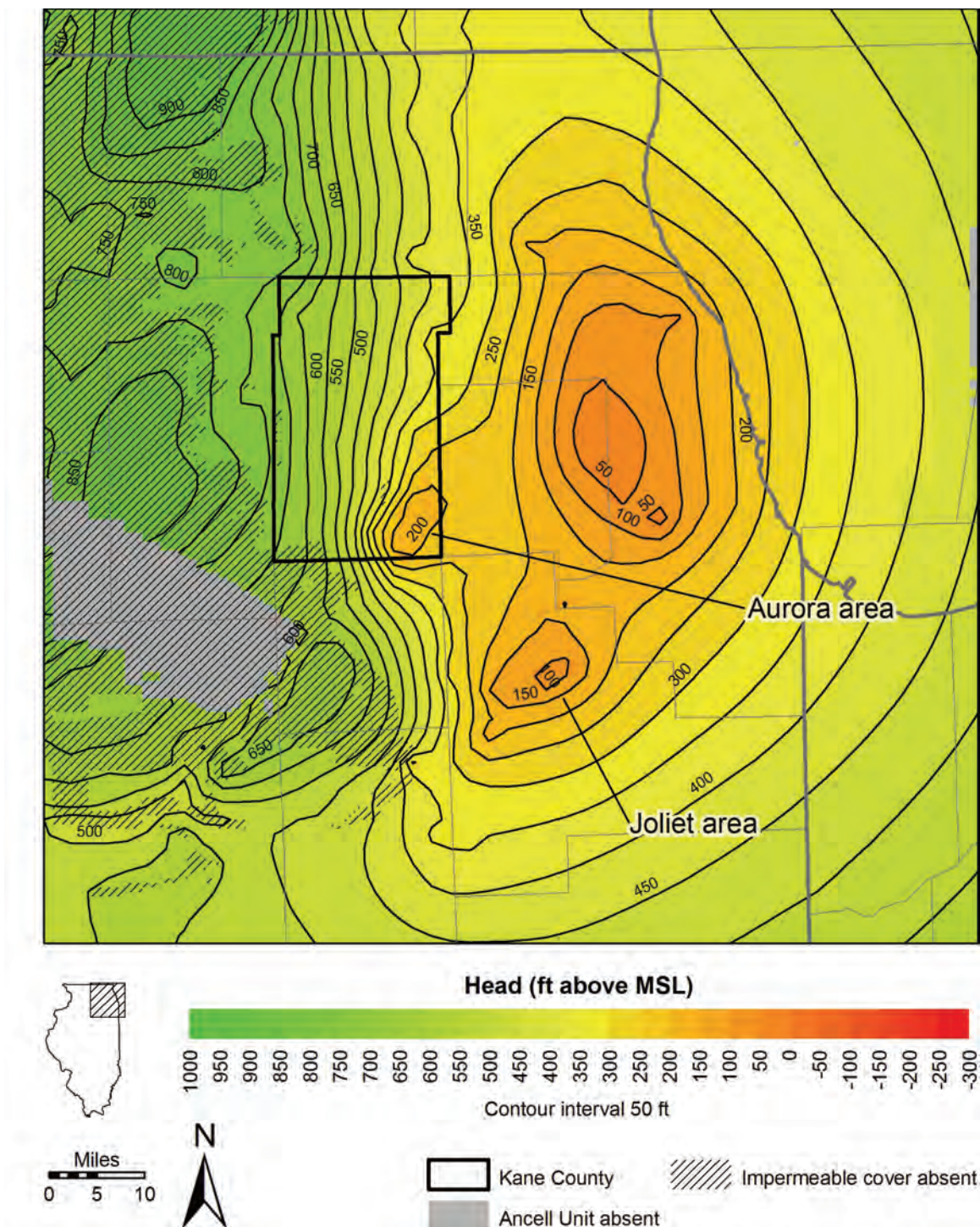


Figure 24. Simulated head in Ancell Unit at the end of 2002.

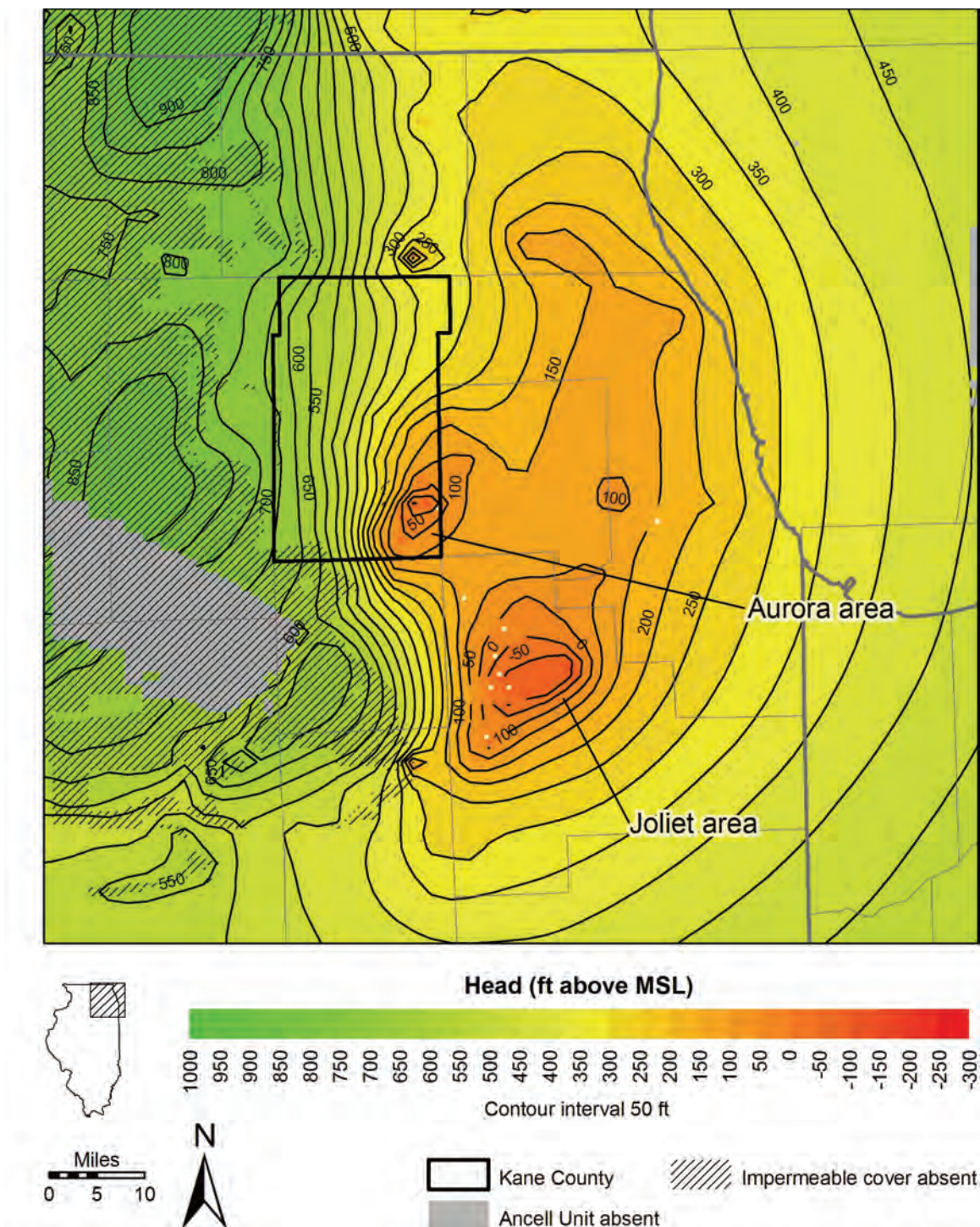


Figure 25. Simulated head in Ancell Unit at the end of 2049, scenario HC.

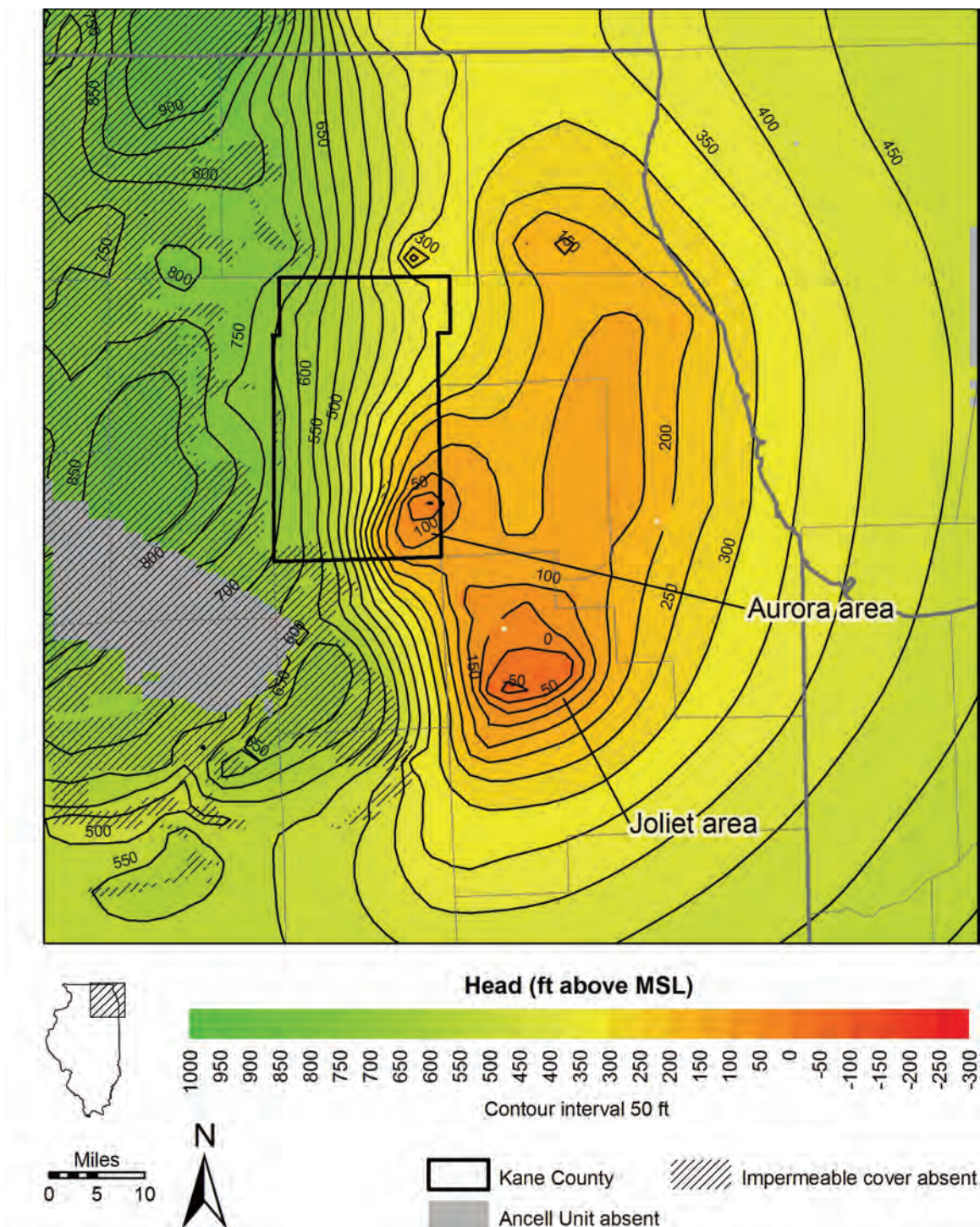


Figure 26. Simulated head in Ancestral Unit at the end of 2049, scenario LC.

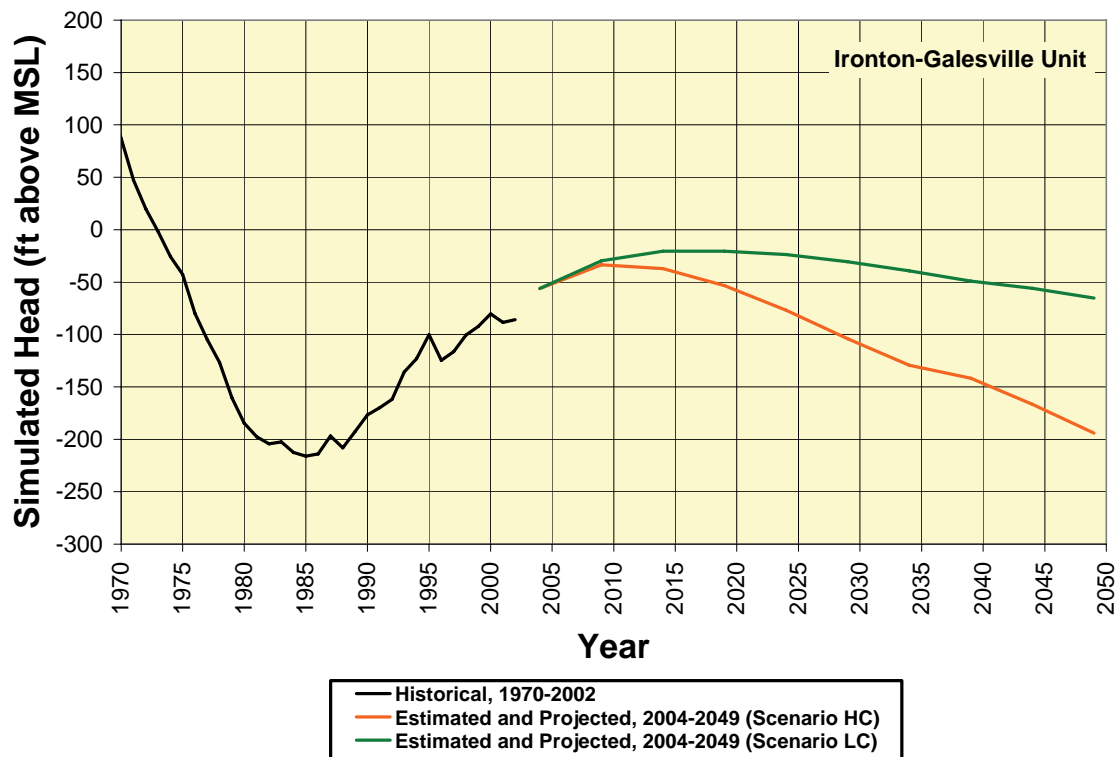
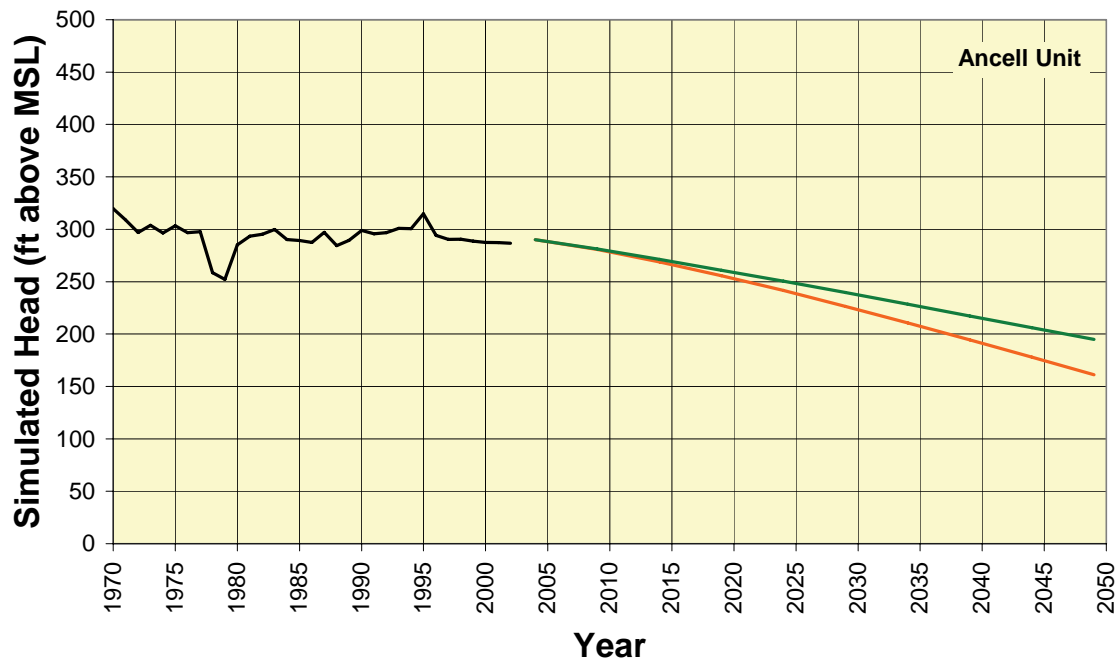


Figure 27. Simulated head from end of 1970 to end of 2049 in Ancell (top) and Ironton-Galesville Units (bottom) at St. Charles. See Figure 10 and Figure 11 for location.

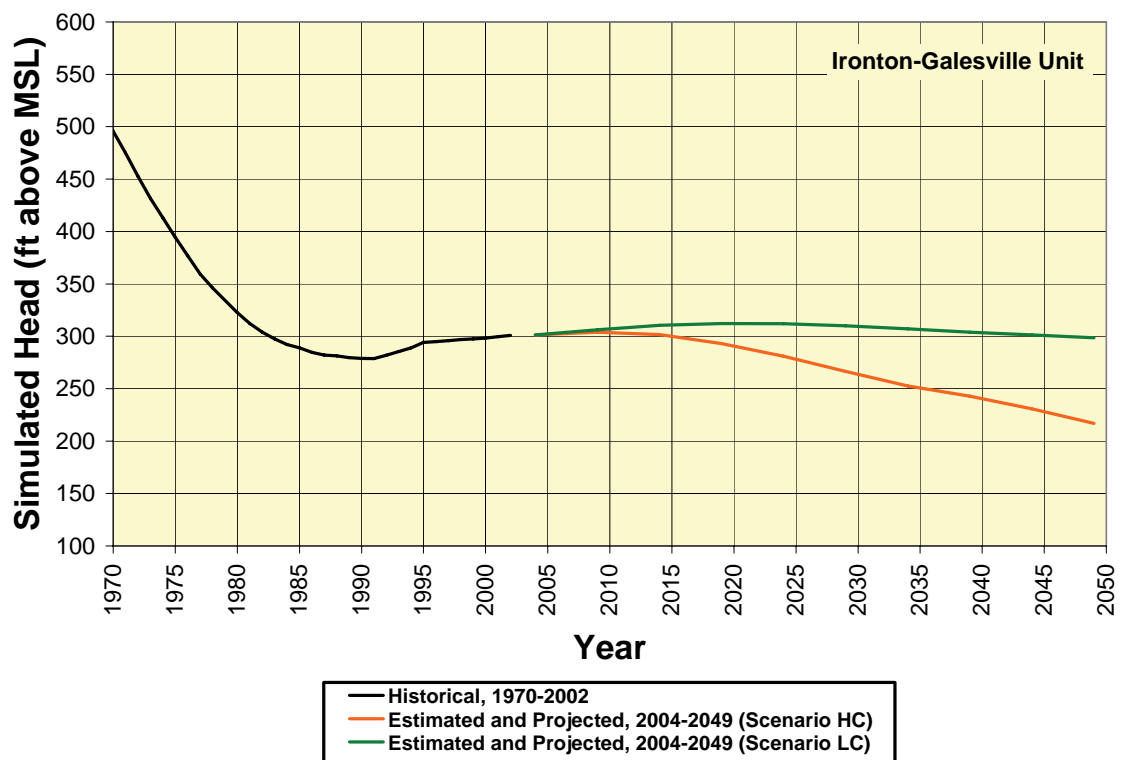
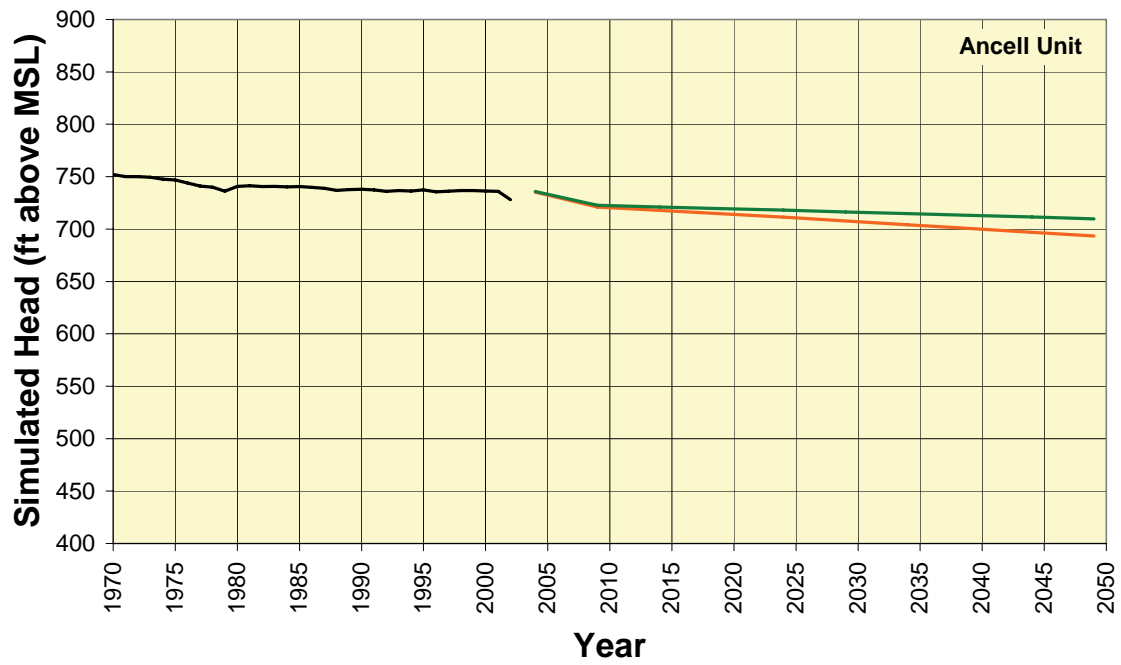


Figure 28. Simulated head from end of 1970 to end of 2049 in Ancell (top) and Ironton-Galesville Units (bottom) at Maple Park. See Figure 10 and Figure 11 for location.

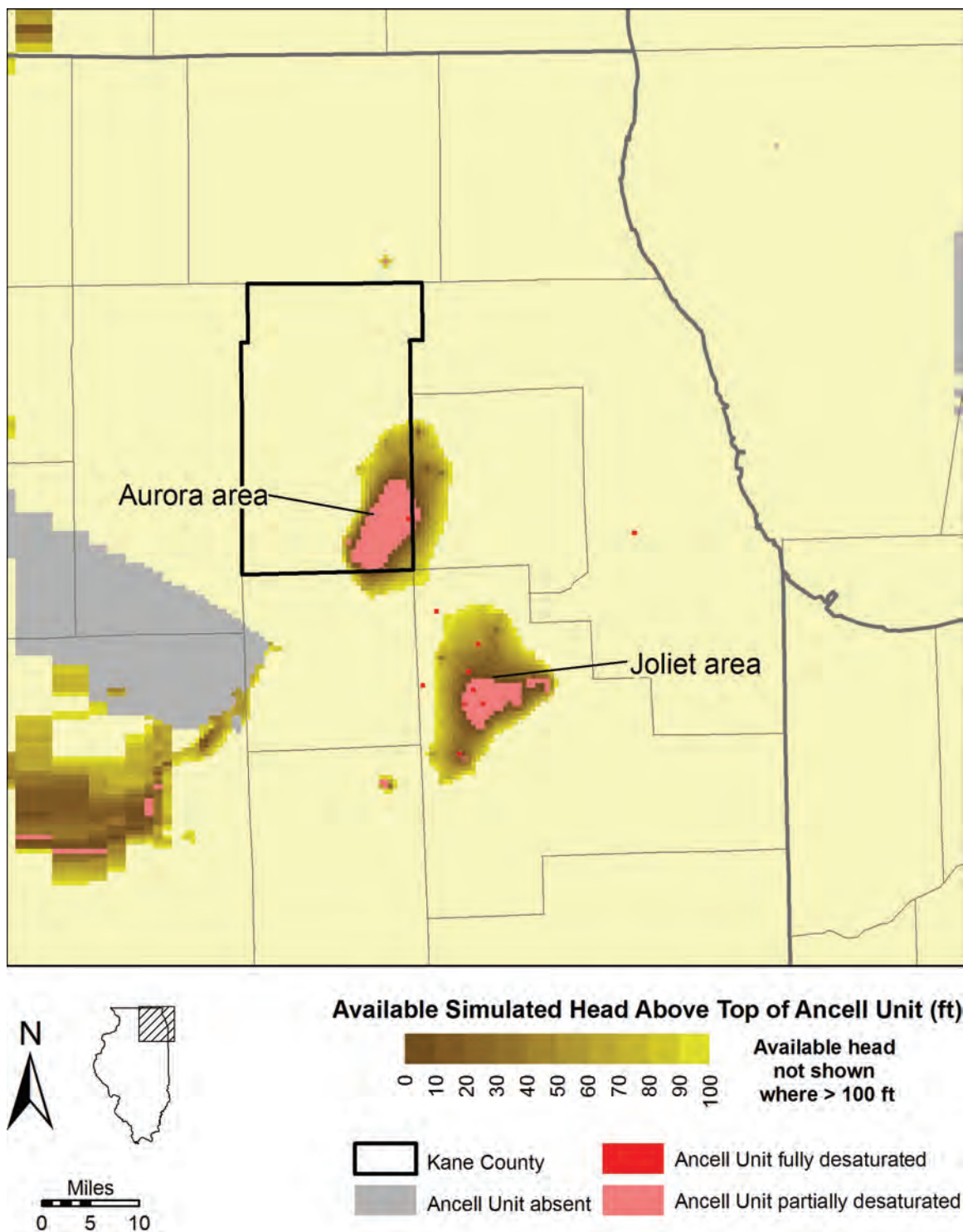


Figure 29. Available simulated head above the top of the Ancell Unit at the end of 2049, scenario HC.

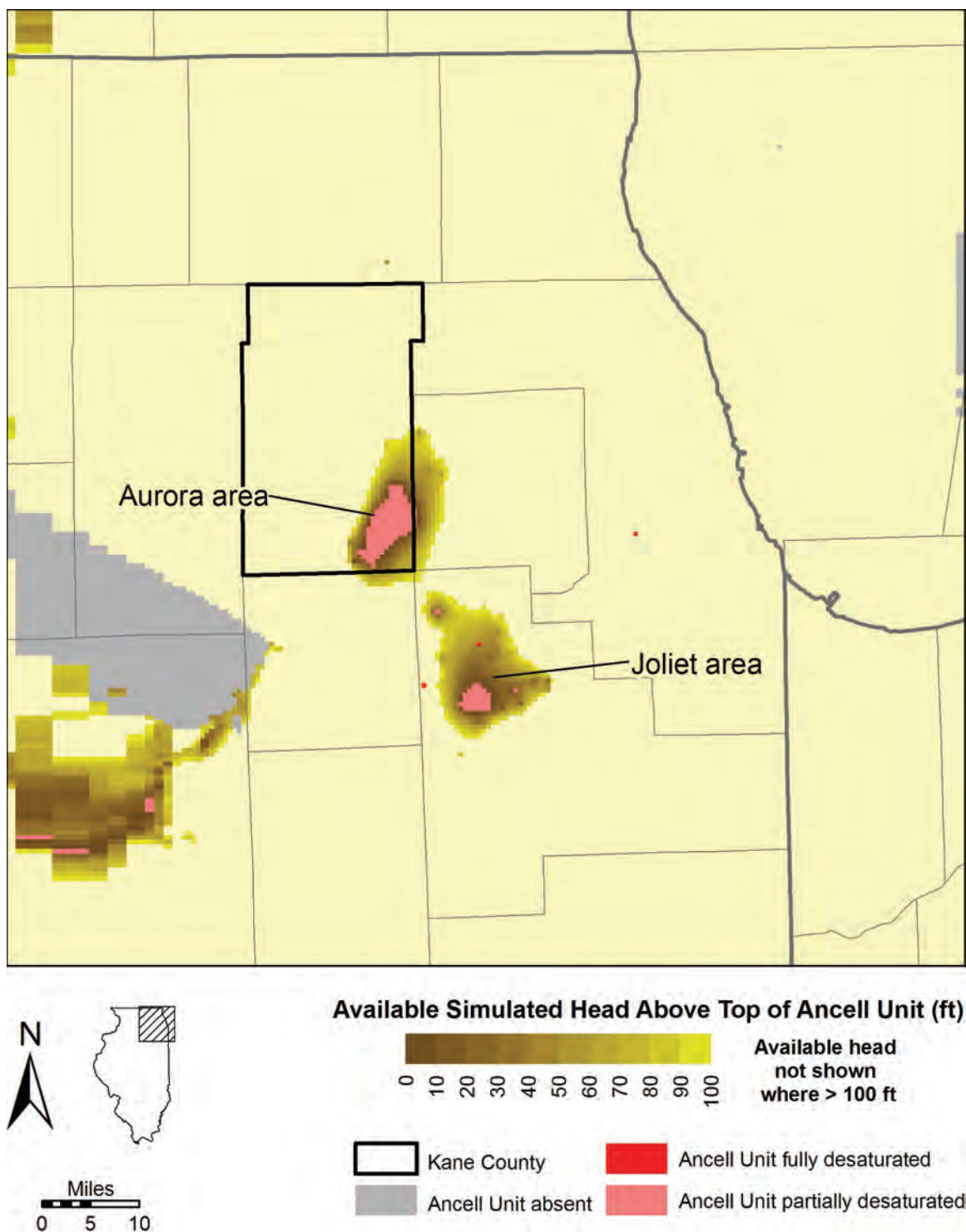


Figure 30. Available simulated head above the top of the Ancell Unit at the end of 2049, scenario LC.

5.3.3. *Head Change in Shallow Aquifers*

Simulations of future scenarios of pumping and recharge using the local-scale model suggest that areas of significant drawdown present in 2003 will expand by 2050 (compare Figure 16 with Figure 31, Figure 32, Figure 33, and Figure 34). These areas include the southeastern McHenry-northeastern Kane County region and the area surrounding West Chicago and Warrenville public-supply wells in west-central DuPage County. The simulations suggest a greater degree of expansion under high-pumping and low-recharge conditions. In contrast to the deep aquifers, recharge rates have an appreciable effect on the simulated heads of the shallow aquifers. Simulated post-2003 drawdown is as high as 40 to 50 ft in 2050 in the area surrounding Algonquin wells 7 and 11. The simulations suggest that a third area of significant drawdown may develop around public-supply wells operated by Batavia and Geneva. This decline is in the area west of Batavia and Geneva discussed previously as a location of significant decline in natural groundwater discharge to Mill Creek in 2003.

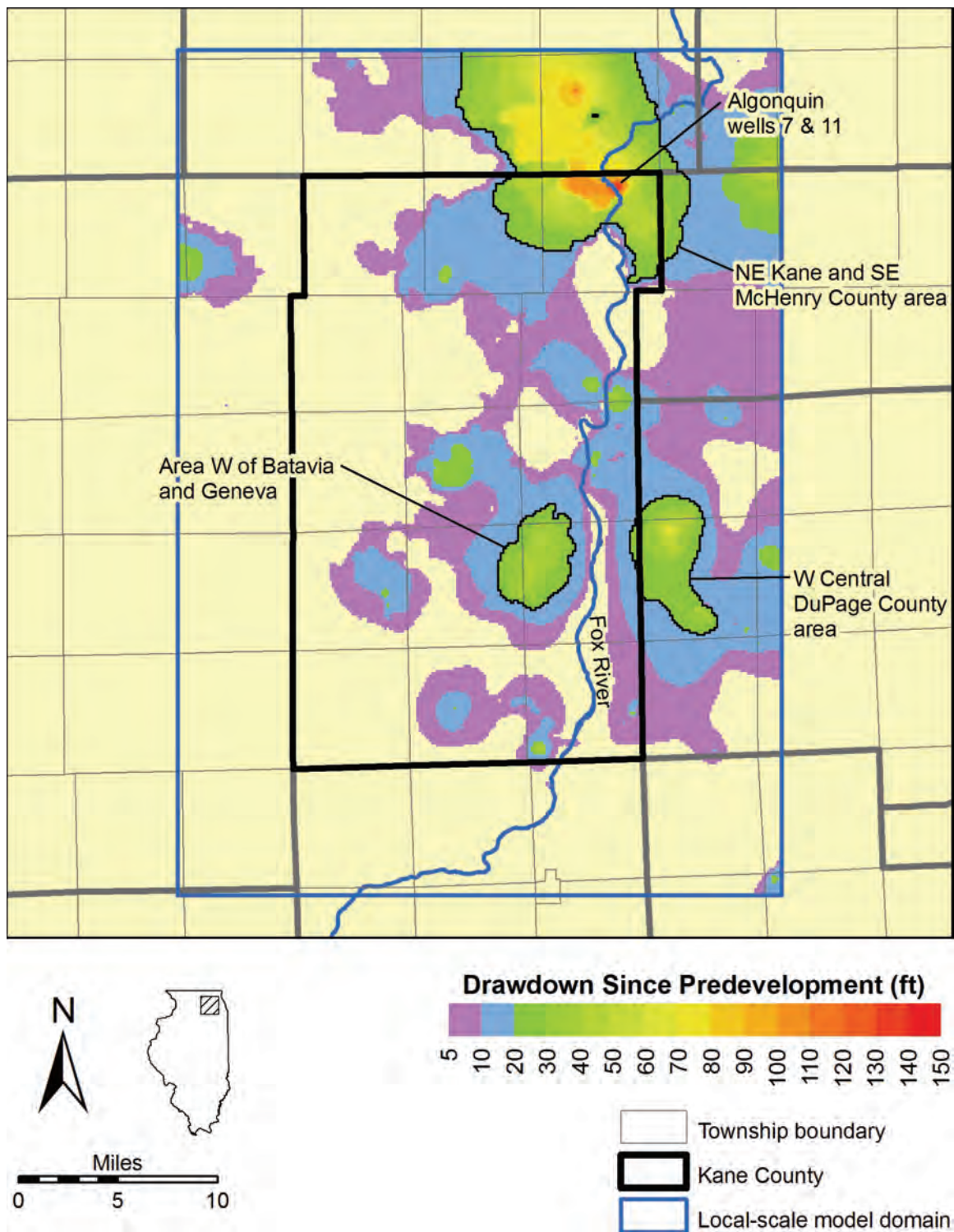


Figure 31. Simulated drawdown in the Shallow Bedrock Aquifer at the end of 2049, scenario HL, with areas of significant drawdown mentioned in the text identified.

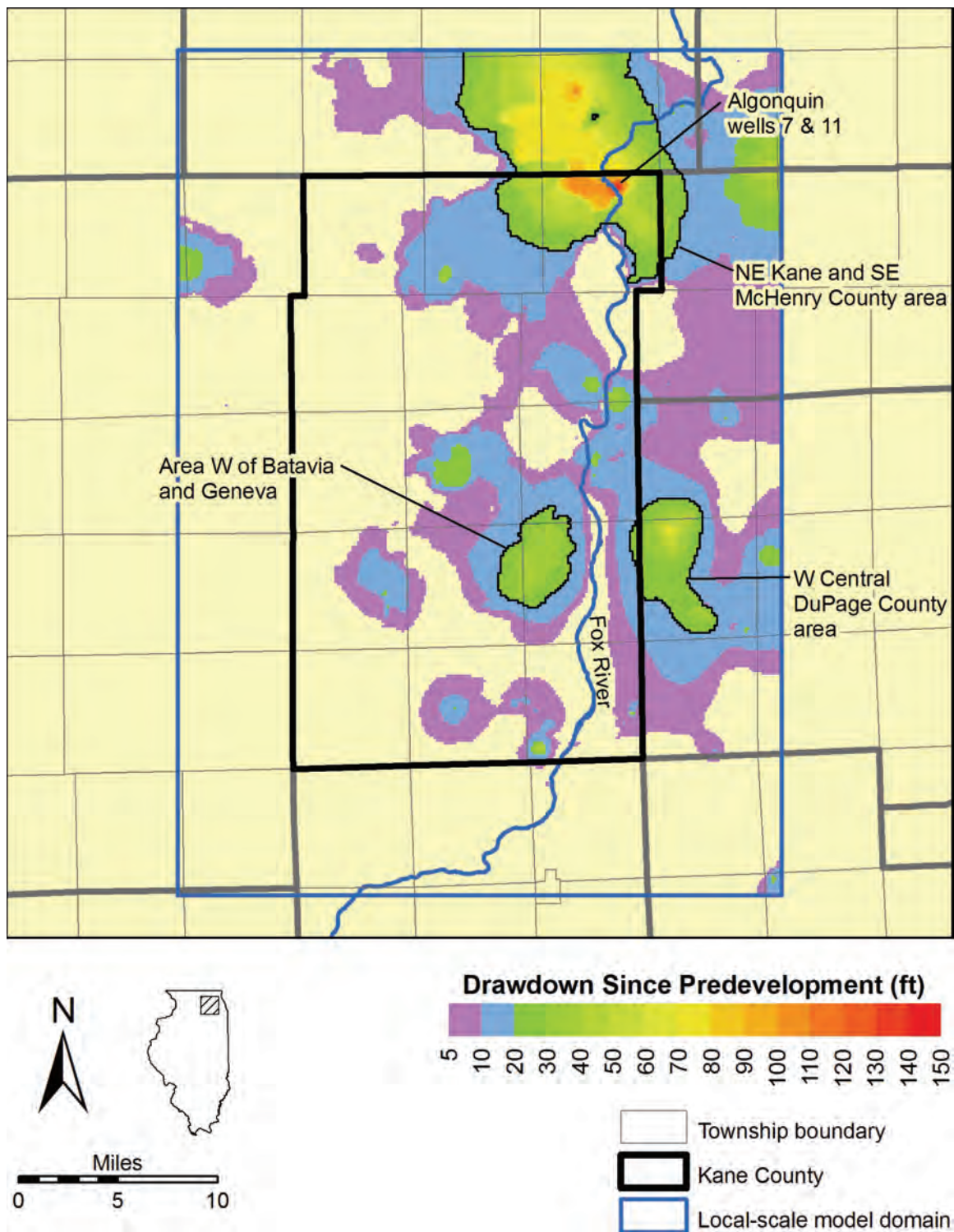


Figure 32. Simulated drawdown in the Shallow Bedrock Aquifer at the end of 2049, scenario HC, with areas of significant drawdown mentioned in the text identified.

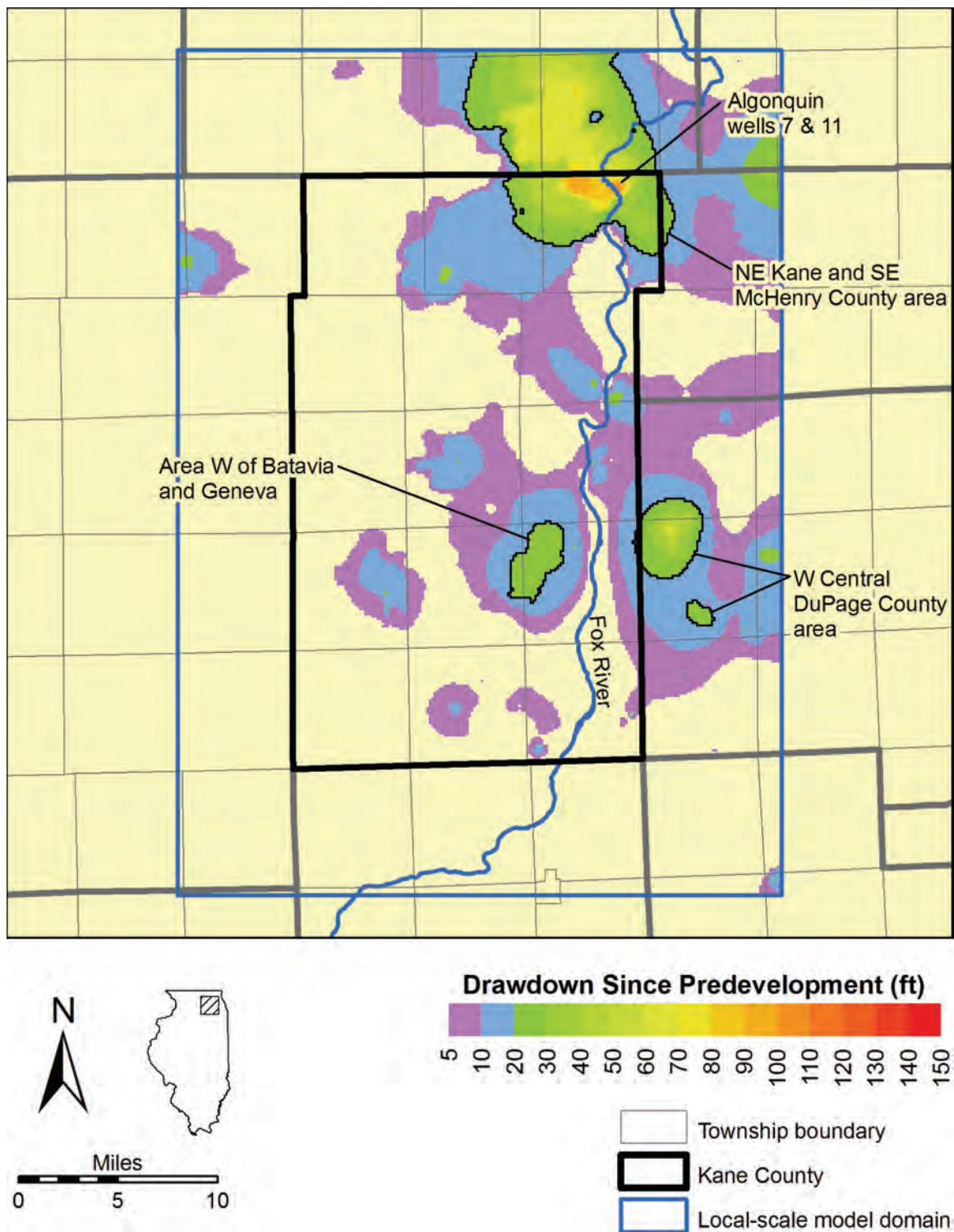


Figure 33. Simulated drawdown in the Shallow Bedrock Aquifer at the end of 2049, scenario LC, with areas of significant drawdown mentioned in the text identified.

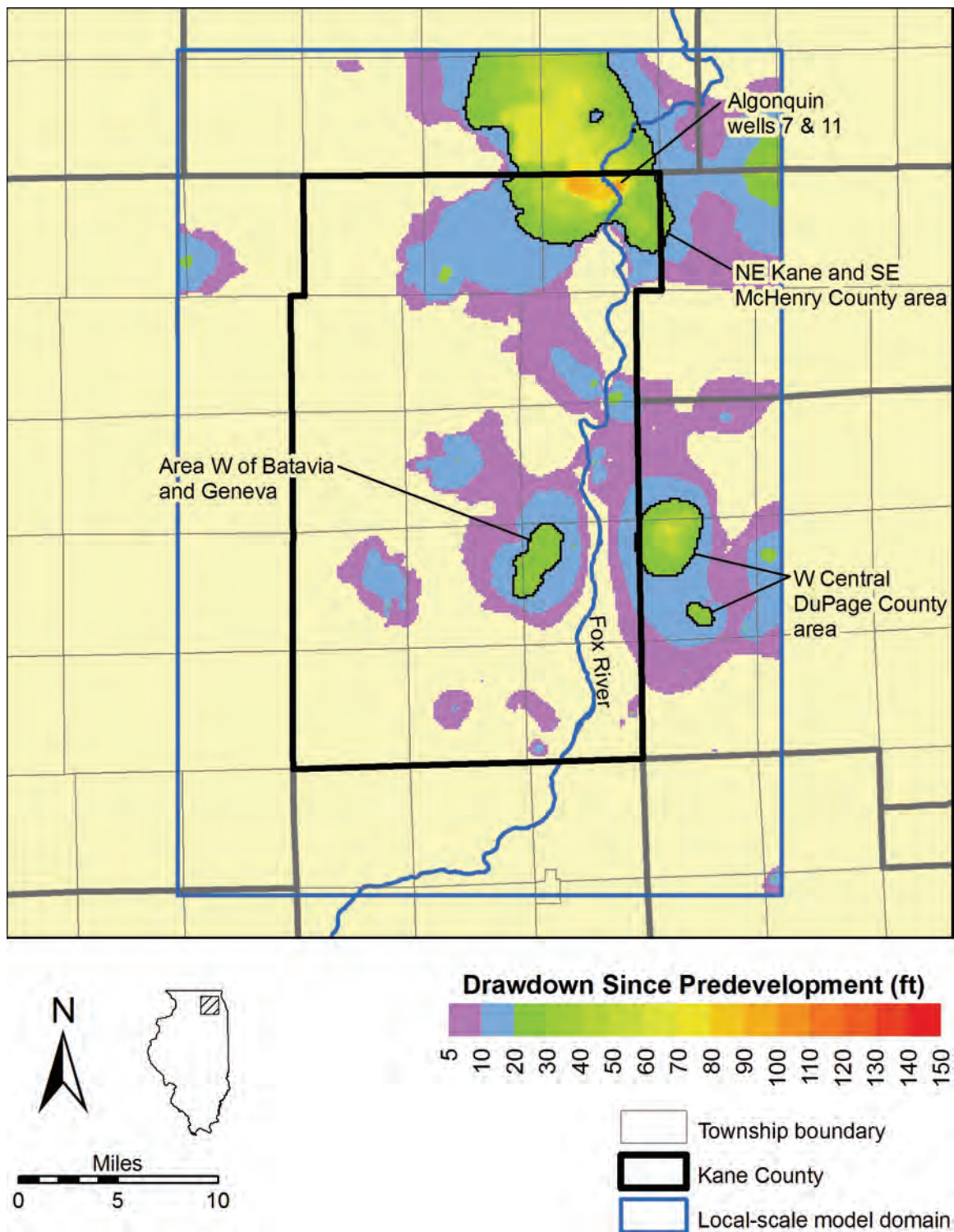


Figure 34. Simulated drawdown in the Shallow Bedrock Aquifer at the end of 2049, scenario LH, with areas of significant drawdown mentioned in the text identified.

5.3.4. *Changes in Streamflow*

Simulations using the local-scale model suggest that changes in recharge rates would impact base flow to streams in the Kane County area to a greater degree than the shallow or deep heads (Figure 35). In all four scenarios, total simulated natural groundwater discharge to streams in the Kane County area is less in 2025 and 2050 than under predevelopment conditions. The simulations suggest that if recharge rates do not change from historical rates, natural groundwater discharge in the Kane County area in 2050 will occur at rates that are 20 to 26 percent lower than estimated predevelopment rates (scenarios LC and HC, respectively). If recharge rates decline to plausibly low rates and pumping is higher (scenario HL), the model suggests that natural groundwater discharge in 2050 in the Kane County area will occur at a rate that is 38 percent lower than estimated predevelopment rates. If recharge rates increase to plausibly high rates and pumping is less (scenario LH), 2050 discharge will be only 8 percent less than estimated predevelopment rates. Discharge of effluent could compensate for future reductions in natural groundwater discharge, but only in areas downstream of wastewater treatment plant outfalls.

Simulated changes in natural groundwater discharge affect streams in the region irregularly, however (Figure 36, Figure 37, Figure 38, Figure 39, and Table 3). Streams experiencing the greatest reduction in groundwater discharge are located in areas of high pumping from the shallow aquifers and where pumped aquifers are hydraulically connected to the streams. Simulations of high-pumping conditions (scenarios HL and HC) show that natural groundwater discharge to Mill Creek could cease entirely upstream of Batavia. This cessation is simulated to occur between 2015 and 2020 under scenario HL, and in 2050 under scenario HC. High-pumping simulations (scenarios HL and HC) suggest that other large reductions in natural groundwater discharge are predicted for the Fox River upstream of Algonquin and the West Branch of the DuPage River upstream of Warrenville. Both areas lie largely outside of Kane County, however, and therefore outside the area of greatest model accuracy. Nevertheless, the fact that the model simulations suggest significant declines in natural groundwater discharge in these areas cannot be dismissed, and additional investigations are warranted.

Simulation of scenario LH suggests that under high-recharge conditions with less pumping, natural groundwater discharge to some streams could increase above predevelopment rates, although the total rate in the Kane County area is less than that of predevelopment.

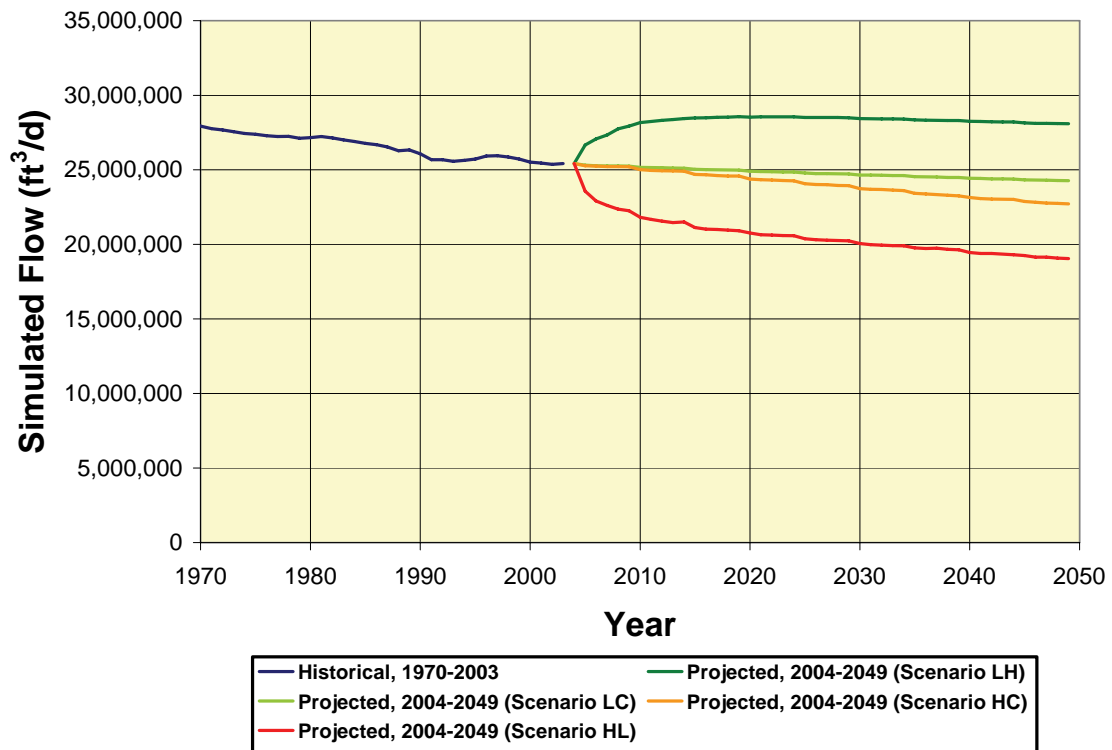


Figure 35. Total natural groundwater discharge to streams in the local-scale model domain.

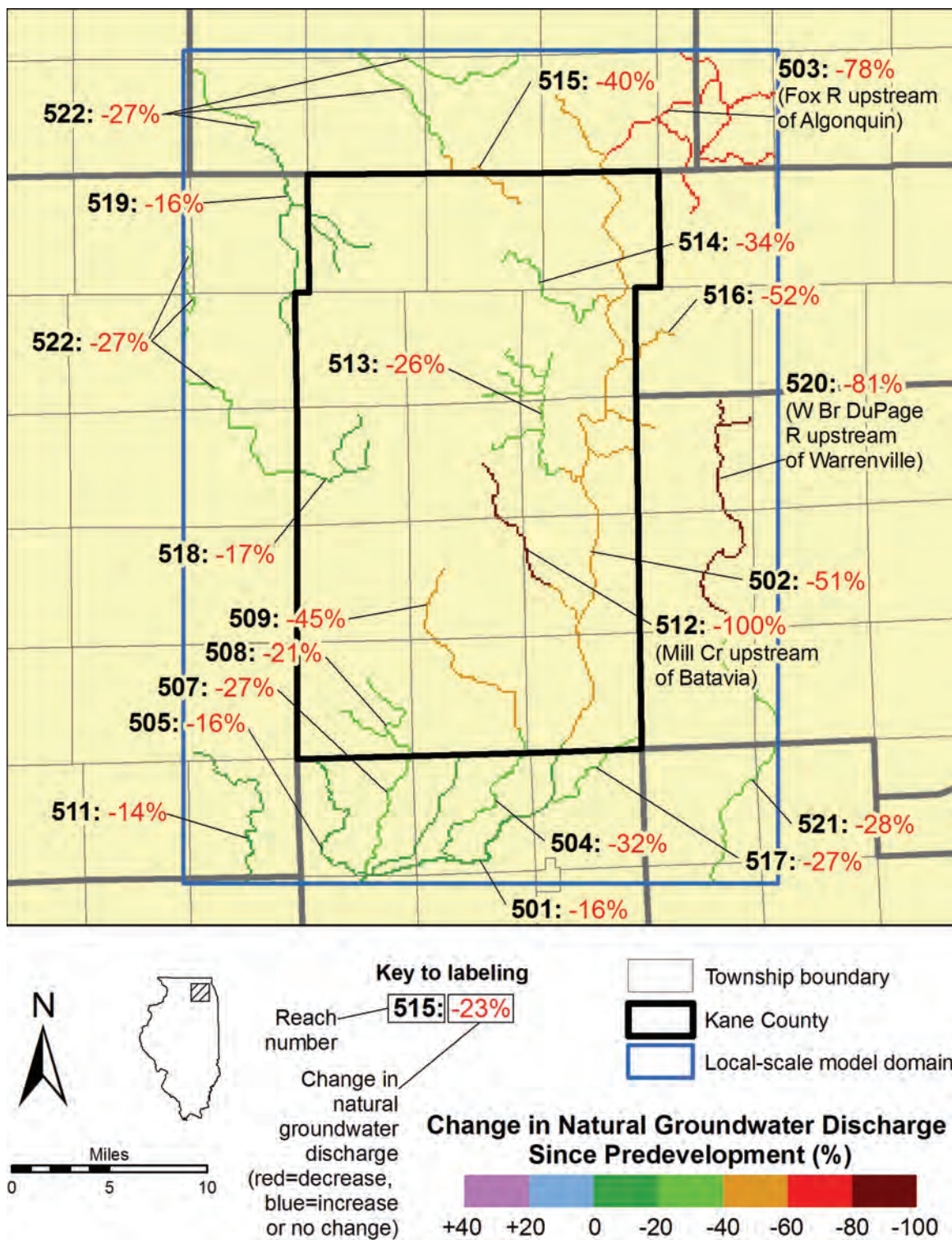


Figure 36. Change in simulated natural groundwater discharge since predevelopment by stream reach in the Kane County area at the end of 2049, scenario HL, with reaches discussed in text identified (see Table 1 for identification of all reaches).

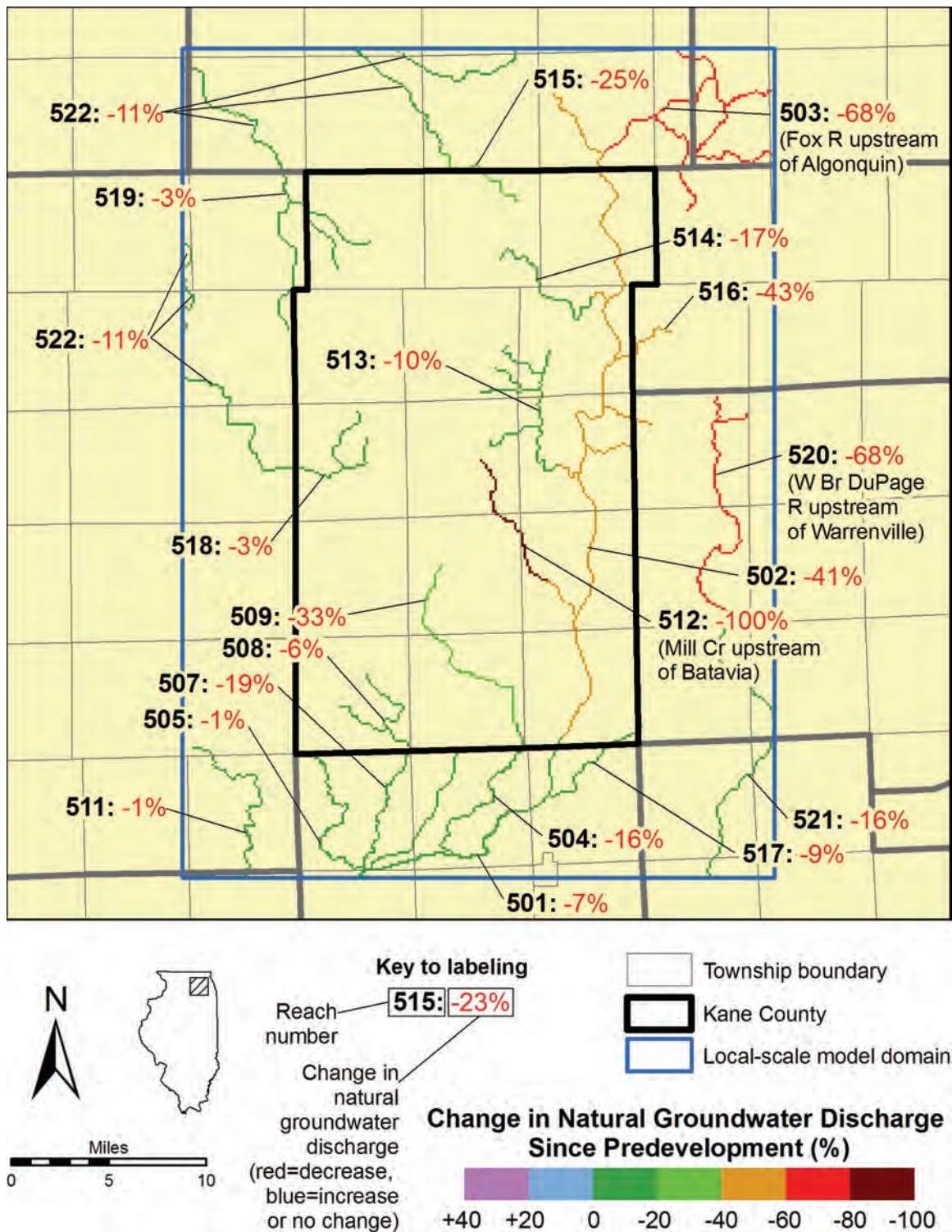


Figure 37. Change in simulated natural groundwater discharge since predevelopment by stream reach in the Kane County area at the end of 2049, scenario HC, with reaches discussed in text identified (see Table 1 for identification of all reaches).

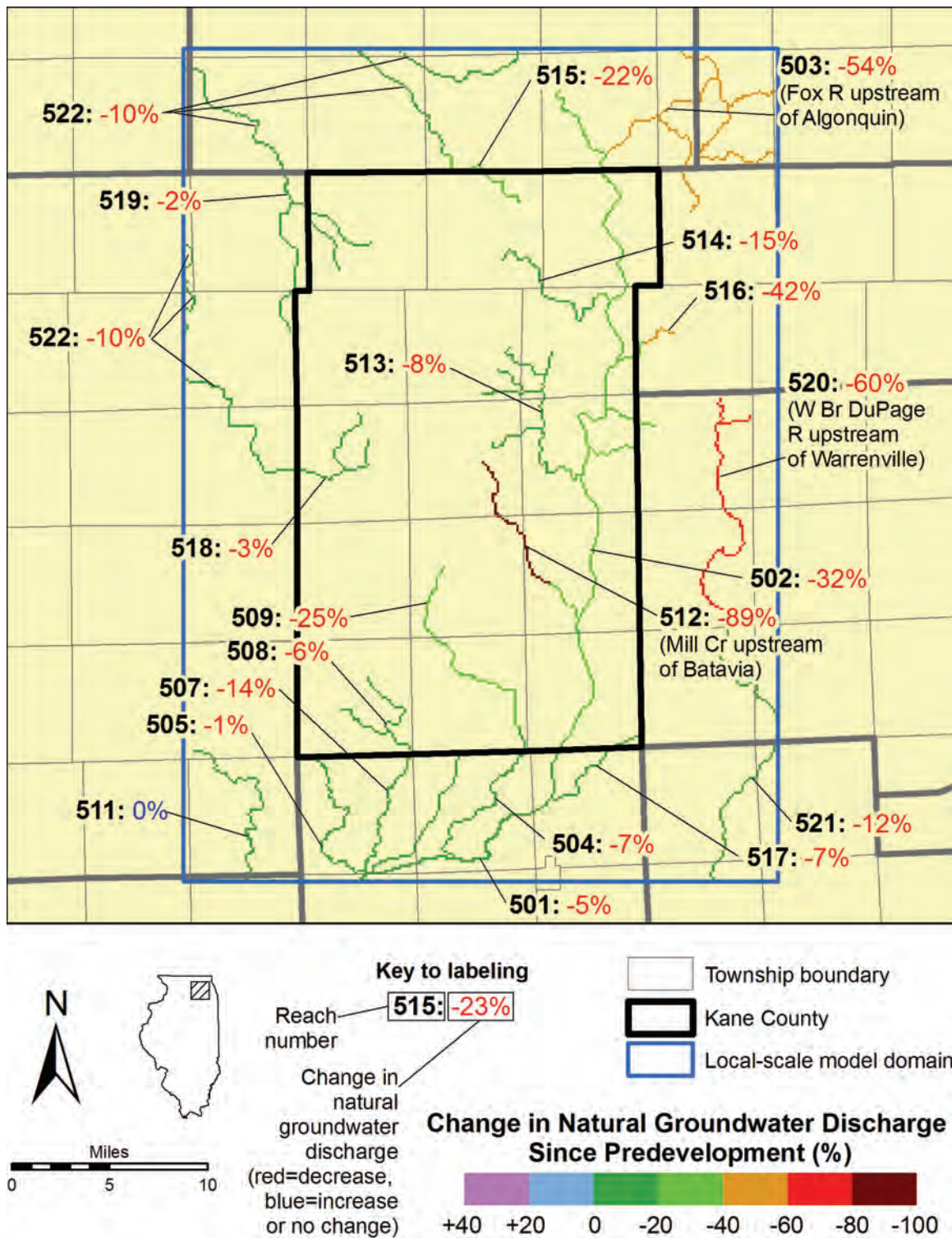


Figure 38. Change in simulated natural groundwater discharge since predevelopment by stream reach in the Kane County area at the end of 2049, scenario LC, with reaches discussed in text identified (see Table 1 for identification of all reaches).

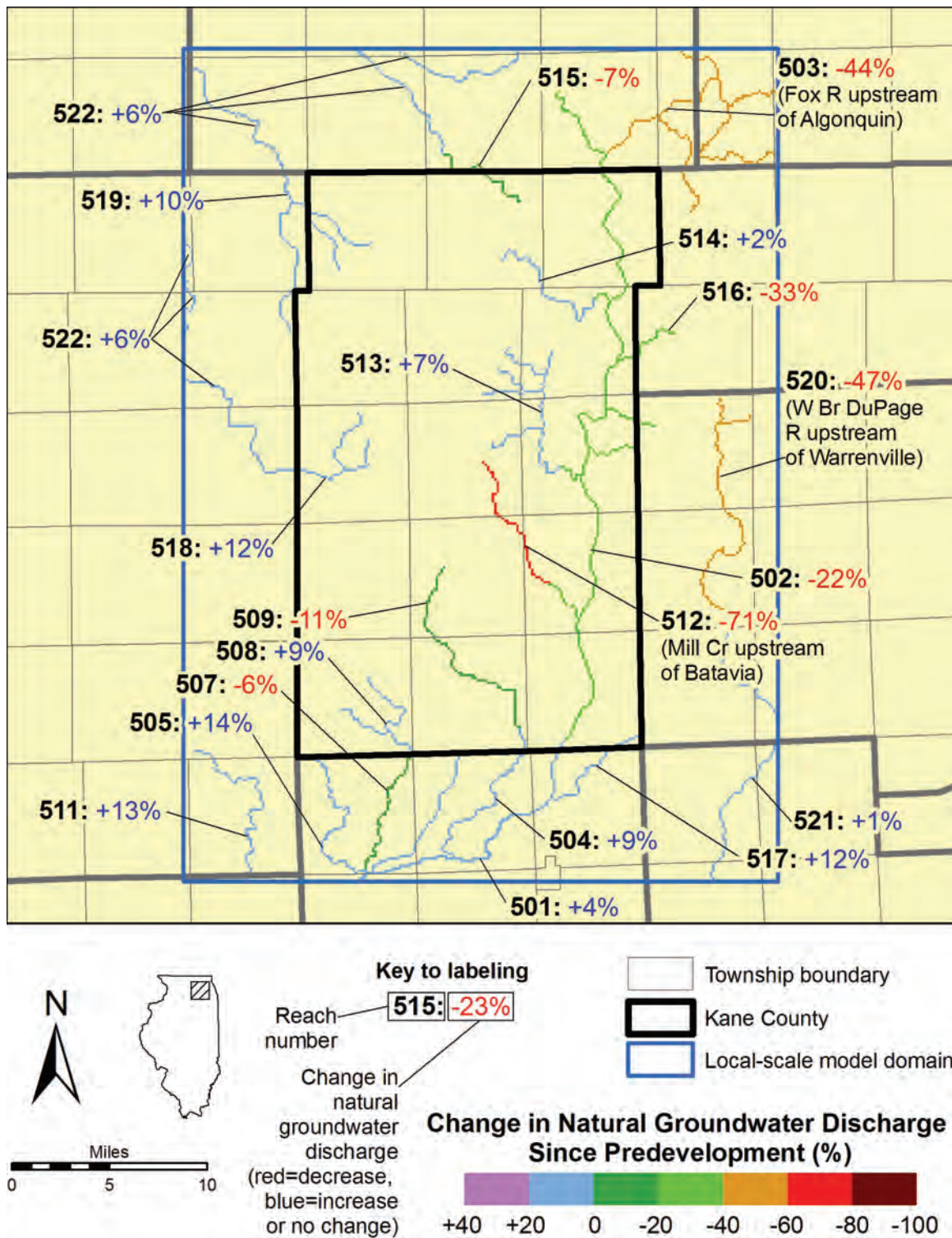


Figure 39. Change in simulated natural groundwater discharge since predevelopment by stream reach in the Kane County area at the end of 2049, scenario LH, with reaches discussed in text identified (see Table 1 for identification of all reaches).

Table 3. Estimated Total Change in Natural Groundwater Discharge at end of 2024 and 2049, by Stream Reach

Reach Number	Principal Streams	Change in Natural Groundwater Discharge Due to Pumping							
		2024				2049			
		HL*	HC	LC	LH	HL	HC	LC	LH
501	Fox River downstream of Montgomery; Big Rock Cr downstream of Kane County boundary	-15%	-6%	-5%	+4%	-16%	-7%	-5%	+4%
502	Fox River from Algonquin to Montgomery; Norton Cr; Brewster Cr; Crystal Cr; lower portions of Mill Cr, Ferson Cr, Poplar Cr, and Tyler Cr	-42%	-32%	-29%	-19%	-51%	-41%	-32%	-22%
503	Fox River upstream of Algonquin; Spring Cr; Flint Cr	-65%	-55%	-50%	-40%	-78%	-68%	-54%	-44%
504	Blackberry Cr from Montgomery to Yorkville	-27%	-11%	-8%	+8%	-32%	-16%	-7%	+9%
505	Little Rock Cr downstream of Kane County boundary	-16%	-1%	-1%	+14%	-16%	-1%	-1%	+14%
507	Big Rock Cr downstream of Kane County boundary	-22%	-14%	-12%	-4%	-27%	-19%	-14%	-6%
508	Big Rock Cr upstream of Kane County boundary; Welch Cr	-19%	-4%	-4%	+10%	-21%	-6%	-6%	+9%
509	Blackberry Cr from Elburn to Montgomery	-37%	-24%	-21%	-8%	-45%	-33%	-25%	-11%
511	Somonauk Cr	-13%	-1%	0%	+12%	-14%	-1%	0%	+13%
512	Mill Cr upstream of Batavia	-100%	-87%	-82%	-64%	-100%	-100%	-89%	-71%
513	Ferson Cr upstream of St Charles; Otter Cr; Stony Cr; Fitchie Cr	-23%	-8%	-7%	+8%	-26%	-10%	-8%	+7%
514	Tyler Cr	-29%	-14%	-14%	+2%	-34%	-17%	-15%	+2%
515	S Br Kishwaukee River upstream of Huntley	-34%	-20%	-19%	-5%	-40%	-25%	-22%	-7%
516	Poplar Cr	-50%	-41%	-41%	-33%	-52%	-43%	-42%	-33%
517	Waubonsie Cr	-25%	-7%	-7%	+11%	-27%	-9%	-7%	+12%
518	Union Ditch No 3; Virgil Ditch No 3; Union-Virgil Ditch No 2	-17%	-2%	-2%	+12%	-17%	-3%	-3%	+12%
519	Upper Coon Cr	-15%	-3%	-2%	+10%	-16%	-3%	-2%	+10%
520	W Br DuPage River upstream of Warrenville	-71%	-58%	-55%	-42%	-81%	-68%	-60%	-47%
521	DuPage River; W Br DuPage River downstream of Warrenville	-25%	-13%	-11%	+1%	-28%	-16%	-12%	+1%
522	Aggregated tributaries of S Br Kishwaukee River outside Kane County	-26%	-10%	-9%	+6%	-27%	-11%	-10%	+6%
	TOTAL	-33%	-21%	-19%	-6%	-38%	-26%	-20%	-8%

* Key to scenarios: HL=high pumping, low recharge; HC=high pumping, model-calibrated recharge; LC=low pumping, model-calibrated recharge; LH=low pumping, high recharge

6. Summary

Computer simulation of plausible scenarios of future pumping and recharge conditions suggests that significant additional drawdown, reduction in stream base flow, and changes in the quality of groundwater withdrawn from deep wells are all possible in parts of the Kane County area before 2050.

- Model simulations suggest that over 500 ft of drawdown and over 1100 ft of drawdown have occurred in the Ancell and Ironton-Galesville Units, respectively, in southeastern Kane County since pumping began in the nineteenth century. These units are the two principal deep aquifers in the region. Drawdown causes water levels in wells open to these aquifers to decline, increasing pumping expenses and, in extreme cases, causing water-supply interruptions that can be addressed only by replacing the wells or lowering the pumps. Drawdown could also lead to increases in salinity of deep well water. Slight increases in total dissolved solids have been recognized in time series of sample results collected at Aurora and Joliet, two locations of large withdrawals from the deep aquifers (Kelly and Meyer, 2005).
- Model simulations suggest that greater than 50 ft of additional drawdown in the deep aquifers will occur between 2002 and 2050 in much of Kane County under both low- and high-pumping conditions. Depending on specific operating rates, additional drawdowns in excess of 50 ft are possible immediately near pumping wells. Drawdown will be greatest in the Aurora area of southeastern Kane County. In addition to reducing well productivity, the additional drawdown may lead to increasing concentrations of radium, barium, arsenic, and salinity in water withdrawn from deep wells.
- Modeling shows that two large areas of significant drawdown (that is drawdown greater than or equal to 20 ft) affected the Kane County area in 2003. Both areas cross the borders of Kane County. One area covers parts of northeastern Kane County and southeastern McHenry County and is a collective response to pumping of wells operated by the Villages of Algonquin, Carpentersville, East Dundee, Lake in the Hills, and the City of Crystal Lake. The second large area of significant shallow aquifer drawdown is a response to pumping by the City of West Chicago and Village of Warrenville and barely crosses the Kane County border with DuPage County to include small parts of the Cities of Batavia and Geneva.
- Simulations of future scenarios of pumping and recharge suggest that areas of significant drawdown in the shallow aquifers present in 2003 will likely expand by 2050. The simulations suggest that a third area of significant shallow aquifer drawdown will likely develop around public-supply wells operated by Batavia and Geneva west of those cities.
- Model simulations suggest that, as of 2003, streamflow capture by pumping had reduced natural groundwater discharge to streams within the local model domain by about 17 percent. This streamflow capture would be observable as a reduction in base flow in streams (that part of streamflow originating as groundwater

discharge). Streamflow accounting models suggest that discharge of effluent may be compensating for the base flow reduction (Knapp et al., 2007).

- Model simulations suggest that the greatest reduction in natural groundwater discharge by 2003 occurred in Mill Creek upstream of Batavia, where simulated capture of streamflow by supply wells operated by the Cities of Batavia and Geneva has reduced groundwater discharge by 68 percent relative to nonpumping conditions.
- Model simulations suggest that, overall, if recharge rates do not change from historical rates, natural groundwater discharge in the Kane County area in 2050 will likely decline to rates that are 20 to 26 percent lower than estimated predevelopment rates.
- If recharge rates decline to plausibly low rates and pumping is high, model simulations suggest that natural groundwater discharge in the Kane County area in 2050 will likely decline by 38 percent from estimated predevelopment rates. If recharge rates increase to plausibly high rates and pumping is low, 2050 discharge may increase to a level that is about 8 percent less than the estimated predevelopment rate.
- Model simulations suggest that natural groundwater discharge to Mill Creek may cease entirely upstream of Batavia before 2050. The model suggests other large reductions in natural groundwater discharge to the Fox River upstream of Algonquin and the West Branch of the DuPage River upstream of Warrenville.

7. Future Work

7.1. Modeling Studies

The models developed for this project are designed for use in future water studies of Kane County and northeastern Illinois and will provide a rational basis for developing policy and management strategies pertaining to water-resources development in the county and region. Withdrawal rates, well locations, source intervals, and other factors may be modified to evaluate the impact of development strategies beyond the four scenarios discussed in this report. In addition, the models can be used to provide boundary fluxes for future high-resolution inset models developed to address a variety of local groundwater issues.

The models and databases developed for this study can be adapted for research on a variety of subjects bearing on water availability in the region. For example, the regional-scale model can be adapted to examine the impact of salty water on deep groundwater circulation in the Mt. Simon Unit and within the Ancell and Ironton-Galesville Units south of the Chicago area. Such an analysis would address the possibility of whether pumping could eventually induce salty water into deep wells in northeastern Illinois, reducing groundwater quality and limiting use of the deep groundwater.

Simulations with the local-scale model suggest that groundwater withdrawals have appreciably reduced natural groundwater discharge to many streams in the Kane County area. The extent to which these reductions are offset by discharges of effluent is not well understood, however, and an investigation of this topic could be a useful contribution to water-resources management in Kane County. Knapp et al. (2007) show that reduction in natural groundwater discharge to the Fox River may be more than offset

by effluent, with low flows in the Fox River possibly higher now than under predevelopment conditions. The opposite could be true for many tributary streams, however. Groundwater that is withdrawn from the tributary watersheds, after distribution through public water systems and treatment as wastewater, is not typically discharged as effluent in the stream reaches affected by the withdrawals. It is instead discharged into another stream, commonly, the Fox River in Kane County.

7.2. Monitoring

Monitoring of aquifer heads should be considered in areas of significant simulated 2003 and future drawdown. At minimum, such monitoring would include installing observation wells open to principal aquifers in problem areas and quarterly measurement of water levels in these wells. Monitoring provides a relatively inexpensive mechanism for early identification of problematic downward water-level trends and establishes head data that are invaluable for future analysis. Streamflow monitoring of streams projected to incur significant simulated baseflow reduction, such as Mill Creek, is also recommended.

7.3. Database Expansion and Improvement

As syntheses of available data, all models can be improved with acquisition of new observations or through novel and alternative approaches to characterizing model input data. In general, the available database for model development suffers from imprecision, geological and geographical bias, sporadic and irregular data collection and compilation efforts, and poor documentation. These shortcomings reflect the fact that data collection, analysis, and mapping have largely been conducted for local studies over a long period of time, using a range of technologies and approaches, and for purposes other than groundwater flow modeling.

The experiences gained through this modeling study suggest that compilation of comprehensive, accurate withdrawal data is needed for database expansion and improvement. As a parameter to which shallow heads and streamflow are highly sensitive, accurate characterization of recharge and discharge is probably the second greatest data need, yet accurate measurement of recharge is problematic and a subject of active research (National Research Council, 2004). Other data that would increase the accuracy and usefulness of groundwater models of Kane County and northeastern Illinois include observations of hydraulic properties of all the modeled units, aquifers and aquitards alike, observations of base flow (natural groundwater discharge) to streams, and water levels in wells. Coordination with authorities in Indiana and Wisconsin in database expansion and improvement would improve the comprehensiveness and quality of the efforts.

Finally, there is a possibility that a thin layer containing arsenic-bearing minerals exists at the top of the Ancell Unit in northeastern Illinois, and pumping-induced reduction of heads in the Ancell could cause arsenic to be released to groundwater from this layer. Such a layer is known to be present in eastern Wisconsin (Schreiber et al., 2000), but there is a need for more comprehensive study to verify the presence of the arsenic-bearing layer in Illinois and confirm that arsenic can be liberated as a consequence of declining heads.

8. References

- Alley, W.M., T.E. Reilly, and O.L. Franke. 1999. *Sustainability of Ground-Water Resources*. United States Geological Survey Circular 1186, Denver, CO.
- Anderson, M.P. and W.W. Woessner. 2002. *Applied groundwater modeling: Simulation of flow and advective transport*. Academic Press, San Diego, CA.
- Arnold, J.G., R.S. Muttiah, and P.M. Allen. 2000. Regional estimation of base flow and groundwater recharge in the Upper Mississippi river basin. *Journal of Hydrology* 227(1):21-40.
- Bloyd, R.M., Jr. 1974. *Summary Appraisals of the Nation's Ground-Water Resources -- Ohio Region*. United States Geological Survey Professional Paper 813-A, Washington, DC.
- Bredehoeft, J.D. 2002. The water-budget myth revisited: Why hydrogeologists model. *Ground Water* 40(4):340-345.
- Bredehoeft, J.D., S.S. Papadopoulos, and H.H. Cooper, Jr. 1982. Groundwater--the water-budget myth. In *Scientific basis of water-resource management*, 51-57. National Academy Press, Washington, DC.
- Cherkauer, D.S. 2001. *Distribution of Ground-Water Recharge in Southeastern Wisconsin*. Wisconsin Department of Natural Resources, Madison, WI.
- Devlin, J.F. and M. Sophocleus. 2005. The persistence of the water budget myth and its relationship to sustainability. *Hydrogeology Journal* 13:549-554.
- Dziegielewski, B., T. Bik, X. Yang, H. Margono, M. Richey, and D. Sherman. 2004. *Countywide Projections of Community Water Supply Needs in the Midwest*. Department of Geography, Southern Illinois University, Carbondale, IL.
- Dziegielewski, B., X. Yang, T. Bik, H. Margono, and M. Richey. 2005. *County-Level Forecasts of Water Use in Illinois: 2005-2025*. Department of Geography, Southern Illinois University, Carbondale, IL.
- Gilkeson, R.H., K. Cartwright, J.B. Cowart, and R.B. Holtzman. 1983. *Hydrogeologic and Geochemical Studies of Selected Natural Radioisotopes and Barium in Groundwater in Illinois*. Illinois State Geological Survey Contract/Grant Report 1983-6, Champaign, IL.
- Harbaugh, A.W., E.R. Banta, M.C. Hill, and C.K. McDonald. 2000. *MODFLOW-2000, The U.S. Geological Survey Modular Ground-Water Model—User Guide to Modularization Concepts and the Ground-Water Flow Processes*. United States Geological Survey Open-File Report 00-92.

Holtschlag, D.J. 1997. *A Generalized Estimate of Ground-Water Recharge Rates in the Lower Peninsula of Michigan*. United States Geological Survey Water-Supply Paper 2437, Washington, DC.

Kelly, W.R. and S.C. Meyer. 2005. *Temporal Changes in Deep Bedrock Groundwater Quality in Northeastern Illinois*. Illinois State Water Survey Contract Report 2005-05, Champaign, IL.

Knapp, H.V., A.M. Russell, J.A. Kramer, and G.P. Rogers. 2007. *Kane County Water Resources Investigations: Surface Water Accounting for Water Supply Planning in Kane County*. Illinois State Water Survey Contract Report 2007-10, Champaign, IL.

McDonald, M.G. and A.W. Harbaugh. 1988. *Techniques of Water-Resources Investigations of the United States Geological Survey. A Modular Three-Dimensional Finite-Difference Ground-Water Flow Model. Book 6, Modeling Techniques. Chapter A1*. United States Geological Survey, Washington, DC.

Meyer, S.C. 2005. Analysis of base flow trends in urban streams, northeastern Illinois, USA. *Hydrogeology Journal* 13(5-6):871-885.

National Research Council. 2004. *Groundwater fluxes across interfaces*. National Academies Press, Washington, DC.

Northeastern Illinois Planning Commission. 2002. *Strategic Plan for Water Resource Management*. Northeastern Illinois Planning Commission, Chicago, IL.

Schreiber, M.E., J.A. Simo, and P.G. Freiberg. 2000. Stratigraphic and geochemical controls on naturally occurring arsenic in groundwater, eastern Wisconsin, USA. *Hydrogeology Journal* 8:161-176.

**Kane County Water Resources Investigations:
Simulation of Groundwater Flow in Kane County and
Northeastern Illinois**

Scott C. Meyer, P.G.
George S. Roadcap, Ph.D., P.G.
Yu-Feng Lin, Ph.D.
Douglas D. Walker, Ph.D.

Contract Report 2009-07

Illinois State Water Survey
A division of the Institute of Natural Resource Sustainability
Champaign, Illinois



Contents

	Page
1. Introduction.....	1
1.1. Purpose	1
1.1.1. Study Objectives	1
1.1.2. Scope and Limitations.....	2
1.2. Acknowledgments.....	3
1.3. Projection and Coordinate System	4
1.4. Location	4
1.5. Population.....	7
1.6. Physical Setting and Drainage	7
1.7. Groundwater Concepts	7
1.7.1. Aquifers and Confining Beds.....	7
1.7.2. Potentiometric Surface Maps	11
1.7.3. Hydraulic Properties	11
1.7.4. Groundwater Recharge and Discharge	13
1.7.5. Effects of Pumping	15
1.8. Overview of Water Resources Available to Kane County	17
1.8.1. Lake Michigan	17
1.8.2. Inland Surface Waters.....	17
1.8.3. Groundwater	18
1.9. Groundwater Development in Kane County Area.....	20
1.10. Previous Studies.....	34
1.10.1. Regional Studies Including Kane County.....	34
1.10.2. Studies Emphasizing Kane County.....	38
2. Model Design	40
2.1. Conceptual Model.....	40
2.1.1. Regional Model Domain.....	44
2.1.1.1. Hydrostratigraphic Nomenclature.....	46
2.1.1.2. Shallow and Deep Aquifers, Units, and Wells	54
2.1.2. Local Model Domain	55
2.1.2.1. Shallow Bedrock Aquifer	55
2.1.2.2. Quaternary Materials	56
2.2. Conceptual Model to Numerical Model.....	60
2.2.1. Grids and Layering	60
2.2.1.1. Regional-Scale Model.....	60
2.2.1.2. Local-Scale Shallow Model.....	64
2.2.2. Geologic Framework	66
2.2.2.1. Regional-Scale Model.....	66
2.2.2.2. Local-Scale Shallow Model.....	68
2.2.3. Hydraulic Conductivity (K)	71
2.2.3.1. Regional-Scale Model.....	71
2.2.3.2. Local-Scale Shallow Model.....	99
2.2.4. Storage Parameters.....	123
2.2.4.1. Regional-Scale Model.....	123

Contents (Continued)

	Page
2.2.4.2. Local-Scale Shallow Model.....	125
2.2.5. Recharge	125
2.2.5.1. Regional-Scale Model.....	125
2.2.5.2. Local-Scale Shallow Model.....	129
2.2.6. Representation of Surface Water	131
2.2.6.1. Regional-Scale Model.....	131
2.2.6.2. Local-Scale Shallow Model.....	135
2.2.7. Representation of Drained Areas	136
2.2.7.1. Regional-Scale Model.....	138
2.2.7.2. Local-Scale Shallow Model.....	140
2.2.8. Withdrawals	140
2.2.9. Boundary Flow into Local Model Area (TMR).....	146
2.3. <i>Model Calibration</i>	147
2.3.1. Regional-Scale Model.....	147
2.3.1.1. Approach.....	147
2.3.1.2. Calibration Targets.....	148
2.3.1.3. Estimated Parameters.....	154
2.3.1.4. Calibration Accuracy and Bias	158
2.3.1.5. Verification	162
2.3.1.6. Sensitivity Analysis	178
2.3.2. Local-Scale Shallow Model.....	180
2.3.2.1. Approach.....	180
2.3.2.2. Calibration Targets.....	182
2.3.2.3. Estimated Parameters.....	182
2.3.2.4. Calibration Accuracy and Bias	187
2.3.2.5. Verification	187
2.3.2.6. Sensitivity Analysis	197
3. Analysis	199
3.1. <i>Introduction</i>	199
3.2. <i>Simulation of Historical Groundwater Conditions</i>	201
3.2.1. Heads.....	201
3.2.1.1. Deep Aquifers	202
3.2.1.2. Shallow Aquifers	211
3.2.2. Streamflow	252
3.2.3. Groundwater Circulation	260
3.2.3.1. Deep Units	266
3.2.3.2. Shallow Units.....	271
3.2.4. Vertical Movement between Shallow and Deep Aquifers.....	271
3.2.5. Comparison with Groundwater Flow Modeling in Southeastern Wisconsin.....	274
3.3. <i>Simulation of Future Groundwater Conditions</i>	279
3.3.1. Transient Simulation of Projected Withdrawals to 2050.....	280
3.3.1.1. Pumping Conditions	280

Contents (Continued)

	Page
3.3.1.2. Recharge Conditions	302
3.3.1.3. Modeling of Pumping/Recharge Scenarios	304
3.3.1.4. Discussion	304
3.3.2. Steady-State Simulation of 2002 Pumping Distribution.....	393
3.4. <i>Capture Zones of High-Capacity Shallow Wells in Kane County</i>	398
4. Summary.....	399
5. Future Work.....	403
5.1. <i>Revision of Existing Regional Model</i>	403
5.2. <i>Modeling Studies</i>	404
5.2.1. Applications	404
5.2.1.1. Existing Models as Rational Basis for Management	404
5.2.1.2. Existing Models as Source of Boundary Conditions for Inset Models.....	404
5.2.2. Research.....	405
5.2.2.1. Groundwater Exchange with Lake Michigan	405
5.2.2.2. Influence of Salinity on Groundwater Flow	405
5.2.2.3. Influence of Sandwich Fault Zone on Groundwater Flow.....	405
5.2.2.4. Relationship between Effluent and Natural Groundwater Discharge	406
5.3. <i>Database Expansion and Improvement</i>	406
5.3.1. Hydraulic Properties and Boundary Conditions	406
5.3.2. Geological Models	409
5.3.3. Calibration Data	409
5.3.4. Sulfide-Cement Horizon at Contact of Galena-Platteville and Ansell Units	410
5.4. <i>Uncertainty Analysis Using Alternative Models</i>	410
5.5. <i>Monitoring</i>	411
6. References.....	411
 Appendix A. Introduction to Groundwater Flow Modeling.....	 A-1
 Appendix B. Development of Withdrawal Database.....	 B-1
 Appendix C. Development of Geologic Framework of Regional Groundwater Flow Model.....	 C-1
 Appendix D. Results of Pumping Tests of Shallow Aquifers in the Kane County Area	 D-1
 Appendix E. Analysis of Calibration Target Errors.....	 E-1
 Appendix F. ISWS Aquifer Code System	 F-1

Contents (Concluded)

	Page
Appendix G. Estimation of Future Pumping	G-1
Appendix H. Capture Zone Delineations.....	H-1
Appendix I. System of Location.....	I-1

List of Figures

	Page
Figure 1. Location of Kane County, Illinois.	6
Figure 2. Municipalities and major roads in the Kane County area.	8
Figure 3. Elevation and drainage in the Kane County area.	9
Figure 4. Major watersheds in the Kane County area.	10
Figure 5. Major aquifers in the Kane County area.	19
Figure 6. Areas of groundwater withdrawal accounting.	22
Figure 7. Groundwater withdrawals in northeastern Illinois, 1964-2003.	23
Figure 8. Withdrawals in 1985 from deep wells in northeastern Illinois.	24
Figure 9. Withdrawals in 2003 from deep wells in northeastern Illinois.	25
Figure 10. Withdrawals in 1985 from shallow wells in northeastern Illinois.	26
Figure 11. Withdrawals in 2003 from shallow wells in northeastern Illinois.	27
Figure 12. Groundwater withdrawals in Kane County, 1964-2003.	28
Figure 13. Withdrawals in 2003 from deep wells in the Kane County area.	30
Figure 14. Withdrawals in 2003 from shallow wells in the Kane County area.	31
Figure 15. Geographic domains of groundwater flow models and lines of cross sections in Figure 16 and Figure 17.	41
Figure 16. Generalized cross section along A-A' (Figure 15) showing domains of groundwater flow models.	42
Figure 17. Generalized cross section along B-B' (Figure 15) showing domains of groundwater flow models.	43
Figure 18. Generalized bedrock geologic index map.	45
Figure 19. Correlation chart, lithostratigraphic nomenclature, and hydrostratigraphic nomenclature employed in regional-scale groundwater flow model.	48
Figure 20. Generalized north-south cross section along A-A' (Figure 15) showing regional hydrostratigraphic units discussed in text.	50
Figure 21. Generalized east-west cross section along B-B' (Figure 15) showing regional hydrostratigraphic units discussed in text.	51
Figure 22. Lithostratigraphic nomenclature and hydrostratigraphic nomenclature employed in local-scale shallow groundwater flow model.	57
Figure 23. Finite-difference grid of regional-scale model.	61
Figure 24. Finite-difference grid of regional-scale model in vicinity of model near field.	62
Figure 25. Layer scheme of regional model.	63
Figure 26. Domain of local-scale shallow model (finite difference grid is too fine to illustrate).	65
Figure 27. Layer scheme of local-scale shallow model.	67
Figure 28. Hypothetical cross section of local model layers 2 through 14 showing modification of layer thicknesses to reduce presence of thin layers in local-scale model.	70
Figure 29. Hydraulic conductivity zonation of regional model layer 20. See Table 4 (pages 94 through 97) for assumed plausible ranges and starting values for calibration for each zone.	72

List of Figures (Continued)

	Page
Figure 30. Hydraulic conductivity zonation of regional model layer 19. See Table 4 (pages 94 through 97) for assumed plausible ranges and starting values for calibration for each zone.	73
Figure 31. Hydraulic conductivity zonation of regional model layer 18. See Table 4 (pages 94 through 97) for assumed plausible ranges and starting values for calibration for each zone.	74
Figure 32. Hydraulic conductivity zonation of regional model layer 17. See Table 4 (pages 94 through 97) for assumed plausible ranges and starting values for calibration for each zone.	75
Figure 33. Hydraulic conductivity zonation of regional model layer 16. See Table 4 (pages 94 through 97) for assumed plausible ranges and starting values for calibration for each zone.	76
Figure 34. Hydraulic conductivity zonation of regional model layer 15. See Table 4 (pages 94 through 97) for assumed plausible ranges and starting values for calibration for each zone.	77
Figure 35. Hydraulic conductivity zonation of regional model layer 14. See Table 4 (pages 94 through 97) for assumed plausible ranges and starting values for calibration for each zone.	78
Figure 36. Hydraulic conductivity zonation of regional model layer 13. See Table 4 (pages 94 through 97) for assumed plausible ranges and starting values for calibration for each zone.	79
Figure 37. Hydraulic conductivity zonation of regional model layer 12. See Table 4 (pages 94 through 97) for assumed plausible ranges and starting values for calibration for each zone.	80
Figure 38. Hydraulic conductivity zonation of regional model layer 11. See Table 4 (pages 94 through 97) for assumed plausible ranges and starting values for calibration for each zone.	81
Figure 39. Hydraulic conductivity zonation of regional model layer 10. See Table 4 (pages 94 through 97) for assumed plausible ranges and starting values for calibration for each zone.	82
Figure 40. Hydraulic conductivity zonation of regional model layer 9. See Table 4 (pages 94 through 97) for assumed plausible ranges and starting values for calibration for each zone.	83
Figure 41. Hydraulic conductivity zonation of regional model layer 8. See Table 4 (pages 94 through 97) for assumed plausible ranges and starting values for calibration for each zone.	84
Figure 42. Hydraulic conductivity zonation of regional model layer 7. See Table 4 (pages 94 through 97) for assumed plausible ranges and starting values for calibration for each zone.	85
Figure 43. Hydraulic conductivity zonation of regional model layer 6. See Table 4 (pages 94 through 97) for assumed plausible ranges and starting values for calibration for each zone.	86

List of Figures (Continued)

	Page
Figure 44. Hydraulic conductivity zonation of regional model layer 5. See Table 4 (pages 94 through 97) for assumed plausible ranges and starting values for calibration for each zone.	87
Figure 45. Hydraulic conductivity zonation of regional model layer 4. See Table 4 (pages 94 through 97) for assumed plausible ranges and starting values for calibration for each zone.	88
Figure 46. Hydraulic conductivity zonation of regional model layer 3. See Table 4 (pages 94 through 97) for assumed plausible ranges and starting values for calibration for each zone.	89
Figure 47. Hydraulic conductivity zonation of regional model layer 2. See Table 4 (pages 94 through 97) for assumed plausible ranges and starting values for calibration for each zone.	90
Figure 48. Hydraulic conductivity zonation of regional model layer 1. See Table 4 (pages 94 through 97) for assumed plausible range and starting value for calibration. ...	91
Figure 49. West-to-east cross section A-A' showing hydraulic conductivity zonation of regional-scale model in the model domain (see Figure 15 for cross section location).	92
Figure 50. South-to-north cross section B'-B showing hydraulic conductivity zonation of regional-scale model in the model domain (see Figure 15 for cross section location).	93
Figure 51. Hydraulic conductivity of local model layer 15 (Shallow Bedrock Aquifer). See Table 5 (pages 100 and 101) for assumed plausible ranges and starting values for calibration for each zone.	102
Figure 52. Hydraulic conductivity zonation of local model layer 14 (Lower Glasford Diamicton Unit). See Table 5 (pages 100 and 101) for assumed plausible ranges and starting values for calibration for each zone.	103
Figure 53. Hydraulic conductivity zonation of local model layer 13 (Lower Glasford Sand Unit). See Table 5 (pages 100 and 101) for assumed plausible ranges and starting values for calibration for each zone.	104
Figure 54. Hydraulic conductivity zonation of local model layer 12 (Middle Glasford Diamicton Unit). See Table 5 (pages 100 and 101) for assumed plausible ranges and starting values for calibration for each zone.	105
Figure 55. Hydraulic conductivity zonation of local model layer 11 (Upper Glasford Sand Unit). See Table 5 (pages 100 and 101) for assumed plausible ranges and starting values for calibration for each zone.	106
Figure 56. Hydraulic conductivity zonation of local model layer 10 (Upper Glasford Diamicton Unit). See Table 5 (pages 100 and 101) for assumed plausible ranges and starting values for calibration for each zone.	107
Figure 57. Hydraulic conductivity zonation of local model layer 9 (Ashmore Unit). See Table 5 (pages 100 and 101) for assumed plausible ranges and starting values for calibration for each zone.	108

List of Figures (Continued)

	Page
Figure 58. Hydraulic conductivity zonation of local model layer 8 (Tiskilwa Unit). See Table 5 (pages 100 and 101) for assumed plausible ranges and starting values for calibration for each zone.	109
Figure 59. Hydraulic conductivity zonation of local model layer 7 (Batestown Sand Unit). See Table 5 (pages 100 and 101) for assumed plausible ranges and starting values for calibration for each zone.	110
Figure 60. Hydraulic conductivity zonation of local model layer 6 (Batestown Diamicton Unit). See Table 5 (pages 100 and 101) for assumed plausible ranges and starting values for calibration for each zone.	111
Figure 61. Hydraulic conductivity zonation of local model layer 5 (Yorkville Sand Unit). See Table 5 (pages 100 and 101) for assumed plausible ranges and starting values for calibration for each zone.	112
Figure 62. Hydraulic conductivity zonation of local model layer 4 (Yorkville Diamicton Unit). See Table 5 (pages 100 and 101) for assumed plausible ranges and starting values for calibration for each zone.	113
Figure 63. Hydraulic conductivity zonation of local model layer 3 (Wadsworth Sand Unit and Beverly Unit). See Table 5 (pages 100 and 101) for assumed plausible ranges and starting values for calibration for each zone.	114
Figure 64. Hydraulic conductivity zonation of local model layer 2 (surficial Henry Unit, Wadsworth Diamicton Unit, and Haeger Unit). See Table 5 (pages 100 and 101) for assumed plausible ranges and starting values for calibration for each zone.....	115
Figure 65. Hydraulic conductivity zonation of local model layer 1 (soil unit and surficial Henry Unit). See Table 5 (pages 100 and 101) for assumed plausible ranges and starting values for calibration for each zone.	116
Figure 66. Index map showing locations of cross sections shown in Figure 67 through Figure 70.	117
Figure 67. West-to-east cross section A-A' showing hydraulic conductivity zonation of local-scale model in northern part of model domain (see Figure 66 for cross section location).	118
Figure 68. West-to-east cross section B-B' showing hydraulic conductivity zonation of local-scale model in central part of model domain (see Figure 66 for cross section location).	119
Figure 69. West-to-east cross section C-C' showing hydraulic conductivity zonation of local-scale model in southern part of model domain (see Figure 66 for cross section location).	120
Figure 70. North-to-south cross section D-D' showing hydraulic conductivity zonation of local-scale model in the model domain (see Figure 66 for cross section location).	121
Figure 71. Recharge rate zonation of regional model.	126
Figure 72. Recharge rate zonation of local-scale model.	130
Figure 73. Area where surface water and drained conditions are simulated in regional model.	132
Figure 74. Representation of surface water in regional model.	133

List of Figures (Continued)

	Page
Figure 75. Representation in the local-scale model, using the MODFLOW river package, of streams having $Q_{7,10}$ greater than zero.	137
Figure 76. Representation of drained areas in regional model.	139
Figure 77. Representation of drained areas and intermittent streams in local-scale model with the MODFLOW drain package.....	141
Figure 78. Deep wells represented in the regional model.....	142
Figure 79. Shallow wells represented in the regional model.	143
Figure 80. Wells represented in the local-scale model.	144
Figure 81. Head targets for calibration of regional predevelopment steady-state model.....	149
Figure 82. Flux targets for calibration of predevelopment steady-state regional model.....	153
Figure 83. Plot showing the goodness of the fit between the steady-state predevelopment target heads and model-calculated heads for the regional-scale model.....	159
Figure 84. Residuals (observed minus simulated values) between target and simulated heads at predevelopment head calibration targets.	161
Figure 85. Comparison of simulated predevelopment base flow to Q_{80} and Q_{50} measurements of streamflow.	163
Figure 86. Head targets, with identification numbers referred to in Section 2.3.1.5, for verification of regional model under transient conditions.	165
Figure 87. Median annual observed water level and simulated water level at shallow head verification location 1115.	166
Figure 88. Median annual observed water level and simulated water level at shallow head verification location 1112.	167
Figure 89. Median annual observed water level and simulated water level at shallow head verification location 1113.	168
Figure 90. Median annual observed water level and simulated water level at deep head verification location 1116.	169
Figure 91. Median annual observed water level and simulated water level at deep head verification location 1118.	170
Figure 92. Median annual observed water level and simulated water level at deep head verification location 1117.	171
Figure 93. Median annual observed water level and simulated water level at deep head verification location 1119.	172
Figure 94. Median annual observed water level and simulated water level at deep head verification location 1120.	173
Figure 95. Median annual observed water level and simulated water level at deep head verification location 1121.	174
Figure 96. Parameter sensitivities for the predevelopment calibration, regional-scale model.....	179

List of Figures (Continued)

	Page
Figure 97. Close similarity of simulated 2003 heads in the Shallow Bedrock Aquifer based on steady-state modeling employing 2003 pumping distribution and rates and transient modeling employing actual 1964-2003 pumping histories.....	181
Figure 98. Head targets for calibration of local-scale model.....	183
Figure 99. Flux targets for calibration of local-scale model.....	184
Figure 100. Calibrated recharge rates in local-scale model.....	186
Figure 101. Plot showing the goodness of the fit between observed 2003 heads and head simulated with 2003 steady-state model.....	188
Figure 102. Residuals between target and simulated heads at 2003 head calibration targets open to model layer 15.....	190
Figure 103. Comparison of simulated base flow to Q_{80} and Q_{50} measurements of streamflow.....	191
Figure 104. Head targets, with identification numbers referred to in Section 2.3.2.5, for verification of local model under transient conditions.	192
Figure 105. Observed and simulated water levels at transient head verification location 95.....	193
Figure 106. Observed and simulated water levels at transient head verification location 171.....	194
Figure 107. Observed and simulated water levels at transient head verification location 196.....	195
Figure 108. Observed and simulated water levels at transient head verification location 2024.....	196
Figure 109. Parameter sensitivities for calibration, local-scale model.	198
Figure 110. Simulated predevelopment head in the Ancell Unit.....	203
Figure 111. Simulated 2002 head in the Ancell Unit.....	204
Figure 112. Simulated drawdown in 1985 in the Ancell Unit.	205
Figure 113. Simulated drawdown in 2002 in the Ancell Unit.	206
Figure 114. Locations of simulated hydrographs shown in Figure 115 and Figure 116.	208
Figure 115. Simulated heads from 1864 through 2002 in the Ancell Unit at selected locations in Kane County.....	209
Figure 116. Simulated heads from 1864 through 2002 in the Ironton-Galesville Unit at selected locations in Kane County.....	210
Figure 117. Available simulated head above the top of the Ancell Unit in 2002 based on regional modeling.	212
Figure 118. Available simulated head above the top of the Ancell Unit under predevelopment conditions based on regional modeling.....	213
Figure 119. Simulated predevelopment head in the Shallow Bedrock Aquifer in the Kane County area.	214
Figure 120. Simulated predevelopment head in the Lower Glasford Sand Unit in the Kane County area.	215
Figure 121. Simulated predevelopment head in the Upper Glasford Sand Unit in the Kane County area.	216

List of Figures (Continued)

	Page
Figure 122. Simulated predevelopment head in the Ashmore Unit in the Kane County area.	217
Figure 123. Simulated predevelopment head in the Batestown Sand Unit in the Kane County area.	218
Figure 124. Simulated predevelopment head in the Yorkville Sand Unit in the Kane County area.	219
Figure 125. Simulated predevelopment head in the Beverly Unit in the Kane County area.	220
Figure 126. Simulated 2003 head in the Shallow Bedrock Aquifer in the Kane County area.	221
Figure 127. Simulated 2003 head in the Lower Glasford Sand Unit in the Kane County area.	222
Figure 128. Simulated 2003 head in the Upper Glasford Sand Unit in the Kane County area.	223
Figure 129. Simulated 2003 head in the Ashmore Unit in the Kane County area.	224
Figure 130. Simulated 2003 head in the Batestown Sand Unit in the Kane County area.	225
Figure 131. Simulated 2003 head in the Yorkville Sand Unit in the Kane County area.	226
Figure 132. Simulated 2003 head in the Beverly Unit in the Kane County area.	227
Figure 133. Simulated drawdown in 2003 in the Shallow Bedrock Aquifer in the Kane County area, with areas of drawdown mentioned in text identified.	229
Figure 134. Simulated drawdown in 2003 in the Lower Glasford Sand Unit in the Kane County area.	230
Figure 135. Simulated drawdown in 2003 in the Upper Glasford Sand Unit in the Kane County area.	231
Figure 136. Simulated drawdown in 2003 in the Ashmore Unit in the Kane County area.	232
Figure 137. Simulated drawdown in 2003 in the Batestown Sand Unit in the Kane County area.	233
Figure 138. Simulated drawdown in 2003 in the Yorkville Sand Unit in the Kane County area.	234
Figure 139. Simulated drawdown in 2003 in the Beverly Unit in the Kane County area.	235
Figure 140. Index map of northeastern Kane County and southeastern McHenry County showing simulated 2003 drawdown in the Shallow Bedrock Aquifer.	236
Figure 141. Locations of simulated hydrographs shown in Figure 142 through Figure 149.	238
Figure 142. Simulated head in the Shallow Bedrock Aquifer at head calibration target 661, located in the Algonquin area of northeastern Kane County, and withdrawals from key nearby wells.	239
Figure 143. Index map of east-central Kane County and west-central DuPage County showing simulated 2003 drawdown in the Shallow Bedrock Aquifer.	240

List of Figures (Continued)

	Page
Figure 144. Simulated heads in the Shallow Bedrock Aquifer at head calibration target 149, located east of Geneva, on the eastern border of Kane County, and withdrawals from key nearby wells.	241
Figure 145. Index map of the South Elgin area showing simulated 2003 drawdown in the Shallow Bedrock Aquifer.	242
Figure 146. Simulated heads in the Shallow Bedrock Aquifer at head calibration target 498, located on the southeast edge of South Elgin.	244
Figure 147. Index map of southeastern Kane and northeastern Kendall Counties showing simulated 2003 drawdown in the Shallow Bedrock Aquifer.	245
Figure 148. Simulated heads in the Shallow Bedrock Aquifer at head calibration target 108, located on the north edge of Montgomery.	246
Figure 149. Simulated heads in the Lower Glasford Sand Unit at head calibration target 154, located west of Batavia.	247
Figure 150. Simulated drawdown in 1964 in the Shallow Bedrock Aquifer in the Kane County area.	248
Figure 151. Simulated drawdown in 1973 in the Shallow Bedrock Aquifer in the Kane County area.	249
Figure 152. Simulated drawdown in 1983 in the Shallow Bedrock Aquifer in the Kane County area.	250
Figure 153. Simulated drawdown in 1993 in the Shallow Bedrock Aquifer in the Kane County area.	251
Figure 154. Stream reaches employed for flow accounting in local-scale model.	253
Figure 155. Estimated total change in natural groundwater discharge caused by pumping, by stream reach, at the end of 2003.	255
Figure 156. Total simulated natural groundwater discharge in local model domain.	257
Figure 157. Total simulated natural groundwater discharge in watersheds covering local model domain.	258
Figure 158. Simulated natural groundwater discharge to Mill Creek upstream of Batavia (reach 512).	259
Figure 159. Simulated natural groundwater discharge to the West Branch of the DuPage River upstream of Warrenville (reach 520).	261
Figure 160. Simulated natural groundwater discharge in the local model domain to Poplar Creek (reach 516).	262
Figure 161. Simulated natural groundwater discharge in the local model domain to the DuPage River and West Branch of the DuPage River downstream of Warrenville (reach 521).	263
Figure 162. Simulated natural groundwater discharge in the local model domain to the Fox River (reaches 501, 502, and 503).	264
Figure 163. Simulated natural groundwater discharge in the local model domain to the Fox River from Algonquin to Montgomery (reach 502).	265
Figure 164. Simulated groundwater flow directions and estimated groundwater flow divides in the Ancell Unit under predevelopment conditions.	267

List of Figures (Continued)

	Page
Figure 165. Simulated groundwater flow directions and estimated groundwater flow divides in the Ancell Unit in 1880.	268
Figure 166. Simulated groundwater flow directions and estimated groundwater flow divides in the Ancell Unit in 1920.	269
Figure 167. Simulated groundwater flow directions and estimated groundwater flow divides in the Ancell Unit in 2002.	270
Figure 168. Simulated 2003 groundwater flow directions in the Shallow Bedrock Aquifer in the Kane County area.	272
Figure 169. Simulated vertical flow across top of Ancell Unit under predevelopment conditions.	273
Figure 170. Simulated vertical flow across top of Ancell Unit in 1985.	275
Figure 171. Simulated vertical flow across top of Ancell Unit in 2002.	276
Figure 172. Areas of flow reversal across the top of the Ancell Unit, from upward under predevelopment conditions to downward in 2002.	277
Figure 173. Areas of downward simulated flow across the top of the Ancell Unit in 2002 where predevelopment vertical flow was negligible (between 10^{-4} ft/d upward and 10^{-4} ft/d downward).	278
Figure 174. Reported and projected groundwater withdrawals from wells supplying the Public Supply, Self-Supplied Commercial and Industrial, and Irrigation sectors in northeastern Illinois, 1964-2050.	282
Figure 175. Reported and projected groundwater withdrawals from shallow wells supplying the Public Supply, Self-Supplied Commercial and Industrial, and Irrigation sectors in northeastern Illinois, 1964-2050.	283
Figure 176. Reported and projected groundwater withdrawals from deep wells supplying the Public Supply, Self-Supplied Commercial and Industrial, and Irrigation sectors in northeastern Illinois, 1964-2050.	284
Figure 177. Reported and projected groundwater withdrawals from wells supplying the Public Supply, Self-Supplied Commercial and Industrial, and Irrigation sectors in Kane County, 1964-2050.	285
Figure 178. Reported and projected groundwater withdrawals from shallow wells supplying the Public Supply, Self-Supplied Commercial and Industrial, and Irrigation sectors in Kane County, 1964-2050.	286
Figure 179. Reported and projected groundwater withdrawals from deep wells supplying the Public Supply, Self-Supplied Commercial and Industrial, and Irrigation sectors in Kane County, 1964-2050.	287
Figure 180. Projected 2025 groundwater withdrawals from wells supplying the Public Supply, Self-Supplied Commercial and Industrial, and Irrigation sectors in the Kane County area, low-pumping conditions.	289
Figure 181. Projected 2025 groundwater withdrawals from wells supplying the Public Supply, Self-Supplied Commercial and Industrial, and Irrigation sectors in the Kane County area, high-pumping conditions.	290

List of Figures (Continued)

	Page
Figure 182. Projected 2050 groundwater withdrawals from wells supplying the Public Supply, Self-Supplied Commercial and Industrial, and Irrigation sectors in the Kane County area, low-pumping conditions.....	291
Figure 183. Projected 2050 groundwater withdrawals from wells supplying the Public Supply, Self-Supplied Commercial and Industrial, and Irrigation sectors in the Kane County area, high-pumping conditions.....	292
Figure 184. 2025 withdrawals simulated in local-scale model, low-pumping conditions.....	293
Figure 185. 2025 withdrawals simulated in local-scale model, high-pumping conditions.....	294
Figure 186. 2050 withdrawals simulated in local-scale model, low-pumping conditions.....	295
Figure 187. 2050 withdrawals simulated in local-scale model, high-pumping conditions.....	296
Figure 188. Total estimated (1964-2003) and projected (2005-2050) withdrawals from deep domestic wells in northeastern Illinois.....	297
Figure 189. Total estimated (1964-2003) and projected (2005-2050) withdrawals from deep domestic wells in Kane County.....	298
Figure 190. Existing deep domestic wells in the Kane County area. Withdrawals during the period 2005-2050 were projected for all of these wells.....	299
Figure 191. Projected deep domestic wells in the Kane County area constructed during the period 2005-2025. Each point may represent several wells.....	300
Figure 192. Projected deep domestic wells in the Kane County area constructed during the period 2005-2050. Each point may represent several wells.....	301
Figure 193. Estimated head change between the end of 2002 and end of 2049 in Ancell Unit under a scenario of high pumping and low recharge rates.	307
Figure 194. Estimated head change between the end of 2002 and end of 2049 in Ancell Unit under a scenario of high pumping and model-calibrated recharge rates.	308
Figure 195. Estimated head change between the end of 2002 and end of 2049 in Ancell Unit under a scenario of low pumping and model-calibrated recharge rates.	309
Figure 196. Estimated head change between the end of 2002 and end of 2049 in Ancell Unit under a scenario of low pumping and high recharge rates.	310
Figure 197. Simulated head in Ancell Unit in 2024 under a scenario of high pumping with low recharge rates.	311
Figure 198. Simulated head in Ancell Unit in 2049 under a scenario of high pumping with low recharge rates.	312
Figure 199. Simulated head in Ancell Unit in 2024 under a scenario of high pumping with model-calibrated recharge rates.	313
Figure 200. Simulated head in Ancell Unit in 2049 under a scenario of high pumping with model-calibrated recharge rates.	314
Figure 201. Simulated head in Ancell Unit in 2024 under a scenario of low pumping with model-calibrated recharge rates.	315

List of Figures (Continued)

	Page
Figure 202. Simulated head in Ancell Unit in 2049 under a scenario of low pumping with model-calibrated recharge rates.	316
Figure 203. Simulated head in Ancell Unit in 2024 under a scenario of low pumping with high recharge rates.	317
Figure 204. Simulated head in Ancell Unit in 2049 under a scenario of low pumping with high recharge rates.	318
Figure 205. Simulated heads from end of 1970 through end of 2049 in Ancell (top) and Ironton-Galesville Units (bottom) at Carpentersville. See Figure 114 for location.	319
Figure 206. Simulated heads from end of 1970 through end of 2049 in Ancell (top) and Ironton-Galesville Units (bottom) at Gilberts. See Figure 114 for location.	320
Figure 207. Simulated head from end of 1970 through end of 2049 in Ancell (top) and Ironton-Galesville Units (bottom) at Hampshire. See Figure 114 for location.	321
Figure 208. Simulated head from end of 1970 through end of 2049 in Ancell (top) and Ironton-Galesville Units (bottom) at Elgin. See Figure 114 for location.	322
Figure 209. Simulated head from end of 1970 through end of 2049 in Ancell (top) and Ironton-Galesville Units (bottom) at Plato Center. See Figure 114 for location.	323
Figure 210. Simulated head from end of 1970 through end of 2049 in Ancell (top) and Ironton-Galesville Units (bottom) at St. Charles. See Figure 114 for location.	324
Figure 211. Simulated head from end of 1970 through end of 2049 in Ancell (top) and Ironton-Galesville Units (bottom) at Maple Park. See Figure 114 for location.	325
Figure 212. Simulated head from end of 1970 through end of 2049 in Ancell (top) and Ironton-Galesville Units (bottom) at Elburn. See Figure 114 for location.	326
Figure 213. Simulated head from end of 1970 through end of 2049 in Ancell (top) and Ironton-Galesville Units (bottom) at Batavia. See Figure 114 for location.	327
Figure 214. Simulated head from end of 1970 through end of 2049 in Ancell (top) and Ironton-Galesville Units (bottom) at Aurora. See Figure 114 for location.	328
Figure 215. Simulated head from end of 1970 through end of 2049 in Ancell (top) and Ironton-Galesville Units (bottom) at Sugar Grove. See Figure 114 for location.	329
Figure 216. Available simulated head above the top of the Ancell Unit at the end of 2024 under a scenario of high pumping with low recharge rates.	330
Figure 217. Available simulated head above the top of the Ancell Unit at the end of 2049 under a scenario of high pumping with low recharge rates.	331
Figure 218. Available simulated head above the top of the Ancell Unit at the end of 2024 under a scenario of high pumping with model-calibrated recharge rates.	332
Figure 219. Available simulated head above the top of the Ancell Unit at the end of 2049 under a scenario of high pumping with model-calibrated recharge rates.	333
Figure 220. Available simulated head above the top of the Ancell Unit at the end of 2024 under a scenario of low pumping with model-calibrated recharge rates.	334
Figure 221. Available simulated head above the top of the Ancell Unit at the end of 2049 under a scenario of low pumping with model-calibrated recharge rates.	335
Figure 222. Available simulated head above the top of the Ancell Unit at the end of 2024 under a scenario of low pumping with high recharge rates.	336

List of Figures (Continued)

	Page
Figure 223. Available simulated head above the top of the Ancell Unit at the end of 2049 under a scenario of low pumping with high recharge rates.	339
Figure 224. Estimated drawdown between the end of 2003 and the end of 2024 in the Shallow Bedrock Aquifer under a scenario of high pumping and low recharge rates. ..	340
Figure 225. Estimated drawdown between the end of 2003 and the end of 2024 in the Shallow Bedrock Aquifer under a scenario of high pumping and model-calibrated recharge rates.	341
Figure 226. Estimated drawdown between the end of 2003 and the end of 2024 in the Shallow Bedrock Aquifer under a scenario of low pumping and model-calibrated recharge rates.	342
Figure 227. Estimated drawdown between the end of 2003 and the end of 2024 in the Shallow Bedrock Aquifer under a scenario of low pumping and high recharge rates. ..	343
Figure 228. Estimated total drawdown at the end of 2024 in the Shallow Bedrock Aquifer under a scenario of high pumping and low recharge rates.....	344
Figure 229. Estimated total drawdown at the end of 2024 in the Shallow Bedrock Aquifer under a scenario of high pumping and model-calibrated recharge rates.	345
Figure 230. Estimated total drawdown at the end of 2024 in the Shallow Bedrock Aquifer under a scenario of low pumping and model-calibrated recharge rates.....	346
Figure 231. Estimated total drawdown at the end of 2024 in the Shallow Bedrock Aquifer under a scenario of low pumping and high recharge rates.....	347
Figure 232. Estimated drawdown between the end of 2003 and the end of 2049 in the Shallow Bedrock Aquifer under a scenario of high pumping and low recharge rates. ..	348
Figure 233. Estimated drawdown between the end of 2003 and the end of 2049 in the Shallow Bedrock Aquifer under a scenario of high pumping and model-calibrated recharge rates.	349
Figure 234. Estimated drawdown between the end of 2003 and the end of 2049 in the Shallow Bedrock Aquifer under a scenario of low pumping and model-calibrated recharge rates.	350
Figure 235. Estimated drawdown between the end of 2003 and the end of 2049 in the Shallow Bedrock Aquifer under a scenario of low pumping and high recharge rates. ..	351
Figure 236. Estimated total drawdown at the end of 2049 in the Shallow Bedrock Aquifer under a scenario of high pumping and low recharge rates.....	352
Figure 237. Estimated total drawdown at the end of 2049 in the Shallow Bedrock Aquifer under a scenario of high pumping and model-calibrated recharge rates.	353
Figure 238. Estimated total drawdown at the end of 2049 in the Shallow Bedrock Aquifer under a scenario of low pumping and model-calibrated recharge rates.....	354
Figure 239. Estimated total drawdown at the end of 2049 in the Shallow Bedrock Aquifer under a scenario of low pumping and high recharge rates.....	355
Figure 240. Locations of simulated hydrographs shown in Figure 241 through Figure 249.....	357
Figure 241. Simulated heads in the Shallow Bedrock Aquifer at head calibration target 661, located in the Algonquin area of northeastern Kane County.....	358

List of Figures (Continued)

	Page
Figure 242. Simulated heads in the Shallow Bedrock Aquifer at head calibration target 278, located in East Dundee, northeastern Kane County.....	359
Figure 243. Simulated heads in the Ashmore Unit at head calibration target 700, located in Carpentersville, northeastern Kane County.	360
Figure 244. Simulated heads in the Shallow Bedrock Aquifer at head calibration target 149, located east of Geneva, on the eastern border of Kane County.	361
Figure 245. Simulated heads in the Shallow Bedrock Aquifer at head calibration target 648, located in Warrenville, DuPage County.	362
Figure 246. Simulated heads in the Lower Glasford Sand Unit at head calibration target 154, located west of Batavia, Kane County.....	364
Figure 247. Simulated heads in the Lower Glasford Sand Unit at head calibration target 158, located west of Geneva, Kane County.	365
Figure 248. Simulated heads in the Shallow Bedrock Aquifer at head calibration target 498, located on the southeast edge of South Elgin.	366
Figure 249. Simulated heads in the Shallow Bedrock Aquifer at head calibration target 108, located on the north edge of Montgomery.....	367
Figure 250. Transmissivity of shallow materials in Kane County, with 2003 withdrawals superimposed.	369
Figure 251. Total natural groundwater discharge to streams in the local-scale model domain.....	370
Figure 252. Estimated post-2003 change in natural groundwater discharge caused by pumping, by stream reach, at the end of 2024 under a scenario of high pumping and low recharge rates.	371
Figure 253. Estimated total change in natural groundwater discharge caused by pumping, by stream reach, at the end of 2024 under a scenario of high pumping and low recharge rates.	372
Figure 254. Estimated post-2003 change in natural groundwater discharge caused by pumping, by stream reach, at the end of 2049 under a scenario of high pumping and low recharge rates.	373
Figure 255. Estimated total change in natural groundwater discharge caused by pumping, by stream reach, at the end of 2049 under a scenario of high pumping and low recharge rates.	374
Figure 256. Estimated post-2003 change in natural groundwater discharge caused by pumping, by stream reach, at the end of 2024 under a scenario of high pumping and model-calibrated recharge rates.	375
Figure 257. Estimated total change in natural groundwater discharge caused by pumping, by stream reach, at the end of 2024 under a scenario of high pumping and model-calibrated recharge rates.	376
Figure 258. Estimated post-2003 change in natural groundwater discharge caused by pumping, by stream reach, at the end of 2049 under a scenario of high pumping and model-calibrated recharge rates.	377

List of Figures (Concluded)

	Page
Figure 259. Estimated total change in natural groundwater discharge caused by pumping, by stream reach, at the end of 2049 under a scenario of high pumping and model-calibrated recharge rates.	378
Figure 260. Estimated post-2003 change in natural groundwater discharge caused by pumping, by stream reach, at the end of 2024 under a scenario of low pumping and model-calibrated recharge rates.	379
Figure 261. Estimated total change in natural groundwater discharge caused by pumping, by stream reach, at the end of 2024 under a scenario of low pumping and model-calibrated recharge rates.	380
Figure 262. Estimated post-2003 change in natural groundwater discharge caused by pumping, by stream reach, at the end of 2049 under a scenario of low pumping and model-calibrated recharge rates.	381
Figure 263. Estimated total change in natural groundwater discharge caused by pumping, by stream reach, at the end of 2049 under a scenario of low pumping and model-calibrated recharge rates.	382
Figure 264. Estimated post-2003 change in natural groundwater discharge caused by pumping, by stream reach, at the end of 2024 under a scenario of low pumping and high recharge rates.	383
Figure 265. Estimated total change in natural groundwater discharge caused by pumping, by stream reach, at the end of 2024 under a scenario of low pumping and high recharge rates.	384
Figure 266. Estimated post-2003 change in natural groundwater discharge caused by pumping, by stream reach, at the end of 2049 under a scenario of low pumping and high recharge rates.	385
Figure 267. Estimated total change in natural groundwater discharge caused by pumping, by stream reach, at the end of 2049 under a scenario of low pumping and high recharge rates.	386
Figure 268. Total natural groundwater discharge to streams in the portion of the Fox River watershed within the local-scale model domain.	391
Figure 269. Simulated natural groundwater discharge to Mill Creek upstream of Batavia (reach 512).	392
Figure 270. Simulated natural groundwater discharge to the Fox River upstream of Algonquin (reach 503).	394
Figure 271. Simulated natural groundwater discharge to the West Branch DuPage River upstream of Warrenville (reach 520).	395
Figure 272. Simulated head in Ancell Unit after extended pumping at 2002 rates with model-calibrated recharge rates.	396
Figure 273. Available simulated head above the top of the Ancell Unit after a period of extended pumping at 2002 rates with model-calibrated-recharge rates.	397

List of Tables

	Page
Table 1. Projection and Coordinate System Used in This Study	5
Table 2. Deep Wells in Kane County That Pumped More Than 100,000 Gallons per Day (gpd) in 2003.....	32
Table 3. Shallow Wells in Kane County That Pumped More Than 100,000 Gallons per Day (gpd) in 2003	33
Table 4. Hydraulic Conductivity Zonation of Regional-Scale Model.....	94
Table 5. Hydraulic Conductivity Zonation of Local-Scale Model	100
Table 6. Starting Values and Plausible Ranges of Storage Parameters Employed in Development of Regional Model.....	124
Table 7. Recharge Zonation of Regional-Scale Model.....	127
Table 8. Starting Values and Plausible Ranges of Leakance (K_v/m) Employed for Representation of Surface Water in Regional Model	135
Table 9. Starting Values and Plausible Ranges of Leakance Employed for Representation of Drained Areas in Regional Model	138
Table 10. Head Targets for Calibration of Predevelopment Steady-State Regional Model	150
Table 11. Flux Targets for Calibration of Predevelopment Steady-State Regional Model	152
Table 12. Median Base Flow and Streamflow Statistics for 50-Year Maximum Period of Record for Six Watersheds in Northern Illinois	152
Table 13. Anisotropy Ratios (K_h/K_v) Used as Constraints for Calibration of Predevelopment Steady-State Regional Model	155
Table 14. Calibration of Horizontal (K_h) and Vertical Hydraulic Conductivity (K_v), Regional-Scale Model.....	156
Table 15. Calibration of Recharge Rates, Regional Model	157
Table 16. Calibration of Leakance (K_v/m) Employed to Represent Surface Water, Regional Model.....	157
Table 17. Calibration of Leakance (K_v/m) Employed to Represent Drained Areas, Regional Model.....	157
Table 18. Statistics Describing Calibration to Predevelopment Head Targets	160
Table 19. Predevelopment Flux Targets and Residuals, Regional Model.....	164
Table 20. Comparison of Simulated Heads and Observed	177
Table 21. Flux Targets for Calibration of Local-Scale Model.....	185
Table 22. Calibration of Horizontal (K_h) and Vertical Hydraulic Conductivity (K_v), Local-Scale Model.....	185
Table 23. Calibration of Recharge Rates, Local-Scale Model.....	185
Table 24. Statistics Describing Steady-State Calibration of Local-Scale Model to 2003 Head Targets	189
Table 25. Simulations Discussed in Section 3	201
Table 26. Principal Streams Included in Reaches Shown in Figure 154 and Figure 155 and Change in Natural Groundwater Discharge since Predevelopment in 2003 (%).....	254
Table 27. Recharge Conditions for Transient Simulation to 2050 using Regional-Scale Model	303

List of Tables (Concluded)

	Page
Table 28. Recharge Conditions for Transient Simulation to 2050 using Local-Scale Model	303
Table 29. Transient Simulations to 2050 using Regional-Scale Model.....	305
Table 30. Stress Periods and Bases for Assumed Pumping Rates for Transient Simulation to 2050	306
Table 31. Estimated Total Change in Natural Groundwater Discharge at Ends of 2024 and 2049, by Stream Reach	387
Table 32. Estimated Post-2003 Change in Natural Groundwater Discharge at Ends of 2024 and 2049, by Stream Reach	388

Glossary

Definition sources: American Geological Institute, Fetter (1988), Heath (1983), and Illinois State Water Survey (2008)

aquifer: A saturated geologic formation that can yield economically useful amounts of *groundwater* to wells, springs, wetlands, or streams.

aquitard: A geologic formation of low permeability that does not yield useful quantities of *groundwater* when tapped by a well and that hampers the movement of water into and out of an *aquifer*.

water availability: The amount of water that occurs in rivers, streams, lakes, reservoirs, and *aquifers* at any given time or over a period of time.

base flow: The sustained *low flow* of a stream, usually originating as *groundwater discharge* to the stream channel.

bedrock: A general term for the consolidated rock that underlies soils or other unconsolidated surficial material (such as *glacial drift*).

capture zone: The portion of the subsurface contributing the *groundwater* withdrawn by a well during a selected time period (for example, five-year capture zone shows the portion of the subsurface contributing the *groundwater* withdrawn by a well over the course of five years of operation).

cone of depression: A three-dimensional representation of the *drawdown* created around a pumping well. Taking the shape of an inverted cone, the *drawdown* is greatest at the pumping well and decreases logarithmically with distance from the pumping well to zero at the *radius of influence*.

confined aquifer: An *aquifer* which is both overlain and underlain by *aquitards*, which is fully saturated (i.e., all pore spaces are filled with water), and within which head is higher than the elevation of the upper boundary of the aquifer.

confining bed: See *aquitard*

confining unit: See *aquitard*

contour line: A line on a cross section or map connecting points of equal value.

desaturation: The act, or the result of the act, of draining pores in a *confined aquifer*, leading to unsaturated conditions within the *aquifer* and thereby causing its conversion to an *unconfined aquifer*.

Glossary (Continued)

discharge: (1) Groundwater that exits the *saturated zone* by processes of seepage, evapotranspiration, or artificial withdrawal (2) the process of removal of groundwater from the *saturated zone*.

discharge area: An area where groundwater exits the *saturated zone* through *evapotranspiration* and/or seepage to springs or stream channels in response to an upward vertical *head gradient*.

drawdown: The reduction of the *water table* of an *unconfined aquifer* or the potentiometric surface of a *confined aquifer* caused by *groundwater* withdrawals from wells.

effluent: Wastewater, treated or untreated, that flows out of a treatment plant, sewer, or industrial outfall. Generally refers to wastes discharged into *surface waters*.

equipotential: A type of *contour line* on a cross section or *potentiometric surface map* along which *head* is equal.

evapotranspiration: The process by which water is returned to the atmosphere by evaporation and transpiration caused by molecular activity at the liquid (water) surface where the liquid turns to vapor. Evaporation occurs at a free-water surface interface; transpiration is essentially the same as evaporation except that the surface from which the water molecules escape is not a free-water surface. The surface for transpiration is largely leaves.

glacial drift: Sediment, including boulders, till, gravel, sand, silt, or clay, transported by a glacier and deposited by or from the ice or by or in water derived from the melting of the ice.

groundwater: Generally all subsurface water as distinct from surface water; specifically, that part of the subsurface water in the *saturated zone*. Groundwater can be hydraulically connected to *surface waters*.

groundwater flow model: An idealized mathematical description of the movement of water through earth materials under a given set of geologic and hydraulic conditions. In common usage, the term is understood to refer to both the computer program that solves the set of equations and to the application of the program to a particular *groundwater* system.

head: The height above a datum plane (commonly mean sea level) of a column of water. Water levels in tightly cased wells indicate head in the *aquifer* to which the well is open.

head gradient: The change in *head* per unit of distance measured in the direction of steepest change. All other factors being equal, *groundwater* flow is directly proportional

Glossary (Continued)

to the head gradient; that is, the steeper the head gradient, the greater the flow. Head gradients are most commonly discussed for lateral distances within units (i.e., a *horizontal head gradient*) and for vertical distances within or across units (i.e., a *vertical head gradient*).

horizontal hydraulic conductivity (K_h): The *hydraulic conductivity* parallel to bedding in horizontally stratified earth materials, frequently orders of magnitude greater than *vertical hydraulic conductivity*.

hydraulic conductivity (K): A *hydraulic property* expressing the capacity of an earth material to transmit *groundwater*, or permeability. It is expressed as the volume of water that will move in a unit time under a unit *head gradient* through a unit area measured at right angles to the direction of flow. In this report, hydraulic conductivities are expressed in units of feet per day (ft/d). Because earth materials are frequently stratified or have a preferred grain orientation, hydraulic conductivity frequently is directional in nature, the most common distinction being between *horizontal* and *vertical hydraulic conductivity* in stratified rocks.

hydraulic gradient: See *head gradient*

hydraulic properties: Numbers describing the capacity of a material to store and transmit water, most notably the *vertical* and *horizontal hydraulic conductivity*, *transmissivity*, *storage coefficient*, and *porosity*.

hydrostratigraphy: *Stratigraphy* based on the hydraulic characteristics of earth materials.

interference: See *well interference*

leakage: (1) The process by which water enters or exits an *aquifer*, generally by vertical movement under the influence of *vertical head gradients* within the *saturated zone* (2) the quantity of water contributed to or removed from an *aquifer*, by movement under the influence of *vertical head gradients* within the *saturated zone*.

leakance: The *vertical hydraulic conductivity* of the streambed or lakebed divided by its thickness. Leakance controls the flow of water between the *saturated zone* and the *surface water*.

lithology: The physical character of a rock or earth material, generally as determined megascopically or with the aid of a low-power magnifier.

lithostratigraphy: *Stratigraphy* based on *lithology*.

low flow: Seasonal and climatic periods during which *streamflows* are notably below average, or the flow rates that occur during such periods.

Glossary (Continued)

porosity (n): A hydraulic property describing the volume of open space (pore space) within a material. It is calculated as the volume of open space divided by the total volume of the material and is sometimes expressed as a percentage.

potentiometric surface: A surface representing the level to which water will rise in tightly cased wells. The *water table* is a potentiometric surface for an *unconfined aquifer*.

potentiometric surface map: A map showing a *potentiometric surface* by means of *contour lines (equipotentials)*.

radius of influence: The horizontal distance (R) from the center of a pumping well to the point where there is no *drawdown* caused by that well, or the limit of its *cone of depression*.

recharge: (1) Water that infiltrates and percolates downward to the *saturated zone* (2) the process by which water infiltrates and percolates downward to the *saturated zone*.

recharge area: An area where *groundwater* moves downward from the *water table* in response to a downward *vertical head gradient*.

saturated zone: The subsurface zone, below the water table, in which all *porosity* is filled with water and within which the water is under pressure greater than that of the atmosphere.

specific storage (S_s): A *hydraulic property* related to the *storage coefficient*, equivalent to the volume of water released from or taken into storage per unit volume of a porous material per unit change in *head*. The specific storage is unitless. *Specific yield* is a term reserved for the specific storage of an *unconfined aquifer*.

specific yield (S_y): A *hydraulic property* describing the capacity of an *unconfined aquifer* material to store water as well as describing the source of water pumped from wells finished in the *aquifer*. It is the ratio of the volume of water the material will yield by gravity drainage to the volume of porous material. The specific yield is unitless. Specific yield is a term reserved for the *specific storage* of an *unconfined aquifer*.

steady-state conditions: As contrasted from *transient conditions*, steady-state conditions are those in which heads and exchange with surface waters in an area do not change over time, having adjusted to the spatial distribution and rates of water inflow and outflow in the area. They describe an equilibrium condition. When stresses change, transient conditions prevail for a time, but given no additional changes, a new equilibrium will become established, and *steady-state conditions* will be re-established.

storage coefficient (S): A *hydraulic property* describing the capacity of an *aquifer* to store water as well as the source of water pumped from wells finished in the *aquifer*. It is the

Glossary (Continued)

volume of water that an *aquifer* releases from or takes into storage per unit surface area per unit change in *head*. The storage coefficient is unitless.

stratigraphy: (1) The arrangement of strata, especially as to the position and order of sequence (2) the branch of geology that deals with the origin, composition, distribution, and succession of strata.

streamflow: The total discharge of water within a watercourse, including runoff, diversions, *effluent*, and other sources.

streamflow capture: The process of reduction of *streamflow* resulting from *groundwater* withdrawals by wells. Streamflow capture occurs both by diversion into wells of *groundwater* that would, under nonpumping conditions, *discharge* to *surface water*, and by inducement of water directly from stream channels.

surface water: An open body of water, such as a stream, lake, reservoir, or wetland.

transient conditions: As contrasted from *steady-state conditions*, transient conditions are hydraulic conditions in which heads and exchange with surface waters change with time as they adjust to a new, or changed, stress, such as the establishment of a new pumping well or a change in withdrawal rate at a new well. If stresses do not change, transient conditions will eventually pass, and a new equilibrium and *steady-state conditions* will be established.

transmissivity (T): A *hydraulic property* that is a measure of the capacity of the entire thickness of an *aquifer* to transmit *groundwater*. It is defined as the rate at which water is transmitted through a unit width of an *aquifer* under a unit *head gradient*, and it is equivalent to the product of the *hydraulic conductivity* and the *aquifer* thickness. In this report, transmissivity is expressed in units of feet squared per day (ft²/d).

unconfined aquifer: An aquifer having no overlying aquitard.

unsaturated zone: A subsurface zone containing water under pressure less than that of the atmosphere, including water held by capillarity, and containing air or gases generally under atmospheric pressure. This zone is limited above by land surface and below by the surface of the *saturated zone* (i.e., the *water table*).

vertical hydraulic conductivity (K_v): *Hydraulic conductivity* perpendicular to bedding in horizontally stratified earth materials, frequently orders of magnitude less than *horizontal hydraulic conductivity*.

water quality: The suitability of water for an intended use. Water that is suitable for irrigation may require treatment to be suitable for drinking. Also refers to a comprehensive description of water composition, e.g., water quality studies.

Glossary (Concluded)

water table: The surface of the *saturated zone*, at which the pressure is equal to that of the atmosphere.

water withdrawal: An amount of water that is withdrawn from *groundwater* or *surface water* sources to meet water demand.

well interference: *Drawdown* caused by a nearby pumping well. Interference between pumping wells can affect well yield and is a factor in well spacing for well field design.

1. Introduction

1.1. Purpose

Kane County is a rapidly growing county in northeastern Illinois, comprising much of the western part of the Chicago metropolitan area. Population growth in this county is projected to increase from 404,119 in 2000 to 718,464 in 2030 (Northeastern Illinois Planning Commission, 2006), but the capacity of the water resources in Kane County to accommodate additional demand is poorly understood. Groundwater withdrawals from the deep bedrock aquifers of northeastern Illinois have long exceeded researchers' estimates of the long-term availability of water from them (Suter et al., 1959; Walton, 1964), yet these estimates are highly uncertain. The estimates also are based on many simplifying assumptions and cannot account for numerous factors affecting groundwater availability to the continually changing network of wells that have operated in the region historically and which will operate here in the future, thus limiting their utility for planning purposes (Walker et al., 2003). Wehrmann et al. (2003) suggest that shallow aquifer withdrawals may approach or exceed estimates of groundwater availability from aquifers in some eastern townships of Kane County, but the approach of their study limits its accuracy on a county scale and does not permit assessment of the hydrologic consequences of pumping from the actual network of wells present in the area. Water from Lake Michigan is used extensively in northeastern Illinois, but whether such water can be used to accommodate demand in Kane County is uncertain. Illinois' present use of Lake Michigan water approaches legally mandated limits, and delivery of Lake Michigan water to Kane County, a comparatively long distance from the lake, would be expensive in relation to developing local water resources.

The projected population growth, limited access to surface water supplies, and uncertainties regarding aquifers prompted an investigation of the water resources of Kane County and surrounding areas. In response, the Illinois State Water Survey (ISWS) and the Illinois State Geological Survey (ISGS) have conducted a series of investigations of surface water, geology, and groundwater resources of the region, supported by the Kane County Development Department and the State of Illinois. These investigations have included streamflow analysis and modeling (Knapp et al., 2007), mapping of groundwater levels (Locke and Meyer, 2007), mapping and modeling of near-surface geology (Dey et al., 2007a; Dey et al., 2007b; Dey et al., 2007c; Dey et al., 2007d; Dey et al., 2007e), analysis of trends in deep groundwater quality (Kelly and Meyer, 2005), and assessment of shallow groundwater quality (Kelly, 2005). This report discusses the final study of this series of investigations: a computer-modeling study of groundwater flow that assimilates the data and knowledge from the preceeding studies and assesses the availability of groundwater in and around Kane County.

1.1.1. Study Objectives

The goal of this study is to assess the current and future status of the groundwater resources of Kane County, Illinois. To achieve this goal, the objectives of this study are to review, document, and archive the hydrogeological data and knowledge for the region; apply a computer modeling of groundwater flow to the regional and local aquifers; use the resulting model to quantify the components of the hydrologic cycle; and use the

model to evaluate the consequences of plausible development and climate scenarios. The models developed in this study integrate the available data and knowledge with a mathematical representation of groundwater flow to yield estimates of recharge rates, assess surface water-groundwater interaction, and estimate leakage between aquifers. The models also are used to delineate capture zones of high-capacity public-supply wells in the shallow aquifers of the county, and to assess the impacts of plausible scenarios of future groundwater development and climate change. A key component of the study is a comprehensive review, archiving, and documentation of data via a modern database and GIS technologies, including a wide range of hydrologic and geologic properties, test data, pumping histories, etc. These databases and GIS coverages, together with the associated groundwater models and geologic models (Dey et al., 2007e) of this study, establish a benchmark and framework for future studies.

1.1.2. Scope and Limitations

This report discusses the development and application of two integrated computer models designed for simulation of groundwater flow (Appendix A) in aquifers supplying Kane County. Although computer models of many of these aquifers have been developed by earlier researchers (Section 1.10), the models described in this report are significantly improved as compared to these earlier models: (1) the horizontal resolution is much finer, giving the model results greater precision; (2) the number of layers is larger, permitting more realistic simulation of groundwater circulation; (3) all major and minor aquifers and aquitards influencing groundwater supply in Kane County are simulated in the integrated models, allowing more realistic simulation of groundwater circulation; (4) groundwater interactions with surface waters are simulated explicitly; and (5) new interpretations of hydraulic parameters affecting groundwater circulation are included.

The models developed for this study have a wide range of applicability for understanding the groundwater resources of the region and their response to management alternatives. The process of developing a model uses the physics of flow through porous media to force the estimates of hydraulic properties, recharge rates, and geology to be consistent with each other and with observations of hydraulic head and flow. As a consequence, the models and their results quantify flow rates, hydraulic head in aquifers, leakage to/from surface-water bodies, and recharge rates within the accuracy of the observations. Model results include maps of groundwater levels and their changes over time, the zones of aquifer desaturation, capture zones for high-capacity wells, changes in rates of groundwater discharge to streams, leakage between aquifers, and the source of water withdrawn from wells. These results should be sufficient for evaluating the impacts of operating wellfields, mapping recharge zones for aquifer protection, estimating the extent of desaturation, and evaluating water-supply management alternatives. Specific levels of accuracy and potential biases in model results are discussed in the sections devoted to model calibration. It should be noted that the models developed for this study are not applicable to analyses requiring extremely high levels of resolution and accuracy. This specifically excludes using the present models for, as examples, assessing the fate and transport of contaminants from point spill events, designing wells beyond screening for locations, or analyzing groundwater flow immediately adjacent to or beneath streams. Similarly, while the models of this study estimate the extent of aquifer desaturation, they cannot be used to assess flow through the unsaturated layers. On the other hand, users

requiring higher resolution and greater accuracy will find that the results and databases of these models provide a framework for creating high-resolution inset models, e.g., to provide geometry and boundary conditions for small-scale detailed models. To enable this onward use, the databases and models have a higher level of detail and documentation than is strictly necessary for the immediate purposes of county-scale planning and management of water resources (see Section 2 and Appendices A through G).

The groundwater flow models developed for this project are available to the public for use in simulating groundwater flow in the region and providing a framework for more detailed, site-specific studies. The models represent a synthesis of data and information available to the authors from 2002 to 2008, and they were developed using procedures and computer software widely accepted during that time period. Users of the models should understand that the models and the analysis based on them should be updated periodically to reflect newly available data, information, and analysis, as well as updated approaches to data synthesis and analysis, modeling techniques, and computer software.

1.2. Acknowledgments

This study was funded by Kane County and the State of Illinois. The views expressed are those of the authors and do not necessarily reflect the views of the sponsor or the ISWS. Paul Schuch of the Kane County Development and Resource Management Department deserves special thanks for his encouragement, assistance, and willingness to coordinate interactions with Kane County officials and stakeholders. The authors thank ISWS Chief Derek Winstanley (now retired), and ISWS Center for Groundwater Science Director Allen Wehrmann for their support and assistance. Derek Winstanley, Allen Wehrmann, Daniel Feinstein (United States Geological Survey, Wisconsin District), Vic Kelson (Wittman Hydro Planning Associates, Bloomington, Indiana), and Jack Wittman (Wittman Hydro Planning Associates, Bloomington, Indiana) reviewed this report and provided encouragement and thoughtful criticism. Lisa Sheppard, Patti Hill, and Sara Olson edited the report, and Sara Olson reviewed the graphics. Numerous individuals at the ISWS contributed to the project. Mark Anliker, Brian Coulson, Eric Hritsuk, Kevin Rennels, Amy Schwarz, and Noe Velazquez all assisted tremendously in the fieldwork necessary for the project. Randy Locke managed and documented an extensive potentiometric mapping effort. Mark Anliker additionally provided analyses of numerous pumping tests conducted in the Kane County area and assisted in compilation of historical groundwater withdrawal data for the project. Brian Dunneback contributed to the potentiometric surface mapping effort by estimating land surface elevations at well locations in the area. University of Illinois student employees Salmaan Akhtar, Sosina Asfaw, and Ye Ge assisted in compiling historical groundwater withdrawal data for the project, and Jonathan Foote developed computer software to estimate groundwater withdrawals in the absence of records. Steve Burch contributed expertise on groundwater flow in the Cambrian and Ordovician bedrock formations of northeastern Illinois.

William S. Dey and Curt Abert of the Illinois State Geological Survey provided analysis of source intervals of wells in the Kane County area and responded to the authors' numerous questions pertaining to the geology of the area. Dave Hart, Timothy Eaton, and Ken Bradbury of the Wisconsin Geological and Natural History Survey, and

Daniel Feinstein and Jim Krohelski of the United States Geological Survey Wisconsin District, contributed hydrogeological data, mapping, and analysis—including computer flow modeling—of great value to the authors not only as a basis for detailed and accurate simulation of groundwater conditions in Wisconsin, but also for the insights they offered in understanding groundwater flow throughout the Upper Midwest region. Mark Basch of the Indiana Department of Natural Resources provided substantial data on groundwater withdrawals in Indiana.

Finally, the authors acknowledge and thank the hundreds of well owners in the Kane County area who permitted use of their wells in this study.

1.3. Projection and Coordinate System

Unless otherwise specified, maps and coordinates in this study are referenced to the projection and coordinate system shown in Table 1, which is sometimes termed the ILLIMAP system.

1.4. Location

Kane County (Figure 1) is located in the Chicago metropolitan area of northeastern Illinois and is bordered by McHenry, DeKalb, Kendall, Cook, and DuPage Counties. The eastern border of Kane County is located about 32 miles west of the Lake Michigan shoreline in Chicago.

Table 1. Projection and Coordinate System Used in This Study

<i>Horizontal Coordinate System Definition:</i>
Planar:
Map Projection:
Map Projection Name: Lambert Conformal Conic
Lambert Conformal Conic:
Standard Parallel: 33.000000
Standard Parallel: 45.000000
Longitude of Central Meridian: -89.500000
Longitude of Projection Origin: 33.000000
False Easting: 2999994.000000
False Northing: 0.000000
<i>Planar Coordinate Information:</i>
Planar Coordinate Encoding Method: coordinate pair
Coordinate Representation:
Abscissa Resolution: 0.001024
Ordinate Resolution: 0.001024
<i>Planar Distance Units: survey feet</i>
<i>Geodetic Model:</i>
Horizontal Datum Name: North American Datum of 1927
Ellipsoid Name: Clarke 1866
Semi-major Axis: 6378206.400000
Denominator of Flattening Ratio: 294.978698

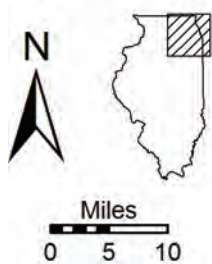
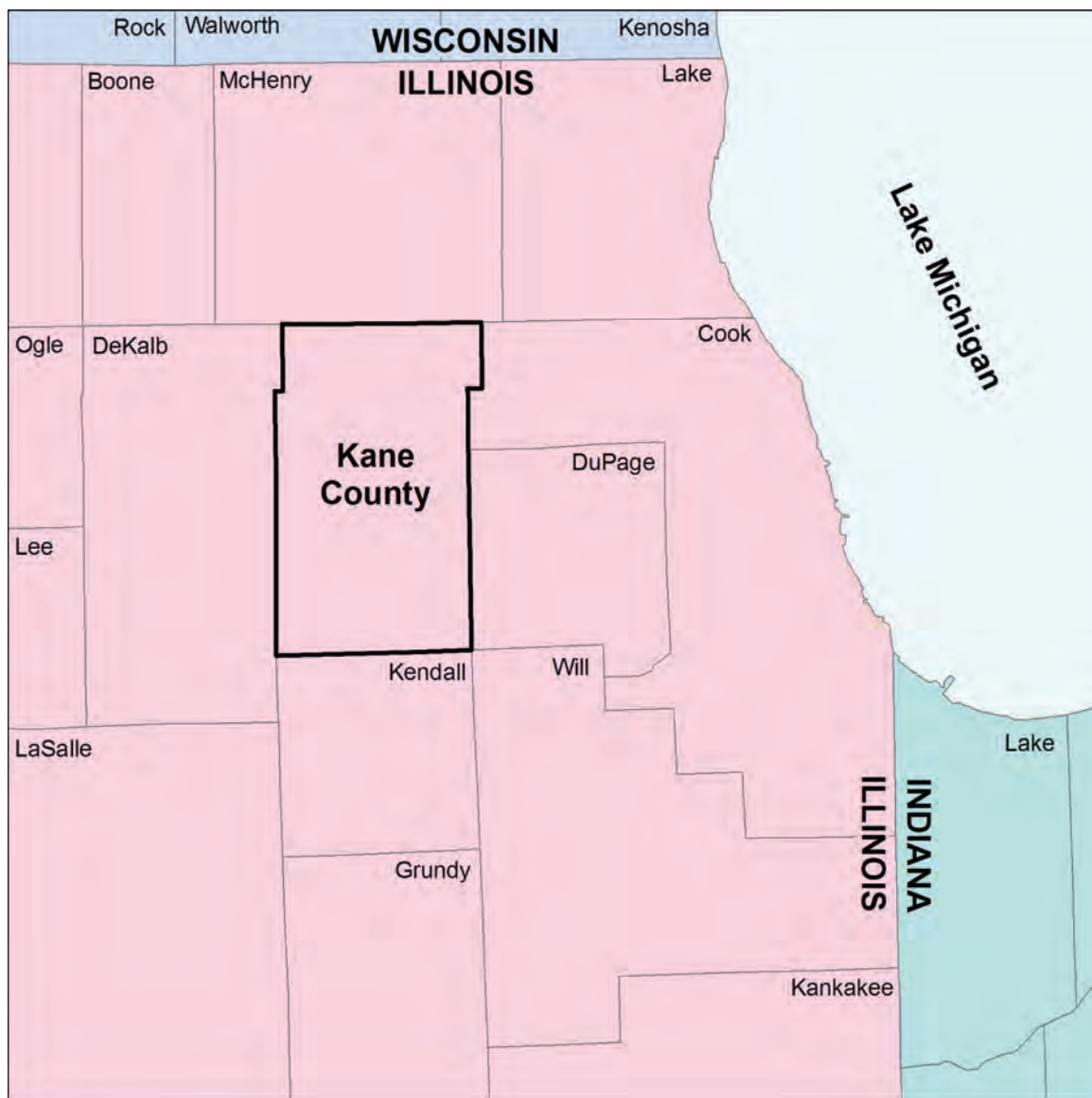


Figure 1. Location of Kane County, Illinois.

1.5. Population

With westward urban expansion of the Chicago metropolitan area, the population of Kane County has grown rapidly from 317,471 in 1990 to 404,119 in 2000 (Northeastern Illinois Planning Commission, 2006; United States Census Bureau, 2004). The estimated 2005 population of the county is 482,113, a 19 percent increase from 2000 (United States Census Bureau, 2004). Most of the county's population resides in the eastern tier of townships, which together encompass about one-third of the county area. In 2000, the population of these eastern townships totaled 354,600, or about 88 percent of the total county population.

Several moderately sized communities are located in Kane County. Communities exceeding 10,000 in the 2000 population include Aurora, Batavia, Carpentersville, Elgin, Geneva, North Aurora, St. Charles, and South Elgin (Figure 2). All of these communities are located in the eastern one-third of Kane County. The Kane County portion of Aurora, the largest city in Kane County, had a population of 100,290 in 2000; the total 2000 population of Aurora, which also incorporates areas of DuPage, Kendall, and Will Counties, was 142,990.

1.6. Physical Setting and Drainage

Land-surface elevations in Kane County range from less than 620 feet (ft) along the Fox River south of Aurora to more than 1060 ft on Marengo Ridge, a prominent north-south trending moraine in northwestern Kane County (Figure 3). Elevations throughout this report are expressed in ft above the National Geodetic Vertical Datum, commonly referred to as mean sea level (MSL).

The Fox River, which flows southward through the eastern part of the county, drains most of the eastern and southern parts of Kane County, an area amounting to about 60 to 70 percent of the county (Figure 3, Figure 4). Tributaries of the Kishwaukee River drain northwestern Kane County, and tributaries of the Des Plaines River drain a limited section of east-central Kane County.

1.7. Groundwater Concepts

1.7.1. Aquifers and Confining Beds

Although nearly all geologic materials will transmit water, the transmission rate varies widely and is dependent on the permeability of the material and the hydraulic pressure gradient. Groundwater moves relatively rapidly through highly permeable materials and relatively slowly through those of lower permeability. An *aquifer* is a layer of saturated geologic materials that, by virtue of its comparatively high permeability, will yield useful quantities of water to a well or spring. Materials that can function as aquifers include sand and gravel, fractured and jointed carbonate rocks (limestone and dolostone), and sandstone. A *confining bed*, *confining unit*, or *aquitard* is a layer of geologic materials having comparatively low permeability, which impedes water movement to and from adjacent aquifers. Materials that can function as confining beds include shale, unweathered and unfractured carbonate rocks (limestone and dolomite), silt, clay, and diamicton (a nonsorted sediment, typically of glacial origin, composed of sand-sized or larger particles dispersed through a fine-grained matrix of clay- and silt-sized particles).

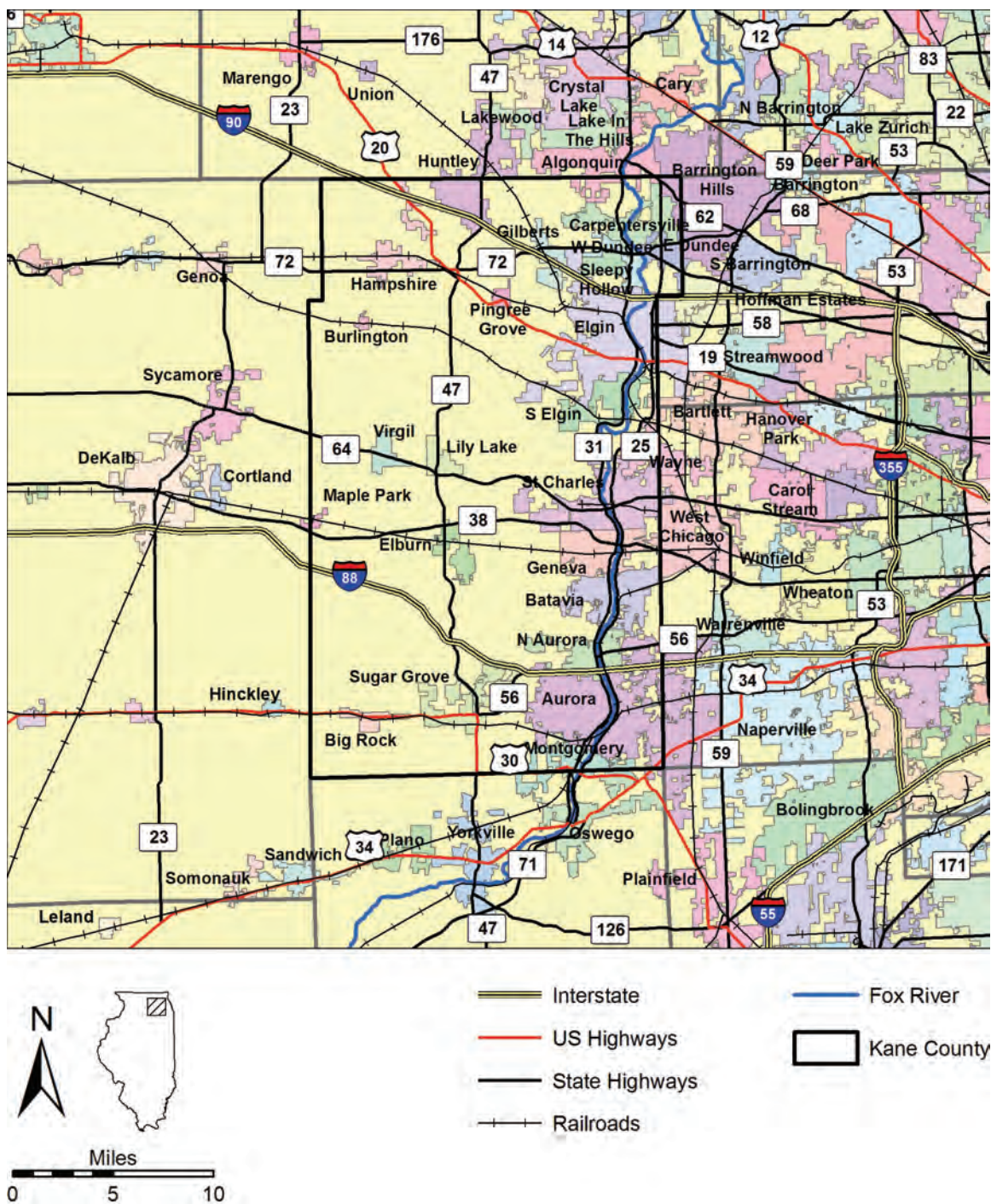


Figure 2. Municipalities and major roads in the Kane County area.

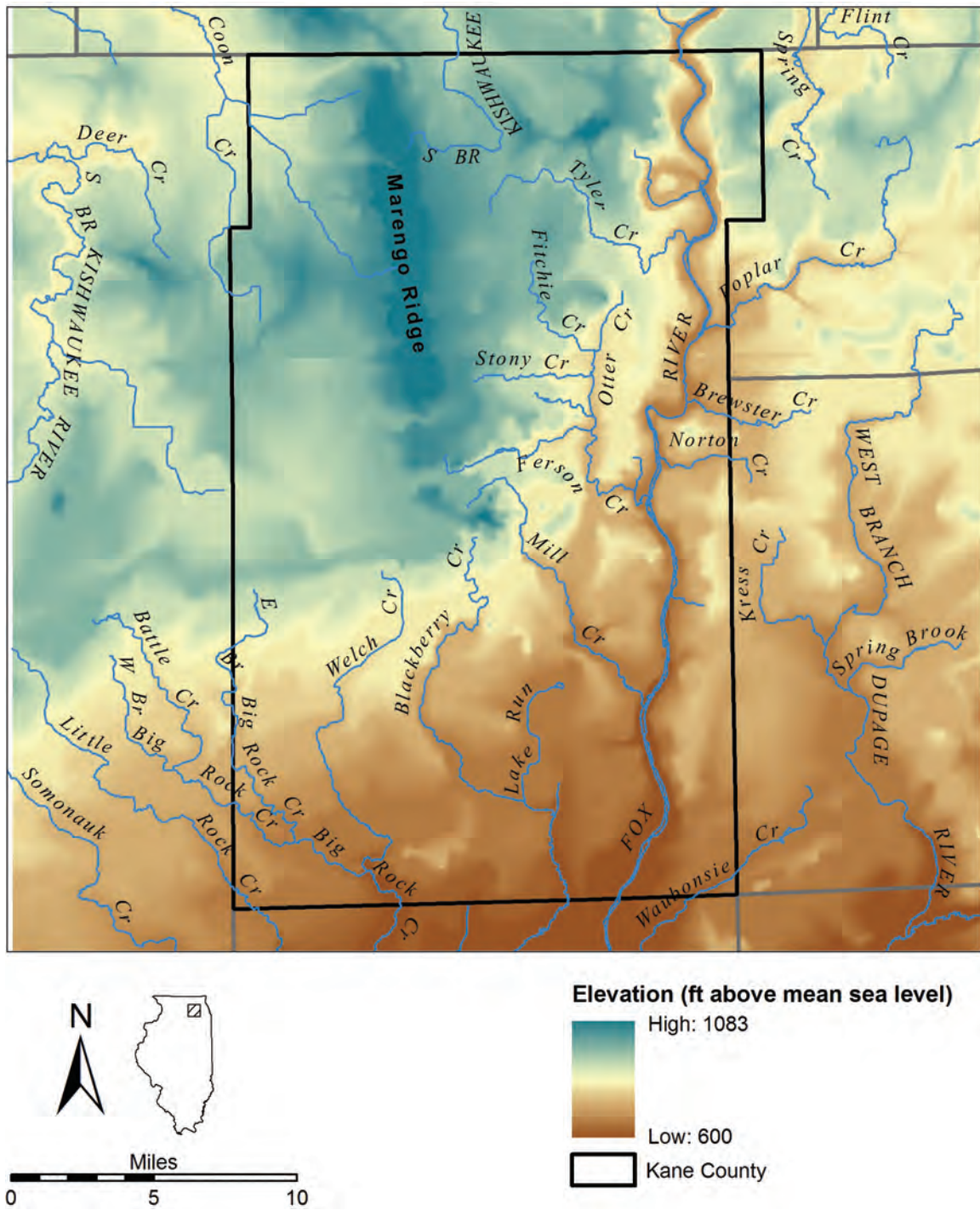


Figure 3. Elevation and drainage in the Kane County area.

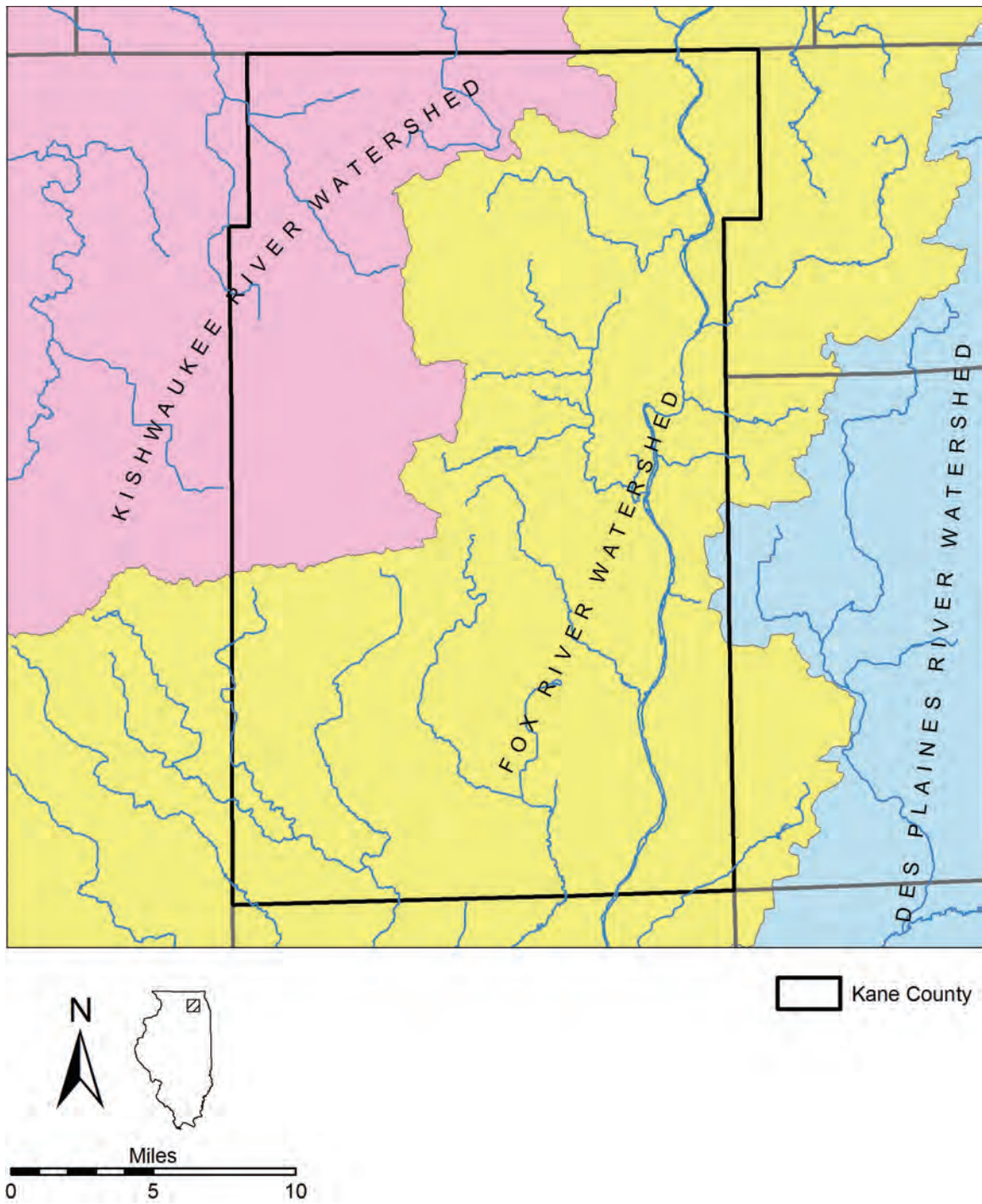


Figure 4. Major watersheds in the Kane County area.

In general, the term *hydrostratigraphy* refers to the study of spatial relationships, both vertical and lateral, of geologic layers grouped by hydraulic characteristics (e.g., aquifers and confining beds).

Aquifers can be unconfined or confined. An *unconfined aquifer* has no overlying confining bed. The water level in a well open to an unconfined aquifer approximates the water table. The water table represents the top of an unconfined aquifer, and as it rises and falls, aquifer thickness increases and decreases, respectively. Unconfined aquifers frequently have a direct hydraulic connection to rivers, lakes, streams, or other surface-water bodies. In such situations, the water level of the surface-water body may closely approximate the water level in the adjacent unconfined aquifer. A *confined aquifer* has confining beds both above and below it. Groundwater in confined aquifers is under pressure, and the water level in wells open to these aquifers will rise above the top of the aquifer.

1.7.2. *Potentiometric Surface Maps*

A *potentiometric surface map* is a contour map of the potentiometric surface of a particular hydrogeologic unit (Fetter, 1988) and illustrates hydraulic head, or the level to which water will rise, in tightly cased wells in that hydrogeologic unit. These maps can be constructed for both confined and unconfined aquifers and are sometimes referred to as water-level maps or head maps. *Contour lines* or *equipotentials* connect points of equal head and represent head values. Groundwater flows from high head to low head, and directions of groundwater flow are perpendicular to equipotentials. A head map can be used to determine groundwater flow directions as well as variations in head distribution.

The potentiometric surfaces of the shallowest aquifers closely approximate land-surface topography. Nearly all topography, including small hills and valleys, is replicated in the potentiometric surface with only a minor dampening of the relief. Dampening of the relief increases in deeper aquifers, so that only large-scale topographic features are replicated in the potentiometric surfaces of deeply buried aquifers.

Heads rise and fall in response to groundwater withdrawals, recharge, evaporation and transpiration, and, in the case of confined aquifers only, aquifer loading (Freeze and Cherry, 1979). Heads typically follow a seasonal cycle that is most noticeable in shallow aquifers and at locations remote from large pumping centers, where pumping effects do not overwhelm natural cycles. Natural declines in heads usually begin in late spring and continue throughout the summer and early fall when rainfall is quickly evaporated or transpired back to the atmosphere by growing plants. Heads begin to rise again in late fall and peak during the spring, when groundwater recharge from rainfall and snowmelt has its greatest effect (Visocky and Schicht, 1969).

1.7.3. *Hydraulic Properties*

The ability of an earth material to store and transmit water is generally a function of its hydraulic conductivity, transmissivity, and storage coefficient.

Hydraulic conductivity is the capacity of an earth material to transmit groundwater. It is expressed as the volume of water that will move in a unit time under a unit hydraulic gradient through a unit area measured at right angles to the directions of flow (Heath, 1983). The terms *head gradient* or *hydraulic gradient* refer to the change in

head per unit of distance measured in the direction of steepest change. All other factors being equal, groundwater flow is directly proportional to the hydraulic gradient; that is, the steeper the hydraulic gradient, the greater the flow. In this report, hydraulic conductivities are expressed in units of feet per day (ft/d). Thus, a 1-ft² area of a material having a hydraulic conductivity of 100 ft/d could transmit 100 ft³ of water during a 1-day period under a hydraulic gradient of 1 ft of head change per ft of horizontal distance (if the 1-ft² area is perpendicular to the hydraulic gradient).

The hydraulic conductivity of a material varies with the density and viscosity of water flowing through the material (which in turn are functions of temperature) as well as with the permeability of the material. For a given temperature, however, hydraulic conductivity is largely a function of permeability. Permeability is, in turn, a function of the size and degree of interconnection of pore spaces. In the unconsolidated sand and gravel aquifers of northeastern Illinois, the porosity consists principally of the voids lying between the sand and gravel grains composing the aquifer framework. The hydraulic conductivity of these materials generally ranges from 10⁰ to 10⁴ ft/d (Heath, 1983). Hydraulic conductivity may range from less than 10⁻⁷ ft/d, in the case of shale and dense, unfractured rocks, to greater than 10⁴ ft/d, in the case of coarse gravels and highly fractured and cavernous rocks (Heath, 1983).

Because earth materials are frequently stratified or have a preferred grain orientation, hydraulic conductivity frequently is directional in nature. The most common distinction is between *horizontal* and *vertical hydraulic conductivity* in stratified rocks, with vertical hydraulic conductivity (hydraulic conductivity perpendicular to bedding) being less than horizontal hydraulic conductivity (hydraulic conductivity parallel to bedding). Horizontal hydraulic conductivity is sometimes orders of magnitude greater than vertical hydraulic conductivity in shaly aquitards, because the long dimensions of the tabular clay mineral crystals composing these rocks are oriented parallel to bedding.

Transmissivity is a measure of the capacity of the entire thickness of an aquifer to transmit groundwater. It is defined as the rate at which water is transmitted through a unit width of an aquifer under a unit hydraulic gradient (Heath, 1983), and it is equivalent to the product of the hydraulic conductivity and the aquifer thickness. In this report, transmissivity is expressed in units of feet squared per day (ft²/d). Whereas hydraulic conductivity may be thought of as an expression of the capacity of a block of aquifer material, 1 ft² in cross-sectional area, transmissivity may be thought of as an expression of the capacity of a slice of the aquifer, 1 ft wide and having a height equal to the aquifer thickness, to transmit water under a unit hydraulic gradient.

The amount of water stored in and released from an aquifer varies with the type of aquifer and the amount of change in the hydraulic head in the aquifer. For confined aquifers, groundwater is stored and released through the elastic expansion and compression of the formation and of water in the pores. The *storage coefficient* is a unitless parameter describing the volume of water released per square foot of aquifer, per foot decrease in hydraulic head. The storage coefficient generally ranges between 10⁻⁵ to 10⁻³ (Heath, 1983) with a typical value in northeastern Illinois of 10⁻⁴ (Suter et al., 1959; Walton, 1964). This means that, as pumping in northeastern Illinois reduces the hydraulic head by 1 ft in a square ft of a confined aquifer, 10⁻⁴ ft³ of groundwater will be released as the water expands and the pore spaces in the aquifer compress. For unconfined aquifers, water is derived principally by gravity draining the pore space in the aquifer,

and the storage is described by the *specific yield*, ranging from 0.1 to 0.3 (Fetter, 1988). Thus, if the head in a 1 ft² area of an unconfined aquifer having a storage coefficient of 0.2 declines 1 ft, then 0.2 ft³ of groundwater has been removed from storage. A hydraulic property related to the storage coefficient is the *specific storage*, which is the amount of water released from or taken into storage per unit volume of a porous medium per unit change in head (Fetter, 1988).

The combination of hydraulic conductivity and the thickness of a streambed or lakebed controls the flow of water between the saturated zone of the subsurface and surface-water features. The vertical hydraulic conductivity of the streambed or lakebed divided by its thickness is referred to as the *leakance*. Field estimates of leakance are generally not available, and this is the case for northeastern Illinois, but typical values for riverbeds assumed to be several feet thick are between 0.1 and 10 feet per day per foot (ft/day-ft) (Calver, 2001).

1.7.4. Groundwater Recharge and Discharge

Groundwater recharge is a process by which water migrates downward through the subsurface and is added to the *saturated zone* in which all pore spaces are filled with water. Although most precipitation runs off to streams or evaporates, some of it percolates downward through the soil and unsaturated zone. A portion of the recharging water taken up by plants is returned to the atmosphere by transpiration. Water that passes through the unsaturated zone reaches the *water table* and is added to the saturated zone. Groundwater recharge occurs most readily where the materials composing the unsaturated zone are relatively permeable and where such factors as slope and land-use practices discourage runoff and uptake of water by plants.

Groundwater eventually discharges to surface-water bodies, including springs, wetlands, streams, rivers, and lakes. Discharge processes sustain flow from springs, maintain saturated conditions in wetlands, and provide base flow of streams and rivers. The groundwater contribution to all streamflow in the United States may be as large as 40 percent (Alley et al., 1999). Groundwater discharge also occurs directly to the atmosphere through evapotranspiration. Pumping of groundwater from wells is also a discharge process.

In Kane County, as in roughly the eastern half of the contiguous United States that is humid, recharge to the saturated zone occurs in all areas between streams or in areas where surface water infiltrates the subsurface. Under predevelopment conditions, discharge from the saturated zone occurs only in streams, lakes, and wetlands together with floodplains and other areas where the saturated zone intersects the land surface or the root zone of plants.

Recharge and discharge also can be considered in terms of movement of water between aquifers. Where downward vertical hydraulic gradients exist (i.e., where heads decrease with depth within the saturated zone), groundwater moves downward from the water table or from a surficial unconfined aquifer to recharge underlying confined aquifers. Where an upward vertical hydraulic gradient exists between a confined aquifer and the land surface, groundwater moves upward from the confined aquifer towards the land surface.

In general, the discharge areas of aquifers become separated by progressively greater distances as aquifer depths increase. The shallowest groundwater, which directly

underlies the water table, is part of a local flow system and discharges to very small ditches and depressions. Recharge to the water table occurs only in the relatively small areas between these local discharge features. Groundwater in more deeply buried confined aquifers is part of a regional flow system and discharges to comparatively large-scale rivers, such as the Fox River, and lakes occupying major valleys and depressions. The recharge areas for these aquifers include the broad areas between the regional discharge features.

Much of Kane County has clay-rich diamicton of low permeability at or near the land surface that inhibits the infiltration of precipitation into underlying aquifers. Prior to European settlement, the county contained vast areas where the water table was at or near the land surface much of the year. To develop the county for agricultural use, extensive networks of tile drains and drainage ditches were constructed. Because the permeability of sand is much greater than that of diamicton, recharge to aquifers will be concentrated in areas with sand at or near the land surface. In some areas, diamictons can be saturated, while underlying sands are only partially saturated or dry.

Groundwater recharge occurs mainly during the spring, when rainfall is high and water losses to evaporation and transpiration are low. Recharge decreases during the summer and early fall when evaporation and transpiration divert most precipitation and infiltrating water back into the atmosphere. Likewise, during winter months surface infiltration is often negligible when soil moisture is frozen, which diverts precipitation into surface-water bodies as runoff. Recharge can occur, however, during mild winters when soil moisture is not frozen (Larson et al., 1997).

Several factors affect the rate of groundwater recharge. Among these are the hydraulic characteristics of the materials both above and below the water table; topography; land cover; vegetation; soil moisture content; depth to the water table; intensity, duration, areal extent, and seasonal distribution of precipitation; type of precipitation (rain or snow); and air temperature (Walton, 1965). Hensel (1992) presented a detailed discussion of groundwater recharge processes in Illinois.

Water managers commonly express concern that groundwater recharge rates and the availability of groundwater are reduced by urban land cover. This belief is understandable since impermeable pavements and rooftops are highly observable features of the urban landscape. However, research from urban areas throughout the world (Brassington and Rushton, 1987; Foster, 1990; Foster et al., 1999; Lerner, 1986; Lerner, 2002; Price and Reed, 1989; Rushton et al., 1988) suggests that leakage from buried pipe networks—principally water distribution systems and storm drains—generates large amounts of recharge in urban areas, more than offsetting the effects of reduced infiltration. So, while decreasing the area of impermeable surfaces and capturing runoff has benefits in terms of reducing storm runoff and improving water quality, the benefits to enhancing recharge are less certain.

Under predevelopment conditions, long-term rates of recharge and discharge are approximately equal, and changes in the quantity of groundwater stored in the saturated zone are negligible. Recharge is provided by infiltration of precipitation and—particularly in arid areas—by loss of water from streams, lakes, and wetlands. Discharge occurs to surface waters through springs and seeps directly to the atmosphere by evapotranspiration, processes that are referred to as “natural” discharge to distinguish

them from well withdrawals, also a discharge process. This equilibrium condition is described by the following equation:

$$\text{Recharge} = \text{"Natural" Discharge}$$

Expressed another way, inflows to the saturated zone (recharge) are equal to outflows from it (discharge by evapotranspiration and through springs and seeps).

1.7.5. *Effects of Pumping*

Groundwater withdrawal from a well causes lowering of heads in the area around the well. This decline in head is called drawdown. In three dimensions, the head distribution surrounding a single pumping well resembles a cone with its apex pointed downward. The lowest head (and greatest drawdown) occurs at the pumping well, and drawdown decreases with distance from the well. The area of lowered heads surrounding pumping wells or a well field is therefore called a cone of depression. In the simplest case—a single well pumping at a uniform pumping rate—the cone of depression typically deepens and widens until gradients are sufficient to divert groundwater into the cone at a rate equivalent to the withdrawal rate, a condition called *equilibrium* or *steady-state*. The size and shape of the cone of depression vary with the hydraulic properties of the subsurface environment, the location of the well in relation to source aquifer boundaries and surface waters in hydraulic connection with the source aquifer, pumping rate and schedule, and other factors. In the common case of numerous, closely spaced wells, which are brought into and out of service over time and are pumped at changing rates, actual equilibrium conditions are rare. Even in some very simple cases—that of a high-capacity well removing water from an aquifer receiving little or no recharge, for example—equilibrium cannot be established, and heads decline until withdrawals from the well cease.

Drawdown is a natural consequence of well withdrawals and cannot be avoided, but excessive drawdown can create problems. The drawdown generated by one well causes water levels to decline in nearby wells. This *interference drawdown* can result in increased pumping expenses and, in more extreme cases, can cause a well to fail to deliver its expected supply. The amount of drawdown that is tolerable, however, depends on local hydrogeologic conditions and individual well construction characteristics such as total depth and pump-setting depth. As discussed in the following paragraphs, drawdown leads to a decrease in natural groundwater discharge. Lastly, changes in groundwater flow resulting from drawdown can sometimes result in deterioration of groundwater quality.

Groundwater withdrawals from a well are initially supplied by a reduction in storage as heads decline in the source aquifer and a cone of depression forms around the well. This reconfiguration of the predevelopment potentiometric surface induces flow of groundwater to the well. In most settings, the removal of groundwater from storage is a transient process, and an increasing proportion of the water withdrawn from the well is supplied by increased groundwater recharge and/or reduction of “natural” groundwater discharge via the predevelopment pathways of springs, seeps, and evapotranspiration. All three components must be considered in any accounting of the water supplied to the well; however,

$$\text{Withdrawal} = \text{Recharge Increase above Predevelopment Rate} + \\ \text{Removal from Storage} + \text{"Natural" Discharge Decrease below Predevelopment Rate}$$

The time required for transient removal of water from storage by a new pumping well to cease and for new equilibrium conditions to become established may range from days to decades. During this time, the cone of depression around the well continues to deepen and widen. In some cases, a new equilibrium cannot be established because predevelopment recharge and discharge rates cannot be altered enough to balance withdrawals.

If a new equilibrium can be established, inflows and outflows will again balance:

$$\text{Withdrawal} = \text{Recharge Increase above Predevelopment Rate} + \\ \text{"Natural" Discharge Decrease below Predevelopment Rate}$$

Thus, long-term pumping of any well or group of wells requires that recharge and/or “natural” discharge rates change and that water be removed from storage. How much water is available long-term—that is, the sustainable pumping rate—depends on how these changes affect the surrounding environment and what the public considers to be acceptable environmental impacts (Alley et al., 1999; Bredehoeft, 2002; Bredehoeft et al., 1982; Devlin and Sophocleus, 2005).

In most settings, withdrawals are accommodated by removal of water from storage and decreased “natural” discharge (Alley et al., 1999). Removal of water from storage causes reduced heads, which may result in increased pumping expenses and in water-supply interruptions where heads decline to the levels of pump intakes. In addition, this head reduction may, in some settings, induce movement of saline water into source aquifers, rendering groundwater pumped from wells unusable or requiring expensive treatment. Decreased “natural” discharge is reflected in reduced streamflow, reduced water levels in lakes and wetlands, reduction of saturated conditions in wetlands, and changes in the vegetation. Such alterations may interfere with instream-flow requirements for fish habitat or other instream environmental needs, ecology of groundwater-dependent habitats such as fens, and availability of surface water for water supply.

This range of pumping effects and their spatial variability illustrate the importance of human judgment in developing sound groundwater management schemes, and they underscore the importance of groundwater flow models as tools for synthesizing a wide range of data, organizing thinking, and mapping and quantifying the diversity of impacts. The simple prescription that groundwater withdrawals are sustainable if they are maintained at or below the recharge rate—the *Water-Budget Myth* (Bredehoeft, 2002; Bredehoeft et al., 1982)—could have unexpected and disastrous impacts if used for long-term groundwater planning and management. In the typical case wherein withdrawals are accommodated by removal of water from storage and decreased “natural” discharge, withdrawals at the rate of predevelopment recharge would likely result in significant drawdown and profound effects on surface waters.

1.8. Overview of Water Resources Available to Kane County

1.8.1. Lake Michigan

Although Kane County has never received water from Lake Michigan, the lake supplies most of the water used in northeastern Illinois (Northeastern Illinois Planning Commission, 2002), and it cannot be dismissed as a water resource available to the county. In 2003, Illinois used 1031 million gallons per day (Mgd) of Lake Michigan water for water-supply purposes in Cook, DuPage, Lake, and Will Counties (Injerd, 2006). To put this figure in context, Kane County used a total of about 61 Mgd in 2003 for water-supply purposes (not including self-supplied farms and domiciles).

The region's use of Lake Michigan for water-supply purposes is limited by legal constraints stemming from the Chicago Sanitary District's reversal of the Chicago and Calumet Rivers in the early 20th Century. This diversion of Lake Michigan water to the Mississippi River watershed provided navigational flow to the Chicago Sanitary and Ship Canal and protected the quality of the City of Chicago's water supply by preventing entry of a significant volume of contaminated surface runoff via the Chicago and Calumet Rivers into Lake Michigan. The diversion also generated considerable litigation before the U.S. Supreme Court when it was challenged by other Great Lakes states (Barker, 1986; Injerd, 1993). As a result of two of these lawsuits, *Wisconsin v. Illinois*, 388 U.S. 426 (1967) and 449 U.S. 48 (1980), the U.S. Supreme Court decreed that the State of Illinois can divert no more than 3200 cubic feet of water per second (cfs) from Lake Michigan, as averaged over a 40-year accounting period (the first 40-year period being measured from the 1980 decree to the year 2020).

Illinois' compliance with these mandatory diversion limits is managed under the state's Level of Lake Michigan Act, 615 ILCS 50/1 *et seq.* (1995). This statute requires all users of Lake Michigan water to possess a valid allocation permit from the Office of Water Resources (OWR) in the Illinois Department of Natural Resources. Because Illinois exceeded its diversion limit during 11 of the 15 years from 1981 to 1995, a Memorandum of Agreement (MOA) was adopted in 1996 between Illinois and the other Great Lakes states under threat of renewed litigation before the Court. Under the MOA, Illinois agreed that it will not only continue to meet its mandated 3200 cfs limit, but also will further reduce its Lake Michigan diversion during the remaining 20-year averaging period of the decree to make up for this overuse.

Lake Michigan water appears to be potentially available to Kane County water systems that can find a willing seller and afford the capital expense of a pipeline and other costs related to use of this water. As of 2006—as a consequence of numerous factors that include lowered lake levels, reduced leakage through lakefront control structures, and reduced water use by the City of Chicago—OWR appears to have accomplished its goal of making up for overuse of Lake Michigan water in the 1980s and 1990s and is optimistic that it can accommodate increasing demand through 2030 by existing permittees (Injerd, 2006). In fact, OWR has issued five new Lake Michigan water allocation permits since 1999.

1.8.2. Inland Surface Waters

Some public water systems and industries in northeastern Illinois obtain water from inland surface waters of the region, including the Calumet Sag Channel, Des Plaines

River, Fox River, Illinois River, and Kankakee River. This total includes very large withdrawals of cooling water for purposes of thermoelectric power generation, of which—in the case of the once-through cooling systems predominating in Illinois power plants—about 3 percent is lost to evaporation, blowdown, drift, and leakage (Dunne and Leopold, 1978; Solley et al., 1998). The remainder is returned to the source stream.

About 23 Mgd was withdrawn from inland surface waters of Kane County in 2003. About 97 percent of this total was withdrawn from the Fox River by the Aurora and Elgin public water systems. Formerly reliant entirely on groundwater, Elgin and Aurora began withdrawing water from the Fox River in 1983 and 1992, respectively. No water is presently withdrawn from inland surface waters of Kane County for purposes of thermoelectric power generation.

1.8.3. *Groundwater*

As will be discussed in greater detail in Section 2.1.1.2, groundwater in Kane County is obtained from aquifers that may be broadly divided into the *shallow aquifers* and *deep aquifers* (Figure 5). The shallow aquifers include unconsolidated Quaternary sand and gravel aquifers and the underlying Shallow Bedrock Aquifer. In a regional context, the sand and gravel aquifers are contained in the materials assigned to the Quaternary Unit (page 54 and Figure 19). Several individual sand and gravel aquifers are recognized in the immediate Kane County area, however, including the Henry Formation and its tongues, and sand and gravel deposits of the Glasford Formation (Figure 22). These sand and gravel aquifers are sporadically distributed across the Kane County area, and—though sometimes separated from one another by relatively impermeable layers of diamicton—they are frequently in hydraulic connection with one another and with the Shallow Bedrock Aquifer. The tops of these aquifers are typically within 300 ft of land surface. The Shallow Bedrock Aquifer consists of 25-125 ft of Paleozoic bedrock underlying the Quaternary materials (pages 44, 53, and 55). The geometry of the Shallow Bedrock Aquifer is defined by the bedrock surface and is a product of weathering and dissolution of the rocks immediately underlying this surface. In Kane County, the Shallow Bedrock Aquifer includes rocks assigned to the regional Silurian-Devonian Carbonate Unit, Maquoketa Unit, and Galena-Platteville Unit—whatever unit is present in the interval of secondary permeability within 25-125 ft of the bedrock surface. Where it consists primarily of rocks of the regional Maquoketa Unit, the Shallow Bedrock Aquifer is less permeable—and less productive—than where it consists of rocks of the regional Silurian-Devonian Carbonate Unit and Galena-Platteville Unit, which, as comparatively pure carbonates, are more susceptible to dissolution than are the shalier rocks of the Maquoketa Unit. The depth to the top of the Shallow Bedrock Aquifer may exceed 300 ft along the axis of Marengo Ridge in northwestern Kane County. The top of the aquifer is at land surface at bedrock outcrops along the Fox River and some of its tributaries (Dey et al., 2004a).

Because the shallow aquifers are frequently in hydraulic connection with one another, and because the shallowest aquifer materials are in hydraulic connection with surface waters, there is an exchange of water between surface waters and the shallow aquifers. This exchange permits wells open to the shallow aquifers to capture surface water, either by inducing flow directly from stream channels or by diverting groundwater

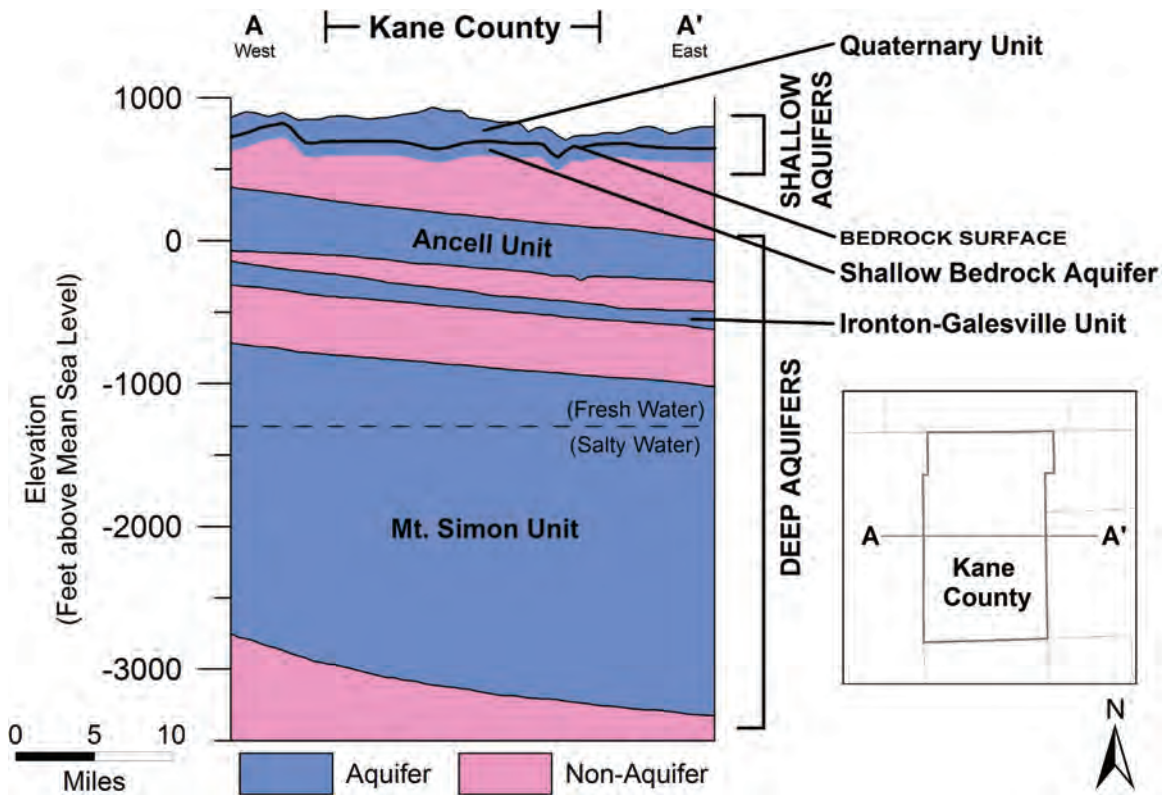


Figure 5. Major aquifers in the Kane County area.

into wells that would otherwise discharge to streams, a process that increases well yields but which may lead to unacceptable reduction of streamflow.

In Kane County, the deep aquifers include, in descending order, the Ancell Unit (consisting of the adjacent Glenwood Formation and St. Peter Sandstone), the Iron-ton-Galesville Unit (consisting of the adjacent Iron-ton and Galesville Sandstones), and the Mt. Simon Unit (consisting of the adjacent Elmhurst Sandstone Member of the Eau Claire Formation and the Mt. Simon Sandstone). It is noteworthy that these aquifers, though “deep”—at least 450 ft in Kane County—are not deep throughout the region or even, for that matter, in northeastern Illinois. For example, the Ancell Unit directly underlies the Quaternary Unit in west-central Kendall County, and may be less than 50 ft deep in that area. It is also noteworthy that the deep aquifers of Kane County are not necessarily aquifers everywhere in the Upper Midwest, and, conversely, the aquitards that separate the deep aquifers of Kane County may, through lateral textural change, become aquifers elsewhere in the region. For example, the Ancell Unit, primarily sandstone in northeastern Illinois, grades southward and eastward to carbonate rocks in Indiana and central Illinois that are not aquifers, and the Eau Claire Unit (the silty aquitard separating the Iron-ton-Galesville and Mt. Simon Units in northeastern Illinois) becomes progressively sandier northward so that in Wisconsin it is a viable aquifer throughout its entire thickness.

Wells targeting the deep aquifers in Kane County are commonly cased through the upper part of the overlying aquitard (referred to in this report as the Maquoketa Unit)

and left open to all underlying units except for the lower part of the St. Peter Sandstone in the Ancell Unit, which is poorly cemented and will otherwise slough into the borehole. This construction practice saves money and permits wells to take advantage of small amounts of water available from the aquitards, as well as aquifers, in the interval underlying the Maquoketa Unit. In some cases, wells drilled to the deep aquifers are also left open to the Shallow Bedrock Aquifer as well, although this practice is discouraged because it permits continuous discharge of groundwater from the shallow aquifers to the deep aquifers when the well is not operating.

Most wells targeting the deep aquifers are not drilled deeper than the base of the Ironton-Galesville Unit. The additional groundwater available from the Mt. Simon Unit has not, historically, been worth the cost of extending wells to this unit. In addition, there are water quality issues associated with groundwater in the Mt. Simon Unit. Suter et al. (1959) and Illinois State Water Survey and Hittman and Associates (1973) reported that total dissolved solids and chloride concentrations greatly increase with depth of penetration into the Mt. Simon Unit. Schicht et al. (1976) presented data from a well near West Chicago (DuPage County) that shows chloride concentrations increasing from 88 milligrams per liter (mg/L) at 450 ft of penetration into the Mt. Simon Unit to 50,500 mg/L at 2190 ft of penetration. Suter et al. (1959) reported that water in the Mt. Simon Unit is too salty for most uses at elevations less than 1275 ft below sea level. As the aquifer elevation increases to the north and west, an increasing thickness of freshwater is observed just below the Eau Claire Unit, permitting some use of the Mt. Simon Unit for water supply in the northernmost extreme of Illinois and in southeastern Wisconsin (Feinstein et al., 2005a). However, even where the top of the Mt. Simon Unit is above 1275 ft below sea level, Schicht et al. (1976) noted that water quality deteriorates with pumping from the unit and attributed this to the upconing of high-chloride waters from the lower parts of the Unit. Sasman et al. (1982) reported that water withdrawn from wells open to this aquifer rapidly becomes saline, prompting users to seal off wells at the bottom of the Ironton-Galesville formation. Barnes (1985) used a two-dimensional, density-dependent model of flow and transport in a vertical cross section to show that salinity in the Elmhurst–Mt. Simon Aquifer could move upward under the influence of pumping, and speculated that vertical jointing might facilitate upward movement of salinity.

1.9. Groundwater Development in Kane County Area

Groundwater development patterns in Kane County and northeastern Illinois for 1964 to 2003 may be ascertained through consultation of the withdrawal database assembled for this project (see Appendix B). For purposes of summarizing groundwater development patterns, wells are broadly subdivided into those open only to the shallow units and those open to the deep units (see Section 2.1.1.2). Note that wells belonging to the second category may be open to the shallow units, as well, because many wells drilled into the Ancell Unit and underlying units also are left open to the Galena-Platteville Unit, and a few are open to units overlying the Galena-Platteville. Withdrawals are compiled for the area of northeastern Illinois shown in Figure 6 and for Kane County. The deep units include the historically productive sandstone aquifers of the Ancell and Ironton-Galesville Units that are frequently lumped as the “Cambrian-Ordovician” or “deep sandstone” aquifers. The interval has been the subject of concern owing to high

rates of withdrawal in the Chicago-Milwaukee area in relation to low rates of vertical leakage into the aquifers, with consequent significant head reduction in the region [see, for example, Burch (2002)].

Sources of the withdrawal data discussed in this section are hardcopy records on file at the ISWS (covering 1964-1979); an electronic database, maintained by the ISWS, of withdrawal data compiled largely from owner-reported withdrawal measurements and estimates (covering 1980-2003); and estimates for years of non-reporting to the ISWS by facility owners (also covering 1980-2003). The completeness of this dataset is not known, but withdrawals during this period are based on sources that sought, and continue to seek, to document withdrawals from all community and non-community public water system wells, wells supplying commercial and industrial facilities having a pump capacity greater than 50 gallons per minute, and irrigation wells having a pump capacity greater than 50 gallons per minute. As such, the data are believed to be a reasonably complete representation of groundwater withdrawals in the region. Estimates are included for wells during years when it is probable that the wells were in use, but withdrawal data were not collected. The accuracy of the data is not known, but it is likely that the reported measurements are accurate to within ± 10 percent of the actual value (United States Department of the Interior Bureau of Reclamation, 1997). The sources, processing, and uncertainty of the withdrawal data are discussed in detail in Appendix B.

Groundwater withdrawals in northeastern Illinois have declined since the 1980s, largely as a consequence of public water systems in Cook, DuPage, and Lake Counties shifting from groundwater to a Lake Michigan water source, but also because of improvements in efficiency, leakage reduction, and deindustrialization (Figure 7). The largest annual declines in total groundwater withdrawals occurred in the early 1990s, when many public water systems in DuPage County shifted to a Lake Michigan source. Declines in withdrawals from wells open to the deep units have been greater than those from wells open only to the shallow units, principally because many of the public water systems that switched to a Lake Michigan water source relied heavily on wells open to the deep units. Comparison of the pumping distribution in 1985 and 2003 shows the effects of the shift to a Lake Michigan water source by many suburban public water systems during the intervening years (Figure 8, Figure 9, Figure 10, and Figure 11). The overall spatial effect of this shift has been to push the band of groundwater withdrawals farther west and south as pipelines deliver Lake Michigan water to inland areas at progressively greater distances from the lake. Principal areas of withdrawals from the deep units remaining in 2003 are (1) Joliet and the industrial corridor along the Chicago Sanitary and Ship Canal in Will County, (2) the Fox River Valley area of southeastern Kane County, and (3) southeastern McHenry County (Figure 9). Large withdrawals from the shallow units are commonplace along a corridor extending practically from the Indiana boundary in Will County northwestward through the Fox River Valley of Kane County and extreme northwestern Cook County (Figure 11).

Kane County has always relied entirely on water from locally available sources, either groundwater sources or the Fox River, and has never received Lake Michigan water. Groundwater withdrawals generally declined from the late 1970s to the early 1990s (Figure 12), but this decline resulted largely from a shift in water source by the large Elgin and Aurora public water systems from groundwater—derived from wells

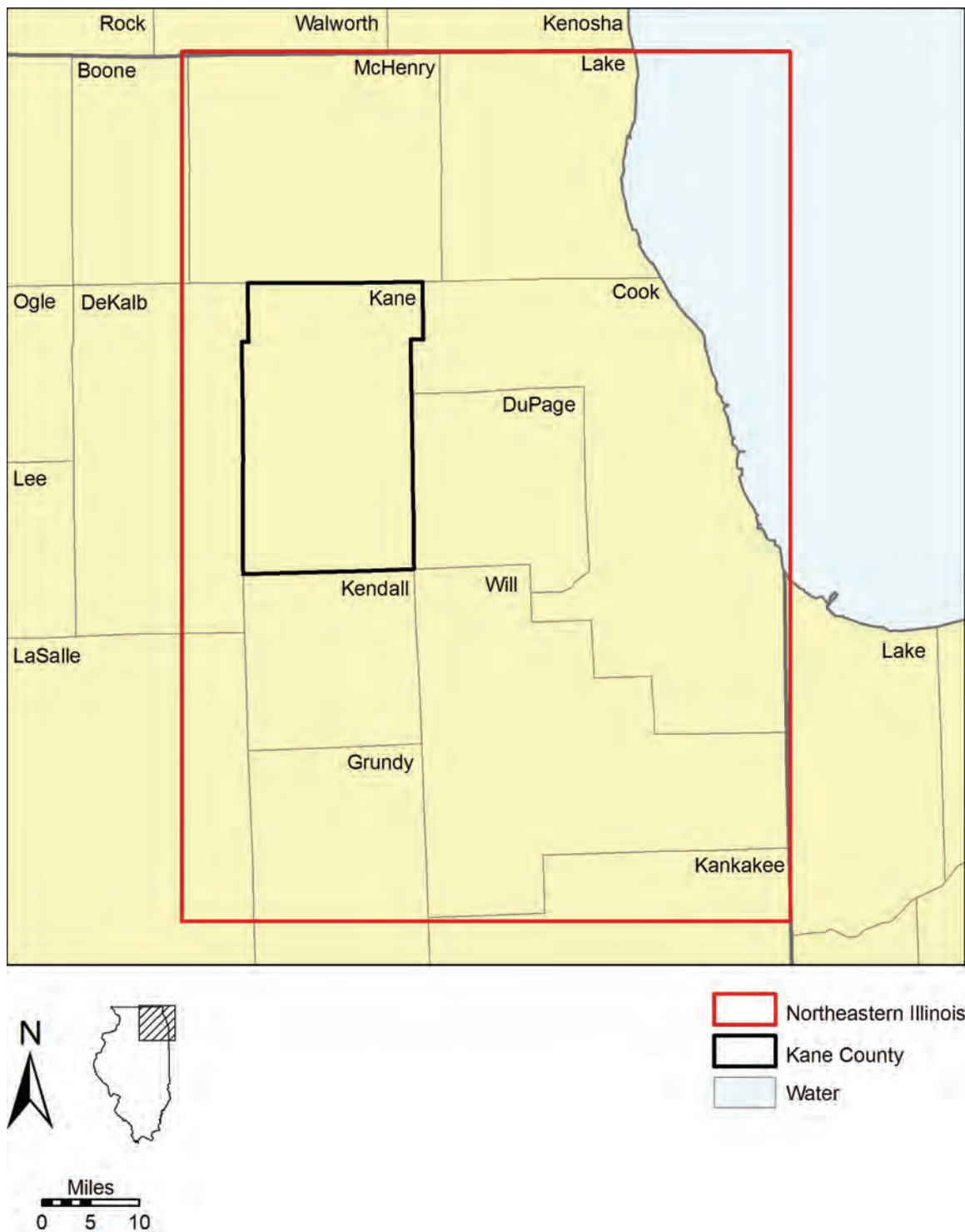


Figure 6. Areas of groundwater withdrawal accounting.

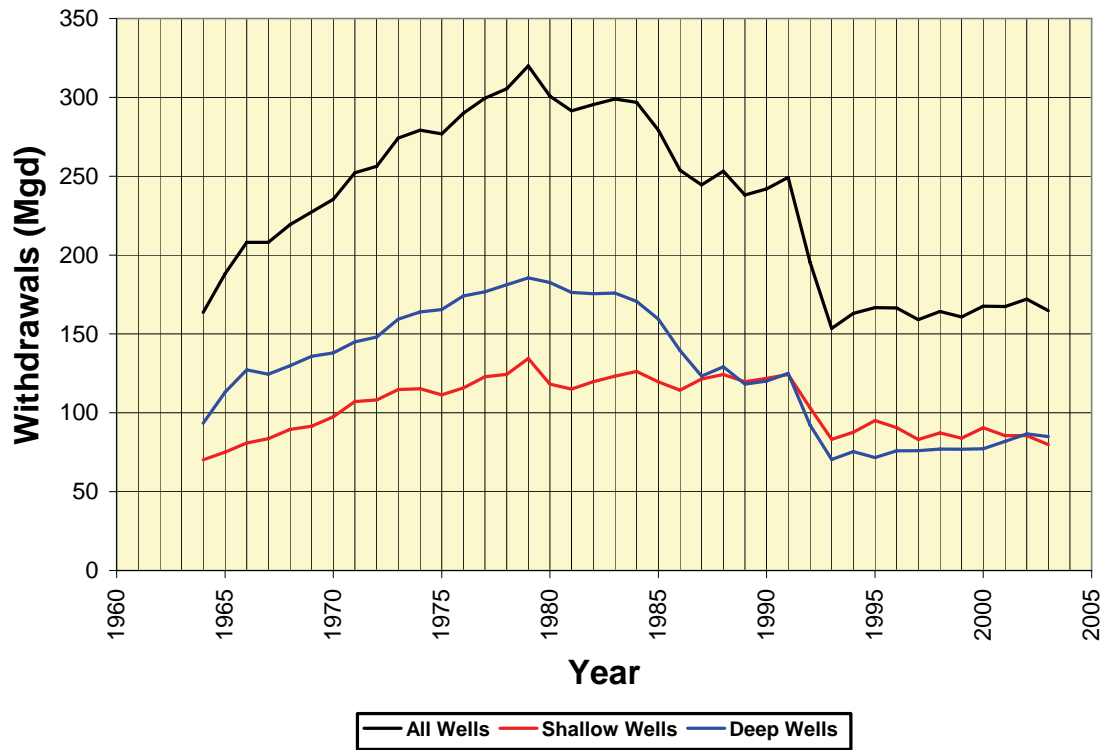


Figure 7. Groundwater withdrawals in northeastern Illinois, 1964-2003.

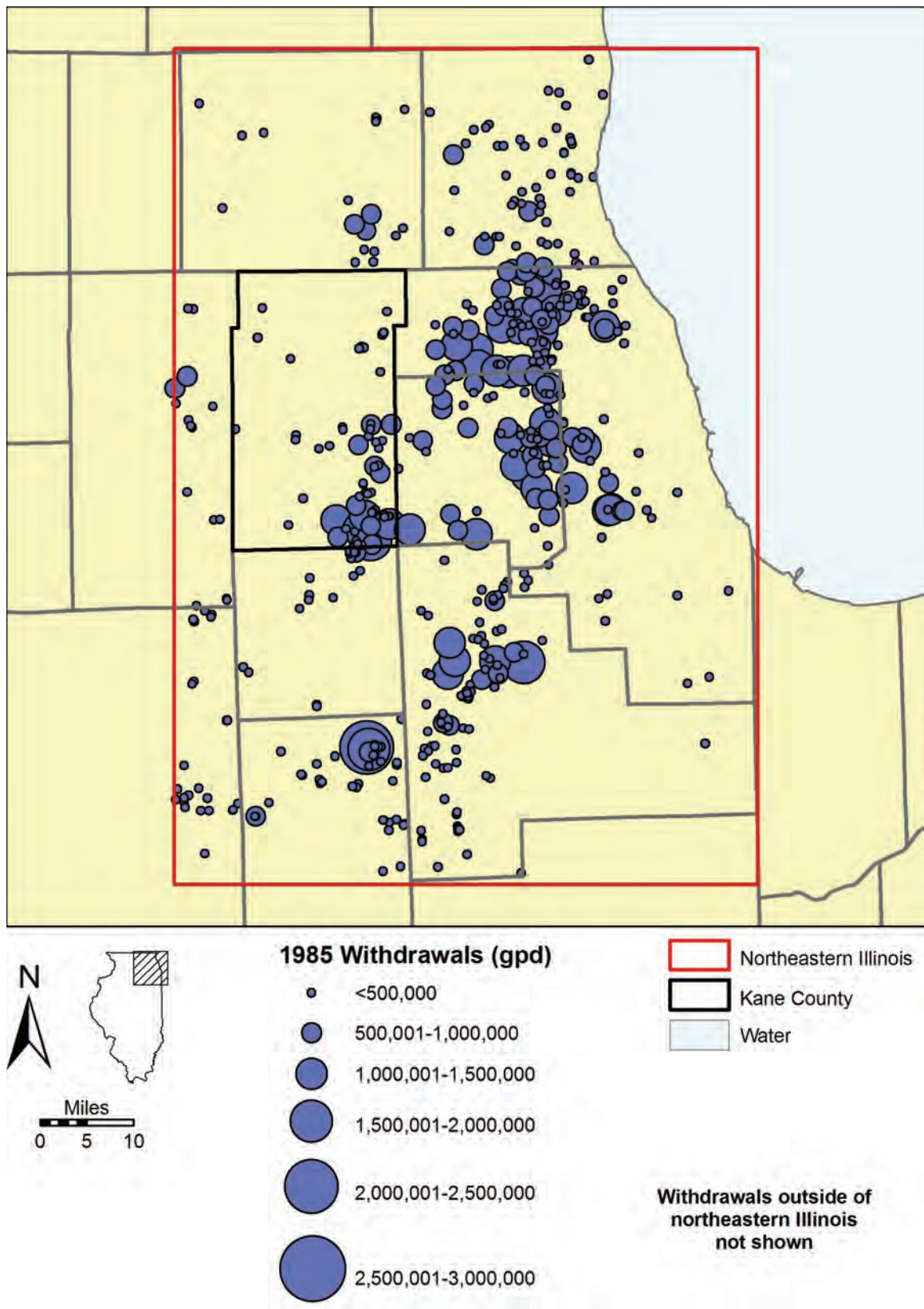


Figure 8. Withdrawals in 1985 from deep wells in northeastern Illinois.

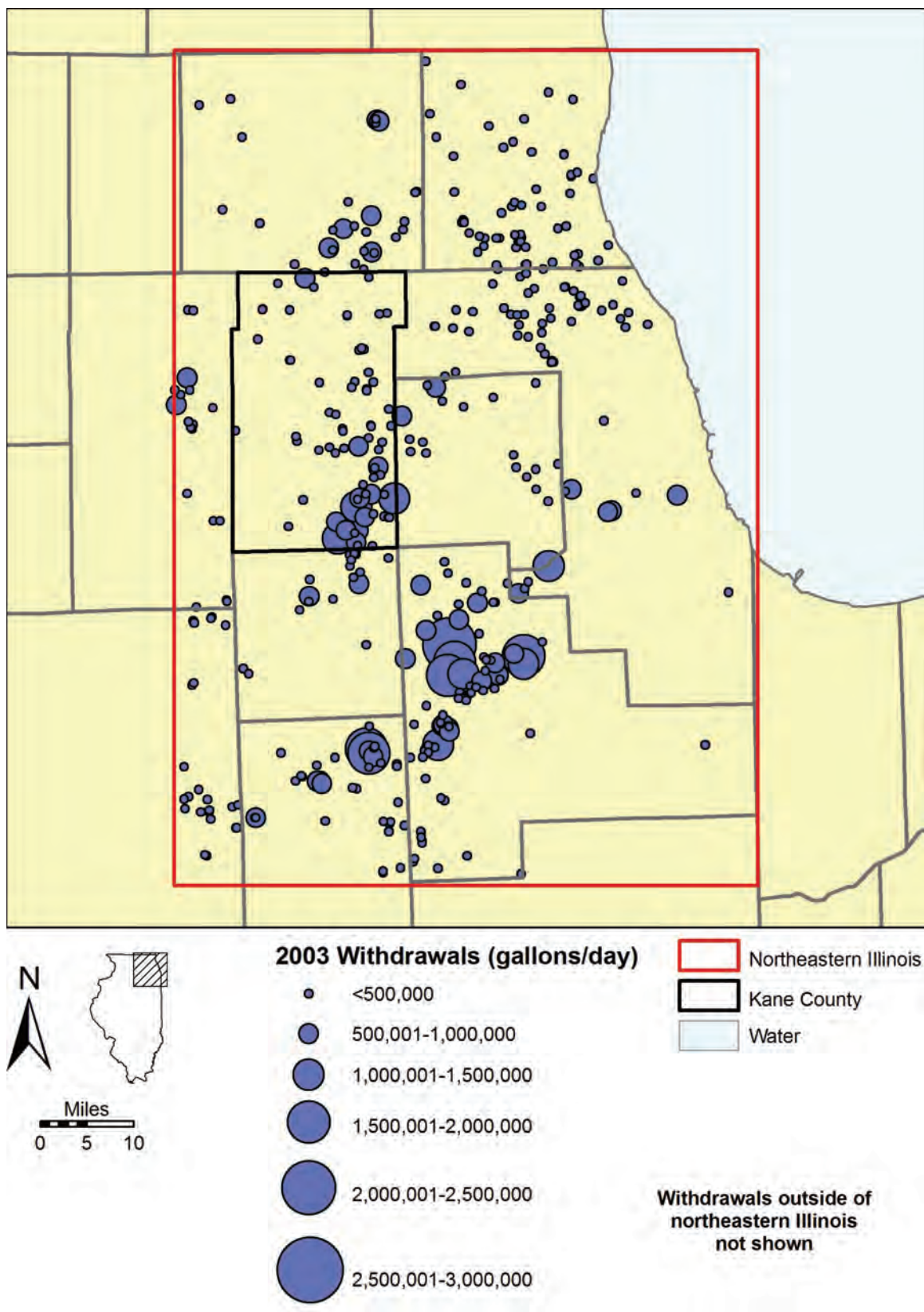


Figure 9. Withdrawals in 2003 from deep wells in northeastern Illinois.

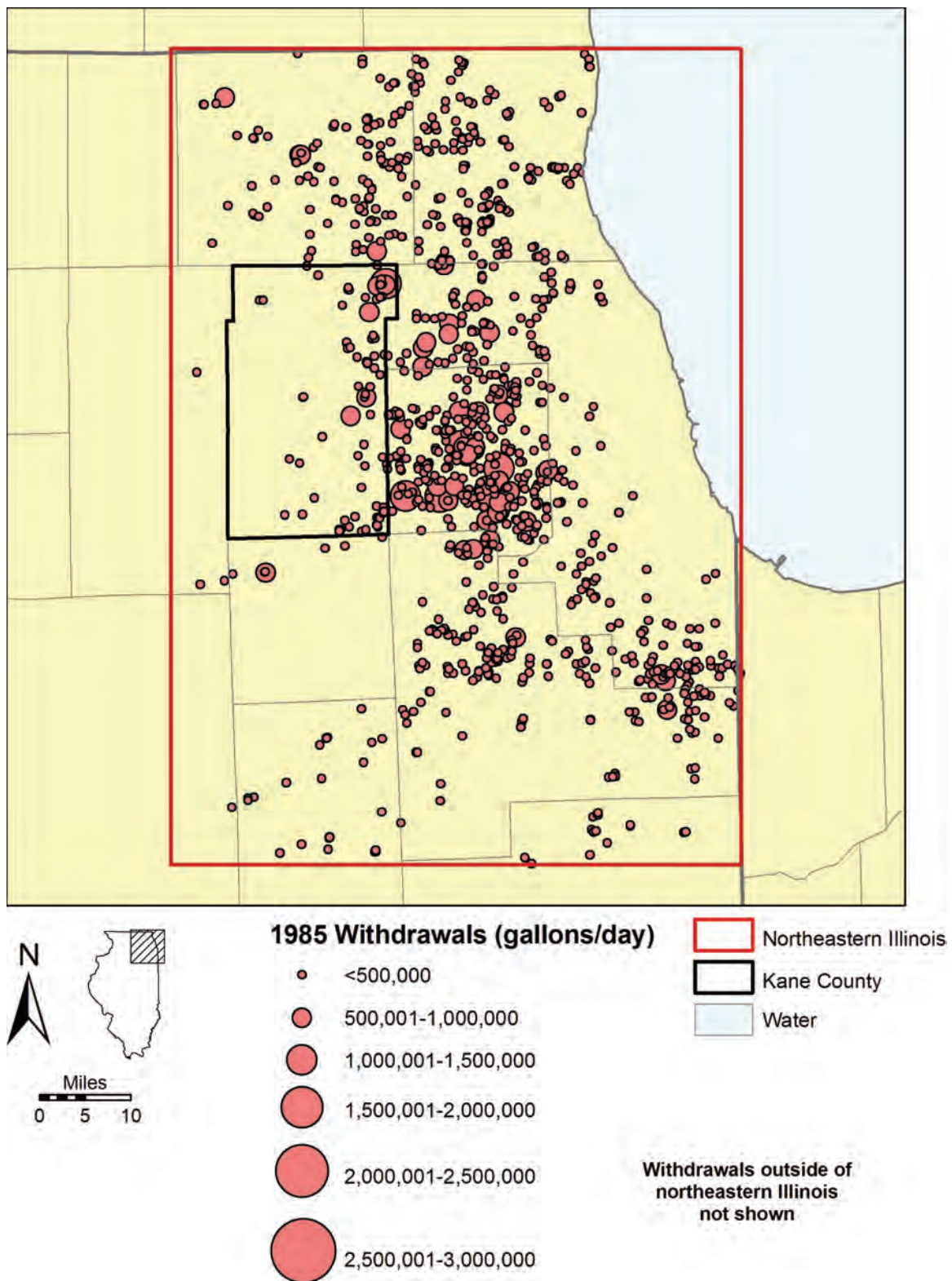


Figure 10. Withdrawals in 1985 from shallow wells in northeastern Illinois.

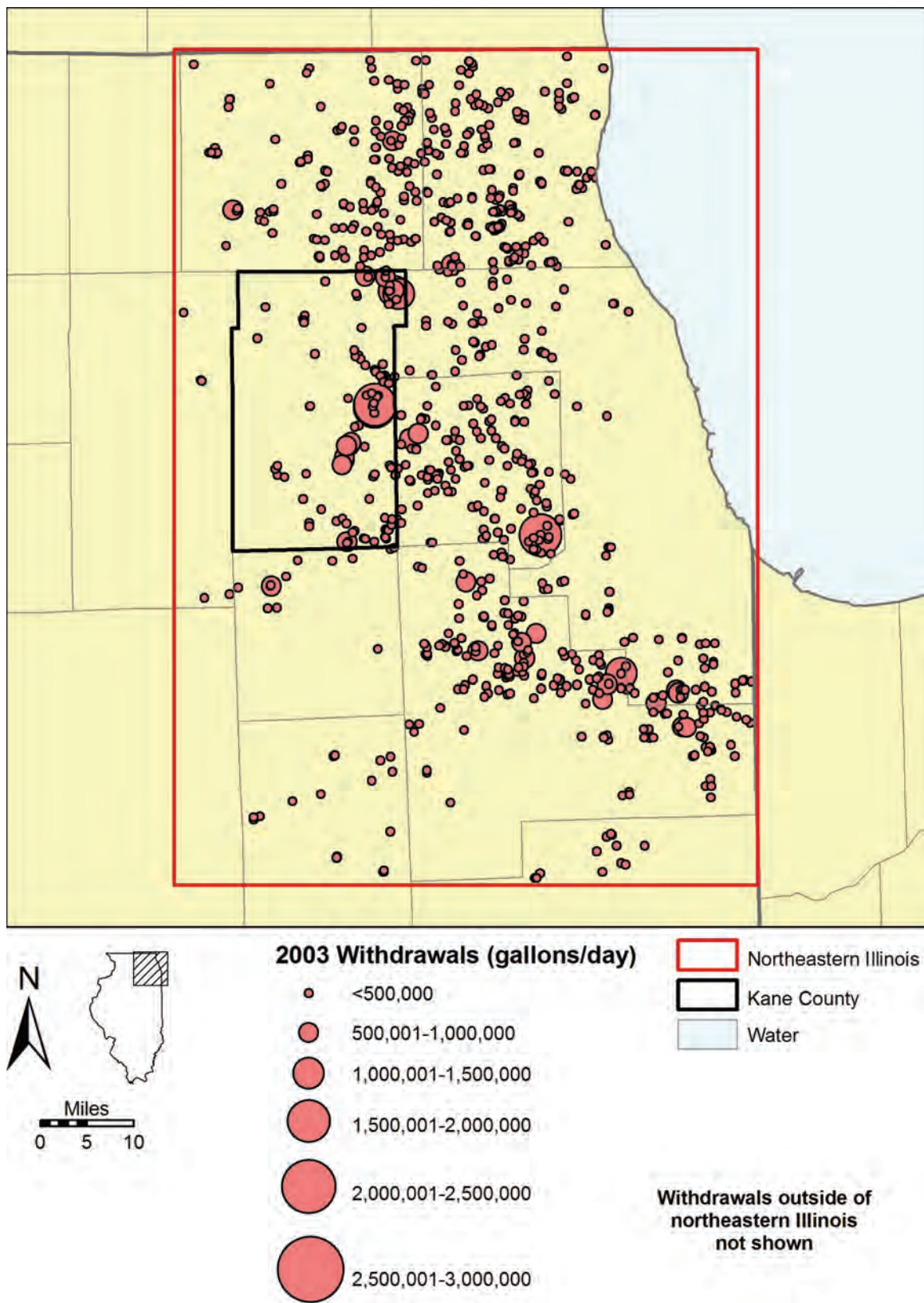


Figure 11. Withdrawals in 2003 from shallow wells in northeastern Illinois.

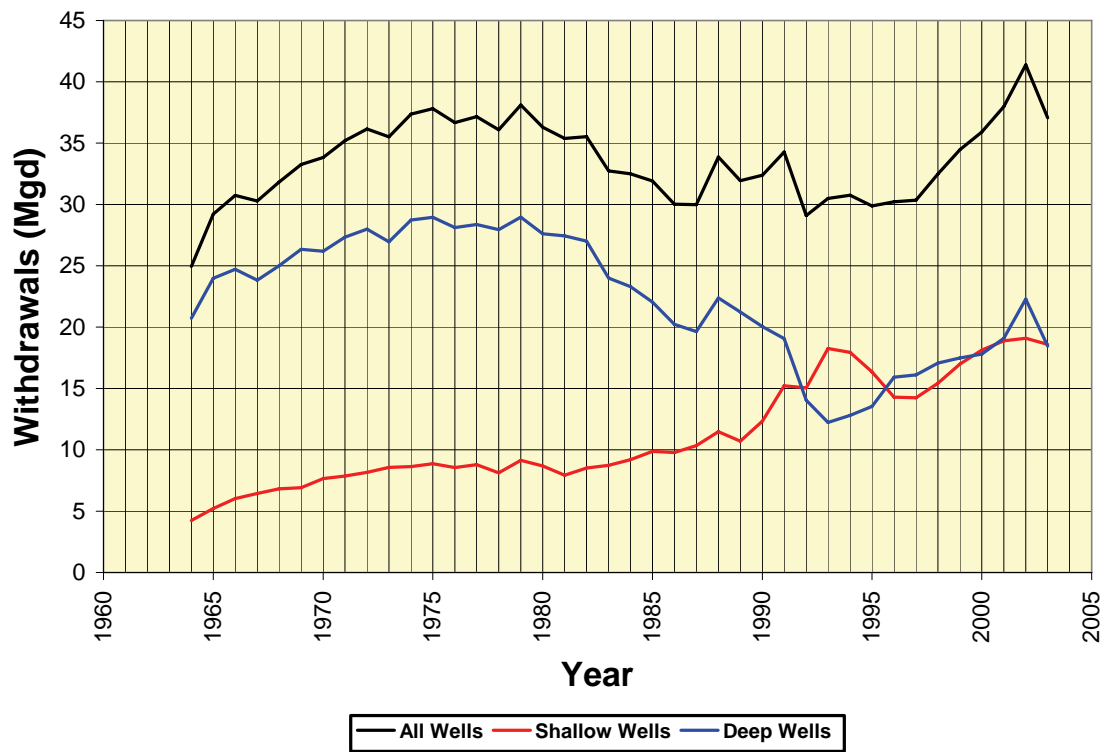


Figure 12. Groundwater withdrawals in Kane County, 1964-2003.

open to the deep units—to the Fox River. Elgin began using water from the Fox River in 1983, and Aurora began in 1992. Groundwater withdrawals have increased dramatically since the mid-1990s to accommodate increases in water demand associated with population growth. Locations of active commercial, industrial, and public water system wells in 2003 are shown in Figure 13 and Figure 14.

Thirty-nine Kane County wells open to the deep units pumped at average rates greater than 100,000 gallons per day (gpd) in 2003, meeting the definition of a high-capacity well based on Illinois' Water Use Act of 1988 (Table 2). The most productive wells are concentrated in the southeastern part of Kane County (Figure 13), where three wells—all supplying Aurora's public water system—pumped at rates greater than 1,000,000 gpd in 2003. Not surprisingly, these very productive wells are open to both the Ancell Unit and Iron-ton-Galesville Unit, the principal “deep bedrock” aquifer units underlying the Galena-Platteville Unit.

Thirty-three Kane County wells open only to the shallow units pumped at average rates greater than 100,000 gpd in 2003 (Table 3). The most productive of these wells supplied the public water systems of Algonquin, Carpentersville, and St. Charles, in the urban corridor of eastern Kane County (Figure 14). Four of these wells are owned by private commercial/industrial concerns and cannot be identified specifically owing to an agreement between them and the ISWS. The most productive of these wells are open to sand and gravel aquifers within the Quaternary Unit.

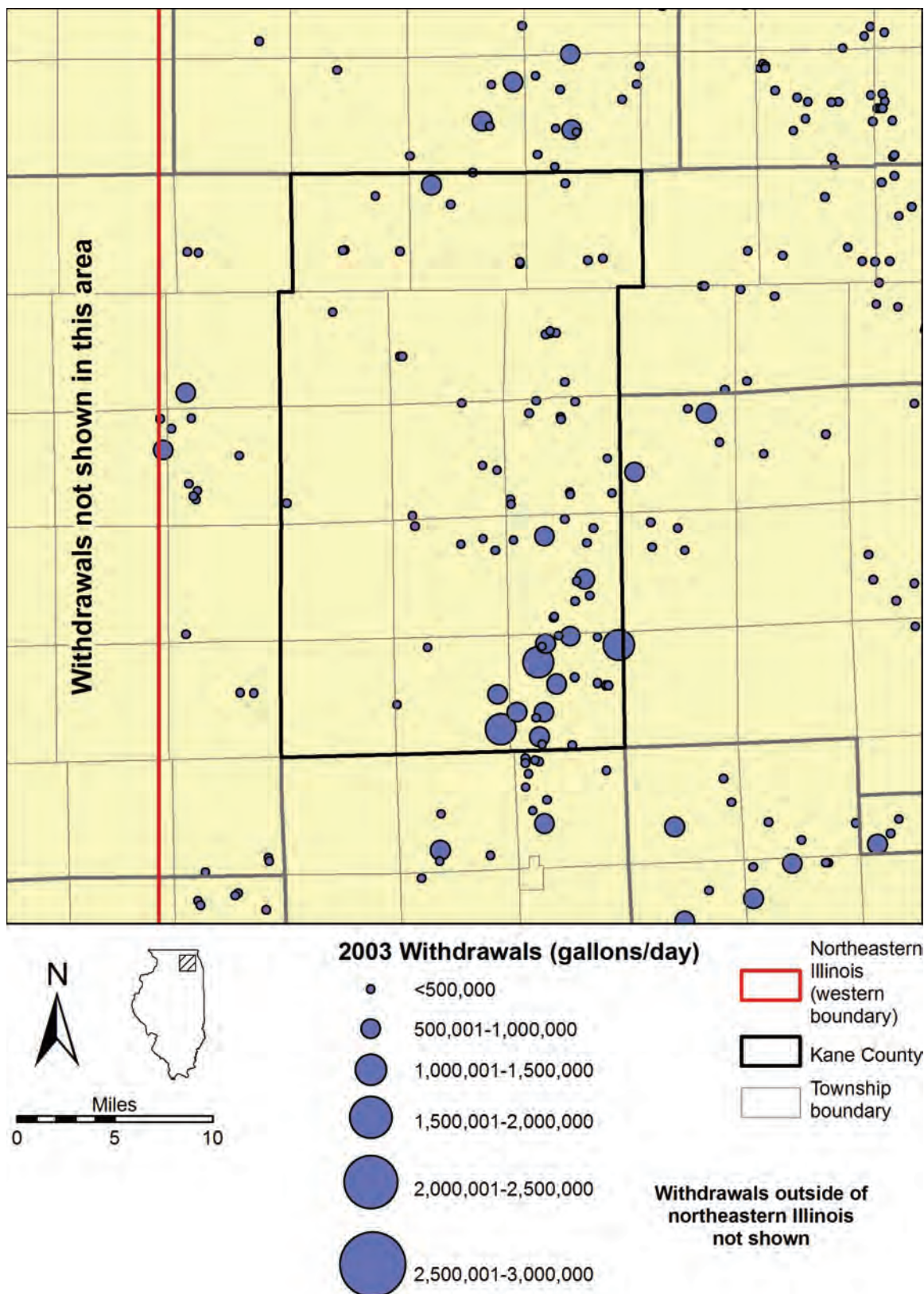


Figure 13. Withdrawals in 2003 from deep wells in the Kane County area.

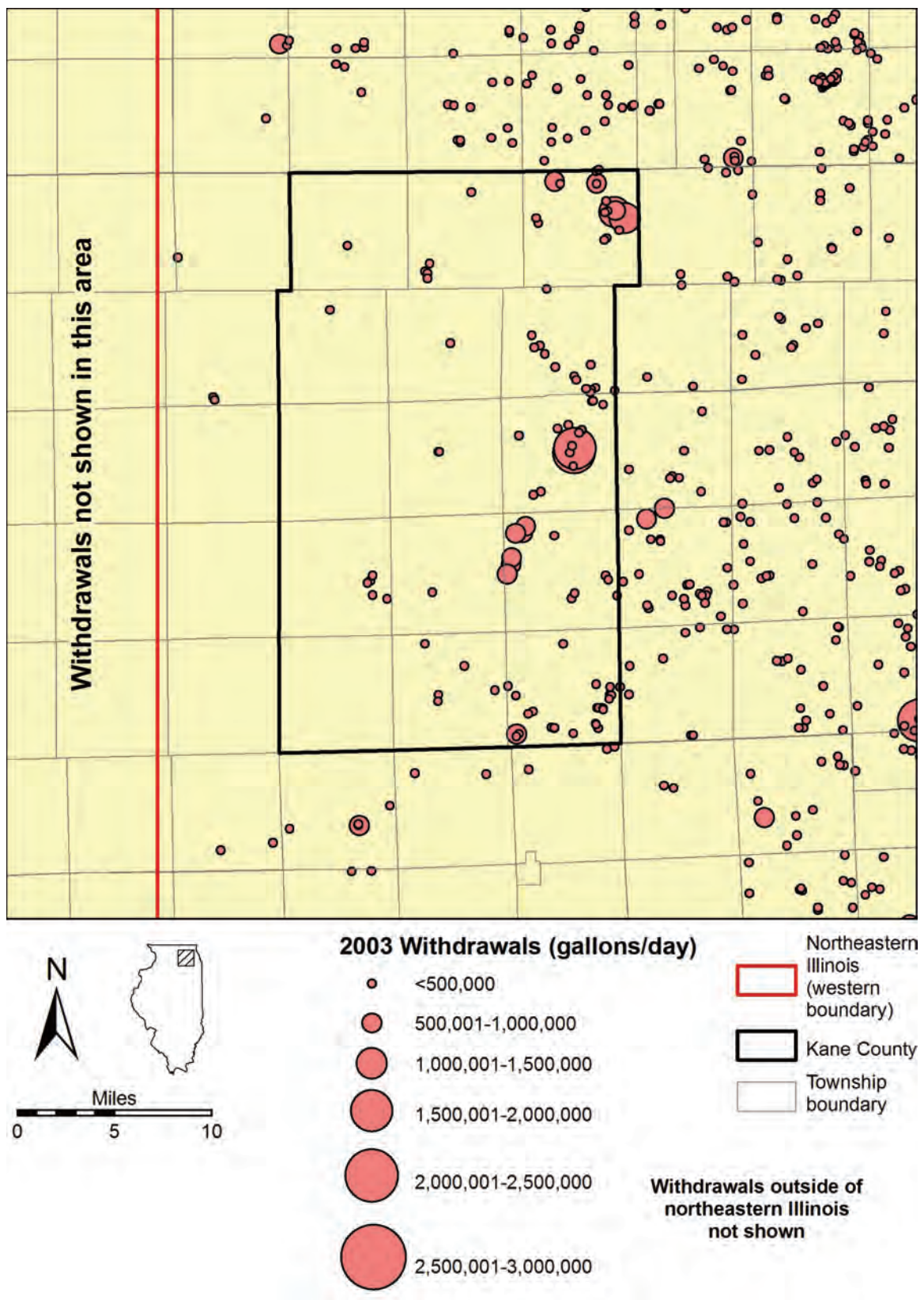


Figure 14. Withdrawals in 2003 from shallow wells in the Kane County area.

**Table 2. Deep Wells in Kane County That Pumped More
Than 100,000 Gallons per Day (gpd) in 2003**

<i>Name and Well Number</i>	<i>Source Interval Hydrostratigraphic Units (see Figure 19)</i>	<i>2003 Withdrawals (gallons per day)</i>
Aurora 20	Ancell through Eau Claire	1,357,651
Aurora 23	Ancell through Eau Claire	1,090,877
Aurora 25	Ancell through Eau Claire	1,047,838
Aurora 15	Ancell through Eau Claire	934,223
Aurora 17	Ancell through Mt. Simon	909,117
Aurora 21	Ancell through Eau Claire	773,415
Geneva 6	Ironton-Galesville through Eau Claire	765,202
North Aurora 5	Ancell through Eau Claire	596,065
Montgomery 4	Ancell through Ironton-Galesville	571,970
Batavia 4	Galena-Platteville through Ironton-Galesville	540,862
Huntley 9	Prairie du Chien-Eminence through Eau Claire	531,877
North Aurora 4	Ancell through Eau Claire	507,636
Aurora 19	Ancell through Ironton-Galesville	503,770
Batavia 2	Galena-Platteville through Mt. Simon	463,436
North Aurora 3	Ancell through Ironton-Galesville	443,517
Batavia 5	Ancell through Eau Claire	419,576
Aurora 24	Ancell	413,331
West Dundee 7	Ancell through Ironton-Galesville	356,605
West Dundee 1	Ancell through Eau Claire	356,605
Montgomery 8	Ancell through Eau Claire	307,529
South Elgin 8	Mt. Simon	305,411
St. Charles 4	Galena-Platteville through Eau Claire	296,816
South Elgin 7	Potosi-Franconia through Ironton-Galesville	286,703
Huntley 7	Prairie du Chien-Eminence through Eau Claire	285,175
Elgin 701	Galena-Platteville through Eau Claire	282,234
Hampshire 6	Maquoketa through Ironton-Galesville	278,122
St. Charles 3	Ancell through Ironton-Galesville	271,978
South Elgin 9	Mt. Simon	271,147
Montgomery 2	Galena-Platteville through Ancell	233,624
Algonquin 10	Prairie du Chien-Eminence through Eau Claire	208,808
Geneva 5	Galena-Platteville through Mt. Simon	199,756
Mill Cr Water Rec Dist 1	Ancell	193,725
Mill Cr Water Rec Dist 2	Ancell	193,725
Elburn 4	Ancell through Ironton-Galesville	192,602
St Charles 8	Galena-Platteville through Eau Claire	191,118
Gilberts 3	Ironton-Galesville through Eau Claire	158,423
Gilberts 4	Ironton-Galesville through Eau Claire	151,504
Elburn 3	Galena-Platteville through Ironton-Galesville	143,715
Wasco Sanitary District 2	Galena-Platteville through Ancell	125,769

Table 3. Shallow Wells in Kane County That Pumped More Than 100,000 Gallons per Day (gpd) in 2003

<i>Name and Well Number</i>	<i>Source Interval Hydrostratigraphic Units (see Figure 19)</i>	<i>2003 Withdrawals (gallons per day)</i>
St. Charles 9	Quaternary	1,568,230
St. Charles 11	Quaternary	1,560,277
Carpentersville 6	Quaternary	1,489,996
Carpentersville 7	Quaternary	1,024,521
Algonquin 7	Quaternary	988,446
Algonquin 9	Quaternary	849,878
Carpentersville 5	Quaternary	736,742
Batavia 7	Quaternary	556,340
Batavia 6	Quaternary	556,340
Batavia 8	Quaternary	556,340
Geneva 8	Quaternary	542,148
Geneva 9	Quaternary	542,148
Geneva 10	Quaternary	542,148
Commercial/Industrial Well	Silurian-Devonian Carbonate through Maquoketa	500,094
South Elgin 4	Quaternary	489,287
Commercial/Industrial Well	Silurian-Devonian Carbonate through Maquoketa	479,256
Sugar Grove 7	Quaternary	426,556
St. Charles 7	Quaternary	411,102
Aurora 101	Quaternary	288,222
Montgomery 13	Maquoketa	255,272
St. Charles 13	Quaternary	249,144
South Elgin 10	Quaternary	245,361
East Dundee 3	Quaternary	244,110
Commercial/Industrial Well	Quaternary	236,550
Algonquin 8	Quaternary	234,672
East Dundee 4	Quaternary	177,643
South Elgin 3	Quaternary	176,445
South Elgin 5	Quaternary	154,782
South Elgin 6	Quaternary	154,771
Sugar Grove 2	Quaternary	148,376
Algonquin 11	Quaternary	144,813
Aurora Country Club 6	Maquoketa	138,898
Commercial/Industrial Well	Quaternary	137,988
Aurora 103	Quaternary	135,258

1.10. Previous Studies

1.10.1. Regional Studies Including Kane County

As an economic and population center, the southern Lake Michigan area has been the focus of numerous regional hydrogeological studies. These studies have included the benchmark study of Suter et al. (1959) that synthesized a diversity of data and analyses regarding hydraulic properties, pumping, potentiometric surfaces, recharge, discharge, groundwater movement, and groundwater quality for each aquifer system in northeastern Illinois. Visocky et al. (1985) provide a more recent synthesis of data and analyses pertaining to the hydrogeology of the Cambrian and Ordovician Systems in northern Illinois. The vertical hydraulic conductivity of the Maquoketa Unit has long been recognized as a key factor influencing the availability of groundwater from underlying units, principally the sandstone aquifers of the Ancell and Ironton-Galesville Units. The first estimate of this variable, still widely cited, was developed by Walton (1960) through analysis of a potentiometric surface map of the underlying units. On the basis of this estimate, Walton (1962; 1965) calculated the downward leakage across the Maquoketa Group under predevelopment conditions and in 1958.

Suter et al. (1959) employed an analytical model of the interval underlying the Maquoketa Unit in northeastern Illinois to estimate the effects of pumping from the 1958 network of wells tapping this interval. The model represented increased recharge in the area lacking Maquoketa Unit cover, west of northeastern Illinois, with a recharge boundary along the western margin of the modeled area. The eastern and southern boundaries of the analytical model were represented with barrier boundaries to simulate declining permeabilities in the Ancell and Ironton-Galesville Units east and south of the Chicago region. Suter et al. (1959) concluded that the 1958 pumping total of approximately 46 Mgd was approximately the maximum that could be withdrawn from the interval without eventually desaturating the vital Ironton-Galesville Unit. Walton (1962) applied flownet analysis to the 1958 potentiometric surface constructed from water-level measurements of wells open to the sub-Maquoketa interval to evaluate the leakage through the Maquoketa confining unit, leading to an update of the analytical model to include the effects of leakage. The revised analytical model assumed a thickness of 200 ft and a vertical hydraulic conductivity of 0.000007 ft/d, but this did not alter the conclusion that 46 Mgd was the maximum sustained yield for the 1958 pumping centers (Walton, 1962; Walton, 1964; Walton and Walker, 1961).

Prickett and Lonquist (1971) used a numerical flow model to refine the analytical modeling of Suter et al. (1959) and extend the represented area to include southeastern Wisconsin, northwestern Indiana, and a larger area of northeastern Illinois. The study used a two-dimensional, finite-difference flow modeling code and a minimum grid resolution of 1 mile. The units between the top of the Galena-Platteville Unit and the base of the Ironton-Galesville Unit were represented as a single, horizontal layer having a uniform thickness of 1025 ft, a homogeneous transmissivity of 2273 ft²/d, and a storage coefficient of 5×10^{-4} . Where the potentiometric surface dropped below the aquifer surface and the aquifer became unconfined, the transmissivity was allowed to vary in proportion to the saturated thickness, and the storage assumed a specific yield of 0.05. Similar to Suter et al. (1959), the model used no-flow boundaries along the southern and eastern margins of the model, but used a recharge area in the northwest corner of the

model to represent the area lacking Maquoketa cover. Using recorded pumping rates up to 1960 and projected pumping rates to 1995, the resulting model predicted large-scale desaturation of the aquifers in the sub-Maquoketa interval in the Chicago area.

Follow-up studies updated the model of Prickett and Lonquist (1971) and used it to predict the aquifer response to changing withdrawal patterns. Schicht et al. (1976) used the model to evaluate alternative management practices. Visocky (1982) used an analytical solution for pumping in Wisconsin, to correct the Suter et al. (1959) maps of observed and predevelopment potentiometric surfaces. Visocky then recalibrated the model of Prickett and Lonquist, adjusting the storage coefficient until the model-simulated potentiometric surface more closely agreed with the corrected maps of Suter et al. (1959). Visocky also calibrated the model to the potentiometric surface observed in 1980. The recalibrated model was then used to predict drawdowns to the year 2020 under various scenarios for the utilization of Lake Michigan allocations.

Young (1976) constructed a numerical groundwater model of the sedimentary rocks underlying the Maquoketa Unit with the objective of predicting drawdown in southeastern Wisconsin through the year 2000. The model domain included northeastern Illinois and southeastern Wisconsin, and it employed a minimum grid resolution of 0.5 miles. All rocks between the base of the Maquoketa and the base of the Mt. Simon Unit were represented as a single, two-dimensional layer, with storage within the confining Maquoketa Unit accounted for explicitly. The modeled layer was heterogeneous, with transmissivity ranging from 668 to 3342 ft²/d, the values in northeastern Illinois being similar to that used by Prickett and Lonquist (1971). The storage coefficient of the layer was specified as 4×10^{-4} , and the specific storage of the confining layer was set to 1×10^{-7} ft⁻¹. Where the heads dropped below the top of the modeled layer so that it became unconfined, the transmissivity was allowed to vary in proportion to the saturated thickness, and the storage assumed a specific yield of 0.05. The model was manually calibrated by adjusting the vertical conductivity of the confining layer to obtain agreement between model-simulated and observed head maps constructed from water-level measurements from wells open to the sub-Maquoketa interval. Where the Maquoketa Unit is present, the calibrated vertical conductivity ranged from 4×10^{-6} to 4×10^{-5} ft/d. In the western region of the model where Maquoketa is absent, the calibrated vertical conductivity ranged from 7×10^{-4} to 3×10^{-3} ft/d.

The model generally simulated greater drawdown than was observed in the system, a discrepancy Young attributed to the fixed location of the potentiometric surface divide at the western edge of the model. Young noted that, in reality, pumping should shift the divide westward and increase recharge to the aquifer, reducing the actual drawdown. Young also commented that "the Galena-Platteville unit does not supply significant quantities of water from storage and ... functions primarily as a semi-confining bed, rather than as part the aquifer." Predictive simulations therefore assumed that conversion to unconfined conditions only occurred after the potentiometric surface reached the bottom of the Galena-Platteville formation. The study assumed that the Milwaukee area would switch to Lake Michigan water by 1990, but withdrawals from the modeled interval otherwise would steadily increase, with projected withdrawals for the year 2000 totaling 95 Mgd in southeastern Wisconsin and 94 Mgd in northeastern Illinois. Model predictions to the year 2000 showed that the shift in withdrawal patterns and general increase in withdrawal rates would result in a westward shift of the

drawdown cone from Waukesha to West Berlin and an increase in total drawdown to 450 ft. The study estimated that 200 ft of drawdown at the state line could be attributed to withdrawals in the Chicago area alone.

Adopting the view that the Galena-Platteville Unit is essentially an aquitard where overlain by the Maquoketa, Burch (1991) revised Prickett and Lonquist's (1971) model of the interval from the base of the Maquoketa to the base of the Ironton-Galesville in the Chicago area. Burch (1991) applied a multi-layer finite-difference model to a domain with the same areal extent and resolution as Prickett and Lonquist's (1971) model. Burch's model used a quasi-three-dimensional approach, representing the system as a stack of two-dimensional aquifers, with flow between units modeled as an instantaneously transferred leakage. Burch (1991) used five layers, representing the Mt. Simon Sandstone and Elmhurst Sandstone Member (Eau Claire Formation); Ironton and Galesville Sandstones; Franconia Formation, Potosi Dolomite, and Eminence Formation; Prairie du Chien Group; and Ancell Group. Each layer varied in thickness and was assigned hydraulic conductivities adapted from Prickett and Lonquist (1971), followed by manual calibration. This quasi-three-dimensional approach permitted an explicit representation of the Prairie du Chien formation, a low-conductivity unit whose thickness varies from zero near Racine, Wisconsin to over 900 ft near Joliet, Illinois.

With hydraulic properties based on newly available aquifer test data and calibration to the observed 1985 potentiometric surface constructed from water-level measurement in wells open to the sub-Maquoketa interval, Burch (1991) used a storage coefficient of 3×10^{-4} and a specific yield of 0.05. The Burch model used an inverse-distance weighting technique to assign withdrawals to model nodes—rather than aggregating wells into pumping centers—and included the Rock River as a series of constant head nodes. The model incorporated reported withdrawal rates for Illinois and Wisconsin up to 1987, and used withdrawal forecasts to estimate drawdown through the year 2010. The model predicted water-level recoveries over a wide area, as much as 600 ft in some places, for the modeled interval in response to a predicted conversion of the source of numerous public water systems to a Lake Michigan water source. Burch (1991) predicted significant water-level recoveries in the Arlington Heights-Wheeling area of western Cook County and DuPage County, while population growth in suburban areas would lead to water level declines in the Aurora, Joliet, and Elmhurst areas.

Mandle and Kontis (1992) constructed a regional model of the aquifers underlying the northern Midwest for the U.S. Geological Survey's Regional Aquifer System Analysis program. The model domain extended from central Missouri to the southern shore of Lake Superior, and from central Michigan to the South Dakota-Minnesota border, covering 378,880 square miles (mi^2). The study used a quasi-three-dimensional, finite-difference flow-modeling code, enhanced to correct the freshwater heads for the density effects of salinity (without modeling the movement of salinity), with a uniform grid resolution of 16 miles. The study represented the shallow and deep bedrock aquifers, from the bottom of the Mt. Simon Formation to ground surface, as a series of two-dimensional layers linked by vertical leakage across the intervening aquitards. Aquifer thicknesses were non-uniform, and the hydraulic conductivities were zoned to reflect regional heterogeneity. The specific storage was 5.5×10^{-7} and where heads dropped below the surface of the Ancell Group and the unit became unconfined, transmissivity varied in proportion to saturated thickness, and the storage was increased

by a factor of 100. The entire upper boundary of the model was assigned a constant head to represent the observed water table surface, under the assumption that drawdown in the uppermost aquifers was negligible on this scale. Major rivers were represented with constant head nodes where they transected the aquifers, otherwise the model boundaries were left as impermeable (no-flow) boundaries. Mandle and Kontis (1992) noted that the model was sensitive to the location of the eastern edge of the domain, and that the smaller domain used by Prickett and Lonnquist (1971) may have influenced that study's predictions for the Chicago area. The model was manually calibrated at steady-state by adjusting the horizontal and vertical conductivities to obtain agreement between the model-simulated and estimated predevelopment potentiometric surfaces, followed by calibration of the storage coefficients to match the 1980 potentiometric surface based on measurements in wells open to the sub-Maquoketa interval. Mandle and Kontis found that, under predevelopment conditions, recharge percolated into the aquifers, eventually discharging into major streams. The model showed that density variations result in significant changes in flow directions in the Michigan and Illinois basins. Under the 1980 pumping conditions, they found that withdrawals had resulted in extensive drawdown in all formations, increasing surface recharge, decreasing discharge to rivers, and reversing flow across aquitards near major pumping centers. This model showed that discharge exceeded recharge to these aquifers, decreasing storage. Mandle and Kontis noted that their model was too coarse to examine important, small-scale flow systems, and addressed neither the three-dimensional nature of this flow system, nor the movement of salinity.

Feinstein et al. (2005a; 2005b) developed a computer model of groundwater flow in southeastern Wisconsin, northeastern Illinois, southern Lake Michigan, northwestern Indiana, and southwestern Michigan. The model represented all rock units from land surface to the bottom of the Mt. Simon Sandstone as three-dimensional layers. Minimum grid resolution was 2500 ft in the model nearfield of southeastern Wisconsin. The model was calibrated under predevelopment steady-state and transient pumping conditions against heads and stream base flow observations. Feinstein et al. concluded that wells in southeastern Wisconsin derived over 80 percent of their water, ultimately, from surface water, including Lake Michigan, in the form of flow induced from surface waters or from capture of groundwater that would have discharged to surface waters under predevelopment conditions. In addition, Feinstein et al. showed that nearly 20 percent of the water withdrawn from deep wells in southeastern Wisconsin—that is, wells open to units below the Maquoketa Group—was derived from outside the region. The modeling showed that, between 1864 and 2000, withdrawals from shallow wells—wells open to the Shallow Bedrock Aquifer and Quaternary sand and gravel aquifers—had caused a reduction of 8.5 percent in discharge of shallow groundwater to Lake Michigan. The most important contributing area for groundwater withdrawals from deep wells was found to be an area of comparatively high leakage to the source units lacking Maquoketa Group cover that was immediately west of major pumping centers in Waukesha County. Finally, the modeling showed that pumping has caused the groundwater flow divide marking the western limit of the diversion area surrounding deep pumping centers in southeastern Wisconsin to shift about 10 miles west from 1864 to 2000.

1.10.2. Studies Emphasizing Kane County

Two published groundwater studies summarize investigations in Kane County and adjacent areas during the late 1980s to collect and analyze data pertinent to siting a superconducting super collider (SSC) then proposed for the area. Visocky and Schulmeister (1988) constructed head maps of the sand and gravel aquifers and the Shallow Bedrock Aquifer, and discussed heads in the underlying, impermeable interval of the Maquoketa and Galena-Platteville Units. Visocky (1990b) discussed water-level measurements from 26 individual and nine nested piezometers finished in the Maquoketa, Galena-Platteville, and Ancell Units. They employed these data to estimate downward leakage across the Maquoketa and Galena-Platteville Units at 5.7×10^{-6} to 1.8×10^{-5} and 1.9×10^{-6} to 3.4×10^{-6} ft/d, respectively. Graese et al. (1988) summarizes a diversity of geological and geotechnical data and analysis, including hydrogeological research, assembled for the SSC-siting effort. This summary includes discussion and mapping of aquifer geometry, hydraulic properties, and head distributions.

Other coincident studies, conducted in the context of concerns over increasing water demand coupled with excessive reliance on the deep aquifers, were concerned with characterizing groundwater availability from locally available shallow aquifers. Curry and Seaber (1990) employed well logs of existing borings, test drilling, and geophysical methods to map the buried bedrock surface and sand and gravel aquifers of Kane County. Gilkeson et al. (1987) and Visocky (1990a) discussed pumping tests of shallow aquifers conducted at probable sites of public-supply well development in the urbanizing Fox River corridor of eastern Kane County, and Visocky (1990a) assessed the shallow aquifer potential yield in the county, revising these estimates upward based on the mapping of Curry and Seaber (1990) showing sand and gravel aquifers of greater lateral extent than previously known. Visocky (1990a) also examined existing chemical analyses to characterize groundwater quality in Kane County. Visocky observed that while concentrations of chlorides, hardness, iron, sulfate, and total dissolved minerals are higher in water from the shallow aquifers than from the deep ones, the quality of the shallow groundwater is generally good, and radium and barium—problematic constituents of deep groundwater—are not present in shallow groundwater.

Three studies have examined aspects of groundwater-supply problems in Campton Township (T 40N, R7E), in central Kane County. Campton Township is an area of relatively dense groundwater development by domestic-supply wells, yet productive, easily accessible, laterally persistent aquifers are absent from the township. As a result, water-supply interruptions are a regular occurrence among existing wells in the township. Benson (1990) compared the advantages of large-diameter bored wells (a well design commonly employed in areas lacking thick, productive aquifers) with small-diameter drilled wells finished in deep, marginally productive rocks of the Maquoketa and Galena-Platteville Units (a common design in Campton Township), and concluded that the large-diameter wells represent a lower-cost alternative to the deep, small-diameter wells. Kay and Kraske (1996) discussed water levels in wells finished in shallow and deep sand and gravel aquifers, the Shallow Bedrock Aquifer, and the comparatively impermeable portion of the Galena-Platteville Unit underlying the Shallow Bedrock Aquifer in Campton Township. Water-level data were employed to construct a 1995 potentiometric surface map showing areas of reduced heads indicative of removal of large amounts of water from storage. Kay et al. (2006) measured water levels in 2002 in wells open to

units as deep as the Ancell Unit in Campton Township and constructed a groundwater flow model of the area. Comparison of the 2002 water-level data with those collected in 1995 by Kay and Kraske (1996) showed large water-level declines during the period in wells open to the Shallow Bedrock Aquifer and impermeable Galena-Platteville Unit, but not in the sand and gravel aquifers or the Ancell Unit. The computer model of Kay et al. (2006) is based on a domain extending about 1.3 miles beyond Campton Township to the north, west, and south, and to the Fox River in the east. Subsurface materials were represented by nine three-dimensional, heterogeneous layers representing subsurface materials between land surface and the base of the Ancell Group. Minimum grid resolution was 500 ft. The model was calibrated, using manual and automated parameter-estimation methods, against water-level and streamflow observations made in 2002. The modeling of Kay et al. (2006) suggested that little recharge within Campton Township penetrates beyond the Shallow Bedrock Aquifer. Similarly, the model predicted little impact of withdrawals from the Ancell Unit on heads in the Shallow Bedrock Aquifer and overlying Quaternary aquifers. Additionally, the modeling suggested that (1) groundwater pumped from the Ancell Unit in Campton Township is from west of the modeled area, and (2) the source of groundwater pumped from the Shallow Bedrock Aquifer and Quaternary aquifers enters those units mainly in the area in the western part of Campton Township and northwest of the township. Finally, the modeling suggested that about 21 percent of the groundwater in the township is discharged to wells, 43 percent is discharged to streams, and 36 percent flows out of the township.

A series of projects were initiated by the ISWS and ISGS in 2002 to provide baseline water-resources data, analyses, and tools for future analyses of water resources available to Kane County. The ISGS reported interim (Dey et al., 2004a; Dey et al., 2004b; Dey et al., 2004c; Dey et al., 2004d; Dey et al., 2005) and final (Abert et al., 2007; Dey et al., 2007a; Dey et al., 2007b; Dey et al., 2007c; Dey et al., 2007d; Dey et al., 2007e) results of geological modeling and mapping efforts conducted for the initiative. Locke and Meyer reported interim (2005) and final (2007) results of efforts to map the potentiometric surfaces of the shallow aquifers of Kane County. Groundwater quality may ultimately affect the availability of groundwater in Kane County. Kelly and Meyer (2005) explored for trends in water quality in groundwater derived from the interval underlying the Maquoketa Unit in northeastern Illinois, a subject of concern since it is plausible that reduction in heads could induce movement of highly mineralized water into northeastern Illinois wells. The available data did not support the existence of such trends in most areas, but data from the two largest deep bedrock pumping centers—Joliet and Aurora—did suggest increasing mineralization. Kelly (2005) sampled wells open to shallow aquifers in Kane County in 2003 and found groundwater quality to be good, generally, with some slight impact in the eastern, urbanized part of the county. Knapp et al. (2007) developed an accounting model for quantifying streamflow in Kane County, as surface water is a crucial element of the Kane County setting and is vital for water supply in Aurora and Elgin, the two largest public water systems in the county.

2. Model Design

The groundwater flow models of this study were constructed using MODFLOW 2000, a computer code developed by the U.S. Geological Survey (McDonald and Harbaugh, 1988). MODFLOW 2000 reads data files describing the area of interest, sets up equations representing groundwater flow, pumping, and interactions of groundwater and surface water, and solves for the estimated hydraulic head and flow. MODFLOW 2000 can simulate *steady-state conditions*, in which hydraulic head and groundwater flow no longer change because they are at equilibrium with the distribution and rates of water inflow and outflow. MODFLOW 2000 can also simulate *transient conditions*, where heads and fluxes change with time as they adjust to new pumping wells or changes in withdrawal rates, recharge, river levels, etc. If stresses do not change, steady-state conditions will eventually be reached as a new equilibrium is reestablished.

Two models of groundwater flow have been developed for this study (Figure 15). The *regional model* covers all aquifers and aquitards over an area that includes northern Illinois, southern Wisconsin, southern Lake Michigan, southwestern Michigan, and northwestern Indiana. The purposes of the regional model are to quantify groundwater flow in the deep aquifer system in northeastern Illinois and to provide boundary conditions for the more detailed *local model* of the shallow aquifers in Kane County. The regional model is designed to be most accurate for the deep aquifers of northeastern Illinois. The extent of the regional model permits simulating distant influences on flow in these aquifers, including the pumping and recharge in Wisconsin and discharge to the Illinois River near LaSalle. The purposes of the local model are to quantify groundwater flow, estimate wellfield capture zones, and evaluate groundwater-surface water interaction in the shallow aquifers of Kane County and the immediately adjacent areas. The two models are linked using *telescopic mesh refinement* (Section A.3), a procedure that ensures that regional patterns of groundwater flow are reflected in the local model. The models constructed for this project simulate all major current and historic groundwater withdrawals in northeastern Illinois and the surrounding areas that could plausibly influence groundwater flow in northeastern Illinois. Flow into and out of major surface-water features are represented using the MODFLOW river and drain packages; the drain package is used to simulate agricultural and urban drainage systems.

2.1. Conceptual Model

The conceptual model is discussed on regional and local scales corresponding to the two groundwater flow models developed for this study (Figure 15). The regional-scale model covers the entire northeastern Illinois region, including portions of Lake Michigan and the neighboring states of Indiana, Michigan, and Wisconsin, and all geologic materials above the impermeable crystalline Precambrian basement (Figure 16, Figure 17). The regional-scale model is most accurate and precise within the detailed *nearfield* region that encompasses northeastern Illinois. Figure 5 illustrates the general conceptual model at the regional scale. At the scale of the regional model, the surficial Quaternary Unit can be regarded as a single aquifer, even though, as discussed in Section 1.8.3, the reality is that this unit consists of a complexly interbedded sequence of unconsolidated, and permeable and impermeable materials functioning as aquifers and aquicludes, respectively.

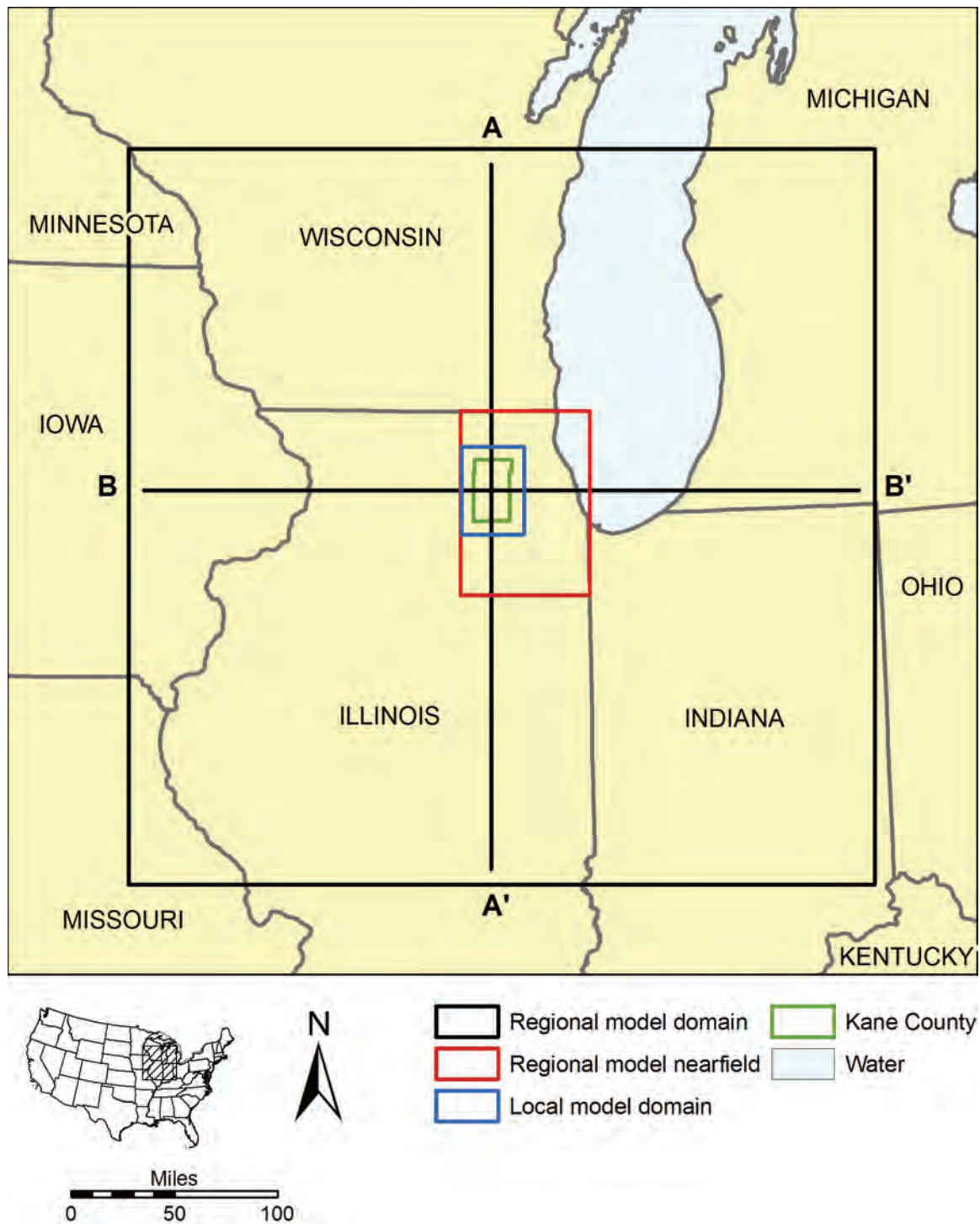


Figure 15. Geographic domains of groundwater flow models and lines of cross sections in Figure 16 and Figure 17.

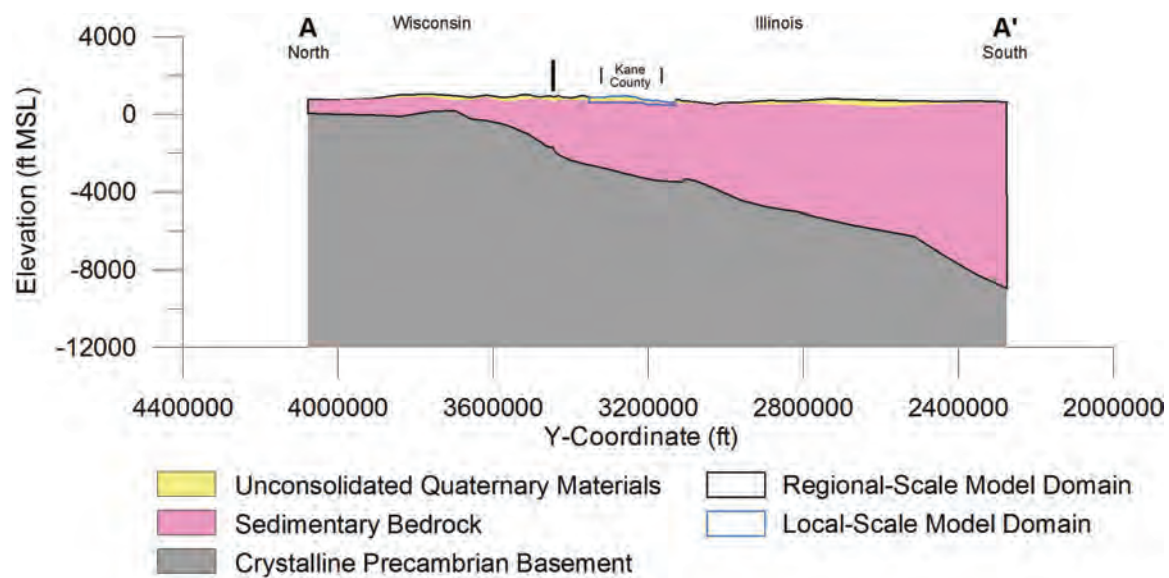


Figure 16. Generalized cross section along A-A' (Figure 15) showing domains of groundwater flow models.

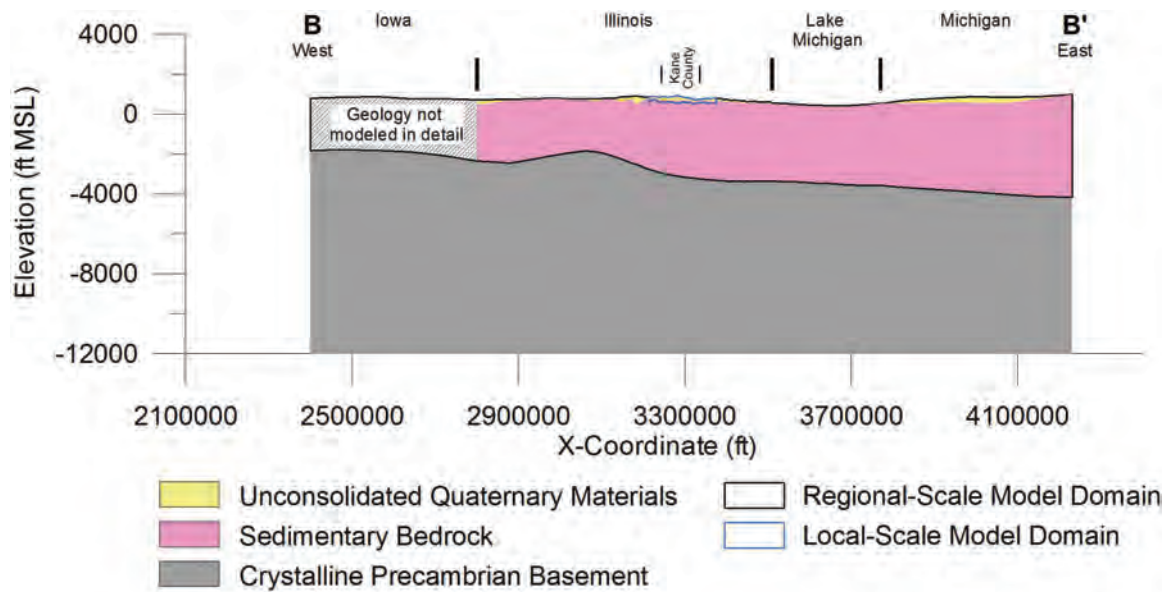


Figure 17. Generalized cross section along B-B' (Figure 15) showing domains of groundwater flow models.

The Quaternary Unit overlies the Shallow Bedrock Aquifer, comprising the uppermost 25-125 ft of bedrock regardless of whether the bedrock consists of Silurian dolomite, interbedded Ordovician Maquoketa Group carbonates and shales, or Ordovician Galena-Platteville dolomite. These shallow aquifers interact with surface water owing to their interconnections with one another and their general proximity to the surface. Deeper aquifers consist of the Ancell Unit, Ironton-Galesville Unit, and Mt. Simon Unit, the last of which is seldom used in northeastern Illinois because of its great depth and because its lower portion contains unacceptably saline groundwater.

Nested within the nearfield region is the local-scale model, which covers Kane County and surrounding areas within a distance of approximately six miles (i.e., the model includes townships that border Kane County). The local-scale model includes only the discontinuous sand and gravel aquifers within the Quaternary Unit of the regional-scale model and the weathered, permeable portion of the underlying sedimentary bedrock (the Shallow Bedrock Aquifer). Sand and gravel aquifers are Quaternary in age (fairly recent in geologic time), typically unconsolidated, and within about 300 ft of land surface. Several individual sand and gravel units, all capable of functioning as aquifers, are present in the Kane County area, including—from the base upward—the Glasford Unit, Ashmore Unit, Batestown Sand Unit, Yorkville Sand Unit, Beverly Unit, Wadsworth Sand Unit, and Surficial Henry Unit. The underlying uppermost sedimentary bedrock consists of dolomites, shales, and sandstones, generally of Silurian and Devonian ages.

2.1.1. Regional Model Domain

Paleozoic sedimentary rocks overlie crystalline Precambrian basement throughout almost the entire regional model domain (Figure 18). These rocks dip gently off the combined Wisconsin and Kankakee Arches into the Michigan Basin to the northeast, and the Illinois Basin to the south. Major faults, most notably the Sandwich Fault Zone in northern Illinois, displace the Paleozoic rocks in some locations. In addition, two small areas of complex folding and faulting—the Des Plaines and Kentland Disturbances—affect the Paleozoic sedimentary cover in northeastern Illinois and northwestern Indiana, respectively (Dietz, 1947; Emrich and Bergstrom, 1962). Both are probable impact structures. Precambrian rocks are poorly known in much of the Midwest because they are concealed by Paleozoic and younger rocks, but in most of these areas the Precambrian rocks are interpreted to be impermeable igneous plutonic and metamorphic rocks (Cannon et al., 1997; Catacosinos and Daniels, 1991; Catacosinos et al., 1990; McGinnis, 1966; Nicholas et al., 1987). Comparatively thin Mesozoic sedimentary rocks overlie the Paleozoic rocks in widely scattered locations, and unconsolidated Quaternary sediments, mostly glacial drift, mantle the older rocks in most of the area. While Precambrian rocks crop out in northern parts of the upper Midwest, their top elevation declines to more than 16,000 ft below sea level in the central Michigan Basin.

Major unconformities separate the sedimentary rocks in the region into depositional sequences generally representing marine transgressive-regressive cycles (Kolata, 1990; Sloss, 1963). Because these major unconformities are often highly eroded surfaces, the basal units of these sequences, such as the Ordovician Ancell Group, can overlie a wide range of lithostratigraphic units and can vary considerably in thickness.

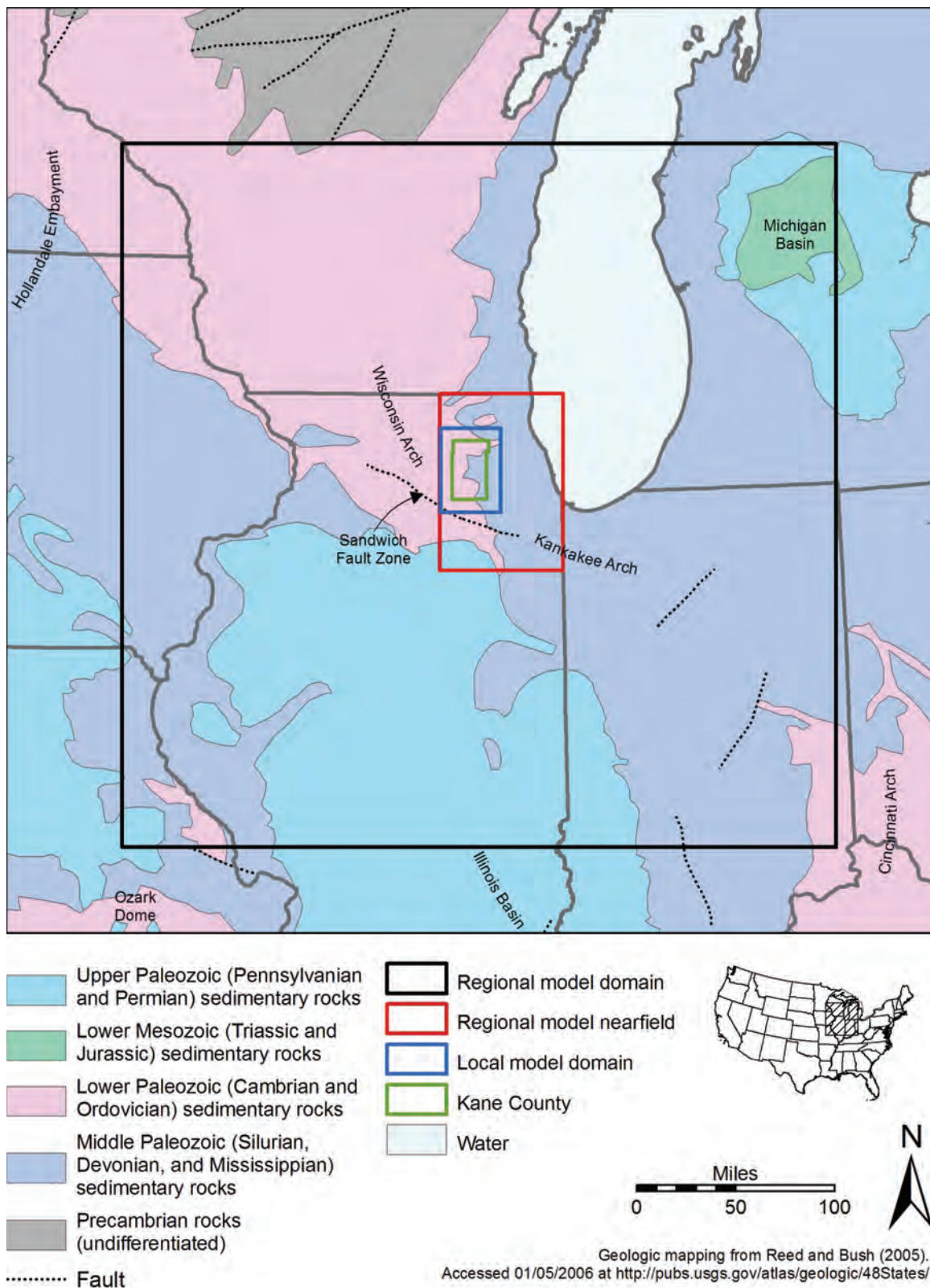


Figure 18. Generalized bedrock geologic index map.

The depositional sequences represented include the Sauk, Tippecanoe, Kaskaskia, Absaroka, Zuni, and Tejas sequences (Sloss, 1963).

2.1.1.1. Hydrostratigraphic Nomenclature

The hydrostratigraphic nomenclature presented in the following paragraphs was developed for this project and is useful for conceptualizing groundwater movement in northeastern Illinois (Figure 19). This nomenclature reflects the layering scheme adopted for project-specific regional groundwater flow modeling. Detailed modeling in other parts of the upper Midwest might be better served by different hydrostratigraphic nomenclature. Cross sections along the lines of section illustrated in Figure 15 are shown in Figure 20 and Figure 21.

The **Mt. Simon Unit** includes the Mt. Simon Sandstone (Cambrian) of the region, primarily fine- to coarse-grained sandstone. Although the term *Mt. Simon Sandstone* is employed widely throughout the region, regional mapping of the Mt. Simon Sandstone and overlying Eau Claire Formation is complicated by differences in the treatment of an interval of comparatively fine-grained sandstone that is assigned to the basal Elmhurst Sandstone Member of the Eau Claire Formation in Illinois. The Elmhurst Member—despite its being included in the lithostratigraphic Eau Claire Formation—is included in the Mt. Simon Unit of the present investigation. In northern Indiana, this interval is likewise included as the lower Eau Claire Formation (Munising Group) (Becker et al., 1978), but in Wisconsin this sandstone interval is included in the Mt. Simon Sandstone (Elk Mound Group). The interval has been included in the lower Eau Claire Formation (Munising Group) of Michigan by numerous researchers (Catacosingos, 1973; Ells, 1967; Western Michigan University Department of Geology, 1981), but more recent studies reflect the Wisconsin interpretation, including the fine sandstone interval as part of the upper Mt. Simon Unit (Catacosingos and Daniels, 1991). The Michigan mapping employed for this project is based on definition of the Mt. Simon-Eau Claire contact that includes the fine-grained sandstone interval in the Eau Claire Formation. The Mt. Simon Unit supplies fresh groundwater to wells in updip areas, primarily in southern Wisconsin. Its use in relatively downdip areas, including most of Illinois, is limited by the presence of saline water in the lower portion or throughout the aquifer (Visocky et al., 1985).

The **Eau Claire Unit** represents the Eau Claire Formation (Cambrian) of Illinois and equivalent lithostratigraphic units in adjacent states. The Eau Claire Unit consists of fine- to medium-grained sandstone with some interbedded gray shale; dolomite, sometimes sandy, with interbedded greenish gray shale; and dolomitic siltstone with interbedded shale. Approximately equivalent lithostratigraphic units include the Eau Claire Formation (Munising Group) of Indiana and Michigan, and the Eau Claire Formation (Elk Mound Group) of Wisconsin. The position of the base of the Eau Claire Unit differs across the region as discussed in the preceding paragraph. Sandy facies of the Eau Claire Unit supply fresh water in updip areas, including much of southern Wisconsin. In northeastern Illinois, such sandy materials occur in the lower Elmhurst Sandstone Member, but use of this member as an aquifer is limited in downdip areas such as northeastern Illinois by high groundwater salinities (Visocky et al., 1985). Other than some updip areas of southern Wisconsin, the Eau Claire Unit in the regional model domain is an aquitard that limits movement of groundwater between overlying and underlying units.

The **Ironton-Galesville Unit** represents the Galesville and Ironton Sandstones (Cambrian) of Illinois and equivalent lithostratigraphic units in adjacent states. Sandstones represented by the Ironton-Galesville Unit are generally fine- to medium-grained and are locally silty and dolomitic. These sandstones become finer-grained southward and eastward from the Wisconsin Arch area, grading into finer-grained siliciclastic rocks and dolomite in central Illinois, central and eastern Indiana, and central Michigan, where the unit cannot be recognized. Rocks assigned to the Ironton-Galesville unit include the Wonewoc Formation (Elk Mound Group) of Wisconsin, the Galesville and Ironton Sandstones (Munising Group) of Indiana, and the Galesville Sandstone (Munising Group) of Michigan. Often used in combination with the Ancell Unit, the Ironton-Galesville Unit is a productive aquifer throughout much of its extent, supplying significant quantities of groundwater to wells in southern Wisconsin and northern Illinois; however, the groundwater within it is too saline for most purposes in down-dip areas of central Illinois, Indiana, and Michigan (Visocky et al., 1985).

The **Potosi-Franconia Unit** represents the Franconia Formation (Cambrian) and overlying Potosi Dolomite (Cambrian) of Illinois and equivalent units in adjacent states. The Franconia is similar to the Eau Claire Formation and consists of poorly-sorted, fine-grained siliciclastic sediments and dolomite that grade southward and eastward from the Wisconsin Arch area to purer dolomite (Willman et al., 1975; Young, 1992). Equivalent lithostratigraphic units include the Tunnel City Group of Wisconsin (Ostrom, 1966; Young and Siegel, 1992) and the Franconia Formation (Munising Group) of Indiana and Michigan. Where the Galesville and Ironton Sandstones are not recognizable in Indiana, equivalents of the Franconia Formation are assigned to the Davis Formation. The Potosi is a fairly pure dolomite throughout its distribution in Illinois, but sand content increases northward (Buschbach, 1964), and the largely dolomitic rocks of the equivalent St. Lawrence Formation (Trempealeau Group) in Wisconsin contain greater quantities of sand, silt, and clay (Young and Siegel, 1992). In Indiana and Michigan, the relatively pure dolomite correlating to the Potosi Dolomite and overlying Eminence Formation in Illinois are not distinguishable, and the two units are therefore lumped as the Potosi Dolomite in Indiana and as the Trempealeau Formation in Michigan (Catacosinos and Daniels, 1991; Droste and Patton, 1985). The Potosi-Franconia Unit supplies groundwater to wells in southern Wisconsin, where coarser-grained and more permeable, siliciclastic materials compose a greater portion of the unit, but the unit supplies little groundwater in other areas. The Potosi-Franconia Unit is the oldest of the hydrostratigraphic units exposed at the bedrock surface in Illinois, where it forms the bedrock surface in a limited area of north-central Illinois on the south side of the Sandwich Fault Zone predominantly in DeKalb, Lee, and Ogle Counties (Kolata et al., 1978; Willman et al., 1975). Where exposed at the bedrock surface, the presence of secondary porosity in these materials probably increases well yields somewhat, but, in general, the Potosi-Franconia Formation is an aquitard throughout its extent in the regional model domain.

The **Prairie du Chien-Eminence Unit** represents the Eminence Formation (Cambrian) of Illinois—together with the laterally equivalent Jordan Sandstone of extreme northwestern Illinois—and the overlying Prairie du Chien Group (Ordovician). The Eminence Formation is a sandy dolomite that becomes less sandy southward and eastward from the Wisconsin Arch area so that it is distinguished with difficulty from

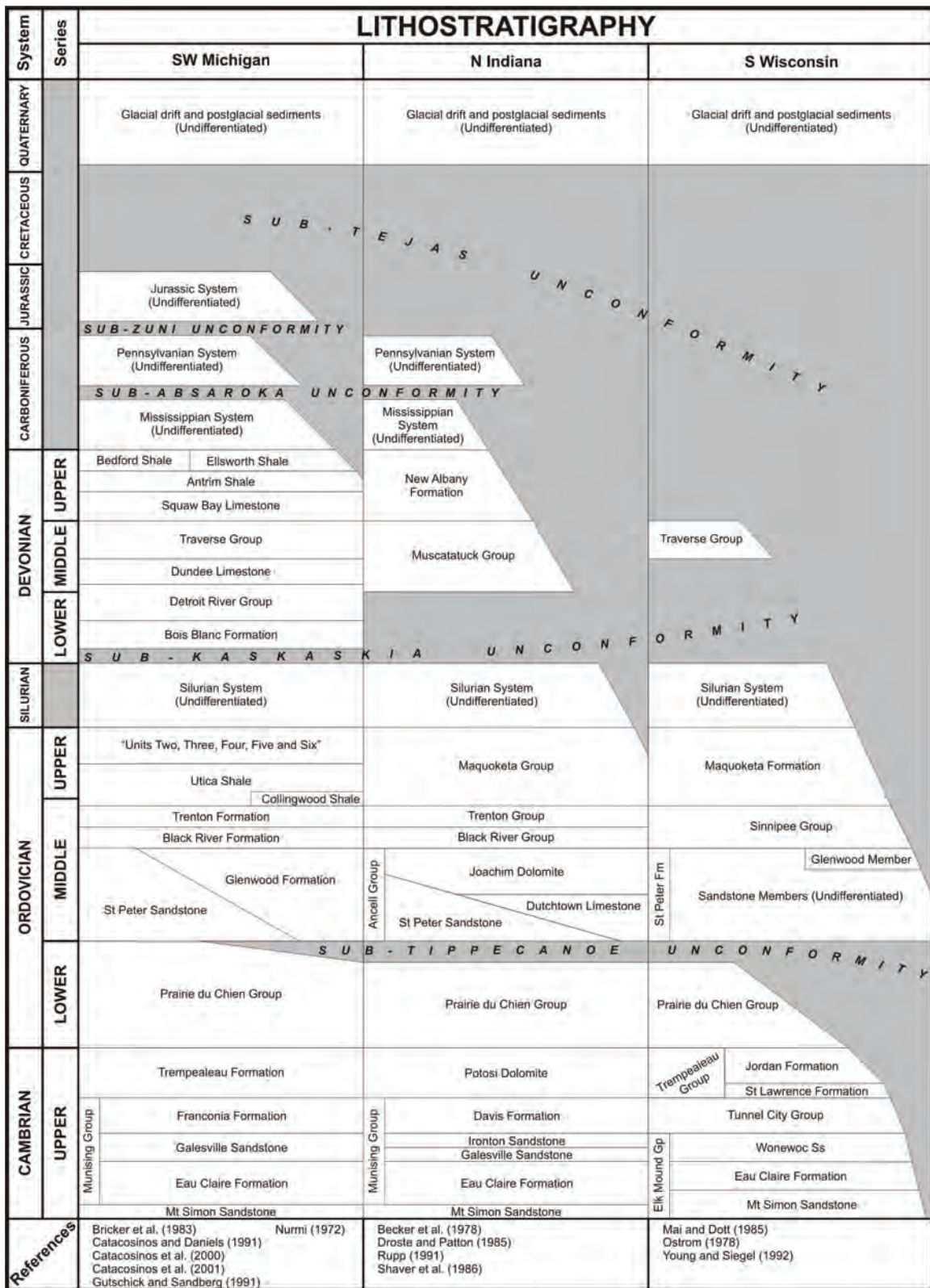


Figure 19. Correlation chart, lithostratigraphic nomenclature, and hydrostratigraphic nomenclature employed in regional-scale groundwater flow model.

LITHOSTRATIGRAPHY		HYDROSTRATIGRAPHIC NOMENCLATURE (THIS REPORT)
Central Illinois	NE Illinois	
Glacial drift and postglacial sediments (Undifferentiated)	Glacial drift and postglacial sediments (Undifferentiated)	Quaternary Unit (QT)
<div style="text-align: center;">SUB-TEJAS UNCONFORMITY</div> Cretaceous System (Undifferentiated)		Upper Bedrock Unit (UB)
<div style="text-align: center;">SUB-ZUNI UNCONFORMITY</div> Pennsylvanian System (Undifferentiated)	Pennsylvanian System (Undifferentiated)	
<div style="text-align: center;">SUB-ABSAROKA UNCONFORMITY</div> Mississippian System (Undifferentiated)		
New Albany Shale Group Cedar Valley Limestone Wapsipinicon Limestone		
<div style="text-align: center;">SUB-KASKASKIA UNCONFORMITY</div> Silurian System (Undifferentiated)	Silurian System (Undifferentiated)	Silurian-Devonian Carbonate Unit (SD)
Maquoketa Group	Maquoketa Group	Maquoketa Unit (MQ)
Galena Group Platteville Group	Galena Group Platteville Group	Galena-Platteville Unit (GP)
Ancell Group Joachim Dolomite Dutchtown Limestone	Ancell Group Glenwood Fm St Peter Sandstone	Ancell Unit (AN)
<div style="text-align: center;">SUB-TIPPECANOE UNCONFORMITY</div> Prairie du Chien Group	Prairie du Chien Group	Prairie du Chien-Eminence Unit (PE)
Eminence Formation	Eminence Formation	Potosi-Franconia Unit (PF)
Potosi Dolomite	Potosi Dolomite	
Franconia Formation	Franconia Formation	Ironton-Galesville Unit (IG)
Ironton Sandstone	Ironton Sandstone	
Galesville Sandstone	Galesville Sandstone	Eau Claire Unit (EC)
Eau Claire Formation	(Undifferentiated)	
Mt Simon Sandstone	Eau Claire Fm Elmhurst Sandstone Member Mt Simon Sandstone	Mt Simon Unit (MS)
Kolata et al. (1990) Willman et al. (1975) Young and Siegel (1992)	Buschbach (1964) Kolata and Graese (1983) Kolata et al. (1990) Willman et al. (1975) Young and Siegel (1992)	

Figure 19. Correlation chart, lithostratigraphic nomenclature, and hydrostratigraphic nomenclature employed in regional-scale groundwater flow model (concluded).

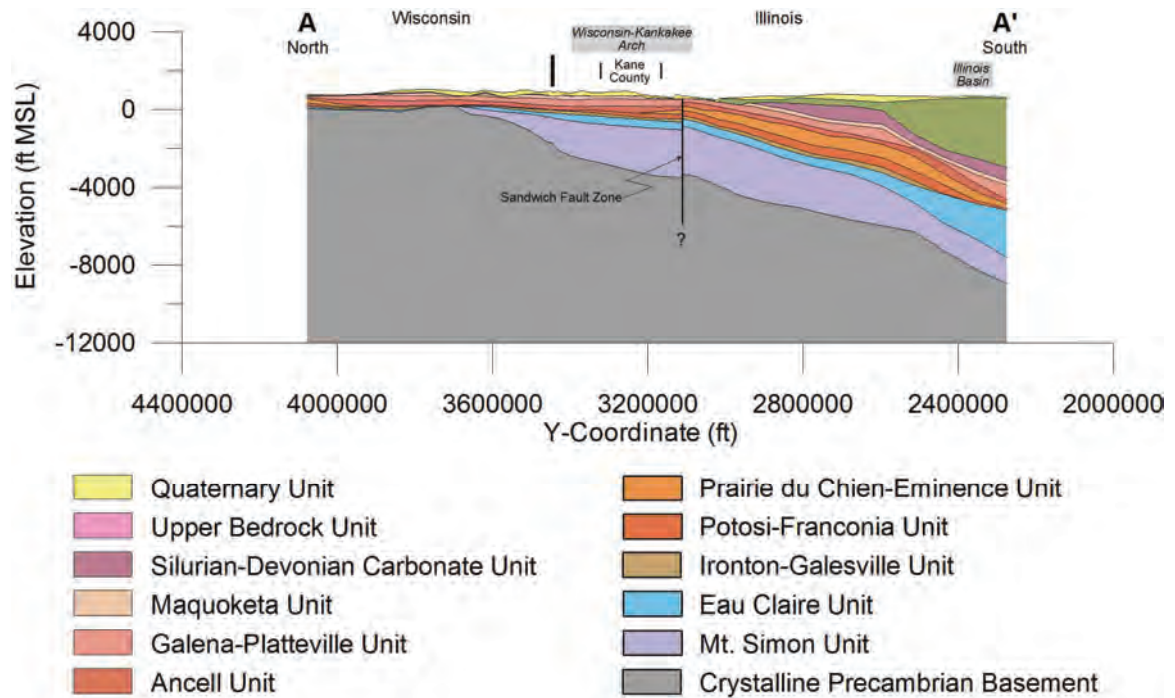


Figure 20. Generalized north-south cross section along A-A' (Figure 15) showing regional hydrostratigraphic units discussed in text.

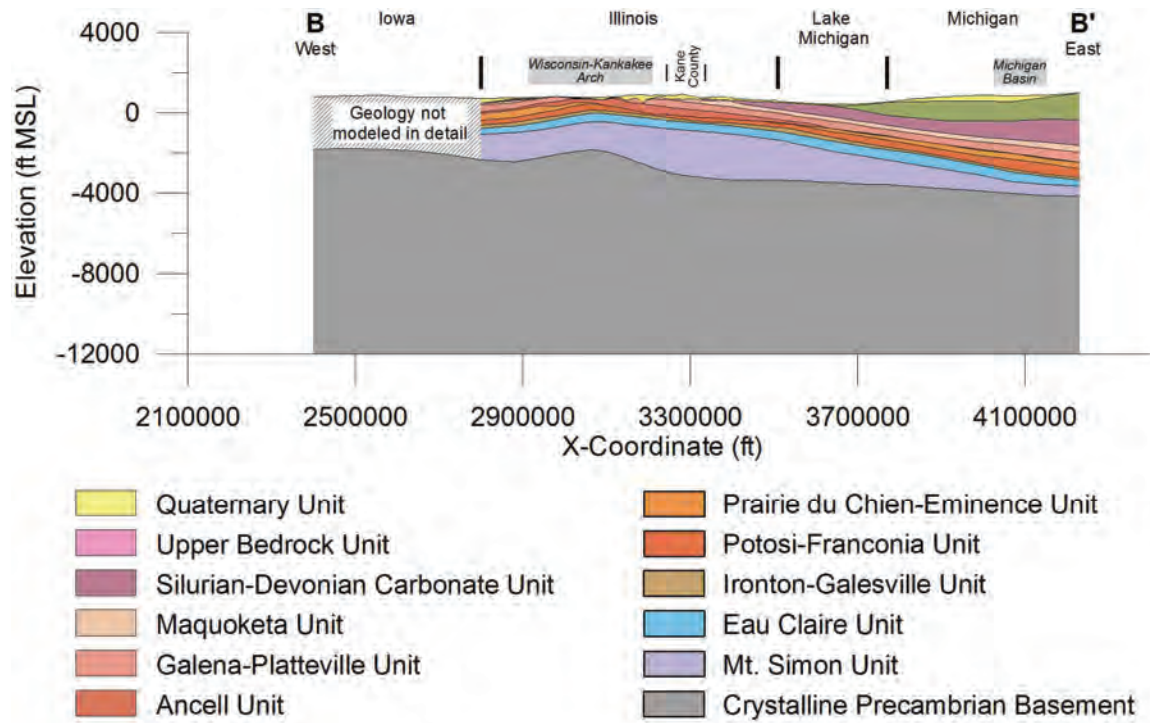


Figure 21. Generalized east-west cross section along B-B' (Figure 15) showing regional hydrostratigraphic units discussed in text.

overlying and underlying dolomites in central Illinois, Indiana, and Michigan (Catacosinos and Daniels, 1991; Droste and Patton, 1985; Willman et al., 1975).

As mentioned in the preceding paragraph, the Eminence and Potosi equivalents in Indiana and Michigan are lumped under the terms Potosi Dolomite and Trempealeau Formation, respectively. The sandy dolomites of the Eminence Formation grade northwestward into a sandstone unit, known as the Jordan Sandstone in Illinois and the Jordan Formation in Wisconsin. The term *Prairie du Chien Group* is employed widely throughout the region. The *Prairie du Chien* consists primarily of finely to coarsely crystalline, cherty dolomite with lenses of sandstone. The *Prairie du Chien-Eminence Unit* is most accurately characterized as an aquitard in the regional model domain, despite the fact that the Jordan Sandstone and other lenses of sandstone within the predominantly dolomitic unit may be important aquifers where present. These sandstones are not well-developed in northeastern Illinois, however. Where exposed at the bedrock surface, secondary porosity permits small groundwater supplies to be obtained from the carbonates of this unit.

The Ancell Group (Ordovician) of Illinois and its equivalents, which contain rocks ranging from sandstone to shale to carbonates, are represented by the **Ancell Unit**. The St. Peter Sandstone composes the entire Ancell Group throughout most of the southern half of northern Illinois. In the northern two to three tiers of counties in Illinois, the upper St. Peter grades laterally into the Glenwood Formation, and in the southern half of Illinois, the St. Peter grades laterally into carbonates of the Dutchtown Limestone and Joaquin Dolomite Members of the Ancell Group (Templeton and Willman, 1963). The St. Peter Sandstone is restricted to the western half of Indiana, where it can compose the entire Ancell Group, although it is commonly overlain by the Joaquin Dolomite. The lower and upper parts of the St. Peter grade eastward in Indiana into carbonates of the Dutchtown Limestone and Joaquin Dolomite, as they do in Illinois (Shaver et al., 1986). In Wisconsin, where the term *St. Peter Formation* replaces the term *Ancell Group*, named sandstone members compose the entire unit on the Wisconsin Arch, and the overlying Glenwood Member comprises a small proportion of the unit in flanking areas. The equivalent rocks in Michigan are assigned to the St. Peter Sandstone and Glenwood Formation, but the term *Ancell Group* is not employed (Bricker et al., 1983; Catacosinos and Daniels, 1991; Catacosinos et al., 2001). Where the St. Peter Sandstone is present in updip areas of Wisconsin and northern Illinois, the Ancell Unit is an important aquifer, supplying many large municipal wells, often in combination with the Ironton-Galesville Unit.

The **Galena-Platteville Unit** represents dolomites of the Platteville and Galena Groups of Illinois and equivalents in the adjacent states. Correlative lithostratigraphic units include carbonates of the Sinnippee Group in Wisconsin (Young and Siegel, 1992), the Black River Group and overlying Trenton Limestone in Indiana (Rupp, 1991; Shaver et al., 1986), and the Black River and Trenton Formations in Michigan (Catacosinos et al., 2001). Throughout the region these rocks consist of relatively pure limestone and dolomite with subordinate amounts of shaly limestone and dolomite. Small to moderate supplies of groundwater are obtained from the upper 50-100 ft of the Galena-Platteville in areas where the unit is exposed at the bedrock surface, and permeability has been increased through secondary porosity development.

In northeastern Illinois, the roughly 50- to 100-ft interval of the bedrock immediately underlying the bedrock surface—in areas where that interval is comprised of carbonate-rich rocks of the Galena-Platteville Unit, Silurian-Devonian Carbonate Unit, and, to a lesser extent, the Maquoketa Unit—is commonly referred to as the *Shallow Bedrock Aquifer*. Indeed, this bedrock interval functions as a single, laterally continuous aquifer by virtue of its proximity to the bedrock surface and consequent secondary porosity development (Csallany and Walton, 1963). Where not present within the interval immediately underlying the bedrock surface—so that it is overlain by the younger Maquoketa Unit, Silurian-Devonian Carbonate Unit, and/or Upper Bedrock Unit—the Galena-Platteville Unit is significantly less permeable and is best considered an aquitard.

The **Maquoketa Unit** represents the Maquoketa Shale Group of Illinois and correlative lithostratigraphic units in the adjacent states. The interval represented by the Maquoketa unit consists predominantly of dolomitic shale, argillaceous dolomite, and argillaceous limestone. Correlative lithostratigraphic units include the Maquoketa Group in Indiana (Shaver et al., 1986) and the Maquoketa Formation in Wisconsin (Young and Siegel, 1992). The Maquoketa Group of Illinois is equivalent to the Collingwood Shale, Utica Shale, and a series of unassigned interbedded shales and carbonates in southwestern Michigan referred to by Nurmi (1972) as Units Two through Six (Catacosinos et al., 1990; Catacosinos et al., 2001; Willman et al., 1975). The Maquoketa Unit is generally considered an important aquitard in the region, although the more carbonate-rich facies of the Maquoketa Unit—where present within 50-100 ft of the bedrock surface—provide small groundwater supplies owing to secondary porosity development (see preceding paragraph on the Galena-Platteville Unit) (Csallany and Walton, 1963). Like the Galena-Platteville Unit, the entire Maquoketa Unit is an aquitard where it is not present in the interval of secondary porosity development near the bedrock surface.

Carbonates deposited during the Silurian and Lower through Middle Devonian are represented by the **Silurian-Devonian Carbonate Unit**. Where both the Silurian and Devonian rocks are present, the interval includes the major sub-Kaskaskia unconformity. The Silurian System consists largely of dolomite, but lesser amounts of shale are present, and the dolomites may be argillaceous, silty, and clean. Thick evaporate sequences are present in the central Michigan Basin, and reef structures are present in many areas. The Lower and Middle Devonian rocks are primarily carbonates and include both limestone and dolomite. They include the Middle Devonian Wapsipinicon Limestone and overlying Cedar Valley Limestone of central Illinois (Willman et al., 1975), the Middle Devonian Muscatatuck Group of northern Indiana (Rupp, 1991), and the Lower and Middle Devonian Bois Blanc Formation, Detroit River Group, Dundee Limestone, and Traverse Group of southwestern Michigan (Catacosinos et al., 1990; Catacosinos et al., 2001). The lower and middle Devonian rocks do not extend into northeastern Illinois, where the Silurian-Devonian Carbonate Unit is composed entirely of Silurian dolomites. Secondary porosity in the 50-100 ft of the Silurian-Devonian Carbonate Unit underlying the bedrock surface—which, together with the 50-100 ft of the Galena-Platteville and Maquoketa Units underlying the bedrock surface, forms the Shallow Bedrock Aquifer (see preceding two paragraphs on the Galena-Platteville and Maquoketa Units)—provides small to moderately large quantities of groundwater to wells in northeastern Illinois (Csallany and Walton, 1963). Where it is overlain by younger rocks of the Upper Bedrock Unit, so that

it is absent from the interval of secondary porosity development near bedrock surface, the Silurian-Devonian Carbonate Unit is most accurately characterized as an aquitard.

The **Upper Bedrock Unit** contains Upper Devonian through Cretaceous rocks of a range of lithologies. Although this sequence includes both aquifers and confining units in areas remote from the model nearfield, its overall hydrologic effect for the underlying units is one of a confining unit, owing to the presence of widespread, impermeable fine siliciclastic materials within it. Since it is the underlying rocks that are of crucial importance in the model nearfield, this entire interval is lumped for the present study. The Upper Devonian and basal Mississippian rocks are generally impermeable shales and include the New Albany Shale Group in Illinois (Willman et al., 1975), the New Albany Formation in Indiana (Shaver et al., 1986), and the Antrim, Ellsworth, and Bedford Shales in Michigan (Catascinos et al., 1990; Catascinos et al., 2001; Gutschick and Sandberg, 1991). The overlying Mississippian rocks include fine- to coarse-grained siliciclastic sediments and carbonates, generally limestones, in complex facies relationships with one another. In general, the siliciclastic sediments within the Mississippian rocks increase and coarsen both upward and northeastward within the region (Harrell and Hatfield, 1991; Rupp, 1991; Shaver et al., 1986). Throughout its distribution in the region, the Pennsylvanian System consists of interbedded sandstones, shale, limestone, and coal. Mesozoic rocks are known only from the northeastern and southwestern corners of the regional model domain, remote from the model nearfield. Shaly sandstone of Jurassic age, present in the central Michigan Basin (Catascinos et al., 2001; Olcott, 1992; Willman et al., 1975), and sand and clayey sand of Cretaceous age, present in southwestern Illinois (Willman et al., 1975), are included in the Upper Bedrock Unit. While the overall hydrologic character of the Upper Bedrock Unit in the region is that of an aquitard, small groundwater supplies are sometimes obtained from sandstones, limestones, and coals within the unit in Illinois and Indiana. Large groundwater supplies are possible from sandstones of the unit in the Michigan Basin (Olcott, 1992).

Quaternary deposits, consisting largely of unconsolidated diamicton, sand, gravel, clay, and silt, are assigned to the **Quaternary Unit**. Most of these materials were deposited during glaciation of the area during the Pleistocene, but post-glacial sand, lacustrine clays and silts, and anthropogenic fill are present in some areas, including the bottom of Lake Michigan (Gross et al., 1970). Where thick and laterally extensive, sand and gravel deposits within the Quaternary Unit can provide large groundwater supplies, but diamicton, clay, and silt beds function as aquitards. The Quaternary Unit is described in greater detail for the Kane County area in the following section.

2.1.1.2. Shallow and Deep Aquifers, Units, and Wells

Because a laterally-extensive impermeable interval underlies the Shallow Bedrock Aquifer throughout Kane County and most of northeastern Illinois, it is possible to make a general distinction between *shallow aquifers* and *deep aquifers* in the region. The *shallow aquifers* include the sand and gravel aquifers of the Quaternary Unit together with the Shallow Bedrock Aquifer, which itself contains parts of the Silurian-Devonian Carbonate Unit, Maquoketa Unit, and Galena-Platteville Unit that are permeable owing to secondary porosity development within about 50-100 ft of the bedrock surface. The *deep aquifers* consist primarily of sandstones underlying the Galena-Platteville, which, in most parts of northeastern Illinois, are limited to the Ancell Unit, Ironton-Galesville Unit, and Mt. Simon Unit. Groundwater circulation in the shallow aquifers is more rapid than

in the deep aquifers owing to their position above the laterally-extensive confining unit underlying the Shallow Bedrock Aquifer. As compared to the deep aquifers, groundwater flow in the shallow aquifers is influenced to a greater extent by surface water and by water table elevation. Residence times within the shallow aquifers are briefer than in the deep aquifers, and pathlines within individual deep aquifers are much longer than in the shallow aquifers.

The authors acknowledge that the distinction between shallow and deep aquifers breaks down outside northeastern Illinois where the Galena-Platteville and overlying units have been removed by pre-Quaternary erosion. The fine-grained, impermeable rocks of the Upper Bedrock Unit directly overlie the Galena-Platteville in much of the area of interest, and in this area the shallow aquifers are limited to the Quaternary Unit and the weathered surface of the bedrock. With few exceptions, the shallow and deep aquifers in northeastern Illinois are separated by the laterally extensive impermeable interval underlying the Shallow Bedrock Aquifer. For the purposes of this study, the terms *shallow* and *deep* are extended to other parts of the regional model domain despite the fact that they do not necessarily accurately describe the positions of the materials in these areas. For example, in southern Wisconsin and in Illinois southwest of the Sandwich Fault, the rocks above the Ancell formation have been removed by erosion; however, the Ancell and underlying aquifers are still referred to as “deep aquifers” despite their shallow depth.

For convenience in discussing groundwater withdrawals in the region, this report extends the distinction between the shallow and deep aquifers to distinguish between *shallow units* and *deep units*, and between *shallow wells* and *deep wells*. The shallow units are those overlying the Ancell Unit, and the deep units are those beneath the Galena-Platteville Unit (Figure 19). In practice, withdrawals from the shallow units are distributed over the units constituting the Shallow Bedrock Aquifer (weathered portions of the Silurian-Devonian Carbonate, Maquoketa, and Galena-Platteville Units). Wells drilled into deep units are sometimes left open all overlying units, thus withdrawals from deep wells can also include withdrawals from shallow units. For the purposes of this study, shallow wells are those open *only* to the shallow units. Deep wells are open to the deep units but also may be open to the shallow units.

2.1.2. Local Model Domain

2.1.2.1. Shallow Bedrock Aquifer

The Shallow Bedrock Aquifer consists of the weathered bedrock underlying the glacial drift in northeastern Illinois (pages 44 and 53). This aquifer (Figure 22) almost everywhere consists of rocks assigned to the Galena-Platteville Unit, Maquoketa Unit, and Silurian-Devonian Carbonate Unit (Dey et al., 2004a; Dey et al., 2004b; Dey et al., 2005). Secondary porosity has developed in the uppermost 25-125 ft of these predominantly carbonate materials, allowing them to function as a single aquifer delimited by the bedrock surface and the depth of secondary porosity. The bottom of the Shallow Bedrock Aquifer is the base of the domain of the local-scale model (Figure 15, Figure 16, and Figure 17). The depth of development of secondary porosity varies by rock type and bedrock topography. Secondary porosity is less developed in the shaly Maquoketa Group than in the purer, more soluble carbonates of the Galena Group and Silurian System (Csallany and Walton, 1963). Bergeron (1981) suggested that secondary

pore development in the Silurian dolomite of Indiana is insignificant deeper than 100 feet beneath the bedrock surface. Graese et al. (1988) reported that the Shallow Bedrock Aquifer in Kane County and adjacent areas is largely contained in the uppermost 50 ft of bedrock regardless of the formation present at the bedrock surface. They also reported that the uppermost bedrock at quarries and in cores showed that the Silurian dolomites are most intensely jointed in the uppermost 40 ft immediately underlying the bedrock surface. Visocky and Schulmeister (1988) considered the depth of the weathered zone in the uppermost bedrock in the Kane County area to be 50 ft. They observed that most borehole data indicate a fractured zone in the upper 25 ft of bedrock, but noted that this fractured zone commonly extends to depths deeper than 50 ft. Kay and Kraske (1996) reported that groundwater flow in the shallow bedrock in Campton Township, Kane County, is predominantly through fracture porosity within 50 ft of the bedrock surface.

In eastern and southern Kane County, Silurian dolomites compose much of the Shallow Bedrock Aquifer. Lower parts of the aquifer in eastern and southern Kane County may include shales and carbonates of the Maquoketa Group. In most of the rest of Kane County, where erosion has removed the Silurian dolomites, Maquoketa Group rocks compose the Shallow Bedrock Aquifer, with the zone of secondary porosity development possibly extending into the underlying dolomite of the Galena Group. In extreme west-central Kane County near Maple Park, erosion has removed both the Silurian dolomites and the Maquoketa Group, and the Shallow Bedrock Aquifer in this area is comprised entirely of Galena Group carbonates. In Kane County, the elevation of the top of the Shallow Bedrock Aquifer ranges from less than 500 ft near Big Rock in the southwest, to more than 800 ft near Burlington in the northwest.

More domestic wells in Kane County appear to be finished in the Shallow Bedrock Aquifer than in all of the sand and gravel aquifers combined. The aquifer also provides water to numerous public water systems in the county.

2.1.2.2. Quaternary Materials

The Quaternary materials of Kane County may exceed 300 ft in thickness (Dey et al., 2004a) and contain numerous stratigraphic units of dissimilar texture and hydrologic character. They are thickest over the axes of moraines and buried bedrock valleys. Sand and gravel aquifers are contained within the Quaternary materials and may be productive aquifers where thick and laterally extensive. The most productive sand and gravel aquifers are typically contained within buried bedrock valleys, where they were deposited by meltwater streams. The most productive sand and gravel aquifers in Kane County are contained within the St. Charles Bedrock Valley, trending northeast-to-southwest across the southern half of the county, and its tributary valleys. Sand and gravel deposits are sometimes separated by layers of fine-grained materials consisting of diamicton and some lacustrine silts and clays. These materials function as aquitards and greatly limit movement of groundwater between sand and gravel units.

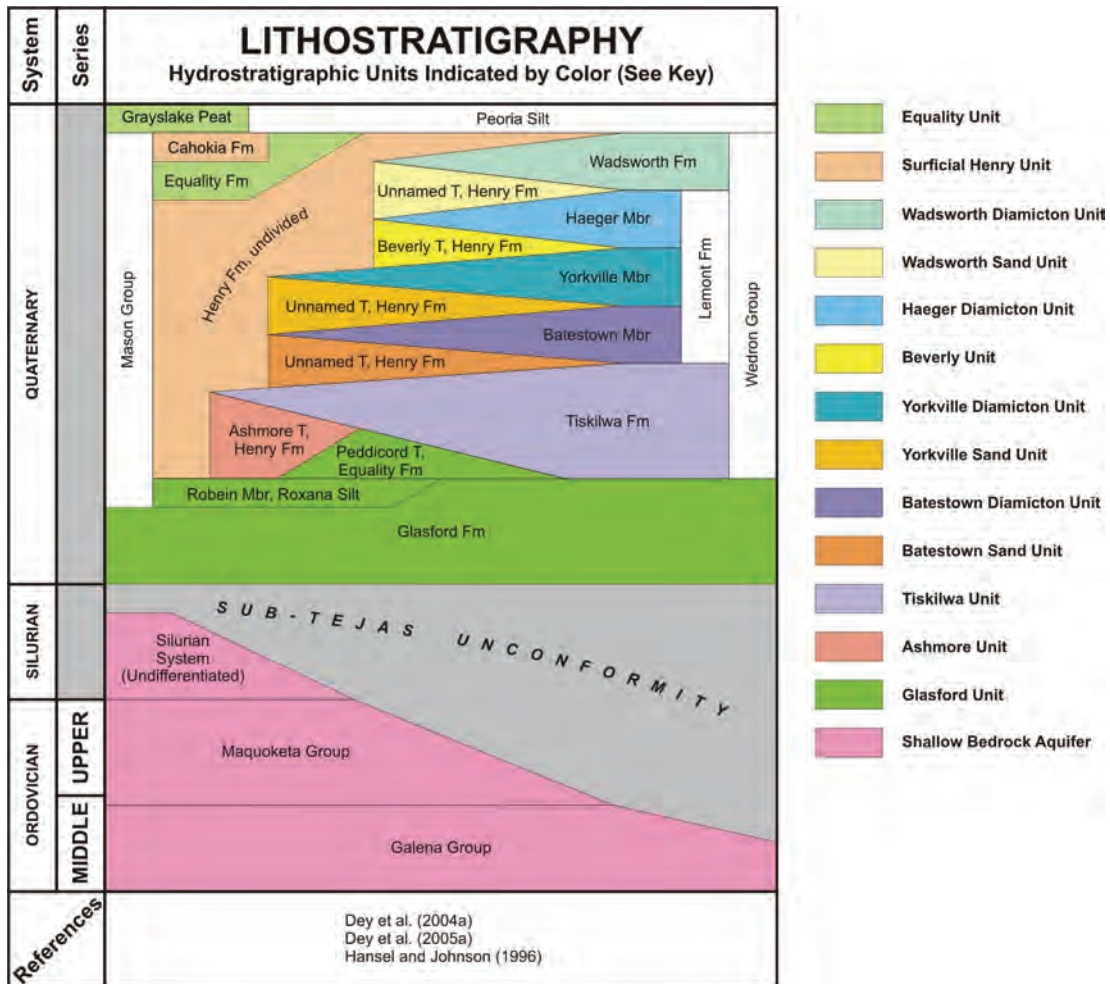


Figure 22. Lithostratigraphic nomenclature and hydrostratigraphic nomenclature employed in local-scale shallow groundwater flow model.

Dey et al. described the Quaternary materials (2004a; 2005) and presented cross sections of them through Kane County (2004c). The summary in the following paragraphs is distilled from these publications. Dey et al. (2004d; 2005) depicted the distribution of the St. Charles, Bloomington, Valparaiso, and Kaneville Aquifers, hydrostratigraphic units originally defined by Curry and Seaber (1990). While the aquifer nomenclature of Dey et al. (2004d; 2005) can be useful, it is not employed in this report because it combines multiple lithostratigraphic units that are not necessarily hydraulically connected or even fully saturated.

The **Glasford Unit** consists primarily of the Glasford Formation, which was deposited during the Illinois Episode and is the oldest of the Quaternary materials present in Kane County (Figure 22). It consists of diamicton, silt, and clay, with abundant lenses of sand and gravel, some of which are thick and productive aquifers. The Glasford Unit includes two thin and sporadically present units, the Robein Member of the Roxana Silt (Mason Group) and the Peddicord Tongue of the Equality Formation (Mason Group). The Glasford Unit is present throughout most of north, west, and central Kane County and forms the surficial unit in the northwestern part of the local model domain.

The Glasford Unit lies comparatively far below the surface and contains numerous lithologic units that are themselves laterally variable. These attributes make mapping the distribution and geometry of lithologies in the Glasford Unit problematic. The ISGS used advanced computer modeling techniques to develop three-layer (Dey et al., 2005) and five-layer (Dey et al., 2007e) simplified models of the Glasford Unit, employing alternating fine- and coarse-grained layers. The five-layer representation of the Glasford Unit (three diamicton layers and two sand and gravel layers) is employed in the local-scale groundwater flow model described in this report.

The Quaternary materials deposited during the Wisconsin Episode are assigned to either the Mason Group or the Wedron Group on the basis of grain-size sorting (Hansel and Johnson, 1996). Deposits comprising similarly sized grains (well-sorted sediments) are assigned to the Mason Group, while those with a range of grain sizes (poorly-sorted sediments) are assigned to the Wedron Group. The Henry Formation (Mason Group) is dominantly sand and gravel deposited by glacial meltwater. The geometry of the sand and gravel Henry Formation is complex because it is discontinuous and may occur at land surface and/or as projecting tongues beneath adjacent diamicton units of the Wedron Formation. Layers of sand and gravel that are comparatively widespread, but occur between named units of the Wedron Formation, are assigned to formally-recognized stratigraphic tongues of the Henry Formation (e.g., the Beverly Tongue of the Henry Formation). Dey et al. (2004a) mapped tongues of the Henry Formation in the local model domain that are not recognized in the formal nomenclature. Since these tongues are of local hydrostratigraphic importance, they are discussed in the following paragraphs and are assigned informal names to facilitate the discussion.

The **Ashmore Unit** consists of the Ashmore Tongue of the Henry Formation (Mason Group), which is a sand and gravel deposit that directly underlies diamicton of the Tiskilwa Formation (Wedron Group). The Ashmore Unit is sporadic throughout most of Kane County, but tends to be thinner in the southeastern part of the county. Thicknesses exceed 80 ft in some parts of northwestern Kane County.

The **Tiskilwa Unit** consists of the Tiskilwa Formation (Wedron Group), the thickest hydrostratigraphic unit in the Kane County area. The Tiskilwa Unit is a diamicton with channel-shaped inclusions of sand and gravel. It exceeds 270 ft in thickness in the Bloomington and Marengo Moraines in northwestern Kane County, but is essentially absent in southeastern Kane County.

The Batestown Member of the Lemont Formation (Wedron Group) overlies the Tiskilwa Formation throughout all but the west-central and northwestern part of the local model domain. The lower portion of the Batestown Member is commonly a sand and gravel tongue of the Henry Formation, although it is not formally recognized as such. This sand and gravel unit, termed the **Batestown Sand Unit**, is tapped as a groundwater source by a limited number of wells. Thickness of the unit may exceed 60 ft in limited areas. The **Batestown Diamicton Unit** comprises the upper part of the Batestown Member, and it is up to 90 ft thick in the local model domain.

The Yorkville Member of the Lemont Formation (Wedron Group) overlies the Batestown Member and is sporadically present in the eastern half of the local model domain. The lower portion of the Yorkville Member is composed of up to 80 ft of sand and gravel that is a tongue of the Henry Formation, although not formally recognized as such. This sand and gravel deposit, termed the **Yorkville Sand Unit**, is not widespread, but is of local hydrostratigraphic importance. The upper Yorkville Member is termed the **Yorkville Diamicton Unit**, and is up to about 100 ft thick in limited areas.

The Beverly Tongue of the Henry Formation overlies the Yorkville Member in the northeastern corner of the local model domain. The Beverly Tongue consists of sand and gravel underlying the Haeger Member of the Lemont Formation (Wedron Group). We term this sand and gravel deposit the **Beverly Unit**. It is up to 80 ft thick.

The overlying **Haeger Unit** consists of the Haeger Member of the Lemont Formation (Wedron Group), a sandy diamicton with abundant, discontinuous lenses of sand and gravel and thin beds of silt and clay. It is present in the northeastern corner of the model domain, where it is up to about 60 ft thick.

The Wadsworth Formation (Wedron Group) occurs in the extreme northeastern corner of the local model domain and, like the Batestown and Yorkville Members of the Lemont Formation, consists of a basal sand and gravel deposit, termed the **Wadsworth Sand Unit**. This sand unit is overlain by the **Wadsworth Diamicton Unit**. The Wadsworth Member is up to about 100 ft thick.

The **Surficial Henry Unit** includes, primarily, Henry Formation (Mason Group) materials that are not overlain by Wedron Group diamicton, and it consists primarily of sand and gravel with subordinate silt and clay. The Surficial Henry Unit also contains coarse-grained post-glacial alluvium, present along stream valleys, assigned to the Cahokia Formation. Finally, the Equality Unit includes, principally, Equality Formation (Mason Group) deposits that are present at or near land surface together with fine-grained facies of the post-glacial Cahokia Formation and Grayslake Peat. The Equality Unit consists mainly of relatively impermeable silt, clay, fine-grained sand, and peat. Note that the Peddicord Tongue of the Equality Formation, a tongue of the Equality Formation occurring beneath the Tiskilwa Formation, is lumped into the Glasford Unit

2.2. Conceptual Model to Numerical Model

2.2.1. *Grids and Layering*

Application of MODFLOW 2000 requires representing the aquifers and aquitards with a multilayer gridwork of blocks or cells known as a finite-difference grid. For the models of this study, the block properties are homogeneous within each block, but vary across the grid in zones to represent variations in hydrogeology. In general, the accuracy of a finite difference model increases with the number of cells, but the computational speed decreases with the number of cells.

The models of this study are three-dimensional, in that they simulate the flow and storage of groundwater in each hydrostratigraphic unit explicitly with one or more model layers. For example, four model layers represent the thick Mt. Simon Unit in the regional-scale model; MODFLOW calculates one head value per cell in each layer, which permits analyzing the vertical difference in heads observed within this thick aquifer. Alternatives to the three-dimensional approach (2D or Quasi-3D approaches) can be appropriate and more computationally efficient, but these omit the layers explicitly representing aquitards and thus ignore transit time and storage within the aquitards. These alternatives also tend to obscure the properties and geometry of units, making the models less useful as a database for subsequent studies. Although the models of this study are three-dimensional, many hydrostratigraphic units are represented with a single model layer and thus only crudely approximate vertical flow within such hydrostratigraphic units. As a consequence, there may be too few layers to resolve vertical flow near partially penetrating wells or immediately beneath streams. Users interested in such complex flow fields will need to develop more detailed models, which the three-dimensional models of this study support by providing a framework of data and boundary conditions.

MODFLOW requires model layers to be continuous across the model domain, but some hydrostratigraphic units are not present throughout the model. Where a hydrostratigraphic unit is absent owing to erosion or nondeposition, the corresponding layer thickness is set to 1 ft and the hydraulic conductivity in an area of absence is set to that of the underlying model layer. This effectively renders the layer transparent to regional groundwater flow and enables MODFLOW to accommodate the area of absence.

2.2.1.1. Regional-Scale Model

Figure 23 illustrates the grid of the regional model, and Figure 24 shows the highly resolved nearfield of the regional model in northeastern Illinois. Figure 25 shows the 20 layers that represent the major aquifers and aquitards of northeastern Illinois, each layer with 221 rows and 170 columns (39,324 cells). The model grid is aligned with the north-south and east-west axes of the ILLIMAP projection and coordinate system (Table 1). In the model nearfield of northeastern Illinois—including all of Cook, DuPage, Kane,

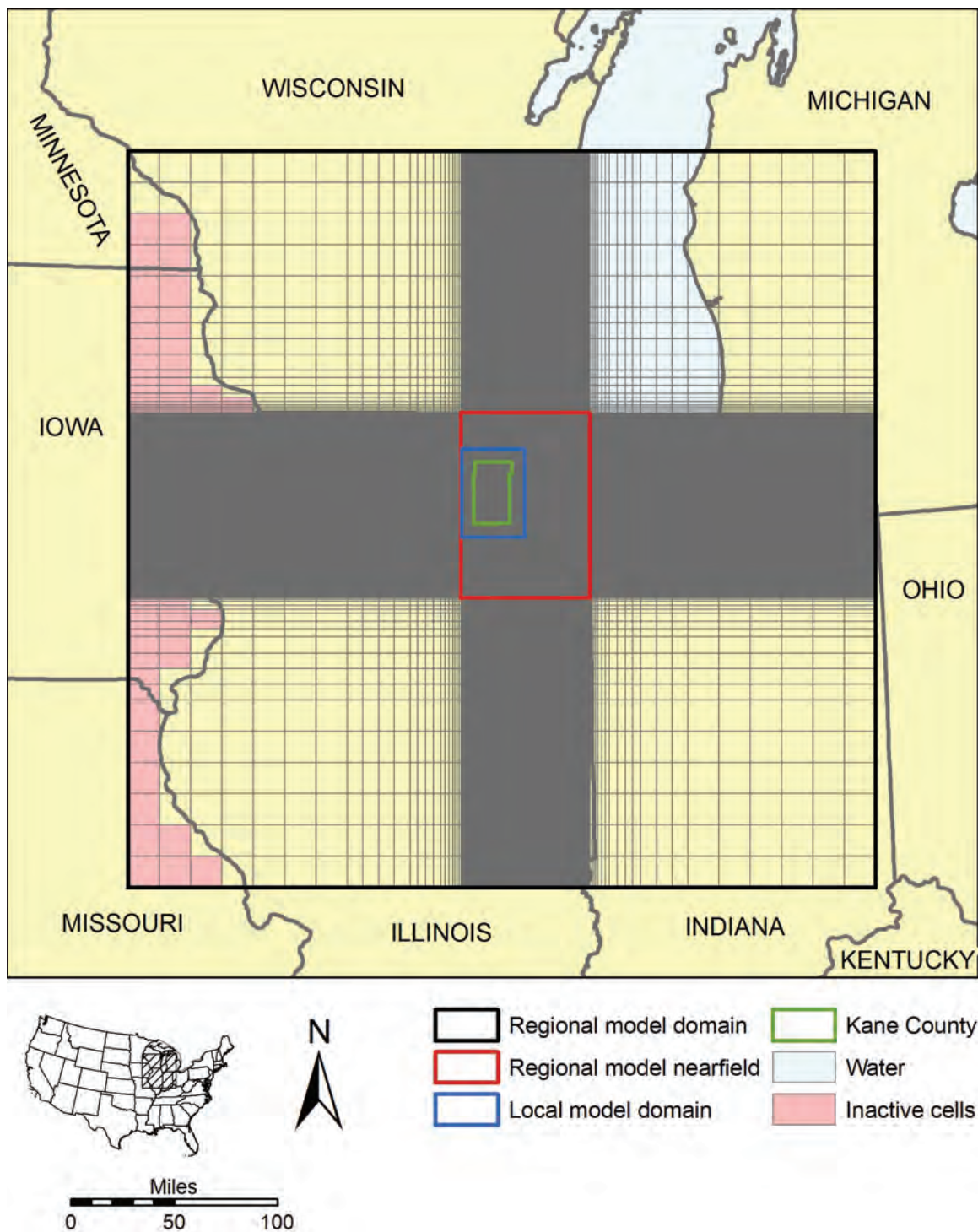


Figure 23. Finite-difference grid of regional-scale model.

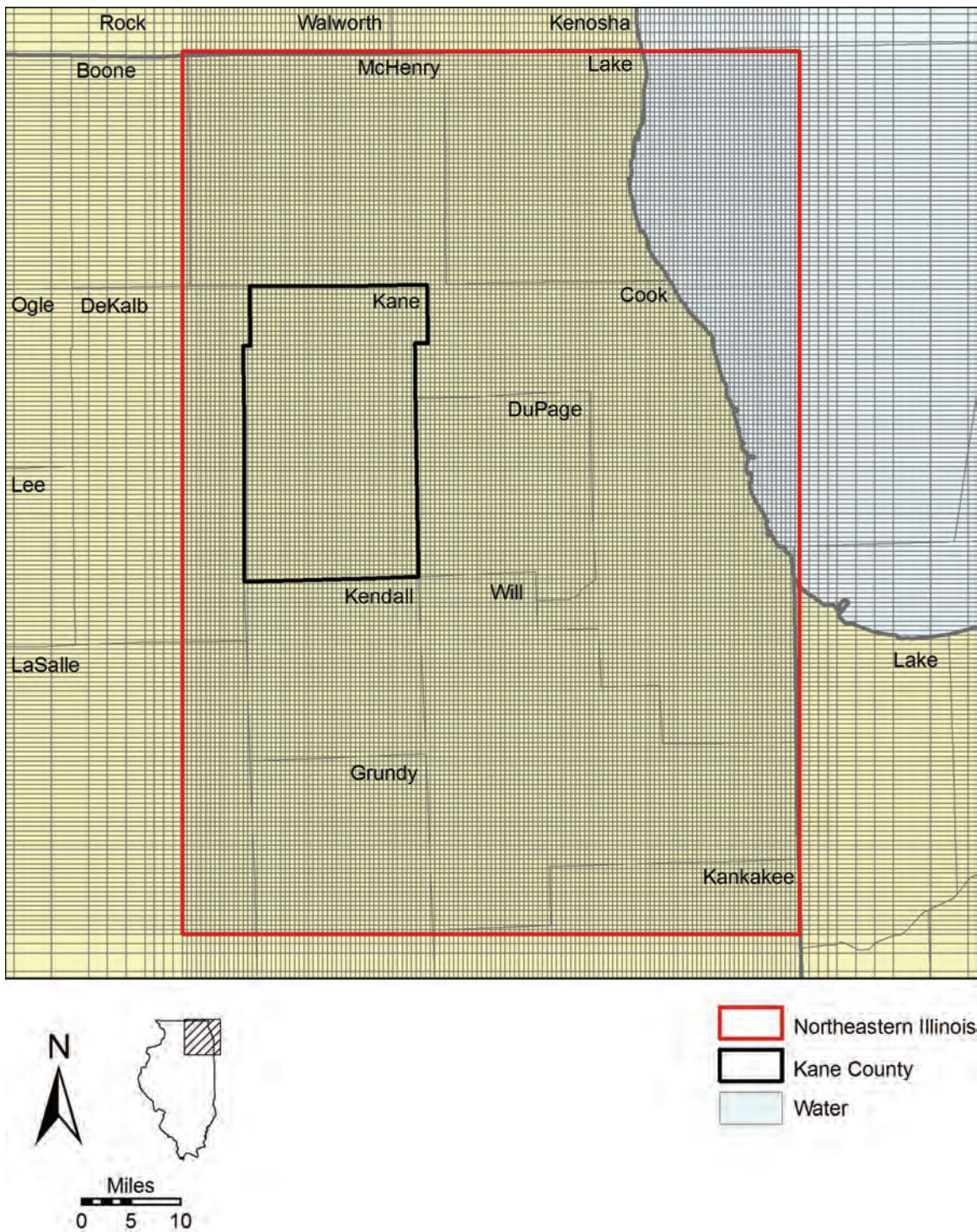


Figure 24. Finite-difference grid of regional-scale model in vicinity of model nearfield.

HYDROSTRATIGRAPHIC UNIT	MODEL LAYER
Quaternary Unit (QT)	1
	2
	3
Upper Bedrock Unit (UB)	4
Silurian-Devonian Carbonate Unit (SD)	5
	6
	7
Maquoketa Unit (MQ)	8
	9
Galena-Platteville Unit (GP)	10
	11
Ancell Unit (AN)	12
Prairie du Chien-Eminence Unit (PE)	13
Potosi-Franconia Unit (PF)	14
Ironton-Galesville Unit (IG)	15
Eau Claire Unit (EC)	16
Mt Simon Unit (MS)	17
	18
	19
	20

Figure 25. Layer scheme of regional model.

Kendall, Lake, McHenry, and Will Counties and parts of several other counties—the x - and y -spacing of cell centers is set to a constant value of 2,500 ft. To improve efficiency, cell sizes are larger at the edges of the model domain where accuracy is less important. Cells west of the Mississippi River are inactive, meaning that they are ignored for purposes of calculating groundwater flow.

2.2.1.2. Local-Scale Shallow Model

The local-scale shallow model represents the hydrogeological system from land surface to the bottom of the Shallow Bedrock Aquifer. The model grid consists of 15 layers, 341 rows, and 243 columns with a uniform horizontal grid spacing of 660 ft (Figure 26). The grid spacing was chosen to maximize the resolution of the model without demanding excessive computational time and computer memory usage when running the model. The grid is aligned with the north-south and east-west axes of the ILLIMAP projection and coordinate system (Table 1). The domain includes all of Kane County and portions of surrounding counties within a distance of about 6 miles of the Kane County boundary.

Layers within the local-scale shallow model are based largely on the hydrostratigraphy of the model domain as described in Section 2.1.2 and illustrated in Figure 22. Several hydrostratigraphic units are aggregated to improve model efficiency. Moreover, the actual, naturally occurring unit geometries are considerably modified to (1) reflect soil development; (2) represent, following Dey et al. (2007e), the complex internal stratigraphy of the Glasford Unit in a simplified fashion as five layers of alternating fine- and coarse-grained materials; (3) adjust the layer bottom elevations in naturally desaturated areas to prevent model cells from drying out during model simulations and creating artificial flow barriers; (4) reduce the number of very thin layers that tend to decrease the numerical stability of the model; and (5) accommodate the change in geologic model resolution when assigning constant flux boundaries via telescopic mesh refinement (TMR) (Figure 27). These modifications are discussed in Section 2.2.2.2.

Local model layer 1 represents the geologic materials exposed at the land surface, including the Surficial Henry Unit, outcrops of stratigraphically lower sand and bedrock units, and the soil developed on top of the glacial diamictos and the Equality Formation. Soil horizons develop on exposed clay deposits through a variety of natural processes, including chemical weathering, fracturing, and root penetration. These processes greatly increase near-surface permeability. Layer 1 has a minimum thickness of 10 ft to allow for the creation of the soil zone and for the insertion of river and drain boundary conditions in a consistent manner throughout the model. The thickness of the soil zone is greater than 10 ft in areas with steep slopes where a thicker soil zone was required to prevent cell desaturation. Where the thickness of layer 1 is less than 10 ft, the bottom elevation of the underlying hydrostratigraphic unit(s) is adjusted downward. Because the Equality Formation is rarely greater than 10 ft, it is modeled as part of the soil zone and not as a separate unit. The hydraulic conductivity of layer 1 is zoned to reflect the uppermost lithology present: (1) the soil zone developed in fine-grained unconsolidated materials of the Equality Unit or any of the diamicton-dominated units described in Section 2.1.2; (2) coarse-grained unconsolidated materials of the Surficial Henry Unit or any of the sand and gravel units described in Section 2.1.2; or (3) the Shallow Bedrock Aquifer.

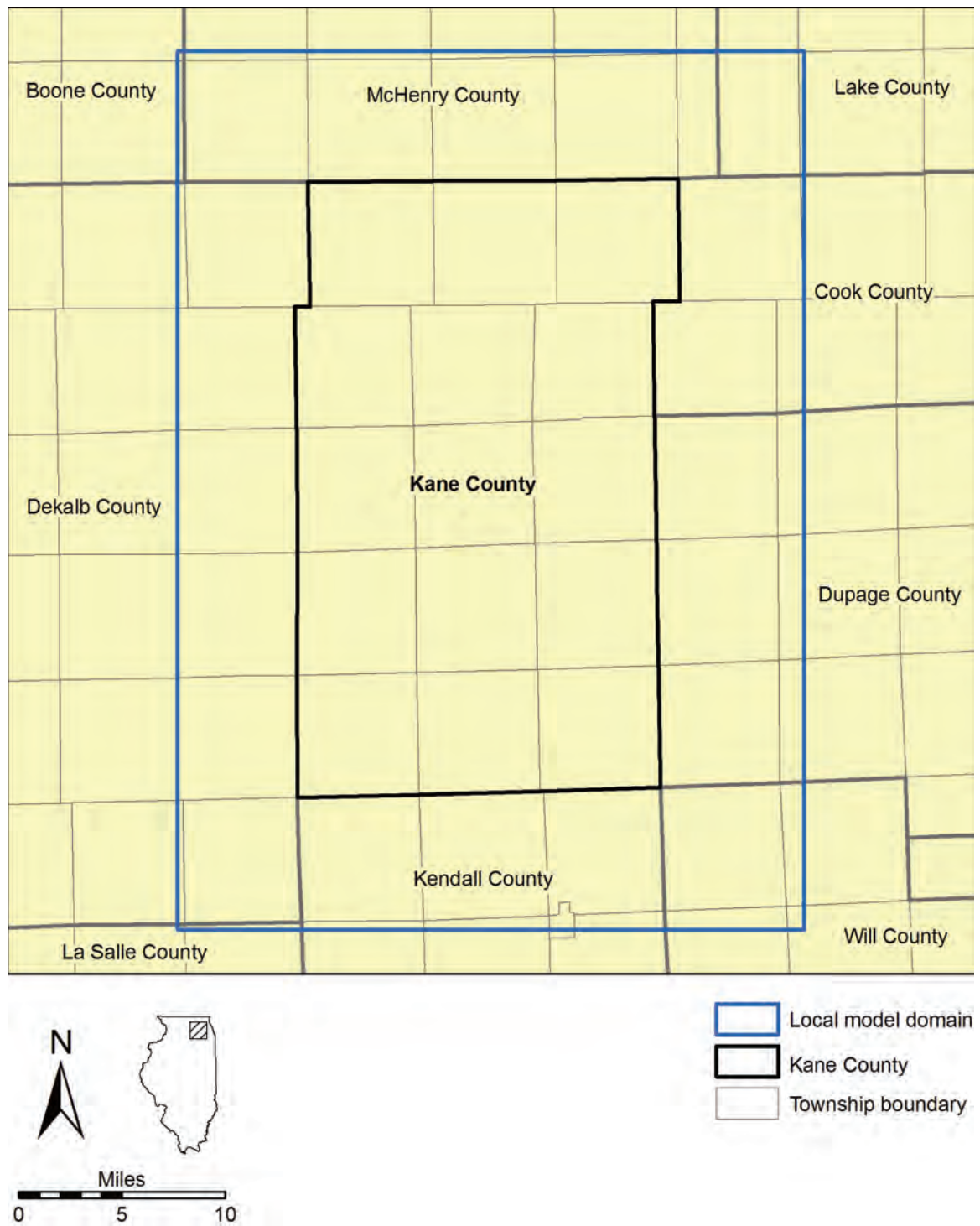


Figure 26. Domain of local-scale shallow model (finite difference grid is too fine to illustrate).

In most of the model domain, local model layer 2 represents the Surficial Henry Unit. In townships of Cook, Lake, and northern DuPage Counties within the local model domain, however, layer 2 represents the aggregated thickness of the Wadsworth and Haeger Diamicton Units. Because there is no significant Equality Formation present in these townships, the Surficial Henry sand could be represented by layer 1. The thickness of the Wadsworth Sand Unit was added to the thickness of the Beverly Unit sand represented by model layer 3 because its thickness is low except in critical recharge areas where it directly overlies the Beverly sand. The Wadsworth Sand Unit is also extensively dewatered naturally and is rarely, if ever, used for water-supply purposes within the local domain. The unit is almost completely absent from Kane County, its distribution being almost entirely limited to the eastern portion of the local domain in Cook, DuPage, and Lake Counties.

Unlike layers 1, 2, and 3, the remaining layers in the local-scale model are not aggregations of hydrostratigraphic units. Layers 4 through 9 represent the Yorkville Diamicton Unit downward through the Ashmore Unit, each model layer representing a single hydrostratigraphic unit. Layers 10 through 14 represent the five alternating fine- and coarse-grained layers of the Glasford Unit as modeled by Dey et al. (2007e). To reflect the dominant lithology present, layers 10 through 14 are termed, respectively, the Upper Glasford Diamicton Unit, Upper Glasford Sand Unit, Middle Glasford Diamicton Unit, Lower Glasford Sand Unit, and Lower Glasford Diamicton Unit (Figure 27). Layer 15 is a uniformly thick 50-ft layer representing the Shallow Bedrock Aquifer.

2.2.2. Geologic Framework

2.2.2.1. Regional-Scale Model

This section summarizes the procedure for developing the geologic framework of the regional groundwater flow model. Refer to Appendix C for a detailed discussion of the development of the model geologic framework. The geologic framework refers to the complete set of estimated elevations defining the tops and bottoms of the hydrostratigraphic units included in the regional model. These elevations were estimated for each active cell in the regional model grid (Figure 23). GIS methods were employed extensively to develop the geologic framework.

Time and cost constraints required that the regional geologic framework be developed from secondary sources, primarily published and unpublished hardcopy maps showing the structure and thickness of lithostratigraphic units recognized in the region, and not primary point data, such as well logs.

The geologic framework of the regional model differs from a standard geologic model in two significant ways. First, elevation estimates are based on the irregular finite-difference flow-modeling grid, which has small cells in a nearfield covering northeastern Illinois and progressively larger cells in all directions outward from the model nearfield, with the largest cells along the model margins (Figure 23). A geologic model developed for most other purposes generally includes elevation estimates based on a regular, evenly-spaced network of nodes. The geologic framework of the regional model is, in fact, based on an irregular-grid geologic model of the regional model domain, which is a set of 12

HYDROSTRATIGRAPHIC UNIT		MODEL LAYER
Soils developed on silts and diamictons		1*
Surficial Henry Unit		
Wadsworth Diamicton Unit		2
Haeger Diamicton Unit		
Wadsworth Sand Unit		3
Beverly Unit		
Yorkville Diamicton Unit		4
Yorkville Sand Unit		5
Batestown Diamicton Unit		6
Batestown Sand Unit		7
Tiskilwa Unit		8
Ashmore Unit		9
Glasford Unit	Upper Glasford Diamicton Unit	10
	Upper Glasford Sand Unit	11
	Middle Glasford Diamicton Unit	12
	Lower Glasford Sand Unit	13
	Lower Glasford Diamicton Unit	14
Shallow Bedrock Aquifer		15

Figure 27. Layer scheme of local-scale shallow model.

polygon-feature ArcGIS shapefiles containing estimates, for each finite-difference cell, of the top elevation of the 11 hydrostratigraphic units and the bottom elevation of the Mt. Simon Unit (Figure 19). Second, since the finite-difference approach requires all layers to be continuous across the entire model domain, even in areas of real-world absence, the model includes an estimate of top elevation of all units in all model cells even though a unit might be absent from an area in the real world. For most hydrostratigraphic units defined for this project, the thickness in an area of absence is 1 foot.

The irregular-grid geologic model was developed for the active cells of the regional groundwater flow model (Figure 23) from a high-resolution geologic model generated for a regular grid having a grid-node spacing of 2500 ft. The node spacing of the high-resolution geologic model was selected because it is identical to the grid-node spacing of the highest resolution portion of the irregular, model-resolution geological model grid. The high-resolution geologic model is a set of 12 point-feature ArcGIS shapefiles containing estimates, for each in the high-resolution grid, of the top elevation of the 11 hydrostratigraphic units and the bottom elevation of the Mt. Simon Unit. Each of these point-shapefiles is referred to in this report as a high-resolution surface model. Each high-resolution surface model was produced by interpolation of point-estimates of the top elevation of the unit, derived from a variety of sources, followed by post-processing of the interpolation results.

As mentioned previously, the irregular-grid geologic model consists of 12 polygon-shapefiles depicting the top elevation of each of the 11 hydrostratigraphic units together with the bottom elevation of the Mt. Simon Unit. The shapefile depicting the elevation of any one of these surfaces—referred to in this report as an irregular-grid surface model—was developed from the high-resolution surface model of the corresponding surface by averaging the elevation estimates of the high-resolution surface model located within each finite-difference cell. Post-processing of these average values permitted each hydrostratigraphic unit to be subdivided into two, three, or four model layers, if necessary, (Figure 25) and allowed these layers to be assigned a minimum thickness of 1 ft in areas of real-world absence of the hydrostratigraphic unit.

2.2.2.2. Local-Scale Shallow Model

The geologic framework of the local-scale model was developed from a geologic model supplied by the ISGS and described by Dey et al. (2007e). The geological data provided by the ISGS consists of top elevations of the model layers illustrated in Figure 27 for the domain illustrated in Figure 26. Elevation data were supplied for locations spaced 660 ft apart corresponding to the centers of grid cells as described in Section 2.2.1.2. Several alterations of the top-elevation data provided by the ISGS were required in order to adapt the geological model for groundwater flow simulation.

Land surface elevations were derived by the ISGS from digital elevation models. Along the major streams with specified river boundary conditions, land surface elevations were manually adjusted to reflect the surface-water elevation shown on the USGS topographic maps.

As described previously (Section 2.2.1.2), although not separately identified and characterized as such by the ISGS, the uppermost portion of the ISGS-provided geologic model was assigned to a surficial “soil layer” (layer 1) in the local-scale groundwater flow model.

The distributions of sand and gravel deposits as depicted in the ISGS geological model were simplified for adaptation as the local-scale groundwater flow model. This was accomplished by restricting the boundaries of model layers representing sand and gravel units (model layers 3, 5, 7, 9, 11, and 13) to areas where the represented unit is greater than 5 ft thick. Areas where these layers are less than 5 ft thick are represented as diamicton. While this simplification removes some areas of probable thin sand and gravel from representation as aquifers, it eliminates numerical problems that might arise from representation of thin, sporadically present, and conjectural sand and gravel deposits in the model.

Initially, to provide for the MODFLOW requirement of continuous model layers, a 1-ft thickness was specified to layers where the ISGS-provided data showed the represented hydrostratigraphic unit(s) to be absent. A similar approach was employed in developing the regional-scale model. To maintain overall thickness, the authors compensated for the additional foot of fictitious material required to represent layers in areas of absence by reducing the thickness of the underlying layer. Where multiple absent zones were stacked, the total correction was made to the nearest underlying layer(s) of sufficient thickness. As will be discussed (Section 2.2.3.2), the absent zones in each model layer were assigned the hydraulic conductivity of the nearest underlying layer having a thickness of 1 ft or more. This approach both satisfies the MODFLOW requirement of continuous model layers and, at the same time, maintains the hydraulic characteristics of the real-world sequence of materials.

To improve the convergence of the model and the representation of flow through thick diamicton units or thinly sandwiched sands, the thickness of adjacent units of like properties were equalized. As shown in Figure 28, cell thicknesses were adjusted upward by summing thicknesses of vertically adjacent layers assigned the same hydraulic conductivity and dividing this aggregate thickness by the number of layers represented. For example, in west-central Kane County the Beverly Unit, Yorkville Diamicton Unit, Yorkville Sand Unit, Batestown Diamicton Unit, and Batestown Sand Unit are all absent and the Tiskilwa Unit (layer 8) is present below the soil zone. Therefore model layers 3 through 7 were all initially assigned a thickness of 1 ft and given the hydraulic conductivity of model layer 8. If a cell in layer 8 is initially 103 ft thick, the adjusted thicknesses of layers 3 through 8 are $108 \div 6$, or 18 ft. None of these adjustments changed the transmissivity of the hydrostratigraphic units represented in the model.

Most of the manual adjustments to model layer elevations conducted by the authors were done to avoid having model cells desaturate in areas where the surficial sand or one of the lower sand or bedrock layers are either naturally dry or only partially saturated. These dry areas occur throughout the model area but are especially concentrated along the Fox River valley where there are sand layers above the elevation of the stream. Dry cells cause two significant problems for finite-difference groundwater flow models developed with MODFLOW: (1) if the dry cell is below an active layer, it will act as a no-flow boundary and not allow any further downward infiltration of water; (2) when the model is running, the model solver may continually try to resaturate these cells and greatly increase the number of iterations necessary to achieve convergence. Dry cells were eliminated by lowering the bottom elevation of the cell to below the water table elevation calculated for the underlying unit. In the lower layers of the model, the problem areas were generally in cells representing diamictons overlying partially

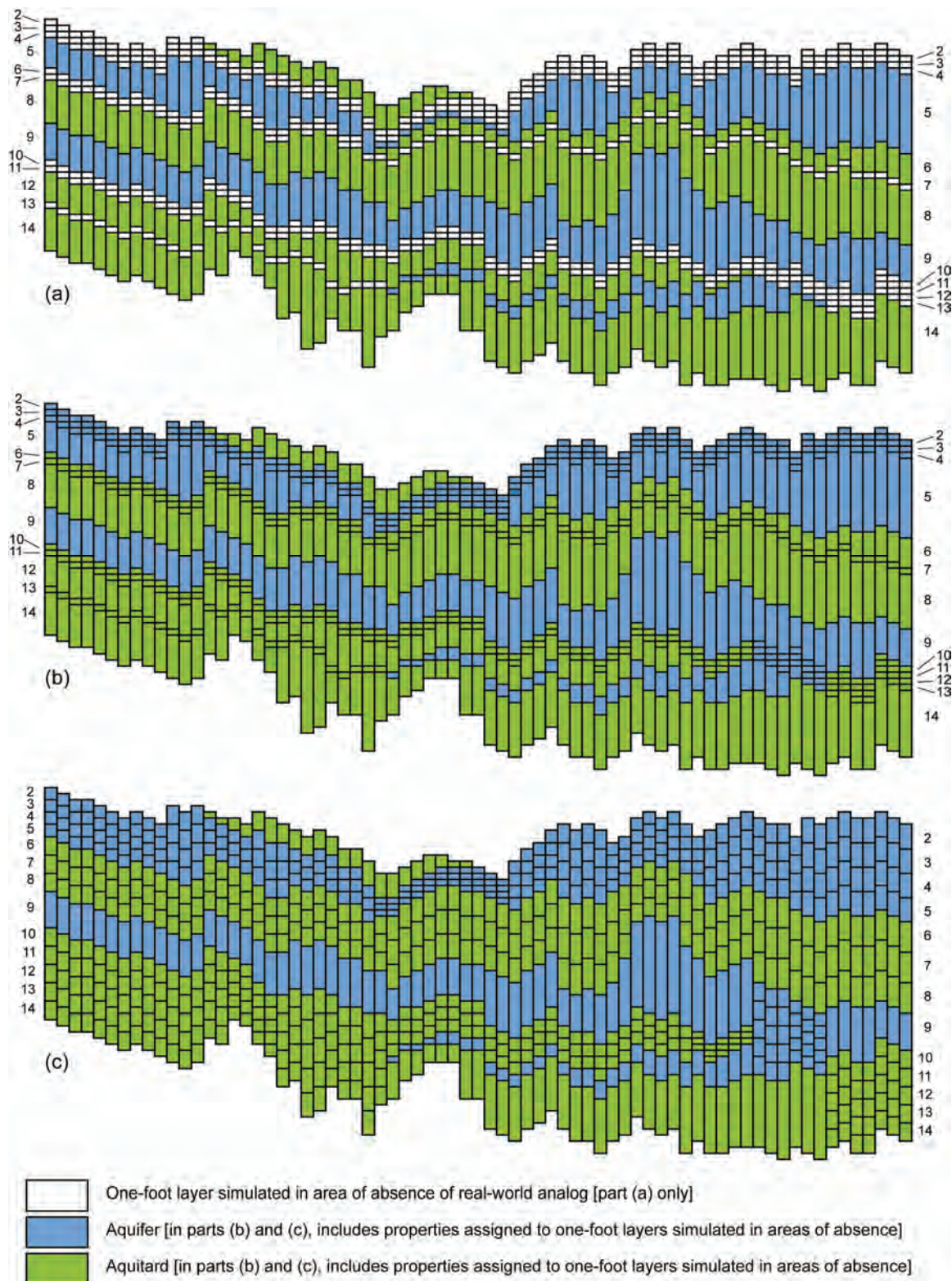


Figure 28. Hypothetical cross section of local model layers 2 through 14 showing modification of layer thicknesses to reduce presence of thin layers in local-scale model.

saturated sands. The conductivities of thin, dry sands along the hill slopes were changed to diamicton to keep the layer saturated. Together, these changes cause the thickness of aquifer material to be less than the observed thickness; however, the saturated transmissivity of the aquifers remains virtually unchanged.

2.2.3. Hydraulic Conductivity (K)

Groundwater models require estimates of horizontal and vertical hydraulic conductivity (K_h and K_v , respectively) of all modeled units in each model domain. In this study, zones of hydraulic conductivity are assigned to model layers to represent large-scale changes in K that reflect differences in weathering, lithology, texture, and depth of burial. Estimates of K_h , K_v , and the anisotropy ratio (K_h/K_v)—and the plausible range of each—were developed for each zone as an initial step in the calibration process. During calibration (Section 2.3), these estimates were changed within the plausible ranges to improve the accuracy of the simulations. The single-value estimates of K_h , K_v , and K_h/K_v that are selected to begin the calibration process are called *starting* or *initial values*, and the values selected through the calibration process are called *calibrated values*. In this study, the anisotropy ratio K_h/K_v was sometimes used for initial estimates of K_h —where K_v was to be based on published estimates—and visa versa.

2.2.3.1. Regional-Scale Model

Starting K values, plausible ranges, and K_h/K_v values for layers in the regional model are based to the extent possible on published and unpublished studies describing the lithology and hydraulic characteristics of the modeled units (Figure 29 through Figure 48 and Table 4). Final, calibrated values of K are shown in Table 14 (Section 2.3.1.3). Note that the zonation of K employs zone numbers simply as identifiers, with no quantitative significance, and the zone numbers appearing in Figure 29 through Figure 48, and in Table 4, do not form a complete sequence from zone 1 to zone 47, since many zone numbers were employed in the model-development process that were later dropped. Note that in areas of absence, model layers are set to a thickness of 1 foot, and the K -zonation in these areas is equivalent to the zonation of the underlying unit. For clarity, K -zonation of areas of absence is not shown in Figure 29 through Figure 48. Figure 49 and Figure 50 show the hydraulic conductivity zonation of the regional model along the lines of section illustrated in Figure 15.

Observations of K on which to base assumed values of K are distributed irregularly. Zonations used in previous modeling studies (Feinstein et al., 2005a; Feinstein et al., 2005b; Mandle and Kontis, 1992; Weaver and Bahr, 1991a; Weaver and Bahr, 1991b) were heavily employed, but differences in layer definitions and model domains sometimes hampered use of these zonation data. For some layers, in some areas, no observations of K are available, so assumed values are founded on estimates based on gross lithology published in widely-accepted textbooks. In other such cases, assumed hydraulic conductivities are based on other zones having similar lithology. For example, zone 31 (layer 13) (Figure 36)—representing weathered dolomites of the Prairie du Chien-Eminence Unit, for which observations of K are not available—is assumed to have the same hydraulic conductivities as zone 23 (layers 10 and 11) (Figure 38 and Figure 39), which represents weathered dolomites of the Galena-Platteville Unit.

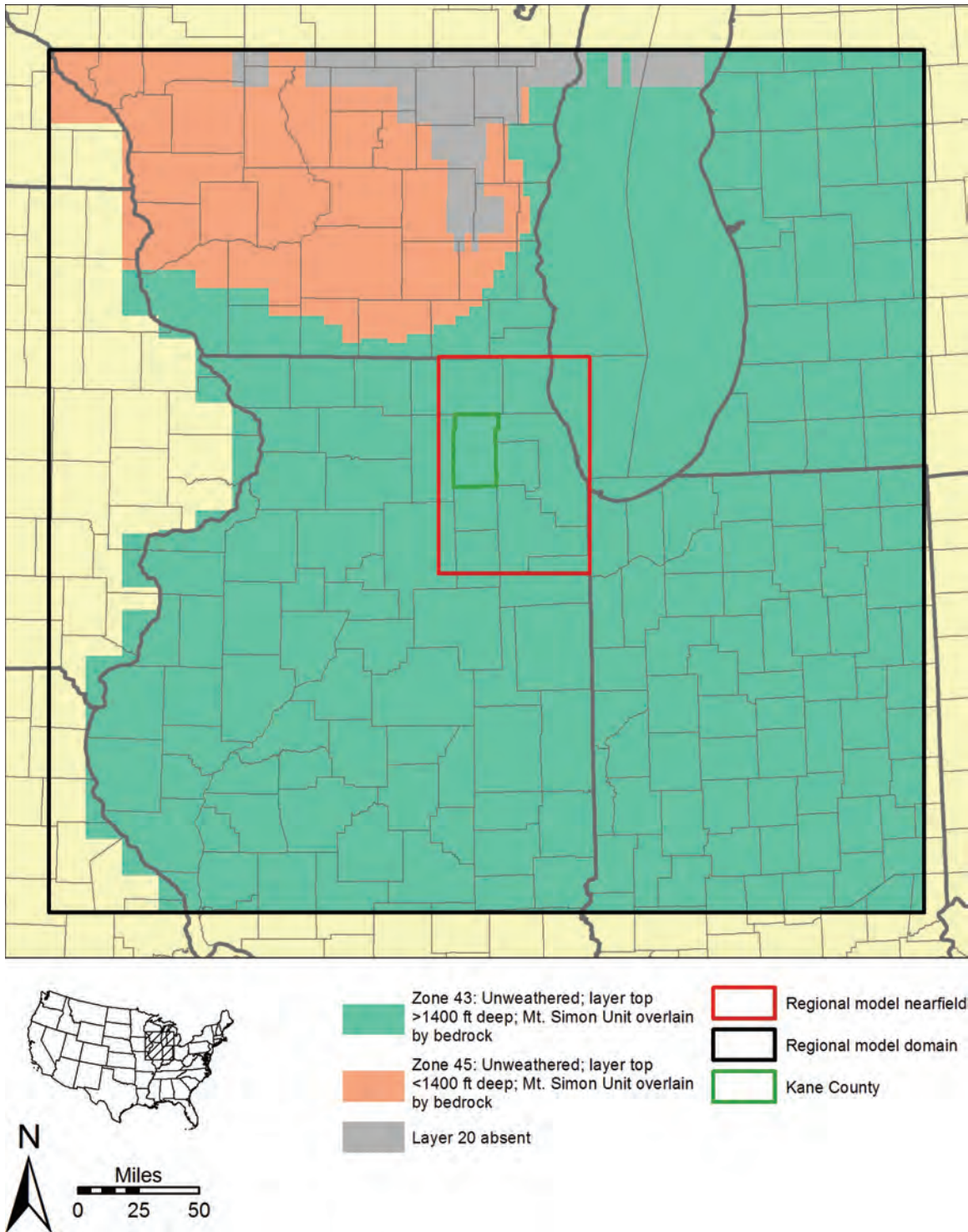


Figure 29. Hydraulic conductivity zonation of regional model layer 20. See Table 4 (pages 94 through 97) for assumed plausible ranges and starting values for calibration for each zone.

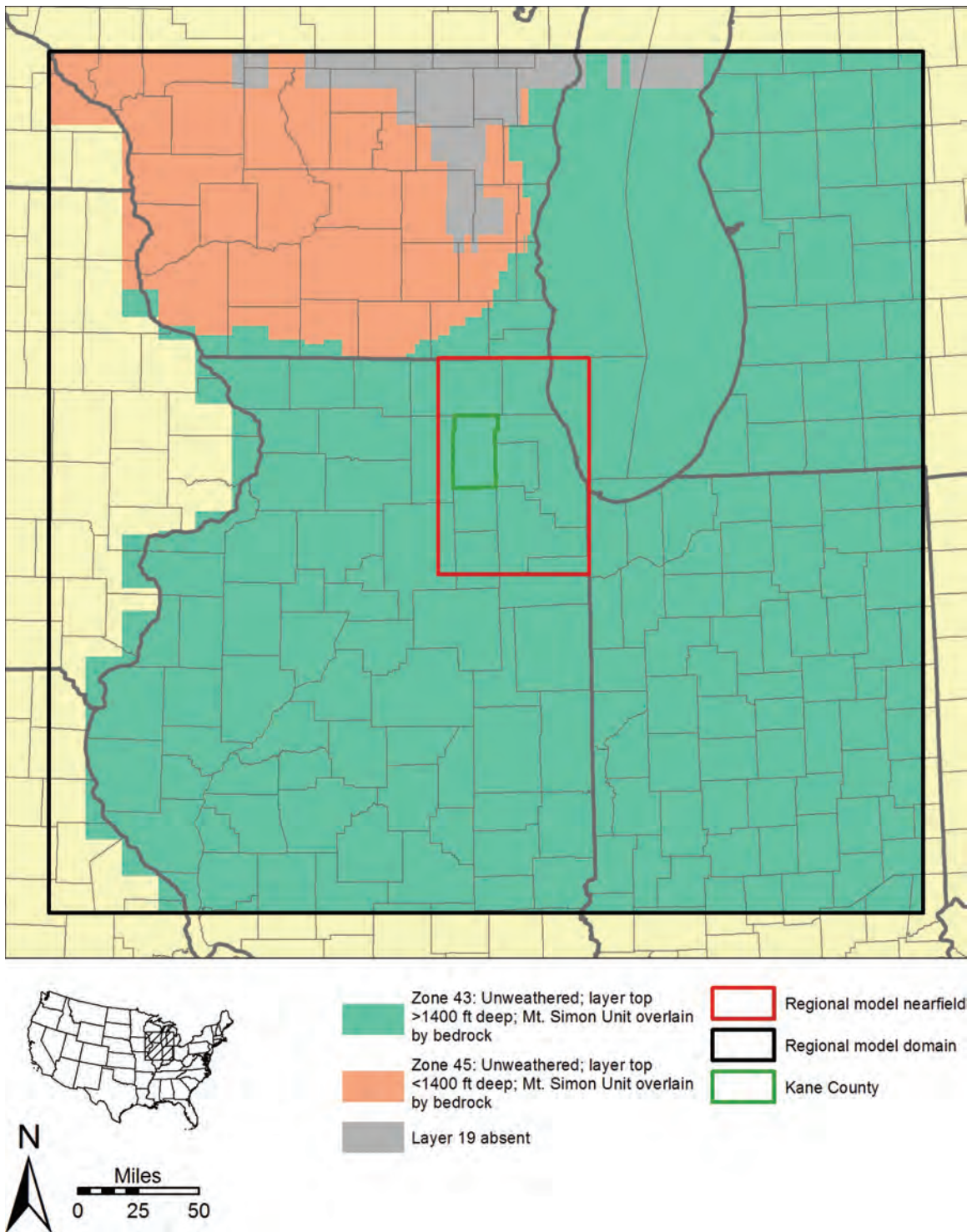


Figure 30. Hydraulic conductivity zonation of regional model layer 19. See Table 4 (pages 94 through 97) for assumed plausible ranges and starting values for calibration for each zone.

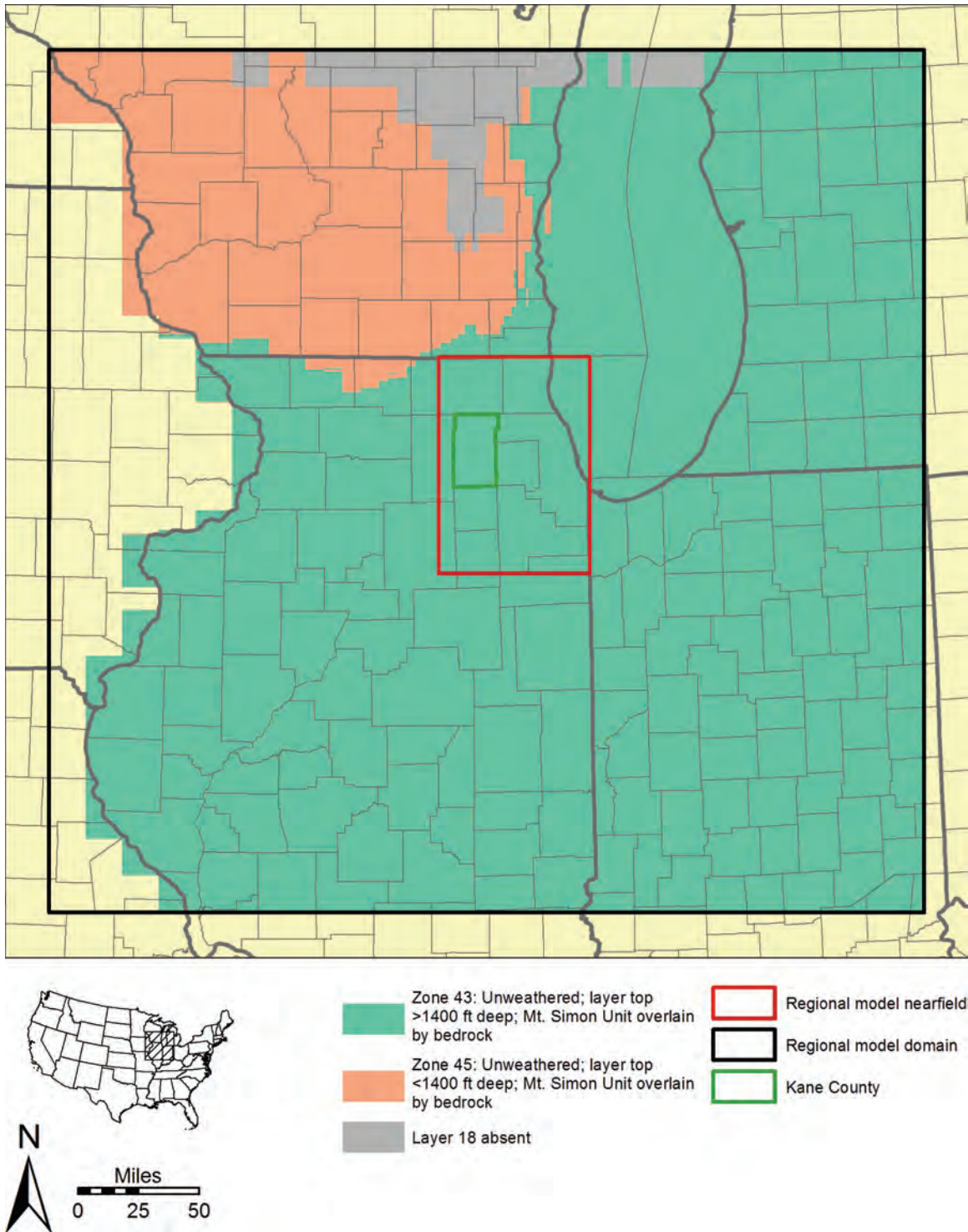


Figure 31. Hydraulic conductivity zonation of regional model layer 18. See Table 4 (pages 94 through 97) for assumed plausible ranges and starting values for calibration for each zone.

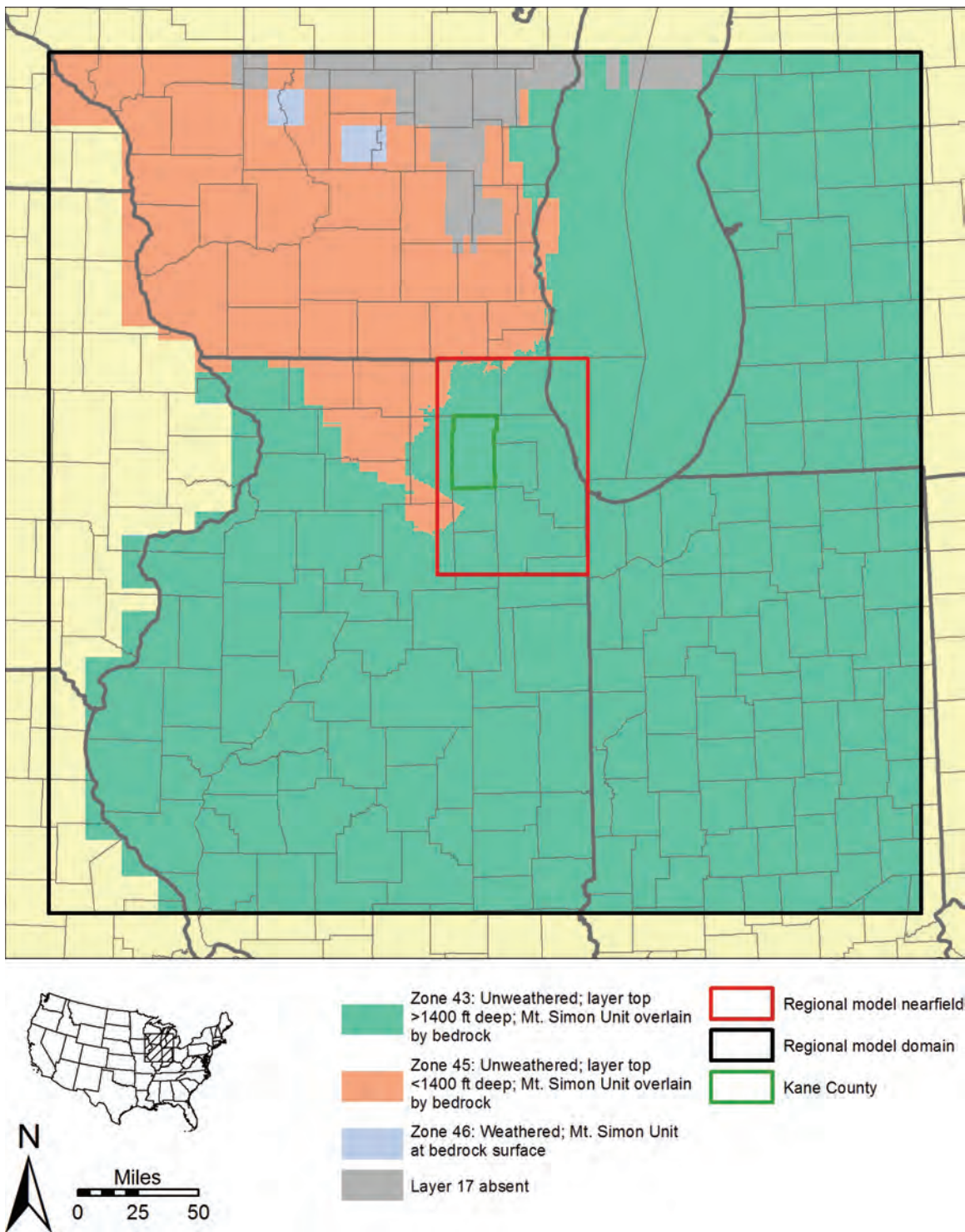


Figure 32. Hydraulic conductivity zonation of regional model layer 17. See Table 4 (pages 94 through 97) for assumed plausible ranges and starting values for calibration for each zone.

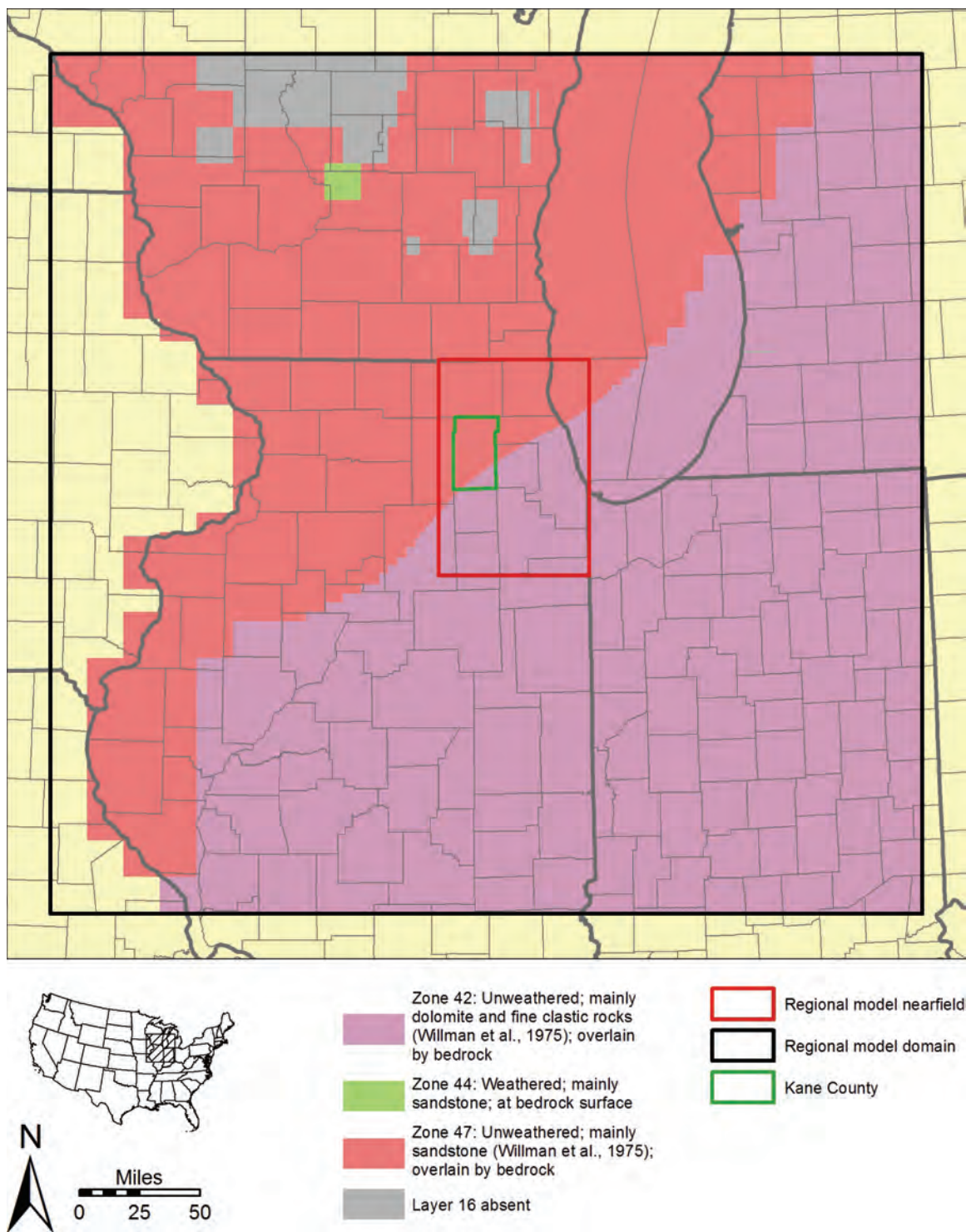


Figure 33. Hydraulic conductivity zonation of regional model layer 16. See Table 4 (pages 94 through 97) for assumed plausible ranges and starting values for calibration for each zone.

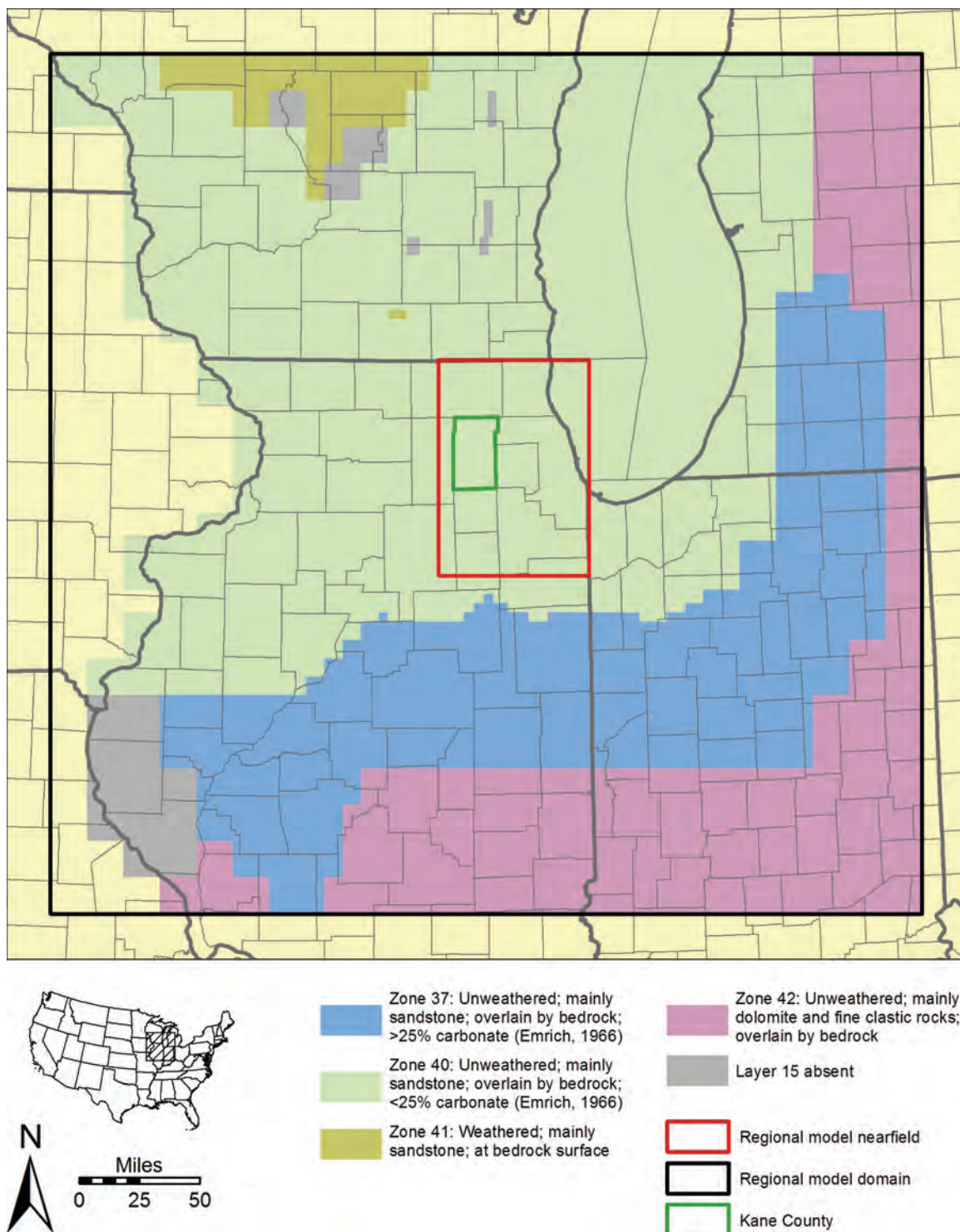


Figure 34. Hydraulic conductivity zonation of regional model layer 15. See Table 4 (pages 94 through 97) for assumed plausible ranges and starting values for calibration for each zone.

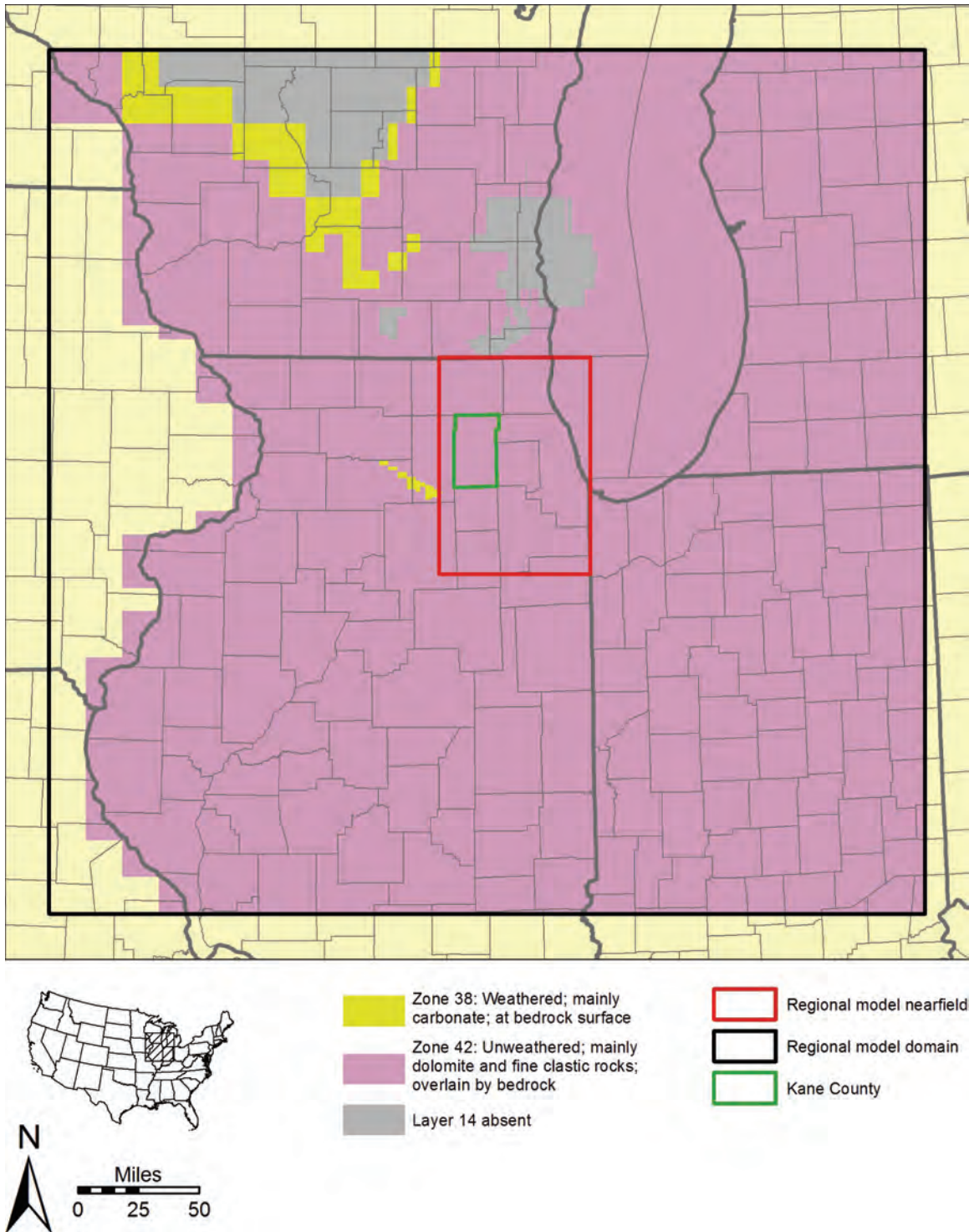


Figure 35. Hydraulic conductivity zonation of regional model layer 14. See Table 4 (pages 94 through 97) for assumed plausible ranges and starting values for calibration for each zone.

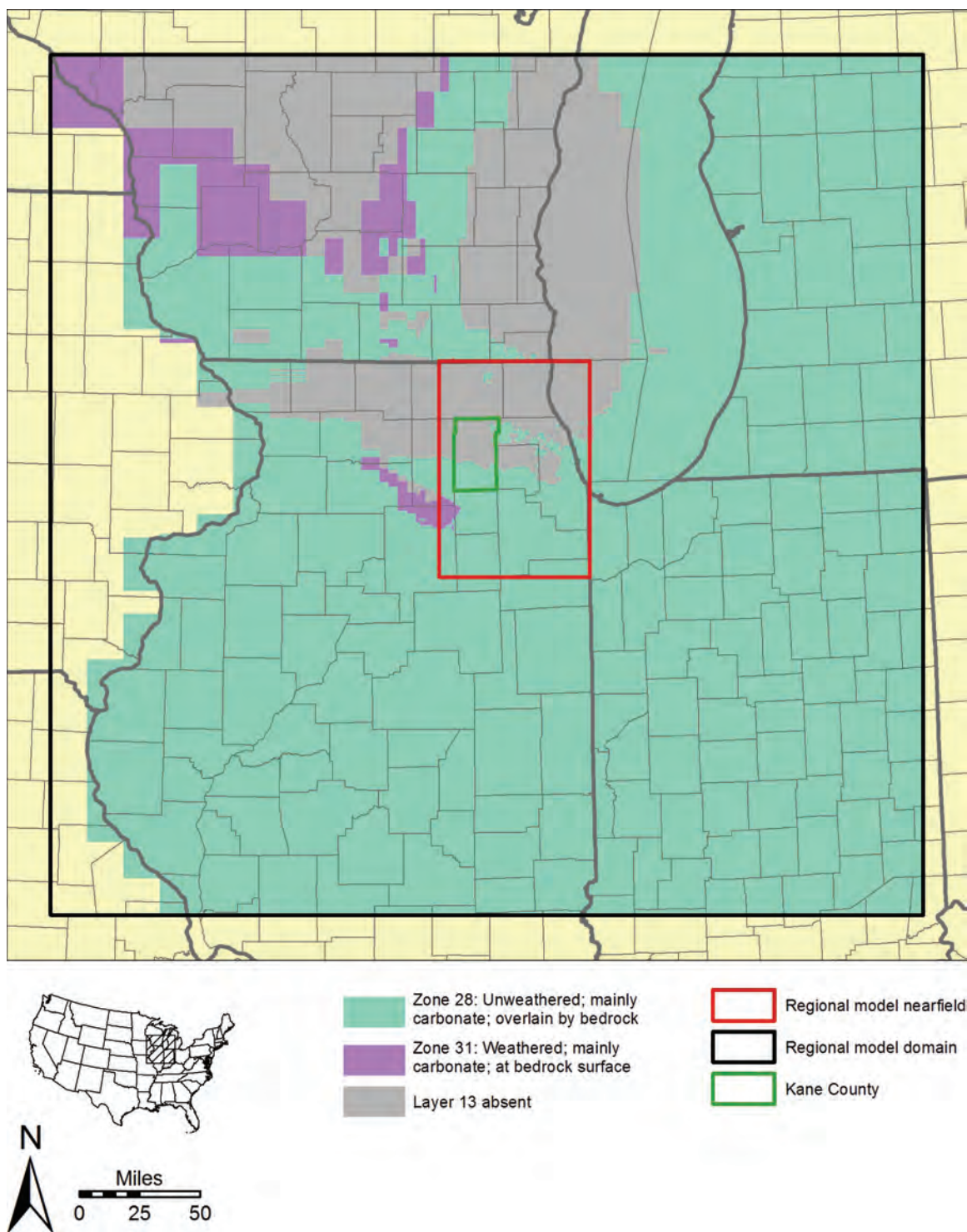


Figure 36. Hydraulic conductivity zonation of regional model layer 13. See Table 4 (pages 94 through 97) for assumed plausible ranges and starting values for calibration for each zone.

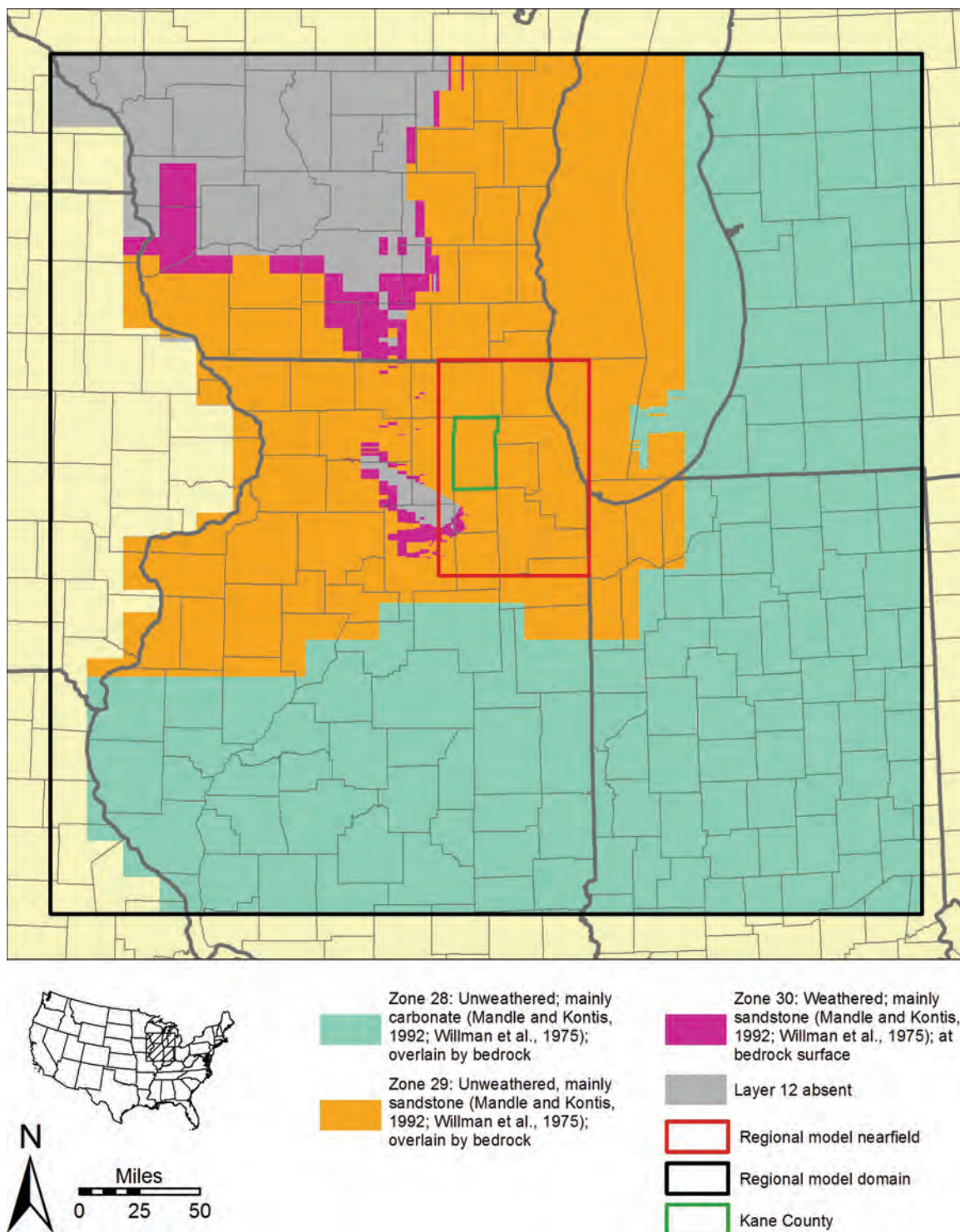


Figure 37. Hydraulic conductivity zonation of regional model layer 12. See Table 4 (pages 94 through 97) for assumed plausible ranges and starting values for calibration for each zone.

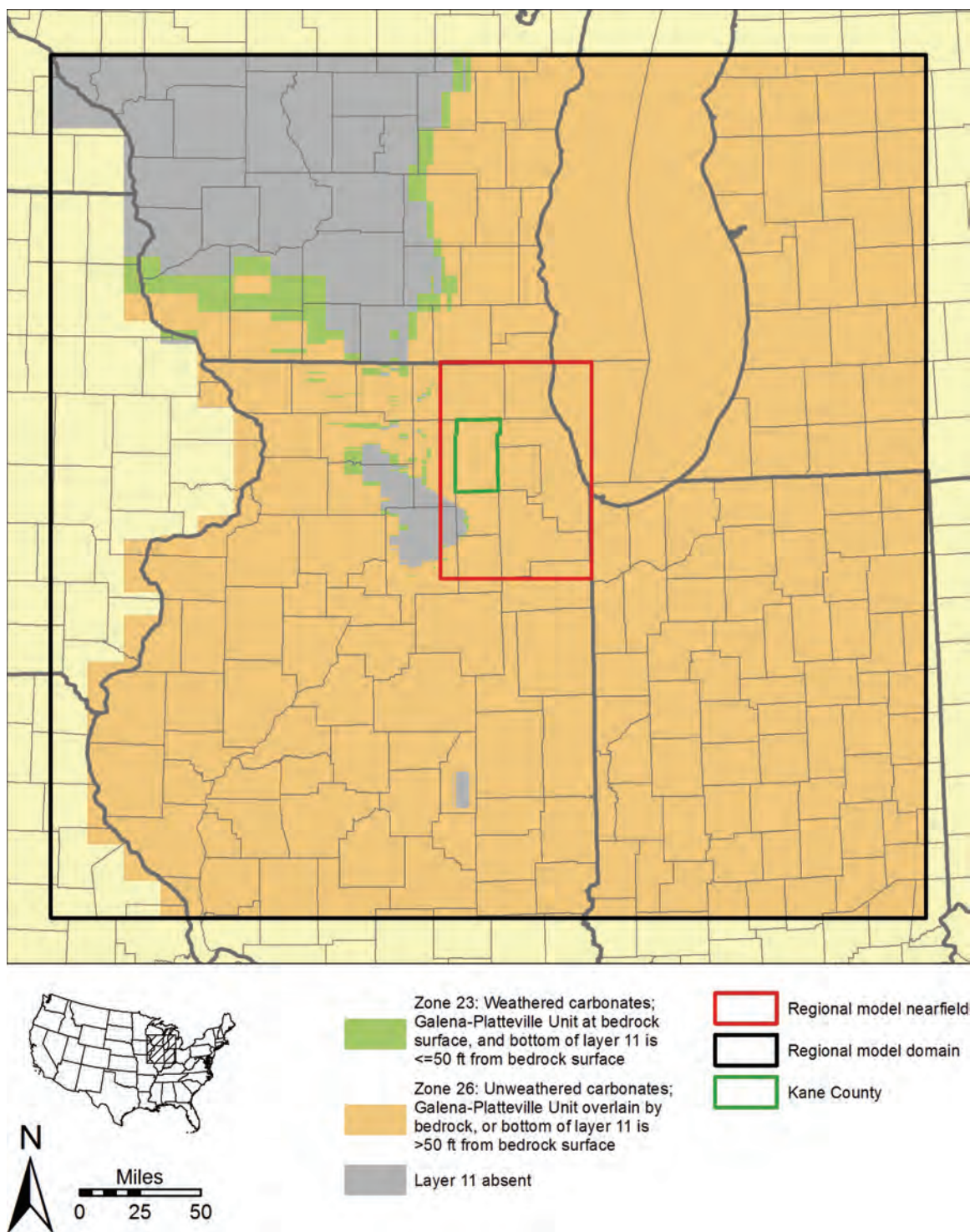


Figure 38. Hydraulic conductivity zonation of regional model layer 11. See Table 4 (pages 94 through 97) for assumed plausible ranges and starting values for calibration for each zone.

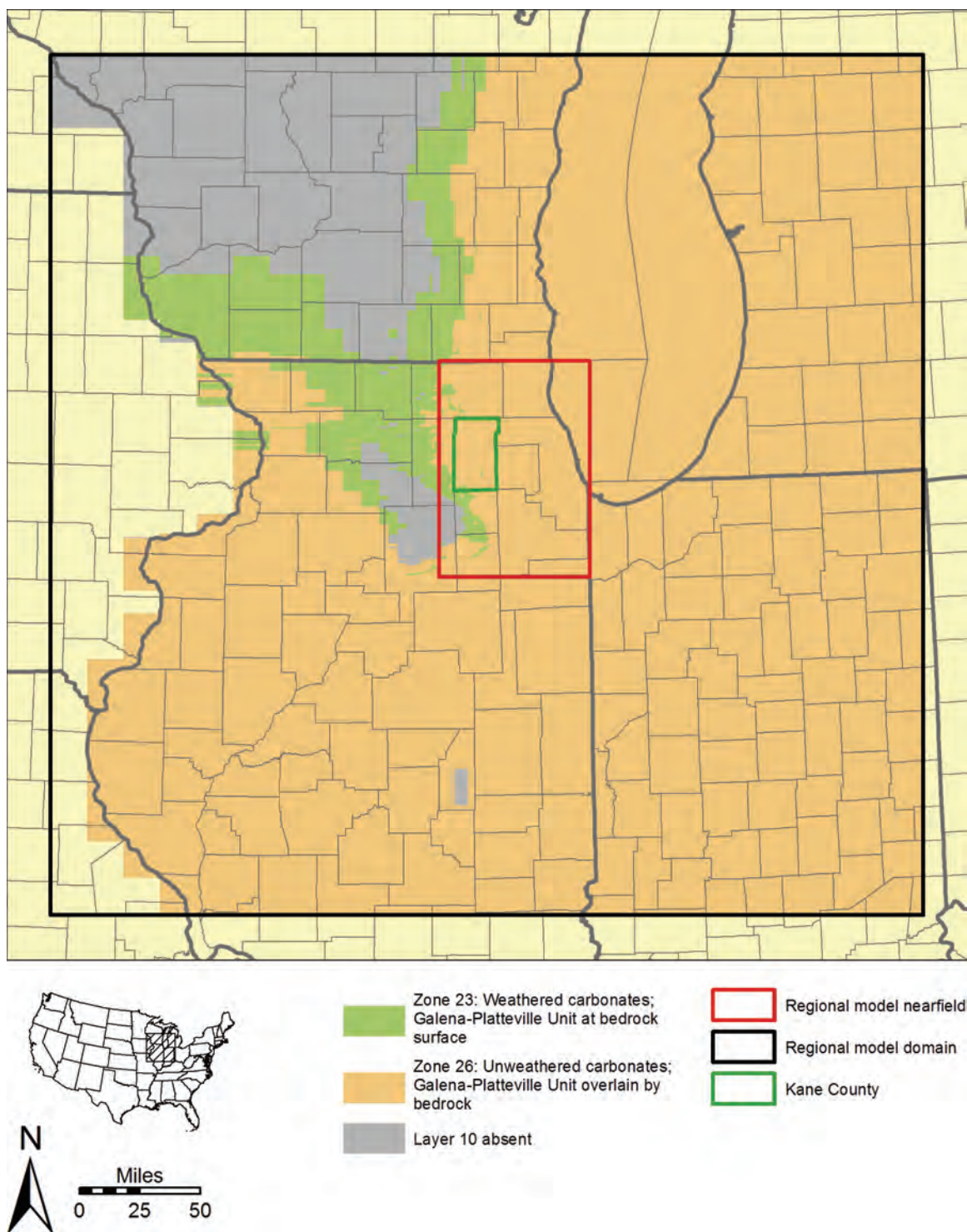


Figure 39. Hydraulic conductivity zonation of regional model layer 10. See Table 4 (pages 94 through 97) for assumed plausible ranges and starting values for calibration for each zone.

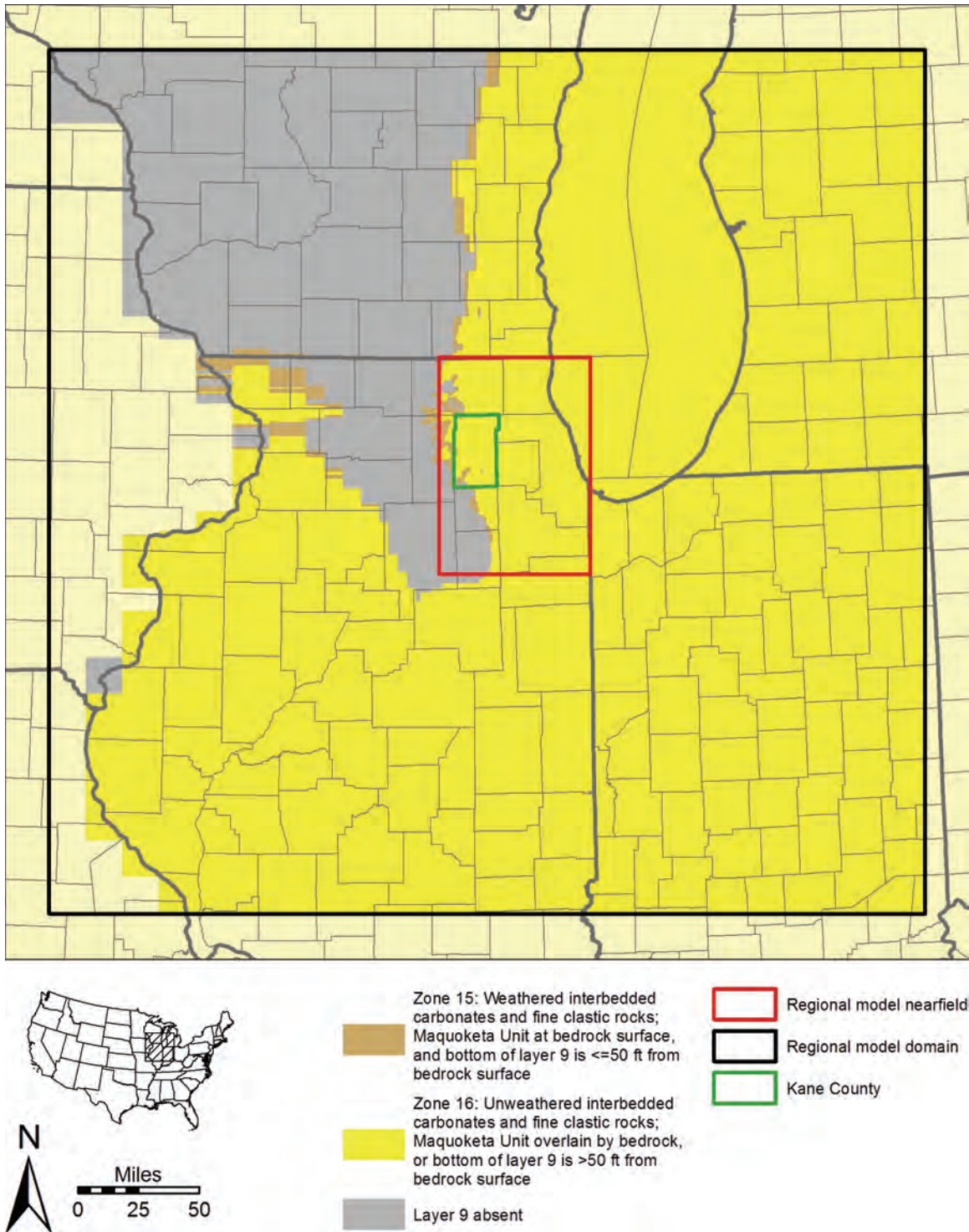


Figure 40. Hydraulic conductivity zonation of regional model layer 9. See Table 4 (pages 94 through 97) for assumed plausible ranges and starting values for calibration for each zone.

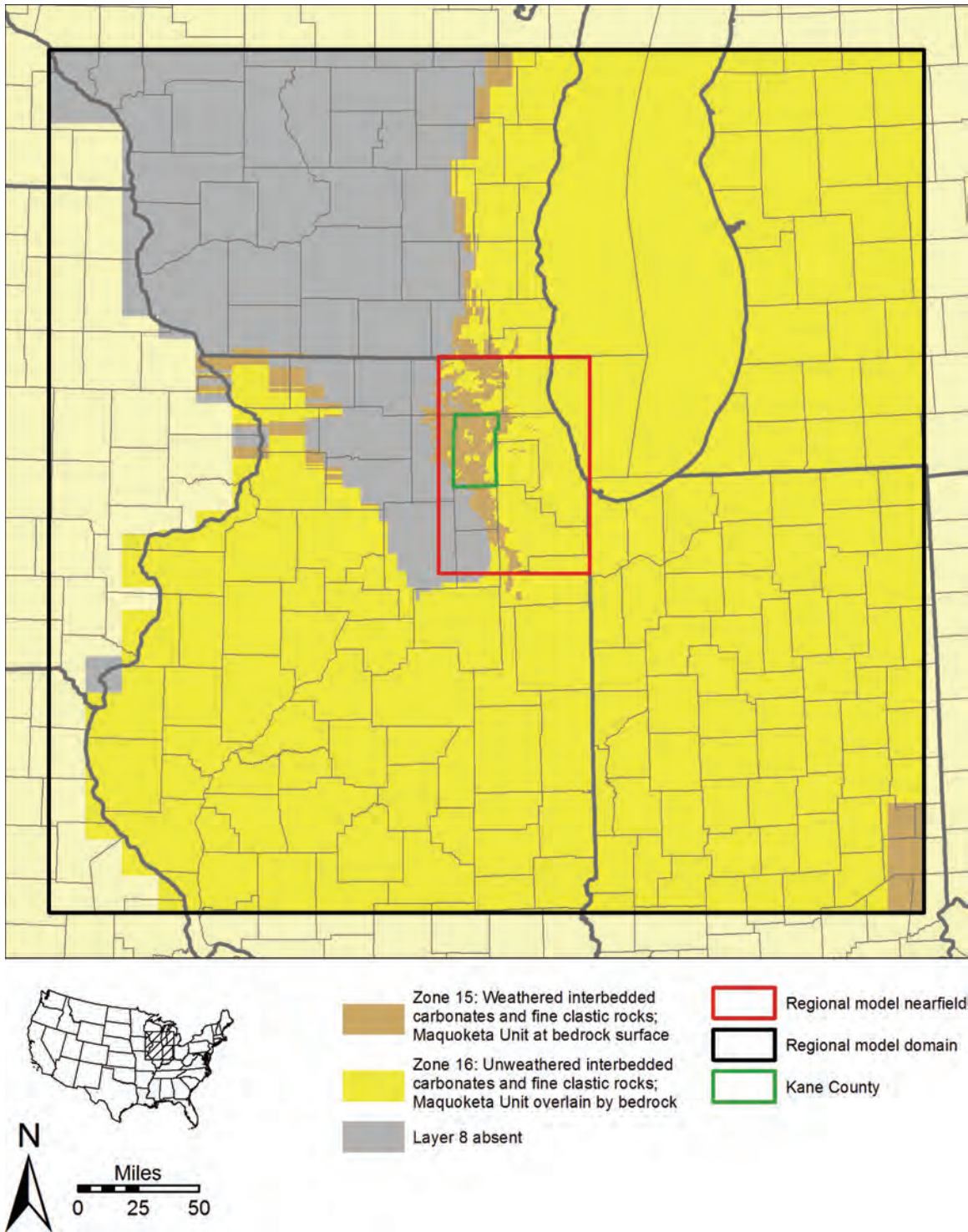


Figure 41. Hydraulic conductivity zonation of regional model layer 8. See Table 4 (pages 94 through 97) for assumed plausible ranges and starting values for calibration for each zone.

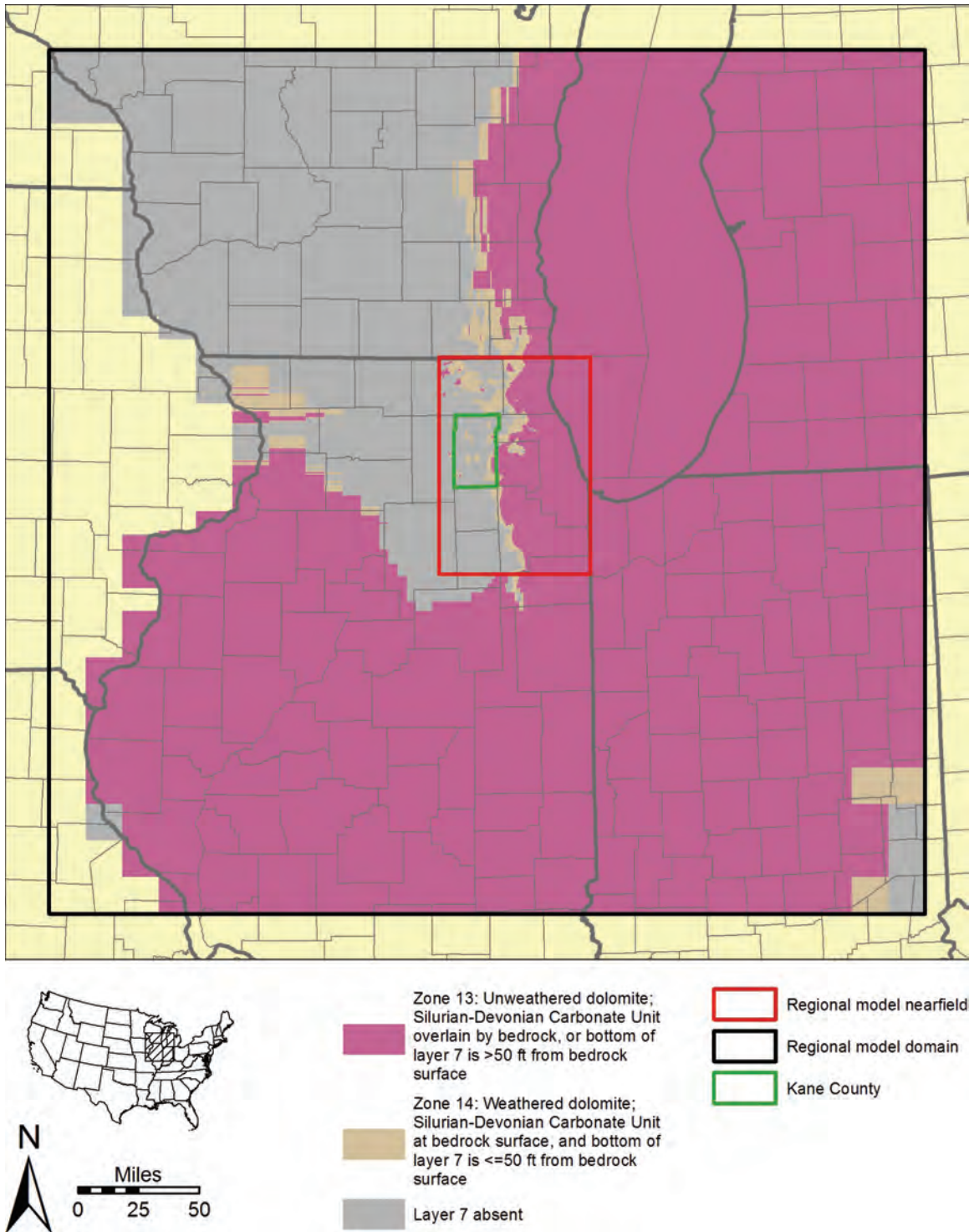


Figure 42. Hydraulic conductivity zonation of regional model layer 7. See Table 4 (pages 94 through 97) for assumed plausible ranges and starting values for calibration for each zone.

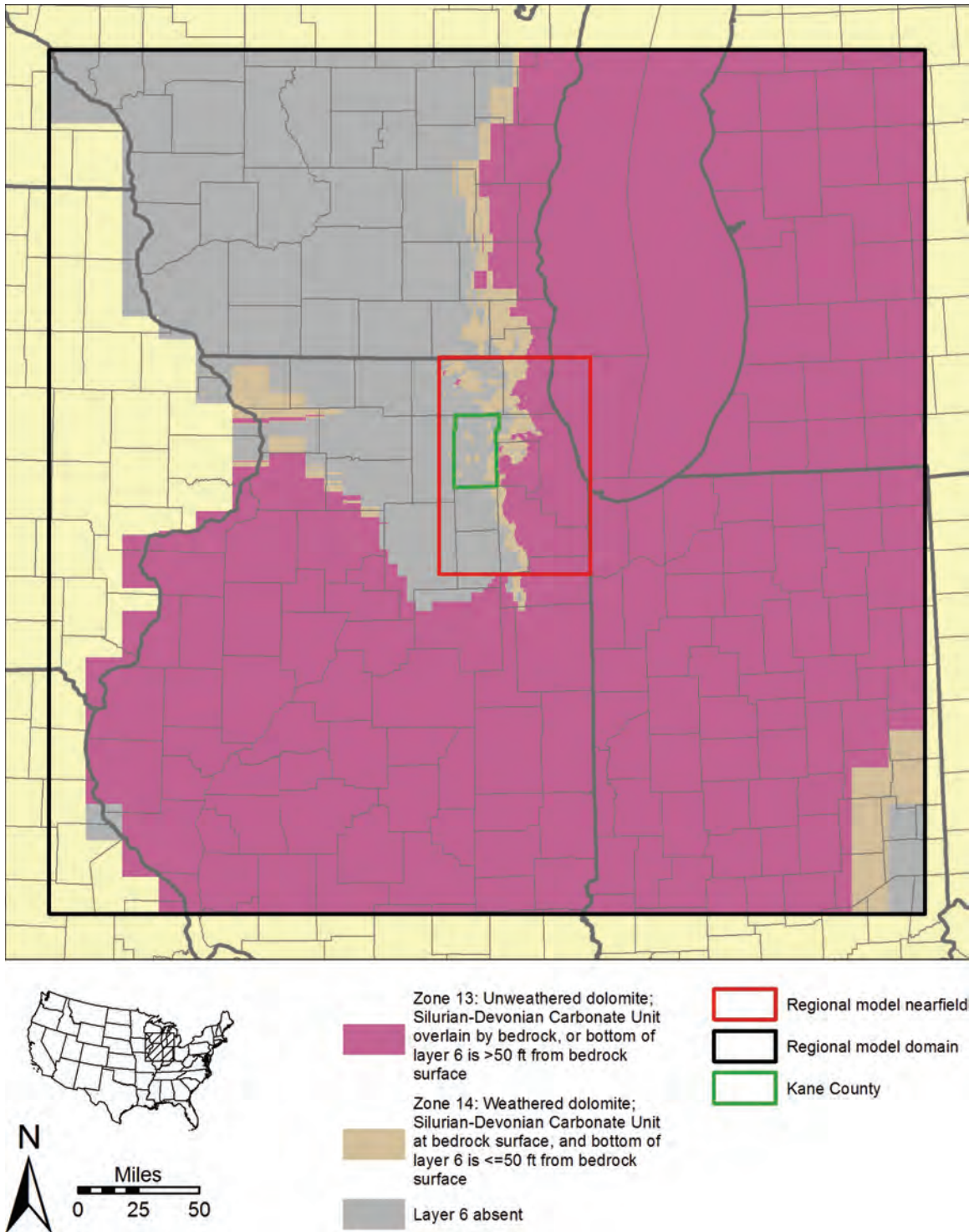


Figure 43. Hydraulic conductivity zonation of regional model layer 6. See Table 4 (pages 94 through 97) for assumed plausible ranges and starting values for calibration for each zone.

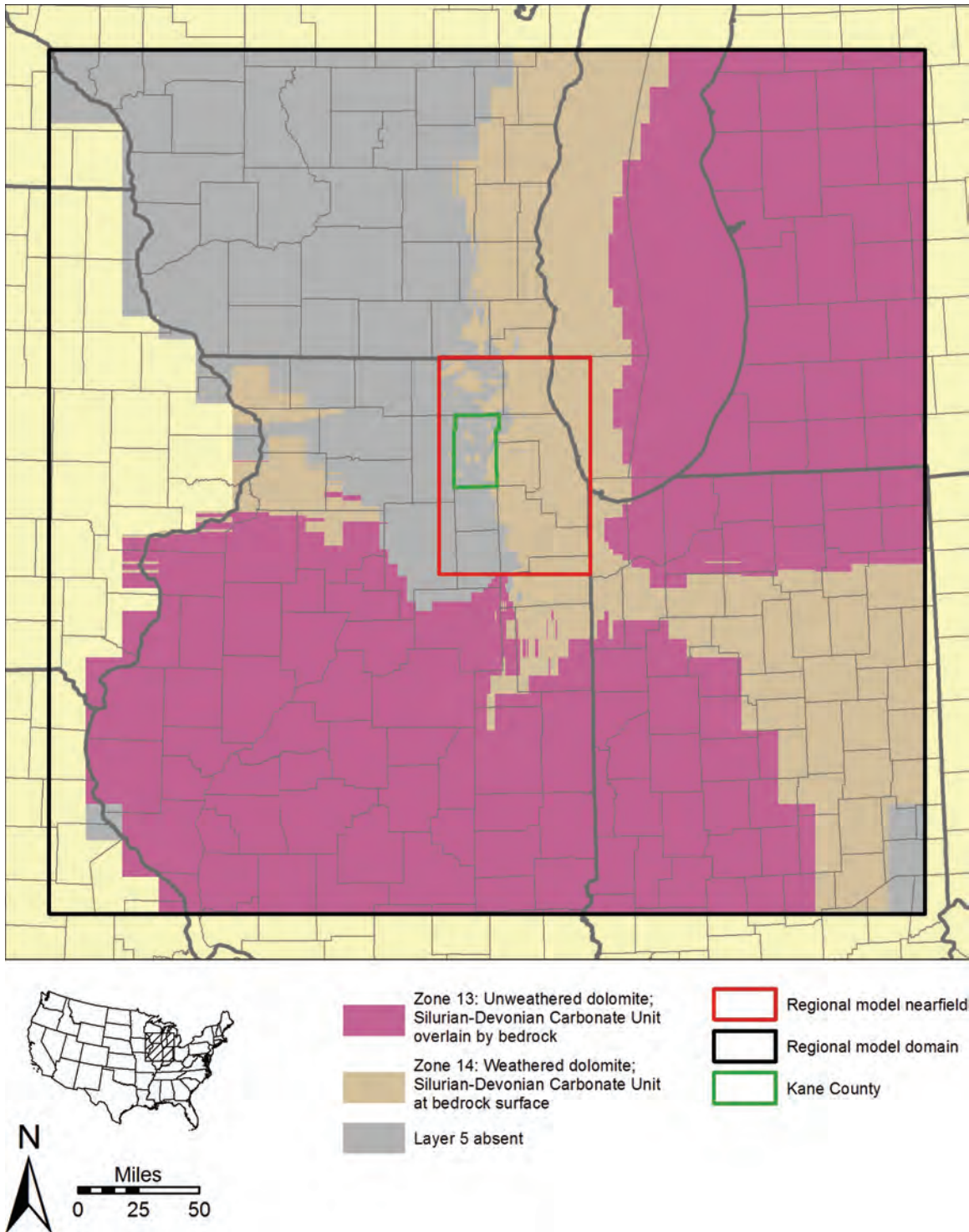


Figure 44. Hydraulic conductivity zonation of regional model layer 5. See Table 4 (pages 94 through 97) for assumed plausible ranges and starting values for calibration for each zone.

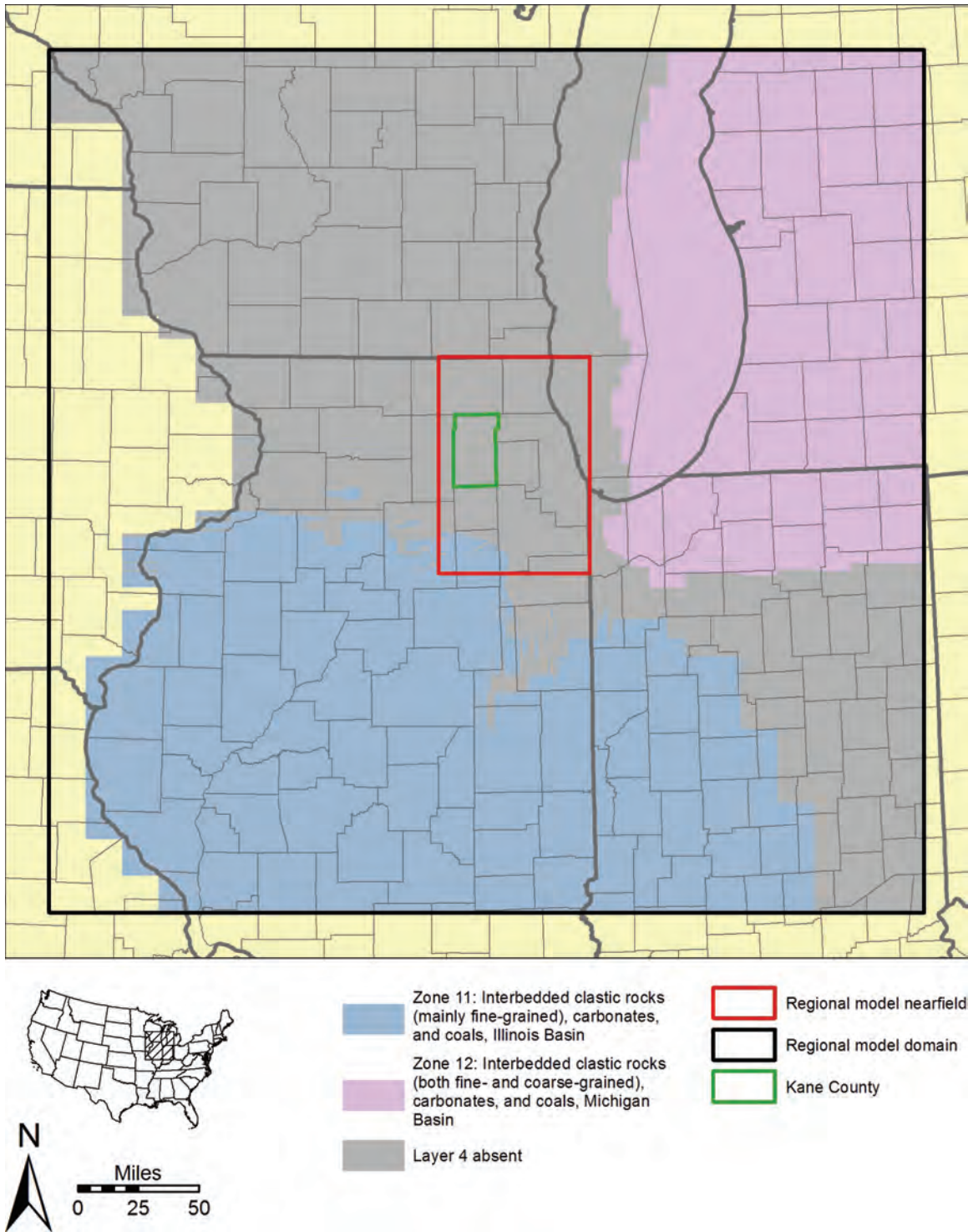


Figure 45. Hydraulic conductivity zonation of regional model layer 4. See Table 4 (pages 94 through 97) for assumed plausible ranges and starting values for calibration for each zone.

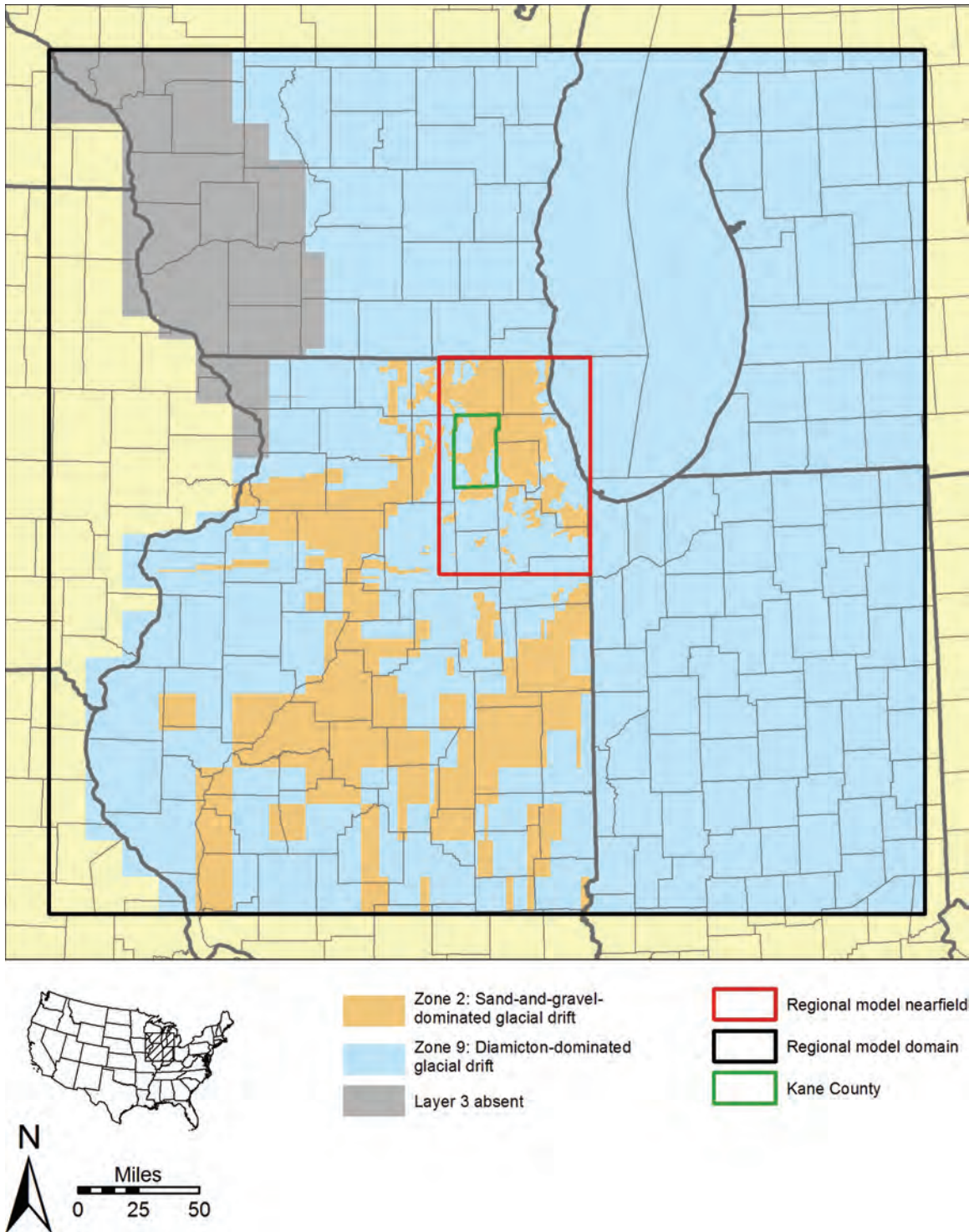


Figure 46. Hydraulic conductivity zonation of regional model layer 3. See Table 4 (pages 94 through 97) for assumed plausible ranges and starting values for calibration for each zone.

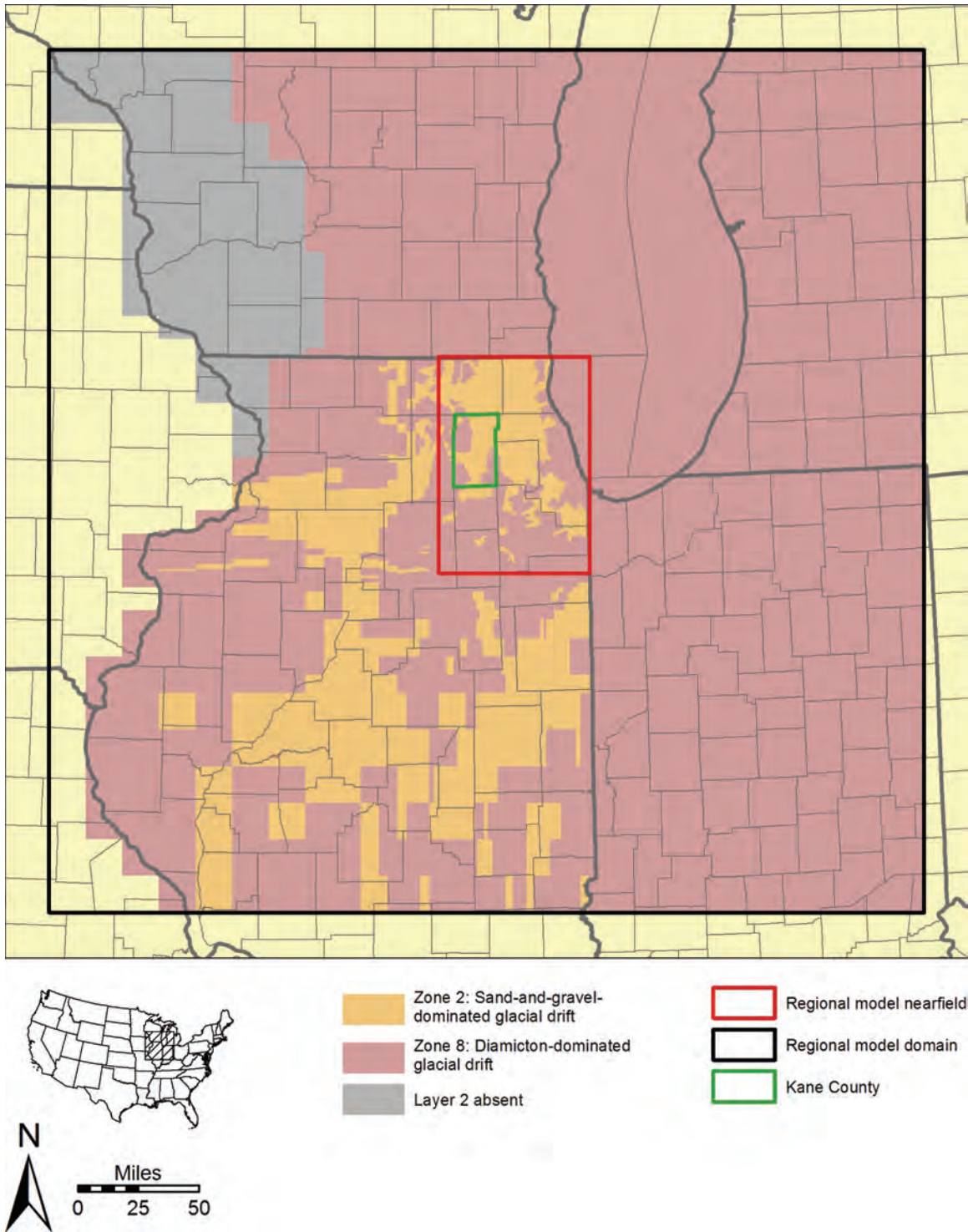


Figure 47. Hydraulic conductivity zonation of regional model layer 2. See Table 4 (pages 94 through 97) for assumed plausible ranges and starting values for calibration for each zone.

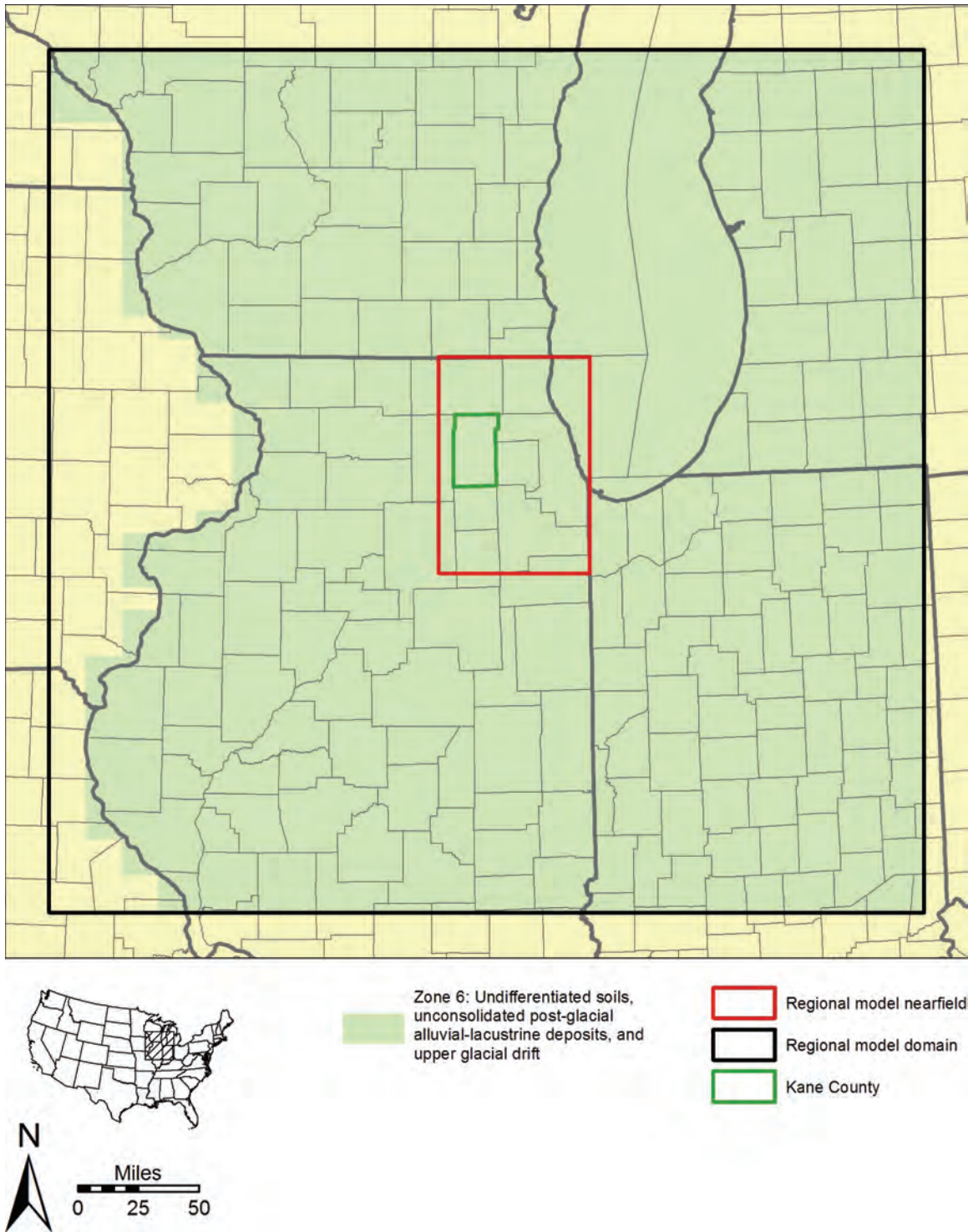


Figure 48. Hydraulic conductivity zonation of regional model layer 1. See Table 4 (pages 94 through 97) for assumed plausible range and starting value for calibration.

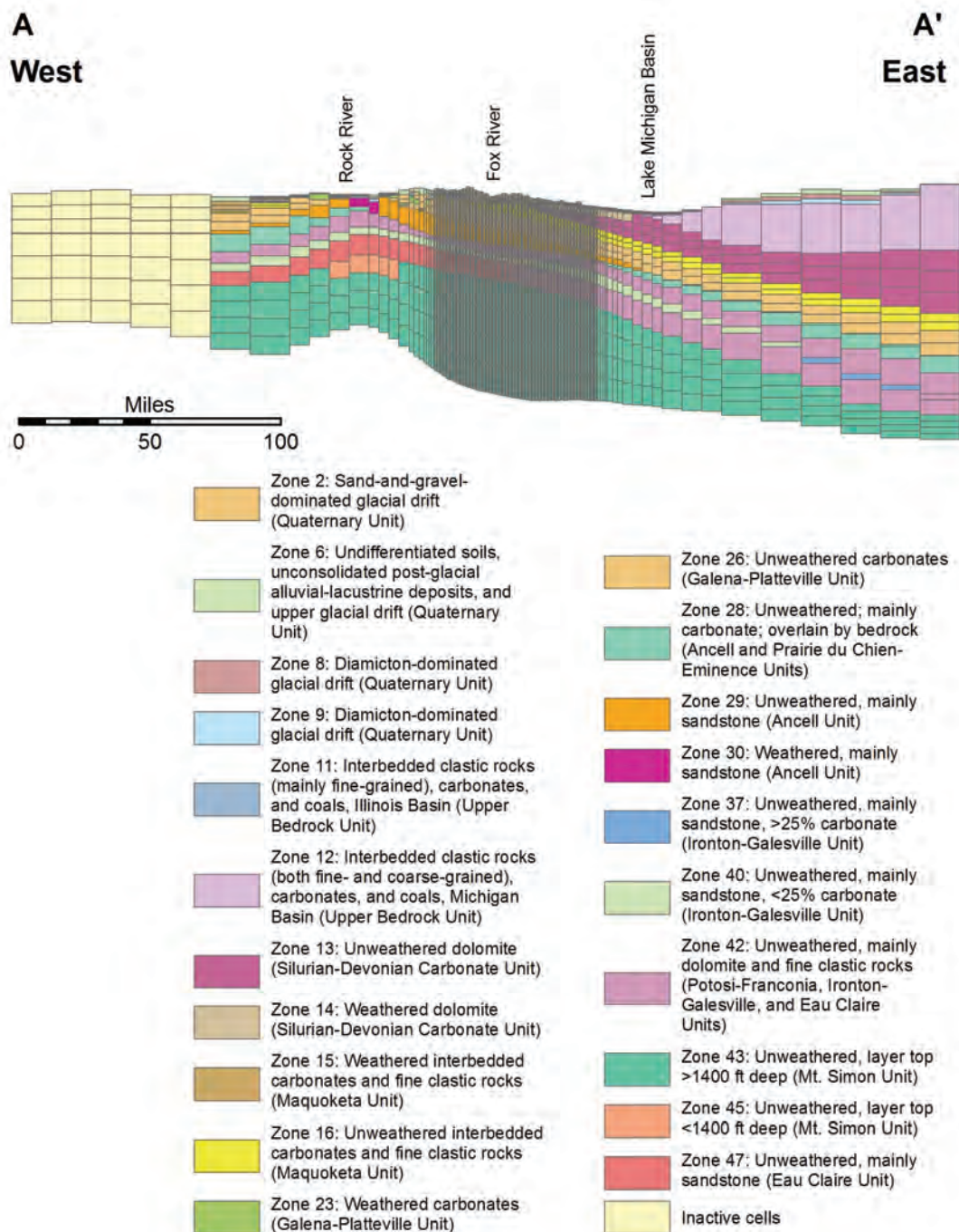


Figure 49. West-to-east cross section A-A' showing hydraulic conductivity zonation of regional-scale model in the model domain (see Figure 15 for cross section location).

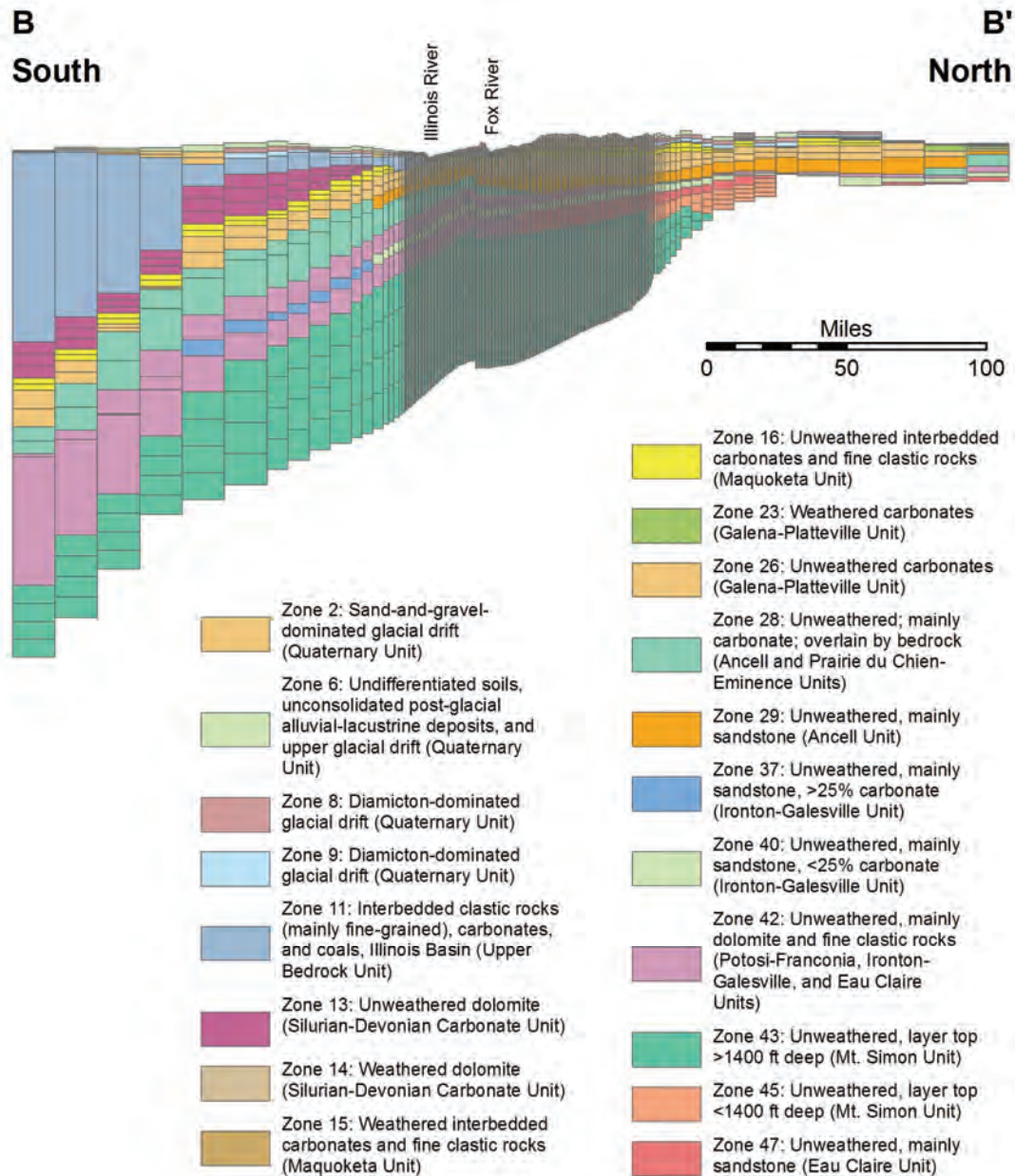


Figure 50. South-to-north cross section B'-B showing hydraulic conductivity zonation of regional-scale model in the model domain (see Figure 15 for cross section location).

Table 4. Hydraulic Conductivity Zonation of Regional-Scale Model

Zone	Description	Parameter	Starting Value	Range	References*
2	Sand and gravel-dominated glacial drift	K_h (ft/d)	1.4×10^2 ft/d	$1.0 \times 10^2 - 3.0 \times 10^2$ ft/d	2, 9, 14
		K_v (ft/d)	2.8×10^0 ft/d	$1.0 \times 10^0 - 6.0 \times 10^0$ ft/d	Estimated from K_h and K_{Iv}/K_v
		K_{Iv}/K_v	50	50 - 100	2, 14
6	Undifferentiated soils, unconsolidated post-glacial alluvial-lacustrine deposits, and upper glacial drift	K_h (ft/d)	1.6×10^0 ft/d	$1.0 \times 10^0 - 5.0 \times 10^0$ ft/d	2, 7
		K_v (ft/d)	1.6×10^{-2} ft/d	$5.9 \times 10^{-3} - 1.0 \times 10^{-1}$ ft/d	Estimated from K_h and K_{Iv}/K_v
		K_{Iv}/K_v	100	50 - 170	2, 3, 8
		K_h (ft/d)	5.0×10^0 ft/d	$1.0 \times 10^0 - 1.6 \times 10^1$ ft/d	2, 4, 7, 16
8	Diamicton-dominated glacial drift (layer 2)	K_v (ft/d)	5.0×10^{-2} ft/d	$5.9 \times 10^{-3} - 3.2 \times 10^{-1}$ ft/d	Estimated from K_h and K_{Iv}/K_v
		K_{Iv}/K_v	100	50 - 170	2, 8
		K_h (ft/d)	1.3×10^1 ft/d	$1.0 \times 10^0 - 1.6 \times 10^1$ ft/d	2, 3, 4, 7, 16
9	Diamicton-dominated glacial drift (layer 3)	K_v (ft/d)	1.3×10^{-1} ft/d	$5.9 \times 10^{-3} - 3.2 \times 10^{-1}$ ft/d	Estimated from K_h and K_{Iv}/K_v
		K_{Iv}/K_v	100	50 - 170	2, 3, 8
		K_h (ft/d)	2.2×10^{-4} ft/d	$1.3 \times 10^{-4} - 1.3 \times 10^{-3}$ ft/d	Estimated from K_v and K_{Iv}/K_v
11	Interbedded clastic rocks (mainly fine-grained), carbonates, and coals, Illinois Basin	K_v (ft/d)	2.2×10^{-6} ft/d	$1.3 \times 10^{-6} - 1.3 \times 10^{-5}$ ft/d	2, 5, 10
		K_{Iv}/K_v	100		6
		K_h (ft/d)	6.9×10^{-4} ft/d	$4.0 \times 10^{-4} - 4.0 \times 10^{-3}$ ft/d	Estimated from K_v and K_{Iv}/K_v
12	Interbedded clastic rocks (both fine- and coarse-grained), carbonates, and coals, Michigan Basin	K_v (ft/d)	6.9×10^{-6} ft/d	$4.0 \times 10^{-6} - 4.0 \times 10^{-5}$ ft/d	2, 5, 10
		K_{Iv}/K_v	100		6
		K_h (ft/d)	1.0×10^0 ft/d	$3.9 \times 10^{-1} - 1.0 \times 10^0$ ft/d	2, 5
13	Unweathered Silurian-Devonian dolomite	K_v (ft/d)	1.0×10^{-3} ft/d	$9.8 \times 10^{-5} - 1.0 \times 10^{-1}$ ft/d	Estimated from K_h and K_{Iv}/K_v
		K_{Iv}/K_v	1000	10 - 4000	2
		K_h (ft/d)	4.0×10^0 ft/d	$1.0 \times 10^0 - 3.0 \times 10^1$ ft/d	2, 3, 13
14	Weathered Silurian-Devonian dolomite	K_v (ft/d)	1.0×10^{-2} ft/d	$2.5 \times 10^{-4} - 3.0 \times 10^0$ ft/d	Estimated from K_h and K_{Iv}/K_v
		K_{Iv}/K_v	400	10 - 4000	2, 13
		K_h (ft/d)	1.0×10^{-1} ft/d	$2.4 \times 10^{-4} - 2.4 \times 10^2$ ft/d	Estimated from K_v and K_{Iv}/K_v
15	Weathered Maquoketa interbedded carbonates and fine clastic rocks	K_v (ft/d)	1.0×10^{-3} ft/d	$4.0 \times 10^{-6} - 4.7 \times 10^{-1}$ ft/d	2, 10
		K_{Iv}/K_v	100	60 - 500	2, 13
		K_h (ft/d)			

**Table 4. Hydraulic Conductivity Zonation of Regional-Scale Model
(Continued)**

Zone	Description	Parameter	Starting Value	Range	References*
16	Unweathered Maquoketa interbedded carbonates and fine clastic rocks	K_h (ft/d)	4.0×10^{-4} ft/d	$2.4 \times 10^{-4} - 6.5 \times 10^{-3}$ ft/d	Estimated from K_v and K_h/K_v
		K_v (ft/d)	6.7×10^{-6} ft/d	$4.0 \times 10^{-6} - 1.3 \times 10^{-5}$ ft/d	2, 5, 10
		K_h/K_v	60	60 – 500	2, 13
23	Weathered Galena-Platteville dolomite	K_h (ft/d)	4.7×10^0 ft/d	$3.0 \times 10^{-1} - 7.1 \times 10^0$ ft/d	2, 7, 13
		K_v (ft/d)	1.6×10^{-1} ft/d	$6.0 \times 10^{-4} - 2.4 \times 10^{-1}$ ft/d	Estimated from K_h and K_h/K_v
		K_h/K_v	30	30 - 500	2, 13
26	Unweathered Galena-Platteville dolomite	K_h (ft/d)	5.0×10^{-2} ft/d	$3.4 \times 10^{-2} - 7.6 \times 10^{-2}$ ft/d	2, 4, 7, 13
		K_v (ft/d)	6.3×10^{-4} ft/d	$6.8 \times 10^{-5} - 2.5 \times 10^{-3}$ ft/d	Estimated from K_h and K_h/K_v
		K_h/K_v	80	30 – 500	2, 13
28	Unweathered Ancell and Prairie du Chien-Eminence, mainly carbonate	K_h (ft/d)	8.0×10^{-1} ft/d	$1.1 \times 10^{-1} - 1.7 \times 10^0$ ft/d	1, 2, 5, 12, 13
		K_v (ft/d)	5.3×10^{-4} ft/d	$7.3 \times 10^{-5} - 1.1 \times 10^{-3}$ ft/d	Estimated from K_h and K_h/K_v
		K_h/K_v	1500		13
29	Unweathered Ancell, mainly sandstone	K_h (ft/d)	1.5×10^0 ft/d	$1.1 \times 10^0 - 1.8 \times 10^0$ ft/d	2, 5, 12, 13
		K_v (ft/d)	7.5×10^{-2} ft/d	$5.5 \times 10^{-3} - 9.0 \times 10^{-2}$ ft/d	Estimated from K_h and K_h/K_v
		K_h/K_v	20	20 - 200	2, 13
30	Weathered Ancell, mainly sandstone	K_h (ft/d)	7.3×10^0 ft/d	$5.4 \times 10^0 - 8.8 \times 10^0$ ft/d	5
		K_v (ft/d)	3.7×10^{-1} ft/d	$2.7 \times 10^{-1} - 4.4 \times 10^{-1}$ ft/d	Estimated from K_h and K_h/K_v
		K_h/K_v	20		13
31	Weathered Prairie du Chien-Eminence, mainly carbonate	K_h (ft/d)	4.7×10^0 ft/d	$3.0 \times 10^{-1} - 3.6 \times 10^1$ ft/d	Based on similarity to Galena-Platteville Unit facies (2, 7, 13)
		K_v (ft/d)	1.6×10^{-1} ft/d	$6.0 \times 10^{-4} - 1.2 \times 10^0$ ft/d	
		K_h/K_v	30	30 – 500	
37	Unweathered Iron-ton-Galesville, mainly sandstone, >25% carbonate (Emrich, 1966)	K_h (ft/d)	3.0×10^0 ft/d	$2.4 \times 10^0 - 4.2 \times 10^0$ ft/d	2, 5, 12
		K_v (ft/d)	6.0×10^{-2} ft/d	$2.4 \times 10^{-2} - 8.4 \times 10^{-2}$ ft/d	Estimated from K_h and K_h/K_v
		K_h/K_v	50	50 – 100	2, 13

**Table 4. Hydraulic Conductivity Zonation of Regional-Scale Model
(Continued)**

Zone	Description	Parameter	Starting Value	Range	References*
38	Weathered Potosi-Franconia, mainly carbonate	K_h (ft/d)	4.7×10^0 ft/d	$3.0 \times 10^{-1} - 3.6 \times 10^1$ ft/d	Based on similarity to Galena-Platteville Unit facies (2, 7, 13)
		K_v (ft/d)	1.6×10^{-1} ft/d	$6.0 \times 10^{-4} - 1.2 \times 10^0$ ft/d	
		K_h/K_v	30	30 - 500	
40	Unweathered Ironton-Galesville, mainly sandstone, <25% carbonate (Emrich, 1966)	K_h (ft/d)	5.3×10^0 ft/d	$2.4 \times 10^0 - 8.4 \times 10^0$ ft/d	2, 5, 12
		K_v (ft/d)	1.1×10^{-1} ft/d	$2.4 \times 10^{-2} - 1.7 \times 10^{-1}$ ft/d	
		K_h/K_v	50	50 - 100	
41	Weathered Ironton-Galesville, mainly sandstone	K_h (ft/d)	8.4×10^0 ft/d	$5.3 \times 10^0 - 8.6 \times 10^0$ ft/d	2, 5, 12
		K_v (ft/d)	1.7×10^{-1} ft/d	$5.3 \times 10^{-2} - 1.7 \times 10^{-1}$ ft/d	
		K_h/K_v	50	50 - 100	
42	Unweathered Potosi-Franconia, Ironton-Galesville, and Eau Claire; mainly dolomite and fine clastic rocks (Willman et al., 1975)	K_h (ft/d)	6.9×10^{-3} ft/d	$4.0 \times 10^{-3} - 4.0 \times 10^{-2}$ ft/d	Estimated from K_v and K_h/K_v
		K_v (ft/d)	6.9×10^{-6} ft/d	$4.0 \times 10^{-6} - 4.0 \times 10^{-5}$ ft/d	
		K_h/K_v	1000		
43	Unweathered Mt. Simon, mainly sandstone, depth >1400 ft	K_h (ft/d)	4.3×10^{-1} ft/d	$1.2 \times 10^{-1} - 6.0 \times 10^{-1}$ ft/d	2, 5
		K_v (ft/d)	2.9×10^{-3} ft/d	$1.2 \times 10^{-5} - 4.0 \times 10^{-3}$ ft/d	
		K_h/K_v	150	150 - 10000	
44	Weathered Eau Claire, mainly sandstone	K_h (ft/d)	3.6×10^0 ft/d	$2.4 \times 10^0 - 8.4 \times 10^0$ ft/d	Based on similarity to Ironton-Galesville Unit facies (2)
		K_v (ft/d)	7.2×10^{-2} ft/d	$4.8 \times 10^{-2} - 1.7 \times 10^{-1}$ ft/d	
		K_h/K_v	50		
45	Unweathered Mt. Simon, mainly sandstone, depth <1400 ft	K_h (ft/d)	4.3×10^0 ft/d	$1.2 \times 10^0 - 6.0 \times 10^0$ ft/d	1, 2, 5, 12
		K_v (ft/d)	2.9×10^{-2} ft/d	$1.2 \times 10^{-4} - 4.0 \times 10^{-2}$ ft/d	
		K_h/K_v	150	150 - 10000	
46	Weathered Mt. Simon, mainly sandstone	K_h (ft/d)	6.0×10^0 ft/d	$1.2 \times 10^0 - 8.6 \times 10^0$ ft/d	2, 5
		K_v (ft/d)	4.0×10^{-2} ft/d	$1.2 \times 10^{-4} - 5.7 \times 10^{-2}$ ft/d	
		K_h/K_v	150	150 - 10000	

**Table 4. Hydraulic Conductivity Zonation of Regional-Scale Model
(Concluded)**

Zone	Description	Parameter	Starting Value	Range	References*
47	Unweathered Eau Claire, mainly sandstone	K_h (ft/d)	7.2×10^{-1} ft/d	$6.0 \times 10^{-1} - 3.6 \times 10^0$ ft/d	2, 13
		K_v (ft/d)	1.4×10^{-2} ft/d	$1.2 \times 10^{-2} - 7.2 \times 10^{-2}$ ft/d	Estimated from K_h and K_h/K_v
		K_h/K_v	50		Based on similarity to Iron-ton-Galesville Unit facies (2)

***References**

1. Eaton et al. (1999)
2. Feinstein et al. (2005a, 2005b)
3. Graese et al. (1988)
4. Kay et al. (2006)
5. Mandle and Kontis (1992)
6. Miller (1984)
7. Mills et al. (2002)
8. Todd (1980)
9. Visocky (1990a)
10. Walton (1960)
11. Walton (1964)
12. Walton and Csallany (1962)
13. Weaver and Bahr (1991a; 1991b)
14. Weeks (1969)
15. Willman et al. (1975)
16. Illinois Environmental Protection Agency (IEPA) database of slug test results summarized by ISGS (personal communication, 2006)

As discussed by Mandle and Kontis (1992), degree of weathering is considered to play a principal role in influencing K, with more weathered units having higher hydraulic conductivities. Thus, areas of bedrock surface exposure of the Ancell Unit downward through the Mt. Simon Unit correspond to zones of higher K in layers 12 through 17, respectively (Figure 32 through Figure 37). Layers 18 through 20, representing the lower 75 percent of the Mt. Simon Unit thickness, do not include such a weathered zone (Figure 29 through Figure 31). The Galena-Platteville Unit, Maquoketa Unit, and Silurian-Devonian Carbonate Unit are each represented by two or more model layers. The uppermost model layers representing each of these units—layers 10, 8, and 5, respectively—are assigned to a higher K zone in areas of bedrock surface exposure of each unit (Figure 39, Figure 41, and Figure 44). Parts of the layers representing the lower portions of these units—layers 11, 9, 7, and 6—are assigned to the higher K zone if the entire layer is within 50 ft of the bedrock surface (Figure 38, Figure 40, Figure 42, and Figure 43). Together, the weathered, high-permeability zones of the Galena-Platteville, Maquoketa, and Silurian-Devonian Carbonate Units approximate the Shallow Bedrock Aquifer of northeastern Illinois (pages 44, 53, and 55). Although the depth below bedrock surface of the higher-permeability interval varies from place to place (published estimates range from about 25 to 125 ft), available research suggests that a depth of 50 ft is a reasonable approximation (Bergeron, 1981; Graese et al., 1988; Kay and Kraske, 1996; Visocky and Schulmeister, 1988; Zeizel et al., 1962).

Lithology is also considered in the assignment of K to bedrock units. The interval included in the Upper Bedrock Unit (model layer 4) is assigned a slightly higher K in the Michigan Basin, where the interval contains more coarse-grained clastic rocks, than in the Illinois Basin (Mandle and Kontis, 1992) (Figure 45). In layer 12, representing the Ancell Unit, zones 28 and 29 (Figure 37) encompass facies of unweathered carbonate and sandstone, respectively (Mandle and Kontis, 1992; Willman et al., 1975). The authors simulate the southward- and eastward- gradation in the lithology of the Ironton-Galesville Unit from sandstone to carbonate to fine-grained clastic rocks (Becker et al., 1978; Catacosinos, 1973; Emrich, 1966) with zones 37, 40, and 42 (layer 15) (Figure 34). Likewise, the southeastward gradation in the lithology of the Eau Claire Unit from sandstone to fine-grained clastic rocks and carbonate (Willman et al., 1975) is simulated with zones 42 and 47 (layer 16) (Figure 33).

As discussed by Mandle and Kontis (1992) and shown by the Illinois State Water Survey and Hittman Associates (1973), hydraulic conductivity of the Mt. Simon Unit is related to the depth of burial. Mandle and Kontis (1992) included this effect by reducing K of the Mt. Simon where the depth of burial was greater than 1400 ft, using a continuously-varying “Delta” factor calculated from the depth of burial of the Mt. Simon. Similarly, the K of each model layer representing the Mt. Simon Unit (layers 17-20) has been adjusted downward in areas where depth of burial of the layer is greater than 1400 ft [compare zones 43 and 45 in layers 17-20 (Figure 29 through Figure 32)].

Zonation of hydraulic conductivity in the Quaternary Unit (model layers 1-3) of the regional model is approximate, since these units are modeled in detail for the Kane County area in the local-scale model. All of model layer 1 (Figure 48) is assigned to a single zone with hydraulic conductivity representative of undifferentiated glacial and postglacial clastic sediments and soils. The deeper Quaternary materials represented by model layers 2 and 3 are segregated in the Illinois portion of the model domain into two

zones on the basis of mapping showing major sand and gravel aquifers (Illinois Department of Natural Resources, 1996) (Figure 46 and Figure 47). The differentiation of model layers 2 and 3 into these two zones—while layer 1 is assigned in its entirety to a single, lower permeability zone—is justified by the general tendency of major sand and gravel deposits to occur in the lower portions of the glacial drift.

2.2.3.2. Local-Scale Shallow Model

Starting K values for layers in the local model are based on pumping tests of wells finished in the shallow aquifers of the local domain, preliminary results of the regional model, and on published studies describing the lithology and hydraulic characteristics of the modeled units. The assumed zonation is summarized in Table 5 and is illustrated in map view (Figure 51 through Figure 65) and in cross sections (Figure 66 through Figure 70). Final, calibrated K values are discussed in Section 2.3.2.3. As in the regional-scale model, hydraulic conductivity is zoned, with zone numbers employed only as identifiers having no quantitative significance. Note that in areas of absence, model layers are set to a thickness of 1 foot, and the K-zonation in these areas is equivalent to the zonation of the underlying unit. Unlike the figures showing the K-zonation employed in the regional-scale model (Figure 29 through Figure 48), the figures showing the K-zonation used in the local-scale model show the complete zonation, even that employed in areas of absence of hydrostratigraphic units represented by the particular model layer. This approach allows for better graphical display of aquifer interconnections.

For purposes of characterizing the hydraulic conductivity of the geologic materials present in the local model domain, this study simplifies the lithostratigraphy of the area to three basic property zones: Shallow Bedrock Aquifer, unconsolidated sand and gravel, and unconsolidated fine-grained materials (chiefly diamicton). Within these basic property zones, additional zones are occasionally specified where field studies, geologic maps, well pumping records, and aquifer tests indicate regions of elevated or reduced conductivity. Within each zone, properties are represented in the model as uniform, with a single effective value calibrated to represent the average, or effective, conductivity of the zone.

Shallow Bedrock The hydraulic conductivity of the Shallow Bedrock Aquifer (local model layer 15) is represented by five zones based on the gross lithology of the upper 50 ft of bedrock (Figure 51). Pumping tests, although few in number, together with observations reported by Graese et al. (1988), suggest that the hydraulic conductivity of the Shallow Bedrock Aquifer in the local model domain is higher than that of the region. Thus, assumed starting values and upper limits of plausible ranges of hydraulic conductivity of local zone 8 is higher than are the values assumed for analogous regional model zone representing the hydraulic conductivity of weathered Silurian-Devonian Carbonate Unit (regional model zone 14) (Figure 40 through Figure 44). Because no pumping test results are available for the weathered Maquoketa Unit or the Galena-Platteville carbonates within the local model domain, the starting values and plausible ranges of hydraulic conductivity of local zones 10 and 12 are identical to calibrated values and assumed ranges for regional model zones 15 and 23 (Figure 38 through Figure 39). Plausible ranges of K for zones 9 and 11—representing the 50 ft of upper bedrock where it contains combinations of lithostratigraphic units—are based largely on assumed values for zones 8 and 12. Because the bedrock units are in the bottom layer of the

Table 5. Hydraulic Conductivity Zonation of Local-Scale Model

Zone	Description	Parameter	Starting Value	Range	References*
1	Soil developed on silts and diamictons	K_h (ft/d)	1×10^{-1}	0.02 – 1.2	1, 4
		K_v (ft/d)	1×10^{-3}	0.001 – 1.2	1, 4
		K_h/K_v	100	40 – 250	2, 8
2	Predominantly sand and gravel in near-surface setting	K_h (ft/d)	1.3×10^2	3.1×10^1 – 4.0×10^2	19 pumping tests in local model domain
		K_v (ft/d)	1.3×10^0	6.0×10^{-4} – 8.0×10^0	Estimated from K_h and K_h/K_v
		K_h/K_v	100	50 – 170	2, 6
3	Predominantly diamicton	K_h (ft/d)	2.7×10^{-2}	3.2×10^{-5} – 6.8×10^1	IEPA database of slug test results summarized by ISGS (personal communication, 2006)
		K_v (ft/d)	2.7×10^{-4}	1.3×10^{-7} – 1.7×10^0	Estimated from K_h and K_h/K_v
		K_h/K_v	100	40 – 250	2, 8
4	Predominantly sand and gravel of typical permeability ¹	K_h (ft/d)	1.3×10^2	3.1×10^1 – 4.0×10^2	19 pumping tests in local model domain
		K_v (ft/d)	1.3×10^0	6.0×10^{-4} – 8.0×10^0	Estimated from K_h and K_h/K_v
		K_h/K_v	100	50 – 170	2, 6
5	Predominantly high-permeability sand and gravel in Ashmore Unit, Carpentersville area	K_h (ft/d)	9.3×10^2	8.6×10^2 – 2.4×10^3	3 specific capacity tests in local model domain
		K_v (ft/d)	9.3×10^0	8.6×10^0 – 1.2×10^3	Estimated from K_h and K_h/K_v
		K_h/K_v	50	2 – 100	2, 9
6	Predominantly high-permeability sand and gravel along axis of St. Charles Bedrock Valley ¹	K_h (ft/d)	1.2×10^3 ft/d	3.1×10^2 – 2.4×10^3	4 pumping tests in local model domain
		K_v (ft/d)	2.3×10^1 ft/d	3.1×10^0 – 1.2×10^3	Estimated from K_h and K_h/K_v
		K_h/K_v	50	2 – 100	2, 9

**Table 5. Hydraulic Conductivity Zonation of Local-Scale Model
(Concluded)**

<i>Zone</i>	<i>Description</i>	<i>Parameter</i>	<i>Starting Value</i>	<i>Range</i>	<i>References*</i>
7	Predominantly very high-permeability sand and gravel in Ashmore Unit, Carpentersville area	K_h (ft/d)	1.2×10^3 ft/d	$3.1 \times 10^2 - 2.4 \times 10^3$	3 specific capacity tests in local model domain
		K_v (ft/d)	2.3×10^1 ft/d	$3.1 \times 10^0 - 1.2 \times 10^3$	Estimated from K_h and K_h/K_v
		K_h/K_v	50	2 – 100	2, 6
8	Upper 50 ft of bedrock is Silurian dolomite	K_h (ft/d)	4.0×10^0	$1.0 \times 10^0 - 3.0 \times 10^1$	2, 3, 8
		K_v (ft/d)	1.0×10^{-2}	$2.5 \times 10^{-4} - 3.0 \times 10^0$	Estimated from K_h and K_h/K_v
		K_h/K_v	400	10 – 4000	2, 8
9	Upper 50 ft of bedrock is Silurian and Maquoketa carbonates and fine clastic rocks	K_h (ft/d)	2.8×10^1	$4.0 \times 10^{-4} - 8.5 \times 10^1$	4 pumping tests in local model domain; estimated ranges for zones 8 and 10
		K_v (ft/d)	7.0×10^{-2}	$6.7 \times 10^{-6} - 8.5 \times 10^0$	
		K_h/K_v	400	10 – 4000	
10	Upper 50 ft of bedrock is Maquoketa Group carbonates and fine clastic rocks, near-surface setting	K_h (ft/d)	1.0×10^{-1}	$2.4 \times 10^{-4} - 2.4 \times 10^2$	Estimated from K_v and K_h/K_v
		K_v (ft/d)	1.0×10^{-3}	$4.0 \times 10^{-6} - 4.7 \times 10^{-1}$	2, 7
		K_h/K_v	100	60 – 500	2, 8
11	Upper 50 ft of bedrock is Maquoketa and Galena-Platteville carbonates and fine clastic rocks	K_h (ft/d)	5.7×10^0	$4.0 \times 10^{-6} - 7.1 \times 10^0$	Starting values are avg of starting values for zones 10 and 12; estimated ranges for zones 10 and 12
		K_v (ft/d)	8.1×10^{-2}	$4.0 \times 10^{-6} - 2.4 \times 10^{-1}$	
		K_h/K_v	65	30 – 500	
12	Upper 50 ft of bedrock is Galena-Platteville carbonates	K_h (ft/d)	4.7×10^0	$3.0 \times 10^{-1} - 7.1 \times 10^0$	2, 5, 8
		K_v (ft/d)	1.6×10^{-1}	$6.0 \times 10^{-4} - 2.4 \times 10^{-1}$	Estimated from K_h and K_h/K_v
		K_h/K_v	30	30 – 500	2, 8

***References**

- | | | |
|------------------------------------|------------------------|-----------------------------------|
| 1. Deniger (2004) | 4. Hendry (1982) | 7. Walton (1960) |
| 2. Feinstein et al. (2005a; 2005b) | 5. Mills et al. (2002) | 8. Weaver and Bahr (1991a; 1991b) |
| 3. Graese et al. (1988) | 6. Todd (1980) | 9. Weeks (1969) |

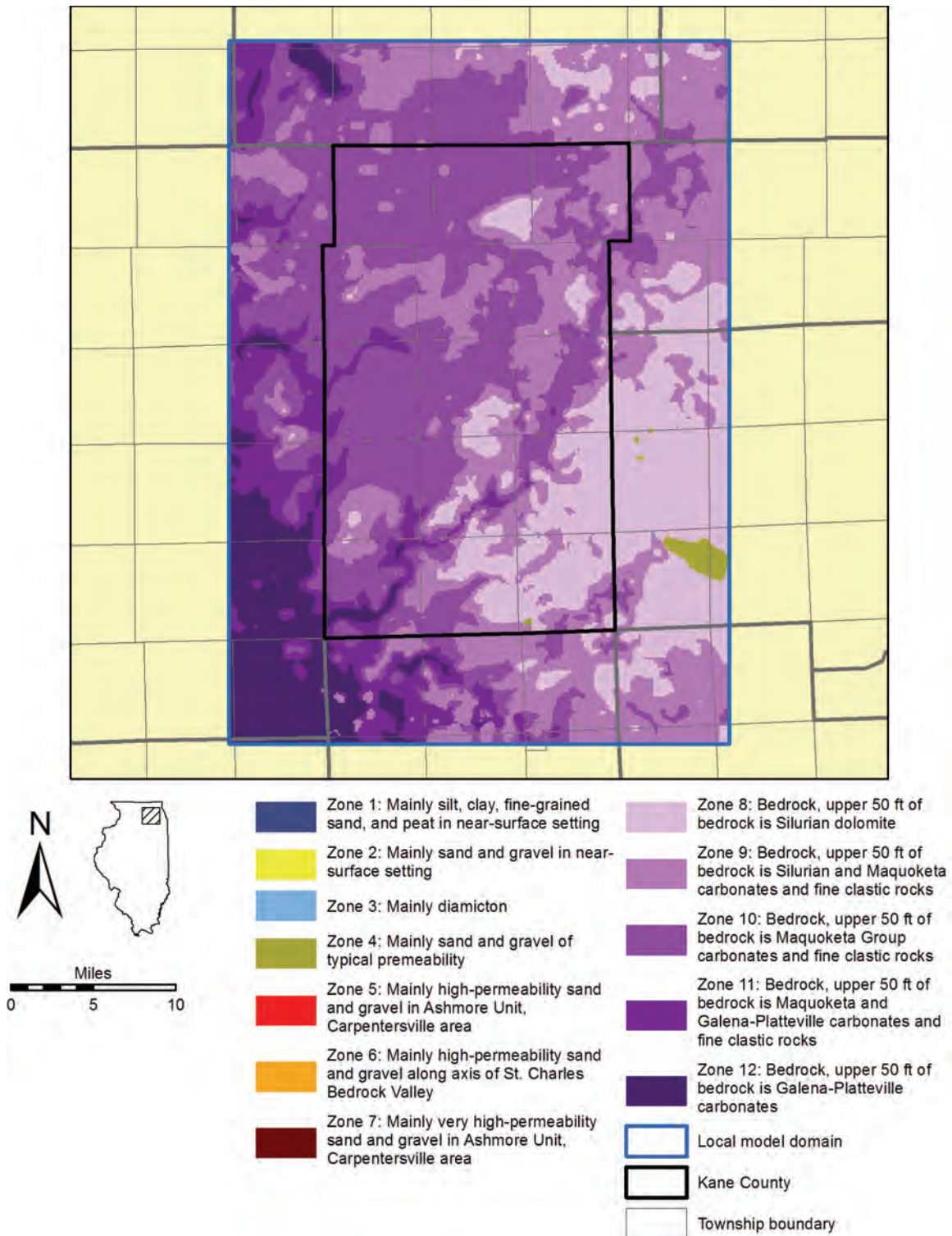


Figure 51. Hydraulic conductivity of local model layer 15 (Shallow Bedrock Aquifer). See Table 5 (pages 100 and 101) for assumed plausible ranges and starting values for calibration for each zone.

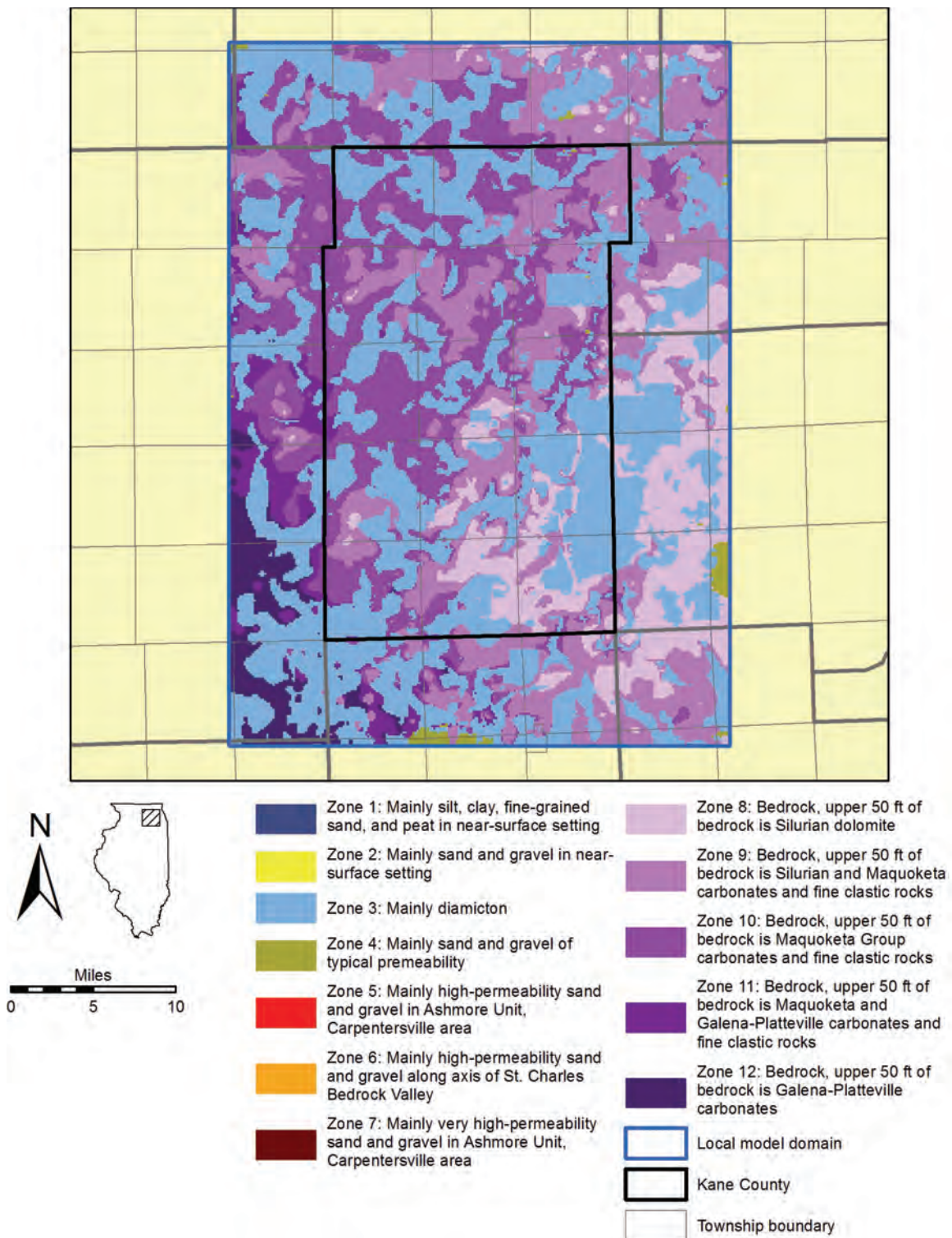


Figure 52. Hydraulic conductivity zonation of local model layer 14 (Lower Glasford Diamicton Unit). See Table 5 (pages 100 and 101) for assumed plausible ranges and starting values for calibration for each zone.

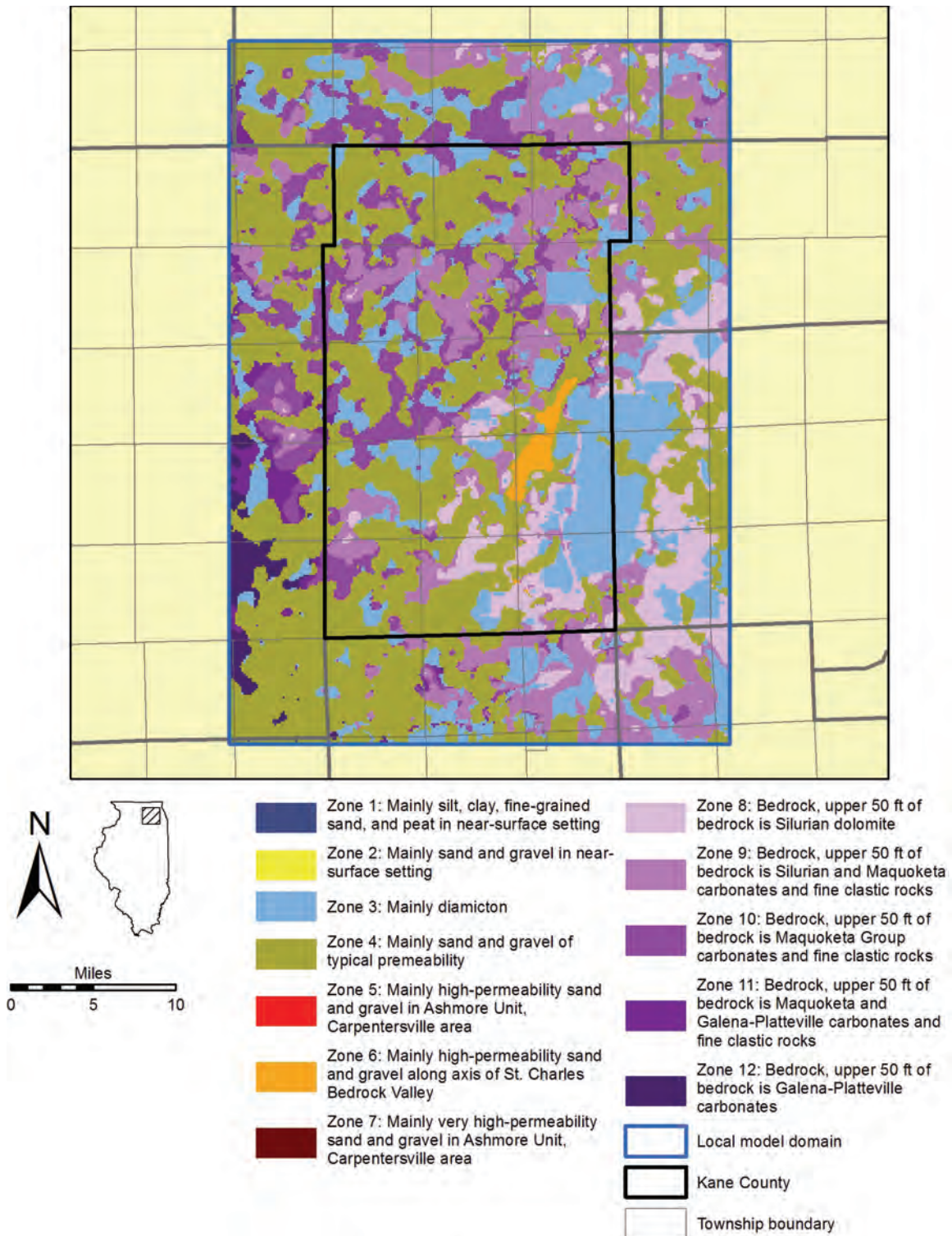


Figure 53. Hydraulic conductivity zonation of local model layer 13 (Lower Glasford Sand Unit). See Table 5 (pages 100 and 101) for assumed plausible ranges and starting values for calibration for each zone.

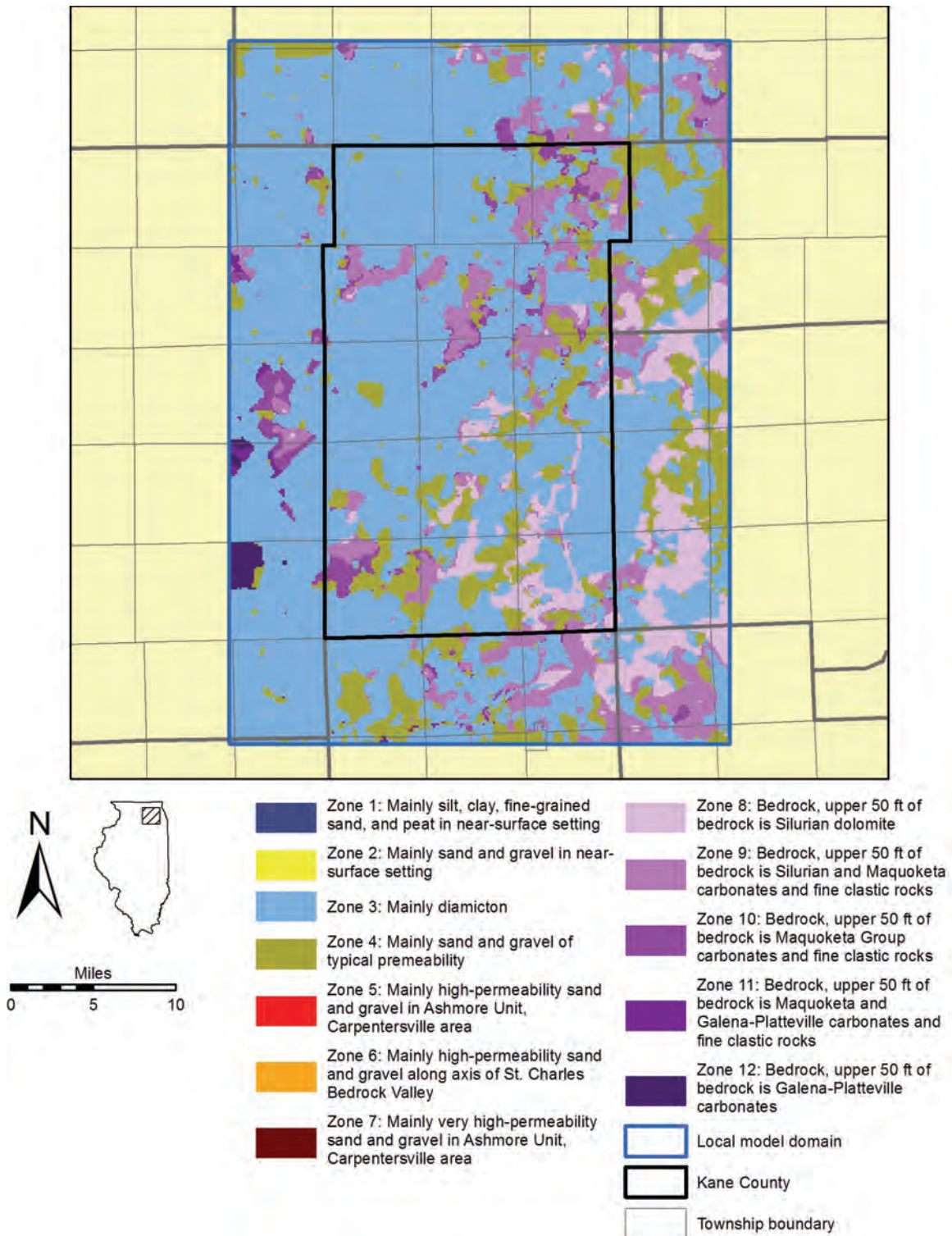


Figure 54. Hydraulic conductivity zonation of local model layer 12 (Middle Glasford Diamicton Unit). See Table 5 (pages 100 and 101) for assumed plausible ranges and starting values for calibration for each zone.

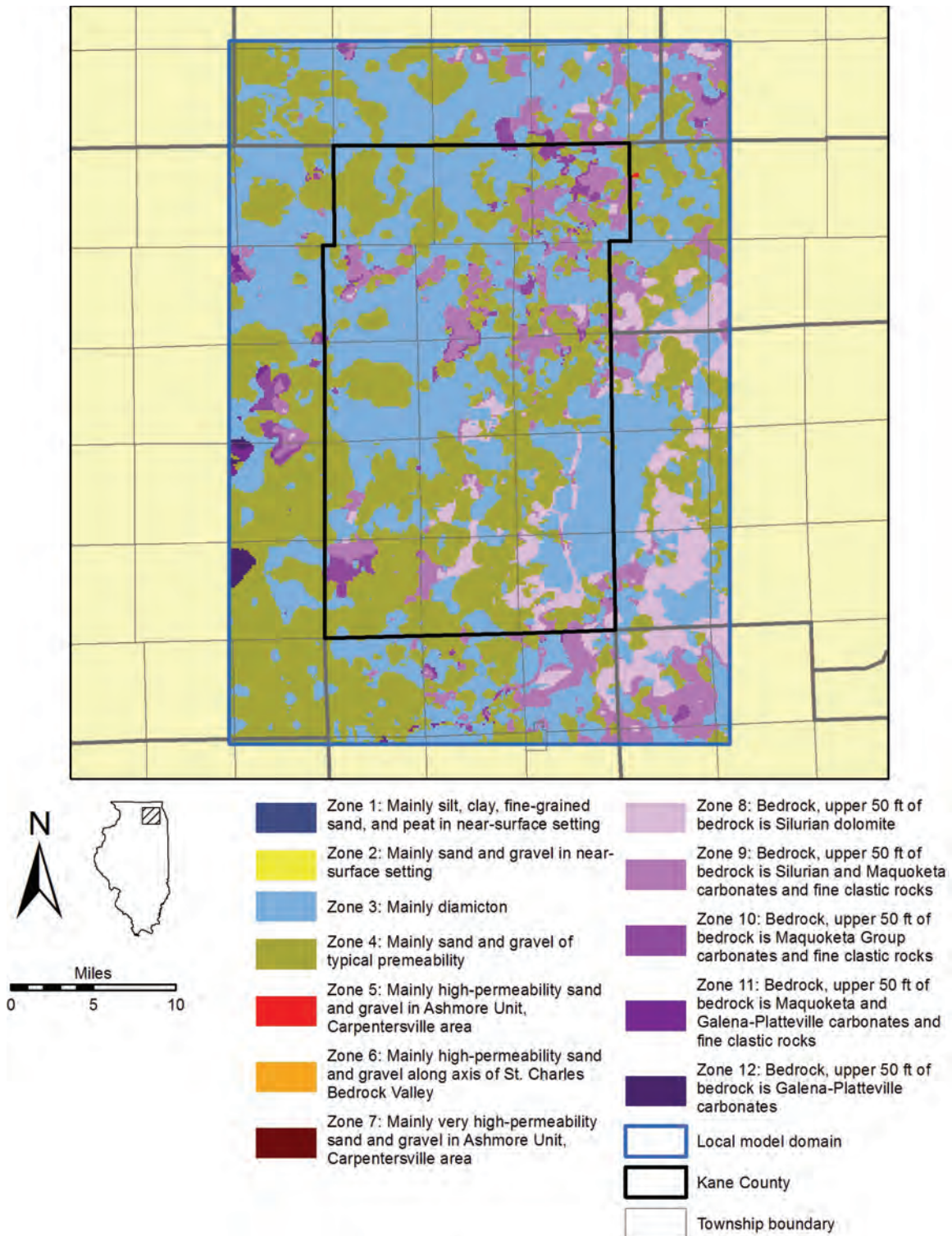


Figure 55. Hydraulic conductivity zonation of local model layer 11 (Upper Glasford Sand Unit). See Table 5 (pages 100 and 101) for assumed plausible ranges and starting values for calibration for each zone.

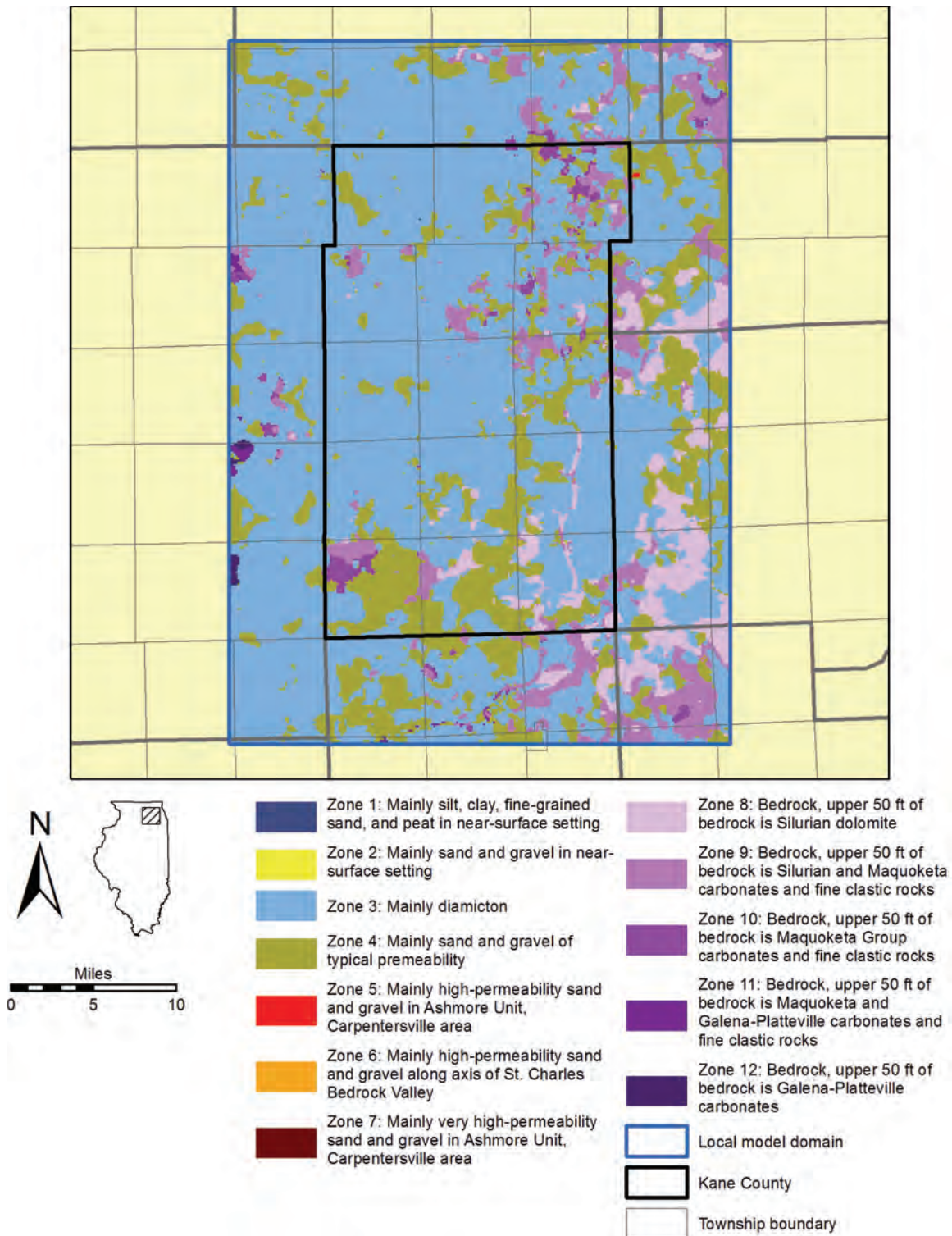


Figure 56. Hydraulic conductivity zonation of local model layer 10 (Upper Glasford Diamicton Unit). See Table 5 (pages 100 and 101) for assumed plausible ranges and starting values for calibration for each zone.

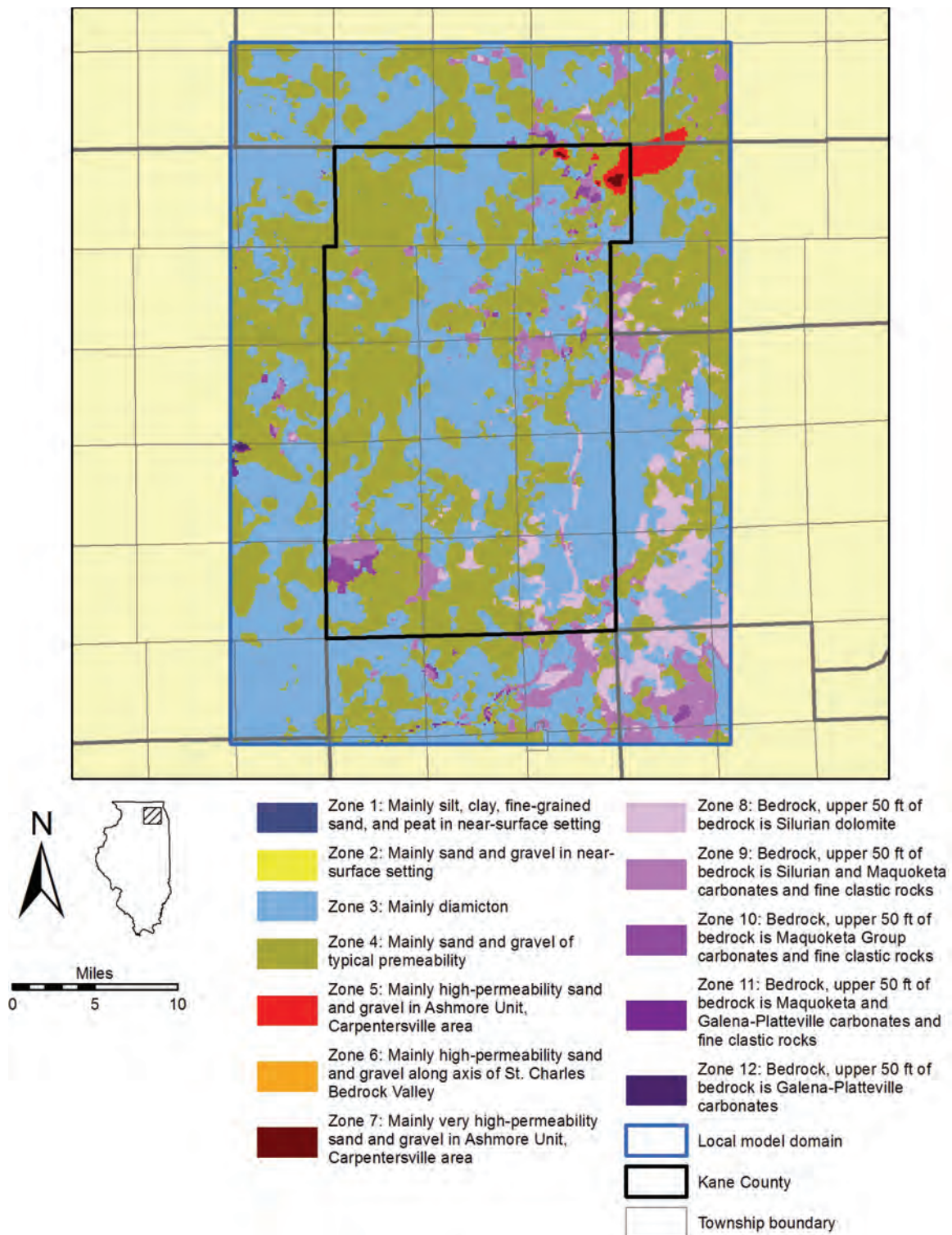


Figure 57. Hydraulic conductivity zonation of local model layer 9 (Ashmore Unit). See Table 5 (pages 100 and 101) for assumed plausible ranges and starting values for calibration for each zone.

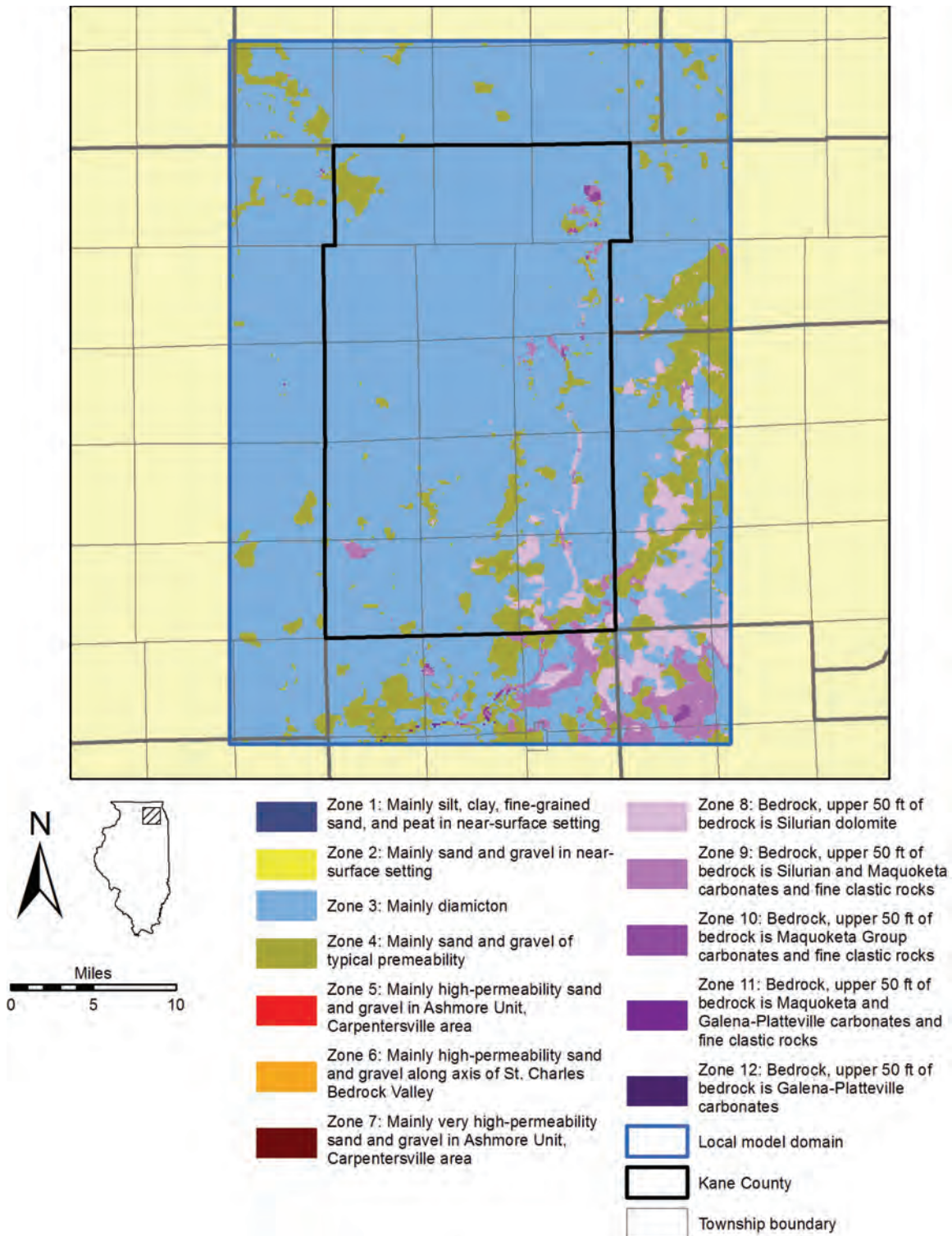


Figure 58. Hydraulic conductivity zonation of local model layer 8 (Tiskilwa Unit). See Table 5 (pages 100 and 101) for assumed plausible ranges and starting values for calibration for each zone.

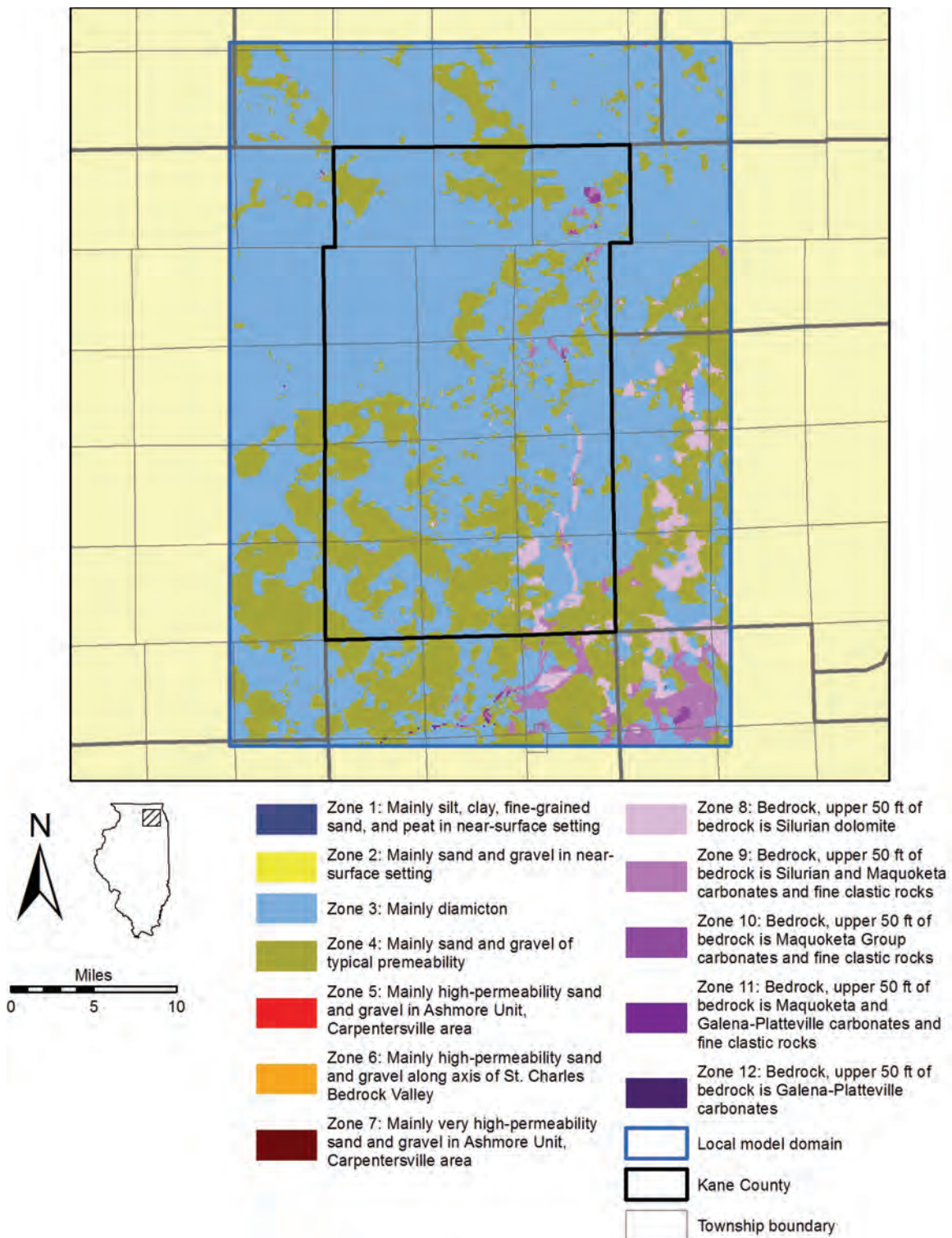


Figure 59. Hydraulic conductivity zonation of local model layer 7 (Batestown Sand Unit). See Table 5 (pages 100 and 101) for assumed plausible ranges and starting values for calibration for each zone.

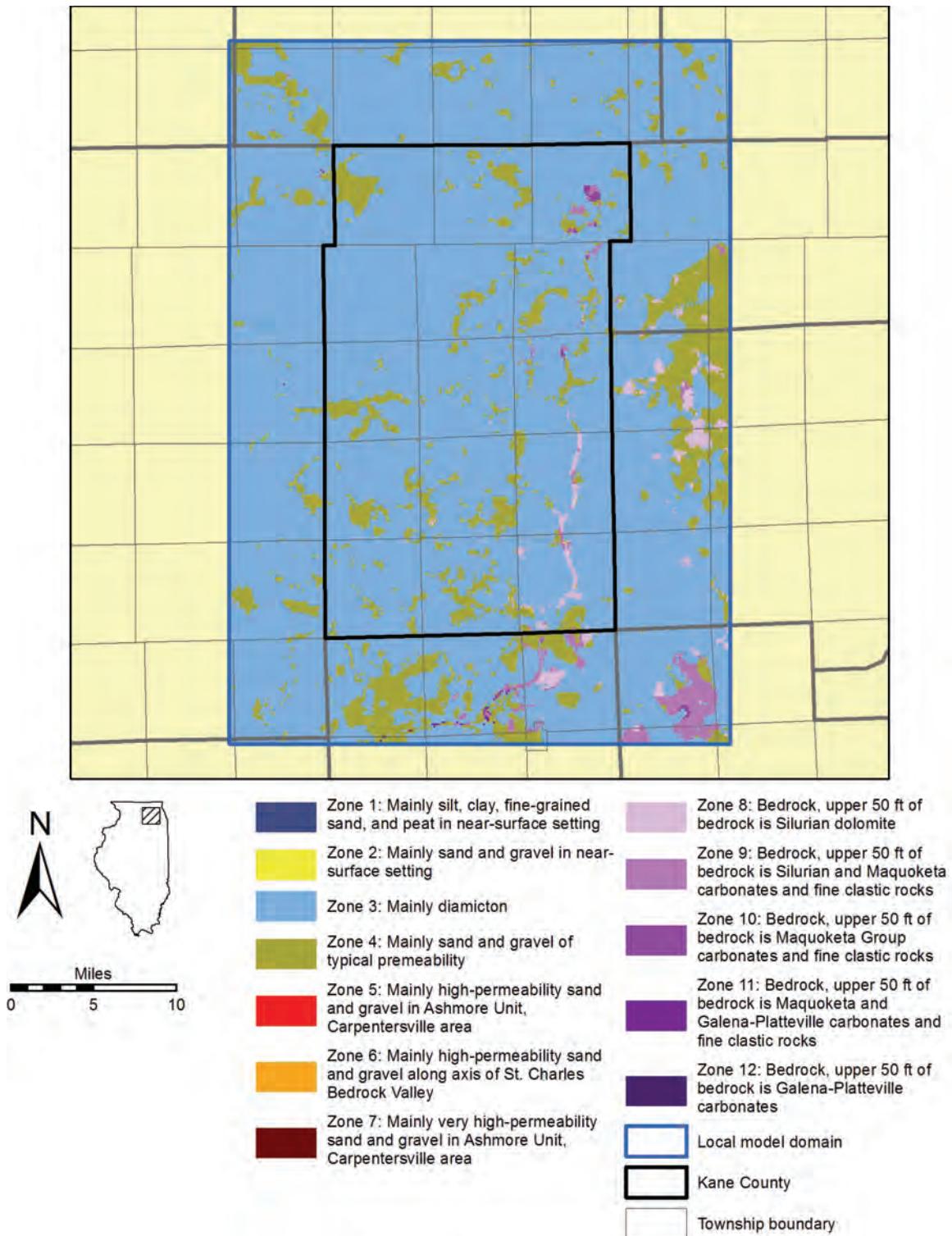


Figure 60. Hydraulic conductivity zonation of local model layer 6 (Batestown Diamicton Unit). See Table 5 (pages 100 and 101) for assumed plausible ranges and starting values for calibration for each zone.

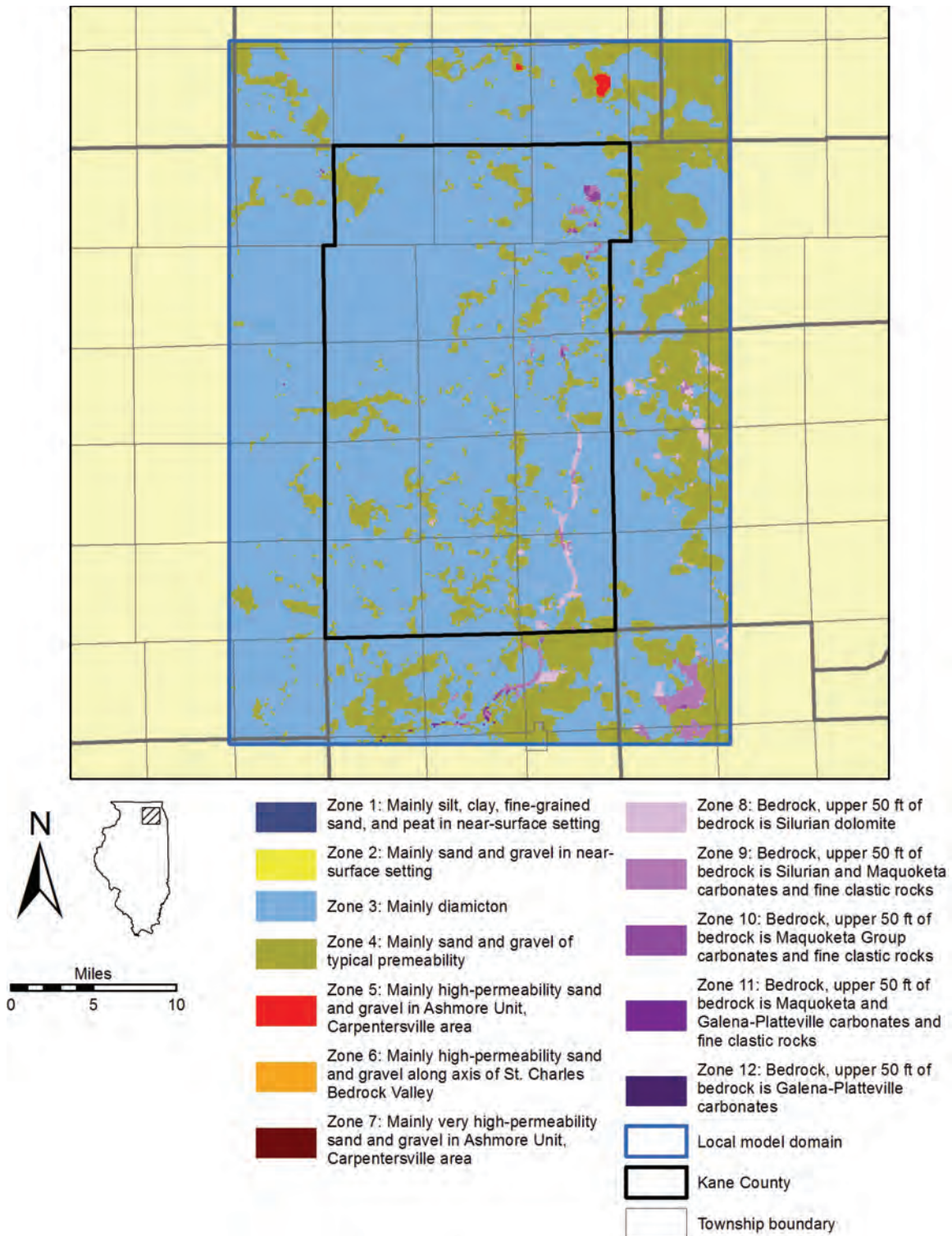


Figure 61. Hydraulic conductivity zonation of local model layer 5 (Yorkville Sand Unit). See Table 5 (pages 100 and 101) for assumed plausible ranges and starting values for calibration for each zone.

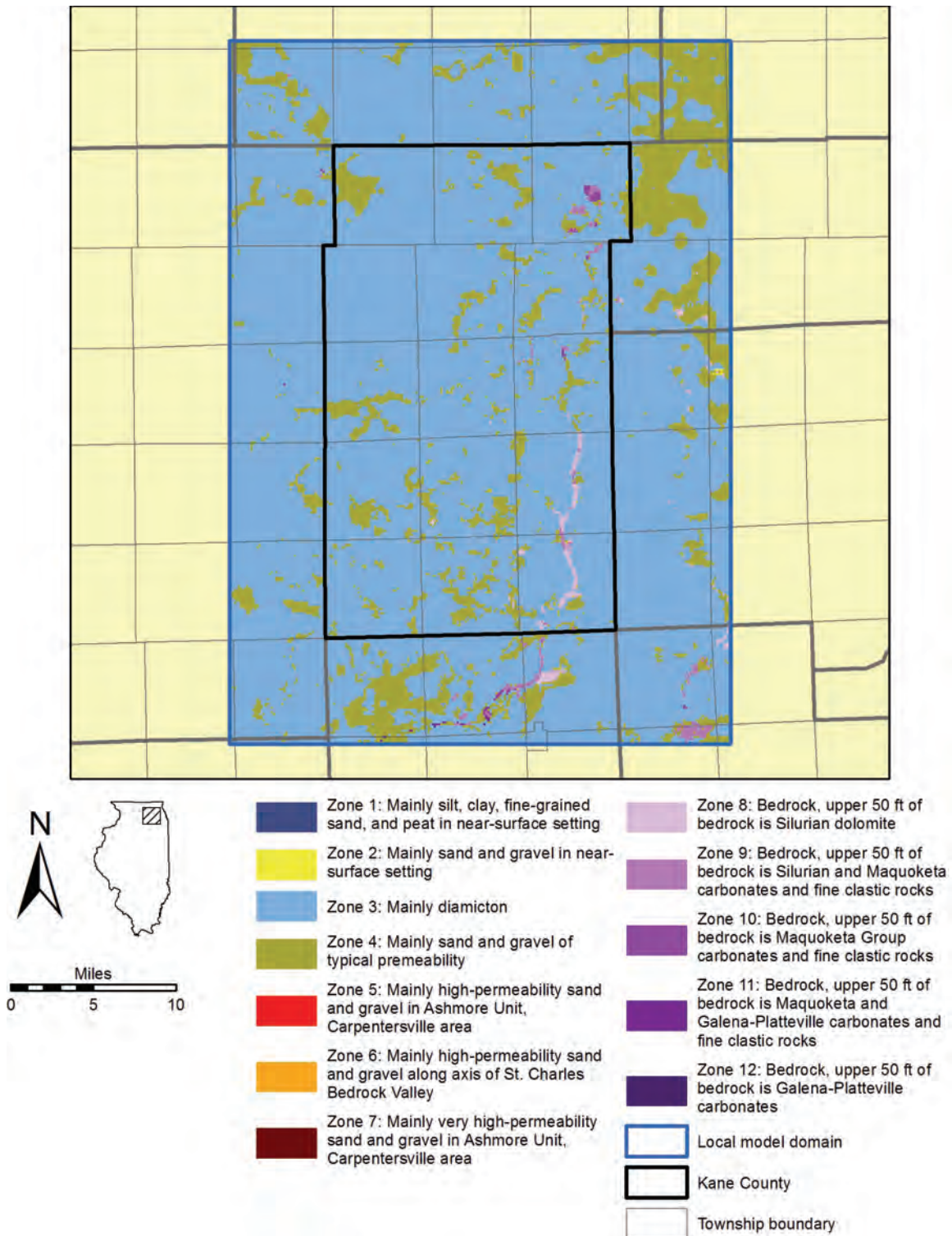


Figure 62. Hydraulic conductivity zonation of local model layer 4 (Yorkville Diamicton Unit). See Table 5 (pages 100 and 101) for assumed plausible ranges and starting values for calibration for each zone.

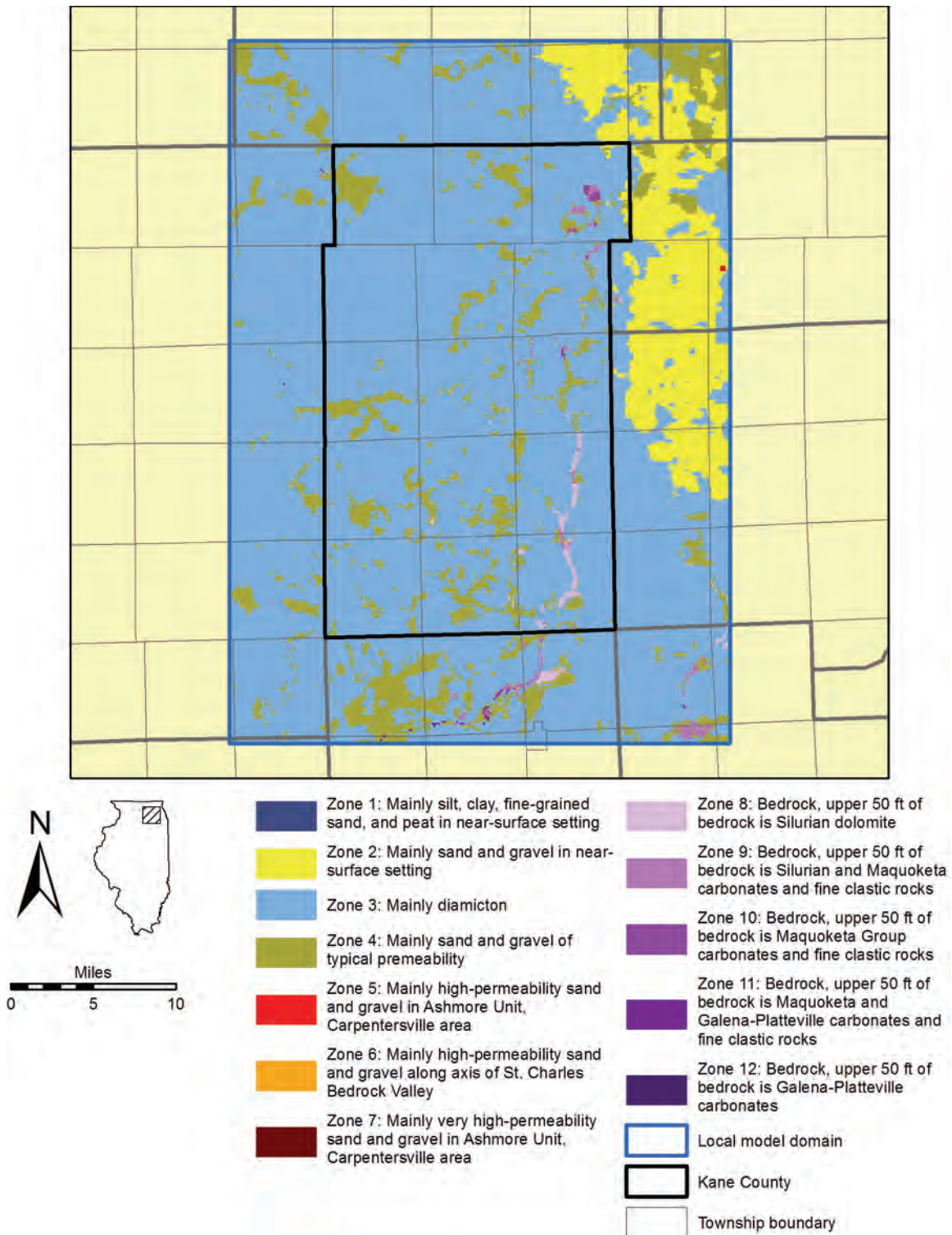


Figure 63. Hydraulic conductivity zonation of local model layer 3 (Wadsworth Sand Unit and Beverly Unit). See Table 5 (pages 100 and 101) for assumed plausible ranges and starting values for calibration for each zone.

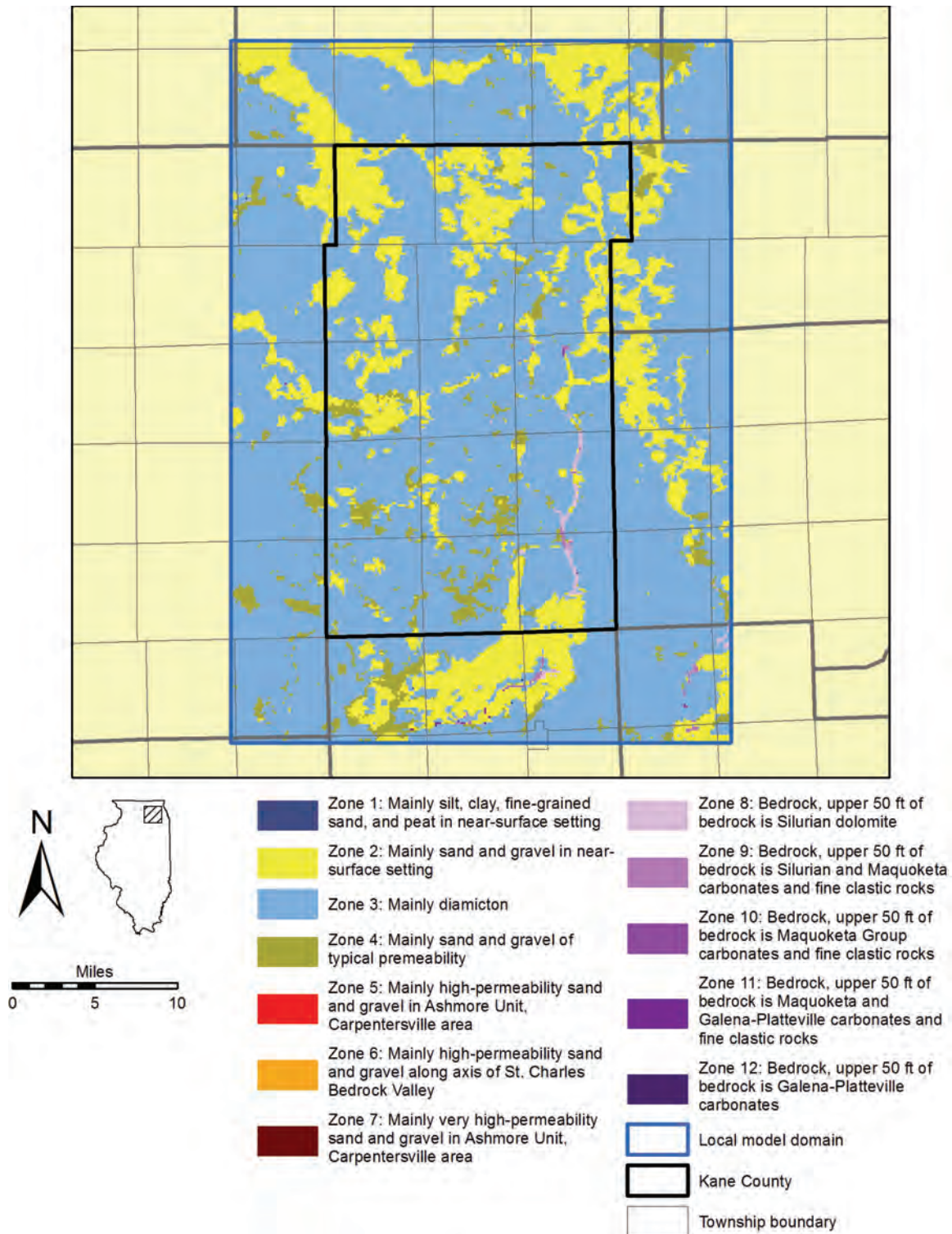


Figure 64. Hydraulic conductivity zonation of local model layer 2 (surficial Henry Unit, Wadsworth Diamicton Unit, and Haeger Unit). See Table 5 (pages 100 and 101) for assumed plausible ranges and starting values for calibration for each zone.

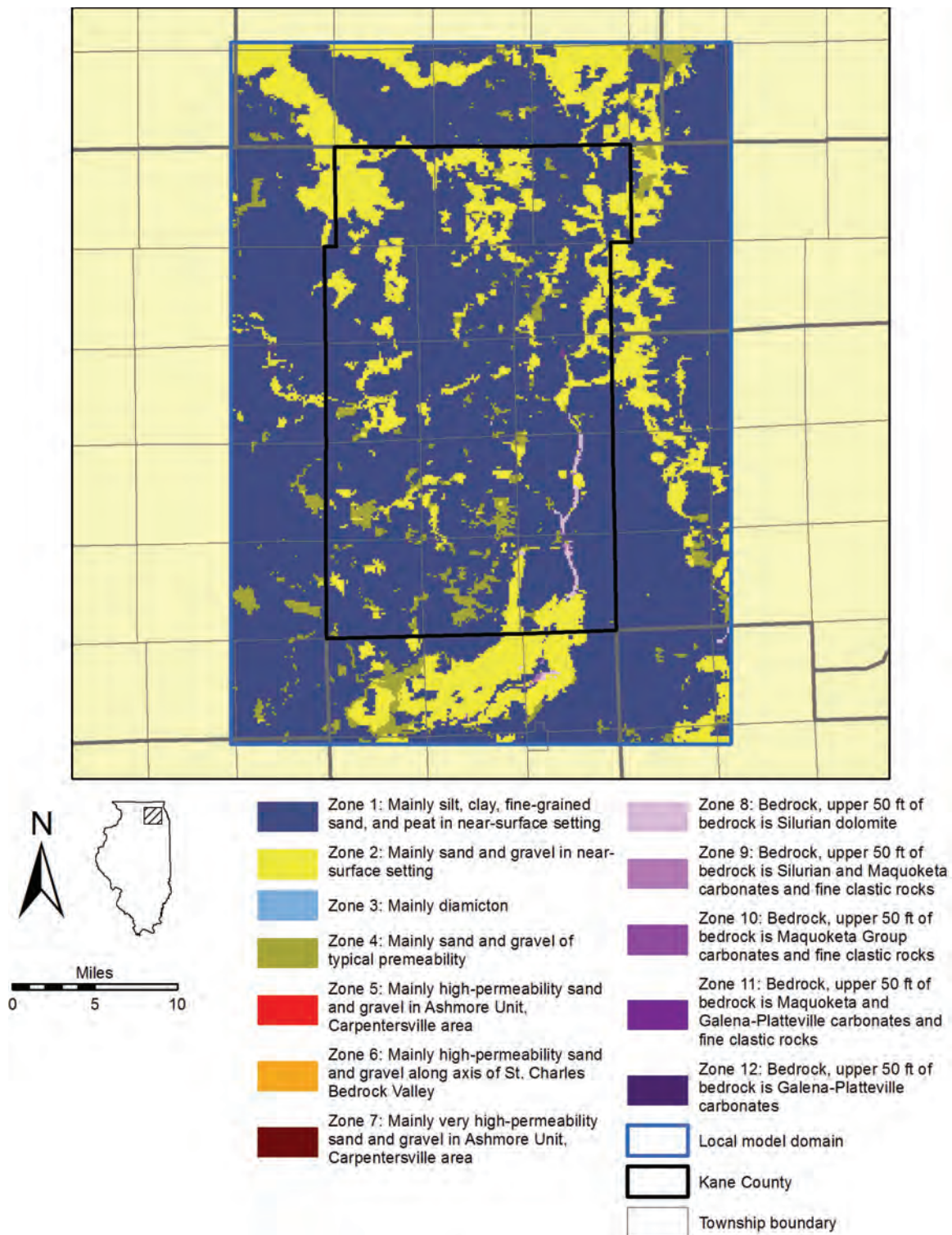


Figure 65. Hydraulic conductivity zonation of local model layer 1 (soil unit and surficial Henry Unit). See Table 5 (pages 100 and 101) for assumed plausible ranges and starting values for calibration for each zone.

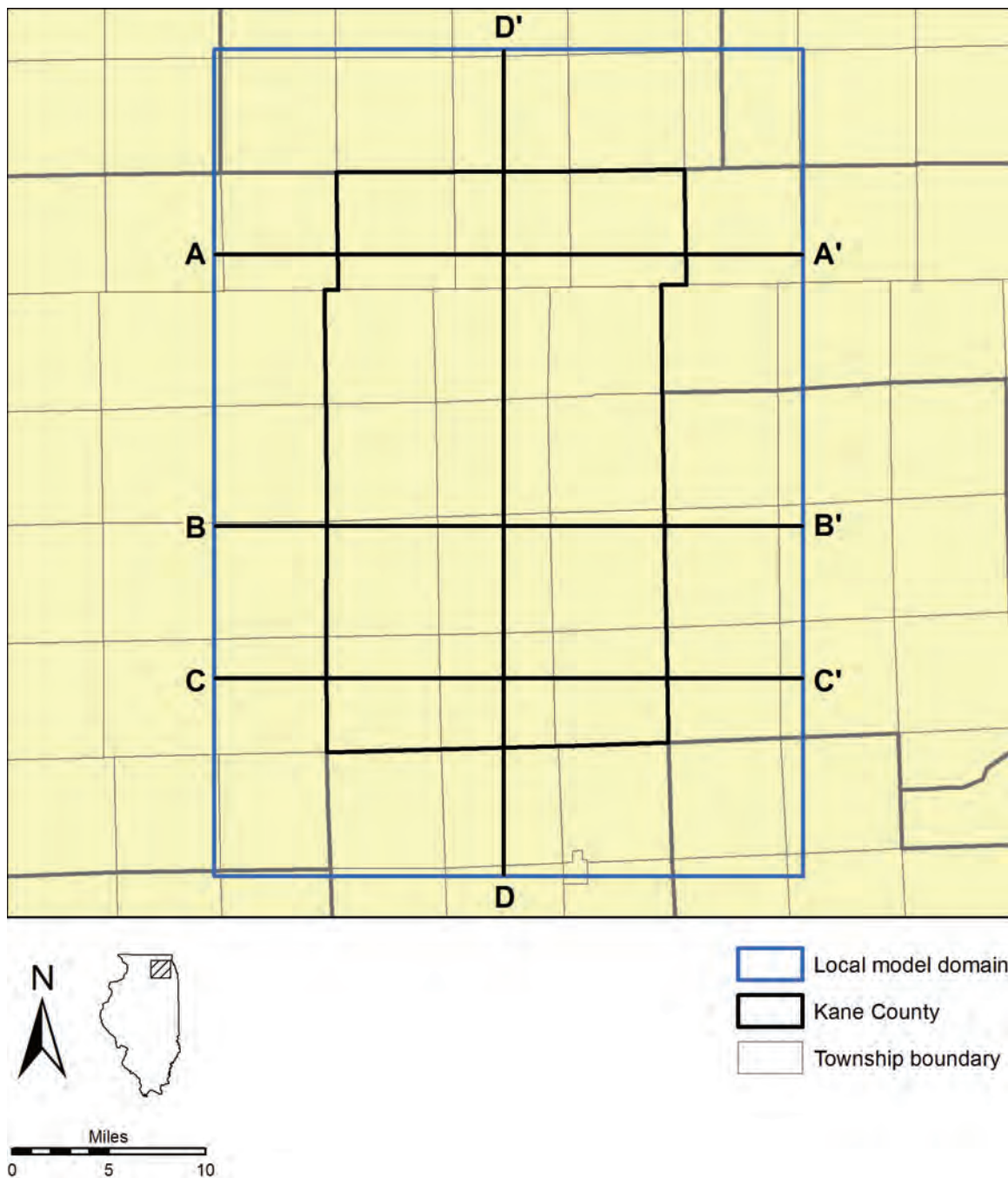


Figure 66. Index map showing locations of cross sections shown in Figure 67 through Figure 70.

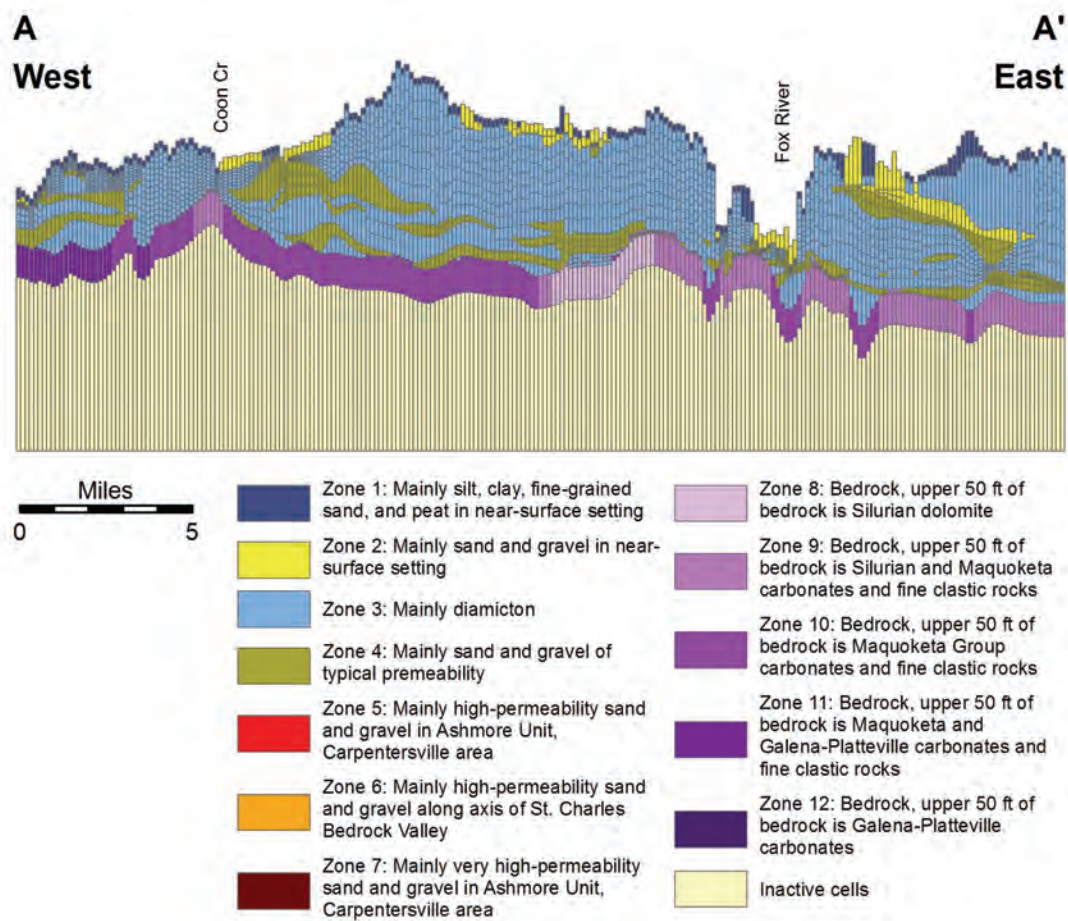


Figure 67. West-to-east cross section A-A' showing hydraulic conductivity zonation of local-scale model in northern part of model domain (see Figure 66 for cross section location).

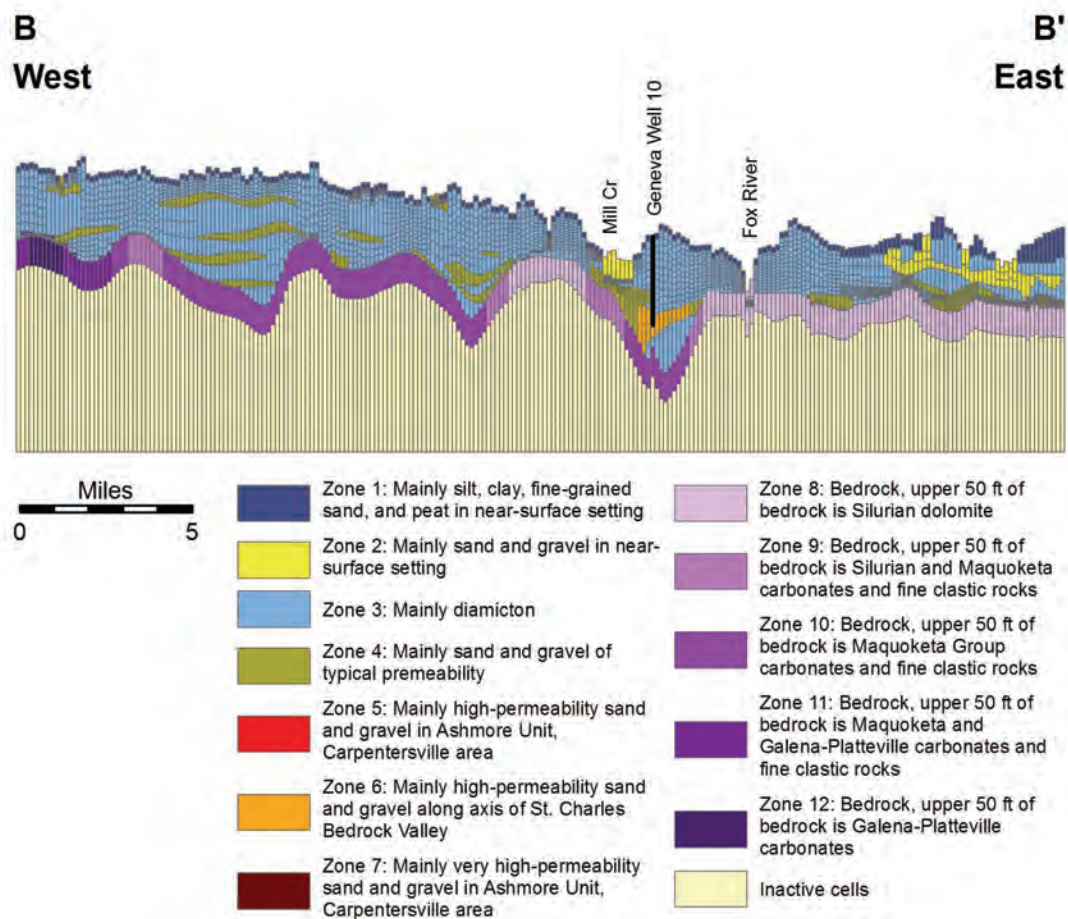


Figure 68. West-to-east cross section B-B' showing hydraulic conductivity zonation of local-scale model in central part of model domain (see Figure 66 for cross section location).

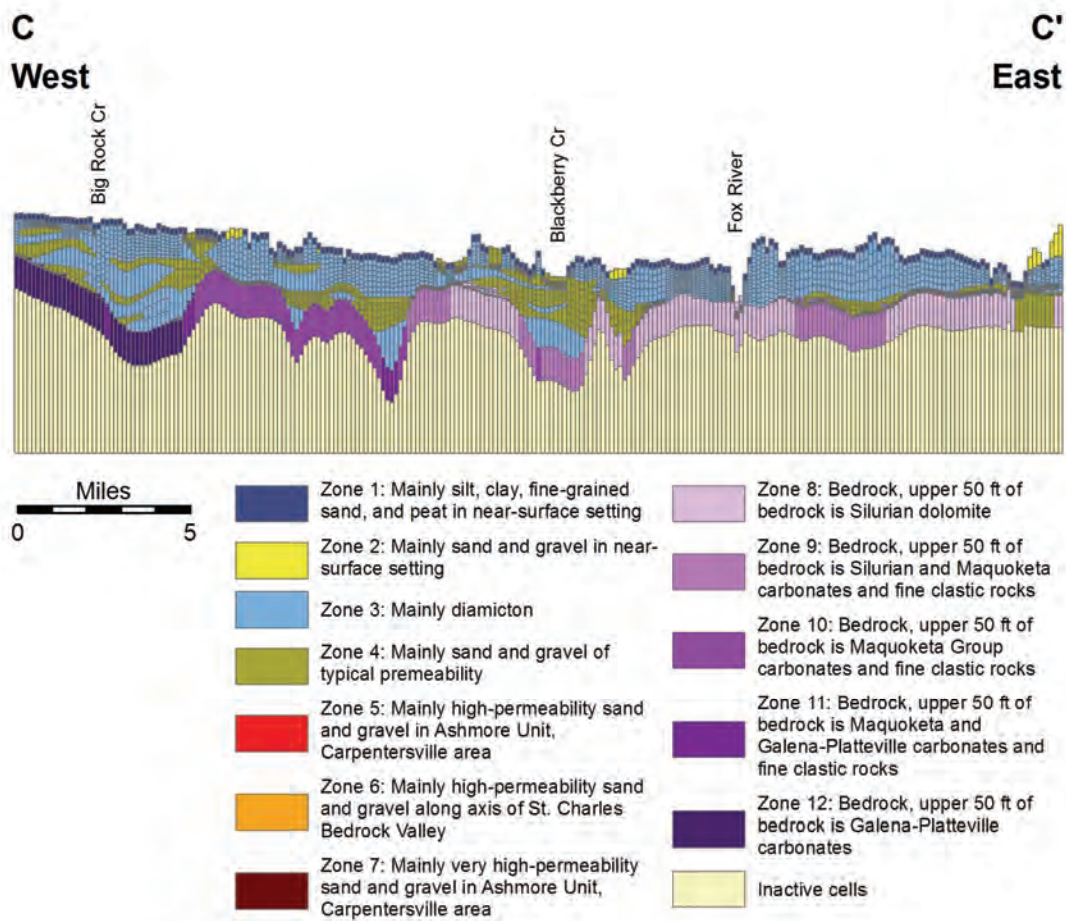


Figure 69. West-to-east cross section C-C' showing hydraulic conductivity zonation of local-scale model in southern part of model domain (see Figure 66 for cross section location).

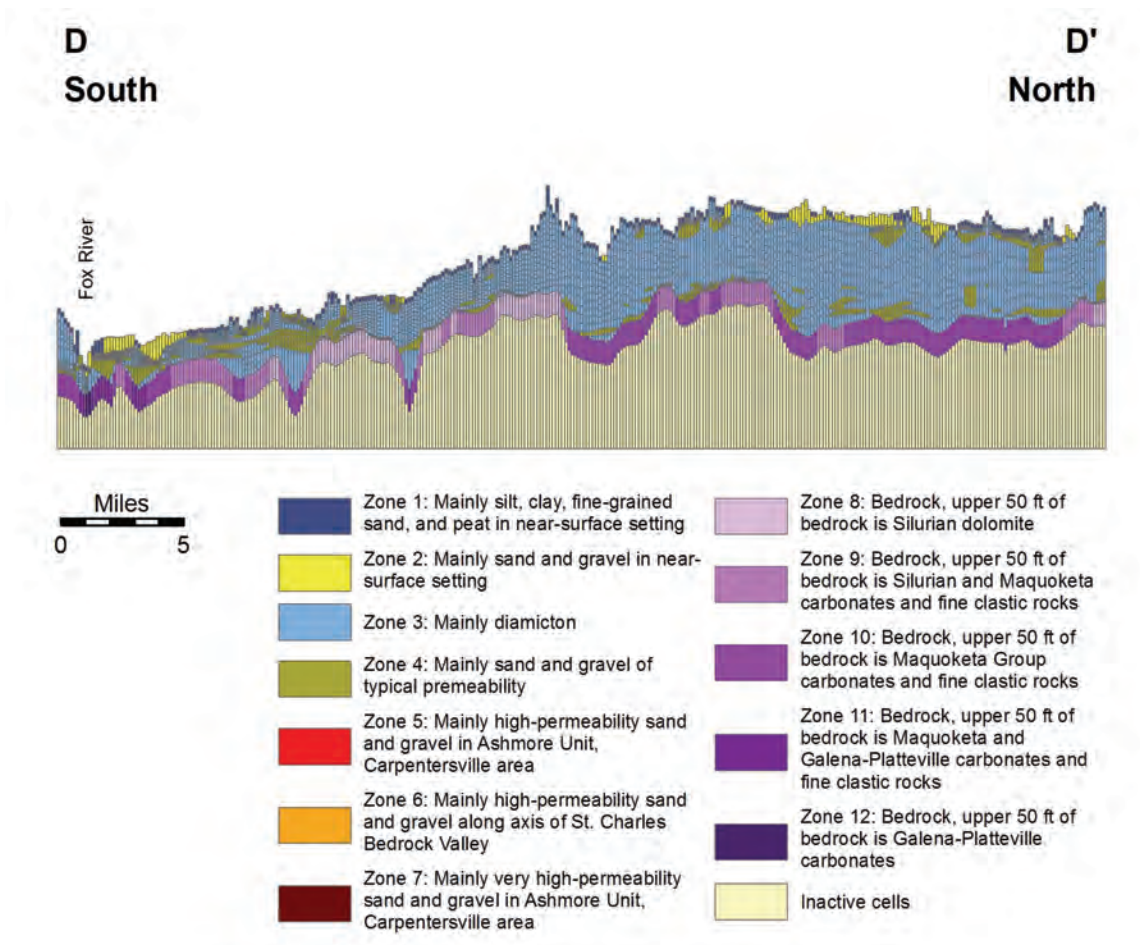


Figure 70. North-to-south cross section D-D' showing hydraulic conductivity zonation of local-scale model in the model domain (see Figure 66 for cross section location).

model, there is no vertical flow across the layer so the K_v values will be poorly constrained and more unreliable than the K_v values of the regional model.

An additional high-conductivity zone (zone 4 in Figure 51), employed in a limited part of the local-scale model domain encompassing part of the West Chicago area of DuPage County, is necessary to maintain simulated heads near observed levels around high-capacity wells in that area. The presence of high shallow bedrock permeability in the West Chicago area is implied by the high pumping capacities for the production wells coupled with relatively low observed drawdowns. For simplicity, the high-conductivity zone is represented with an existing zone used to represent the sand and gravel. Although the accuracy of the assumed distribution of the high-permeability zones and the values of hydraulic conductivity assumed for them is uncertain, the authors believe that the effect on model accuracy within the Kane County portion of the local model domain is negligible.

Sand and Gravel The location and extent of the basic property zones representing unconsolidated sand and gravel and unconsolidated fine-grained materials are based on the geologic model of the Kane County area developed by the ISGS (Dey et al., 2007e). The aquifers as defined by Curry and Seaber (1990)—the St. Charles, Valparaiso, Kaneville, and Bloomington aquifers—were not used in developing the property zones because they are aggregations of multiple sand and gravel layers. The hydraulic conductivity of unconsolidated sand and gravel is represented principally with two zones. Zone 4 represents more deeply buried sand and gravel simulated as layers 3, 5, 7, 9, 11, and 13, and zone 2 represents the surficial Henry Unit simulated in layers 1 and 2. Starting values and plausible ranges for hydraulic conductivities of zones 2 and 4 are based primarily on pumping test data, which is on file at the ISWS (Appendix D), supplemented by published literature (Table 5, Figure 53, Figure 55, Figure 57, Figure 59, Figure 61, Figure 63, and Figure 65). The pumping test data typically consist of constant-rate tests with multiple observation wells. For the purposes of this project, these archival data were reinterpreted using AquiferWin32 (Environmental Simulations Inc., 2001), a software package for type-curve interpretation of hydraulic tests. At many of the tested wells, the available data include data from multiple observation wells and repeated tests, each of which may be interpreted for estimates of hydraulic properties in the region surrounding the tested well. The representative hydraulic conductivity for each well is taken as the median of the estimates available at each well, yielding a set of 24 estimates based on aquifer test data. The median of these estimates is 175 ft/day, and they range from 30 to 2381 ft/day. The range of the estimates within a zone provides the bounds used to constrain the calibration of the local model.

Three additional zones, 5, 6, and 7, are selectively employed to represent areas of elevated permeability in layers 9 and 13. Geologic logs and aquifer tests indicate the presence of these deposits of highly conductive, bouldery sand and gravel in limited areas. One of these occurs in the lower Glasford sand (local model layer 13) within a portion of the St. Charles bedrock valley in east-central Kane County near and within the cities of St. Charles, Geneva, Batavia, and Aurora where highly productive wells are reported. A zone of elevated hydraulic conductivity (zone 6) within local model layer 13 was therefore defined to simulate the presence of these highly conductive materials (Figure 53). Two additional high-conductivity zones (zones 5 and 7) were defined within the Ashmore Unit (local model layer 9) near Carpentersville (Figure 57), where the

Ashmore Unit supports high pumping rates from public-supply wells. Unfortunately, pumping test data are not available as a basis for inferring the hydraulic conductivity of these materials. The hydraulic conductivity of the high-conductivity zones within the Ashmore Unit (local model layer 9) in this area was therefore inferred from specific-capacity data from Carpentersville wells 5, 6, and 7 (Figure 57). These specific capacities suggest conductivities appropriate for the coarse gravel indicated by geologic logs of the wells.

Diamicton The hydraulic conductivity of fine-grained diamictons have been found in field studies of glacial tills in Wisconsin and Alberta to be extremely low (Hendry, 1982; Simpkins and Bradbury, 1992). The low values of these materials are also suggested by a database of Illinois Environmental Protection Agency slug test results compiled by the ISGS (ISGS, personal communication, 2006). Unweathered and unfractured till had the lowest hydraulic conductivity of 3×10^{-5} ft/d to 9×10^{-5} ft/d. Near the surface of an exposed till, weathering and fracturing produces a secondary permeability structure that increases the hydraulic conductivity to 1×10^{-3} ft/d. Large-scale fractures can increase this value to 0.06 ft/d. Because of their great thicknesses, the diamicton layers in Kane County are likely to have a hydraulic conductivity in the range of an unfractured or slightly fractured till except at the surface (Figure 52, Figure 54, Figure 56, Figure 58, Figure 60, Figure 62, Figure 64). Few observations of anisotropy of such materials are available, so K_v values must be inferred from mass balance and modeling studies. In central Illinois, Wilson et al. (1998) used a K_v value of 4×10^{-4} ft/d to model vertical flow through the Glasford and Wedron Formation that is similar to these materials as they occur in Kane County. The soil developed on the fine-grained silts and diamictons are represented by zone 1 (Figure 65). Saturated soils in Kane County that are classified with very slow to moderate permeabilities have a K range of 0.02 to 1.2 ft/d (Deniger, 2004).

2.2.4. Storage Parameters

2.2.4.1. Regional-Scale Model

Starting values and plausible ranges of specific storage (S_s) are based on published studies in the region (Feinstein et al., 2005a; Feinstein et al., 2005b; Foley et al., 1953; Mandle and Kontis, 1992) and on the results of pumping tests conducted in the local-scale model domain. Values are specified for three hydrostratigraphic intervals, reflecting reduction in storage with burial (Table 6). Specific storage of model layers 1-3 (the Quaternary Unit) is inferred from the median of the interpreted pumping tests in sand and gravel aquifers in the local-scale model domain. Starting and minimum specific storage of model layers 4-11 (the mainly dolomitic and fine clastic interval overlying the deep aquifers consisting of the Upper Bedrock Unit downward through the Galena-Platteville Unit) and model layers 12-20 (the deep interval containing the sandstone bedrock aquifers and intervening carbonates and fine clastic rocks) are based on inferences reported by Feinstein et al. (2005a; 2005b). These are, in turn, based on pumping test results in southeastern Wisconsin reported by Foley et al. (1953). The maximum specific storage of the interval is reported by Mandle and Kontis (1992), and is based on geomechanical arguments articulated in their report.

Table 6. Starting Values and Plausible Ranges of Storage Parameters Employed in Development of Regional Model

Model Layer	Specific Storage (S_s) (fr^{-1})			Apparent Specific Yield (S_{ya})			Effective Porosity (n)		
	Starting Value	Range	References	Starting Value	Range	References	Starting Value	Range	References
1	5.7×10^{-6}	$3.7 \times 10^{-7} - 1.8 \times 10^{-5}$	Pumping tests in local-scale shallow model domain	1.5×10^{-1}	$1.2 \times 10^{-1} - 2.3 \times 10^{-1}$	Feinstein et al. (2005a; 2005b), Meyer (1998), Weeks (1969)	2.3×10^{-1}	$1.0 \times 10^{-1} - 3.5 \times 10^{-1}$	Meyer (1998), Driscoll (1986)
2									
3									
4	2.6×10^{-7}	$1.9 \times 10^{-7} - 5.5 \times 10^{-7}$	Feinstein et al. (2005a; 2005b), Foley (1953), Mandel and Kontis (1992)	1.0×10^{-2}	$8.0 \times 10^{-3} - 1.5 \times 10^{-2}$	Feinstein et al. (2005a; 2005b), range assumed to be 80 to 150% of initial value as for model layers 1-3	4.0×10^{-2}	$6.0 \times 10^{-3} - 6.2 \times 10^{-2}$	Meyer (1998), Roadcap (1990)
5									
6									
7									
8									
9									
10									
11									
12	2.6×10^{-7}	$1.9 \times 10^{-7} - 5.5 \times 10^{-7}$	Feinstein et al. (2005a; 2005b), Foley (1953), Mandel and Kontis (1992)	5.0×10^{-2}	$2.9 \times 10^{-2} - 8.3 \times 10^{-2}$	Feinstein et al. (2005a; 2005b), Prickett and Lonquist (1971), S_{ya} assumed to be $S \times 100$	5.0×10^{-2}	$2.9 \times 10^{-2} - 8.3 \times 10^{-2}$	Walton (1964), range assumed to be identical to range of S_{ya}
13									
14									
15									
16									
17									
18									
19									
20									

Starting values and range for the apparent specific yield (S_{ya}) are based on published modeling studies and values inferred from analog field sites, and are assigned to the same hydrostratigraphic intervals as the specific storage. For model layers 1-3, the initial value is the calibrated value from the modeling study of Feinstein et al. (2005a; 2005b). The maximum is based on the assumption that the S_{ya} can be no greater than the effective porosity, which Meyer (1998) estimated to be 0.225 based on the range cited by Driscoll (1986). The minimum S_{ya} is from a series of aquifer tests in central Wisconsin (Weeks, 1969). For model layers 4-11, the initial value of S_{ya} is taken from the modeling study of Feinstein et al. (2005a; 2005b), and the range is scaled proportionately from the range used for model layers 1-3. For model layers 12-20, the initial value of S_{ya} is taken from the modeling studies of Feinstein et al. (2005a; 2005b) and Prickett and Lonquist (1971), which assume S_{ya} is 100 times the storage coefficient. The range is inferred similarly by multiplying the minimum and maximum values of the storage coefficient by 100, using an average thickness of 1500 ft.

Since local studies of porosity do not exist, assumed porosity values are general values based on general ranges from the literature for materials of similar lithology.

2.2.4.2. Local-Scale Shallow Model

Starting values and plausible ranges of S_s , S_{ya} , and n are identical to those specified for regional model development for the Quaternary Unit as summarized in Table 6.

2.2.5. *Recharge*

Recharge rates in both the regional- and local-scale models were zoned to reflect the geographical variability of recharge rates resulting from differences in geology (specifically, permeability of near-surface materials), topography, vegetation, land cover, and other factors. As will be discussed, the bases for the recharge zonations employed in the regional- and local-scale models differ, as does the procedure for calibration of the recharge rates assigned to these zones.

2.2.5.1. Regional-Scale Model

Recharge rates are assigned on a zoned basis in the vicinity of the regional model nearfield, and to areas bordering Lake Michigan (Figure 71, Table 7). Recharge is represented implicitly in the model farfield using constant head cells at land surface, similar to the modeling study of Mandle and Kontis (1992). These cells will automatically calculate the recharge necessary to maintain the water table in this area, which is typically reported to be near land surface and relatively steady through time. Lake Michigan is represented using constant head cells. For the most part, the recharge zonation is adapted, as described in the following paragraphs, from comparatively recent watershed-based mapping of recharge rates by Arnold et al. (2000), Cherkauer (2001), and Holtschlag (1997), who estimated recharge rates for large, sometimes interstate watersheds through analysis of long periods of streamflow records in the Upper Mississippi Basin, southeastern Wisconsin, and Lower Peninsula of Michigan, respectively. It was necessary to use the more dated analysis of Bloyd (1974) to specify recharge rates in more marginal areas of the Wabash River Basin in Indiana (see zone 3 in Figure 71). Zone delineations correspond with watershed outlines. Because the recharge zones correspond with large watershed areas, the recharge rates assigned to

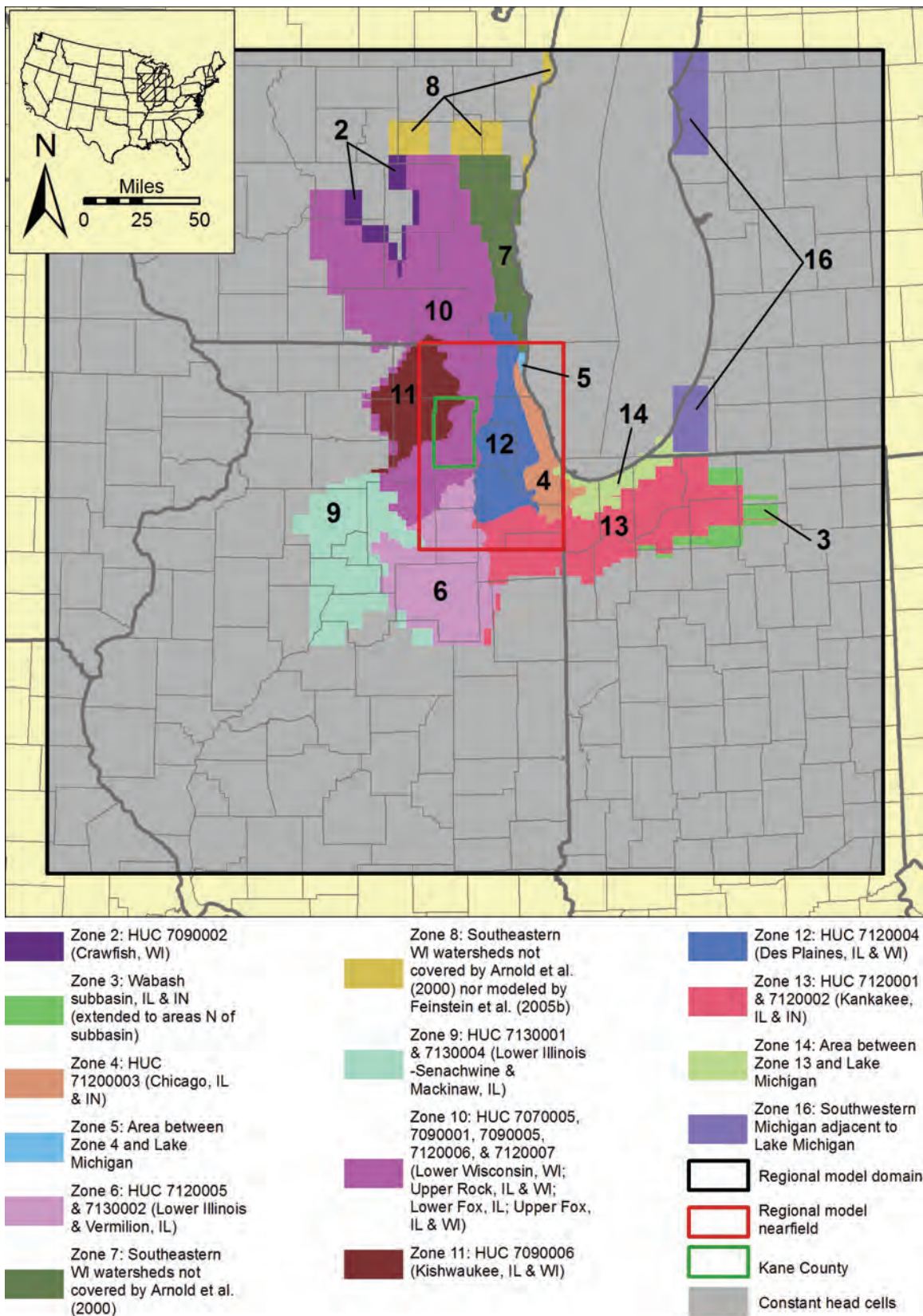


Figure 71. Recharge rate zonation of regional model.

Table 7. Recharge Zonation of Regional-Scale Model

Zone	Region	Starting Value	Range	Reference
2	HUC 7090002 (Crawfish, WI)	6.74×10^{-4} ft/d	±20%	Arnold et al. (2000)
3	Wabash subbasin, IL & IN (extended to areas N of subbasin)	9.98×10^{-4} ft/d	±20%	Bloyd (1974)
4	HUC 71200003 (Chicago, IL & IN)	2.25×10^{-4} ft/d	±20%	Arnold et al. (2000)
5	Area between Zone 4 and Lake Michigan	2.25×10^{-4} ft/d	±20%	Zone 4 (Arnold et al., 2000)
6	HUC 7120005 & 7130002 (Lower Illinois & Vermilion, IL)	6.74×10^{-4} ft/d	±20%	Arnold et al. (2000)
7	Southeastern WI watersheds not covered by Arnold et al. (2000)	7.46×10^{-4} ft/d	±20%	Model-calibrated values (Feinstein et al., 2005a)
8	Southeastern WI watersheds not covered by Arnold et al. (2000) nor modeled by Feinstein et al. (2005b)	1.03×10^{-3} ft/d	±20%	Average for southeastern WI watersheds (Cherkauer, 2001)
9	HUC 7130001 & 7130004 (Lower Illinois-Senachwine & Mackinaw, IL)	1.12×10^{-3} ft/d	±20%	Arnold et al. (2000)
10	HUC 7070005, 7090001, 7090005, 7120006, & 7120007 (Lower Wisconsin, WI; Upper Rock, IL & WI; Lower Fox, IL; Upper Fox, IL & WI)	1.57×10^{-3} ft/d	±20%	Arnold et al. (2000)
11	HUC 7090006 (Kishwaukee, IL & WI)	2.02×10^{-3} ft/d	±20%	Arnold et al. (2000)
12	HUC 7120004 (Des Plaines, IL & WI)	1.12×10^{-3} ft/d	±20%	Arnold et al. (2000)
13	HUC 7120001 & 7120002 (Kankakee, IL, IN, & MI; Iroquois, IL & IN)	2.92×10^{-3} ft/d	±20%	Arnold et al. (2000)
14	Area between Zone 13 and Lake Michigan	2.25×10^{-4} ft/d	±20%	Zone 4 (Arnold et al., 2000)
16	Southwestern Michigan adjacent to Lake Michigan	2.11×10^{-3} ft/d	±20%	Average of area- weighted estimates for SW MI watersheds (Holtschlag, 1997)

them represent average rates. Actual recharge rates within the watershed may vary considerably from these average rates based on geology, slope, land cover, and other factors. Other supporting data were derived from groundwater flow modeling of southeastern Wisconsin (Feinstein et al., 2005a; Feinstein et al., 2005b). Final, calibrated values of recharge are discussed in Section 2.3.1.3.

Where applicable, the authors employed the mapping by Arnold et al. (2000), who used the soil and water assessment tool model (SWAT) to estimate recharge rates for United States Geological Survey (USGS) Hydrologic Unit Codes (HUCs) in the Upper Mississippi Basin, as the basis for recharge rates in the regional-scale model. In some cases, recharge rates were assigned only for parts of watersheds examined by Arnold et al. (2000), the remainder of these watersheds being represented by constant head cells. Examples include the watersheds of the Crawfish River (part of which is represented by zone 2), Mackinaw River (partly in zone 9), and the lower Wisconsin and lower Rock Rivers (partly in zone 10). For lack of more recent estimates, the recharge rate estimated by Arnold et al. (2000) for the Chicago River watershed (zone 4) was employed in adjacent zones 5 and 14. Use of this relatively low recharge rate in zone 14 is consistent with the observation of the Indiana Governor's Water Resource Study Commission (1980) that the surficial materials in the lakeshore area of northwestern Indiana consist of poorly drained clay.

Groundwater flow modeling of southeastern Wisconsin (Feinstein et al., 2005a; Feinstein et al., 2005b), together with a supporting recharge rate study of southeastern Wisconsin (Cherkauer, 2001), were employed as the basis for the recharge rates assumed for zones 7 and 8. The assumed recharge rate in zone 7 is a simple average of calibrated recharge rates from 5864 cells of the groundwater flow model of southeastern Wisconsin developed by Feinstein et al. (2005a; 2005b) within the area of zone 7. Zone 8 is assigned a recharge rate that is the average of recharge rates estimated for southeastern Wisconsin watersheds by Cherkauer (2001), as employed by Feinstein et al. (2005a; 2005b) in portions of the southeastern Wisconsin model domain not within watersheds studied directly by Cherkauer (2001).

Recharge rates estimated from analyses published by Bloyd (1974) and Holtschlag (1997) were employed in limited areas. The recharge rate assigned to zone 3 is identical to the recharge rate estimated for the Wabash sub-basin of the Ohio River basin in Illinois, Indiana, and Ohio by Bloyd (1974). The northern part of zone 3, however, includes a very limited number of cells that do not fall in the Wabash sub-basin; these cells were, nevertheless, assigned the Wabash sub-basin recharge rate on the basis of their proximity to the Wabash sub-basin. The recharge rate assigned to zone 16 is based on an area-weighted average of recharge rates estimated for southwestern Michigan watershed by Holtschlag (1997).

Just as for hydraulic conductivity, estimates of recharge rates (*starting* or *initial values*) and plausible ranges were developed for each recharge zone in the regional-scale model as an initial step in the calibration process. Because large numbers of independent observations of recharge are not available, and to account for uncertainty in the estimates of recharge employed as starting values, a speculative plausible range of ± 20 percent is applied to all starting values. In the process of calibration (Section 2.3), these estimates were changed, honoring the plausible ranges, to improve the accuracy of the simulations.

2.2.5.2. Local-Scale Shallow Model

With the availability of the detailed geologic and surface-water models for Kane County, recharge rates are zoned based on the surficial geologic material and calibrated to streamflow rates. Soil developed on the fine-grained diamictons is assigned a lower recharge rate, and comparatively permeable sands and gravels are assigned higher recharge rates (Figure 72). This segregation of recharge rates removes the constraint of using an averaged value for an entire watershed such as those estimated by Arnold et al. (2000) or Cherkauer (2001). Because the recharge process is time- and scale-dependant, recharge values must match the time and scale of the model. For this model, the authors chose to calibrate recharge rates to the average of the Q_{80} and Q_{50} (i.e., flows that are exceeded by 80 percent and 50 percent, respectively, of the observed streamflows) in the streams as determined by Knapp et al. (2007). As discussed in section 2.3.1.2, this flux target for baseflow is consistent with the study of Meyer (2005) for watersheds in Illinois and is similar to the approach used by Feinsein et al. (2005a; 2005b).

The recharge rate through the glacial diamictons reflects several water-exchange processes among the the overlying soil, surface waters, and the atmosphere. These processes include infiltration, evaporation, transpiration, drainage into field tiles, and lateral flow into ditches. These processes cause the surficial water table to annually fluctuate between land surface in winter and the depth of the drainage tiles in summer. Because the average depth to water in the wells measured for this study is 46 feet, the water table fluctuation at the surface will have only a minimal impact on the vertical flow gradient across the diamicton. To model this system, a sufficiently large recharge rate was used to keep the soil zone saturated and to exceed the downward flow rate of water across the diamicton. The excess recharge either flows laterally into the next model cell or is carried off by the river or drain boundary condition assigned within the model cell. By using this modeling approach, the net downward recharge is controlled more by the relatively low vertical permeability of the diamicton than by the assigned recharge rates. Previous recharge estimates for a glacial till plain vary from 2×10^{-4} ft/d for a model calibrated to $Q_{7,10}$ flows (Wilson et al., 1998) to 8×10^{-4} ft/d for flownet analyses in Will and Cook Counties (Roadcap et al., 1993) and DuPage County (Sasman et al., 1981).

The recharge rate to the surficial sand and gravel was assigned an initial value that is higher than the watershed average values of Arnold et al. (2000) or Cherkauer (2001) in order to balance the relatively lower recharge rates assigned to fine-grained soils. Recharge rates to outcrops of sand and gravel are difficult to determine in northeastern Illinois because the outcrops do not cover entire watersheds. Estimates of recharge for the large sandy watersheds in Mason County range from 1.3×10^{-3} to 5.4×10^{-3} ft/d depending on the amount of precipitation (Clark, 1994). During the calibration process, two additional recharge zones (3 and 4) were created based on local hydrologic conditions. The lower recharge rate of zone 3 is applied to isolated bodies of surficial sand and gravel that are not connected to surface waters or larger bodies of saturated sand and gravel. Zone 3 also includes the sand plain along Coon Creek that is heavily dissected by ditches. Conversely, the higher recharge rate of zone 4 is applied to isolated outcrops of sands connected to buried aquifers that are able to accept the additional flow. Some areas where the surficial sand is thick and the water table is below the assumed evapotranspiration limiting depth of 10 ft were also assigned the higher rate.

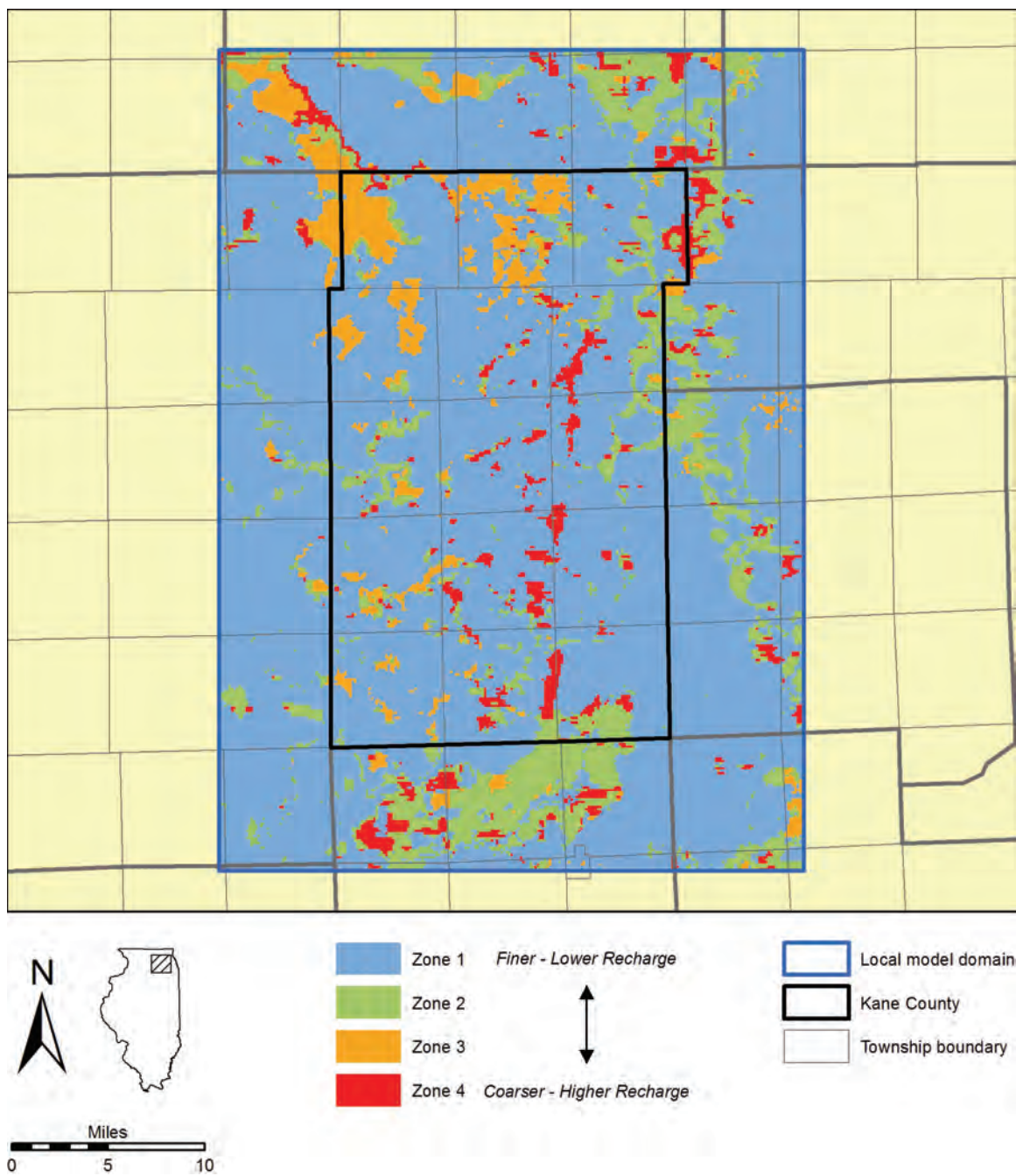


Figure 72. Recharge rate zonation of local-scale model.

2.2.6. Representation of Surface Water

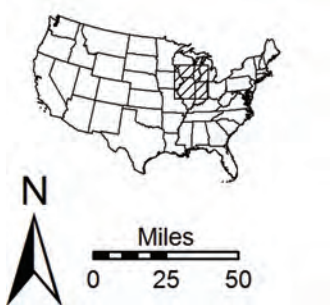
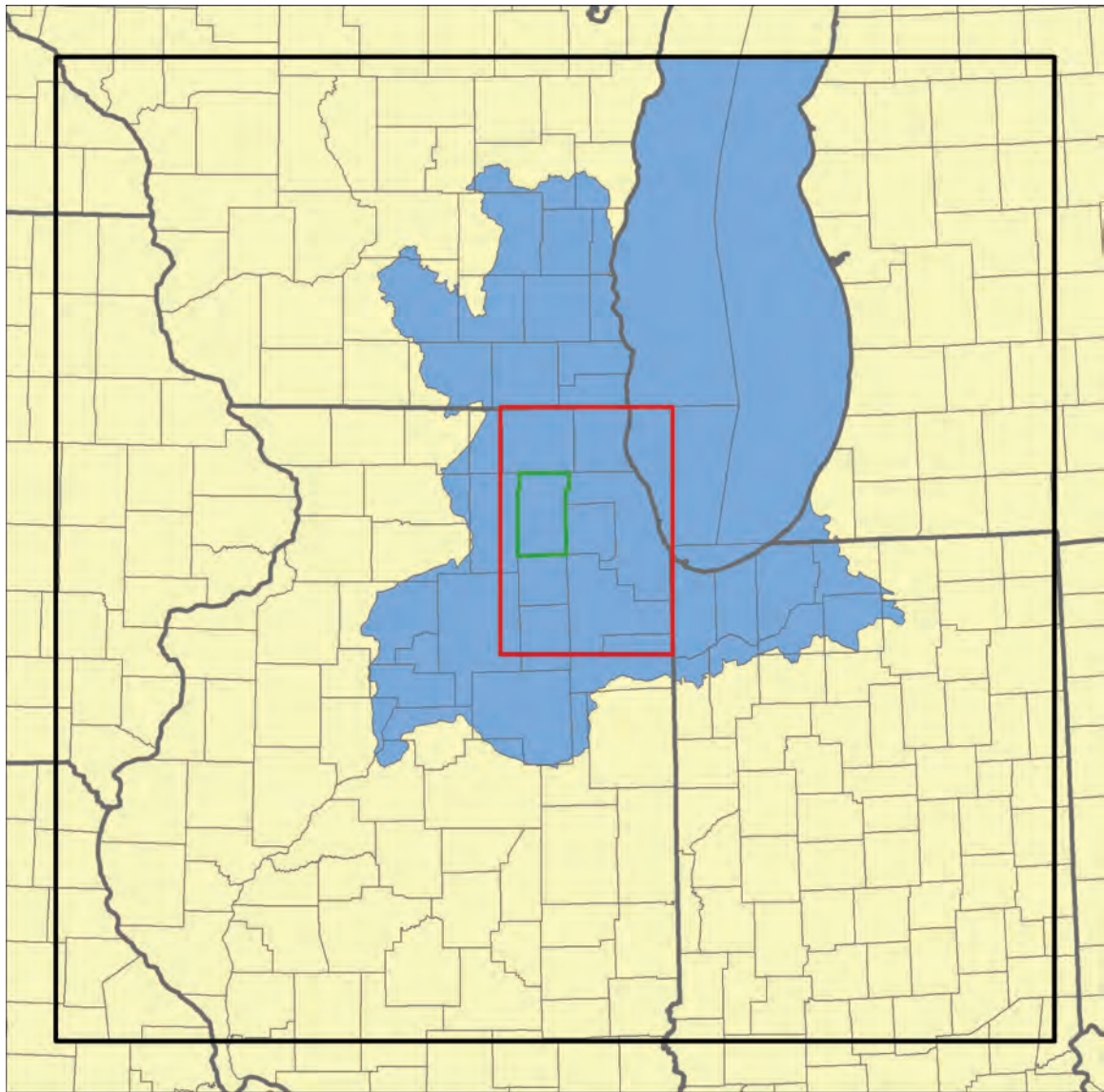
Surface waters interact with the groundwater and are therefore represented in both regional and local-scale groundwater flow models using the MODFLOW *river package* and *drain package*. Packages are modules within the MODFLOW groundwater flow program that control input and output for various aspects of the model such as internal boundary conditions. In general, cells represented with the river package (river cells) can both discharge water to the subsurface and receive water from it, but cells represented with the drain package (drain cells) only receive water from the subsurface. This section describes the procedures used to identify cells representing surface water in the models and the assumptions regarding the hydraulic characteristics of these cells.

2.2.6.1. Regional-Scale Model

Surface water (as well as drained conditions, discussed in Section 2.2.7.1) is represented within an irregular area, delineated using watershed boundaries, surrounding the nearfield of the model (Figure 73) and encompassing Lake Michigan and the following USGS hydrologic units: 7090001, 4040003, 7120006, 4040002, 7120004, 7090006, 7120003, 4040001, 7120007, 7120001, 7130001, 7120005, and 7130002. Except for its inclusion of Lake Michigan and a small corner of southwestern Michigan, this area is employed for representation of shallow aquifer withdrawals in the regional model, as well, and in that context is referred to as the shallow aquifer withdrawal accounting region (SAWAR) [Appendix B].

Streams and lakes are simulated in the model using the MODFLOW river and drain packages. The river package is employed to simulate permanent lakes and permanent streams—that is, streams having a 7-day, 10-year low flow ($Q_{7,10}$) greater than zero, and the drain package is used to simulate intermittent streams—those having a $Q_{7,10}$ of zero. Use of both the river and drain packages requires that model cells be identified as river or drain cells, and then—for the cells so identified—that parameters controlling the interaction of groundwater and surface water at the location be specified. Locations of all surface-water features simulated in the model, either as river or drain cells, were obtained using the medium-resolution USGS National Hydrography Dataset (NHD), a GIS resource providing a wide range of information on surface waters throughout the United States. Stream reaches in the NHD having a $Q_{7,10}$ greater than zero (represented using the river package) were identified using published maps providing regional streamflow data, including those by Singh et al. (1988a; 1988b) and Singh and Ramamurthy (1993) covering Illinois, Fowler and Wilson (1996) covering Indiana, and Holmstrom (1978) covering southeastern Wisconsin. The remaining streams were simulated using the drain package. All lakes included in the NHD were simulated using the river package.

For river cells, MODFLOW requires specification of the surface-water elevation, lake or stream-bottom elevation, and lake or streambed conductance (a function of lake or streambed area, vertical hydraulic conductivity, and thickness). For purposes of model development and calibration, river cells were divided into three categories: (1) those representing streams having $Q_{7,10}$ greater than zero; (2) inland lakes; and (3) Lake Michigan (Figure 74). Surface-water elevation, lake or stream-bottom elevation, and initial values of lake or streambed conductance were specified somewhat differently for these three categories of river cells, and conductance of each category was calibrated






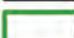
-  Area of surface water simulation
-  Regional model nearfield
-  Regional model domain
-  Kane County

Figure 73. Area where surface water and drained conditions are simulated in regional model.

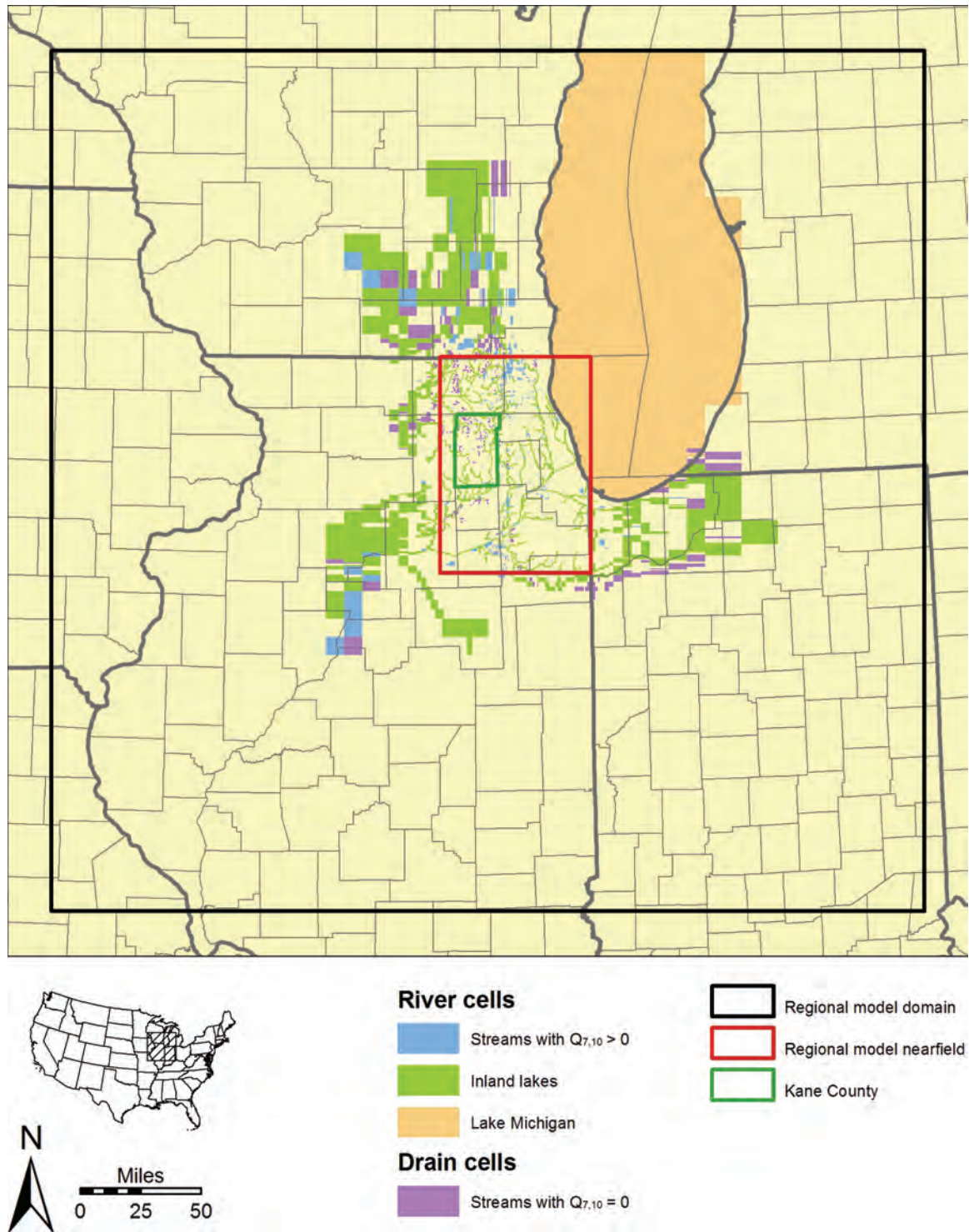


Figure 74. Representation of surface water in regional model.

independently of the other two (Table 8). For all three categories, surface-water elevation was specified as land surface elevation based on USGS Digital Elevation Model (DEM) data. Stream-bottom elevation was set at 1 ft below surface-water elevation for river cells representing streams having $Q_{7,10}$ greater than zero. Lake bottom elevation was set at 3 ft below surface-water elevation for river cells representing inland lakes, and, for those representing Lake Michigan, lake bottom elevation was set at an estimate of actual Lake Michigan bottom elevation based on mapping of Lake Michigan bathymetry (National Oceanic and Atmospheric Administration Satellite and Information Service, 1996). Surface-water elevation and lake or stream-bottom elevation were not changed during the calibration process.

Estimation of initial values of conductance and subsequent calibration required several data-processing steps. For river cells representing inland lakes and Lake Michigan, the lakebed area was estimated for each cell using mapped areas from the NHD and a GIS technique to estimate the lakebed area within each river cell. For cells representing streams having $Q_{7,10}$ greater than zero, streambed area data are not readily available, and an estimate of streambed area in each river cell was therefore developed from estimates of stream length and width. Streambed length was estimated using the mapped reach length as depicted in the NHD. Streambed width was estimated using a GIS technique, described by Bartosova et al. (2004), that employed the NHD and observations of stream width at 85 gaging stations in the area of surface-water simulation (Figure 73) to establish an empirical relationship between stream width at a location and the arbolate sum (the sum of the length of reaches upstream of a location). NHD stream reaches were divided into segments corresponding to the portions falling within individual regional model cells. Using width estimates determined for the NHD reaches, total streambed area for each model cell was computed. Conductance (C) is equal to bed area multiplied by the bed leakance, with leakance defined as bed vertical hydraulic conductivity divided by bed thickness:

$$C = A \times \left(\frac{K_v}{m} \right)$$

Where:

A = bed area

K_v = bed vertical hydraulic conductivity

m = bed thickness

Leakance was calibrated for all river cells, and since it is the product of leakance and bed area (which is fixed for each cell), conductance was indirectly calibrated along with leakance. For cells representing streams having $Q_{7,10}$ greater than zero, the initial value of leakance was set to 10^0 feet per day per foot (ft/d-ft); for cells representing inland lakes and Lake Michigan, leakance was set to 10^{-2} ft/d-ft. These choices are consistent with field and laboratory determinations, as well as modeling results, showing that riverbed leakances worldwide generally fall between 10^{-1} to 10^1 ft/d-ft (Calver, 2001). The plausible ranges of leakance for all three categories were set at 1 percent to 1000 percent of the initial value (10^{-2} to 10^1 ft/d-ft for streams having $Q_{7,10}$ greater than

zero, and 10^{-4} to 10^{-1} ft/d-ft for inland lakes and Lake Michigan). Recent modeling in southeastern Wisconsin (Feinstein et al., 2005a) employed a streambed leakance of 5.0×10^0 ft/d-ft and leakances of 5.0×10^{-2} to 5.0×10^{-1} ft/d-ft for the centers and perimeters of lakes, respectively. The authors of the southeastern Wisconsin model acknowledge that streambed leakance in their model is set high, so we selected a plausible range that allowed calibration of streambed leakance to a value lower than 5.0×10^0 ft/d-ft. We selected a plausible range of leakances for inland lakes and Lake Michigan that permits calibration to a lower leakance than employed in the Wisconsin model and that accommodates, in a single value, lateral differences in leakance between the centers and perimeters of lakes.

Small streams—those having a $Q_{7,10}$ equal to zero—are represented using the MODFLOW drain package (Figure 74). For each drain cell, MODFLOW requires that a drain elevation be specified. This elevation was estimated as the land surface elevation based on USGS DEM data. Also required is a conductance value, which—as described for river cells representing streams having $Q_{7,10}$ greater than zero—was based on an estimate of streambed area determined from an empirical relationship of streambed width and arbolate sum (Bartosova et al., 2004). As discussed previously, conductance is equal to streambed area multiplied by leakance, and it is leakance that was calibrated. Based on the references discussed in the preceding paragraph, the initial value of leakance assigned to these drain cells was set to 1 ft/d-ft, and the plausible range was set at 1 percent to 1000 percent of the initial value, or 10^{-2} to 10^1 ft/d-ft (Table 8).

2.2.6.2. Local-Scale Shallow Model

Surface water (as well as drained conditions, discussed in Section 2.2.7.1) is represented throughout the local-scale model domain. Just as for the regional model, streams are simulated in the local-scale model using the MODFLOW river and drain packages. The river package is employed to simulate permanent streams (streams having a 7-day, 10-year low flow [$Q_{7,10}$] greater than zero), and the drain package is used to simulate intermittent streams (those having $Q_{7,10}$ equal to zero). The locations of all

Table 8. Starting Values and Plausible Ranges of Leakance (K_v/m) Employed for Representation of Surface Water in Regional Model

<i>MODFLOW Package</i>	<i>Category</i>	<i>Leakance (ft/d-ft)</i>		<i>References</i>
		<i>Starting Value</i>	<i>Range</i>	
River	Streams with $Q_{7,10} > 0$	10^0	$10^{-2} - 10^1$	Calver (2001), Feinstein et al. (2005a; 2005b)
	Inland lakes	10^{-2}	$10^{-4} - 10^{-1}$	
	Lake Michigan	10^{-2}	$10^{-4} - 10^{-1}$	
Drain	Streams with $Q_{7,10} = 0$	10^0	$10^{-2} - 10^1$	

streams simulated in the model, either as river or drain cells, were obtained using the medium-resolution USGS NHD. Stream reaches in the NHD having $Q_{7,10}$ greater than zero (represented using the river package) were identified using field observations under low-flow conditions, published maps [(Singh et al. (1988a; 1988b); Singh and Ramamurthy (1993)], and on statistical modeling of streamflow in the Kane County area (Knapp et al., 2007). Because upstream reaches can dry up, these reaches are simulated using the drain package to prevent the model from inducing water out of a dry creek. The exception to this is Mill Creek, where pools of stagnant water have been observed at low flow, suggesting that this creek may act as a recharge basin for the Batavia and Geneva wellfields.

As discussed in the previous section, MODFLOW requires that river cells include specification of the surface-water elevation, stream-bottom elevation, and streambed conductance (a function of lake or streambed area, vertical hydraulic conductivity, and thickness). For river cells in the local-scale model (Figure 75), surface-water elevations were based on the elevation contours shown on the USGS topographic maps. River cell elevations were interpolated with a uniform gradient between cells with known elevations. Stream-bottom elevations were set at 3 ft below surface-water elevation. Because of the ample scouring of native materials, we assume the streams with $Q_{7,10}$ greater than zero represent the water table and are well connected to the adjacent groundwater. Therefore, a sufficiently large ($10,000 \text{ ft}^2/\text{d}$) bed conductance was used so the flow of groundwater into or out of the streams is not impeded. For a few cells along Mill Creek and the Fox River in east-central Kane County, bed conductance was reduced to $1000 \text{ ft}^2/\text{d}$ during the calibration process to prevent excessive stream leakage. The conductances of two cells along the DuPage River near the edge of the model were increased to help supply water to wells in an area that was historically overpumped.

Small streams—those having a $Q_{7,10}$ equal to zero—are represented using the MODFLOW drain package (Section 2.2.7.2).

2.2.7. Representation of Drained Areas

Agricultural drainage systems (tile drains) and urban storm water systems have significantly changed the hydrologic cycle in the upper Midwest from its predevelopment condition. Each of these engineered drainage systems has lowered the water table, altering the circulation of groundwater and profoundly affecting the shallow groundwater system near the water table.

Areas with urban and agricultural drainage systems are represented in both the regional- and local-scale models using the MODFLOW drain package, as was employed to represent small streams having $Q_{7,10}$ equal to zero (Section 2.2.6). Drain cells were assigned a leakance that was calibrated or altered within a plausible range of values to improve agreement between observations and model simulations of groundwater flow. This section describes the identification of cells representing drained areas in the models and the assumptions regarding the characteristics of these cells, including the initial assumed values and plausible ranges of leakance.

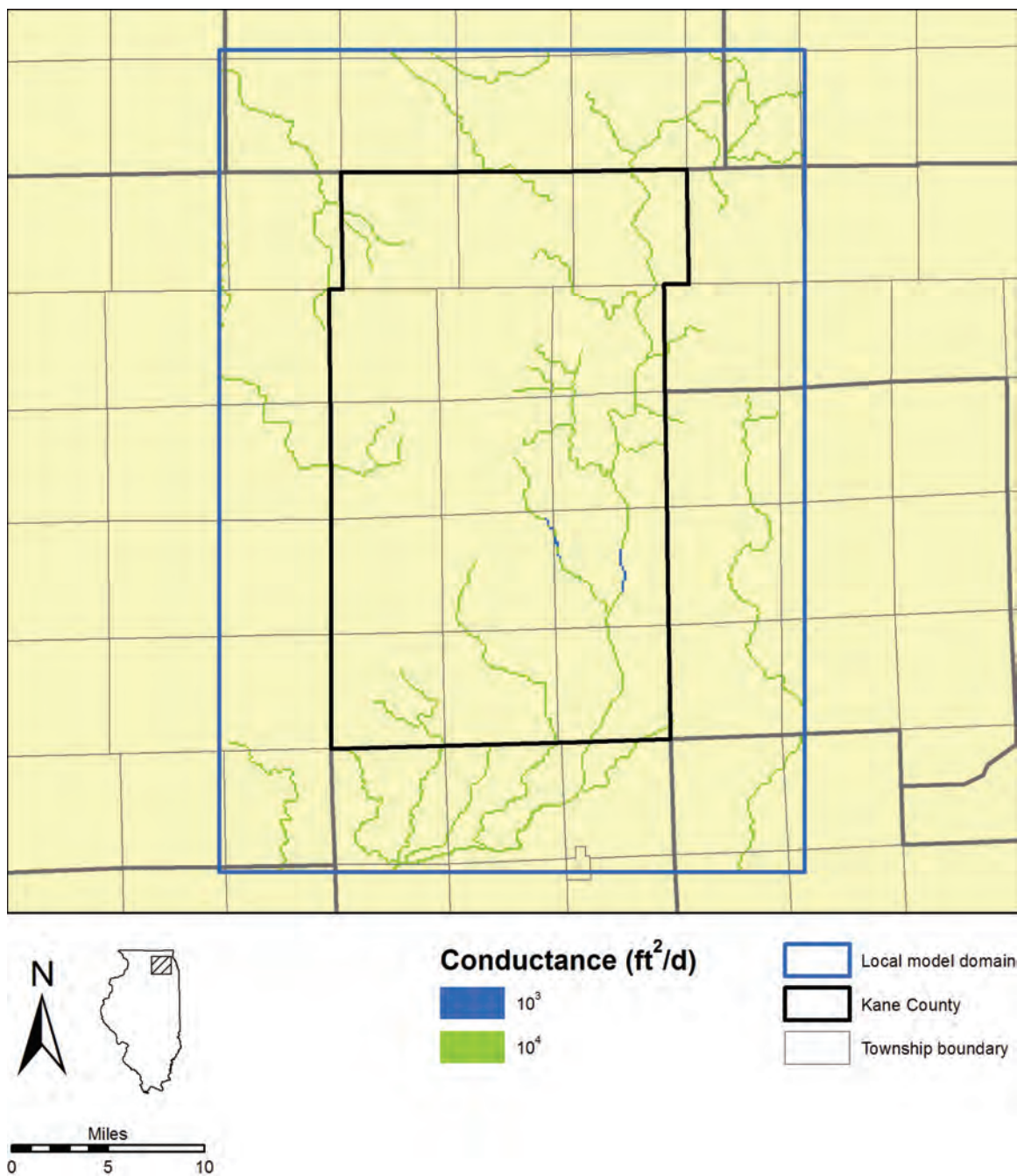


Figure 75. Representation in the local-scale model, using the MODFLOW river package, of streams having $Q_{7,10}$ greater than zero.

2.2.7.1. Regional-Scale Model

Surface water and drained conditions are simulated in an irregular area defined with watershed boundaries surrounding the regional model nearfield (Figure 73). A polygon shape file representing the 1990 incorporated areas having a population greater than 50,000 (ESRI Bureau of Transportation Statistics, 1990) was employed to identify model cells in areas of urban drainage (Figure 76). Although this method of selection does not simulate the expansion of urban drainage systems accompanying regional development, the 1990 incorporated areas represent a reasonable approximation of current urban drainage in the region. Simulation of predevelopment and historical drainage conditions is left to future analyses. Areas of probable agricultural drainage were identified using a shape file depicting soil characteristics as mapped in the United States Department of Agriculture State Soil Geographic (STATSGO) database (United States Department of Agriculture Natural Resources Conservation Service, 1994). This shapefile was consulted to identify polygons (those not already representing urban drainage) representing soil associations with more than 50 percent somewhat poorly drained soil types. Like the method of selection of cells representing urban drainage, this method cannot permit identification of changing areas of agricultural drainage; however, it does allow for more accurate simulation of groundwater flow under the present regime (and probably the future regime) of intensive agriculture in rural areas.

MODFLOW requires that drain elevation and conductance be specified for all drain cells, and these parameters were assigned uniformly for each of the two categories of drain cells. Both categories of drain cells were assigned an elevation equal to 3 ft below land surface as estimated from USGS DEM data. Initial values of leakance for both categories of drain cell were set to 1 ft/d-ft, and the plausible range was set at 1 percent to 1000 percent of the initial value, or 0.01 to 10 ft/d-ft (Table 9). Drain output was routed to the appropriate stream, based on the location of the drain cell relative to watershed boundaries, so that it could be included in flux estimates employed in model calibration.

Table 9. Starting Values and Plausible Ranges of Leakance Employed for Representation of Drained Areas in Regional Model

<i>Category</i>	<i>Leakance (ft/d-ft)</i>		<i>References</i>
	<i>Starting Value</i>	<i>Range</i>	
Urban drainage	10 ⁰	10 ⁻² – 10 ¹	Calver (2001), Feinstein et al. (2005a; 2005b)
Agricultural drainage	10 ⁰	10 ⁻² – 10 ¹	

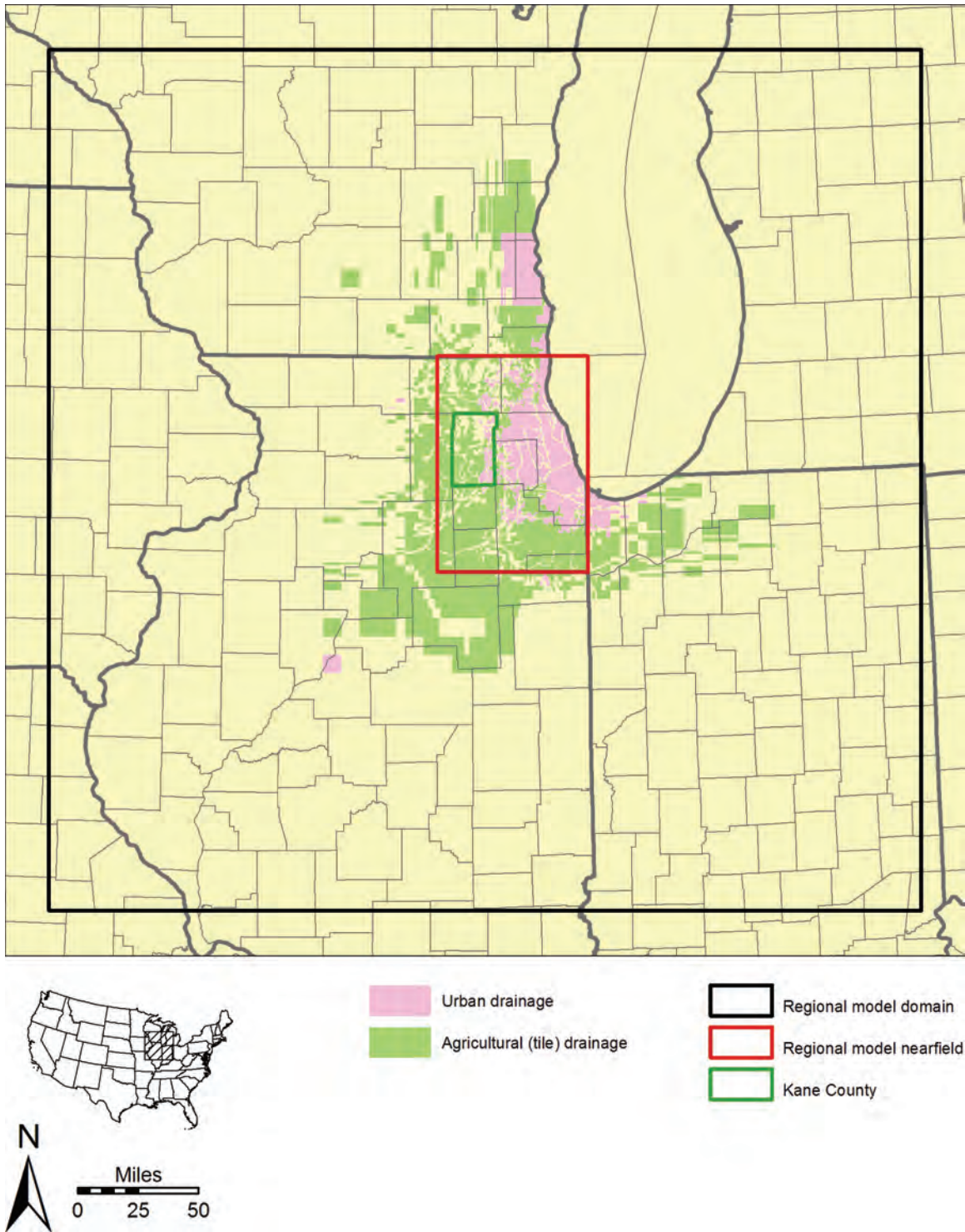


Figure 76. Representation of drained areas in regional model.

2.2.7.2. Local-Scale Shallow Model

Drained conditions are simulated throughout the local model domain using the MODFLOW drain package (Figure 77). Drains simulated in the model represent three hydrologic features: the intermittent streams in the USGS database (those having $Q_{7,10}$ equal to zero), agricultural tile drains, and urban drainage. Drain locations were determined using available GIS resources depicting urban areas together with the ISGS-provided geological model (Section 2.2.2.2). Areas of probable drainage by agricultural tiles were specified using the outline of the soil developed from the diamictos (hydraulic conductivity zone 1) in model layer 1 (Figure 65). The authors consider the methodology of employing the ISGS-provided geological model to identify areas of probable agricultural drainage in the local model domain to be more accurate than the soils mapping used to identify these areas in the regional model domain. As described for the regional model (Section 2.2.7.1), a polygon shape file representing the 1990 incorporated areas having a population greater than 50,000 (ESRI Bureau of Transportation Statistics, 1990) was employed to identify model cells for representation as areas of urban drainage (Figure 77). Although this method of selection does not permit simulation of the expansion of the urban drainage systems accompanying development of the region, the 1990 incorporated areas represent a reasonable approximation of current urban drainage in the region and therefore permit more accurate simulation of current groundwater flow at the possible expense of accurate simulation of predevelopment and historical conditions.

Conceptually, the drains in the low permeability soil are designed to carry excess recharge out of layer 1, keep the water table below land surface, and contribute to the total flow balance of the streams within the watersheds. Therefore, the conductances of these drains were set at a value high enough to accommodate all of the incoming recharge flux if necessary. With the drain set of 3 ft below the land surface elevation and a recharge flux of less than $300 \text{ ft}^3/\text{d}$, the resulting conductance value is $100 \text{ ft}^2/\text{d}$. Sizing the conductance value to the flux in these cells also improved the numerical stability of the model. Like the river cells, the drain cells in more permeable sand and gravels were assigned a high enough conductance value ($1 \times 10^4 \text{ ft}^2/\text{d}$) so flow into the drains would not be impeded. As in the regional model, drain output was routed to the appropriate stream, based on the location of the drain cell relative to watershed boundaries, so that it could be included in flux estimates employed in model calibration.

2.2.8. *Withdrawals*

Groundwater withdrawal data were compiled for a total of 10,980 wells and for an additional group of seven “pumping centers” employed to represent pre-1964 withdrawals from deep wells in northeastern Illinois (Appendix B). Withdrawals from all of these wells and pumping centers were simulated in the regional groundwater flow model (Figure 78, Figure 79), and withdrawals from wells open only to the shallow aquifers were simulated in the local-scale model (Figure 80). For purposes of simulating withdrawals from wells open to multiple layers, the groundwater flow modeling software employed for this study [Groundwater Vistas (Environmental Simulations Inc., 2005)] apportions withdrawals on the basis of the transmissivities of the intercepted layers.

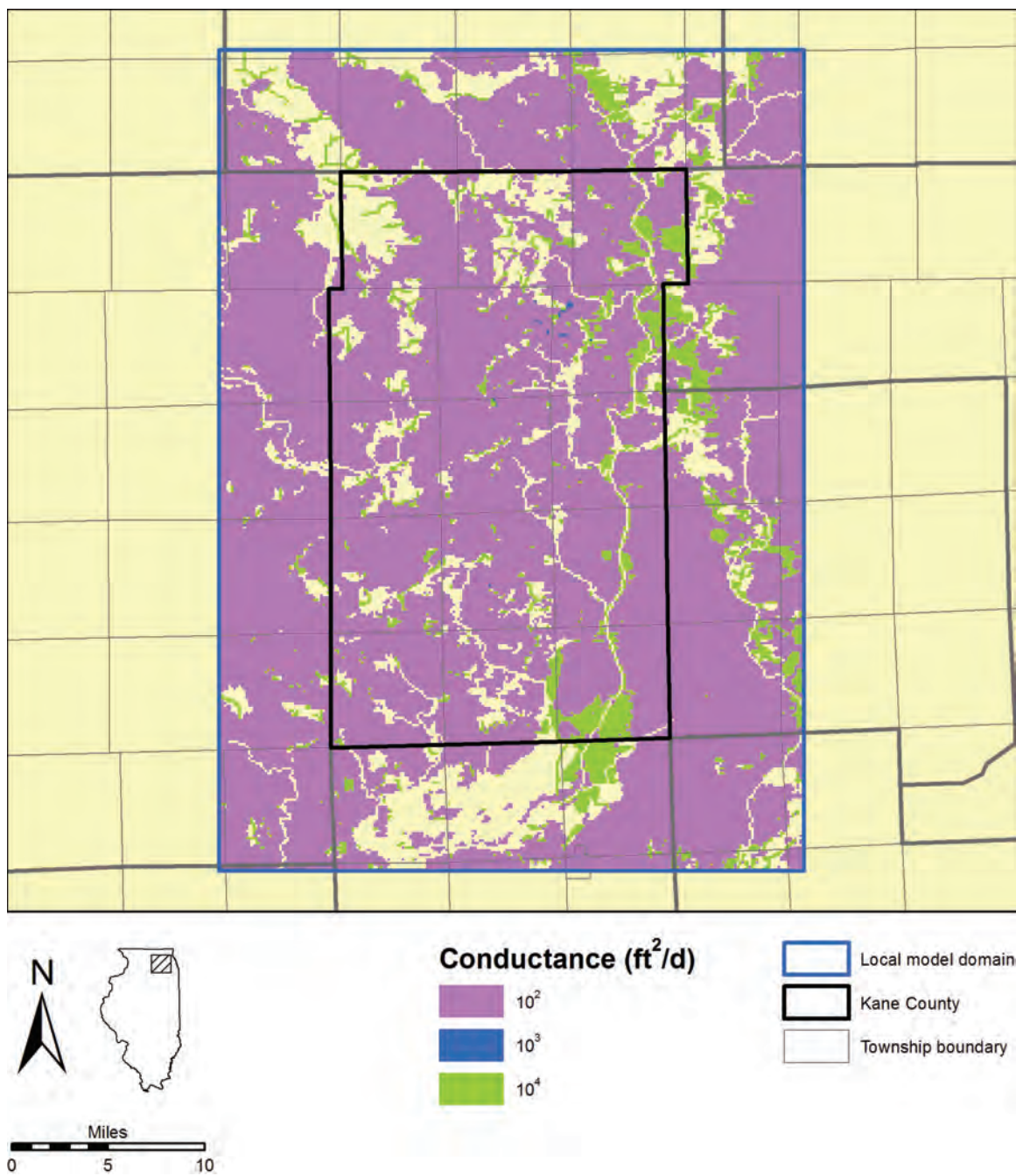


Figure 77. Representation of drained areas and intermittent streams in local-scale model with the MODFLOW drain package.

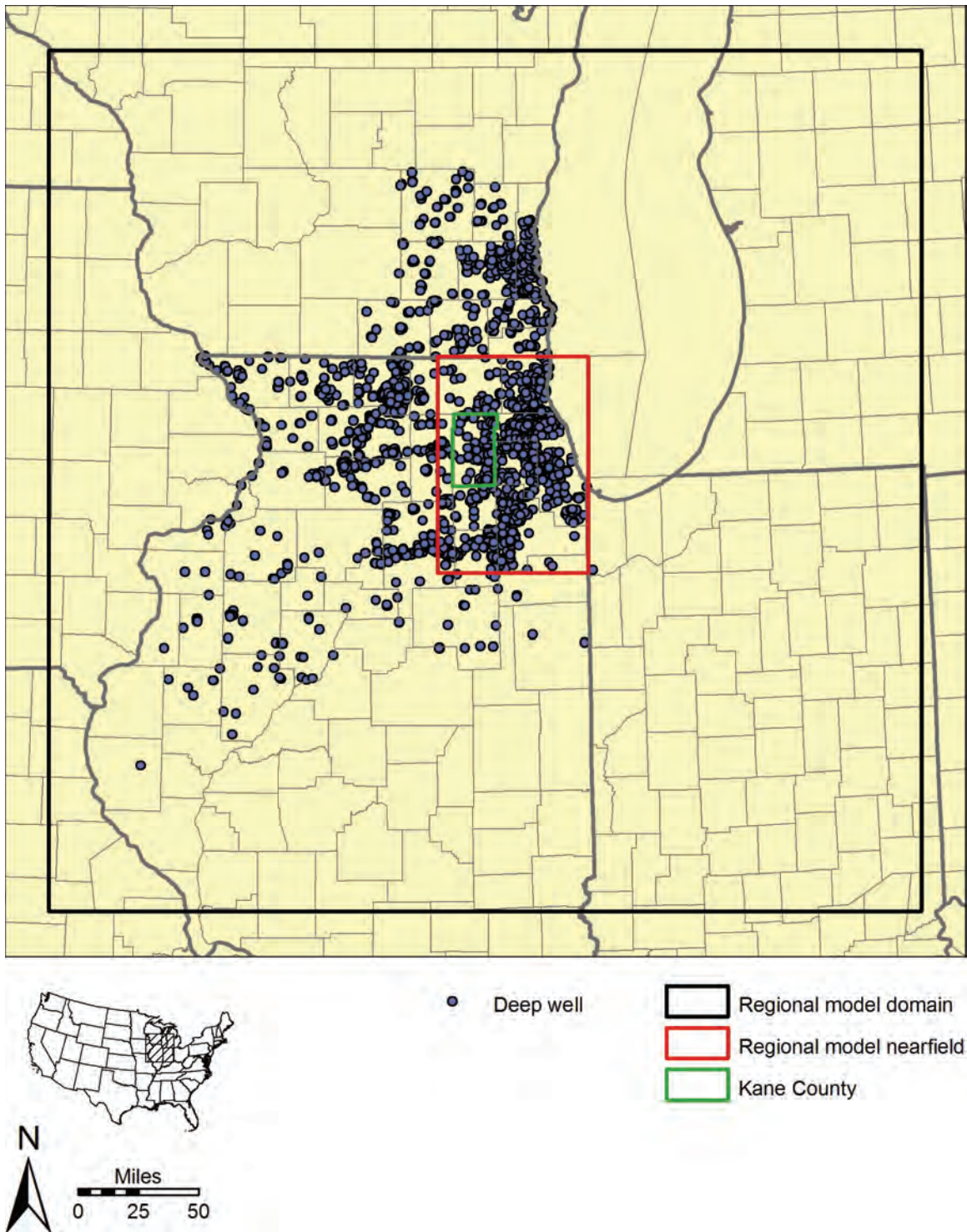


Figure 78. Deep wells represented in the regional model.

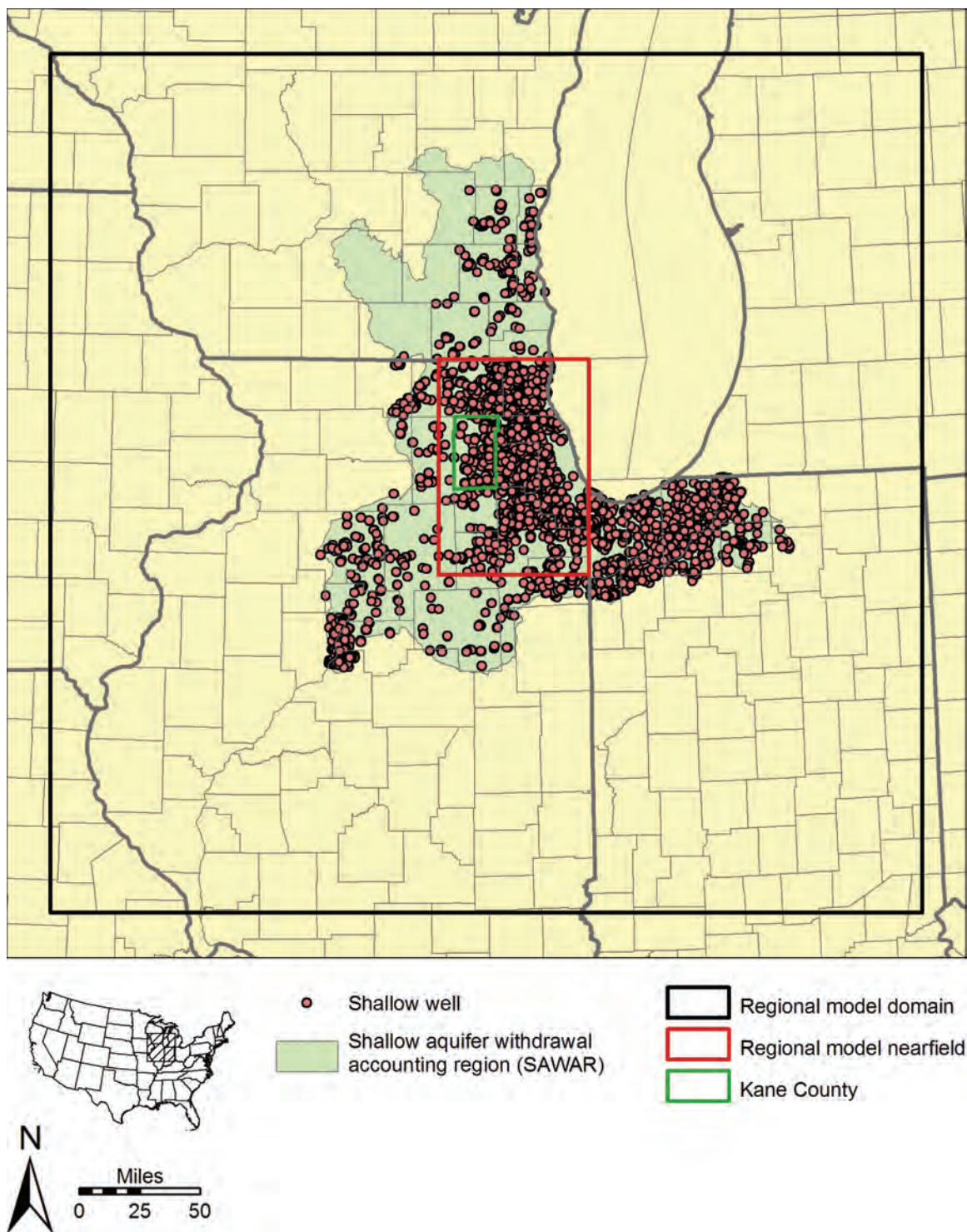


Figure 79. Shallow wells represented in the regional model.

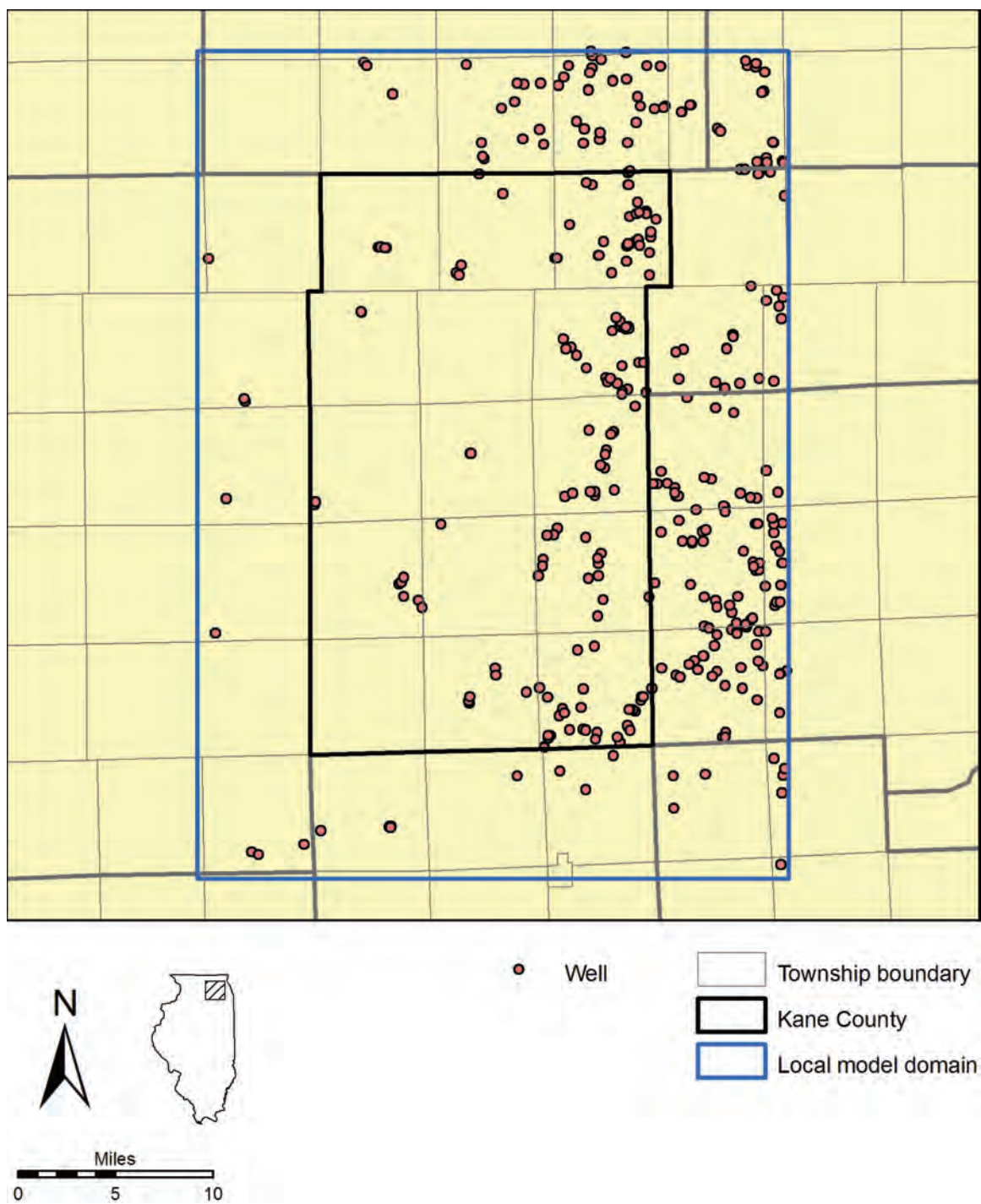


Figure 80. Wells represented in the local-scale model.

The geographic, hydrogeologic, and temporal scope of the withdrawals represented in the regional- and local-scale models is not comprehensive. However, the dataset is considered to be comprehensive enough to adequately represent the major influences on groundwater flow in the regional model nearfield of northeastern Illinois. Withdrawals are omitted for several reasons: (1) inclusion of a truly comprehensive representation of groundwater withdrawals would strain computational resources and add significantly to computation time; (2) withdrawals at distant locations, at low rates, in the distant past, and from rapidly-recharged aquifers would have little impact on present groundwater flow in the model nearfields; and (3) the task of making assumptions regarding locations, rates, timing, and hydrostratigraphic sources of withdrawals in the absence of readily available data from existing databases would strain the project budget and schedule. Thus, existing databases of groundwater withdrawals in the regional model domain were reviewed, and if omissions in these databases were judged to be significant to modeling groundwater flow in the model nearfields, withdrawals were assumed in order to address the omissions. A detailed description of the data sources and processing used in compiling the withdrawal database is included in Appendix B.

The geographic scope of the withdrawals simulated in the regional model includes the central and northern portions of Illinois and Indiana and the southern portion of Wisconsin. Withdrawals in Michigan are not represented. Withdrawals from deep wells in Illinois and Indiana are sometimes omitted owing to irregular availability of historical withdrawal data, as discussed in Appendix B. Because it is unlikely that withdrawals from distant shallow wells would affect heads in the regional model nearfield, shallow wells in Illinois and Indiana are represented only if they are located within the following USGS hydrologic units in the immediate vicinity of northeastern Illinois: 7090001, 4040003, 7120006, 4040002, 7120004, 7090006, 7120003, 4040001, 7120007, 7120001, 7130001, 7120005, and 7130002. This area is referred to as the SAWAR.

Deep wells represented in the regional model are illustrated in Figure 78. The time period represented by these withdrawals differs by state. Withdrawals from deep wells in Illinois are represented for the period 1864-2003. Deep wells active during the period 1864-1963 are represented by seven idealized pumping centers, with pumping totals at these seven centers equivalent to aggregated total deep well withdrawals from surrounding areas. These aggregated withdrawals are intended to represent withdrawals within Cook, DuPage, Kane, Lake, McHenry, and Will Counties of northeastern Illinois. Wells active during the period 1964-2003 are represented individually. Deep well withdrawals during the period 1964-1979 in Illinois that are represented in the regional model are limited to wells located in the following 20 northern Illinois counties: Boone, Carroll, Cook, DeKalb, DuPage, Grundy, Jo Daviess, Kane, Kankakee, Kendall, Lake, La Salle, Lee, McHenry, Ogle, Rock Island, Stephenson, Whiteside, Will, and Winnebago. Most deep well withdrawals in the state occur within this area. Deep well withdrawals from Illinois wells during the period 1980-2003 are represented in the entire portion of Illinois within the regional model domain. Numerous deep domestic wells are located in the regional model nearfield, and, despite the comparatively low rate of withdrawals from the wells, these wells were identified—and withdrawals from them were estimated—for the period 1875-2003. A total of 5686 deep wells are simulated in the groundwater flow modeling, including 3060 domestic wells.

Mineralized water from deep wells in Indiana is unacceptable for most uses, such that the deep units are largely unused in that state. Only one deep well in Indiana is represented in the regional model; this is the only deep well included in a database of groundwater withdrawals obtained from the Indiana Department of Natural Resources (personal communication, 2002). The withdrawal record for this well covers the period 1985-2002. Deep wells in southeastern Wisconsin are represented for the period 1864-2002 in this dataset. Data from other parts of Wisconsin are not available.

Shallow well withdrawals simulated in the regional model are limited to the SAWAR (Figure 79). Pre-1964 withdrawals in Illinois and Indiana from shallow wells within the SAWAR are not represented, and withdrawals from 1964 to 2002 are irregularly represented. Shallow well withdrawals in Illinois during the period 1964-1979 are represented only for the portion of the SAWAR within the following counties: Boone, Cook, DeKalb, DuPage, Grundy, Kane, Kankakee, Kendall, Lake, La Salle, Lee, McHenry, Ogle, Will, and Winnebago. Shallow well withdrawals within the entire Illinois portion of the SAWAR are represented in the model for the period 1980-2002. Shallow well withdrawals within the Indiana portion of the SAWAR are represented in the model only for the period 1985-2002. Shallow wells in southeastern Wisconsin are represented for the period 1864-2002. Data from other parts of Wisconsin are not available. A total of 5294 shallow wells are simulated in the groundwater flow modeling.

Only withdrawals from the Shallow Bedrock Aquifer and overlying Quaternary sand and gravel aquifers are simulated in the local-scale groundwater flow model. To reduce model complexity, shallow wells pumped at very low average annual rates of withdrawal (less than 10 gallons per minute during all annual accounting periods of the well's period of record) were omitted from the local-scale model. The omitted wells withdrew less than 0.5 percent of total shallow withdrawals from the domain in 2003.

In contrast to the regional-scale model whose withdrawals cover the period ending with 2002, shallow withdrawals simulated in the local-scale model extend through 2003. This difference was necessitated by the availability of withdrawal data at the time of model development and by the requirements for model calibration. At the time of model development, when data were compiled for the regional-scale model, only 2002 data were available from Indiana and Wisconsin. This period was acceptable for regional model calibration because no regional calibration target data were obtained after 2002; post-2002 withdrawal data would be irrelevant for calibration purposes. However, the local-scale model was initiated later than the regional-scale model, when 2003 withdrawal data for Illinois were available. These 2003 data were essential for model calibration because the head data used for calibration were measured in fall 2003.

2.2.9. Boundary Flow into Local Model Area (TMR)

The amount of groundwater flowing across the lateral and bottom boundaries of the local-scale model was obtained from the regional-scale model using an approach of telescopic mesh refinement (TMR) (Appendix A). The appropriate directional flux from a cell in the regional model was apportioned and assigned as a constant flux (well) to the corresponding boundary cells in the local-scale model. The lateral fluxes from Quaternary layers in the regional model (regional model layers 1-3) were apportioned to Quaternary layers in the local model (local model layers 1-14). Likewise, the lateral and vertical fluxes in the weathered bedrock aquifer in the regional model (layers 5-11) were

apportioned and assigned to local model layer 15. Some of the cell fluxes from the regional model required editing to fit the framework of the local model, such as where local model boundaries split adjacent river cells in the regional model. To prevent cells from going dry, fluxes were not apportioned to some of the cells near the surface that represent soils or diamictons. The total lateral fluxes across the boundary of the local model equals about 1,300,000 ft³/d (9.5 Mgd) inward and about 2,300,000 ft³/d (17.5 Mgd) outward for a net loss of about 1,000,000 ft³/d (8.0 Mgd). The vertical exchange with the deeper bedrock equals about 1,500,000 ft³/d (11.0 Mgd) upward and about 3,200,000 ft³/d (24.0 Mgd) downward for a net loss of 1,700,000 ft³/d (13.0 Mgd). The TMR fluxes from the regional model do not change sufficiently enough under different modeled historical and future pumping conditions to warrant assigning new fluxes to the local model for transient modeling.

2.3. Model Calibration

Groundwater flow models undergo a process of *calibration* in which system geometry and properties, initial and boundary conditions, and stresses are adjusted so that the model simulations are as realistic as possible (Hill and Tiedeman, 2007). The preceding sections of the report have discussed the initial adaptation of the model geometry and boundaries to the hydrology, geology, and stresses. This included improving the numerical stability of the model by adapting model layers to address gaps in hydrostratigraphic units and tuning the numerical representation of unconfined aquifers. This section of the report discusses the calibration of model parameters using an automated procedure for parameter estimation, also known in groundwater modeling as the inverse solution. Automated estimation of parameters runs the model many times, adjusting parameter values until model simulations approximate a set of observations of head and groundwater discharge referred to as *calibration targets*. These calibration targets have associated errors that are the result of measurement errors, unmodeled temporal and spatial variability, and other factors (Anderson and Woessner, 2002). The quality of the calibration can be judged in part with respect to these errors, since the accuracy of the model-simulated heads and flows can be no better than that of the calibration targets. This section discusses the parameter estimation for the regional and local models, including the selection and use of calibration targets, the sensitivity of key parameters, and the accuracy and bias of the resulting calibration.

2.3.1. Regional-Scale Model

2.3.1.1. Approach

Parameter estimation for the regional model began by manual adjustment to develop an initial set of model parameters capable of simulating heads and flows under steady-state conditions during predevelopment (pre-1864). This consisted of altering horizontal hydraulic conductivity K_h , vertical hydraulic conductivity K_v , leakance, and recharge within plausible ranges until model simulations were numerically stable and approximated the calibration targets. Calibration targets for the regional model were observations of predevelopment heads, base flow in streams, and their associated errors. The process of parameter estimation was then continued automatically using PEST (Watermark Numerical Computing, 2005), a software package that runs the model many times, adjusting parameters until no further improvement with respect to the calibration

targets can be achieved. Within PEST, calibration targets were weighted to emphasize accuracy in the model nearfield and to preserve calibration targets considered to be more reliable. PEST also employed anisotropy ratios (K_h/K_v) as prior information to constrain estimates of K_h and K_v within the hydraulic conductivity zones. As noted in Section 2.2.3.1, these anisotropies were taken from published field and modeling studies within the regional model domain. PEST results were assessed graphically and statistically, and sensitivity analyses were conducted to ascertain the sensitivity of the model to changes in the parameter estimates.

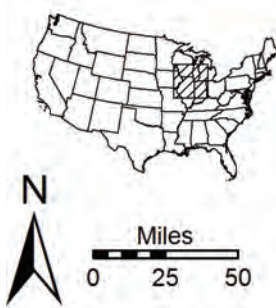
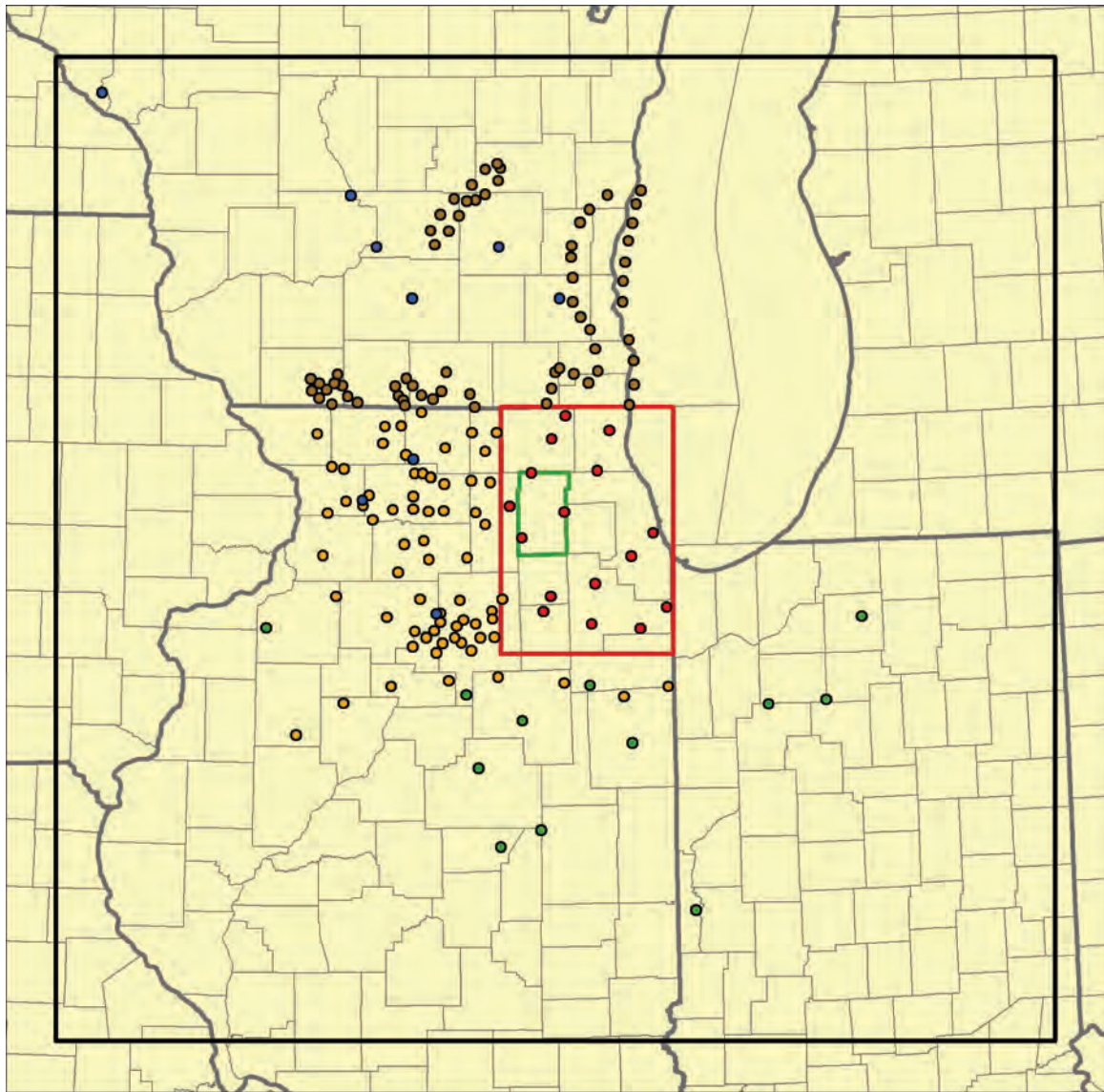
Model calibration was verified by comparing transient simulations to the time series of heads observed in the model nearfield during the period 1864 to 2002 (the period of transient groundwater flow conditions). The adequacy of the calibration and verification was evaluated by comparing the calibration errors relative to the errors in the calibration targets (Appendix E). This sequence of steady-state *predevelopment calibration* and *transient verification* is essentially as discussed in Anderson and Woessner (2002).

2.3.1.2. Calibration Targets

Most calibration targets for hydraulic head in the regional model were obtained from Stephen L. Burch of the ISWS (personal communication, 2002), who compiled these estimates of predevelopment head for use in developing a computer model of deep groundwater flow in the Chicago area (Burch, 1991) (Figure 81, Table 10). Burch compiled the data from head maps developed by other, earlier researchers (Anderson, 1919; Suter et al., 1959; Visocky et al., 1985; Weidman and Schultz, 1915). Although these observations were for the aggregated deep sandstone aquifer, for the purposes of calibrating the regional model, the head data provided by Burch were assigned as calibration targets to regional model layer 12 (Ansell Unit). This assignment is justified by borehole studies which indicate that, outside of regions with intense pumping, differences between the hydraulic heads of the Ansell and Ironton-Galesville are small (Nicholas et al., 1987). The similarity in heads between deep aquifers prior to pumping was confirmed by transient model simulations of historical pumping. No head maps were available for units above the Maquoketa Unit, but the heads in these near-surface units are highly correlated with surface topography and the elevation of streams and lakes.

The set of calibration targets for head in the regional model included 21 estimates of predevelopment head in the Mt. Simon Unit assembled by Mandle and Kontis (1992) and Bond (1972), all of which were assigned to regional model layer 17 (upper Mt. Simon Unit). Bond (1972) corrected his Mt. Simon head measurements for the greater density of the saline groundwater present in the Mt. Simon, but Mandle and Kontis (1992) did not correct their head observations for density. Correction of the head measurements for density revises the observed value of head upward.

The head-calibration targets were weighted so that the calibration process emphasized the targets in northeastern Illinois. Because they were not corrected for density, the Mt. Simon head estimates from Mandle and Kontis (1992) were considered to be the least reliable and therefore were weighted the least.



- Burch (personal communication, 2002), after Anderson (1919), Suter et al. (1959), and Visocky et al. (1985); NE Illinois; Model Layer 12
 - Burch (personal communication, 2002), after Anderson (1919), Suter et al. (1959), and Visocky et al. (1985); Illinois (excluding NE); Model Layer 12
 - Burch (personal communication, 2002), after Weidman and Schultz (1915); Wisconsin; Model Layer 12
 - Bond (1972), Density-corrected Mt. Simon, Model Layer 17
 - Mandle and Kontis (1992), Uncorrected Mt. Simon, Model Layer 17
- Regional model nearfield
- Regional model domain
- Kane County

Figure 81. Head targets for calibration of regional predevelopment steady-state model.

**Table 10. Head Targets for Calibration of Predevelopment
Steady-State Regional Model**

<i>Data Source</i>	<i>Description</i>	<i>Number</i>	<i>Model Layer</i>	<i>Relative Weight</i>
Burch (personal communication, 2002 [after Anderson (1919), Suter et al. (1959), and Visocky et al. (1985)])	Composite head in Cambrian and Ordovician units (NE Illinois)	16	12	40
Burch (personal communication, 2002 [after Anderson (1919), Suter et al. (1959), and Visocky et al. (1985)])	Composite head in Cambrian and Ordovician units, Illinois (excluding NE Illinois)	69	12	4
Burch (personal communication, 2002 [after Weidman and Schultz (1915)])	Composite head in Cambrian and Ordovician units (Wisconsin)	65	12	2
Bond (1972)	Head in Mt. Simon (density-corrected)	12	17	2
Mandle and Kontis (1992)	Head in Mt. Simon (not density-corrected)	9	17	1

The calibration targets for head have associated errors that vary with location, the degree of heterogeneity, and measurement error. For the regional-scale model, the greatest model resolution is in northeastern Illinois where the total error of head targets in the units underlying the Maquoketa is estimated to be 82 ft (errors for head targets in units overlying the Maquoketa are discussed in the sections describing the local model). As the model grid spacing increases and the open interval of observation wells expands to include multiple formations, the error of the calibration targets for head will increase. Thus, calibration targets at depth in the farfield of the domain may have errors of more than 200 ft. Additional details on the inference of errors associated with calibration targets are presented in Appendix E.

Calibration of the regional model also used calibration targets for groundwater flux representing the long-term average of groundwater discharge, or base flow, to streams and drains. Unfortunately, no predevelopment streamflow observations are available for this region and modern streamflow is influenced by the extensive alteration of the watershed with drains, land-use changes, diversions, etc. Similar to Feinstein et al. (2005a; 2005b), this study is forced to infer predevelopment base flow from modern USGS streamflow data. Eight watersheds were selected along streams in and around the model nearfield (Table 11 and Figure 82) whose gage records had a sufficiently long period of record to infer long-term streamflow statistics. Similar to Feinstein et al. (2005a; 2005b), flux targets are inferred from the Q_{80} and Q_{50} (the 80th and 50th percentiles of the distribution), shown in units of cubic feet per day (ft³/d) in Table 11, of observed streamflows. In addition, streamflow records of six watersheds in northern Illinois were examined and graphical methods of hydrograph separation were used to

estimate base flow rates. Base flow in three of these watersheds, those in northeastern Illinois, is discussed by Meyer (2005). While the base flow varies continuously in time through a wide range, the median base flow for the period of record of each watershed is consistently centered between Q_{80} and Q_{50} , shown in units of cubic feet per second (ft^3/s) in Table 12. This study therefore estimates the long-term average of base flow as the arithmetic average of the observed Q_{80} and Q_{50} , and uses that average as the calibration target for flux in each of the selected watersheds. These average values were calculated from stream gage data except for those calculated for Coon Creek and Ferson Creek, where Q_{80} and Q_{50} were estimated using a regression model for streamflow in Kane County developed by the ISWS (Knapp et al., 2007). Errors associated with all calibration targets are inferred from the error variances of the ILSAM regression model, as discussed in Appendix E. Table 9 presents the calibration targets for flux and the associated errors for each watershed.

Calibration targets for flux were weighted to emphasize fitting the four targets in the Kane County area (gage locations 1, 2, 3, and 5 in Figure 82). Targets in other parts of northeastern Illinois were weighted less, and targets in Wisconsin were weighted the least. The calibration targets for flux were assigned lower weights than the head calibration targets to normalize calibration errors [i.e., to put flux calibration errors (in ft^3/day) and head calibration errors (in ft) on the same scale]. Weights for the calibration targets for flux were also lower than the head targets to acknowledge the approximate nature of calibrating a predevelopment model against fluxes inferred from modern streamflow data. As with the weights on the calibration targets for head, the weights for the flux targets were tuned during parameter estimation to achieve stable estimates for model parameters.

We calibrated the regional model to predevelopment head and base flow targets because, as predevelopment measurements and estimates, these targets represent steady-state, not transient, conditions. Use of these predevelopment targets required only that PEST repeat a steady-state solution of the regional-scale model, a much faster computational process than repeating numerous transient model runs. Maps and measurements of head during the period of transient hydrologic conditions in the deep aquifers are available for several different times [e.g., Burch (2002)]; instead of being used for calibration, we employ observations of head during this period for transient verification of the regional model (Section 2.3.1.5).

**Table 11. Flux Targets for Calibration of Predevelopment
Steady-State Regional Model**

<i>Gage Name</i>	<i>Q₈₀ (ft³/d)</i>	<i>Q₅₀ (ft³/d)</i>	<i>Q Target (ft³/d)</i>	<i>Q Target Error (ft³/d)</i>	<i>Relative Weight</i>
Blackberry Cr near Yorkville, IL	907,200	3,542,400	2,224,800	266,976	5.71×10^{-4}
Ferson Cr near St Charles, IL	578,880	1,771,200	1,175,040	317,261	7.75×10^{-4}
Boone Cr near McHenry, IL	578,880	864,000	721,440	194,789	3.95×10^{-4}
Coon Cr at Riley, IL	829,440	2,505,600	1,667,520	450,230	9.27×10^{-4}
Skokie River near Highland Park, IL	501,120	1,166,400	833,760	100,051	7.98×10^{-5}
Weller Cr at Des Plaines, IL	101,952	293,760	197,856	23,742.7	9.69×10^{-5}
Turtle Cr at Carvers Rock Rd near Clinton, WI	5,184,000	7,862,400	6,523,200	1,761,264	4.11×10^{-5}
White River near Burlington, WI	2,246,400	5,097,600	3,672,000	991,440	7.76×10^{-5}

**Table 12. Median Base Flow and Streamflow Statistics for 50-Year Maximum
Period of Record for Six Watersheds in Northern Illinois**

<i>Gage Name</i>	<i>USGS Gage Number</i>	<i>Q₈₀ (ft³/s)</i>	<i>Q₅₀ (ft³/s)</i>	<i>Median Base Flow (ft³/s)</i>
East Branch Panther Creek near El Paso	5566500	0.34	4.5	3.24
Gimlet Creek near Sparland	5559000	0	0.9	0.5
Terry Creek near Custer Park	5526500	1.4	4.45	3.455
McDonald Creek near Mt. Prospect	5529500	0.44	2.2	1.49
Tinley Creek near Palos Park	5536500	0.84	3.4	2.06
Weller Creek at Des Plaines	5530000	0.5	1.7	0.96

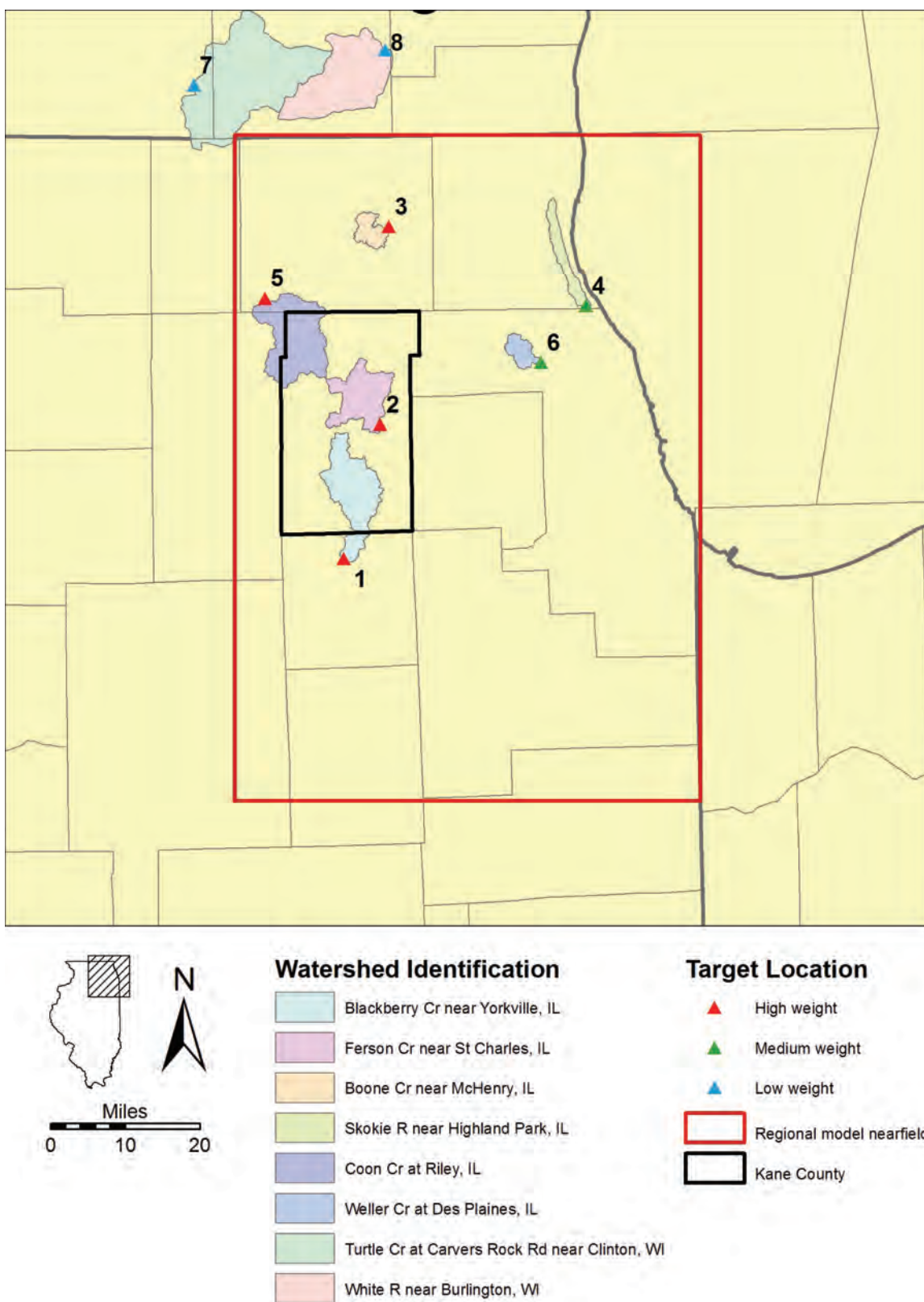


Figure 82. Flux targets for calibration of predevelopment steady-state regional model.

2.3.1.3. Estimated Parameters

Initial trials of automated parameter estimation for the regional model showed that the parameter estimation problem was poorly posed. This was evidenced by many parameter estimates reaching the plausibility bounds and other parameters having little effect on the agreement between model simulations and calibration targets. These characteristics are not uncommon in applications of parameter estimation (Hill and Tiedeman, 2007), and in this case were attributed to estimating too many parameters with an insufficient number of, and poorly located, calibration targets. Additional calibration targets were not available in appropriate locations, and attempts to eliminate insensitive parameters did not sufficiently constrain the remaining estimates. Parameter estimation often requires prior information to sufficiently constrain parameter estimates (Carrera and Neuman, 1986), and such prior information was available as estimates of the anisotropy ratio of horizontal to vertical hydraulic conductivity (K_h/K_v). The initial values and ranges of anisotropies were based on published modeling and field studies in the region (Feinstein et al., 2005a; Feinstein et al., 2005b; Weaver and Bahr, 1991a; Weaver and Bahr, 1991b; Weeks, 1969), and were specified for each of the hydraulic conductivity zones discussed in Section 2.2.3.1. Lower weights were assigned to prior estimates of anisotropy inferred from studies at analog sites outside the region. PEST uses prior information like a calibration target, favoring K_h and K_v values that yield anisotropies close to the initial anisotropy values. Prior information on anisotropy provides a high degree of correlation between estimates of K_h and K_v while still allowing the anisotropy ratio to be calibrated within a plausible range. The weights on the prior anisotropies were gradually increased for successive attempts at automated estimation until PEST found a stable set of estimated parameters.

The final estimates for parameters are shown in Table 14, Table 15, Table 16, and Table 17. For most of the parameters, the final estimates differ by 1 to 5 percent from their initial values. The final estimate of K_v for zone 9 (1.3×10^{-3} ft/d) is slightly less than the lower plausibility bound for the zone (5.9×10^{-3} ft/d); however, owing to the high sensitivity of the model to this parameter (discussed in Section 2.3.1.6), the value of 1.3×10^{-3} ft/d was accepted. The final estimates of recharge in zones 2, 3, 8, and 16 differ by 20 percent from the initial values, having reached their plausibility bounds. These recharge zones are at the extreme margins of the detailed representation of surface flow, and are not critical to the accuracy of the model. Taken together, the results of parameter estimation indicate that, although estimates are constrained by prior information, PEST is still free to find a solution that matches the calibration targets. The results also indicate that follow-up studies should be directed toward augmenting the set of calibration targets with many more observations of head and flux, and that alternative calibration strategies should be attempted.

Although storage parameters were not calibrated, manual adjustment of storage parameters during transient verification of the regional calibration (Section 2.3.1.5) suggested that no net improvement in model accuracy was achieved by alteration of specific storage from the starting values shown in Table 6.

**Table 13. Anisotropy Ratios (K_h/K_v) Used as Constraints for Calibration of
Predevelopment Steady-State Regional Model**

<i>Zone</i>	<i>Model Layers</i>	<i>Figures Illustrating Zones</i>	<i>Value</i>	<i>Relative Weight</i>
2	2, 3	Figure 46, Figure 47	50	500
6	1	Figure 48	100	500
8	2	Figure 47	100	500
9	3	Figure 46	100	500
13	5, 6, 7	Figure 42, Figure 43, Figure 44	1000	500
14	5, 6, 7	Figure 42, Figure 43, Figure 44	400	500
15	8, 9	Figure 40, Figure 41	100	500
16	8, 9	Figure 40, Figure 41	60	500
23	10, 11	Figure 38, Figure 39	30	500
26	10, 11	Figure 38, Figure 39	80	500
28	12, 13	Figure 36, Figure 37	1500	500
29	12	Figure 37	20	500
37	15	Figure 34	50	500
40	15	Figure 34	50	500
41	15	Figure 34	50	500
42	14, 15, 16	Figure 33, Figure 34, Figure 35	1000	500
11	4	Figure 45	100	100
12	4	Figure 45	100	100
30	12	Figure 37	20	100
31	13	Figure 36	30	100
38	14	Figure 35	30	100
43	17, 18, 19, 20	Figure 29, Figure 30, Figure 31, Figure 32	150	100
44	16	Figure 33	50	100
45	17, 18, 19, 20	Figure 29, Figure 30, Figure 31, Figure 32	150	100
46	17, 18, 19, 20	Figure 29, Figure 30, Figure 31, Figure 32	150	100
47	16	Figure 33	50	100

Table 14. Calibration of Horizontal (K_h) and Vertical Hydraulic Conductivity (K_v), Regional-Scale Model

<i>Zone*</i>	<i>K_h</i>		<i>K_v</i>	
	<i>Starting Value (ft/d)</i>	<i>Calibrated Value (ft/d)</i>	<i>Starting Value (ft/d)</i>	<i>Calibrated Value (ft/d)</i>
2	1.4×10^2	1.4×10^2	2.8×10^0	2.8×10^0
6	1.6×10^0	1.6×10^0	1.6×10^{-2}	1.6×10^{-2}
8	5.0×10^0	4.8×10^0	5.0×10^{-2}	4.8×10^{-2}
9	1.3×10^1	1.3×10^1	1.3×10^{-1}	1.3×10^{-1}
11	2.2×10^{-4}	2.1×10^{-4}	2.2×10^{-6}	2.1×10^{-6}
12	6.9×10^{-4}	6.8×10^{-4}	6.9×10^{-6}	6.8×10^{-6}
13	1.0×10^0	1.0×10^0	1.0×10^{-3}	1.0×10^{-3}
14	4.0×10^0	4.0×10^0	1.0×10^{-2}	1.0×10^{-2}
15	1.0×10^{-1}	9.4×10^{-2}	1.0×10^{-3}	9.4×10^{-4}
16	4.0×10^{-4}	4.0×10^{-4}	6.7×10^{-6}	6.6×10^{-6}
23	4.7×10^0	5.0×10^0	1.6×10^{-1}	1.7×10^{-1}
26	5.0×10^{-2}	5.0×10^{-2}	6.3×10^{-4}	6.2×10^{-4}
28	8.0×10^{-1}	7.9×10^{-1}	5.3×10^{-4}	5.3×10^{-4}
29	1.5×10^0	1.5×10^0	7.5×10^{-2}	7.5×10^{-2}
30	7.3×10^0	7.2×10^0	3.7×10^{-1}	3.6×10^{-1}
31	4.7×10^0	4.8×10^0	1.6×10^{-1}	1.6×10^{-1}
37	3.0×10^0	3.0×10^0	6.0×10^{-2}	5.9×10^{-2}
38	4.7×10^0	5.7×10^0	1.6×10^{-1}	1.9×10^{-1}
40	5.3×10^0	5.2×10^0	1.1×10^{-1}	1.0×10^{-1}
41	8.4×10^0	7.1×10^0	1.7×10^{-1}	1.4×10^{-1}
42	6.9×10^{-3}	6.8×10^{-3}	6.9×10^{-6}	6.8×10^{-6}
43	4.3×10^{-1}	4.3×10^{-1}	2.9×10^{-3}	2.9×10^{-3}
44	3.6×10^0	3.6×10^0	7.2×10^{-2}	7.2×10^{-2}
45	4.3×10^0	4.2×10^0	2.9×10^{-2}	2.8×10^{-2}
46	6.0×10^0	7.6×10^0	4.0×10^{-2}	5.0×10^{-2}
47	7.2×10^{-1}	7.2×10^{-1}	1.4×10^{-2}	1.4×10^{-2}

*See Figure 29 through Figure 48 for zone locations.

Table 15. Calibration of Recharge Rates, Regional Model

<i>Zone*</i>	<i>Initial Value (ft/d)</i>	<i>Calibrated Value (ft/d)</i>
2	6.7×10^{-4}	5.4×10^{-4}
3	1.0×10^{-3}	8.0×10^{-4}
4	2.3×10^{-4}	2.3×10^{-4}
5	2.3×10^{-4}	2.3×10^{-4}
6	6.7×10^{-4}	7.0×10^{-4}
7	7.5×10^{-4}	7.7×10^{-4}
8	1.0×10^{-3}	1.2×10^{-3}
9	1.1×10^{-3}	1.1×10^{-3}
10	1.6×10^{-3}	1.6×10^{-3}
11	2.0×10^{-3}	2.0×10^{-3}
12	1.1×10^{-3}	1.1×10^{-3}
13	2.9×10^{-3}	2.9×10^{-3}
14	2.3×10^{-4}	2.3×10^{-4}
16	2.1×10^{-3}	1.7×10^{-3}

*See Figure 71 for zone locations.

Table 16. Calibration of Leakance (K_v/m) Employed to Represent Surface Water, Regional Model

<i>MODFLOW Package</i>	<i>Category</i>	<i>Initial Value (ft/d-ft)</i>	<i>Calibrated Value (ft/d-ft)</i>
River	Streams with $Q_{7,10} > 0$	1	1.00488
	Inland lakes	0.01	0.009823
	Lake Michigan	0.01	0.009915
Drain	Streams with $Q_{7,10} = 0$	1	1.03073

Table 17. Calibration of Leakance (K_v/m) Employed to Represent Drained Areas, Regional Model

<i>Category</i>	<i>Initial Value (ft/d-ft)</i>	<i>Calibrated Value (ft/d-ft)</i>
Urban drainage	1	1.08145
Agricultural drainage	1	1.48848

2.3.1.4. Calibration Accuracy and Bias

The calibration accuracy of the regional model can be understood through graphical and statistical comparisons to predevelopment calibration targets. Figure 83 presents the first of these comparisons, a plot of observed head versus model-predicted head at each calibration target in the regional model along with a diagonal line that denotes the one-to-one relationship of perfect agreement. In general, the closer the symbol to the diagonal line, the better the simulation. Overall, the plot shows good agreement between observed and model-calculated heads, with the points scattered around the line. As intended in the model design, the best agreement is in the model nearfield of northeastern Illinois, reflecting the higher weighting of the head calibration targets in that area, all of which are assigned to model layer 12.

Table 18 presents statistics of the *residuals*—the differences between target and model-calculated values—for the predevelopment head calibration targets for the five subpopulations of head targets discussed previously and shown in Figure 81 and Table 10. The residual mean of -34.3 ft (Table 18) indicates that the model tends to overestimate head on average, but the residual mean of 9.8 ft for nearfield targets shows that the model slightly underestimates head in northeastern Illinois. The mean absolute error (MAE) describes the average magnitude of the residual in either a negative or positive direction. In the model nearfield of northeastern Illinois, the MAE is 28.1 ft. In the model farfield and in the Mt. Simon Unit, the MAE increases, indicating poorer agreement between calculated and observed heads. To compare goodness of fit between subpopulations of head calibration targets, the MAE may be normalized by dividing by the total range of observed heads, with the result expressed as a percentage. For the entire population of head targets, the model simulates predevelopment heads adequately (11 percent). Of all subpopulations of head calibration targets, the nearfield targets are fit best (19 percent), but other subpopulations, except the Mt. Simon Unit targets (Mandle and Kontis, 1992), are fit comparably. The comparatively low value of this statistic calculated for all targets (11 percent) reflects the influence of the large number of comparatively well-simulated heads and the large range of target values. Note that both the mean residual and the MAE for northeastern Illinois are less than the estimated error (82 ft for head targets in units underlying the Maquoketa). This indicates that the model is at least as accurate as the observations of head, and suggests that improvements to the model will require more accurate head observations.

Figure 84 illustrates the geographic distribution of residuals for the predevelopment head calibration targets. The symbols in Figure 84 denote whether the simulated values differ from the target value by an amount greater than the MAE (red if residual is negative or blue if residual is positive) or less than the MAE (no shading). As shown in Figure 83 and discussed previously, the distribution of residuals (Figure 84) suggests good agreement between the simulated and target values in northeastern Illinois and in most of the onshore portion of southeastern Wisconsin. The model tends to overestimate heads (negative residual) in most other areas with the exception of east-central Illinois, where it underestimates heads.

The set of calibration targets also included eight predevelopment flux targets located in and around northeastern Illinois (Figure 82 and Table 11). The model

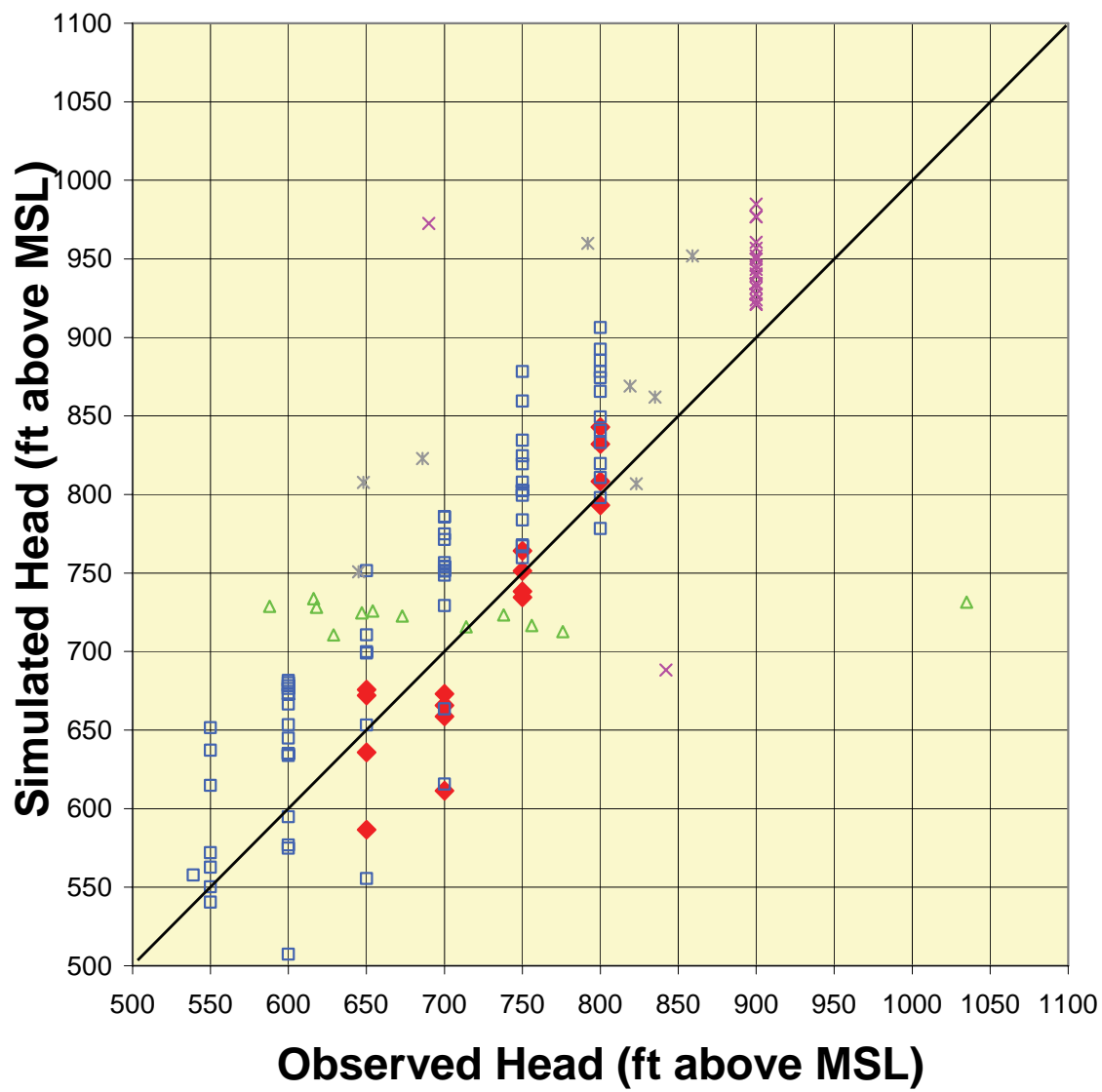


Figure 83. Plot showing the goodness of the fit between the steady-state predevelopment target heads and model-calculated heads for the regional-scale model.

Table 18. Statistics Describing Calibration to Predevelopment Head Targets

<i>Statistical Measure</i>	<i>NE Illinois [Burch (personal communication, 2002) after Anderson (1919), Suter et al. (1959), and Visocky et al. (1985)]</i>	<i>Illinois, excluding NE [Burch (personal communication, 2002) after Anderson (1919), Suter et al. (1959), and Visocky et al. (1985)]</i>	<i>Wisconsin [Burch (personal communication, 2002) after Weidman and Schultz (1915)]</i>	<i>Mt. Simon Unit (Bond, 1972)</i>	<i>Mt. Simon Unit (Mandle and Kontis, 1992)</i>	<i>All Head Targets</i>
Number of target heads	16	69	72	12	11	180
Residual mean (feet)	9.8	-43.2	-36.7	-19.2	-43.2	-34.3
Mean absolute error (feet)	28.1	54.7	45.5	89.4	142.7	56.3
Minimum residual (feet)	-42.9	-128.3	-132.0	-140.8	-282.6	-282.6
Maximum residual (feet)	88.6	94.4	141.0	303.6	377.4	377.4
Range of target values (feet)	150.0	261.0	200.0	447.0	214.0	496.0
Mean absolute error/Range	19%	21%	23%	20%	67%	11%
Calibration target error (feet) (Appendix E)	±82	±200	±200	±200	±200	±200

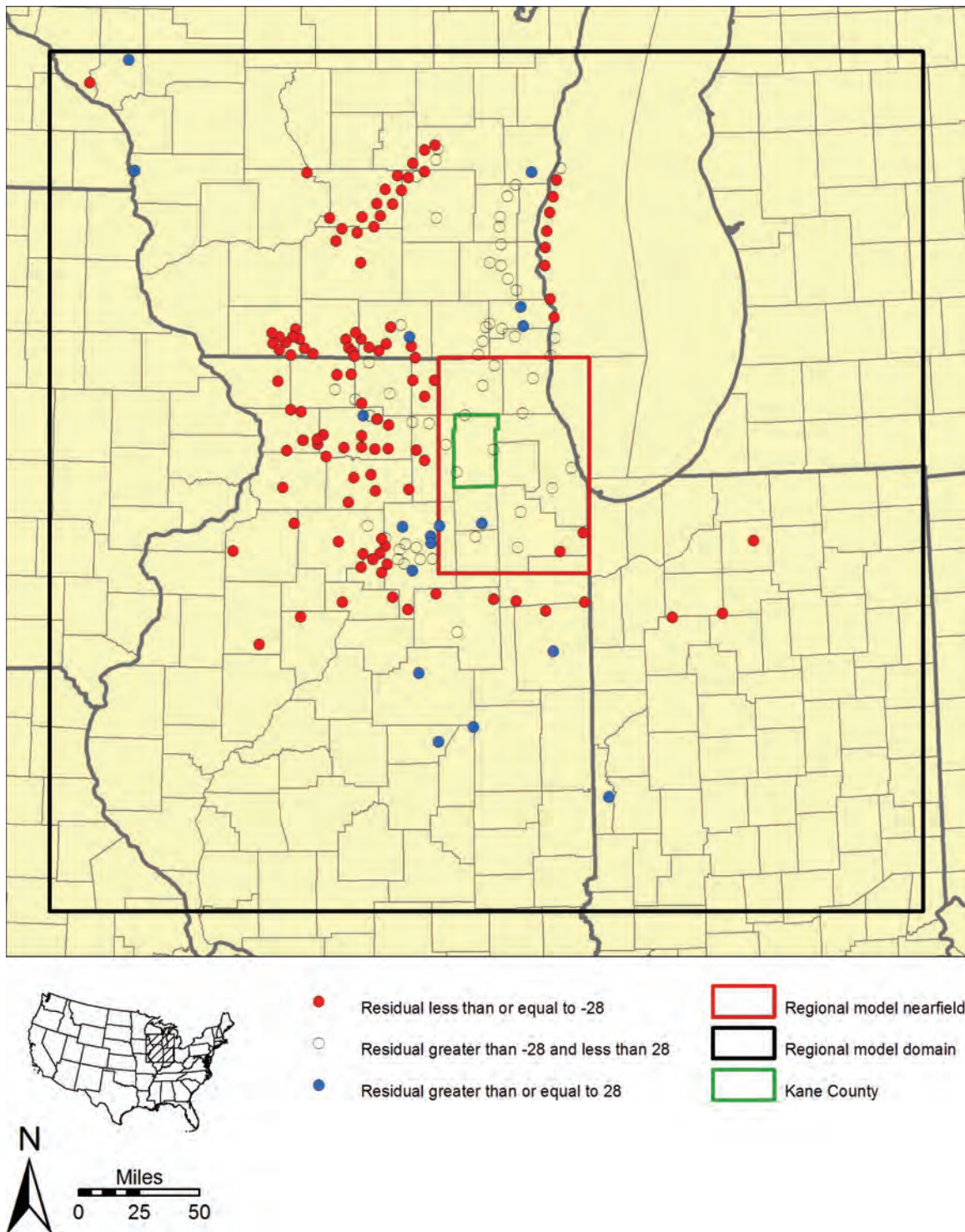


Figure 84. Residuals (observed minus simulated values) between target and simulated heads at predevelopment head calibration targets.

simulated flux is between the Q_{80} and Q_{50} values (the target range for calibration) at three of the eight flux targets in the region, and is within 12 percent of the target at three of the four high-weighted flux targets in the Kane County area (Figure 85 and Table 18). Model-simulated flux exceeds Q_{50} at two of the northeastern Illinois targets, and it underestimates Q_{80} at one of them (Skokie River near Highland Park, where the simulated flux indicates loss of water from the stream to groundwater). The model-simulated flux slightly exceeds Q_{50} at both of the flux targets in southeastern Wisconsin. This is attributed to the relative coarseness of the model grid in this area, the challenges of inferring predevelopment baseflow from modern streamflow data, and the approximate nature of using Q_{80} and Q_{50} to infer baseflow. As intended in the design of the regional model, the model-simulated fluxes generally agree with observed fluxes in the Kane County area. Three of the four targets in Kane County have calibration residuals of less than 12 percent, which is less than or equal to the estimated errors for the calibration targets (12 percent; see Appendix E). Further refinements are left to the local-scale model, whose increased resolution more accurately represents the geology and surface-water bodies.

2.3.1.5. Verification

After completing the steady-state calibration of the regional model, the calibrated model was verified by comparing a simulation of the region's pumping history against observed water levels at wells during the simulated pumping period. The purposes of this transient verification are to confirm the parameter estimates of the steady-state calibration and to build confidence in the calibrated model. Transient simulations require additional model parameters, the specific storage (S_s) and the specific yield, which govern aquifer storage and thus the rate of aquifer response to pumping. Ideally, the storage parameters will have highly reliable estimates such that their inclusion is the only change necessary for the calibrated model to match the observed transient heads, and thus the model can be considered verified (Anderson and Woessner, 2002). Groundwater withdrawal records from Illinois, Indiana, and Wisconsin were used to synthesize a pumping history (Appendix B), and estimates of storage parameters were taken from aquifer tests and published reports (Table 6). The verification targets consisted of measured water levels at selected ISWS observation wells in the regional model nearfield (Figure 86). Additional comparison was made with head measurements obtained from the deep USGS test well located at Zion, IL (Figure 86).

Time series of model-simulated and median annual observed heads (calculated from several measurements per year) were plotted together and compared visually for model verification. The comparison is limited by the long open intervals of the observation wells, so that the observed water levels are actually composites of heads in all of the intercepted layers. Consequently, model accuracy must be judged by comparing observed heads against the set of model-calculated heads, one series for each model layer intercepted by the open interval of the observation well. Such plots, with model-calculated heads determined using starting—and final—values of S_s (Table 6) are shown in Figure 87 through Figure 95. Although MODFLOW packages are available that permit simulating wells intersecting more than one model layer and interformational flow along boreholes, such refinements are left to future investigations.

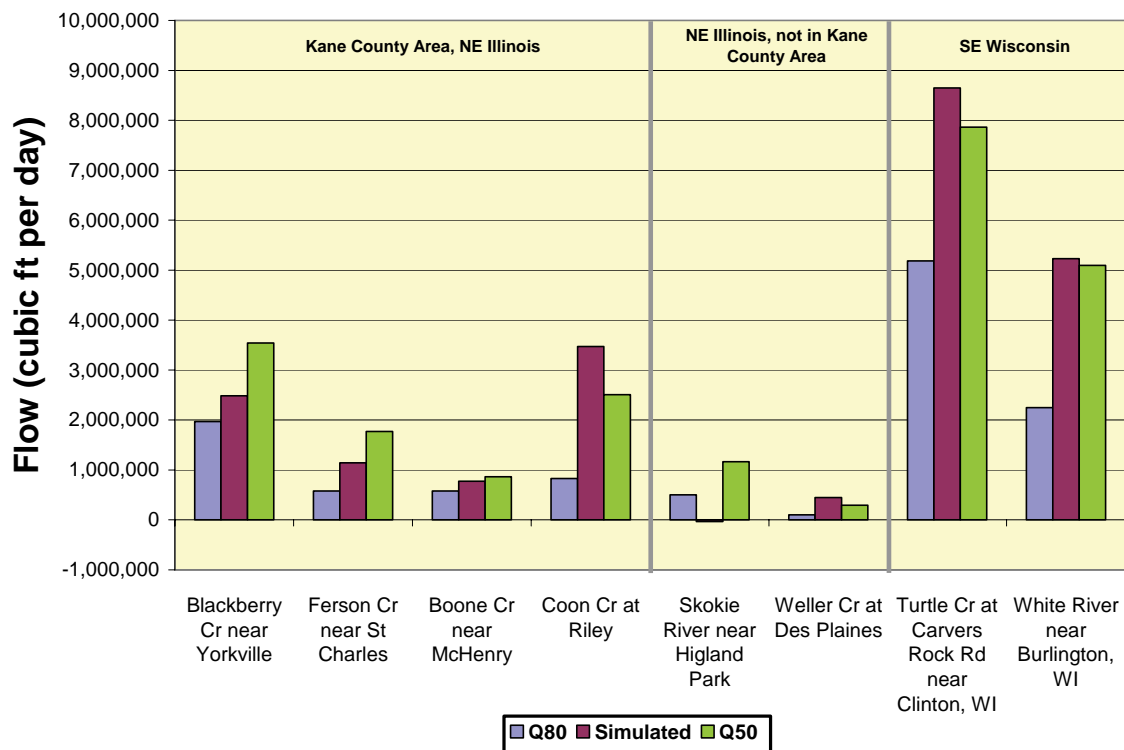


Figure 85. Comparison of simulated predevelopment base flow to Q_{80} and Q_{50} measurements of streamflow.

Table 19. Predevelopment Flux Targets and Residuals, Regional Model

<i>Gage Name</i>	<i>Q Target (ft³/d)</i>	<i>Q Simulated (ft³/d)</i>	<i>% Q Residual (Residual/Target)</i>
Blackberry Cr near Yorkville, IL	2,224,800	2,485,380	-11.71
Ferson Cr near St Charles, IL	1,175,040	1,139,601	3.02
Boone Cr near McHenry, IL	721,440	774,249	7.32
Coon Cr at Riley, IL	1,771,200	3,473,639	-108.31
Skokie River near Highland Park, IL	833,760	-35,665	104.28
Weller Cr at Des Plaines, IL	197,856	445,664	-125.25
Turtle Cr at Carvers Rock Rd near Clinton, WI	6,523,200	8,644,875	-32.53
White River near Burlington, WI	3,672,000	5,228,461	-42.39

Figure 87 shows model results at observation well 1115 in Woodstock (McHenry County). The well is finished in an unconsolidated, sand and gravel aquifer of the Quaternary Unit assigned to model layer 3. The comparison of observed and model-calculated heads in Figure 87 shows that the difference between observed and model-calculated heads at well 1115 is greatest in 1964 and that this difference decreases during the period 1964-1970. After 1970, the model accuracy does not generally improve. This pattern of increasing, then stable, levels of model accuracy suggests that omitting most withdrawals from model layers 1-11 prior to 1964 reduces the accuracy of model results until transient pumping effects are reduced (see Section 2.2.6 and Appendix B); rates for 1952-1962 are estimated at 1 to 2 Mgd in Woodstock public water supply wells (Prickett et al., 1964). It is likely that including pre-1964 withdrawals in the shallow model layers would improve accuracy prior to 1970, but it is unlikely that including these early withdrawals would improve the accuracy of the post-1970 model simulations.

Figure 88 and Figure 89 illustrate regional model results at two observation wells open to the Silurian-Devonian Carbonate Unit (model layers 5, 6, and 7). Disagreement between observed and model-calculated heads at these wells is pronounced and reveals several features of the regional model that limit its accuracy, particularly in the shallower model layers. One source of inaccuracy is omitting withdrawals prior to 1964 from wells open to model layers above layer 12, as discussed in the preceding paragraph. Another limitation of the present model is that it does not simulate unsaturated flow (although recent extensions of MODFLOW address this). This is illustrated by the comparison of heads at well 1112 (Figure 88), located in Chicago Heights (Cook County). Large-scale withdrawals from the Silurian-Devonian Carbonate Unit of this area, begun in the late 19th century, had, by 1962, resulted in desaturation of more than 150 ft of the Silurian-Devonian Carbonate Unit in Chicago Heights (Prickett et al., 1964). This zone of desaturation was probably not remedied until Lake Michigan water was brought to

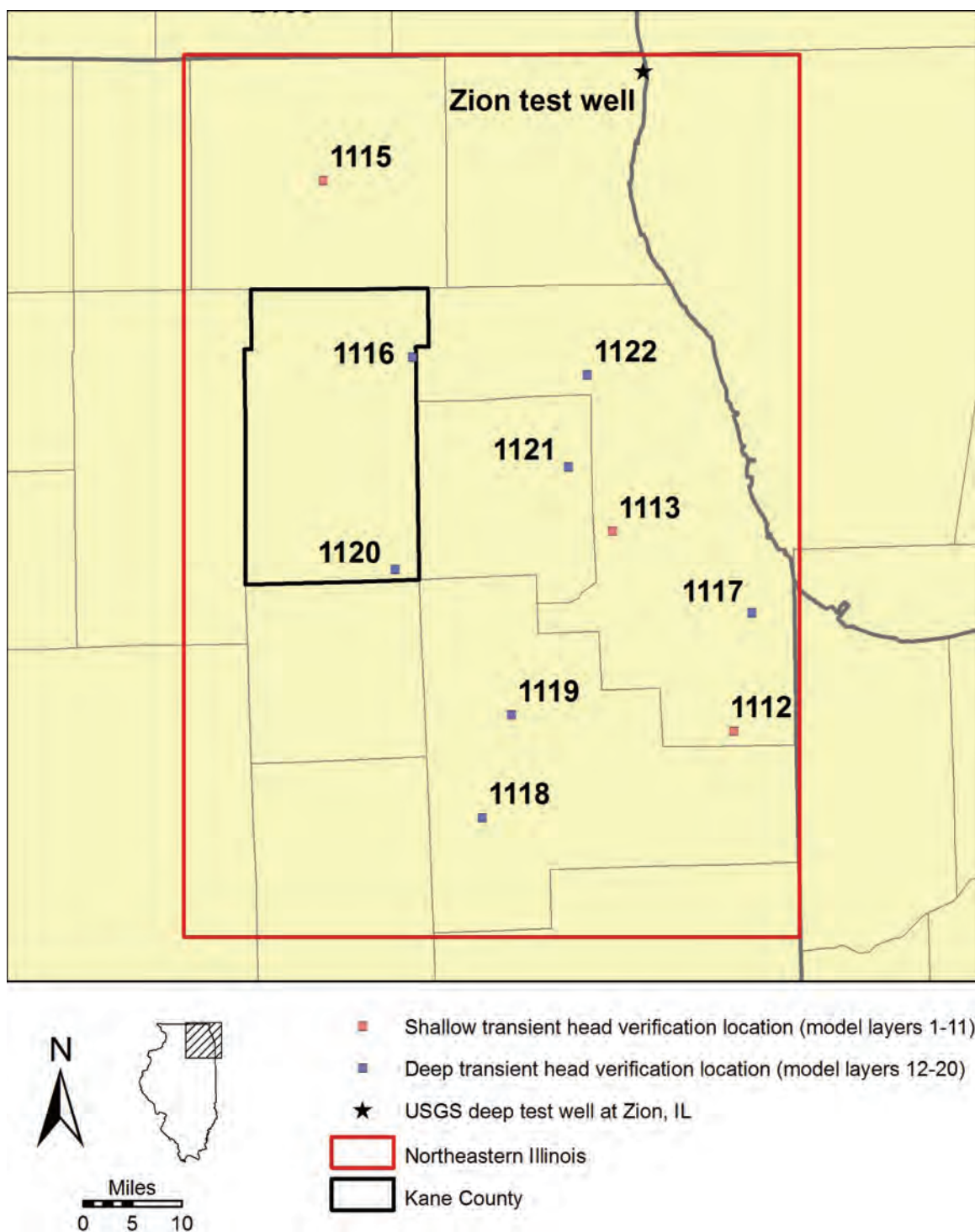


Figure 86. Head targets, with identification numbers referred to in Section 2.3.1.5, for verification of regional model under transient conditions.

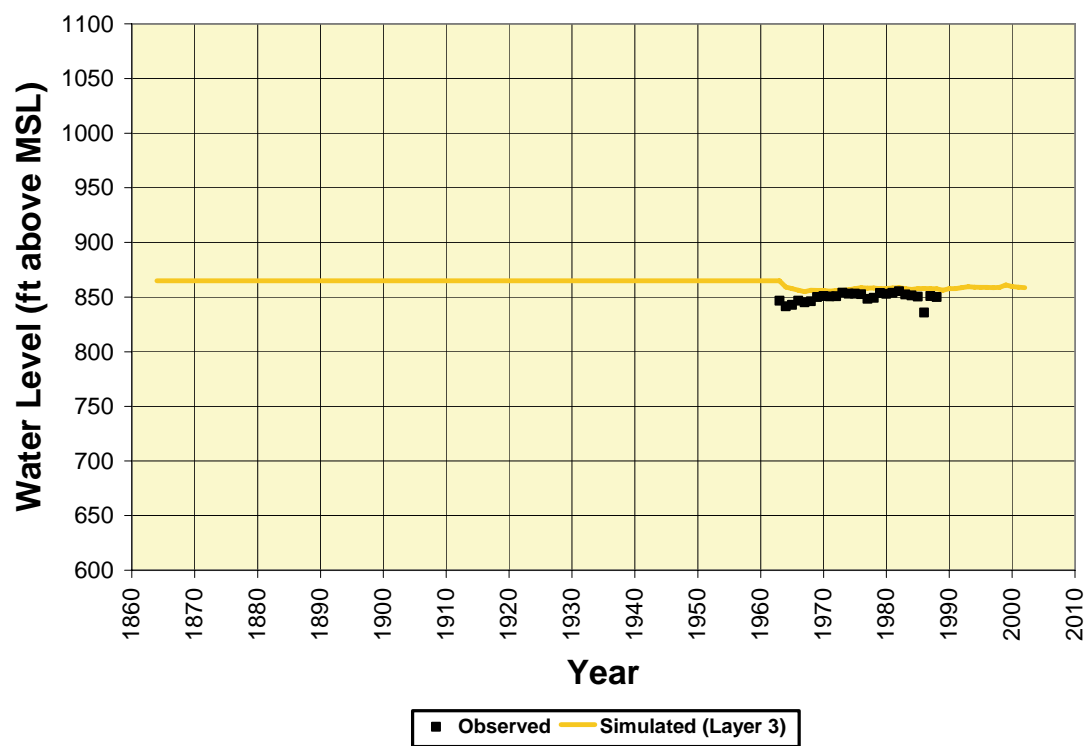


Figure 87. Median annual observed water level and simulated water level at shallow head verification location 1115.

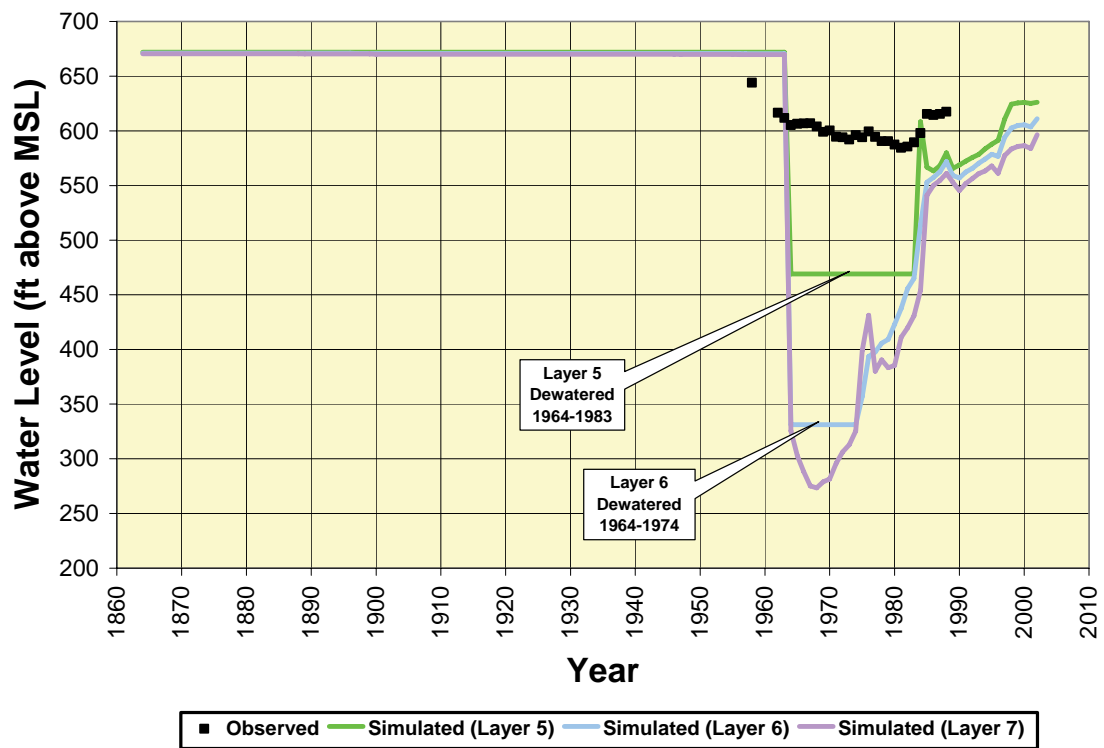


Figure 88. Median annual observed water level and simulated water level at shallow head verification location 1112.

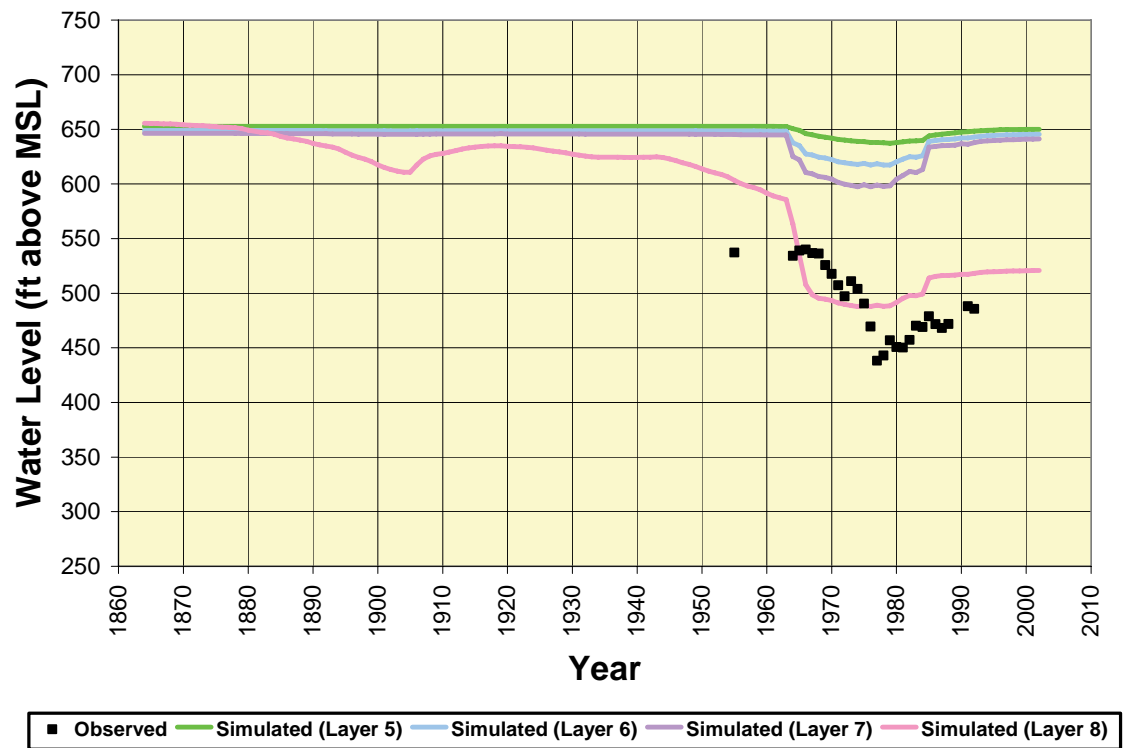


Figure 89. Median annual observed water level and simulated water level at shallow head verification location 1113.

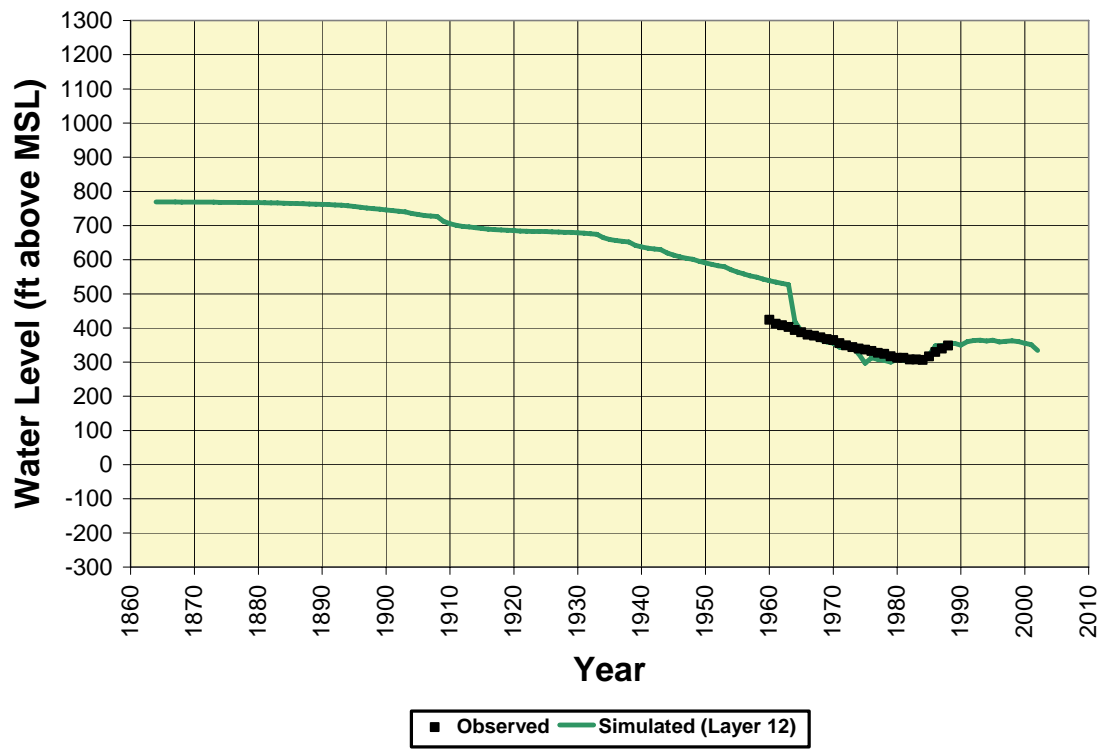


Figure 90. Median annual observed water level and simulated water level at deep head verification location 1116.

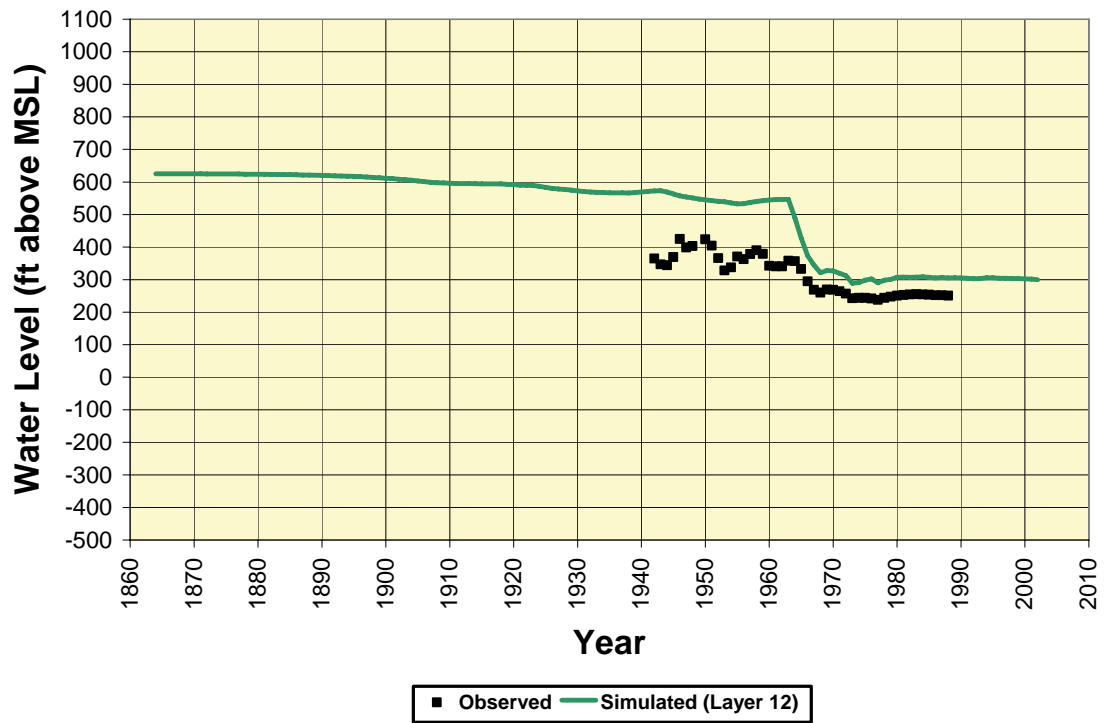


Figure 91. Median annual observed water level and simulated water level at deep head verification location 1118.

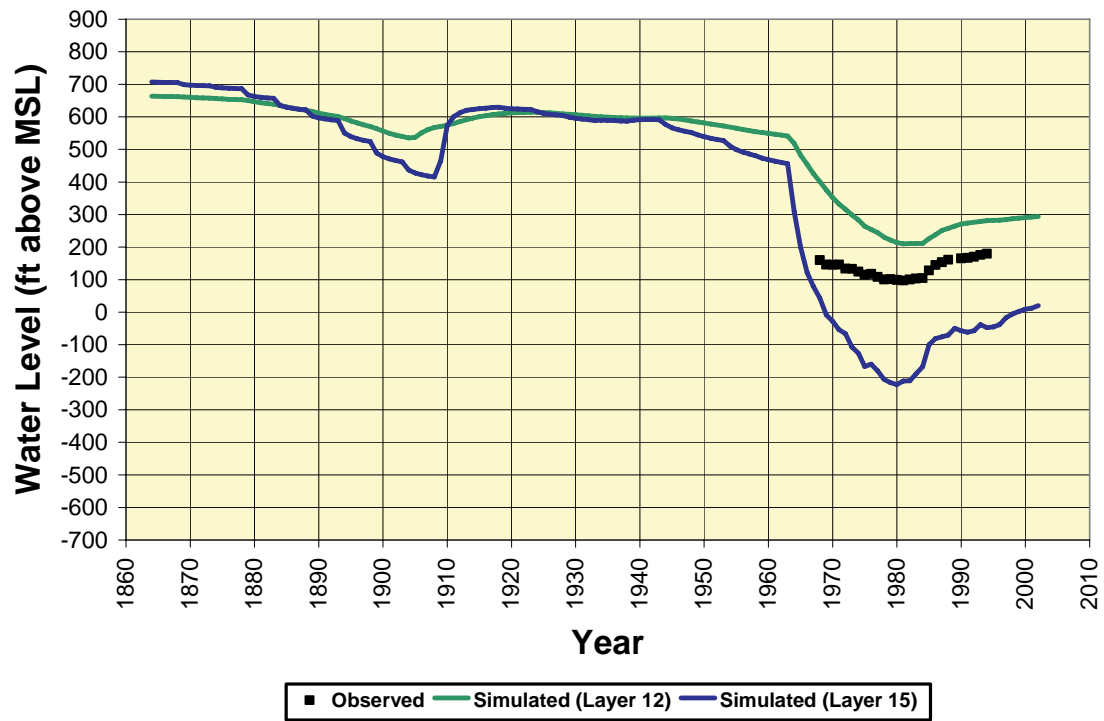


Figure 92. Median annual observed water level and simulated water level at deep head verification location 1117.

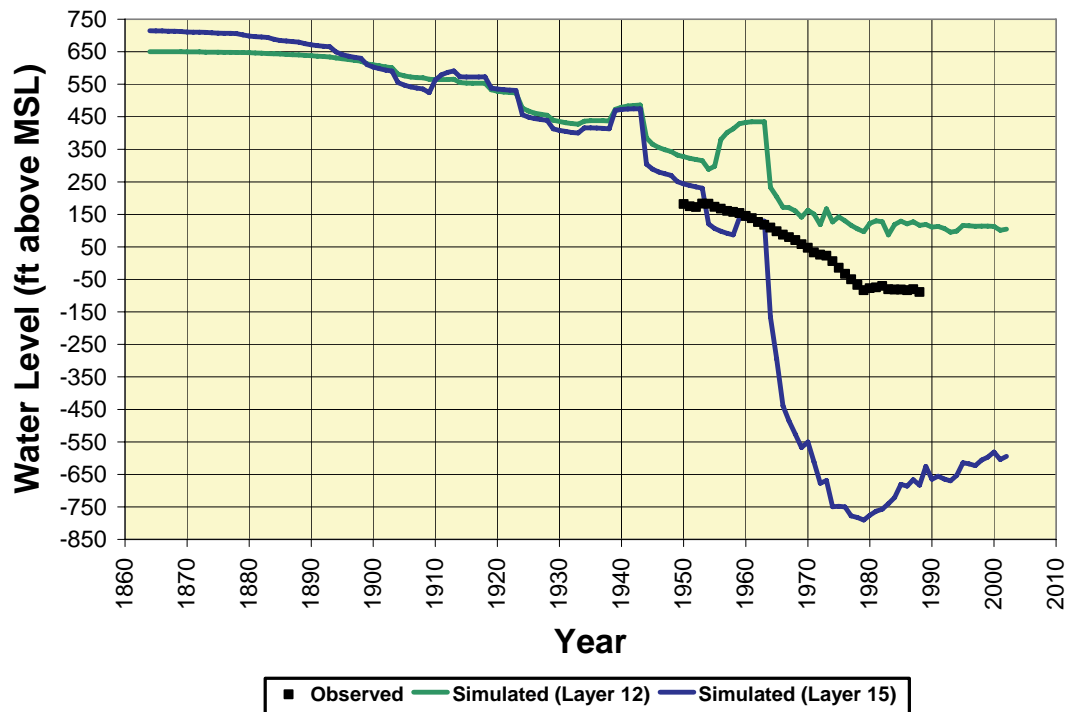


Figure 93. Median annual observed water level and simulated water level at deep head verification location 1119.

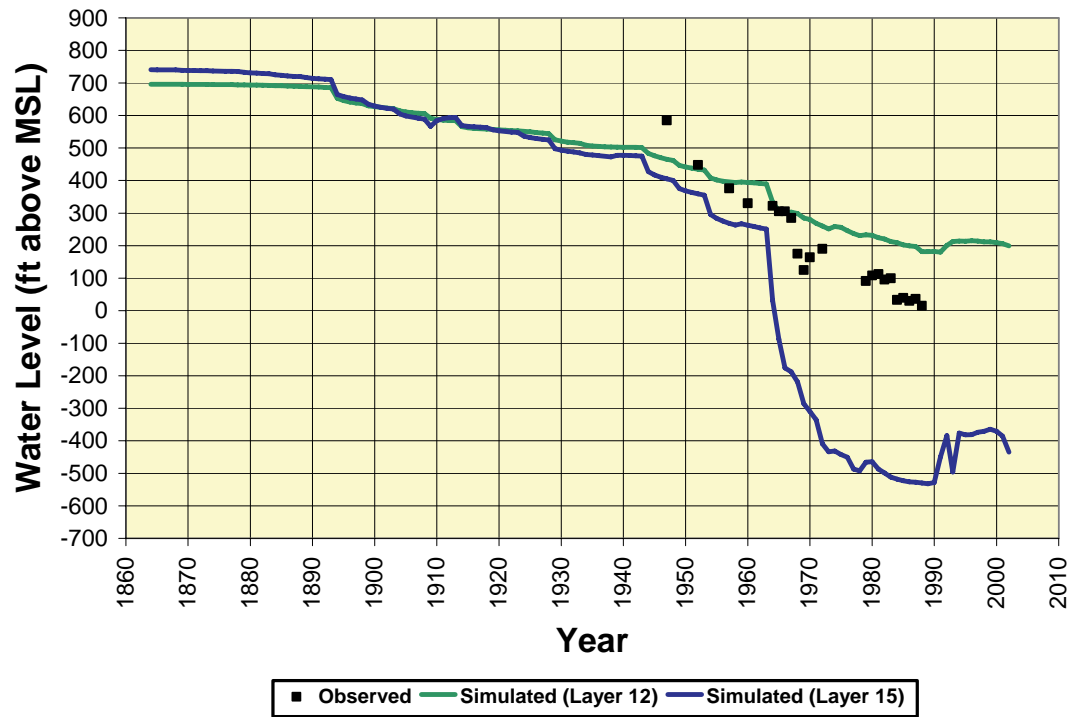


Figure 94. Median annual observed water level and simulated water level at deep head verification location 1120.

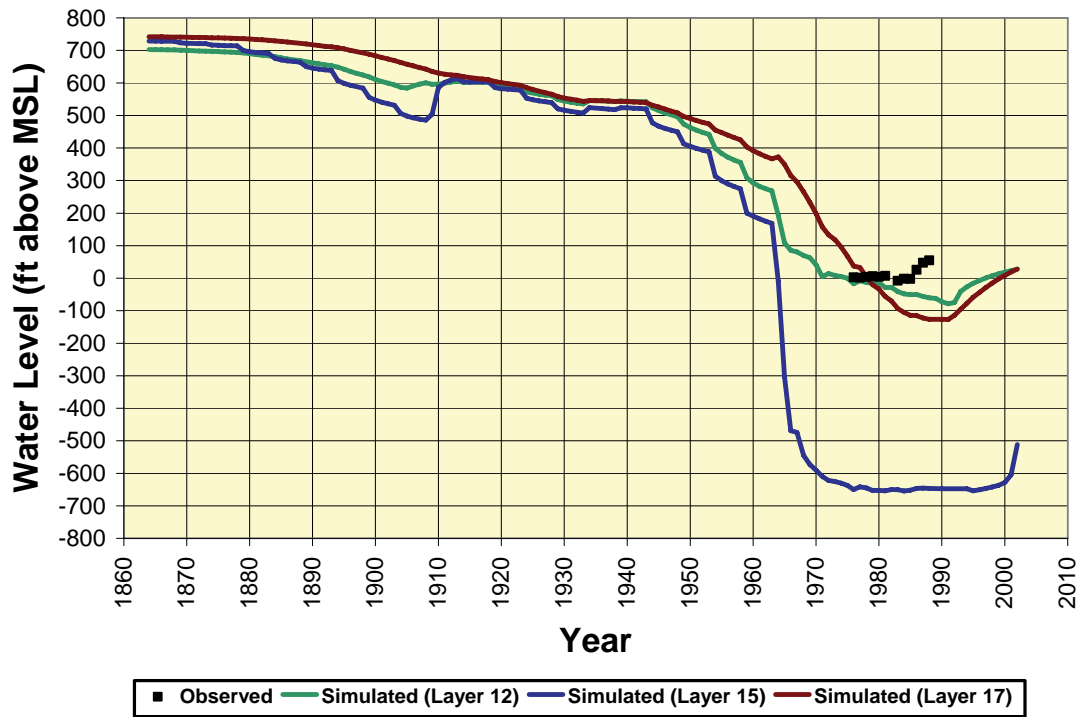


Figure 95. Median annual observed water level and simulated water level at deep head verification location 1121.

Chicago Heights in the mid-1980s. Although it is likely that unsaturated flow of water from adjacent materials, including a thick, extensive basal sand and gravel aquifer (Prickett et al., 1964; Roadcap et al., 1993), would have restored some groundwater to the Silurian-Devonian Carbonate Unit and increased heads within it, lateral flow through unsaturated areas is not simulated in this model. Consequently, while the model-calculated heads in the Silurian-Devonian Carbonate Unit at well 1112 accurately show the unit to be partially desaturated during the period 1964-1983, it is likely that the model underestimates observed heads in well 1112. As noted above, the model does not simulate interformational flow of groundwater along boreholes, and this could cause the difference between observed and model-calculated heads at observation well 1112. In the case of well 1112, it is entirely plausible that groundwater moved up the borehole to saturate overlying, desaturated materials during the period of heavy pumping ending in 1984. This process would supplement water derived by unsaturated flow from above to increase heads in the Silurian-Devonian Carbonate Unit.

Observed and model-calculated heads at observation well 1113 (Figure 89), located in LaGrange (Cook County), also disagree significantly. Well 1113 is open to the Silurian-Devonian Carbonate Unit and the upper part of the Maquoketa Unit (model layers 5-8). Like the Chicago Heights area, the LaGrange-Western Springs area of Cook and DuPage Counties was the location of significant withdrawals from the Silurian-Devonian Carbonate Unit during much of the 20th century. These large withdrawals continued until 1984, when LaGrange shifted the source of its public water supply to Lake Michigan. Like the Chicago Heights area, more than 150 ft of the Silurian-Devonian Carbonate Unit was desaturated in the LaGrange-Western Springs area in 1962 (Prickett et al., 1964). The differences between observed and model-calculated heads at well 1113 and the absence of a desaturated region in the simulations of the Silurian-Devonian Carbonate Unit are attributed to omitting most pre-1964 withdrawals. It is plausible that the observed head in well 1113, which is much lower than model-calculated heads in the Silurian-Devonian Carbonate Unit, is strongly influenced by non-simulated downward borehole transfers of groundwater from the Silurian-Devonian Carbonate Unit to the Maquoketa Unit.

Figure 90 through Figure 95 show regional model results at observation wells open to deeper model layers (layers 10-17). To simplify these figures, only simulated heads for the model layers that are aquifers in northeastern Illinois, that is, the Ancell Unit, Ironton-Galesville Unit, and upper Mt. Simon Unit (model layers 12, 15, and 17, respectively) are shown. As mentioned previously, observed water levels in deep wells are composites of heads in all units intercepted by the open borehole, particularly the heads in the aquifers. Thus, we expect the observed water levels to be between the simulated heads in the borehole-intercepted aquifers. The plots in Figure 90 through Figure 95 do, in fact, show approximate agreement between observed water levels and model-calculated heads in the aquifers to which the wells are reported to be open, with the observed water level between the simulated aquifer heads for the most part. A portion of the disagreement between the simulated heads in intercepted units and the observed water levels is attributed to uncertainty in the head calibration targets, estimated in the nearfield at 82 ft for single-aquifer deep wells distant from pumping (more comparable to Figure 90 and Figure 91) and 200 ft for multiple-aquifer deep wells close to pumping (comparable to Figure 92 through Figure 95) (Appendix E).

Much of the remaining difference between observed composite water levels and simulated heads in intercepted aquifers may be attributable to interformational transfer of groundwater, via open boreholes, between deep aquifers. This effect is not simulated by the regional model, and although a detailed analysis of its effects is beyond the scope of the project, the authors can offer a speculative, qualitative assessment of the effect of these transfers on deep aquifer head. Since most deep wells in northeastern Illinois are open only to the Ancell and Ironton-Galesville Units, not the deeper Mt. Simon Unit, model-simulated heads (e.g., Figure 90 through Figure 94) suggest that the transfer of water along most deep boreholes is downward, from the Ancell Unit (with higher simulated head) to the Ironton-Galesville (with lower simulated head).

This transfer is equivalent to constantly pumping water from the Ancell Unit and injecting the water into the Ironton-Galesville. With the influence of unsimulated downward transfers of groundwater in the thousands of deep wells in northeastern Illinois, then, actual head is likely to be lower in the Ancell and higher in the Ironton-Galesville than the heads simulated with the regional model. In wells open to the Mt. Simon Unit as well as the Ancell and Ironton-Galesville (e.g., Figure 95), some upward transfer of water from the Mt. Simon may also occur. The overall hydrologic effect of such interformational transfers of groundwater is to equalize the head between the deep aquifers.

This conjectured relationship is corroborated by heads observed by the USGS in discrete, packed-off intervals in a deep test well at Zion, Lake County, Illinois (Nicholas et al., 1987) (Figure 86). The USGS drilled this test well in 1980 to a depth of 3,475 ft, penetrating 40 ft of Precambrian granite. Portions of the Zion well were isolated from the rest of the open interval of the well using packers so that heads could be measured in the isolated intervals. This is the only well in the model nearfield from which such data are available. Observed and simulated heads at the Zion well are shown in Table 20. The data show that the range of observed heads in the deep aquifers at Zion is far less than that of the simulated heads. The lesser range of observed deep aquifer heads is consistent with the conjectured equalization of head through interformational transfers of groundwater. Still, since the magnitude of the residuals at the Zion location, which range from about 7 ft (layer 12) to 149 ft (layer 20), is also consistent with the calibration target errors calculated for nearfield wells in Appendix E, the residuals at Zion may simply reflect the components of error considered in the Appendix E calculation. These error components include unmodeled temporal variability, measurement error, errors due to vertical averaging over long piezometer intervals (not including the effect of interformational borehole transfers of groundwater), unmodeled heterogeneity, and interpolation error. The residuals between the observed and simulated heads at Zion suggest the regional model accuracy is greatest for model layer 12, and that the accuracy declines downward.

Table 20. Comparison of Simulated Heads and Observed Heads at USGS Zion Test Well

<i>Model Layer</i>	<i>1982 Simulated Head (ft above MSL)</i>	<i>Median Observed Head in 1982 (ft above MSL)</i>	<i>Residual (ft)</i>
12	376.877686	370.25	-6.63
15	271.804169	366.38	94.58
17	273.054138	373.435	100.38
20	275.779572	424.655	148.88

Trends in observed and model-calculated heads in deep wells match one another more closely in the period following the mid-1970s, although in some cases the trends agree closely at earlier times (e.g., Figure 90 and Figure 93). The gradual improvement in model accuracy through the 1960s and early 1970s probably reflects the transition from representing pre-1964 pumping at seven aggregated pumping centers to representing it at actual well locations from 1964 onward (see Section 2.2.6 and Appendix B). In the case of at least one deep observation well south of Joliet (Figure 91), the scattered plot of observed heads appears to document pre-1964 withdrawals at the observation well itself, or in its immediate vicinity. It is likely that the regional model overestimates head in the source interval of the observation well because these withdrawals are aggregated with other withdrawals in the Joliet area and simulated collectively at the Joliet pumping center, located 12 miles north of the observation well. For the most part, the model calculated heads at the deep observation wells are not affected by omitting unsaturated flow from the model, as discussed in regard to shallow observation well 1112 (Figure 88). With one exception—well 1121 (Figure 95)—the open intervals of these wells do not intercept layers that the regional model simulates as desaturated. At well 1121, the regional model indicates that the upper part of the Galena-Platteville Unit is desaturated, but it is doubtful that unsaturated flow across this layer—even if simulated—could explain the disagreement between the observed and model-calculated heads at the well, since the origin of any unsaturated flow entering the Galena-Platteville would be the relatively impermeable Maquoketa Unit. The Maquoketa would be expected to release a negligible amount of water to the underlying Galena-Platteville.

After successive trials of alternative values of storage parameters, no improvement in model accuracy—as judged by comparison against the observed heads—could be realized by changing storage parameters from the assumed starting values (Table 6). The transient verification also shows that the model is more accurate for deeper model layers (layers 10-15), although accuracy for the deepest model layers (layers 16-20) can not be ascertained with the available calibration targets. The verification is somewhat confounded by the averaging effect of observation wells with long open intervals, but it should be noted the residuals still are generally less than the errors in the calibration targets for head (200 ft, including this averaging effect; see Appendix E). The simulated trends echo the observed trends in head with increasing accuracy up to present day, suggesting that the model can be considered verified within the limits of the existing data.

2.3.1.6. Sensitivity Analysis

Following calibration of the regional model, the output of PEST (Watermark Numerical Computing, 2005) for the final parameter estimates under predevelopment conditions was used for sensitivity analysis. The purpose of this sensitivity analysis is to quantify the uncertainty in the calibrated model caused by uncertainty in the estimates of aquifer properties (Anderson and Woessner, 2002). This information helps illustrate which parameters are affected by which calibration targets, and helps evaluate the worth of additional parameter measurements and observations of calibration targets in improving model accuracy. For the regional model, the sensitivities of the estimated parameters were grouped as:

- horizontal hydraulic conductivity of the shallow units (shallow K_h),
- horizontal hydraulic conductivity of the deep units (deep K_h),
- vertical hydraulic conductivity of the shallow units (shallow K_v),
- vertical hydraulic conductivity of the deep units (deep K_v),
- leakance of streambeds, lakebeds, and drains (leakance), and
- recharge for all zones (recharge).

PEST computed the relative sensitivities (i.e., the change in the objective function per unit change in the parameter, divided by the parameter value), and the average relative sensitivity was calculated for each of the above groups. Since the calibration targets are weighted differently, the results also are grouped by the calibration targets being matched to assist in understanding the sensitivities. These target groups are:

- composite head in Cambrian-Ordovician units (northeastern Illinois, highly weighted),
- composite head in Cambrian-Ordovician units (Illinois, excluding northeastern Illinois),
- composite head in Cambrian-Ordovician units (Wisconsin),
- head in Mt. Simon (density-corrected, highly weighted),
- head in Mt. Simon (not density-corrected),
- flux, Illinois (near Kane County, highly weighted),
- flux, Illinois (not near Kane County),
- flux (Wisconsin),
- anisotropy ratio (K_h/K_v) (high reliability, highly weighted), and
- anisotropy ratio (K_h/K_v) (low reliability)

Note that the anisotropy ratios are listed with the calibration targets, since they are used as prior information in this study and thus are matched as part of the objective function of PEST. Figure 96 summarizes the sensitivities, where the total bar length is the sum of the average relative sensitivities of 11 groups of calibration targets to variation in each of six parameter groups. Thus, for any individual parameter group, the length of each bar segment in Figure 96 is equivalent to the average relative sensitivity of a specific calibration target group to changes in that parameter group. Overall, the most sensitive parameter group is the hydraulic conductivities in the vertical plane for the shallow units (shallow K_v), where the sensitivity is dominated by the group of calibration

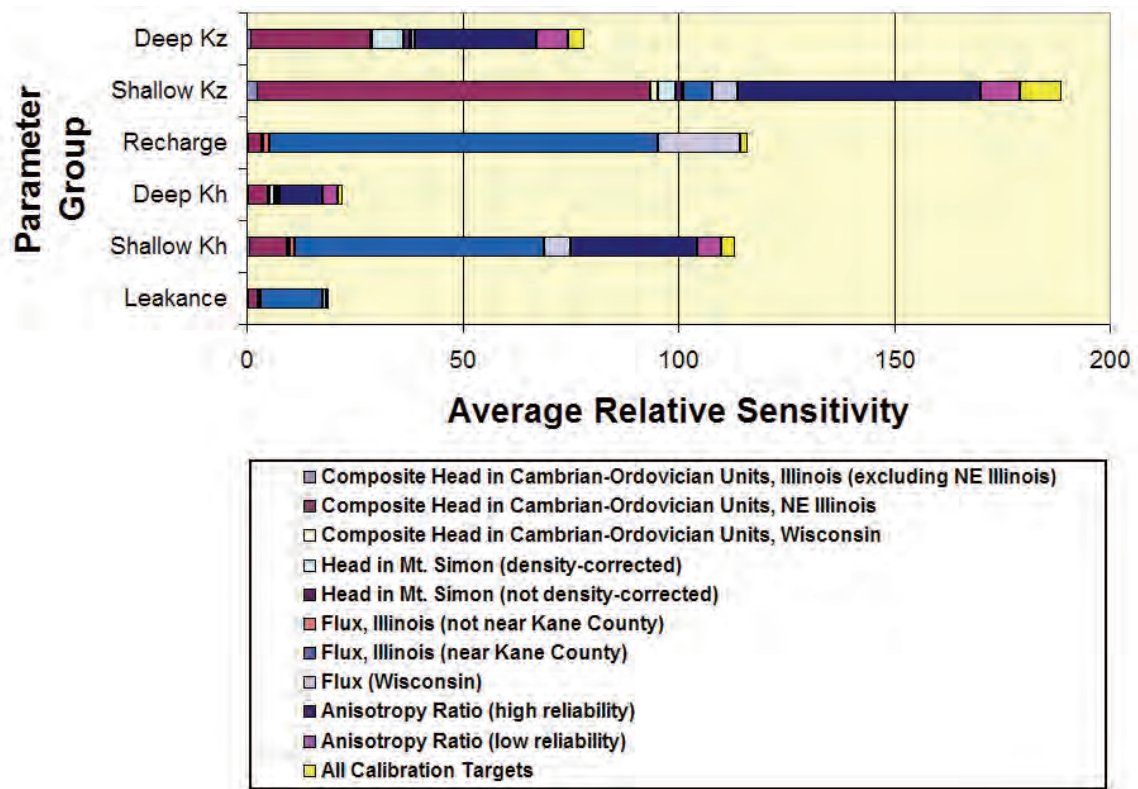


Figure 96. Parameter sensitivities for the predevelopment calibration, regional-scale model.

targets for heads in the Cambrian-Ordovician Units in northeastern Illinois. This suggests that the vertical conductivities are the most important control on downward flow from the shallow aquifers to the underlying sandstone aquifers. The next most sensitive parameter groups are the recharge estimates and the horizontal conductivities of the shallow units, whose sensitivity is dominated by the calibration targets for flux near Kane County. This is reasonable, since the flux targets are in the uppermost active layer of the model and there were no predevelopment head data available to be included as calibration targets in the shallow aquifers. The match of the model to the anisotropy priors is sensitive to the hydraulic conductivity parameters, a consequence of the weighting of these priors to stabilize the parameter estimates. While this suggests that the anisotropy prior information is a controlling factor in the parameter estimation, it should be noted that it is generally the minor contributor to the sensitivity.

2.3.2. *Local-Scale Shallow Model*

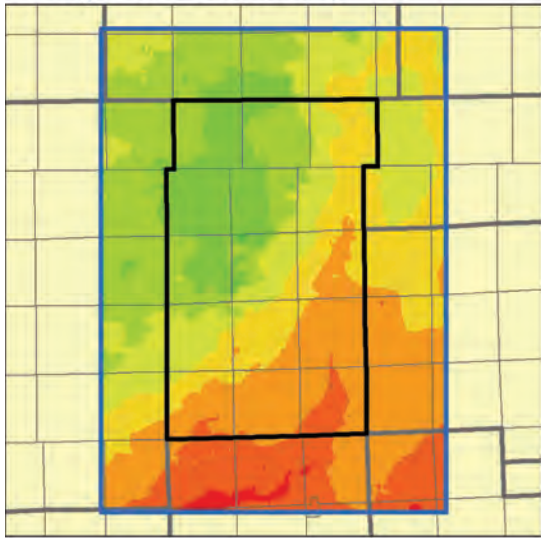
2.3.2.1. Approach

The approach to calibrating the local model differs somewhat from that used for the regional model due to differences in model resolution and data availability at the differing scales of representation. The local-scale model was calibrated by adjusting model parameters until the steady-state simulation of 2003 pumping conditions closely reproduced a set of calibration targets. The model was calibrated against measurements of head in the shallow aquifers obtained in fall 2003 and against estimates of flux, or base flow in streams, obtained from statistical modeling of streamflow in the Kane County area (Knapp et al., 2007), together with estimates of their associated errors. A steady-state calibration to predevelopment conditions was not attempted owing to the lack of either observed or conjectural predevelopment heads.

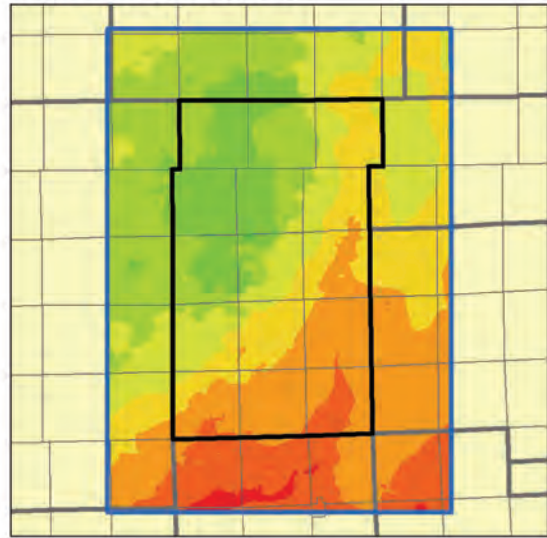
Steady-state calibration using the 2003 pumping distribution is an appropriate approach for the local-scale model because heads in the shallow aquifers adjust to a steady state fairly rapidly with changes in pumping owing to their connection to surface waters and, in the humid eastern United States, the relative proximity of surface waters to points of withdrawal. In other words, heads in the shallow aquifers are controlled by surface-water elevations and rapidly adjust to changes in pumping. Support for this view is offered by the close similarity of simulated steady-state heads in the Shallow Bedrock Aquifer calculated from 2003 pumping rates and distribution and simulated transient heads calculated from the actual pumping history (Figure 97).

Just as for the regional-scale model, initial steady-state calibration to 2003 pumping conditions was conducted manually, by altering K_h , K_v , leakance, and recharge within plausible ranges until the model simulations were numerically stable and approximated the calibration targets. The calibration process was continued using the nonlinear parameter-estimation software PEST (Watermark Numerical Computing, 2005) until no further improvement with respect to the calibration targets could be achieved. Within PEST, calibration targets were weighted to emphasize accuracy within Kane County. Calibration results were assessed graphically and statistically, and sensitivity analyses were conducted to ascertain the sensitivity of the model to changes in the calibrated parameters. Transient verification of the steady-state calibration was performed by comparing 2003 results of *transient* simulations of historical pumping from 1964 through 2003 against (1) the fall 2003 head measurements and flux estimates based on

Steady-State Simulation



Transient Simulation



Head in 2003 (ft above MSL)

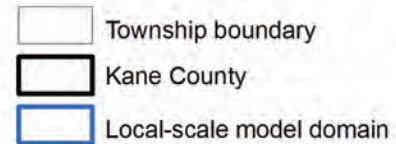


Figure 97. Close similarity of simulated 2003 heads in the Shallow Bedrock Aquifer based on steady-state modeling employing 2003 pumping distribution and rates and transient modeling employing actual 1964-2003 pumping histories.

statistical modeling (i.e., the same targets used for steady-state calibration), and (2) time-series of shallow aquifer head data compiled from published reports and well records. The adequacy of the calibration and verification was evaluated by comparing the calibration errors relative to the errors in the calibration targets (Appendix E).

2.3.2.2. Calibration Targets

Head targets for calibration of the local-scale model were based on water-level measurements from the shallow aquifers collected in fall 2003 (Locke and Meyer, 2007). The set of calibration targets included 782 head measurements within the local model domain (Figure 98), observed in domestic water-supply wells open to the Shallow Bedrock Aquifer and open to sand and gravel units. For automated parameter estimation using PEST, head calibration targets were weighted to emphasize accuracy in Kane County. Based on the error analysis discussed in Appendix E, the total error associated with the head calibration targets in the local-scale model is 29 ft.

The local-scale model was also calibrated against targets for groundwater flux representing long-term average base flow in eight watersheds in the model domain (Figure 99). Similar to the regional model, flux targets for the local model are inferred as the arithmetic average of Q_{80} and Q_{50} as an estimate of the long-term average of groundwater discharge to streams and agricultural drains. In contrast with the regional model, where the flux targets were inferred from USGS stream gages, flux targets for the local model were developed using ILSAM, the statistical model of Kane County streamflow during the period from 1948 through 2004 (Knapp et al., 2007) (Table 21). Unlike the raw USGS gage data used for the flux targets of the regional model, the ILSAM estimates of Q_{80} and Q_{50} exclude the effects of diversions, effluent, and Stratton Dam (on the Fox River upstream of Kane County), and thus are appropriate for developing flux calibration targets. The errors associated with these flux targets are inferred from the ILSAM variances for Q_{80} and Q_{50} (Appendix E), and vary depending on the subsoil permeability within each watershed (Table 11). For automated estimation of parameters using PEST, the calibration targets for flux were assigned lower weights than the head calibration targets to normalize calibration errors (i.e., to put calibration errors of ft^3/day and ft/day on the same scale).

2.3.2.3. Estimated Parameters

Final, calibrated values of hydraulic conductivity and recharge rates are shown in Table 22 and Table 23. As discussed in Section 2.2.5.2, two additional recharge zones were created during the calibration process based on local hydrologic conditions (Figure 100). A lower recharge rate is applied to isolated bodies of surficial sand and gravel that are not connected to surface waters or larger bodies of saturated sand and gravel and a higher recharge rate is applied to isolated outcrops of sands connected to buried aquifers that are able to accept the additional flow. Calibrated recharge rates are also illustrated in Figure 100. Leakance values were not changed from starting values.

The transient verification procedure (Section 2.3.2.5) did not result in alteration of specific storage from the starting value shown for the Quaternary Unit in Table 6.

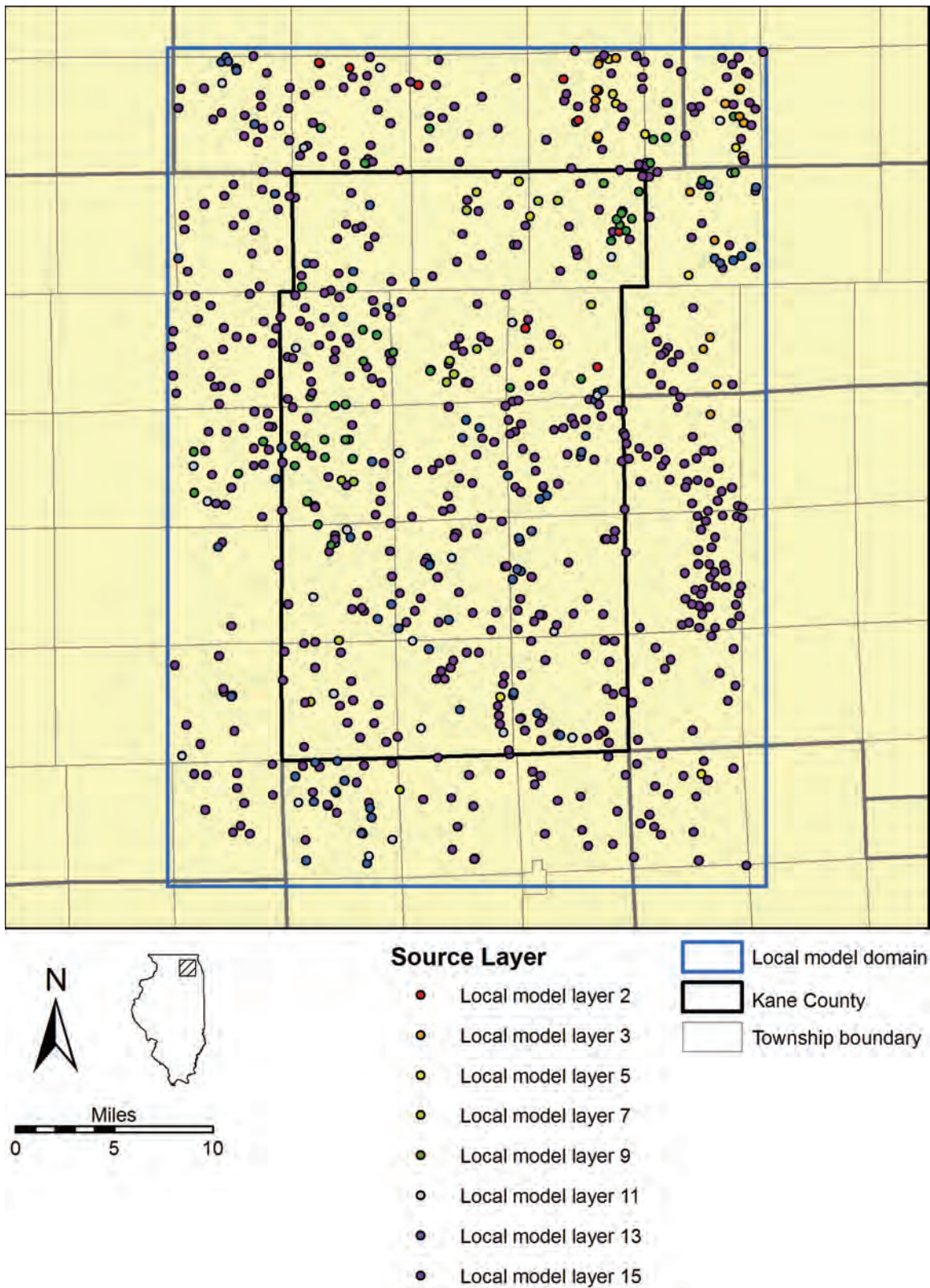


Figure 98. Head targets for calibration of local-scale model.

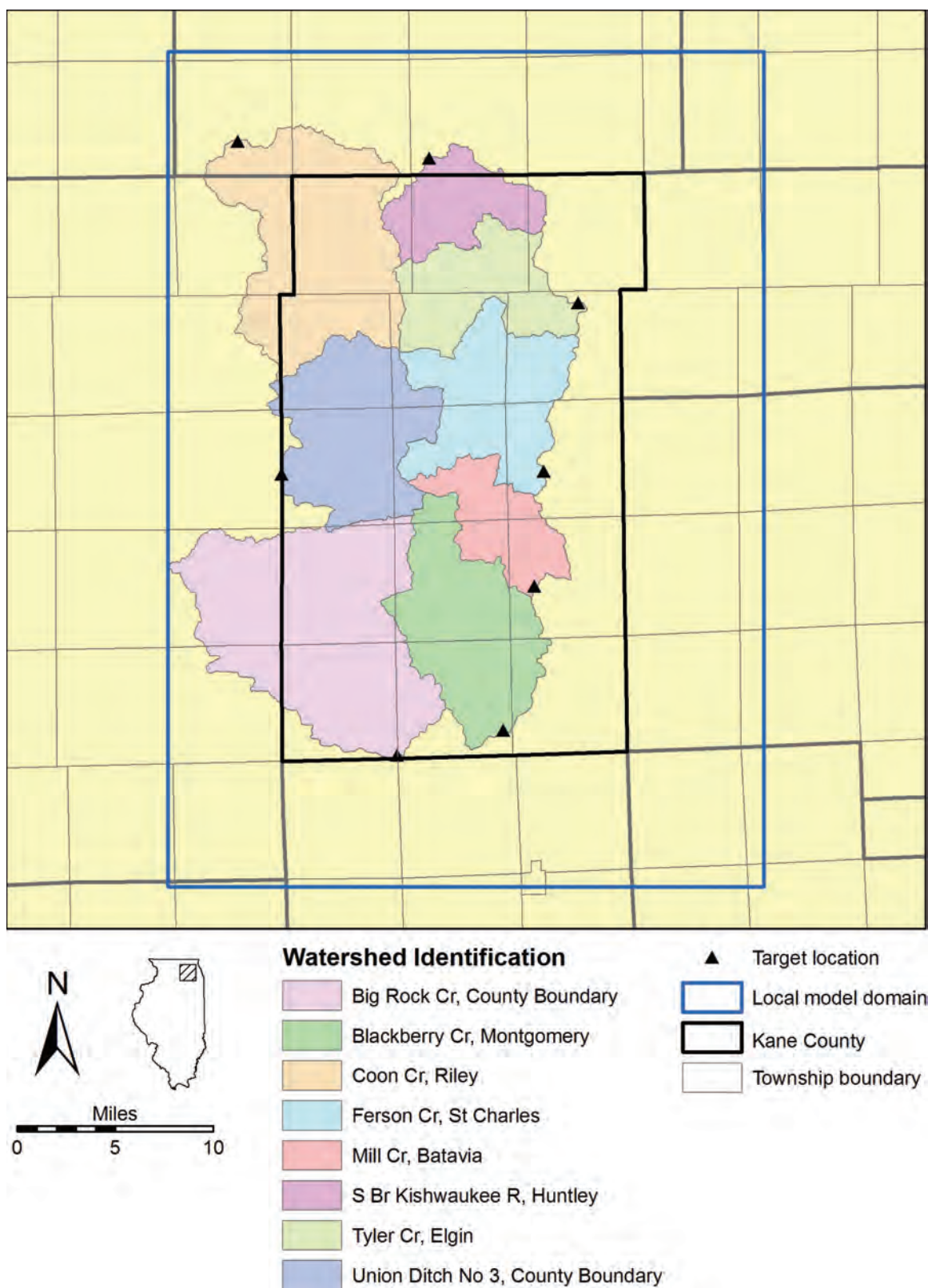


Figure 99. Flux targets for calibration of local-scale model.

Table 21. Flux Targets for Calibration of Local-Scale Model

<i>Watershed</i>	<i>Q₈₀ (ft³/d)</i>	<i>Q₅₀ (ft³/d)</i>	<i>Q Target (ft³/d)</i>	<i>Q Target Error (ft³/d)</i>
Big Rock Cr	362,880	2,220,480	1,291,680	155,002
Blackberry Cr	907,200	2,073,600	1,490,400	178,848
Coon Cr	829,440	2,505,600	1,667,520	450,230
Ferson Cr	578,880	1,771,200	1,175,040	317,261
Mill Cr	103,680	561,600	332,640	39,916.8
S Br Kishwaukee River	129,600	725,760	427,680	51,321.6
Tyler Cr	267,840	915,840	591,840	71,020.8
Union Ditch No 3	362,880	1,702,080	1,032,480	123,898

Table 22. Calibration of Horizontal (K_h) and Vertical Hydraulic Conductivity (K_v), Local-Scale Model

<i>Zone*</i>	<i>K_h</i>		<i>K_v</i>	
	<i>Starting Value (ft/d)</i>	<i>Calibrated Value (ft/d)</i>	<i>Starting Value (ft/d)</i>	<i>Calibrated Value (ft/d)</i>
1	1.0×10^{-1}	1.0×10^{-1}	1.0×10^{-2}	1.0×10^{-3}
2	1.0×10^2	6.0×10^1	1.0×10^1	6.0×10^{-1}
3	5.0×10^{-4}	3.6×10^{-4}	2.0×10^{-4}	3.6×10^{-4}
4	1.0×10^2	8.1×10^1	1.0×10^1	8.0×10^0
5	1.0×10^3	1.1×10^3	2.0×10^1	1.2×10^1
6	1.0×10^3	4.1×10^2	2.0×10^1	6.4×10^0
7	1.5×10^3	2.0×10^3	3.0×10^1	2.0×10^1
8	3.0×10^1	2.5×10^1	3.0×10^{-1}	1.0×10^0
9	3.0×10^1	2.5×10^1	3.0×10^{-1}	1.0×10^0
10	9.4×10^{-2}	6.5×10^{-2}	9.4×10^{-4}	1.3×10^{-3}
11	5.0×10^0	7.0×10^0	1.6×10^{-1}	2.3×10^{-1}
12	5.0×10^0	7.0×10^0	1.6×10^{-1}	2.3×10^{-1}

Table 23. Calibration of Recharge Rates, Local-Scale Model

<i>Zone*</i>	<i>Initial Value Range (ft/d)</i>	<i>Calibrated Value (ft/d)</i>
1	2.0×10^{-4} to 8.0×10^{-4}	5.0×10^{-4}
2	1.3×10^{-3} to 5.4×10^{-3}	2.5×10^{-3}
3	Modified from zone 2	8.0×10^{-4}
4	Modified from zone 2	4.0×10^{-3}

*See Figure 72 for zone locations.

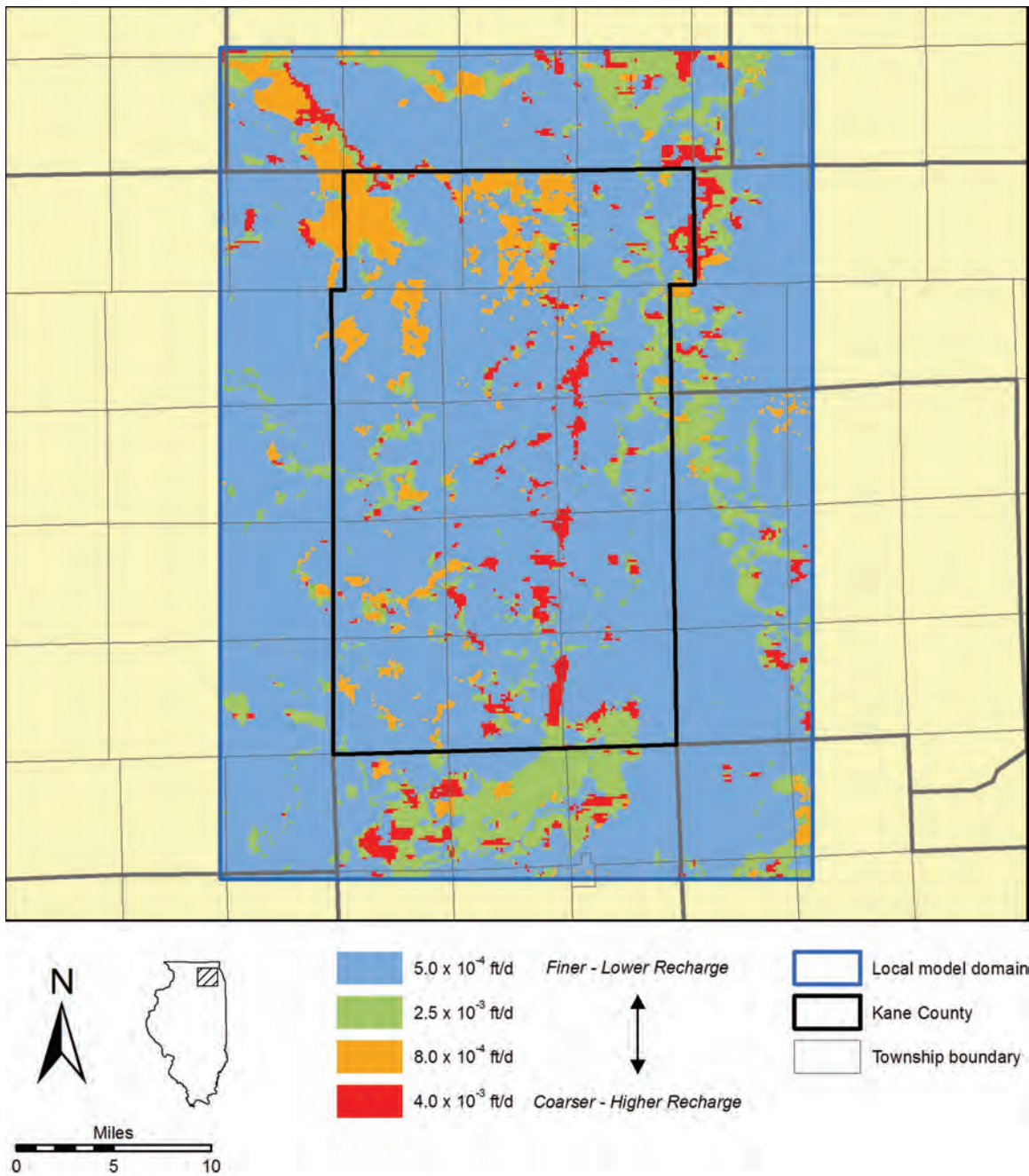


Figure 100. Calibrated recharge rates in local-scale model.

2.3.2.4. Calibration Accuracy and Bias

Accuracy of the steady-state calibration of the local-scale model against observed 2003 head targets is analyzed both graphically and statistically. The analysis shows that the local-scale model simulates heads and fluxes within the accuracy of the calibration target data and that the calibration has little overall bias. Observed and model-calculated heads are compared in Figure 101 by plotting one against the other. Target locations are shown in Figure 98. Overall, the agreement between the points in this plot with a line marking a one-to-one relationship is good, and little bias, which would display as a preponderance of points plotting either above or below the one-to-one line, is apparent.

Residual statistics (see Section 2.3.1.4) corroborate this assessment. Minimal bias in the model-calculated heads is indicated by the residual mean of 0.59 ft (Table 24). The mean absolute error (MAE) describes how much the model-calculated heads differ from target values in either a negative or positive direction. This statistic shows that model-calculated heads differ from target heads by an average of 9.6 ft, well less than the minimum error of the set of head targets employed in the calibration, 29 ft (see Appendix E). To illustrate goodness of fit normalized for the natural range of heads, the mean absolute error can be divided by the total range of observed heads and expressed as a percentage. For the entire population of head targets, this calculation shows that the local-scale model simulates 2003 heads very well (2.8 percent). Figure 102, a map of residuals for the 2003 head calibration targets open to model layer 15, suggests that the residuals have little systematic geographic bias. The symbols in Figure 102 denote whether the simulated values differ from the target value by an amount greater than the MAE (red if residual is negative or blue if residual is positive) or less than the MAE (no shading).

Figure 103 shows that simulated steady-state fluxes for 2003 pumping conditions fall within the target range from Q_{80} to Q_{50} at all of the eight flux calibration locations shown in Figure 99.

The mass balance error for the 2003 simulation is 0.13 percent. Total simulated inflows to the local model domain included 3.3×10^7 ft³/d (249 Mgd) from recharge, 1.1×10^6 ft³/d (8 Mgd) from steam leakage, and 2.7×10^6 ft³/d (20 Mgd) from regional groundwater flow. Total simulated outflows from the local model domain included 2.7×10^7 ft³/d (204 Mgd) to streams, 4.3×10^6 ft³/d (32 Mgd) to water-supply wells, and 5.5×10^6 ft³/d (41 Mgd) to regional groundwater flow.

2.3.2.5. Verification

Following steady-state calibration under 2003 pumping conditions, the local-scale model was verified by comparing the simulated pumping history of the Kane County area against observed water levels at four locations within the local model domain. As discussed previously for the regional model (Section 2.3.1.5), the purposes of transient verification are to confirm the parameter estimates of the steady-state calibration and build confidence in the calibrated model. For the transient simulations, pumping histories were estimated from available data as discussed in Appendix B, and storage parameters are based on aquifer tests and published reports (Table 6). The verification targets consist of four series of three or more water-level measurements assembled from well records and ISWS potentiometric-surface-mapping studies (Locke and Meyer, 2007; Meyer, 1998; Sasman et al., 1981; Visocky and Schulmeister, 1988) (Figure 104).

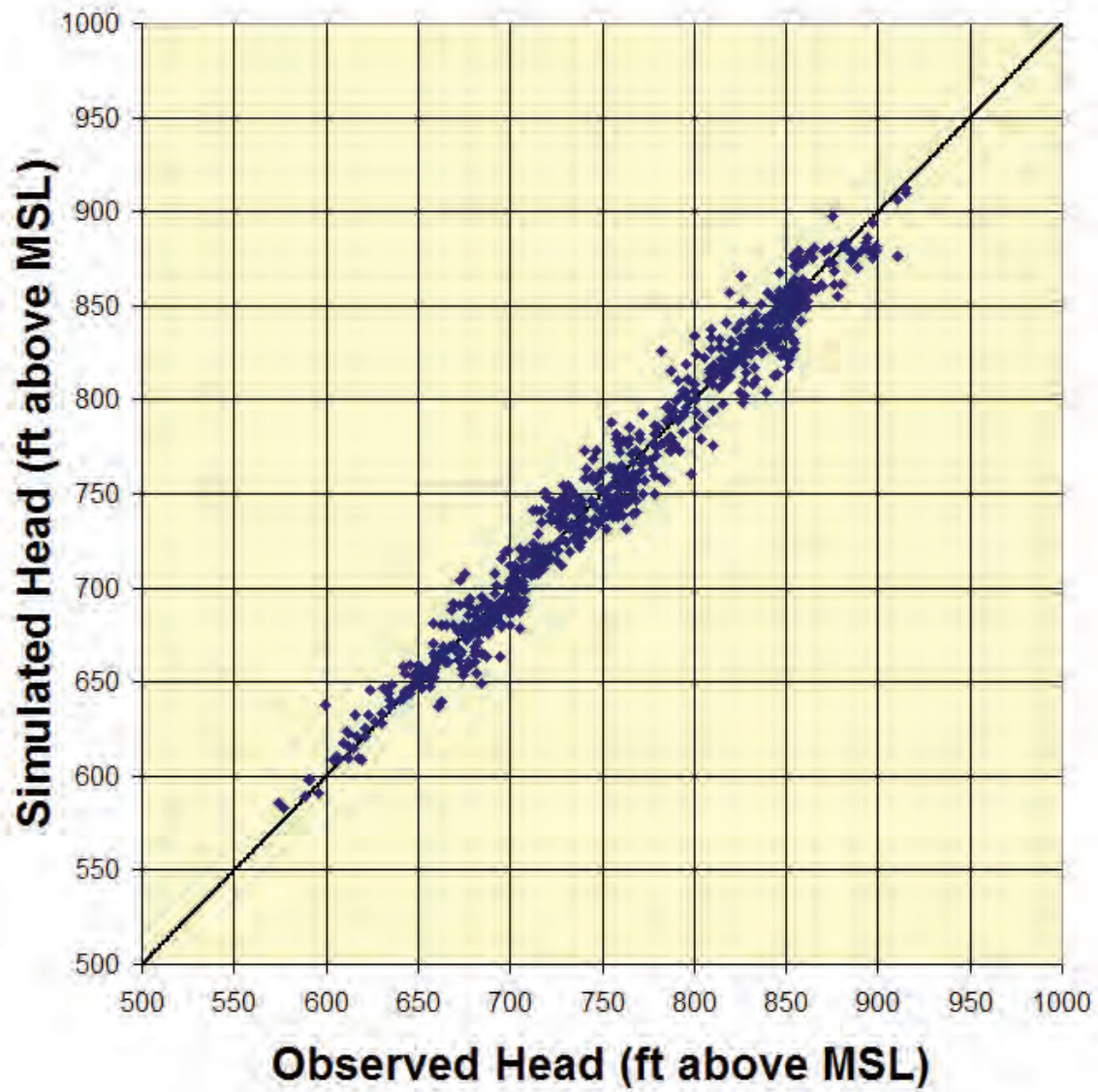


Figure 101. Plot showing the goodness of the fit between observed 2003 heads and head simulated with 2003 steady-state model.

**Table 24. Statistics Describing Steady-State Calibration of
Local-Scale Model to 2003 Head Targets**

<i>Statistical Measure</i>	<i>Value</i>
Number of target heads	782
Residual mean (feet)	0.59
Mean absolute error (feet)	9.60
Minimum residual (feet)	-44
Maximum residual (feet)	38
Range of target values (feet)	341
Mean absolute error/Range	2.8%
Calibration target error (feet) (Appendix E)	±29

The comparison is limited to wells open to the Shallow Bedrock Aquifer since adequate time series of water-level measurements from other units are not available.

Time series of model-simulated and observed heads were plotted together and compared visually for model verification (Figure 105 through Figure 108). The plots show good agreement between simulated and observed values with all but one data point (the first data point in Figure 107) plotting within the average local model head calibration target uncertainty of 29 ft discussed in Appendix E. Thus, although it is impossible to separate the sources of uncertainty in the model output, it is possible to attribute the disagreement between simulated and target values almost entirely to calibration target error. The greater improved agreement between simulated and measured heads evident at locations having comparatively long observation histories (Figure 105 and Figure 106) indicate that the model simulates head better for the period after about 1970. This is likely due to the greater accuracy and comprehensiveness of the pumping database for the post-1970 period. Although the simulated values in Figure 105 through Figure 108 are generally less than the observed values, it is noteworthy that the mean error of the local scale model (0.4 ft) indicates that the model on the whole only slightly underestimates head.

Manual adjustments of storage parameters evaluated the sensitivity and the potential improvements in the accuracy of the transient simulations. No net improvement in the transient simulations was observed for reasonable variations in the storage parameters, thus the transient verification procedure did not result in alteration of specific storage from the starting value for the Quaternary Unit shown in Table 6.

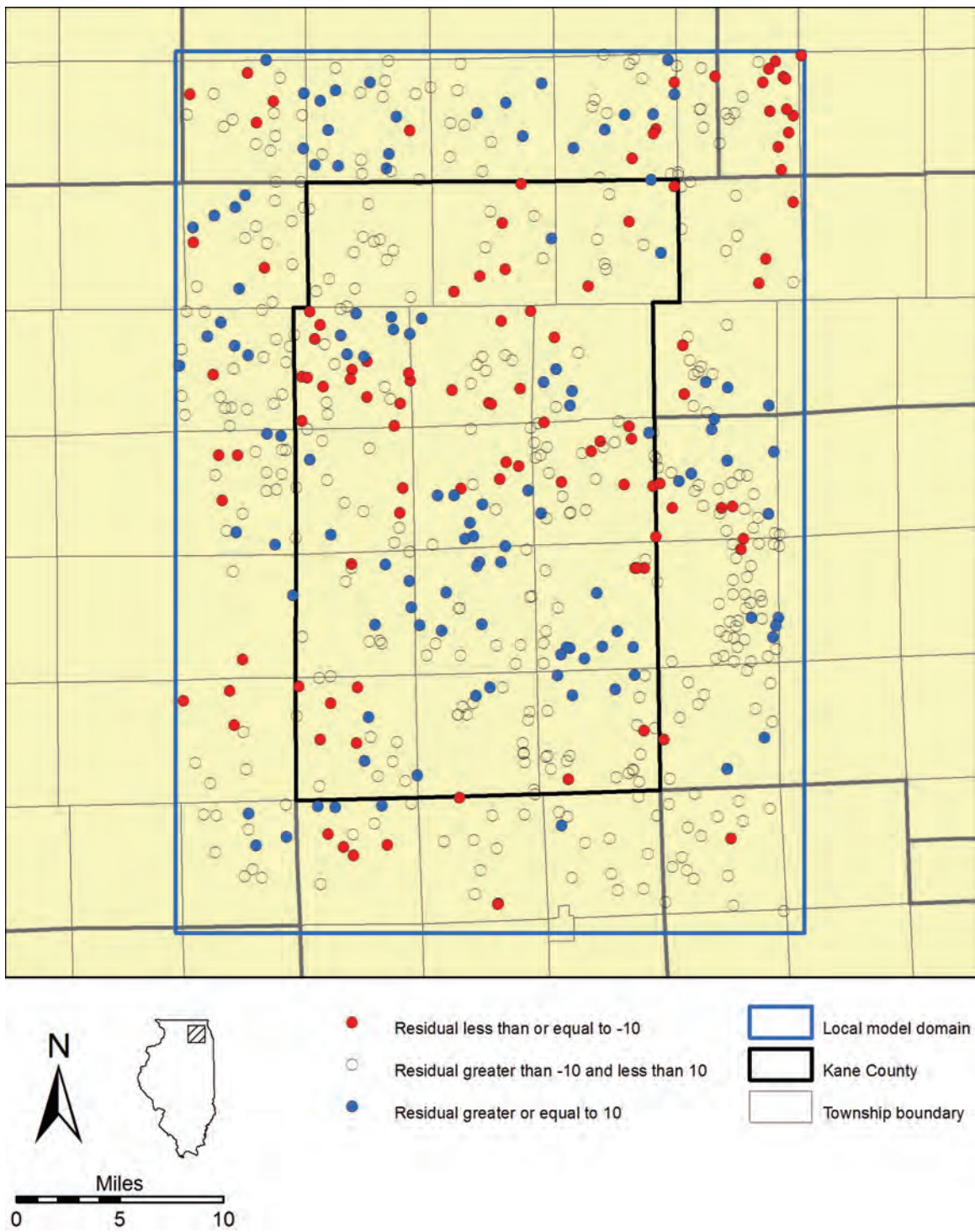


Figure 102. Residuals between target and simulated heads at 2003 head calibration targets open to model layer 15.

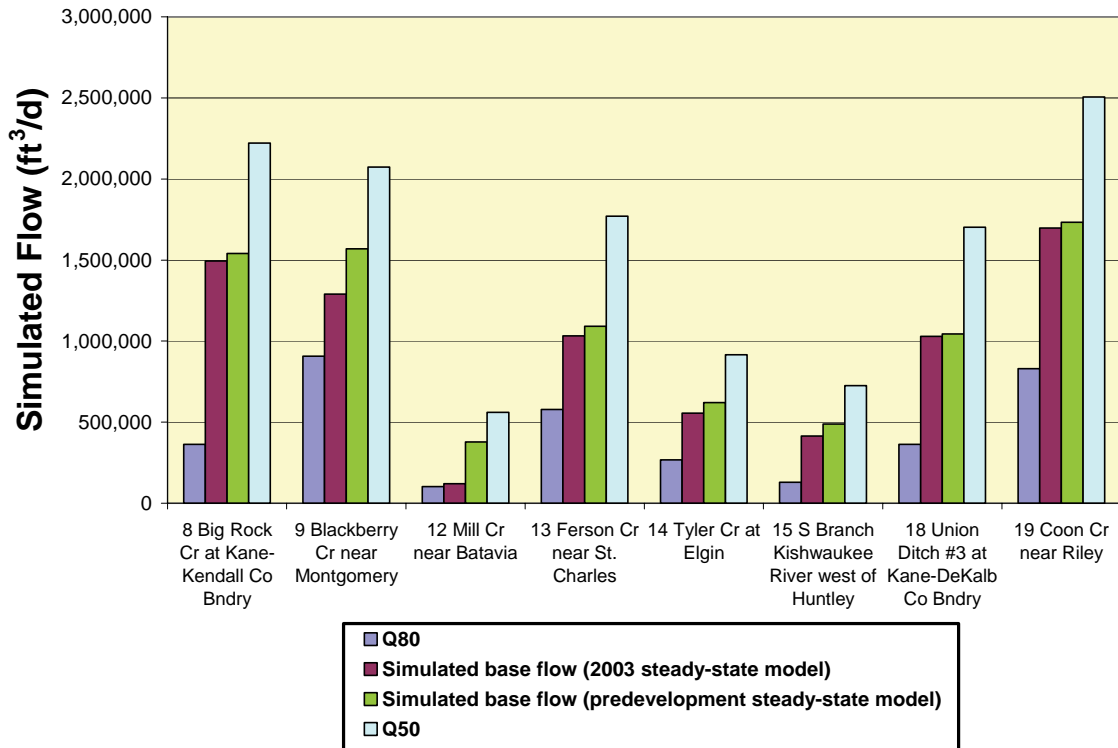


Figure 103. Comparison of simulated base flow to Q_{80} and Q_{50} measurements of streamflow.

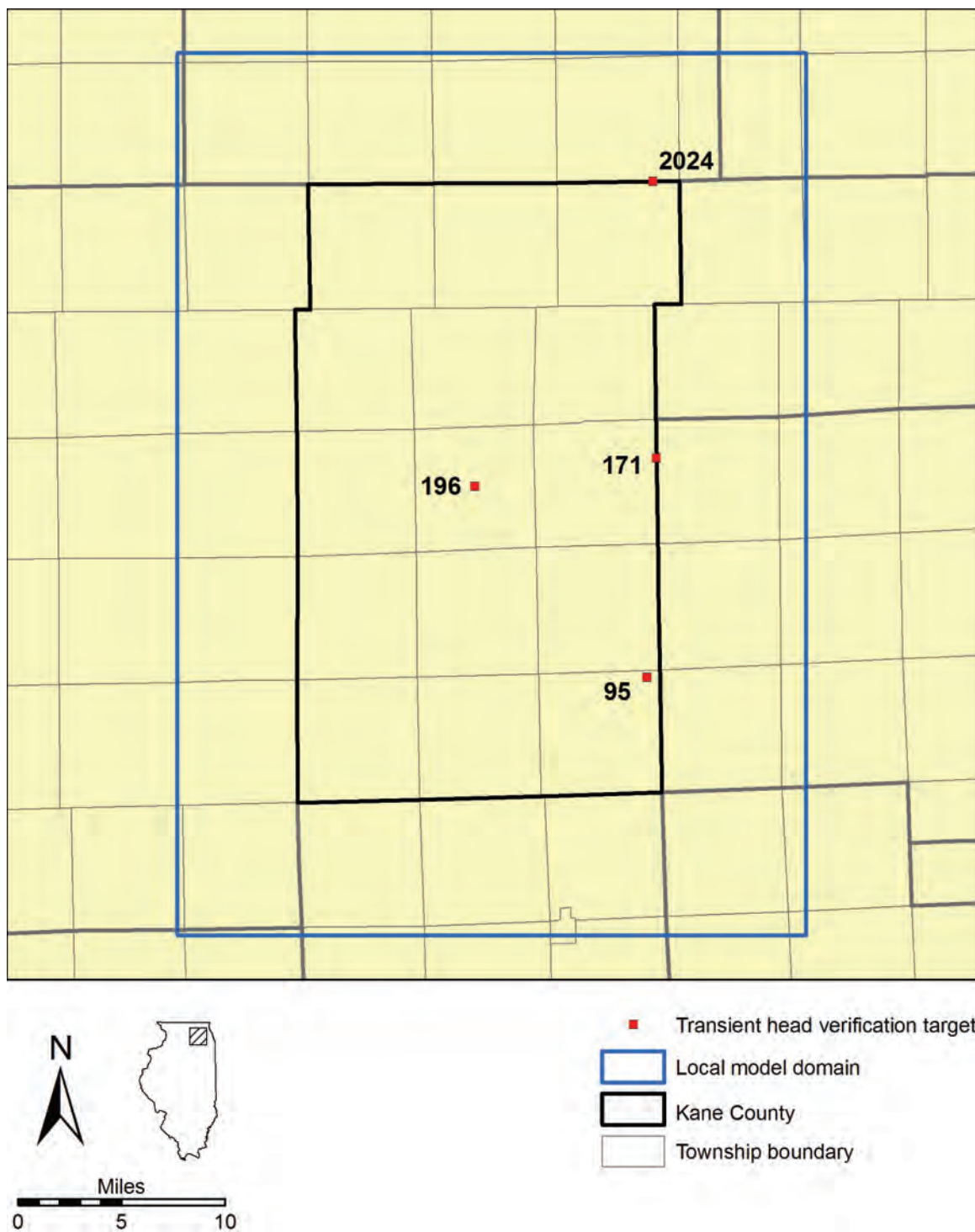


Figure 104. Head targets, with identification numbers referred to in Section 2.3.2.5, for verification of local model under transient conditions.

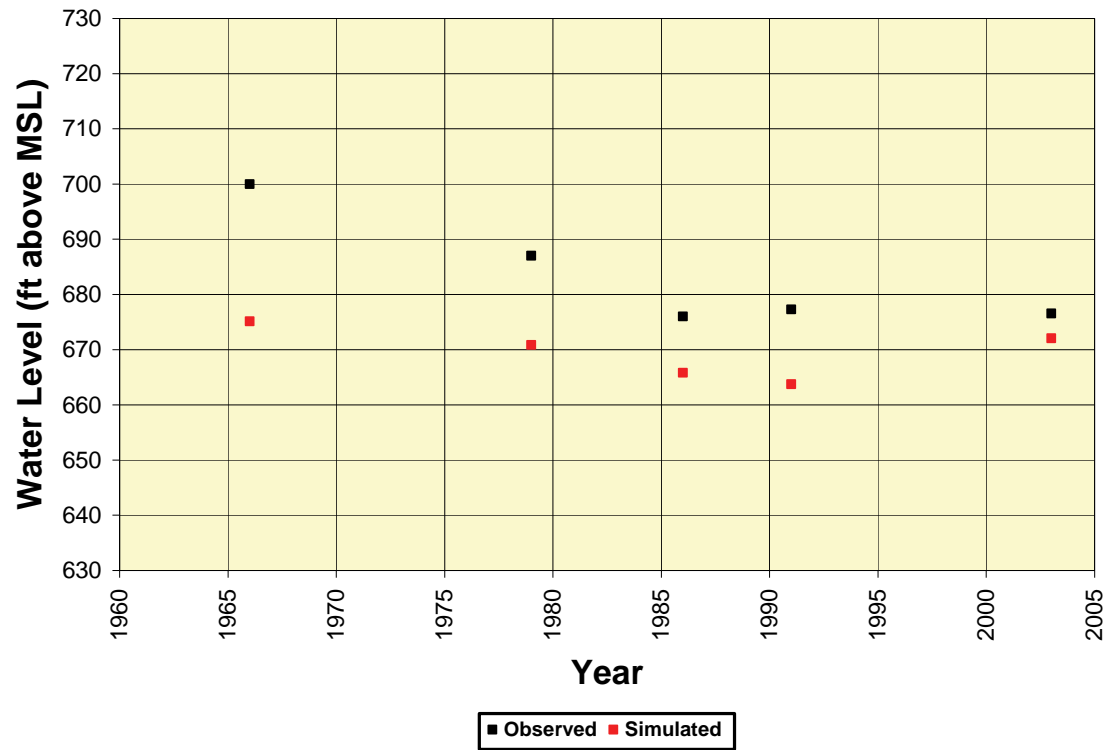


Figure 105. Observed and simulated water levels at transient head verification location 95.

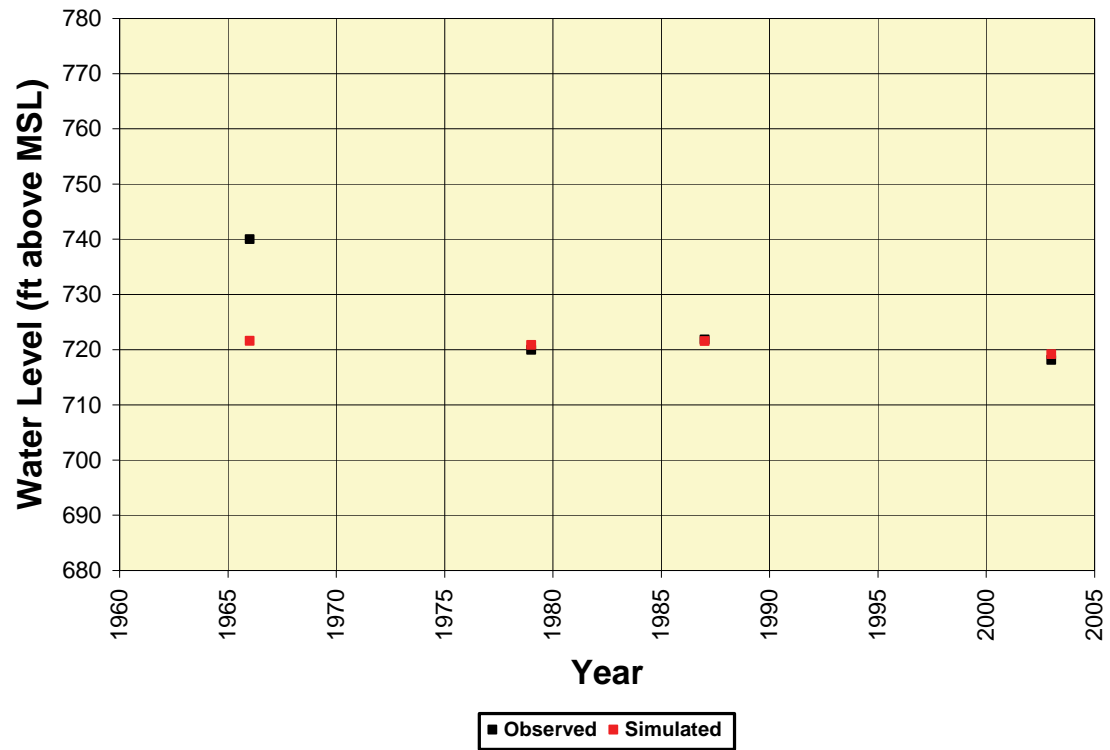


Figure 106. Observed and simulated water levels at transient head verification location 171.

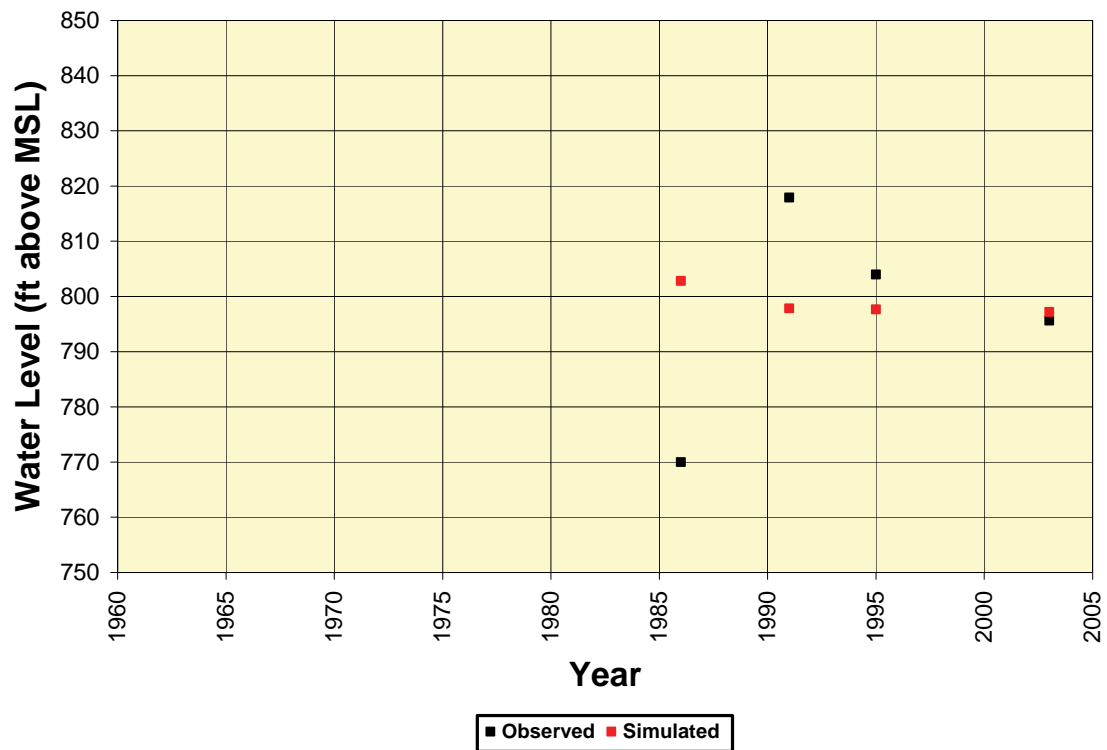


Figure 107. Observed and simulated water levels at transient head verification location 196.

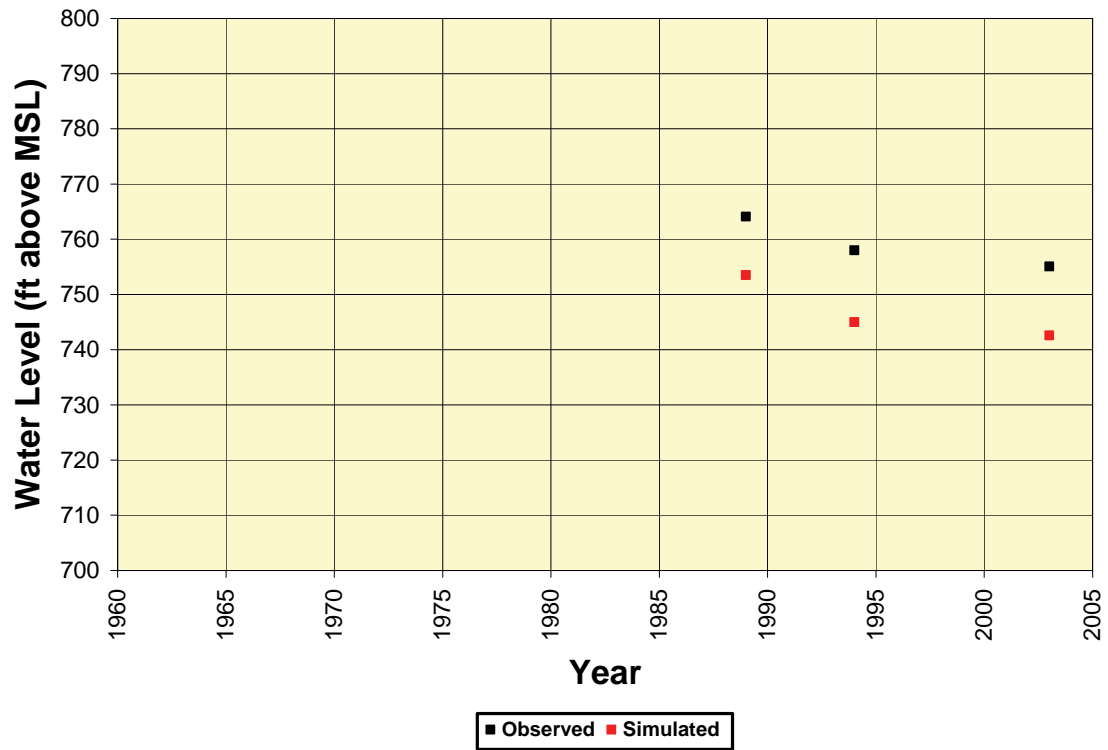


Figure 108. Observed and simulated water levels at transient head verification location 2024.

2.3.2.6. Sensitivity Analysis

Similar to the procedure used for the regional model, the program PEST (Watermark Numerical Computing, 2005) was used for a sensitivity analysis to quantify the uncertainty in the calibrated model caused by uncertainty in the estimates of aquifer properties. Parameters with the highest sensitivities warrant additional future observation and measurement to improve model accuracy. For the local model, the sensitivities of the following parameters were calculated:

- horizontal hydraulic conductivity (K_h) for all the sands,
- horizontal hydraulic conductivity (K_h) for the diamicton,
- horizontal hydraulic conductivity (K_h) for each bedrock unit,
- vertical hydraulic conductivity (K_v) for all the sands,
- vertical hydraulic conductivity (K_v) for the diamicton,
- recharge for all zones.

The sensitivity of the soil parameters and the vertical flow parameters in the bedrock units were not analyzed because of the large number of boundary conditions and the lack of true vertical flow across these units. As discussed in Section 2.2.6 the leakances of the rivers and drains were set sufficiently high as to not impede flow and thus were not used as calibration parameters.

The PEST-computed relative sensitivities are summarized in Figure 109. The most sensitive parameters are the horizontal hydraulic conductivity of the Maquoketa Formation and the vertical hydraulic conductivity of the diamictons. The sensitivity of the model to the Maquoketa Formation is likely the result of the complex relationships among the hydrologic units in Kane County. Many of the thicker lenses of Glasford sand overlying the Maquoketa Formation are contained within small bedrock valleys that generally run northeast to southwest and are generally perpendicular to the slope of the land surface and the principal direction of groundwater flow. Thus, the small intervening bedrock upland areas composed of Maquoketa material act as groundwater flow barriers that can significantly increase upgradient hydraulic heads.

As discussed in Section 2.2.6, the amount of recharge flowing through the diamictons is principally controlled by the low vertical permeability of the unit. Because the diamictons cover most of Kane County, the model is more sensitive to the K_v of the diamicton than the recharge rates.

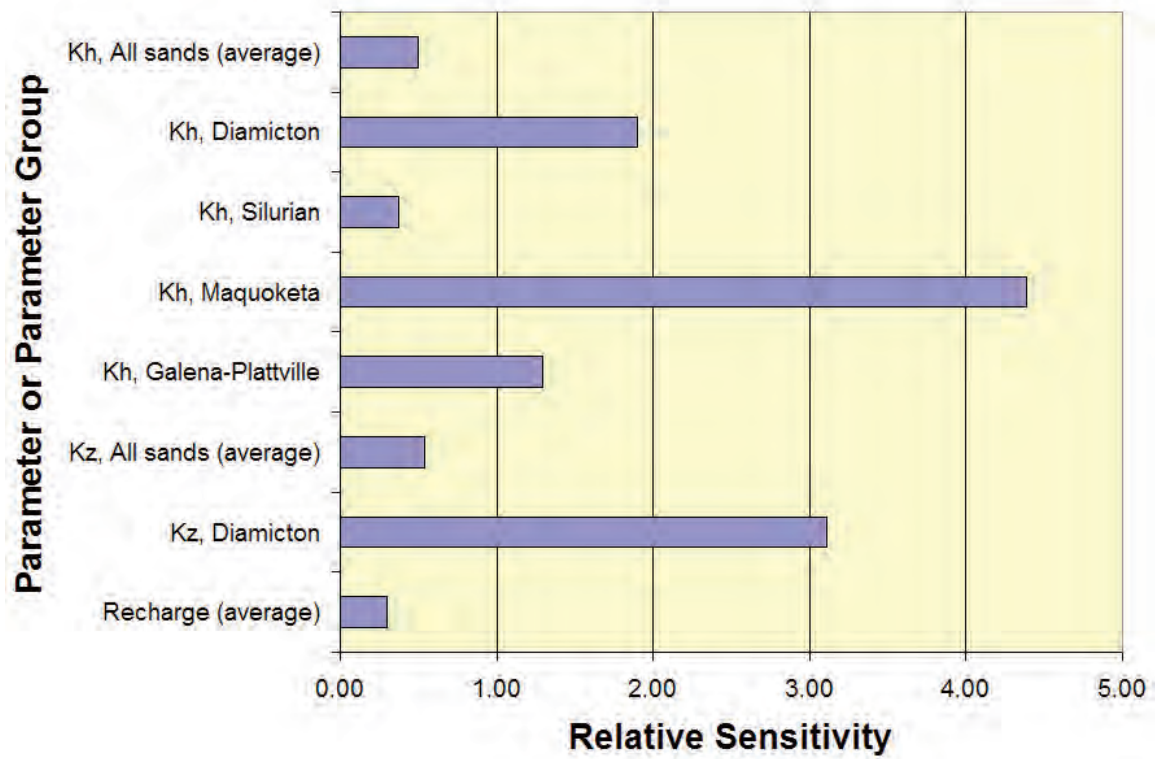


Figure 109. Parameter sensitivities for calibration, local-scale model.

3. Analysis

3.1. Introduction

This section discusses results of model simulations of historical groundwater conditions (Section 3.2) and estimated future groundwater conditions (Section 3.3). The modeling of historical conditions, carried out using both regional-scale and local-scale models, simulates pumping between 1864 (when large-scale pumping is considered to have begun in northeastern Illinois) and the present. This simulation of history is transient in that pumping for each well represented in the model is varied annually as indicated by the database of groundwater withdrawals assembled for this project (Section 2.2.8 and Appendix B). Only pumping rates are changed from year to year in this model; all other parameters remain constant through time, including recharge. The historical simulation provides insight into the principal influences on groundwater flow in Kane County and the region, and it permits identification of locations of extreme impacts where planning and monitoring efforts might be directed.

Simulations of future conditions based on projected pumping have a number of unavoidable uncertainties that arise from our inability to understand, measure, or completely represent all the features of the true system (Gorelick, 1997). These uncertainties in groundwater models may be categorized as either *parameter uncertainty* or *conceptual uncertainty* (Neuman and Wierenga, 2003). *Parameter uncertainties* reflect our imperfect knowledge of the input parameters of the model (hydraulic conductivity, recharge, pumping rates, top and bottom elevations of aquifers, etc.) and the simulated variables (hydraulic heads and flows). Calibrating the model reduces the uncertainty of input parameters, but parameter uncertainty cannot be eliminated due to errors in the observations used for calibration. *Conceptual uncertainties* arise from our imperfect knowledge of which processes to include in the model, thus expert judgment must be used, introducing the possibility of judgment errors.

Both parameter and conceptual uncertainty are present in the study models; although neither can be eliminated, the impacts of uncertainties on the simulations of projected pumping can be assessed. The formal approach to uncertainty analysis would be to determine the probabilities of the range of model simulations and summarize their range using confidence intervals. The distribution of the simulations could then be used to assess the range of possible outcomes and rationally evaluate the risks associated with management alternatives (Pappenberger and Beven, 2006). Unfortunately, the current technology for assigning probabilities to the simulations of groundwater models requires either much simpler models with restrictive assumptions or massive repetition of calculations. An alternative is to bound the range of plausible simulations of projected pumping rates using high and low values of the most sensitive parameters and assumptions (Walker et al., 2003). Although probabilities cannot be assigned to these bounds, they do qualitatively express the reliability of model simulations for use in evaluating management alternatives (Wittman, personal communication, 2007). Calibration of the model shows that, although recharge is not necessarily the most sensitive model parameter, the model is highly sensitive to changes in recharge within its plausible range. Uncertainties in recharge also arise from conceptual uncertainties associated with potential increases or decreases in precipitation due to climate variability.

An additional conceptual uncertainty is that associated with future pumping rates; simulated heads are highly sensitive to these rates. For the purposes of this study, the qualitative range of predictive uncertainty will be expressed using variations in both recharge and pumping rates. Other hydraulic parameters in the model are held constant over time.

Five different simulations of future conditions were conducted using the regional- and local-scale models (Table 25). Four of these are transient simulations that continue the historical simulation forward to 2050, and the fifth is a steady-state simulation that illustrates the impact of pumping currently active wells continuously, for an extended, indefinite time period, until heads no longer decline and equilibrium is reached. The four transient scenarios simulate two different future pumping conditions—*high pumping* and *low pumping*—and three different future recharge conditions intended to represent possible impacts of climate change on the groundwater system—*model-calibrated (historical) recharge*, *high recharge*, and *low recharge*. Future pumping and recharge conditions were characterized on the basis of published literature. The distinction between the simulated *high-* and *low-pumping conditions* is based on whether improvements in water conservation, begun during the historical period, are continued to 2050. Under *high-pumping conditions*, the improvements are not continued, but they are continued under *low-pumping conditions*. For two of the future transient simulations, each of these pumping conditions is simulated under *model-calibrated recharge* conditions. *Model-calibrated recharge conditions* are the recharge rate distribution that was selected through the model calibration process. Since calibration is based on reproducing observations of head and streamflow during the historical period, the *model-calibrated recharge conditions* are considered to be representative of effective recharge rates during the historical period—a period ending in 2002 for the regional model and in 2003 for the local model.

For one of the transient simulations, *high-pumping conditions* and *low-recharge conditions* were simulated. This simulation represents a more resource-intensive scenario of future groundwater conditions since inflow to the system (recharge) is reduced and groundwater withdrawals are elevated. The last of the four transient simulations represents a less resource-intensive scenario and is a simulation of *low-pumping conditions* and *high-recharge conditions*. The four scenarios simulated by transient modeling were chosen to represent plausible well configurations and pumping rates as well as likely recharge rates, taking into account the potential for climate change to affect recharge. Together, the output from model simulation of these scenarios is representative of the plausible range of future groundwater conditions in the region. Note that this project does not conduct transient simulations of intermediate scenarios represented by the combinations of (1) *high pumping* and *high recharge* and (2) *low pumping* and *low recharge*. The final, fifth simulation of future groundwater conditions is a steady-state simulation of all wells active in 2002. This simulation illustrates the impacts of pumping these wells continuously, at the rates reported for 2002, for an extended period ending when steady-state conditions have been reached—that is, when equilibrium has been reached and heads no longer decline.

Table 25. Simulations Discussed in Section 3

<i>Time Period</i>	<i>Simulation Approach</i>	<i>Pumping Conditions</i>	<i>Recharge Conditions</i>
Historical	Transient	Historical	Calibrated
Future	Transient	High	Low
		High	Calibrated
		Low	Calibrated
		Low	High
	Steady-State	Historical (2002)	Calibrated

For both the historical and future simulations, the discussion and illustrations in this section emphasize the simulated potentiometric surfaces, simulated available head above the top of the Ancell Unit (which, as will be discussed, would be disadvantageous to desaturate), temporal changes in simulated head (i.e., drawdown and recovery), and temporal changes in simulated natural groundwater discharge to streams. Planning and management efforts can be directed toward mitigating impacts in areas affected to a degree that is judged unacceptable by residents, managers, and policymakers.

3.2. Simulation of Historical Groundwater Conditions

Large-scale groundwater withdrawals began in northeastern Illinois in about 1864. This section describes the impacts of these withdrawals using simulations from the regional-scale and local-scale groundwater flow models. These impacts include those on heads, on groundwater flow directions and locations of groundwater divides, and on vertical movement between shallow and deep aquifers.

3.2.1. Heads

Impacts of pumping on heads are discussed with reference to regional-scale modeling results for the year 2002 and local-scale modeling results for the year 2003. Although these results reflect pumping conditions in two different years, they represent results based on the most recent pumping data available at the time of model development. The results also reflect multiple-year trends and current aquifer conditions. Indiana and Wisconsin pumping data were available only for the period ending in 2002 when the regional-scale model was assembled, but Illinois data were available for the period ending in 2003 when the local-scale model was developed. In fact, the 2003 withdrawal data were essential for calibrating the local-scale model, because head measurements used for calibration were obtained in fall 2003.

This report frequently discusses simulated *predevelopment heads*. It is emphasized that these predevelopment heads are estimated by removing all pumping stresses from the models, but other boundary conditions are not changed. Thus, the heads characterized as *predevelopment* in this report are, more accurately, simulated *nonpumping heads* given modern drainage, surface water, and recharge conditions. These values are referred to as simulated *predevelopment heads* rather than *nonpumping heads* because the former language is thought to be more efficient and less ambiguous.

3.2.1.1. Deep Aquifers

Simulated predevelopment (pre-1864) and 2002 heads in the Ancell Unit, which includes the important St. Peter Sandstone Aquifer, are shown in Figure 110 and Figure 111. Simulated heads in other deep aquifers display a similar distribution. Heads are strongly influenced by topography and surface water in the area where the Maquoketa and Upper Bedrock Units are absent, largely west of the regional model nearfield. Pumping has had a limited effect on groundwater flow in that area owing to the wells and comparatively good hydraulic connection between shallow parts of the flow system (surface water and the shallow aquifers). In the area of Maquoketa and Upper Bedrock presence, the simulated predevelopment potentiometric surface of the Ancell Unit is smoother.

Model simulation shows that the upper Illinois and lower Fox Rivers function as regional discharge areas for the deep aquifers in the western part of northeastern Illinois owing to the absence of Maquoketa and Upper Bedrock Units. Although absence of these impermeable units is sporadic along the Illinois River, the absence is sufficient to allow groundwater discharge from the deep bedrock aquifers into the river. Despite significant pumping since 1864, the model suggests that discharge into the Illinois and Fox Rivers persists. The simulated 2002 head distribution, however, suggests that the Illinois River in the area of Maquoketa absence in Grundy County has converted from a discharge area to a recharge area as a consequence of large withdrawals from the deep aquifers to the northeast, principally the Joliet area.

Pumping of wells open to the deep aquifers has resulted in several hundred feet of drawdown in simulated Ancell Unit heads in northeastern Illinois (Figure 112 and Figure 113) and has established a steep, generally west-to-east gradient in the portion of the area bordering the area of Maquoketa and Upper Bedrock Unit absence (Figure 111), including almost all of Kane County. Decline of simulated heads in the area of absence of the Maquoketa and Upper Bedrock Units is negligible, however. Centers of simulated drawdown in northeastern Illinois shifted west and southwest from 1985 to 2002, reflecting cessation of public water system withdrawals from the deep aquifers—in exchange for Lake Michigan water—in central Lake County, northwestern Cook County, DuPage County, and southern Cook County. Centers of simulated 1985 drawdown are located in the Mount Prospect-Elk Grove Village area of northwestern Cook County, the Elmhurst area of eastern DuPage County, Joliet, and Aurora (Figure 112). By 2002, simulated drawdown was reduced throughout a large portion of northeastern Illinois, and simulated heads had recovered in the Mount Prospect-Elk Grove Village and Elmhurst drawdown centers such that the formerly-distinct cones of depression had merged into a single, smoother feature (Figure 113). Simulated drawdown increased from 1985 to 2002 in the vicinity of Joliet and Aurora, however, where pumping from the deep bedrock continued. It is noteworthy that modeling shows that a large cone of depression, centered in the Elmhurst area, remains despite the cessation of most deep bedrock pumping there by 1993. The model suggests that this subdued recovery reflects the relatively small rates of leakage that are possible across overlying and underlying confining units and the general low rates of lateral inflow.

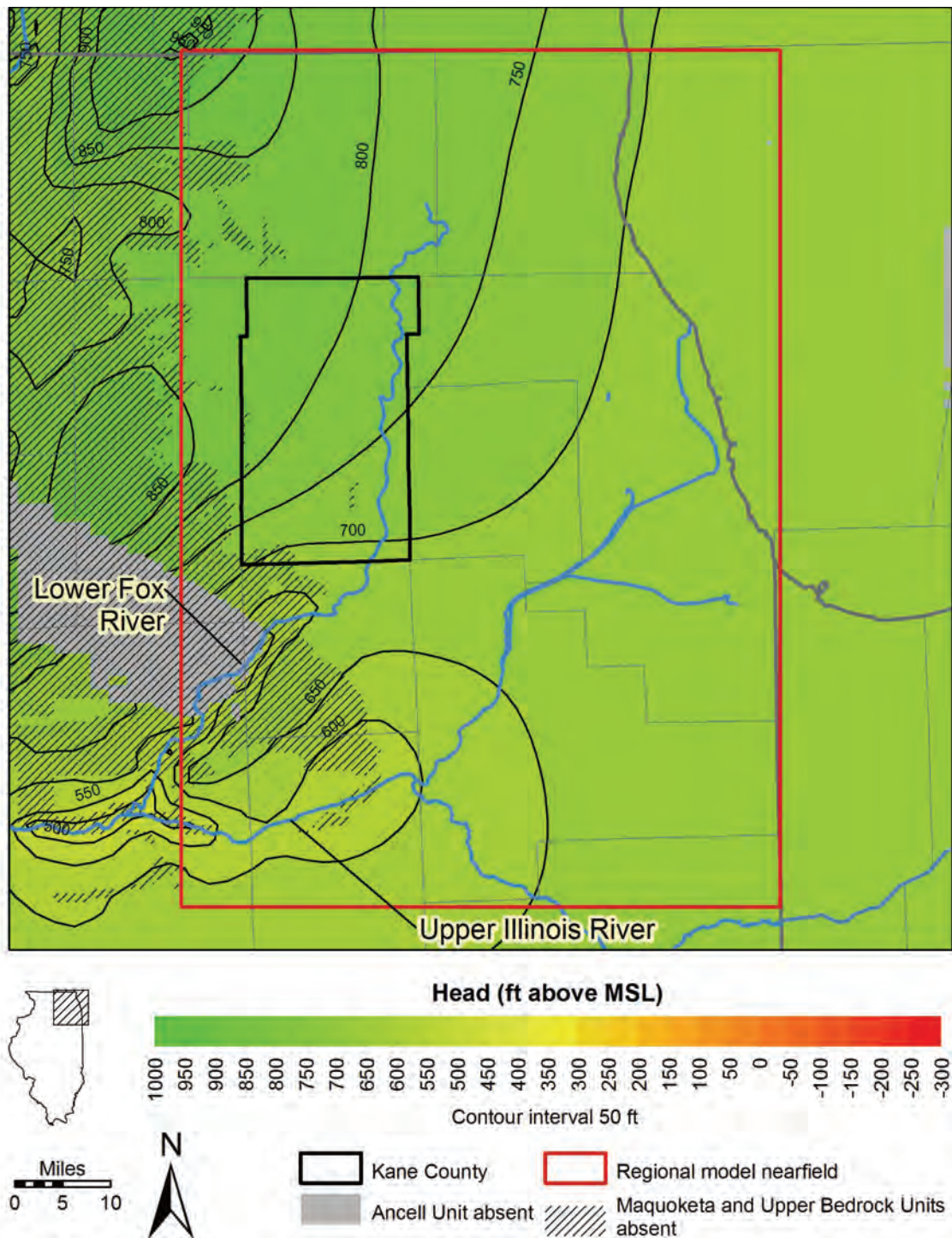


Figure 110. Simulated predevelopment head in the Ancell Unit.

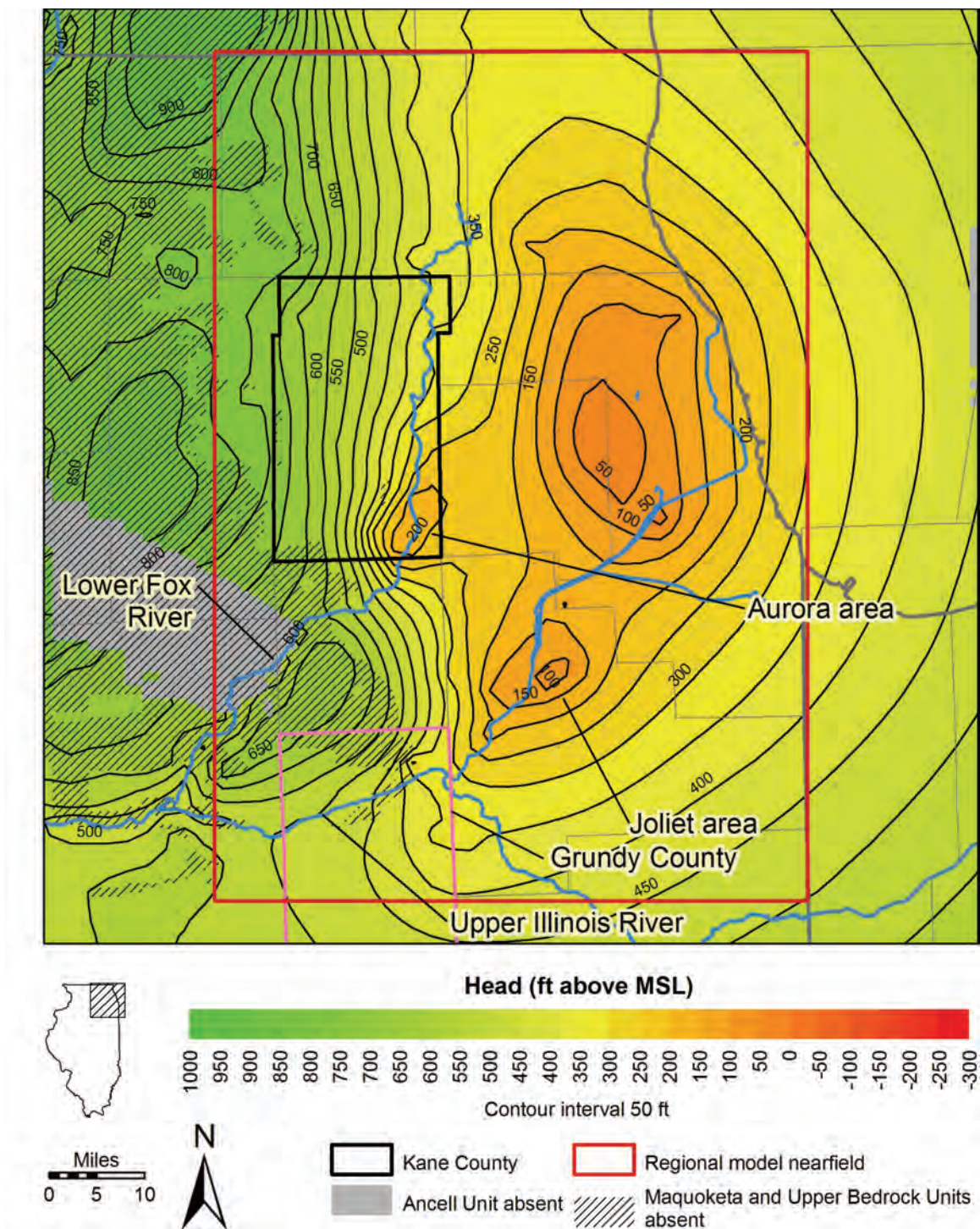


Figure 111. Simulated 2002 head in the Ancell Unit.

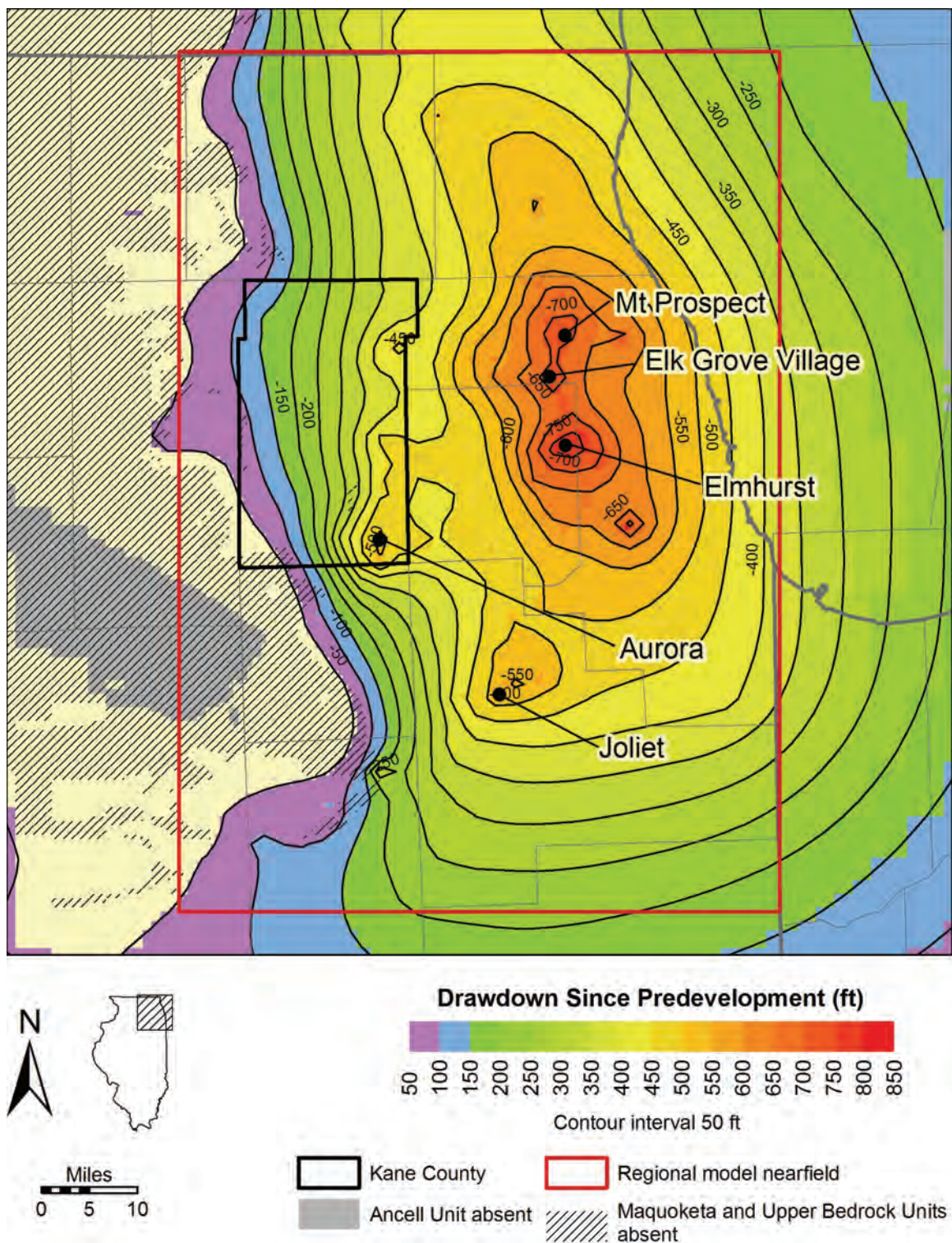


Figure 112. Simulated drawdown in 1985 in the Ancell Unit.

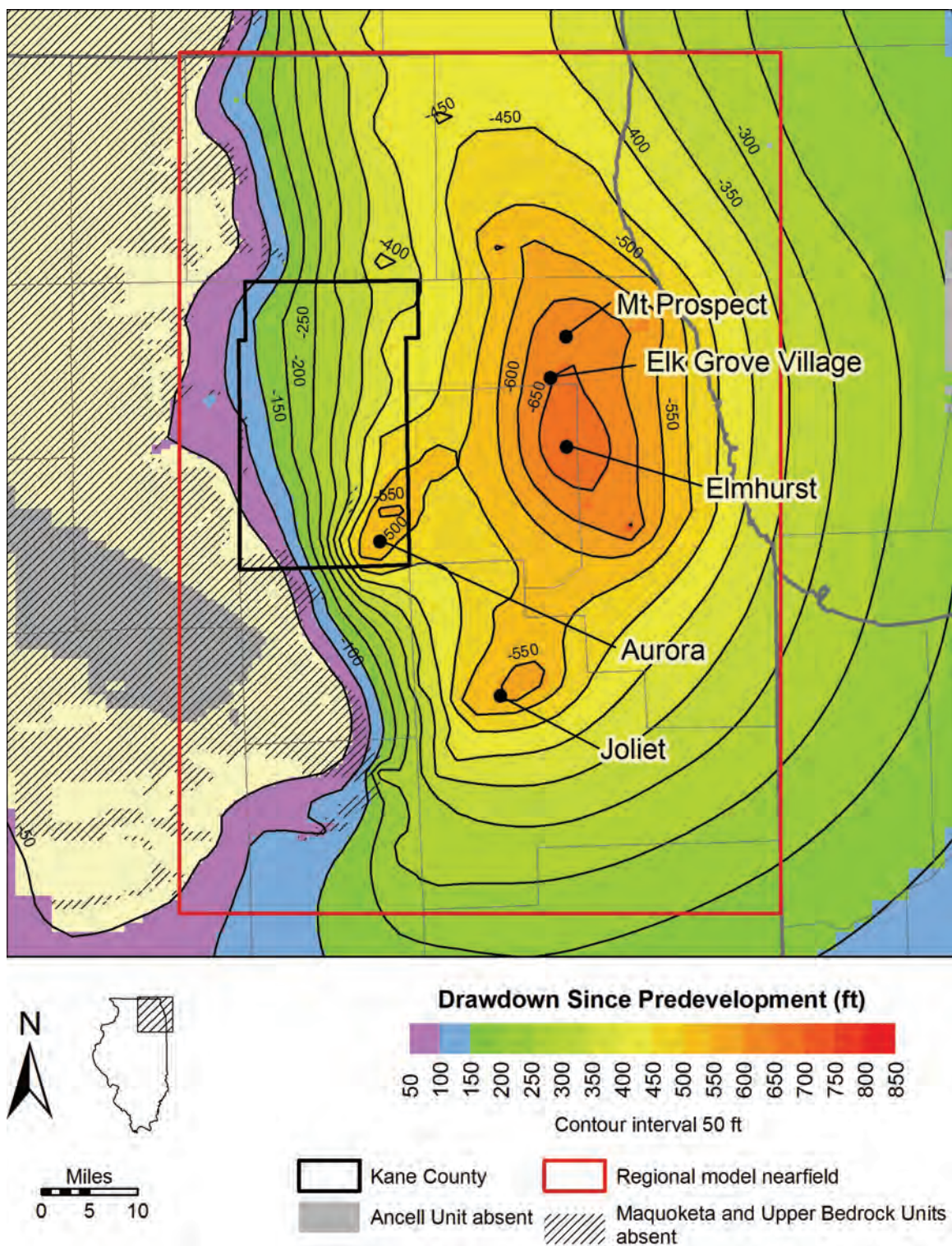


Figure 113. Simulated drawdown in 2002 in the Ancell Unit.

Simulated heads from 1864 through 2002 in the Ancell Unit and Ironton-Galesville Unit—the two principal deep bedrock aquifers—at selected locations in Kane County (Figure 114) are shown in Figure 115 and Figure 116. Trends in simulated heads reflect both regional and local pumping trends as well as proximity to the area of absence of the Maquoketa and Upper Bedrock Unit, where deep bedrock heads are heavily influenced by shallow aquifer heads and surface water, as discussed in the preceding paragraphs. It is also noteworthy that the trends in simulated heads reflect the approach to simulating withdrawals, with pre-1964 withdrawals aggregated into seven pumping centers, and 1964-2002 withdrawals modeled at reported well locations. In general, less simulated drawdown occurs, as might be expected, in areas distant from deep bedrock in areas closer to the area of absence of the Maquoketa and Upper Bedrock Units. Thus, simulated drawdown has been greater at Aurora, Batavia, St. Charles, and Elgin (comparatively near large deep bedrock pumping centers outside of Kane County as well as locations of deep bedrock pumping in their own right) than at Maple Park, Hampshire, and Elburn. Aurora, Batavia, and Elgin, moreover, are locations of aggregated centers of pre-1964 pumping. Simulated drawdown at Maple Park has been comparatively insignificant because it is close to areas of Maquoketa and Upper Bedrock Unit absence and because deep bedrock pumping there has been minor. Overall, simulated drawdown in the Ancell Unit has been less than in the Ironton-Galesville Unit. Local pumping trends are apparent in the simulated head trends illustrated in Figure 115 and Figure 116. For example, while recovery of simulated heads is apparent at several of the locations, it has been somewhat greater at Elgin and Aurora, where deep bedrock withdrawals were reduced when the two communities began using Fox River water for public supply in 1983 and 1992, respectively.

It is possible for pumping from units overlain by aquitards to reduce heads so far that one or more pumped units become partially or completely desaturated. Pore spaces are drained in the desaturated unit, resulting in establishment of a second water table at depth. Desaturation of an aquifer can reduce the production capacity of a well because it reduces the contributing saturated thickness (and hence, the transmissivity) of the aquifer.

There are also possible water-quality consequences of desaturation of the deep units. In northeastern Illinois, it is possible that desaturation of the contact between the Galena-Platteville Unit and the Ancell Unit could reduce water quality in wells open to the interval. Exposure to oxygen of a sulfide-cement horizon (SCH) near the contact of the Galena-Platteville Unit and the Ancell Unit appears related to concentrations of arsenic as high as 12,000 micrograms per liter ($\mu\text{g/L}$) in groundwater withdrawn from wells finished in the Ancell Unit in eastern Wisconsin (Schreiber et al., 2000). The SCH there is typically about 10 feet or less in thickness and is marked by arsenic-bearing secondary pyrite and marcasite. Schreiber et al. (2000) concluded that, in the most severe cases of arsenic contamination, the arsenic is released to water in these wells in the immediate vicinity of the borehole through the introduction of air to the SCH where the static water level is at or near the SCH. Lasemi (personal communication, 2005) found abundant pyrite in the lower 1-2 ft of the Platteville Group in five cores from southwest Kane County and southeast DeKalb County, but noted that the relationship between this pyritic interval and the SCH in Wisconsin is not clear. It is also unclear whether the pyritic interval in Illinois contains arsenic, as it does in Wisconsin. Lastly, since most deep wells in northeastern Illinois (except domestic deep wells) are open to both the

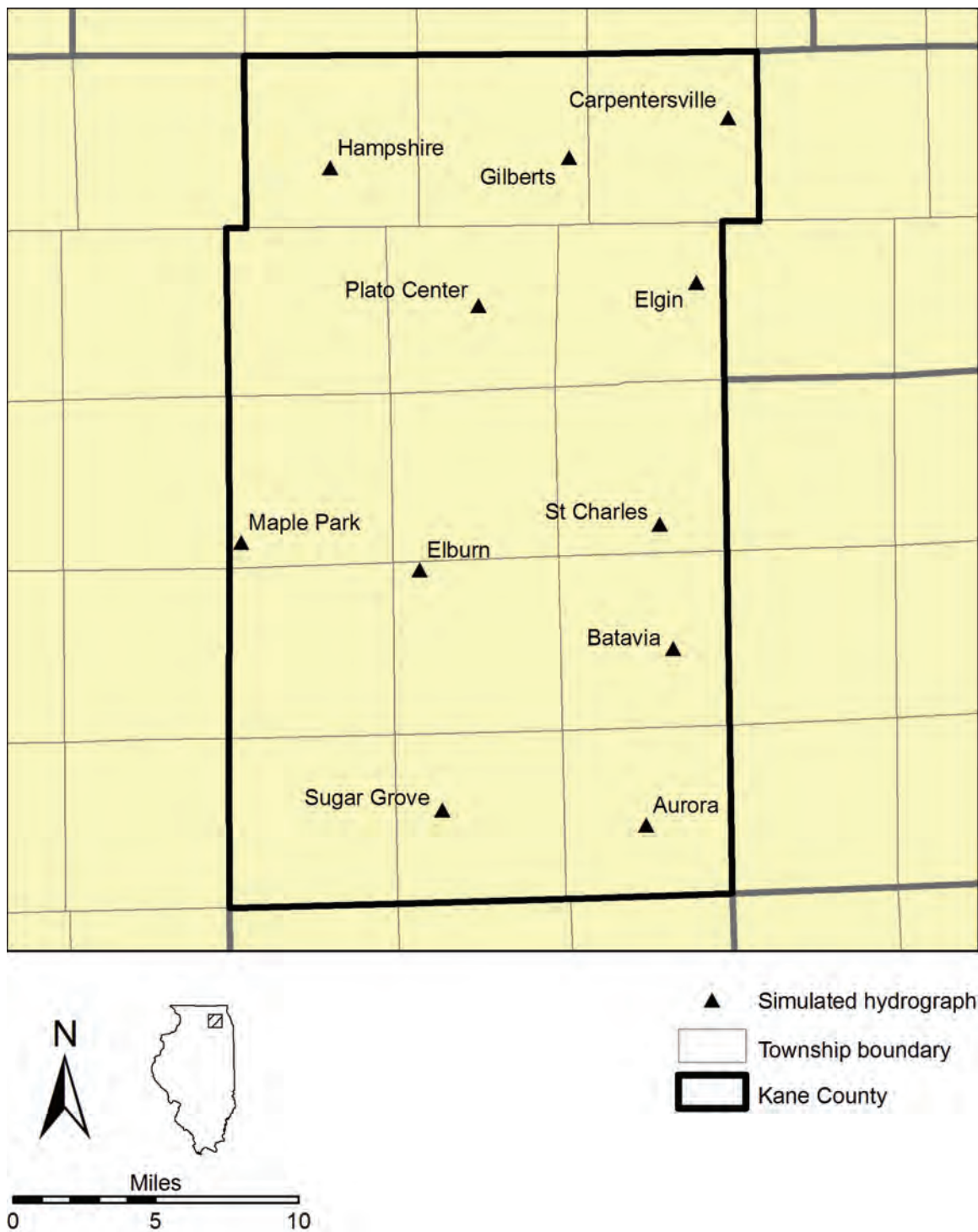


Figure 114. Locations of simulated hydrographs shown in Figure 115 and Figure 116.

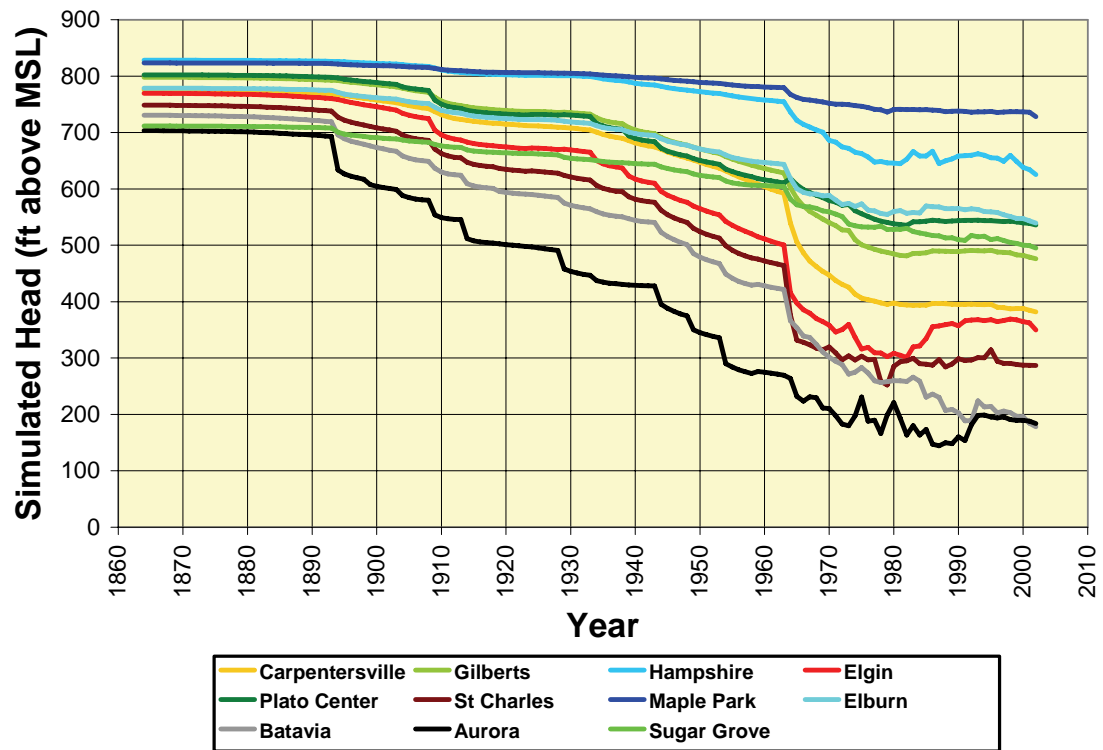


Figure 115. Simulated heads from 1864 through 2002 in the Ancell Unit at selected locations in Kane County.

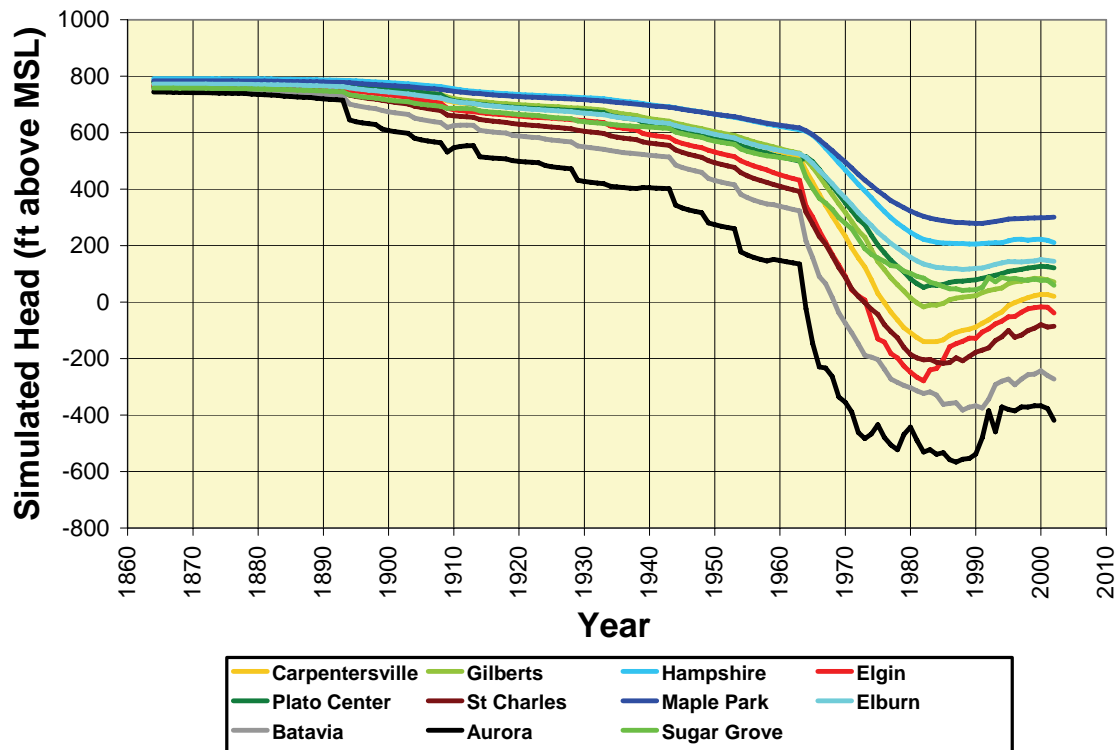


Figure 116. Simulated heads from 1864 through 2002 in the Ironton-Galesville Unit at selected locations in Kane County.

Ancell Unit and the Ironton-Galesville Unit, desaturation of the Ansell Unit would increase the proportion of Ironton-Galesville groundwater withdrawn from these wells. This increased proportion of Ironton-Galesville groundwater may reduce water quality, because the Ironton-Galesville groundwater is believed to be poorer in quality than the Ansell Unit groundwater, containing, most notably, high concentrations of dissolved radium and barium (Gilkeson et al., 1983). Thus, with desaturation of the Ansell Unit, the quality of water pumped from deep wells would be expected to more closely resemble the poorer-quality Ironton-Galesville groundwater.

Regional model output suggests that, as of 2002, Ansell Unit head has declined to less than 100 ft above MSL in the Aurora area, and is within 40 ft of the top of the Ansell at some locations (Figure 117). In this area, it is plausible that Ansell heads are near enough to the top of the Ansell that atmospheric oxygen could conceivably be introduced to the critical interval during pumping. Areas having less than 100 ft of available simulated head above the top of the Ansell are speculative in geometry because of the limited resolution of the regional model and because MODFLOW does not explicitly simulate flow through unsaturated materials such as the desaturated portions of the Galena-Platteville Unit overlying the Ansell. Nonetheless, the model-predicted areas where Ansell head is within 100 ft of the top of the Ansell do represent a hydrologic condition that bears monitoring and further investigation for protection both of well production capacity and water quality. The model suggests that a large area having simulated 2002 Ansell head within 100 ft of the top of the Ansell exists in the vicinity of the lower Fox and upper Illinois Rivers in Kendall and LaSalle Counties (Figure 118). Model simulations suggest, however, that this head condition existed in the lower Fox-upper Illinois River area prior to development owing to the nearness in that area of the top of the Ansell to land surface. Whether this is an area where water quality problems could develop is not known. In part of this area, the top of the Ansell has been removed by erosion, and the problematic interval is absent. In other parts of the area, the model suggests that the top of the Ansell has always been unsaturated, possibly reducing or eliminating the risk to water quality.

3.2.1.2. Shallow Aquifers

Simulated predevelopment heads are very similar to simulated 2003 heads in the shallow aquifers (i.e., the Shallow Bedrock Aquifer, Lower and Upper Glasford Sand Units, Ashmore Unit, Batestown Sand Unit, Yorkville Sand Unit, and Beverly Unit; compare Figure 119 through Figure 125 to Figure 126 through Figure 132). Local-scale modeling results suggest that a major control on drawdown surrounding shallow wells in the Kane County area is the hydraulic connectivity of the well to surface-water bodies. Where hydraulic connections are distant, drawdown surrounding a well is greater, because the cone of depression must grow to a larger size before sufficient water is captured to balance withdrawals. The scale of the drawdown in the local model is considerably less than that of the regional model; however, the scale of available drawdown (head above the top of the aquifer) is also considerably less. Thus, a smaller drawdown in a shallow system can have a potentially larger impact on water availability than a much larger drawdown in the deep bedrock aquifer. In general, the higher permeability of the shallow aquifers allows for much greater pumping rates than what the same amount of drawdown would support in the deeper aquifers.

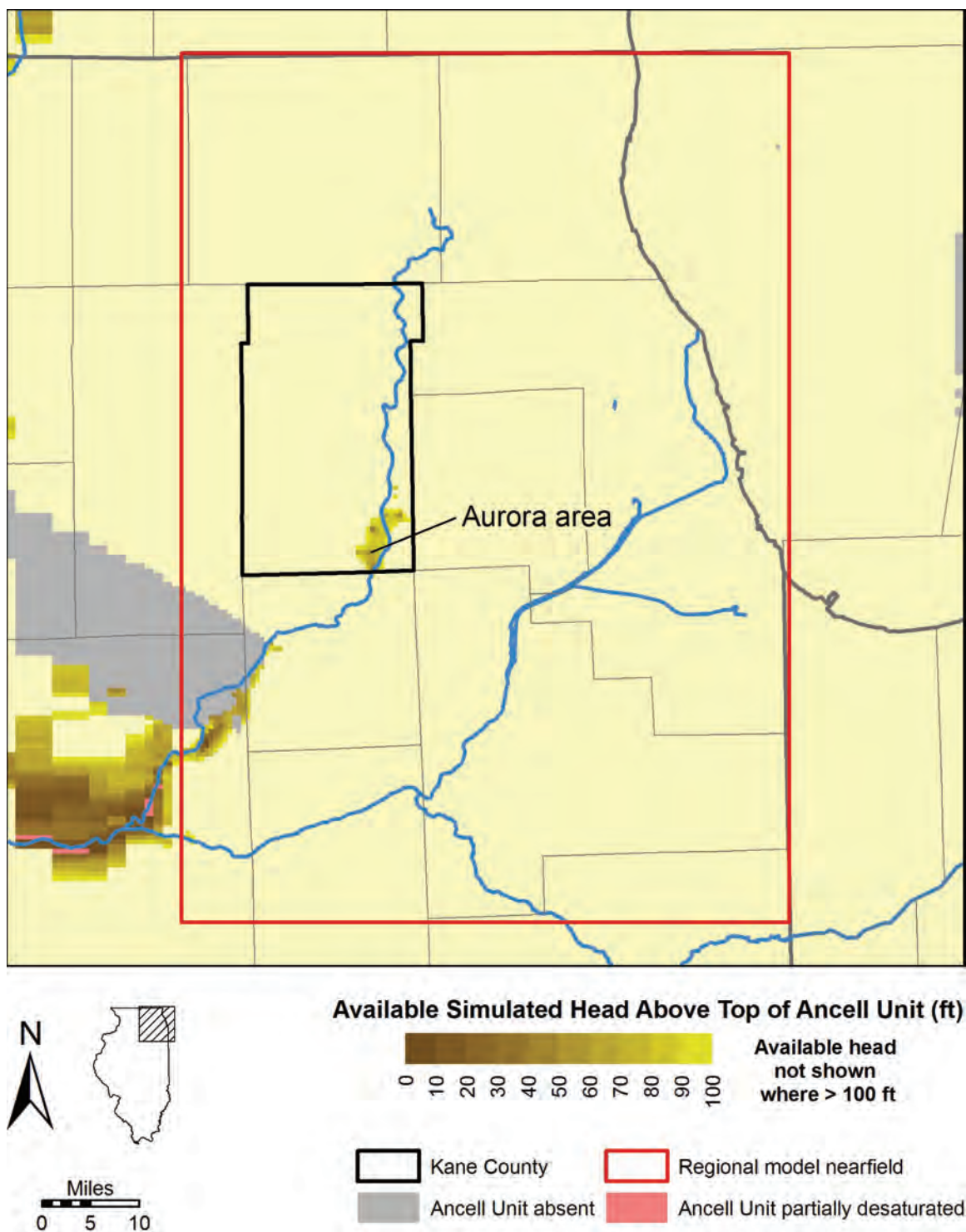


Figure 117. Available simulated head above the top of the Ancell Unit in 2002 based on regional modeling.

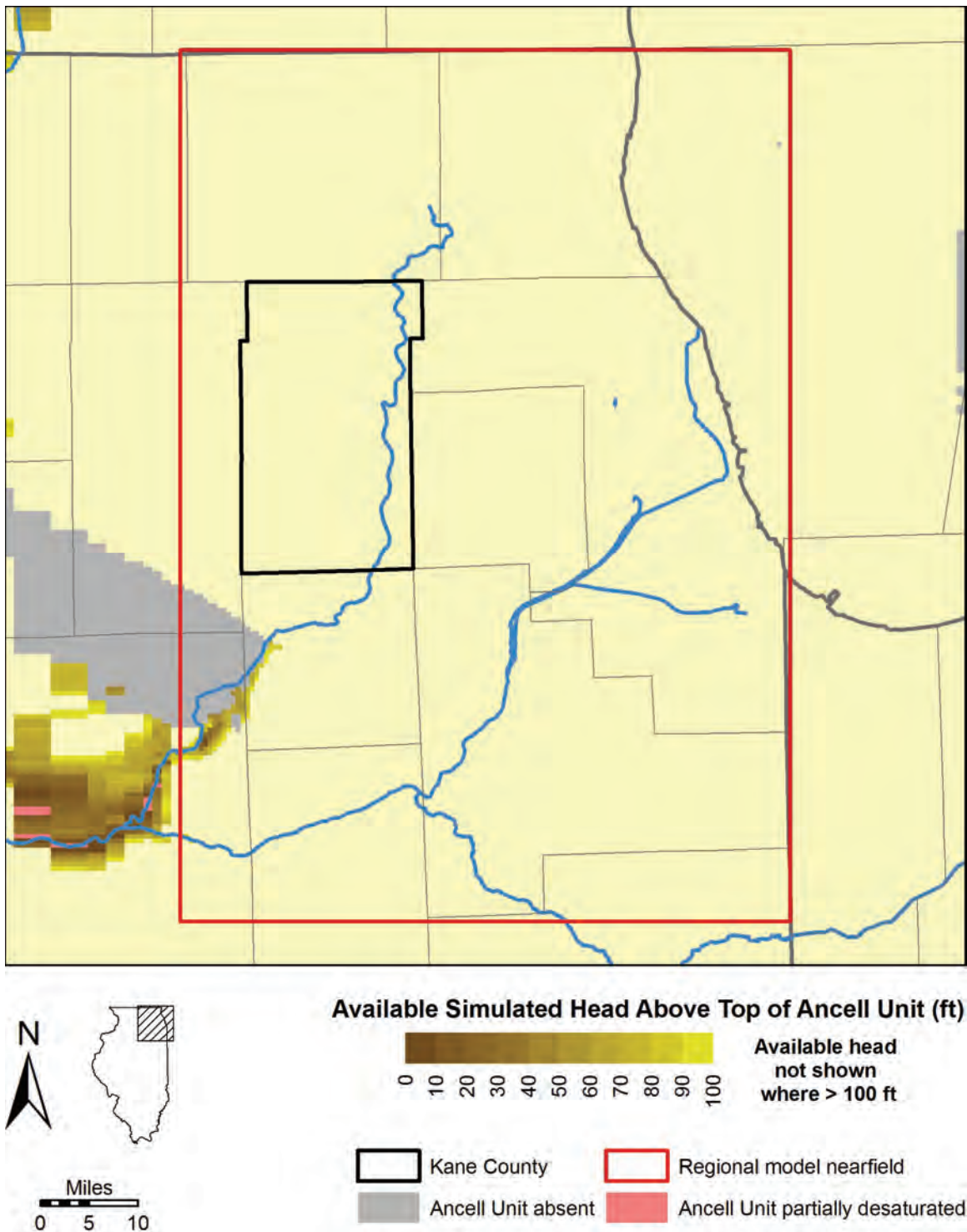


Figure 118. Available simulated head above the top of the Ancell Unit under predevelopment conditions based on regional modeling.

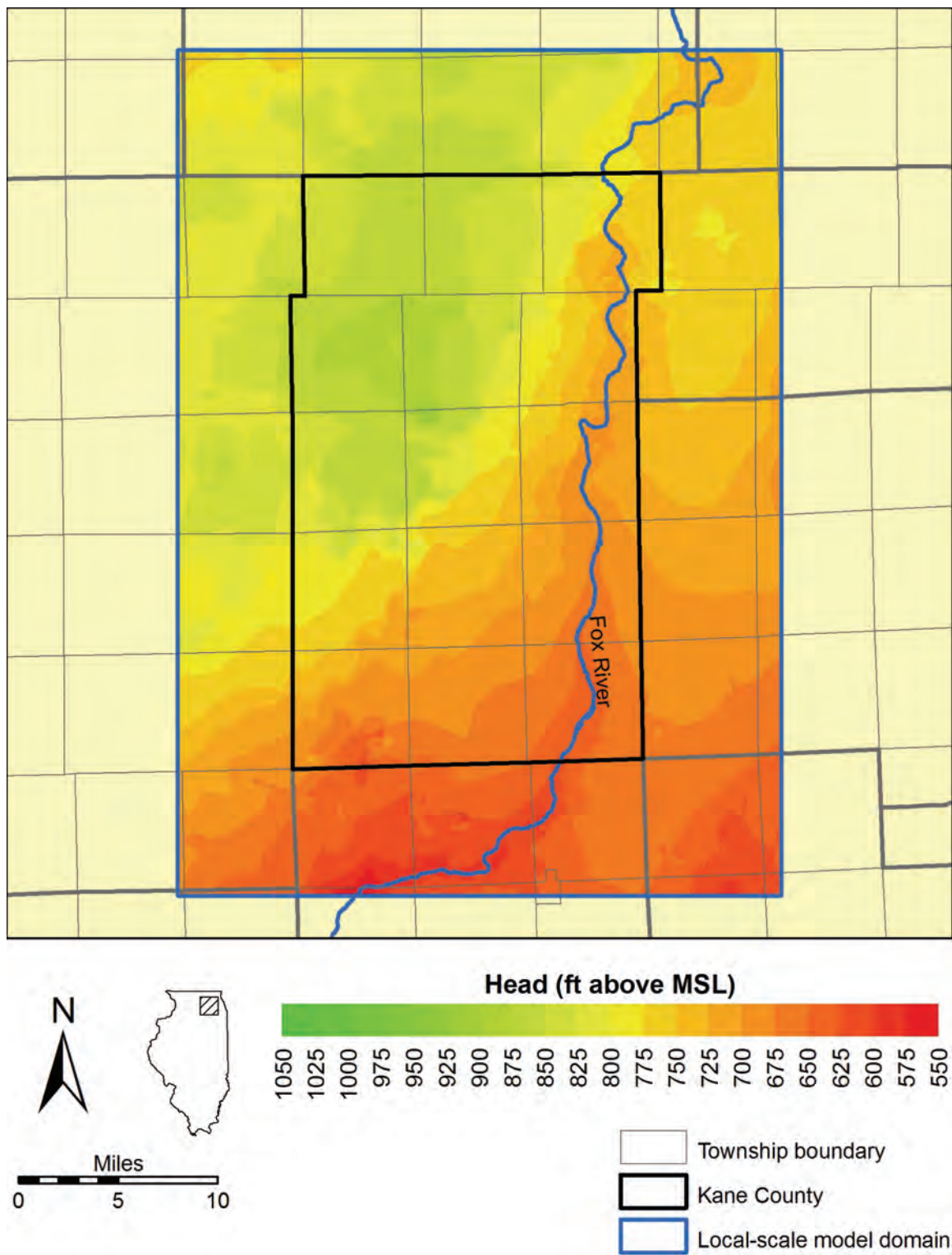


Figure 119. Simulated predevelopment head in the Shallow Bedrock Aquifer in the Kane County area.

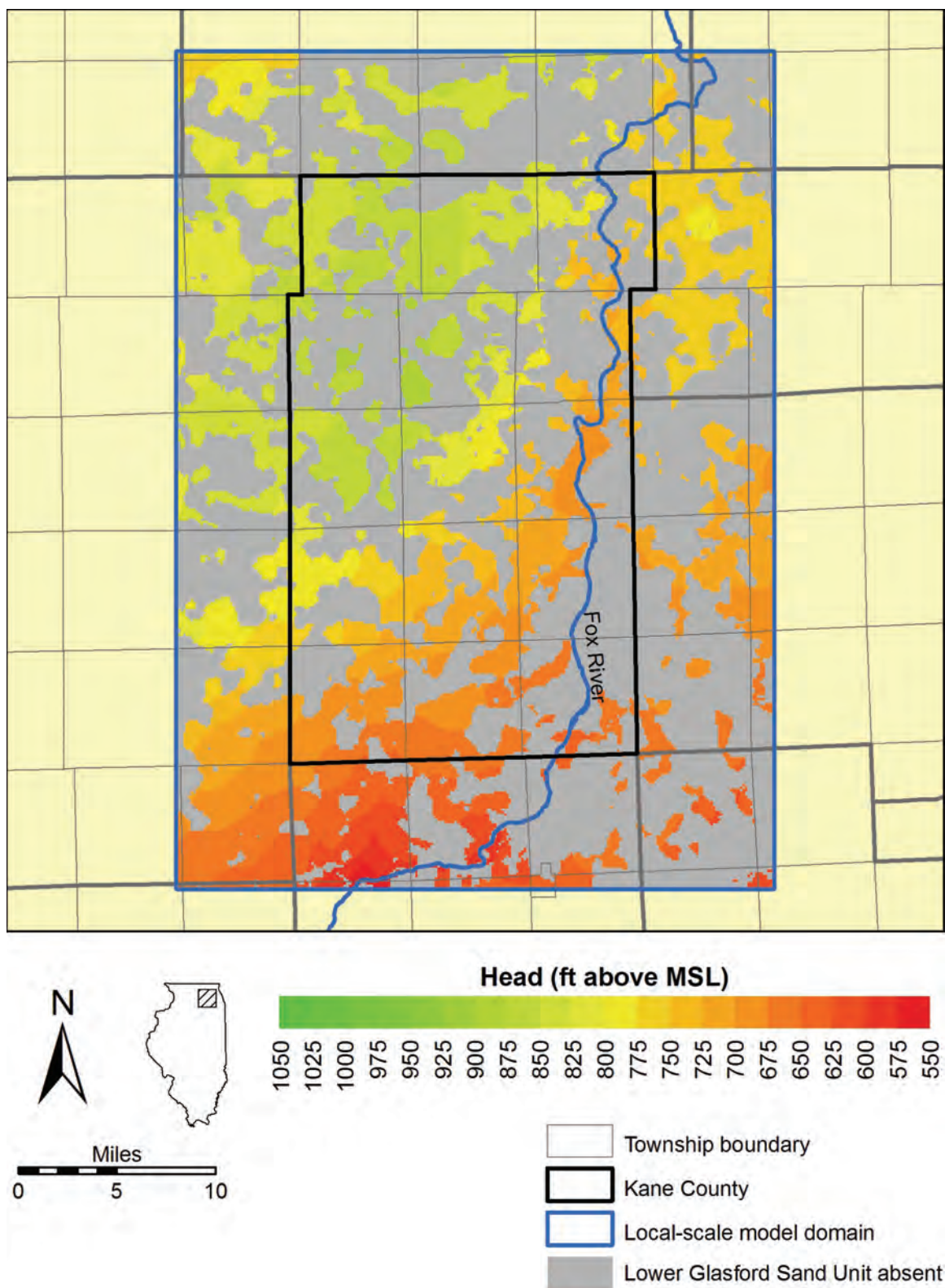


Figure 120. Simulated predevelopment head in the Lower Glasford Sand Unit in the Kane County area.

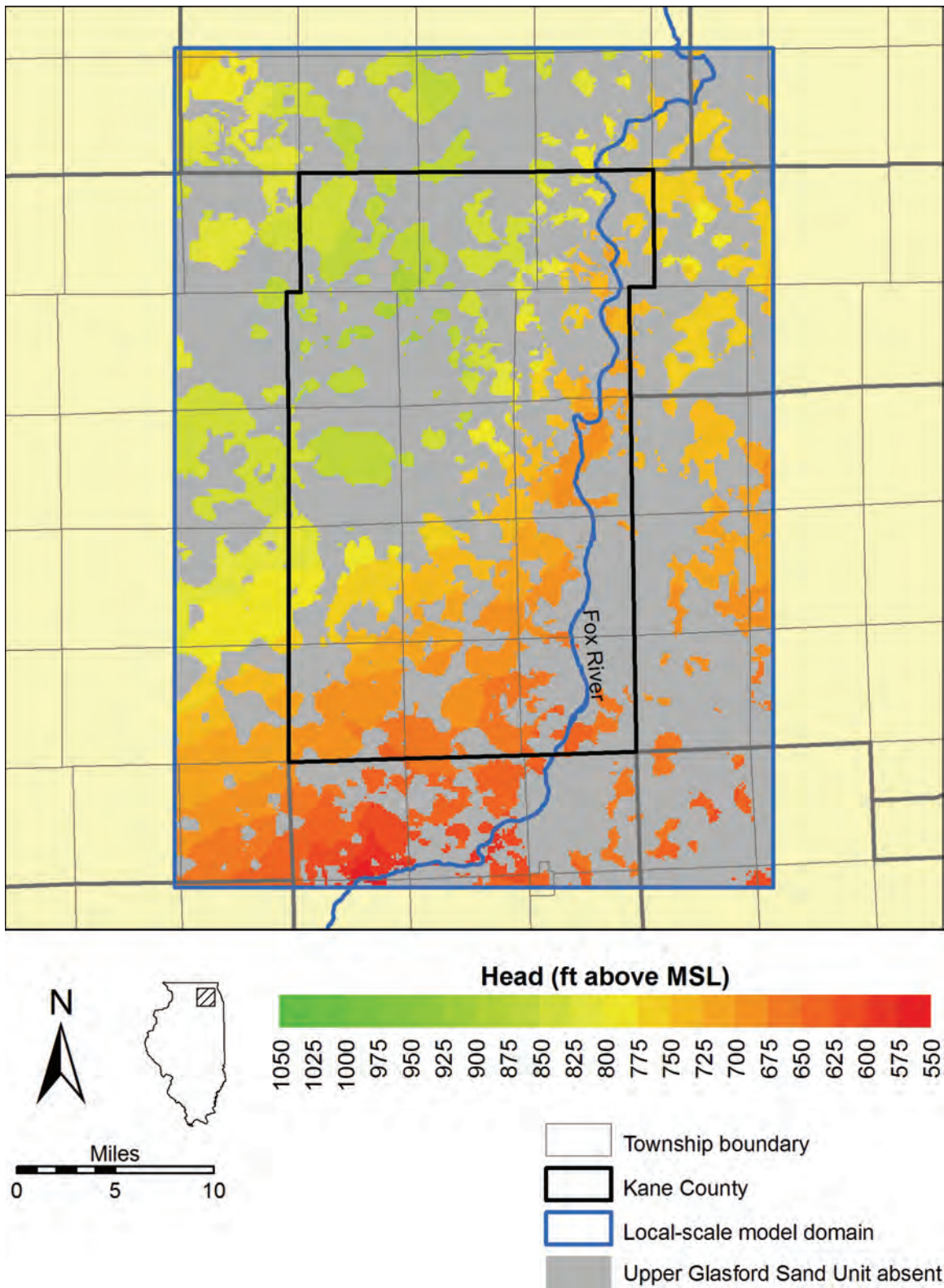


Figure 121. Simulated predevelopment head in the Upper Glasford Sand Unit in the Kane County area.

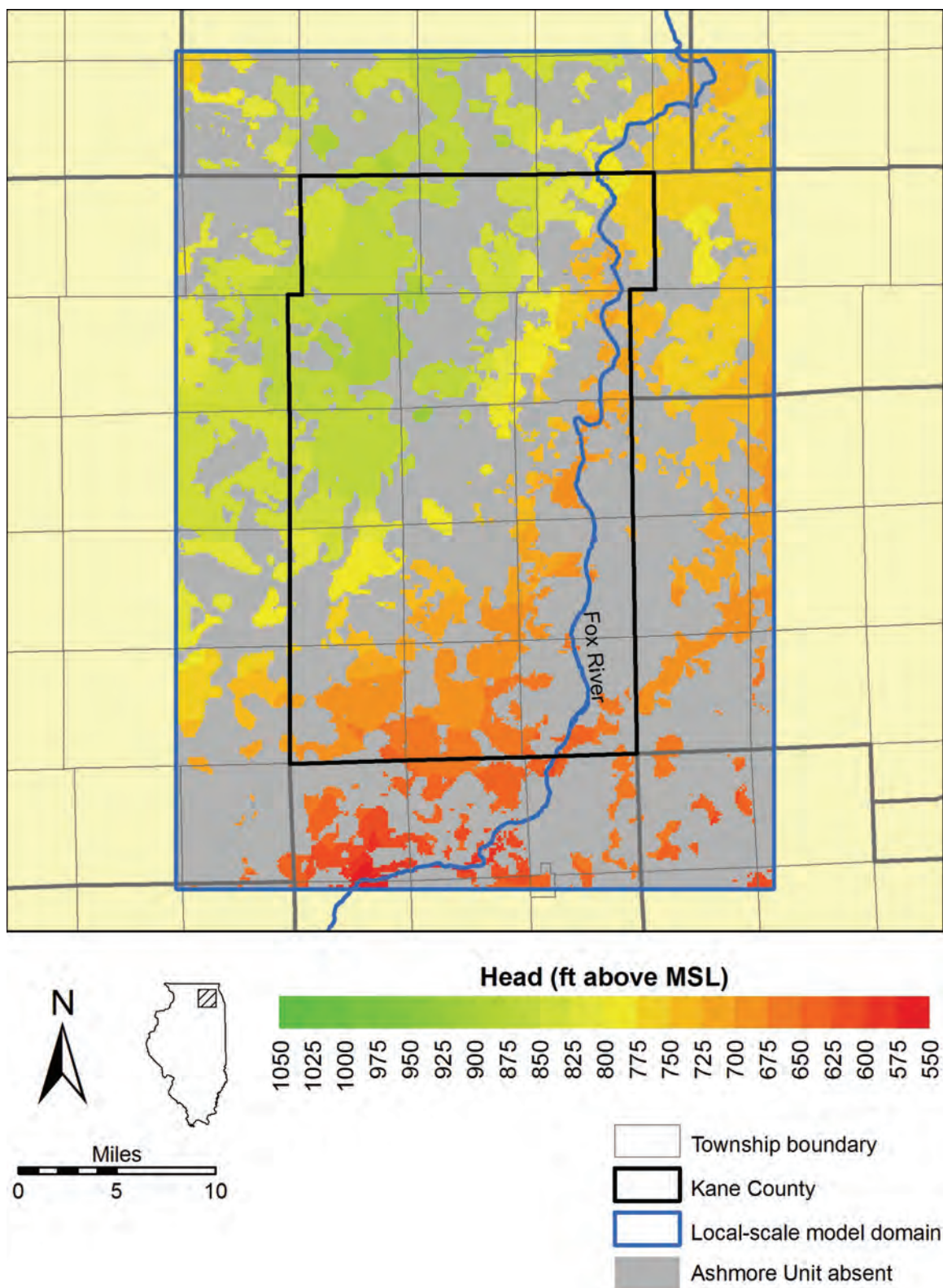


Figure 122. Simulated predevelopment head in the Ashmore Unit in the Kane County area.

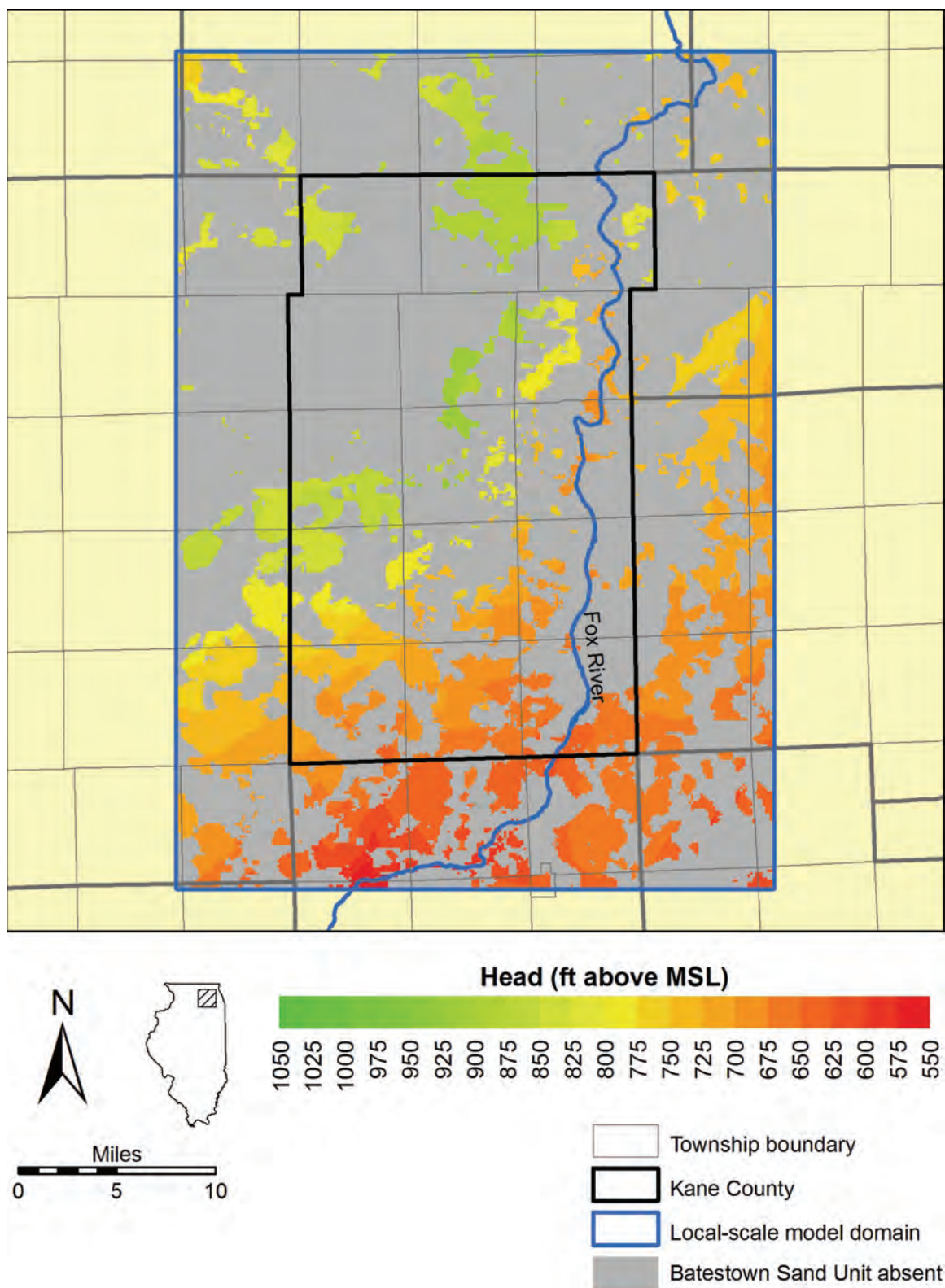


Figure 123. Simulated predevelopment head in the Batestown Sand Unit in the Kane County area.

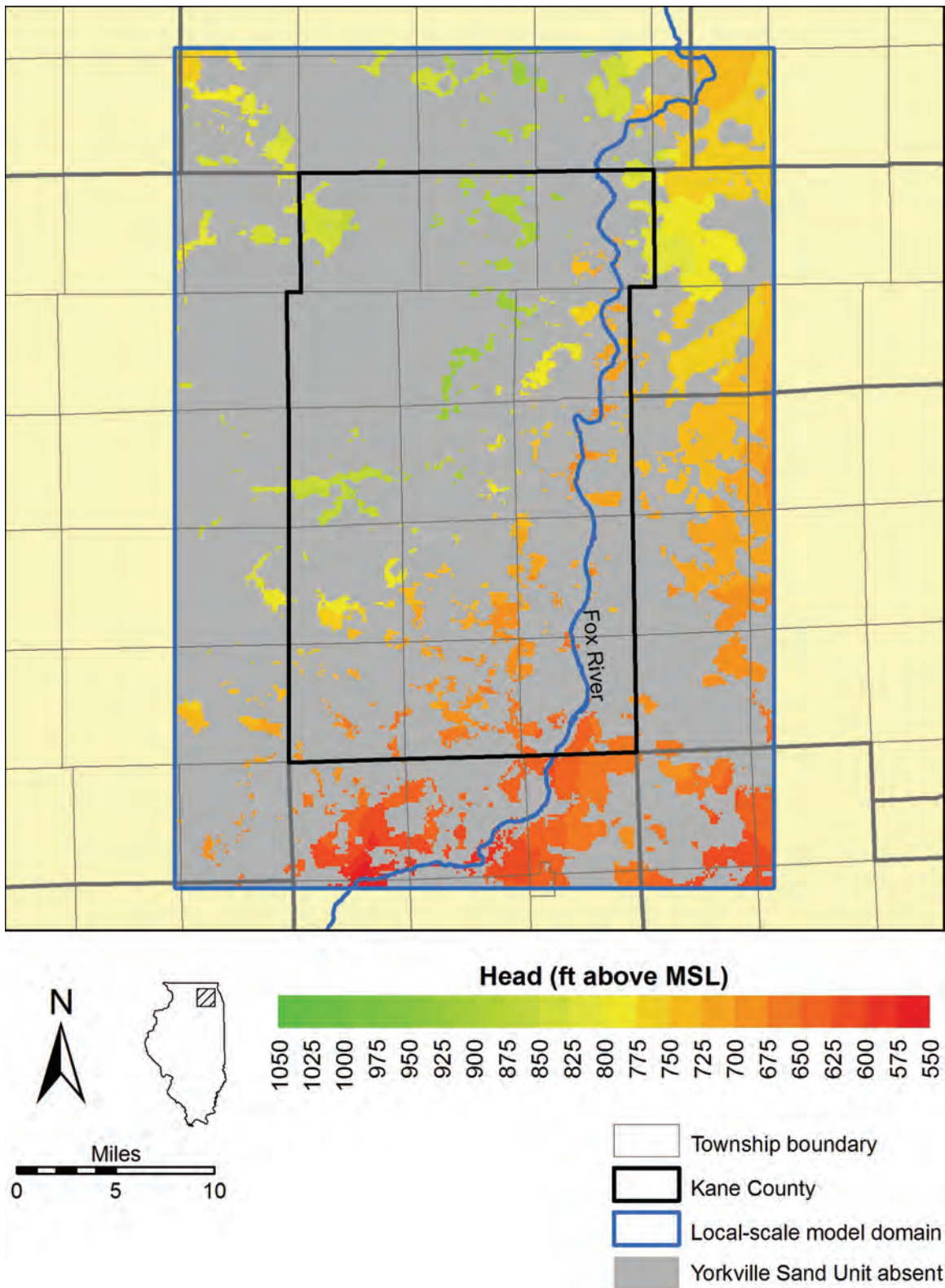


Figure 124. Simulated predevelopment head in the Yorkville Sand Unit in the Kane County area.

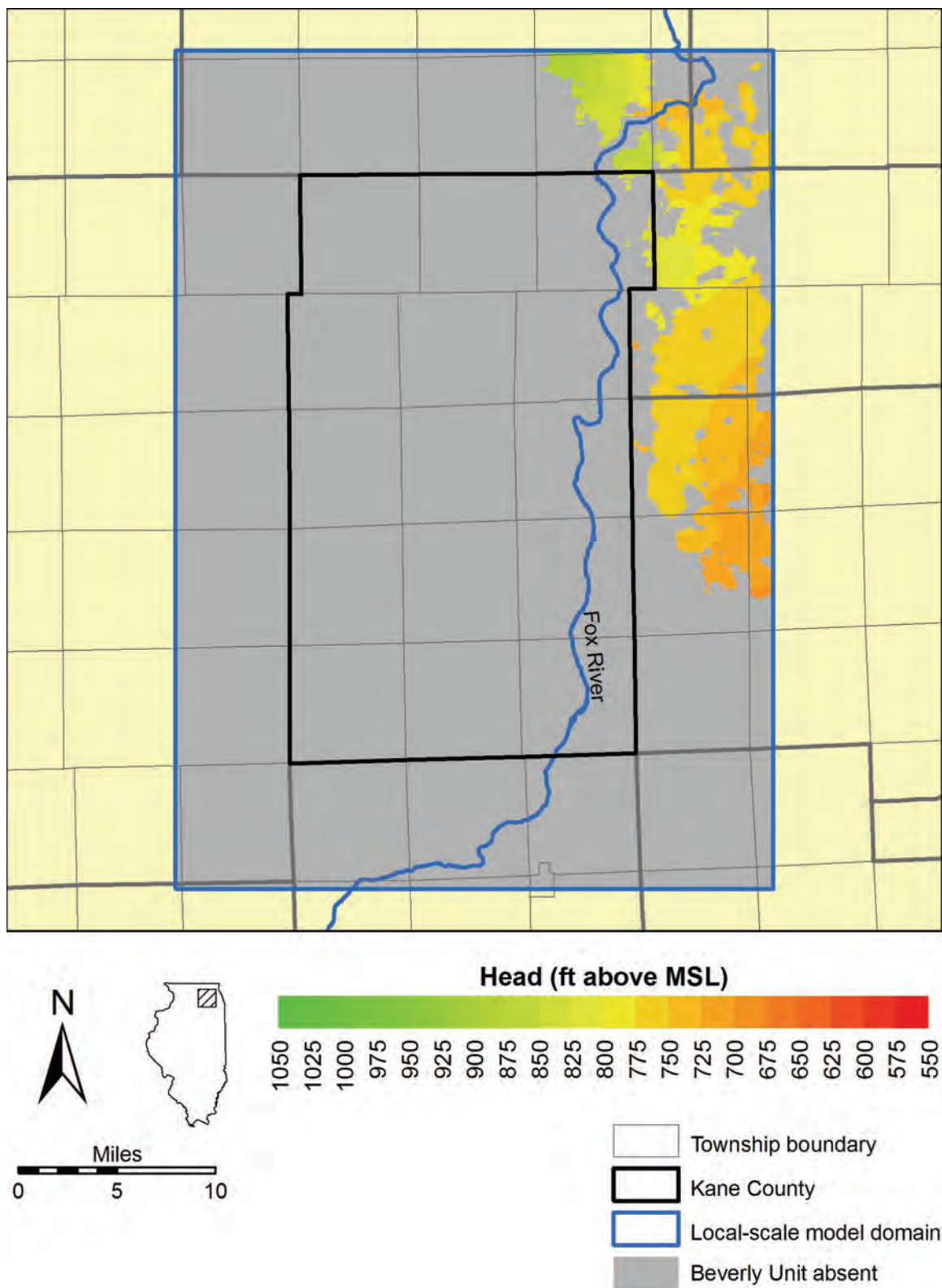


Figure 125. Simulated predevelopment head in the Beverly Unit in the Kane County area.

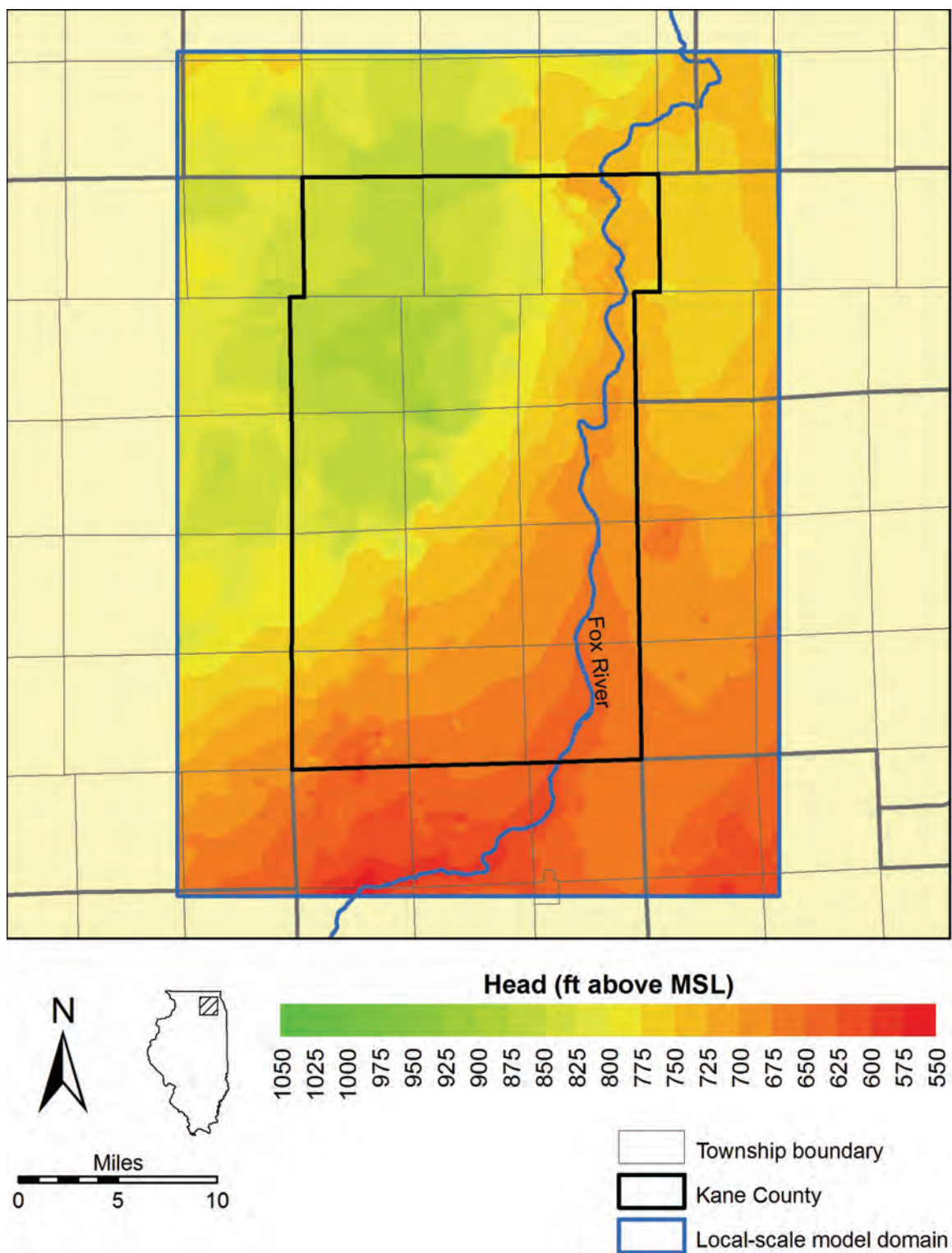


Figure 126. Simulated 2003 head in the Shallow Bedrock Aquifer in the Kane County area.

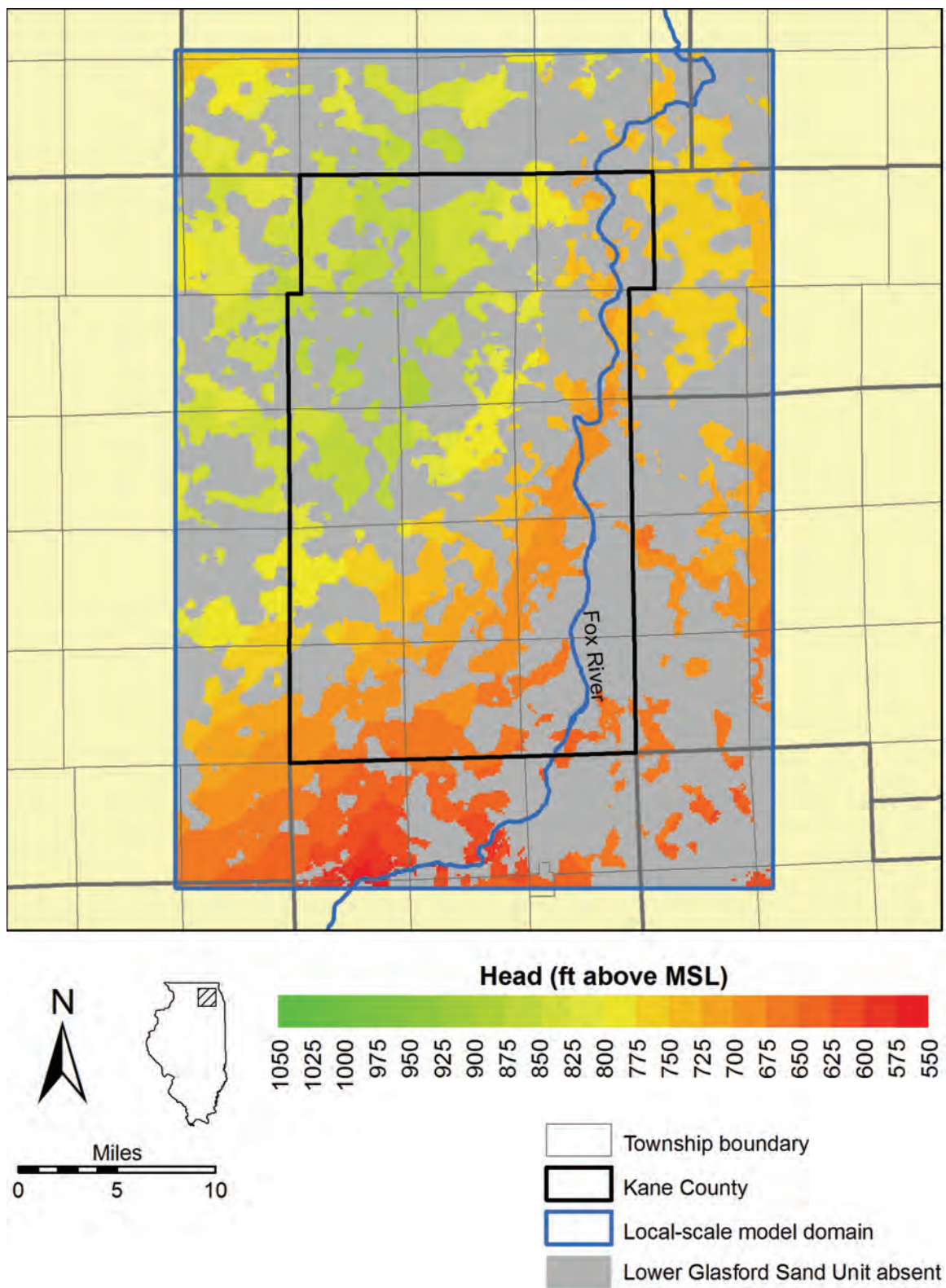


Figure 127. Simulated 2003 head in the Lower Glasford Sand Unit in the Kane County area.

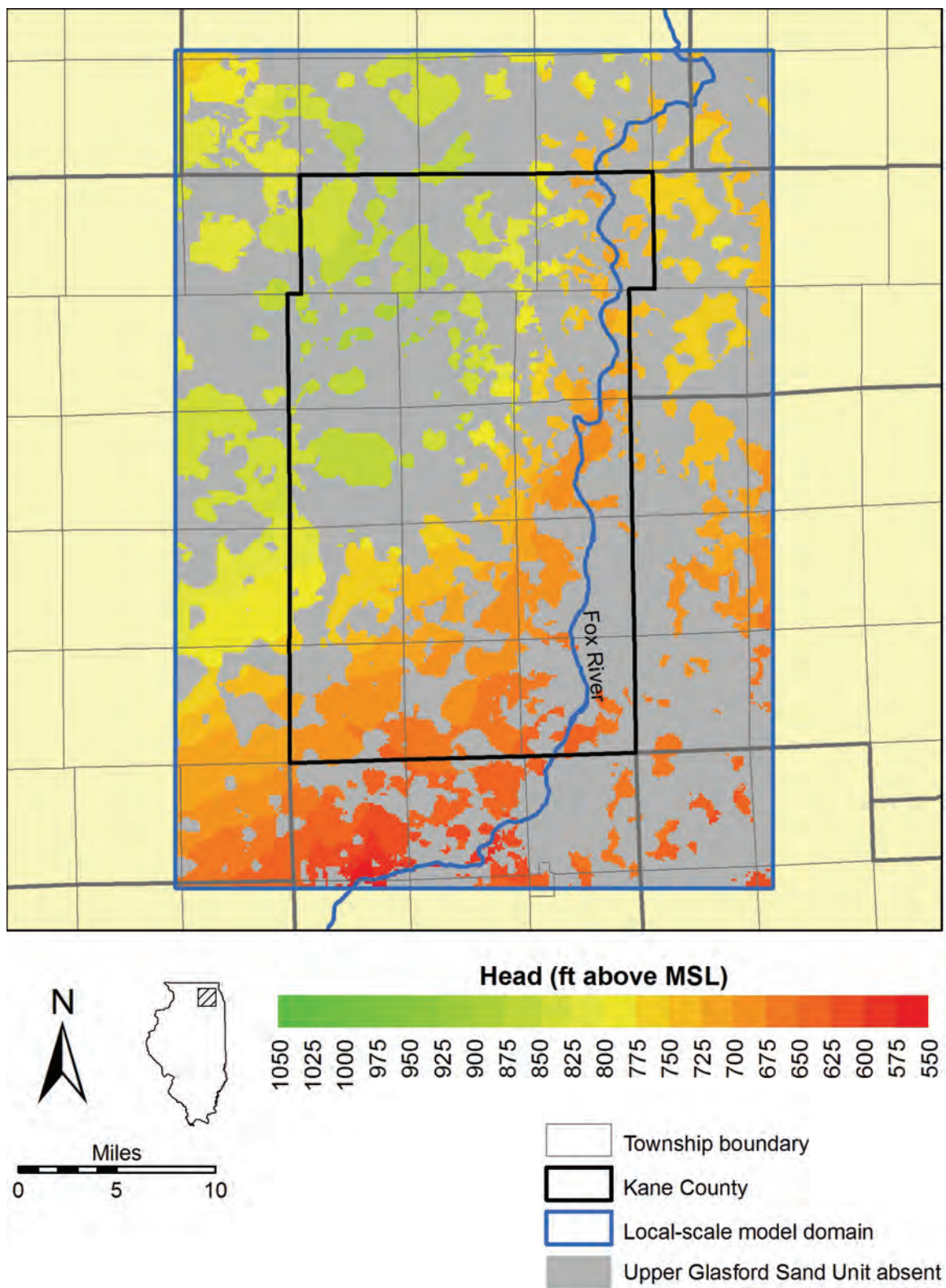


Figure 128. Simulated 2003 head in the Upper Glasford Sand Unit in the Kane County area.

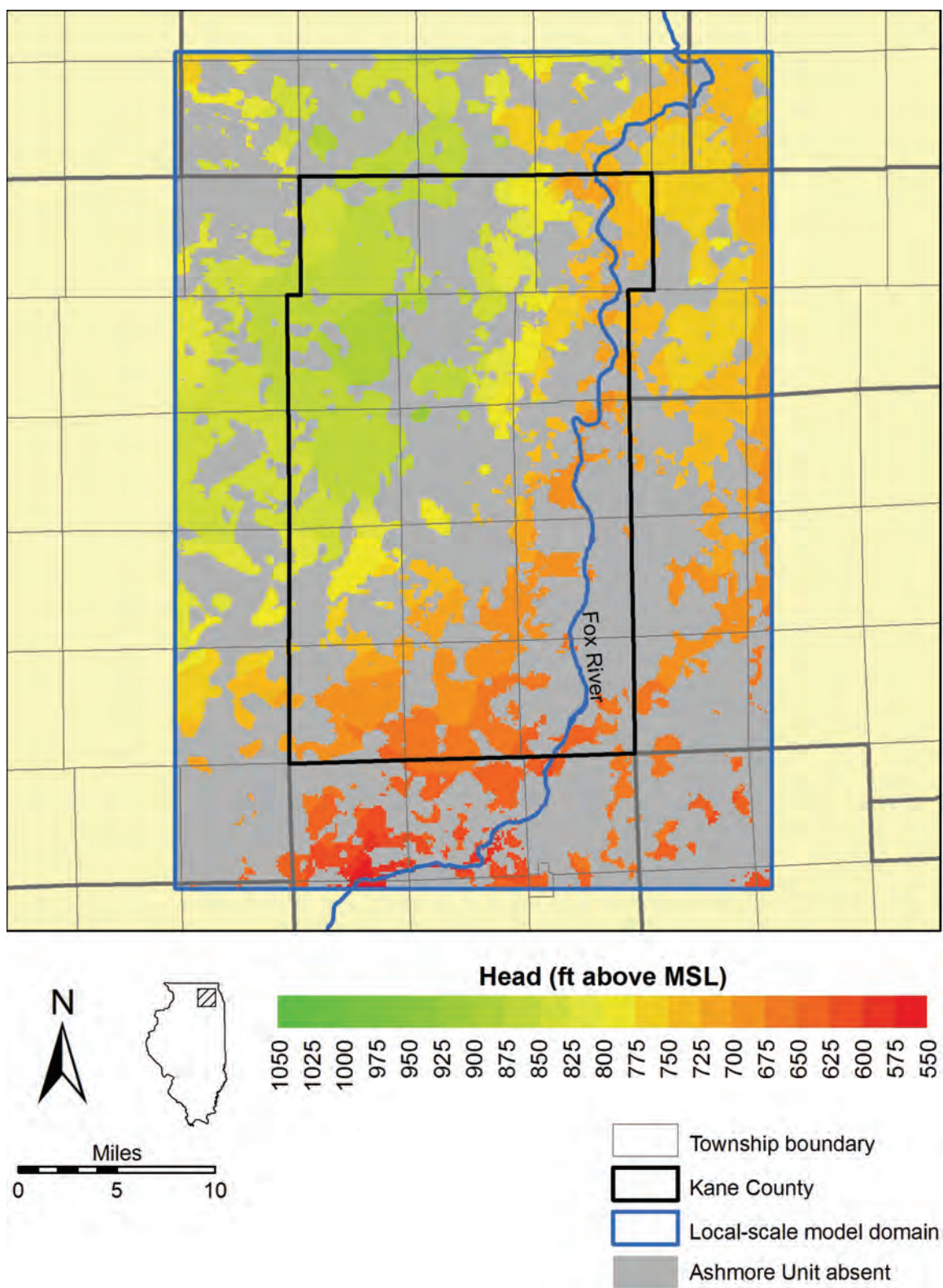


Figure 129. Simulated 2003 head in the Ashmore Unit in the Kane County area.

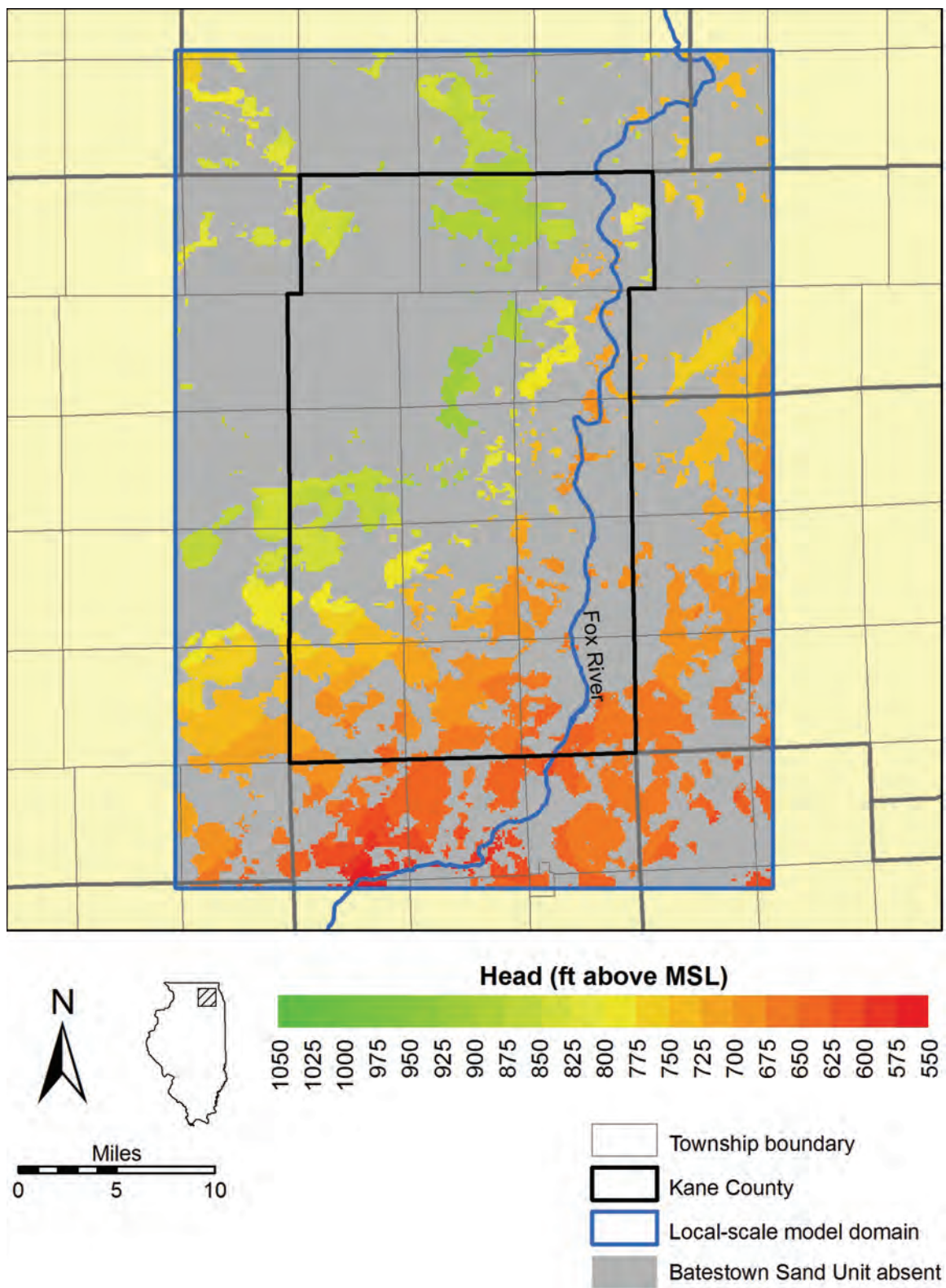


Figure 130. Simulated 2003 head in the Batestown Sand Unit in the Kane County area.

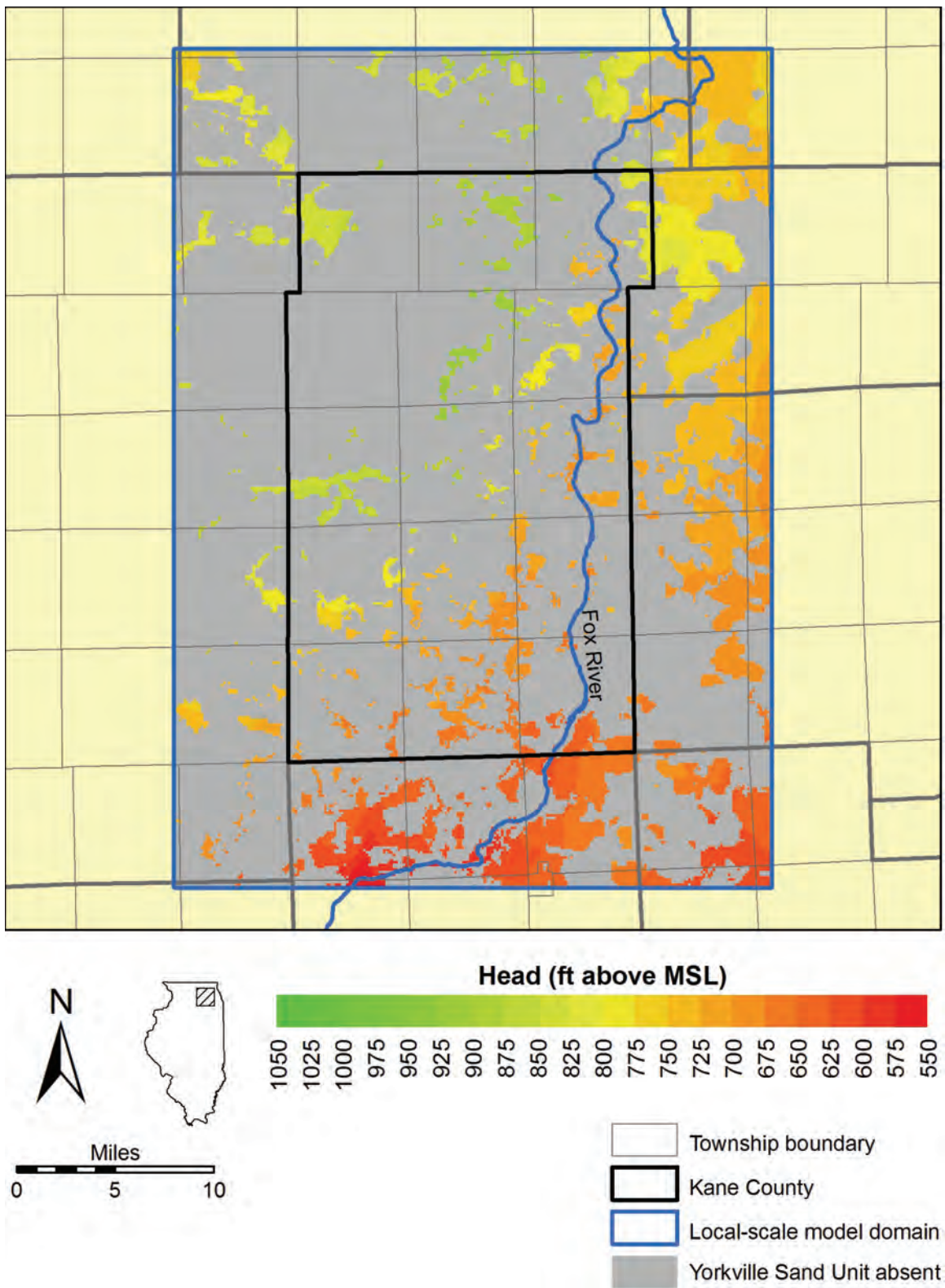


Figure 131. Simulated 2003 head in the Yorkville Sand Unit in the Kane County area.

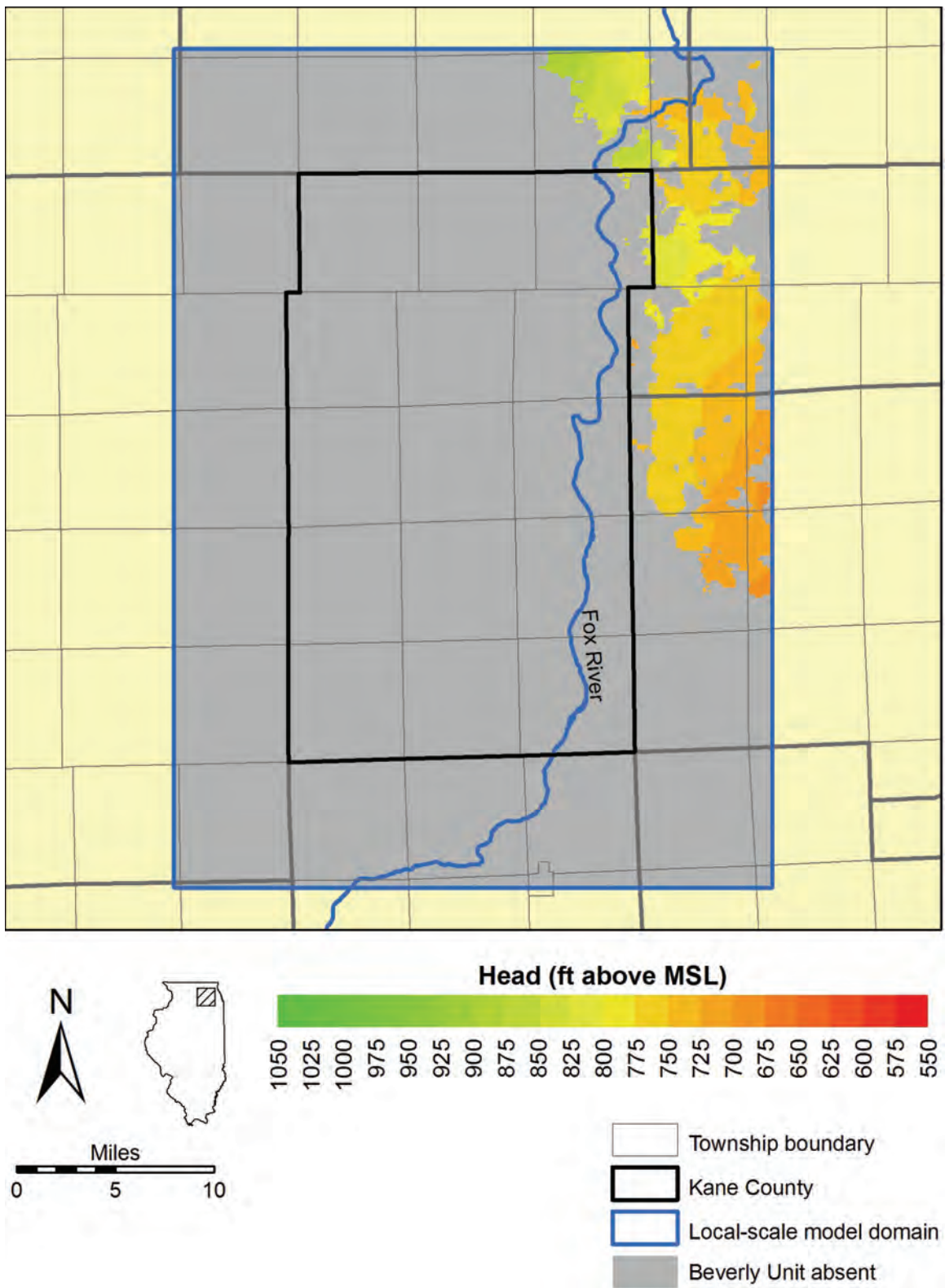


Figure 132. Simulated 2003 head in the Beverly Unit in the Kane County area.

Simulated heads in the shallow aquifers are typified by a pattern of high heads in northwestern Kane County that decline toward the south and east to lows along the Fox River. The simulated head distribution resembles topography, with the resemblance decreasing downward so that, while small topographic features are reflected in the potentiometry of the shallowest aquifers, only the larger features are mimicked by that of the more deeply-buried aquifers. The model suggests that the similarity in simulated heads between the lower units reflects numerous hydraulic connections between the aquifers (i.e., areas where the thickness of intervening aquitards is zero). The resemblance between simulated shallow aquifer heads and topography suggests a circulation pattern of recharge in upland areas and discharge to wells and to permanent surface waters in intervening low areas.

Within the shallow aquifers of the Kane County area, simulated drawdown is generally greater in the more deeply buried sub-Tiskilwa aquifers (Shallow Bedrock Aquifer, Lower and Upper Glasford Sand Units, and Ashmore Unit; Figure 133 through Figure 136) than in the aquifers nearer the surface (Batestown Sand Unit, Yorkville Sand Unit, and Beverly Unit; Figure 137 through Figure 139). The model simulations suggest that this pattern reflects the importance of the sub-Tiskilwa aquifers as water-supply sources as well as the importance of the Tiskilwa Unit in Kane County as a confining unit separating underlying aquifers from surface waters. Although in comparison with the deep aquifers, all of the shallow aquifers have closely-spaced hydraulic connections with surface waters, the Tiskilwa Unit, as the thickest, most continuous shallow aquitard in the Kane County area, isolates, to a degree, the sub-Tiskilwa aquifers from the controlling effect of surface waters on drawdown. In general, the greatest simulated drawdown occurs at and near wells pumping from the shallow aquifers in areas of low source aquifer transmissivity and without nearby hydraulic connections to permanent surface waters.

Not surprisingly, most areas of simulated drawdown exceeding 5 ft in 2003 in the Kane County area are located in the more heavily developed eastern part of Kane County and adjacent parts of DuPage and McHenry Counties (Figure 133 through Figure 139). Even with the comparatively heavy pumping in eastern Kane County, the regulating effect on heads of hydraulic connections with surface water is clearly evident in the reduction in simulated drawdown to zero near the Fox River in many areas. Drawdown at any one location is typically associated with pumping at one or, at most, a very few nearby wells.

Within the local model domain, the largest area of significant simulated drawdown (defined, for purposes of this report, as drawdown exceeding 20 ft) encompasses much of northeastern Kane County and adjacent southeastern McHenry County (Figure 140). This area surrounds public water-supply wells operated by the Villages of Algonquin, Carpentersville, East Dundee, Lake in the Hills, and the City of Crystal Lake. The most severe simulated drawdown, which exceeds 80 ft, occurs in the area of Algonquin wells 7, 8, 9, and 11. The modeling suggests that the magnitude of the simulated drawdown in the area of the Algonquin wells, which are finished in the Ashmore and Upper Glasford Sand Units, reflects the lack of an efficient hydraulic connection between these source aquifers and surface water. Simulated head in the Shallow Bedrock Aquifer at head calibration target 661, located approximately midway between Algonquin wells 8 and 9 (to the west) and Algonquin wells 7 and 11 (to the east)

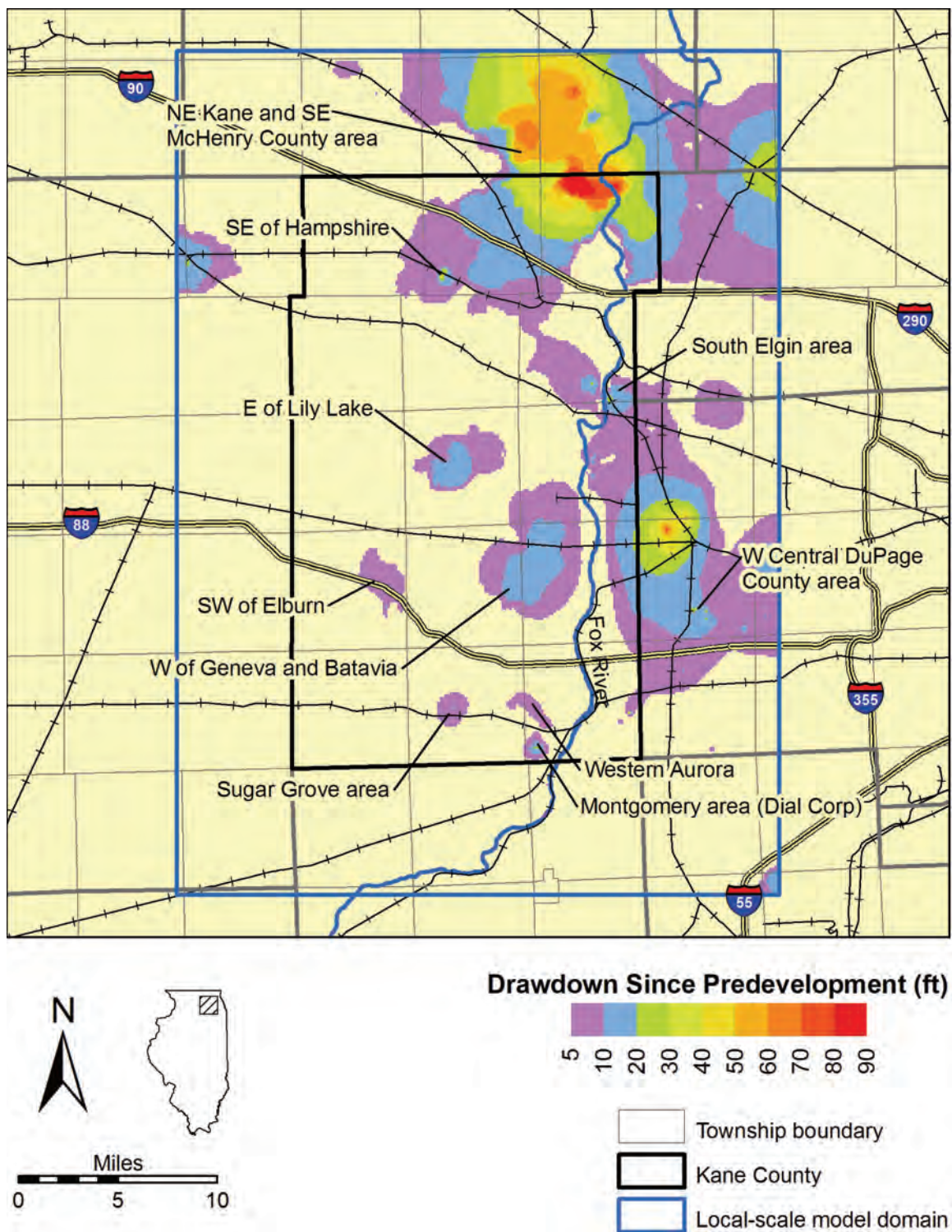


Figure 133. Simulated drawdown in 2003 in the Shallow Bedrock Aquifer in the Kane County area, with areas of drawdown mentioned in text identified.

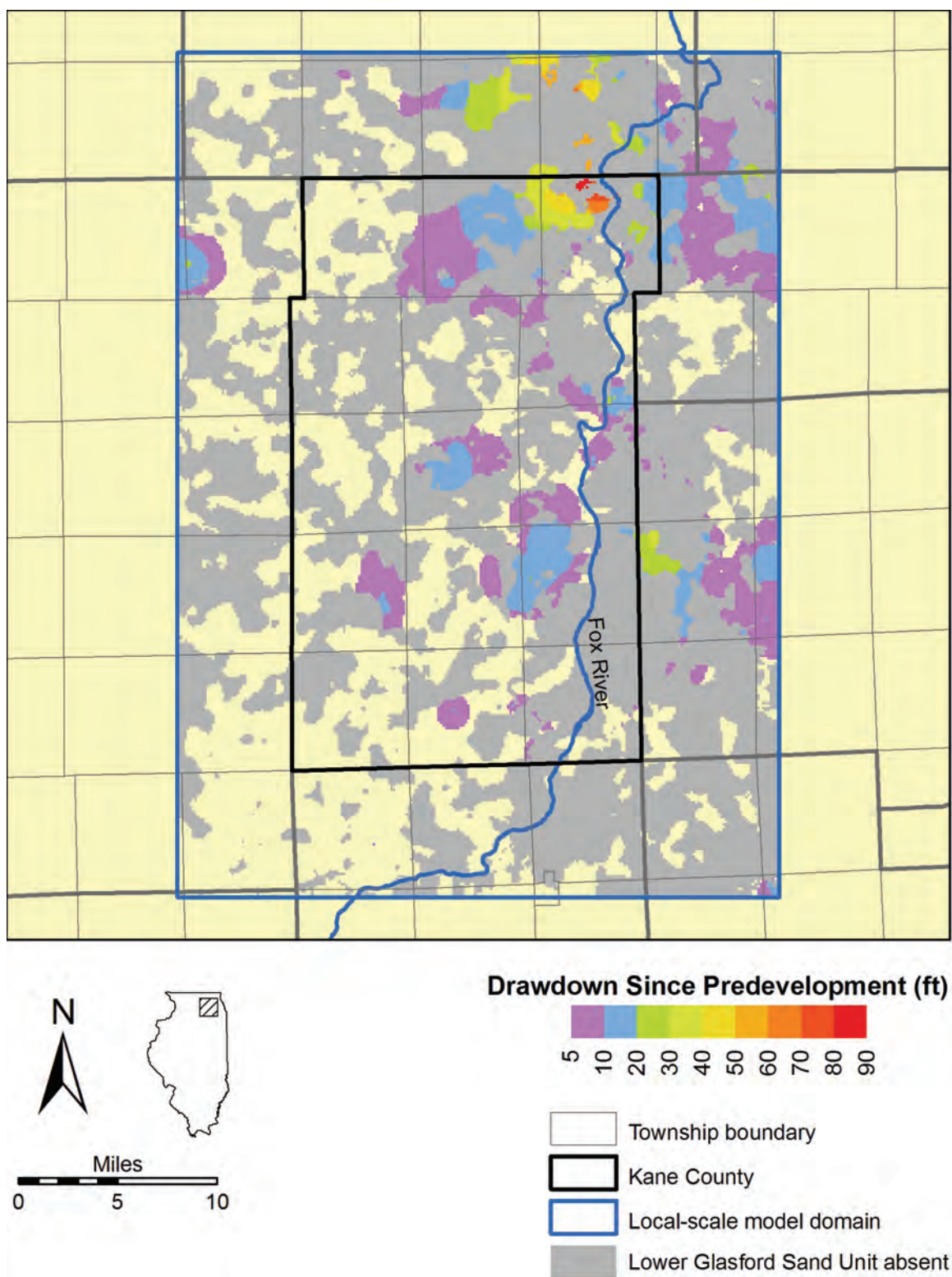


Figure 134. Simulated drawdown in 2003 in the Lower Glasford Sand Unit in the Kane County area.

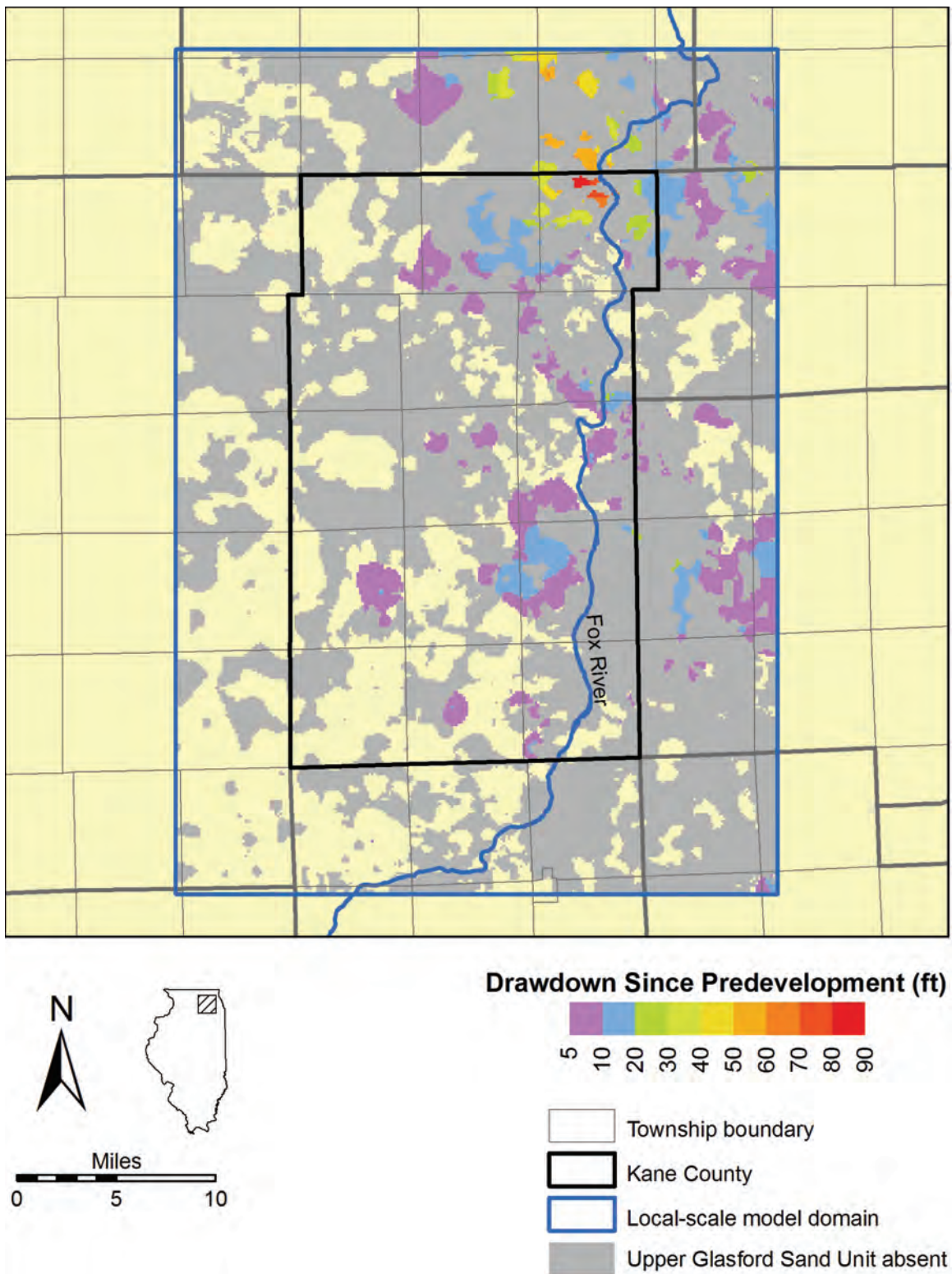


Figure 135. Simulated drawdown in 2003 in the Upper Glasford Sand Unit in the Kane County area.

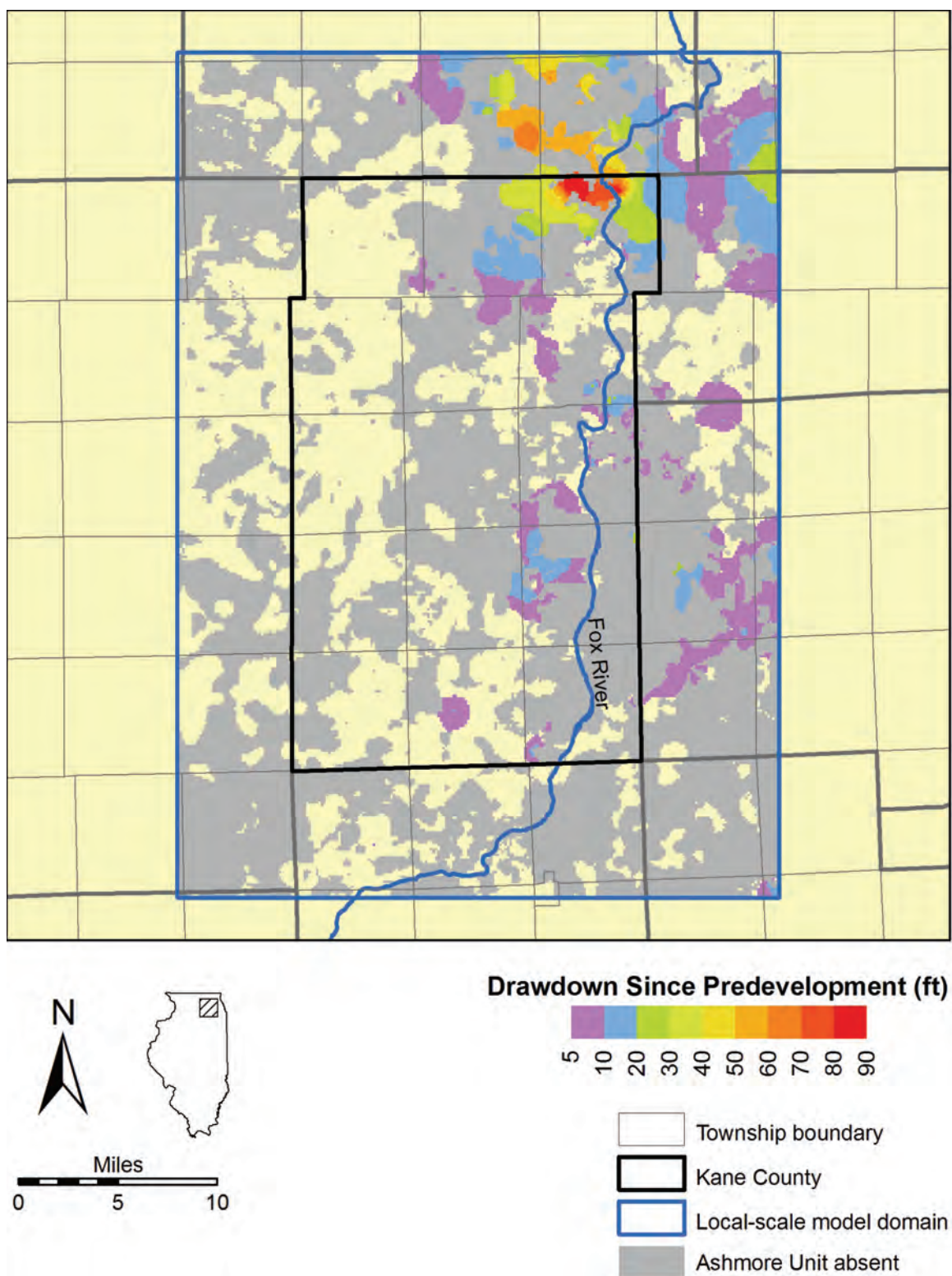


Figure 136. Simulated drawdown in 2003 in the Ashmore Unit in the Kane County area.

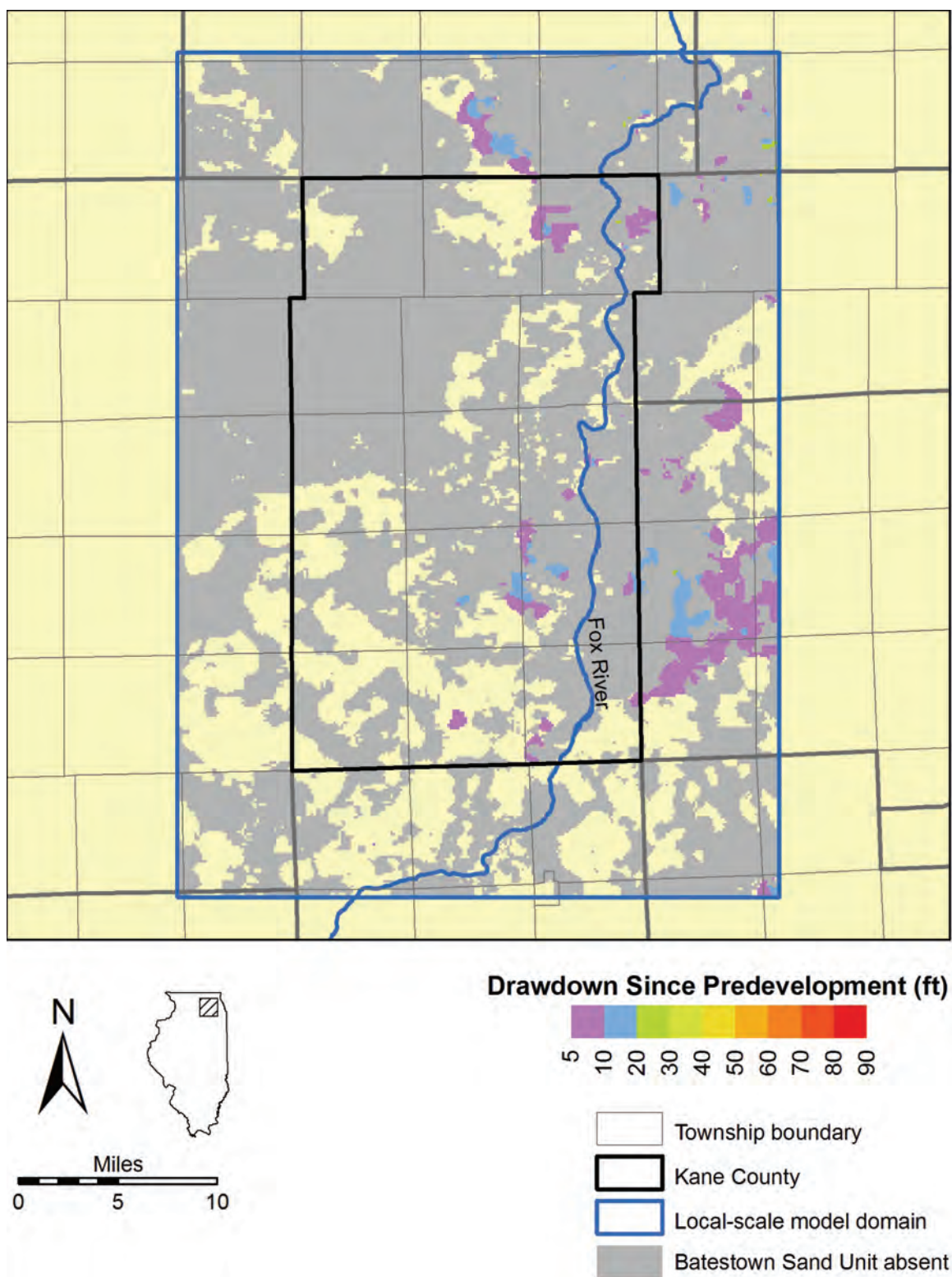


Figure 137. Simulated drawdown in 2003 in the Batestown Sand Unit in the Kane County area.

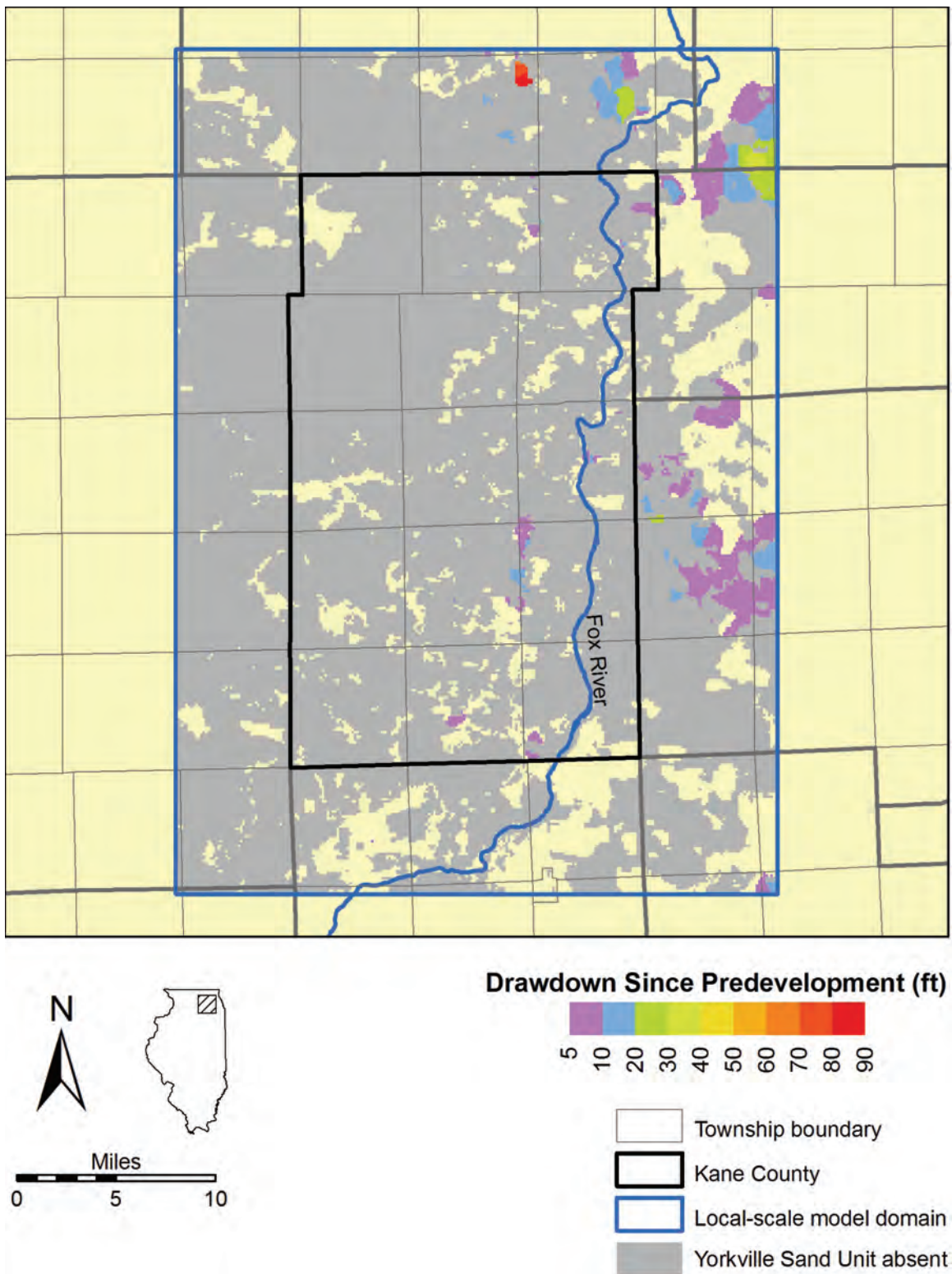


Figure 138. Simulated drawdown in 2003 in the Yorkville Sand Unit in the Kane County area.

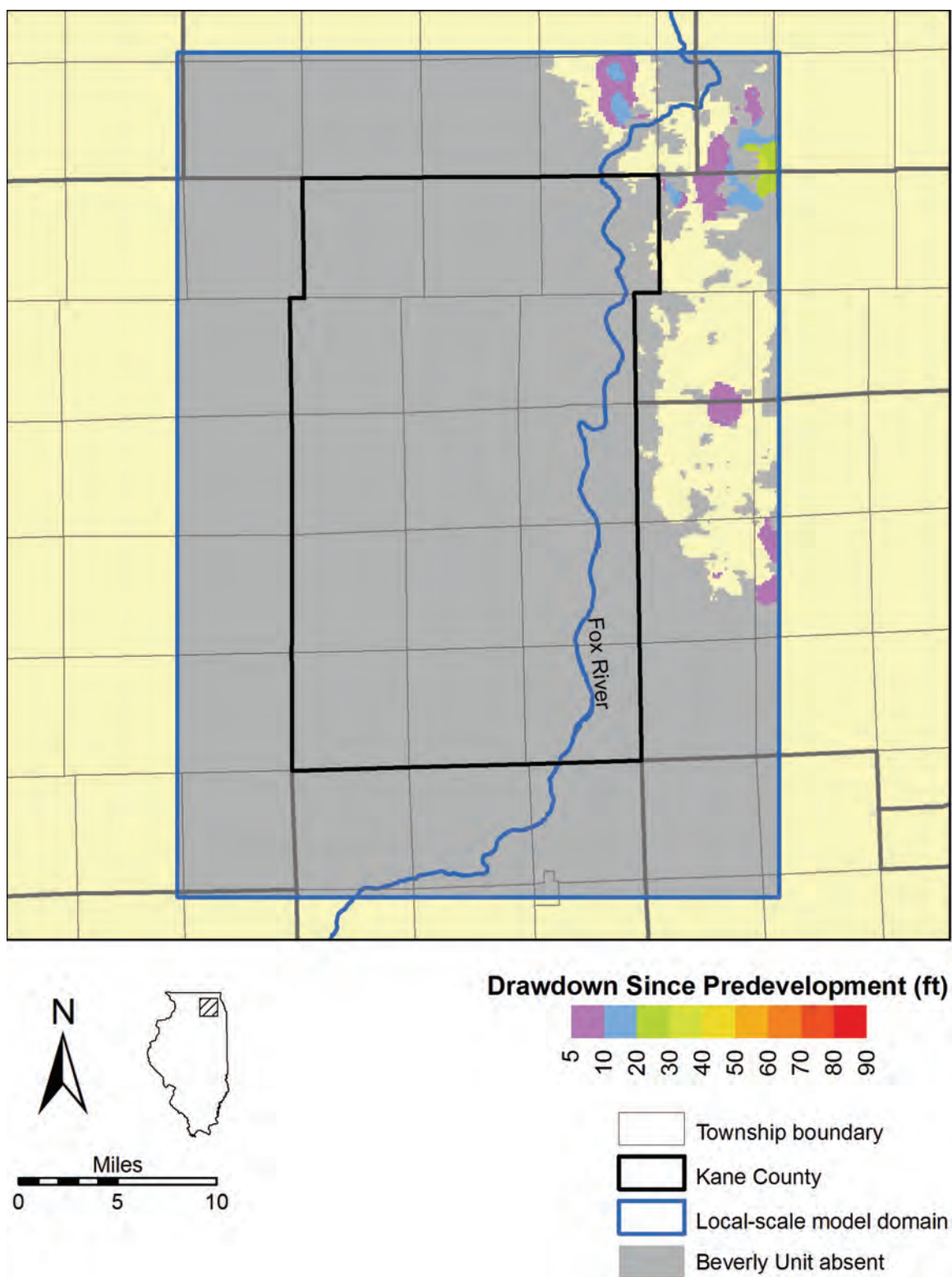


Figure 139. Simulated drawdown in 2003 in the Beverly Unit in the Kane County area.

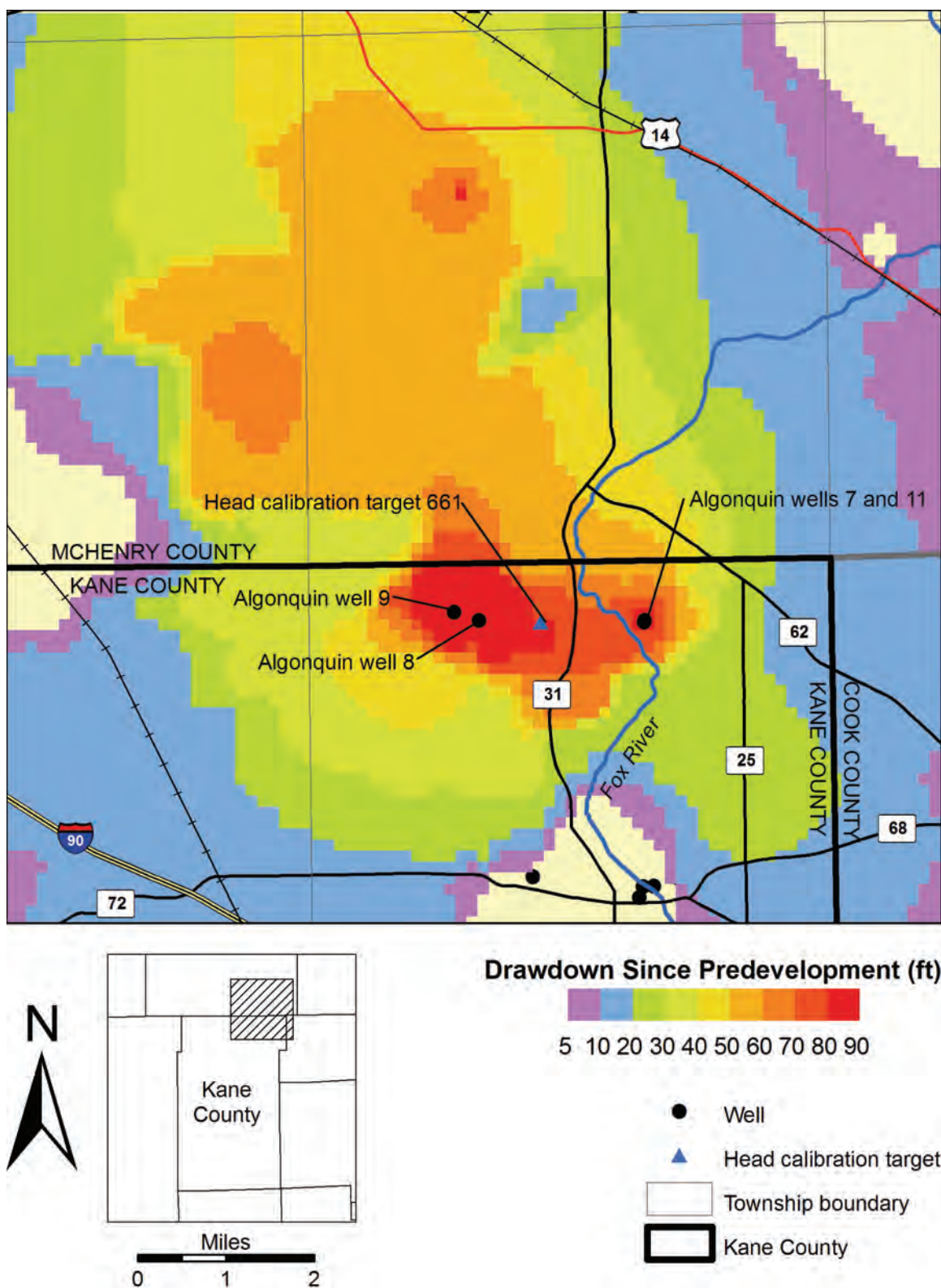


Figure 140. Index map of northeastern Kane County and southeastern McHenry County showing simulated 2003 drawdown in the Shallow Bedrock Aquifer.

(Figure 141, Figure 142), suggests that, while heads have declined slowly at that location since 1964, drawdown greatly increased in 1995, when Algonquin wells 8 and 9 were brought into service. Total withdrawals from the two wells nearly doubled from 1998 to 2000, from about 0.6 to 1.1 Mgd, causing over 20 ft of additional drawdown at calibration target 661.

A second large area of significant simulated drawdown occurs in west-central DuPage County and east-central Kane County, including parts of the Cities of Batavia and Geneva (Figure 143). This area is centered on West Chicago wells 6, 7, and 8, which are finished in the Shallow Bedrock Aquifer. An additional smaller area of significant simulated drawdown surrounds Warrenville wells 4, 8, and 10, which are also finished in the Shallow Bedrock Aquifer. That both the West Chicago and Warrenville wells are finished in the Shallow Bedrock Aquifer, which is less permeable than sand and gravel aquifers present elsewhere in the Kane County area, partially explains the magnitude of simulated drawdown in the area, but does not offer a complete explanation. Model simulations suggest that the comparatively great distance of the West Chicago and Warrenville wells from hydraulically connected surface water is the major factor explaining the significant drawdown at these wells. The West Chicago wells are more or less centered between the Fox River and the West Branch of the DuPage River, but model simulations suggest that they are too distant (2 to 3 miles) from these streams for streamflow capture to offset drawdown. Likewise, modeling suggests that the Warrenville wells, which are less than about 0.5 miles from the West Branch of the DuPage River, cannot capture significant streamflow because the hydraulic connection of the Shallow Bedrock Aquifer with the stream is sporadic, and the hydraulically-connected Fox River, over 5 miles west, is too distant to offset drawdown. Figure 144 shows simulated heads in the Shallow Bedrock Aquifer at head calibration target 149, along the eastern border of Kane County, within the area of significant simulated drawdown surrounding the West Chicago wells. The figure suggests a strong correlation between pumping from West Chicago wells 6, 7, and 8 and heads in the Shallow Bedrock Aquifer at calibration target 149.

Remaining areas of significant simulated drawdown in 2003 in the Kane County area are much more limited than those discussed in the preceding two paragraphs. Two small areas, considered together here, surround South Elgin well 4 (on the west side of the Fox River) and South Elgin wells 3, 6, and 10 (east of the Fox River) in east-central Kane County (Figure 145). These wells are finished in the Ashmore Unit and the Upper and Lower Glasford Sand Units, which—since they are hydraulically connected to one another in the South Elgin area and effectively respond to pumping as a single aquifer—are referred to in this paragraph as the Sub-Tiskilwa Aquifer. The South Elgin wells are only about 0.3 to 0.5 miles from the Fox River. Modeling suggests that the relatively large magnitude of the simulated drawdown at the wells appears to be related to the poor hydraulic connection of the Fox River to the Sub-Tiskilwa Aquifer in the immediate vicinity of the South Elgin wells, which is at best discontinuous. This discontinuous connection causes greater drawdown around the South Elgin wells than it would were a more continuous connection present, as is the case in most of the local model domain. For example, simulated 2003 drawdown at St. Charles wells 9 and 11 is less than 20 ft. These wells are a little more than 3 miles downstream from South Elgin wells 3, 6, and 10, but in an area of continuous hydraulic connection between the source aquifer and the

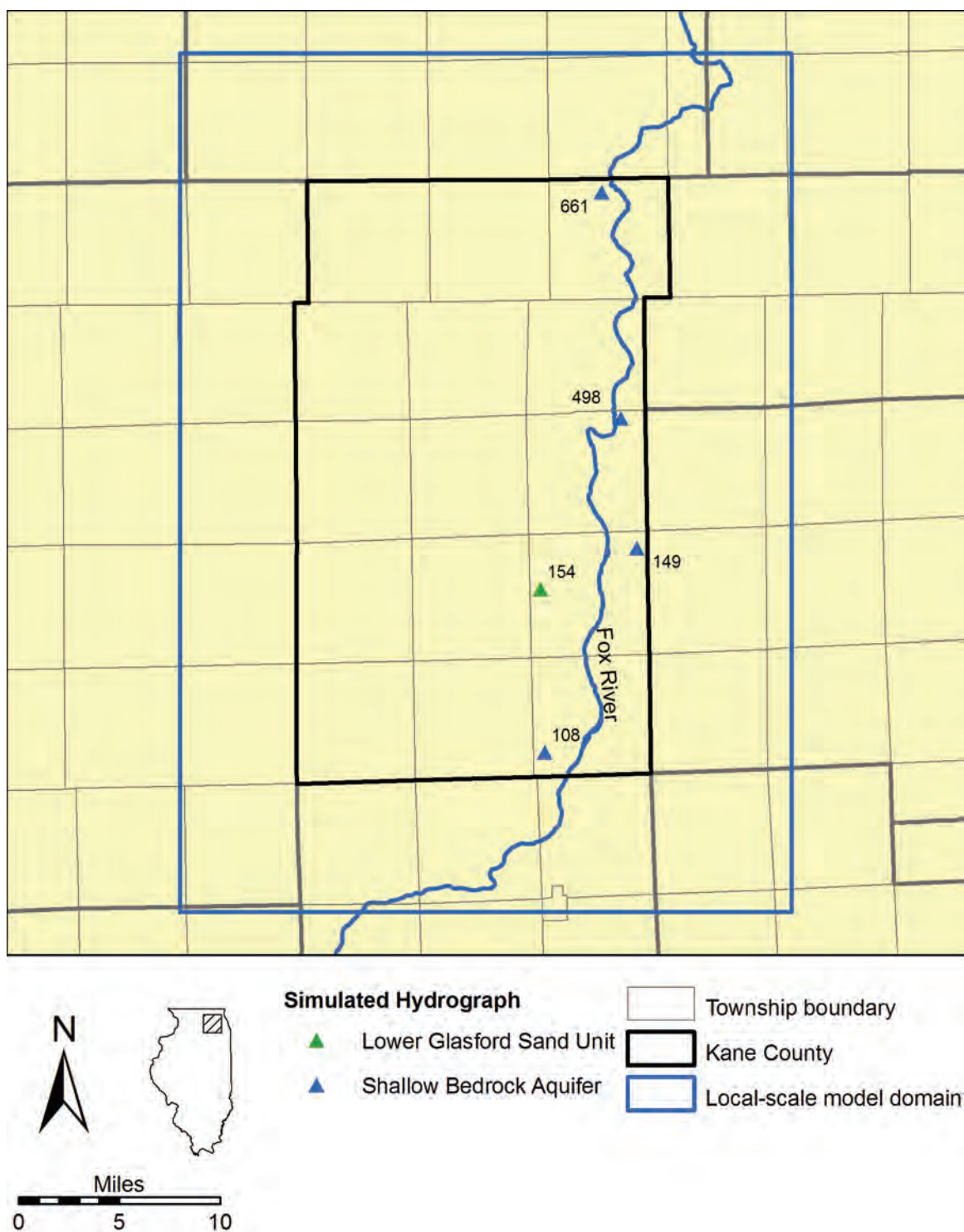


Figure 141. Locations of simulated hydrographs shown in Figure 142 through Figure 149.

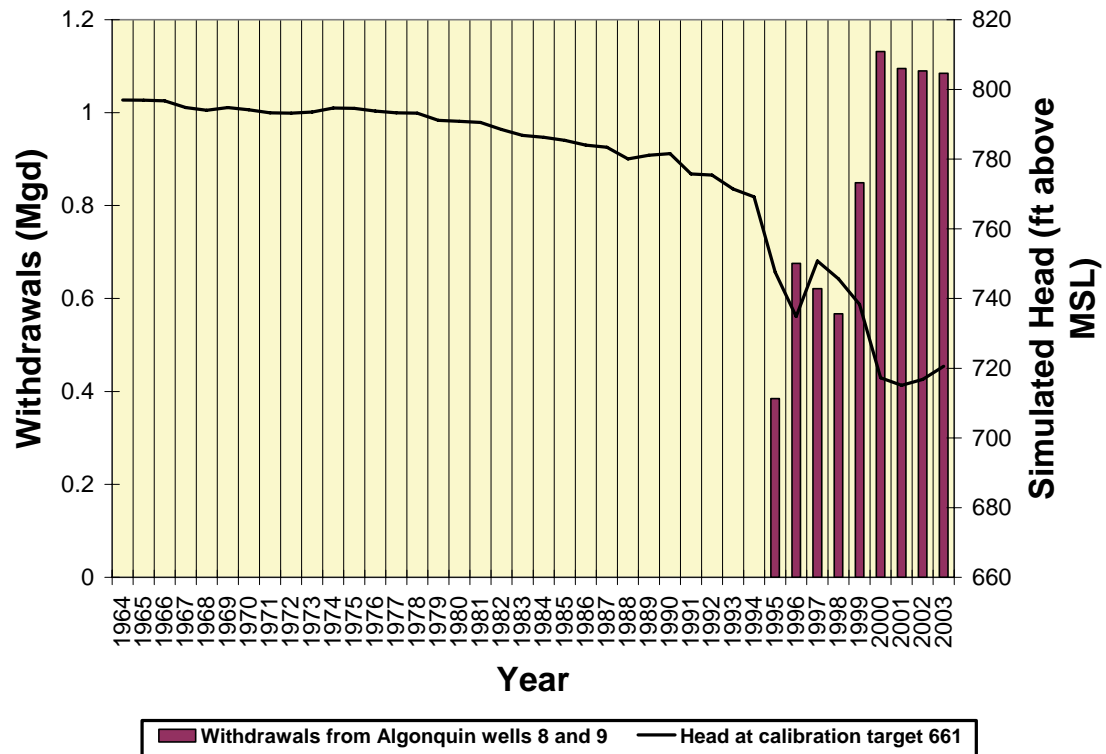


Figure 142. Simulated head in the Shallow Bedrock Aquifer at head calibration target 661, located in the Algonquin area of northeastern Kane County, and withdrawals from key nearby wells.

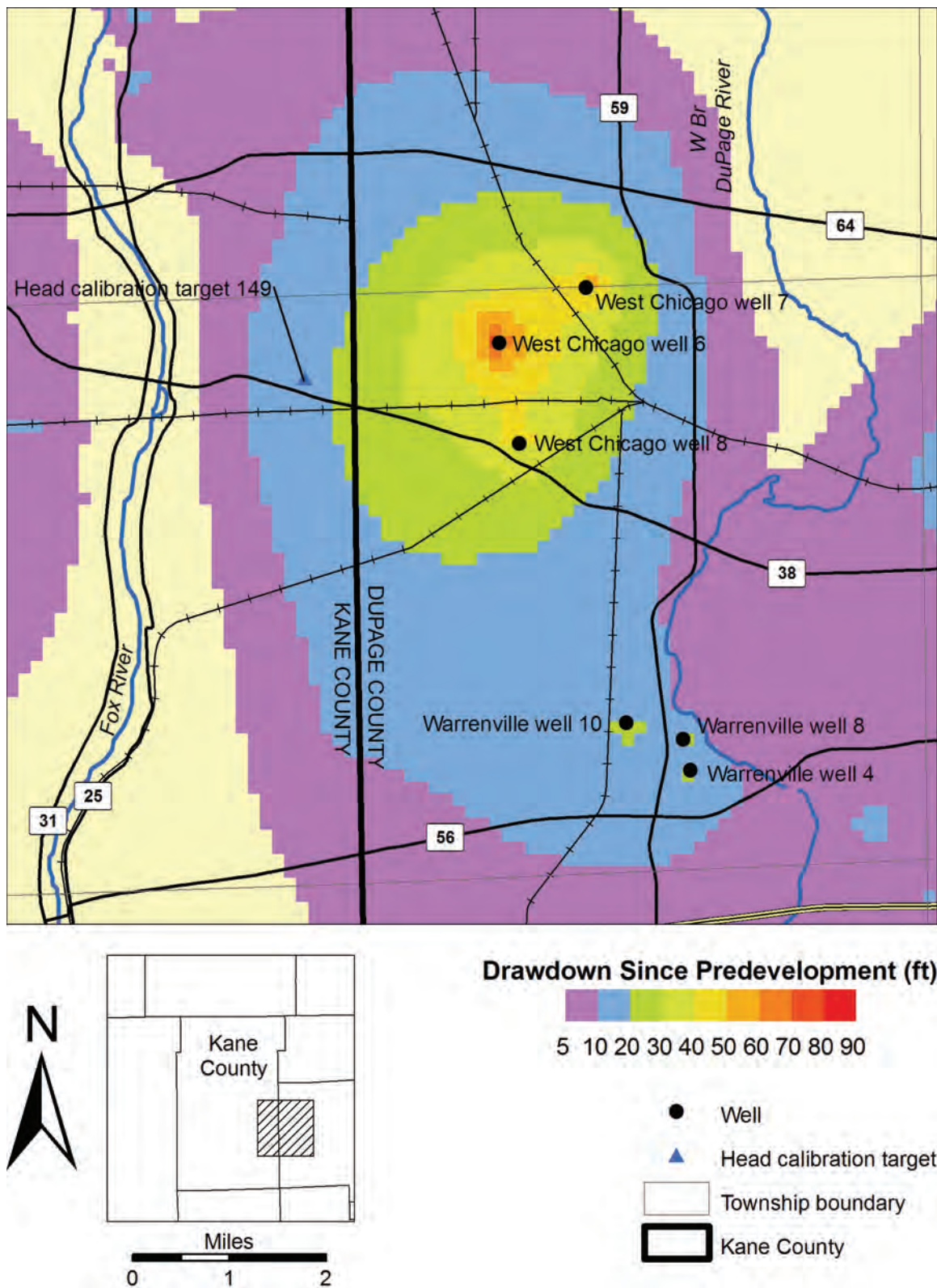


Figure 143. Index map of east-central Kane County and west-central DuPage County showing simulated 2003 drawdown in the Shallow Bedrock Aquifer.

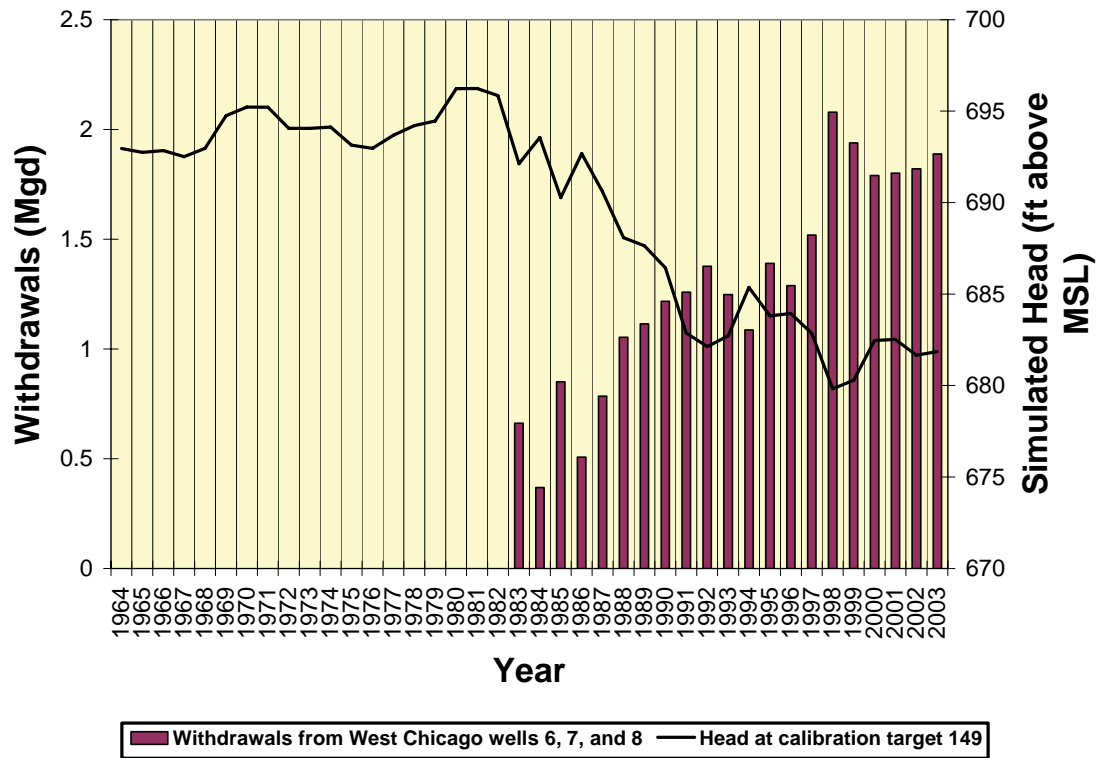


Figure 144. Simulated heads in the Shallow Bedrock Aquifer at head calibration target 149, located east of Geneva, on the eastern border of Kane County, and withdrawals from key nearby wells.

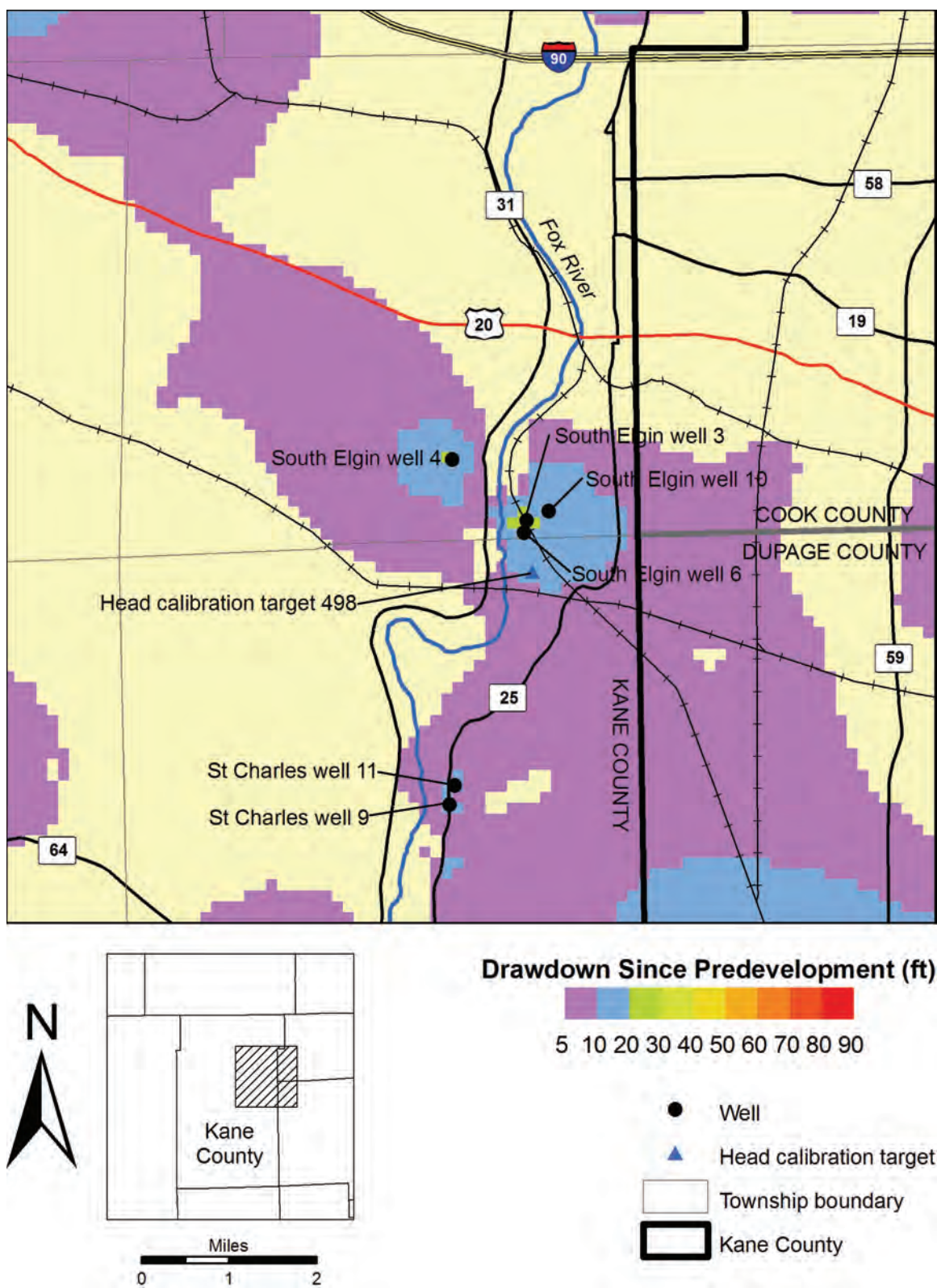


Figure 145. Index map of the South Elgin area showing simulated 2003 drawdown in the Shallow Bedrock Aquifer.

Fox River. The lesser drawdown surrounding the St. Charles wells occurs despite the fact that the wells, which are only about 1200 ft apart, pumped from the Upper and Lower Glasford Sand Units nearly three times as much as the four South Elgin wells in 2003. Simulated head in the Shallow Bedrock Aquifer at head calibration target 498, located about 2400 to 8300 ft from South Elgin wells 3, 4, 6, and 10, is illustrated in Figure 146.

The final area of significant simulated drawdown in 2003 surrounds Dial Corporation wells 1, 2, and 3 in Montgomery, southeastern Kane County (Figure 147). Like the South Elgin area, the area of simulated drawdown exceeding 20 ft around these wells is very limited. Model simulations suggest that heads in the area (for example, at head calibration target 108, in the Shallow Bedrock Aquifer a few hundred ft north of the Dial wells) have declined slowly since 1964 and chiefly reflect fluctuations in pumping at the Dial Corporation wells (Figure 148). Simulated drawdown is less than 5 ft along Blackberry Creek, to the west of the Dial wells, suggesting that hydraulic connections to the creek supply much of the water withdrawn from the wells.

Not surprisingly given the population growth of the Kane County region, local-scale model simulations suggest that areas affected by more than 5 ft of drawdown have increased in the Kane County area from 1964 through 2003. During this period, withdrawals from shallow wells in Kane County more than quadrupled, expanding from about 4 to 19 Mgd (Figure 12). The pattern of expansion of the affected areas is exemplified by maps of simulated drawdown in the Shallow Bedrock Aquifer in 1964, 1973, 1983, 1993 (Figure 150 through Figure 153), and 2003 (Figure 133). In general, model simulations suggest that areas of simulated drawdown exceeding 5 ft expand westward into Kane County from DuPage and Cook Counties, and southward from southeastern McHenry County during this period. They also develop at these locations:

- west of Geneva and Batavia (where Geneva wells 8, 9, and 10, and Batavia wells 6, 7, and 8, withdraw water from the Upper and Lower Glasford Sand Units)
- western Aurora (where Aurora wells 101, 103, and 119, and Aurora Country Club wells 5 and 6, withdraw water from the Upper and Lower Glasford Sand Units and the Shallow Bedrock Aquifer)
- east of Lily Lake (where Ferson Creek Utilities Corporation wells 2 and 3 withdraw water from the Lower Glasford Sand Unit)
- Sugar Grove (where Sugar Grove wells 2 and 7 withdraw water from the Upper and Lower Glasford Sand Units)
- southwest of Elburn (where Duntelman Turf Farm wells 1, 2, 3, and 4 withdraw water from the Upper and Lower Glasford Sand Units).

Two areas of drawdown in the Hampshire and Huntley areas, reduced in size during the 1964-2003 period, reflecting retirement of shallow public and commercial supply wells (not shown in Figure 133).

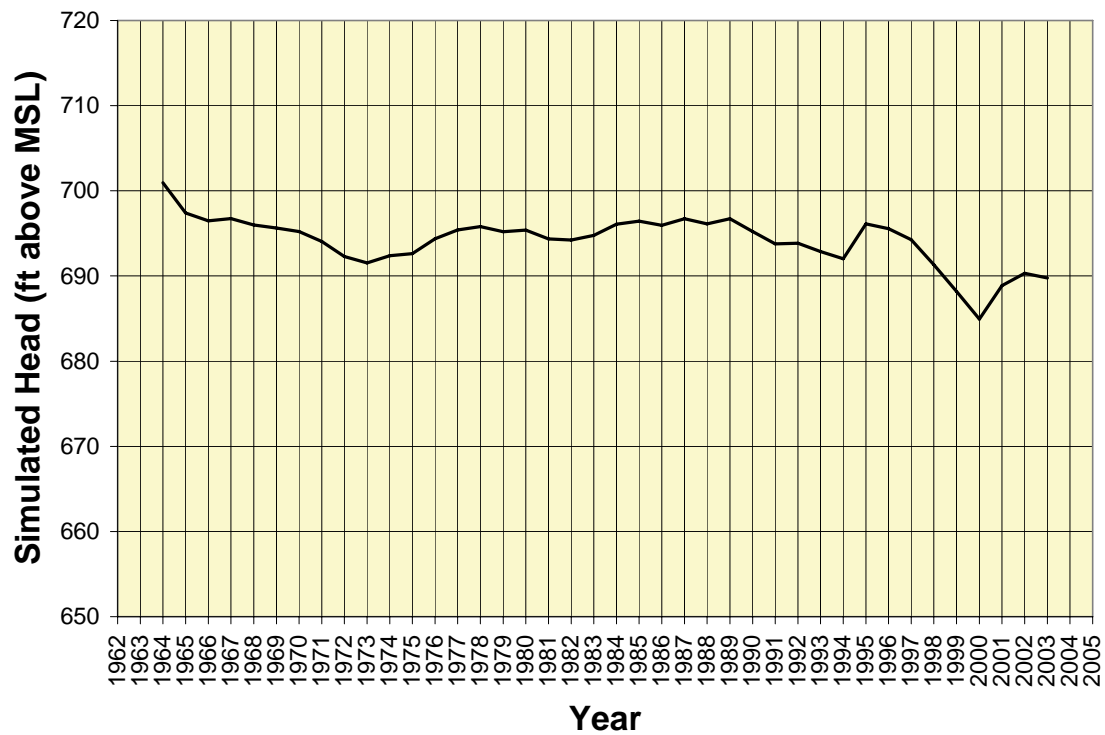


Figure 146. Simulated heads in the Shallow Bedrock Aquifer at head calibration target 498, located on the southeast edge of South Elgin.

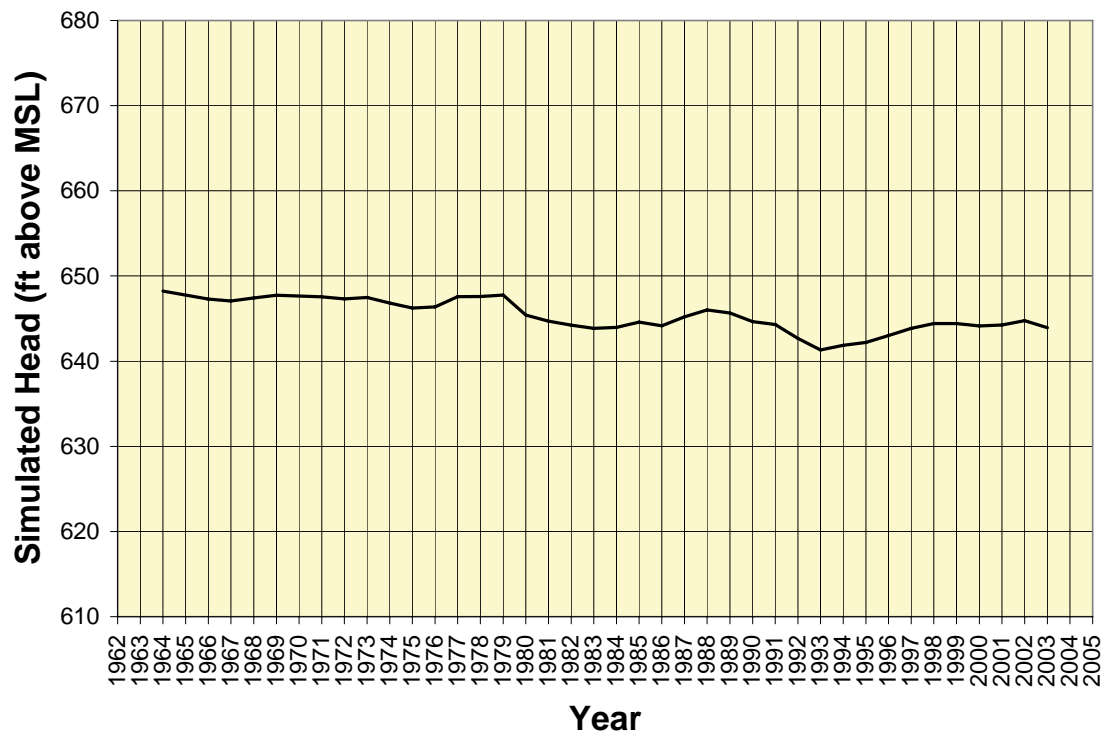


Figure 148. Simulated heads in the Shallow Bedrock Aquifer at head calibration target 108, located on the north edge of Montgomery.

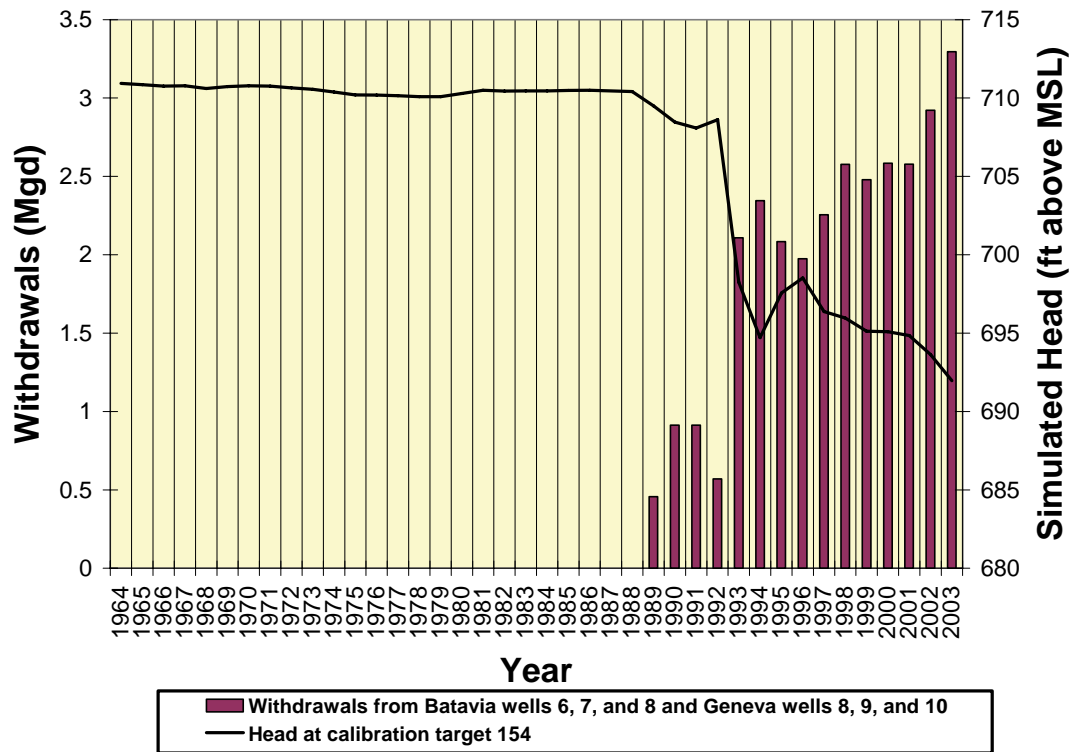


Figure 149. Simulated heads in the Lower Glasford Sand Unit at head calibration target 154, located west of Batavia.

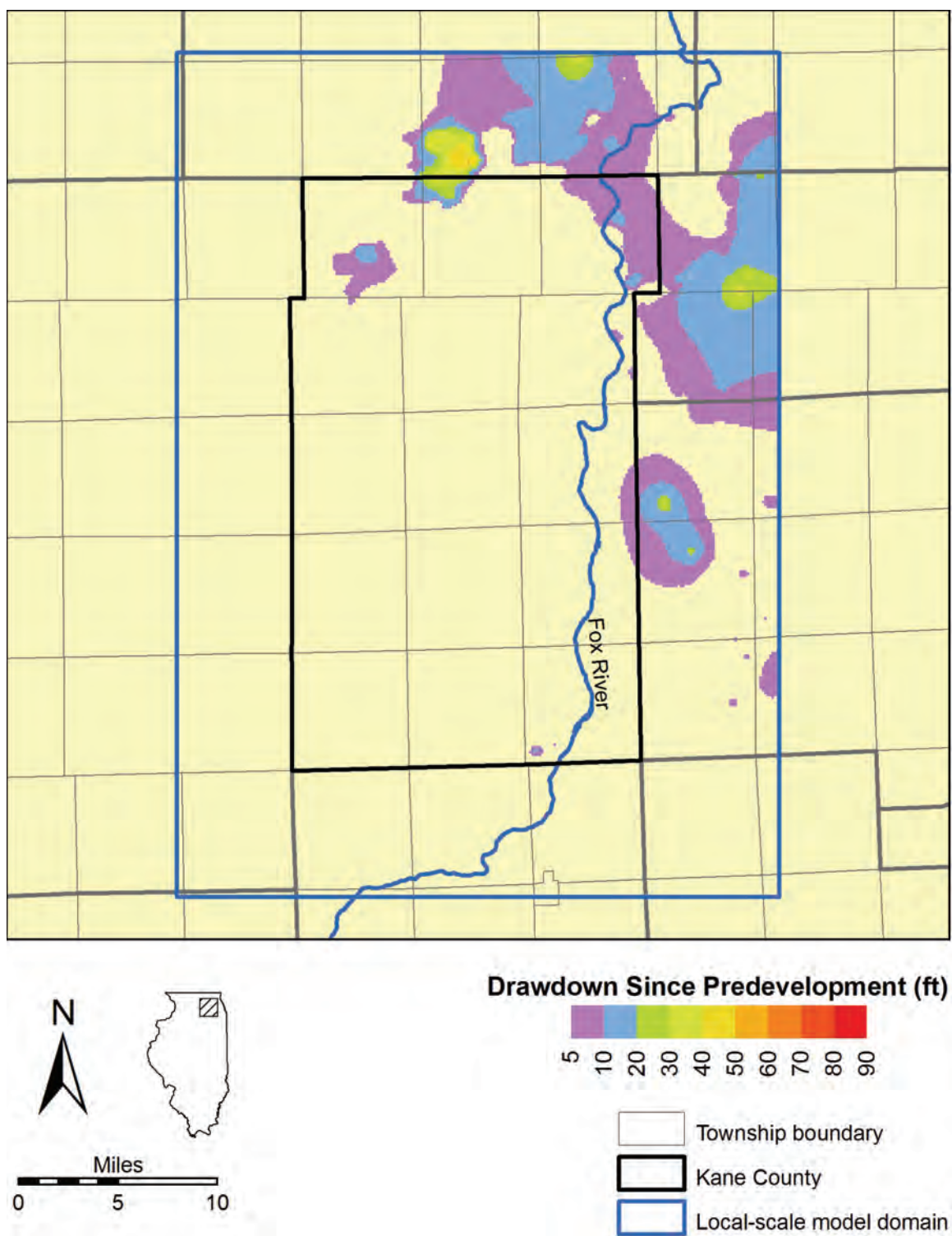


Figure 150. Simulated drawdown in 1964 in the Shallow Bedrock Aquifer in the Kane County area.

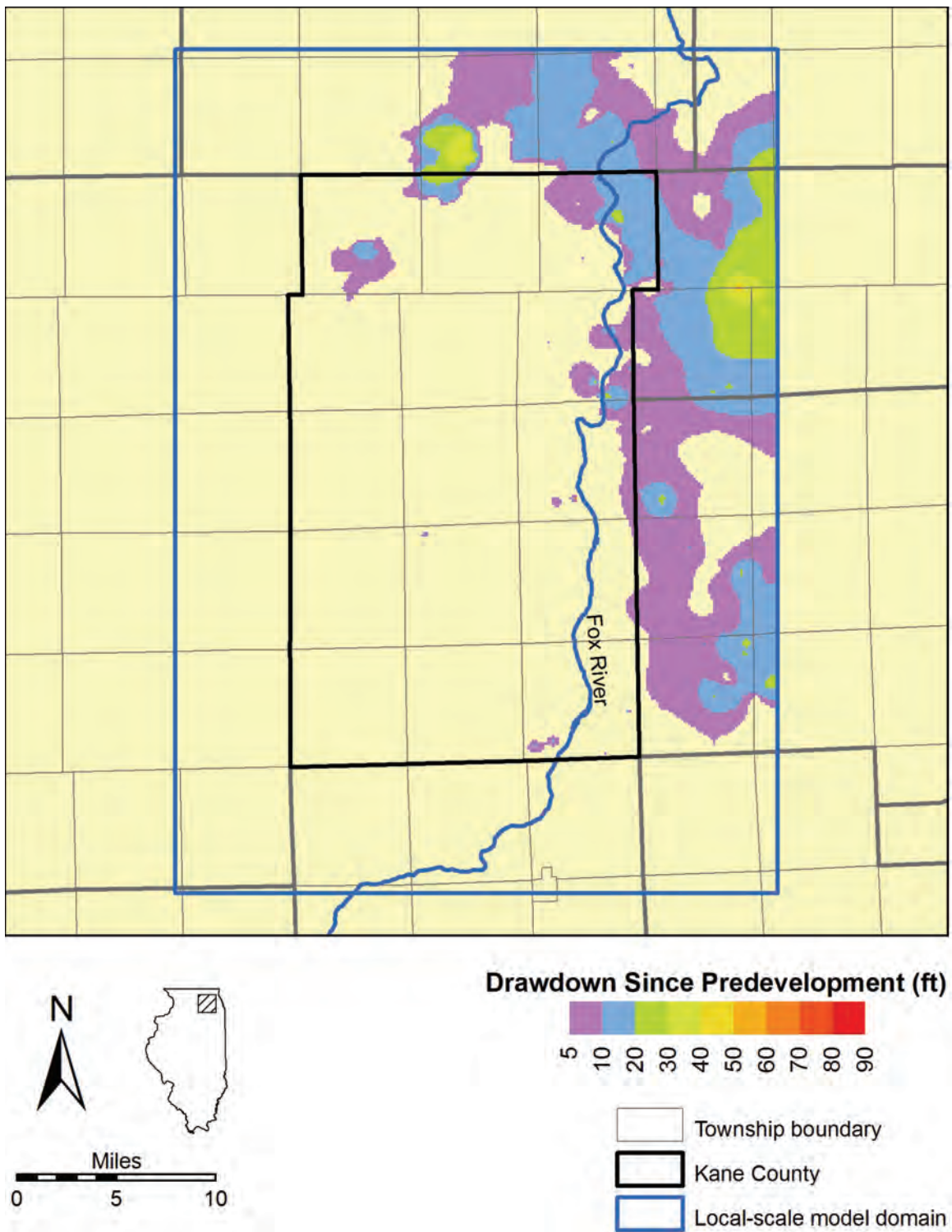


Figure 151. Simulated drawdown in 1973 in the Shallow Bedrock Aquifer in the Kane County area.

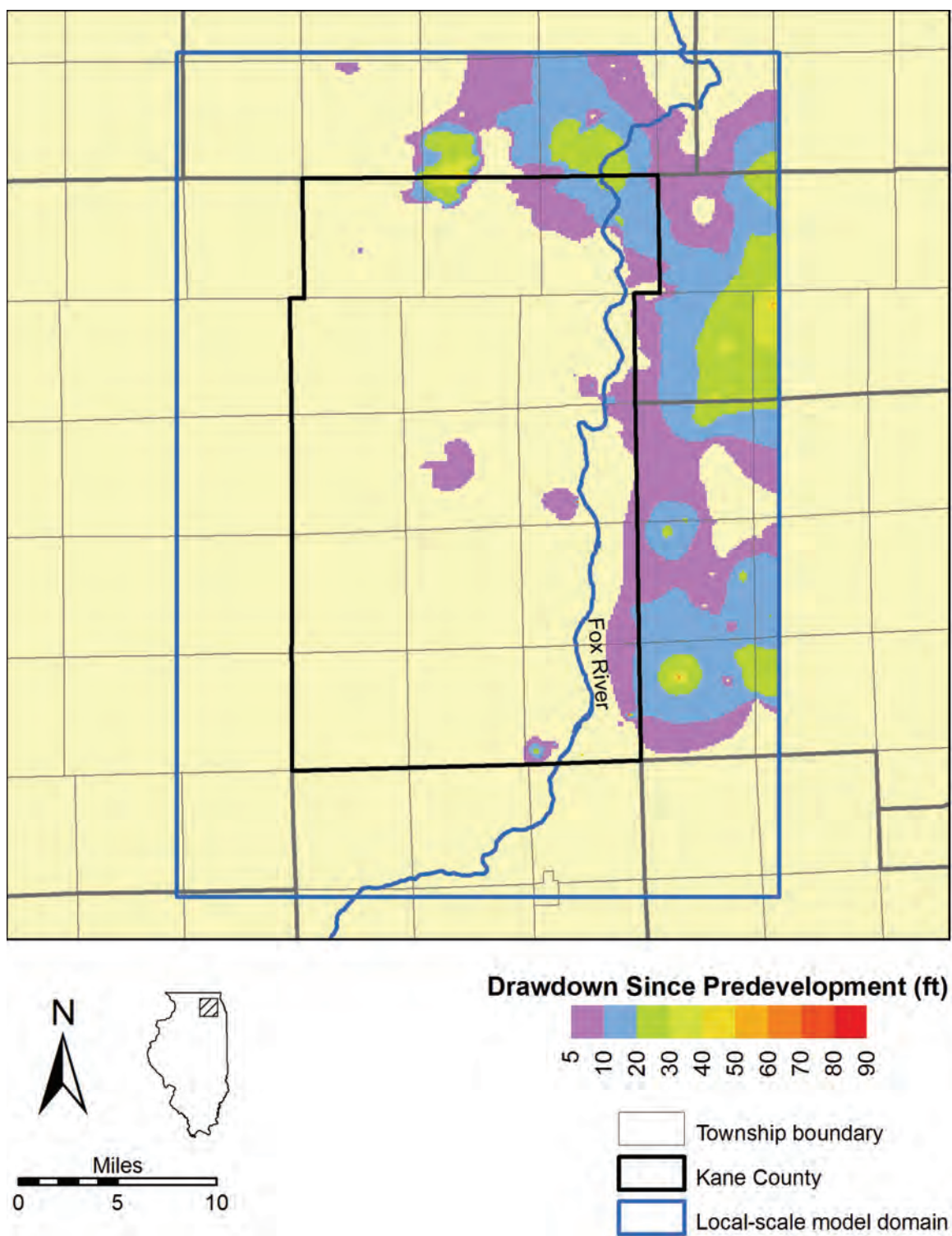


Figure 152. Simulated drawdown in 1983 in the Shallow Bedrock Aquifer in the Kane County area.

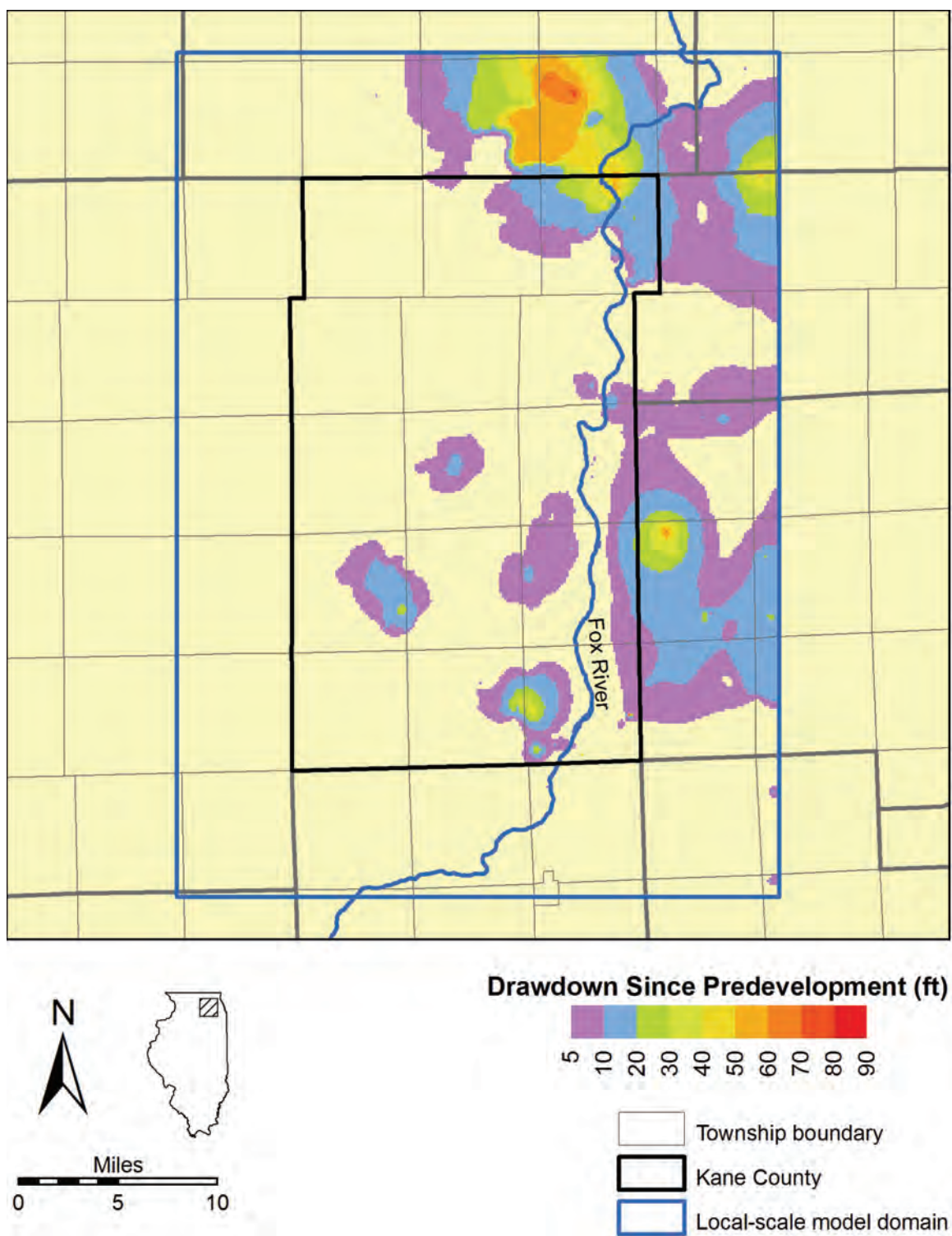


Figure 153. Simulated drawdown in 1993 in the Shallow Bedrock Aquifer in the Kane County area.

The region of simulated drawdown west of the cities of Batavia and Geneva deserves additional discussion because it is an area of concentrated pumping, fairly recently begun, supplying two of Kane County's largest communities. Batavia wells 6, 7, and 8 and Geneva wells 8, 9, and 10 began pumping groundwater from the Upper and Lower Glasford Sand Units in the area west of the communities, along the axis of the St. Charles Bedrock Valley, in 1989. Pumping by Batavia and Geneva is illustrated in Figure 149, which also illustrates simulated heads in the Lower Glasford Sand Unit at head calibration target 154, west of Batavia. By 2003, pumping by Batavia and Geneva from the Glasford sands located along the St. Charles Valley had expanded to more than 3 Mgd furnished by six wells. Despite this significant pumping, however, modeling suggests that drawdown in the area surrounding the wells has not exceeded 20 ft, probably because the sand and gravel supplying the wells is highly conductive and because (as will be discussed in Section 3.2.2) hydraulic connection of the Glasford sands to Mill Creek permit a large proportion of the well yield to be derived from captured streamflow, rather than aquifer storage.

3.2.2. *Streamflow*

Strong hydraulic connections between the shallow aquifers and surface water reduce drawdown in the aquifer but also tend to reduce groundwater discharge to streams and can reduce streamflow. This reduction is accomplished by diverting groundwater that, under predevelopment conditions, would have discharged to streams, and by inducing flow directly out of surface waters (see Section 3.2.1.2). Thus, the pumping—artificial groundwater discharge—causes a reduction in natural groundwater discharge. This reduction is referred to as *streamflow capture*. Streamflow capture is observable as a reduction in base flow. Following a period of transient reduction of heads, most of the water withdrawn by wells is accounted for by reduced base flow, the remainder being accommodated by reduced storage. The cone of depression surrounding a well will deepen and widen until the change of head within it causes an amount of water equivalent to the amount withdrawn from the well to be diverted from predevelopment streamflow and storage.

The local-scale model permits estimation of the change in natural groundwater discharge to the stream reaches shown in Figure 154 and described in Table 26. These estimates (Figure 155, Table 26) approximate the change in natural groundwater discharge to the reaches caused by pumping. Without additional modeling to characterize changes in recharge and drainage conditions through time, they can be regarded only as rough estimates of change in natural groundwater discharge since predevelopment, because predevelopment hydrologic conditions cannot be truly known owing to the lack of observations of the predevelopment environment. The estimates of change in natural groundwater discharge provided by the model do not account for surface withdrawals (such as occur from the Fox River at Elgin and Aurora) or effluent (discharged into streams or applied as irrigation at numerous locations in Kane County). It is important to note that the changes in simulated natural groundwater discharge illustrated in Figure 155 and Table 26 are only equivalent to changes in base flow along the particular reach shown. For the stream reaches that have separate upstream reaches or that have watersheds not entirely within the model domain (501-504, 507, 511, and 520-522), the

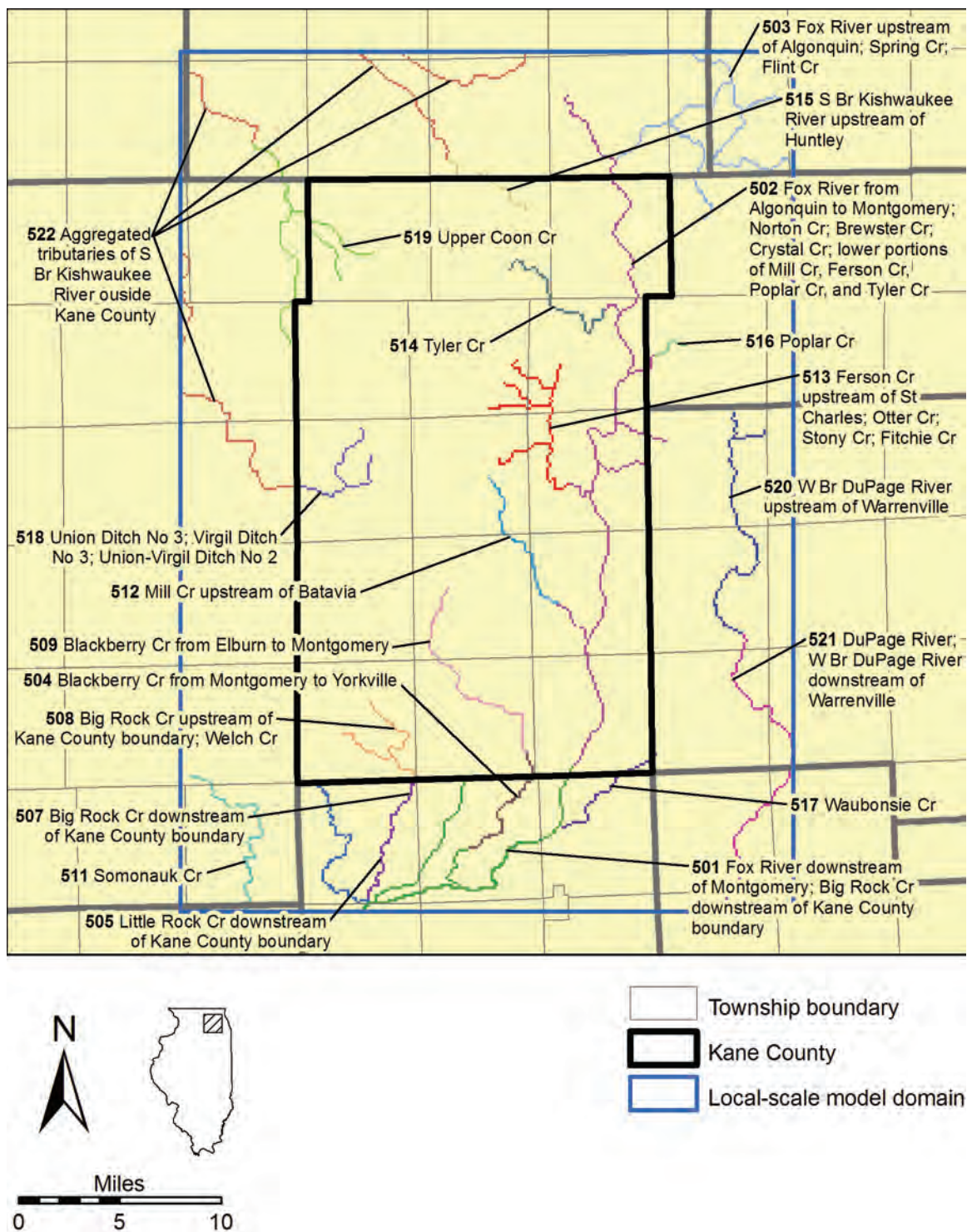


Figure 154. Stream reaches employed for flow accounting in local-scale model.

**Table 26. Principal Streams Included in Reaches
Shown in Figure 154 and Figure 155 and Change in Natural Groundwater
Discharge since Predevelopment in 2003 (%)**

<i>Reach Number</i>	<i>Principal Streams</i>	<i>Natural Groundwater Discharge</i>		
		<i>Predevelopment</i>	<i>2003</i>	<i>Change</i>
501	Fox River downstream of Montgomery; Big Rock Cr downstream of Kane County boundary	3,058,783	2,908,083	-5%
502	Fox River from Algonquin to Montgomery; Norton Cr; Brewster Cr; Crystal Cr; lower portions of Mill Cr, Ferson Cr, Poplar Cr, and Tyler Cr	5,911,827	4,406,876	-25%
503	Fox River upstream of Algonquin; Spring Cr; Flint Cr	2,754,773	1,477,822	-46%
504	Blackberry Cr from Montgomery to Yorkville	523,720	481,652	-8%
505	Little Rock Cr downstream of Kane County boundary	729,978	724,670	-1%
507	Big Rock Cr downstream of Kane County boundary	989,856	884,754	-11%
508	Big Rock Cr upstream of Kane County boundary; Welch Cr	1,540,121	1,494,689	-3%
509	Blackberry Cr from Elburn to Montgomery	1,569,068	1,290,106	-18%
511	Somonauk Cr	554,272	551,936	0%
512	Mill Cr upstream of Batavia	378,494	121,024	-68%
513	Ferson Cr upstream of St Charles; Otter Cr; Stony Cr; Fitchie Cr	1,090,815	1,033,021	-5%
514	Tyler Cr	621,083	555,593	-11%
515	S Br Kishwaukee River upstream of Huntley	488,396	413,769	-15%
516	Poplar Cr	323,175	190,455	-41%
517	Waubonsie Cr	453,537	417,734	-8%
518	Union Ditch No 3; Virgil Ditch No 3; Union-Virgil Ditch No 2	1,043,596	1,029,184	-1%
519	Upper Coon Cr	1,733,411	1,696,750	-2%
520	W Br DuPage River upstream of Warrenville	986,100	473,999	-52%
521	DuPage River; W Br DuPage River downstream of Warrenville	1,994,171	1,752,033	-12%
522	Aggregated tributaries of S Br Kishwaukee River outside Kane County	3,167,406	2,920,689	-8%

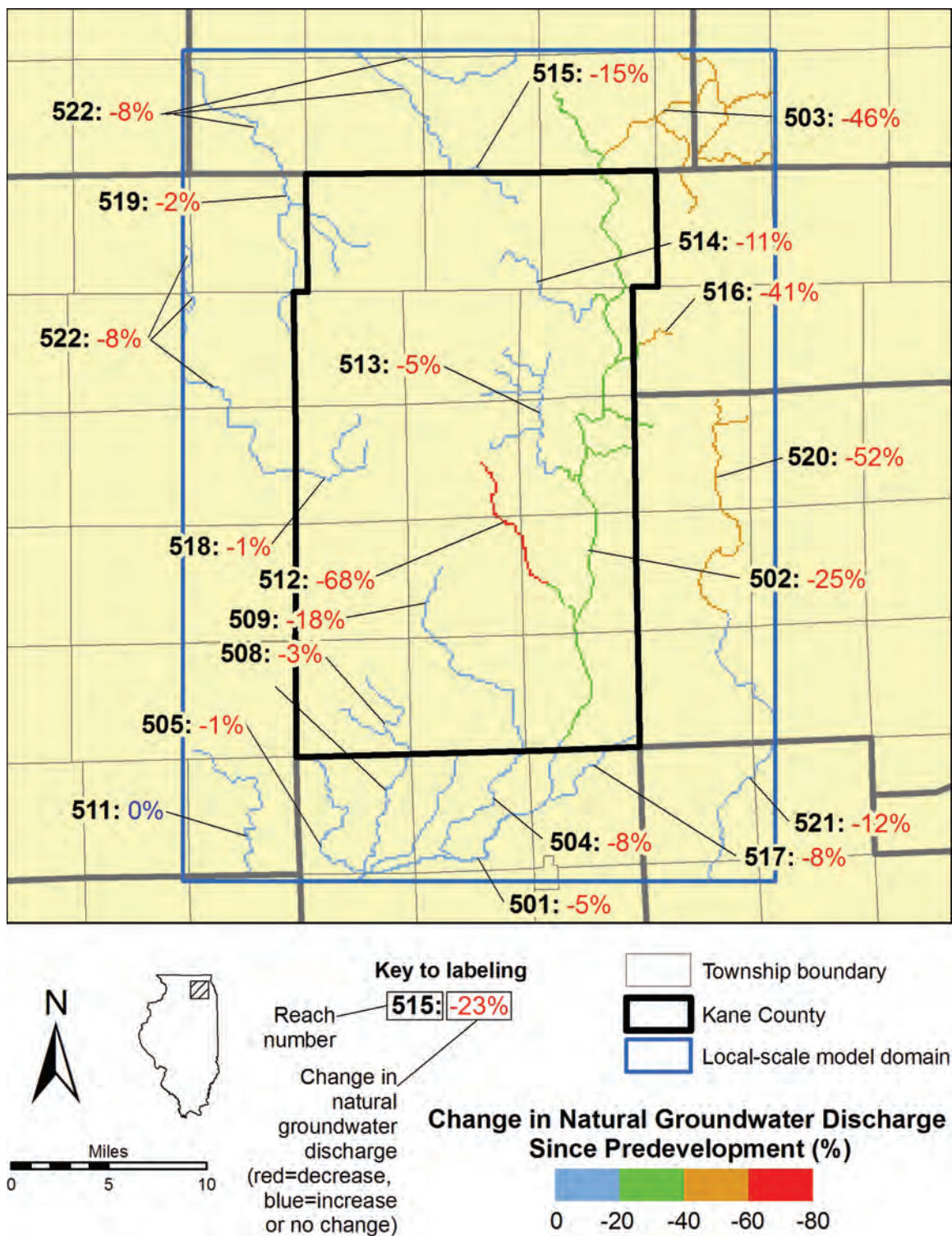


Figure 155. Estimated total change in natural groundwater discharge caused by pumping, by stream reach, at the end of 2003.

values in Figure 155 and Table 26 should not be regarded as changes in base flow, but merely changes in natural groundwater discharge to the stream reach.

It is also noteworthy that effluent can compensate for the reduction of streamflow caused by a reduction in natural groundwater discharge, but the degree to which this compensation occurs in Kane County area streams has not been investigated. Even if the volume of reduced flow is wholly compensated for by effluent, it is likely that differences in quality exist between the effluent and natural groundwater discharge that may affect the stream environment. Also, replacement of natural groundwater discharge as a sustaining source of streamflow with effluent, which enters streams at sporadically distributed points, may lead to irregularly distributed low flows, especially when combined with sporadically distributed surface intakes along the stream.

On the whole, the local-scale model suggests that in 2003 pumping has reduced natural groundwater discharge by about 17 percent in Kane County (Figure 156). Model simulations suggest that the reductions differ across the Kane County area, however, reflecting the irregular distribution of shallow pumping and variable hydrogeology (Figure 155, Table 26). In general, the greatest reductions in natural groundwater discharge occur in the areas of greatest groundwater withdrawals. The model suggests that, as of 2003, for the three watersheds partially covered by the local model domain (Figure 4), the portion of the Des Plaines watershed within the domain has, with a change of -25 percent, experienced the greatest reduction in simulated natural groundwater discharge due to pumping (Figure 157). Simulated natural groundwater discharge in the Fox watershed, which dominates the local domain, has declined by about 19 percent due to pumping, while simulated natural discharge in the comparatively rural Kishwaukee watershed has declined by about 6 percent due to pumping.

In 2003, for the stream reaches shown in Figure 154, the greatest reduction in simulated natural groundwater discharge due to pumping occurred along Mill Creek (reach 512), in east-central Kane County, where model results suggest that about 68 percent of base flow had been diverted into water-supply wells (Figure 155, Figure 158, and Table 26). It is noteworthy that this watershed is the location of Batavia wells 6, 7, and 8 and Geneva wells 8, 9, and 10, which began withdrawing water from the Upper and Lower Glasford Sand Units in 1989 and, as of 2003, obtained more than 3 Mgd from these wells. Given the scale of these withdrawals, simulated drawdown in the vicinity of the wells has been comparatively low, less than 20 ft (see page 252). Model results suggest that the low drawdown in the vicinity of the wells is at least partly attributable to the Batavia and Geneva wells capturing water from Mill Creek (either by diverting groundwater that would otherwise discharge to Mill Creek or by inducing leakage from the stream). In 2003, withdrawals from the six Batavia and Geneva supply wells totaled about 3.3 Mgd, and simulated base flow reduction since 1988 due to pumping on Mill Creek was about 1.7 Mgd. That pumping and base flow reduction are not equivalent suggests that a portion of the withdrawals from the Batavia and Geneva wells is derived from reduction of groundwater discharge in adjacent watersheds. Indeed, mapping of simulated changes in drain output suggests that a portion of the yield of the Batavia and Geneva wells is obtained from the Ferson and Blackberry Creek watersheds (drained by reaches 513 and 509, respectively), immediately north and south of the Mill Creek watershed. Simulated base flow reduction due to pumping between 1988 and 2003 in reaches 513 and 509 is about 1.3 Mgd. The total 1988-2003 base flow reduction due to

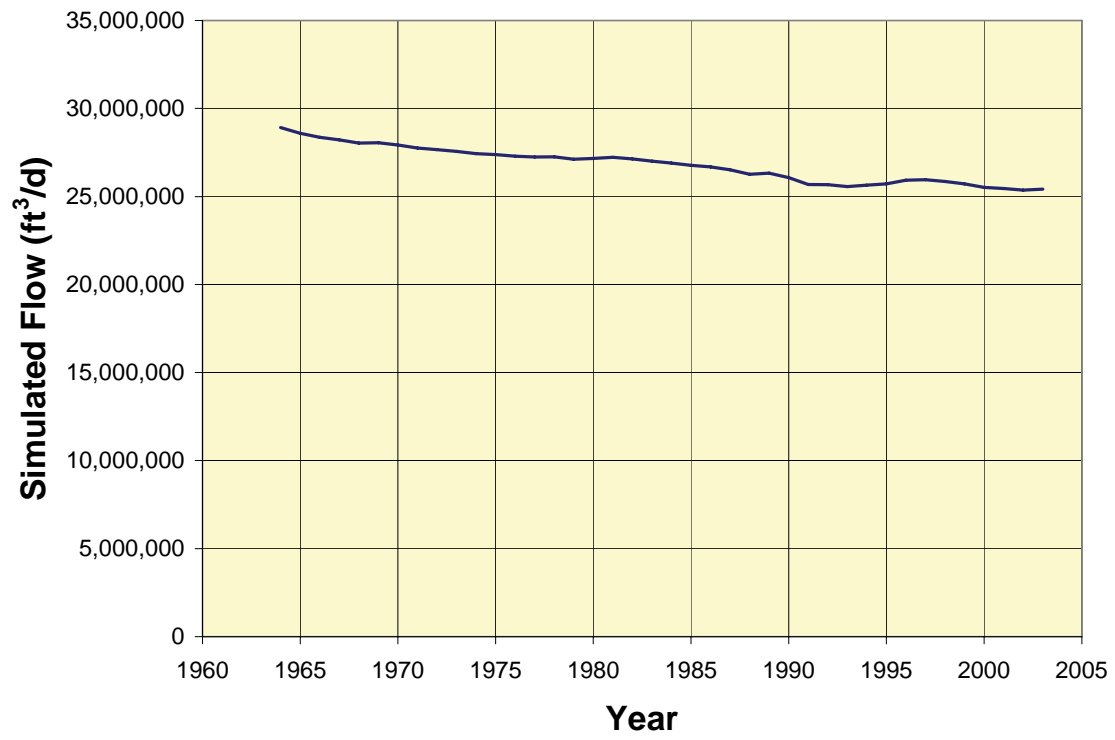


Figure 156. Total simulated natural groundwater discharge in local model domain.

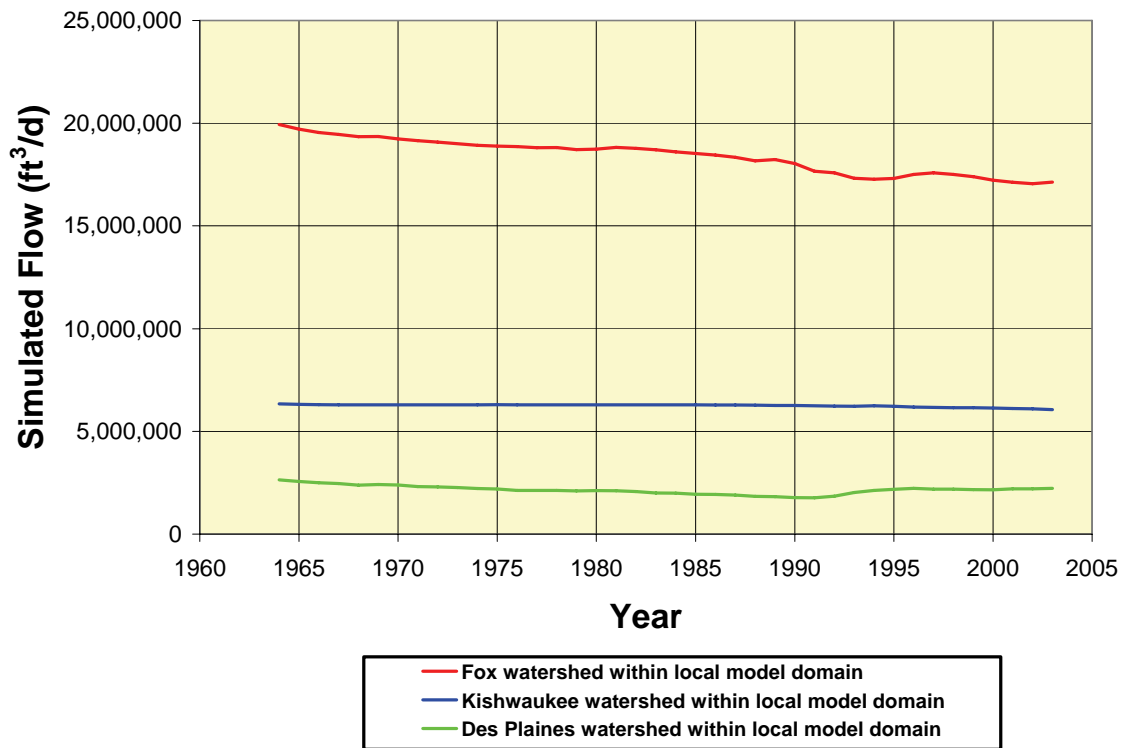


Figure 157. Total simulated natural groundwater discharge in watersheds covering local model domain.

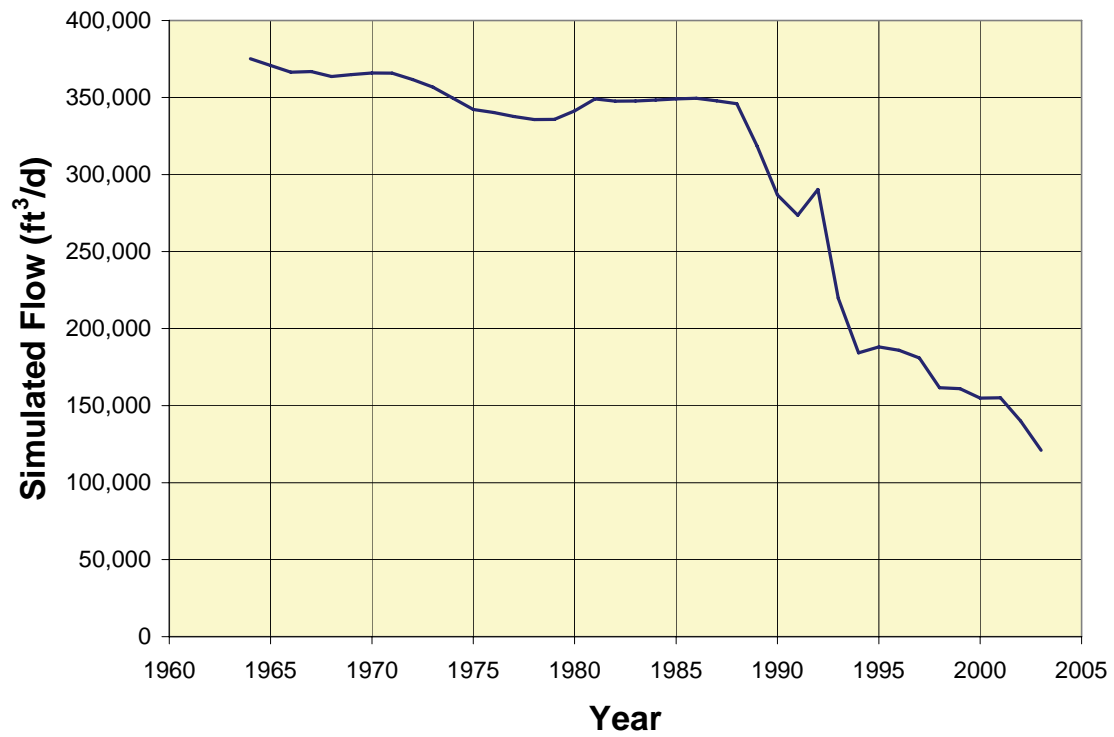


Figure 158. Simulated natural groundwater discharge to Mill Creek upstream of Batavia (reach 512).

pumping in Mill Creek, Ferson Creek, and Blackberry Creek (upstream of Montgomery) was simulated at about 3.0 Mgd, which is much closer to the total 2003 withdrawal of 3.3 Mgd, and even closer to the 2002 withdrawal of about 2.9 Mgd, suggesting that the difference between 2003 pumping and simulated natural discharge reduction of about 0.3 Mgd was contributed from aquifer storage and streamflow reduction in the nearby watershed of the main stem of the Fox River.

Model results suggest that pumping has caused a reduction in natural groundwater discharge to the West Branch of the DuPage River (reach 520) upstream of Warrenville, of about 52 percent in 2003 (Figure 155, Table 26, and Figure 159). Simulations suggest that streamflow here has recovered some since 1990, when natural groundwater discharge to the stream had been reduced by about 61 percent due to pumping. The modeling suggests that this recovery reflects reduced pumping in the area resulting principally from a 1992 shift by many DuPage County public water systems from groundwater to a Lake Michigan water source. Model simulation suggests comparable recoveries of natural groundwater discharge to the portions of the watersheds of Poplar Creek (reach 516) (Figure 160) and of the DuPage River and lower portion of the West Branch DuPage River downstream of Warrenville (reach 521) (Figure 161). Model simulations suggest that the post-1990 increase in natural groundwater discharge to reach 521 reflects the same 1992 shift to a Lake Michigan water source in DuPage County that affected reach 520. Similarly, increases in simulated natural groundwater discharge to Poplar Creek (reach 516) began in the mid-1980s, when several northwest Cook County public water systems shifted from groundwater to a Lake Michigan water source.

Reduction in simulated natural groundwater discharge due to pumping in 2003 to the main stem of the Fox River in the local model domain (reaches 501-503) was appreciable—about 25 percent (Figure 162). Reduction varied along the stream from about 46 percent upstream of Algonquin (reach 503), to about 25 percent in the reach between Algonquin and Montgomery (reach 502) (Figure 163), to about 5 percent downstream of Montgomery (reach 501). These reductions reflect the irregular distribution of wells and hydraulic connections between source aquifers and the river along the Fox Valley.

3.2.3. *Groundwater Circulation*

As discussed in Section 1.7.2, groundwater flows from areas of high head to areas of low head. Thus, the simulated head distributions described in Section 3.2.1 are expressed as groundwater circulation patterns that may themselves be divided into flow systems, separated by *groundwater divides*, which range from local to regional in scale (see Section 1.7.4). Typically, flow systems in shallow materials are localized and increase in size with depth of burial. Groundwater divides, particularly those separating regional flow systems, do not necessarily coincide with surface-water divides. Groundwater circulation in the deep and shallow units in the Kane County area is illustrated in this section of the report using simulated flow arrows denoting directions of groundwater flow.

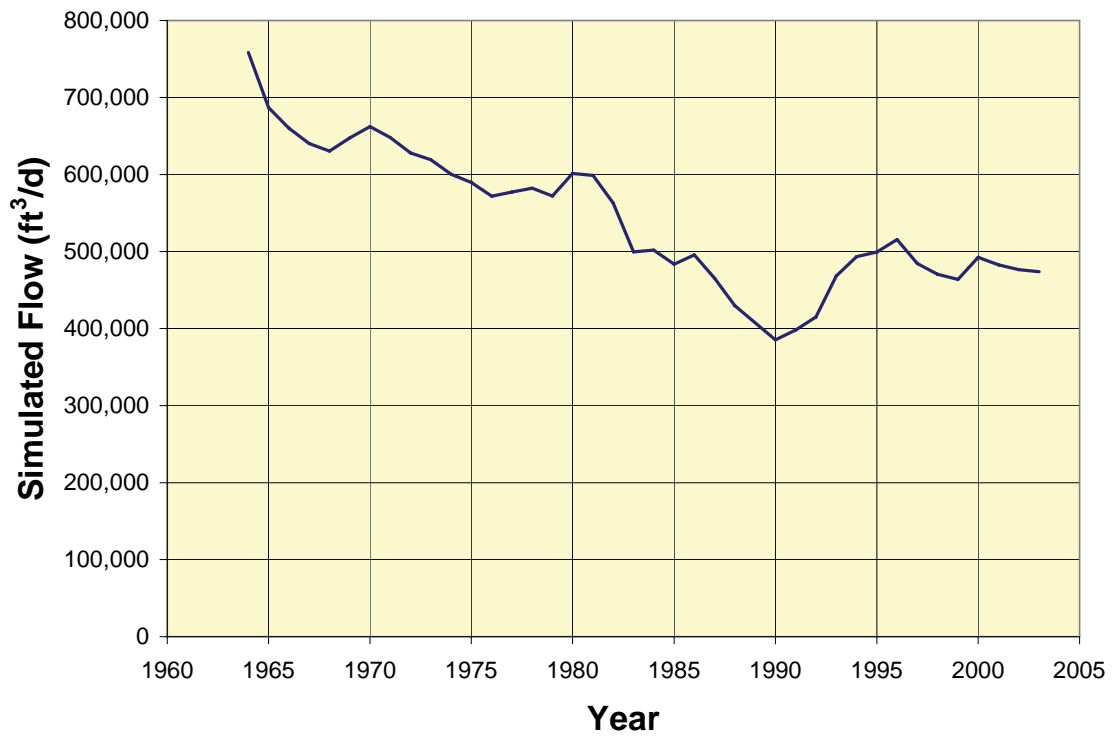


Figure 159. Simulated natural groundwater discharge to the West Branch of the DuPage River upstream of Warrenville (reach 520).

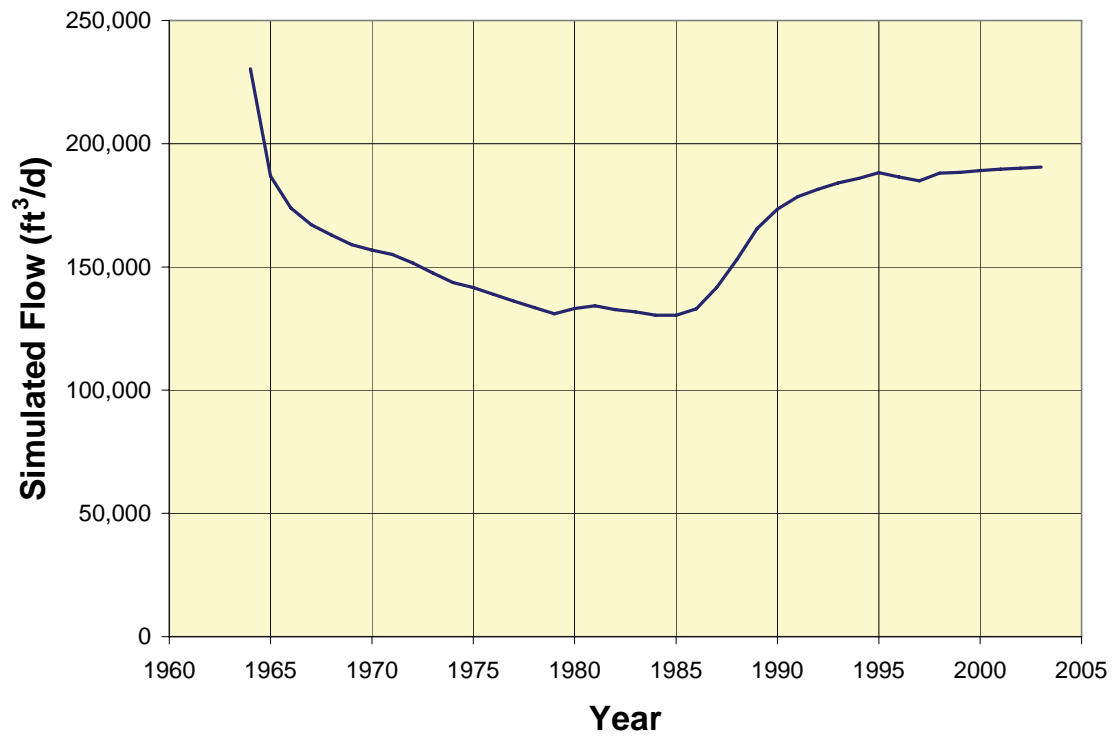


Figure 160. Simulated natural groundwater discharge in the local model domain to Poplar Creek (reach 516).

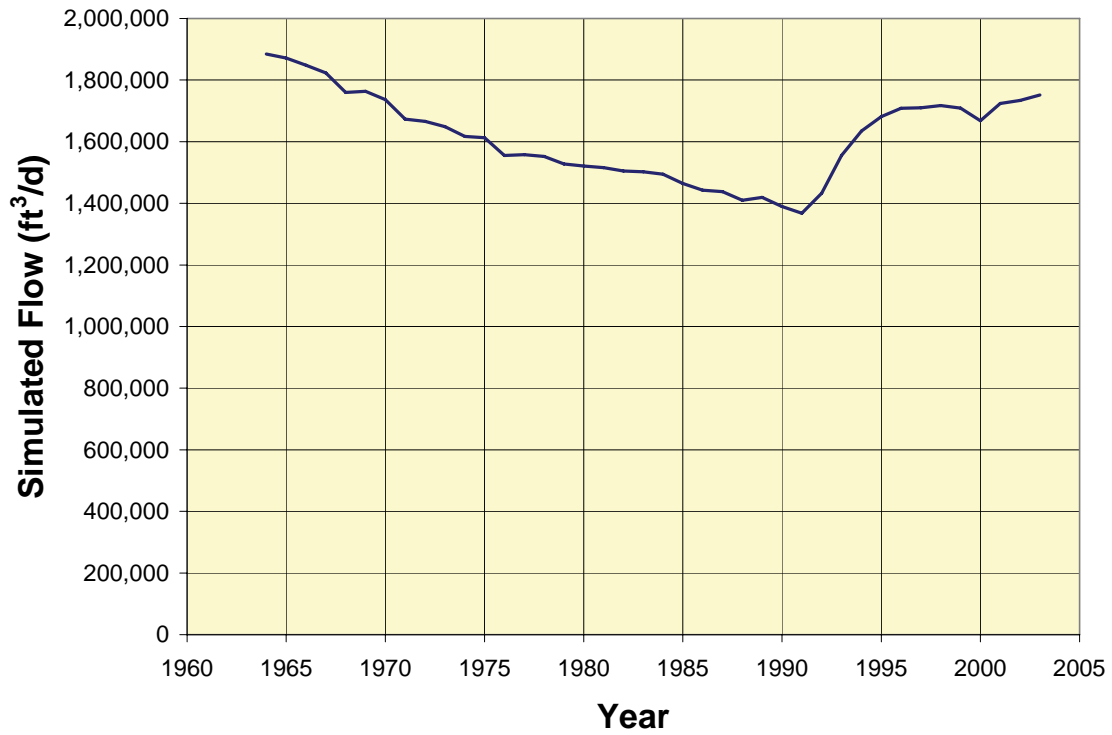


Figure 161. Simulated natural groundwater discharge in the local model domain to the DuPage River and West Branch of the DuPage River downstream of Warrenville (reach 521).

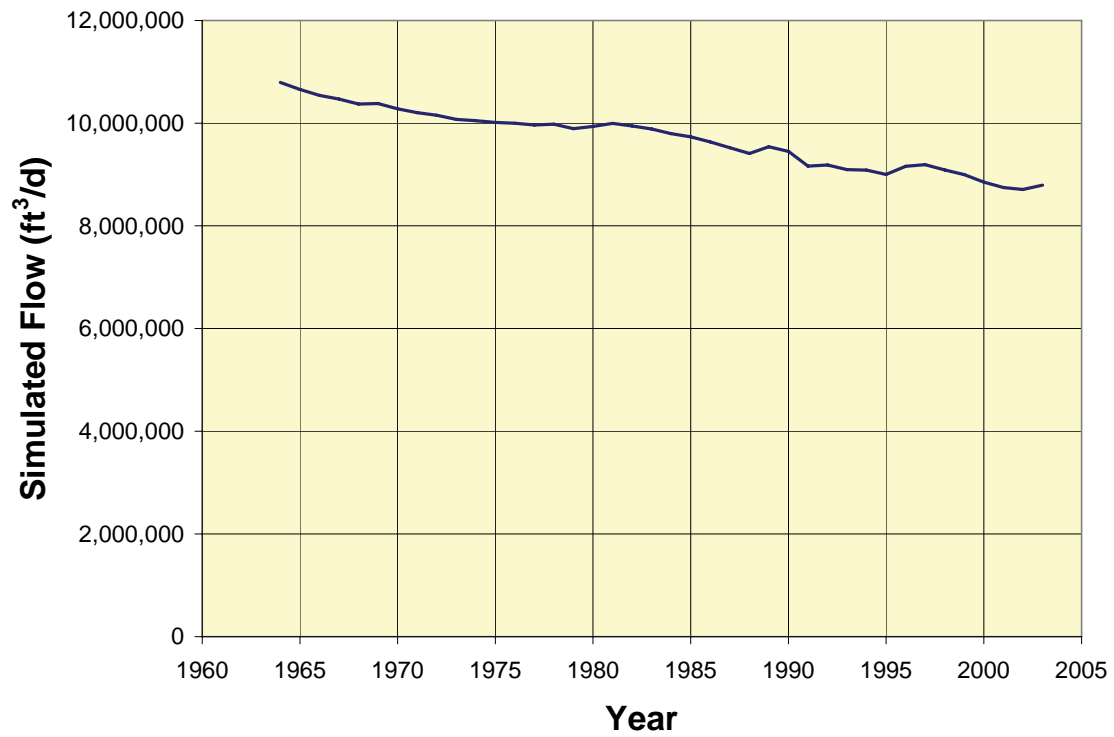


Figure 162. Simulated natural groundwater discharge in the local model domain to the Fox River (reaches 501, 502, and 503).

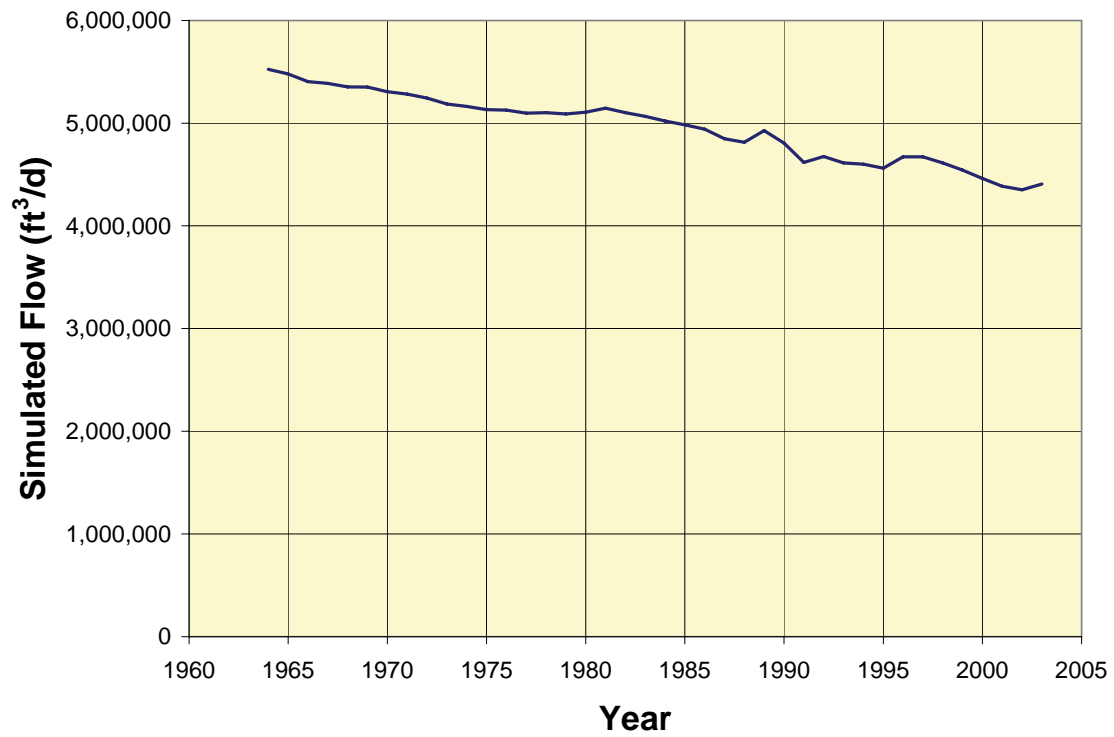


Figure 163. Simulated natural groundwater discharge in the local model domain to the Fox River from Algonquin to Montgomery (reach 502).

3.2.3.1. Deep Units

Groundwater circulation in the Ancell Unit, determined from simulations using the regional-scale model, is discussed here as representative of circulation in most of the deep aquifers. Prior to development, groundwater in the deep aquifers of northeastern Illinois (as exemplified by the Ancell Unit in Figure 164) discharged into (1) streams at westward locations lacking cover by the Maquoketa and Upper Bedrock Units, and (2) Lake Michigan to the east. A groundwater flow divide separated the deep groundwater discharging into these two sinks. In the northern part of northeastern Illinois, this divide approximated the edge of the area of cover by the Maquoketa Unit, as it did in southeastern Wisconsin (Feinstein et al., 2005a; 2005b). Under the influence of important discharge areas along the lower Fox and upper Illinois Rivers, the divide diverged from the position along the zero-edge of the Maquoketa Unit in present east-central DeKalb County and, from there, trended southeastward into Indiana.

The area west of the divide thus encompassed both topographically driven local flow systems, west of the area of cover by the Maquoketa and Upper Bedrock Units (where leakage to the Ancell Unit was comparatively high, as were groundwater velocities in the Ancell), and a single, regional-scale flow system in the area of Maquoketa/Upper Bedrock cover that was driven by discharge to streams in the area lacking cover. Leakage rates in the latter area were low, and flow toward the western discharge areas was comparatively sluggish. The most important discharge locations were the lower Fox and upper Illinois Rivers, where the Ancell subcrops the Quaternary Unit and, in some areas, is exposed at land surface, so that discharge was unimpeded or less impeded by overlying units.

Pumping resulted in the addition of a third diversion area, in which groundwater was diverted to water-supply wells, to the predevelopment pattern of discharge to streams and Lake Michigan. In reality, pumping resulted in the addition of multiple diversion areas, each surrounding a well; because the individual diversion areas were concentrated geographically, coalesced fairly rapidly, and supplied wells, they may reasonably be considered together. New groundwater divides appeared that separated the area of diversion to wells from the predevelopment areas of discharge to streams to the west and Lake Michigan to the east. By 1880, the area of diversion to wells occupied a significant portion of the area which, under predevelopment conditions, had contributed groundwater to Lake Michigan (Figure 165). By 1920, the groundwater divide separating diversion to wells from natural diversion to Lake Michigan had moved completely out of northeastern Illinois (Figure 166). This fairly rapid eastward movement of the divide reflects the fact that the predevelopment hydraulic gradient was very gentle initially in the area having Maquoketa/Upper Bedrock cover, and that pumping easily shifted the gradient as a consequence of very low leakage rates through the bedrock units overlying the Ancell.

With the addition of pumping in western and southern pumping centers in the collar counties, pumping during the 20th century caused the position of the deep groundwater flow divide to shift westward and southward so that, by 2002, it was located, for the most part, outside of the regional model nearfield (Figure 167). East of the divide, the groundwater is captured entirely by wells. In general, pumping has caused the divide to move westward to a location that is roughly coincident with the zero edge of

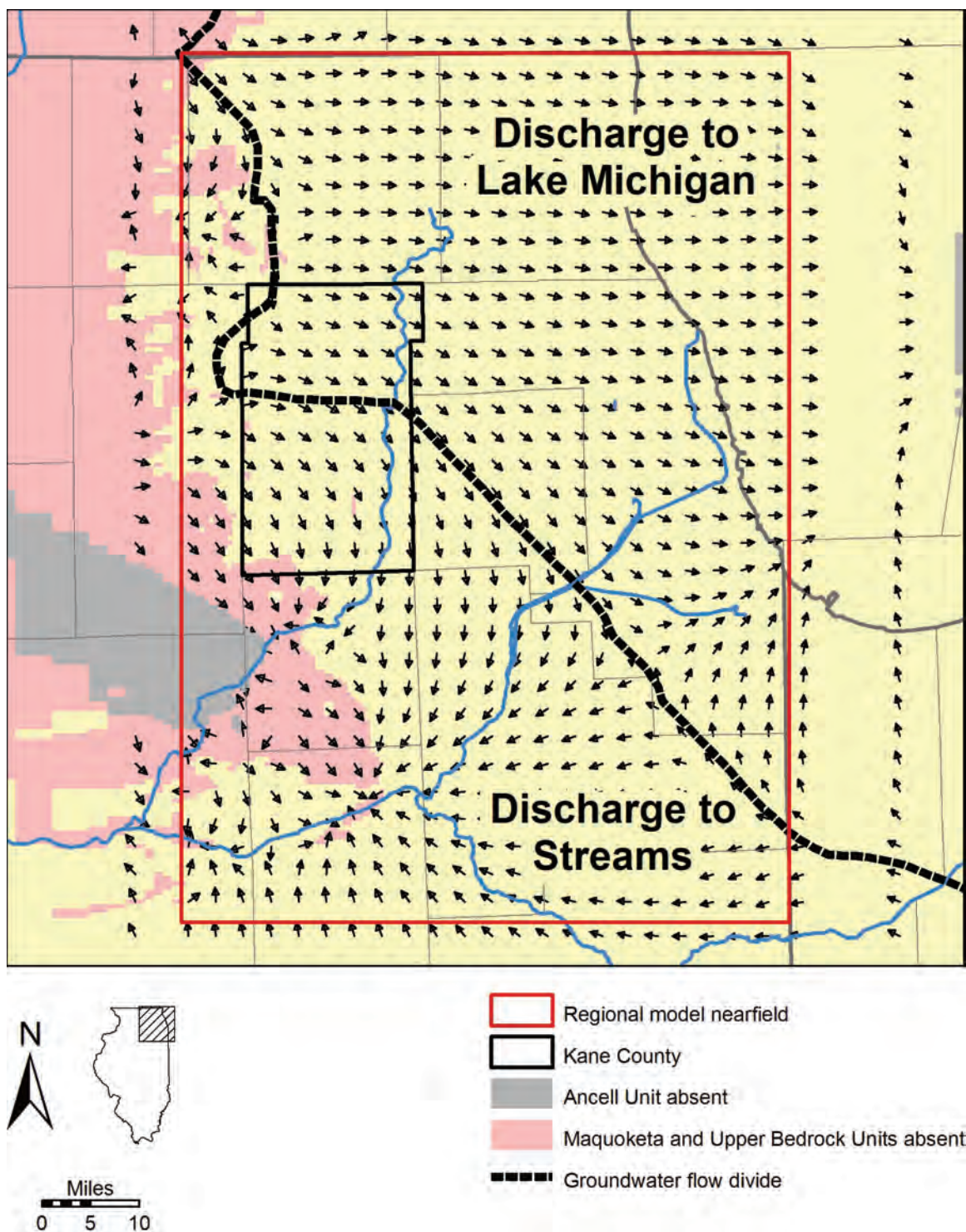


Figure 164. Simulated groundwater flow directions and estimated groundwater flow divides in the Ancell Unit under predevelopment conditions.

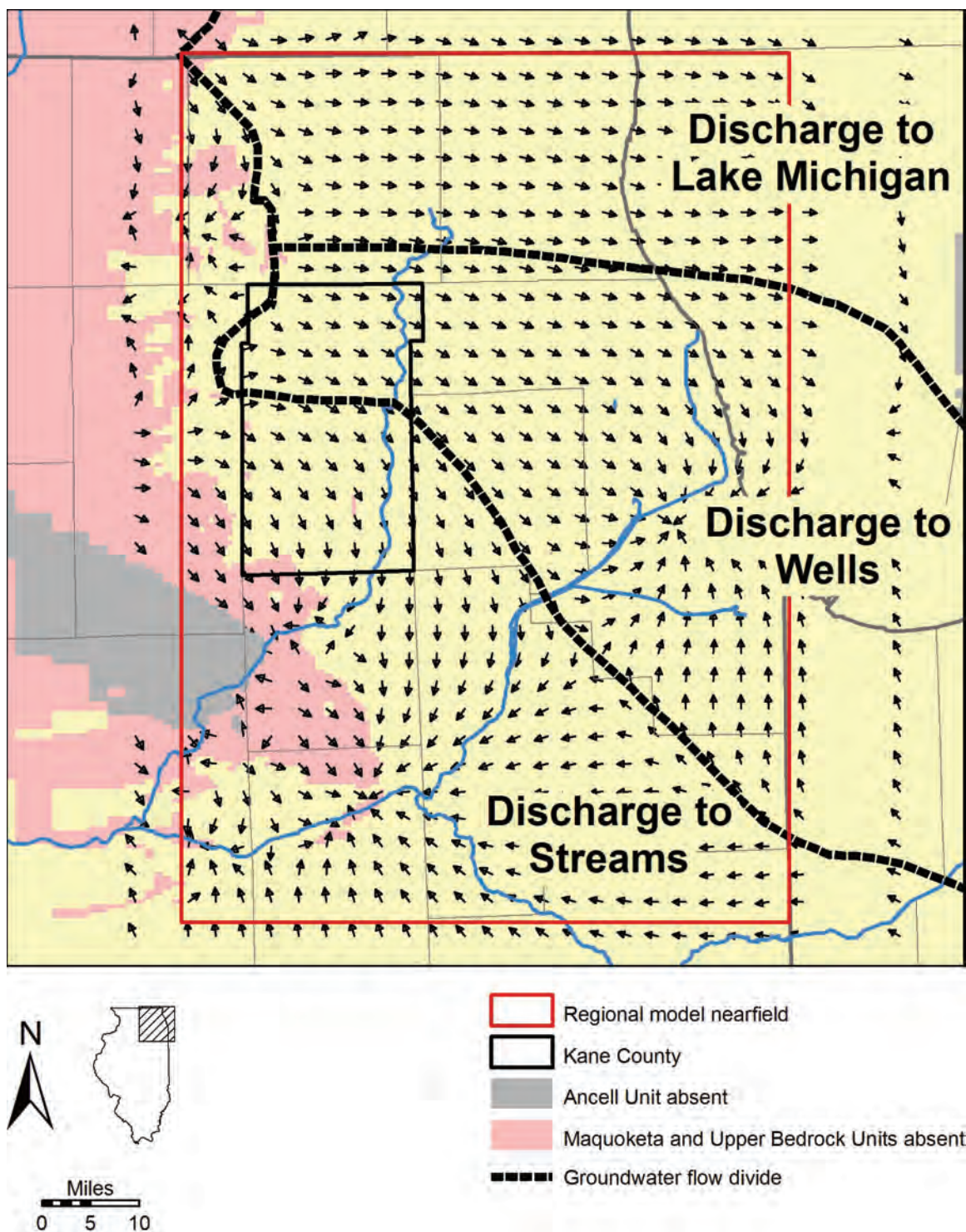


Figure 165. Simulated groundwater flow directions and estimated groundwater flow divides in the Ancell Unit in 1880.

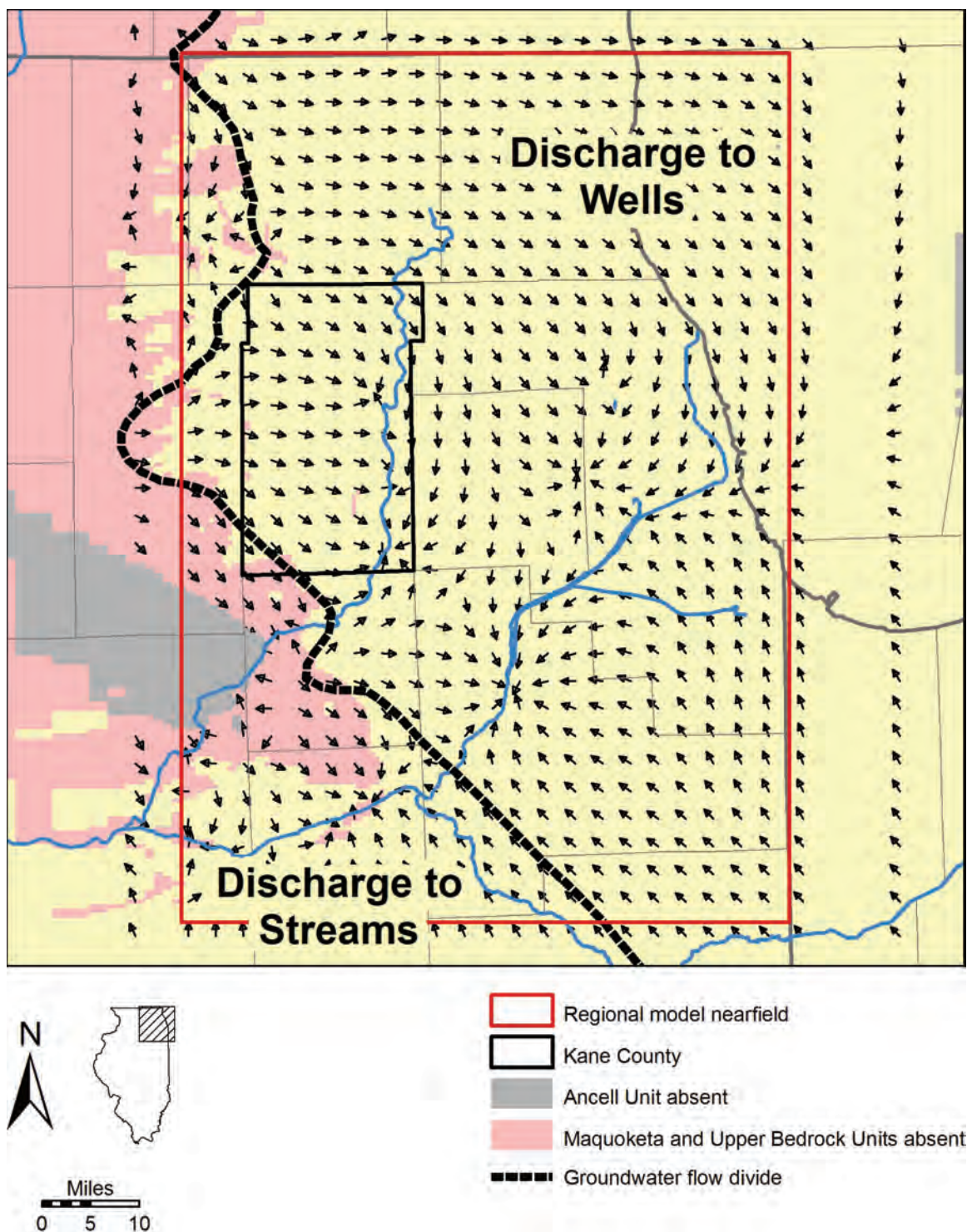


Figure 166. Simulated groundwater flow directions and estimated groundwater flow divides in the Ancell Unit in 1920.

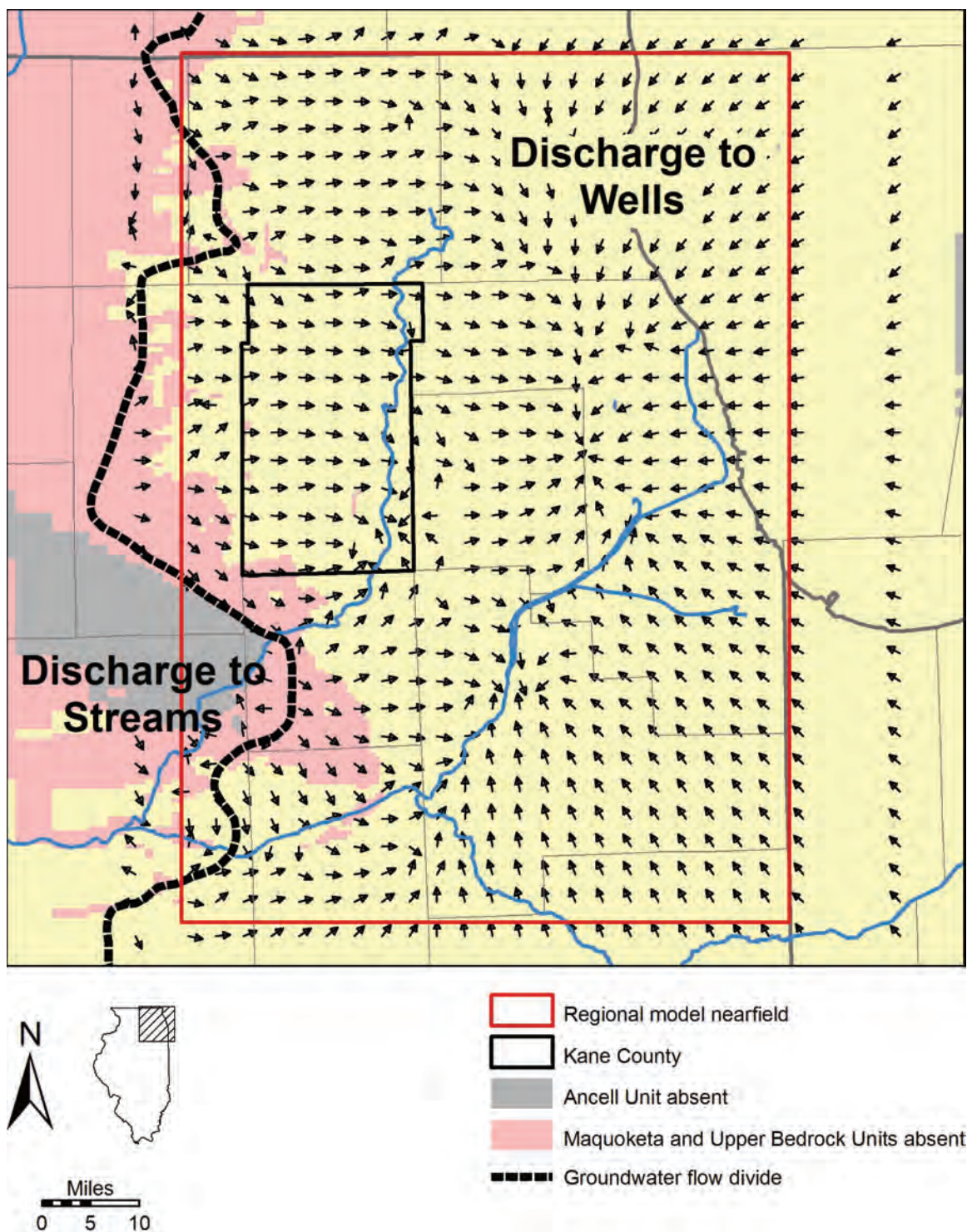


Figure 167. Simulated groundwater flow directions and estimated groundwater flow divides in the Ancell Unit in 2002.

the combined Maquoketa and Upper Bedrock Units. In some areas where the Galena-Platteville overlies the Ancell Unit, slightly reducing leakage to the Ancell from the surface, the divide has even moved slightly beyond this zero edge, but, in general, the comparatively high rates of leakage in the area lacking Maquoketa/Upper Bedrock cover have caused the zero edge of these units to function as a stopping point for the westward migration of the flow divide. In the northern part of the nearfield, where the predevelopment divide was closely associated with the zero edge of the Maquoketa Unit, the divide has shifted less than 5 miles westward since predevelopment. In the southern part of the nearfield, however, where the predevelopment divide was located in the area of cover by the Maquoketa and Upper Bedrock Units, the divide has shifted tens of miles westward to approximately the zero edge of Maquoketa/Upper Bedrock cover. The greater westward migration of the divide in the southern part of the nearfield signifies the very low rates of leakage in the area of Maquoketa/Upper Bedrock cover that, under predevelopment conditions, had discharged to streams, principally the lower Fox and upper Illinois Rivers.

3.2.3.2. Shallow Units

Both and regional and local-scale modeling suggests that, prior to development, topography, geology, and locations of surface-water bodies exerted strong control over directions of shallow groundwater flow. Shallow groundwater in Kane County circulated within numerous local-scale flow systems that received recharge locally and discharged into local surface-water bodies. As an example, Figure 168 shows flow directions in the Shallow Bedrock Aquifer under predevelopment conditions determined using the local-scale model. Flow directions vary considerably across the Kane County area. Flow directions in shallower sand and gravel units are, in general, even more variable than those in the Shallow Bedrock Aquifer, reflecting flow within even smaller local flow systems.

Pumping has had little effect on simulated directions of flow in the shallow aquifers at the resolution of the local-scale model. This reflects the relative proximity of hydraulic connections between the shallow aquifers and surface waters.

3.2.4. *Vertical Movement between Shallow and Deep Aquifers*

Under predevelopment conditions, model simulations suggest that exchange of groundwater between the shallow and deep aquifers was limited to the area where the Maquoketa and Upper Bedrock Units are absent or very thin and vertical leakage was more-or-less unimpeded (Figure 169). In this area, groundwater circulated in local flow cells, and flux across the top of the Ancell Unit shifted from downward to upward across comparatively short lateral distances. In most of the area depicted in Figure 169, modeling suggests that flux of groundwater across the top of the Ancell Unit occurred at low rates, but in limited areas, rates can be more substantial (greater than 0.001 ft/d), both under predevelopment conditions as well as under conditions of pumping from the deep aquifers. Highest rates of simulated flux across the top of the Ancell occur in the area where the Ancell is exposed at the bedrock surface, in the southwestern part of the regional model nearfield and immediately west of there. Greatest simulated flux occurs where the Ancell Unit is overlain by stream channels, most notably those of the lower Fox River and upper Illinois River.

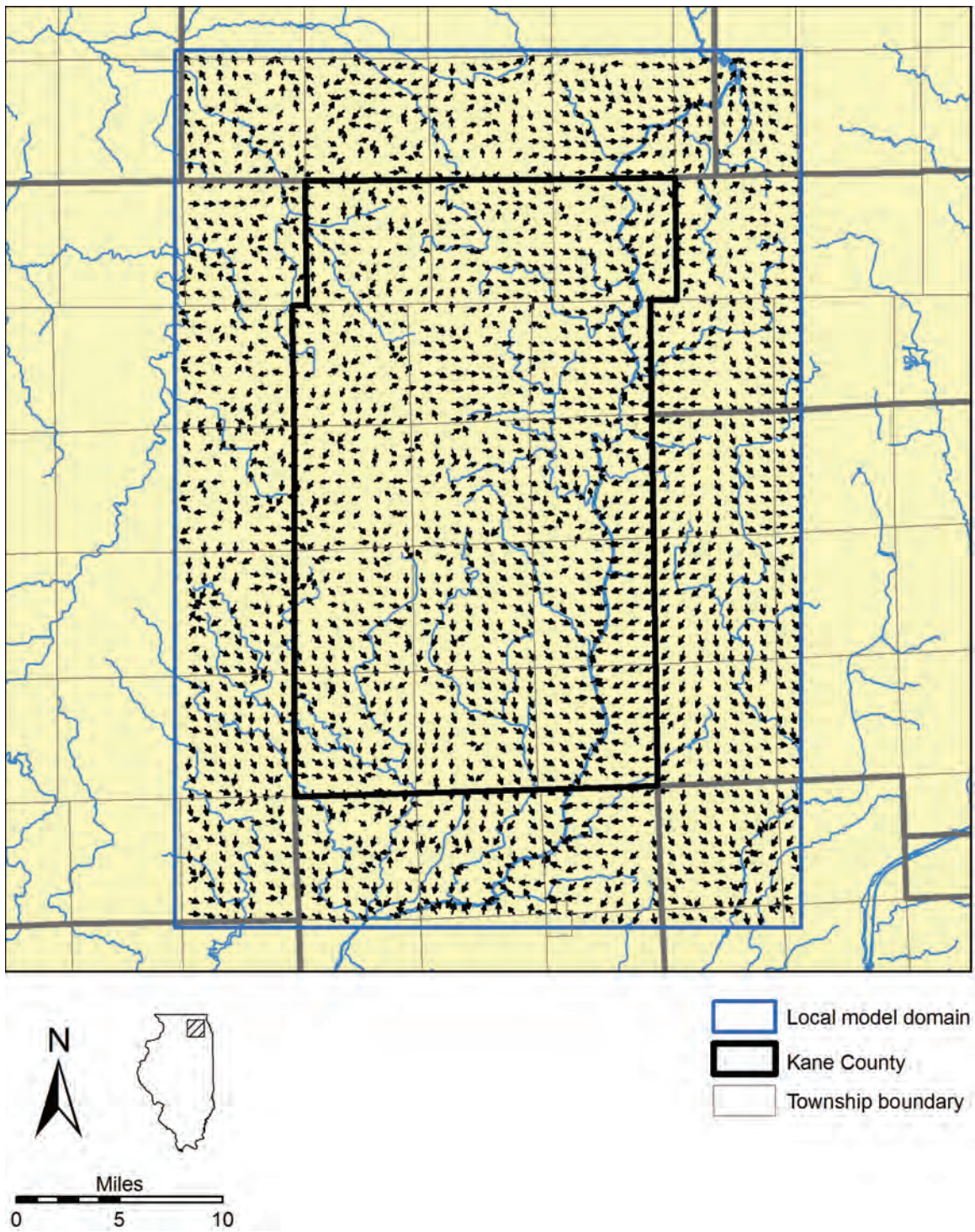


Figure 168. Simulated 2003 groundwater flow directions in the Shallow Bedrock Aquifer in the Kane County area.

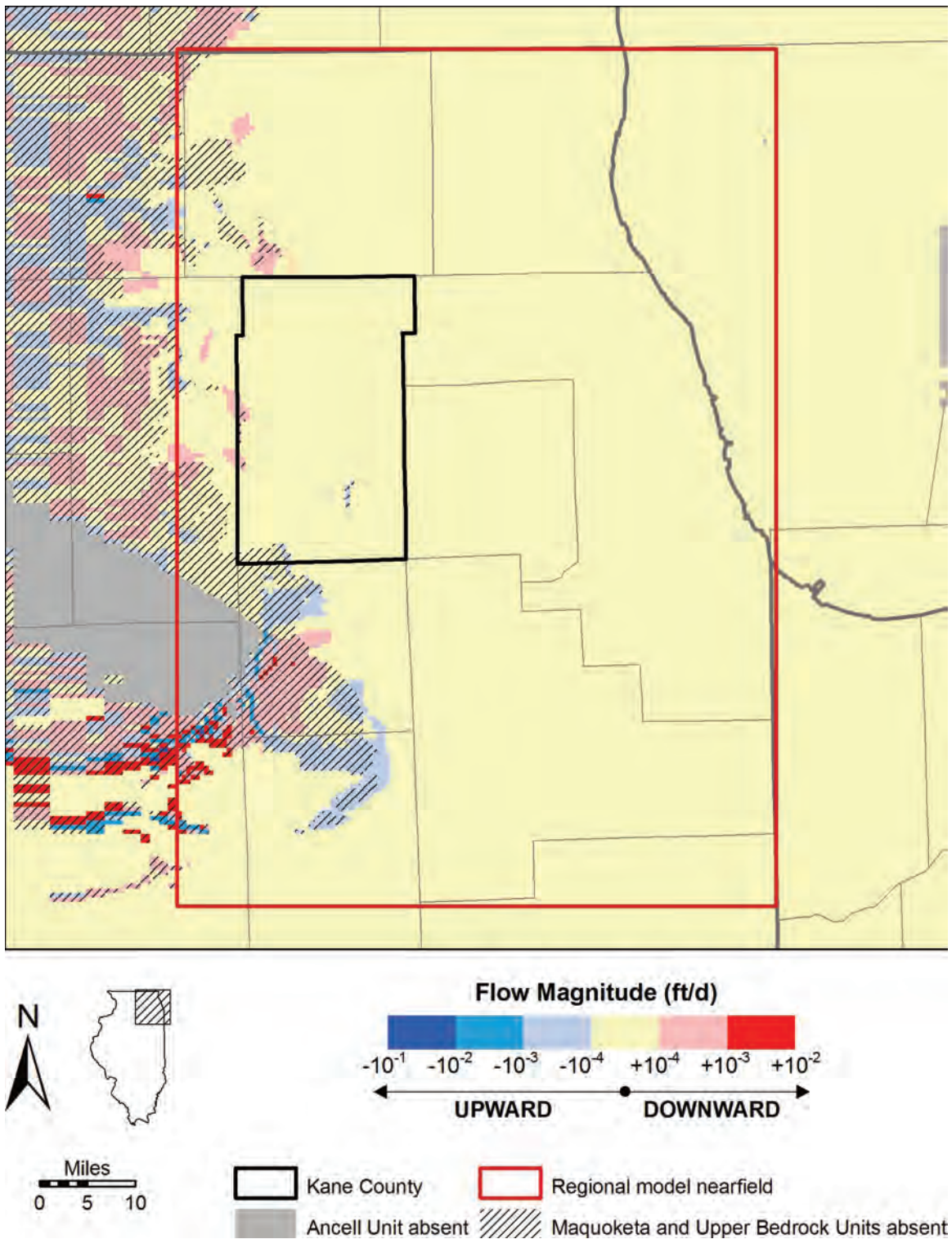


Figure 169. Simulated vertical flow across top of Ancell Unit under predevelopment conditions.

Pumping from the deep aquifers increases simulated downward flow across the top of the Ancell Unit. Model simulations suggest that downward flow increases where large withdrawals result in significant downward vertical hydraulic gradients, even in the area of Maquoketa/Upper Bedrock cover. The simulations further suggest that where the upper Galena-Platteville becomes desaturated (green areas of Figure 170 and Figure 171), the resulting interruption of the vertical hydraulic gradient causes flux to drop to zero as the MODFLOW model cells become inactive dry cells. Because the vertical hydraulic gradient is greatest at the margins of the desaturated areas, limited areas of very high simulated downward flow are sometimes present in these marginal locations. Simulation of the reduction in deep aquifer withdrawals during the 1980s and early 1990s causes a reduction in the area of downward flow across the top of the Ancell. By 2002, upward flow becomes established, in response to recovery of Ancell heads, in limited areas of Cook County (Figure 171).

Model simulations show that pumping causes an increase in downward flow in areas where predevelopment flux was also downward, while in other areas it causes an outright reversal of flow across the top of the Ancell, so that the direction of movement shifted from upward under predevelopment conditions to downward with pumping stress (Figure 172). In still other areas pumping causes downward flow to occur where predevelopment flow magnitude had been negligible (less than 0.0001 ft/d) (as shown for 2002 in Figure 173). Reversal of simulated predevelopment upward flow is most notable in north-central Grundy County, south-central Kendall County, and northwestern Kendall County, where model simulations suggest that the reversal is a consequence of head reduction caused by pumping at Joliet and Aurora (Figure 172). Simulations suggest that downward flow becomes established in an area of negligible predevelopment flux across the top of the Ancell in the area extending from northern Will County northward through eastern Kane and western DuPage Counties, a region of high pumping from the deep aquifers, and is scattered in other locations near large pumping centers (Figure 173).

3.2.5. *Comparison with Groundwater Flow Modeling in Southeastern Wisconsin*

The output of the regional-scale model was compared with the output of recent groundwater-flow modeling centered on southeastern Wisconsin (Feinstein et al., 2005b) along the boundary of northeastern Illinois and southeastern Wisconsin, which is approximately the boundary of the nearfields of the two models. Since the two models were developed to provide accurate simulation of groundwater flow in these nearfield areas, the scope of this comparison is limited in this nearfield-boundary area. The comparison is also limited in scope to simulated heads in the deep units, since the approach adopted for the present study was to employ the local-scale shallow model to provide accurate simulation of shallow groundwater flow, and the local-scale model domain is located some distance from the state boundary. For purposes of conciseness, in this discussion the southeastern Wisconsin model described by Feinstein et al. (2005a; 2005b) is referred to as the *Wisconsin model* and the regional-scale model developed for the present study as the *Illinois model*.

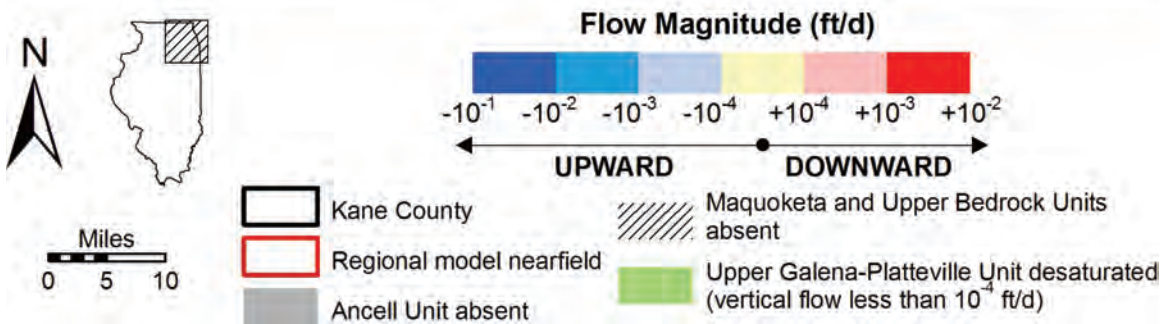
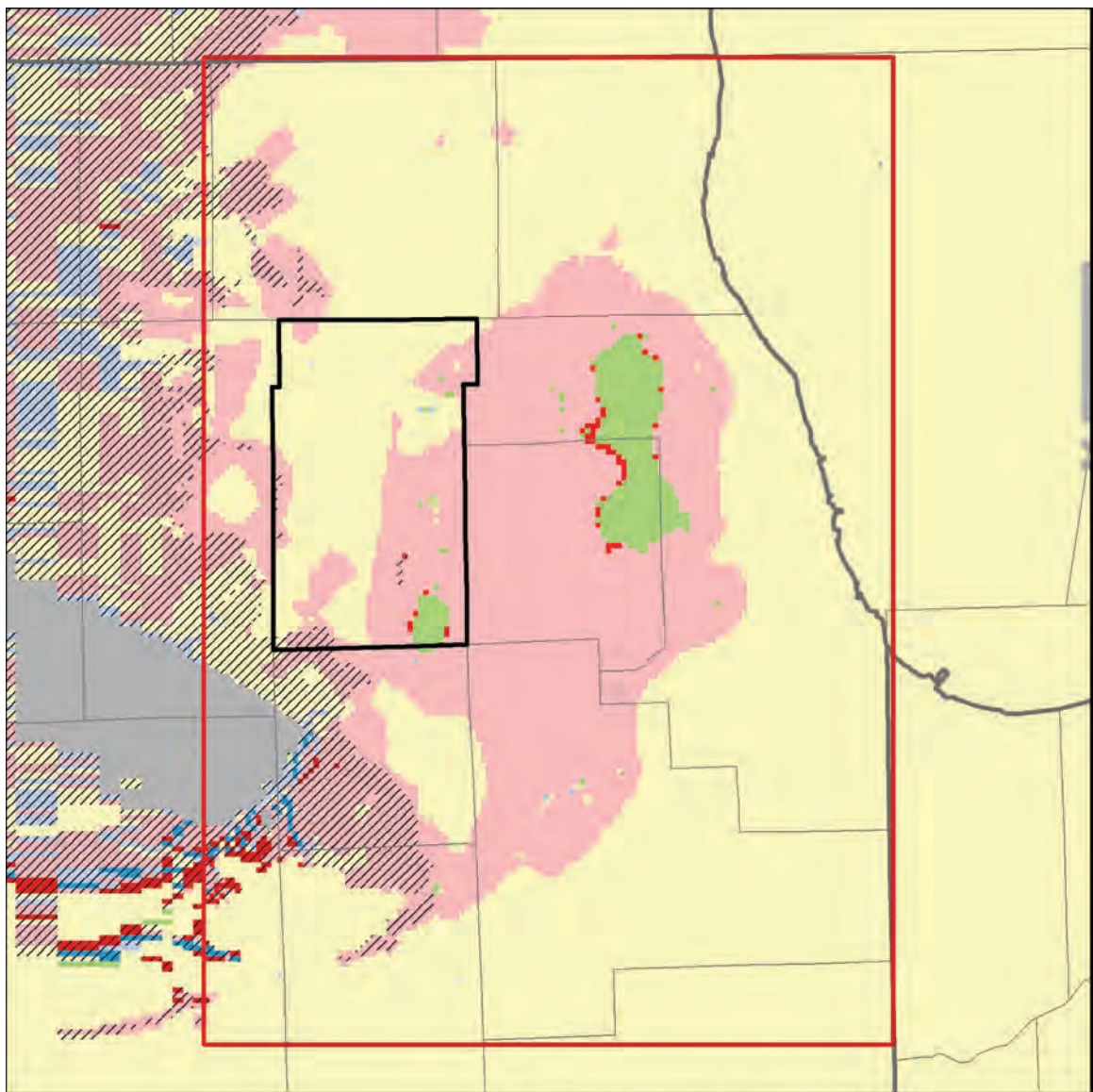


Figure 170. Simulated vertical flow across top of Ancell Unit in 1985.

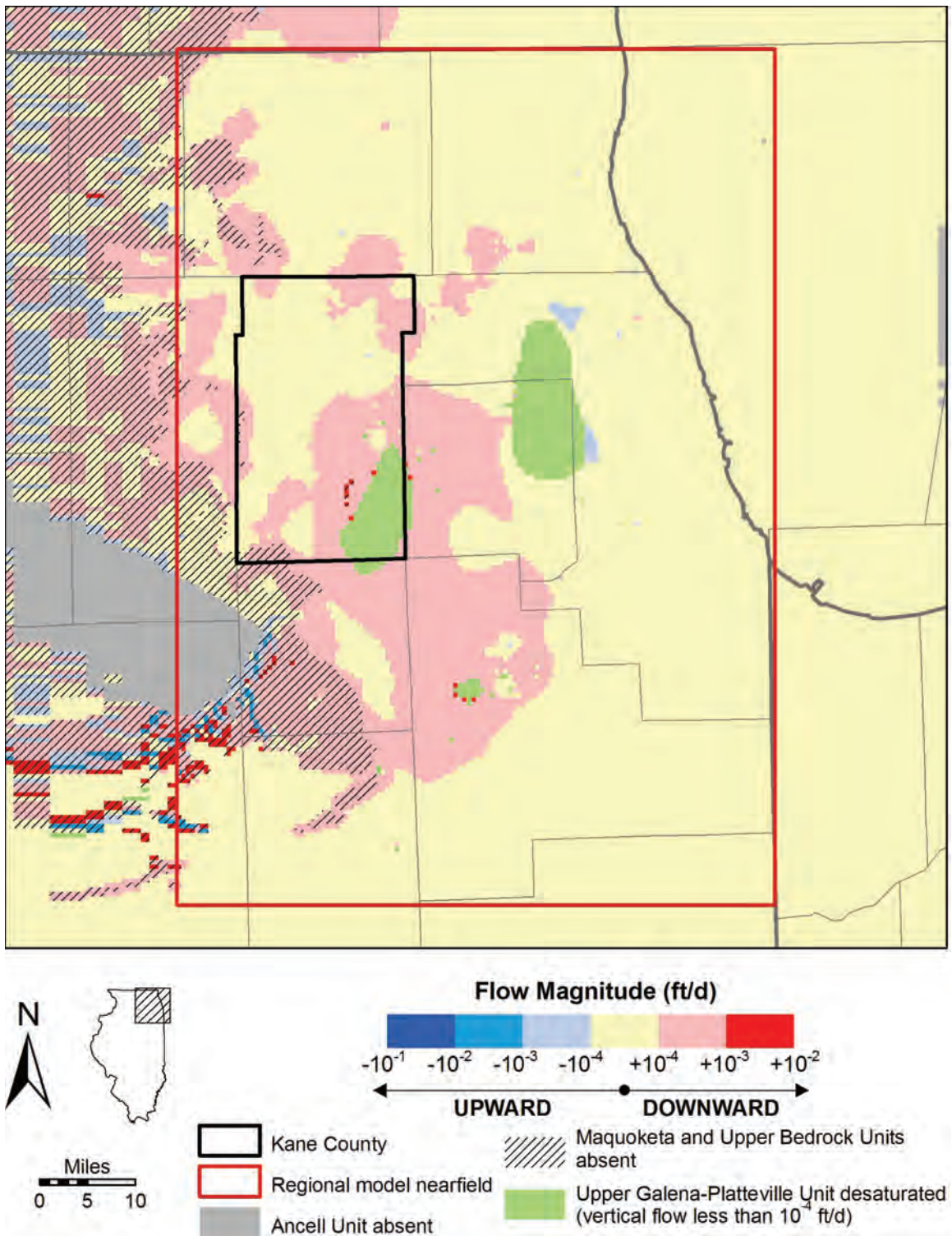


Figure 171. Simulated vertical flow across top of Ancell Unit in 2002.

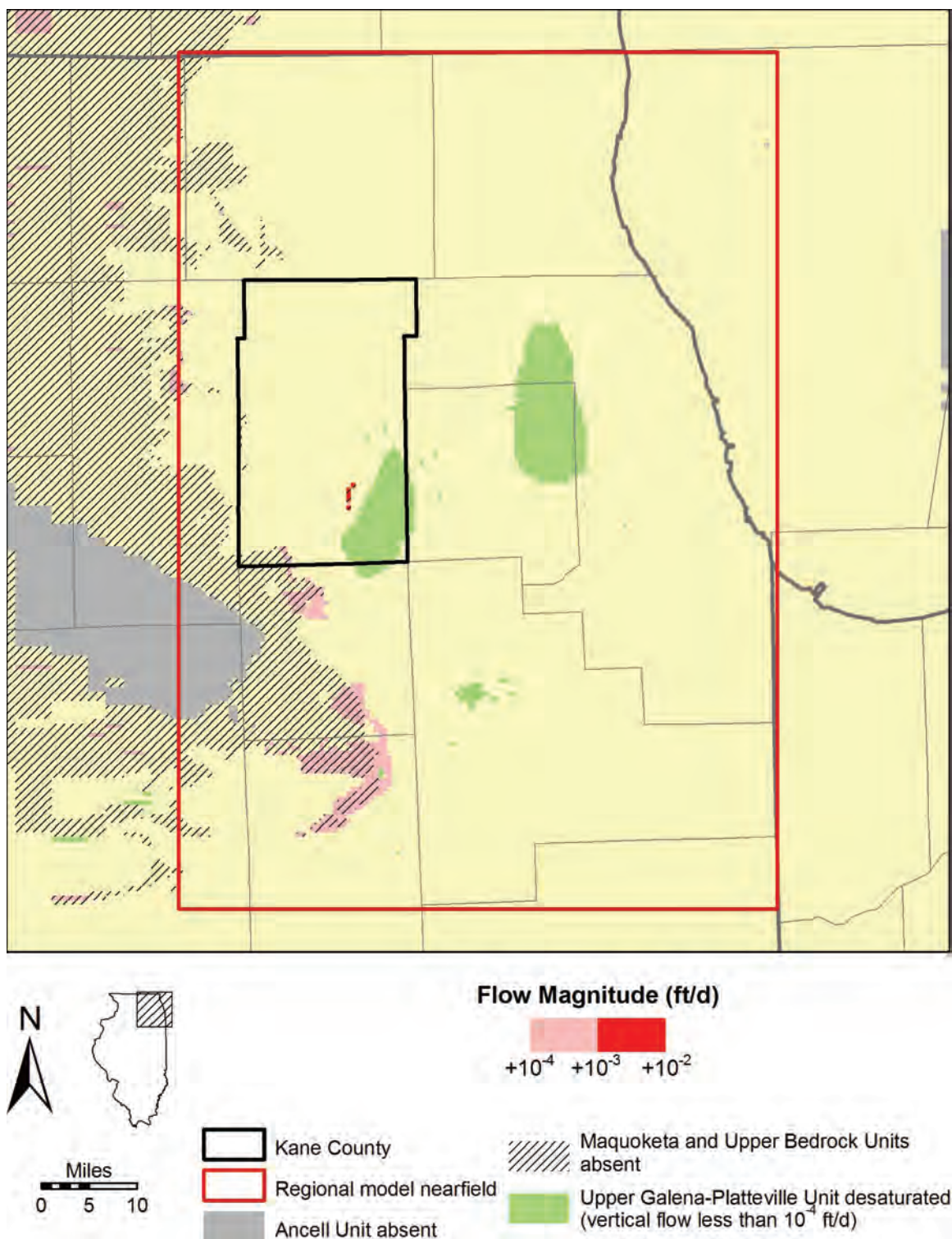


Figure 172. Areas of flow reversal across the top of the Ansell Unit, from upward under predevelopment conditions to downward in 2002.

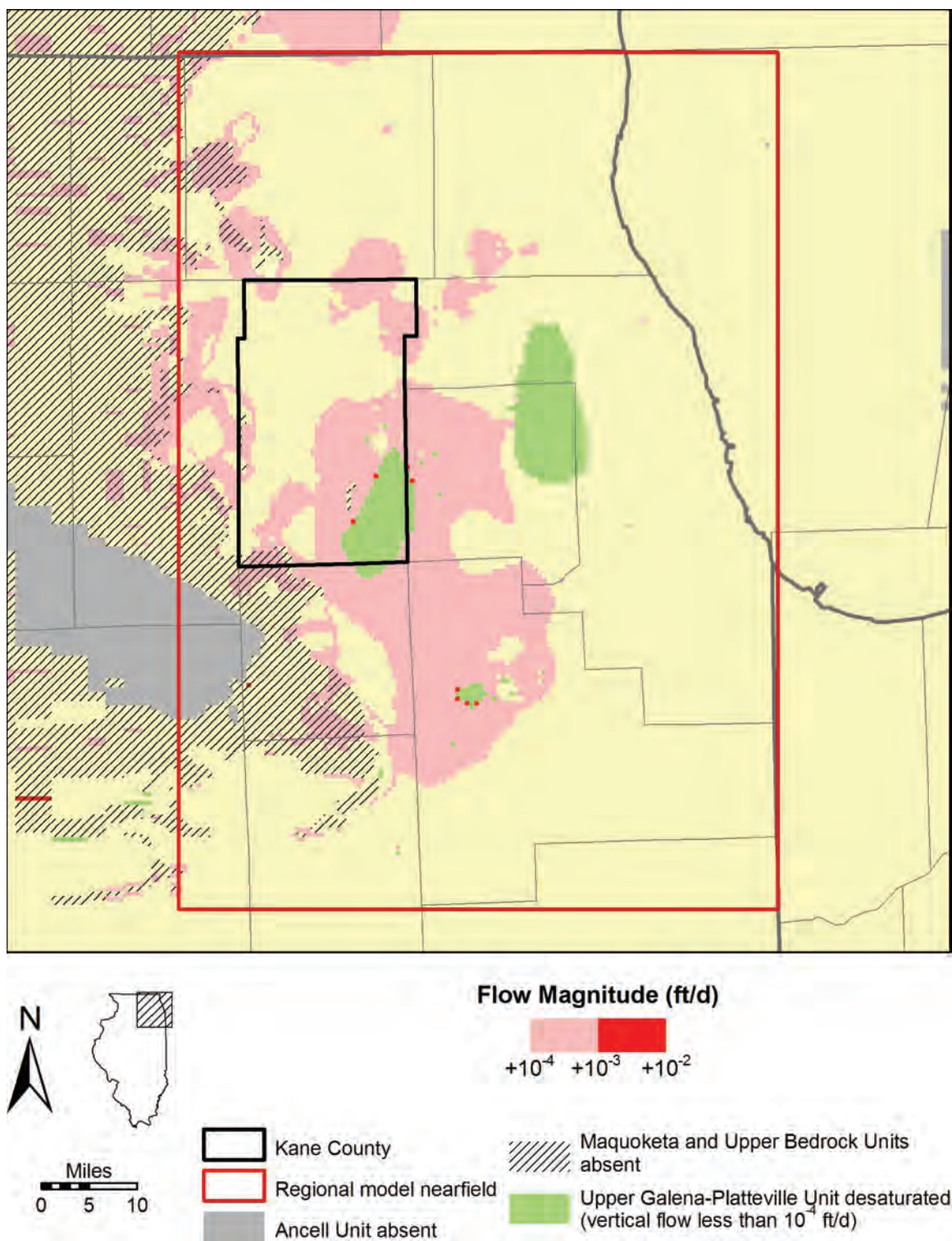


Figure 173. Areas of downward simulated flow across the top of the Ansell Unit in 2002 where predevelopment vertical flow was negligible (between 10⁻⁴ ft/d upward and 10⁻⁴ ft/d downward).

The comparison shows little difference in simulated predevelopment heads in the nearfield boundary area, but the simulated heads in deep units for the period of historical pumping ending in 2002 are generally lower in the Illinois model than in the Wisconsin model. Within individual hydrostratigraphic units, the difference in head increases with distance from the area of absence of the Maquoketa and Upper Bedrock Units. The difference in simulated heads also increases downward, so that while most head differences in the boundary area vary by less than 200 ft in the Ancell Unit, some differences in the Ironton-Galesville Unit exceed 400 ft. Head differences in the Mt. Simon appear to be on the order of the Ironton-Galesville differences, but quantification is problematic because of variations between the models in the definitions of model layers making up the Mt. Simon Unit. Differences in the direction of the horizontal head gradient also increase downward. Simulated Ancell Unit potentiometric surfaces in the two models are similar, sloping generally from west to east in the boundary area. While the simulated Ironton-Galesville potentiometric surface of the Wisconsin model slopes from west to east, however, that of the Illinois model generally slopes from northwest to southeast.

Though similar in most respects, there are numerous subtle differences between the models that could contribute to the differences described in the preceding paragraph. These differences include similar, but differing geologic frameworks, representations of surface water and drained areas, and zonations of hydraulic parameters, including recharge, hydraulic conductivity, and specific storage. The authors believe, however, that significant differences in the model output arise from time resolution employed to represent groundwater withdrawals in the two models. The Wisconsin model employs much lower resolution time discretization in simulating withdrawals than does the Illinois model, possibly causing the model to underestimate drawdown. The Wisconsin model simulates pumping from 1864 through 2002 with 16 stress periods, each divided into five time steps, whereas the Illinois model employs 139 stress periods divided into 300 time steps each. As described by Andersen (1993), MODFLOW underestimates drawdown to an increasing degree with decreasing time resolution.

3.3. Simulation of Future Groundwater Conditions

While single-value estimates (e.g., estimate of aquifer yield, sustained yield, practical sustained yield) appear on first glance to offer water managers a simple, objective tool with which to guide groundwater development, such estimates have been widely discredited for failing to take into account realistic pumping networks, changes in recharge and natural discharge rates with pumping, transient conditions, and for relying on implicit value judgments (Alley et al., 1999; Bredehoeft, 2002; Sophocleus, 2000; Walker et al., 2003; Wood, 2001).

Rather than a single-value estimate of groundwater availability, this report presents model estimates of the impacts of plausible pumping and recharge conditions on future heads and streamflow. Plausible estimates of low- and high-pumping conditions, as well as low, model-calibrated, and high-recharge conditions, are simulated. *Model-calibrated recharge rates* are the rates determined through the calibration process and are representative of average recharge during the historic period. Estimates of low- and high-recharge conditions are based on observations of the range of recharge rates in the region and are intended to reflect the possible impacts of climate change. For purposes of this

report, a specific simulated combination of pumping and recharge conditions is referred to as a *scenario*. Thus, for example, the combination of high-pumping and low-recharge conditions is referred to as the *high-pumping, low-recharge scenario*.

Four scenarios are simulated, but the models may be adapted to simulate a wide range of other scenarios. These include two scenarios that assume *model-calibrated recharge* (i.e., no impact of climate variability) for two different trends in the growth of groundwater pumping (described as *low-* and *high-pumping conditions* in the preceding paragraph). A third scenario, the most resource-intensive of the four, assumes *high-pumping conditions* and *low recharge*. The last scenario, the least resource-intensive, assumes *low-pumping conditions* and *high recharge*. The four scenarios simulated for the investigation were chosen to represent plausible well configurations and pumping rates as well as likely recharge rates, taking into account the potential for climate change to affect recharge. Together, the output from model simulation of these scenarios is representative of the plausible range of future groundwater conditions in the region.

Scenarios of future pumping and recharge are simulated through transient modeling using both regional-scale and local-scale models. The simulation period ends at the start of 2050. In addition, the regional-scale model was employed for steady-state simulation of the 2002 well network. The steady-state simulation illustrates the effects of long-term pumping at 2002 rates from the 2002 network of wells on deep aquifer heads.

3.3.1. *Transient Simulation of Projected Withdrawals to 2050*

3.3.1.1. Pumping Conditions

Details of the development of projections of future pumping are discussed in Appendix F. This section summarizes the procedure of developing the estimates and discusses the magnitude, range, and distribution of projected withdrawals. Section 3.3.1.3 discusses adaptation of the projected withdrawals for modeling. As discussed above, estimates of both high and low pumping were developed for use in simulation of future conditions.

Each set of estimates includes a projected pumping rate for each well for the years 2005 through 2050, at five-year intervals. The scenarios include projections of withdrawals from public water system wells; major commercial, industrial, and irrigation wells; and from domestic wells in northeastern Illinois open to the Ansell and underlying hydrostratigraphic units. Well locations and source intervals are based on the locations and source intervals of wells active during 2000-2003 and on estimates of 1974-2003 drilling rates of domestic wells open to the Ansell and underlying hydrostratigraphic units. It is emphasized that these estimates are uncertain and that the simulated future drawdown approximated for these pumping scenarios does not take into account the installation of wells at new locations and changing proportions of withdrawals between wells.

Pumping rates assigned to the wells are based on (1) forecasts of county-level water use in the Public Supply water-use sector, Self-Supplied Commercial and Industrial sector, and Irrigation sector developed by Dziegielewski et al. (2005) for Illinois and by Dziegielewski et al. (2004) for Indiana and Wisconsin; (2) plausible estimates of withdrawals from domestic wells based on USGS estimates of per capita self-supplied domestic water use [in Dziegielewski et al. (2005)]; and (3) an estimate of the number of persons supplied by domestic wells (Illinois Department of Energy and Natural

Resources, 1998). Estimates of low pumping based on county-level water-use estimates for Illinois counties by Dziegielewski et al. (2005) that assume modest improvements in water conservation (improvements that have affected water use in the Public Supply and Self-Supplied Commercial and Industrial sectors from 1985 through 2000) will continue. High-pumping estimates are based on county-level estimates for Illinois counties by Dziegielewski et al. (2005) that assume that these improvements in water conservation in the Public Supply and Self-Supplied Commercial and Industrial sectors do not continue beyond 2000. Thus, the low-and high-pumping conditions differ only with respect to projected groundwater withdrawals in Illinois counties in the Public Supply and Self-Supplied Commercial and Industrial sectors. Only a single estimate of future pumping was developed for all other wells (i.e., irrigation wells in Illinois, all wells in Indiana and Wisconsin, and for domestic deep wells).

The county-level water-use estimates of Dziegielewski et al. (2004) and Dziegielewski et al. (2005)—and, by extension, the well-by-well withdrawal projections developed for this study—are based on sophisticated analyses of water use in the region. County-level estimates of water use in the Public Supply and Self-Supplied Commercial and Industrial sectors are based on multivariate statistical models that incorporate a range of socioeconomic, climatic, demographic, and geographic variables. County-level estimates of irrigation water use are based on a method that incorporates projections of total cropland acres, projections of percentage of irrigated cropland, estimates of golf course acreage, and estimates of “normal” precipitation. Estimates of future water withdrawals from domestic wells were developed for this study on the basis of USGS estimates of per-capita demand from self-supplied domestic wells from 1960 through 2000 [reported by Dziegielewski et al. (2005)], and an estimate of 3.4 persons supplied by each well (Illinois Department of Energy and Natural Resources, 1998). Per-capita demand from such wells is projected to increase from about 98 gallons per day (gpd) in 2000 to 171 gpd in 2005.

Comparison of projected 2005-2050 withdrawals and reported 1964-2003 withdrawals from wells serving the Public Supply, Self-Supplied Commercial and Industrial, and Irrigation sectors validates the plausibility of the projections and illustrates the significant difference that carrying forward the water-conservation trend makes to aggregate withdrawals in Kane County and northeastern Illinois. Aggregate withdrawals as estimated for the low and high pumping scenarios in the regional model nearfield of northeastern Illinois (Figure 6) diverge from the 2003 reported withdrawal of about 164 Mgd to about 197 Mgd (low pumping conditions) and 293 Mgd (high pumping conditions) in 2050 (Figure 174). Projected withdrawals in 2050 from shallow wells range from about 103 to 146 Mgd (Figure 175), and those from deep wells range from about 94 to 147 Mgd (Figure 176). Aggregate 2050 withdrawals from all Kane County wells serving the Public Supply, Self-Supplied Commercial and Industrial, and Irrigation sectors range from about 53 to 73 Mgd (Figure 177). Projected 2050 Kane County withdrawals from shallow wells range from about 26 to 36 Mgd (Figure 178). Those from deep wells range from about 27 to 37 Mgd (Figure 179). Because the projected pumping conditions are based on existing well locations, the locations of the largest projected withdrawals in Kane County are in the presently urbanized eastern one-third of the county, reflecting the limitations of the projection procedure to accommodate

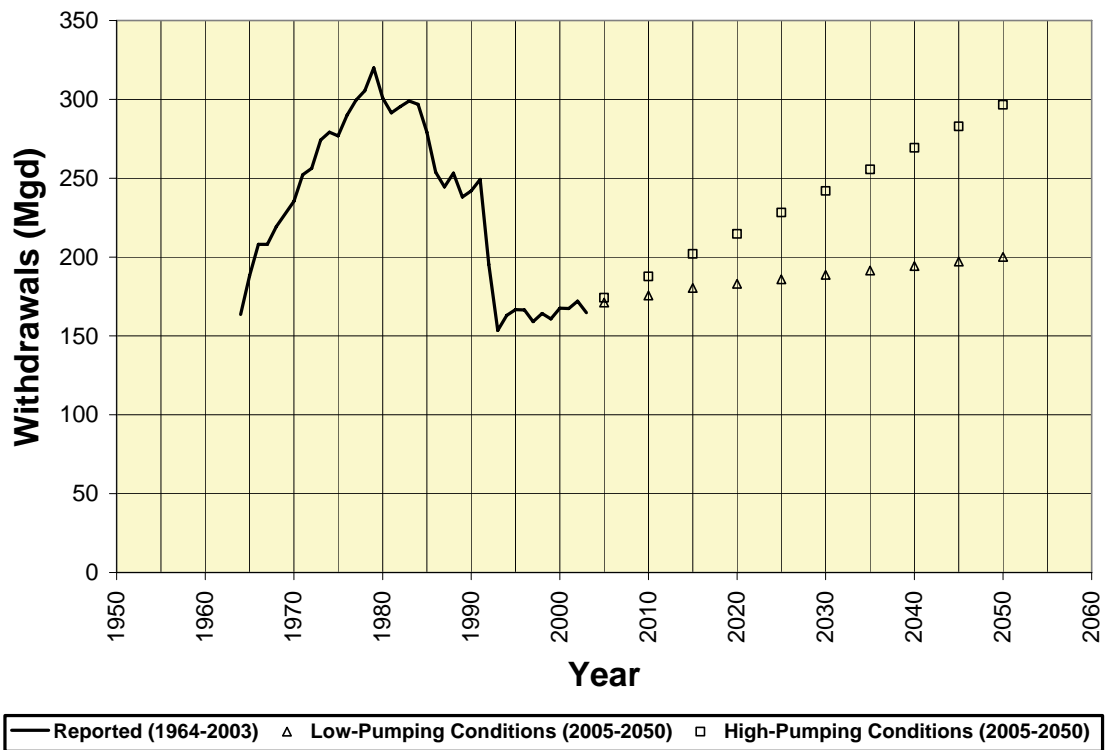


Figure 174. Reported and projected groundwater withdrawals from wells supplying the Public Supply, Self-Supplied Commercial and Industrial, and Irrigation sectors in northeastern Illinois, 1964-2050.

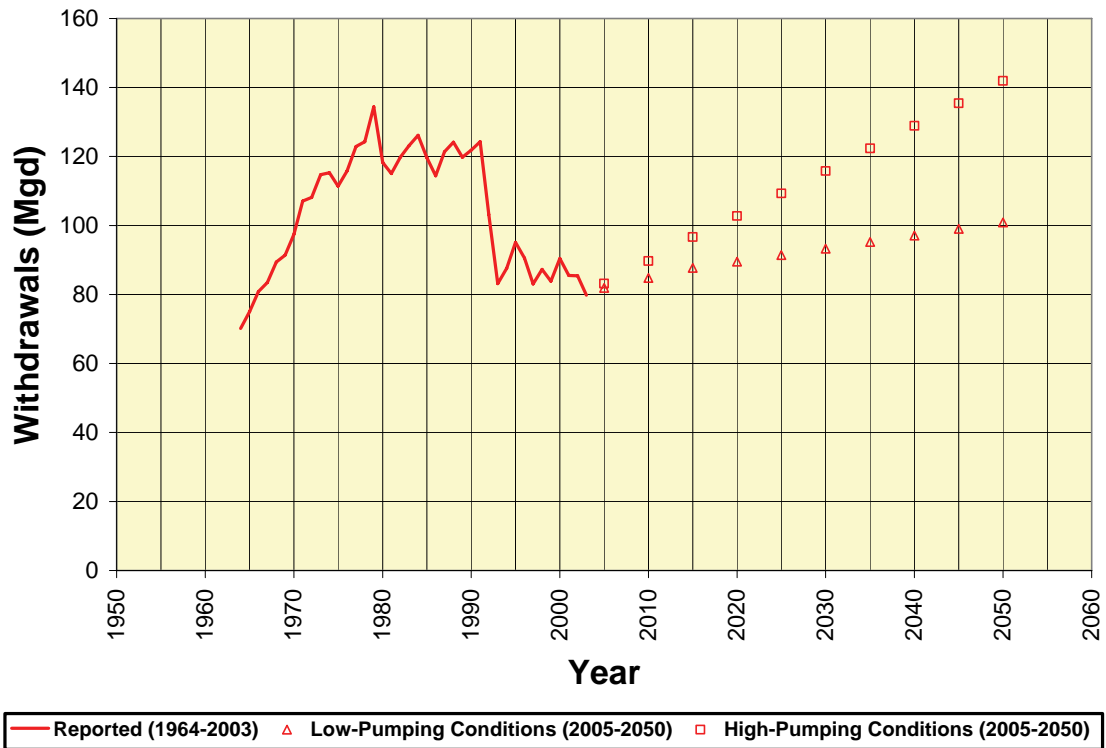


Figure 175. Reported and projected groundwater withdrawals from shallow wells supplying the Public Supply, Self-Supplied Commercial and Industrial, and Irrigation sectors in northeastern Illinois, 1964-2050.

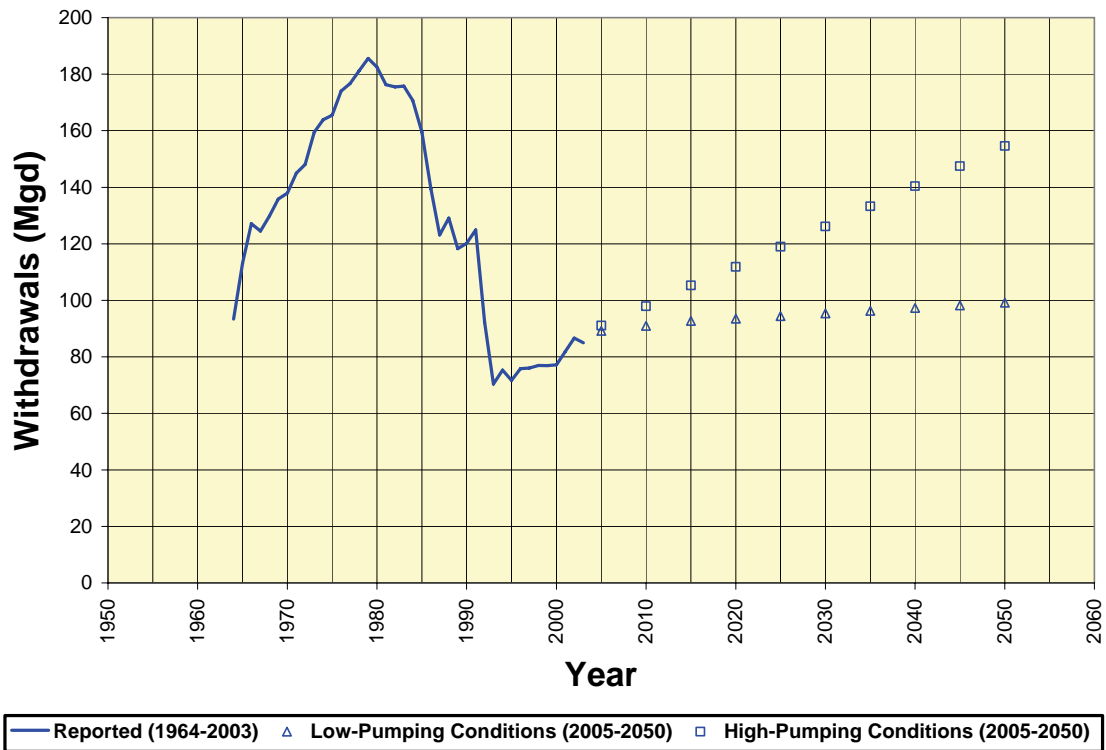


Figure 176. Reported and projected groundwater withdrawals from deep wells supplying the Public Supply, Self-Supplied Commercial and Industrial, and Irrigation sectors in northeastern Illinois, 1964-2050.

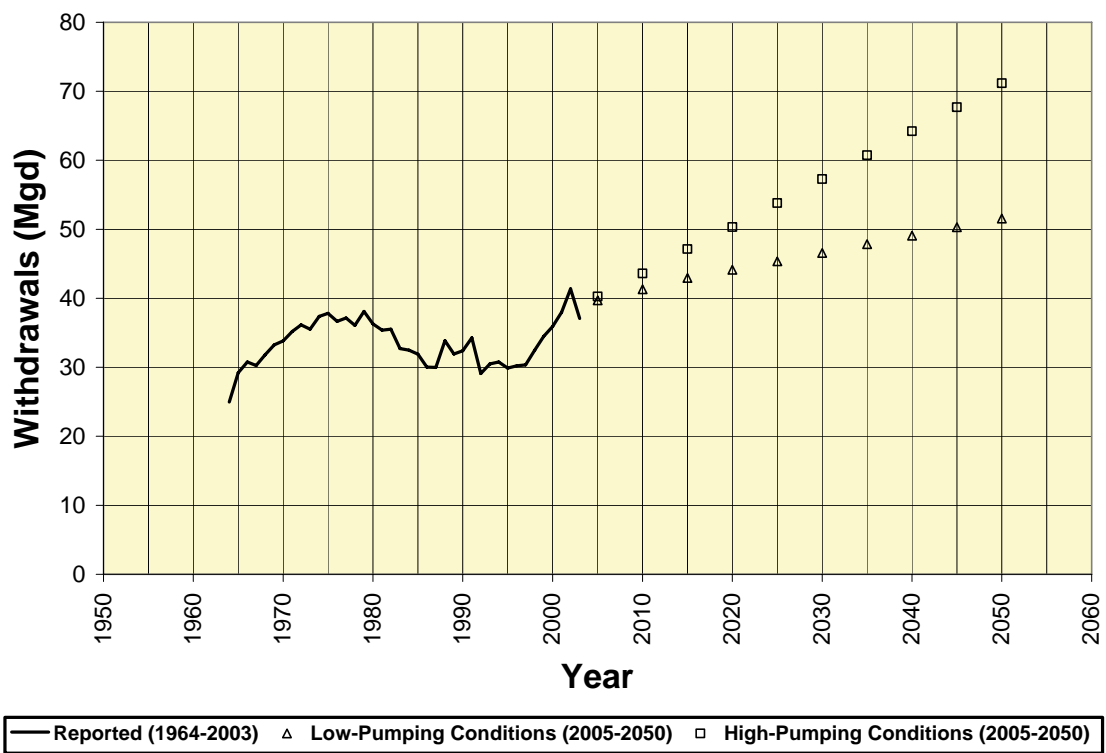


Figure 177. Reported and projected groundwater withdrawals from wells supplying the Public Supply, Self-Supplied Commercial and Industrial, and Irrigation sectors in Kane County, 1964-2050.

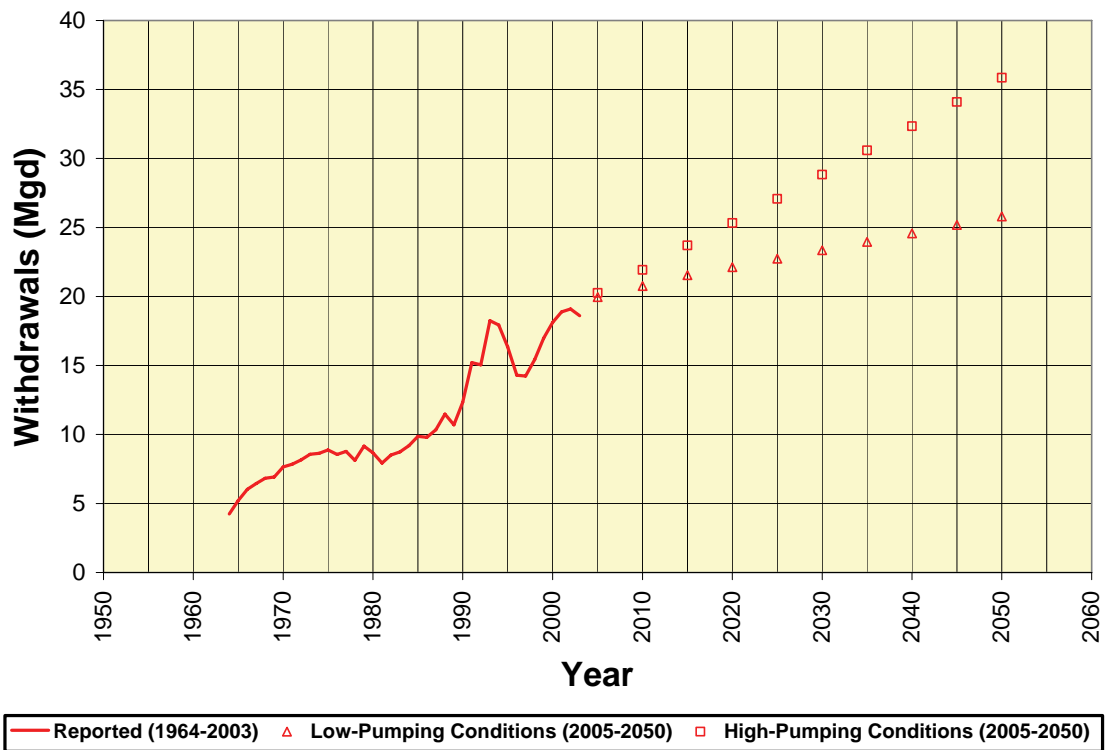


Figure 178. Reported and projected groundwater withdrawals from shallow wells supplying the Public Supply, Self-Supplied Commercial and Industrial, and Irrigation sectors in Kane County, 1964-2050.

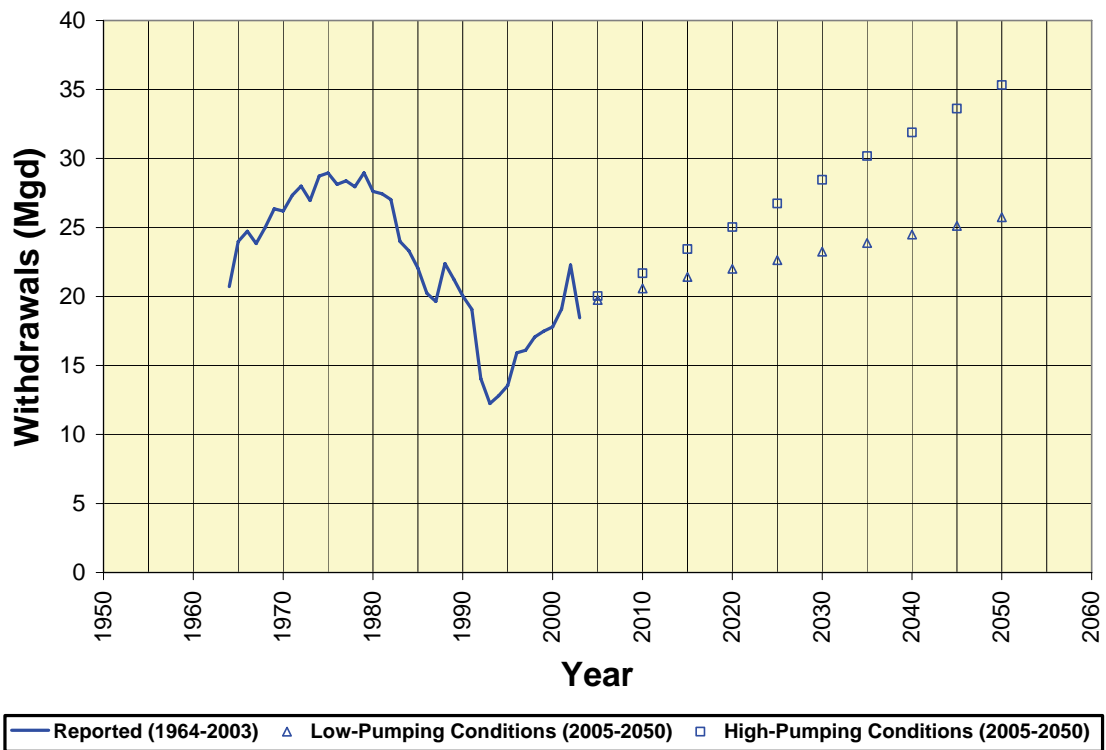


Figure 179. Reported and projected groundwater withdrawals from deep wells supplying the Public Supply, Self-Supplied Commercial and Industrial, and Irrigation sectors in Kane County, 1964-2050.

westward urbanization of the county (Figure 180, Figure 181, Figure 182, and Figure 183).

Limitations imposed by assigned boundary conditions (that is, river and drain cells) in the local-scale model required that we limit projected pumping rates through 2050 for certain wells (Figure 184 through Figure 187) to reported 2003 rates, rather than employ the higher 2005-2050 rates determined for these wells for both low- and high-pumping conditions through the procedure described in Appendix G. These adjustments were employed for local-scale modeling only and were not used in regional-scale modeling. Experiments with the local-scale model showed that the higher pumping rates caused such extreme drawdown that the model failed to function because the assigned boundary conditions became invalid, and the model could not consequently simulate the complete period ending in 2050. The wells for which future pumping rates were limited at 2003 rates include the following: Algonquin 8 and 9; Crystal Lake 15; and West Chicago 6, 7, and 8. These wells are all located in areas of significant drawdown in 2003 as described in Section 3.2.1.2.

Compared to projected withdrawals from deep wells serving the Public Supply, Self-Supplied Commercial and Industrial, and Irrigation sectors, those from domestic deep wells are comparatively small. These withdrawals may have important local effects, however. Projected withdrawals from these domestic wells in northeastern Illinois—both existing and newly-constructed during the period 2005-2050—are 1.3 percent of total projected withdrawals from deep wells serving the Public Supply, Self-Supplied Commercial and Industrial, and Irrigation sectors in 2005. For the year 2050, these proportions increase to 2.3 percent (high pumping conditions) and 3.6 percent (low pumping conditions). The growth in this proportion reflects both projected drilling of new deep domestic wells and the projected growth of per-capita water use from self-supplied domestic wells (see Appendix B and Appendix G). In Kane County, withdrawals from deep domestic wells are projected to be 0.6 percent of total projected withdrawals from deep wells serving the Public Supply, Self-Supplied Commercial and Industrial, and Irrigation sectors in 2005. For the year 2050, these proportions increase to 0.9 percent (high pumping conditions) and 1.2 percent (low pumping conditions). Total estimated (1964-2003) and projected (2005-2050) withdrawals from deep domestic wells in northeastern Illinois and Kane County (Figure 6) are shown in Figure 188 and Figure 189. The break in slope between Kane County 1964-2003 estimated withdrawals and 2005-2050 projected withdrawals reflects the fact that the 1974-2003 drilling rate of deep wells in Kane County, which was used to estimate withdrawals from newly constructed wells, underestimates drilling rates in the county over shorter, more recent time periods (Figure 189). The distribution of existing and anticipated deep domestic wells in the Kane County area (Figure 190 depicting existing deep domestic wells, Figure 191 depicting new deep domestic wells drilled by 2025, and Figure 192 depicting new wells deep domestic drilled by 2050) reflects the high current density and high drilling rates of these wells in suburban residential areas of Kane County where productive shallower aquifers are largely absent.

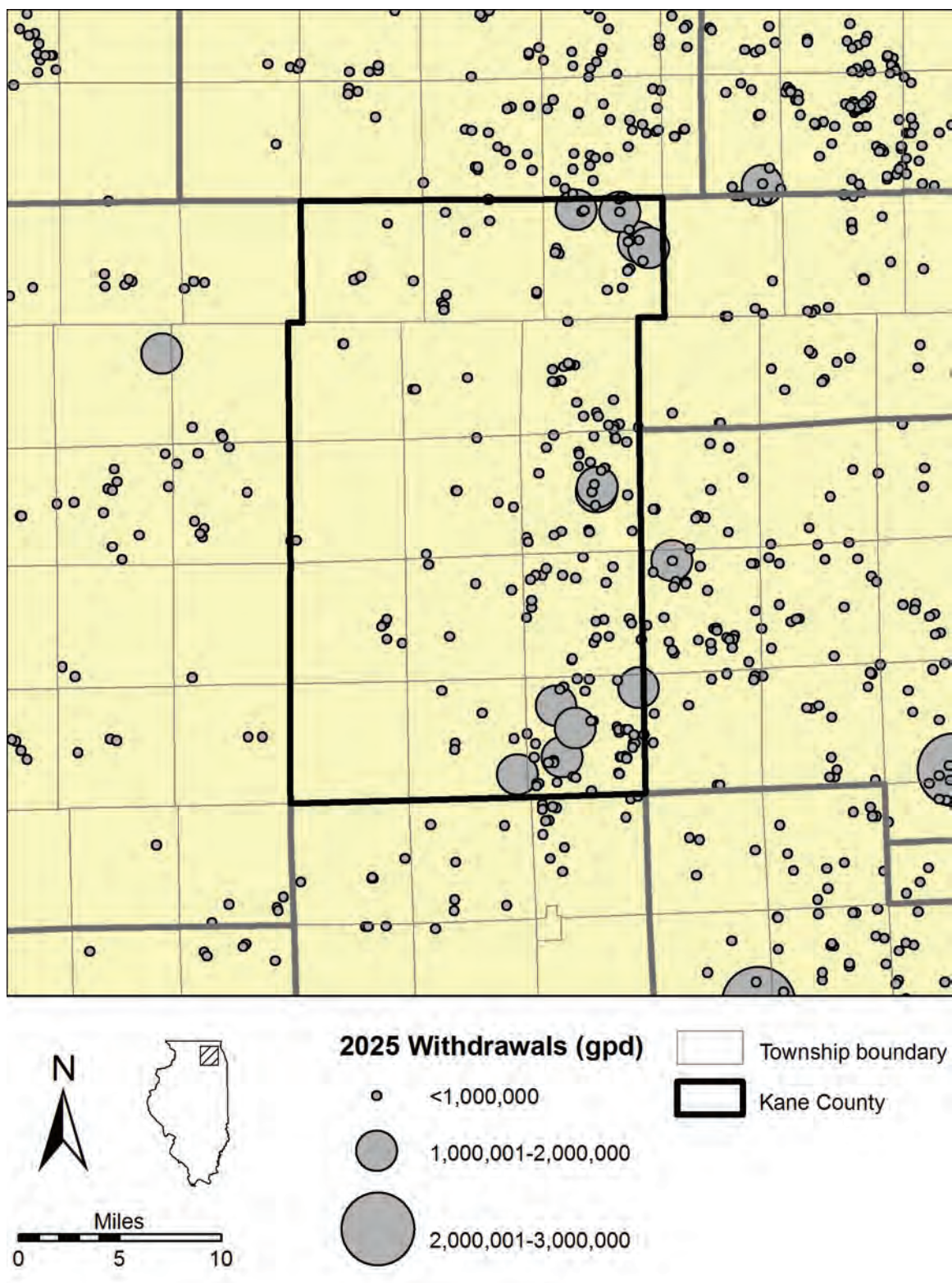


Figure 180. Projected 2025 groundwater withdrawals from wells supplying the Public Supply, Self-Supplied Commercial and Industrial, and Irrigation sectors in the Kane County area, low-pumping conditions.

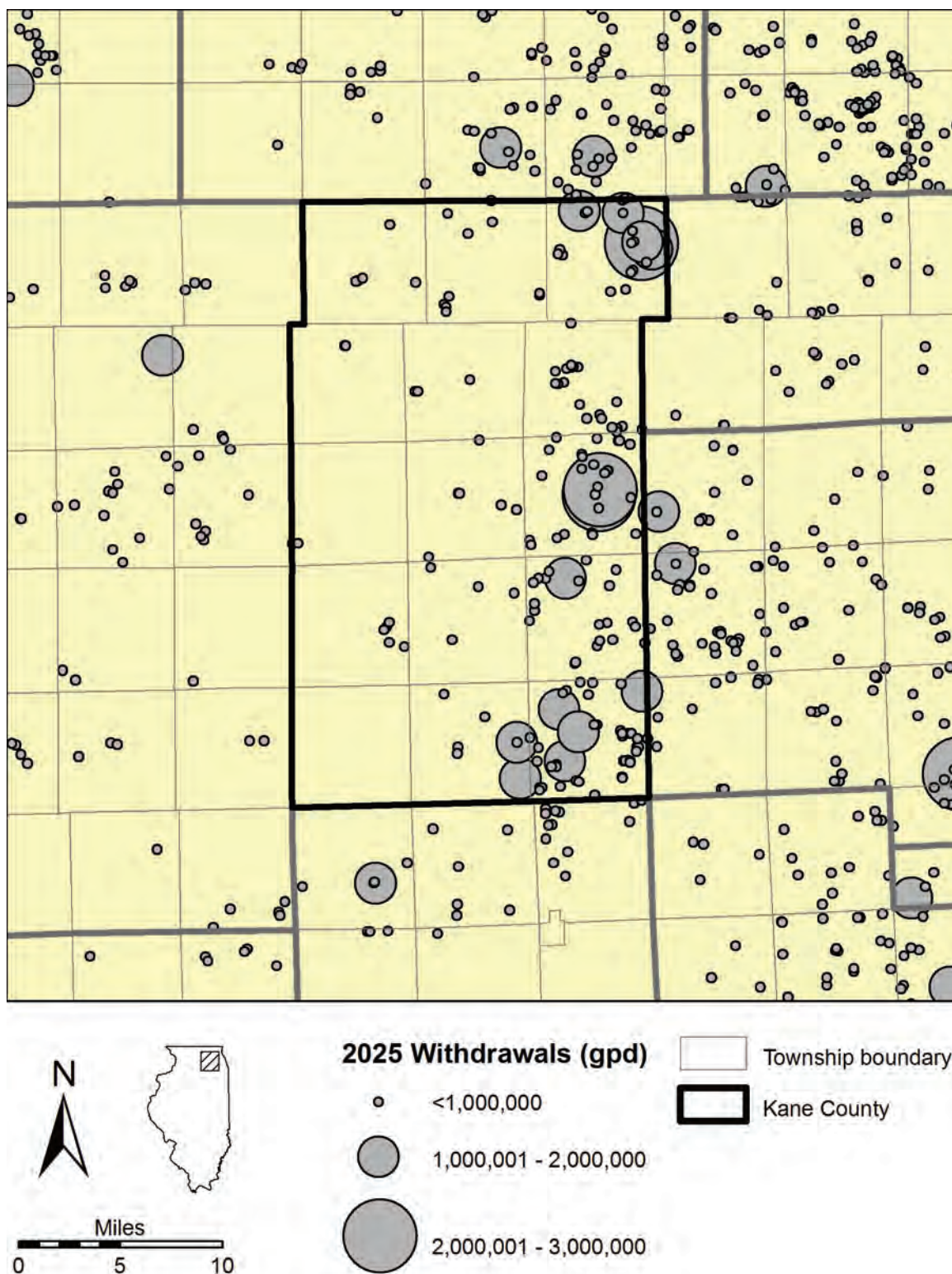


Figure 181. Projected 2025 groundwater withdrawals from wells supplying the Public Supply, Self-Supplied Commercial and Industrial, and Irrigation sectors in the Kane County area, high-pumping conditions.

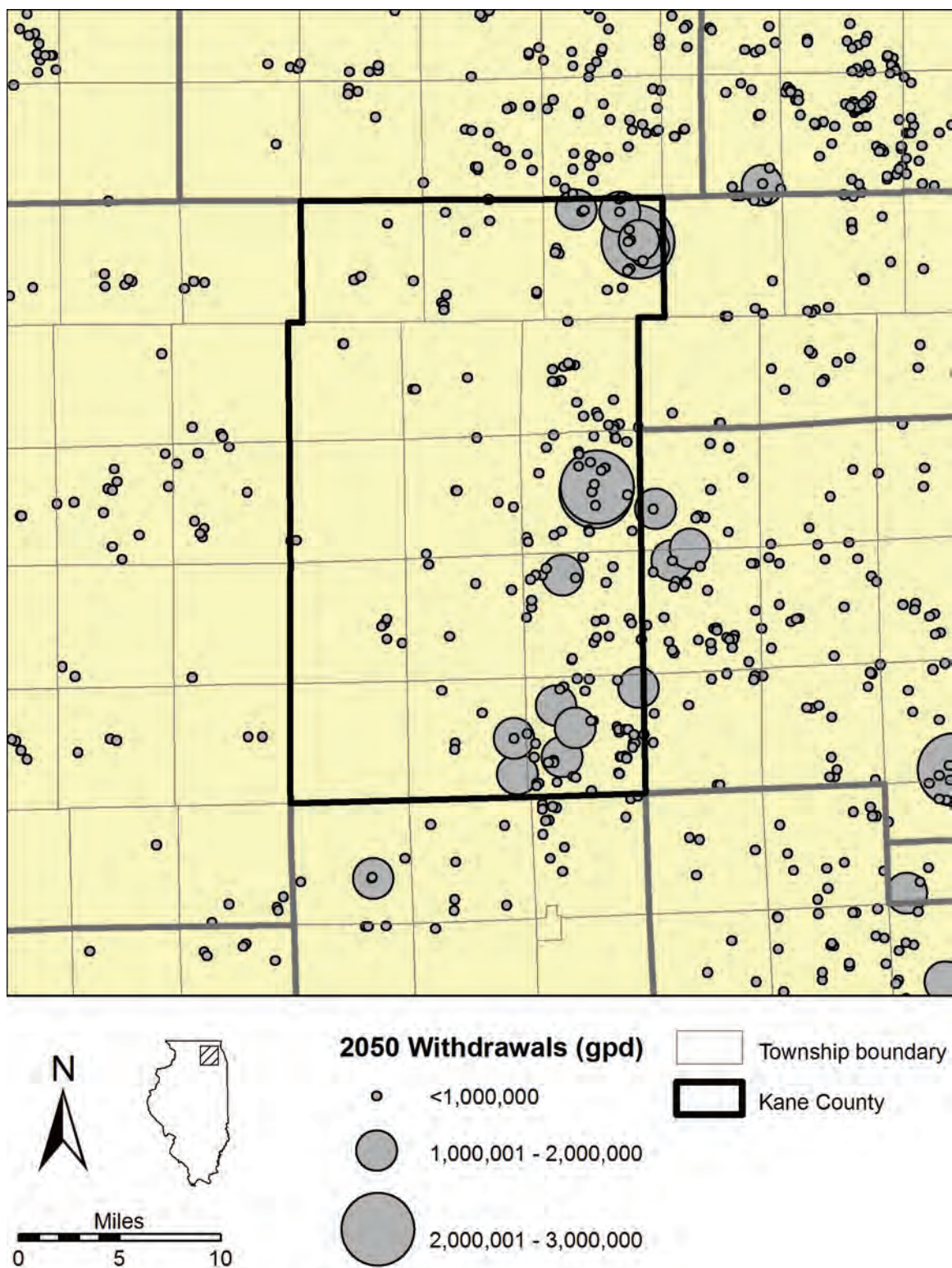


Figure 182. Projected 2050 groundwater withdrawals from wells supplying the Public Supply, Self-Supplied Commercial and Industrial, and Irrigation sectors in the Kane County area, low-pumping conditions.

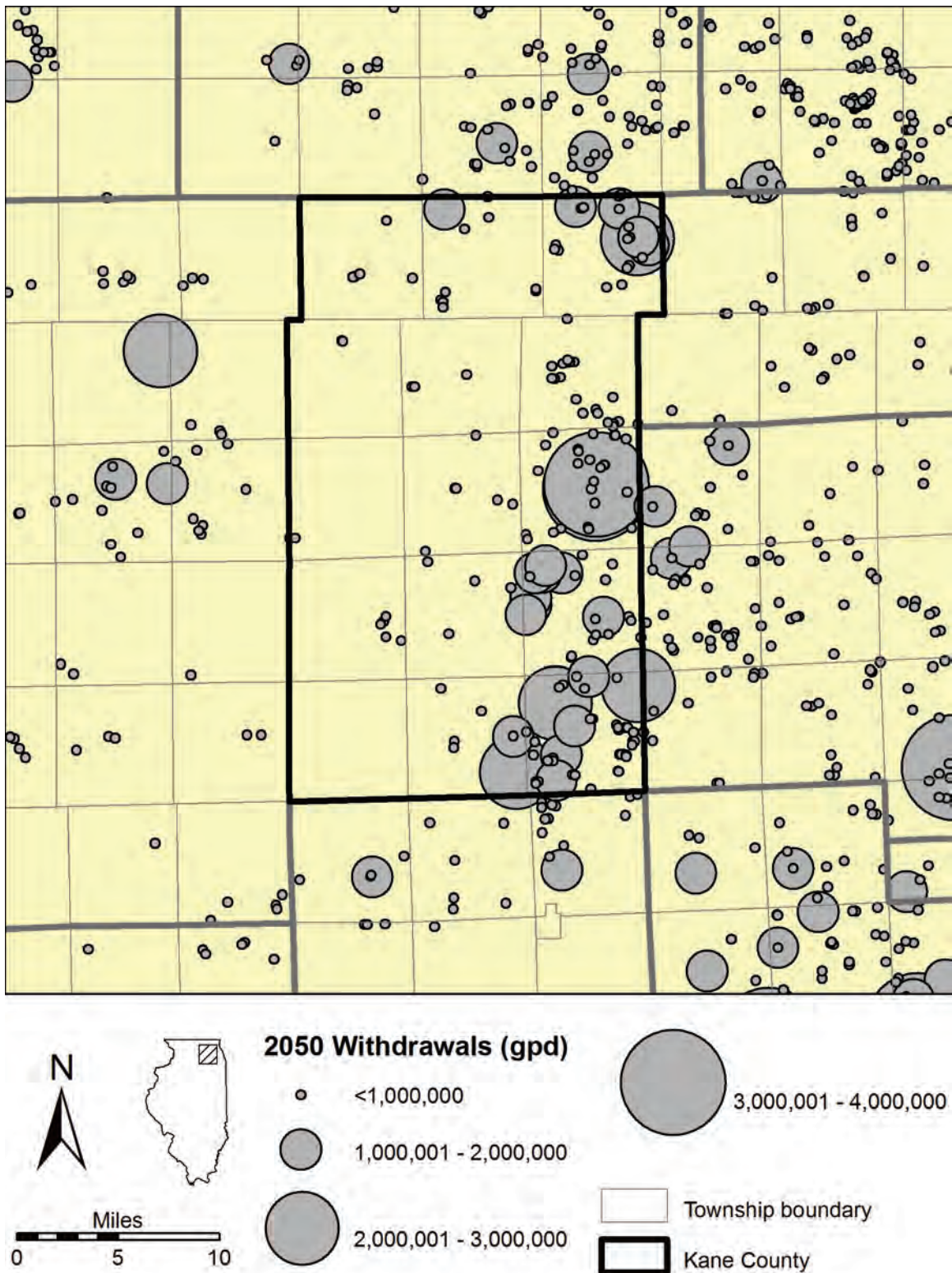


Figure 183. Projected 2050 groundwater withdrawals from wells supplying the Public Supply, Self-Supplied Commercial and Industrial, and Irrigation sectors in the Kane County area, high-pumping conditions.

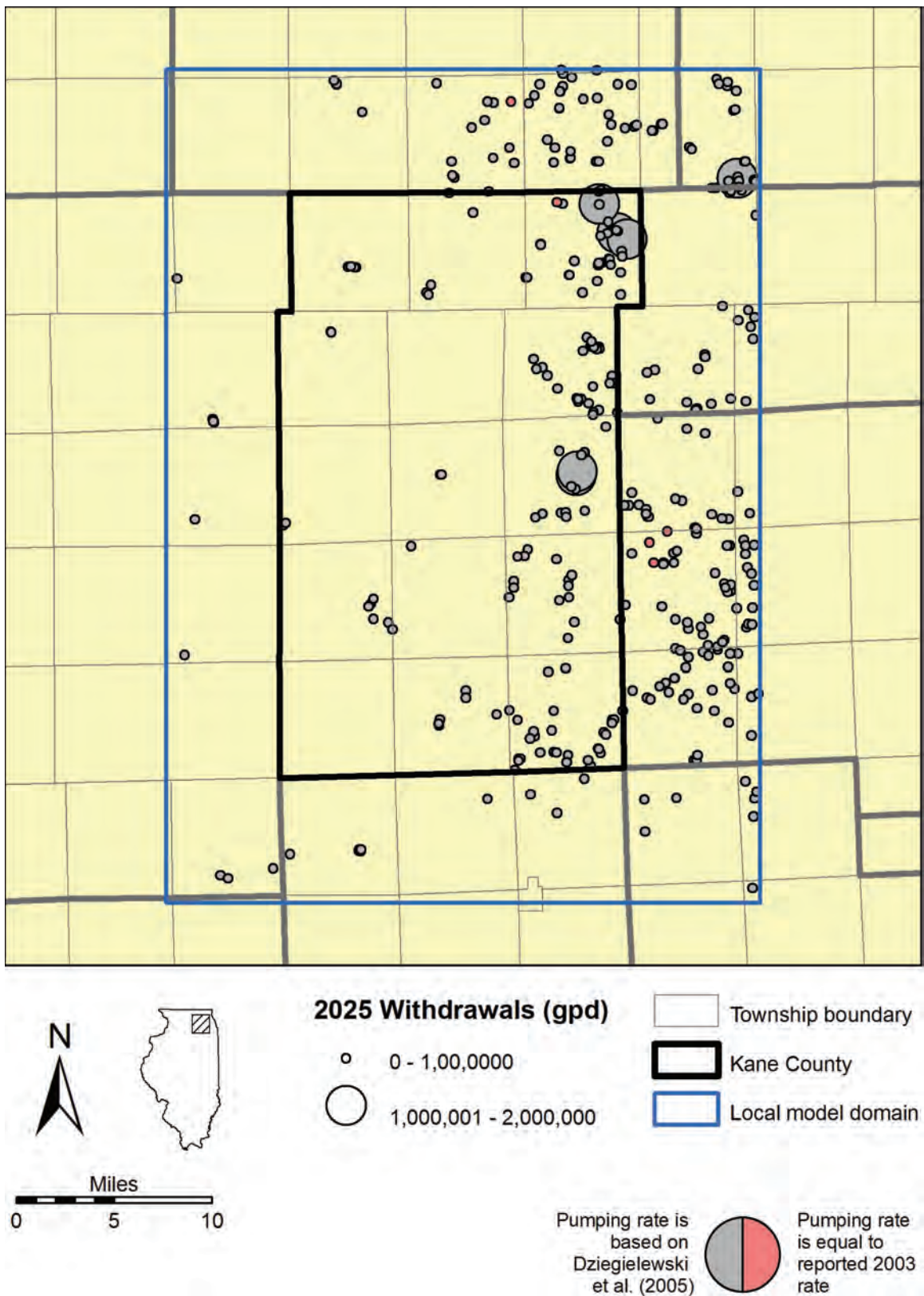


Figure 184. 2025 withdrawals simulated in local-scale model, low-pumping conditions.

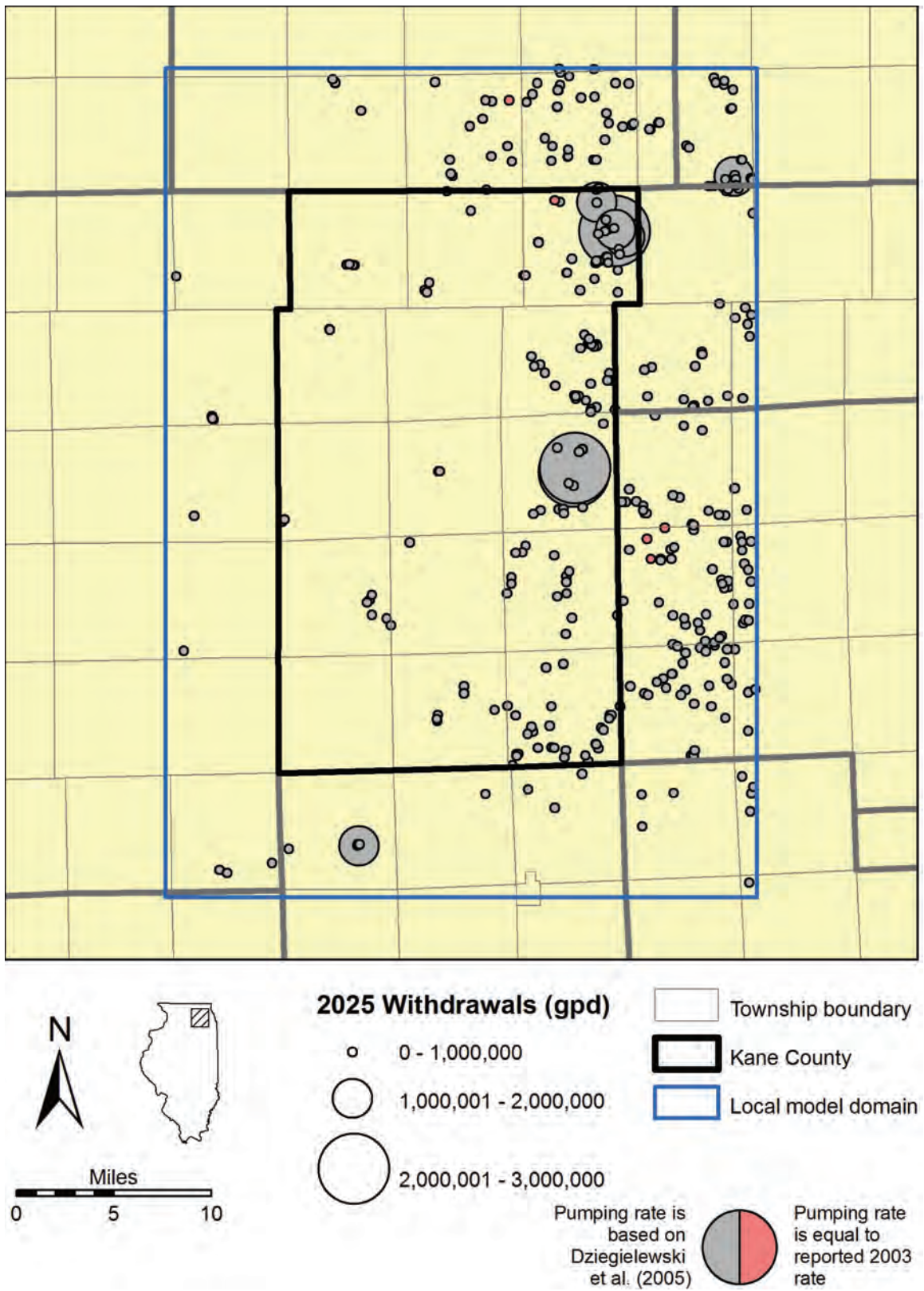


Figure 185. 2025 withdrawals simulated in local-scale model, high-pumping conditions.

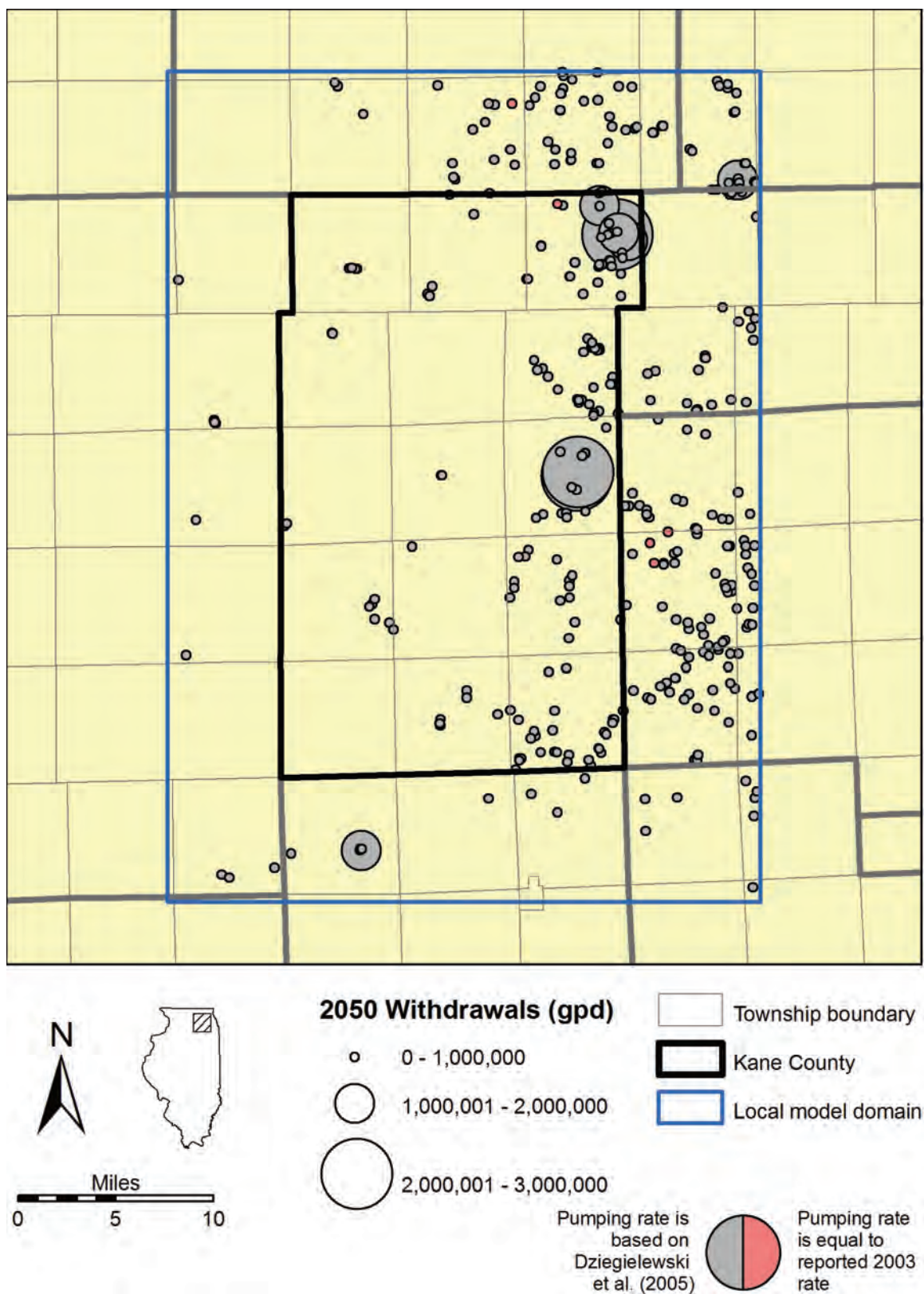


Figure 186. 2050 withdrawals simulated in local-scale model, low-pumping conditions.

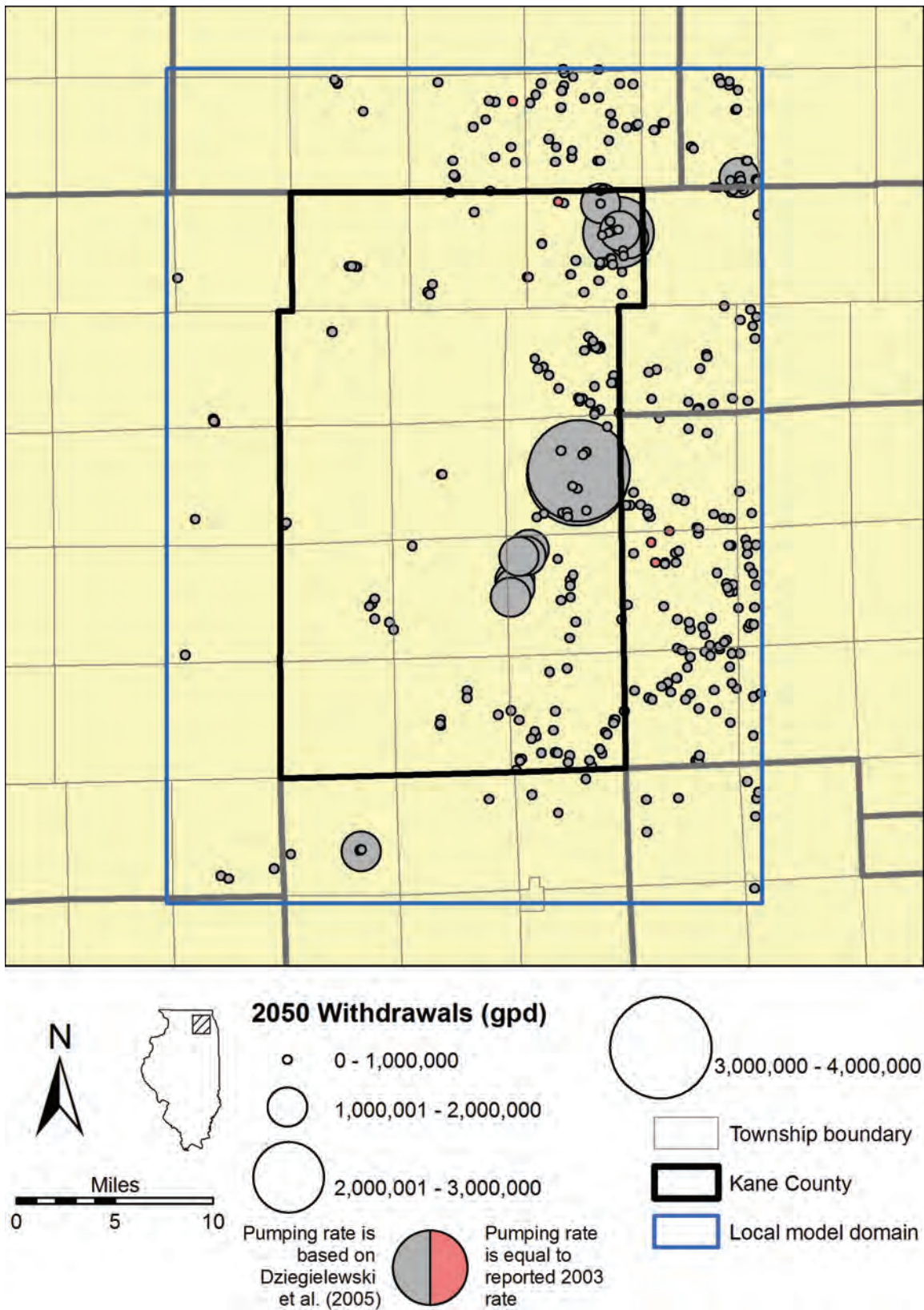


Figure 187. 2050 withdrawals simulated in local-scale model, high-pumping conditions.

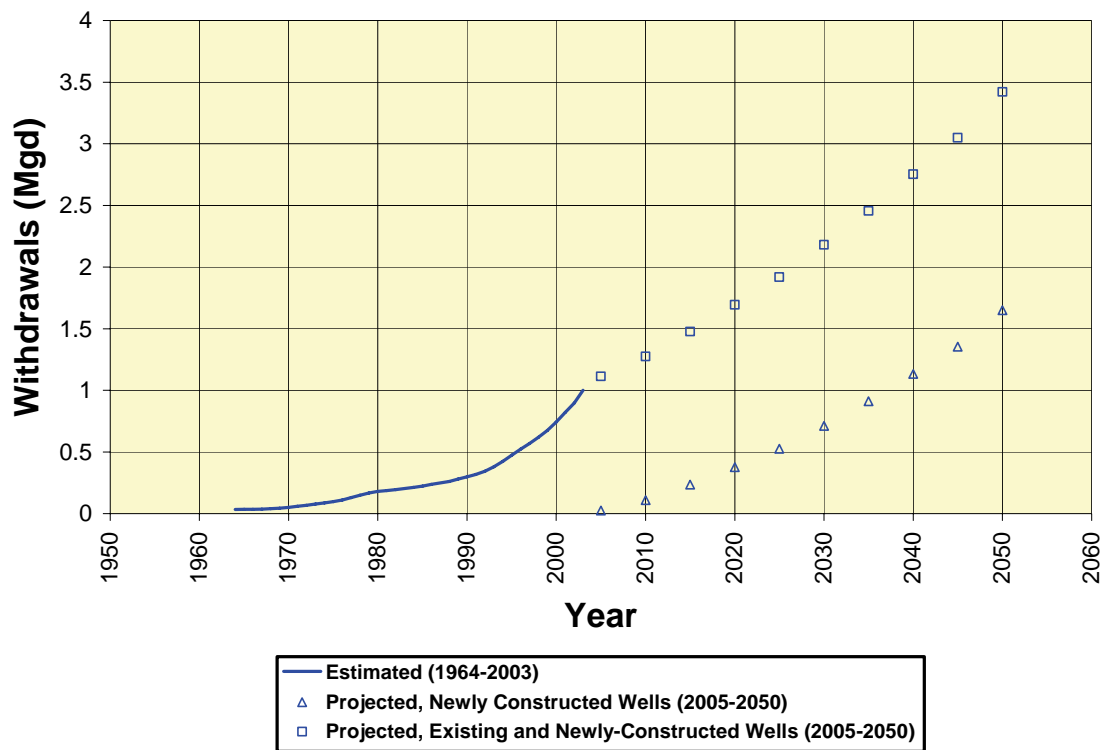


Figure 188. Total estimated (1964-2003) and projected (2005-2050) withdrawals from deep domestic wells in northeastern Illinois.

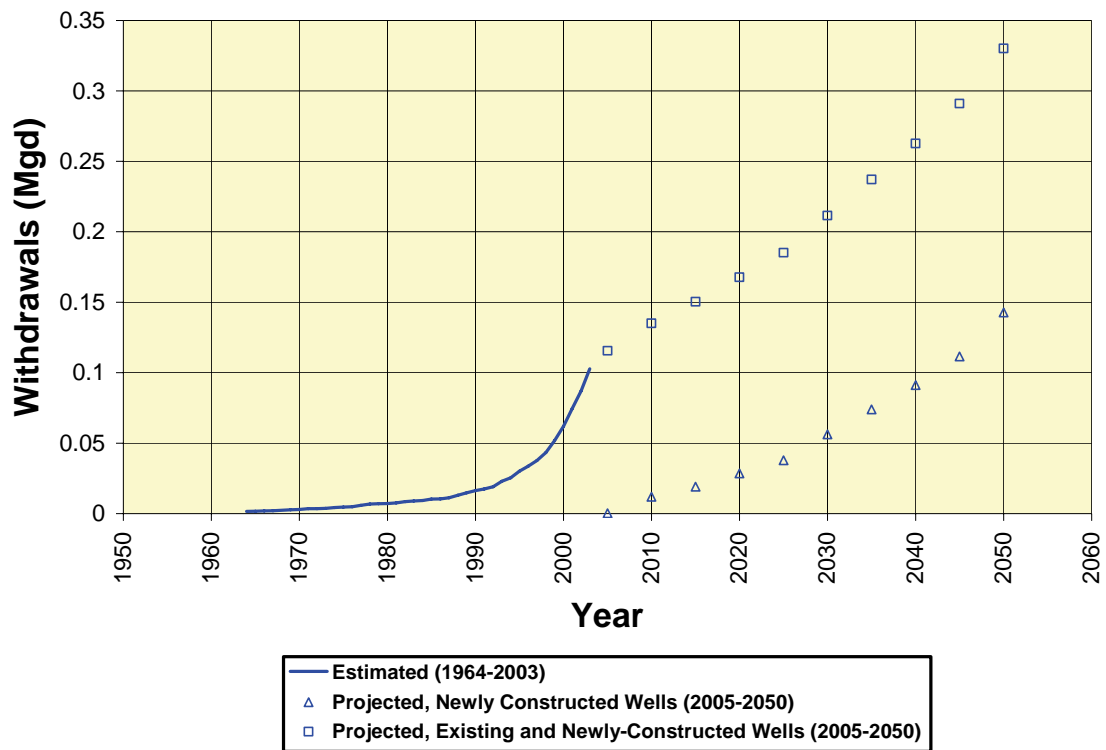


Figure 189. Total estimated (1964-2003) and projected (2005-2050) withdrawals from deep domestic wells in Kane County.

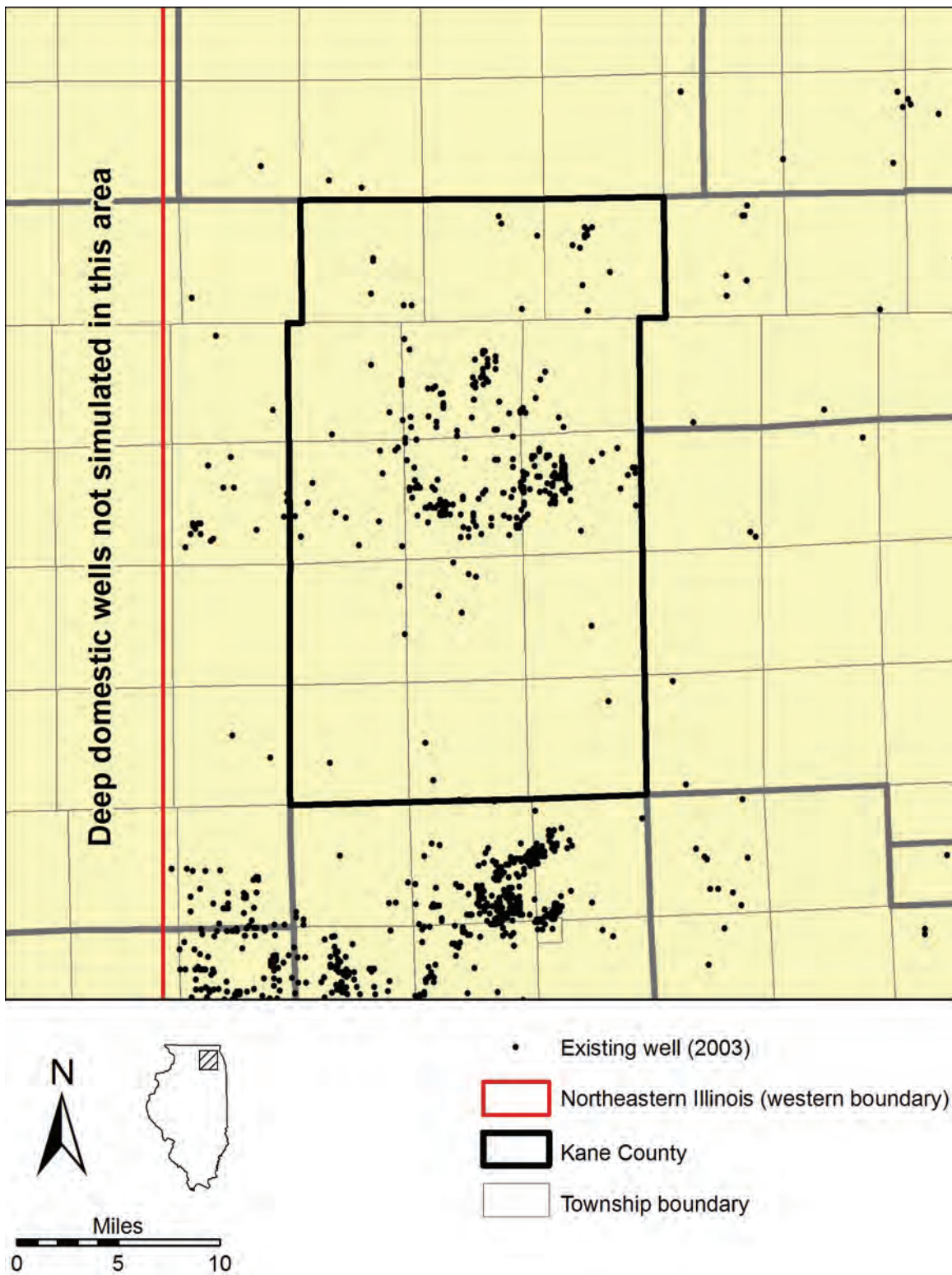


Figure 190. Existing deep domestic wells in the Kane County area. Withdrawals during the period 2005-2050 were projected for all of these wells.

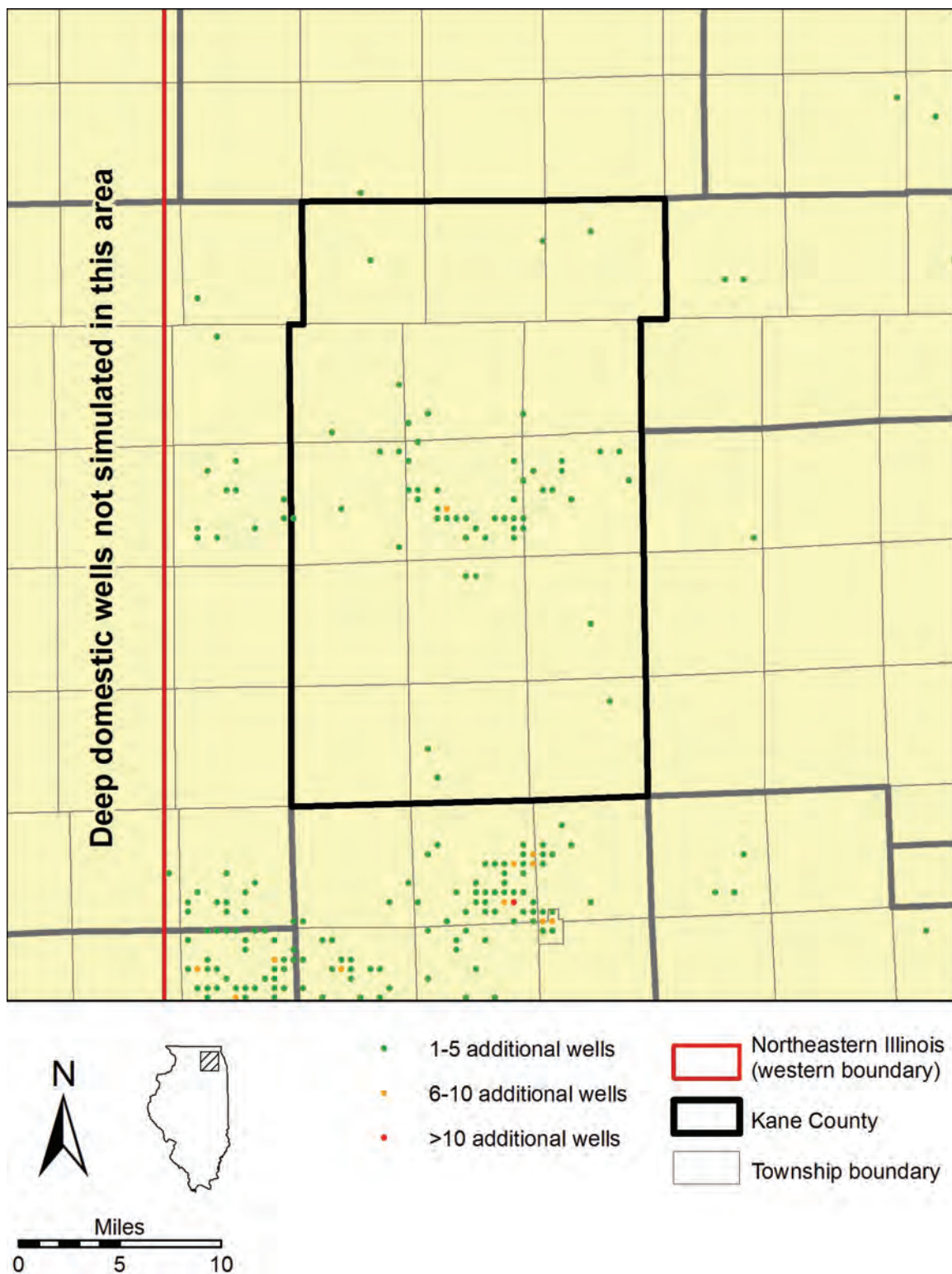


Figure 191. Projected deep domestic wells in the Kane County area constructed during the period 2005-2025. Each point may represent several wells.

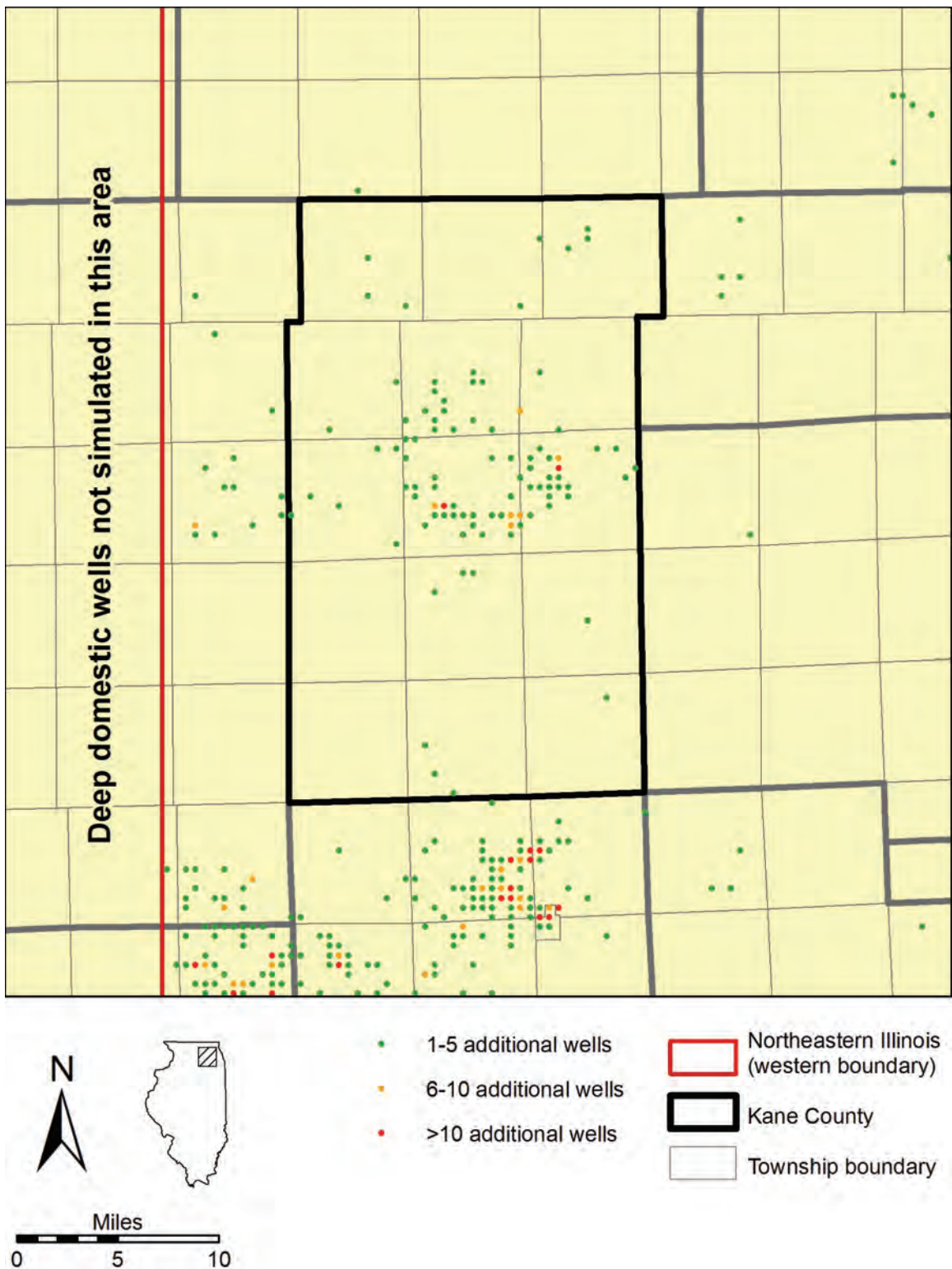


Figure 192. Projected deep domestic wells in the Kane County area constructed during the period 2005-2050. Each point may represent several wells.

3.3.1.2. Recharge Conditions

Three sets of assumed recharge conditions are considered in the analysis. The first, which is referred to as *calibrated-recharge conditions*, assumes that recharge rates will remain at the model-calibrated rates for the period ending 2050. The second set, which we term *high-recharge conditions*, assumes that recharge will increase to plausibly high rates in 2003 and that these rates are maintained to 2050. The third set is referred to as *low-recharge conditions*, in which recharge rates decline to plausibly low rates in 2003 and that these low rates are maintained to 2050. Recharge rates employed in the regional- and local-scale models differ because the basis for the zonation differs: in the regional model (Table 27), the zonation is based on watershed outlines, while in the local-scale model (Table 28), the zonation is based on hydrogeology—principally the texture of the near-surface materials. For both the regional- and local-scale models, the high and low recharge rates are specified for the recharge zonations discussed in Section 2.2.5 (Figure 71 and Figure 72).

The high and low recharge rates employed for projection modeling using the regional-scale model (Table 27) are based mostly on the high and low recharge rates specified in the literature that was the source of the initial recharge rates used for model calibration. There are two exceptions. First, for regional model zone 3, the authors specified a low recharge rate equivalent to the low plausibility bound as set for calibration (that is, 0.000798 ft/d, which is 20 percent less than the initial recharge rate set for calibration). The authors chose this value because the minimum rate specified for this zone by Bloyd (1974) (0.000998 ft/d)—the reference used to justify the initial rate set for calibration—is *higher* than the minimum rate set for calibration (0.000798 ft/d), and because the minimum rate set for calibration ended up being selected as the calibrated recharge rate. Thus, the same recharge rates were employed for zone 3 to represent both calibrated and low recharge conditions. Second, for regional zone 8, we selected a high recharge rate equivalent to the high plausibility bound set for calibration (0.001232 ft/d, or 20 percent more than the initial rate specified for calibration). Similar to the situation for regional zone 3, the high plausibility bound for calibration of regional zone 8 (0.001232 ft/d) is *higher* than the maximum rate specified by Cherkauer (2001) (0.001027 ft/d), which is the reference used to justify the initial rate specified for calibration of regional zone 8. Therefore, the same recharge rates were employed for regional zone 8 to represent both calibrated- and high-recharge conditions.

The high and low recharge rates employed for projection modeling using the local-scale model (Table 28) are based on the difference between the calibrated, high, and low recharge rates specified for recharge zones 10 and 11 of the regional model, which correspond to the Lower Fox and Kishwaukee basins and are the two recharge zones covering the area of the local-scale model domain. Arnold et al. (2000) indicate that, for regional zones 10 and 11, plausibly low and high recharge rates are about 12 percent lower and higher than the recharge rates selected through regional model calibration. Thus, for each of the four recharge zones employed in the local-scale model, we have specified low and high recharge rates that are about 12 percent lower and higher than the recharge rates selected through calibration of the *local*-scale model (Table 28).

Varying the recharge conditions in modeling future groundwater flow in the Kane County areas serves two purposes. First, it acknowledges model uncertainty by altering a parameter type that has a significant effect on model calibration accuracy as indicated by

**Table 27. Recharge Conditions for Transient Simulation to
2050 using Regional-Scale Model**

<i>Zone¹</i>	<i>Assumed Recharge Rate (ft/d)</i>		
	<i>Low-Recharge Conditions</i>	<i>Calibrated-Recharge Conditions</i>	<i>High-Recharge Conditions</i>
2	0.000449	0.000539	0.000899
3	0.000798 ²	0.000798	0.001361
4	0.000009	0.000225	0.000449
5	0.000009	0.000229	0.000449
6	0.000449	0.000702	0.000899
7	0.000228	0.000767	0.002282
8	0.000746	0.001232	0.001232 ²
9	0.000899	0.001111	0.001348
10	0.001348	0.001573	0.001798
11	0.001798	0.002020	0.002247
12	0.000899	0.001124	0.001348
13	0.002697	0.002894	0.003146
14	0.000009	0.000231	0.000449
16	0.001155	0.001692	0.003240

¹See Figure 71 for zone locations.

²Equivalent to calibrated recharge rate.

**Table 28. Recharge Conditions for Transient Simulation to
2050 using Local-Scale Model**

<i>Zone¹</i>	<i>Assumed Recharge Rate (ft/d)</i>		
	<i>Low-Recharge Conditions</i>	<i>Calibrated-Recharge Conditions</i>	<i>High-Recharge Conditions</i>
1	0.000440	0.000500	0.000560
2	0.002200	0.002500	0.002800
3	0.000700	0.000800	0.000900
4	0.003500	0.004000	0.004500

¹See Figure 72 for zone locations.

sensitivity analyses. Second, it acknowledges that climate variability may affect recharge rates in the region.

3.3.1.3. Modeling of Pumping/Recharge Scenarios

Six possible combinations of the future pumping and recharge conditions discussed in Sections 3.3.1.1 and Section 3.3.1.2 are possible. These may be arranged along a gradient of resource-use intensity as shown in Table 29, the combination of high pumping and low recharge being the most resource intensive and that of low pumping and high recharge being the least resource intensive. Of these six possible combinations of future pumping and recharge conditions, four are simulated for this project, with two combinations of intermediate resource-use intensity not simulated.

For simulations employing the regional-scale model, initial conditions were assumed to be the simulated conditions at the end of 2002 discussed in Section 3.2.1.1. For simulations employing the local-scale model, initial conditions are assumed to be nonpumping conditions. The pumping rate for simulated Indiana and Wisconsin wells during the years 2003 and 2004 was assumed to be equal to the estimated 2005 pumping rate discussed in Section 3.3.1.1 and Appendix F (Table 30). Pumping rates for 2003 and 2004 for the simulated Illinois wells are reported 2003 withdrawal rates, or, if a facility did not report withdrawals for 2003, estimated rates based on reported values for earlier years. For each five-year period beginning in 2005, the assumed pumping rate is the rate assumed for the beginning year of the period as discussed in section 3.3.1.1 and Appendix F. Thus, for the period 2005-2009, the pumping rate estimated for 2005 was employed in the simulation. Simulations conclude at the end of 2049, with the estimated 2045 pumping rate employed for the period 2045-2049. In text and figures, results labeled as 2025 refer to simulation results for the beginning of that year, and those marked 2050 likewise refer to model results for the beginning of 2050.

3.3.1.4. Discussion

Figure 193 through Figure 196 show simulated Ancell Unit head change between the end of 2002 and the end of 2049, based on regional-scale model simulation for each of the four simulated scenarios shown in Table 29. For brevity, of all the deep units, only Ancell Unit heads are illustrated because they are representative of simulated heads in deeper units and because, as the shallowest of the major deep aquifers, the Ancell Unit is most jeopardized by head reductions that could ultimately reduce well yields. Simulated Ancell Unit heads for each of the modeled scenarios are shown in Figure 197 through Figure 204. For comparison, simulated Ancell Unit heads at the end of 2002 are shown in Figure 114. Figure 205 through Figure 215 illustrate simulated head in the Ancell Unit and Ironton Galesville Unit at selected locations in Kane County shown in Figure 114. Available head above the top of the Ancell Unit, including estimated areas of desaturation of the Ancell, is illustrated in Figure 216 through Figure 222. The areas of Ancell desaturation shown in these figures are equivalent to areas of desaturation of the basal Galena-Platteville Unit—a critical horizon because its desaturation may result in increased arsenic concentrations in groundwater withdrawn from deep wells (see page 207).

Table 29. Transient Simulations to 2050 using Regional-Scale Model

<i>Pumping Conditions</i>	<i>Recharge Conditions</i>	<i>Intensity of Resource Use</i>	<i>Simulated</i>	<i>Figures and Tables</i>
High	Low	Most	Yes	Figure 193, Figure 197, Figure 198, Figure 205-Figure 215, Figure 216, Figure 217, Figure 224, Figure 228, Figure 232, Figure 236, Figure 241, Figure 251, Figure 252, Figure 255, Figure 268, Figure 271, Table 31, Table 32
High	Calibrated	Intermediate	Yes	Figure 194, Figure 199, Figure 200, Figure 218, Figure 219, Figure 225, Figure 229, Figure 233, Figure 237, Figure 241, Figure 251, Figure 256, Figure 259, Figure 268, Figure 271, Table 31, Table 32
High	High		No	
Low	Low		No	
Low	Calibrated		Yes	Figure 195, Figure 201, Figure 202, Figure 220, Figure 221, Figure 226, Figure 230, Figure 234, Figure 238, Figure 241, Figure 251, Figure 260, Figure 263, Figure 268, Figure 271, Table 31, Table 32
Low	High	Least	Yes	Figure 196, Figure 203, Figure 204, Figure 205, Figure 215, Figure 222, Figure 223, Figure 227, Figure 231, Figure 235, Figure 239, Figure 241, Figure 251, Figure 264, Figure 267, Figure 268, Figure 271, Table 31, Table 32

Table 30. Stress Periods and Bases for Assumed Pumping Rates for Transient Simulation to 2050

<i>Stress Period</i>				<i>Basis for Assumed Pumping Rates</i>
<i>Regional Model ID</i>	<i>Local Model ID</i>	<i>Starts Jan. 1</i>	<i>Ends Dec. 31</i>	
1	40	2003	2004	Reported or estimated 2003 pumping (IL), estimated 2005 pumping (IN, WI)
2	41	2005	2009	Estimated 2005 pumping
3	42	2010	2014	Estimated 2010 pumping
4	43	2015	2019	Estimated 2015 pumping
5	44	2020	2024	Estimated 2020 pumping
6	45	2025	2029	Estimated 2025 pumping
7	46	2030	2034	Estimated 2030 pumping
8	47	2035	2039	Estimated 2035 pumping
9	48	2040	2044	Estimated 2040 pumping
10	49	2045	2049	Estimated 2045 pumping

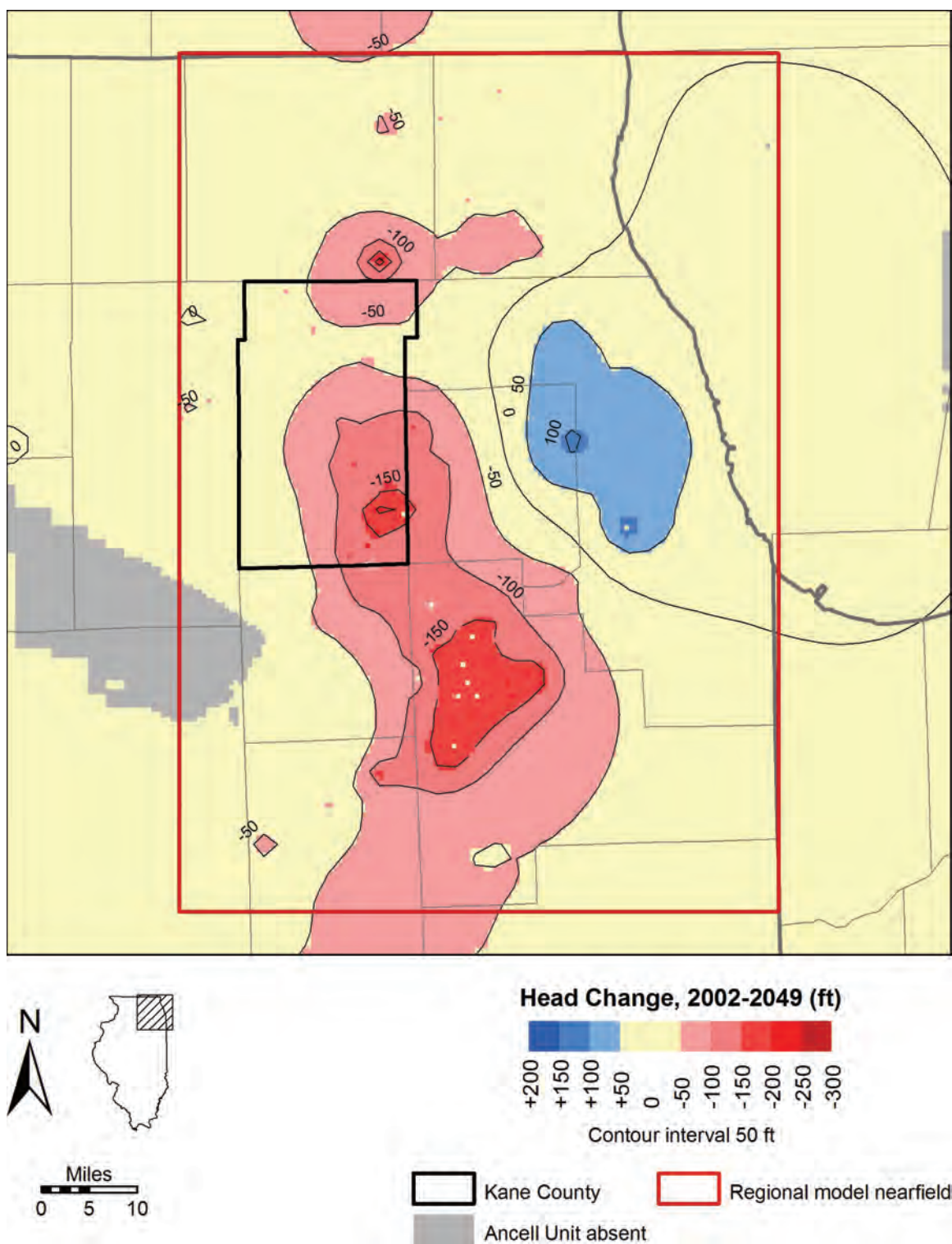


Figure 193. Estimated head change between the end of 2002 and end of 2049 in Ancell Unit under a scenario of high pumping and low recharge rates.

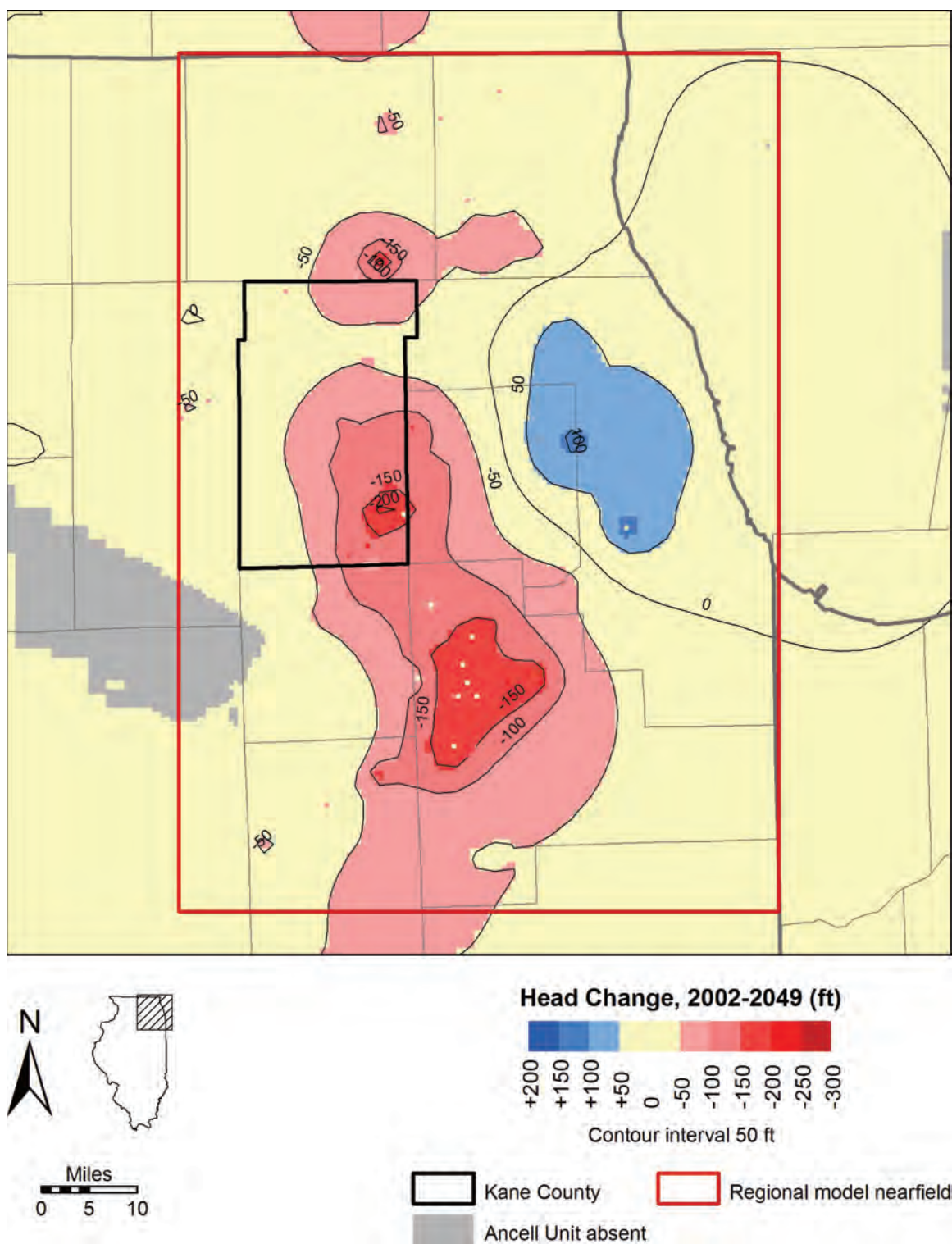


Figure 194. Estimated head change between the end of 2002 and end of 2049 in Ancell Unit under a scenario of high pumping and model-calibrated recharge rates.

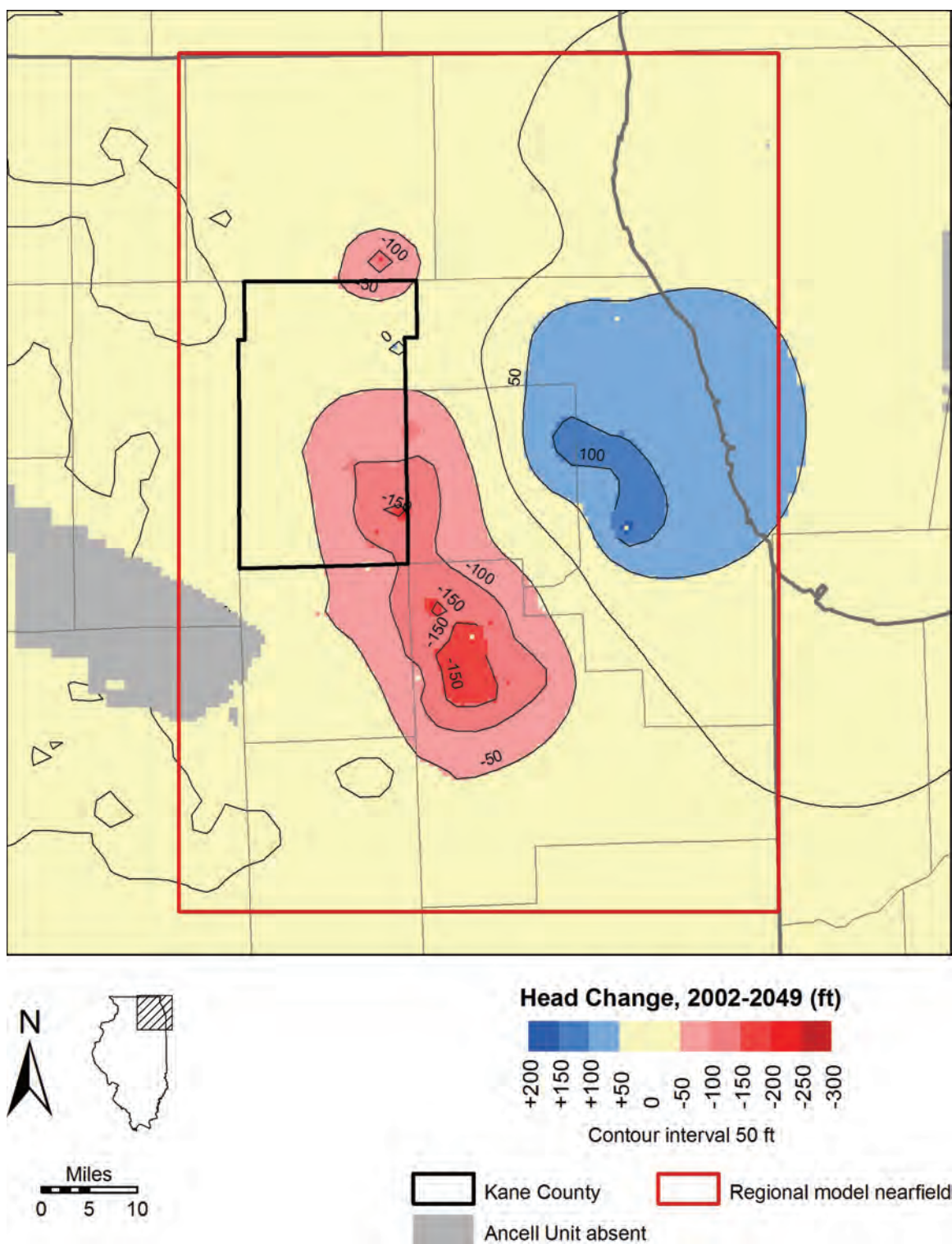


Figure 195. Estimated head change between the end of 2002 and end of 2049 in Ancell Unit under a scenario of low pumping and model-calibrated recharge rates.

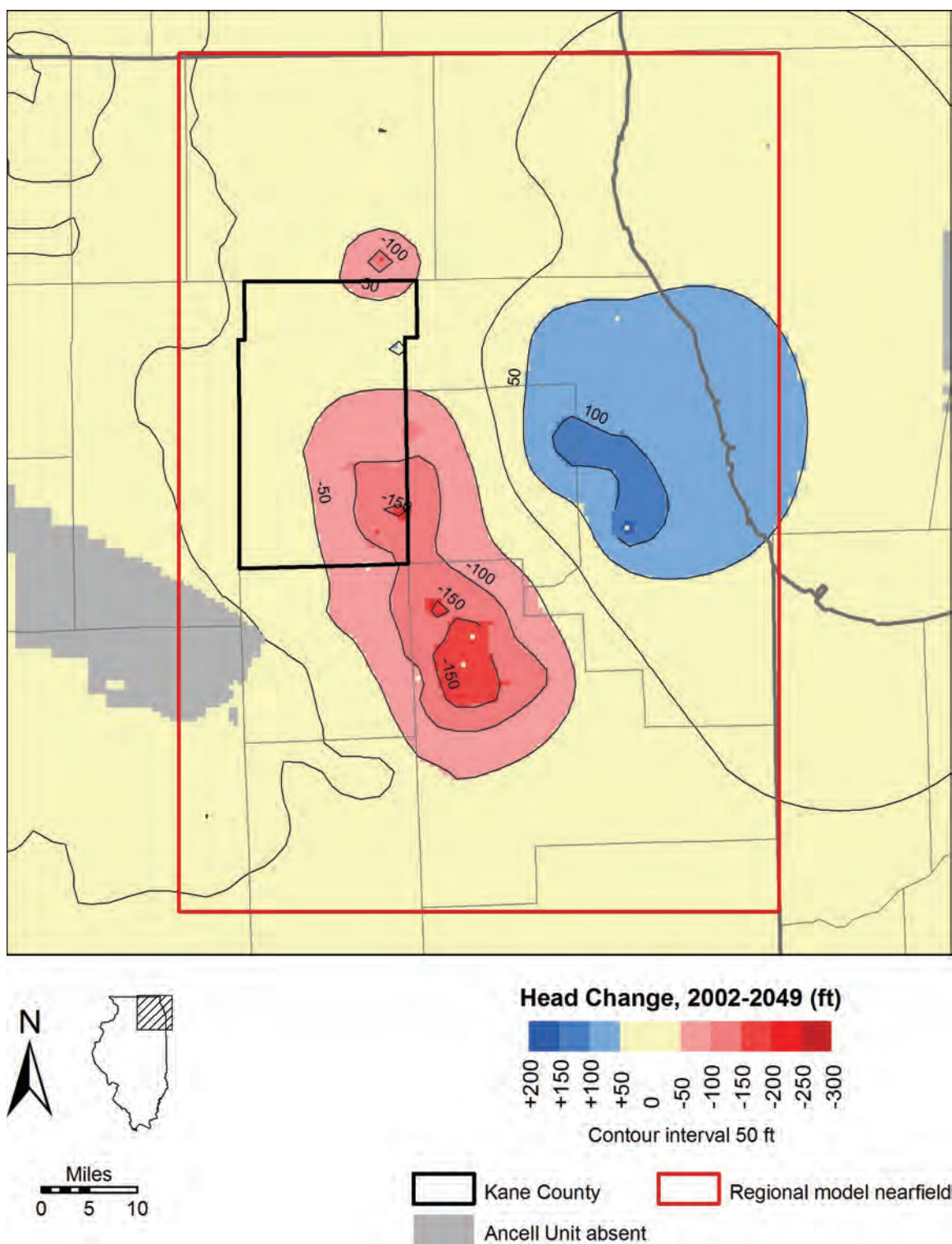


Figure 196. Estimated head change between the end of 2002 and end of 2049 in Ancell Unit under a scenario of low pumping and high recharge rates.

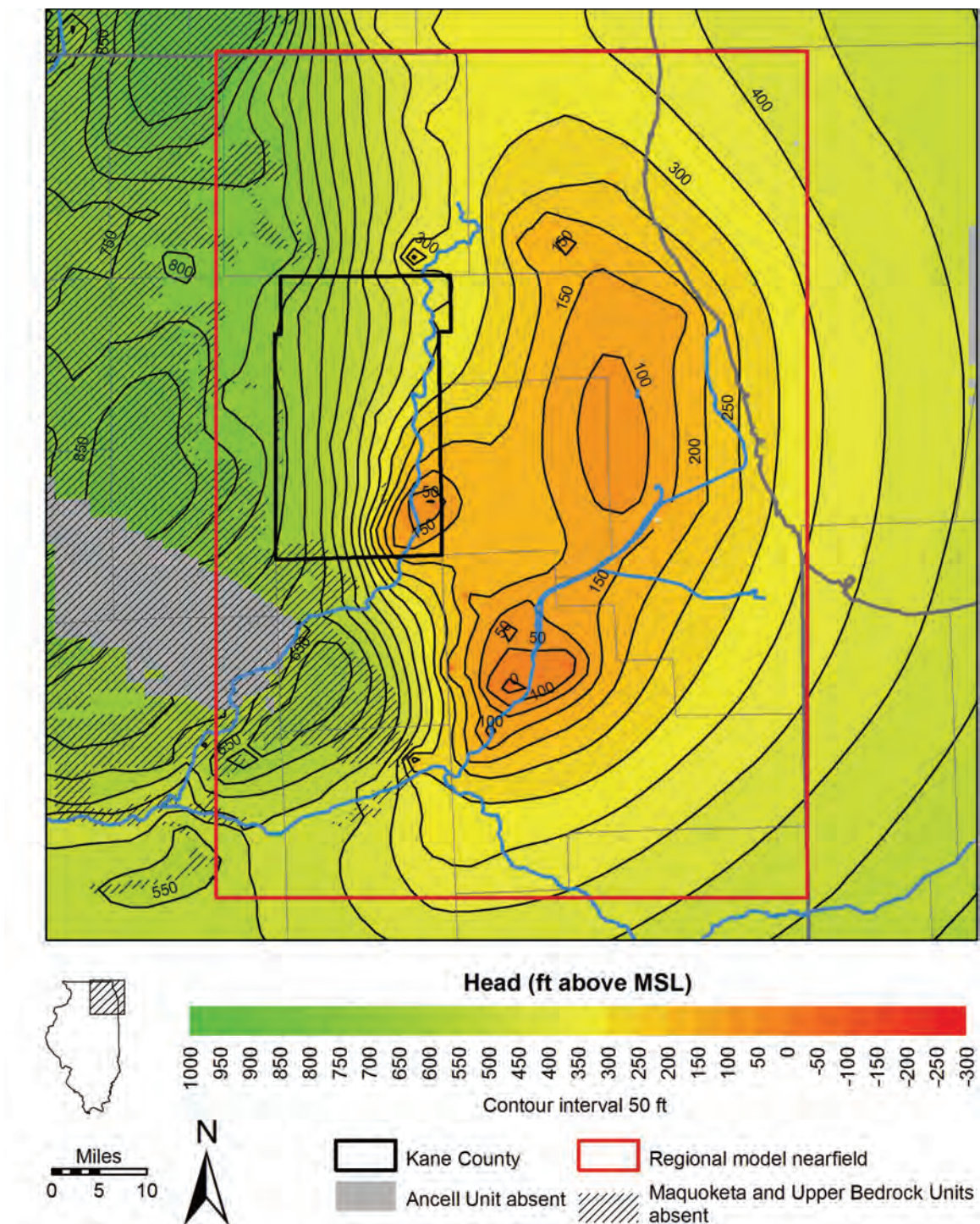


Figure 197. Simulated head in Ancell Unit in 2024 under a scenario of high pumping with low recharge rates.

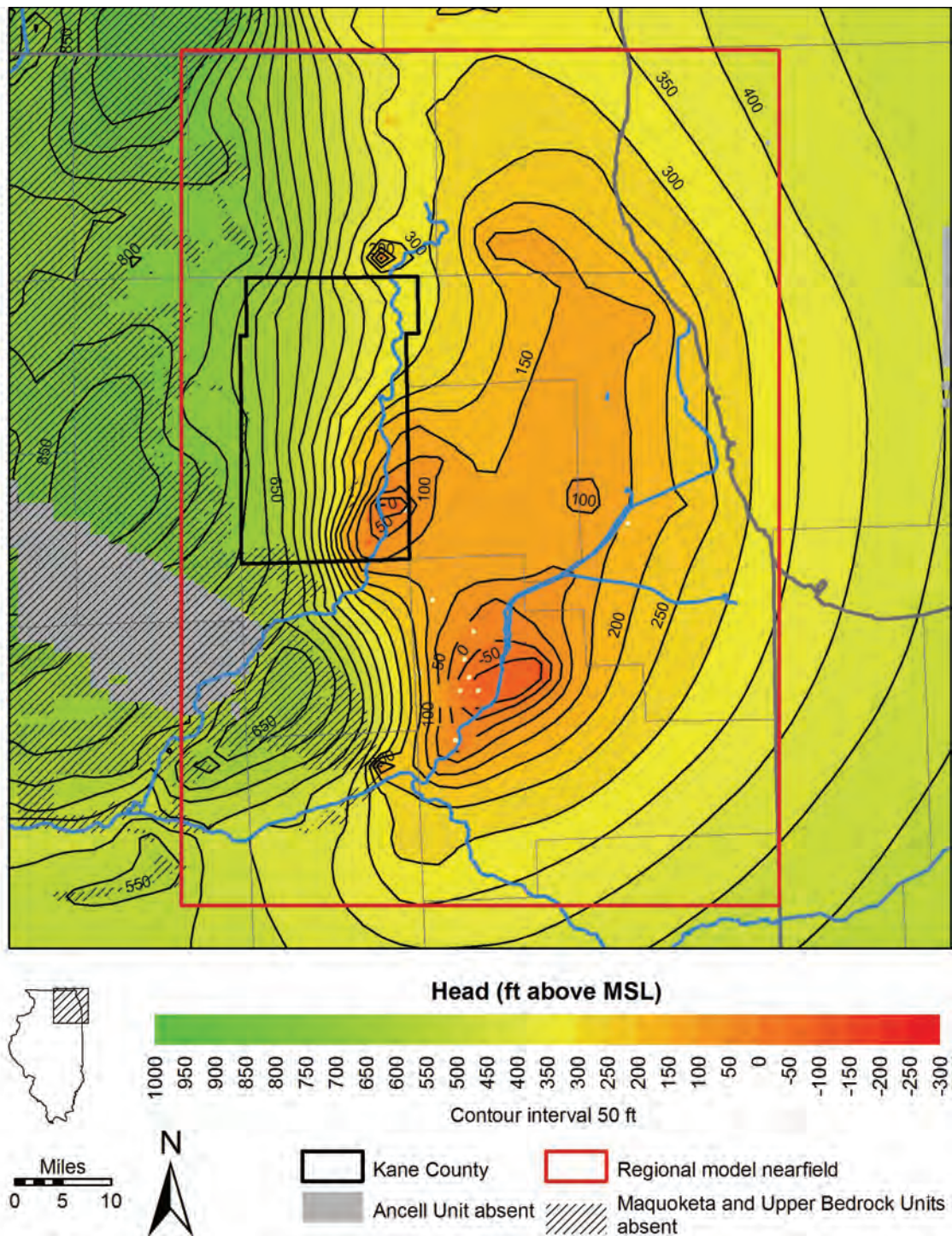


Figure 198. Simulated head in Ancell Unit in 2049 under a scenario of high pumping with low recharge rates.

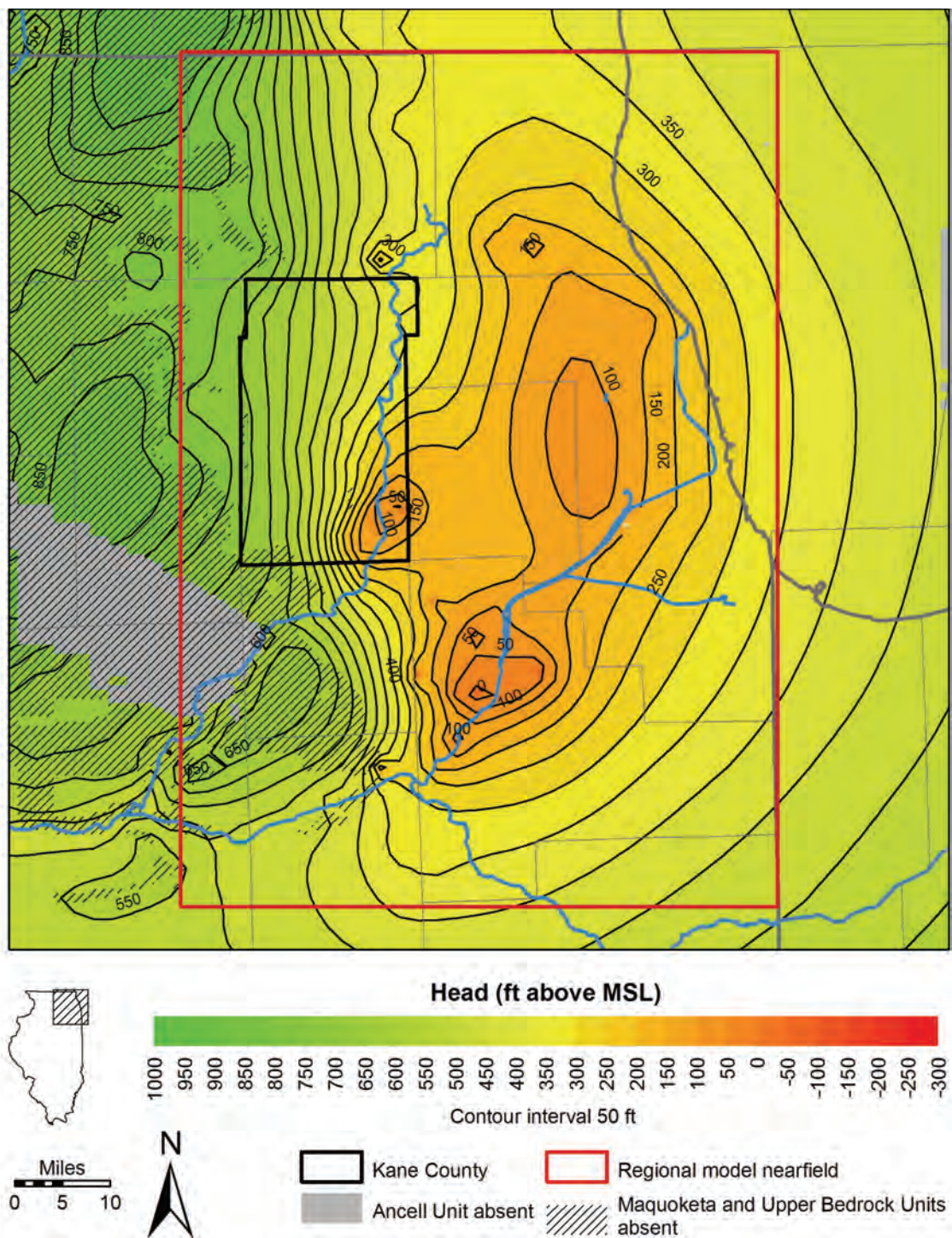


Figure 199. Simulated head in Ancell Unit in 2024 under a scenario of high pumping with model-calibrated recharge rates.

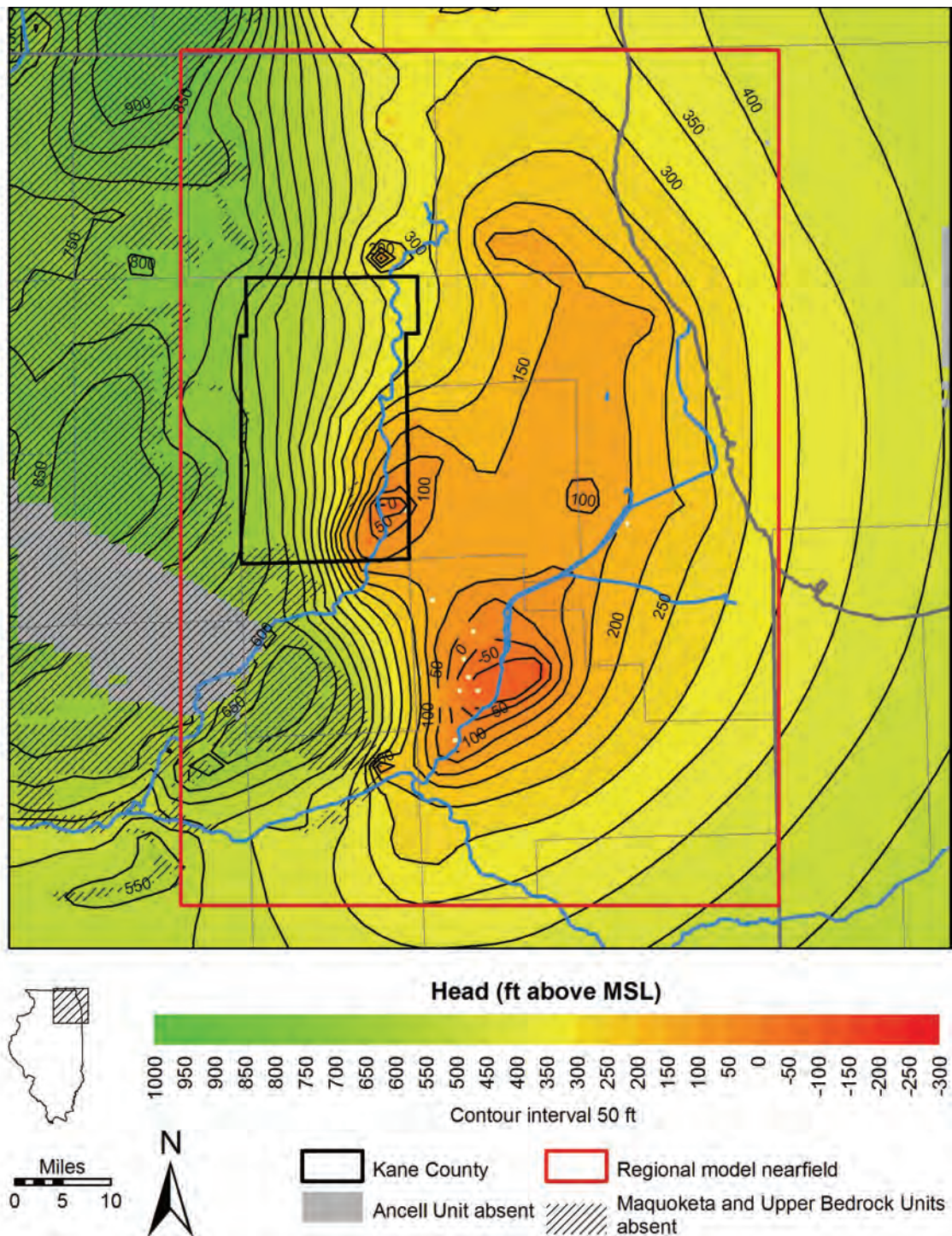


Figure 200. Simulated head in Ancell Unit in 2049 under a scenario of high pumping with model-calibrated recharge rates.

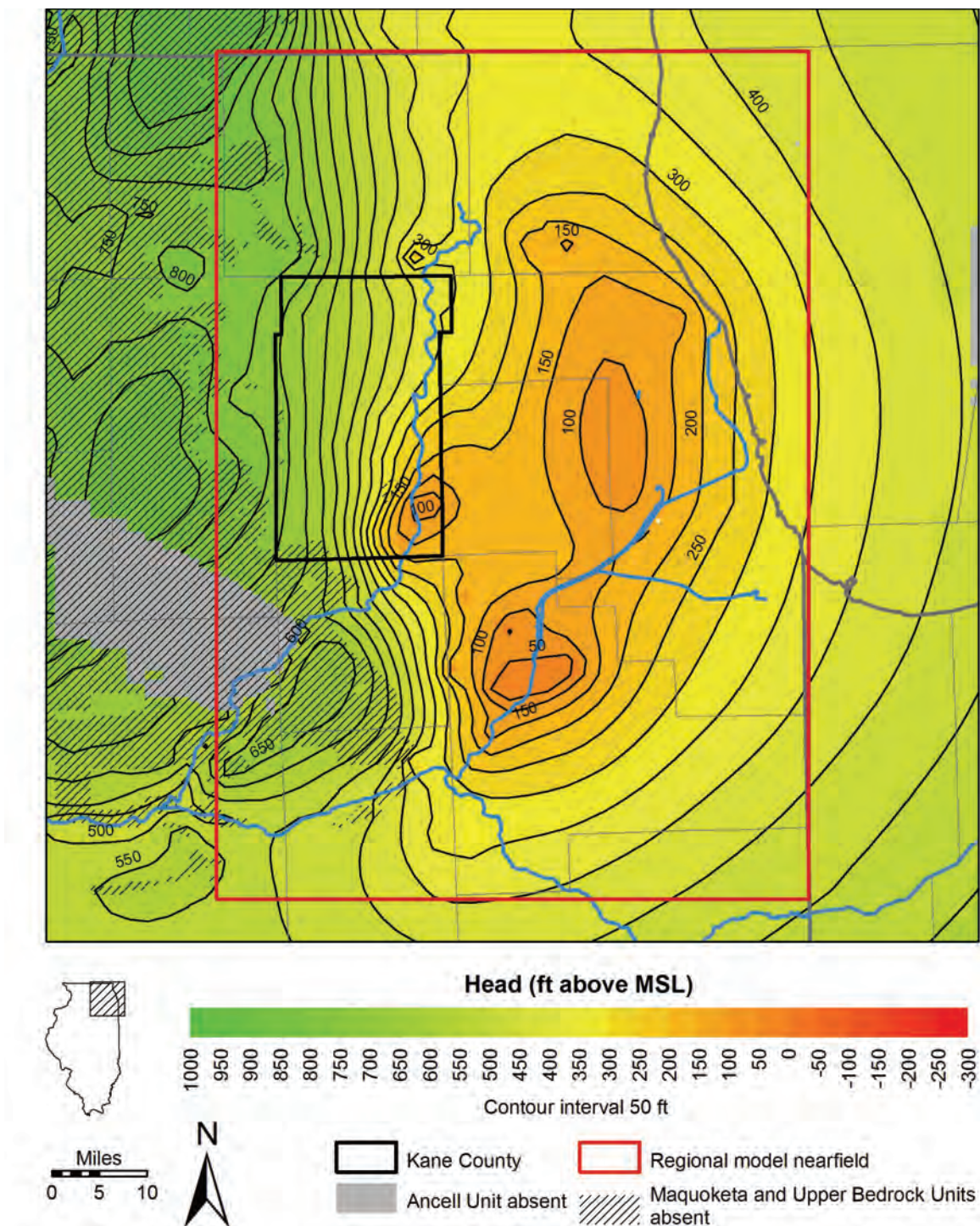


Figure 201. Simulated head in Ancell Unit in 2024 under a scenario of low pumping with model-calibrated recharge rates.

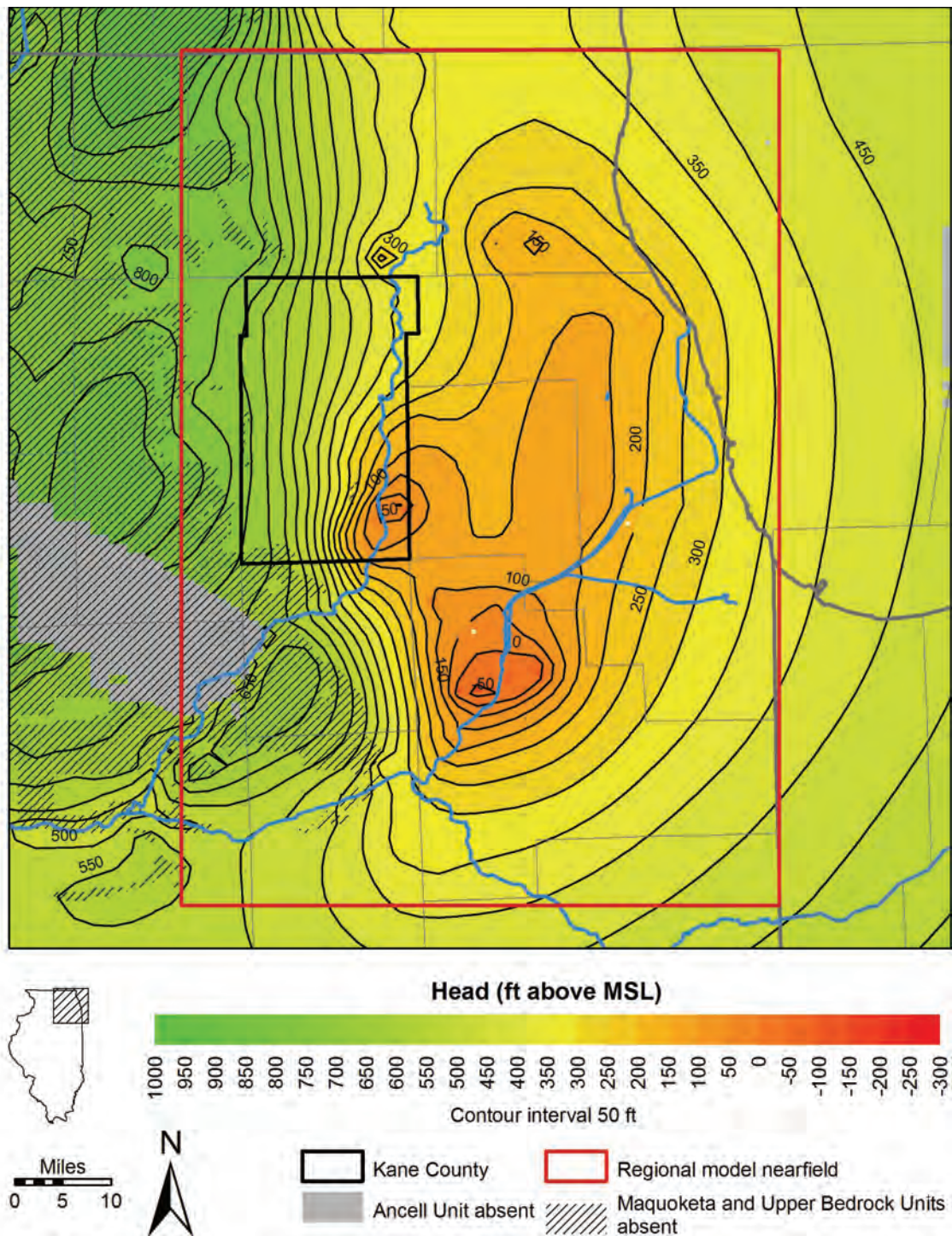


Figure 202. Simulated head in Ancell Unit in 2049 under a scenario of low pumping with model-calibrated recharge rates.

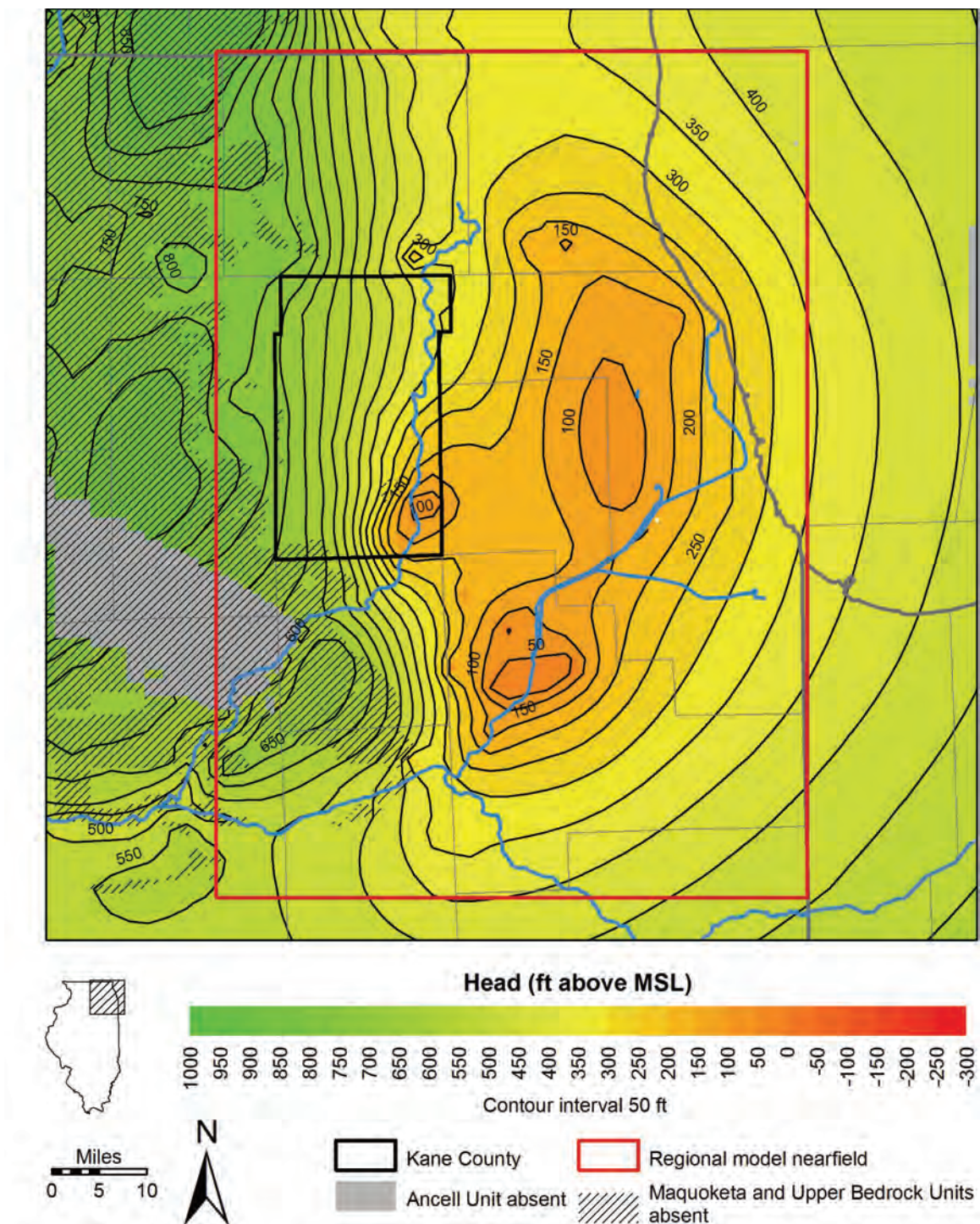


Figure 203. Simulated head in Ancell Unit in 2024 under a scenario of low pumping with high recharge rates.

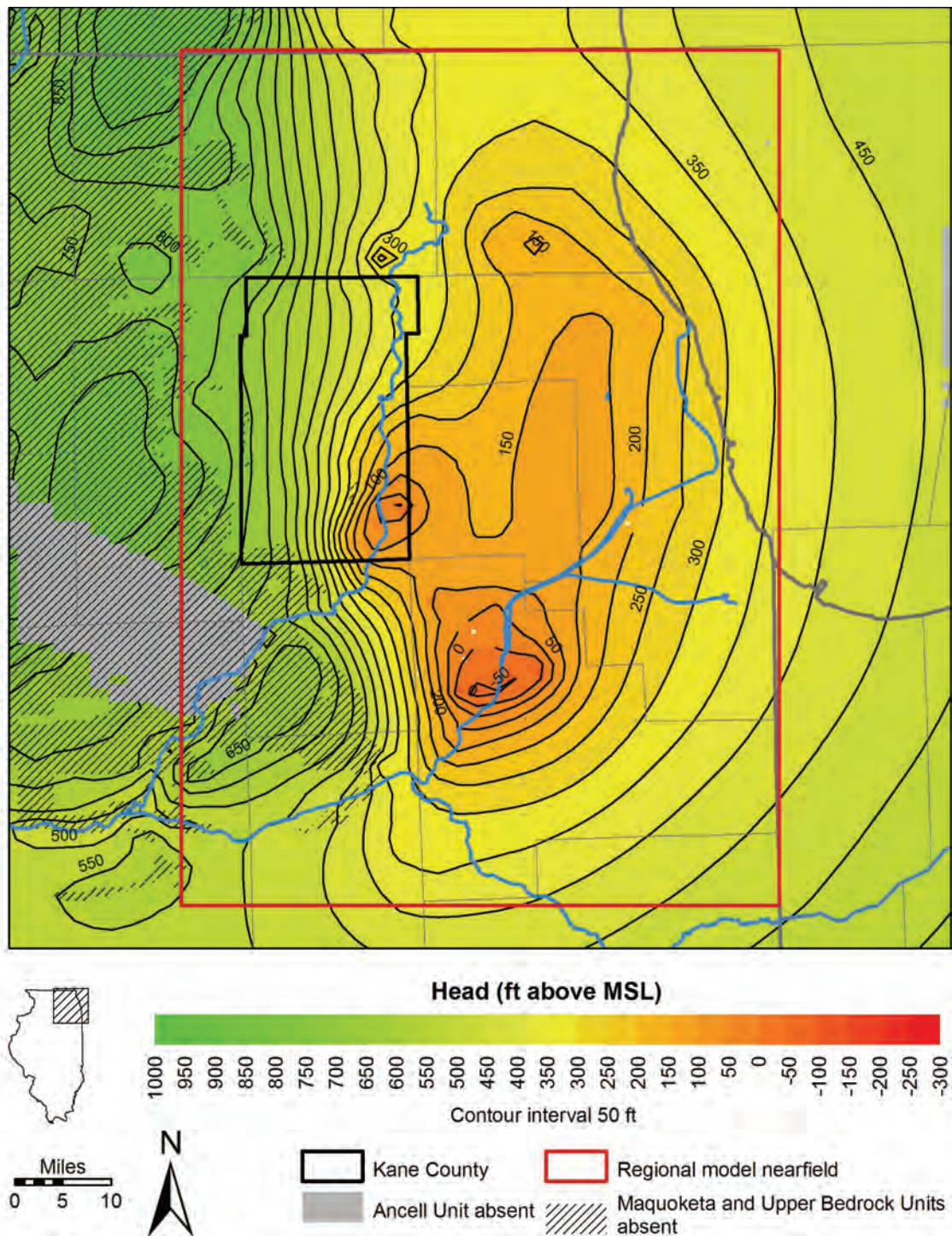


Figure 204. Simulated head in Ancell Unit in 2049 under a scenario of low pumping with high recharge rates.

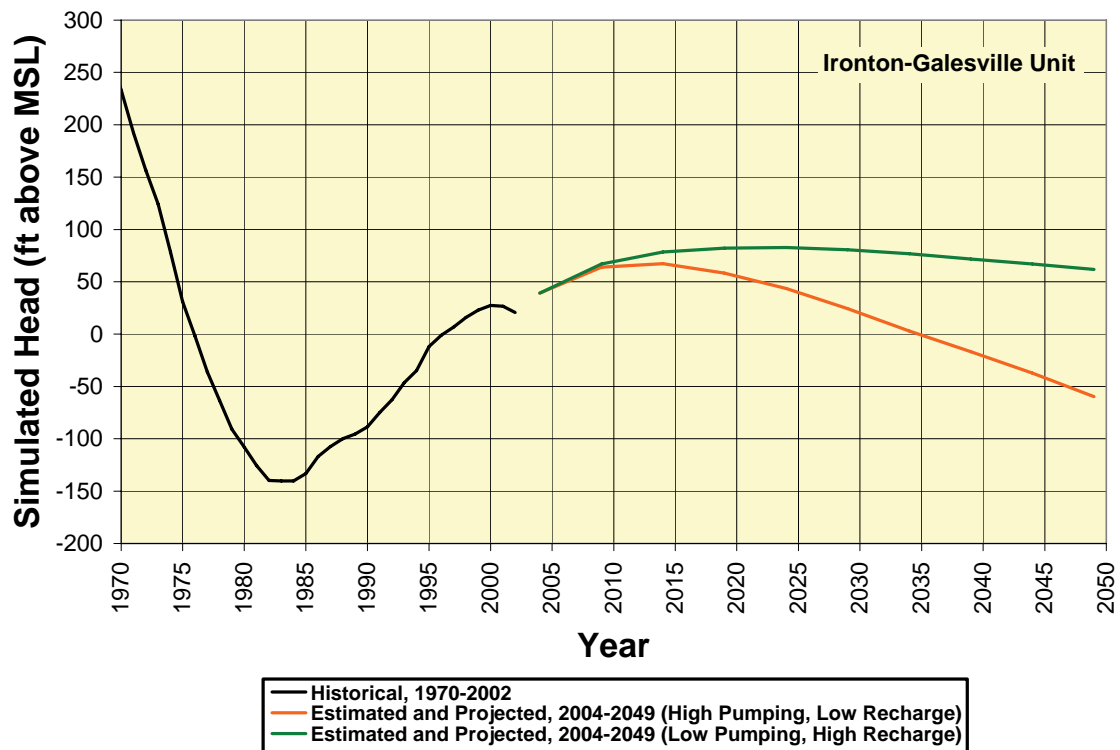
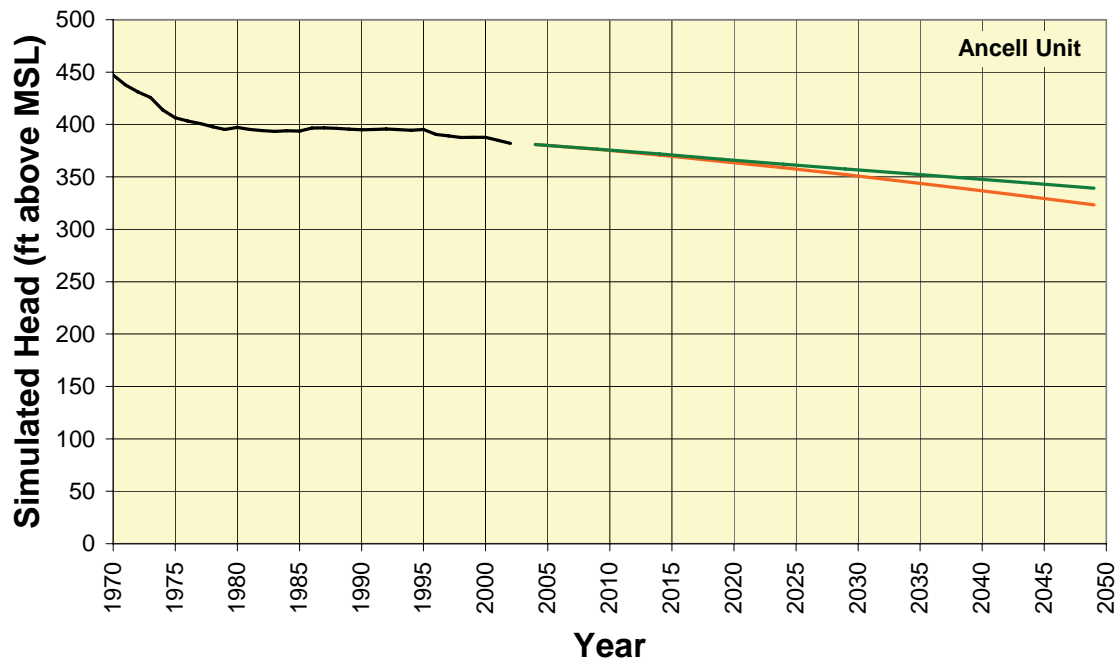


Figure 205. Simulated heads from end of 1970 through end of 2049 in Ancell (top) and Ironton-Galesville Units (bottom) at Carpentersville. See Figure 114 for location.

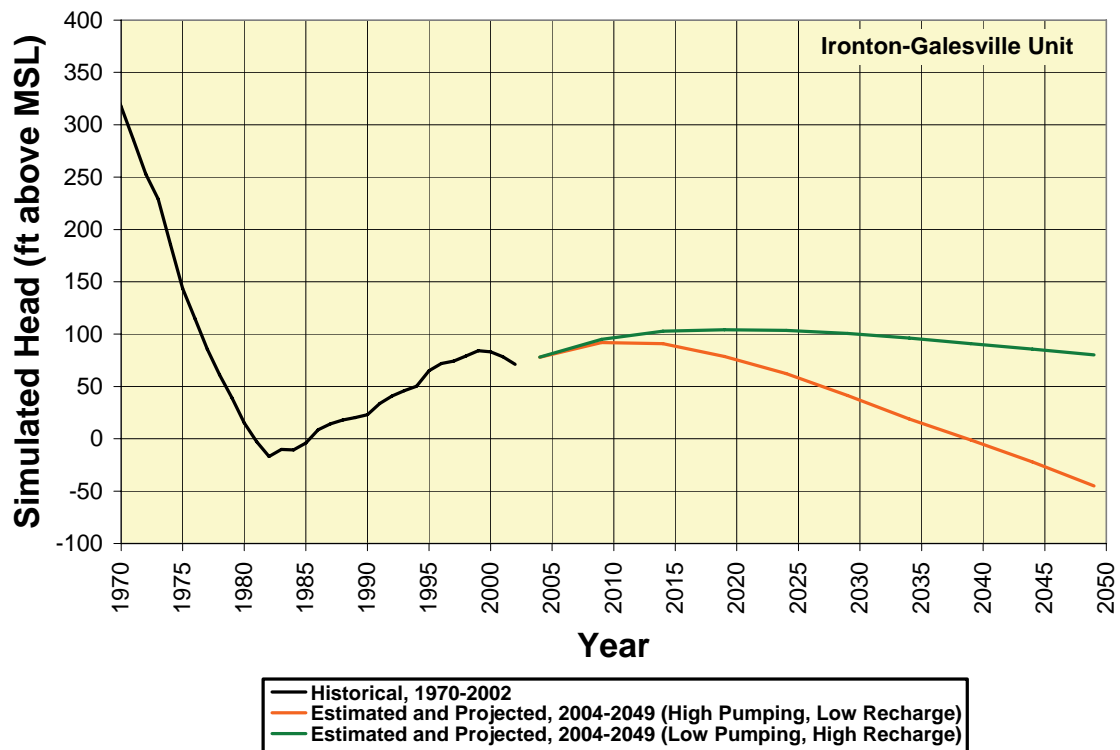
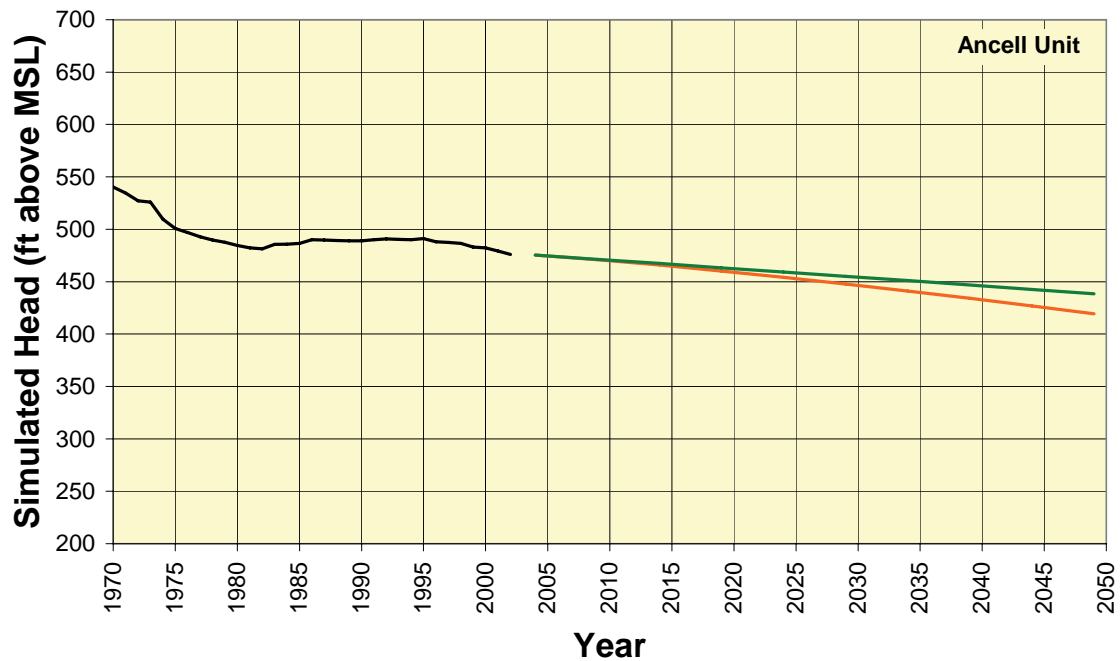


Figure 206. Simulated heads from end of 1970 through end of 2049 in Ancell (top) and Ironton-Galesville Units (bottom) at Gilberts. See Figure 114 for location.

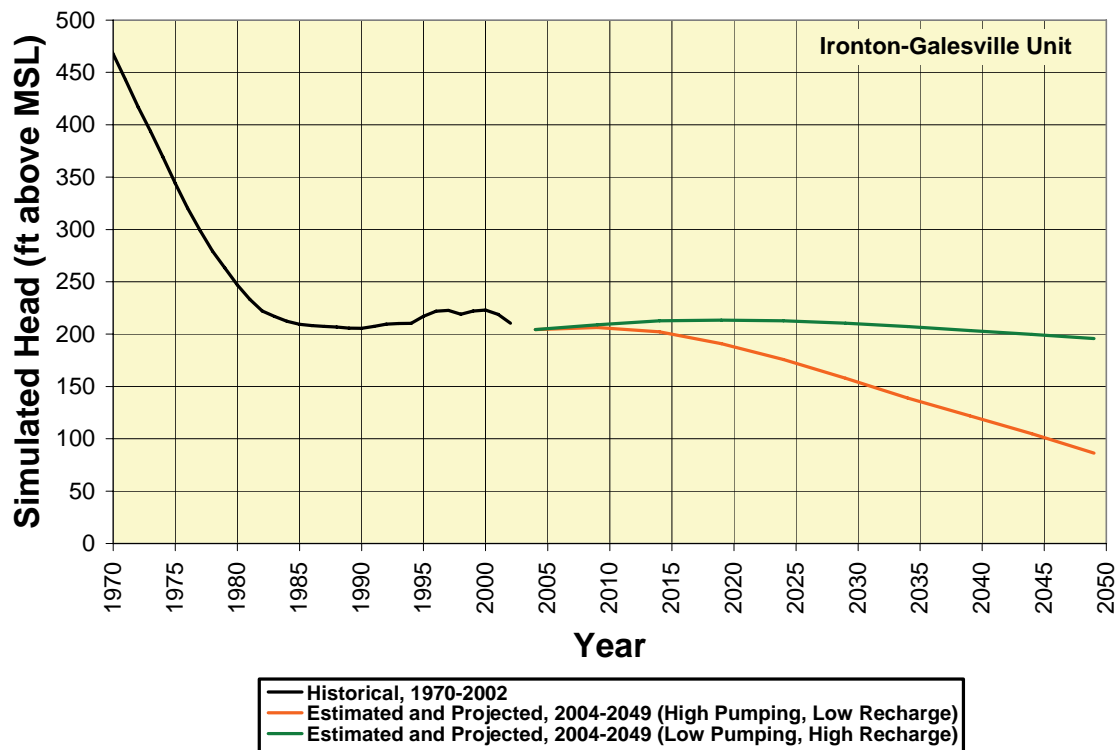
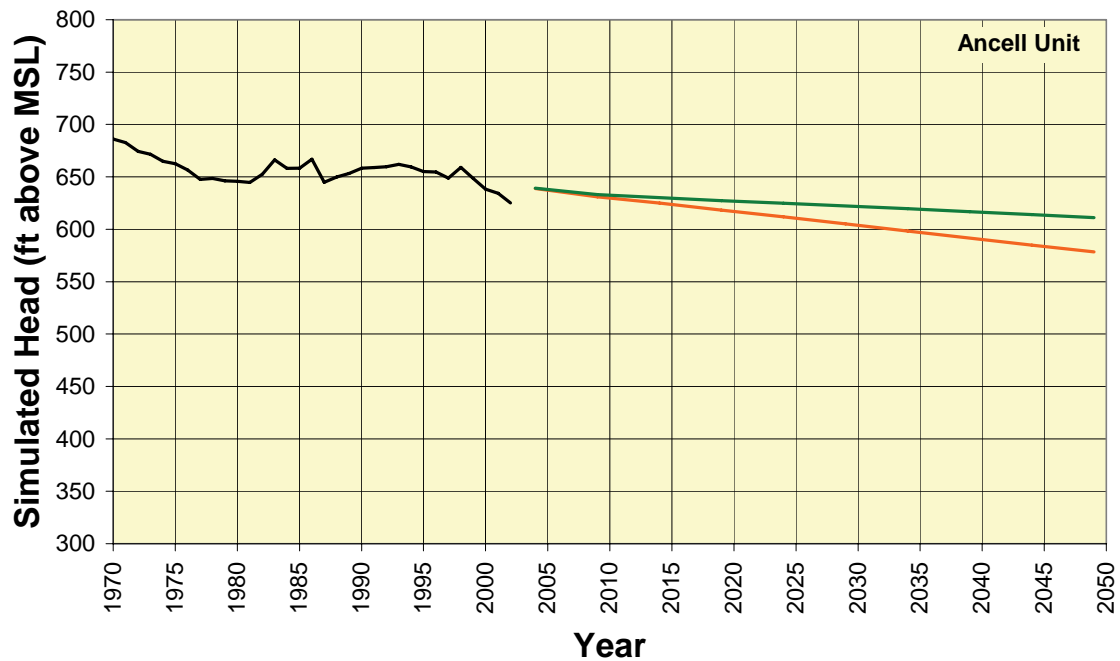


Figure 207. Simulated head from end of 1970 through end of 2049 in Ancell (top) and Ironton-Galesville Units (bottom) at Hampshire. See Figure 114 for location.

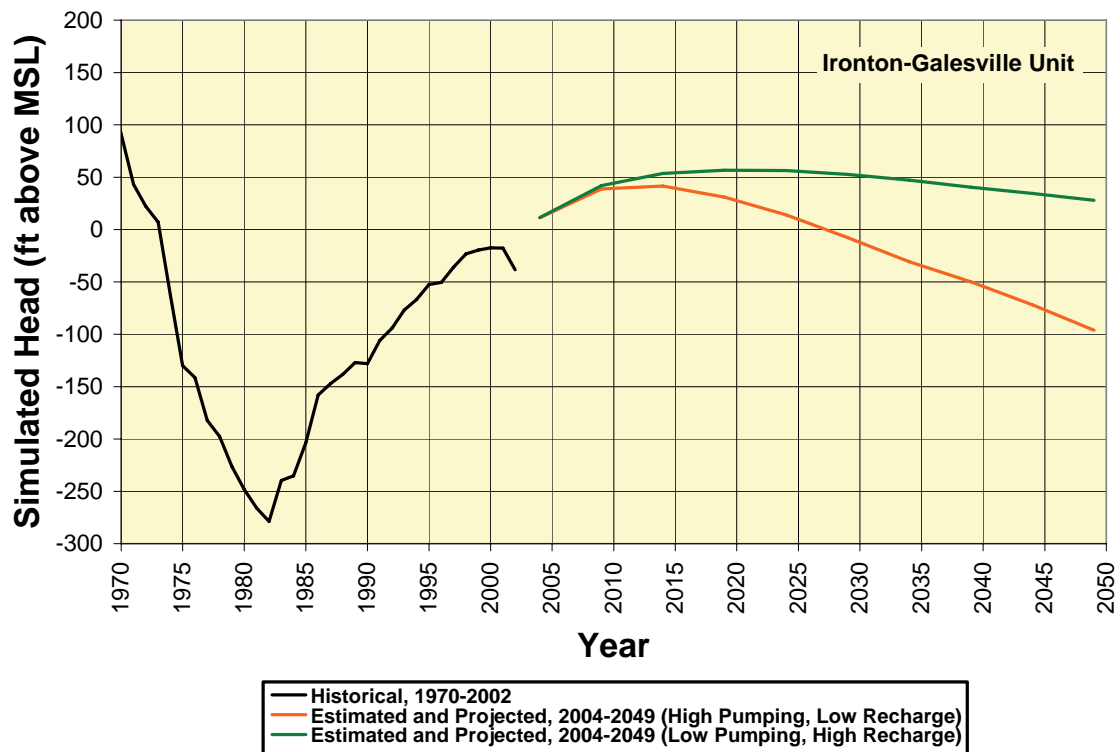
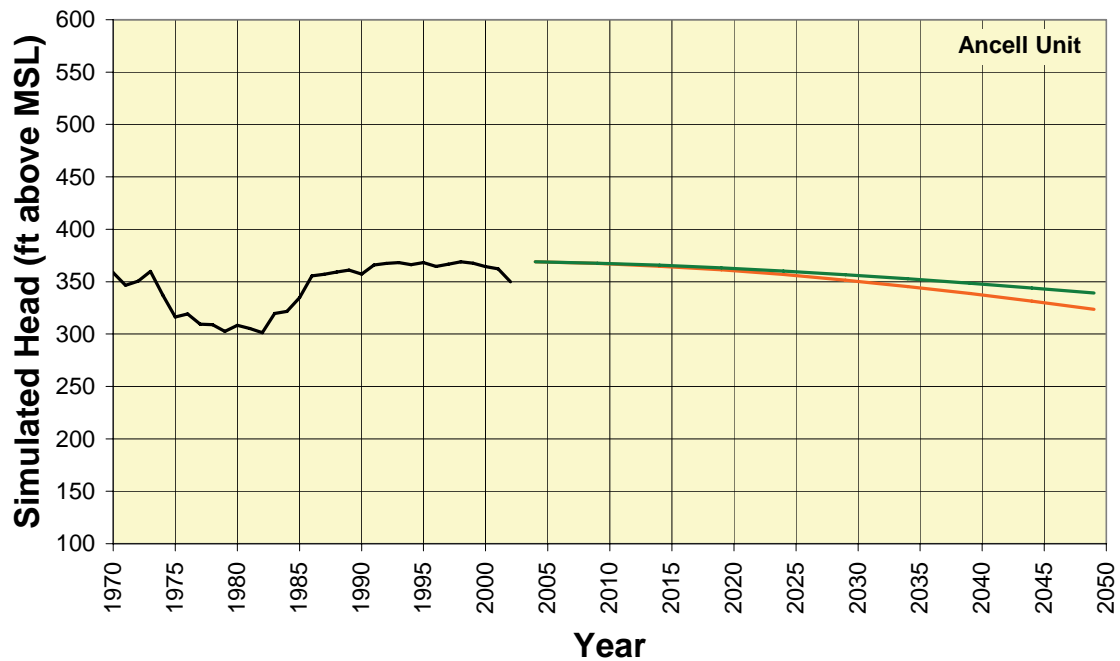


Figure 208. Simulated head from end of 1970 through end of 2049 in Ancell (top) and Ironton-Galesville Units (bottom) at Elgin. See Figure 114 for location.

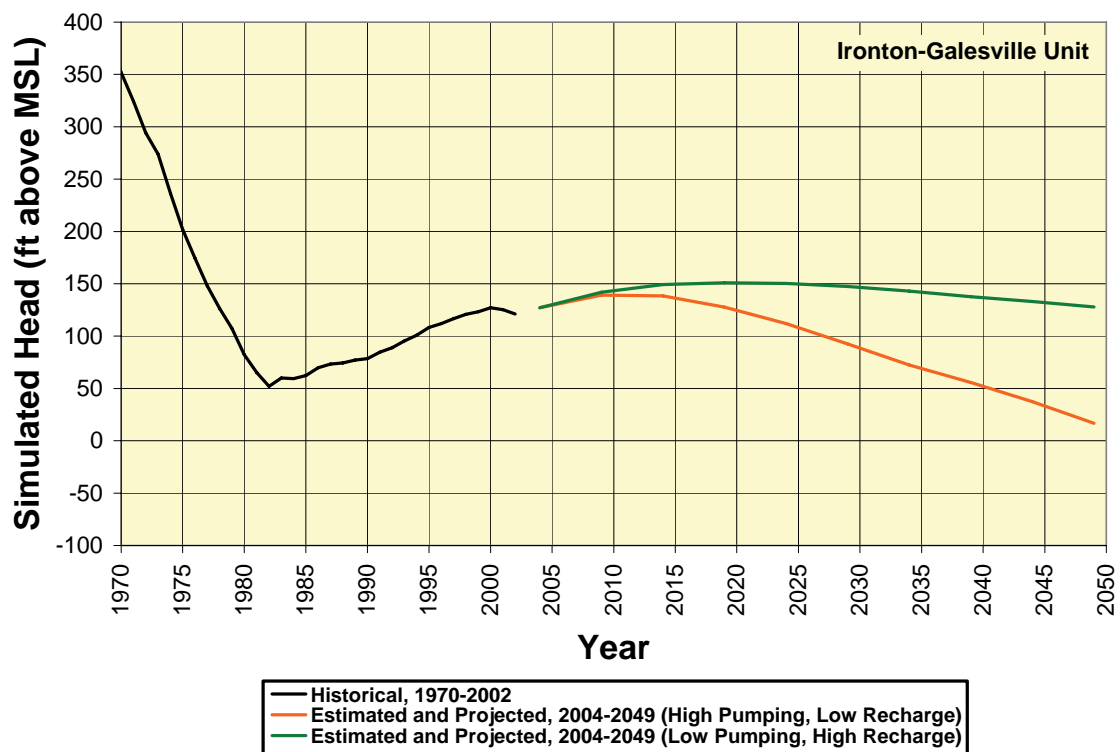
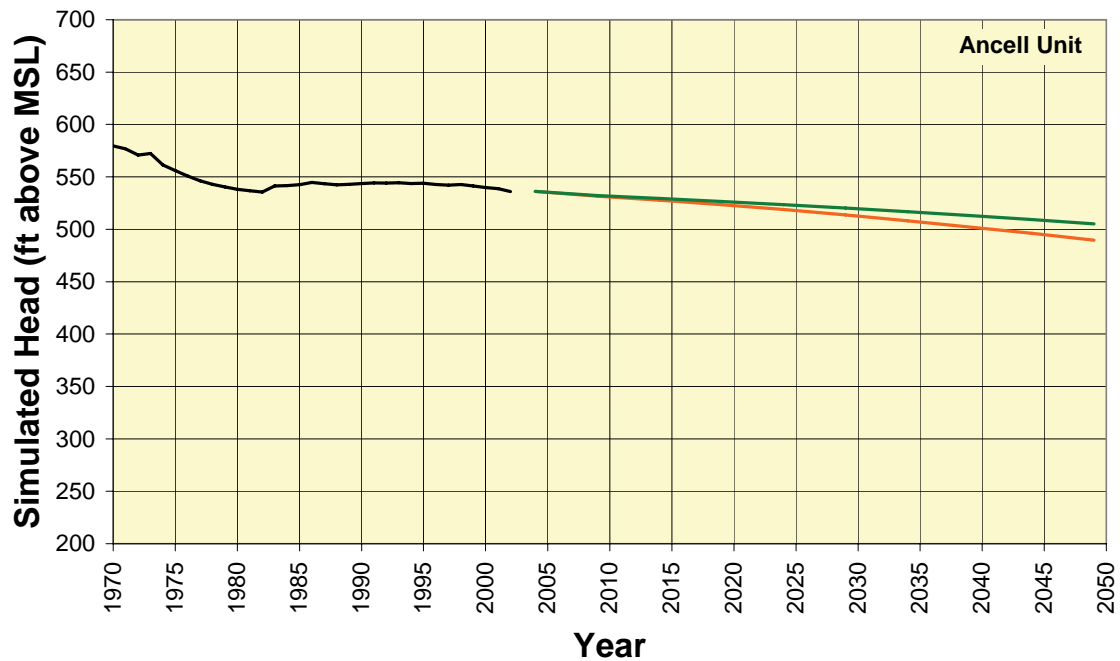


Figure 209. Simulated head from end of 1970 through end of 2049 in Ancell (top) and Ironton-Galesville Units (bottom) at Plato Center. See Figure 114 for location.

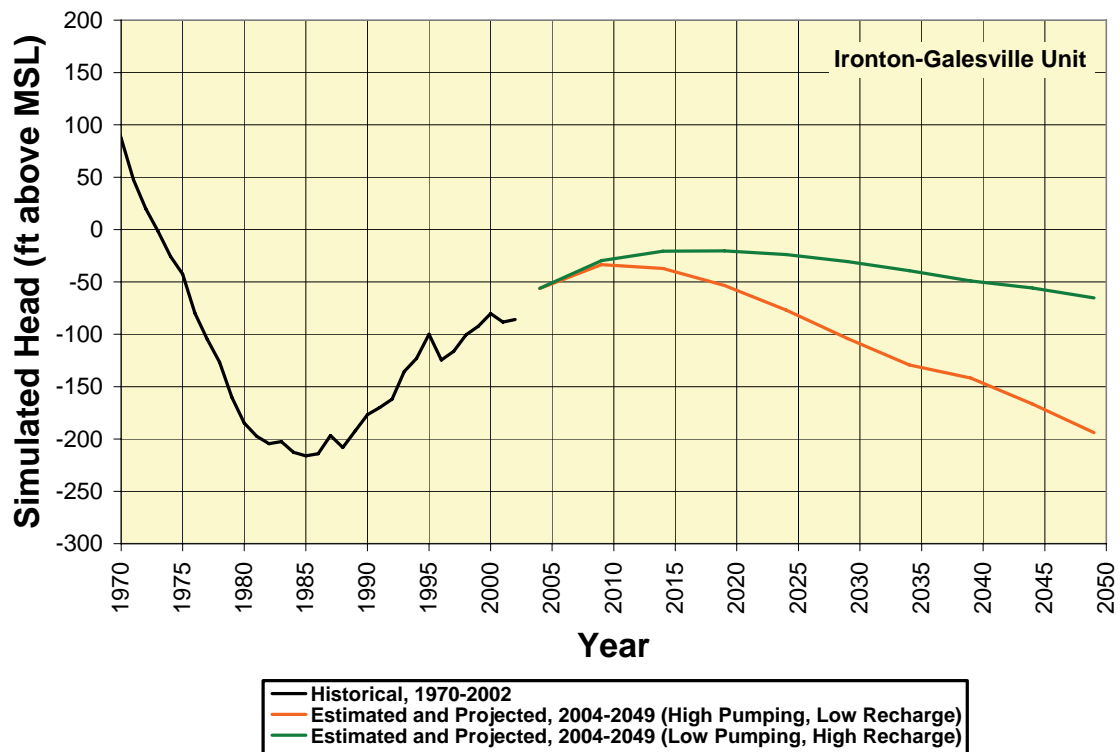
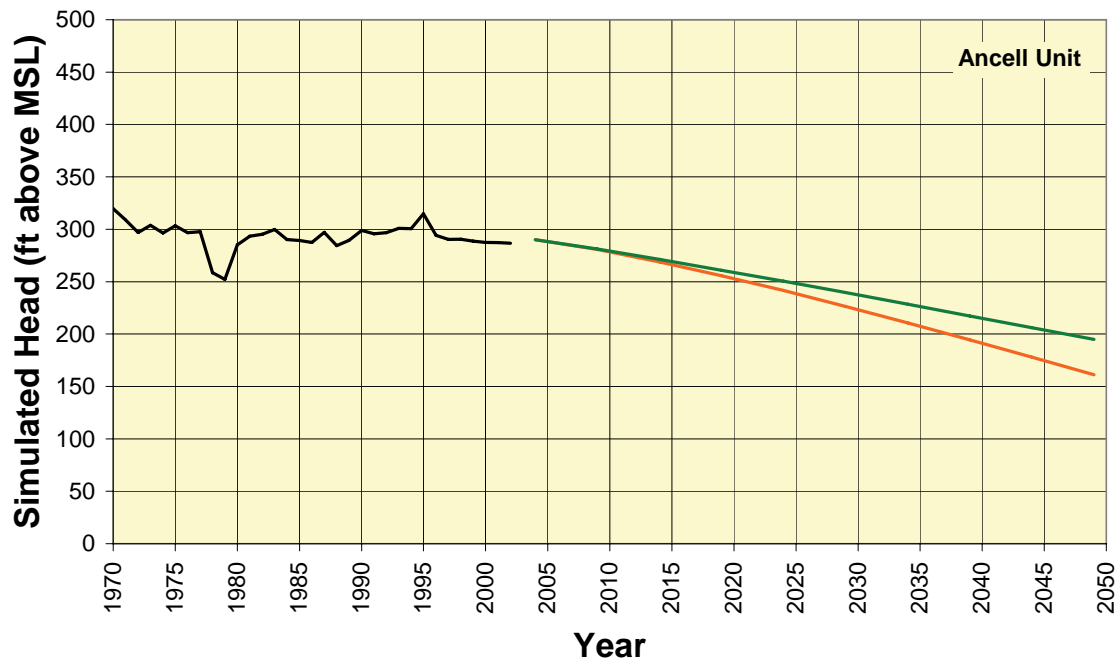


Figure 210. Simulated head from end of 1970 through end of 2049 in Ancell (top) and Ironton-Galesville Units (bottom) at St. Charles. See Figure 114 for location.

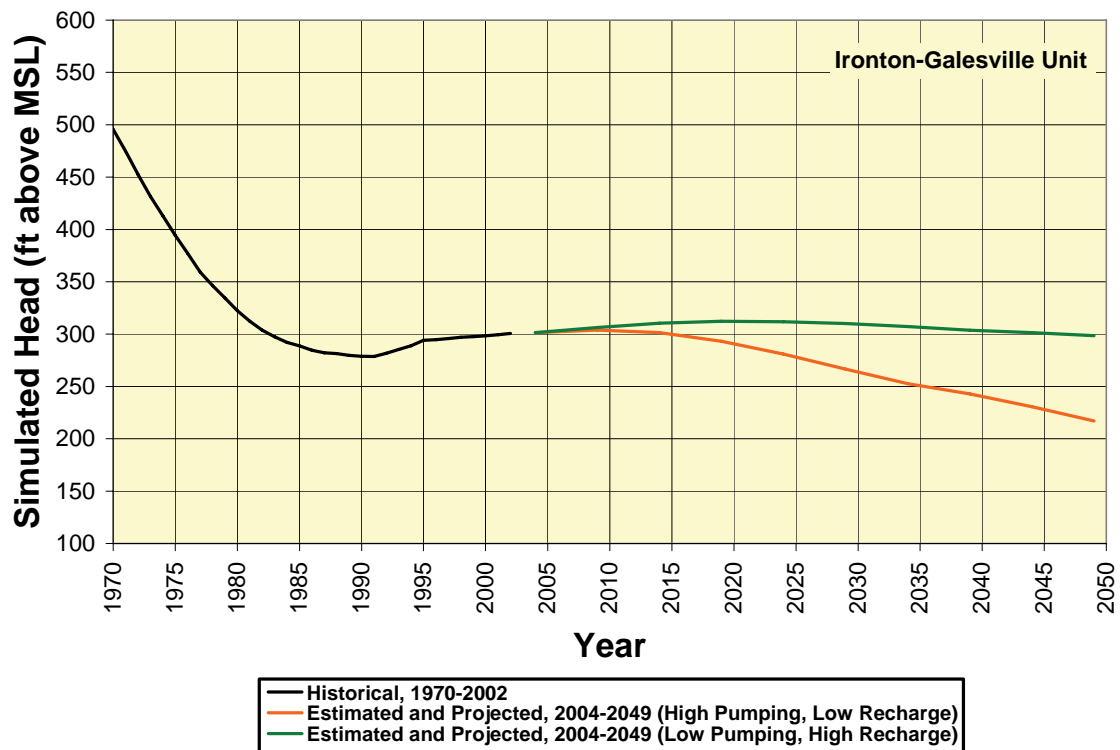
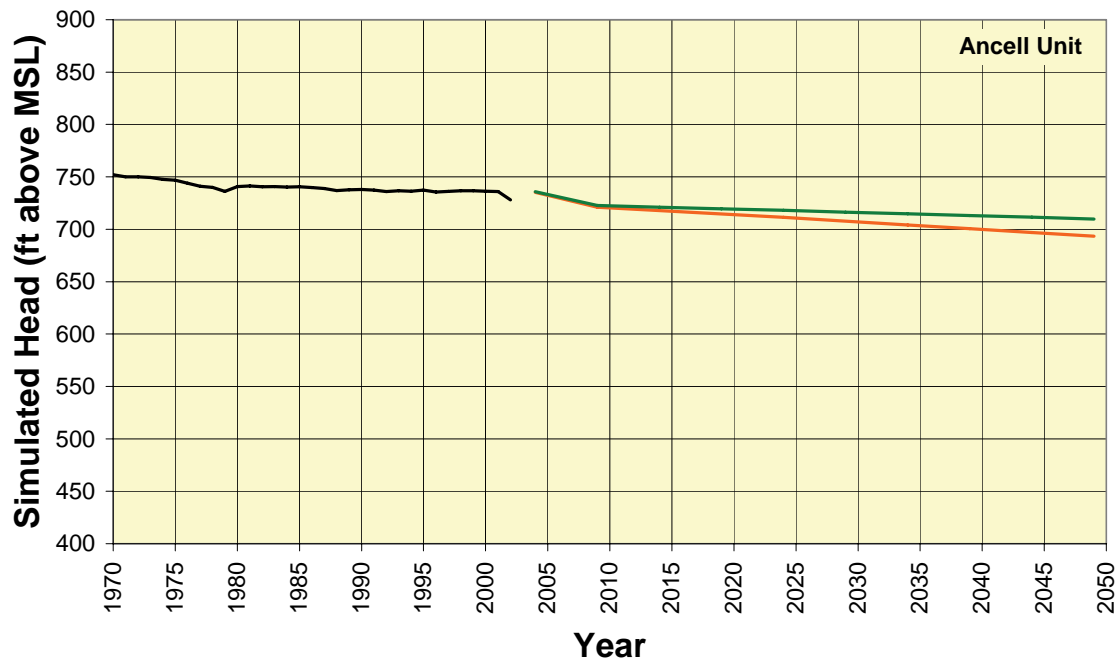


Figure 211. Simulated head from end of 1970 through end of 2049 in Ancell (top) and Ironton-Galesville Units (bottom) at Maple Park. See Figure 114 for location.

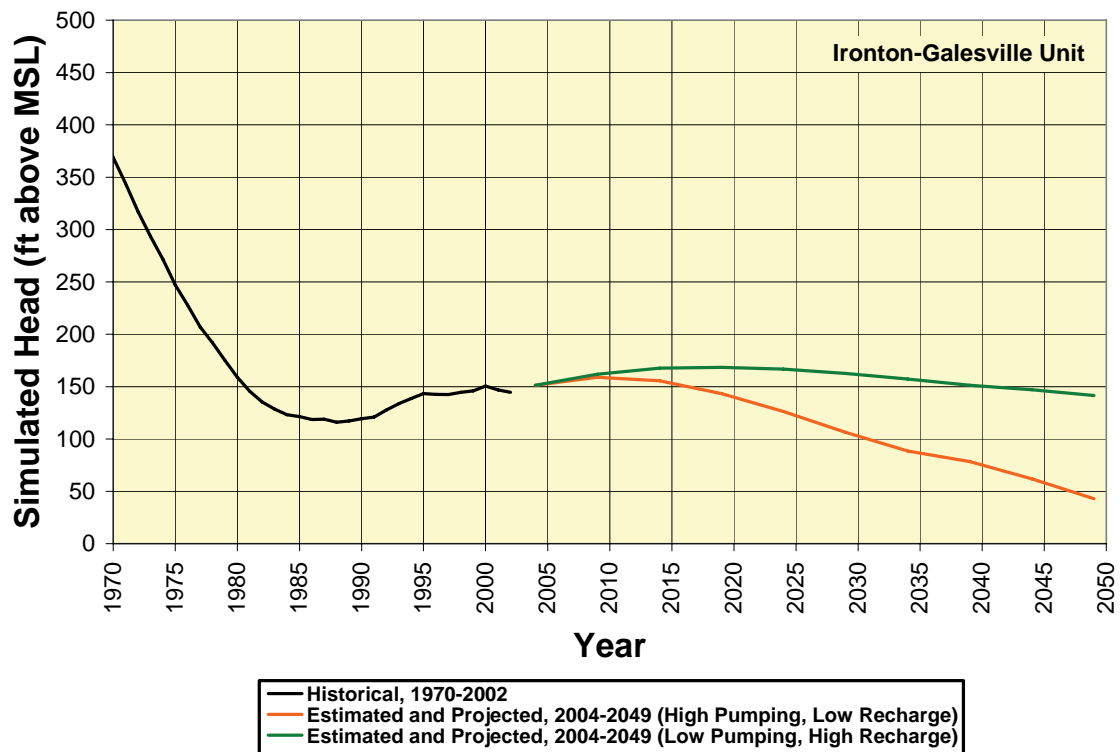
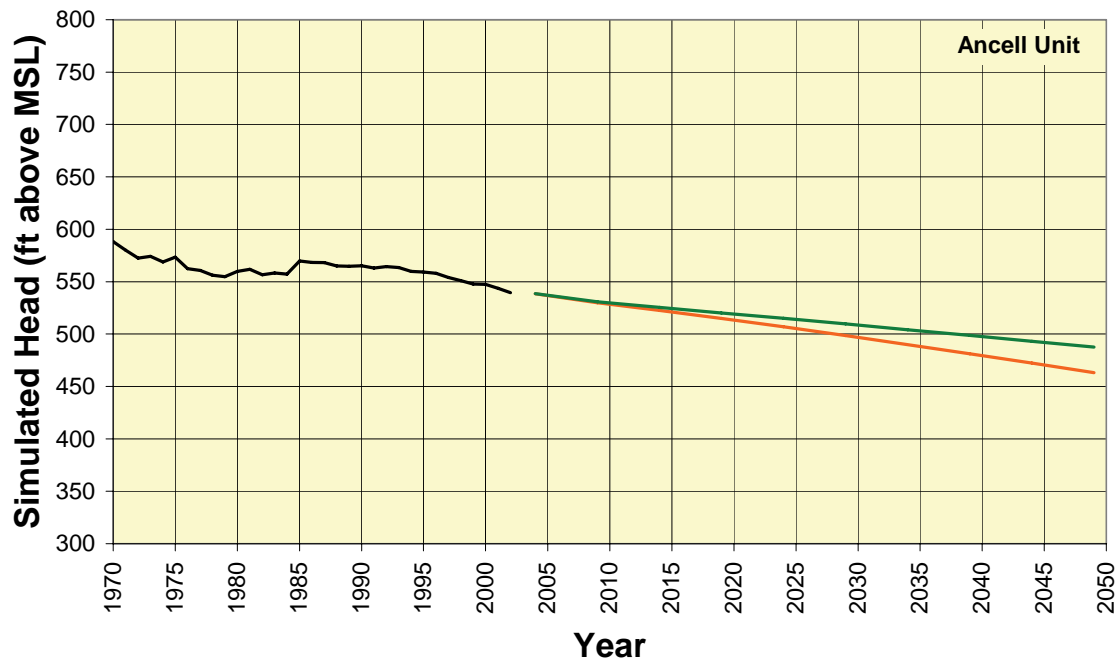


Figure 212. Simulated head from end of 1970 through end of 2049 in Ancell (top) and Ironton-Galesville Units (bottom) at Elburn. See Figure 114 for location.

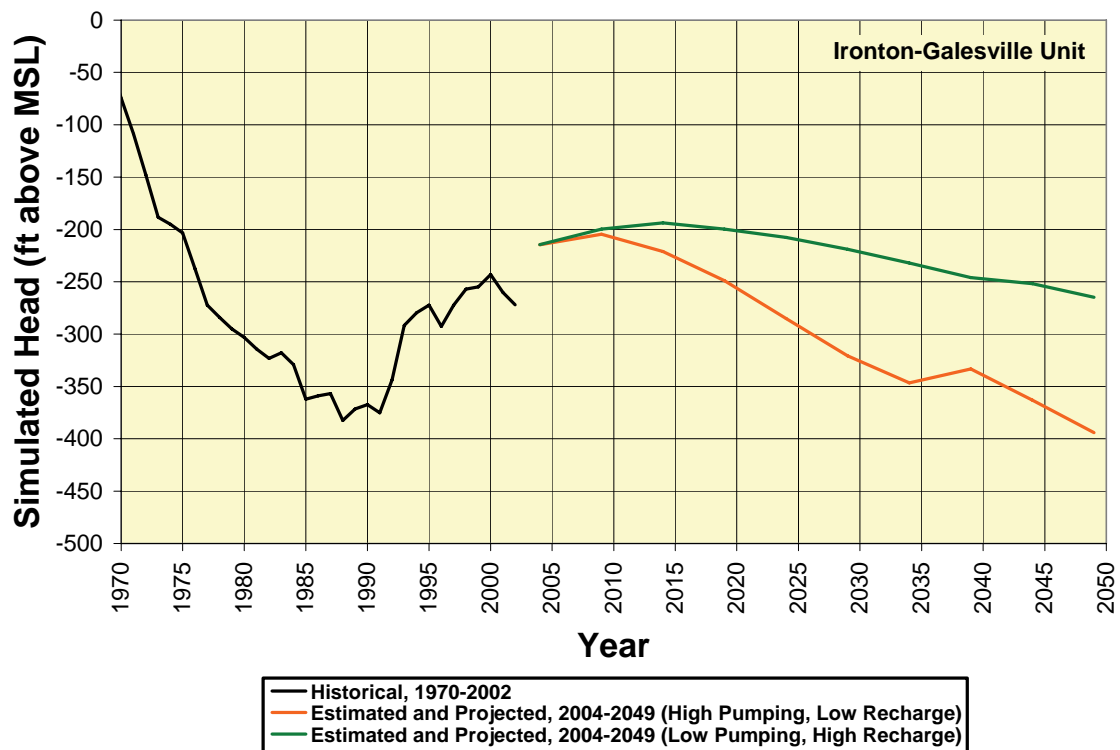
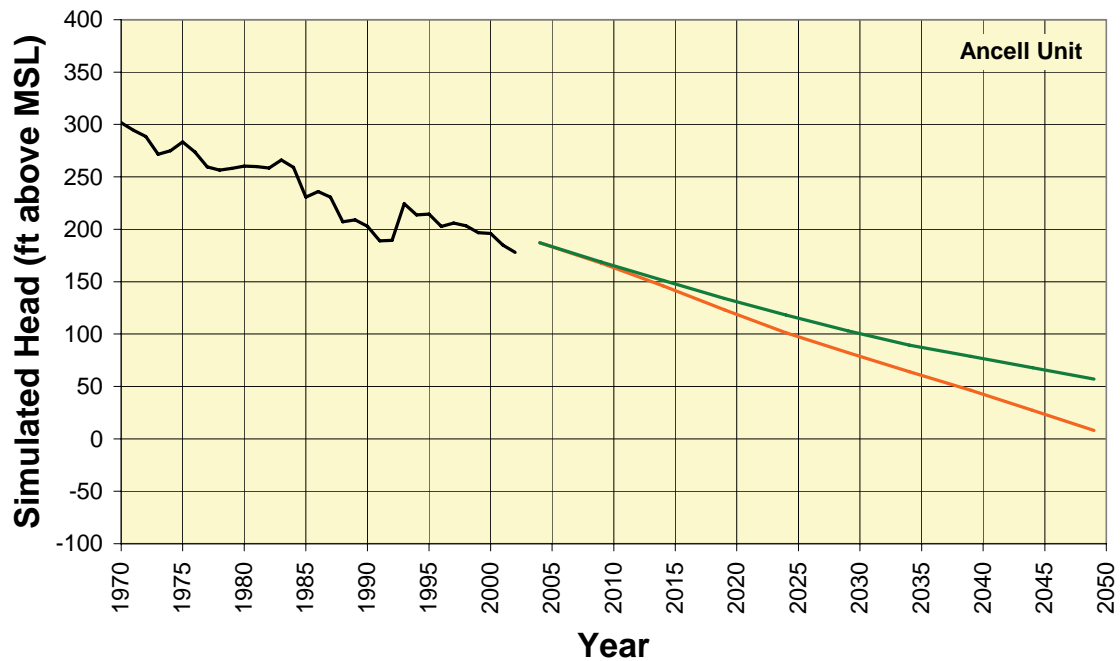


Figure 213. Simulated head from end of 1970 through end of 2049 in Ancell (top) and Ironton-Galesville Units (bottom) at Batavia. See Figure 114 for location.

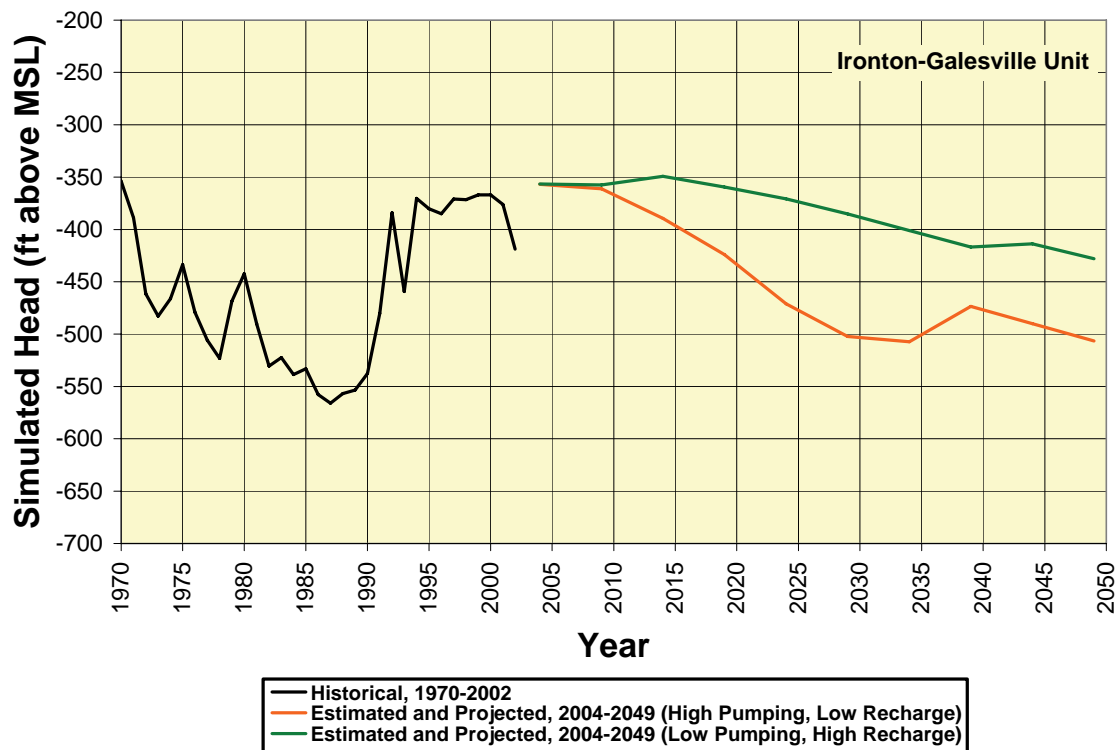
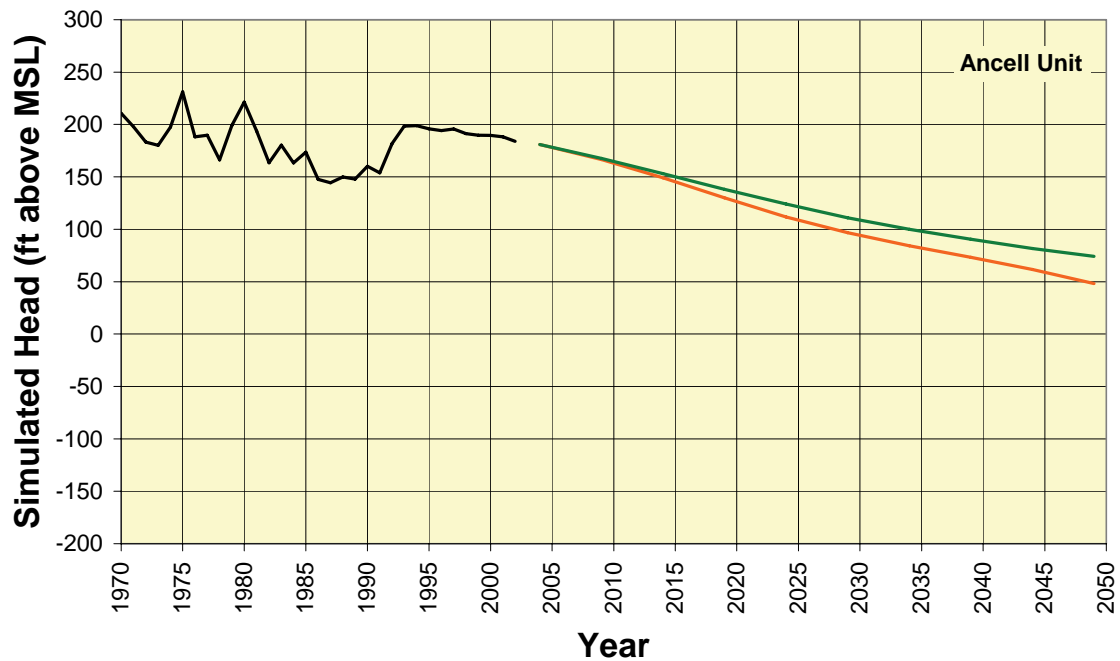


Figure 214. Simulated head from end of 1970 through end of 2049 in Ancell (top) and Ironton-Galesville Units (bottom) at Aurora. See Figure 114 for location.

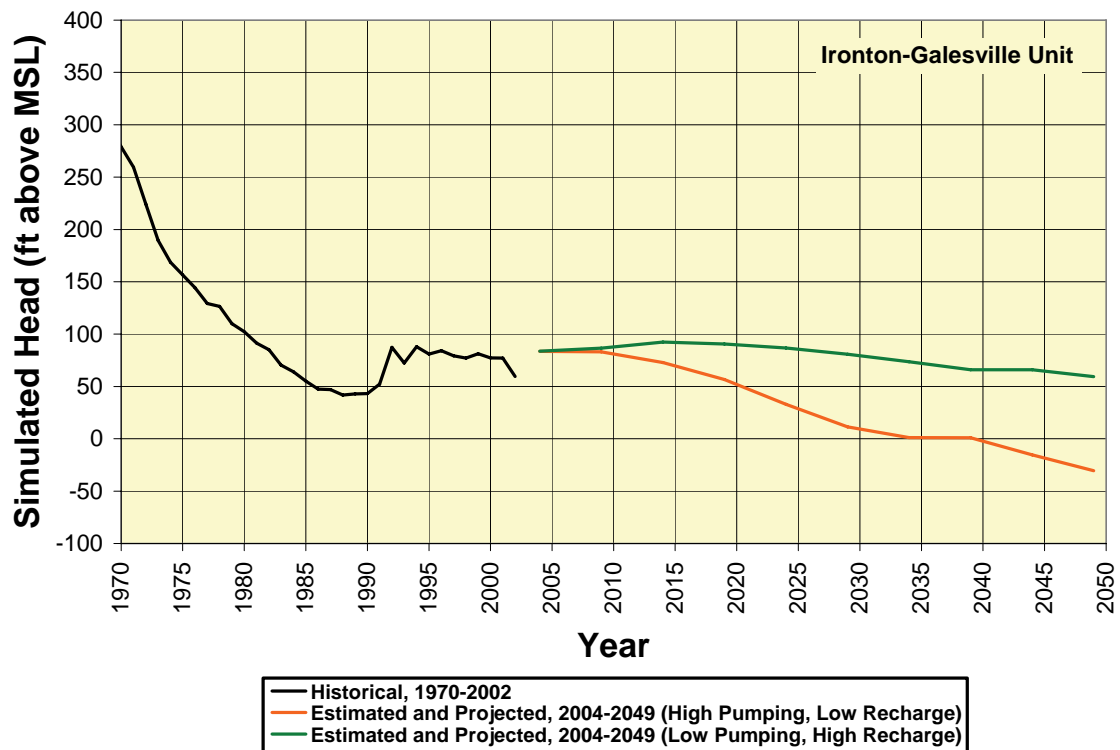
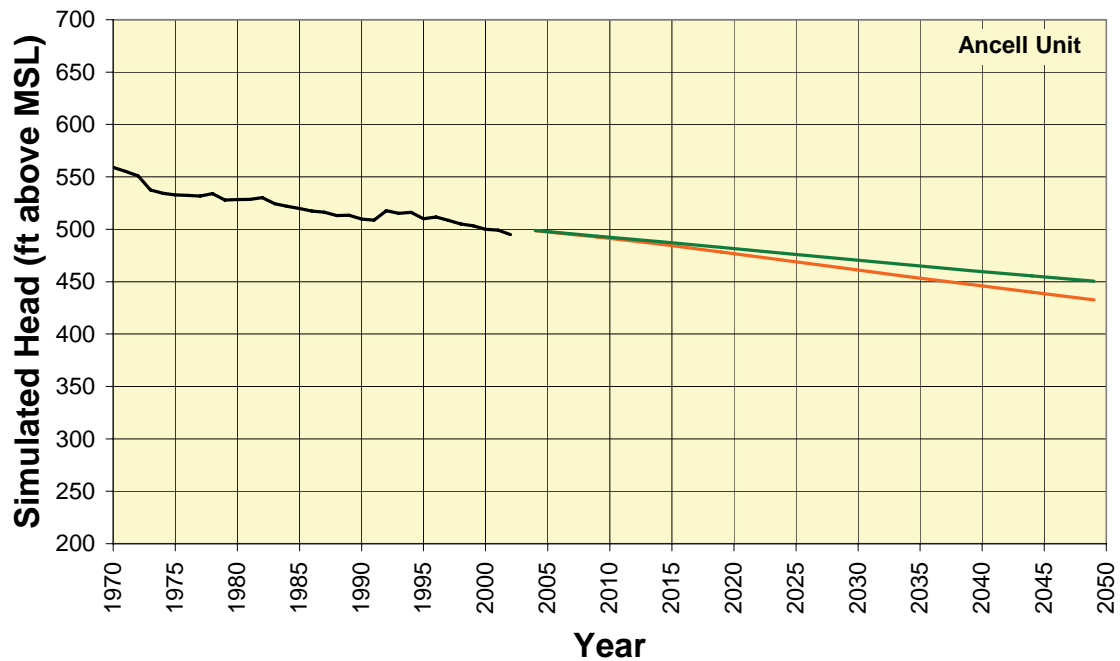


Figure 215. Simulated head from end of 1970 through end of 2049 in Ancell (top) and Ironton-Galesville Units (bottom) at Sugar Grove. See Figure 114 for location.

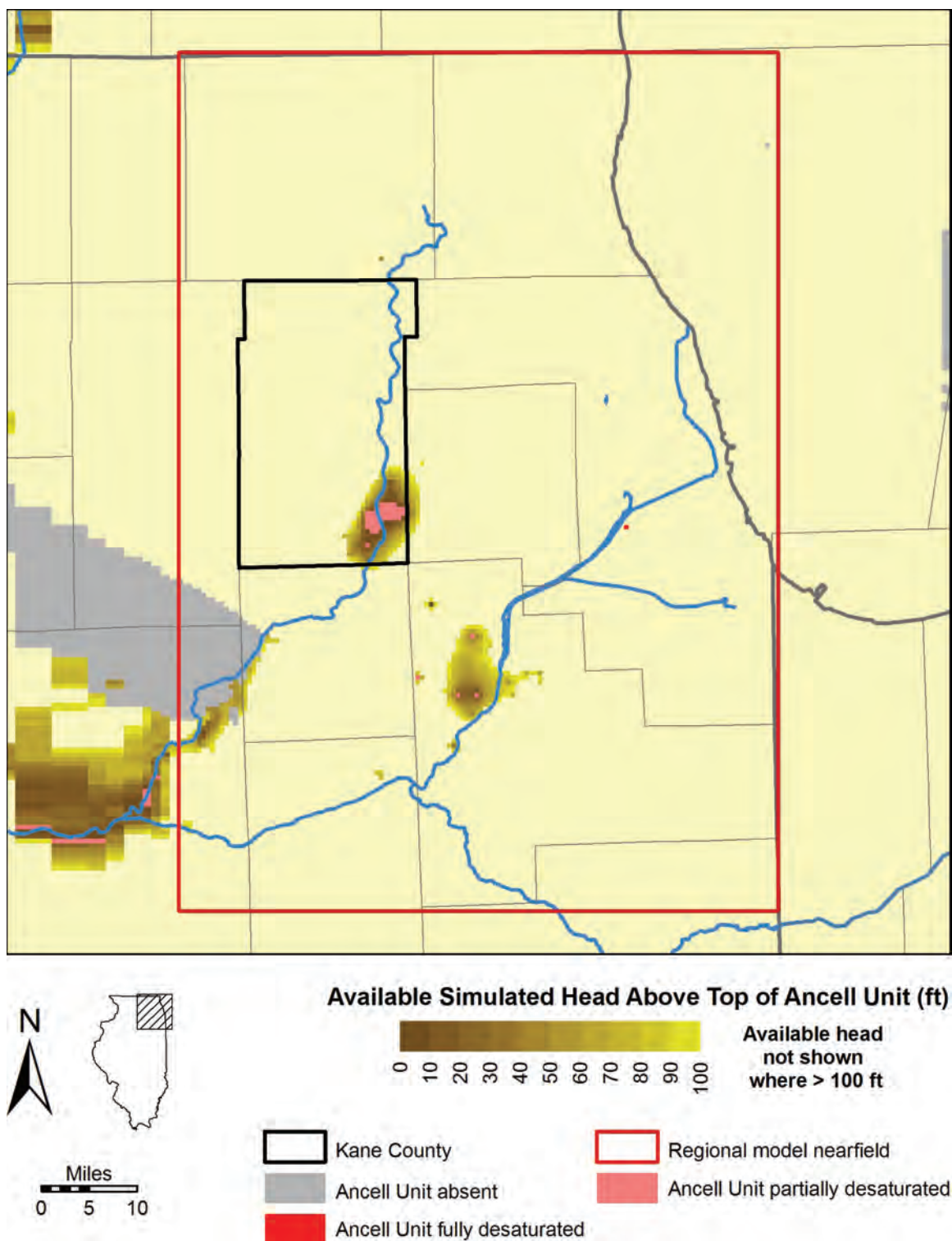


Figure 216. Available simulated head above the top of the Ancell Unit at the end of 2024 under a scenario of high pumping with low recharge rates.

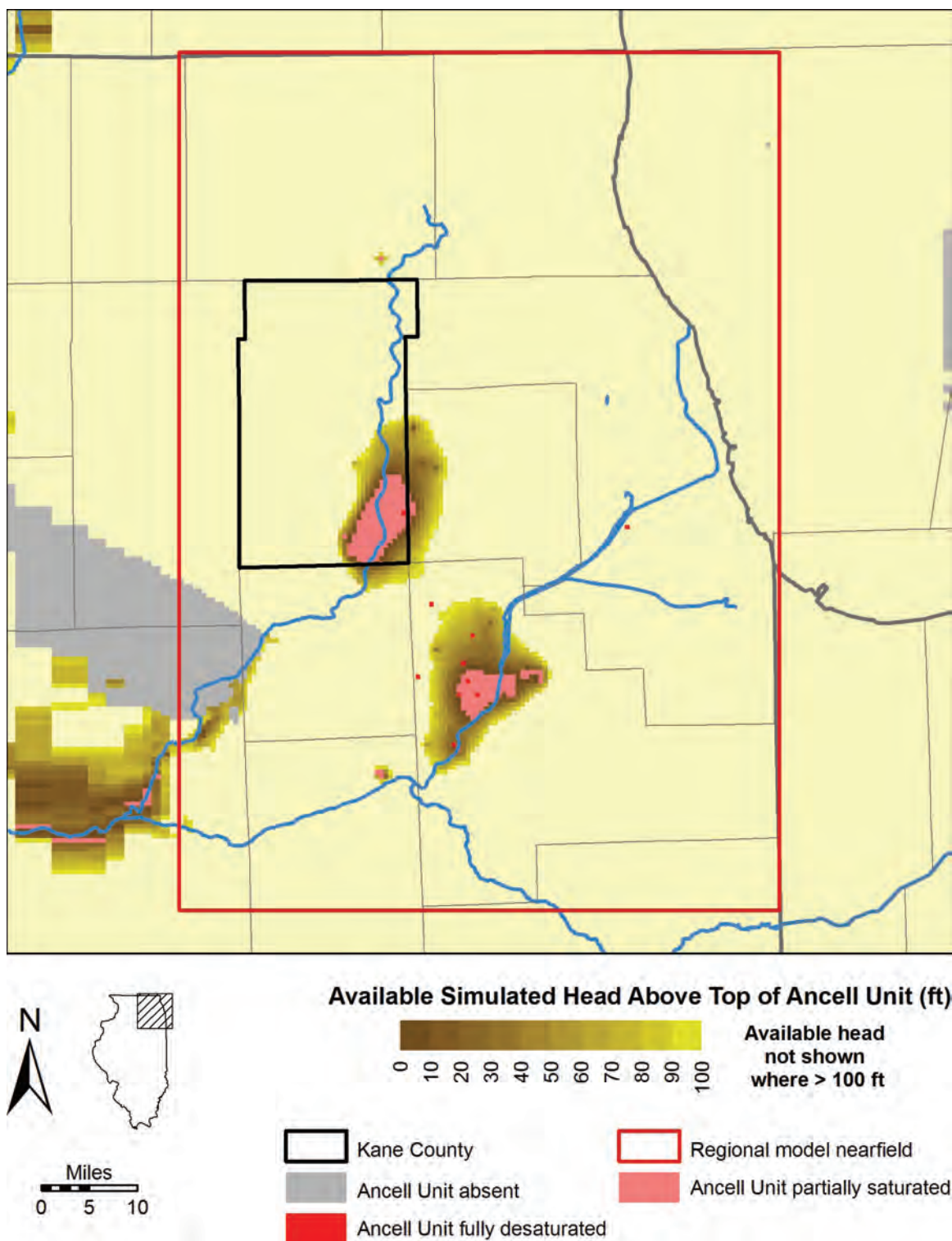


Figure 217. Available simulated head above the top of the Ancell Unit at the end of 2049 under a scenario of high pumping with low recharge rates.

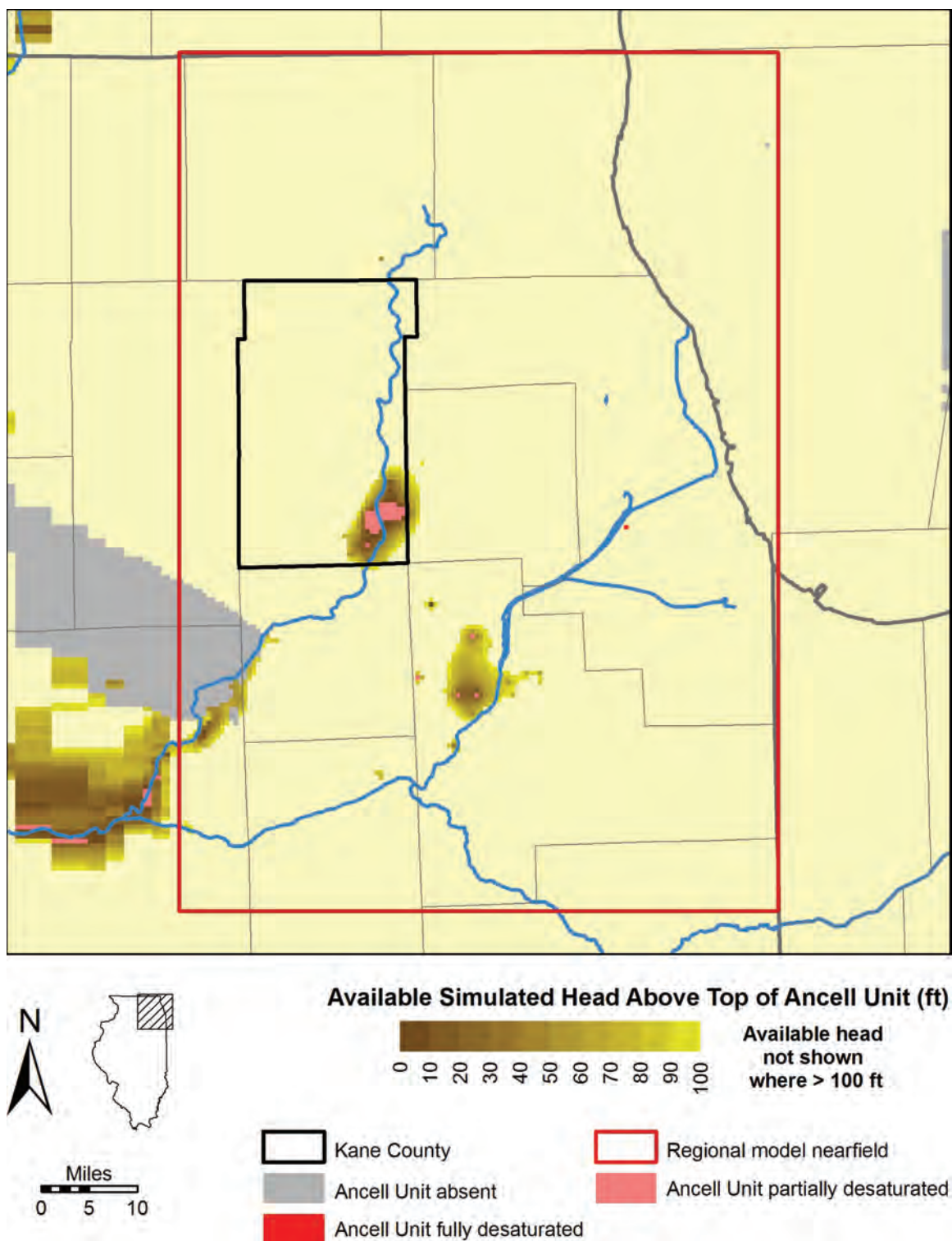


Figure 218. Available simulated head above the top of the Ancell Unit at the end of 2024 under a scenario of high pumping with model-calibrated recharge rates.

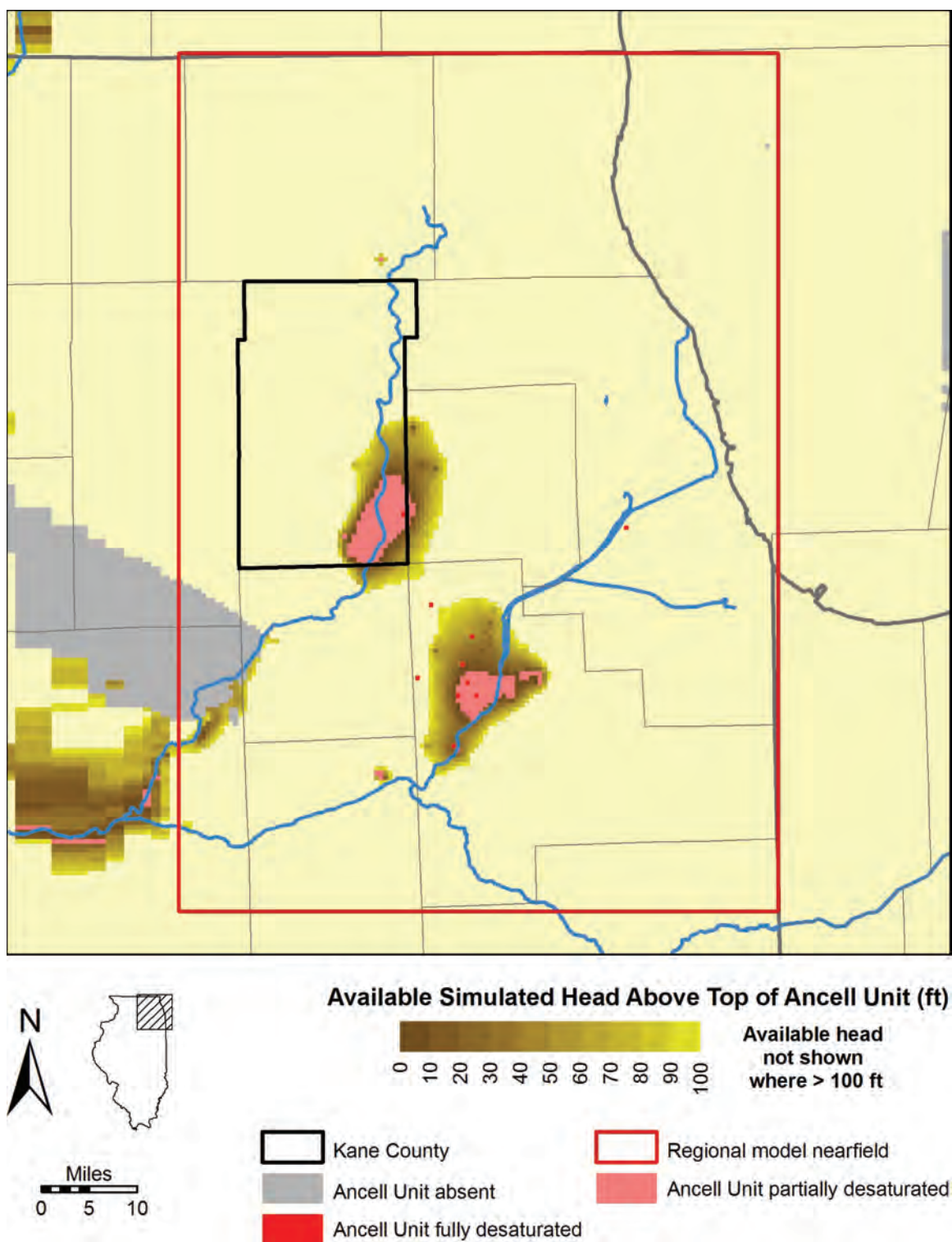


Figure 219. Available simulated head above the top of the Ancell Unit at the end of 2049 under a scenario of high pumping with model-calibrated recharge rates.

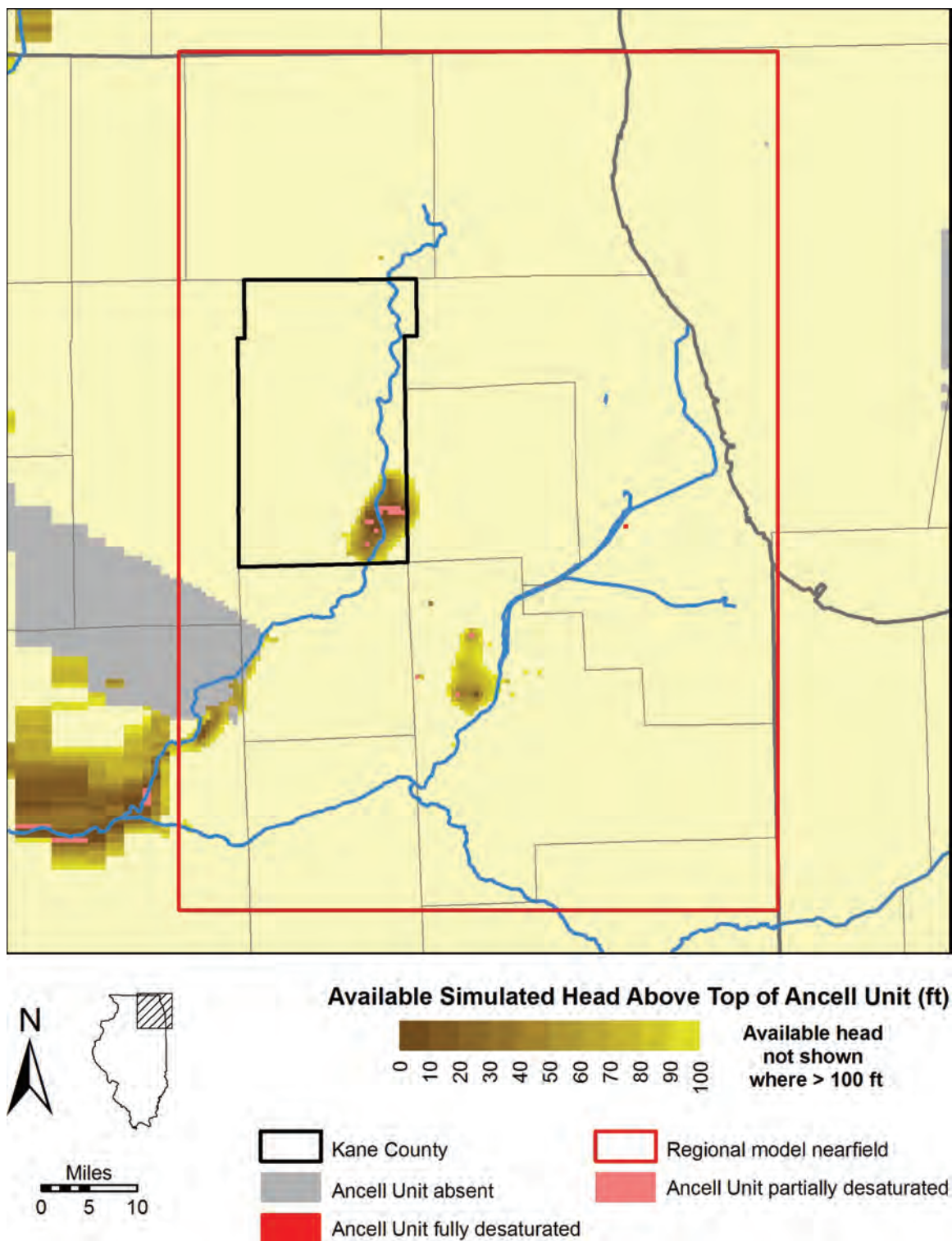


Figure 220. Available simulated head above the top of the Ancell Unit at the end of 2024 under a scenario of low pumping with model-calibrated recharge rates.

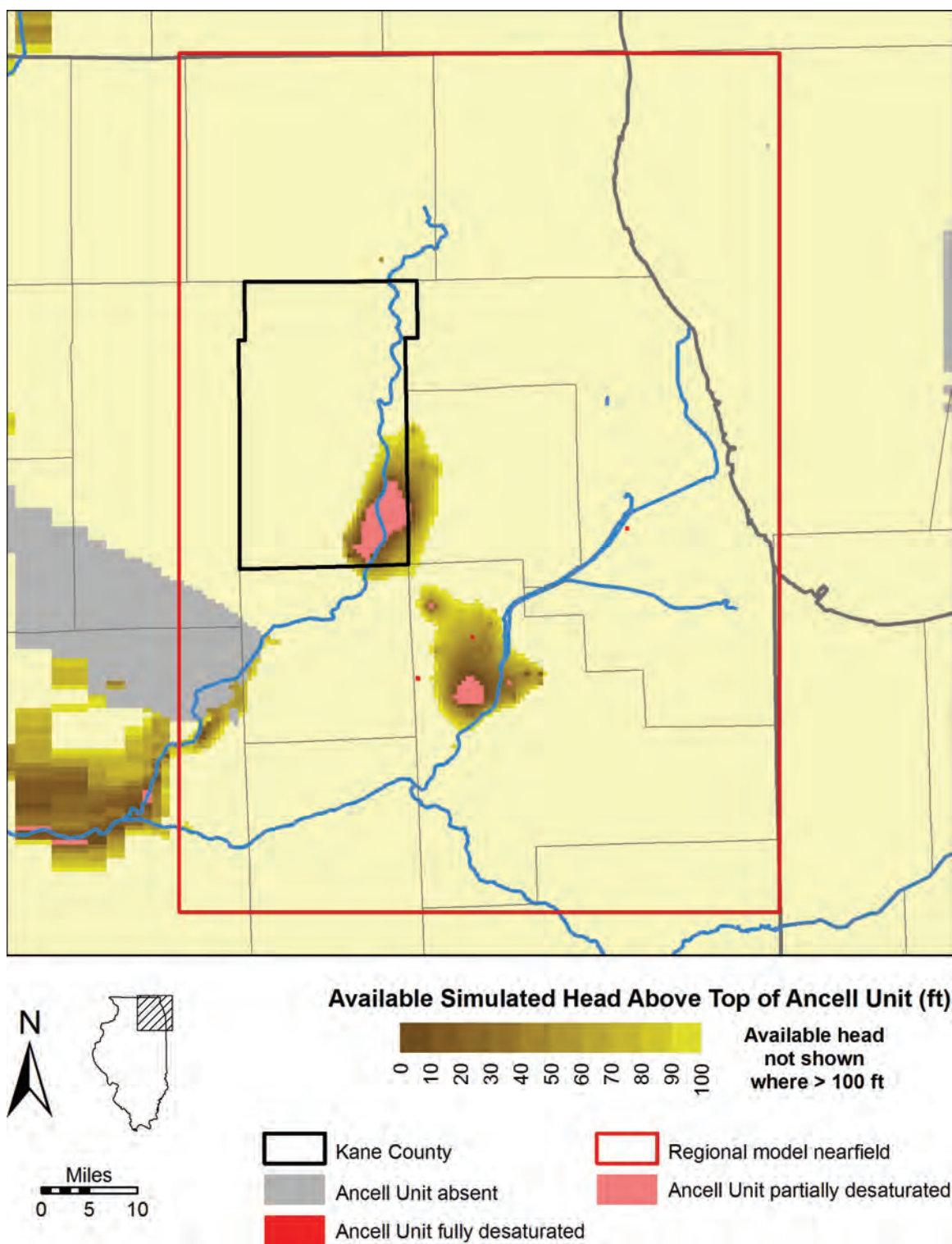


Figure 221. Available simulated head above the top of the Ancell Unit at the end of 2049 under a scenario of low pumping with model-calibrated recharge rates.

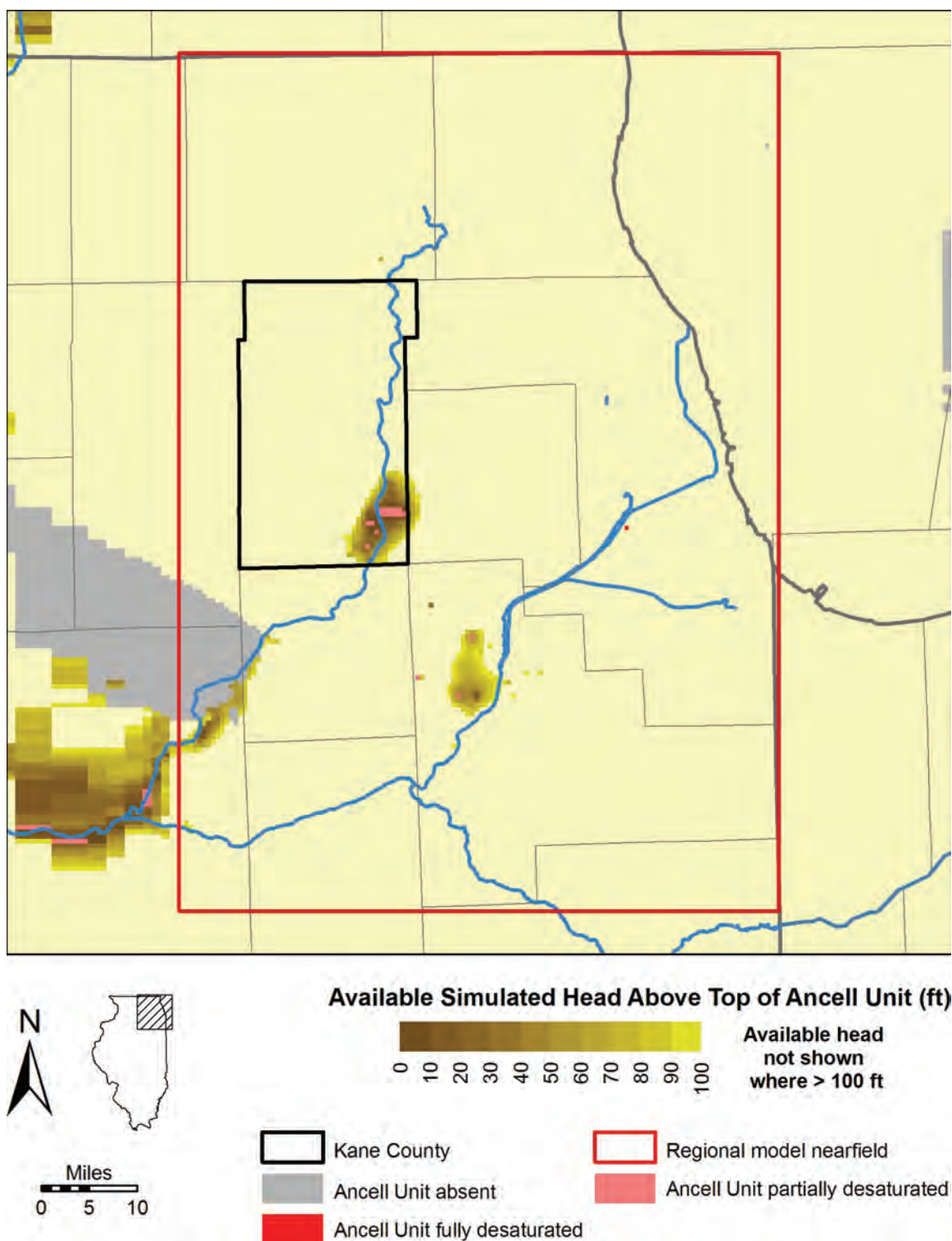


Figure 222. Available simulated head above the top of the Ancell Unit at the end of 2024 under a scenario of low pumping with high recharge rates.

Model simulations suggest that Ancell Unit heads will decline over much of northeastern Illinois through 2049, even under the least resource-intensive scenario of low pumping and high recharge (Figure 193 through Figure 196). Simulated drawdown is most pronounced in northern Will County and southeastern Kane County, where large withdrawals in the vicinity of Joliet and Aurora are projected. Simulated drawdown occurs in all of Kane County, and simulated declines exceed 50 ft in much of the county. Although simulated post-2002 drawdown is greater under high-pumping conditions (Figure 193 and Figure 194), it exceeds 100 ft at the end of 2049 in the immediate vicinities of Joliet and Aurora even under low-pumping conditions (Figure 195 and Figure 196). Model simulations suggest continued recovery of head, exceeding 100 ft in some places in eastern DuPage and much of Cook Counties in response to reduced pumping in the eastern part of northeastern Illinois begun in the 1980s (see Section 1.9). This recovery is limited, however, and simulated heads (Figure 197 through Figure 204) in the area of recovery remain far below predevelopment levels (Figure 110) even as late as 2049. The model suggests that recovery is limited because numerous wells to the west, most notably a north-south chain of wells extending from Crystal Lake southward to Joliet, capture eastward flow from the area lacking cover by the Maquoketa and Upper Bedrock Units, leaving only vertical leakage across overlying and underlying confining units to restore heads in the Ancell in areas to the east where withdrawals were reduced. In general, however, the combined effects of continued head decline in the Joliet and Aurora areas and continued recovery of heads in the eastern part of northeastern Illinois results in a westward and southwestward shift of the deepest parts of the Chicago area cone of depression to apices in the Joliet and Aurora areas (Figure 197 through Figure 204). Model simulations show that changes in recharge rates affect heads in the deep aquifers very little in the approximate half-century represented.

Simulated hydrographs in Figure 205 through Figure 215 illustrate in detail, for the Kane County locations shown in Figure 114, the trends discussed in the preceding paragraph. Each figure shows simulated heads in the Ancell and Ironton-Galesville Units from the end of 2004 to the end of 2049. For reference, simulated heads under the historical pumping conditions from the end of 1970 through the end of 2002 also are illustrated. For simplicity, only simulated heads for the most and least resource-intensive scenarios (Table 29) are illustrated, because heads simulated for the intermediate resource-intensive scenarios differ negligibly from the most and least resource-intensive scenarios. Model simulations predict a continued decline in Ancell Unit head through the end of 2049 for both the high-pumping, low-recharge and low-pumping, high-recharge scenarios, with greatest simulated head declines in the eastern part of Kane County, nearer the locations of large predicted withdrawals from the deep aquifers and more distant from the high-leakage area lacking Maquoketa-Upper Bedrock Unit cover to the west. Under the low-pumping, high-recharge scenario, total simulated Ancell Unit head declines between the end of 2002 and the end of 2049 range from about 26 ft at Maple Park to about 130 ft at Batavia. Under the high-pumping, low-recharge scenario, these declines range from about 42 ft at Maple Park to 179 ft at Batavia.

At most locations in Kane County, the model suggests that recovery of Ironton-Galesville heads, begun in the 1980s, will continue at decreasing rates, and then heads will begin to decline again. Renewed decline of simulated Ironton-Galesville heads begins earlier (2010-2015) under the high-pumping, low-recharge scenario than under the

low-pumping, high-recharge scenario (2020-2025). Under the low-pumping, high-recharge scenario, the renewed decline in simulated Ironton-Galesville head at Carpentersville and Elgin begins late enough and occurs at such a low rate relative to the preceding recovery that simulated heads are slightly higher in 2049 than in 2004. This unexpected result partially reflects the significant recovery of simulated Ironton-Galesville heads in northeastern Kane County that resulted from partial conversion of the Elgin water supply to a Fox River source in the early 1980s. At other locations, however, simulated heads in the Ironton-Galesville are forecast to be significantly lower at the end of 2049 than the end of 2004. Of the locations shown in Figure 114, simulated head declines are greatest at Aurora and Batavia owing to their proximity to important deep wells. Under the low-pumping, high-recharge scenario, simulated Ironton-Galesville head declines about 72 ft at Aurora between the end of 2002 and the end of 2049, and under the high-pumping, low-recharge scenario, the simulated decline from 2002 levels ranges from about 84 ft at Maple Park to about 180 ft at Batavia.

The simulations suggest that Ancell Unit head will decline to within 100 ft of the top of the Ancell Unit, and that the upper Ancell Unit will become desaturated in the Aurora and Joliet areas before 2050, even under the least resource-intensive scenario of low pumping and high recharge (Figure 216 through Figure 223). These developments could result in elevated arsenic, radium, and barium in groundwater withdrawn from deep wells (page 207) and reduced deep well yields. Note that the area of low available simulated head surrounding the lower Fox and upper Illinois Rivers is a feature that modeling suggests was present before pumping began (see Figure 118) and changes in well yield and groundwater quality would not, therefore, be expected in that area.

Simulated drawdown in the shallow aquifers is less than in the deep aquifers, as shown by forecasted drawdown in the Shallow Bedrock Aquifer at the end of 2024 and 2049 (Figure 224 through Figure 239). The major source aquifers for water supply (the Ashmore Unit, Upper and Lower Glasford Sand Units, and the Shallow Bedrock Aquifer) remain fully saturated through 2049 even under the most resource-intensive model scenario of high pumping and low recharge. However, to keep the model cells saturated and prevent production wells from going dry and shutting off, pumping rates for eight wells in Algonquin, Crystal Lake, and West Chicago were held constant at 2003 rates (Section 3.3.1.3). As was the case for historic drawdown (Section 3.2.1.2), simulated post-2003 drawdown (Figure 224 through Figure 227, Figure 232 through Figure 235) in the shallow aquifers generally increases with depth of burial; thus, simulated post-2003 drawdown is generally greater in the Shallow Bedrock Aquifer than in any of the overlying sand and gravel aquifers. Rates of simulated drawdown are low enough, however, that despite continued head decline after 2003, the general predevelopment pattern of high heads in northwestern Kane County declining toward the south and east is maintained through 2049. Although rates of recharge make a slight difference in the amount of simulated drawdown, model simulations suggest that pumping rates exert a much more important influence on the magnitude of simulated drawdown at any single location and on the areal extent of simulated cones of depression.

Areas of significant simulated total drawdown at the end of 2024 and 2049 (Figure 228 through Figure 231, Figure 236 through Figure 239)—defined for purposes of this report as drawdown greater than 20 ft—are mostly more extensive versions of the areas of significant simulated drawdown in 2003 discussed previously (Section 3.2.1.2),

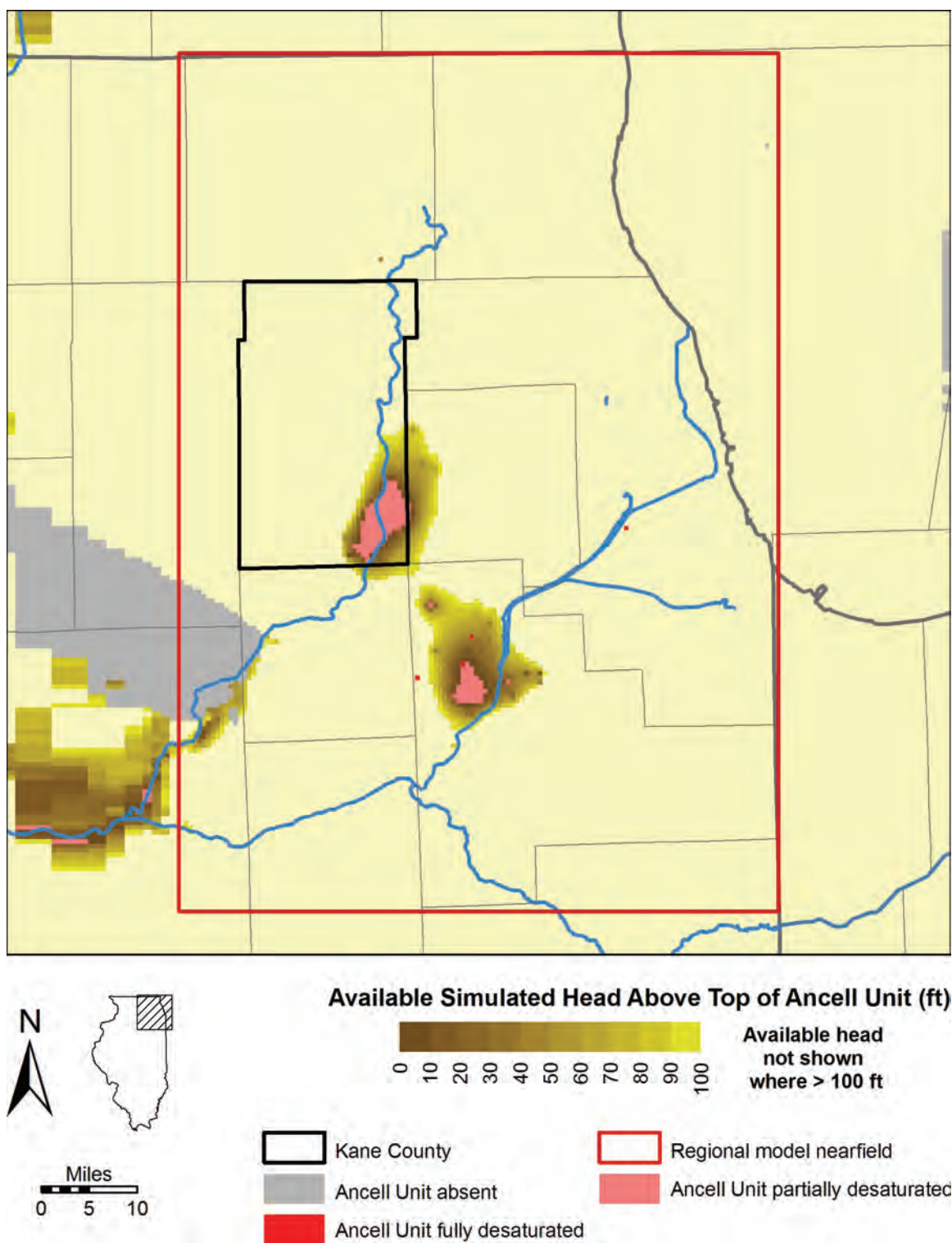


Figure 223. Available simulated head above the top of the Ancell Unit at the end of 2049 under a scenario of low pumping with high recharge rates.

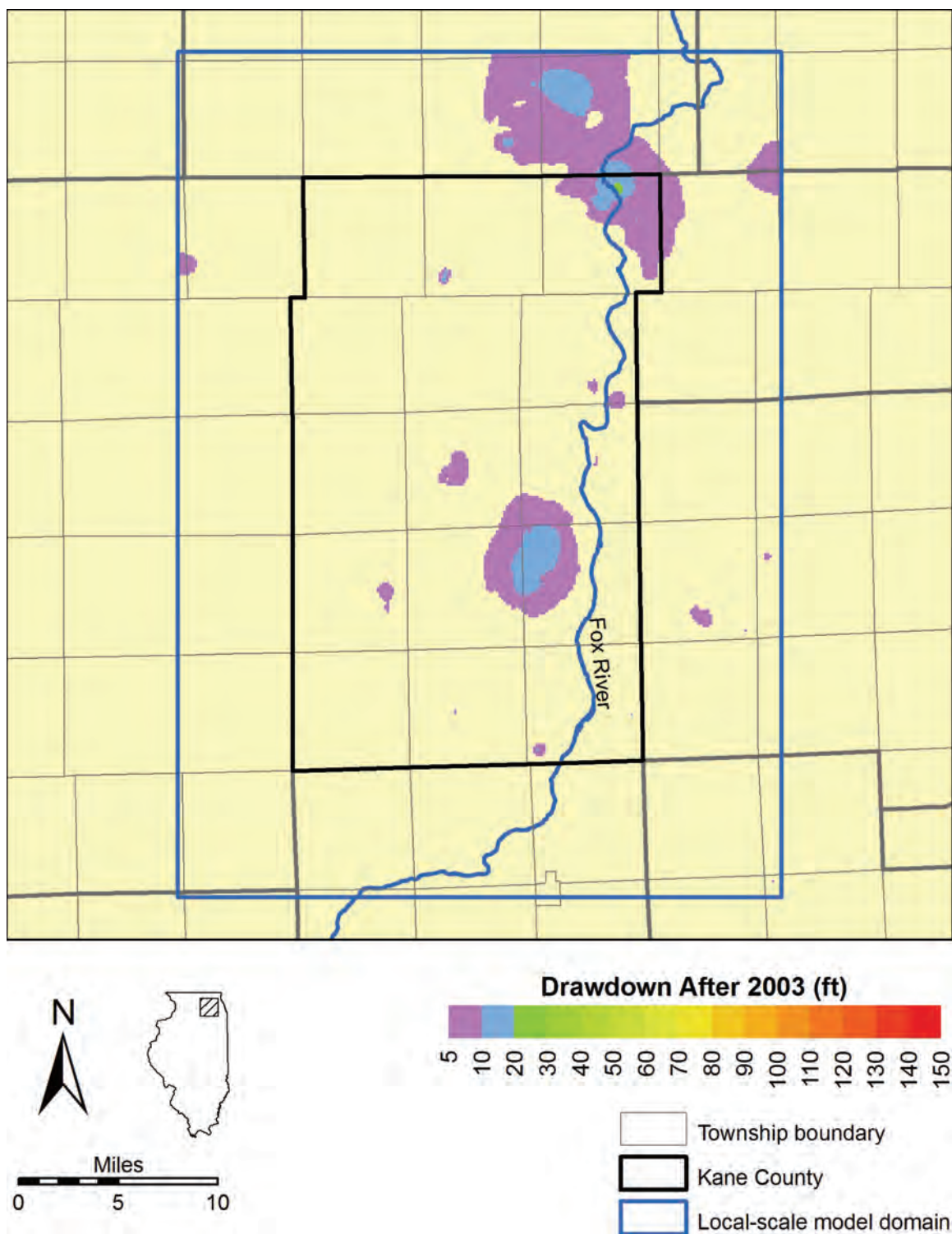


Figure 224. Estimated drawdown between the end of 2003 and the end of 2024 in the Shallow Bedrock Aquifer under a scenario of high pumping and low recharge rates.

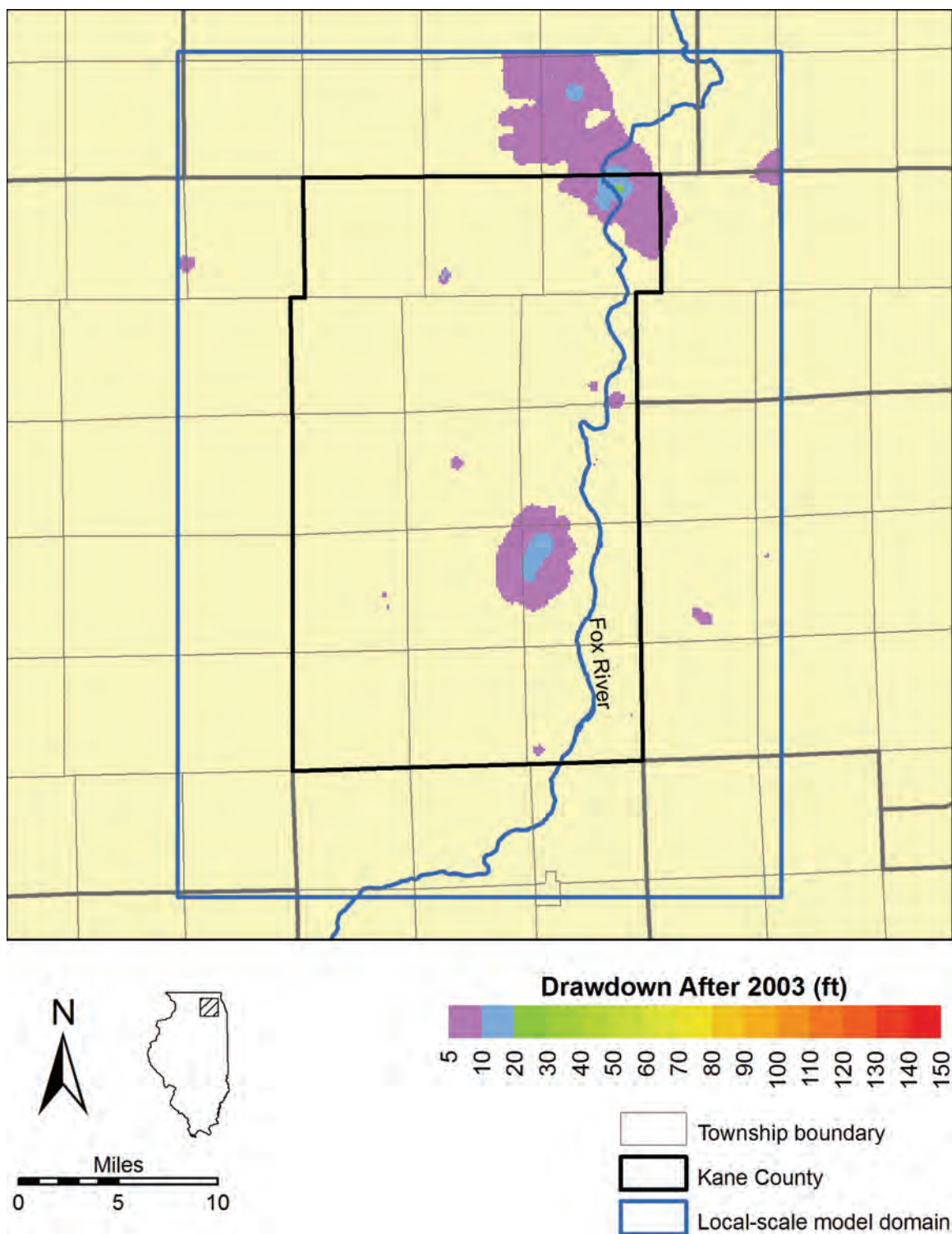


Figure 225. Estimated drawdown between the end of 2003 and the end of 2024 in the Shallow Bedrock Aquifer under a scenario of high pumping and model-calibrated recharge rates.

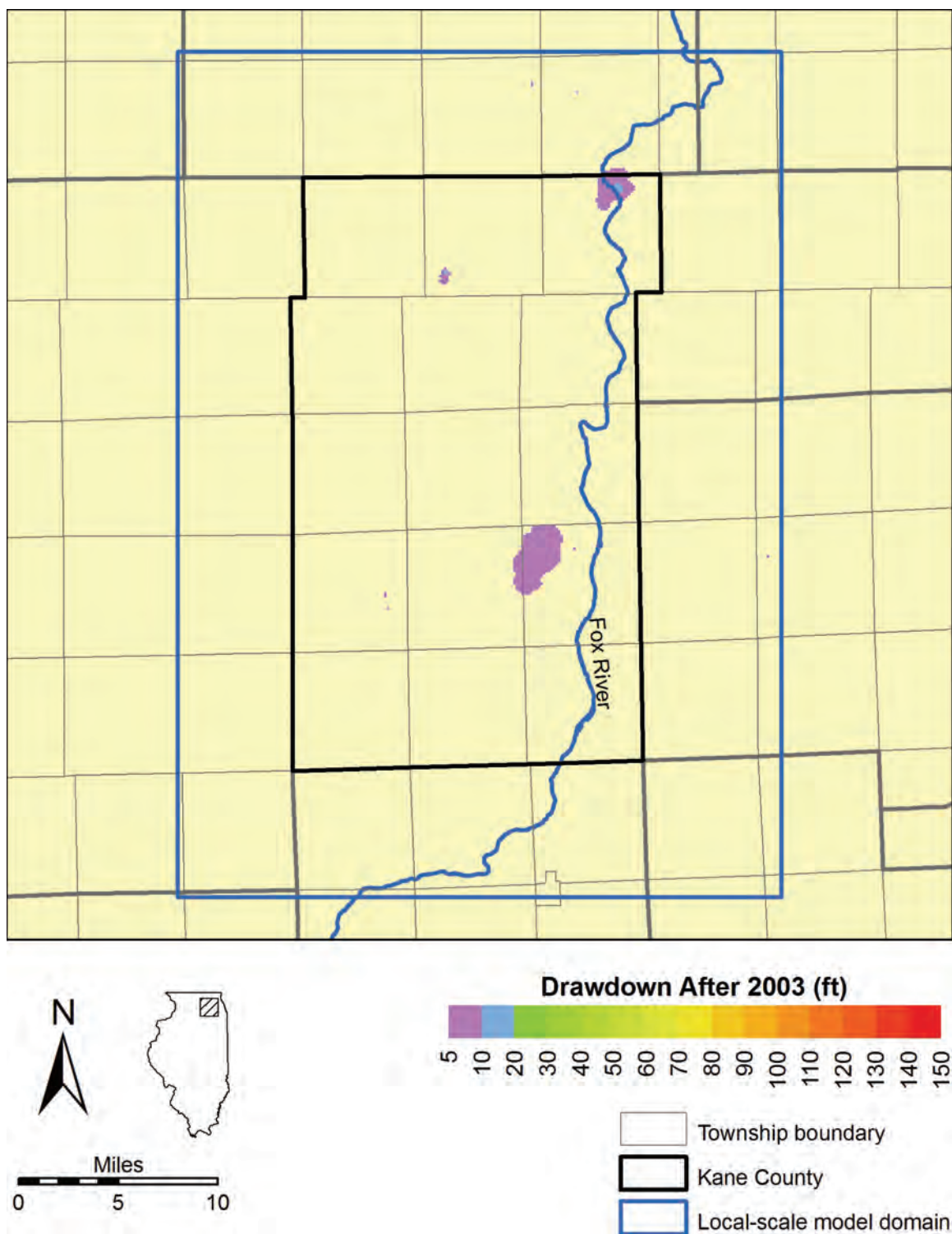


Figure 226. Estimated drawdown between the end of 2003 and the end of 2024 in the Shallow Bedrock Aquifer under a scenario of low pumping and model-calibrated recharge rates.

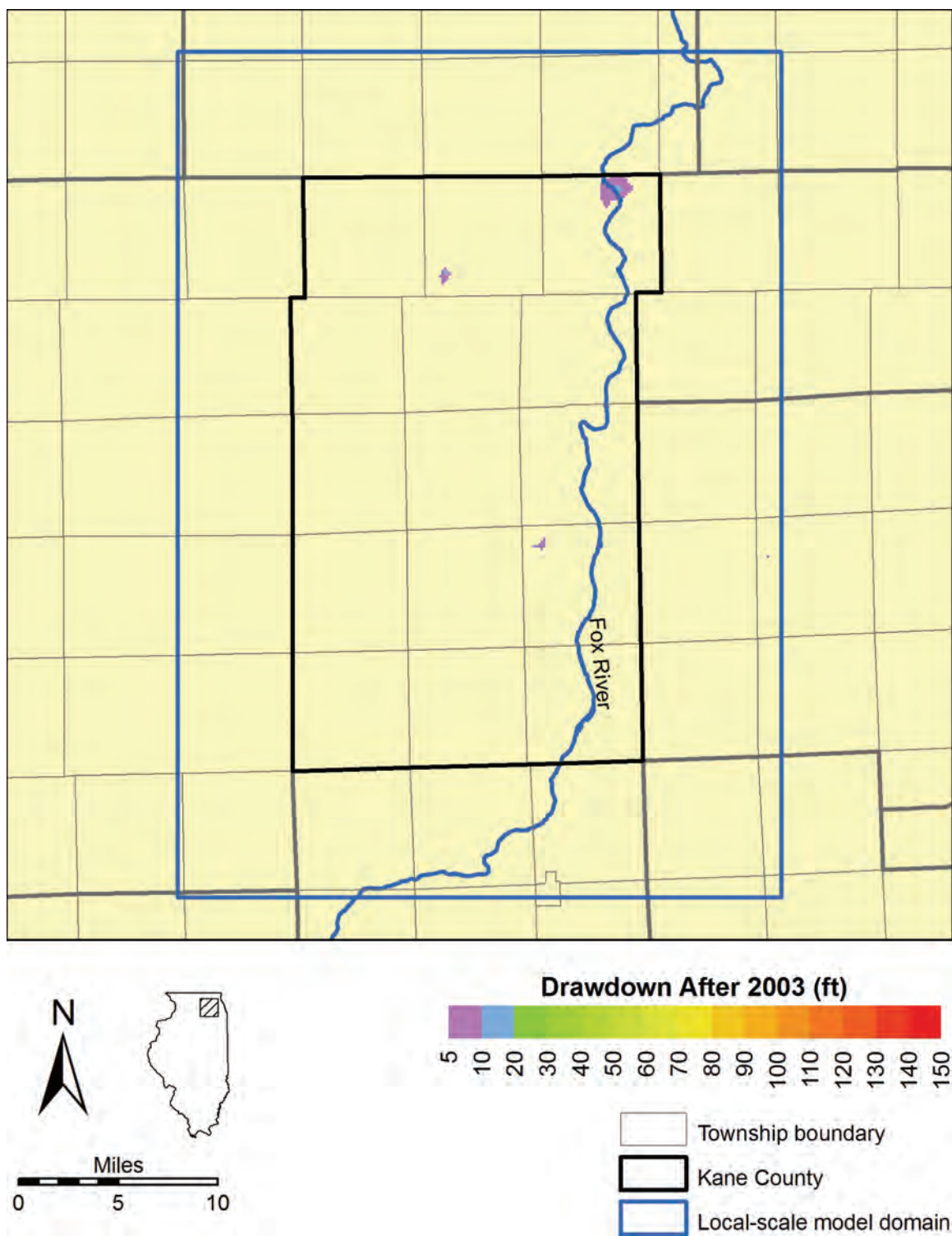


Figure 227. Estimated drawdown between the end of 2003 and the end of 2024 in the Shallow Bedrock Aquifer under a scenario of low pumping and high recharge rates.

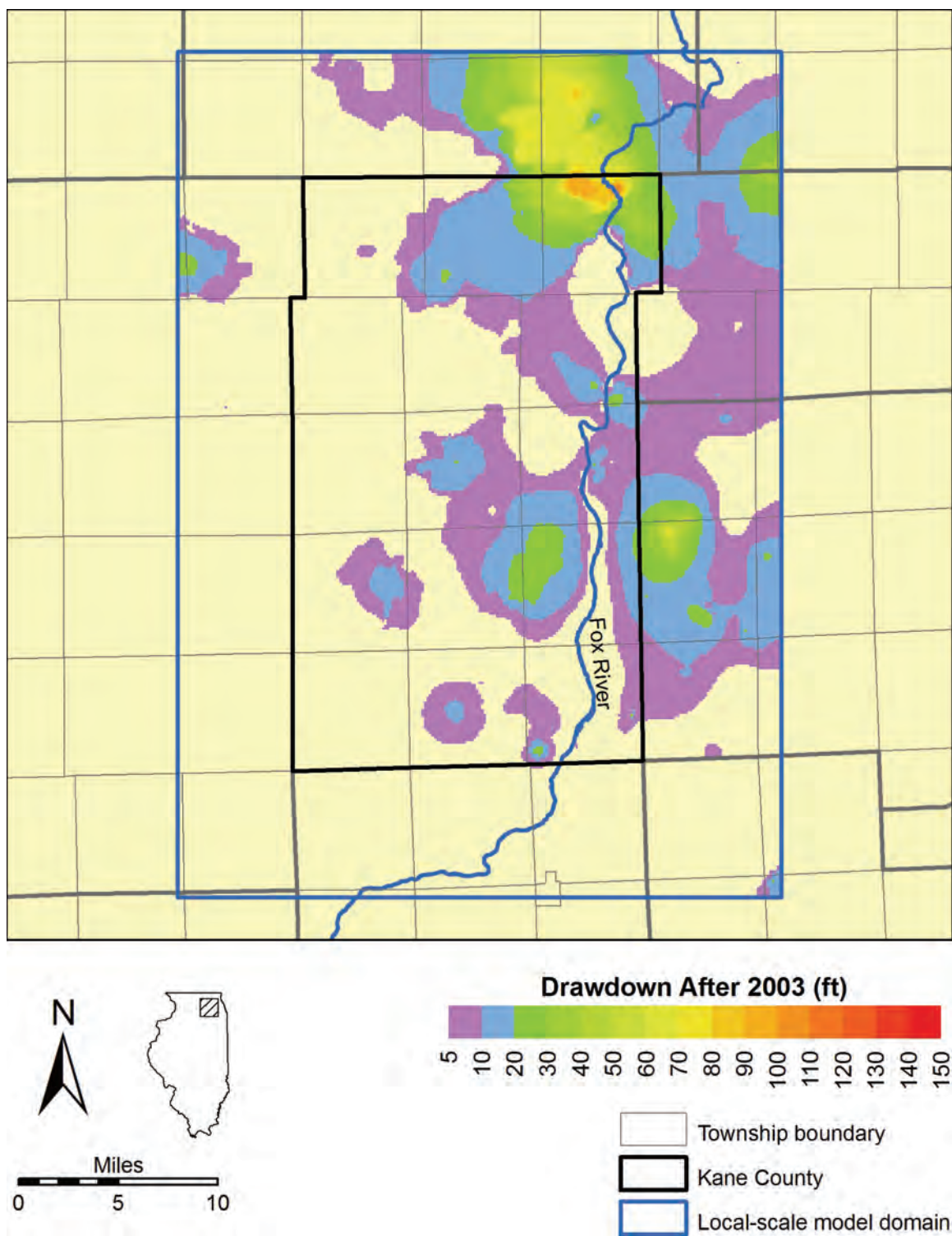


Figure 228. Estimated total drawdown at the end of 2024 in the Shallow Bedrock Aquifer under a scenario of high pumping and low recharge rates.

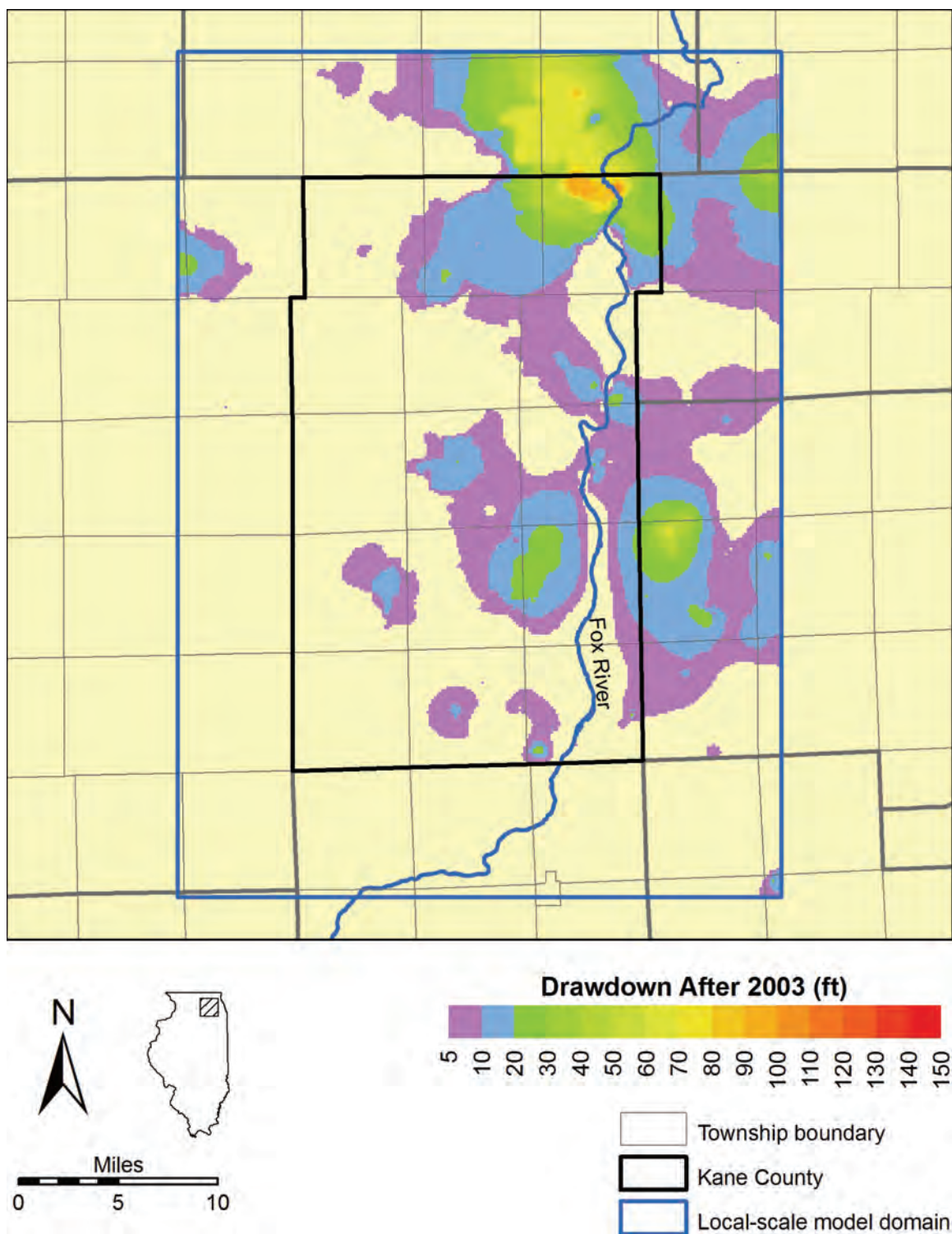


Figure 229. Estimated total drawdown at the end of 2024 in the Shallow Bedrock Aquifer under a scenario of high pumping and model-calibrated recharge rates.

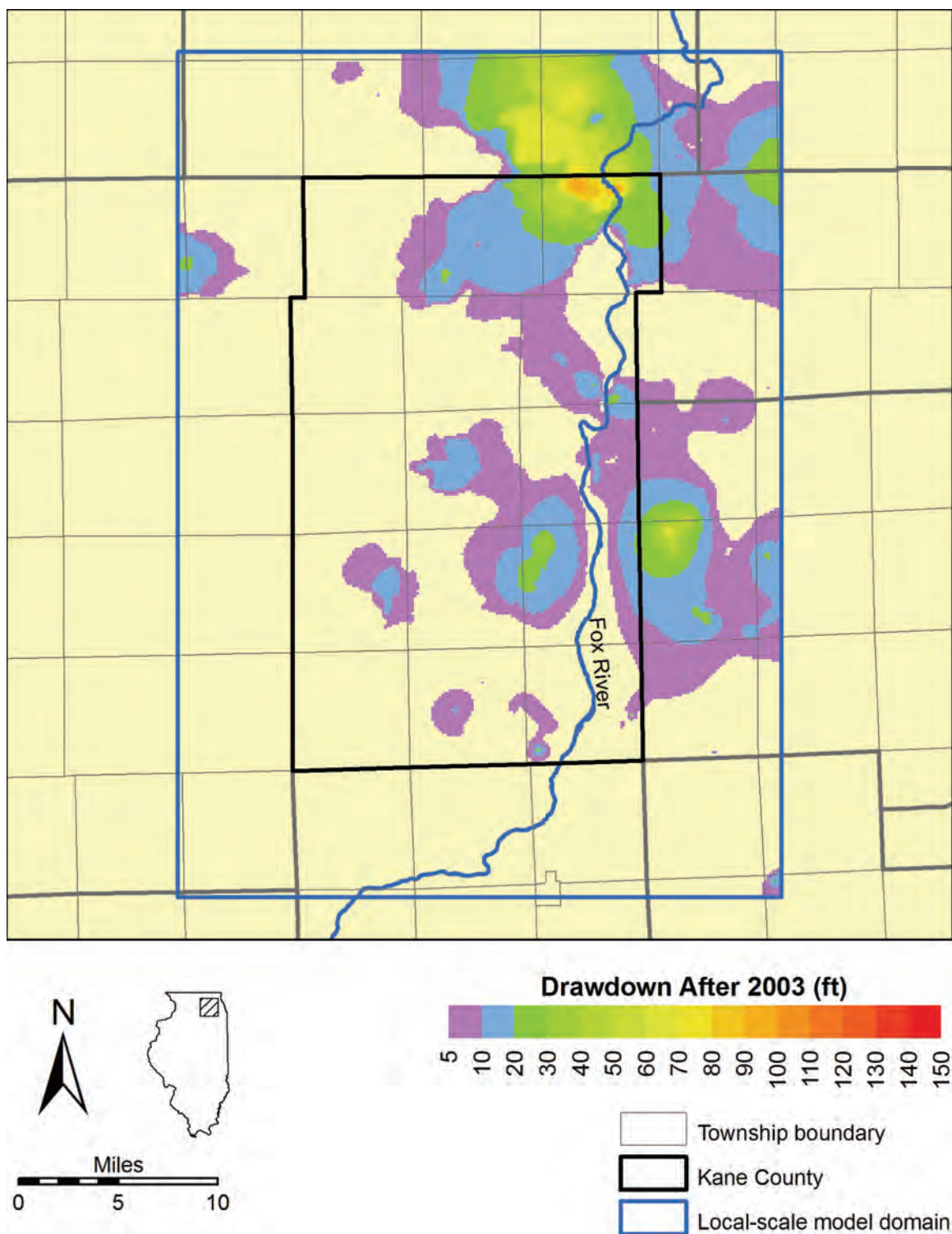


Figure 230. Estimated total drawdown at the end of 2024 in the Shallow Bedrock Aquifer under a scenario of low pumping and model-calibrated recharge rates.

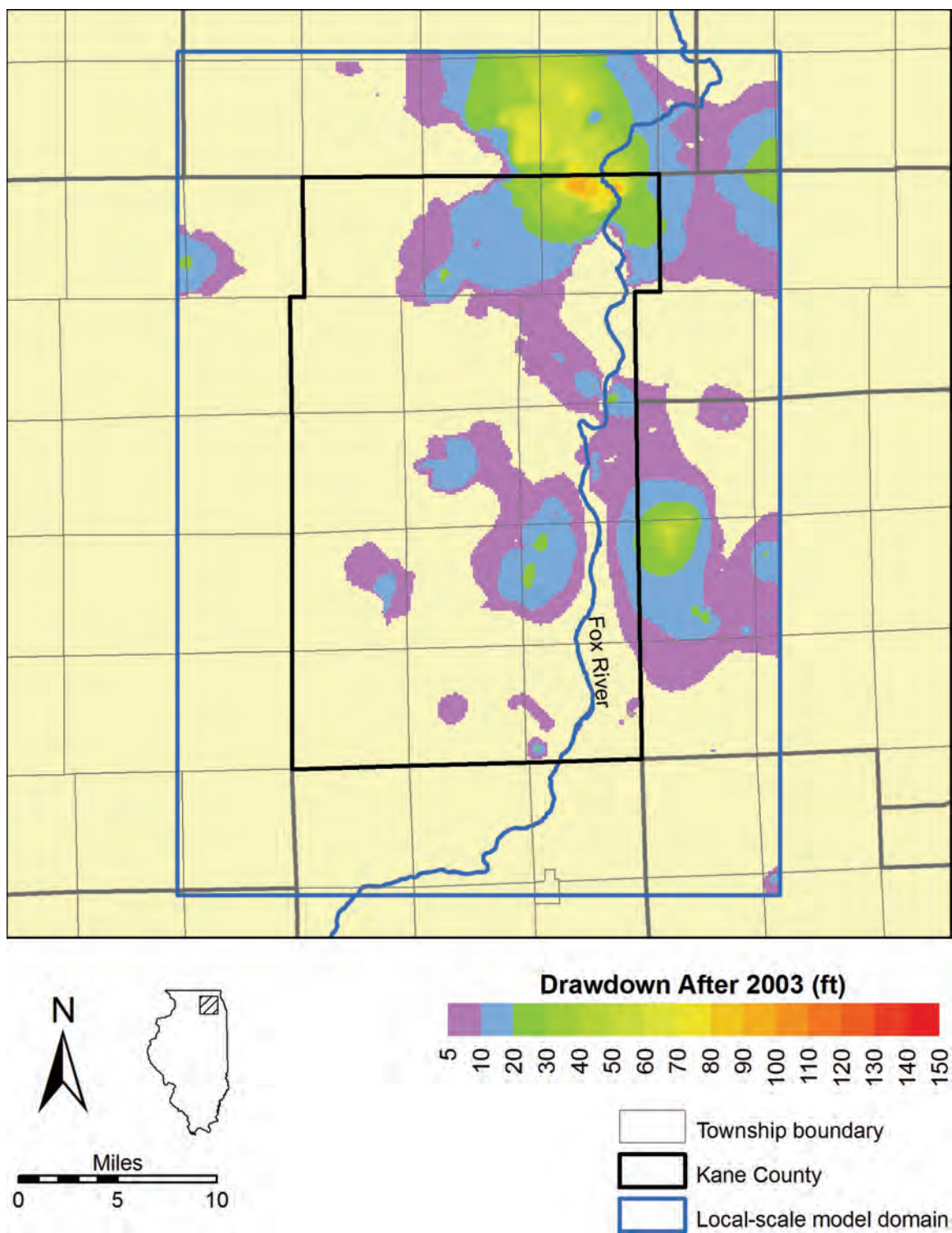


Figure 231. Estimated total drawdown at the end of 2024 in the Shallow Bedrock Aquifer under a scenario of low pumping and high recharge rates.

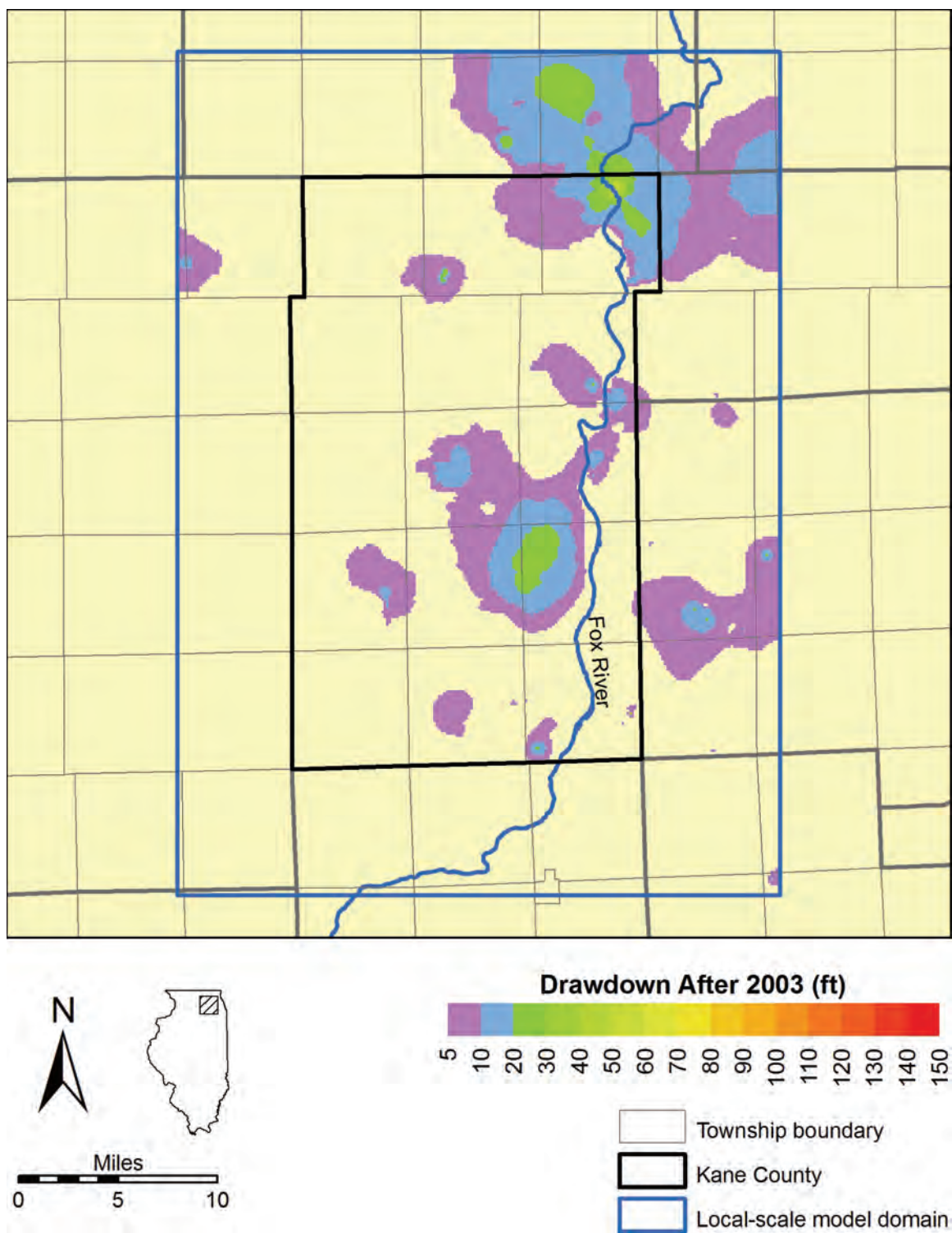


Figure 232. Estimated drawdown between the end of 2003 and the end of 2049 in the Shallow Bedrock Aquifer under a scenario of high pumping and low recharge rates.

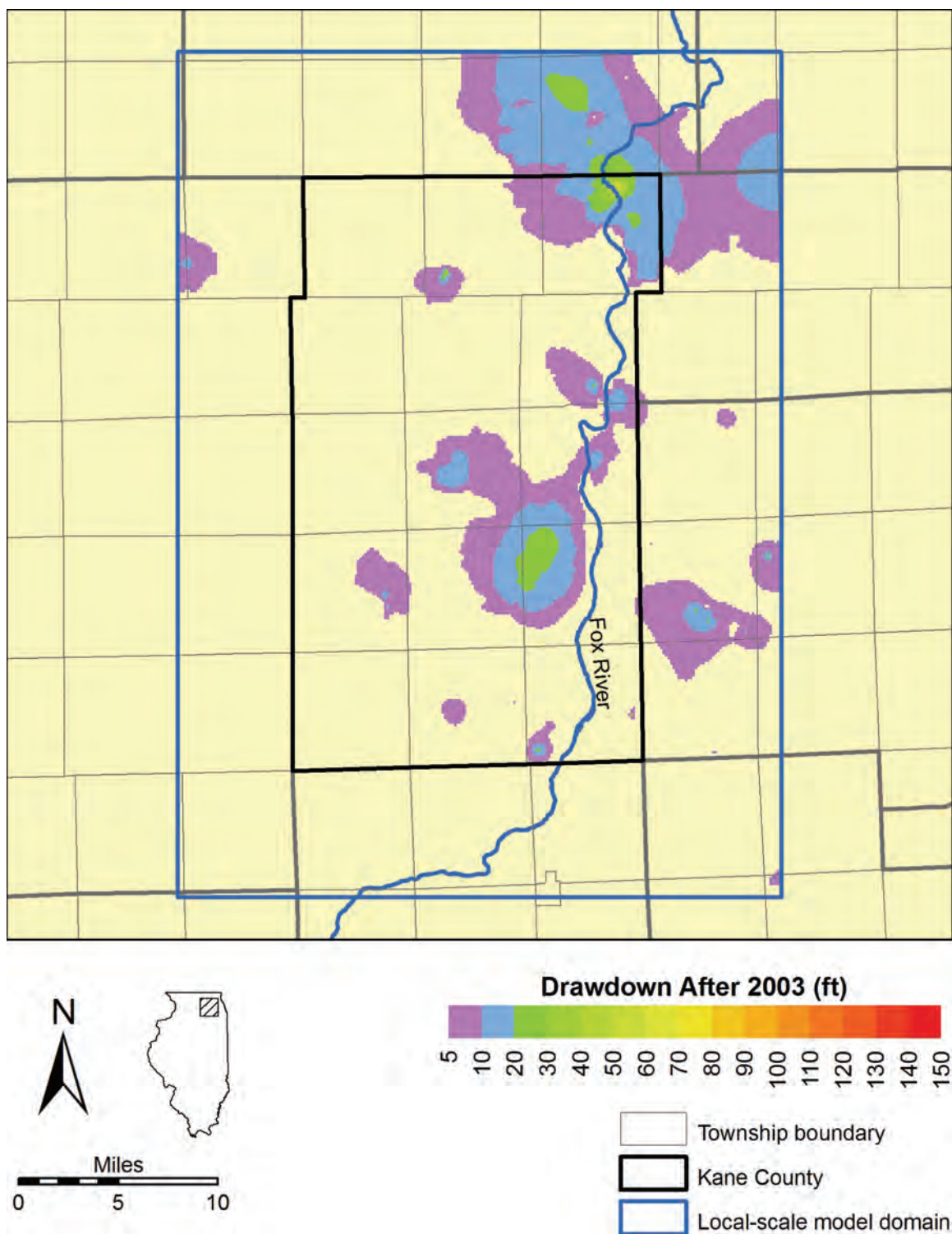


Figure 233. Estimated drawdown between the end of 2003 and the end of 2049 in the Shallow Bedrock Aquifer under a scenario of high pumping and model-calibrated recharge rates.

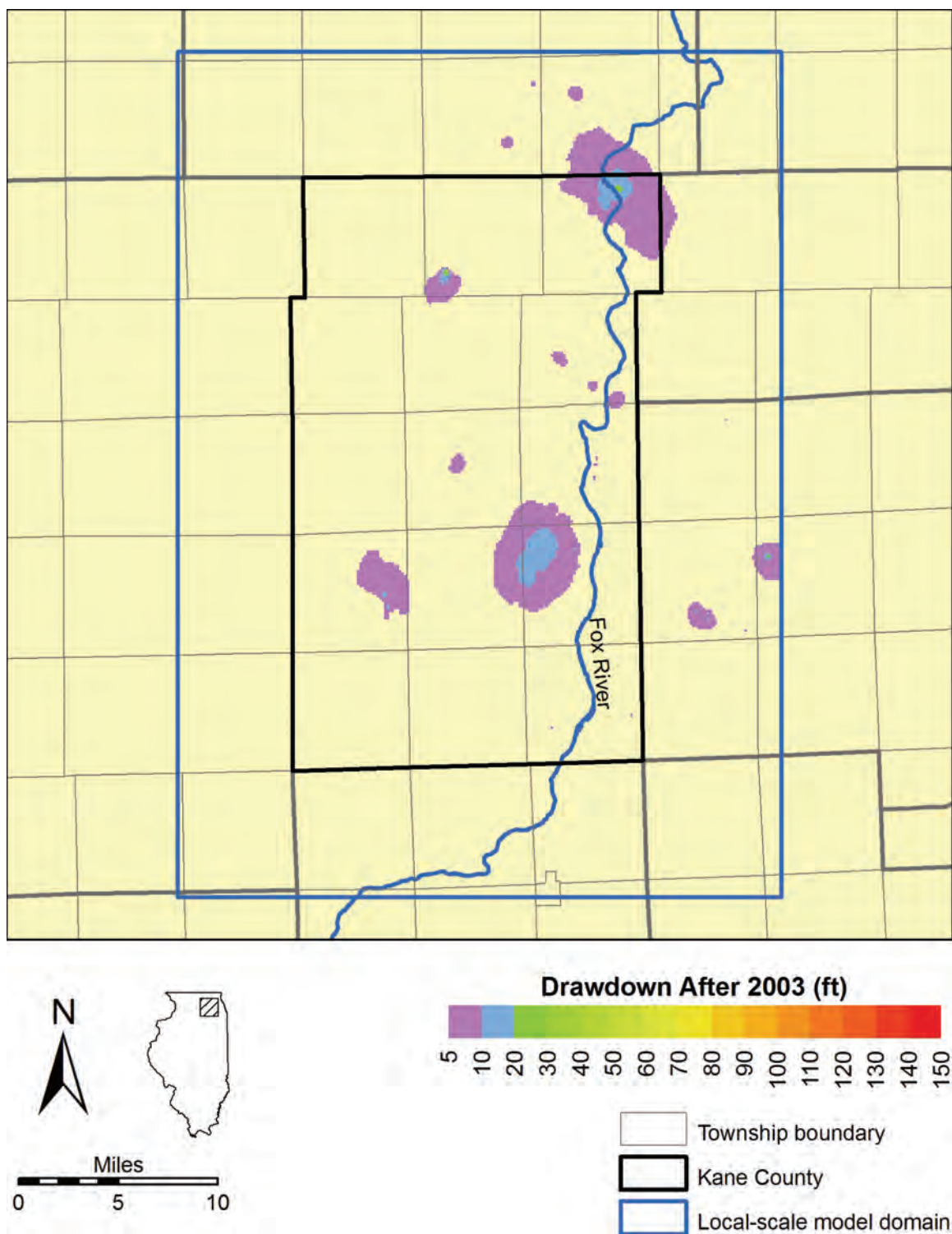


Figure 234. Estimated drawdown between the end of 2003 and the end of 2049 in the Shallow Bedrock Aquifer under a scenario of low pumping and model-calibrated recharge rates.

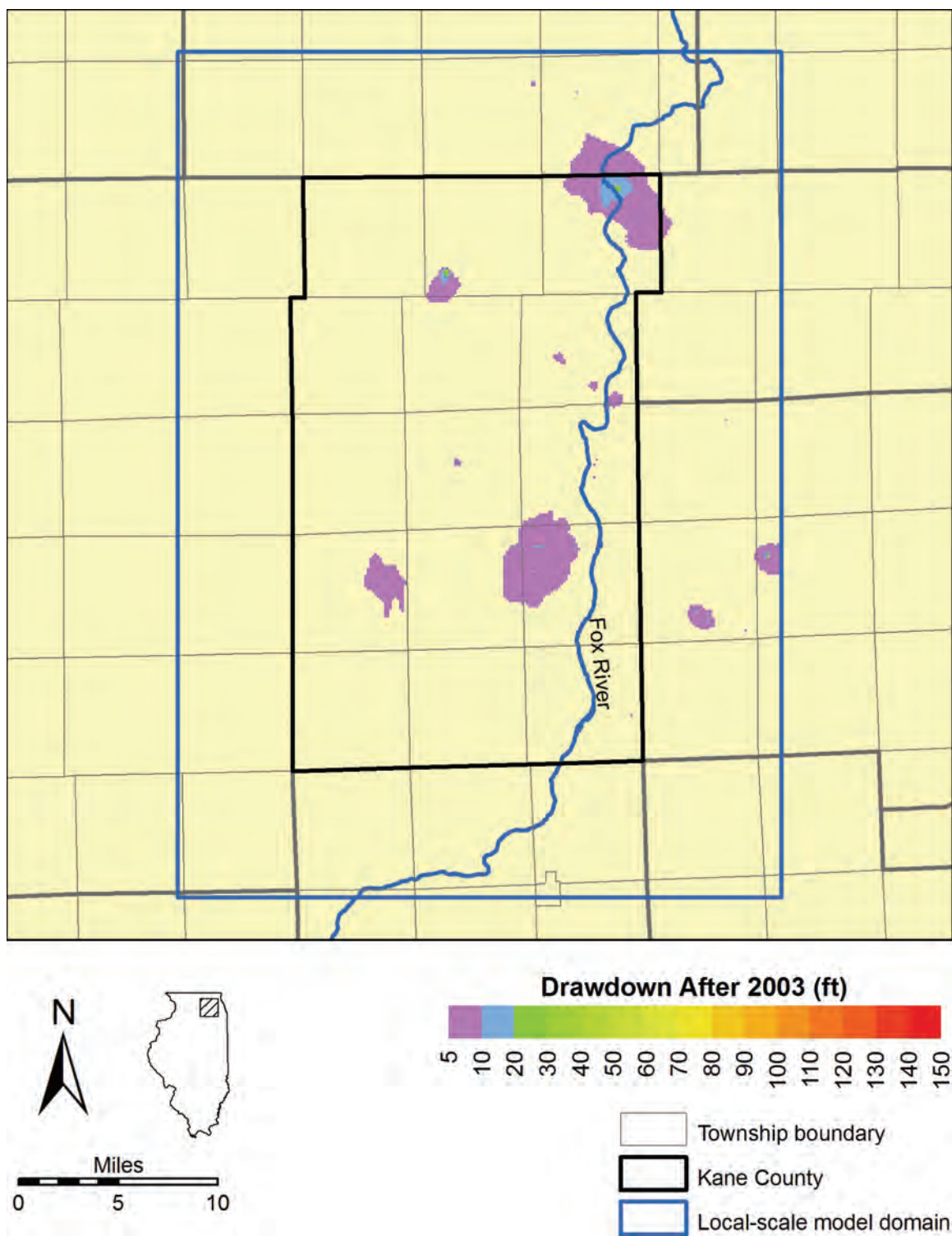


Figure 235. Estimated drawdown between the end of 2003 and the end of 2049 in the Shallow Bedrock Aquifer under a scenario of low pumping and high recharge rates.

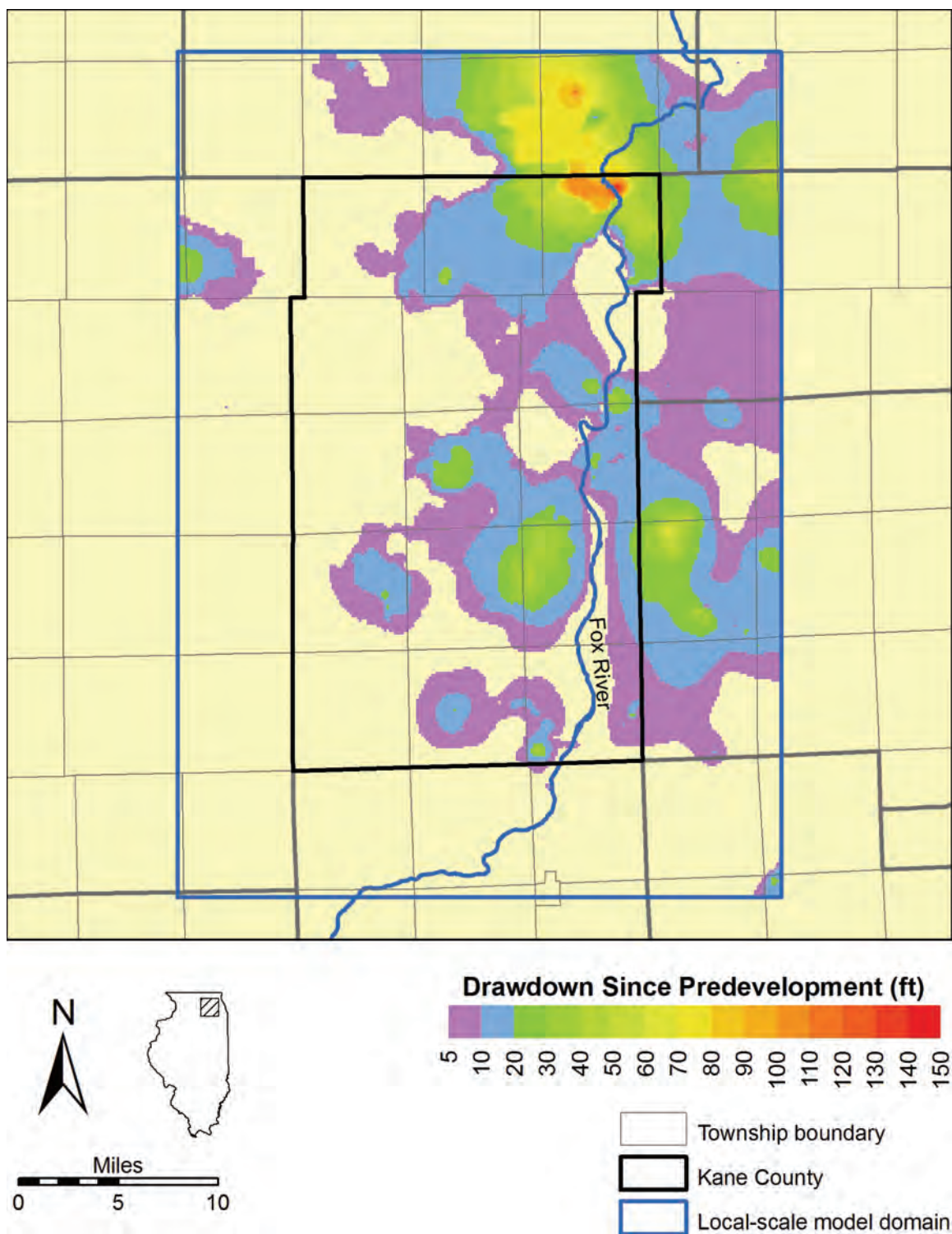


Figure 236. Estimated total drawdown at the end of 2049 in the Shallow Bedrock Aquifer under a scenario of high pumping and low recharge rates.

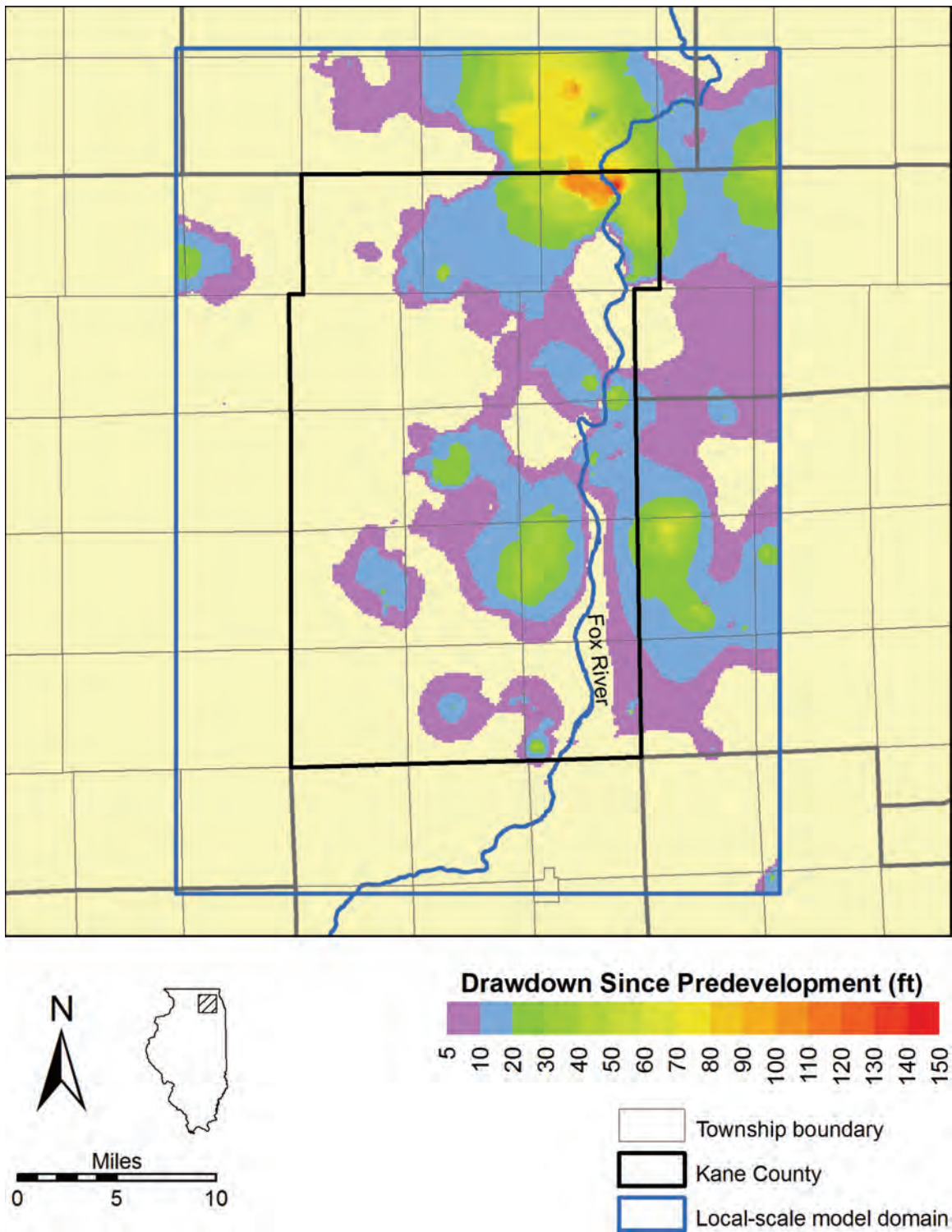


Figure 237. Estimated total drawdown at the end of 2049 in the Shallow Bedrock Aquifer under a scenario of high pumping and model-calibrated recharge rates.

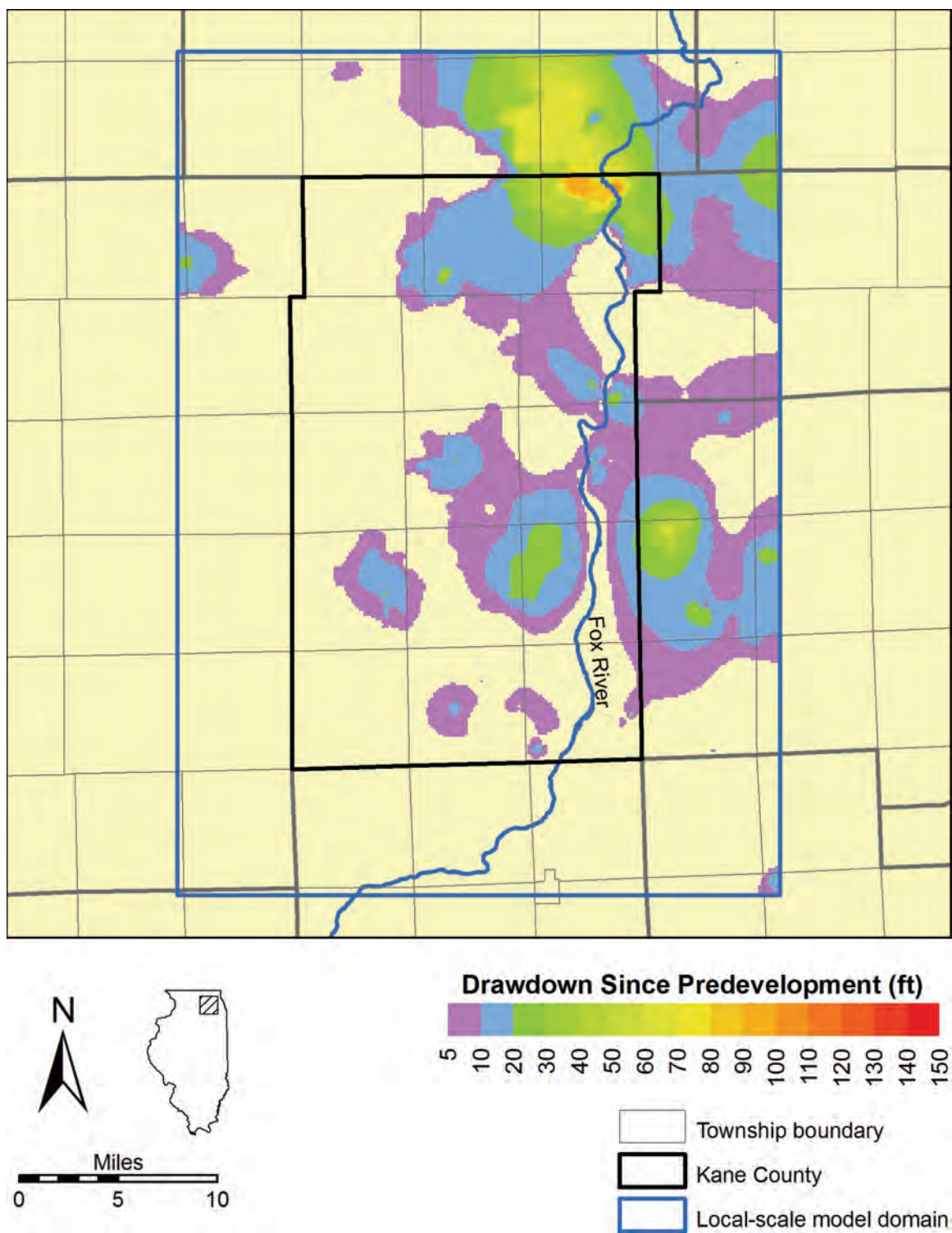


Figure 238. Estimated total drawdown at the end of 2049 in the Shallow Bedrock Aquifer under a scenario of low pumping and model-calibrated recharge rates.

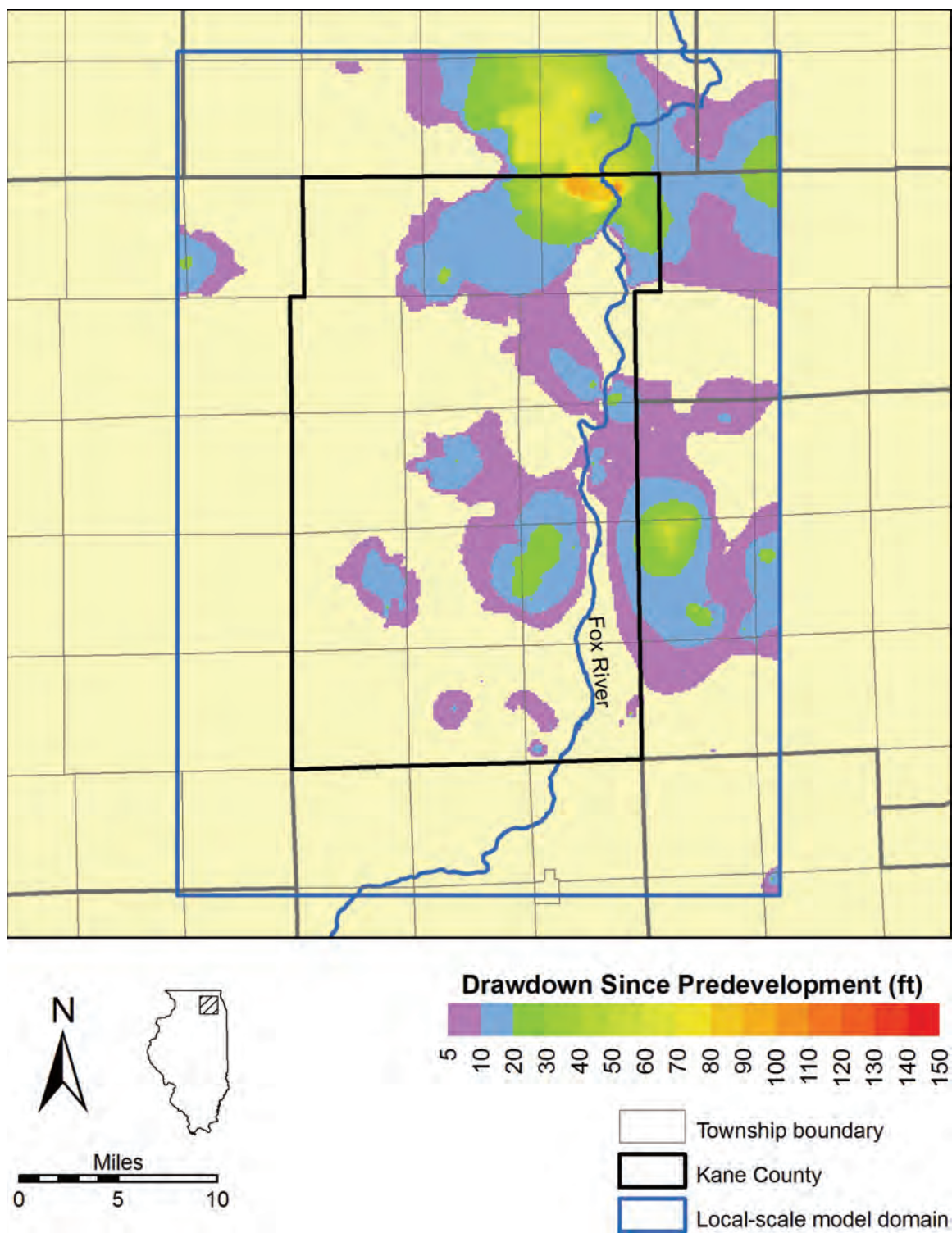


Figure 239. Estimated total drawdown at the end of 2049 in the Shallow Bedrock Aquifer under a scenario of low pumping and high recharge rates.

though new areas of significant simulated drawdown appear. This correspondence in location is not surprising owing to the fact that the simulated pumping conditions are based on rates and locations of pumping during the period 2000 through 2003.

The area of northeastern Kane County and southeastern McHenry County (page 228) remains the most extensive single area of significant simulated drawdown in the area, even with simulated pumping through 2049 from Algonquin wells 8 and 9 fixed at 2003 rates. The model suggests that, under conditions of high pumping and both model-calibrated (i.e., "normal" historic) recharge and low recharge, over 20 ft of post-2003 drawdown will occur in the immediate vicinity of Algonquin well 11 by 2025. Also by 2025, the area of significant post-2003 simulated drawdown surrounding Algonquin well 11 expands and merges (under low-recharge conditions), or nearly merges (under model-calibrated recharge conditions), with a nearby area of significant post-2003 simulated drawdown surrounding Carpentersville wells 6 and 7. Under high-pumping and low-recharge conditions, total simulated drawdown at the end of 2049 is about 112 ft at Algonquin well 11, at the apex of the simulated cone of depression in northeastern Kane and southeastern McHenry Counties, whereas total simulated drawdown is about 82 ft under low-pumping and high-recharge conditions. Simulated hydrographs at head calibration targets 661, 278, and 700 (Figure 240 through Figure 243) illustrate simulated head at locations within the northeastern Kane-southeastern McHenry cone of depression from 1964 through 2049. Simulated heads in the Shallow Bedrock Aquifer at head target 661 (Figure 241), the historic heads at which were discussed in Section 3.2.1.2, decline little during the post-2003 period as compared to the historic period from 1980 through 2003. This relatively small predicted decline is largely a consequence of maintaining withdrawals at 2003 rates during the post-2003 period. Simulated heads at targets 278 and 700 (Figure 242 and Figure 243) are strongly influenced by pumping at Carpentersville wells 6 and 7, the response at target 700 being more pronounced owing to its proximity to the Carpentersville wells.

The area of significant simulated drawdown surrounding West Chicago wells 6, 7, and 8—largely in DuPage County east of Batavia and Geneva and previously discussed on page 237—remains after 2003 despite simulated pumping rates for the West Chicago wells being fixed at 2003 rates. Note that geographically separated areas of simulated drawdown exceeding 20 ft surrounding the West Chicago and Warrenville wells are discussed collectively here, as on page 237, as a single area of significant simulated drawdown. In reality, these areas remain separate except during later stress periods under high-pumping conditions. Maximum simulated drawdown in the West Chicago-Warrenville area occurs at West Chicago well 6. Under high-pumping, low-recharge conditions, the model suggests that about 8 ft of post-2003 drawdown and about 77 ft of total drawdown due to pumping will occur at that location by the end of 2049. Under low-pumping, high-recharge conditions, about 2 ft of post-2003 drawdown is suggested by the model by the end of 2049, for total simulated drawdown due to pumping of about 72 ft. Simulated heads in the Shallow Bedrock Aquifer at head targets 149 and 648 (Figure 240, Figure 244, and Figure 245), located respectively on the western and southern edges of the West Chicago-Warrenville drawdown center, illustrate head change through time in the area. In general, simulated head change at these targets is small owing to their distance from the West Chicago and Warrenville pumping centers and to the maintenance of assumed future pumping rates at 2003 levels. Head target 149 is included

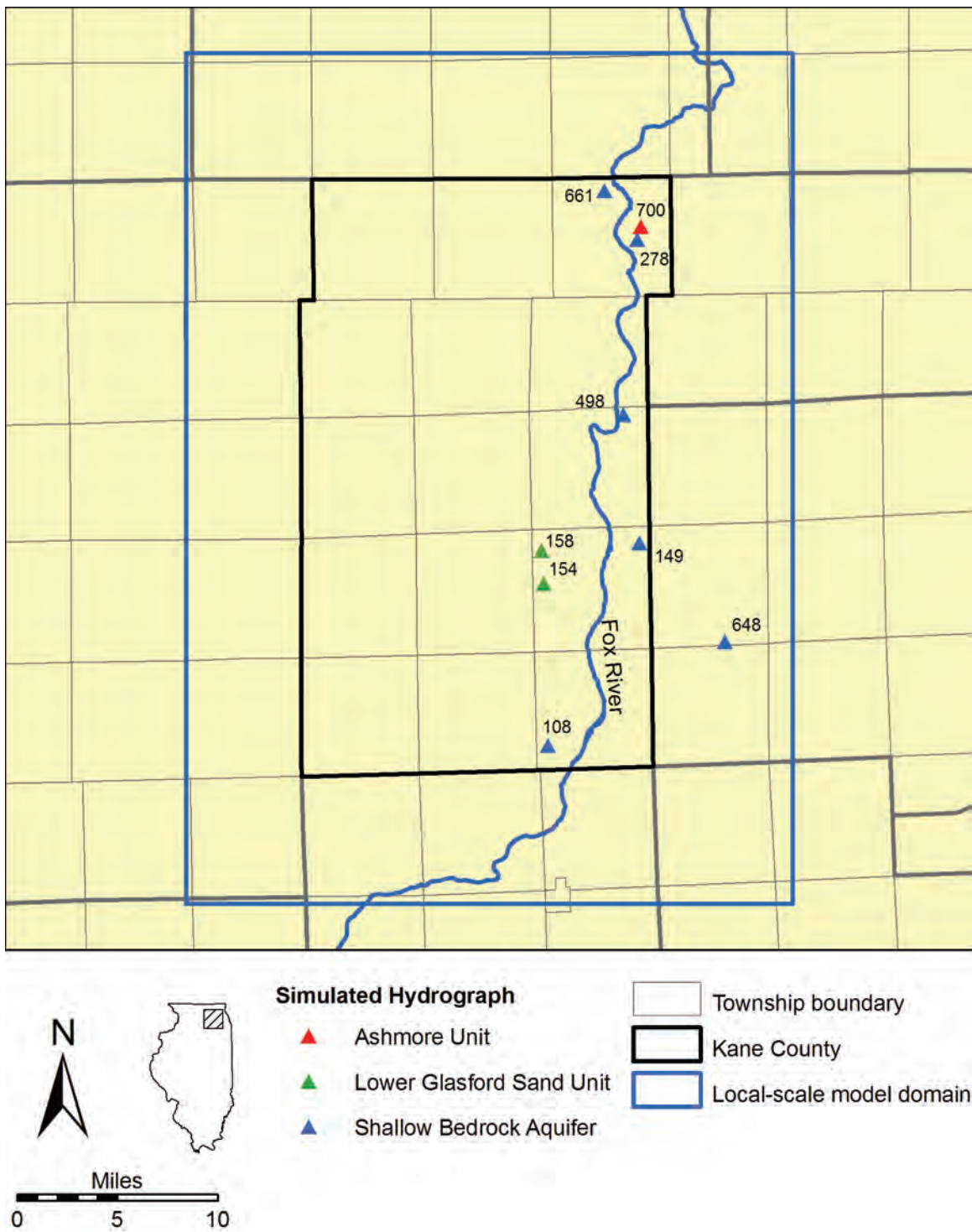


Figure 240. Locations of simulated hydrographs shown in Figure 241 through Figure 249.

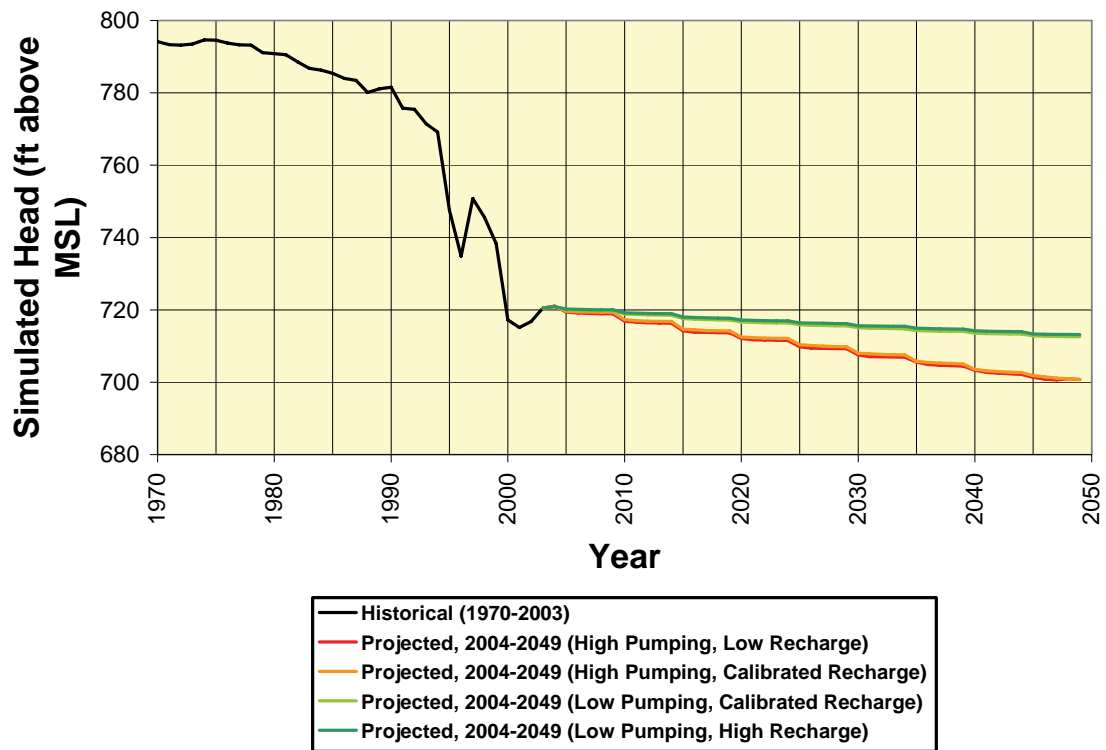


Figure 241. Simulated heads in the Shallow Bedrock Aquifer at head calibration target 661, located in the Algonquin area of northeastern Kane County.

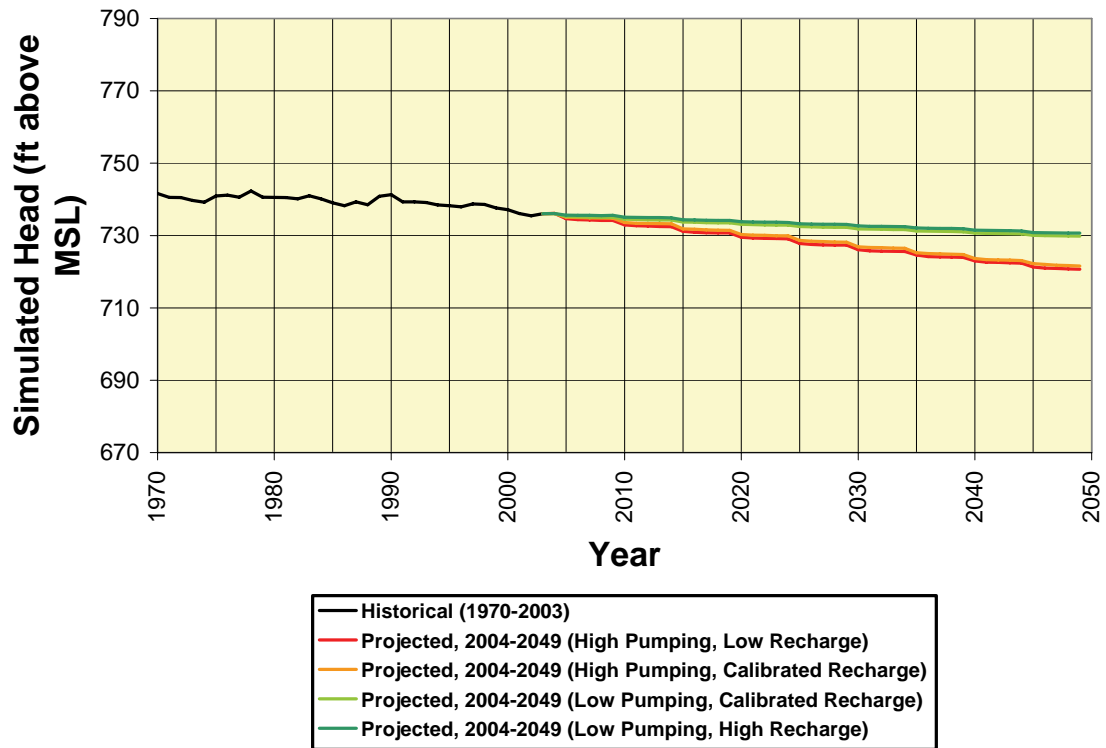


Figure 242. Simulated heads in the Shallow Bedrock Aquifer at head calibration target 278, located in East Dundee, northeastern Kane County.

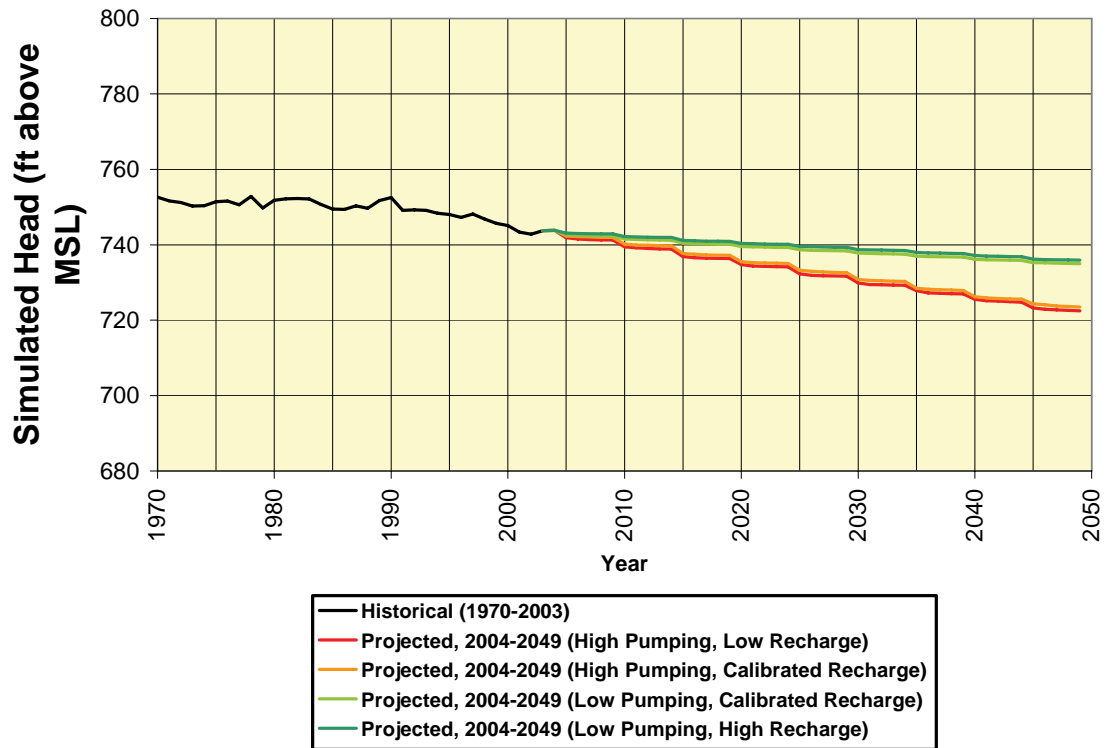


Figure 243. Simulated heads in the Ashmore Unit at head calibration target 700, located in Carpentersville, northeastern Kane County.

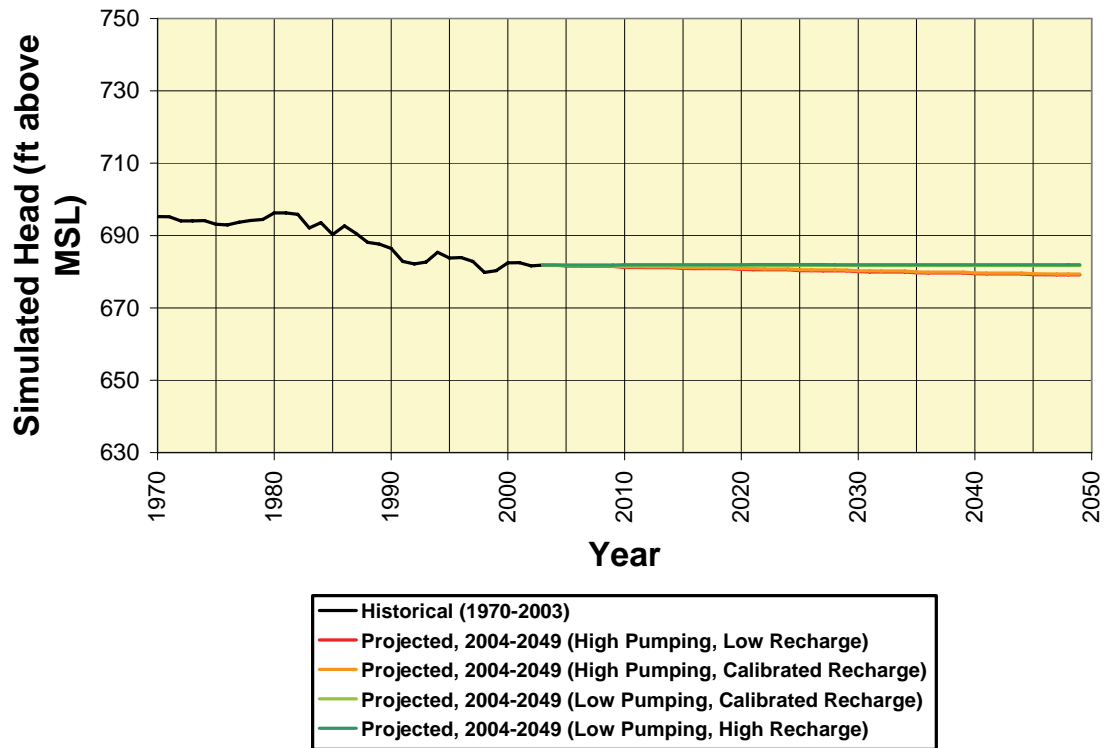


Figure 244. Simulated heads in the Shallow Bedrock Aquifer at head calibration target 149, located east of Geneva, on the eastern border of Kane County.

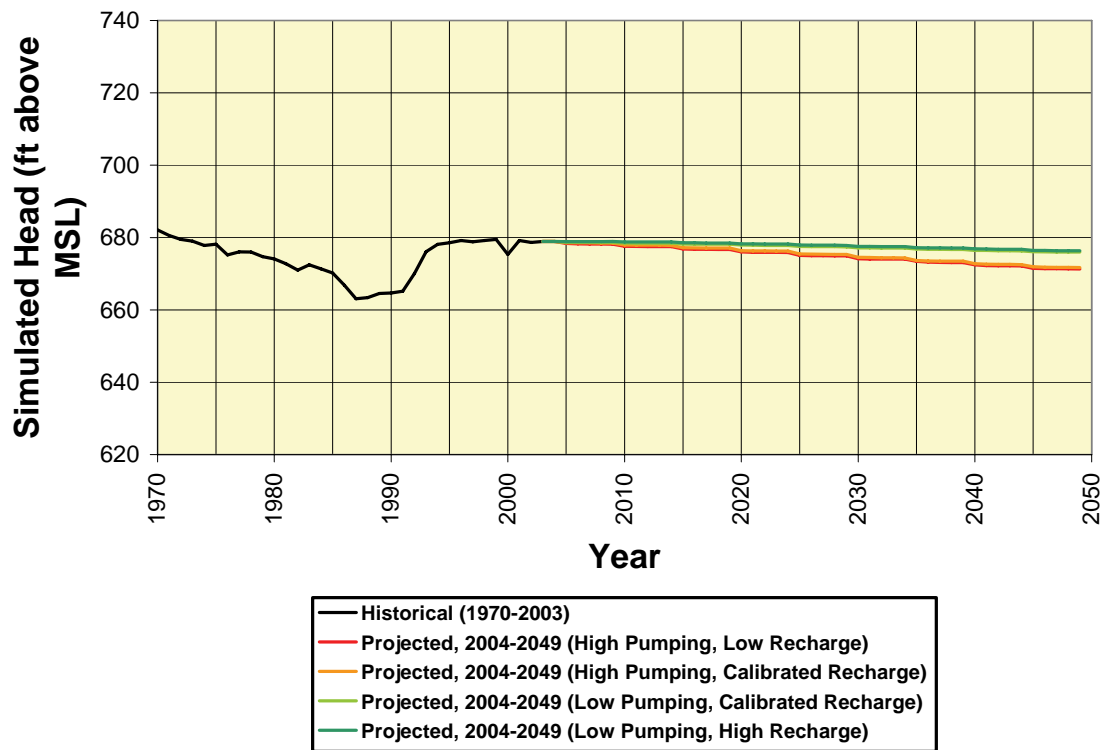


Figure 245. Simulated heads in the Shallow Bedrock Aquifer at head calibration target 648, located in Warrenville, DuPage County.

in this report because it illustrates the effect of West Chicago and Warrenville pumping in Kane County.

Model simulations suggest that a third large area of significant drawdown will develop after 2025 west of the cities of Batavia and Geneva under high-pumping conditions and both model-calibrated and low-recharge conditions. Post-2003 simulated drawdown in this area results principally from pumping from the Upper and Lower Glasford Sand Units at Batavia wells 6, 7, and 8 and Geneva wells 8, 9, and 10. The area was discussed previously in conjunction with 2003 drawdown (page 252) and base flow reduction in Mill Creek (page 256). Significant simulated drawdown develops in the Batavia-Geneva well field area before 2025. Separate areas of significant simulated drawdown first develop around each community's well field, and these two separate drawdown centers merge into a single area by 2025 in all but the low-pumping, high-recharge scenario. By 2050, in all four simulated scenarios, a single area of significant simulated drawdown surrounds both well fields. Greatest post-2003 simulated drawdown and total simulated drawdown in 2050 occur at Batavia well 6, where the model suggests about 11 to 33 ft of post-2003 simulated drawdown, for a total simulated drawdown due to pumping of about 29 to 50 ft. Simulated hydrographs at head targets 154 and 158—located in the Batavia and Geneva well fields, respectively—illustrate simulated head change in the Lower Glasford Sand Unit through time (Figure 240, Figure 246, and Figure 247).

Remaining areas of significant simulated drawdown at the end of 2049 are much more limited in area than those in northeastern Kane-southeastern McHenry Counties, the West Chicago area, and the Batavia-Geneva well field area. Two areas of significant simulated drawdown in South Elgin in existence in 2003 (page 237), one surrounding South Elgin well 4 (on the west side of the Fox River) and the other surrounding South Elgin wells 3, 6, and 10 (on the east side of the river), remain through 2049 under all four simulated scenarios. Significant simulated drawdown on the east side of the river affects a larger area owing to the greater magnitude of pumping there, but the areas of simulated drawdown on opposite sides of the river do not merge, even as late as 2050, because the wells are able to capture streamflow from the Fox River to supply part of their yields. Estimated post-2003 simulated drawdown in the Shallow Bedrock Aquifer at the end of 2049 at head target 498, located east of the Fox River on the southeast side of South Elgin, ranges from about 4 to 12 ft, with total simulated drawdown due to pumping ranging from about 16 to 23 ft (Figure 248). The area of significant simulated drawdown in 2003 surrounding Dial Corporation wells 1, 2, and 3 in Montgomery—discussed on page 243—is maintained and slightly expanded under high-pumping conditions, but it disappears under low-pumping conditions. Indeed, as shown by simulated heads in the Shallow Bedrock Aquifer at nearby head target 108 (Figure 249), simulated heads in the vicinity of the Dial Corporation wells, while continuing to decline under high-pumping conditions, actually rise 1 to 2 ft, depending on recharge conditions, under low-pumping conditions. This effect reflects the fact that pumping from the Dial wells is projected to decline under low-pumping conditions.

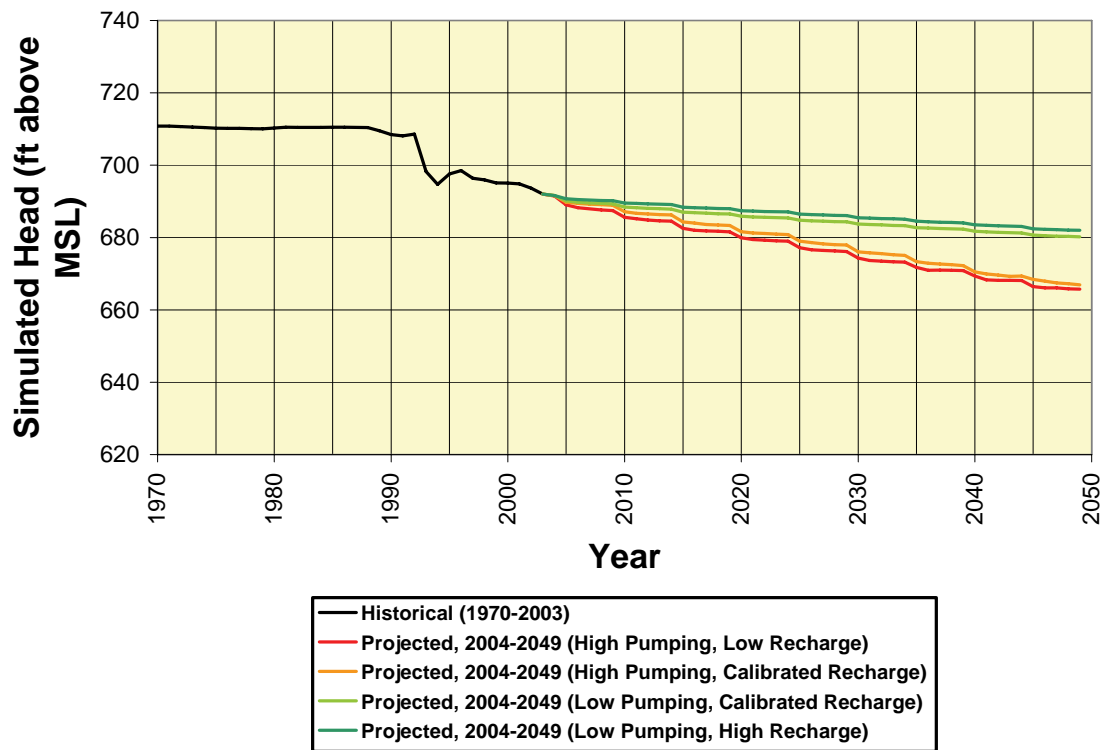


Figure 246. Simulated heads in the Lower Glasford Sand Unit at head calibration target 154, located west of Batavia, Kane County.

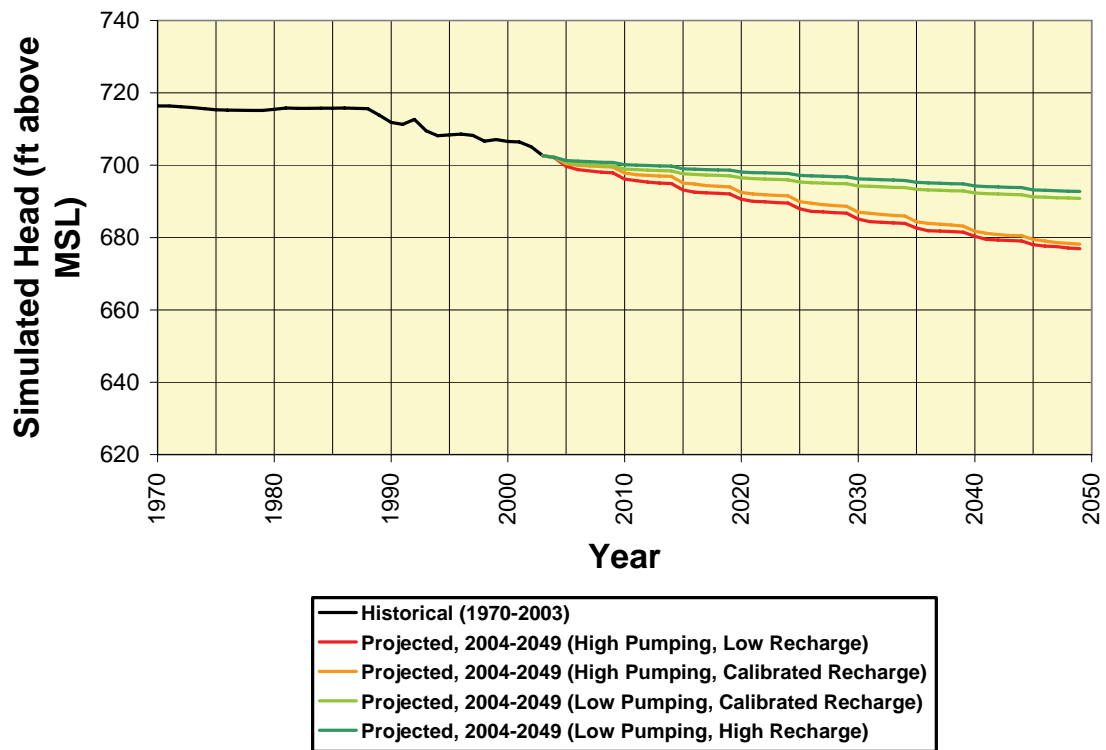


Figure 247. Simulated heads in the Lower Glasford Sand Unit at head calibration target 158, located west of Geneva, Kane County.

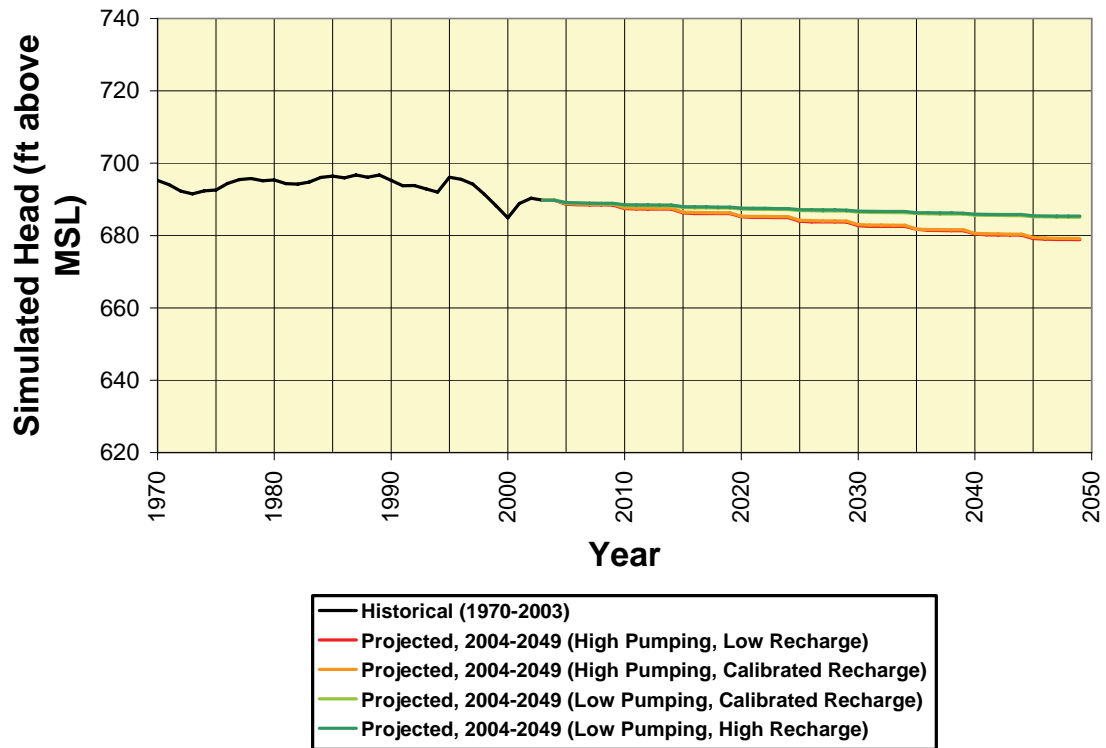


Figure 248. Simulated heads in the Shallow Bedrock Aquifer at head calibration target 498, located on the southeast edge of South Elgin.

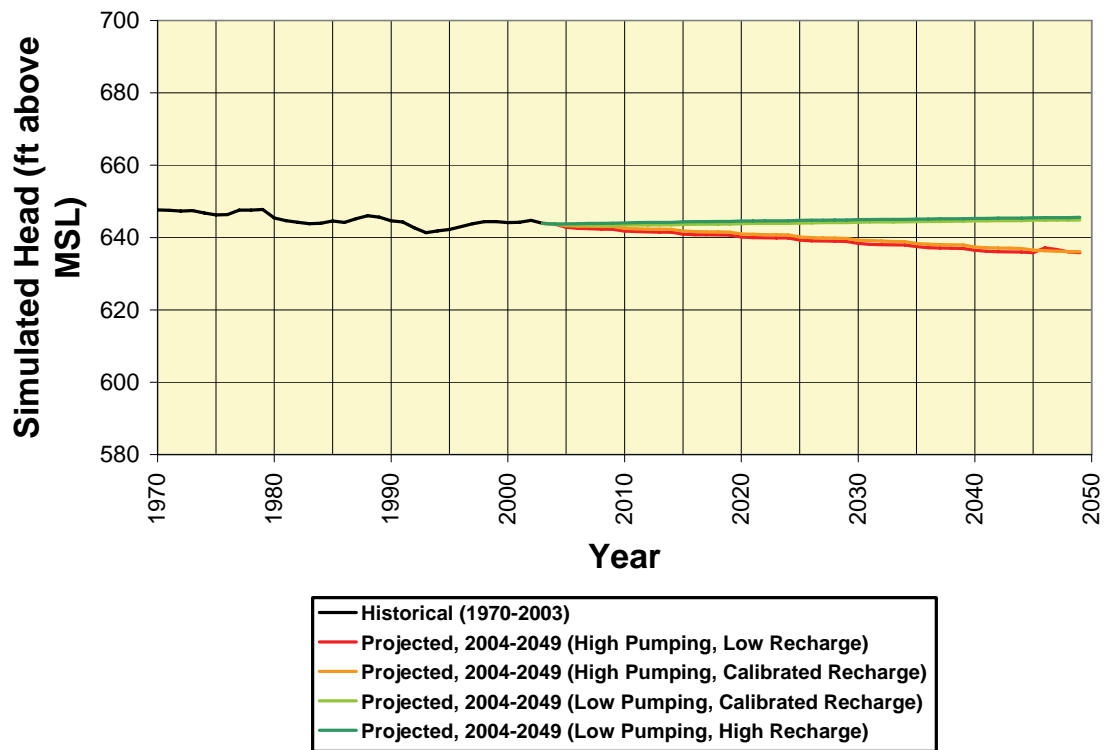


Figure 249. Simulated heads in the Shallow Bedrock Aquifer at head calibration target 108, located on the north edge of Montgomery.

Modeling results suggest that new areas of significant drawdown may develop after 2003 in the vicinity of Lily Lake, near irrigation wells operated by Hampshire farms between Hampshire and Pingree Grove in the vicinity of irrigation wells operated by Dunteman Turf Farm southwest of Elburn, in St. Charles, and in Sugar Grove. The largest of these is the one in the vicinity of Lily Lake, which surrounds Ferson Creek Utilities Corporation wells 2 and 3, both of which obtain groundwater from the Lower Glasford Sand Unit. The other areas of significant drawdown are very small and notably include two small, separate but closely spaced areas in St. Charles, one surrounding St. Charles wells 9 and 11, and the second surrounding an irrigation well operated by the St. Charles Country Club. Records show that St. Charles wells 9 and 11 each pumped more than 1.5 Mgd in 2003, the greatest production of any shallow wells in Kane County that year. Simulated pumping from each well from 2045 through 2049 is 2.1 to 2.9 Mgd under low- and high-pumping conditions, respectively.

Typical approaches to reducing drawdown are to reduce pumping rates in problem areas and relocate water-supply wells to areas of less drawdown. Unfortunately, mapping the overall transmissivity of the shallow materials (the Shallow Bedrock Aquifer and all Quaternary materials) in the local model domain suggests that the most productive shallow aquifers in Kane County are already developed by wells (Figure 250). New drilling may reveal unmapped intervals of high transmissivity, but it is likely, given the large number of wells that have already been drilled in the area, that such intervals will be limited in area and incapable of supporting large groundwater withdrawals over a long time period.

Model simulations suggest that, for the scenarios which assume historical recharge rates (scenarios *HC* and *LC* in Table 31 and Table 32), natural groundwater discharge in the Kane County area at the end of 2024 would be 2 to 5 percent below 2003 rates, and at the end of 2049 it would be 5 to 11 percent below 2003 rates (Figure 251), depending on pumping conditions. For each of the four simulated scenarios of pumping and recharge, model-suggested changes in natural groundwater discharge to streams are shown in four figures. Figure 252 through Figure 255 show changes in simulated natural groundwater discharge for the high-pumping, low-recharge scenario, and the following groups of four figures illustrate results for the high-pumping, model-calibrated recharge scenario (Figure 256 through Figure 259); the low-pumping model-calibrated recharge scenario (Figure 260 through Figure 263); and the low-pumping, high-recharge scenario (Figure 264 through Figure 267). For each scenario, the figures show post-2003 change in natural groundwater discharge at the end of 2024 (Figure 252, Figure 256, Figure 260, and Figure 264); change in natural groundwater discharge since predevelopment at the end of 2024 (Figure 253, Figure 257, Figure 261, and Figure 265); post-2003 change in natural groundwater discharge at the end of 2049 (Figure 254, Figure 258, Figure 262, and Figure 266); and change in natural groundwater discharge since predevelopment at the end of 2049 (Figure 255, Figure 259, Figure 263, and Figure 267). In addition, changes in simulated natural groundwater discharge since predevelopment are shown in Table 31, and changes after 2003 are shown in Table 32.

Model simulations suggest, not surprisingly, that climate variability, simulated as changes in recharge, could have a significant effect on natural groundwater discharge to streams throughout the Kane County area. Simulated high-recharge conditions actually cause simulated groundwater discharge to many streams to rise above simulated 2003

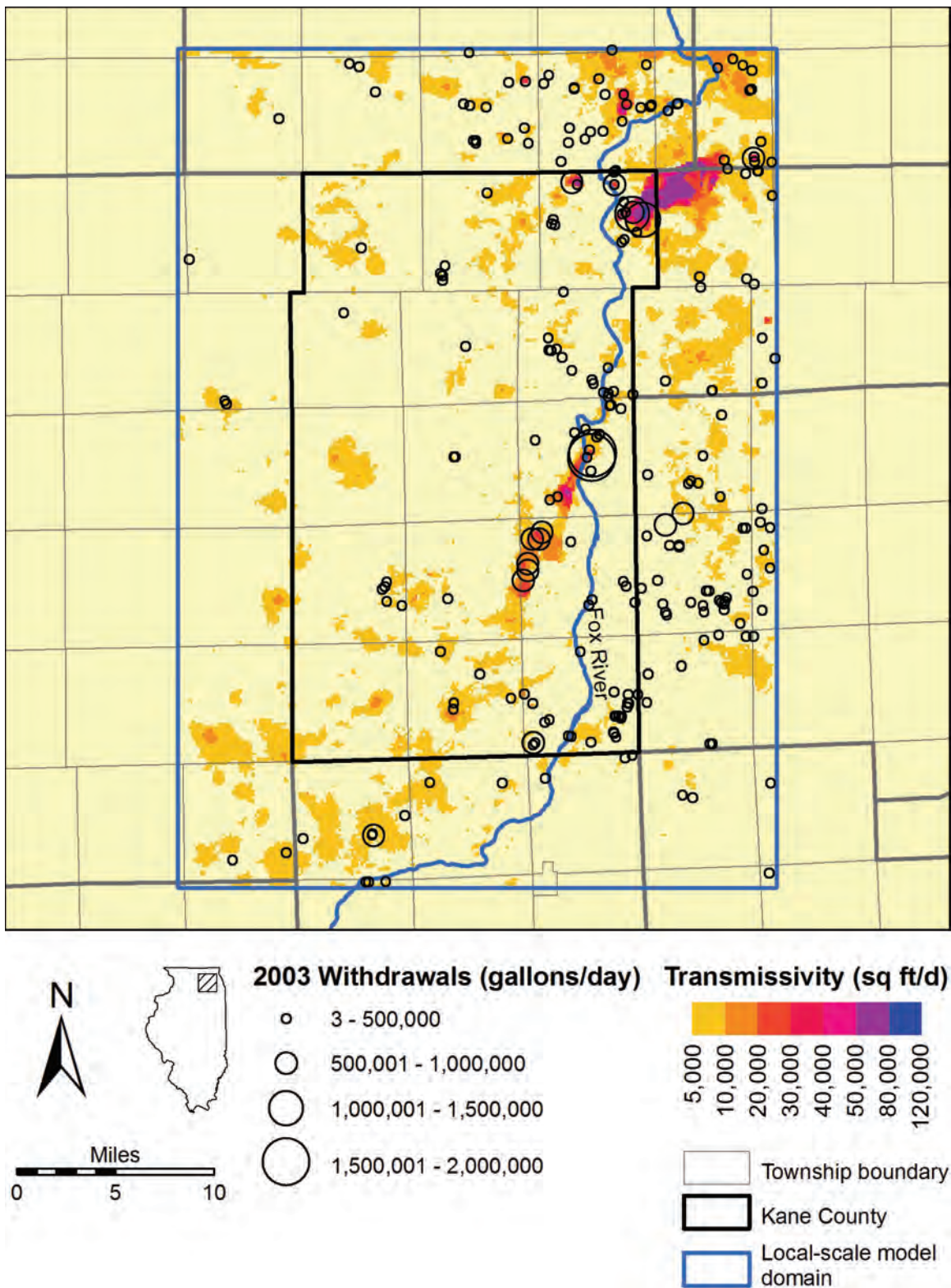


Figure 250. Transmissivity of shallow materials in Kane County, with 2003 withdrawals superimposed.

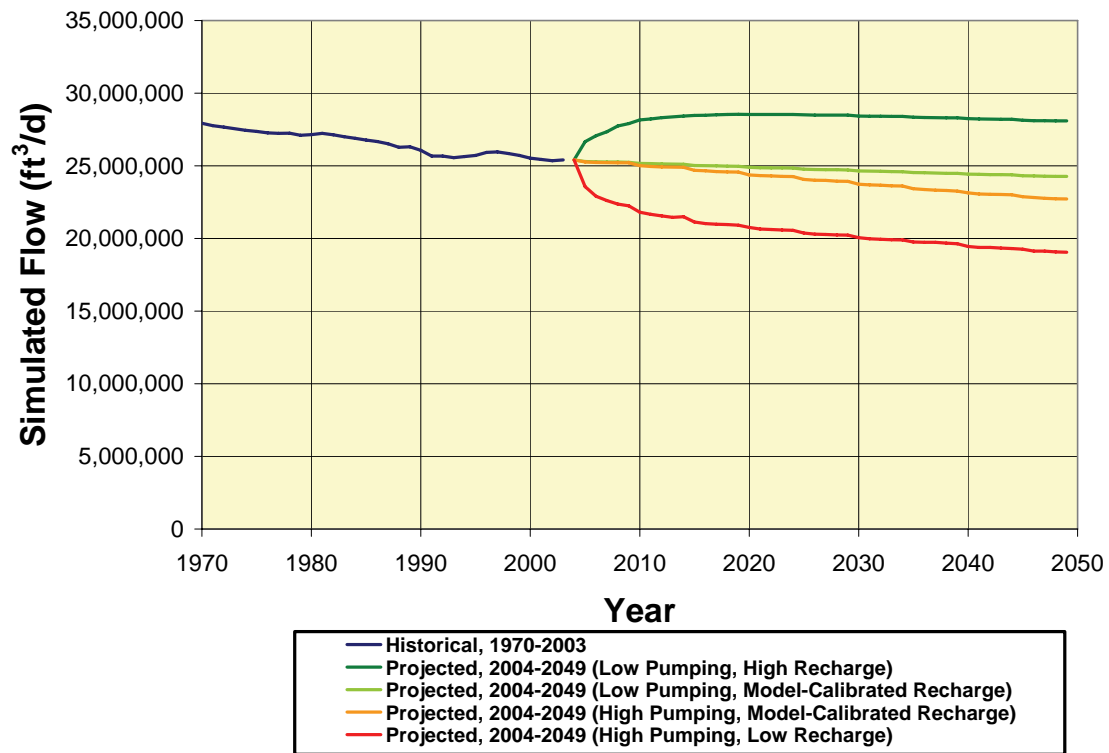


Figure 251. Total natural groundwater discharge to streams in the local-scale model domain.

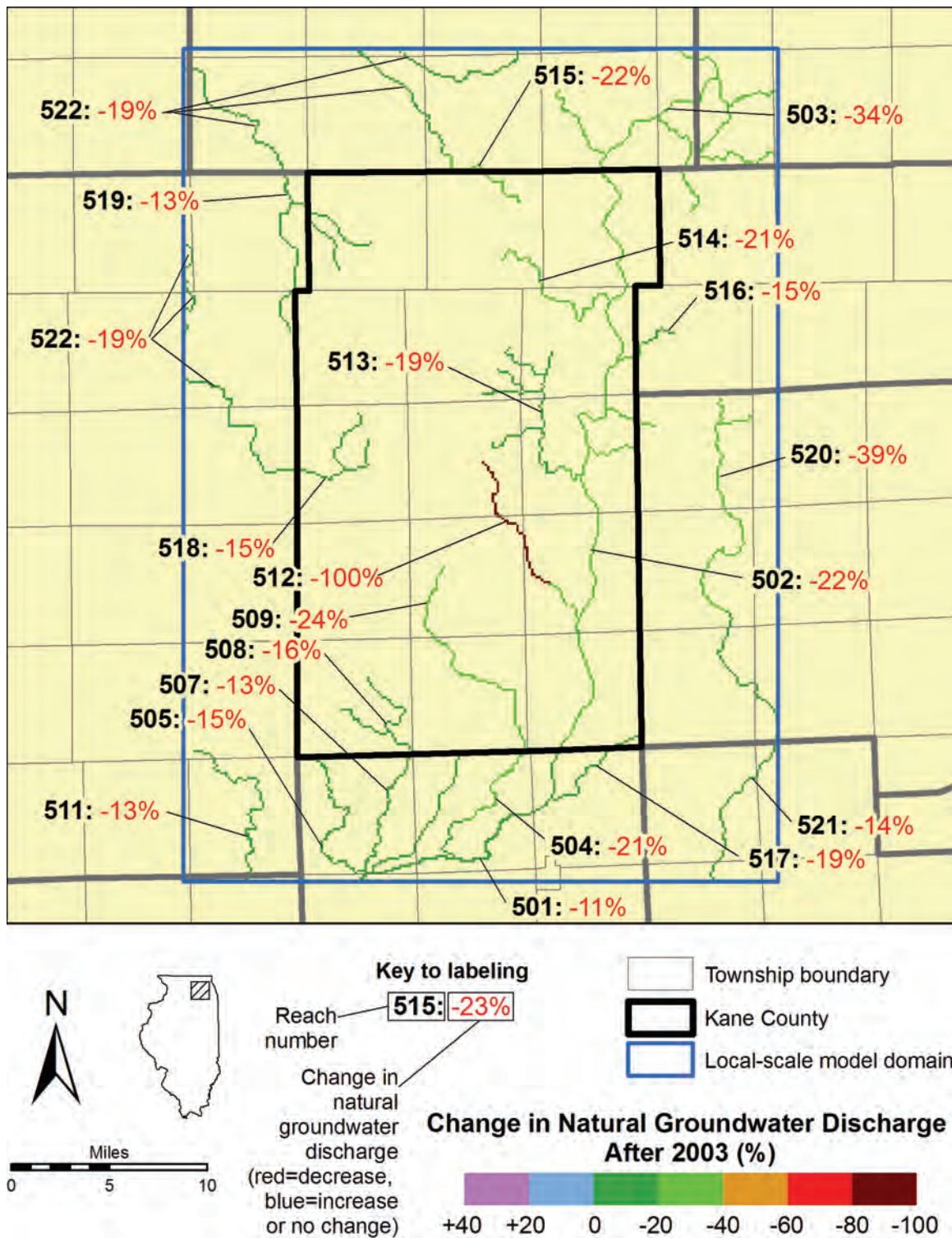


Figure 252. Estimated post-2003 change in natural groundwater discharge caused by pumping, by stream reach, at the end of 2024 under a scenario of high pumping and low recharge rates.

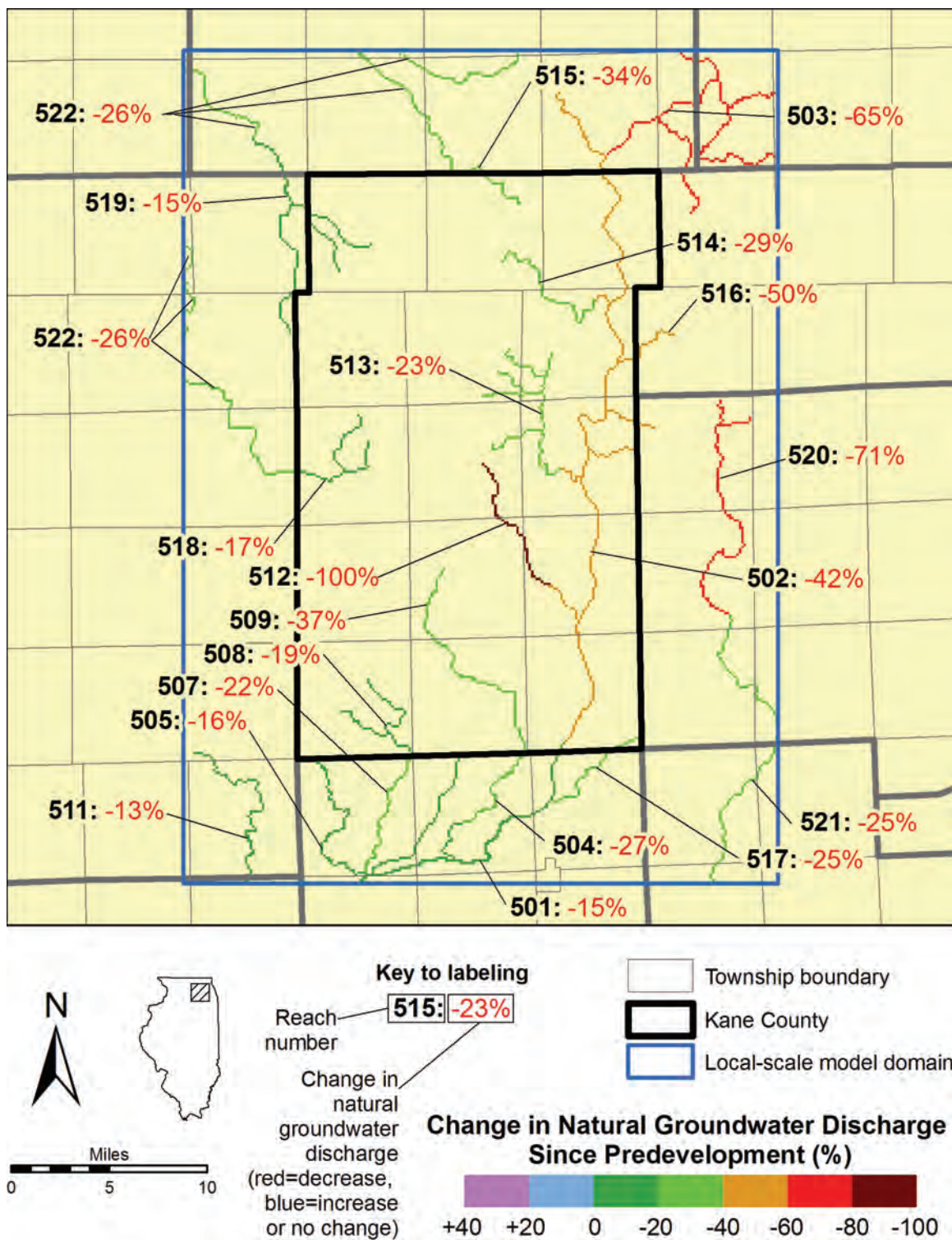


Figure 253. Estimated total change in natural groundwater discharge caused by pumping, by stream reach, at the end of 2024 under a scenario of high pumping and low recharge rates.

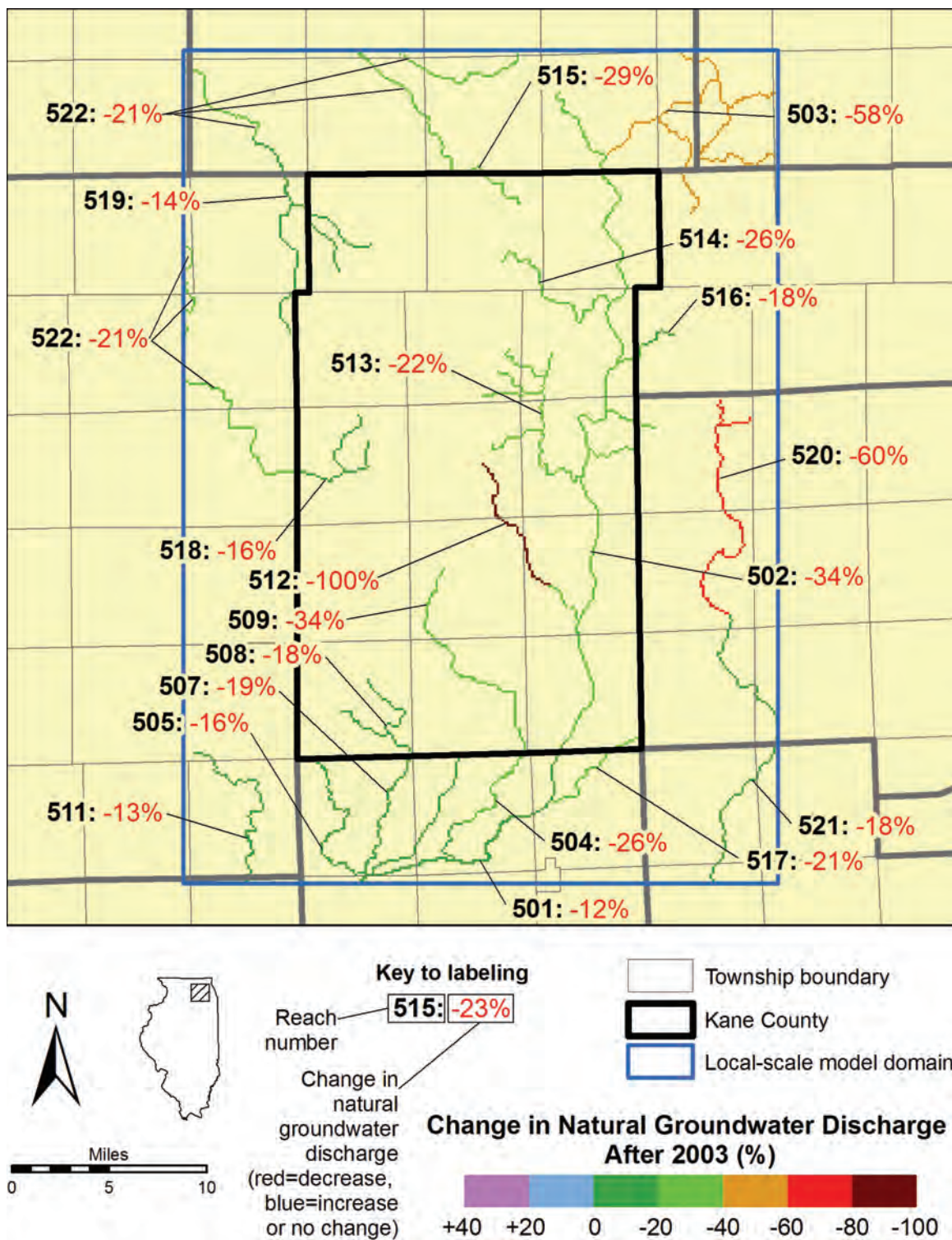


Figure 254. Estimated post-2003 change in natural groundwater discharge caused by pumping, by stream reach, at the end of 2049 under a scenario of high pumping and low recharge rates.

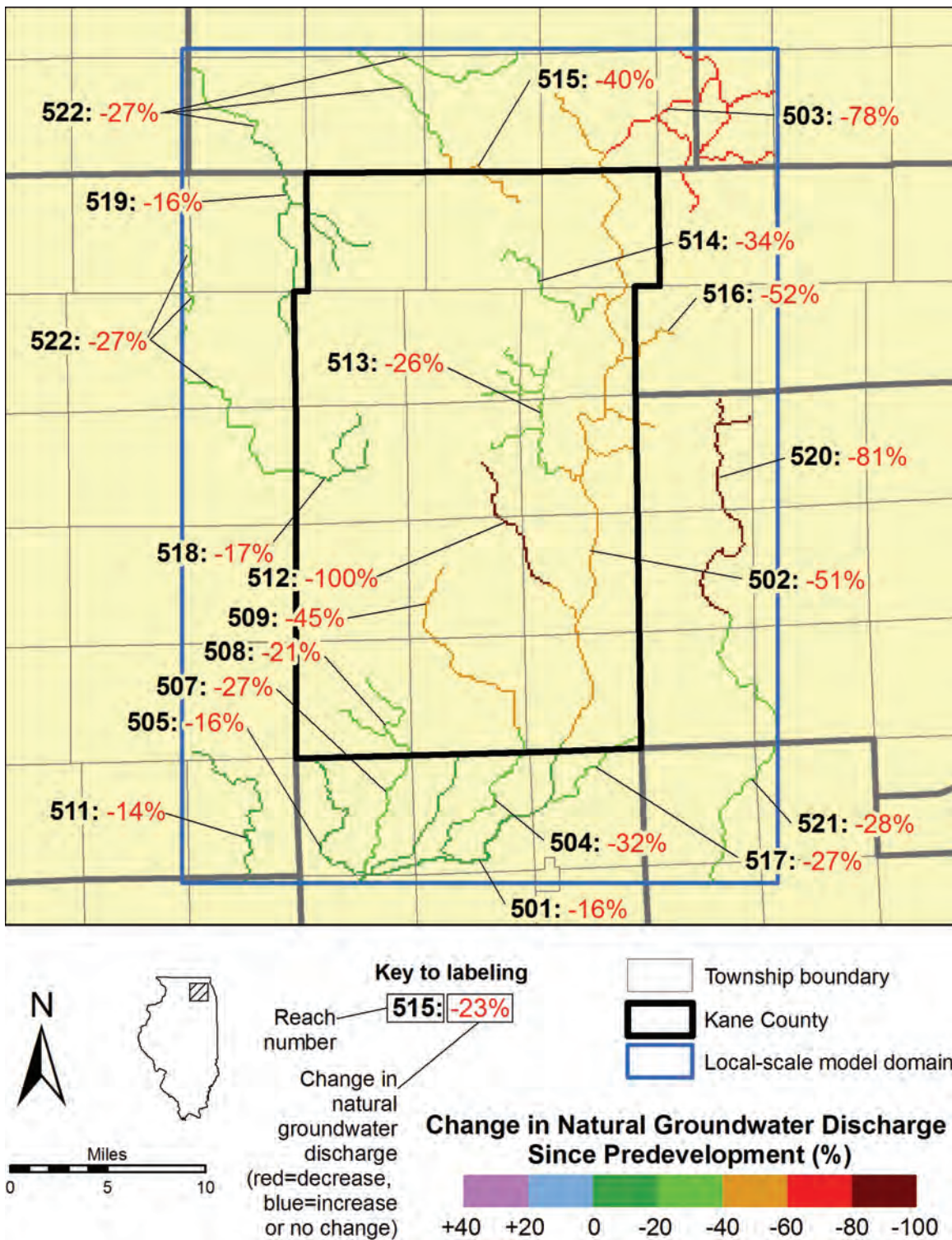


Figure 255. Estimated total change in natural groundwater discharge caused by pumping, by stream reach, at the end of 2049 under a scenario of high pumping and low recharge rates.

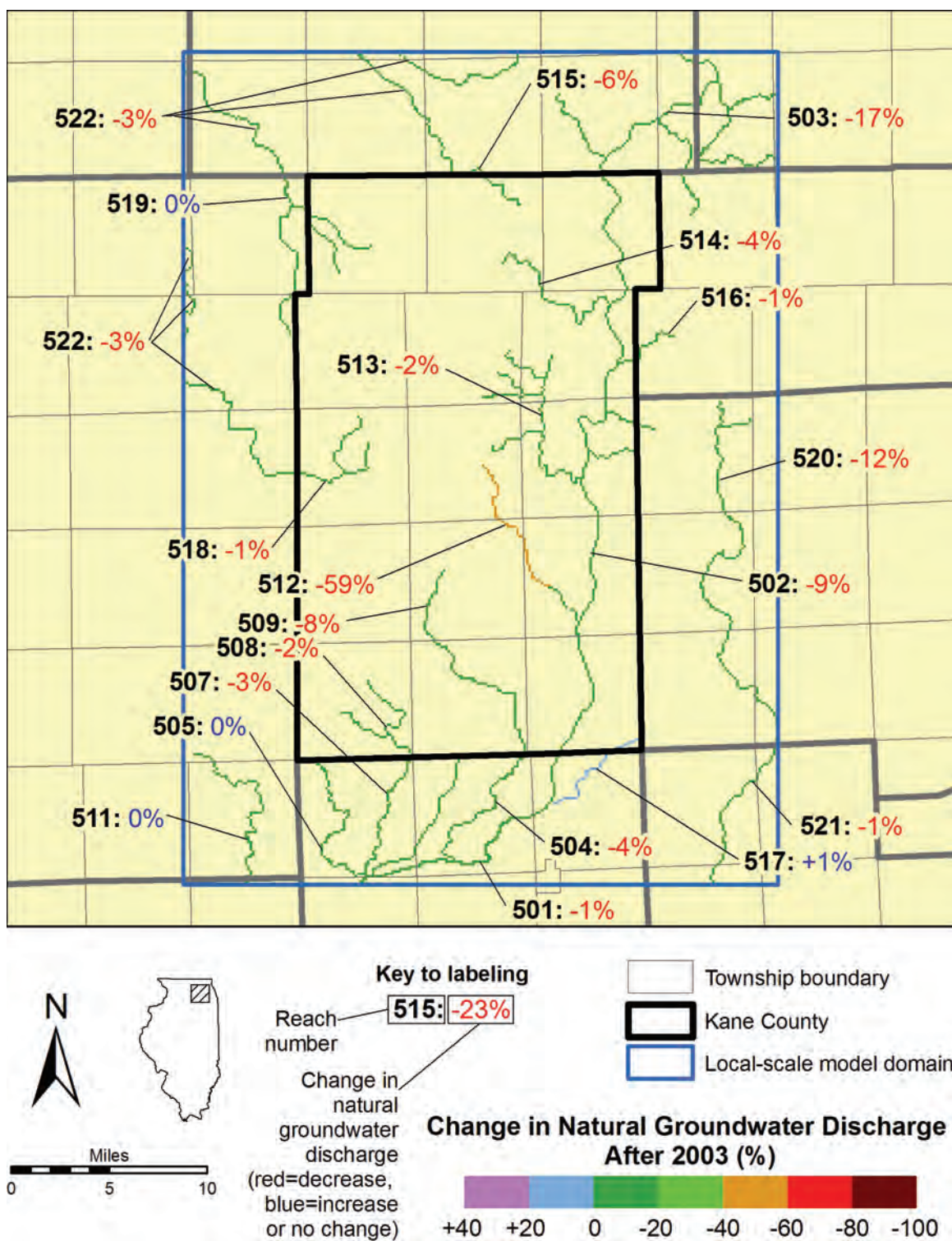


Figure 256. Estimated post-2003 change in natural groundwater discharge caused by pumping, by stream reach, at the end of 2024 under a scenario of high pumping and model-calibrated recharge rates.

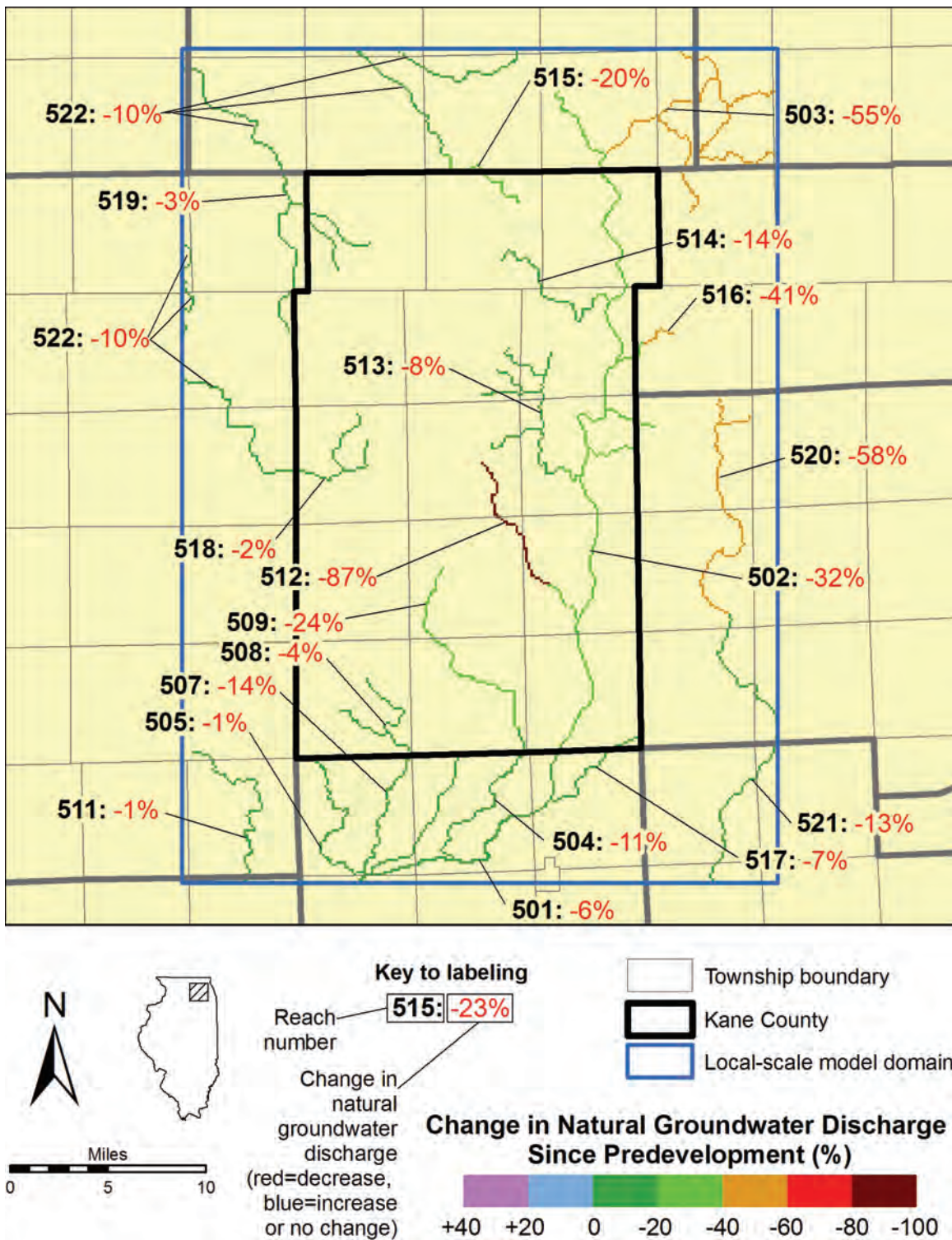


Figure 257. Estimated total change in natural groundwater discharge caused by pumping, by stream reach, at the end of 2024 under a scenario of high pumping and model-calibrated recharge rates.

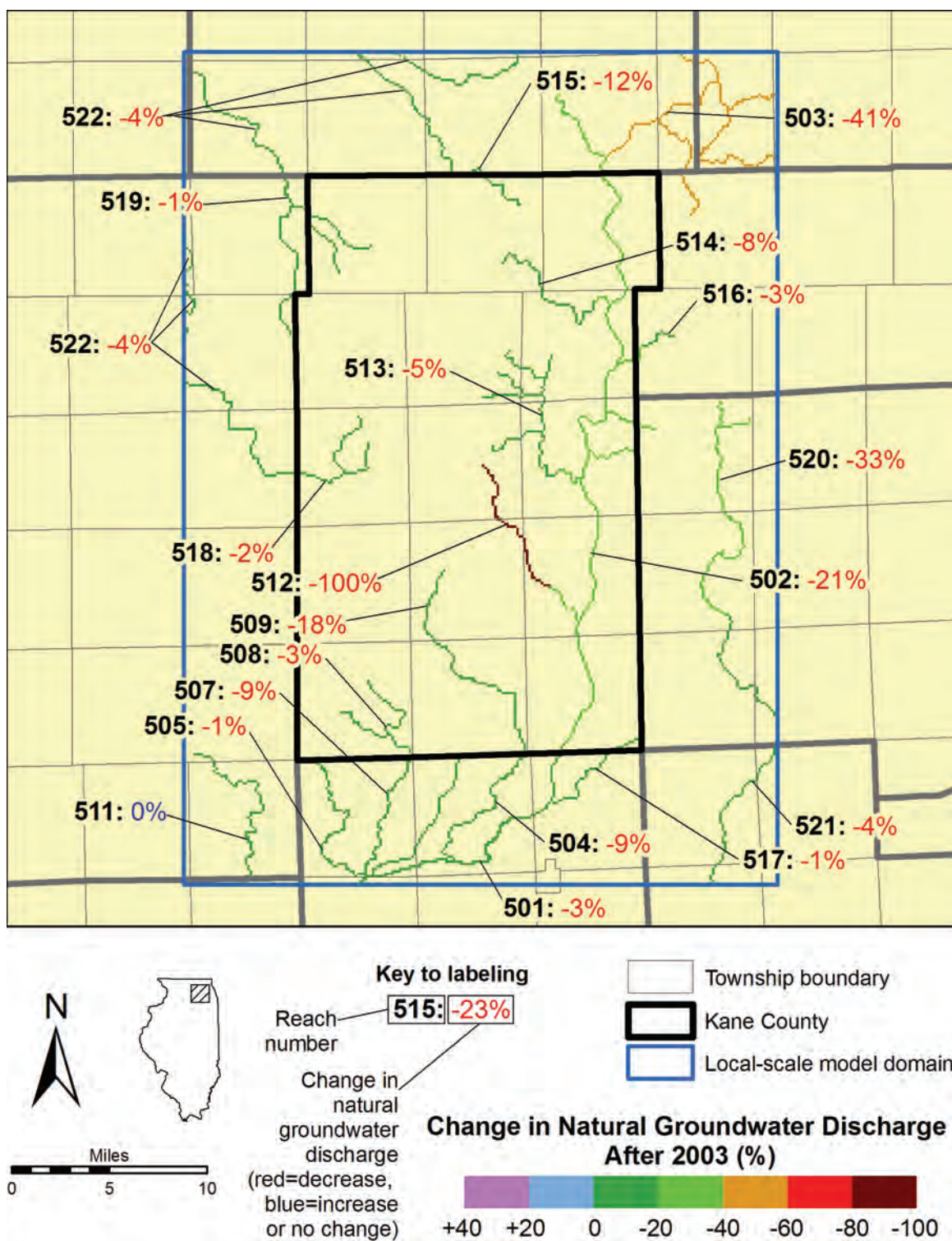


Figure 258. Estimated post-2003 change in natural groundwater discharge caused by pumping, by stream reach, at the end of 2049 under a scenario of high pumping and model-calibrated recharge rates.

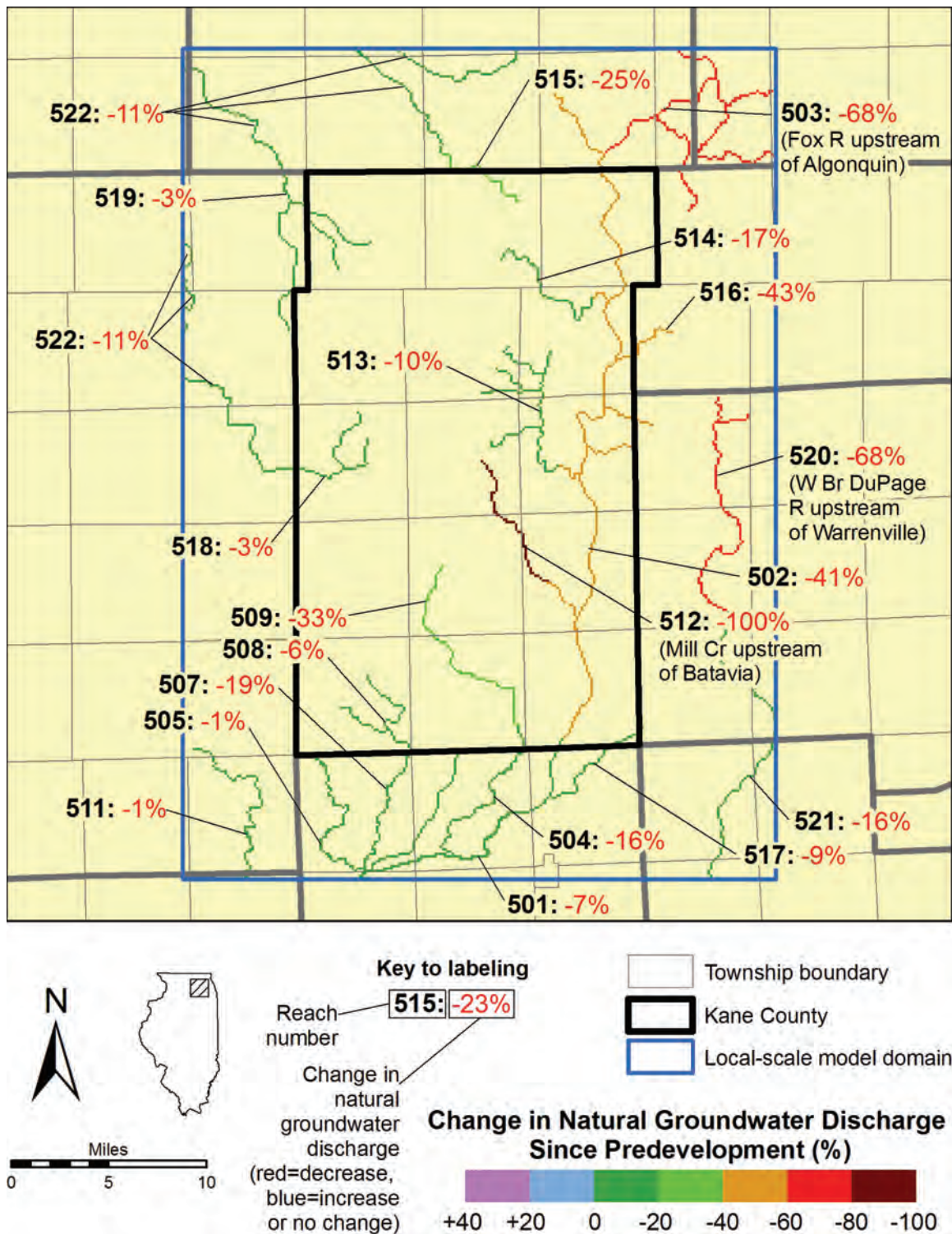


Figure 259. Estimated total change in natural groundwater discharge caused by pumping, by stream reach, at the end of 2049 under a scenario of high pumping and model-calibrated recharge rates.

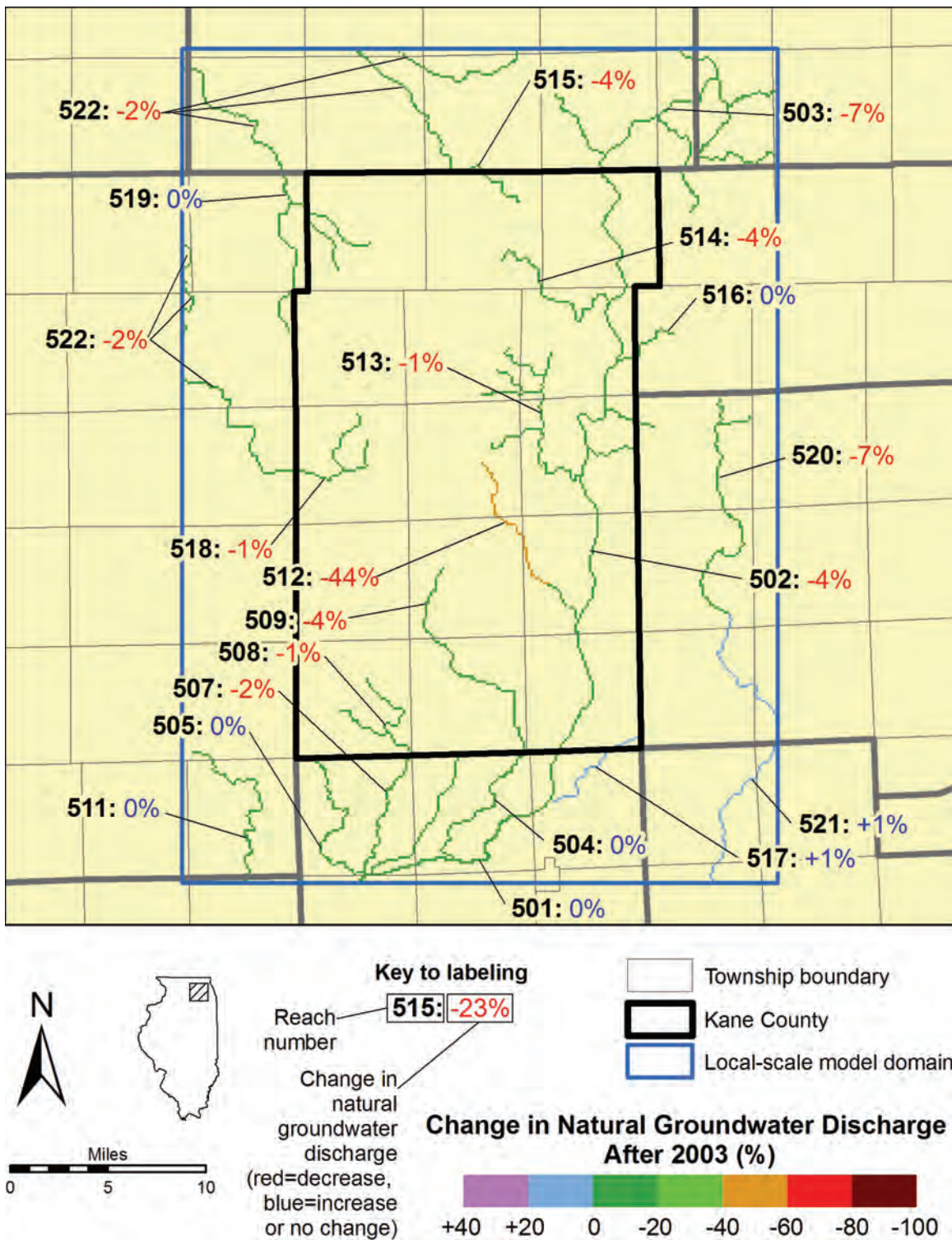


Figure 260. Estimated post-2003 change in natural groundwater discharge caused by pumping, by stream reach, at the end of 2024 under a scenario of low pumping and model-calibrated recharge rates.

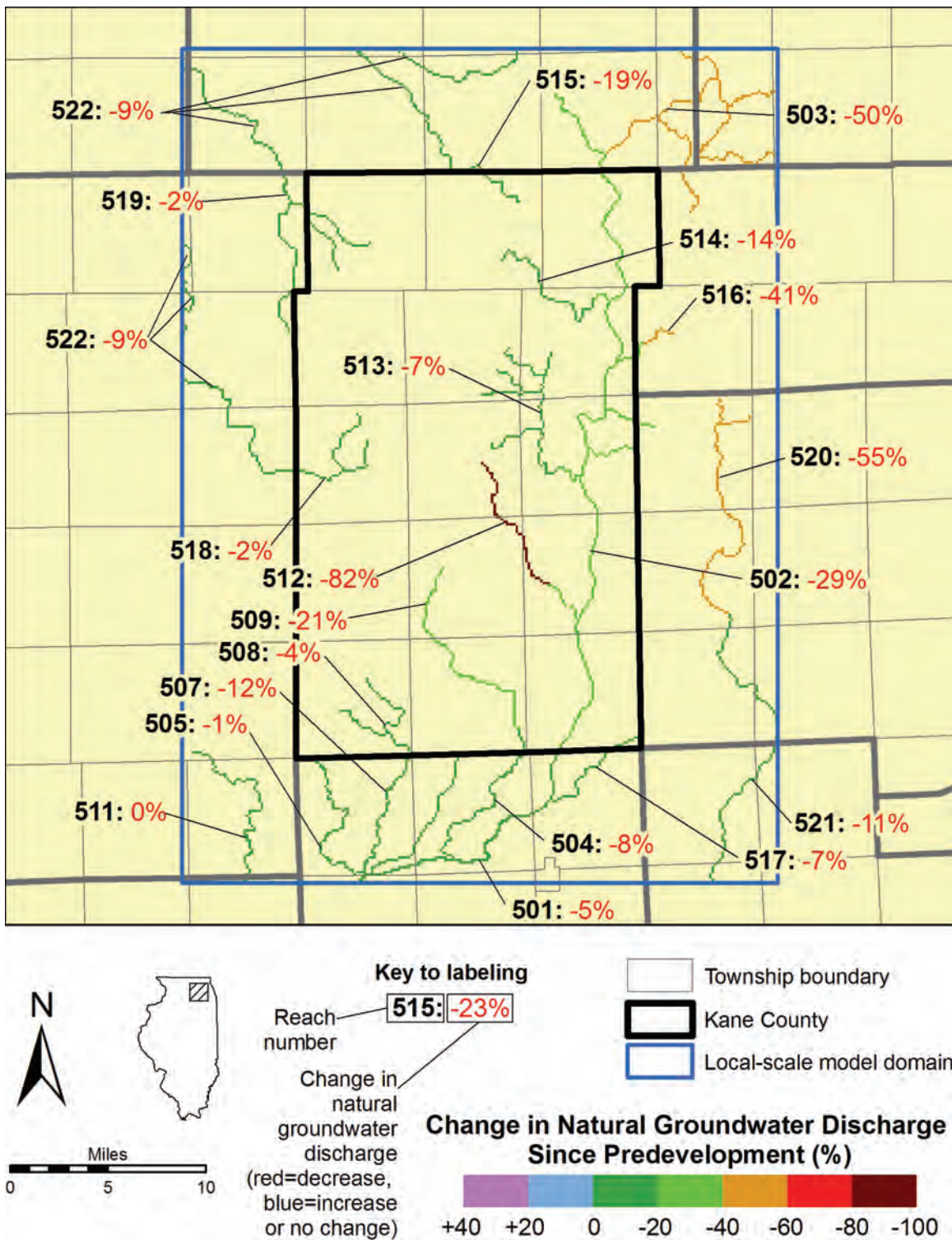


Figure 261. Estimated total change in natural groundwater discharge caused by pumping, by stream reach, at the end of 2024 under a scenario of low pumping and model-calibrated recharge rates.

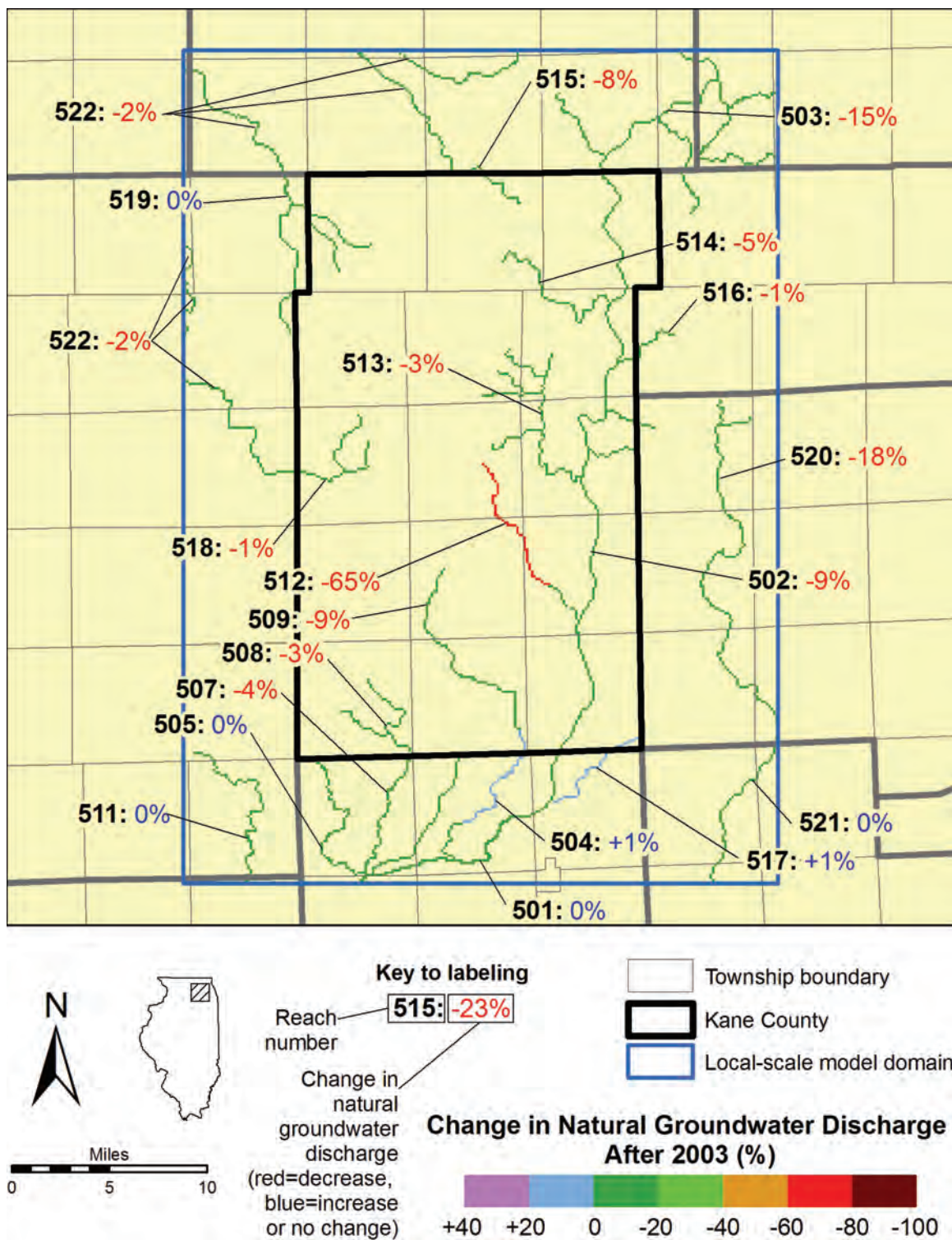


Figure 262. Estimated post-2003 change in natural groundwater discharge caused by pumping, by stream reach, at the end of 2049 under a scenario of low pumping and model-calibrated recharge rates.

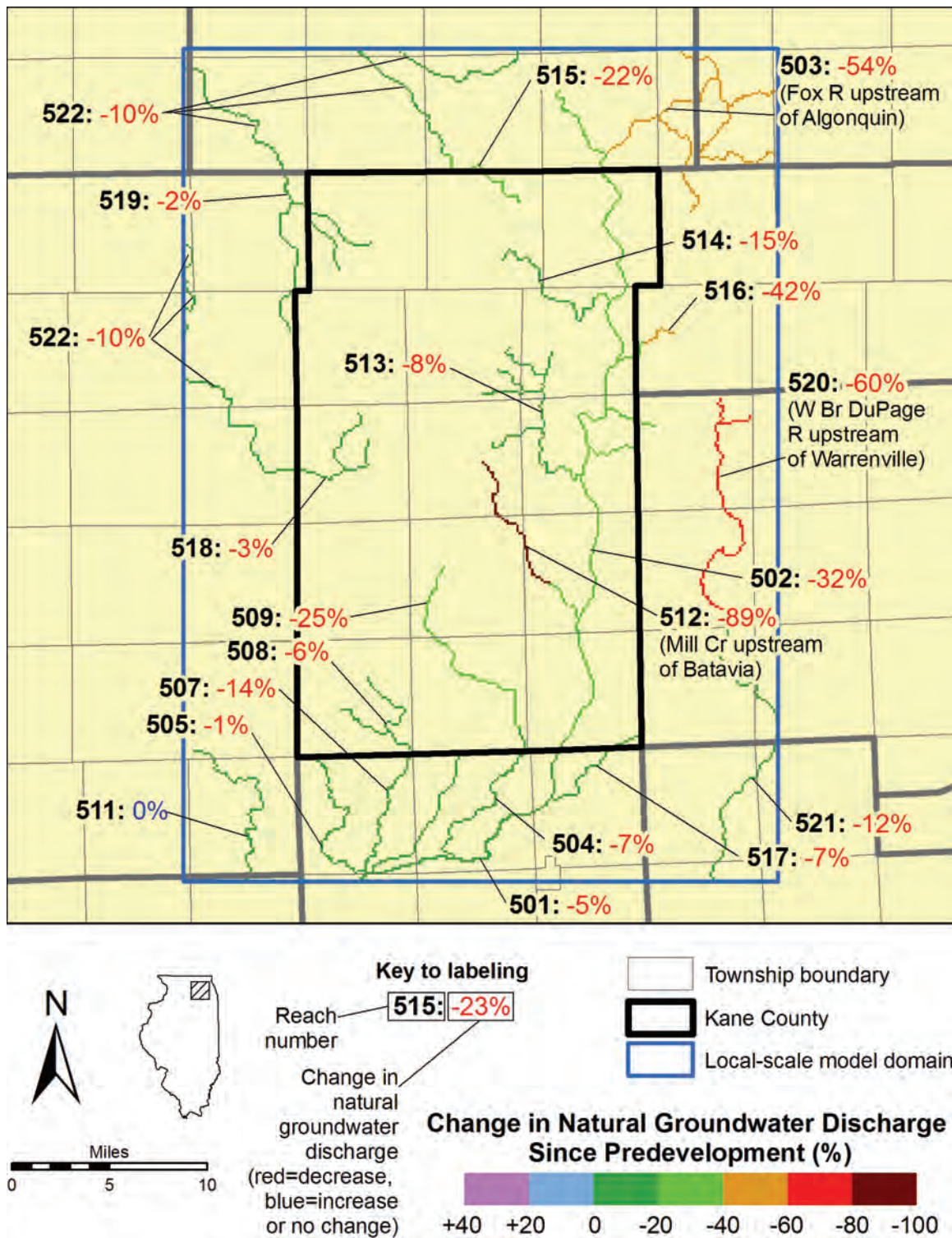


Figure 263. Estimated total change in natural groundwater discharge caused by pumping, by stream reach, at the end of 2049 under a scenario of low pumping and model-calibrated recharge rates.

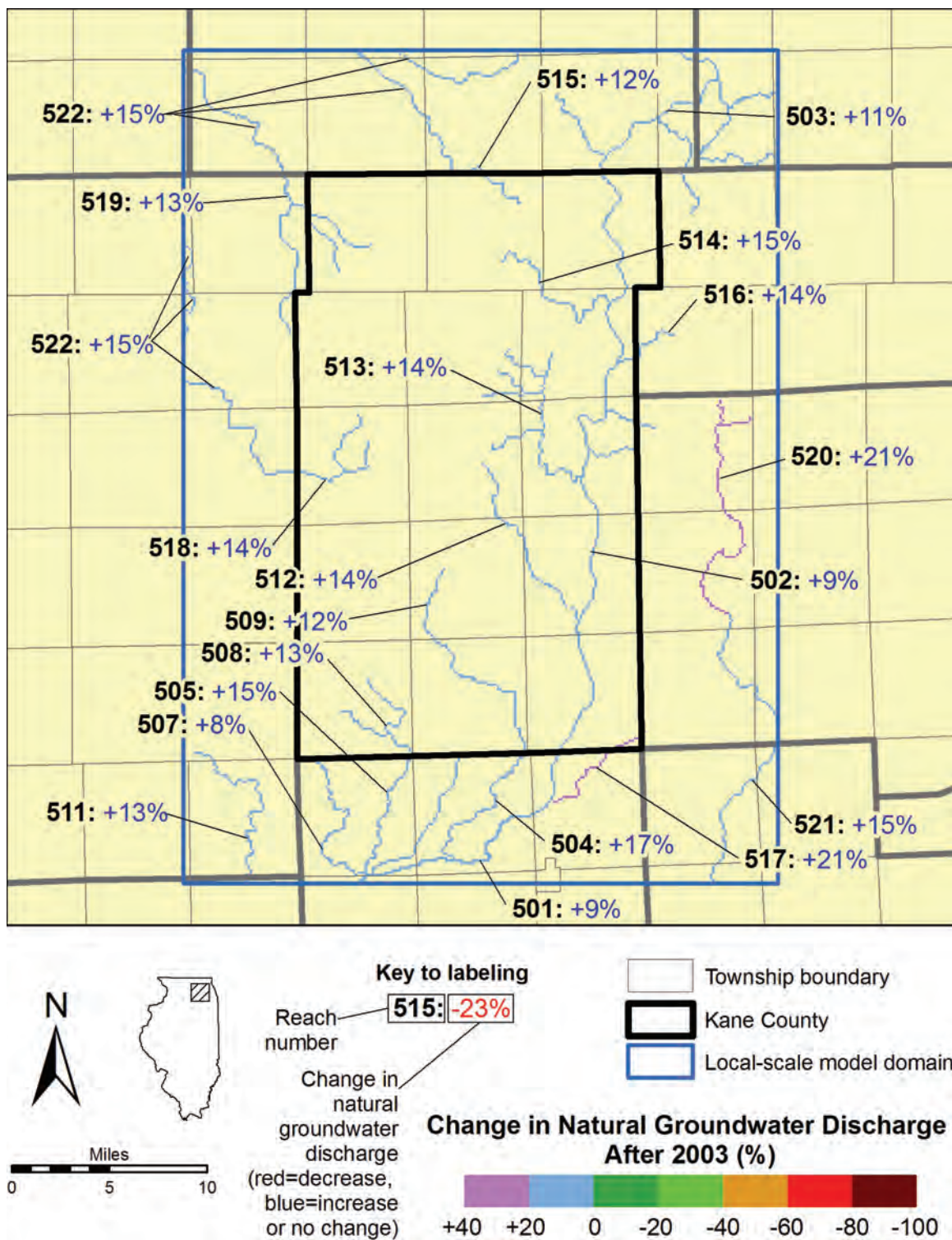


Figure 264. Estimated post-2003 change in natural groundwater discharge caused by pumping, by stream reach, at the end of 2024 under a scenario of low pumping and high recharge rates.

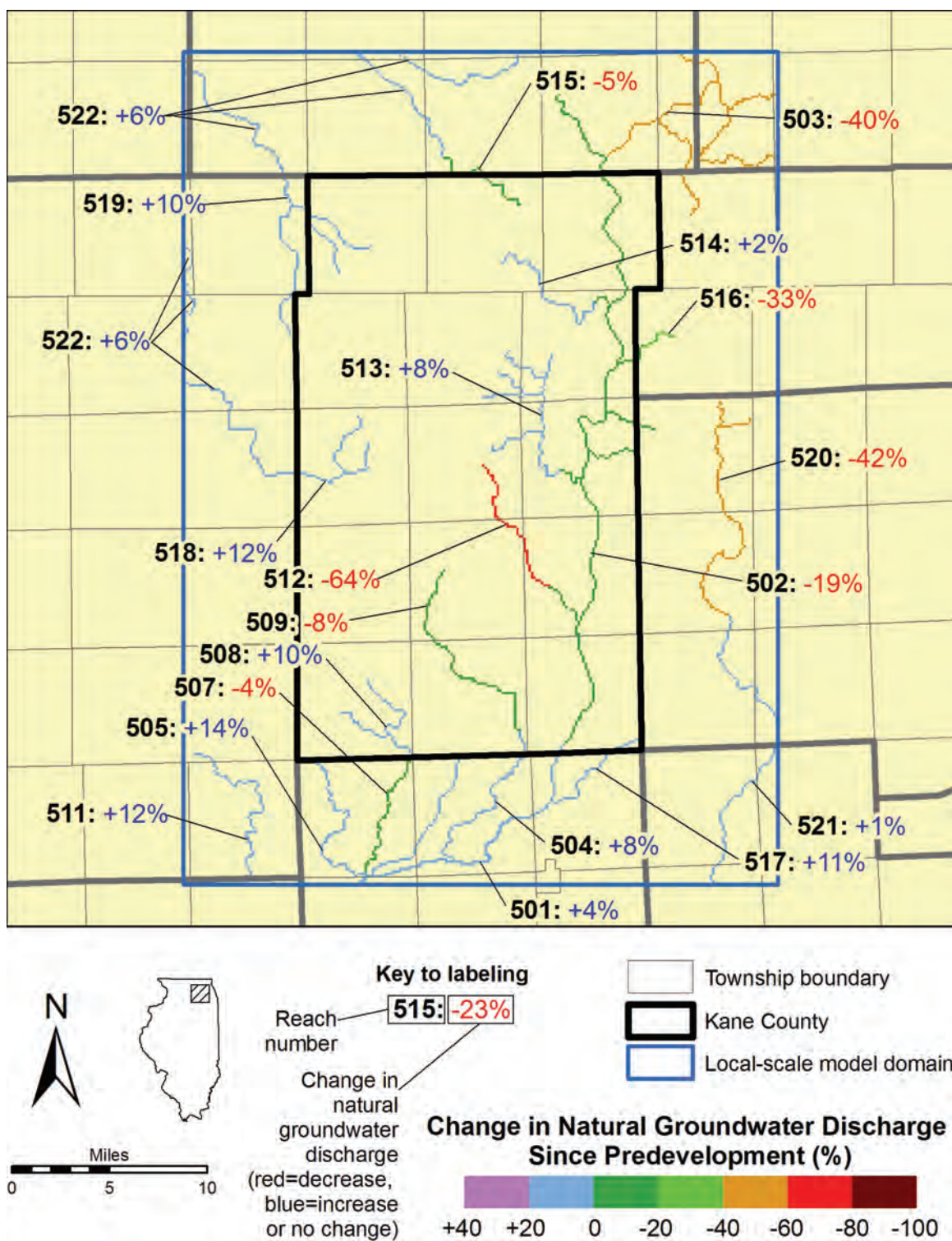


Figure 265. Estimated total change in natural groundwater discharge caused by pumping, by stream reach, at the end of 2024 under a scenario of low pumping and high recharge rates.

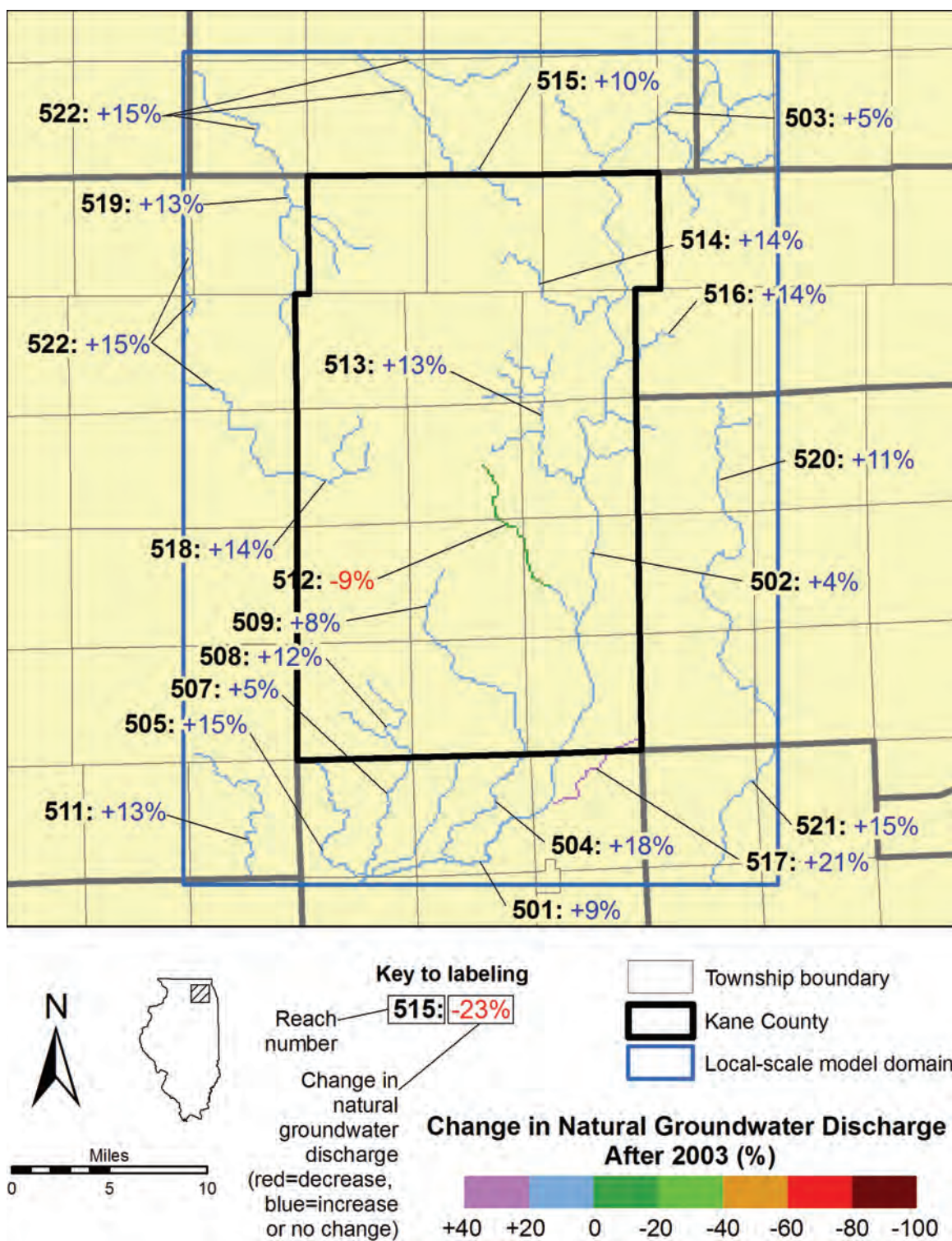


Figure 266. Estimated post-2003 change in natural groundwater discharge caused by pumping, by stream reach, at the end of 2049 under a scenario of low pumping and high recharge rates.

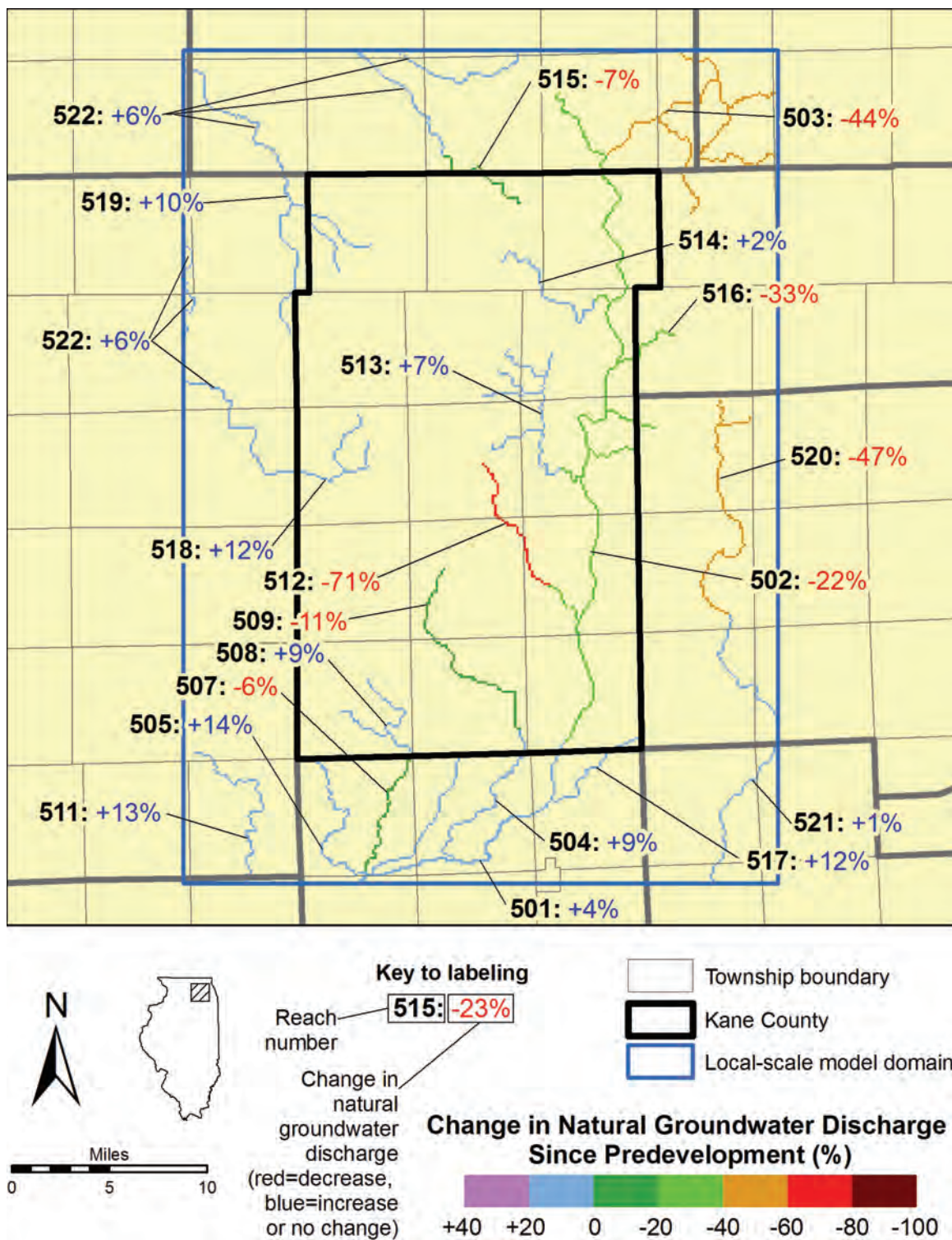


Figure 267. Estimated total change in natural groundwater discharge caused by pumping, by stream reach, at the end of 2049 under a scenario of low pumping and high recharge rates.

Table 31. Estimated Total Change in Natural Groundwater Discharge at Ends of 2024 and 2049, by Stream Reach

Reach Number	Principal Streams	Change in Natural Groundwater Discharge Due to Pumping							
		2024				2049			
		HL*	HC	LC	LH	HL	HC	LC	LH
501	Fox River downstream of Montgomery; Big Rock Cr downstream of Kane County boundary	-15%	-6%	-5%	+4%	-16%	-7%	-5%	+4%
502	Fox River from Algonquin to Montgomery; Norton Cr; Brewster Cr; Crystal Cr; lower portions of Mill Cr, Ferson Cr, Poplar Cr, and Tyler Cr	-42%	-32%	-29%	-19%	-51%	-41%	-32%	-22%
503	Fox River upstream of Algonquin; Spring Cr; Flint Cr	-65%	-55%	-50%	-40%	-78%	-68%	-54%	-44%
504	Blackberry Cr from Montgomery to Yorkville	-27%	-11%	-8%	+8%	-32%	-16%	-7%	+9%
505	Little Rock Cr downstream of Kane County boundary	-16%	-1%	-1%	+14%	-16%	-1%	-1%	+14%
507	Big Rock Cr downstream of Kane County boundary	-22%	-14%	-12%	-4%	-27%	-19%	-14%	-6%
508	Big Rock Cr upstream of Kane County boundary; Welch Cr	-19%	-4%	-4%	+10%	-21%	-6%	-6%	+9%
509	Blackberry Cr from Elburn to Montgomery	-37%	-24%	-21%	-8%	-45%	-33%	-25%	-11%
511	Somonauk Cr	-13%	-1%	0%	+12%	-14%	-1%	0%	+13%
512	Mill Cr upstream of Batavia	-100%	-87%	-82%	-64%	-100%	-100%	-89%	-71%
513	Ferson Cr upstream of St Charles; Otter Cr; Stony Cr; Fitchie Cr	-23%	-8%	-7%	+8%	-26%	-10%	-8%	+7%
514	Tyler Cr	-29%	-14%	-14%	+2%	-34%	-17%	-15%	+2%
515	S Br Kishwaukee River upstream of Huntley	-34%	-20%	-19%	-5%	-40%	-25%	-22%	-7%
516	Poplar Cr	-50%	-41%	-41%	-33%	-52%	-43%	-42%	-33%
517	Waubonsie Cr	-25%	-7%	-7%	+11%	-27%	-9%	-7%	+12%
518	Union Ditch No 3; Virgil Ditch No 3; Union-Virgil Ditch No 2	-17%	-2%	-2%	+12%	-17%	-3%	-3%	+12%
519	Upper Coon Cr	-15%	-3%	-2%	+10%	-16%	-3%	-2%	+10%
520	W Br DuPage River upstream of Warrenville	-71%	-58%	-55%	-42%	-81%	-68%	-60%	-47%
521	DuPage River; W Br DuPage River downstream of Warrenville	-25%	-13%	-11%	+1%	-28%	-16%	-12%	+1%
522	Aggregated tributaries of S Br Kishwaukee River outside Kane County	-26%	-10%	-9%	+6%	-27%	-11%	-10%	+6%
	TOTAL	-33%	-21%	-19%	-6%	-38%	-26%	-20%	-8%

*Key to scenarios: HL=high pumping, low recharge; HC=high pumping, model-calibrated-recharge; LC=low pumping, model-calibrated-recharge; LH=low pumping, high recharge

Table 32. Estimated Post-2003 Change in Natural Groundwater Discharge at Ends of 2024 and 2049, by Stream Reach

Reach Number	Principal Streams	Change in Natural Groundwater Discharge Due to Pumping							
		2024				2049			
		HL*	HC	LC	LH	HL	HC	LC	LH
501	Fox River downstream of Montgomery; Big Rock Cr downstream of Kane County boundary	-11%	-1%	0%	+9%	-12%	-3%	0%	+9%
502	Fox River from Algonquin to Montgomery; Norton Cr; Brewster Cr; Crystal Cr; lower portions of Mill Cr, Ferson Cr, Poplar Cr, and Tyler Cr	-22%	-9%	-4%	+9%	-34%	-21%	-9%	+4%
503	Fox River upstream of Algonquin; Spring Cr; Flint Cr	-34%	-17%	-7%	+11%	-58%	-41%	-15%	+5%
504	Blackberry Cr from Montgomery to Yorkville	-21%	-4%	0%	+17%	-26%	-9%	+1%	+18%
505	Little Rock Cr downstream of Kane County boundary	-15%	0%	0%	+15%	-16%	-1%	0%	+15%
507	Big Rock Cr downstream of Kane County boundary	-13%	-3%	-2%	+8%	-19%	-9%	-4%	+5%
508	Big Rock Cr upstream of Kane County boundary; Welch Cr	-16%	-2%	-1%	+13%	-18%	-3%	-3%	+12%
509	Blackberry Cr from Elburn to Montgomery	-24%	-8%	-4%	+12%	-34%	-18%	-9%	+8%
511	Somonauk Cr	-13%	0%	0%	+13%	-13%	0%	0%	+13%
512	Mill Cr upstream of Batavia	-100%	-59%	-44%	+14%	-100%	-100%	-65%	-9%
513	Ferson Cr upstream of St Charles; Otter Cr; Stony Cr; Fitchie Cr	-19%	-2%	-1%	+14%	-22%	-5%	-3%	+13%
514	Tyler Cr	-21%	-4%	-4%	+15%	-26%	-8%	-5%	+14%
515	S Br Kishwaukee River upstream of Huntley	-22%	-6%	-4%	+12%	-29%	-12%	-8%	+10%
516	Poplar Cr	-15%	-1%	0%	+14%	-18%	-3%	-1%	+14%
517	Waubonsie Cr	-19%	+1%	+1%	+21%	-21%	-1%	+1%	+21%
518	Union Ditch No 3; Virgil Ditch No 3; Union-Virgil Ditch No 2	-15%	-1%	-1%	+14%	-16%	-2%	-1%	+14%
519	Upper Coon Cr	-13%	0%	0%	+13%	-14%	-1%	0%	+13%
520	W Br DuPage River upstream of Warrenville	-39%	-12%	-7%	+21%	-60%	-33%	-18%	+11%
521	DuPage River; W Br DuPage River downstream of Warrenville	-14%	-1%	+1%	+15%	-18%	-4%	0%	+15%
522	Aggregated tributaries of S Br Kishwaukee River outside Kane County	-19%	-3%	-2%	+15%	-21%	-4%	-2%	+15%
	TOTAL	-19%	-5%	-2%	+12%	-25%	-11%	-5%	+11%

*Key to scenarios: HL=high pumping, low recharge; HC=high pumping, model-calibrated-recharge; LC=low pumping, model-calibrated-recharge; LH=low pumping, high recharge

rates and predevelopment discharge rates, even with increasing pumping (Figure 264 through Figure 267, Table 31, Table 32). In some stream reaches in the eastern part of the local model domain (Poplar Creek, reach 516; West Branch DuPage River below Warrenville, reach 521; and Waubonsie Creek, reach 517), where nearby post-2003 groundwater withdrawals are projected at rates lower than historical rates, model simulations suggest possible small post-2003 increases in groundwater discharge even under model-calibrated recharge rates (Figure 256, Figure 260, Figure 262). For simulations based on low and model-calibrated recharge rates, reduction in simulated natural groundwater discharge, like simulated shallow aquifer drawdown, is greatest in the eastern portion of the local model domain because this area contains a greater concentration of pumping than the remainder of the model domain.

For the most resource-intensive scenario (high pumping and low recharge, *HL* in Table 31 and Table 32), domain-wide change in natural groundwater discharge since predevelopment is estimated at -33 percent at the end of 2024 and -38 percent at the end of 2049. Domain-wide post-2003 change in natural groundwater discharge is estimated at -19 percent at the end of 2024 to -25 percent at the end of 2049. Model-suggested changes since predevelopment for individual stream reaches range from -13 percent (Somonauk Creek, reach 511) to -100 percent (Mill Creek, reach 512) at the end of 2024 (Figure 253). Model simulations suggest Mill Creek will convert from a gaining stream (one that receives groundwater discharge from the subsurface) to a losing stream (one that provides groundwater recharge to the subsurface). Changes in simulated discharge from 2003 rates range from -11 percent (Fox River below Montgomery) to -100 percent (Mill Creek) by the end of 2024 (Figure 252), and from -12 to -100 percent for the same two streams at the end of 2049 (Figure 254).

Simulations based on model-calibrated recharge conditions (*HC* and *LC* in Table 31 and Table 32) suggest a general reduction in natural groundwater discharge in most stream reaches in the Kane County area. Moreover, in local areas of heavy pumping from the shallow aquifers, streamflow capture by wells may add significantly to reduction in natural groundwater discharge under model-calibrated and low-recharge conditions. For the two simulated scenarios based on model-calibrated recharge rates, the model suggests that domain-wide changes in natural groundwater discharge after predevelopment will range from -19 to -21 percent at the end of 2024 and from -20 to -26 percent by 2050 (Table 31). Total change after 2003 for these two scenarios is estimated at -2 to -5 percent at the end of 2024 and -5 to -11 percent at the end of 2049 (Table 32).

For the scenarios based on model-calibrated recharge rates, model-suggested change from predevelopment natural groundwater discharge rates ranges, for high-pumping conditions, from -1 percent (Little Rock Creek in Kendall County, Somonauk Creek) to -87 percent (Mill Creek) at the end of 2024 (Figure 257) and, for low-pumping conditions, from 0 percent (Somonauk Creek) to -82 percent (Mill Creek) at the end of 2024 (Figure 261). Simulated change since predevelopment at the end of 2049 for scenarios based on model-calibrated recharge rates ranges from -1 percent (Little Rock Creek in Kendall County, Somonauk Creek) to -100 percent (Mill Creek) for high-pumping conditions (Figure 259). For low-pumping conditions, change since predevelopment at the end of 2049 range from 0 to -89 percent (Somonauk Creek and Mill Creek, respectively) (Figure 263). Model-suggested changes from 2003 rates of natural groundwater discharge range, for high-pumping conditions, from +1 percent

(Waubonsie Creek) to -59 percent (Mill Creek) at the end of 2024 (Figure 256) and from 0 percent (Somonauk Creek) to -100 percent (Mill Creek) at the end of 2049 (Figure 258). For the low pumping, model-calibrated recharge scenario, model-suggested changes from 2003 rates of natural groundwater discharge range from +1 percent (Waubonsie Creek, and DuPage River below Warrenville, reach 521) to -44 percent (Mill Creek) by 2024 (Figure 260). For this scenario, model-suggested changes from 2003 rates range from +1 percent (Waubonie Creek; Blackberry Creek below Montgomery, reach 504) to -65 percent (Mill Creek) by 2049 (Figure 262).

As mentioned previously, simulation of the low-pumping, high-recharge scenario (scenario *LH* in Table 31 and Table 32) suggests that an increase in recharge could lead to an increase in natural groundwater discharge in many streams in the Kane County area. Indeed, the modeling suggests that an increase in recharge, begun in 2004, could cause natural groundwater discharge to some streams to increase to rates exceeding predevelopment rates. Domain-wide rates of natural groundwater discharge are still projected to decline under this scenario, however, to rates that are, at the end of 2024, 6 percent less than predevelopment rates and, at the end of 2049, 8 percent less than predevelopment rates. The model-suggested rate of domain-wide natural groundwater discharge is, at the end of 2024, 12 percent *more* than the 2003 rate, however, and is, at the end of 2049, 11 percent more than the 2003 rate. Total change in simulated natural discharge ranges from +14 percent (Little Rock Creek in Kendall County, reach 505) to 64 percent (Mill Creek) at the end of 2024 (Figure 265) and from +14 to -71 percent for the same two streams at the end of 2049 (Figure 267).

Since the Fox River watershed is the principal watershed within the local model domain, simulated natural groundwater discharge in the portion of it within the local domain (Figure 268) resembles that in the local model domain as a whole (Figure 251). For the range of scenarios examined for this project, model-suggested changes from rates of predevelopment natural groundwater discharge within the Fox watershed range from -10 to -35 percent at the end of 2024 and from -12 to -41 percent at the end of 2049. Model-suggested changes from predevelopment discharge rates for scenarios based on model-calibrated recharge rates range from -21 to -23 percent at the end of 2024 and from -23 to -30 percent at the end of 2049.

The model suggests extreme reductions in natural groundwater discharge to Mill Creek upstream of Batavia, an area and stream discussed previously (Section 3.2.1.2, page 252; Section 3.2.2, page 256) for the impacts on head and streamflow of historic pumping from municipal wells operated by the Cities of Batavia and Geneva. The reduction in simulated natural discharge to Mill Creek increases with increased pumping to such an extent that under high-pumping, low-recharge conditions, the model suggests that Mill Creek will convert from a gaining to a losing stream between 2014 and 2020 (Figure 269). Under a scenario of high pumping and model-calibrated-recharge rates, the model suggests that this will occur around 2050. Just as with any loss of groundwater discharge, conversion of Mill Creek to a losing stream has implications for streamflow, particularly low flows, and water quality. In addition, yields of the Batavia and Geneva municipal wells, and any other wells in the area, could be reduced at times when sufficient runoff is not present in the Mill Creek channel to sustain heads in source aquifers.

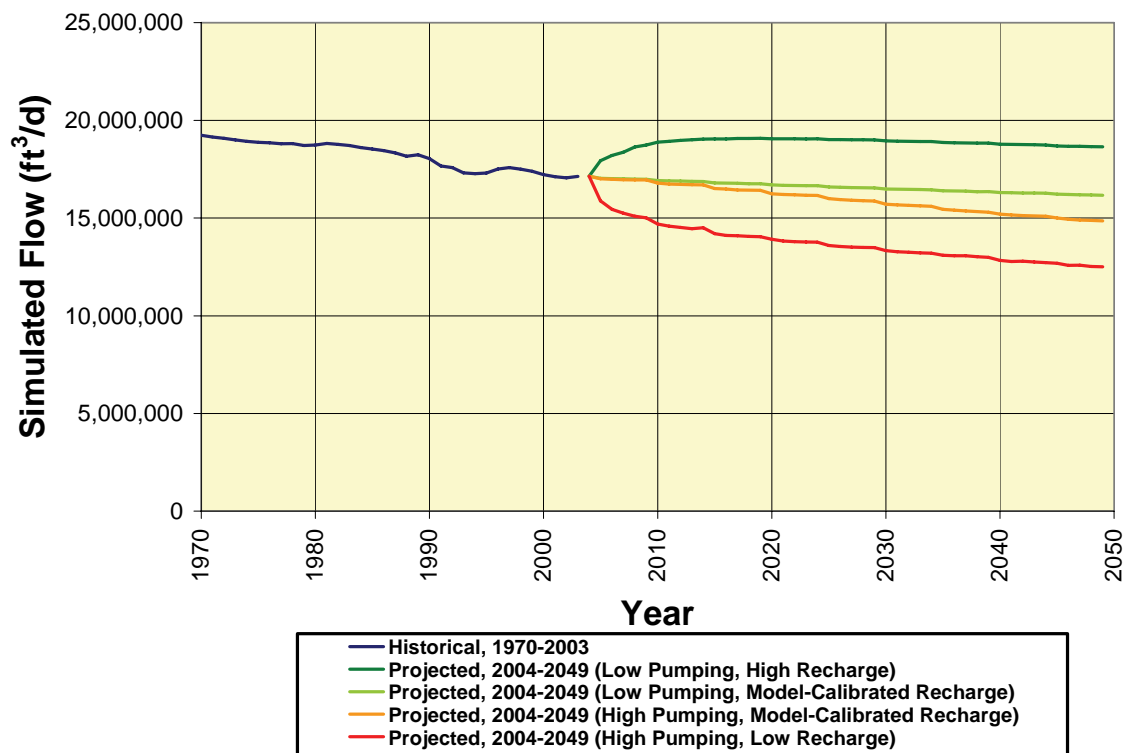


Figure 268. Total natural groundwater discharge to streams in the portion of the Fox River watershed within the local-scale model domain.

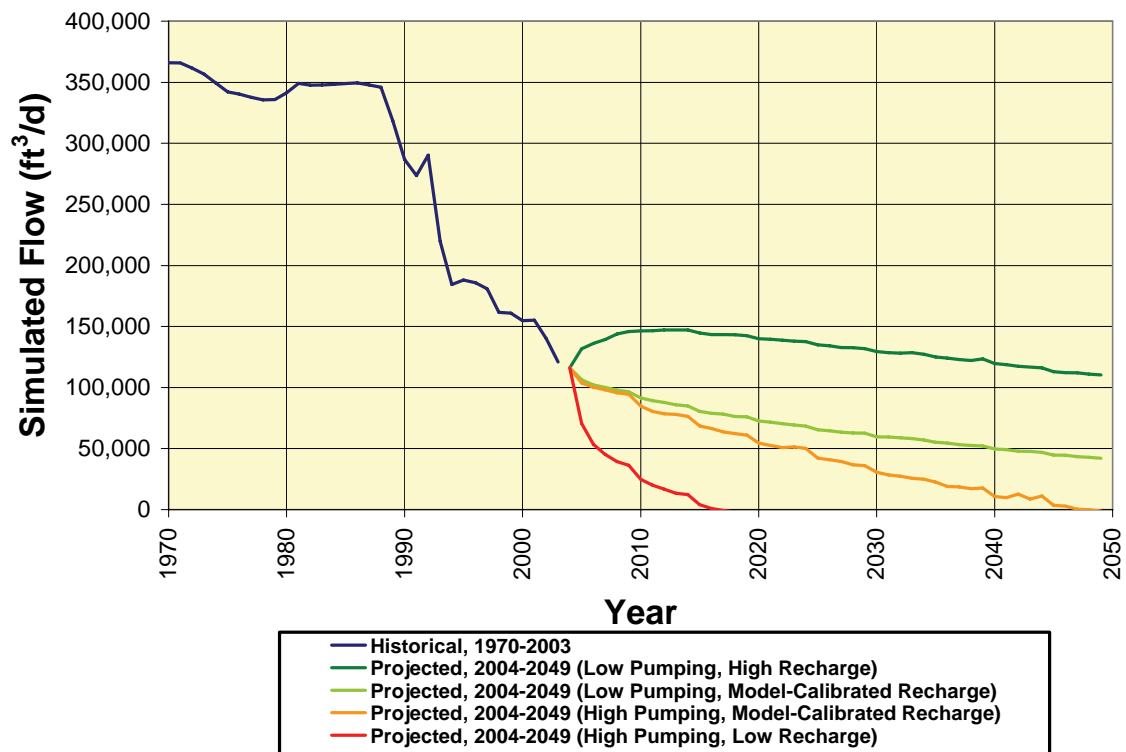


Figure 269. Simulated natural groundwater discharge to Mill Creek upstream of Batavia (reach 512).

Other large reductions in natural groundwater discharge are suggested for the Fox River within the local model domain upstream of Algonquin (reach 503) and the West Branch DuPage River upstream of Warrenville (reach 520). These stream reaches are both outside of Kane County, but a reduction in one of them—the Fox upstream of Algonquin—would affect Fox River conditions in downstream areas that include Kane County. Model simulations suggest that natural groundwater discharge to the Fox River upstream of Algonquin could decline as much as 65 percent below the predevelopment rate at the end of 2024 and 78 percent below the predevelopment rate at the end of 2049 (Figure 270). Model simulations suggest that natural groundwater discharge to the West Branch DuPage River upstream of Warrenville could decline as much as 71 percent below the predevelopment rate at the end of 2024 and 81 percent below the predevelopment rate at the end of 2049 (Figure 271). It is worth noting that both areas discussed in this paragraph lie largely outside Kane County, and therefore outside the area of greatest model accuracy. Nevertheless, the fact that the model simulations suggest significant declines in natural groundwater discharge in these areas cannot be dismissed, and additional investigations are warranted.

3.3.2. Steady-State Simulation of 2002 Pumping Distribution

Water managers often wish to know the impacts of extended pumping from the current well network and at current rates, so for this study the simulated impacts of extended pumping of the 2002 well network at 2002 rates are presented. Although such a steady-state pumping scenario is unrealistic, its examination is helpful because the results illustrate groundwater conditions after transient contributions from groundwater storage are exhausted, when withdrawals from wells are compensated for entirely by increases from predevelopment recharge rates and decreases from predevelopment discharge rates (see Section 1.7.5). Under such conditions, maximum reductions of both of heads and streamflow have occurred. The results presented here thus offer water managers a glimpse of the ultimate consequences of a strict business-as-usual scenario in which pumping conditions are maintained precisely as they were in 2002, and they are an indication of whether the 2002 pumping configuration is truly sustainable. In contrast, the transient results presented in Section 3.3 are based on more realistic forecasts for future pumping, but they extend only to the mid-21st century. It is noteworthy that depletion of storage in the deep aquifers could take a long time, perhaps centuries, and existing simulations do not indicate how long the process could take.

The regional model simulation suggests severe head reductions in the Ancell Unit that result in partial to complete desaturation of the Ancell Unit in the Joliet and Aurora areas in response to large withdrawals at these locations (Figure 272 and Figure 273). Simulated Ancell Unit head declines to within 100 ft of the top of the Ancell Unit in a broad area of northeastern Illinois. These head reductions could result in elevated arsenic, radium, and barium in groundwater withdrawn from deep wells (page 207) and reduced deep well yields. Based on the outcomes discussed in this paragraph, then, it is concluded that the 2002 pumping configuration is not sustainable, but it is stressed that it is not known how long it would take to achieve the conditions shown in Figure 272 and Figure 273.

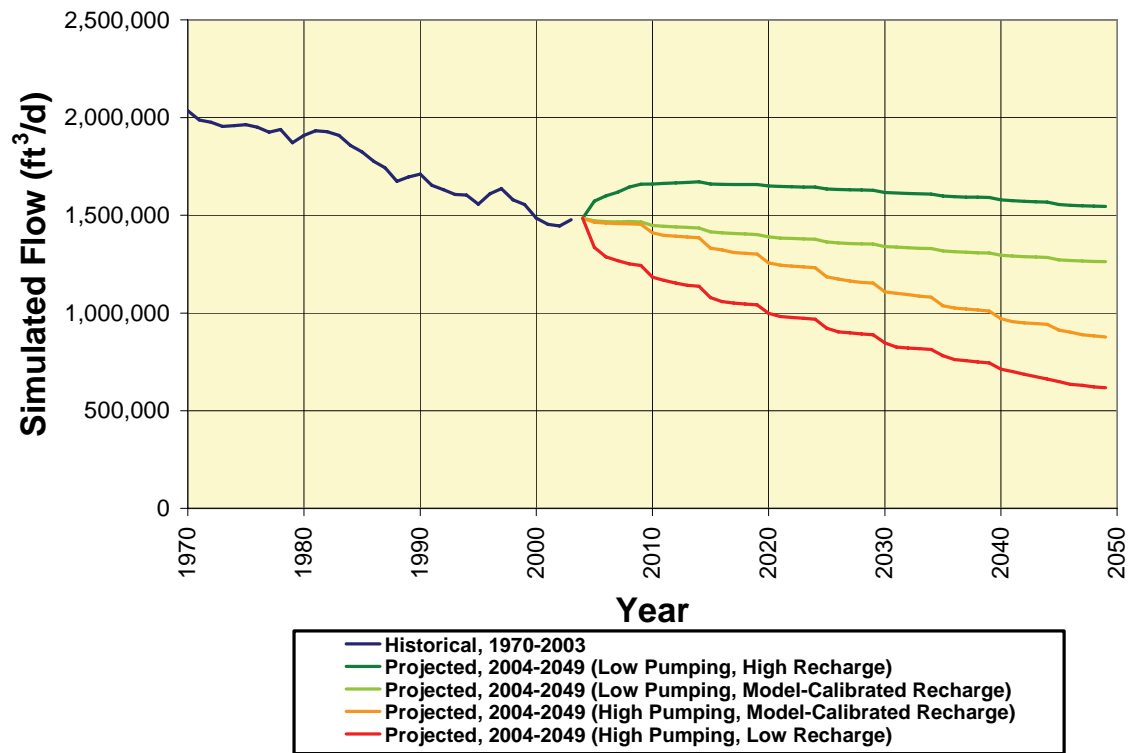


Figure 270. Simulated natural groundwater discharge to the Fox River upstream of Algonquin (reach 503).

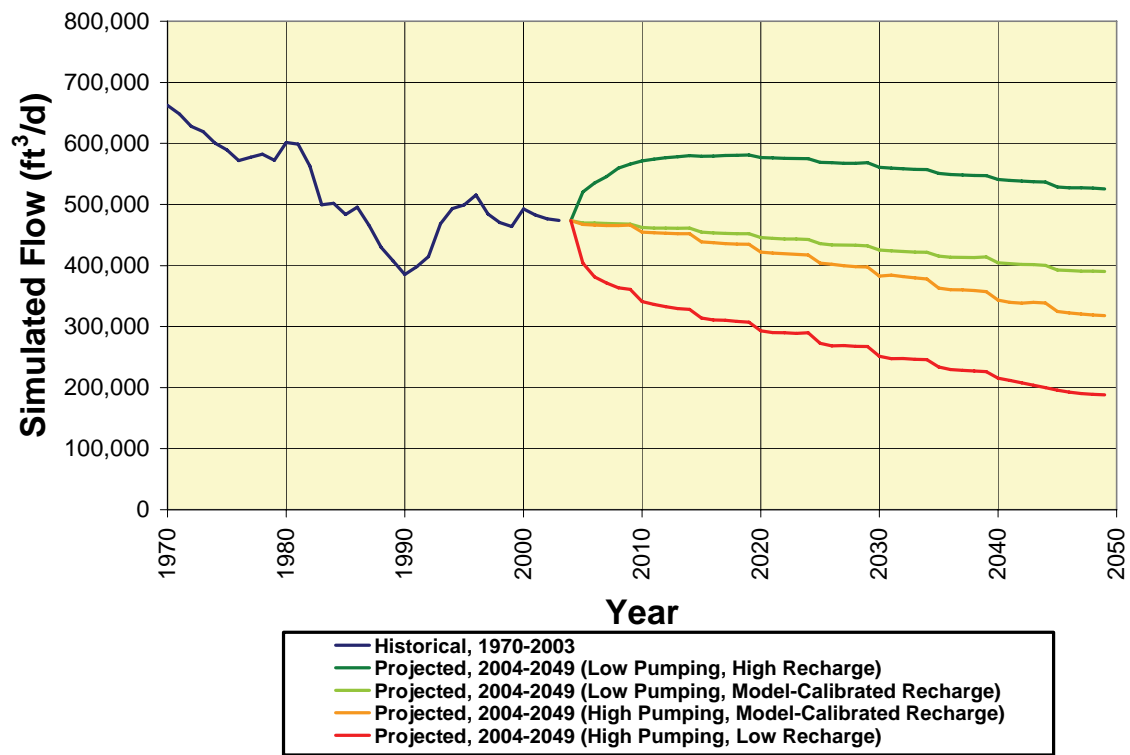


Figure 271. Simulated natural groundwater discharge to the West Branch DuPage River upstream of Warrenville (reach 520).

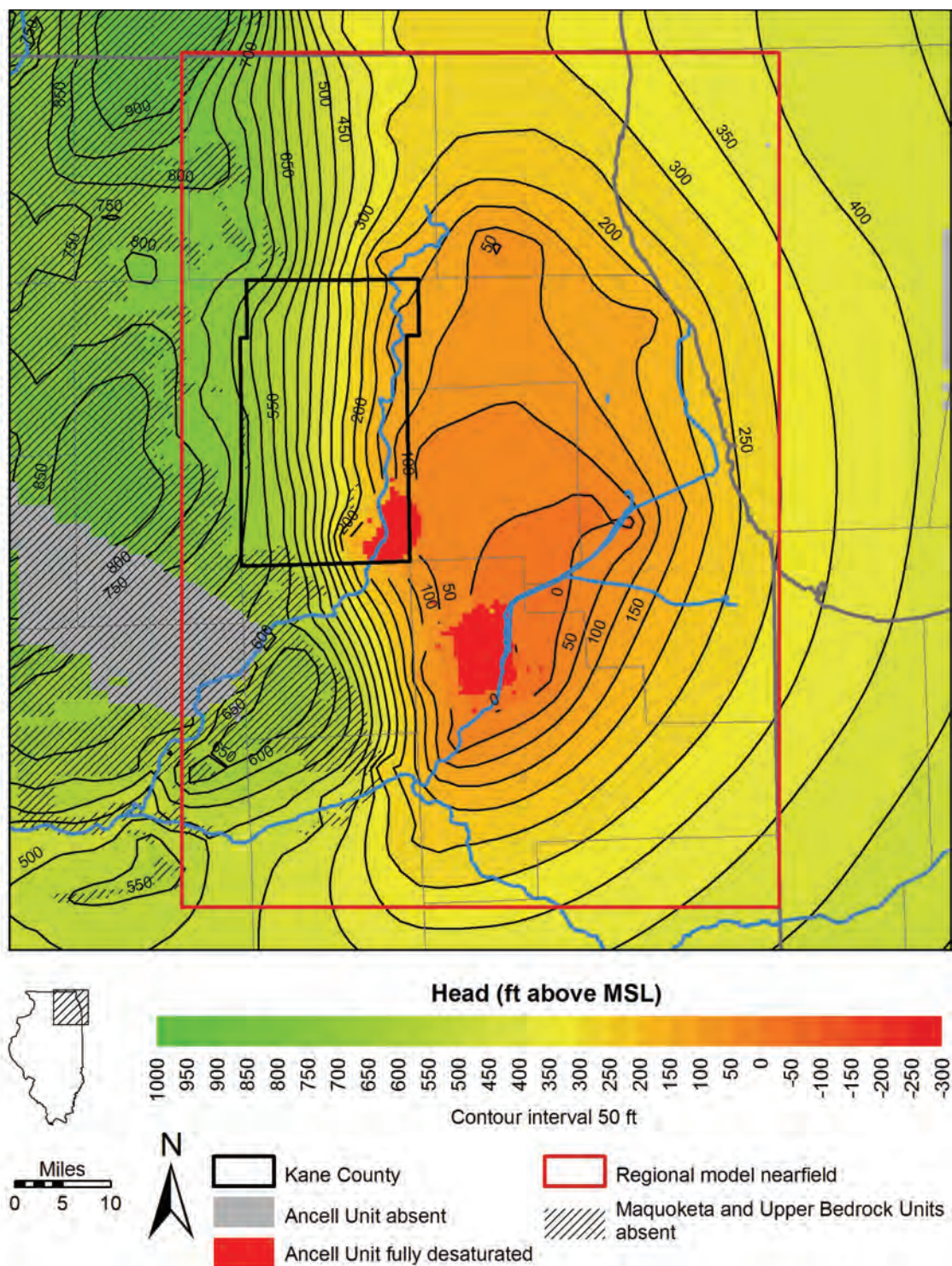


Figure 272. Simulated head in Ancestral Unit after extended pumping at 2002 rates with model-calibrated recharge rates.

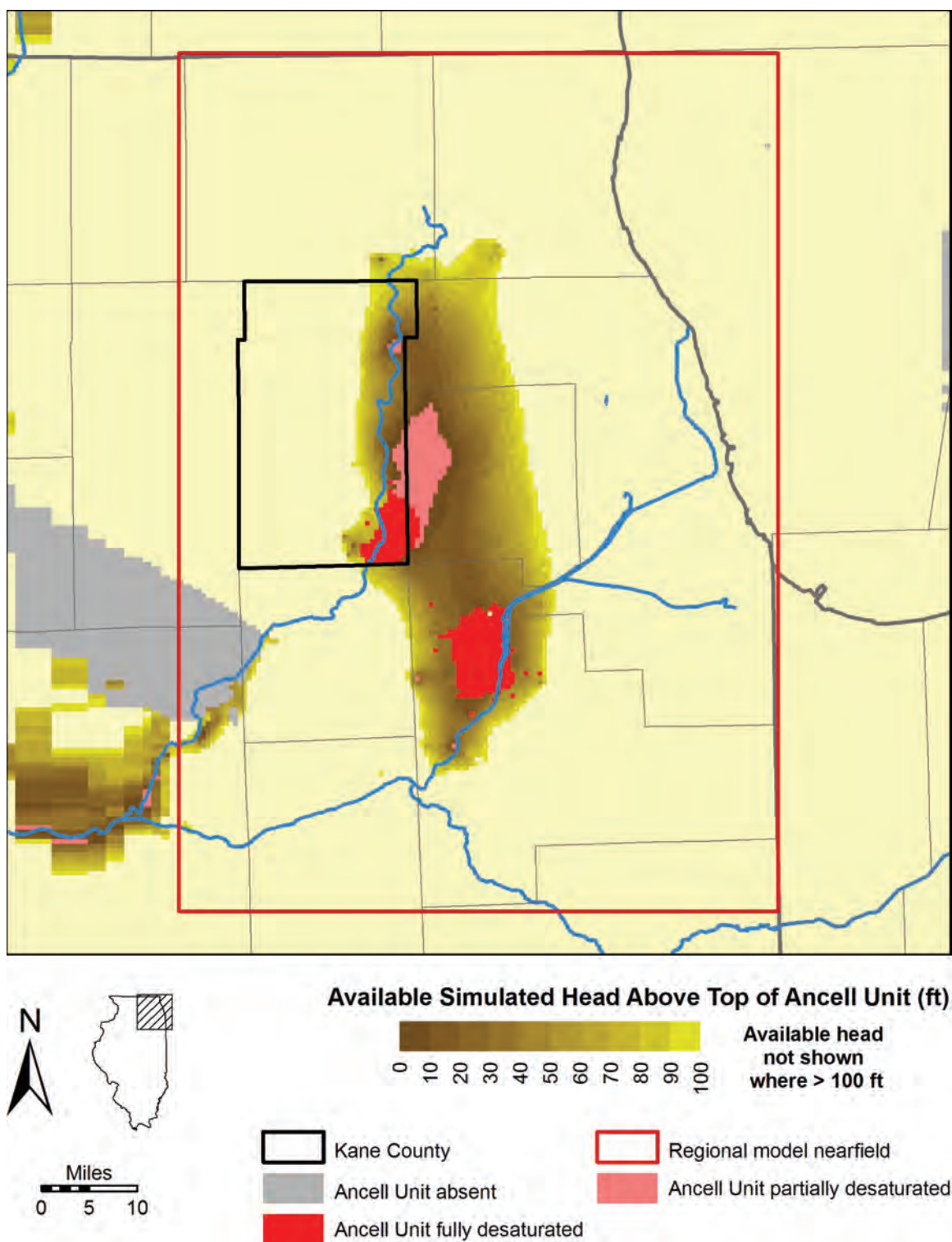


Figure 273. Available simulated head above the top of the Ancell Unit after a period of extended pumping at 2002 rates with model-calibrated-recharge rates.

3.4. Capture Zones of High-Capacity Shallow Wells in Kane County

The term *capture zone* is used with both three-dimensional and two-dimensional meanings. In its three-dimensional sense, the capture zone of a pumping well is that portion of the subsurface in which groundwater flow is toward the open interval of the well. Thus, it is a depiction of the portion of the subsurface contributing groundwater to the well. In its more commonly used, two-dimensional sense, the capture zone of a pumping well is the map view, or the two-dimensional projection, of the three-dimensional portion of the subsurface in which groundwater flow is toward the well. In this report, the term capture zone is used in the two-dimensional sense. Capture zones are important tools for groundwater protection because contaminants within a capture zone and within the source aquifer for the well (and sometimes within bordering hydrostratigraphic units, depending on local conditions) will move toward the pumping well and can eventually appear in the groundwater pumped from the well. The capture zone generally extends upgradient from the pumping well to the edge of the source aquifer or to a groundwater divide. Thus, capture zones are generally asymmetrical.

Capture zones are usually defined in terms of time of travel. A time-related capture zone is the map projection of the portion of the subsurface that contributes the groundwater withdrawn from a well during a defined time period. For example, a five-year time-related capture zone—commonly referred to as a *five-year capture zone*—is the map projection of the portion of the subsurface that contributes the groundwater to a well within five years. In other words, groundwater within the five-year capture zone will be withdrawn from the well within five years. It is noteworthy that the capture zone does not communicate information on the portion of the subsurface that contributes this groundwater, but rather, is a map projection of contributing portion of the subsurface. This three-dimensional entity includes the aquifer(s) to which the well is open (the source aquifer) and may also include bordering aquitards and aquifers that are hydraulically connected to the source aquifer at a distance from the pumped well.

Five-year and 20-year capture zone estimations for shallow Kane County public water-supply wells that pumped more than 100,000 gpd in 2003 (Table 3) are shown in Appendix H. These capture zones were delineated by employing the steady-state local-scale shallow model, with 2003 pumping rates, and backward tracking particles from well open intervals for periods of five years and 20 years. The endpoints of the particle pathlines define the capture zone.

4. Summary

- The Illinois State Water Survey has developed and calibrated two numerical groundwater flow models to accurately represent groundwater circulation in the aquifers supplying water to Kane County. A *regional-scale model* simulates groundwater flow in all materials overlying the Precambrian basement in much of the upper Midwest, but results from this model are most accurate in a highly resolved nearfield area that includes Cook, DuPage, Kane, Kendall, Lake, McHenry, and Will Counties and parts of several other counties in northeastern Illinois. A second, higher-resolution *local-scale model* simulates groundwater flow in the shallow, unconsolidated materials and underlying upper bedrock in Kane County and its immediate vicinity. The models are three-dimensional and are linked using telescoping mesh refinement so that distant influences on groundwater flow are represented in the local-scale model, even though these influences might operate well outside the local-scale model domain. Both models are three-dimensional and transient, containing an accurate history of groundwater withdrawals in the region. Both simulate exchange of water between surface-water features and groundwater. Both models accurately reproduce measured and estimated water levels and base flow in streams under predevelopment and pumping conditions. Hydraulic conductivities in the models accurately reflect values and anisotropy ratios documented in the literature. The models provide a tool for simulating groundwater flow in Kane County and northeastern Illinois under a wide variety of user-specified conditions, and they provide a framework for detailed investigations of specific areas and for development of higher-resolution inset models.
- Under predevelopment conditions, the groundwater circulation pattern in northeastern Illinois, including Kane County, was the product of topography, geology, and the locations and elevations of surface-water bodies. Groundwater in the shallow aquifers circulated within local flow cells and discharged to surface waters throughout the region. Local circulation also predominated within the deep aquifers in the western edge of the region, where impermeable rocks of the Upper Bedrock and Maquoketa Units are absent. In most of northeastern Illinois, however, the presence of the impermeable Upper Bedrock and Maquoketa Units greatly reduced exchange of water between the deep aquifers on the one hand, and the shallow aquifers and surface waters on the other. Circulation within the deep aquifers in the area occurred on a regional scale and at comparatively sluggish rates under the influence of gentle hydraulic gradients. A flow divide crossed the area of confinement by the Upper Bedrock and Maquoketa Units that separated groundwater that would eventually discharge into Lake Michigan from that flowing toward western discharge locations along streams in the area lacking Maquoketa and Upper Bedrock cover, particularly the upper Illinois and lower Fox Rivers.
- Pumping profoundly changed the predevelopment pattern of groundwater circulation within the deep aquifers in the area of cover by the Upper Bedrock and Maquoketa Units, but changes have been much more subtle in the area lacking Upper Bedrock-Maquoketa cover because heads in that area are maintained by

high rates of leakage to the deep aquifers from surface waters and the shallow aquifers. In the area of Upper Bedrock-Maquoketa cover, drawdown in the Ancell Unit, which is representative of the deep aquifers, exceeded 650 ft relative to predevelopment levels.

- Within the overall Chicago-area cone of depression, locations of greatest drawdown in the deep aquifers have been responsive to shifts in locations of pumping. Greatest drawdown in the early 1980s, prior to the importation of Lake Michigan water (with consequent retirement of numerous wells tapping the deep bedrock aquifers), was in Cook and eastern DuPage Counties. Although significant drawdown remained in that area in 2002, some recovery had occurred in response to limited vertical leakage and lateral flow. Drawdown continued in Aurora and Joliet, where deep aquifer withdrawals have persisted and even increased since the 1980s.
- Deep aquifer heads in Kane County are generally lowest in the southeastern part of the county, which is both near to high-capacity deep wells inside and outside Kane County and more distant from the area of high leakage to the deep aquifers mainly west of Kane County. Significant recovery of heads has occurred at Aurora and Elgin in response to partial shifts by these communities to use of the Fox River for water supply.
- By 2002, regional modeling suggests that partial desaturation of the upper Galena-Platteville Unit had occurred, principally in three areas: eastern DuPage and northwestern Cook Counties, the Aurora area, and the Joliet area. The model suggests that large-scale desaturation of the base of the Galena-Platteville Unit and of the Ancell Unit had not occurred by 2002, but simulated Ancell Unit heads had declined to within 100 ft of the top of the Ancell Unit in the Aurora area. Such proximity of simulated Ancell Unit heads and the top of the Ancell Unit could result in water-quality reduction—specifically an increase in dissolved arsenic concentration—in water withdrawn from deep wells in the areas of reduced available head.
- Deep aquifer withdrawals resulted in the superposition of an area of diversion to wells on a predevelopment flow regime in which a groundwater flow divide separated northeastern Illinois into an area of discharge to Lake Michigan and an area of discharge to streams in the western part of the area, principally the lower Fox and upper Illinois Rivers. The area of diversion to wells has expanded to encompass the entire area of predevelopment discharge to Lake Michigan in the vicinity of northeastern Illinois. The edge of Upper Bedrock-Maquoketa cover has limited westward expansion of the area of diversion to wells, because comparatively high rates of leakage in the area have largely maintained predevelopment heads, but some westward expansion of the diversion area has occurred, particularly west of the large Aurora and Joliet pumping centers.
- In the shallow aquifers, pumping has caused less drawdown than in the regional aquifers, but in localized areas the drawdown is a greater proportion of the available drawdown than in the deep regional aquifers. Smaller drawdowns occur because the aquifers are more permeable and because heads in the shallow aquifers are regulated by comparatively closely spaced hydraulic connections with surface waters. Thus, instead of creating large drawdown, withdrawals from

- the shallow aquifers result in reduced streamflow and declining water levels in lakes and wetlands. Capture of surface waters occurs both by establishment of hydraulic gradients that induce flow directly out of surface-water bodies and by diversion into wells of flow that would otherwise discharge to surface waters.
- Several factors affect the amount of drawdown surrounding shallow wells in the Kane County area, but the most important are pumping rate (positively correlated with drawdown), source aquifer transmissivity (negatively correlated with drawdown), and distance to hydraulic connections with permanent surface waters (positively correlated with drawdown). In general, greater drawdown has occurred in the aquifers underlying the Tiskilwa Unit—a widespread, low-permeability unit that isolates these aquifers from surface waters—in the eastern part of Kane County where pumping rates are greater. Greatest drawdown has occurred in the Shallow Bedrock Aquifer, an aquifer of comparatively low transmissivity.
 - Significant areas of drawdown in the shallow aquifers of Kane County (here defined as areas where drawdown in 2003 exceeds 20 ft) occur (1) in northeastern Kane County and southeastern McHenry County; (2) surrounding public water system wells of the Cities of Warrenville and West Chicago in west-central DuPage County; (3) surrounding South Elgin public water system wells on both sides of the Fox River; and (4) surrounding Dial Corporation water-supply wells in the Montgomery area of southeastern Kane County. The areas of significant drawdown in northeastern Kane and southeastern McHenry Counties and surrounding the Warrenville and West Chicago wells are significantly larger than those surrounding the South Elgin and Dial Corporation wells.
 - Mapping of transmissivities of the Shallow Bedrock Aquifer and overlying Quaternary materials, based on the local-scale model, suggests addressing current and future simulated drawdown by simply relocating water-supply wells to undeveloped areas may not be feasible. Most areas of high transmissivity are already developed by wells.
 - Drawdown in the shallow aquifers of the Kane County area has generally increased since 1964, reflecting an increase in shallow pumping from 4 to 19 Mgd within the county during this time period. Also, areas of drawdown exceeding 5 ft expanded westward into Kane County from DuPage and Cook Counties and southward from southeastern McHenry County.
 - Model simulations suggest that, at the end of 2003, pumping had reduced natural groundwater discharge in the local-scale model domain by about 17 percent. Because natural groundwater discharge sustains streamflow during dry periods, the reduction would be observable as a reduction in stream base flow. The greatest reduction in base flow occurs in Mill Creek, where model simulations suggest that at the end of 2003, capture of streamflow by public water system wells supplying Batavia and Geneva has reduced base flow by about 68 percent. Other stream reaches which model simulations suggest have been significantly affected by reductions in natural groundwater discharge include the West Branch of the DuPage River upstream of Warrenville and the Fox River upstream of Algonquin. Streamflow modeling has suggested that effluent from wastewater treatment plants could compensate for reductions in natural groundwater discharge downstream of treatment plant outfalls (Knapp et al., 2007).

- Simulation of future pumping shows that heads in the deep aquifers will decline in much of northeastern Illinois through 2049 under scenarios of both low and high pumping and that changing recharge rates would have only a negligible affect on deep heads within that time frame. Head declines are greater under the scenario of high pumping. In general, the combined effects of continued pumping at high rates in the Joliet and Aurora areas, and continued recovery of heads in the eastern part of northeastern Illinois, results in a westward and southwestward shift of the deepest parts of the Chicago area cone of depression to apices in the Joliet and Aurora areas. Under both low- and high-pumping scenarios, Ancell and Ironton-Galesville head declines between the ends of 2002 and 2049 will exceed 150 ft in the projected pumping centers of Joliet and Aurora. Continued recovery is forecasted in eastern DuPage and much of Cook Counties in response to reductions in pumping since the 1980s in those areas. The recovery is limited, however, by the limited capacity of the deep units to transmit water eastward from the high-leakage area to the west, where the impermeable Upper Bedrock and Maquoketa Units are absent and by capture of most of this eastward flow by large-capacity wells extending from Crystal Lake southward to Joliet. Estimated Ancell Unit head declines will exceed 50 ft in much of Kane County and will exceed 150 ft in the southeastern part of the county. In many areas, recovery of Ironton-Galesville heads, begun in the 1980s, is forecasted to end before 2025, and heads will then begin to decline again.
- Simulation of future pumping suggests that Ancell Unit head will decline to within 100 ft of the top of the Ancell Unit, and that the upper Ancell Unit will become desaturated in the Aurora and Joliet areas before 2050. Such desaturation could result in reduced well yields and elevated arsenic, radium, and barium concentrations in groundwater withdrawn from deep wells. Model simulations suggest that the areas of desaturation will expand through the end of the simulation period (2049). These areas are greater in size under the high pumping conditions.
- Simulation of future withdrawals suggests that drawdown in the shallow aquifers will generally be less than in the deep aquifers owing to the effect of closely spaced hydraulic connections between the shallow aquifers and surface waters. These closely spaced hydraulic connections facilitate the process of streamflow capture by shallow wells, permitting the wells to obtain their yields with less reliance on removal of water from aquifer storage—the process causing drawdown—than deep wells. Local-scale model simulations suggest that the major aquifers remain fully saturated when future withdrawals are limited to 2003 rates at Algonquin wells 8 and 9, Crystal Lake well 15, and West Chicago wells 6, 7, and 8. Areas of future drawdown greater than 20 ft are mostly more extensive versions of areas of significant 2003 drawdown. A new area of significant drawdown is predicted to develop west of Batavia and Geneva surrounding public-supply wells operated by the two communities. Model simulations also suggest that pumping in this area causes significant reduction of natural groundwater discharge to Mill Creek.
- Simulation of future withdrawals suggests that withdrawals from shallow wells will, in the local model domain, cause reduction of natural groundwater discharge

to streams at rates that are, at the end of 2049, 8 to 38 percent lower than rates of discharge under simulated predevelopment conditions. Reduction of natural groundwater discharge to streams is expected to be greatest in the eastern part of the local model domain, where shallow withdrawals are projected to be greatest. Under the low pumping, high recharge scenario, rates of groundwater discharge to many streams would increase to levels greater than rates under nonpumping conditions and rates of recharge effective historically. Under high pumping conditions, groundwater discharge to Mill Creek upstream of Batavia would cease before 2050 due to pumping from public-supply wells operated by Batavia and Geneva.

- Simulation of the long-term impacts of extended pumping of the 2002 network of pumping wells, carried to a steady state at the 2002 rates, shows that such development would result in complete desaturation of the Ancell Unit in the Aurora and Joliet areas, partial desaturation of the Ancell Unit in adjacent areas, and reductions of Ancell Unit head to within 100 ft of the top of the Ancell over a large part of northeastern Illinois. This desaturation will greatly reduce well yields and could result in elevated arsenic, radium, and barium concentrations in groundwater withdrawn from deep wells. It is not known how long it would take to reach these steady-state conditions.

5. Future Work

Possibilities for future work fall into several categories: (1) revision of the existing regional model; (2) studies that employ the existing models, possibly with slight revision; (3) database expansion and improvement; (4) development of alternative modeling codes; (5) uncertainty analysis using alternative models; and (6) monitoring. Considerable overlap between these categories exists, and efforts in one category may feed back to others.

5.1. Revision of Existing Regional Model

Although not critical for Kane County, the existing regional model could be revised, using readily available data, to more accurately simulate groundwater flow in other parts of the northeastern Illinois region. Note that revision of the model implies recalibration. Revising the model so that surface water and drained conditions are represented as boundary conditions in the lower Rock River watershed, west of the area where surface water and drained conditions are represented in the current model, would provide more accurate simulations in DeKalb County, a rapidly-growing county at the western margin of the Chicago metropolitan region. The lower Rock River watershed is important with regard to groundwater availability at pumping centers in the more urbanized areas to the east because the lack of Maquoketa and Upper Bedrock Unit cover in much of the watershed permits comparatively high rates of leakage to the deep aquifers. In addition, representation of the lower Rock River watershed as constant head cells in the present regional-scale model forces simulated streamflow to higher-than-observed rates at some locations in northwestern Kane County.

It would be possible, using groundwater flow modeling of southeastern Wisconsin (Feinstein et al., 2005a; Feinstein et al., 2005b), to refine the hydraulic conductivity

zonation of layers 1, 2, and 3 (the Quaternary Unit) to reflect thick sand and gravel deposits in southeastern Wisconsin. This would probably improve simulation accuracy in the northern part of the regional model nearfield, along the Illinois-Wisconsin boundary, particularly in the shallow units.

Revision of the existing regional model to simulate interformational transfer of groundwater via open boreholes is also suggested. Numerous such boreholes exist in northeastern Illinois, and transfers of groundwater, most notably between the Ancell and Ironton-Galesville Units, could affect heads in the region. The existing model does not simulate such transfers.

The models developed in this study have assumed that groundwater flow is dominated by flow within the saturated portions of the aquifers, and have ignored flow through unsaturated zones. This assumption is justified by the relatively low flow rates through unsaturated material, and is a common assumption for studies of aquifers in humid regions. However, it is possible that modeling downward flow through the dewatered regions indicated by regional model simulations may improve the representation of wells simulated as going dry. This suggests that future enhancement of the models might include the use of MODFLOW modules that include flow through the unsaturated zone.

5.2. Modeling Studies

5.2.1. Applications

5.2.1.1. Existing Models as Rational Basis for Management

The models developed for this project are designed for use in future water studies of Kane County and northeastern Illinois and will provide a rational basis for formation of policy and management strategies pertaining to water-resources development in the county and region. Useful modeling studies might include simulation of alternative scenarios of future conditions in order to test development strategies for impacts. Such simulations have been generated for this study (see Appendix G and Section 3.3.1), but they are limited to four scenarios that are themselves based on numerous simplifying assumptions. More detailed scenarios, based on input from individual communities, and possibly employing wells at new locations would likely generate more accurate forecasts of future groundwater conditions. Simulations could be conducted for extended periods to evaluate impacts beyond the mid-21st century (the time horizon employed for transient simulations conducted for this project) and could employ alternative recharge scenarios to simulate climate change impacts.

5.2.1.2. Existing Models as Source of Boundary Conditions for Inset Models

Both the regional-scale and local-scale models can be used to provide boundary fluxes for future high-resolution inset models. Such model integration, accomplished using the approach of telescopic mesh refinement as discussed in Appendix A, permits distant influences on groundwater flow to be represented in a rational and non-arbitrary manner in the inset models.

5.2.2. *Research*

5.2.2.1. Groundwater Exchange with Lake Michigan

Lake Michigan is a water resource of paramount value to the region. The lake interacts with groundwater, receiving groundwater discharge directly or indirectly via tributary streams. Also, depending on local conditions, Lake Michigan is a source of recharge. The interaction of the Great Lakes with groundwater is acknowledged by U.S. and Canadian Great Lake states and provinces in its 2001 Great Lakes Charter Annex (International Joint Commission, 2001), which includes protection of groundwater quantity and quality as vital for preservation of the lakes. The regional-scale model can be used to estimate changes in groundwater exchange with Lake Michigan resulting from historical and future groundwater pumping in the region. Groundwater flow modeling indicates that total direct and indirect groundwater discharge to Lake Michigan in the seven counties of southeastern Wisconsin in 2000 was about 91.5 percent of the predevelopment rate (Feinstein et al., 2005b).

5.2.2.2. Influence of Salinity on Groundwater Flow

Saline water is present in lower portions of the Mt. Simon Unit and in downdip areas of the important deep aquifers, including the Ancell Unit, Ironton-Galesville Unit, and Mt. Simon Unit. Because it is denser than fresh water, this saline water influences groundwater circulation, yet the saline water is not represented in modeling developed for this project. Deep saline groundwater also is a concern because pumping in northeastern Illinois could eventually induce saline water into deep wells, reducing groundwater quality and limiting use of the deep groundwater. By employing different modeling codes, more accurate modeling that explicitly includes saline water could be generated, and the potential for saline water to enter deep wells in northeastern Illinois could be evaluated. However, the modeling process would be computationally demanding. Preliminary simulations could be developed using available head data and groundwater quality data from the Mt. Simon Unit and downdip portions of other bedrock units, which are scarce, but these simulations would be limited in accuracy until additional head and groundwater quality data became available. Acquisition of this additional data is recommended in Section 5.3.

5.2.2.3. Influence of Sandwich Fault Zone on Groundwater Flow

The hydraulic character of the Sandwich Fault Zone may not be as represented in the regional groundwater flow model, which treats it simply as a planar displacement feature juxtaposing model layers having differing hydraulic properties but with no unique intrinsic hydraulic properties of its own. It is conceivable, however, that rocks within the fault zone could have either higher or lower hydraulic conductivity than surrounding rocks, owing to fracturing (which would increase permeability) and mineral precipitation within fractures (which would decrease permeability). Although observations of the hydraulic character of the fault zone are not available (see Section 5.3), preliminary models could be calibrated, using the existing regional-scale model together with assumed values of hydraulic conductivity representative of either a high- or low-permeability fault zone to test the effect on groundwater circulation in the region. Acquisition of additional data on the hydraulic properties of the Sandwich Fault Zone might provide a rational justification for one or the other representation of the fault zone

(simple displacement feature versus high- or low-permeability zone); such acquisition is recommended in Section 5.3.

5.2.2.4. Relationship between Effluent and Natural Groundwater Discharge

Simulations with the local-scale model suggest that groundwater withdrawals have appreciably reduced natural groundwater discharge to many streams in the Kane County area. The extent to which these reductions are offset by discharges of effluent is not well understood, however, and an investigation of this topic could be a useful contribution to water-resources management in Kane County. Knapp et al. (2007) show that reduction in natural groundwater discharge to the Fox River may be more than offset by effluent, with low flows in the Fox River possibly higher now than under predevelopment conditions. The opposite could be true for many tributary streams, however. Groundwater that is withdrawn from the tributary watersheds, after distribution through public water systems and treatment as wastewater, is not typically discharged as effluent in stream reaches affected by the withdrawals. It is instead discharged into another stream; in Kane County, the receiving stream is commonly the Fox River.

5.3. Database Expansion and Improvement

One of the outcomes of this modeling study and the related data collection and analysis is to evaluate the worth of additional data, including the value of additional monitoring and measurement. Scientists and engineers are always tempted to ask for additional data, but it is important to identify those data that will do the most to improve model accuracy by investigating alternative conceptual models, provide additional calibration targets, or quantify heterogeneity. In general, the available database for justification of the hydraulic parameters, boundary conditions, and conceptual models suffers from imprecision, geological and geographical bias, sporadic and irregular data collection and compilation efforts, and poor documentation. These shortcomings reflect the fact that data collection, analysis, and mapping have largely been conducted for local studies over a long period of time, using a range of technologies and approaches, and for purposes other than groundwater flow modeling. Compounding these problems is the fact that the region covers four states, each with different governmental and institutional authorities responsible for hydrogeological research and data collection, and has at its center a notable absence of data in the area of Lake Michigan.

This category of future work covers an array of efforts including field studies; identification, compilation, and possible reanalysis of archived data and information; revision of existing governmental and institutional database-compilation practices; and compilation of comprehensive datasets. In this section, the term *database* is used, then, with its most expansive meaning, and includes the complete array of published, unpublished, digital, and hardcopy data, information, mapping, and analysis employed to justify the hydraulic parameters, boundary conditions, and conceptual models that are synthesized as groundwater flow models.

5.3.1. Hydraulic Properties and Boundary Conditions

The experiences gained through this modeling study suggest that, arguably, the most significant need for database expansion and improvement is for compilation of comprehensive, accurate withdrawal data. The analysis of alternative scenarios of future

pumping (Section 3.3) clearly shows that pumping rate uncertainty is responsible for much of the uncertainty in possible outcomes. This also applies to simulations of aquifer history, where the aquifer simulations have anomalous changes in drawdown that are solely a function of the assumed distribution of pumping. Historic pumping simulated by the models is limited in accuracy. For example, pre-1985 pumping in Indiana and pre-1964 shallow pumping in Illinois are not simulated, and pre-1964 pumping from deep wells in Illinois is aggregated at seven fictitious pumping centers. The limited accuracy of the simulated historic pumping is largely a product of the lack of readily available data, but it might be possible to fill gaps in the record with assumptions or with withdrawal data from historic pumping records that could be discovered through a well-organized research effort. Both efforts would require extensive research using hardcopy records, possibly at several local and state facilities. Improvement of the database of historic pumping would be of greatest value in simulating groundwater flow in the deep units, because, as contrasted from shallow groundwater flow, deep groundwater flow requires significant time to reach a steady state following changes in pumping rates and locations.

Simulation accuracy could be enhanced by improvement of existing withdrawal databases, which might also involve changes in institutional/governmental requirements for reporting of groundwater withdrawals. In general, regional groundwater flow modeling in the urban corridor surrounding southern Lake Michigan, which covers an area extending from Michigan through Indiana and Illinois to Wisconsin, would benefit from a consistent approach to withdrawal measurement, reporting, and data compilation by all states surrounding the lake. Currently, reporting of groundwater withdrawals in Illinois is voluntary, and many of the largest users choose not to report.

As a parameter to which shallow heads and streamflow are highly sensitive, accurate characterization of recharge—and discharge (including withdrawals), which must balance recharge—is probably the second greatest data need, yet accurate measurement of recharge is problematic and a subject of active research (National Research Council, 2004). Recharge rates employed in both the regional- and local-scale models are based on watershed-scale estimates that do not portray the local variability arising from such factors as vegetation, land cover, slope, and geology. Studies directed toward detailed characterization of recharge rates in the region would be of enormous value in future modeling studies. Further, current research into climate variability suggests that the climatic factors affecting recharge might be dramatically different in the future, yet the relationship between climate and recharge is not clear. Reducing uncertainties in recharge and discharge—or at least understanding their impact on model predictions—will require continued monitoring and analysis of streamflow, monitoring wells, and soil moisture probes to assess the temporal variability of the water table. Quantifying recharge and discharge also will require supporting models to assimilate and interpret the data.

Future modeling in the region would benefit from systematic research on the hydraulic properties of all the modeled units, aquifers and aquitards alike. This research would logically include an effort devoted to identification and reanalysis using a consistent approach of available pumping and slug tests from the entire multi-state region. Other efforts would be devoted to field studies directed toward observation of hydraulic properties of units that are, at best, poorly understood hydraulically. For example, the aquitard consisting of unweathered Silurian-Devonian Carbonate Unit,

Maquoketa Unit, and Galena-Platteville Unit underlying the Shallow Bedrock Aquifer exerts a significant influence on groundwater circulation within the major deep aquifers of northeastern Illinois (the Ancell, Ironton-Galesville, and Mt. Simon Units), yet the hydraulic character of this interval is poorly known. As another example, despite the importance of the Ironton-Galesville Unit as an aquifer, little is known about the hydraulic characteristics of the Ironton-Galesville, because most tested wells open to the aquifer are also open to the Ancell Unit. It is impossible from testing of such wells to compute hydraulic properties specific to the Ironton-Galesville. Finally, field studies to improve characterization of the hydraulic properties of the Sandwich Fault Zone might provide justification for one of the conceptual models of the fault zone discussed in Section 5.2.2.3 (simple planar displacement, high conductivity zone, or low conductivity zone), or it might suggest another conceptual model entirely.

Additional field studies would provide needed observational data to support improvement of the local-scale model and the development of new models of shallow materials. The available pumping tests of the shallow materials within the local model domain include comparatively few high-quality tests, and many units have not been tested. Diamicton units, for example, exert a major influence on shallow groundwater movement, yet their hydraulic characteristics are not well understood. In general, the spatial variability of the hydraulic conductivity of the vitally important sand and gravel aquifers is not well known and is only hinted at by differences in productivity of individual wells. For example, a high hydraulic conductivity is conjectured for the sand and gravel aquifer supplying the highly productive Carpentersville wells, yet high-quality pumping tests are not available to document this supposition. The horizontal and vertical distributions of hydraulic conductivity of the widely used Shallow Bedrock Aquifer are poorly documented by available high-quality pumping tests, which are sparsely distributed, influenced by overlying sand and gravel aquifers, and are from wells open to bedrock intervals that frequently extend downward into the underlying aquitard. Additional field studies would provide much-needed observational data to support improvement of the local-scale model and the development of new models of shallow materials.

With the exception of pumping rates, the hydraulic parameters and boundary conditions in both the regional- and local-scale models do not change with time, and they reflect modern conditions (roughly those of the late 20th century). Yet land cover changes associated with settlement, urbanization, and agricultural development have had significant hydrologic impacts, and more accurate model simulations might be possible if the models could portray historically accurate changes in such characteristics as recharge rates and drained area, both of which have probably changed with urbanization and agricultural development in the region. Such an effort would require extensive research into land cover changes and estimation of hydraulic characteristics of historic land cover regimes.

The locations and characteristics of drained areas in the model domains are poorly known and, for this project, are based on soils and urban-area mapping and on general assumptions regarding agricultural and urban drainage systems in the region. The actual locations of the many drainage systems are not documented, and the locations and characteristics of agricultural drains are, in particular, debatable. Future modeling would

benefit from mapping of both agricultural and urban drainage systems and field studies to support accurate characterization of these systems.

As discussed in Section 5.2.2.2, the effect of saline water in downdip areas and in the Mt. Simon Unit on groundwater flow is not simulated directly in the regional-scale groundwater flow model. The accuracy of additional modeling to simulate these effects would be severely limited without acquisition of groundwater quality data from the downdip areas and from the Mt. Simon Unit. These data could also be useful in accurately simulating the effects of the Sandwich Fault Zone on groundwater flow in the region. Some newly acquired water-quality data from current studies of carbon sequestration by the ISGS might be useful for modeling the effects of salinity in the Sandwich Fault Zone.

5.3.2. Geological Models

The regional- and local-scale models are each based on a single geological model, or geological framework. In reality, subsurface geology is a subject of continuing scientific inquiry, and interpretations of the geometries and relationships of stratigraphic units are numerous and continually evolving. Each different interpretation of the geology is equivalent to a different conceptual model (see Section 2.1), and each interpretation employed in a groundwater flow model would result in different simulations of groundwater flow, although the differences might be subtle. The only way to evaluate the uncertainty generated by the conceptual model is by developing separate groundwater flow models based on each separate conceptual model, then comparing the results. Such an undertaking would be helpful in understanding the uncertainty of model simulations, but it would require considerable effort.

5.3.3. Calibration Data

The regional- and local-scale models are calibrated to observations of streamflow and head, but these observations are limited in their applicability for model calibration, many having been collected for other purposes. Future modeling could benefit from focused monitoring efforts, begun in the present, to acquire and compile higher-quality data for model calibration. Sites having suitable long-term streamflow data, useful for estimating the component of groundwater discharge known as base flow (discussed as a research need with recharge on page 407), are sparsely distributed in the northeastern Illinois region, the historical gage network having been monitored sporadically. Calibration of future models and model characterization of streambed properties would benefit from expansion of the existing gage network and a commitment to long-term data collection by monitoring authorities. Further, studies to quantify actual groundwater discharge to streams in the region would be helpful for calibration of future models to fluxes. Lacking more accurate estimates of base flow, the regional- and local-scale models of the present study were calibrated, somewhat speculatively, to the range of streamflow between Q_{80} and Q_{50} .

There is no alternative to employing speculative predevelopment heads for steady-state calibration of the regional-scale model under nonpumping conditions, but head data for transient calibration of the model under pumping conditions could be improved. These data were collected from a sparse network of active or retired supply wells frequently open to numerous hydrostratigraphic units, giving them a very low level

of reliability for calibration (Appendix E). In addition, collection of water-level data from the wells occurred sporadically, and some of the wells served as water-supply wells during the time the water-level data were collected, limiting their usefulness for model calibration. Future model development would greatly benefit from systematic, long-term collection of head data from a network of dedicated observation wells open to single hydrostratigraphic units and not subject to pumping. Installation, protection, and measurement of monitoring wells are relatively inexpensive for the shallow, unconsolidated aquifers, but can be very expensive for the deep aquifers. Here, collaborating with owners of existing deep wells may permit converting old wells into monitoring wells at a minimal cost. Heads in these wells should be observed at least quarterly to permit use of the data for transient model calibration. Some head data from deep hydrostratigraphic units, most notably the Mt. Simon Unit, have been collected recently by the ISGS in conjunction with studies of carbon sequestration, and these data could be useful for further calibration and improvement of the regional-scale groundwater flow model and for modeling of salinity in the deep units as discussed above (Section 5.2.2.2).

Long-term, rather than sporadic, monitoring of water levels in these observation wells would be critical for the data to be most useful for model calibration, requiring a commitment to the effort from monitoring authorities. Moreover, the wells in such a network would probably need to be constructed, at considerable expense, as it is unlikely that a suitable number of retired deep water-supply wells, open to single hydrostratigraphic units, will ever become available for use as observation wells in the region. It is practical for water-supply purposes to leave deep wells open to all rocks underlying the Maquoketa Unit.

5.3.4. Sulfide-Cement Horizon at Contact of Galena-Platteville and Ancell Units

As described in Section 3.3.1, research suggests that reduction of heads to a position near the contact of the Galena-Platteville and Ancell Units has led to increased arsenic concentrations in groundwater pumped from deep wells in northeastern Wisconsin (Schreiber et al., 2000). The source of the arsenic may be a thin interval of sulfide minerals [the sulfide-cement horizon (SCH)] at the contact between the Galena-Platteville and Ancell, which releases arsenic under oxidizing conditions. Although preliminary studies suggest that the SCH is present in Illinois (Lasemi, personal communication, 2005), there is a need for more comprehensive study to verify the presence of the SCH in Illinois and confirm that the SCH contains arsenic that can be liberated as a consequence of declining heads. Combined geochemical and flow modeling could help determine how much arsenic is released and how the concentration would be diluted by water from the other formations.

5.4. Uncertainty Analysis Using Alternative Models

Numerous revisions of parameter zonations, boundary conditions, and conceptual models are justifiable solely on the basis of existing data, and alternative calibration weighting schemes employing the existing calibration targets are also justifiable. Expansion and improvement of the database for model development, as recommended in Section 5.3, would justify additional parameter zonations, boundary conditions, and conceptual models and might suggest still more calibration weighting schemes. In

summary, it is possible—and will continue to be possible—to develop a multitude of alternative, justifiable models on the basis of observational data available now and in the future. Each of these models would yield somewhat different results. Although considerable effort would be required to develop a large number of alternative models using present methods, statistical analysis of simulations generated using a group of such models would prove valuable in understanding the uncertainty of model predictions.

5.5. Monitoring

Monitoring of aquifer heads should be considered in areas of significant simulated 2003 and future drawdown. Such monitoring would require installation of observation wells open to principal source aquifers in problem areas and quarterly measurement of water levels in these wells. Monitoring provides a relatively inexpensive mechanism for early identification of problematic downward water-level trends and establishes a database of irreplaceable historic head data. Streamflow monitoring of streams projected to incur significant simulated base flow reduction, such as Mill Creek, is also advisable.

6. References

Abert, C.C., W.S. Dey, A.M. Davis and B.B. Curry. 2007. *Three-Dimensional Geologic Model, Kane County, Illinois*. Illinois State Geological Survey Illinois County Geologic Map ICGM Kane-3D, Champaign, IL.

Alley, W.M., T.E. Reilly and O.L. Franke. 1999. *Sustainability of Ground-Water Resources*. United States Geological Survey Circular 1186, Denver, CO.

Andersen, P.F. 1993. *A Manual of Instructional Problems for the U.S.G.S. MODFLOW Model*. Robert S. Kerr Environmental Research Laboratory, Office of Research and Development, United States Environmental Protection Agency Dynamac Contract 68-C8-0058, Ada, OK.

Anderson, C.B. 1919. *Artesian Waters of Northeastern Illinois*. Illinois State Geological Survey Bulletin 34, Urbana, IL.

Anderson, M.P. and W.W. Woessner. 2002. *Applied groundwater modeling: Simulation of flow and advective transport*. Academic Press, San Diego, CA.

Arnold, J.G., R.S. Muttiah and P.M. Allen. 2000. Regional estimation of base flow and groundwater recharge in the Upper Mississippi river basin. *Journal of Hydrology* 227(1):21-40.

Barker, J. 1986. Lake Diversion at Chicago. *Case Western Reserve Journal of International Law* 18:203-218.

- Barnes, M.J. 1985. *The Extent and Behavior of the Mineralized Water in the Mt. Simon Formation, Northeastern Illinois*. M.S. Thesis. Department of Geology and Environmental Sciences, Northern Illinois University, DeKalb, IL.
- Bartosova, A., S. McConkey, Y.F. Lin and D.D. Walker. 2004. Using NHD to estimate stream geometry characteristics for MODFLOW. In *Geographic information systems and water resources III: AWRA Spring Specialty Conference, May 17-19, 2004, Nashville Tennessee*, 7. American Water Resources Association, Middleburg, VA.
- Becker, L.E., A.J. Hreha and T.A. Dawson. 1978. *Pre-Knox (Cambrian) Stratigraphy in Indiana*. Indiana Department of Natural Resources Geological Survey Bulletin 57, Bloomington, IN.
- Benson, C.R. 1990. Evaluation of Water-Supply and Well Designs for Campton Township in Kane County, Illinois. Illinois State Water Survey Contract Report 494, Champaign, IL.
- Bergeron, M.P. 1981. *Effect of Irrigation Pumping on the Ground-Water System in Newton and Jasper Counties, Indiana*. United States Geological Survey Water-Resources Investigations Report 81-38, Indianapolis, IN.
- Bloyd, R.M., Jr. 1974. *Summary Appraisals of the Nation's Ground-Water Resources -- Ohio Region*. United States Geological Survey Professional Paper 813-A, Washington, DC.
- Bond, D.C. 1972. *Hydrodynamics in deep aquifers of the Illinois Basin*. Illinois State Geological Survey Circular 470, Urbana, IL.
- Brassington, F.C. and K.R. Rushton. 1987. Rising water table in central Liverpool. *Quarterly Journal of Engineering Geology* 20:151-158.
- Bredehoeft, J.D. 2002. The water-budget myth revisited: why hydrogeologists model. *Ground Water* 40(4):340-345.
- Bredehoeft, J.D., S.S. Papadopoulos and H.H. Cooper, Jr. 1982. Groundwater--The water-budget myth. In *Scientific basis of water-resource management*, 51-57. National Academy Press, Washington, DC.
- Bricker, D.M., R.L. Milstein and J. C.R. Reszka. 1983. *Selected Studies of Cambro-Ordovician Sediments within the Michigan Basin*. Michigan Department of Natural Resources Geological Survey Division Report of Investigation 26, Lansing, MI.
- Burch, S.L. 1991. The New Chicago Model: A Reassessment of the Impacts of Lake Michigan Allocations on the Cambrian-Ordovician Aquifer System in Northeastern Illinois. Illinois State Water Survey Research Report 119, Champaign, IL.

- Burch, S.L. 2002. A Comparison of Potentiometric Surfaces for the Cambrian-Ordovician Aquifers of Northeastern Illinois, 1995 and 2000. Illinois State Water Survey Data/Case Study 2002-02, Champaign, IL.
- Buschbach, T.C. 1964. *Cambrian and Ordovician Strata of Northeastern Illinois*. Illinois State Geological Survey Report of Investigation 218, Urbana, IL.
- Calver, A. 2001. Riverbed permeabilities: information from pooled data. *Ground Water* 39(4):546-553.
- Cannon, W.F., T.H. Kress, D.M. Sutphin, G.B. Morey, J. Meints and R.D. Barber-Delach. 1997. Digital Geologic Map and Mineral Deposits of Minnesota, Wisconsin, and Michigan (Version 3.0) (Downloadable GIS Data). *United States Geological Survey*, <http://pubs.usgs.gov/of/1997/of97-455/> (accessed April 4, 2006).
- Carrera, J. and S.P. Neuman. 1986. Estimation of aquifer parameters under transient and steady state conditions: 2. Uniqueness, stability, and solution. *Water Resources Research* 22(2):211-227.
- Catacosinos, P.A. 1973. Cambrian lithostratigraphy of Michigan Basin. *American Association of Petroleum Geologists Bulletin* 57(12):2404-2418.
- Catacosinos, P.A. and P.A. Daniels, Jr. 1991. Stratigraphy of Middle Proterozoic to Middle Ordovician formations of the Michigan basin. In *Early sedimentary evolution of the Michigan basin*, 53-71. Edited by P.A. Catacosinos and P.A. Daniels. Geological Society of America Special Paper 256. Geological Society of America, Boulder, CO.
- Catacosinos, P.A., P.A. Daniels, Jr. and W.B. Harrison, III. 1990. Structure, Stratigraphy, and Petroleum Geology of the Michigan Basin. In *Interior Cratonic Basins*, 561-601. Edited by M.W. Leighton, D.R. Kolata, D.F. Oltz and J.J. Eidel. American Association of Petroleum Geologists Memoir 51. American Association of Petroleum Geologists, Tulsa, OK.
- Catacosinos, P.A., W.B. Harrison, III, R.F. Reynolds, D.B. Westjohn and M.S. Wollensak. 2001. *Stratigraphic Lexicon for Michigan*. Michigan Department of Environmental Quality Geological Survey Division Bulletin 8, Lansing, MI.
- Cherkauer, D.S. 2001. *Distribution of Ground-Water Recharge in Southeastern Wisconsin*. Wisconsin Department of Natural Resources, Madison, WI.
- Clark, G.R. 1994. Mouth of the Mahomet Regional Groundwater Model, Imperial Valley Region of Mason, Tazewell, and Logan Counties, Illinois. Illinois Department of Transportation, Division of Water Resources, Springfield, IL.
- Csallany, S. and W.C. Walton. 1963. *Yields of Shallow Dolomite Wells in Northern Illinois*. Illinois State Water Survey Report of Investigation 46, Champaign, IL.

Curry, B.B. and P.R. Seaber. 1990. *Hydrogeology of Shallow Groundwater Resources, Kane County, Illinois*. Illinois State Geological Survey Contract/Grant Report 1990-1, Champaign, IL.

Deniger, J.A. 2004. *Soil Survey of Kane County, Illinois*. United States Department of Agriculture-Natural Resources Conservation Service in cooperation with Illinois Agricultural Experiment Station.

Devlin, J.F. and M. Sophocleus. 2005. The persistence of the water budget myth and its relationship to sustainability. *Hydrogeology Journal* 13:549-554.

Dey, W.S., A.M. Davis and B.B. Curry. 2007a. *Aquifer Sensitivity to Contamination, Kane County, Illinois*. Illinois State Geological Survey Illinois County Geologic Map ICGM Kane-AS, Champaign, IL.

Dey, W.S., A.M. Davis and B.B. Curry. 2007b. *Bedrock Geology, Kane County, Illinois*. Illinois State Geological Survey Illinois County Geologic Map ICGM Kane-BG, Champaign, IL.

Dey, W.S., A.M. Davis and B.B. Curry. 2007c. *Major Quaternary Aquifers, Kane County, Illinois*. Illinois State Geological Survey Illinois County Geologic Map ICGM Kane-QA, Champaign, IL.

Dey, W.S., A.M. Davis, B.B. Curry and C.C. Abert. 2007d. *Geologic Cross Sections, Kane County, Illinois*. Illinois State Geological Survey Illinois County Geologic Map ICGM Kane-CS, Champaign, IL.

Dey, W.S., A.M. Davis, B.B. Curry, D.A. Keefer and C.C. Abert. 2007e. *Kane County Water Resources Investigations: Final Report on Geologic Investigations*. Illinois State Geological Survey Contract Report 2007, Champaign, IL.

Dey, W.S., A.M. Davis, B.B. Curry and J.C. Sieving. 2004a. *Kane County Water Resources Investigations: Interim Report on Geologic Investigations*. Illinois State Geological Survey Open File Series 2004-9, Champaign, IL.

Dey, W.S., A.M. Davis, B.B. Curry and J.C. Sieving. 2004b. *Preliminary Bedrock Geology Map, Kane County, Illinois*. Illinois State Geological Survey Illinois Preliminary Geologic Map IPGM Kane-BG, Champaign, IL.

Dey, W.S., A.M. Davis, B.B. Curry and J.C. Sieving. 2004c. *Preliminary Geologic Cross Sections, Kane County, Illinois*. Illinois State Geological Survey Illinois Preliminary Geologic Map IPGM Kane-CS, Champaign, IL.

Dey, W.S., A.M. Davis, B.B. Curry and J.C. Sieving. 2004d. *Preliminary Map of Major Quaternary Aquifers, Kane County, Illinois*. Illinois State Geological Survey Illinois Preliminary Geologic Map IPGM Kane-QA, Champaign, IL.

Dey, W.S., A.M. Davis, B.B. Curry and J.C. Sieving. 2005. *Kane County Water Resources Investigations: Interim Report on Three-dimensional Geologic Modeling*. Illinois State Geological Survey Open File Series 2005-6, Champaign, IL.

Dietz, R.S. 1947. Meteorite impact suggested by orientation of shatter cones at the Kentland, Indiana, disturbance. *Science* 105(2714):42-43.

Driscoll, F.G., ed. 1986. *Groundwater and Wells*. Johnson Division, St. Paul, MN.

Droste, J.B. and J.B. Patton. 1985. *Lithostratigraphy of the Sauk Sequence in Indiana*. Indiana Department of Natural Resources Geological Survey Occasional Paper 47, Bloomington, IN.

Dunne, T. and L.B. Leopold. 1978. *Water in Environmental Planning*. W.H. Freeman and Company, San Francisco, CA.

Dziegielewski, B., T. Bik, X. Yang, H. Margono, M. Richey and D. Sherman. 2004. *Countywide Projections of Community Water Supply Needs in the Midwest*. Department of Geography, Southern Illinois University, Carbondale, IL.

Dziegielewski, B., X. Yang, T. Bik, H. Margono and M. Richey. 2005. *County-Level Forecasts of Water Use in Illinois: 2005-2025*. Department of Geography, Southern Illinois University, Carbondale, IL.

Eaton, T.T., K.R. Bradbury and T.J. Evans. 1999. *Characterization of the Hydrostratigraphy of the Deep Sandstone Aquifer in Southeastern Wisconsin*. Wisconsin Geological and Natural History Survey Open-File Report 1999-02, Madison, WI.

Ells, G.D. 1967. Correlation of Cambro-Ordovician rocks in Michigan Basin. In *Correlation Problems of the Cambrian and Ordovician Outcrop Areas, Northern Michigan*, 42-57. Edited by M.E. Ostrom, A.E. Slaughter and others. Michigan Basin Geological Society Annual Field Excursion Guidebook. Michigan Basin Geological Society, Lansing, MI.

Emrich, G.H. 1966. *Ironton and Galesville (Cambrian) Sandstones in Illinois and Adjacent Areas*. Illinois State Geological Survey Circular 403, Urbana, IL.

Emrich, G.H. and R.E. Bergstrom. 1962. Des Plaines Disturbance, northeastern Illinois. *Geological Society of America Bulletin* 73:959-968.

Environmental Simulations Inc. 2001. AquiferWin32 Version 2.36.

Environmental Simulations Inc. 2005. Groundwater Vistas Version 4.19.

ESRI Bureau of Transportation Statistics. 1990. U.S. Urbanized Areas. *ESRI, Inc.*, <http://www.esri.com/data/index.html> (accessed January 1, 2003).

Feinstein, D.T., T.T. Eaton, D.J. Hart, J.T. Krohelski and K.R. Bradbury. 2005a. Regional aquifer model for southeastern Wisconsin; Report 1: Data collection, conceptual model development, numerical model construction, and model calibration. Wisconsin Geological and Natural History Survey administrative report prepared for Southeastern Wisconsin Regional Planning Commission.

Feinstein, D.T., T.T. Eaton, D.J. Hart, J.T. Krohelski and K.R. Bradbury. 2005b. *Regional aquifer model for southeastern Wisconsin; Report 2: Model results and interpretation*. Wisconsin Geological and Natural History Survey administrative report prepared for Southeastern Wisconsin Regional Planning Commission.

Fetter, C.W. 1988. *Applied Hydrogeology*. MacMillan, New York, NY.

Foley, F.C., W.C. Walton and W.J. Drescher. 1953. *Ground-water Conditions in the Milwaukee-Waukesha Area, Wisconsin*. United States Geological Survey Water-Supply Paper 1229, Washington, DC.

Foster, S.S.D. 1990. Impacts of urbanisation on groundwater. In *Hydrological processes and water management in urban areas*, 187-207. Edited by H. Massing, J. Packman and F.C. Zuidema. IAHS Publication 198.

Foster, S.S.D., B.L. Morris and P.J. Chilton. 1999. Groundwater in urban development - a review of linkages and concerns. In *Impacts of urban growth on surface water and groundwater quality*, 3-12. Edited by J.B. Ellis. IAHS Publication 259.

Fowler, K. and J. Wilson. 1996. *Low-Flow Characteristics of Indiana Streams*. United States Geological Survey Water Resources Investigations Report 96-4128.

Freeze, R.A. and J.A. Cherry. 1979. *Groundwater*. Prentice-Hall, Inc., Englewood Cliffs, NJ.

Gilkeson, R.H., K. Cartwright, J.B. Cowart and R.B. Holtzman. 1983. *Hydrogeologic and Geochemical Studies of Selected Natural Radioisotopes and Barium in Groundwater in Illinois*. Illinois State Geological Survey Contract/Grant Report 1983-6, Champaign, IL.

Gilkeson, R.H., S.S. McFadden, D.E. Laymon and A.P. Visocky. 1987. Hydrogeological Evaluation of Groundwater Resources in Buried Bedrock Valleys, Northeastern Illinois. In *Proceedings of the NWWA FOCUS Conference on Midwestern Ground Water Issues*, 145-167. National Water Well Association, Dublin, OH.

- Gorelick, S.M. 1997. Incorporating uncertainty into aquifer management models. In *Subsurface Flow and Transport: A Stochastic Approach*, 101-112. Edited by G. Dagan and S. Neuman. Cambridge Univ. Press, Cambridge.
- Graese, A.M., R.A. Bauer, B.B. Curry, R.C. Vaiden, W.G. Dixon, Jr. and J.P. Kempton. 1988. *Geological-Geotechnical Studies for Siting the Superconducting Super Collider in Illinois: Regional Summary*. Illinois State Geological Survey Environmental Geology Notes 123, Champaign, IL.
- Gross, D.L., J.A. Lineback and W.A. White. 1970. *Preliminary Stratigraphy of Unconsolidated Sediments From the Southwestern Part of Lake Michigan*. Illinois State Geological Survey Environmental Geology Notes 30, Urbana, IL.
- Gutschick, R.C. and C.A. Sandberg. 1991. Late Devonian history of Michigan Basin. In *Early sedimentary evolution of the Michigan basin*, 181-202. Edited by P.A. Catacosinos and P.A. Daniels. Geological Society of America Special Paper 256. Geological Society of America, Boulder, CO.
- Hansel, A.K. and W.H. Johnson. 1996. Wedron and Mason Groups: Lithostratigraphic Reclassification of Deposits of the Wisconsin Episode, Lake Michigan Lobe Area. Illinois State Geological Survey Bulletin 104, Champaign, IL.
- Harrell, J.A. and C.B. Hatfield. 1991. Mississippian System of the Michigan Basin; Stratigraphy, sedimentology, and economic geology. In *Early sedimentary evolution of the Michigan basin*, 53-71. Edited by P.A. Catacosinos and P.A. Daniels. Geological Society of America Special Paper 256. Geological Society of America, Boulder, CO.
- Heath, R.C. 1983. *Basic Ground-Water Hydrology*. United States Geological Survey Water-Supply Paper 2220, Washington, DC.
- Hendry, M.J. 1982. Hydraulic conductivity of a glacial till in Alberta. *Ground Water* 20(2):162-169.
- Hensel, B.R. 1992. *Natural Recharge of Groundwater in Illinois*. Illinois State Geological Survey Environmental Geology Notes 143, Champaign, IL.
- Hill, M.C. and C.R. Tiedeman. 2007. *Effective Groundwater Model Calibration*. John Wiley and Sons, Hoboken, NJ.
- Holmstrom, B. 1978. *Low-Flow Characteristics of Streams in the Rock-Fox River Basin, Wisconsin*. United States Geological Survey Open-File Report 78-85, Madison, WI.
- Holtschlag, D.J. 1997. *A Generalized Estimate of Ground-Water Recharge Rates in the Lower Peninsula of Michigan*. United States Geological Survey Water-Supply Paper 2437, Washington, DC.

Illinois Department of Energy and Natural Resources. 1998. Fox River Area Assessment. Volume 2: Water Resources. Illinois Department of Natural Resources Critical Trends Assessment Program Document. Springfield, IL.

Illinois Department of Natural Resources. 1996. Major Sand and Gravel Aquifers, Illinois Geographic Information System, Volume I (GIS Data on CD-ROM). *Illinois Department of Natural Resources* (May 1996).

Illinois State Water Survey. 2008. Glossary. *Illinois State Water Survey*, <http://www.sws.uiuc.edu/wsp/faq/glossary.asp> (accessed October 10, 2008).

Illinois State Water Survey and Hittman Associates. 1973. *Feasibility Study on Desalting Brackish Water from the Mt. Simon Aquifer in Northeastern Illinois*. Illinois State Water Survey Contract Report 153, Champaign, IL.

Indiana Governor's Water Resource Study Commission. 1980. *The Indiana Water Resource: Availability, Uses, and Needs*. Indiana Department of Natural Resources, Indianapolis, IN.

Injerd, D. 1993. Lake Michigan Water Diversion: A Case Study. *Buffalo Environmental Law Journal* 1:307-315.

Injerd, D. 2006. Status Report: Illinois' Compliance with the U.S. Supreme Court Decree and Lake Michigan Water Allocation. Illinois Department of Natural Resources, Office of Water Resources, Chicago, IL.

International Joint Commission. 2001. The Great Lakes Charter Annex: A Supplementary Agreement to the Great Lakes Charter.

Kay, R.T., L.D. Arihood, T.L. Arnold and K.K. Fowler. 2006. *Hydrogeology, Water Use, and Simulated Ground-Water Flow and Availability in Campton Township, Kane County, Illinois*. United States Geological Survey Scientific Investigations Report 2006-5076, Reston, VA.

Kay, R.T. and K.A. Kraske. 1996. *Ground-Water Levels in Aquifers Used for Residential Supply, Campton Township, Kane County, Illinois*. United States Geological Survey Water-Resources Investigations Report 96-4009, DeKalb, IL.

Kelly, W.R. 2005. *Shallow Groundwater Quality Sampling in Kane County, October 2003*. Illinois State Water Survey Contract Report 2005-07, Champaign, IL.

Kelly, W.R. and S.C. Meyer. 2005. *Temporal Changes in Deep Bedrock Groundwater Quality in Northeastern Illinois*. Illinois State Water Survey Contract Report 2005-05, Champaign, IL.

- Knapp, H.V., A.M. Russell, J.A. Kramer and G.P. Rogers. 2007. *Kane County Water Resources Investigations: Surface Water Accounting for Water Supply Planning in Kane County*. Illinois State Water Survey Contract Report 2007-10, Champaign, IL.
- Kolata, D.R. 1990. Overview of Sequences. In *Interior Cratonic Basins*, 59-73. Edited by M.W. Leighton, D.R. Kolata, D.F. Oltz and J.J. Eidel. American Association of Petroleum Geologists Memoir 51. American Association of Petroleum Geologists, Tulsa, OK.
- Kolata, D.R., T.C. Buschbach and J.D. Treworgy. 1978. *The Sandwich Fault Zone of Northern Illinois*. Illinois State Geological Survey Circular 505, Urbana, IL.
- Larson, D.R., J.P. Kempton and S.C. Meyer. 1997. *Geologic, Geophysical, and Hydrologic Investigations for a Supplemental Municipal Groundwater Supply, Danville, Illinois*. Illinois State Geological Survey and Illinois State Water Survey Cooperative Groundwater Report 18, Champaign, IL.
- Lerner, D.N. 1986. Leaking pipes recharge groundwater. *Ground Water* 24(5):654-662.
- Lerner, D.N. 2002. Identifying and quantifying urban recharge: a review. *Hydrogeology Journal* 10:143-152.
- Locke, R.A., II and S.C. Meyer. 2005. Kane County Water Resources Investigations: Interim Report on Shallow Aquifer Potentiometric Surface Mapping. Illinois State Water Survey Contract Report 2005-04, Champaign, IL.
- Locke, R.A., II and S.C. Meyer. 2007. *Kane County Water Resources Investigations: Final Report on Shallow Aquifer Potentiometric Surface Mapping*. Illinois State Water Survey Contract Report 2007-06, Champaign, IL.
- Mandle, R.J. and A.L. Kontis. 1992. Simulation of Regional Ground-Water Flow in the Cambrian-Ordovician Aquifer System in the Northern Midwest, United States. United States Geological Survey Professional Paper 1405-C, Washington, DC.
- McDonald, M.G. and A.W. Harbaugh. 1988. Techniques of Water-Resources Investigations of the United States Geological Survey. A Modular Three-Dimensional Finite-Difference Ground-Water Flow Model. Book 6, Modeling Techniques. Chapter A1. United States Geological Survey, Washington, DC.
- McGinnis, L.D. 1966. *Crustal Tectonics and Precambrian Basement in Northeastern Illinois*. Illinois State Geological Survey Report of Investigation 219, Urbana, IL.
- Meyer, S.C. 1998. *Ground-Water Studies for Environmental Planning, McHenry County, Illinois*. Illinois State Water Survey Contract Report 630, Champaign, IL.

- Meyer, S.C. 2005. Analysis of base flow trends in urban streams, northeastern Illinois, USA. *Hydrogeology Journal* 13(5-6):871-885.
- Miller, R.T. 1984. Anisotropy in the Ironton and Galesville Sandstones near a thermal-energy-storage well, St. Paul, Minnesota. *Ground Water* 22(5):532-537.
- Mills, P.C., J.E. Nazimek, K.J. Halford and D.J. Yeskis. 2002. *Hydrogeology and simulation of ground-water flow in the aquifers underlying Belvidere, Illinois*. United States Geological Survey Water-Resources Investigations Report 01-4100, Urbana, IL.
- National Oceanic and Atmospheric Administration Satellite and Information Service. 1996. Bathymetry of Lake Michigan. *National Oceanic and Atmospheric Administration*, <http://map.ngdc.noaa.gov/website/mgg/greatlakesbathy/viewer.htm> (accessed August 9, 2005).
- National Research Council. 2004. *Groundwater fluxes across interfaces*. National Academies Press, Washington, DC.
- Neuman, S. and P. Wierenga. 2003. *A Comprehensive Strategy of Hydrogeologic Modeling and Uncertainty Analysis for Nuclear Facilities and Sites*. United States Nuclear Regulatory Commission Office of Nuclear Regulatory Research NUREG/CR-6805, Washington, DC.
- Nicholas, J.R., M.G. Sherrill and H.L. Young. 1987. *Hydrogeology of the Cambrian-Ordovician Aquifer System at a Test Well in Northeastern Illinois*. United States Geological Survey Water-Resources Investigations Open-File Report 84-4165, Urbana, IL.
- Northeastern Illinois Planning Commission. 2002. *Strategic Plan for Water Resource Management*. Northeastern Illinois Planning Commission.
- Northeastern Illinois Planning Commission. 2006. Northeastern Illinois Planning Commission 2030 Forecasts of Population, Households, and Employment by County and Municipality. *Northeastern Illinois Planning Commission*, http://www.chicagoareapanning.org/data/forecast/2030_revised/ (accessed February 28, 2007).
- Nurmi, R.D. 1972. *Upper Ordovician Stratigraphy of the Southern Peninsula of Michigan*. M.S. Thesis. Department of Geology, Michigan State University, East Lansing, MI.
- Olcott, P.G. 1992. *Groundwater Atlas of the United States. Segment 9. Iowa, Michigan, Minnesota, Wisconsin*. United States Geological Survey Hydrogeologic Investigations Atlas 730-J, Reston, VA.

Ostrom, M.E. 1966. *Cambrian Stratigraphy in Western Wisconsin*. Wisconsin Geological and Natural History Survey Information Circular 7, Madison, WI.

Pappenberger, F. and K.J. Beven. 2006. Ignorance is bliss: Or seven reasons not to use uncertainty analysis. *Water Resources Research* 42(5):W05302.
doi:10.1029/2005WR004820.

Price, M. and D.W. Reed. 1989. The influence of mains leakage and urban drainage on groundwater levels beneath conurbations in the UK. *Proceedings - Institution of Civil Engineers (Design and Construction)* 86 (part 1):31-39.

Prickett, T.A., L.R. Hoover, W.H. Baker and R.T. Sasman. 1964. *Ground-Water Development in Several Areas of Northeastern Illinois*. Illinois State Water Survey Report of Investigation 47, Champaign, IL.

Prickett, T.A. and C.G. Lonnquist. 1971. *Selected Digital Computer Techniques for Groundwater Resource Evaluation*. Illinois State Water Survey Bulletin 55, Champaign, IL.

Roadcap, G.S. 1990. An evaluation of wellhead-protection area delineation methods as applied to municipal wells in the leaky-confined carbonate-bedrock aquifer at Richwood, Ohio. M.S. Thesis. Department of Geology and Mineralogy, The Ohio State University, Columbus, OH.

Roadcap, G.S., S.J. Cravens and E.C. Smith. 1993. Meeting the Growing Demand for Water: An Evaluation of the Shallow Ground- Water Resources in Will and Southern Cook Counties, Illinois. Illinois State Water Survey Research Report 123, Champaign, IL.

Rupp, J.A. 1991. *Structure and Isopach Maps of the Paleozoic Rocks of Indiana*. Indiana Department of Natural Resources Geological Survey Special Report 48, Bloomington, IN.

Rushton, K.R., M.W. Kawecki and F.C. Brassington. 1988. Groundwater model of conditions in Liverpool sandstone aquifer. *Journal of the Institution of Water and Environmental Management* 2(1):67-84.

Sasman, R.T., C.R. Benson, R.S. Ludwigs and T.L. Williams. 1982. *Water-Level Trends, Pumpage, and Chemical Quality in the Cambrian- Ordovician Aquifer in Illinois, 1971-1980*. Illinois State Water Survey Circular 154, Champaign, IL.

Sasman, R.T., R.J. Schicht, J.P. Gibb, M.O. Hearn, C.R. Benson and R.S. Ludwig. 1981. *Verification of the Potential Yield and Chemical Quality of the Shallow Dolomite Aquifer in DuPage County, Illinois*. Illinois State Water Survey Circular 149, Champaign, IL.

Schicht, R.J., J.R. Adams and J.B. Stall. 1976. *Water Resources Availability, Quality, and Cost in Northeastern Illinois*. Illinois State Water Survey Report of Investigation 83, Champaign, IL.

Schreiber, M.E., J.A. Simo and P.G. Freiberg. 2000. Stratigraphic and geochemical controls on naturally occurring arsenic in groundwater, eastern Wisconsin, USA. *Hydrogeology Journal* 8:161-176.

Shaver, R.H., C.H. Ault, A.M. Burger, D.D. Carr, J.B. Droste, D.L. Eggert, H.H. Gray, D. Harper, N.R. Hasenmueller, W.A. Hasenmueller, A.S. Horowitz, H.C. Hutchison, B.D. Keith, S.J. Keller, J.B. Patton, C.B. Rexroad and C.E. Wier. 1986. *Compendium of Paleozoic Rock-Unit Stratigraphy in Indiana - A Revision*. Indiana Department of Natural Resources Geological Survey Bulletin 59, Bloomington, IN.

Simpkins, W.W. and K.R. Bradbury. 1992. Groundwater flow, velocity, and age in a thick, fine-grained till unit in southeastern Wisconsin. *Journal of Hydrology* 132:283-319.

Singh, K. and G. Ramamurthy. 1993. *7-Day, 10-Year Low Flows of Streams in Northeastern Illinois*. Illinois State Water Survey Contract Report CR-545, rev 2003, Champaign, IL.

Singh, K., G. Ramamurthy and I. Seo. 1988a. 7-Day, 10-year Low Flows in the Rock, Spoon, La Moine, and Kaskaskia Regions: Map 1 Rock River Region, rev. 2002. Illinois State Water Survey Contract Report 440, Champaign, IL.

Singh, K., G. Ramamurthy and I. Seo. 1988b. 7-day, 10-year Low Flows of Streams in the Kankakee, Sangamon, Embarras, Little Wabash, and Southern Regions: Map 3 Kankakee Region, Illinois State Water Survey. Illinois State Water Survey Contract Report 441, Champaign, IL.

Sloss, L.L. 1963. Sequences in the cratonic interior of North America. *Geological Society of America Bulletin* 74:93-113.

Solley, W.B., R.R. Pierce and H.A. Perlman. 1998. *Estimated Use of Water in the United States in 1995*. United States Geological Survey Circular 1200, Denver, CO.

Sophocleus, M. 2000. From safe yield to sustainable development of water resources - the Kansas experience. *Journal of Hydrology* 235:27-43.

Suter, M., R.E. Bergstrom, H.F. Smith, G.H. Emrich, W.C. Walton and T.E. Larson. 1959. *Preliminary Report on the Ground-Water Resources of the Chicago Region, Illinois*. Illinois State Water Survey and Illinois State Geological Survey Cooperative Ground-Water Report 1, Urbana, IL.

Templeton, J.S. and H.B. Willman. 1963. *Champlainian Series (Middle Ordovician) in Illinois*. Illinois State Geological Survey Bulletin 89, Urbana.

Todd, D.K. 1980. *Groundwater Hydrology*. John Wiley and Sons, Inc., New York, NY.

United States Census Bureau. 2004. Census 2000 Data for the State of Illinois. *United States Census Bureau*, <http://www.census.gov/census2000/states/il.html> (accessed August 24, 2006).

United States Department of Agriculture Natural Resources Conservation Service. 1994. *State Soil Geographic (STATSGO) Data Base Data Use Information*. United States Department of Agriculture Natural Resources Conservation Service Miscellaneous Publication 1492, Fort Worth, TX.

United States Department of the Interior Bureau of Reclamation. 1997. *Water Measurement Manual*. U.S. Government Printing Office, Washington, DC.

Visocky, A.P. 1982. *Impact of Lake Michigan Allocations on the Cambrian-Ordovician Aquifer System*. Illinois State Water Survey Contract Report 292, Champaign, IL.

Visocky, A.P. 1990a. Hydrology and Water Quality of Shallow Ground-Water Resources in Kane County, Illinois. Illinois State Water Survey Contract Report 500, Champaign, IL.

Visocky, A.P. 1990b. Summary of Monthly Water-Level Data for the Superconducting Super Collider Study Area in Illinois. Illinois State Water Survey Contract Report 489, Champaign, IL.

Visocky, A.P. and R.J. Schicht. 1969. *Groundwater Resources of the Buried Mahomet Bedrock Valley*. Illinois State Water Survey Report of Investigation 62, Champaign, IL.

Visocky, A.P. and M.K. Schulmeister. 1988. *Ground-Water Investigations for Siting the Superconducting Super Collider in Northeastern Illinois*. Illinois State Water Survey Circular 170, Champaign, IL.

Visocky, A.P., M.G. Sherrill and K. Cartwright. 1985. *Geology, Hydrology, and Water Quality of the Cambrian and Ordovician Systems in Northern Illinois*. Illinois State Geological Survey and Illinois State Water Survey Cooperative Groundwater Report 10, Champaign, IL.

Walker, D.D., S.C. Meyer and D. Winstanley. 2003. Uncertainty of estimates of groundwater yield for the Cambrian-Ordovician Aquifer in northeastern Illinois. In *Groundwater Quality Modeling and Management Under Uncertainty, Proceedings of the Probabilistic Approaches & Groundwater Modeling Symposium held during the World Water and Environmental Resources Congress in Philadelphia, Pennsylvania, June 24-*

26, 2003, 273-283. Edited by S. Mishra. American Society of Civil Engineers, Reston, VA.

Walton, W.C. 1960. *Leaky Artesian Aquifer Conditions in Illinois*. Illinois State Water Survey Report of Investigation 39, Champaign, IL.

Walton, W.C. 1962. *Selected Analytical Methods for Well and Aquifer Evaluation*. Illinois State Water Survey Bulletin 49, Champaign, IL.

Walton, W.C. 1964. Future water-level declines in deep sandstone wells in Chicago region. *Ground Water* 2(1):13-20.

Walton, W.C. 1965. *Ground-Water Recharge and Runoff in Illinois*. Illinois State Water Survey Report of Investigation 48, Champaign, IL.

Walton, W.C. and S. Csallany. 1962. *Yields of Deep Sandstone Wells in Northern Illinois*. Illinois State Water Survey Report of Investigation 43, Champaign, IL.

Walton, W.C. and W.H. Walker. 1961. Evaluating wells and aquifers by analytical methods. *Journal of Geophysical Research* 66(10).

Watermark Numerical Computing. 2005. PEST Version 9.00.

Weaver, T.R. and J.M. Bahr. 1991a. Geochemical evolution in the Cambrian-Ordovician sandstone aquifer, eastern Wisconsin: 1. Major ion and radionuclide distribution. *Ground Water* 29(3):350-356.

Weaver, T.R. and J.M. Bahr. 1991b. Geochemical evolution in the Cambrian-Ordovician sandstone aquifer, eastern Wisconsin: 2. Correlation between flow paths and ground-water chemistry. *Ground Water* 29(4):510-515.

Weeks, E.P. 1969. Determining the ratio of horizontal to vertical permeability by aquifer-test analysis. *Water Resources Research* 5(1):196-214.

Wehrmann, H.A., S.V. Sinclair and T.P. Bryant. 2003. *An Analysis of Groundwater Use to Aquifer Potential Yield in Illinois*. Illinois State Water Survey Contract Report 2004-11, Champaign, IL.

Weidman, S. and A.R. Schultz. 1915. *The Underground and Surface Water Supplies of Wisconsin*. Wisconsin Geological and Natural History Survey Bulletin 35, Madison, WI.

Western Michigan University Department of Geology. 1981. Hydrogeologic Atlas of Michigan prepared for United States Environmental Protection Agency, Underground Injection Control Program. Western Michigan University, Kalamazoo, MI.

Willman, H.B., E. Atherton, T.C. Buschbach, C. Collinson, J.C. Frye, M.E. Hopkins, J.A. Lineback and J.A. Simon. 1975. *Handbook of Illinois Stratigraphy*. Illinois State Geological Survey Bulletin 95, Urbana, IL.

Wilson, S.D., G.S. Roadcap, B.L. Herzog, D.R. Larson and D. Winstanley. 1998. Hydrogeology and Ground-water Availability in Southwest McLean and Southeast Tazewell Counties. Part 2: Aquifer Modeling and Final Report. Illinois State Water Survey Cooperative Groundwater Report 19, Champaign, IL.

Wood, W. 2001. Water sustainability - science or management. *Ground Water* 39(5):641.

Young, H.L. 1976. *Digital-Computer Model of the Sandstone Aquifer in Southeastern Wisconsin*. Southeastern Wisconsin Regional Planning Commission Technical Report 16, Waukesha, WI.

Young, H.L. 1992. Summary of Ground-Water Hydrology of the Cambrian-Ordovician Aquifer System in the Northern Midwest, United States. United States Geological Survey Professional Paper 1405-A, Washington, DC.

Young, H.L. and D.I. Siegel. 1992. *Hydrogeology of the Cambrian-Ordovician Aquifer system in the Northern Midwest, United States*. United States Geological Survey Professional Paper 1405-B, Washington, DC.

Zeisel, A.J., W.C. Walton, R.T. Sasman and T.A. Prickett. 1962. *Ground-Water Resources of DuPage County, Illinois*. Illinois State Water Survey and Illinois State Geological Survey Cooperative Ground-Water Report 2, Urbana, IL.

Appendix A. Introduction to Groundwater Flow Modeling

Scientists and engineers often cannot directly analyze natural systems because they are too complex or cumbersome, and instead must use models to describe and analyze the systems. The modeling process begins with the development of a conceptual model, which is a summary of the major components of the system and the processes that link them. The conceptual model of the aquifers of interest to this study identifies the aquifers and their extent, the associated surface-water bodies, the stresses of pumping and recharge, and the physical process of water moving through porous media. The conceptual model is quantified by a mathematical model, which is the set of equations representing the physics, properties, stresses, geometry, etc. of the system. The solution of the mathematical model yields the hydraulic heads and flow rates corresponding to the conceptual model, which can be used to simulate the aquifers' responses to projected stresses. Solving the many interrelated equations of a detailed mathematical model is a tedious task that is commonly addressed by programming a computer. Computer programs for modeling groundwater flow, or modeling codes, represent generic sets of physical properties that can be adapted to a specific system by assigning parameters that describe the system and its stresses. The modeling code and the input parameters for a specific groundwater system are collectively referred to as the model. That is, the code is written once, but the model is designed and built for each specific application (Anderson and Woessner, 2002).

A.1. Finite-Difference Groundwater Flow Modeling

Representing the irregular geometries and spatial variability of aquifers and surface-water bodies frequently results in a complex mathematical model whose solution requires special techniques. In this study, the mathematical model is solved using the finite-difference method, a technique that mathematicians classify as a numerical solution. The finite-difference method begins by superimposing a checkerboard-like grid on the modeled region and dividing the aquifers into a set of finite differences, or blocks. Each block represents an aquifer volume of homogeneous properties where the hydraulic head will be determined. The hydraulic head in each block is governed by classical equations for mass conservation and flow in porous media that depend on the aquifer properties and the hydraulic head in the surrounding blocks. To this are added mathematical constraints known as boundary conditions to represent sources, sinks, and aquifer limits (recharge, wells, rivers, etc.). Because the hydraulic head in each block depends on the head in the surrounding blocks, the equations for the block are an interrelated set that must be solved simultaneously. Various mathematical tricks are employed to solve the set of equations to yield a solution for the hydraulic head at each block center and the flow rates among all components of the modeled system. Changes in the system with time can be found by repeating the finite difference solution for a series of time steps for a so-called transient solution. In this instance, the hydraulic head in the blocks during each time step depends on changes in the boundary conditions (e.g., pumping rates), the amount of water released from storage, and the hydraulic heads of the previous time step. The computational burden increases dramatically with the number of blocks in the grid and the number of time steps in the transient simulation.

A.2. Data Requirements of Groundwater Flow Modeling

A detailed finite-difference model can faithfully represent the system and provide a highly resolved simulation of groundwater flow in the region of interest. But in addition to the computational burden, every block and time step require input parameters. For a site-specific modeling study, inferring these parameters requires data and information on surface hydrology, geology, and pumping history. Further, calibrating the model and building confidence in its results also require observations of hydraulic head and discharge to streams for comparison to model simulations. In short, an extensive, detailed model requires supporting databases and software to manage input parameters and interpret the results. While there are extensive databases available at the regional scale related to, for example, geology, hydrology, and topography, developing a groundwater model generally requires developing supporting databases for local details and pumping history.

Every finite-difference model requires defining the rows, columns, and layers of the grid. This grid definition is largely developed from the geologic model, with the top and bottom surfaces of hydrostratigraphic units used to define the grid layers, so that each block corresponds to a specific portion of the modeled system. Model grids generally have greater resolution in the area of interest (for increased precision) and near pumping wells (for increased accuracy). Grid resolution is decreased in areas of peripheral interest to reduce the computational burden.

Hydraulic properties must also be assigned to each block, including hydraulic conductivities, storage properties (specific storage and specific yield), and effective porosities. Because these can be highly variable and observations are sparse, hydraulic properties are inferred from the statistics of interpreted field tests, previous modeling studies, and from studies in neighboring regions. In this modeling study, and in many others, hydraulic properties are assigned using a zoned approach, with zone boundaries based on geology. For example, research may show that areas of bedrock-surface exposure of a model layer are more permeable as a consequence of weathering, so these areas of exposure are defined as a zone, and that zone is assigned a single value of hydraulic conductivity reflecting the increased permeability. Lithology can also be used as a basis for zone definition.

Hydrologic data are taken from various sources to develop the groundwater model. Boundary conditions representing surface-water bodies and their elevations are taken from digital maps. Streamflow statistics are used to determine plausible ranges of base flow for use in calibrating the models. Maps of low-flow characteristics are used to identify streams to be represented as drains that go dry under conditions of low recharge or high pumping. Hydraulic head measurements in wells (water level measurements) are interpreted to create the potentiometric surface maps used in developing the conceptual model and initial conditions. Estimates of groundwater recharge are developed from streamflow statistics, rainfall data, and watershed characteristics. Recharge estimates are difficult to come by, and the estimation techniques are an area of active research (National Research Council, 2004). Water level measurements are also used directly in calibrating and verifying groundwater flow models. Ideally, such hydrologic data are available for each stream and aquifer at a high level of resolution in space and time. Groundwater salinity and temperature are used indirectly to adjust the hydraulic conductivity at great depth, and to evaluate the effect of unmodeled movement of salinity.

Drained areas are challenging to characterize in general, because their locations are rarely mapped and difficult to detect. Locations are typically inferred from soil maps and topography, and drain elevations, based on typical practices in Illinois, are assumed to be below the depth of

freezing (that is, about 3 ft). The drain leakance is typically calibrated to maintain base flow, balance recharge, and imitate natural wetlands.

Wells can have an enormous affect on the model results, and require several types of data. This includes the location of the well and aquifers from which it withdraws water (the open, or screened, interval). The operating interval and rate need to be taken from owner surveys or inferred from population data. The same information set is required for any hypothesized wells to be simulated in projections into the future.

A.3. Nested Models and Telescopic Mesh Refinement

The design of the finite-difference grid for a model must balance the needs for accuracy and precision with the need to include regional flow patterns in the model. Satisfying both of these objectives would result in an extensive, detailed model grid with the associated burdens of slow computational times, large memory requirements, extensive datasets, and cumbersome data processing tasks. An alternative strategy is to first simulate the regional flow pattern with a coarse-grid model, then create a second, local-scale model with a finely spaced grid for the area of interest. The models are joined, or nested, by taking simulated flows or heads from the regional model and applying these along the edges of the local model as boundary conditions. This strategy, known as *telescopic mesh refinement* (TMR), reduces the computational burden while providing the necessary detail in the area of interest (Ward et al., 1987). The challenge of TMR is to design the local model grid such that the local model boundaries need not be updated to reflect transient effects or changed scenarios. In practice, this can be achieved by positioning the edges of the local model at natural boundaries (e.g., low permeability strata, rivers) and maintaining a buffer zone between the area of interest and the edges of the local model. TMR boundaries can be assembled from regional model simulations using a model post-processor such as Groundwater Vistas (Environmental Simulations Inc., 2005) or using spreadsheets and GIS as necessary. Regardless of the time step of the regional model used for TMR or the data processing approach, the analyst must verify that TMR boundaries accurately transfer the regional conditions to the local model and that only trivial changes occur along the TMR boundary as the local model simulates transient conditions or pumping changes (Anderson and Woessner, 2002).

A.4. Model Calibration

Calibration is the process of adjusting the components and input parameters of the model so that values simulated by the model match the equivalent values measured in the field. Calibration is necessary in groundwater modeling because the modeled process is complex and the simulated values of hydraulic head and flow are more easily measured than the input parameters of hydraulic conductivity, storage parameters, recharge, and leakage (Hill, 1998). Although one perspective is that calibration is only the so-called inverse problem (given the model results and some target observations of head and flow, find the set of input parameters) (Anderson and Woessner, 2002), this report uses model calibration to refer to the following:

- checking data discrepancies (for example, missing records, aquifer assignment errors, etc.);
- managing strata that are discontinuous;
- choosing approaches for representing desaturating aquifers;
- refining parameter zones;
- fine-tuning the numerical algorithms for a stable solution;

- assigning weights to target observations;
- calculating the sensitivity of the results to the input parameters;
- adjusting input parameters to match model-simulated values to observed values (the inverse solution);
- assessing the plausibility and uncertainty of input parameters;
- testing alternative models (e.g., zonation of parameters, weighting schemes);
- examining model errors;
- transient verification; and
- assessing the sensitivity of model projections to uncertain input parameters.

The inverse solution itself can be a trial-and-error manual adjustment of input parameters, or an automatic process of multivariate nonlinear weighted regression. The calibration process ensures that the model is as accurate as the observations, provides an independent verification, and quantifies the effects of known uncertainties on the model predictions.

A.5. Applications of Groundwater Flow Modeling

Groundwater flow models have various uses in research and engineering. As interpretive tools, models are useful for error-checking and assimilating field data. Such interpretive models also evaluate the adequacy of the conceptual model, determine the sensitivity of model results to input parameters, and quantify the flow between various components of the hydrologic system. Model sensitivity analyses can assess the worth of additional data and thus help design field studies to improve the understanding of the modeled system. Interpretive models can be further developed into predictive models that assess the consequences of changing pumping schemes or recharge. For example, a predictive groundwater model can simulate changes in hydraulic head and groundwater discharge to streams that correspond to changes in groundwater withdrawal strategies. Regional and local-scale groundwater flow models also provide a starting point for site-scale detailed models of well fields or of subsurface contamination. There are also a variety of uses for groundwater models in the analysis of generic research problems.

A.6. Uncertainty

Uncertainty in models of natural systems arises from our inability to understand, measure, or completely represent all the features of the true systems (Gorelick, 1997). Uncertainties in groundwater models may be categorized as either *parameter uncertainty* or *conceptual uncertainty* (Neuman and Wierenga, 2003). *Parameter uncertainties* reflect our imperfect knowledge of both the input parameters of the model (hydraulic conductivity, recharge, pumping rates, aquifer geometry, etc.) and the variables the model simulates (hydraulic heads and flow rates). For example, field studies yield estimates of the hydraulic conductivity, but hydraulic conductivity varies by location such that a complete characterization is impossible. Further, field studies of hydraulic conductivity are plagued by scale effects and simple measurement errors. Calibrating model results to field observations can reduce the uncertainty of the input hydraulic conductivity, but the observations themselves also include errors such that the calibrated values retain uncertainty. That is, input parameters for the model can only be known within a range of values justified by field studies and calibration. *Conceptual uncertainties* arise from our imperfect knowledge of the processes governing the modeled system, which forces us to make assumptions regarding what processes to include in the model. In practice, conceptual models are based on expert judgment and can be evaluated to quantify the possible impact of

conceptual uncertainties. For example, this study assumes that the dominant groundwater flow processes for this system are saturated, isothermal flow, driven by hydraulic gradients at relatively low velocities. The effects of salinity, temperature, and flow through unsaturated zones are not included because these processes are generally believed to have minor influences on the aquifers of this system (Feinstein et al., 2005a; Feinstein et al., 2005b; Mandle and Kontis, 1992). The impact of these conceptual uncertainties on the model can be quantified by ancillary calculations, but evaluating conceptual model uncertainty is an area of ongoing research (Neuman and Wierenga, 2003). It is important to note that both categories of uncertainty are present in the models of this study, and cannot be avoided; in short, “With any model, we get uncertainty for free” (Gorelick, 1997).

The groundwater flow models developed for this study embody the conceptual models developed from expert judgment and use the sets of calibrated model parameters, thus they represent the best understanding of the system. However, the conceptual and parameter uncertainties imply that reasonable variations of the expected-case model will yield a range of plausible predictions rather than a single prediction. The formal approach to uncertainty analysis would be to determine the probabilities of these predictions and summarize their range using, for example, confidence intervals. Such estimates could then be used by decision-makers to assess the reliability of model predictions and rationally evaluate the risks associated with management alternatives (Pappenberger and Beven, 2006). Unfortunately, the current technology for assigning probabilities to detailed groundwater models requires repeating the simulation many times (a so-called Monte Carlo analysis), an exercise that is beyond the scope of the current study. An alternative is to create a limited set of simulations that bound the range of plausible predictions using the most sensitive parameters and assumptions (Walker et al., 2003). Although probabilities cannot be assigned to these bounds, they do qualitatively express the reliability of model predictions for use in evaluating management alternatives (Wittman, personal communication, 2007). This study uses the parameter sensitivities calculated during model calibration to select the most sensitive parameters and then repeats the predictive simulations to estimate the range of model predictions.

A.7. References

Anderson, M.P. and W.W. Woessner. 2002. *Applied groundwater modeling: Simulation of flow and advective transport*. Academic Press, San Diego, CA.

Feinstein, D.T., T.T. Eaton, D.J. Hart, J.T. Krohelski, and K.R. Bradbury. 2005a. *Regional Aquifer Model for Southeastern Wisconsin; Report 1: Data Collection, Conceptual Model Development, Numerical Model Construction, and Model Calibration*. Wisconsin Geological and Natural History Survey administrative report prepared for Southeastern Wisconsin Regional Planning Commission.

Feinstein, D.T., T.T. Eaton, D.J. Hart, J.T. Krohelski, and K.R. Bradbury. 2005b. *Regional Aquifer Model for Southeastern Wisconsin; Report 2: Model Results and Interpretation*. Wisconsin Geological and Natural History Survey administrative report prepared for Southeastern Wisconsin Regional Planning Commission.

Gorelick, S.M. 1997. Incorporating uncertainty into aquifer management models. In *Subsurface flow and transport: A stochastic approach*, 101-112. Edited by G. Dagan and S. Neuman. Cambridge Univ. Press, Cambridge.

Hill, M.C. 1998. *Methods and Guidelines for Effective Model Calibration*. United States Geological Survey Water-Resources Investigations Report 98-4005, Denver, CO.

Mandle, R.J. and A.L. Kontis. 1992. *Simulation of Regional Ground-Water Flow in the Cambrian-Ordovician Aquifer System in the Northern Midwest, United States*. United States Geological Survey Professional Paper 1405-C, Washington, DC.

National Research Council. 2004. *Groundwater fluxes across interfaces*. National Academies Press, Washington, DC.

Neuman, S. and P. Wierenga. 2003. *A Comprehensive Strategy of Hydrogeologic Modeling and Uncertainty Analysis for Nuclear Facilities and Sites*. United States Nuclear Regulatory Commission Office of Nuclear Regulatory Research NUREG/CR-6805, Washington, DC.

Pappenberger, F. and K.J. Beven. 2006. Ignorance is bliss: Or seven reasons not to use uncertainty analysis. *Water Resources Research* 42(5):W05302. doi:10.1029/2005WR004820.

Walker, D.D., S.C. Meyer, and D. Winstanley. 2003. Uncertainty of estimates of groundwater yield for the Cambrian-Ordovician Aquifer in northeastern Illinois. In *Groundwater Quality Modeling and Management Under Uncertainty, Proceedings of the Probabilistic Approaches & Groundwater Modeling Symposium held during the World Water and Environmental Resources Congress in Philadelphia, Pennsylvania, June 24-26, 2003*, 273-283. Edited by S. Mishra. American Society of Civil Engineers, Reston, VA.

Ward, D.S., D.R. Buss, J.W. Mercer, and S.S. Hughes. 1987. Evaluation of a groundwater corrective action at the Chem-Dyne hazardous waste site using a telescope mesh refinement modeling approach. *Water Resources Research* 23(4):603-617.

Appendix B. Development of Withdrawal Database

B.1. Data Sources

B.1.1. Illinois

B.1.1.1. Data Obtained from Previous Modeling Studies

Withdrawal rates for Illinois wells during the period 1864 through 1963 were obtained as an electronic file from Stephen L. Burch of the Illinois State Water Survey (ISWS) (personal communication, 2002). Data derived from this source represent withdrawals from deep wells that were active during this period. Pumping activity is represented by seven idealized pumping centers, with pumping totals equivalent to aggregated total deep well withdrawals from surrounding areas. These aggregated withdrawals are intended to represent those within the area of Cook, DuPage, northern Grundy, Kane, Kendall, Lake, McHenry, and Will Counties, Illinois.

These data were employed in a previous modeling study by Burch (1991). Burch had obtained the values from an even earlier modeling study by Prickett and Lonquist (1971), who appear to have approximated the 1864-1958 values from plots of withdrawal rates published by Suter et al. (1959) and based the 1959-1963 withdrawal rates on pumping data collected by the ISWS. Prickett and Lonquist (1971) also augmented the pumping records published by Suter et al. (1959) by adding a time record of approximate withdrawal rates at a seventh pumping center (Batavia) to the previous six pumping centers, each referred to by city name (Chicago, Joliet, Elmhurst, Des Plaines, Elgin, and Aurora) (Figure B-1).

B.1.1.2. Hardcopy Data

Hardcopy records of groundwater withdrawals in 20 northern Illinois counties, compiled by the ISWS, were entered into a computer database and employed to represent groundwater withdrawals in Illinois during 1964 through 1979 (Figure B-2). These withdrawal records represent wells supplying community and non-community public water systems; commercial and industrial facilities; and irrigation systems for nurseries, athletic fields, and golf courses, but not grain crops such as corn and soybeans. The records were the basis for discussions of groundwater withdrawals in northern Illinois appearing in ISWS reports published in the 1960s, 1970s, and 1980s (Sasman and Baker, 1966; Sasman et al., 1962a; Sasman et al., 1974; Sasman et al., 1973; Sasman et al., 1982; Sasman et al., 1977; Sasman et al., 1967; Sasman et al., 1961; Sasman et al., 1962b).

All records of withdrawals from deep wells in the hardcopy dataset were included in the modeling database. Records of withdrawals from shallow wells were included in the modeling database only if the wells are located within the area of the shallow aquifer withdrawal accounting region (SAWAR), a region delineated for this project using the natural hydrologic boundaries of watersheds and enclosing the regional model nearfield (Figure B-3). The SAWAR was employed to limit the scope of the database to include shallow wells only if the wells are near enough to the nearfield of the regional model that they would be likely to influence groundwater flow in the area. The SAWAR was trimmed to exclude a small area of the watershed-delimited area in extreme southwestern Michigan.

B.1.1.3. ISWS Public-Industrial-Commercial Survey (PICS) Database

Withdrawal rates for Illinois wells within the regional model domain during the period 1980 through 2003 were obtained from the ISWS Public-Industrial-Commercial Survey (PICS) Database (Figure B-4). This Microsoft Access (Microsoft Corporation, 2003a) database is compiled from withdrawal data collected annually through the ISWS Illinois Water Inventory Program (IWIP) by voluntary submission of a form tailored to each (known) major water user in the state. For the year 2000, IWIP received a 70 percent return on inquiries sent to 2832 facilities. Withdrawals are estimated for non-respondents on the basis of data submitted during previous years, so that a fairly complete water use picture for any one year is compiled. Large changes in reported water use (> 10 percent) from one year to the next trigger a follow-up call to the facility operator to verify the accuracy of the reported withdrawal rates and to inquire about reasons for growth or decline.

All records of withdrawals from deep wells were included in the modeling database, but records of withdrawals from shallow wells were included in the modeling database only if the wells are located within the SAWAR (Figure B-3).

B.1.1.4. Assumed Withdrawals from Additional Deep Wells in Northeastern Illinois

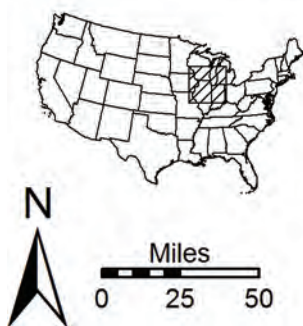
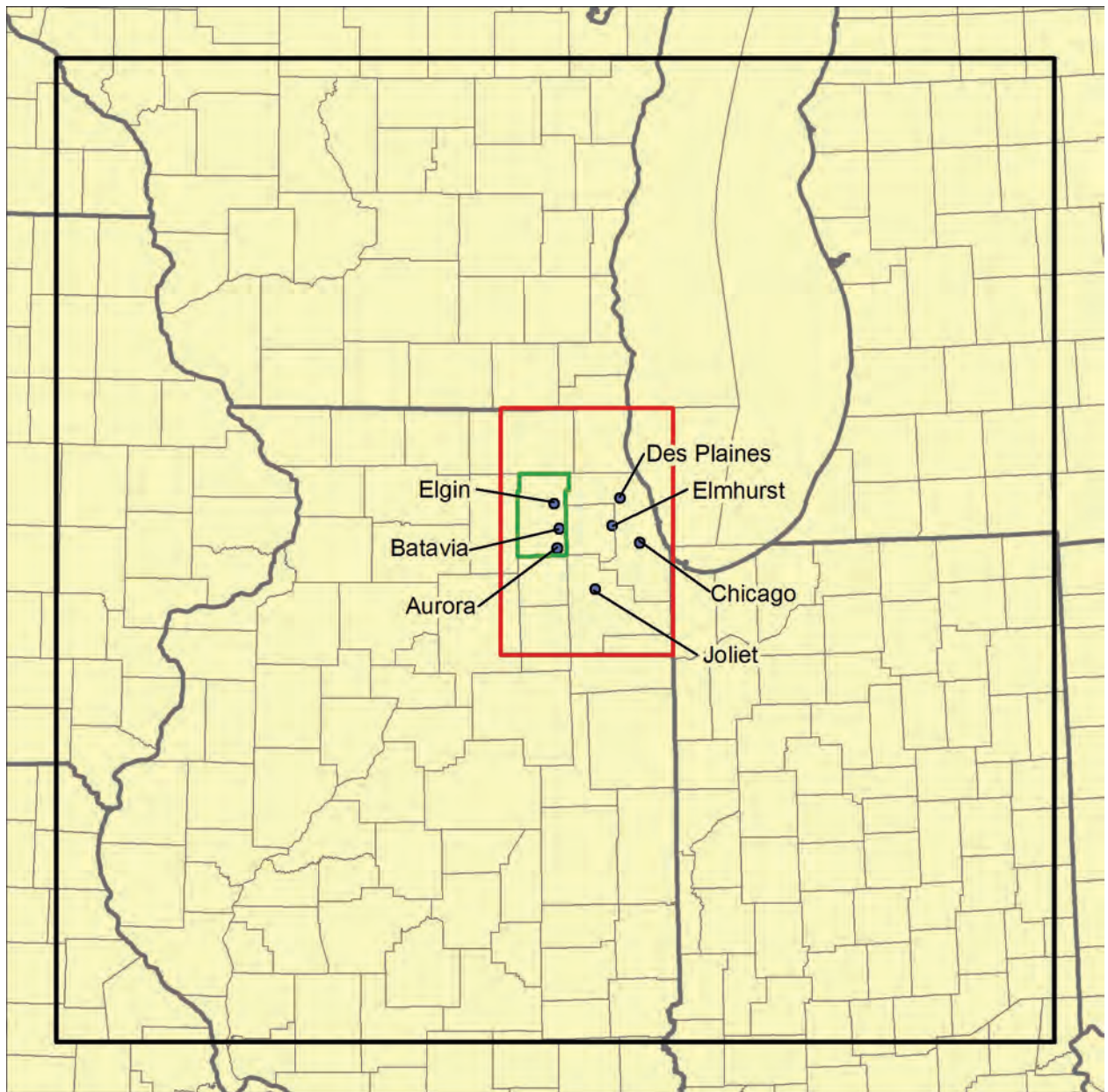
Withdrawal rates from other Illinois wells were estimated for the years 1864 through 2003. Withdrawals were estimated for deep wells represented by records in the ISWS Private Well Database, a database generally containing records of low-capacity wells supplying households and commercial facilities. Withdrawals were not estimated for shallow wells because about 85 to 90 percent of groundwater withdrawn from such wells is estimated to be returned to the shallow units via on-site wastewater disposal (Pebbles, 2003; United States Environmental Protection Agency Region V, 1975), with little net effect on groundwater flow.

B.1.2. *Indiana*

All withdrawal data for Indiana wells were obtained from a database of groundwater withdrawals purchased from the Indiana Department of Natural Resources in June 2003 (personal communication, 2003). All records of withdrawals from deep wells in the Indiana database were included in the modeling database, although only a single such well was recorded in the database. Records of withdrawals from shallow wells were included in the modeling database only if the wells are located within the SAWAR (Figure B-3). The database is limited to records of withdrawals during the years 1985 through 2002. Earlier records of withdrawals from Indiana wells are not available.

B.1.3. *Wisconsin*

Withdrawal rates for wells in Wisconsin were obtained from groundwater flow model input files received from the Wisconsin Geological and Natural History Survey (personal communication, 2002) and developed to model groundwater flow in southeastern Wisconsin as described by Feinstein et al. (2005a; 2005b). These files represent average annual withdrawal rates from wells only in southeastern Wisconsin for 1864 through 2002. Withdrawal rates in the files are aggregated into time steps of durations ranging from 5 to 20 years.



- Pumping center
- Regional model domain
- Regional model nearfield
- Kane County

Figure B-1. Locations of pumping centers represented by Illinois withdrawal data derived from earlier modeling studies.

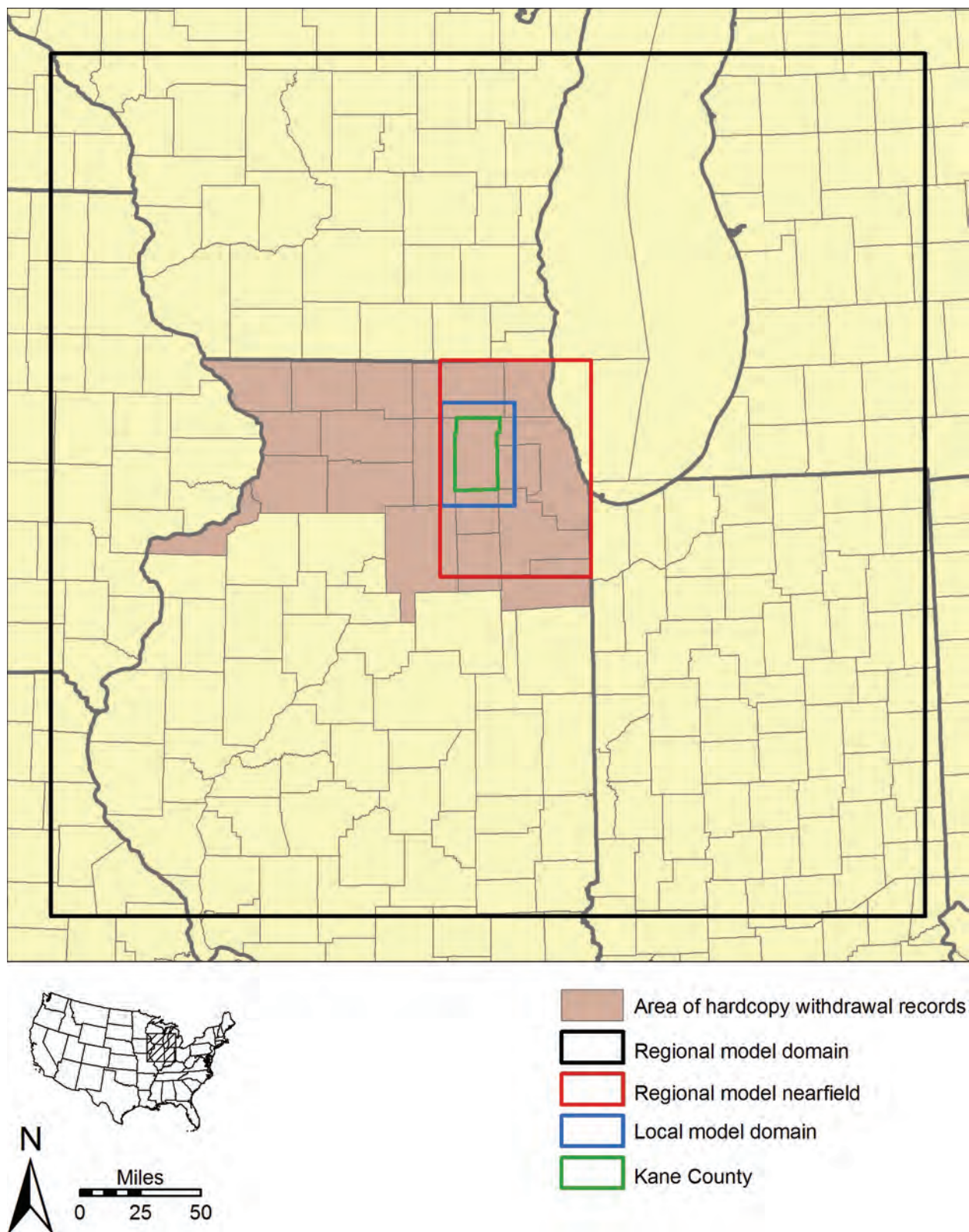


Figure B-2. Area of hardcopy withdrawal records used to represent groundwater withdrawals in Illinois from 1964 through 1979.

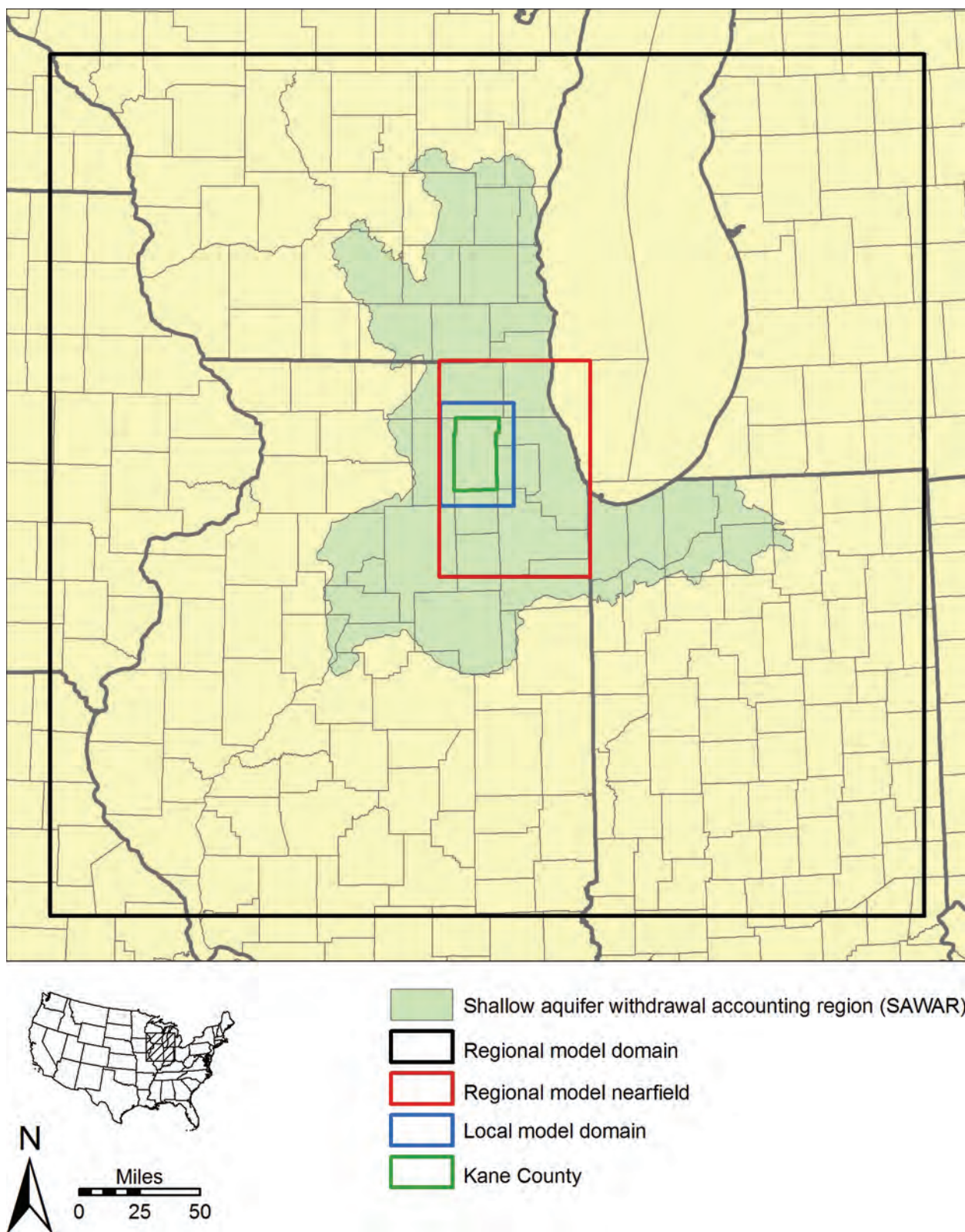


Figure B-3. Shallow aquifer withdrawal accounting region (SAWAR).

B.2. Data Processing

B.2.1. Illinois

B.2.1.1. Data Obtained from Previous Modeling Studies

Withdrawal data provided by Burch (personal communication, 2002) specified pumping center locations as row and column coordinates for his model (Burch, 1991). These location coordinates were converted to the ILLIMAP coordinate system in the present study using Appendix B in Burch's report (Burch, 1991), which lists ILLIMAP x - and y -coordinates for the rows and columns in his model.

Withdrawal totals for the seven pumping centers covered by the dataset showed withdrawals from the hydrostratigraphic units between the top of the Ancell Unit and the bottom of the Ironton-Galesville Unit. The withdrawal totals did not include the component of water contributed from overlying and underlying units to the wells represented in the dataset, many of which were open to bedrock units as shallow as the Silurian-Devonian Carbonate Unit and as deep as the Mt. Simon Unit (Suter et al., 1959). The withdrawal totals were therefore increased, using data given in Suter et al. (1959) to reflect water contributed to the wells by units above the Ancell Group and below the Ironton-Galesville Sandstone. Plots of pumping through time at the six pumping centers described by Suter et al. (1959) (their Figure 36, page 61) suggest that the proportion of water derived from the overlying and underlying units is approximately constant through time. For the present study, total rates of groundwater withdrawal at the pumping centers were based on the 1958 proportions given in Figure 37 (page 62) of Suter et al. (1959) (Table B-1). Since the Batavia pumping center was not considered by Suter et al. (1959), total groundwater withdrawals were based on the average of the proportion of groundwater pumped from the Ancell to Ironton-Galesville interval estimated by Suter et al. for the nearby Elgin and Aurora pumping centers. A total of 700 annual withdrawal records was obtained from the data compiled for previous modeling studies.

Since the pumping centers are meant to simulate deep wells open to all aquifers from the top of the Silurian-Devonian Carbonate Unit downward through the Mt. Simon Unit, the seven pumping centers were assumed to be open to model layers 5 through 17. The source interval was assumed to extend no deeper than model layer 17 since only the upper portion of the Mt. Simon Unit contains fresh water in Illinois (Illinois State Water Survey and Hittman Associates, 1973; Schicht et al., 1976; Suter et al., 1959).

B.2.1.2. Hardcopy Data

Data from the hardcopy records employed to represent groundwater withdrawals in Illinois from 1964 through 1979 were entered into electronic spreadsheets using Microsoft Excel (Microsoft Corporation, 2003b) and then imported into a Microsoft Access database application (Microsoft Corporation, 2003a) for additional data processing. The hardcopy records represent withdrawals from 3223 wells.

The entered withdrawal records required augmentation with (1) x - and y -coordinates in the ILLIMAP projection (see Table B-1) of the wells represented in the hardcopy records; and (2) characterization of the source interval of the represented wells. If the wells were included in the network of wells that were the source of water-level measurements for shallow-aquifer potentiometric-surface mapping in Kane County (Locke and Meyer, 2005), the x - and y -coordinates were based on surveying conducted for the mapping effort. Otherwise, the coordinates and open-interval characterizations were obtained from existing ISWS electronic

databases, if records of the wells were included in these other databases. In instances wherein records of the wells were not present in the other databases, or wherein the existing databases do not include records of the wells, assumptions were made to compensate for the missing data. The two existing ISWS databases consulted for the project are (1) the PICS (Public-Industrial-Commercial) Database, a database generally containing records of high-capacity wells supplying public water systems and self-supplied industrial and commercial facilities (see Section B.1.1.3); and (2) the Private Well Database, a database generally containing records of low-capacity wells supplying households and commercial facilities. Although the populations of wells recorded in these two databases are generally mutually exclusive, a small overlap exists, and in the event that a record of the same well appears in both databases, preference was given to the data included in the more detailed PICS Database. A hardcopy record of withdrawals from a well was linked to an entry in the PICS or Private Well Database on the basis of information on the hardcopy record, which usually included the following: owner name; local well identification number; location description giving county name, township, range, section, and 10-acre plot (Appendix I); dates of drilling and abandonment; and a rough characterization of the open interval. Of the 3223 wells represented by the hardcopy withdrawal records, 2728 (85 percent) are represented by records in the PICS Database, and 456 (14 percent) are represented in the Private Well Database, leaving only 39 wells (1 percent) not recorded in either database.

Although both the PICS and Private Well Databases contain fields for ILLIMAP x - and y -coordinates, these fields are not always completed. When the fields are completed, the basis for the coordinate determinations is not documented, but interviews with ISWS staff indicate that most of these entries are computer estimates based on reported location descriptions giving county name, township, range, section, and 10-acre plot (Appendix I), as well as footages from section corners sometimes reported on well records. In a few cases, the coordinates are based on optical surveying. If the fields are completed in the PICS and/or Private Well Databases for a well represented by a hardcopy withdrawal record, the x - and y -coordinates were copied, giving preference to the entries in the PICS Database in the event that the well is recorded in both databases. If ILLIMAP coordinates are not listed in the PICS and Private Well Databases, the coordinates were estimated using ISWS and ISGS computer programs that base coordinate determinations on county name, township, range, section, and 10-acre plot (Appendix I). The estimated coordinates correspond to the center of the described 10-acre plot. It was necessary to use both ISWS and ISGS programs to generate ILLIMAP coordinates, since the ISWS program, which was given preference, was not yet functional for all areas of Illinois. In a few cases, a plot designator was missing from all location descriptions, both in the hardcopy withdrawal record and the existing ISWS electronic databases. In such cases, the ISWS files were searched for location information permitting identification of the 10-acre plot in which the well is located. If such information was not available, coordinates were calculated for the center of the section in which the well is located. In still rarer cases, both section and plot designators were not available, thus coordinates were calculated for the center of the township in which the well is located. As mentioned in the preceding paragraph, if the well location was surveyed for purposes of potentiometric surface mapping (Locke and Meyer, 2005), the x - and y -coordinates assigned to the well were based on surveying conducted for the mapping effort.

For the 39 wells represented by hardcopy withdrawal records that are not recorded in either the ISWS PICS or Private Well Databases, computer estimates of the x - and y -coordinates of the wells were developed using location data included on the hardcopy withdrawal records. These annotations are typically adequate for estimation of coordinates, but in some cases they do

not identify the 10-acre plot in which the well is located. In these cases, coordinates were calculated for the center of the section in which the well is located, as discussed in the preceding paragraph.

Source interval characterizations, in the form of four-digit aquifer codes consistent with ISWS conventions (Appendix F), were assigned to the wells recorded in the ISWS PICS Database on the basis of entries in a field in that database containing such codes. This field is not always completed, however, and many aquifer codes used in the PICS Database denote unspecified stratigraphic units within an interval encompassing several stratigraphic units, requiring substitution of a secondary aquifer code (here referred to as a *project aquifer code*) denoting a specific interval directly translatable to the layer scheme of the regional model. For example, the aquifer code 6080 is often employed in the PICS Database to indicate a source interval understood to be the interval commonly recognized in Illinois as the “deep bedrock”—an interval including any unit underlying the Ordovician Maquoketa Group (including the Eau Claire Formation and Mt. Simon Sandstone, despite the fact that the two-character code 80 is meant to denote Cambrian units above the Eau Claire Formation). Of the 2728 wells having hardcopy withdrawal records covering the period 1964-1979 and appearing in the PICS Database, 190 had been assigned such nonspecific aquifer codes in the PICS Database. Each of these wells was researched using hardcopy well logs and other records on file at the ISWS, electronic database records of nearby wells, annotations on the withdrawal records themselves, and available geologic mapping in order to substitute a project aquifer code that could be directly translated to a source interval characterization based on the layer scheme of the regional model (Table B-3). Of the 2728 wells having hardcopy withdrawal records and appearing in the PICS Database, 12 had been assigned no aquifer code in the PICS Database. These wells were similarly researched, and a project aquifer code was assumed that could be directly translated to the layer scheme of the regional model.

The 456 wells having hardcopy withdrawal records and are recorded in the ISWS Private Well Database were assigned a four-digit aquifer code consistent with ISWS conventions (Appendix F) as an intermediate step toward characterizing the source intervals using the model layer scheme of the regional model. These assignments were based principally on hardcopy well logs and other records on file at the ISWS, annotations on the withdrawal records themselves, and available geologic mapping. Similarly, the 39 wells not recorded in either the ISWS PICS or Private Well Databases were assigned annotations on the hardcopy withdrawal records and well construction conventions in nearby areas, most notably at the facility served by the well.

Four-digit ISWS standard aquifer codes, which were specific enough to permit translation to the regional model layer scheme, were assigned to the 3223 wells represented by the hardcopy records containing 1964-1979 withdrawal data. These codes were then translated to open interval characterizations referencing the regional model layer scheme. Open intervals were characterized by identifying the uppermost and lowermost model layers to which each well is open based on the key shown in Table B-4. Several assumptions guided this translation. First, wells assigned aquifer codes denoting an open interval in the Quaternary Unit were considered to be open to model layers 2 and 3, but not model layer 1—the uppermost one-third of the Unit. Without consulting records of the many wells open to the Quaternary Unit, we consider it improbable that most of these wells are open to the shallowest Quaternary materials. Second, wells assigned aquifer codes indicating an open interval extending into the Elmhurst Member of the Eau Claire Formation or Mt. Simon Formation were assumed to be open to model layer 17, which represents the upper one-fourth of the Mt. Simon Unit (equivalent to the Mt. Simon Formation).

Although it is possible that some of these wells do not penetrate the Mt. Simon Formation, without consulting numerous individual well logs the authors assume that most or all of the wells do penetrate the Mt. Simon Formation. Third, wells assigned four-digit aquifer codes indicating that exposure to any stratigraphic unit represented by multiple model layers (other than the Quaternary Unit and Mt. Simon Unit as discussed above) are considered to be open to all of the layers representing that unit. For example, wells assigned code 61 are assumed to be exposed to both model layers 8 and 9, representing the Maquoketa Group.

A total of 37,800 annual withdrawal records were obtained from the hardcopy data. The distribution of the wells covered by these data is shown in Figure B-5 and Figure B-6.

Table B-1. Proportion of Groundwater Derived from (1) Ancell Unit through Ironton-Galesville Unit (Column D) and (2) Units above Ancell Unit and Below Ironton-Galesville Unit (Column E) at Northeastern Illinois Pumping Centers (Suter et al., 1959)

<i>Pumping Center</i>	<i>Column A: 1958 Total, Silurian-Devonian Carbonate Unit through Mt. Simon Unit (ft³/d) (Suter et al., 1959)¹</i>	<i>Column B: 1958 Total, Ancell Unit through Ironton-Galesville Unit (ft³/d) (Suter et al., 1959)¹</i>	<i>Column C: Ratio of 1958 Totals [A/B])</i>	<i>Column D: Proportion Derived From Ancell Unit through Ironton-Galesville Unit (%) [B/(A+B)]</i>	<i>Column E: Proportion Derived From Units Above Ancell Unit and Below Ironton-Galesville Unit (%) [A/(A+B)]</i>
Aurora	1871800	976010	1.92	52%	48%
Chicago	3128580	1470700	2.13	47%	53%
Des Plaines	909160	467950	1.94	51%	49%
Elgin	1082970	548170	1.98	51%	49%
Elmhurst	1310260	708610	1.85	54%	46%
Joliet	1871800	1550920	1.21	83%	17%

¹Figure 37, page 62 (Suter et al., 1959)

Table B-2. Watersheds Included in the Shallow Aquifer Withdrawal Accounting Region (SAWAR)

<i>Eight-Digit Hydrologic Unit Code</i>	<i>Cataloging Unit Name (Seaber et al., 1987)</i>
07090001	Upper Rock. Illinois, Wisconsin.
04040003	Milwaukee. Wisconsin.
07120006	Upper Fox. Illinois, Wisconsin.
04040002	Pike-Root. Illinois, Wisconsin.
07120004	Des Plaines. Illinois, Wisconsin.
07090006	Kishwaukee. Illinois, Wisconsin.
07120003	Chicago. Illinois, Indiana.
04040001 ¹	Little Calumet-Galien. Illinois, Indiana, Michigan.
07120007	Lower Fox. Illinois.
07120001 ¹	Kankakee. Illinois, Indiana, Michigan.
07130001	Lower Illinois-Senachwine Lake. Illinois.
07120005	Upper Illinois. Illinois.
07130002	Vermilion. Illinois.

¹Trimmed to exclude portion of watershed in Michigan

Table B-3. Project Aquifer Codes Substituted for Nonspecific Aquifer Codes Appearing in ISWS PICS Database

<i>Nonspecific Aquifer Code from PICS Database</i>	<i>Project Aquifer Code</i>	<i>Number of Wells</i>
__97	6697	3
6060	6366	10
6060	6666	2
6070	6370	3
6080	6161	1
6080	6166	1
6080	6365	4
6080	6366	49
6080	6381	3
6080	6383	2
6080	6387	54
6080	6393	23
6080	6397	2
6080	6566	4
6080	6666	7
6080	6681	1
6080	6687	7
6080	6693	2
6080	6697	2
6080	7087	1
6080	7187	2
6087	6387	1
6090	6393	6
6093	6393	1
6097	6397	1
__66	6366	1
__97	6697	3

Table B-4. Characterization of Source Interval Based on ISWS Aquifer Code

<i>Project Aquifer Code</i>	<i>Uppermost Model Layer</i>	<i>Lowermost Model Layer</i>
0101	2	3
0104	2	3
0105	2	3
0106	2	3
0109	2	3
0150	2	7
0156	2	7
0161	2	9
0163	2	11
0165	2	11
0166	2	12
2020	4	4
2061	4	9
2063	4	11
2065	4	11
2066	4	12
3040	4	4
4051	4	7
4066	4	12
4087	4	15
5050	5	7
5063	5	11
5065	5	11
5066	5	12
5156	5	7
5161	5	9
5163	5	11
5166	5	12
5171	5	13
5173	5	13
5193	5	16
5555	5	7
5556	5	7
5650	5	7
5656	5	7
5661	5	9
5663	5	11
5665	5	11
5666	5	12
5671	5	13
5675	5	13
5680	5	15

**Table B-4. Characterization of Source Interval Based on ISWS Aquifer Code
(Continued)**

<i>Project Aquifer Code</i>	<i>Uppermost Model Layer</i>	<i>Lowermost Model Layer</i>
5681	5	14
5683	5	14
5687	5	15
5693	5	16
5697	5	17
6065	10	11
6066	10	12
6161	8	9
6163	8	11
6165	8	11
6166	8	12
6171	8	13
6175	8	13
6187	8	15
6193	8	16
6197	8	17
6363	10	11
6365	10	11
6366	10	12
6370	10	13
6370	10	13
6371	10	13
6373	10	13
6375	10	13
6381	10	14
6383	10	14
6387	10	15
6393	10	16
6397	10	17
6565	10	11
6566	10	12
6573	10	13
6575	10	13
6581	10	14
6587	10	15
6593	10	16
6597	10	17
6666	12	12
6670	12	13
6671	12	13
6673	12	13
6675	12	13

**Table B-4. Characterization of Source Interval Based on ISWS Aquifer Code
(Continued)**

<i>Project Aquifer Code</i>	<i>Uppermost Model Layer</i>	<i>Lowermost Model Layer</i>
6681	12	14
6683	12	14
6687	12	15
6693	12	16
6697	12	17
7073	13	13
7075	13	13
7080	13	15
7087	13	15
7093	13	16
7097	13	17
7171	13	13
7173	13	13
7175	13	13
7177	13	13
7181	13	14
7187	13	15
7193	13	16
7197	13	17
7373	13	13
7375	13	13
7377	13	13
7381	13	14
7387	13	15
7393	13	16
7575	13	13
7581	13	14
7587	13	15
7593	13	16
7597	13	17
7777	13	13
7787	13	15
7793	13	16
7797	13	17
8181	13	14
8187	13	15
8193	13	16
8197	13	17
8387	14	15
8393	14	16
8397	14	17
8787	15	15

**Table B-4. Characterization of Source Interval Based on ISWS Aquifer Code
(Concluded)**

<i>Project Aquifer Code</i>	<i>Uppermost Model Layer</i>	<i>Lowermost Model Layer</i>
8793	15	16
8797	15	17
9397	16	17
9797	17	17

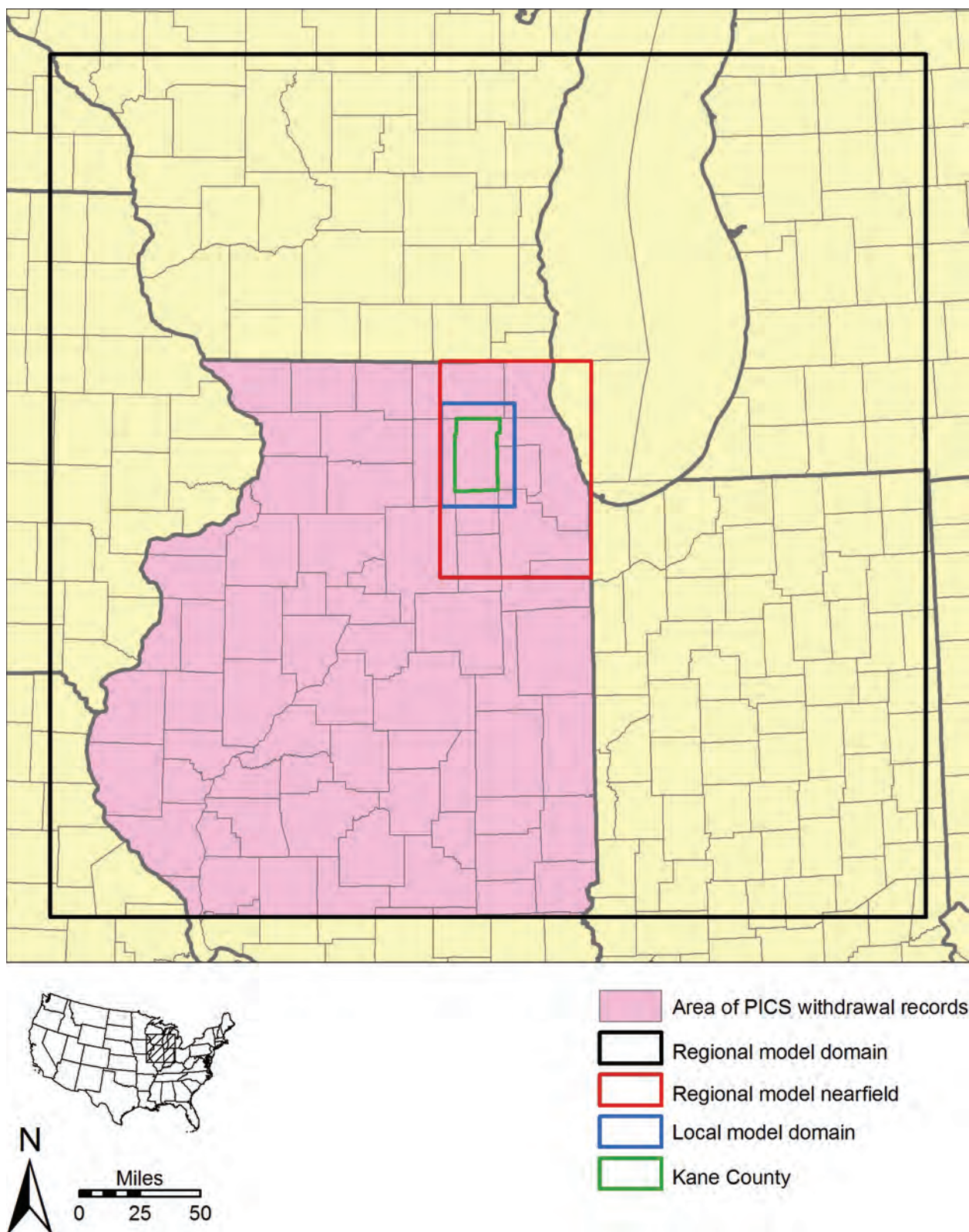


Figure B-4. Area of withdrawal records obtained from the ISWS PICS Database used to represent groundwater withdrawals in Illinois from 1980 through 2003.

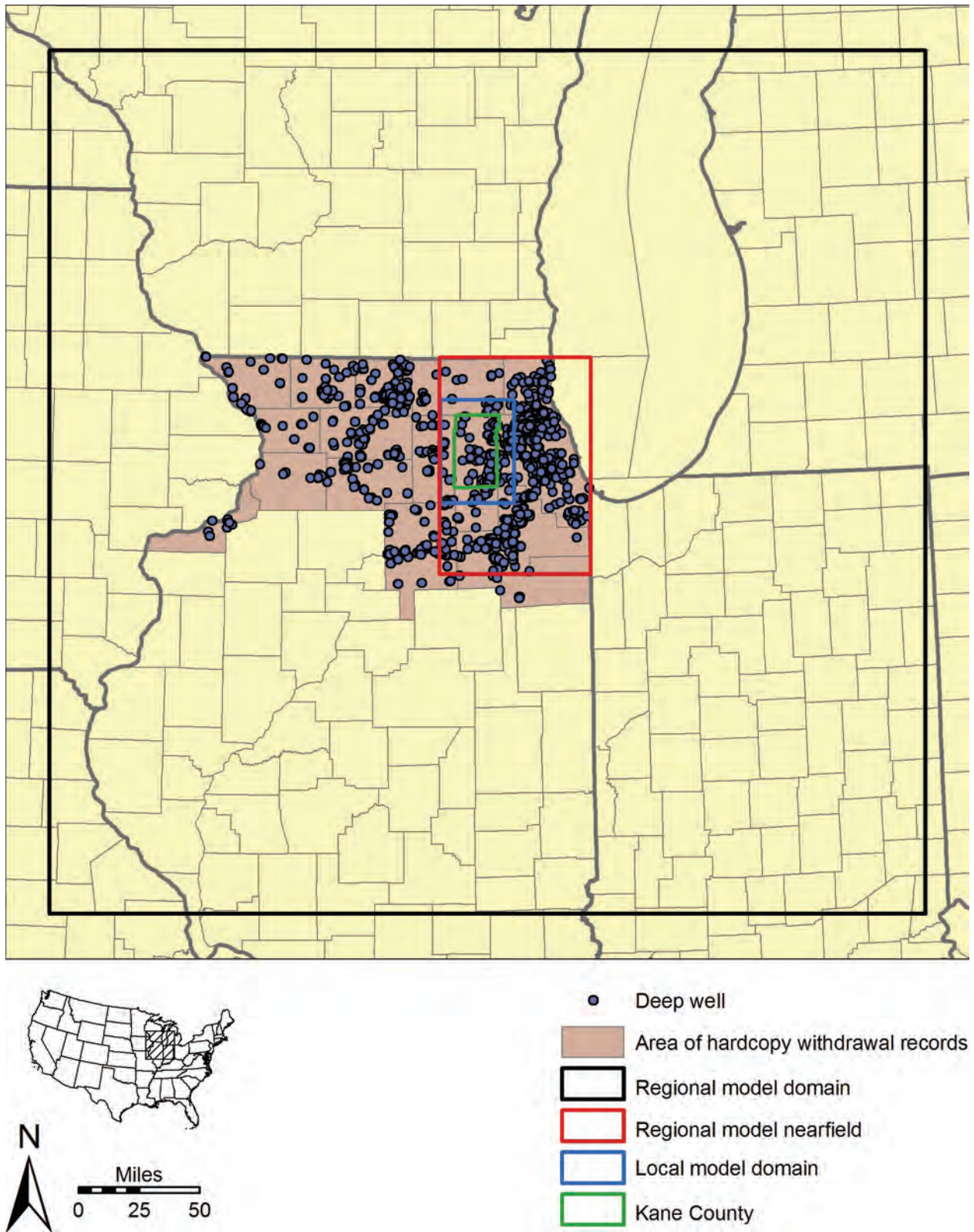


Figure B-5. Deep wells in Illinois having withdrawals documented by hardcopy records spanning the period 1964-1979.

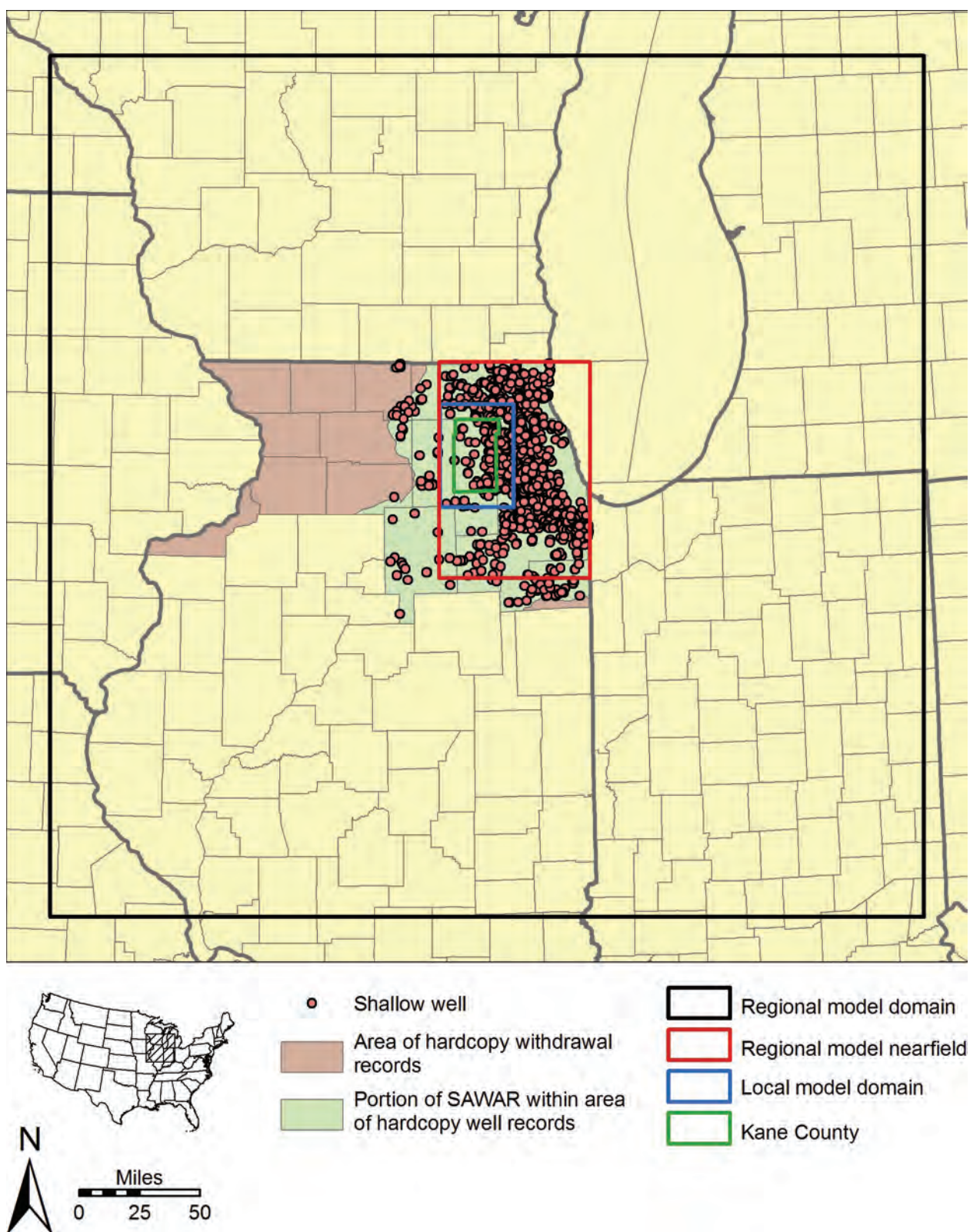


Figure B-6. Shallow wells in Illinois having withdrawals documented by hardcopy records spanning the period 1964-1979.

B.2.1.3. ISWS Public-Industrial-Commercial Survey (PICS) Database

Withdrawal data derived from the ISWS PICS Database were processed in much the same way as the hardcopy-derived data discussed in the previous section. In order to employ the data in project groundwater flow modeling, many withdrawal records obtained by querying the PICS Database required augmentation with (1) ILLIMAP x - and y -coordinates and (2) characterization of the source interval of the represented wells. The PICS Database contains ILLIMAP coordinates for many, but not all, of the wells represented in it, and these coordinates are employed in project modeling if available; it was necessary to estimate the missing coordinates. Similarly, ISWS aquifer codes (Appendix F) are contained in the PICS Database for some, but not all, wells. If suitably specific, these aquifer codes were employed directly for source interval characterization, but—as discussed in the preceding section—many of the aquifer codes used in the PICS Database denote unspecified stratigraphic units within an interval encompassing several stratigraphic units. For wells for which the PICS Database contains a non-specific aquifer code, it was necessary to substitute a project aquifer code denoting a specific interval that is directly translatable to the layer scheme of the regional model.

If ILLIMAP coordinates were not listed in the PICS Database, they were estimated using ISWS and ISGS computer programs that base coordinate determinations on county name, township, range, section, and 10-acre plot (Appendix I), as discussed in the preceding section on 1964-1979 Illinois withdrawal data derived from hardcopy sources. If a well location was surveyed for purposes of potentiometric surface mapping (Locke and Meyer, 2005), the x - and y -coordinates assigned to the well are based on surveying conducted for the mapping effort.

Using the same approach discussed in the preceding section, source interval characterizations, in the form of four-digit aquifer codes consistent with ISWS conventions (Appendix F), were assigned to withdrawal records obtained from the ISWS PICS Database on the basis of entries in a field in that database containing such codes. The PICS Database entries were used without alteration if they were specific enough to permit direct translation to the regional model layer scheme. Based on research of hardcopy well logs and other records on file at the ISWS, electronic database records of nearby wells, and available geologic mapping, project aquifer codes were substituted for nonspecific aquifer codes in the PICS Database. Of the 5222 wells for which withdrawal records were obtained from the PICS Database, 192 were assigned such nonspecific aquifer codes in the database. Each of these wells was assigned a project aquifer code that could be directly translated to a source interval characterization based on the layer scheme of the regional model (Figure B-3). Of the 5222 wells for which withdrawal records were obtained from the PICS Database, 84 were assigned no aquifer code in the PICS Database. A project aquifer code was also assumed for these wells.

In order to more completely represent recent groundwater use in the Illinois portion of the regional model domain, groundwater withdrawals were estimated for the years 1980 through 2003 for selected wells listed in the ISWS PICS Database, using an automated procedure. Withdrawals were estimated for wells during years when a facility (for example, a public water system or industrial/commercial facility) did not report withdrawals to the ISWS. The PICS Database contains a field indicating the status of a well and containing a one-character code such as *A* (abandoned), *U* (unused), *E* (emergency), etc. This field was employed to further restrict the population of wells for which estimates were developed to wells having a status code of *I* (in use). Application of the above criteria resulted in the identification of a population of wells for which withdrawal estimates were needed and, for each well, a year or years for which withdrawal estimates were needed.

Estimates of annual withdrawals were developed for 1323 of the 5222 wells for which withdrawal data were obtained from the PICS Database. Alternatively, 8379 estimates were developed for this project from the PICS Database data, as compared to 86,306 reported withdrawal values used for this project from the database. An estimation window was defined for each of these wells using initiation and sealing dates contained in the PICS Database as the first and last years of the window. In cases wherein these fields are not completed, the first year of the estimation window was assumed to be 1980 and the last year was assumed to be 2003. Estimates were developed using one of three different approaches designed for the following situations (Figure B-7): (1) the estimate was for one or more years at the start of the estimation window, with reported withdrawals available only for later years; (2) the estimate was for one or more years at the end of the estimation window, with reported withdrawals available only for earlier years; or (3) the estimate was for one or more years within the estimation window, with reported withdrawals available for both earlier and later years. Withdrawals for years at the start of the estimation window were estimated to be equal to the first year of reported withdrawals for the well. Similarly, withdrawals for years at the end of the estimation window were estimated to be equal to the last year of reported withdrawals. Withdrawals for years within the estimation window, with reported withdrawals available for both earlier and later years, were estimated by linear interpolation. Figure B-8 shows the sum of estimated withdrawals based on ISWS PICS Database records and the total of the estimates and the reported withdrawal values obtained from the PICS Database for the project.

Distribution of wells covered by the PICS Database withdrawal records and associated estimates are shown in Figure B-9 and Figure B-10.

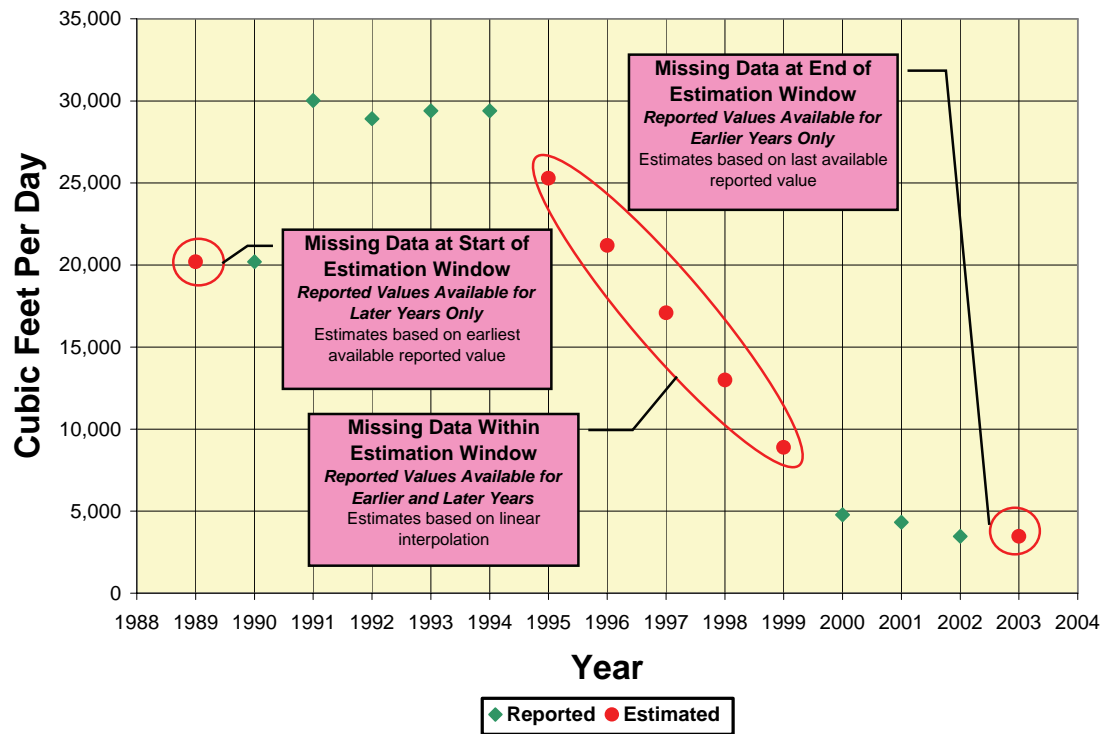


Figure B-7. Example of methods used for estimation of 1980-2003 Illinois withdrawals for years of non-reporting by facilities to the Illinois Water Inventory Program, which provides data to the ISWS PICS Database.

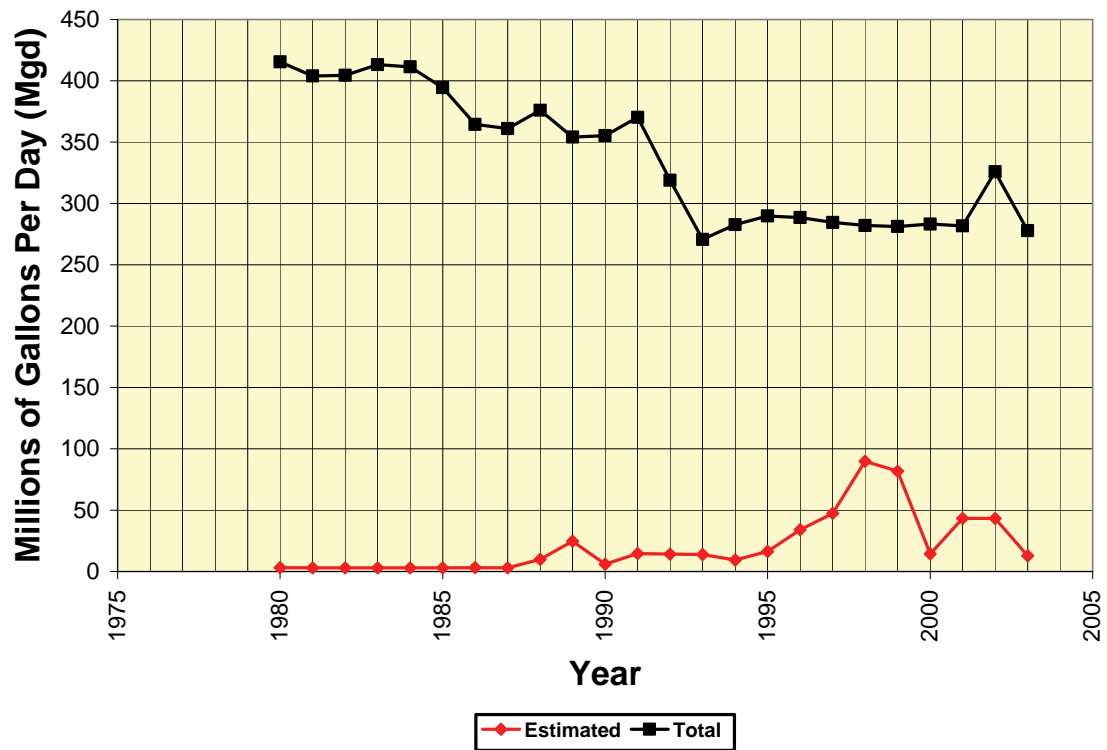


Figure B-8. Estimated withdrawals from wells recorded in ISWS PICS Database represented in the regional model, 1980-2003, and total withdrawals, including both reported and estimated withdrawals.

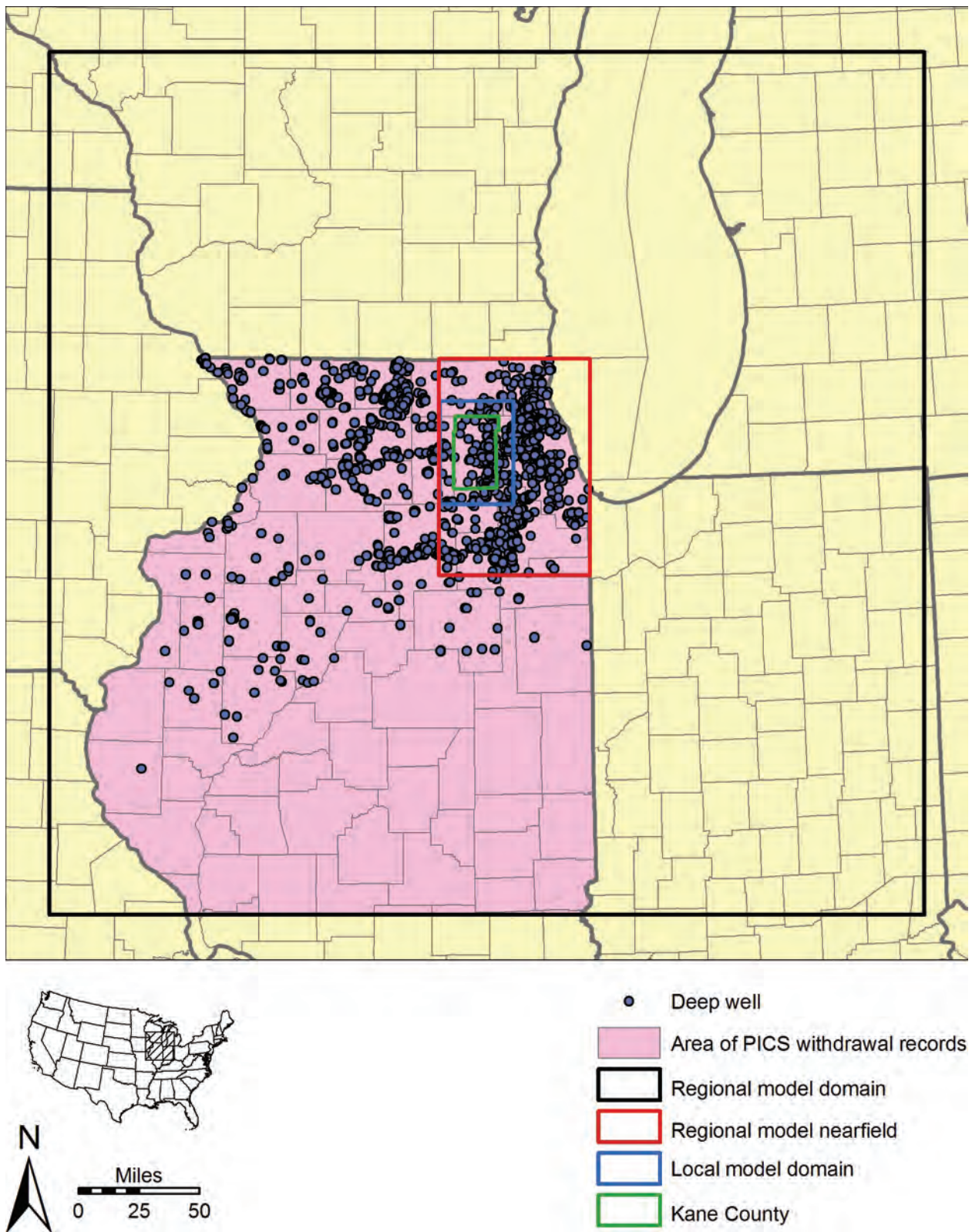


Figure B-9. Deep wells in Illinois having 1980-2003 withdrawals documented by ISWS PICS Database.

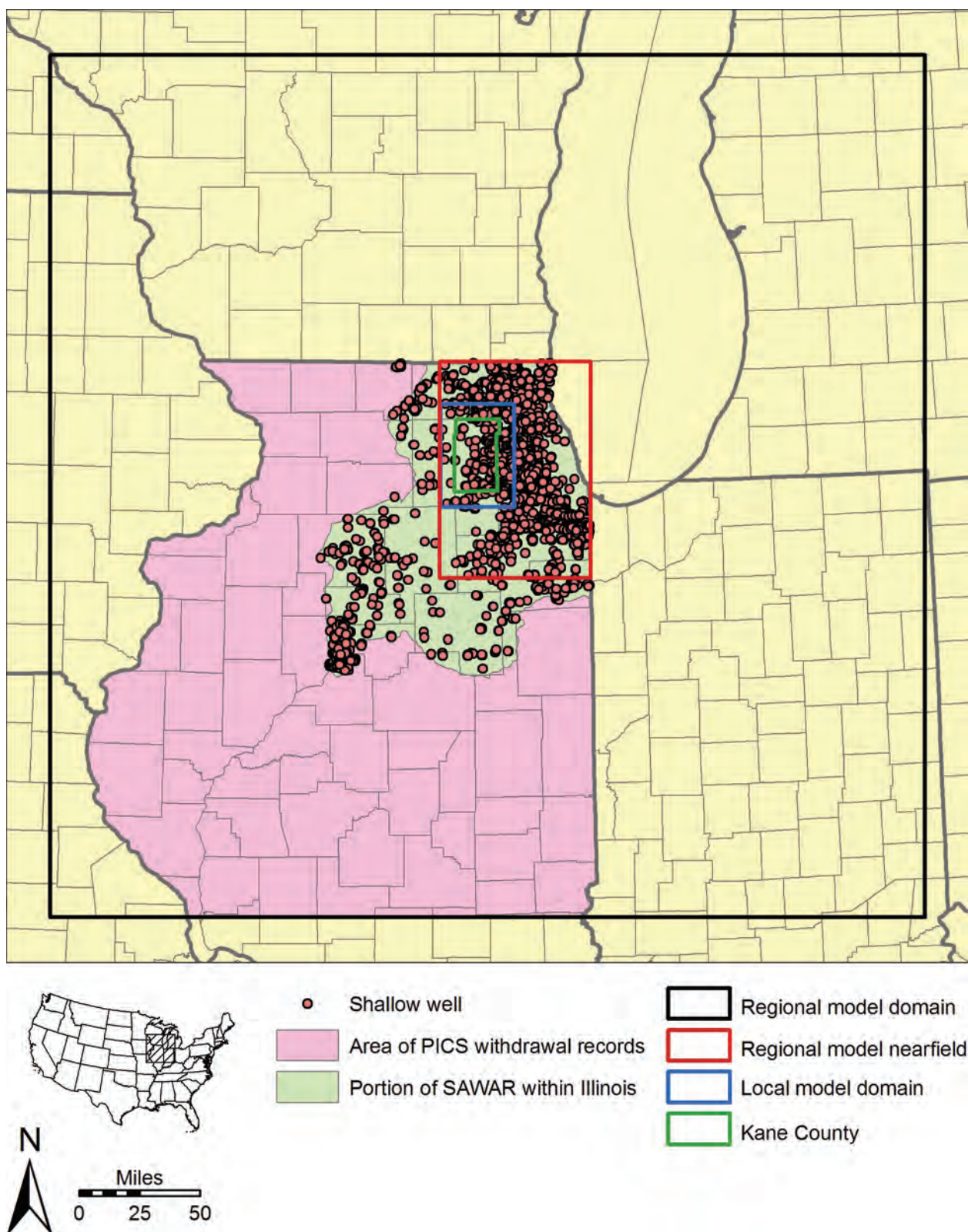


Figure B-10. Shallow wells in Illinois having 1980-2003 withdrawals documented by ISWS PICS Database.

B.2.1.4. Assumed Withdrawals from Deep Domestic Wells in Northeastern Illinois

The ISWS Private Well Database was queried to obtain a list of domestic and commercial water-supply wells within counties partially or completely contained within the nearfield of the regional groundwater flow model (the Illinois counties of Boone, Cook, DeKalb, DuPage, Grundy, Kane, Kankakee, Kendall, Lake, LaSalle, McHenry, and Will). The query results were reduced to a manageable size by applying rough depth criteria to remove records of wells of insufficient depth to penetrate the bottom of the Galena-Platteville Unit. Thus records of wells in Cook, Lake, and Will Counties were removed from the list if their depth was less than 500 feet (ft), and records of wells in DuPage, Kane, and McHenry Counties were removed if they were shallower than 400 ft. Stricter criteria were applied later to eliminate additional wells not penetrating the bottom of the Galena-Platteville Unit. All wells in Boone, DeKalb, Grundy, Kankakee, Kendall, and LaSalle Counties were retained in the query results.

If not already included in the query results, ILLIMAP x - and y -coordinates were estimated for these wells using ISWS and ISGS computer programs that base coordinate determinations on county name, township, range, section, and 10-acre plot (Appendix I). The estimated coordinates correspond to the center of a 10-acre plot.

These coordinates permitted the query results, modified to remove shallow wells, to be imported and plotted in ArcGIS, converted to shapefile format and further modified. First, the query results were reduced by removing all records of wells located outside the regional model nearfield. Second, a spatial join was executed to add estimates of the elevation of the top of each regional model layer, and the bottom of model layer 20, to the attribute table of the shapefile of wells within the regional model nearfield. The approximate bottom elevation of each of the wells included in the shapefile was calculated by subtracting the well depth from the top elevation of model layer 1 (land surface). Wells having a bottom elevation less than the top elevation of model layer 12 (the bottom of the Platteville Group) were selected from the shapefile and then exported as another shapefile representing only sub-Platteville domestic and commercial water-supply wells in the regional model nearfield.

Further data processing was necessary to characterize the open intervals of the deep wells and permit their inclusion in the regional groundwater flow model. Ideally, open intervals could be characterized using casing depth and well depth data, both of which are represented by fields in the ISWS Private Well Database. Unfortunately—though well depth is known for all of the 3762 wells in the shapefile of deep wells—casing-depth data is available only for 903 of these wells. Therefore, the relationship between the open interval of the 903 wells having both casing and well depth data was examined to determine the most likely open interval in the wells lacking casing depth data. This relationship was analyzed independently for each of the Quaternary subcrop belts present in the regional model nearfield and, where Pennsylvanian rocks are present in the nearfield, for each Pennsylvanian subcrop belt. Employing elevation data for land-surface and the tops of the hydrostratigraphic units used in the regional groundwater flow model, differences in elevation between casing bottom, well bottom, and the tops of the hydrostratigraphic units were calculated for each of the 903 wells having documented casing and wells depths. Median differences in elevation were calculated from these data; from these medians, the most probable open interval was deduced for deep wells in each subcrop belt (Table B-5, Table B-6). All wells lacking casing depth data in the ISWS Private Well Database were then segregated by subcrop belt, and the uppermost model layer of the open interval of typical deep wells in that well's subcrop belt (Table B-7) was assumed to be the uppermost model layer of each of these wells. Well depth data were available for all 3762 wells, and the lowermost

model layer to which the well was open was determined by comparing the difference in elevation between the well bottom and the tops of the hydrostratigraphic units. The lowermost model layer to which the well was open was assumed to be the deepest model layer for which this elevation difference was zero or negative. For example, if well bottom elevation was estimated at 100 ft above mean sea level (MSL) at a location where the tops of model layers 12 and 13 were at elevations of 150 ft and 50 ft above MSL, respectively, the lowermost model layer to which the well is open was assumed to be model layer 12. The elevation difference between the well bottom and the top of this layer would be -50 ft, while the difference between the well bottom and the top of model layer 13 would be +50 ft.

After augmenting the file of 3762 deep wells with x- and y-coordinates and open interval characterizations, the file was reduced to only those recognized as domestic wells in the ISWS Private Well Database. Thus, irrigation and commercial/industrial wells—wells already included in the withdrawal database for the project—were removed from the file. This reduced the number of wells represented in the file to 3060 (Figure B-11).

Withdrawal rates for the wells are based on linear interpolation of estimates of per-capita self-supplied domestic water use developed at five-year increments for the period 1960-2000 by the United States Geological Survey (USGS) and reported by Dziegielewski et al. (2005) (Figure B-12), together with the assumption that each well supplies 3.4 people (Illinois Department of Energy and Natural Resources, 1998). Pre-1960 per-capita withdrawal rates are assumed to have been equal to the 1960 rate determined by linear interpolation of the USGS estimates [5.2 cubic feet per day (ft^3/d)], but per capita rates between 1960 and 2003 are assumed to have increased in a linear fashion from 5.2 to 13.6 ft^3/d . Withdrawals from the wells were assumed to have occurred for the entire year of drilling and to have been zero during the year of sealing. The ISWS Private Well Database reliably includes the year of drilling of these wells, but a field devoted to housing sealing date data is completed for only a small minority of wells. If the sealing date was not available, the well was assumed to be in service through the year 2003. Per-capita self-supplied domestic water use rates for the period 2005-2050, based on linear interpolation of the 1960-2000 USGS estimates, are employed in pumping forecasts discussed in Appendix G.

Table B-5. Median Distance Between Casing Bottom and Top of Hydrostratigraphic Units for Deep Wells Listed in the ISWS Private Well Database in Northeastern Illinois

Subcrop Belt (Overlying Unit/ Underlying Unit)	No. of Wells	Median Distance (ft) Between Casing Bottom and Top of Hydrostratigraphic Unit										
		QT*	UB	SD	MQ	GP	AN	PE	PF	IG	EC	MS
QT/SD*	77	-420	-288	-287	-201	-37	300	478	641	827	954	1367
UB/SD	0											
QT/MQ	466	-273.5	-170	-169	-166	-41	318	600	684	903	1034	1442
UB/MQ	17	-163	-124	-51	-48	12	351	610	918	1255	1418	1866
QT/GP	29	-145	-30	-29	-26	-24	179	409	669	963	1106	1508
UB/GP	76	-226	-135.5	-36.5	-33.5	-31.5	71.5	354.5	697	1021.5	1183.5	1594
QT/AN	91	-155	-66	-65	-62	-60	-58	-13	352	628	786	1175
UB/AN	5	-279	-95	-46	-43	-41	-39	146	550	833	974	1385
QT/PE	142	-103.5	-32.5	-31.5	-28.5	-26.5	-24.5	-23.5	314	587	748.5	1134.5

*See Figure 25 for key to acronyms

Table B-6. Median Distance Between Well Bottom and Top of Hydrostratigraphic Units for Deep Wells Listed in the ISWS Private Well Database in Northeastern Illinois

Subcrop Belt (Overlying Unit/ Underlying Unit)	No. of Wells	Median Distance (ft) Between Well Bottom and Top of Hydrostratigraphic Unit										
		QT*	UB	SD	MQ	GP	AN	PE	PF	IG	EC	MS
QT/SD*	77	-800	-649	-648	-579	-399	-50	125	274	446	589	998
UB/SD	0											
QT/MQ	466	-640	-543	-542	-539	-392	-34	232	326	525	640	1042
UB/MQ	17	-560	-551	-454	-451	-397	-62	205	518	849	1021	1468
QT/GP	29	-440	-350	-349	-346	-344	-85	119	374	654	804	1192
UB/GP	76	-360	-261.5	-185	-182	-180	-59	176	570	892.5	1047	1481.5
QT/SP	91	-200	-102	-101	-98	-96	-94	-58	288	577	716	1110
UB/SP	5	-360	-197	-127	-124	-122	-120	54	463	753	894	1305
QT/PJ	142	-140	-69.5	-68.5	-65.5	-63.5	-61.5	-60.5	270	545	699.5	1087.5

*See Figure 25 for key to acronyms

Table B-7. Assumed Open Intervals of Deep Wells in Northeastern Illinois Lacking Casing-Depth Data Based on Data in Table B-5 and Table B-6

<i>Subcrop Belt (Overlying Unit/ Underlying Unit)</i>	<i>Assumed Open Interval</i>	
	<i>Uppermost Model Layer</i>	<i>Lowermost Model Layer</i>
QT/SD*	10	12
UB/SD	10	12
QT/MQ	10	12
UB/MQ	8	12
QT/GP	10	12
UB/GP	10	12
QT/SP	13	13
UB/SP	12	12
QT/PJ	13	13

*See Figure 25 for key to acronyms

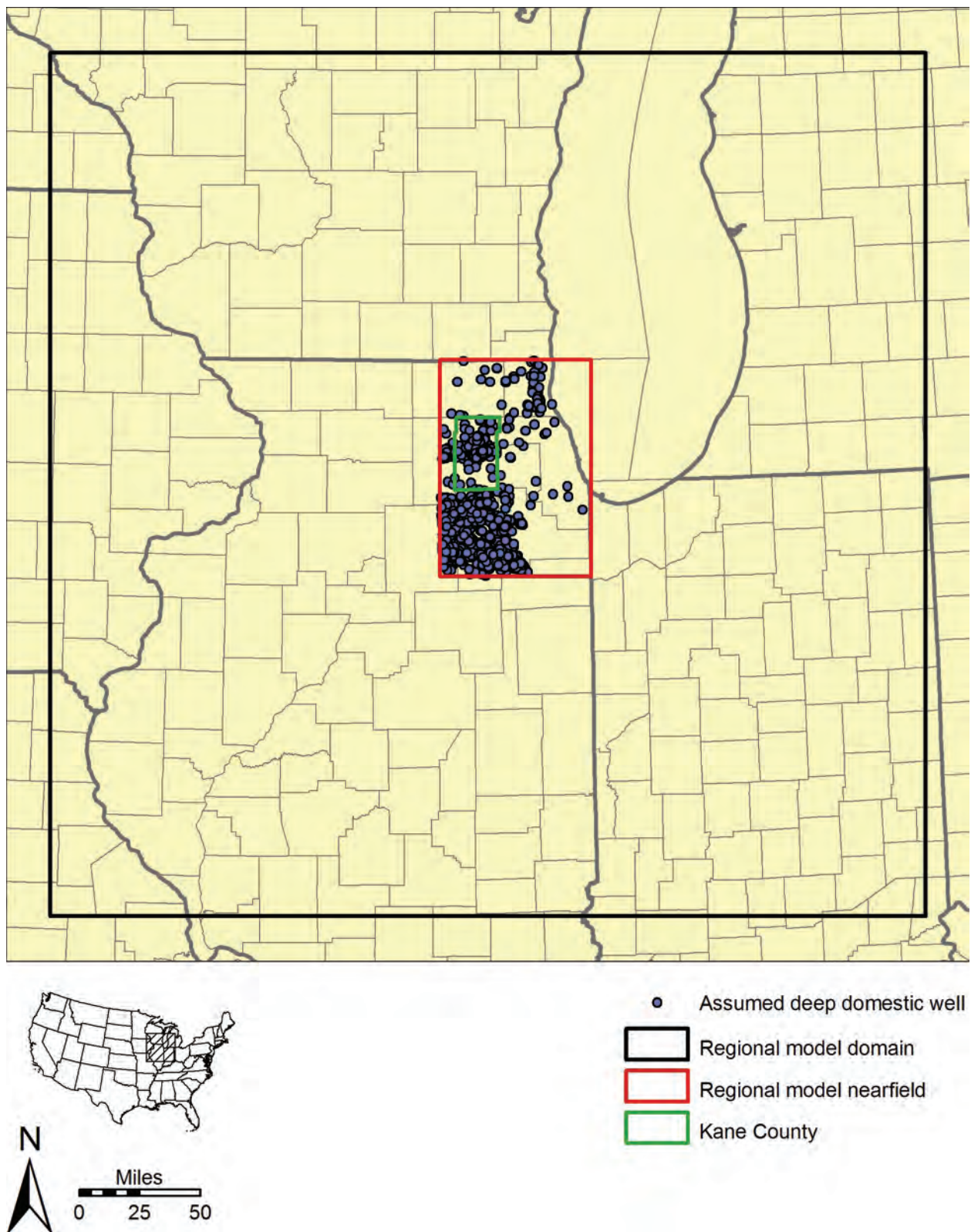


Figure B-11. Deep domestic wells.

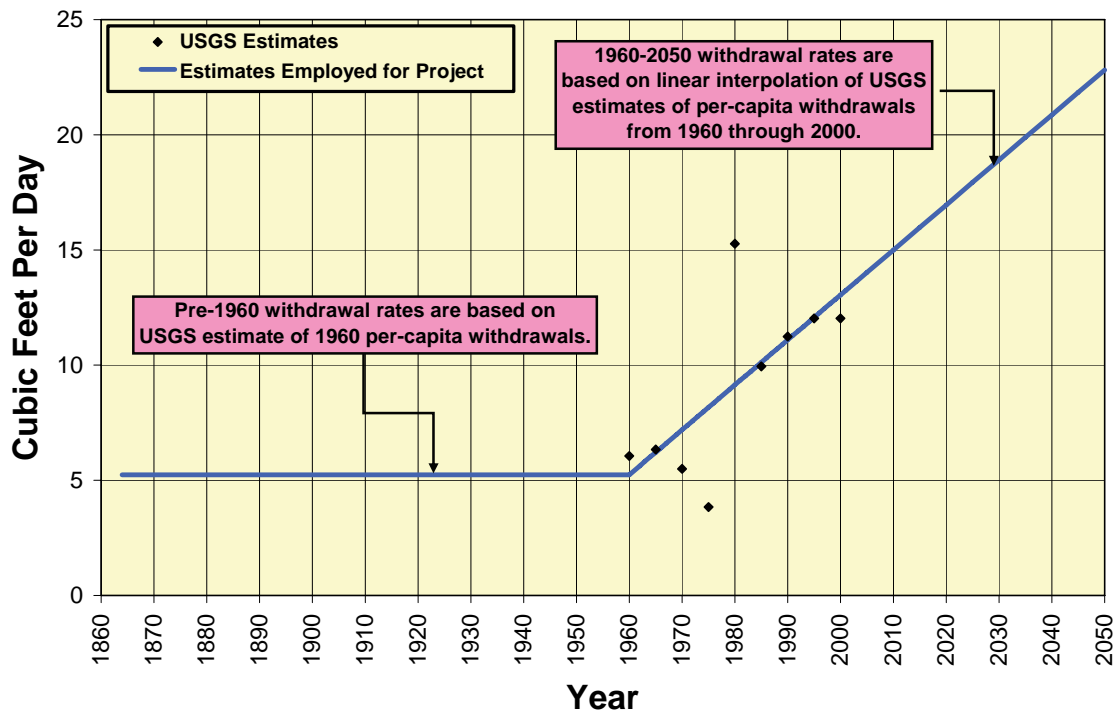


Figure B-12. Estimated per-capita self-supplied domestic withdrawal rates.

B.2.2. Indiana

Data purchased from the Indiana Department of Natural Resources mainly required processing to assign the represented wells ILLIMAP x - and y -coordinates and to characterize the open intervals of the wells using model layers.

The Indiana withdrawal database contained fields for the x - and y -coordinates of wells, but these coordinates were referenced to the NAD 1927 UTM Zone 16N projection and coordinate system used by the State of Indiana. A GIS procedure was employed to generate ILLIMAP coordinates for the Indiana wells. First, the Indiana wells were saved as an ArcGIS point-shapefile format referencing their native UTM projection and coordinate system. This shapefile was then imported into an ArcGIS data frame that had been assigned the ILLIMAP projection and coordinate system. Next, the imported data were exported as a point-shapefile referenced to the ILLIMAP system. Finally, fields for the ILLIMAP x - and y -coordinates were added to the attribute table of this shapefile, and these fields were populated using VBA scripts to calculate x - and y -coordinates of the data points.

The open intervals of the Indiana wells were characterized using aquifer codes consistent with ISWS standards (see Appendix F) that could be directly translated to a characterization referencing the layers of the regional groundwater flow model (Table B-4). These aquifer codes were assigned on the basis of a rough characterization of the open intervals of the wells by the

Indiana authorities, on the depths of the wells as indicated by the database as received, and on regional geological information.

Indiana wells represented in the withdrawal database are shown in Figure B-13 and Figure B-14. Only a single deep Indiana well is included in the database.

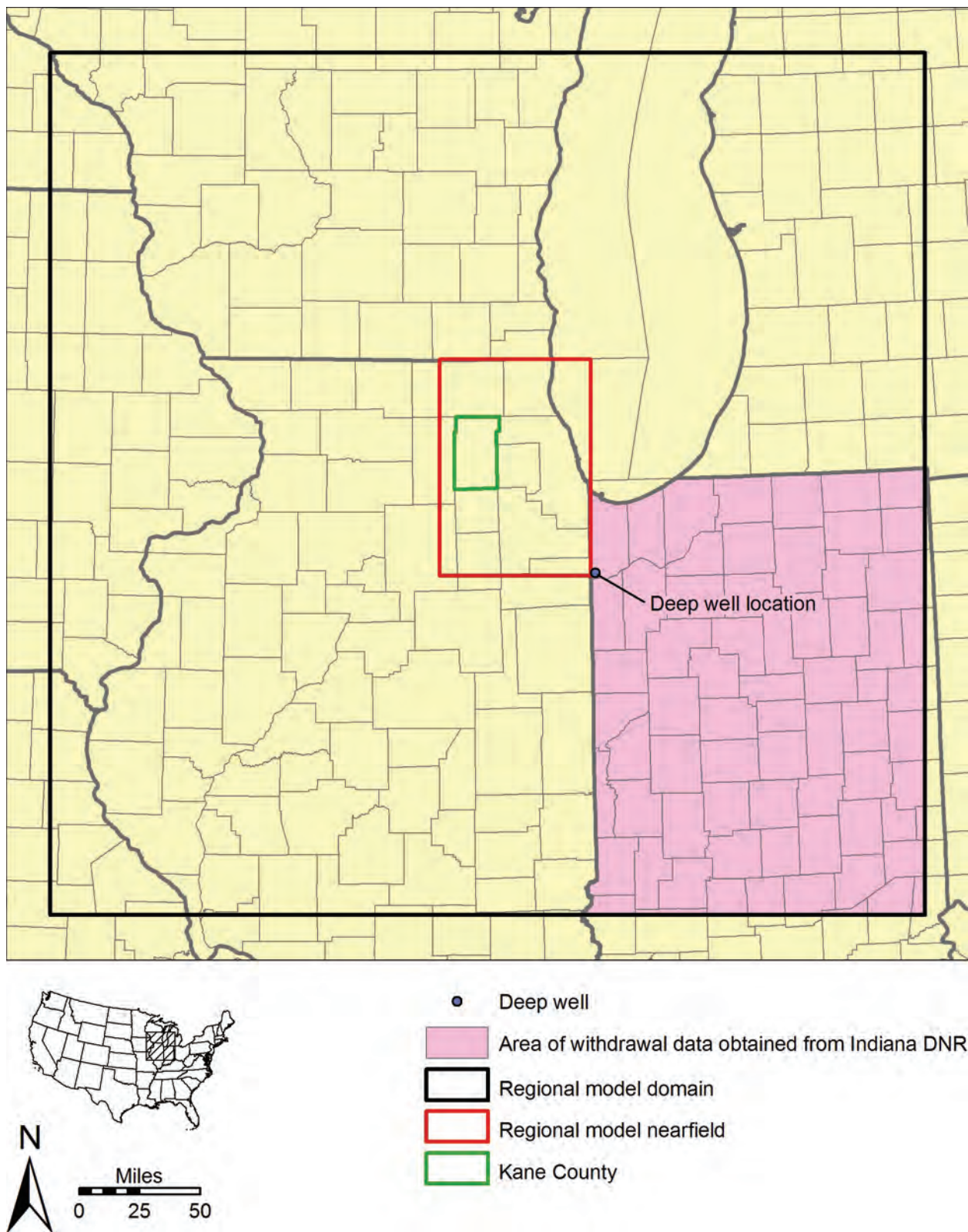


Figure B-13. Deep well in Indiana having 1985-2002 withdrawals documented by Indiana Department of Natural Resources database.

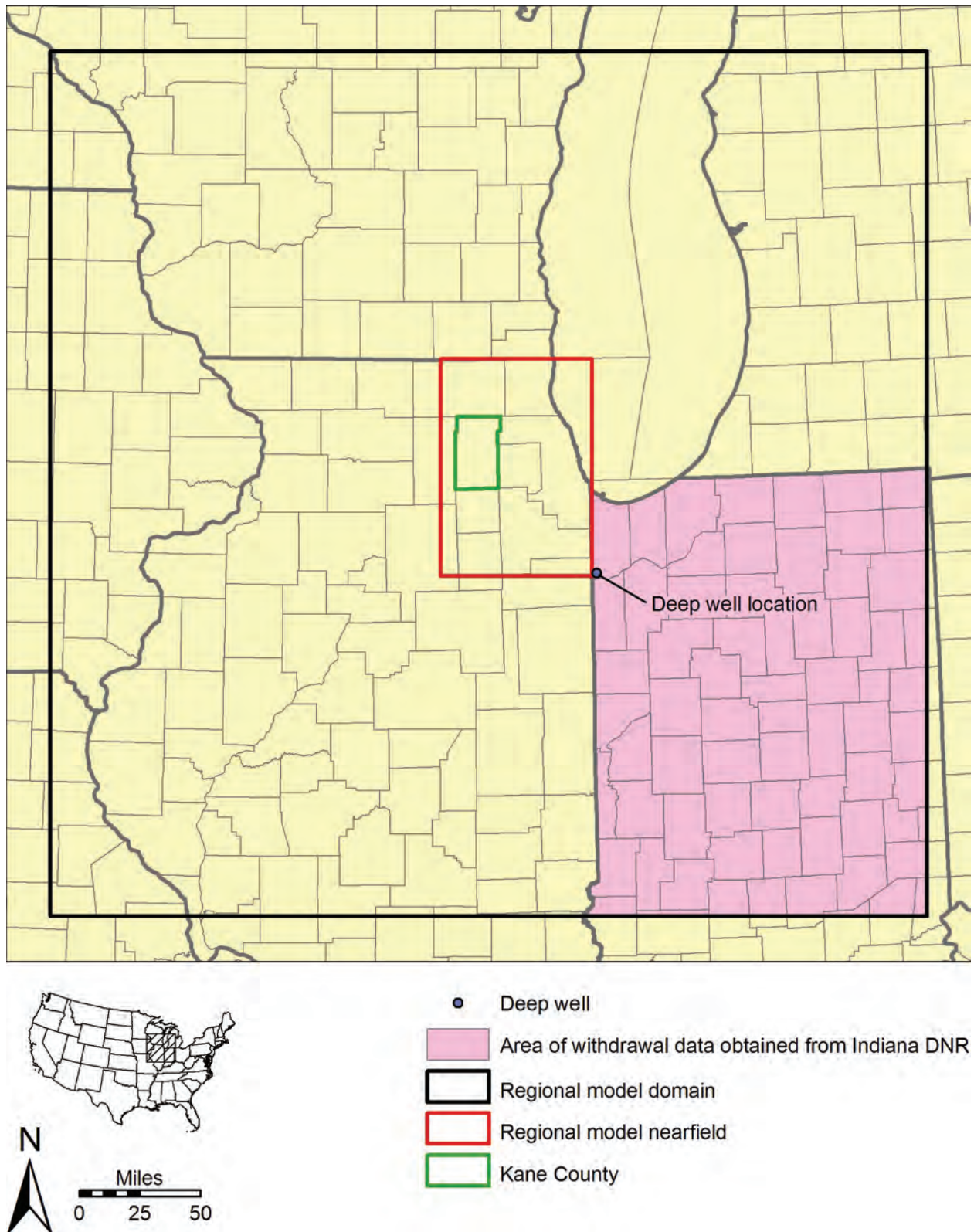


Figure B-14. Shallow wells in Indiana having 1985-2002 withdrawals documented by Indiana Department of Natural Resources database.

B.2.3. Wisconsin

Wisconsin withdrawal data were received from the Wisconsin Geological and Natural History Survey in two separate files, each representing a separate group of wells. In one file, open intervals were characterized using top and bottom elevations of the open interval. In the second file, open intervals were characterized using the uppermost and lowermost model layer to which each well was open, referencing the layer nomenclature employed in the project for which the file was developed (Feinstein et al., 2005a; Feinstein et al., 2005b). The wells in the second file were universally open to the same interval of Cambrian and Ordovician bedrock, an interval corresponding to layers 12 through 20 of the regional groundwater flow model developed for the present study. In both files, withdrawal rates were given as average withdrawal rates for stress periods of 2 to 20 years' duration covering the period 1864 through 2002.

Like the Indiana wells, it was necessary to assign ILLIMAP *x*- and *y*-coordinates to the Wisconsin wells represented in the two files. Coordinates included in the files, as received from the Wisconsin Geological and Natural History Survey, referenced the Wisconsin Transverse Mercator (WTM) projection and coordinate system. The files were saved as an ArcGIS shapefile referenced to the WTM system, and this shapefile was then imported into a data frame referencing the ILLIMAP system. The Wisconsin well locations were then exported as a shapefile referencing the ILLIMAP projection and coordinate system. Fields to contain the ILLIMAP *x*- and *y*-coordinates were then added to the attribute table of the latter shapefile, and these fields were populated using VBA scripts to calculate *x*- and *y*-coordinates of the data points.

Stress-period averages were disaggregated and incorporated into the database as the withdrawal rate for each year of the stress period. For example, the pumping rate for a well given by the Wisconsin Geological and Natural History Survey for the stress period 1971 through 1980 was assumed to be the pumping rate for each year of the period 1971 to 1980.

The open-interval characterizations provided by the Wisconsin Geological and Natural History Survey as elevations were not altered and were retained in the project database as the basis for input of the wells into the regional groundwater flow model. The open interval characterizations of wells provided as model layers—universally layers 13 through 16 of the Wisconsin modeling effort—were altered to the model layer designations used for the modeling project described in the present study (layers 12 through 20).

The Wisconsin wells represented in the provided dataset include both shallow and deep wells. Since the area covered by the dataset is roughly coincident with the portion of the shallow aquifer withdrawal accounting region (SAWAR) within Wisconsin, no effort was made to remove shallow wells falling outside this region.

Locations of the Wisconsin wells provided by the Wisconsin Geological and Natural History Survey, and included in the modeling database, are shown in Figure B-15 and Figure B-16.

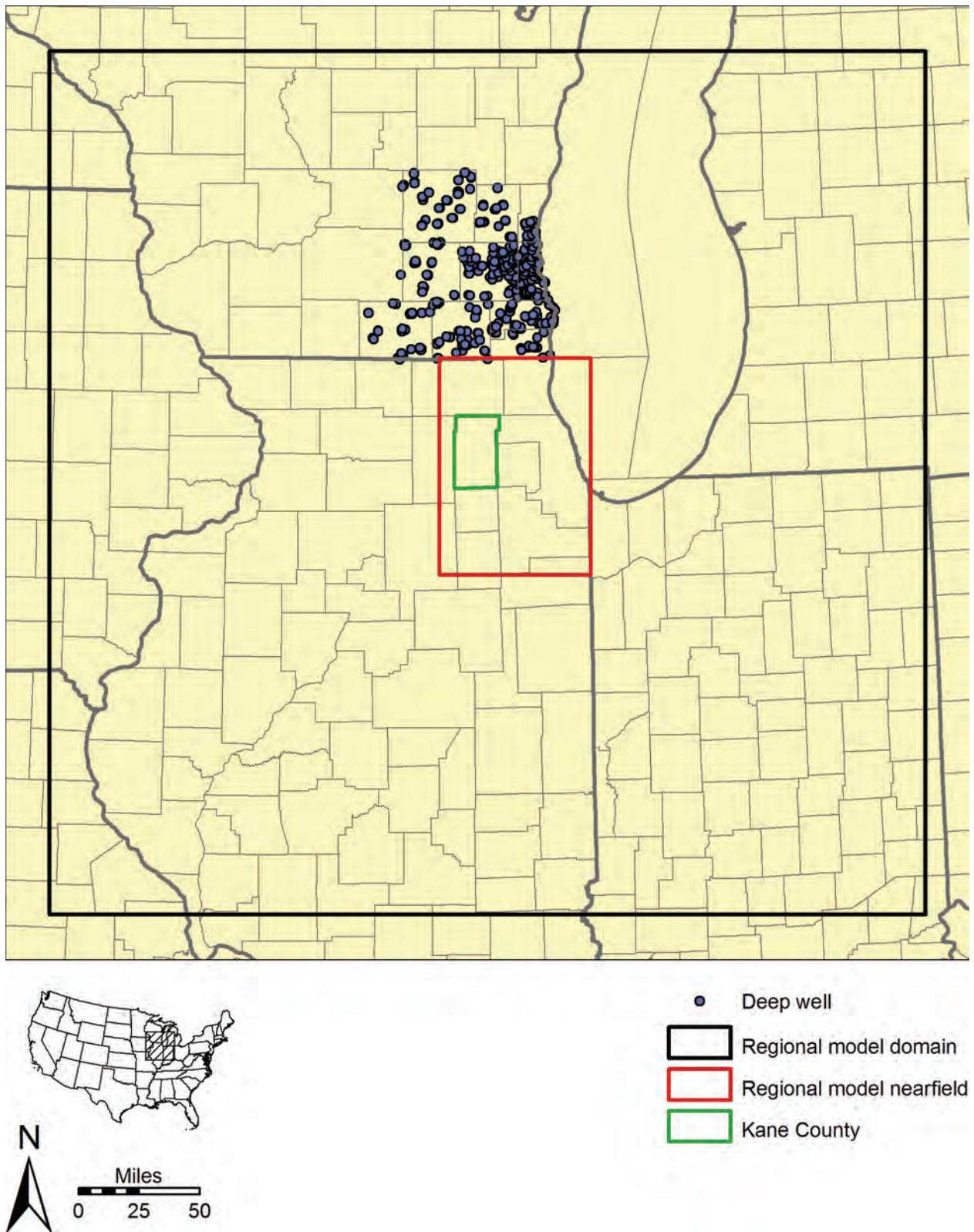


Figure B-15. Deep wells in Wisconsin having 1984-2002 withdrawals documented by records obtained from the Wisconsin Geological and Natural History Survey.

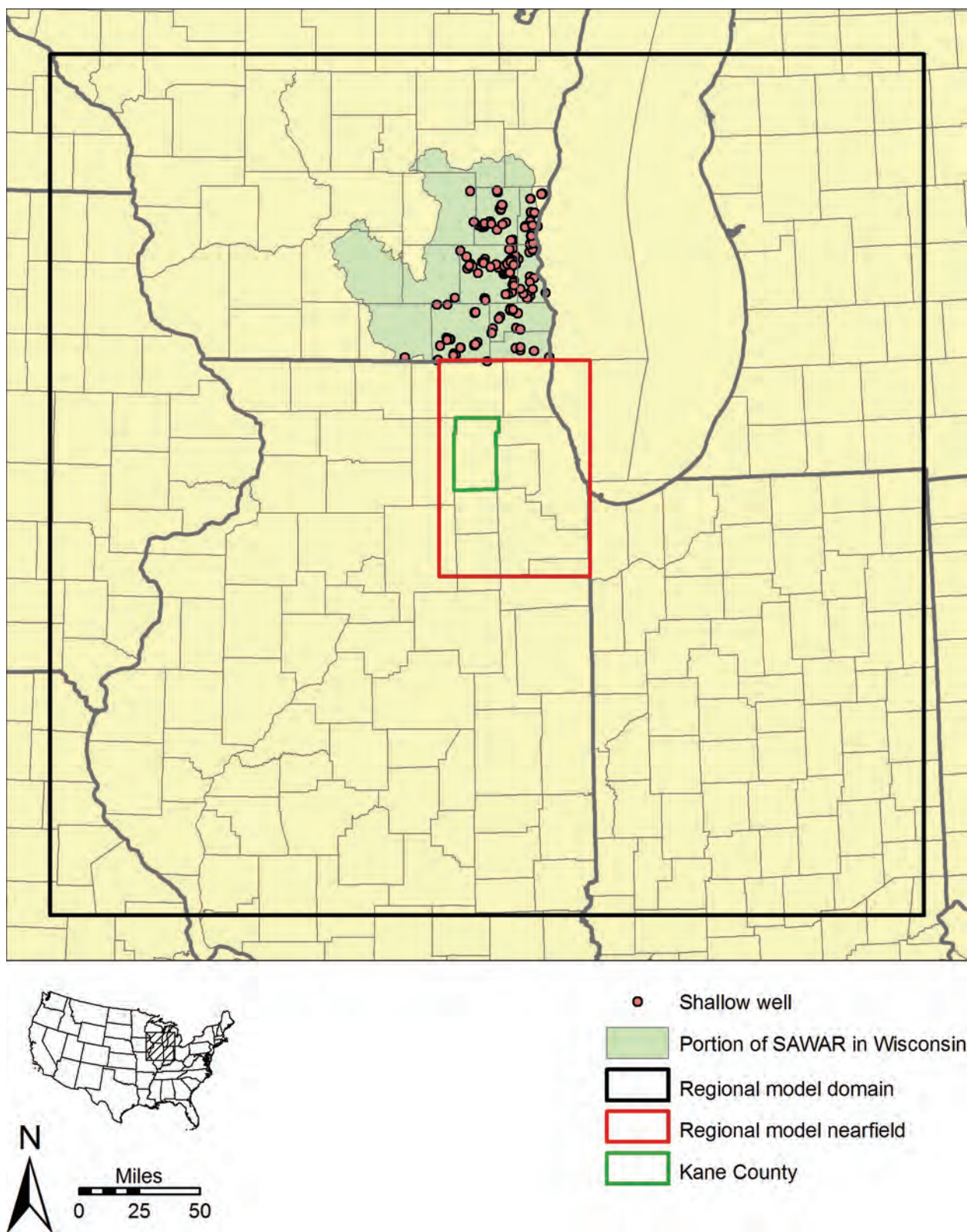


Figure B-16. Shallow wells in Wisconsin having 1984-2002 withdrawals documented by records obtained from the Wisconsin Geological and Natural History Survey.

B.3. Uncertainties

The following section discusses uncertainties associated with the withdrawal data compiled for the modeling effort. Two aspects of uncertainty are discussed below: uncertainty of withdrawal rate data and positional accuracy.

A third aspect—completeness—is commented upon here. The principal withdrawal datasets consulted for this study—pre-1964 Illinois data obtained from previous modeling studies, Illinois data for the period 1964-1979 obtained from hardcopy records, data obtained from the ISWS PICS Database for the period 1980-2003, and withdrawal data obtained from Indiana authorities for the period 1985-2002 and from Wisconsin authorities for the period 1864-2002—are thought by their compilers to represent the majority of withdrawals in these areas during the time periods covered. It is acknowledged that some withdrawals—particularly during years earlier in the history of the groundwater development of the region—have been missed by the compilers of these datasets, but quantification of the completeness of the datasets is beyond the scope of this study. With the exception of withdrawals from domestic wells open to the sub-Platteville interval in the regional model nearfield, withdrawals from domestic wells are not included in the datasets. Withdrawals were not estimated for domestic wells open to shallower units because 85 to 90 percent of the relatively small quantities of groundwater withdrawn from such wells would be returned via on-site wastewater disposal systems to the shallow interval from which they were obtained (Pebbles, 2003; United States Environmental Protection Agency Region V, 1975), with little net effect on groundwater flow.

B.3.1. Illinois

B.3.1.1. Data Obtained from Previous Modeling Studies

Suter et al. (1959) do not estimate the uncertainty of the withdrawal estimates in northeastern Illinois that are employed to represent withdrawals in groundwater flow modeling developed for the present project from 1864 through 1958. Nor do Prickett and Lonquist (1971), who employed the estimates of Suter et al. (1959) in groundwater flow modeling and whose pumping estimates for the period 1959 through 1963 are employed in the present study. Suter et al. (1959) described a procedure that would seem to imply a high degree of uncertainty, however, indicating that their plots of withdrawals

were constructed by piecing together fragments of information on pumpage found in published reports and in the files of the State Water Survey, by making evaluations based on the number of wells, their reported yields, and their time of construction, and by taking into consideration population growth and per capita consumption.

Furthermore, Suter et al. (1959) indicate that, although records of withdrawals are fairly complete for the period 1942 through 1958, “very few records of pumpage are available for years prior to 1942.” Adding to the uncertainty of the 1864-1963 period is the probability that withdrawal data employed for the present study—received in the form of digital files—were estimated from small plots appearing in the 1959 report of Suter et al. Finally, for the present study, these estimates were revised upward using a rough approximation to reflect contributions to pumping from deep wells by units overlying the Ancell Group and underlying the Ironton-Galesville Sandstone.

With the lack of source documentation of the 1864-1963 withdrawal estimates and the procedures used to generate them, estimation of uncertainty is problematic. A component of uncertainty exists that is associated with the measurement of withdrawals during this time period, and this component of uncertainty—as opposed to those associated with documentation and reporting procedures and with estimation of withdrawals based on population growth, per-capita consumption, and numbers of wells—is quantified in the literature. The United States Department of the Interior Bureau of Reclamation (1997) estimates that most flow-measurement devices produce accuracies of ± 5 percent, but accuracy declines to ± 10 percent when instruments are not maintained, when they are inappropriate for site conditions, and when they are deployed in nonstandard installations. It is probable, owing to improvements in flow-measurement technology, that accuracies of measured withdrawals are poorer with increasing age. Solely on the basis of the accuracy of flow-measurement devices, it is probable that the pre-1964 withdrawal data employed in the present study are only accurate to ± 10 percent.

Burch (1991), who also relied on the early Illinois withdrawal data ultimately derived from the plots of Suter et al. (1959), evaluated the accuracy of published estimates of early withdrawals by comparing published estimates of withdrawals in ISWS reports covering the period 1964-1980 with estimates developed from tabulations of detailed hardcopy withdrawal data covering the same time period. Burch (1991) found that the difference between the published estimates and the tabulations increased from 2 percent in 1980 to 22 percent in 1964. This analysis suggests an uncertainty in excess of ± 20 percent for the pre-1964 withdrawal estimates employed for the present study.

Withdrawals for the period 1864-1963 are not assigned to actual well locations but are rather aggregated at seven northeastern Illinois pumping centers. The locations of six of these pumping centers were selected by Suter et al. (1959), with a seventh added by Prickett and Lonnquist (1971), to best represent actual pumping in northeastern Illinois. The x - and y -coordinates selected by Burch (1991) are employed to represent these pumping centers. Since the coordinates do not represent actual well locations, the positional accuracy of these coordinates is not discussed further. Detailed withdrawal data, representing reported withdrawals at actual well locations, are employed for the post-1963 period, allowing the groundwater flow models nearly 40 years to adjust to detailed pumping conditions. It is acknowledged that model accuracy for the period ending 1963 is limited owing to the simplified representation of pumping conditions for that period.

B.3.1.2. Hardcopy Data

The uncertainty of withdrawals documented in hardcopy form by the ISWS for the period 1964-1979 varies with year, facility, and well. These withdrawal data consist of measurements from water meters or estimates by water managers, reported to the ISWS, as well as estimates by ISWS researchers themselves. Withdrawals from public water system wells are nearly always metered in cities, but many smaller villages operate without meters, and withdrawals from wells operated by self-supplied industrial and commercial facilities and from irrigation wells are not typically metered. The United States Department of the Interior Bureau of Reclamation (1997) estimates that most water measurement devices have an accuracy of ± 5 percent, but this accuracy declines to ± 10 percent when instruments are not maintained, when they are inappropriate for site conditions, and when they are deployed in nonstandard installations. Metering devices, installations, and procedures are not documented, and undoubtedly vary between facilities and wells, so it is not possible to quantify the uncertainty of these measurements. Accuracies of estimated withdrawals are not known. Based on the accuracy estimates of the Bureau of

Reclamation and the likelihood that estimated withdrawals are less accurate than measurements using water meters, it is probably safe to assume that the hardcopy withdrawal data are accurate only to within ± 10 percent.

For the vast majority of wells documented by hardcopy withdrawal records, locational coordinates are largely accurate to the 10-acre plot within which the well is reported to be located (Appendix I). Still, the locations of some wells are not known to the 10-acre plot, but rather only to the section or, in a few cases, the township. For the majority of wells, wherein the locational coordinates are accurate to within a reported 10-acre plot, the x - and y -coordinates have an accuracy of about ± 500 ft. In the worst cases, wherein the coordinates are accurate only to within a reported township, the accuracy of the x - and y -coordinates declines to about $\pm 22,500$ ft. It is acknowledged that the reported locations of these wells may be erroneous, but this source of uncertainty is not evaluated. In other, comparatively rare, cases, well locations are known by surveying and are more accurate, typically within ± 100 ft, but possibly within ± 20 ft (Locke and Meyer, 2005).

B.3.1.3. ISWS Public-Industrial-Commercial Survey (PICS) Database

Like that of the withdrawal data derived from hardcopy data discussed in the preceding section, the uncertainty of the withdrawal data obtained from the ISWS PICS Database varies with year, facility, and well. This is because the data consist of measurements obtained using a variety of undocumented devices, installations, and procedures, together with estimates by reporting water managers and former ISWS staff. Thus, as for the hardcopy withdrawal data, it is probably safe to assume that the PICS withdrawal data are accurate only to within ± 10 percent (United States Department of the Interior Bureau of Reclamation, 1997). Cross-validation analysis against reported rates of a sample of 94 withdrawal estimates, developed for this study using the procedure illustrated in Figure B-7, shows that the median error of the estimates to be about -2 percent.

Positional accuracy of the wells documented in the ISWS PICS Database is also similar to that of the wells documented by hardcopy records. Most of the locational coordinates are accurate to the 10-acre plot within which the well is reported to be located, and the x - and y -coordinates of such wells have an accuracy of about ± 500 ft. This accuracy declines in instances wherein the 10-acre plot location is not known and is at its worst when even the section is unknown, so that the well is arbitrarily located at the center of a township; in the latter case, the accuracy of the x - and y -coordinates declines to about $\pm 22,500$ ft. The accuracy of surveyed coordinates is better, typically within ± 100 ft, but possibly within ± 20 ft (Locke and Meyer, 2005).

B.3.1.4. Assumed Withdrawals from Deep Domestic Wells in Northeastern Illinois

Withdrawals from deep domestic wells are based on a single estimate of 3.4 people served by each well (Illinois Department of Energy and Natural Resources, 1998), an estimate of per capita withdrawals based on interpolation of USGS estimates of self-supplied domestic per capita withdrawals from 1960 through 2000 [as reported by Dziegielewski et al. (2005)] (Figure B-12), and an assumed pumping period extending from the year of drilling to the year of sealing as shown by records in the ISWS Private Well Database. The uncertainty in these withdrawal estimates is considerable. The year of sealing of most wells listed in the ISWS Private Well Database is often not recorded, and the well has, consequently, been assumed to be active through the year 2003. It is likely that many such wells have actually been sealed, however, and the pumping rate is zero rather than the assumed rate. Countering this uncertainty in the pumping

period is the likelihood that the records of the Private Well Database are incomplete, and that there are more deep domestic wells present than are actually recorded.

For purposes of illustrating the considerable uncertainty associated with the estimates of withdrawals from deep domestic wells, one can examine some simple, but likely, possibilities. First, it is very likely, as mentioned in the preceding paragraph, that withdrawals from many wells are zero—100 percent less than the assumed per-well rate—because they have been sealed. On the other hand, if one assumes (1) the highest USGS estimate of self-supplied domestic water use (15.3 ft³/d per capita) rather than the per-capita rate estimated through interpolation (Figure B-12) and (2) that a well supplies a moderately large family of six rather than the assumed 3.4. It is demonstrable that the assumed per-well rate might be 100 percent more than the assumed rate and—for years prior to 1961 for which a low per-capita water usage of about 5.2 ft³/d was assumed (Figure B-12)—the actual per-well withdrawal rate might be over 400 percent more than the assumed rate.

Locational coordinates are accurate to the 10-acre plot within which the well is reported to be located, so the *x*- and *y*-coordinates of such wells have an accuracy of about ± 500 ft.

B.3.2. Indiana

Indiana groundwater withdrawal data are submitted by water managers to the Indiana Department of Natural Resources. It is probable that these submitted withdrawal data consist of measurements obtained through a wide range of procedures, using a variety of measurement devices and installations, as well as estimates. It is likely that these data are accurate only to within ± 10 percent (United States Department of the Interior Bureau of Reclamation, 1997). Positional accuracy is not documented.

B.3.3. Wisconsin

Withdrawal data received from the Wisconsin Geological and Natural History Survey include estimates and measurements obtained using a wide range of procedures, devices, and installations, and accuracy probably varies considerably with facility, well, and year. Like the Illinois data obtained from previous modeling studies, these estimates cover a long period beginning in 1864. The early estimates, in particular, are probably quite uncertain, possibly in excess of ± 20 percent, as discussed in the section on Illinois data obtained from previous modeling studies. The accuracy of later estimates is probably better, possibly within ± 10 percent (United States Department of the Interior Bureau of Reclamation, 1997). Positional accuracy is not documented.

B.4. References

- Burch, S.L. 1991. *The New Chicago Model: A Reassessment of the Impacts of Lake Michigan Allocations on the Cambrian-Ordovician Aquifer System in Northeastern Illinois*. Illinois State Water Survey Research Report 119, Champaign, IL.
- Dziegielewski, B., X. Yang, T. Bik, H. Margono, and M. Richey. 2005. *County-Level Forecasts of Water Use in Illinois: 2005-2025*. Department of Geography, Southern Illinois University, Carbondale, IL.
- Feinstein, D.T., T.T. Eaton, D.J. Hart, J.T. Krohelski, and K.R. Bradbury. 2005a. *Regional Aquifer Model for Southeastern Wisconsin; Report 1: Data Collection, Conceptual Model Development, Numerical Model Construction, and Model Calibration*. Wisconsin Geological and Natural History Survey administrative report prepared for Southeastern Wisconsin Regional Planning Commission.
- Feinstein, D.T., T.T. Eaton, D.J. Hart, J.T. Krohelski, and K.R. Bradbury. 2005b. *Regional Aquifer Model for Southeastern Wisconsin; Report 2: Model Results and Interpretation*. Wisconsin Geological and Natural History Survey administrative report prepared for Southeastern Wisconsin Regional Planning Commission.
- Illinois Department of Energy and Natural Resources. 1998. *Fox River Area Assessment. Volume 2: Water Resources. Illinois Department of Natural Resources Critical Trends Assessment Program Document*. Springfield, IL.
- Illinois State Water Survey and Hittman Associates. 1973. *Feasibility Study on Desalting Brackish Water from the Mt. Simon Aquifer in Northeastern Illinois*. Illinois State Water Survey Contract Report 153, Champaign, IL.
- Locke, R.A., II and S.C. Meyer. 2005. *Kane County Water Resources Investigations: Interim Report on Shallow Aquifer Potentiometric Surface Mapping*. Illinois State Water Survey Contract Report 2005-04, Champaign, IL.
- Pebbles, V. 2003. *Measuring and Estimating Consumptive Use of the Great Lakes Water*. Great Lakes Commission, Ann Arbor, MI.
- Prickett, T.A. and C.G. Lonquist. 1971. *Selected Digital Computer Techniques for Groundwater Resource Evaluation*. Illinois State Water Survey Bulletin 55, Champaign, IL.
- Sasman, R.T. and W.H. Baker, Jr. 1966. *Ground-Water Pumpage in Northeastern Illinois through 1963*. Illinois State Water Survey Report of Investigation 52, Champaign, IL.
- Sasman, R.T., W.H. Baker, Jr., and W.P. Patzer. 1962a. *Water-Level Decline and Pumpage During 1961 in Deep Wells in the Chicago Region, Illinois*. Illinois State Water Survey Circular 85, Champaign, IL.

- Sasman, R.T., C.R. Benson, and G.L. Dzursin. 1974. *Groundwater Pumpage in Northern Illinois, 1960-1970*. Illinois State Water Survey Report of Investigation 73, Champaign, IL.
- Sasman, R.T., C.R. Benson, G.L. Dzursin, and N.E. Risk. 1973. *Water-Level Decline and Pumpage in Deep Wells in Northern Illinois, 1966- 1971*. Illinois State Water Survey Circular 113, Champaign, IL.
- Sasman, R.T., C.R. Benson, R.S. Ludwigs, and T.L. Williams. 1982. *Water-Level Trends, Pumpage, and Chemical Quality in the Cambrian-Ordovician Aquifer in Illinois, 1971-1980*. Illinois State Water Survey Circular 154, Champaign, IL.
- Sasman, R.T., C.R. Benson, J.S. Mende, N.F. Gangler, and V.M. Colvin. 1977. *Water-Level Decline and Pumpage in Deep Wells in the Chicago Region, 1971- 1975*. Illinois State Water Survey Circular 125, Champaign, IL.
- Sasman, R.T., C.K. McDonald, and W.R. Randall. 1967. *Water-Level Decline and Pumpage in Deep Wells in Northeastern Illinois, 1962-1966*. Illinois State Water Survey Circular 94, Champaign, IL.
- Sasman, R.T., T.A. Prickett, and R.R. Russell. 1961. *Water-Level Decline and Pumpage During 1960 in Deep Wells in the Chicago Region, Illinois*. Illinois State Water Survey Circular 83, Champaign, IL.
- Sasman, R.T., W.H. Baker, Jr., and W.P. Patzer. 1962b. *Water-Level Decline and Pumpage During 1961 in Deep Wells in the Chicago Region, Illinois*. Illinois State Water Survey Circular 85, Champaign, IL.
- Schicht, R.J., J.R. Adams, and J.B. Stall. 1976. *Water Resources Availability, Quality, and Cost in Northeastern Illinois*. Illinois State Water Survey Report of Investigation 83, Champaign, IL.
- Seaber, P.R., F.P. Kapinos, and G.L. Knapp. 1987. *Hydrologic Unit Maps*. United States Geological Survey Water-Supply Paper 2294, Reston, VA.
- Suter, M., R.E. Bergstrom, H.F. Smith, G.H. Emrich, W.C. Walton, and T.E. Larson. 1959. *Preliminary Report on the Ground-Water Resources of the Chicago Region, Illinois*. Illinois State Water Survey and Illinois State Geological Survey Cooperative Ground-Water Report 1, Urbana, IL.
- United States Department of the Interior Bureau of Reclamation. 1997. *Water Measurement Manual*. U.S. Government Printing Office, Washington, DC.
- United States Environmental Protection Agency Region V. 1975. *Great Lakes Basin Framework Study Appendix 6: Water Supply—Municipal, Industrial, Rural*. Great Lakes Basin Commission, Ann Arbor, MI.

Appendix C. Development of Geologic Framework of Regional Groundwater Flow Model

C.1. High-Resolution Geologic Model

The high-resolution geologic model is a set of 12 high-resolution surface models of individual surfaces, here referred to as *high-resolution surface models* (Table C-1), representing the top elevations of each of the 11 model hydrostratigraphic units and the bottom elevation of the Mt. Simon Unit. Each high-resolution surface model consists of a point-feature shapefile containing an estimate of the elevation of the surface at each point in the regional model domain. Each model was produced by interpolation of point-estimates of the top elevation of the unit (*interpolation source data*), derived from a variety of sources, followed by post-processing of the interpolation results. The accuracy of each high-resolution surface model is greatest in the area of active model cells east of the Mississippi River.

Because the finite-difference groundwater flow modeling approach requires that the models of all hydrostratigraphic units extend across the entire model domain, each of the 11 high-resolution surface models includes estimates of the surface elevation both in areas where the unit is present and in areas where it is absent. Top-elevation estimates in the area of absence of a hydrostratigraphic unit are essentially equal to those of the underlying unit, implying a thickness of zero for the unit in its area of absence. The high-resolution surface model of the top of the Upper Bedrock Unit is equivalent to a model of bedrock surface, which is present in the real world throughout the regional model domain. Likewise, the high-resolution surface model of the base of the Mt. Simon Unit is equivalent to a model of the Precambrian surface, which is also present throughout the model domain.

Except for the high-resolution surface model of the top of the Quaternary Unit—a special case developed from surface-elevation data and Lake Michigan bathymetric data—each high-resolution surface model was developed through interpolation of three general types of source data (Figure C-1). In areas east of the Mississippi River (the active cells of the regional model), structure data were used as estimates of the top elevation of the unit in areas where the unit is present, but not exposed at the bedrock surface. In areas west of the Mississippi River, structure data were used as estimates of the top elevation of the unit in all areas where the unit is present, whether or not it is exposed at the bedrock surface. Estimates of bedrock-surface elevation were employed as interpolation source data in areas of bedrock-surface exposure east of the Mississippi River. For the model of the top of the Upper Bedrock Unit, these consist principally of data derived from bedrock-surface topographic maps. For models of the other units, the bedrock-surface estimates consist of point data selected and clipped from the model of the Upper Bedrock Unit, which was completed early in the process. Estimates of the elevation of the underlying unit were generally used as interpolation source data in areas of absence of a unit. These consist of point data selected and clipped from the high-resolution surface model of the underlying unit developed earlier in the overall process.

Following interpolation, the provisional high-resolution surface model was adjusted using the previously developed high-resolution surface model of an overlying unit, or, more commonly, previously developed high-resolution surface models of both an overlying and underlying unit. Because the procedure of developing each high-resolution surface model employed previously developed high-resolution surface models, order of development of the high-resolution surface models was important to compiling an accurate high-resolution geologic

model (Table C-2). For example, high-resolution surface modeling of the top of the Upper Bedrock Unit employed data from the high-resolution surface model of the top of the Quaternary Unit, requiring that the Quaternary Unit model be completed first. The portion of each high-resolution surface model corresponding to the area of active cells east of the Mississippi River was clipped as an *active-cell high-resolution surface model* and was employed for development of the irregular-grid geologic model.

Most of the data processing leading to the high-resolution geologic model was conducted using ArcGIS version 9.1 (Environmental Systems Research Institute, 2005) and Surfer version 8 (Golden Software Inc., 2002). The terms shapefile and coverage as used in this report refer to proprietary data formats employed in ArcGIS.

Table C-1. Specialized Terminology Employed in Discussion of Geological Modeling

<i>Term</i>	<i>Definition</i>
Active-cell high-resolution surface model	Point-shapefile created from a <i>high-resolution surface model</i> containing estimates of the elevation of a hydrostratigraphic horizon at nodes in the part of the regional model domain east of the Mississippi River.
High-resolution geologic model	Set of 12 <i>high-resolution surface models</i> of the tops of each of the 11 hydrostratigraphic units and the bottom of the Mt. Simon Unit.
High-resolution surface model	Point-shapefile containing estimates of the elevation of a hydrostratigraphic horizon at nodes spaced 762 m (2500 ft) apart across the entire regional model domain.
Interpolation source data	Data sources for point-format estimates of the elevation of a hydrostratigraphic horizon that are interpolated to develop a <i>provisional high-resolution surface model</i> . Examples include high-resolution surface models, hardcopy structure-contour or bedrock-topography maps, polyline-feature shapefiles depicting bedrock topography, and point-shapefiles created by adding or subtracting thickness and structure data.
Irregular-grid geologic model	Set of 12 <i>irregular-grid surface models</i> , in Microsoft Excel format, of the tops of each of the 11 hydrostratigraphic units and the bottom of the Mt. Simon Unit.
Irregular-grid surface model	Estimates of the elevation of a hydrostratigraphic horizon for each active cell in the irregular finite-difference groundwater flow modeling grid in Microsoft Excel format. Elevation estimates are adjusted from a provisional irregular-grid surface model to accommodate a minimum model layer thickness of one foot.
Provisional high-resolution surface model	Point-shapefile containing results of interpolation of <i>interpolation source data</i> that have not been adjusted to remove <i>stratigraphic violations</i> .
Provisional irregular-grid surface model	Polygon-shapefile containing estimates of the elevation of a hydrostratigraphic horizon for each active cell in the irregular finite-difference groundwater flow modeling grid. Elevation estimates are averages for each cell of estimated elevations in an active-cell high-resolution surface model.
Stratigraphic violation	An inconsistency between two or more depictions of geologic structure (for example, hardcopy structure-contour maps, polyline-format digital structure-contour data, point-format digital interpolated elevation results, etc.) implying that one surface is at a higher elevation than another surface that is stratigraphically higher.

Table C-2. Order of Development and Interpolation Source Data of High-Resolution Surface Models

Order	High-Resolution Surface Model (HRSM)	General Description of Interpolation Source Data		
		Unit is Present (Not Exposed at Bedrock Surface)	Unit Exposed at Bedrock-Surface	Unit Absent
1	Top of Quaternary Unit (Land Surface)	NA ¹	NA	NA
2	Top of Upper Bedrock Unit (Bedrock Surface)	NA	Bedrock-surface elevation data	Bedrock-surface elevation data; Top of Quaternary Unit (HRSM) in driftless area
3	Base of Mt. Simon Unit (Precambrian Surface)	Precambrian top-elevation estimates	Top of Upper Bedrock Unit (Bedrock Surface) (HRSM) ²	NA
4	Top of Mt. Simon Unit	Mt. Simon Unit top-elevation estimates	Top of Upper Bedrock Unit (Bedrock Surface) (HRSM)	Base of Mt. Simon Unit (Precambrian Surface) (HRSM)
5	Top of Silurian-Devonian Carbonate Unit (First Iteration)	Silurian-Devonian Carbonate Unit top-elevation estimates	Top of Upper Bedrock Unit (Bedrock Surface) (HRSM)	Top of Mt. Simon Unit (HRSM)
6	Top of Eau Claire Unit	Eau Claire Unit top-elevation estimates	Top of Silurian-Devonian Carbonate Unit (First Iteration) (HRSM)	Top of Mt. Simon Unit (HRSM)
7	Top of Ironton-Galesville Unit	Ironton-Galesville Unit top-elevation estimates		Top of Eau Claire Unit (HRSM)
8	Top of Potosi-Franconia Unit	Potosi-Franconia Unit top-elevation estimates		Top of Ironton-Galesville Unit (HRSM)
9	Top of Prairie du Chien-Eminence Unit	Prairie du Chien-Eminence Unit top-elevation estimates		Top of Potosi-Franconia Unit (HRSM)
10	Top of Ancell Unit	Ancell Unit top-elevation estimates		Top of Prairie du Chien-Eminence Unit (HRSM)
11	Top of Galena-Platteville Unit	Galena-Platteville Unit top-elevation estimates		Top of Ancell Unit (HRSM)
12	Top of Maquoketa Unit	Maquoketa Unit top-elevation estimates		Top of Galena-Platteville Unit (HRSM)
13	Top of Silurian-Devonian Carbonate Unit (Second Iteration)	Silurian-Devonian Carbonate Unit top-elevation estimates	Top of Upper Bedrock Unit (Bedrock Surface) (HRSM)	Top of Maquoketa Unit (HRSM)

¹NA: not applicable

²Used in areas of Precambrian bedrock-surface exposure.

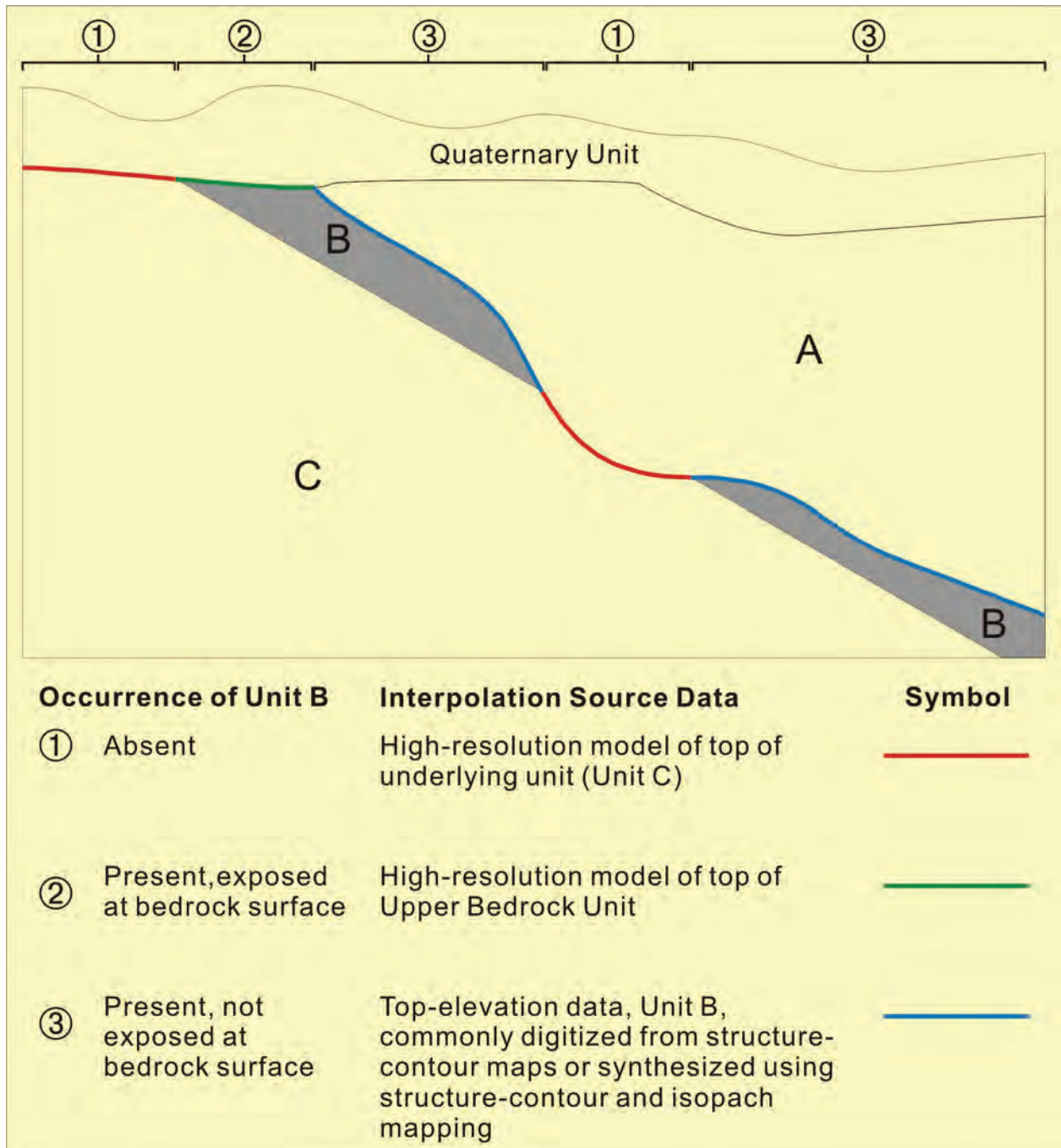


Figure C-1. General categories of source data employed for interpolation in area of active model cells.

C.1.1. Development of Required Geologic Mapping Elements

The high-resolution geologic modeling methodology required development and compilation of (1) mapping of bedrock-surface exposures of the hydrostratigraphic units; (2) mapping of areas of absence of the hydrostratigraphic units; and (3) mapping of fault features to be used as breaklines in the interpolation procedure. As described in the preceding section, mapping of areas of bedrock-surface exposure and areas of absence were employed to select elevation data from previously developed high-resolution surface models for use in the interpolation process. Mapping of fault features allowed the interpolation process to replicate escarpments along the selected faults.

C.1.1.1. Bedrock-Surface Exposures

Delineation of areas of bedrock-surface exposure—areas of outcrop and Quaternary subcrop—relied heavily on GIS-format state geologic maps of Illinois (Illinois Department of Natural Resources, 1996a) and Indiana (Gray et al., 2002) as well as a GIS-format geologic map of the Lake Superior area of Michigan, Minnesota, and Wisconsin (Cannon et al., 1997). Bedrock-surface exposures were delineated only in the portion of the regional model domain east of the Mississippi River because the trans-Mississippi area was designated as inactive. In the trans-Mississippi area, where estimated elevations of tops of hydrostratigraphic units are irrelevant, interpolation source data in areas of bedrock-surface exposure are based on structure-contour maps.

With one exception, the use of different mapping units by the authors of the geologic maps of Illinois, Indiana, and the Lake Superior area was not problematic, since the hydrostratigraphic units employed in the modeling effort are often aggregations of the lithostratigraphic mapping units used in the maps (Table C-3). The exception pertains to the Cambrian lithostratigraphic units, in which both the Illinois and Lake Superior-area geologic mapping aggregate into a single Cambrian mapping unit (Cambrian rocks are not exposed at the bedrock surface in Indiana). The regional modeling effort, however, includes Cambrian lithostratigraphic units in several hydrostratigraphic units, and development of the high-resolution geologic model consequently required that bedrock-surface exposures be delineated for these units. Numerous published and unpublished resources were employed to subdivide the mapped Cambrian bedrock-surface exposure into exposures of hydrostratigraphic units used in the modeling effort. The resulting maps of bedrock-surface exposures were saved as polygon-shapefiles for later use in data processing.

Except for a single outlier where the Franconia Formation crops out (Willman et al., 1975), Cambrian rocks crop out or subcrop the Quaternary in a small portion of Illinois immediately south of the Sandwich Fault Zone, where Cambrian bedrock-surface exposure includes the upper portion of the Franconia Formation, the Potosi Dolomite, and the Eminence Formation (Kolata et al., 1978; Willman et al., 1975). No published or unpublished resource displays the areas of bedrock-surface exposure of these formations within the Cambrian bedrock-surface exposure south of the Sandwich Fault. However, it is reasonable to conclude that rocks assigned in this paper to the Potosi-Franconia Unit make up most of the areal extent of exposure. This conclusion is based on the fact that the uneroded Potosi Dolomite thickness in the area—on the order of 150 ft—is about three times greater than that of the Eminence Formation (Willman et al., 1975), together with the fact that an unknown thickness of the Franconia Formation is reportedly exposed here. In the absence of detailed mapping of the Cambrian exposure, then, it is assumed that the entire area of the mapped Cambrian bedrock-surface exposure south of the

Sandwich Fault is a bedrock-surface exposure of the Potosi-Franconia Unit. For purposes of geologic modeling, this assumption results in an underestimation of the bedrock-surface exposure of the Prairie du Chien-Eminence Unit and an overestimation of the bedrock-surface exposure of the Potosi-Franconia Unit, since a portion of the mapped Cambrian bedrock-surface exposure must be occupied by dolomites of the Eminence Formation. The bedrock-surface exposure of the Prairie du Chien-Eminence Unit was assumed to be equivalent to the mapped area of Prairie du Chien exposure. From a hydrologic standpoint, however, this inaccuracy is probably of little importance, because the dolomites of both the Potosi-Franconia and Prairie du Chien-Eminence Units are hydraulically similar, and the mapping errors are compensatory: the overall bedrock-exposure of the two units honors the geologic mapping.

Unpublished structure-contour mapping (United States Geological Survey [USGS], Wisconsin District, personal communication, 2002), used for developing a regional groundwater-flow model of the Cambrian and Ordovician aquifers of the U.S. upper Midwest (Young, 1992), permitted the large Cambrian bedrock-surface exposure in Wisconsin to be disaggregated into bedrock-surface exposures of hydrostratigraphic units employed in the present modeling study. This mapping included delineations of areas of absence of equivalents of the Eau Claire Unit, Ironton-Galesville Unit, and Potosi-Franconia Unit.

The areas of absence illustrated on these maps were digitized for the present study, and these were displayed in an ArcGIS map file together with the Wisconsin Cambrian bedrock-surface exposure from Cannon et al. (1997). The area of bedrock-surface exposure of the Potosi-Franconia Unit was then approximated by erasing the area of absence of the Potosi-Franconia Unit (digitized from the unpublished USGS mapping) from the Cambrian bedrock-surface exposure (Cannon et al., 1997). Similarly, the area of bedrock-surface exposure of the Ironton-Galesville Unit was approximated as the portion of the Cambrian bedrock-surface exposure where the unpublished mapping showed (1) the Ironton-Galesville Unit to be present and (2) the Potosi-Franconia Unit to be absent. The bedrock-surface exposure of the Eau Claire Unit was approximated as the portion of the Cambrian bedrock-surface exposure where the unpublished mapping showed (1) the Eau Claire Unit to be present, (2) the Ironton-Galesville Unit to be absent, and (3) the Potosi-Franconia Unit to be absent. Finally, the bedrock-surface exposure of the Mt. Simon Unit was approximated as the portion of the Cambrian bedrock-surface exposure where the unpublished mapping showed the Eau Claire, Ironton-Galesville, and Potosi-Franconia Units to all be absent.

As was the case with the assumption regarding mapped Cambrian bedrock-surface exposures in Illinois, this set of assumptions regarding the Wisconsin exposure probably overestimates the bedrock-surface exposure of the Potosi-Franconia Unit at the expense of that of the Prairie du Chien-Eminence Unit. The Cambrian Eminence Formation and equivalent Jordan Formation in Wisconsin must occupy a portion of the mapped Cambrian bedrock-surface exposure, yet the assumption employed here assigns this area to the bedrock-surface exposure of the Potosi-Franconia Unit. Unlike the stratigraphically deeper units, a suitable map illustrating the area of absence of the Prairie du Chien-Eminence Unit in Wisconsin was not available, so—as was the assumption in Illinois—the area of exposure of the Prairie du Chien-Eminence Unit was assumed to be the mapped area of exposure of the Prairie du Chien Group only.

Table C-3 summarizes the aggregation of mapped geologic units in the Illinois, Indiana, and Lake Superior area geologic mapping into bedrock-surface exposures of the hydrostratigraphic units employed in the study. Offsets of contacts between mapped units at boundaries between the areas covered by the geologic maps were minor and not corrected since

these offsets would ultimately be of little importance following the averaging process leading to the irregular-grid geologic model. The resulting maps of bedrock-surface exposure areas were saved as ArcGIS polygon-shapefiles. They were generally created by selecting and—in ArcGIS Editor— copying polygons from the Illinois, Indiana, and Lake Superior area GIS-format geologic maps and pasting them into a polygon-shapefile developed for the bedrock-surface exposure of each hydrostratigraphic unit. The polygons within each of these shapefiles were then clipped using a polygon-shapefile of the regional model domain and, for clarity and ease of use, combined into a single feature.

The highly disruptive but very limited effects of the Des Plaines and Kentland Disturbances were removed from the bedrock-surface exposure mapping, effectively removing their effects from the resulting high-resolution and irregular-grid geologic models. The bedrock-surface manifestations of these features were removed because their local-scale structural effects are so poorly understood that the regional-scale structure-contour mapping that is the basis for much of the geologic modeling ignores them. Without detailed contour mapping of the subsurface structure of these features, use of the conflicting bedrock-surface exposure patterns and structure-contour data in the geologic-modeling procedure presented here would lead to an improbable rendering of the geologic structure. Removal of these probable impact features from the geologic models was viewed as acceptable for purposes of this project since their effect on regional groundwater circulation is probably negligible. The bedrock-exposure mapping of the Des Plaines Disturbance shown in the mapping of the Illinois Department of Natural Resources (1996a) was altered to remove effects of the feature on bedrock-surface geology by cutting polygons in the Disturbance representing rocks assigned to the Upper Bedrock, Maquoketa, and Ancell Units from the shapefiles developed to show bedrock-surface exposure of these units and pasting the cut polygons into the shapefile representing bedrock-surface exposure of the Silurian-Devonian Carbonate Unit. A similar approach was employed to alter the real-world bedrock-exposure pattern at the Kentland Disturbance. Here, polygon in the Disturbance representing rocks assigned to the Maquoketa Unit were cut and pasted into the shapefile representing the bedrock-surface exposure of the Silurian-Devonian Carbonate Unit. The bedrock-surface exposure patterns of the Des Plaines Disturbance and Kentland Disturbance were thus altered to resemble the bedrock surface of the surrounding, undisturbed areas.

The geologic modeling procedure required that bedrock-surface exposure patterns be assumed in areas for which bedrock-surface geologic mapping is not available, principally the area of Lake Michigan, and in Wisconsin, Lakes Winnebago, Butte des Morts, Winneconne, and Poygan, for which bedrock-surface geology is not mapped by Cannon et al. (1997). The only unmapped contact that was estimated under the area of Lake Michigan was that between the Upper Bedrock Unit and the Silurian-Devonian Carbonate Unit. This was estimated with professional judgment informed by the mapping of adjacent onshore areas by Cannon et al. (1997), Gray et al. (2002), and the Illinois Department of Natural Resources (1996a). Professional judgment was also employed to estimate contacts at the bases of the Silurian-Devonian Carbonate Unit, Maquoketa Unit, Galena-Platteville Unit, Ancell Unit, Prairie du Chien-Eminence Unit, Potosi-Franconia Unit, Ironton-Galesville Unit, and Eau Claire Unit under the areas of Lakes Winnebago, Butte des Morts, Winneconne, and Poygan. The estimated positions of these contacts are based on the mapping of Cannon et al. (1997) and the bedrock-surface exposure patterns estimated for Cambrian hydrostratigraphic units described previously.

C.1.1.2. Areas of Absence

Delineations of areas of absence were employed to select points as interpolation source data from a previously developed high-resolution surface model of an underlying unit. Areas of absence may be broadly subdivided into two categories. The first category consists of areas where older, stratigraphically deeper units are exposed at the bedrock surface. For example, the Eau Claire Unit is absent in areas where the Mt. Simon Unit and Precambrian rocks are exposed at the bedrock surface. The second category consists of areas where a unit is absent from the subsurface interval beneath the bedrock surface, either as a consequence of nondeposition or complete removal by erosion. For example, the Prairie du Chien-Eminence Unit is absent from a large area of northern Illinois and southern Wisconsin where it was completely removed by erosion prior to deposition of the Ancell Unit and its equivalents. In this area of absence, the Ancell Unit rests directly on the Potosi-Franconia and older units. Delineation of the areas of absence of each hydrostratigraphic unit required, then, aggregation of mapping showing bedrock-surface exposures of all older units (the first category of areas of absence) together with mapping showing areas of absence in the subsurface interval that is deeper than the bedrock surface (the second category).

For each hydrostratigraphic unit, mapping of bedrock-surface exposures of the older hydrostratigraphic units was compiled, with one exception, from the polygon-shapefiles depicting these exposures developed as described in the preceding section of this report. The exception is the Quaternary Unit, which is absent from a large driftless area in the northwestern part of the regional model domain that includes extreme northwestern Illinois and much of southwestern Wisconsin. The area of absence of the Quaternary Unit was mapped by digitizing as a polygon the driftless area of Wisconsin from a hardcopy Quaternary geologic map of Wisconsin (Wisconsin Geological and Natural History Survey and Wisconsin Department of Administration State Planning Office, 1976), digitizing as a polygon the driftless area of Illinois from a polyline-shapefile illustrating the bedrock-topography of Illinois (Illinois Department of Natural Resources, 1996b), and merging the two.

The second category of areas of absence are known with less certainty than are the first category, which are better understood from observation of outcrops and the logs of large numbers of shallow wells penetrating the bedrock surface. Nonetheless, resources are available, including structure-contour, isopach, and geologic mapping of significant unconformities (subcrop mapping), that allow an approximation of these areas of absence.

Unpublished structure-contour mapping (USGS, Wisconsin District, personal communication, 2002), used for developing a regional groundwater-flow model of the Cambrian and Ordovician aquifers of the U.S. upper Midwest (Young, 1992), illustrated approximate areas of absence of the Mt. Simon Unit, Eau Claire Unit, Ironton-Galesville Unit, Potosi-Franconia Unit, and Prairie du Chien-Eminence Unit in Wisconsin. These were digitized from the hardcopy maps as separate polygon shapefiles.

In Illinois, erosion preceding deposition of the Tippecanoe, Kaskaskia, and Absaroka Sequences resulted in complete removal, in certain areas, of some of the hydrostratigraphic units employed in this study; published subcrop mapping of each of these sequences was employed to delineate areas of absence. Mapping by Willman et al. (1975) shows that non-deposition was only a small influence on the configuration of areas of absence in Illinois.

Tippecanoe-Sequence subcrop mapping by Buschbach (1964) and Willman et al. (1975) was used as a basis for delineating areas of absence of the Prairie du Chien-Eminence Unit in northern Illinois (Figure C-2, Figure C-3). Unfortunately, the aggregation of lithostratigraphic

units into subcrop-mapping units employed in these maps is inconsistent. The Tippecanoe-Sequence subcrop map of Buschbach (1964), which is limited in scope to a seven-county area of northeastern Illinois, employs lithostratigraphic mapping units that are directly applicable to this study, lumping the Eminence Formation with the Gunter Sandstone and Oneota Dolomite (the lower members of the Prairie du Chien Group) so that the Potosi Dolomite subcrop shown in the map illustrates precisely the area of absence of the Prairie du Chien-Eminence Unit of this study. The map of Willman et al. (1975), which is not only more recently published—and presumably more accurate—than that of Buschbach (1964), but also covers all of northern Illinois, lumps the Eminence Formation and Potosi Dolomite into a mapping unit that is problematic in that it includes parts of two hydrostratigraphic units employed in the present study. The subcrop patterns of the Oneota-Gunter-Eminence and Potosi mapping units of Buschbach (1964) strongly resemble those of the Oneota-Gunter and Eminence-Potosi mapping units of Willman et al. (1975), respectively, in the northeastern Illinois area mapped in both studies.

The failure of these studies to adjust their subcrop mapping to the use of differing mapping units that aggregate the Eminence Formation with the overlying lower Prairie du Chien Group on the one hand (Buschbach, 1964), and with the underlying Potosi Dolomite on the other (Willman et al., 1975), suggests that the similar lithologies of the Potosi Dolomite, Eminence Formation, and Prairie du Chien Group render these units problematic to distinguish in drilling records. For purposes of groundwater flow modeling, the similar lithologies and comparable depth of burial of all of these units suggest that they are hydraulically comparable.

In the absence of more recent Tippecanoe-Sequence subcrop mapping that makes use of mapping units that are consistent with hydrostratigraphic units employed in the present study, then the authors have chosen to employ the more areally extensive subcrop map of Willman et al. (1975) as a guide to areas of absence of the Prairie du Chien-Eminence Unit, digitizing as a polygon-shapefile the mapped Eminence-Potosi and Franconia subcrops as approximations of areas of absence of the Prairie du Chien-Eminence Unit. A similar assumption was employed to delineate bedrock-surface exposures of the Prairie du Chien-Eminence and Potosi-Franconia Units, as discussed previously. If the subcrop map of Willman et al. (1975) is accurate, the described use of the map would result in an underestimation of the area of absence of the Prairie du Chien-Eminence Unit and an overestimation of the area of absence of the Potosi-Franconia Unit, since a portion of the mapped Eminence-Potosi subcrop must be occupied by dolomites of the Eminence Formation. The subcrop of the Prairie du Chien-Eminence Unit is assumed to be equivalent to the mapped area of the Prairie du Chien subcrop. From a hydrologic standpoint, however, this inaccuracy is probably of little importance, because the dolomites of both the Potosi-Franconia and Prairie du Chien-Eminence Units are hydraulically similar, and the mapping errors are compensatory: the overall Tippecanoe-Sequence subcrop of the two units honors the geologic mapping.

The approximate areas of absence of the Prairie du Chien-Eminence Unit in Wisconsin (digitized from unpublished mapping (USGS, Wisconsin District, personal communication, 2002) and in Illinois [digitized from Tippecanoe-Sequence subcrop mapping (Willman et al., 1975)] were revised slightly using professional judgment informed by a generalized mapping by Droste and Shaver (1983) and Droste and Patton (1985). This revision was necessary because the original digitized outlines, reflecting the mapped areas of the source data, abruptly terminate the areas of absence along the Illinois-Wisconsin boundary. Revision resulted in a more plausible estimation of the area of absence of the Prairie du Chien-Eminence Unit that crosses the state boundary and extends beneath a large part of southern Lake Michigan.

Kaskaskia-Sequence subcrop mapping (Willman et al., 1975) shows an area of extreme western Illinois where middle Devonian carbonates—the basal rocks of the Kaskaskia Sequence in that area—rest directly on the Galena Group. In this area the Maquoketa Group and Silurian dolomites have been completely removed by pre-Kaskaskia erosion. In terms of the hydrostratigraphic nomenclature employed in this study, the Silurian-Devonian Carbonate Unit rests directly on the Galena-Platteville Unit in this area, and the Maquoketa Unit is absent. The area where the Kaskaskia Sequence is subcropped by the Galena Group depicted by Willman et al. (1975) was therefore digitized as a polygon-shapefile showing an area of absence of the Maquoketa Unit.

Absaroka-Sequence subcrop mapping (Willman et al., 1975) show adjacent subcrop belts in an area of north-central Illinois where Pennsylvanian rocks of the Absaroka Sequence rest directly on the Ancell Group, the Galena and Platteville Groups, and the Maquoketa Group. In the Ancell Group subcrop, the Upper Bedrock Unit rests directly on the Ancell Unit, and the Silurian-Devonian Carbonate Unit, Maquoketa Unit, and Galena-Platteville Unit are absent, having been completely removed by erosion prior to deposition of the Absaroka Sequence. The Upper Bedrock Unit rests directly on the Galena-Platteville Unit where the Absaroka Sequence is subcropped by the Galena and Platteville Groups, and the Silurian-Devonian Carbonate Unit and Maquoketa Unit are absent. Finally, in the Maquoketa Group subcrop, the Upper Bedrock Unit rests directly on the Maquoketa Unit, and the Silurian-Devonian Carbonate Unit is absent. Thus, the Ancell Group subcrop, the Galena and Platteville Group subcrop, and the Maquoketa subcrop depicted by Willman et al. (1975) were digitized as a single polygon-shapefile illustrating an area of absence of the Silurian-Devonian Carbonate Unit. The Galena and Platteville Group subcrop as well as the Ancell Group subcrop were digitized as a polygon-shapefile illustrating an area of absence of the Maquoketa Unit. Lastly, the Ancell Group subcrop was digitized as a polygon-shapefile delineating an area of absence of the Galena-Platteville Unit.

With a single exception, all of the hydrostratigraphic units beneath the Quaternary Unit were deposited across all of Illinois, so that the principal generator of areas of absence in Illinois has been erosion during the periods of time between deposition of the Sauk, Tippecanoe, Kaskaskia, and Absaroka Sequences. A comparatively small area of absence of the Silurian-Devonian Carbonate Unit resulting partly from non-deposition is present in the southwestern part of the regional model domain in western Illinois along the Mississippi River. In this area, pre-Kaskaskia erosion completely removed Silurian dolomites, and Middle Devonian carbonates—the basal rocks of the Kaskaskia Sequence in the region—were not deposited. This area of absence of the Silurian-Devonian Carbonate Unit was delineated by processing polygon-shapefiles digitized from maps by Willman et al. (1975) showing the outline of the area of non-deposition of the Middle Devonian carbonates and the outline of the Maquoketa and Galena Group subcrops of the Kaskaskia Sequence. These shapefiles were processed by clipping the portion of the polygon delineating the area of non-deposition of the Middle Devonian carbonates within the polygon showing the Maquoketa and Galena Group subcrops of the Kaskaskia Sequence.

Areas of absence through erosion or nondeposition belonging to the second category described previously—those lying below the bedrock surface—do not significantly affect the distribution of the hydrostratigraphic units in Indiana and Michigan. Rupp (1991) reported that the Ancell Group in Indiana is missing in places that are areally small and poorly known and therefore are not documented in his structure-contour and isopach maps of the unit. Because the

level of detail required by the groundwater flow model is low, particularly in the model farfield of Indiana, like Rupp, these comparatively small areas of absence have been ignored. Pre-Tippecanoe, pre-Kaskaskia and pre-Absaroka erosion has affected the distribution of some lithostratigraphic units in Indiana and Michigan, but it has not completely removed any of the aggregate hydrostratigraphic units (Droste and Patton, 1985; Droste and Shaver, 1983; Rupp, 1991).

Areas of absence were delineated to a limited extent in the inactive portion of the regional model domain west of the Mississippi River. If such areas of absence were identified in the unpublished structure-contour maps used extensively for interpolation source data in this area (USGS, Wisconsin District, personal communication, 2002), their outlines were digitized as polygon-shapefiles as areas of absence. Areas of absence were delineated in the southwestern part of Minnesota because that area is covered by the Lake Superior area geologic mapping of Cannon et al. (1997; Droste and Patton, 1985) used for delineation of bedrock-surface exposures and areas of absence in Michigan and Wisconsin, but no special effort was made to digitize areas of absence from geologic maps covering the portions of Iowa and Missouri within the regional model domain. This sacrifice, made to address time and budget constraints, was viewed as acceptable chiefly because geologic model accuracy in the inactive portion of the groundwater flow model corresponding to the trans-Mississippi River area is irrelevant to the functioning of the groundwater flow model. The inclusion of points from the high-resolution surface model of an underlying unit for representation of a unit's elevation in an area of absence of the unit might, in some cases, have resulted in a small improvement in high-resolution surface model accuracy along the western boundary of the area of active cells (the Mississippi River). This improvement in high-resolution surface model accuracy would have a negligible effect on the irregular-grid model and on groundwater flow modeling results in the model nearfield.

Table C-3. Key to Aggregation of Geologic Mapping Units to Hydrostratigraphic Units

<i>Hydrostratigraphic Unit</i>	<i>Illinois (Illinois Department of Natural Resources, 1996a)</i>	<i>Indiana (Gray et al., 2002)</i>	<i>Lake Superior Area (Michigan and Wisconsin) (Cannon et al., 1997)</i>
Upper Bedrock Unit	All Cretaceous units All Pennsylvanian units All Mississippian units All Upper Devonian units	All Pennsylvanian units All Mississippian units Ellsworth Shale (Devonian) Antrim Shale (Devonian) New Albany Shale (Devonian)	All Jurassic units All Pennsylvanian units All Mississippian units Ellsworth Shale (Devonian) Antrim Shale (Devonian)
Silurian-Devonian Carbonate Unit	All Middle Devonian units All Silurian units	Muscatatuck Group (Devonian) All Silurian units	Traverse Group (Devonian) All Silurian units
Maquoketa Unit	Maquoketa Group (Ordovician)	All Ordovician units	Maquoketa Formation (Ordovician)
Galena-PlattevilleUnit	Galena-Platteville Group (Ordovician)	(Not exposed at bedrock surface)	Sinnipee Group (Ordovician)
Ancell Unit	Ancell Group (Ordovician)		Ancell Group (Ordovician)
Prairie du Chien-Eminence Unit	Prairie du Chien Group (Ordovician) (see text)		Prairie du Chien Group (Ordovician) (see text)
Potosi-Franconia Unit	All Cambrian units (see text)		None. The aggregate Cambrian mapping unit was subdivided as described in the text.
Ironton-Galesville Unit	(Not exposed at bedrock surface)		All Precambrian units
Eau Claire Unit			
Mt. Simon Unit			
Precambrian (not a modeled hydrostratigraphic unit)			

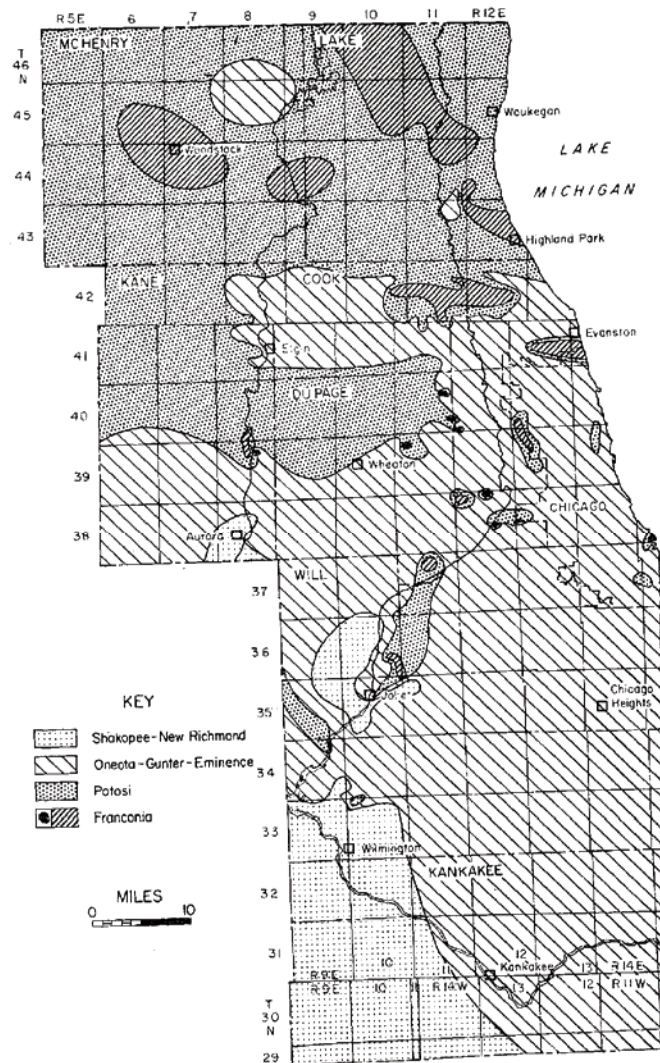


Figure C-2. Tippecanoe-Sequence subcrop map of northeastern Illinois (Buschbach, 1964). The Shakopee, New Richmond, Oneota, and Gunter units are formations within the Prairie du Chien Group.

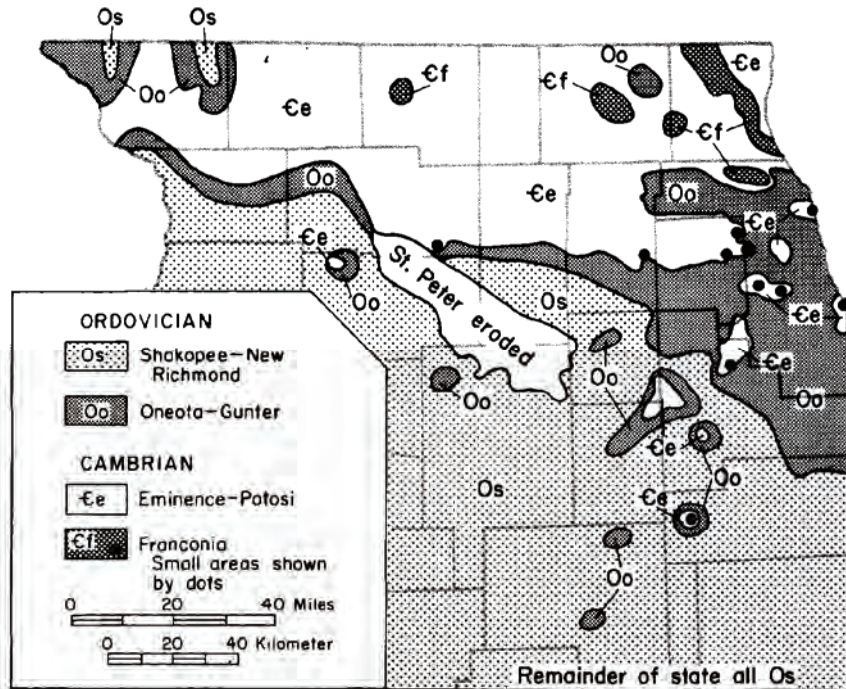


Figure C-3. Tippecanoe-Sequence subcrop map of northern Illinois (Willman et al., 1975). The Shakopee, New Richmond, Oneota, and Gunter units are formations within the Prairie du Chien Group.

C.1.1.3. Faults to be Modeled as Breakline Features

The interpolation algorithm selected for development of many of the high-resolution surface models, inverse distance to a power, permits the incorporation of faults into the interpolation process as features known as *breaklines*. In estimating a value at a given location, the search pattern of the interpolation algorithm is restricted from searching the input data on the opposite side of a breakline.

Faults were selected for explicit treatment as breaklines if they were included on structure-contour mapping used as source data for the project. All other faulting affecting the regional model domain is assumed to be represented accurately enough for purposes of groundwater flow modeling through structure contouring. The faults included as breaklines are the Plum River Fault and Sandwich Fault Zones in Illinois and the Royal Center, Fortville, and Mt. Carmel Faults in Indiana (Figure C-4). These faults offset the tops of the Silurian-Devonian Carbonate Unit and all underlying units. The Plum River Fault and the Sandwich Fault Zone, simplified to a single trace, were digitized from mapping by Visocky et al. (1985). Incorporation of the Sandwich Fault Zone in the geologic modeling as a single surface, rather than as a set of surfaces, required some simplification, using professional judgment, of the outcrop patterns illustrated in geologic mapping by the Illinois Department of Natural Resources (1996a) in the immediate vicinity of the fault zone. Indiana fault locations were digitized from mapping by Rupp (1991).



Figure C-4. Faults included as surfaces of displacement.

C.1.2. *Compilation of Interpolation Source Data*

The general procedure for developing each high-resolution surface model began with compiling estimates, as ArcGIS point-shapefiles in a consistent projection and coordinate system, of the top elevation of the surface from available digital and hardcopy sources. These compiled estimates constitute the *interpolation source data* that were interpolated to generate the high-resolution surface model. If available, digital source data, such as digital bedrock-surface topographic mapping, often required projection and transformation to the Lambert conic conformal projection used for the project (referred to as the *Illimap projection* in this report) as well as conversion from raster to vector-point format or conversion from vector-polyline to vector-point format. Hardcopy source data required digitization as polylines, followed by conversion to a vector-point format.

Source data were irregularly employed from areas outside of the regional model domain. If they were available, and if time and budget constraints permitted, source data were employed from areas outside the regional model domain, but the high-resolution and, ultimately, the irregular-grid model were developed only for the area of active model cells (i.e., the portion of the regional model domain east of the Mississippi River). The selected interpolation algorithms consider the source data from outside the regional model domain only in a limited fashion, but their inclusion in the interpolation process marginally improves the model accuracy along the edges of the regional model domain.

Most of the hardcopy maps digitized for the project are contoured maps of the tops of the hydrostratigraphic units employed in the study, either bedrock-topography or structure-contour maps. In a few cases, however, structure-contour maps were not available for the tops of hydrostratigraphic units, requiring digitization of isopach maps of one or more lithostratigraphic units and synthesis of the missing structure data. This synthesis was accomplished through a process of addition or subtraction of the thickness data to or from an adjacent, previously generated, high-resolution surface model or a digitized structure-contour map of another lithostratigraphic surface. For example, since a structure-contour map of the top of the Eau Claire Group in Indiana was not available, but an isopach map of the Eau Claire Group was available, the isopach map was digitized, and the thickness data were then interpolated. The interpolated thickness data—a thickness model of the Eau Claire Group—was then added to the previously generated high-resolution surface model of the Mt. Simon Unit to synthesize top elevation data for the Eau Claire Unit in Indiana. These data were in turn used as source data for interpolation of the high-resolution surface model of the Eau Claire Unit. Top-elevation data that were synthesized by adding or subtracting thickness data to or from a structure-contour map were saved as a point-feature shapefile.

In many cases, it was necessary for digitized structure-contour and isopach maps to be augmented, using professional judgment, with additional contours to provide enough data for ensuing interpolation procedures to generate geologically plausible results from the interpolation source data. This augmentation was made necessary because experiments with the selected interpolation algorithms showed that data derived from the relatively widely separated contours on some of the digitized maps did not adequately constrain the interpolation results. Specifically, the interpolation results using only the contour data digitized from the source maps sometimes strayed from the values of adjacent contours in the maps so that the resulting surface was not a plausible model of the data represented by the map. Interpolated surfaces based only on the map contours were especially implausible in the case of elevations interpolated in the vicinity of faults, where the search pattern of the selected interpolation algorithm is restricted to only one

side of the fault, further limiting the already sparse availability of data on which to base the interpolation result. Time and budget constraints sometimes limited the labor-intensive augmentation process to the model nearfield and to portions of the regional model domain near faults. The added contours were constructed to depict simple surfaces honoring the map contours with minimal added perturbations between the map contours.

Some editing of contours digitized from structure-contour maps used as source data was necessary to correct *stratigraphic violations* and adjust elevations in the vicinity of areas of absence. For purposes of this report, a *stratigraphic violation* occurs between two depictions of geologic structure (e.g., hardcopy structure-contour maps, polyline-format digital structure-contour data, point-format digital interpolated elevation results, etc.) when they imply that one surface is at a higher elevation than another surface that is stratigraphically higher. For example, a stratigraphic violation occurs where structure-contour maps of the tops of the Ancell Group and the Platteville Group show that the top of the Ancell Group is at a higher elevation than the top of the Platteville Group. Adjustment of contours was also necessary in the vicinity of areas of absence delineated in some structure-contour maps employed as source data. Although consistent mapping requires that structure contours at the edge of an area of absence show the elevation of the top of a mapped unit to be the same as that shown on a structure-contour map of the immediately underlying stratigraphic unit, some maps employed as source data for this study rarely meet this requirement. Thus, the digitized structure contours were repositioned, in as minimal a way as possible, to consistently and plausibly depict elevations in the vicinity of mapped areas of absence.

Before using them as interpolation source data, the elevation estimates in both point- and polyline-feature shapefiles were erased from a buffer area along state boundaries and—if fault features had displaced the surface to be modeled—from a narrow buffer on either side of faults. This removal of source data was necessary to eliminate direct juxtaposition of structure interpretations by different state and federal mapping authorities, causing differences in interpretations between mapping authorities to be resolved by the interpolation algorithm. Direct juxtaposition of competing interpretations would result in an implausible simulation of surface by the interpolation process. One buffer was employed to erase data in a 50,000-ft buffer *outside* the Illinois boundary. Erasing these data effectively forces the interpolation process to give priority to interpretations by Illinois mapping authorities in areas near the Illinois boundary. Prioritization was preferred for Illinois-based interpretations because they probably are more accurate for the parts of the model nearfield (northeastern Illinois) abutting Indiana, Lake Michigan, and Wisconsin than would be interpretations resolved mathematically by the interpolation algorithm. As the center of the Chicago metropolitan area, northeastern Illinois has been the subject of numerous geologic studies, and the authors preferred that the interpolation results prioritize interpretations of Illinois mapping authorities in the region. A second buffer was employed to erase data in a 50,000-ft strip straddling the Indiana-Michigan boundary and the Lake Michigan shoreline of Indiana, Michigan, and Wisconsin. By erasing data from a 25,000-ft strip on each side of the boundaries separating these areas, this buffer results in the interpolation algorithm giving equal priority to the competing interpretations on either side of the boundaries.

Since digitizing of structure contours and editing of the digitized polylines representing them results in polyline vertices being placed precisely on fault features employed as breaklines, polyline segments were erased in a 7,000-ft buffer on either side of the fault features to eliminate vertices located directly on the faults. Vertices located precisely on the fault features would interfere with the interpolation process, because the search pattern of the algorithm seeks

elevation data on one side of a fault, and a vertex located precisely on the fault would be employed by the algorithm to estimate elevations on both sides of the fault, resulting in implausible interpolation results. Buffers were employed to erase polyline segments along faults as a step in compiling the interpolation source data for all high-resolution surface models except those of the tops of the Quaternary and Upper Bedrock Units, which are unaffected by displacement along the faults.

After erasing point data and polyline segments from along state boundaries and, if necessary, from fault areas, an ArcGIS tool was employed to convert the polyline-shapefiles to point-shapefiles consisting of the polyline vertices. Fields were added to the attribute tables of these point-feature shapefiles to hold the x - and y -coordinates of the individual points, and another ArcGIS tool was used to populate these fields with the coordinates. If not already present, such fields were also added to the attribute tables of any point-feature shapefiles developed using thickness data for use as interpolation source data, and these fields were populated with x - and y -coordinates of the points. At the conclusion of this step, all interpolation source data consisted of point-feature shapefiles containing fields for x - and y -coordinates and a field for the elevation of the hydrostratigraphic unit to be modeled. All of these point-feature shapefiles were then exported in text format, and in Surfer, the contents of the files were appended to one another and saved in comma-delimited (.csv) format.

As previously discussed, digital source data were employed from previously completed high-resolution surface models for development of each high-resolution surface model (Table C-2). These data were selected from the previously completed high-resolution surface models using polygon-shapefiles depicting the areas of bedrock-surface exposure and absence of the surface to be modeled. The selected features were then exported in text format. In Surfer, the contents of these text files were then appended to the .csv file described in the previous paragraph, and the combined file was used as input for the interpolation process.

A polygon-shapefile of the bedrock-surface exposures of the unit was employed to select points from the previously developed high-resolution surface model of the top of the Upper Bedrock Unit (which is equivalent to a model of the bedrock surface) that fall within the bedrock-surface exposures. For example, points for development of the high-resolution surface model of the top of the Eau Claire Unit were selected from the high-resolution surface model of the top of the Upper Bedrock Unit if they fell within the polygons included in the shapefile of the bedrock-surface exposures of the Eau Claire Unit. Use of these data in the interpolation process forces the interpolation to duplicate bedrock-surface configuration in the area of bedrock-surface exposure.

Polygon-shapefiles of areas of absence were used to select points from a previously developed high-resolution surface model of an underlying unit. For example, points for development of the Eau Claire high-resolution surface model were selected from the high-resolution surface model of the top of the Mt. Simon Unit if they fell within polygons included in the shapefile of areas of absence of the Eau Claire Unit. These data force the interpolation process to duplicate the configuration of the top of the underlying unit in the areas of absence. Such duplication provides laterally extensive elevation estimates covering areas of real-world absence—a requirement of finite-difference groundwater flow modeling—and implies zero thickness, essentially, in the areas of absence. Later data processing, done in conjunction with development of the irregular-grid geologic model, assigns a minimum thickness of 1 ft to each unit in its area of absence.

C.1.3. Interpolation

A provisional high-resolution surface model was then interpolated from the compiled interpolation source data. Different interpolation algorithms employing different parameters were employed for the high-resolution surface models. A kriging algorithm was employed if the real-world surface was not displaced by faulting, but an inverse-distance algorithm was used if fault escarpments were present on the surface. The kriging algorithm was preferred if the interpolation process was not intended to duplicate fault escarpments because it provides a more realistic simulation of a geologic surface. Otherwise, the inverse-distance algorithm was employed since this algorithm can take into account breakline features and thereby generate a simulated surface that includes escarpments along faults.

A 2500-ft interpolation-node spacing was employed in all interpolations, and bounding coordinates were selected so that the interpolation results for all high-resolution surface models were consistently located at the same *x*- and *y*-coordinates. In most cases, the bounding coordinates were selected so that the area covered by the interpolation results was equivalent to the regional model domain, but in some cases, interpolation results were desired for smaller parts of the regional model domain, such as the Lake Michigan basin, and the bounding coordinates were adjusted accordingly. Parameters of the principal interpolation algorithms employed are shown in Table C-4 and Table C-5.

The quality of the interpolation resulting in each provisional high-resolution surface model was assessed using a cross-validation process (Table C-6). The cross-validation process reports statistics based on the interpolation error at a subset of *N* source data points (residual *Z*). Surfer computes each residual *Z* by removing the first observation from the subset of source data and using the remaining data and the specified algorithm to interpolate a value at the first observation location. The interpolation error is calculated using the following relationship:

$$\text{interpolation error} = \text{interpolated value} - \text{observed value}$$

The first observation is then returned to the dataset, and the interpolation error is computed with the second observation removed from the subset of source data. The process is then repeated with the third, fourth, fifth observations, etc., and removed all the way up to and including the *N*th observation. With completion of this process, *N* interpolation errors have been computed, and statistics are generated based on these errors, the most significant of which are included in Table C-6. These statistics show that the selected interpolation algorithms adequately predict an observed value when the observation has been removed from the interpolation source data and all other interpolation source data are retained. Correlation statistics show the spatial correlations between the residual *Z* and the (*x*, *y*) coordinates and elevation (*z*-coordinate) of the removed source data point are near zero.

C.1.4. Processing of Provisional High-Resolution Surface Models

Each provisional high-resolution surface model was adjusted, generally using previously generated high-resolution surface models of one overlying and one underlying surface (Table C-7). The previously generated high-resolution surface models were employed as upper and lower constraints on plausible values of the elevation of the provisional high-resolution surface model that was the subject of the adjustment. Less typically, the provisional high-resolution surface model was adjusted using only a single previously generated high-resolution surface model of an

overlying surface as an upper constraint on the plausibility of the provisional high-resolution surface model that was the subject of the adjustment.

This adjustment was undertaken to eliminate stratigraphic violations between the provisional high-resolution surface model and the high-resolution surface models of the overlying and underlying units. These stratigraphic violations occur for two main reasons. The most numerous stratigraphic violations fall in the immediate vicinity of areas of absence of the unit that is the subject of the adjustment, where interpolation source data were imported from the high-resolution surface model of the underlying unit. Because the interpolation algorithms employed for this study are not designed to strictly honor the input data, comparison of the provisional high-resolution surface model in an area of absence with the high-resolution surface model of the underlying unit (the very data used as a source for the provisional high-resolution surface model) reveals numerous small differences—both positive and negative, and always less than 0.3 m (1 ft)—between the surface models. It is the negative differences that are identified as stratigraphic violations and that are the basis for adjustment of the provisional high-resolution surface model.

The second category of stratigraphic violations result from stratigraphic violations inherited from the structure-contour mapping digitized as source data for development of the high-resolution surface models. Many, perhaps most, of these structure-contour maps were not developed in concert with one another so as to assure an absence of stratigraphic violations. Structure-contour mapping used as source data for the project was selected with care so as to avoid stratigraphic violations, but for many areas the available structure-contour mapping is limited. In some cases where structure-contour mapping was unacceptable, structure data for use as interpolation sources were synthesized by adding or subtracting thickness data to or from structure data. In other cases, the mapping—after digitization—was edited manually, based on professional judgment, to eliminate stratigraphic violations. But in still other cases in the model farfield far from northeastern Illinois, source data were not synthesized or corrected to circumvent stratigraphic violations. Stratigraphic violations between the provisional high-resolution surface model and the high-resolution surface models of overlying and underlying surfaces resulting from violations in the source data typically affect smaller areas than the first category of violations and are restricted to the model farfield, but the violations may exceed 30 m (100 ft).

As mentioned in the preceding paragraph, the interpolation process sometimes generates provisional elevation estimates in areas of absence that imply a small (<0.3 m or 1 ft) thickness of the unit. For purposes of this project, this error is acceptable, because it is a requirement of the finite-difference groundwater flow modeling code that model layers be present at all locations within the model domain, even in areas of real-world absence. Model layers are therefore assigned a consistently applied minimum thickness in such areas of absence. In this project, that minimum thickness is 1 ft. Since the thicknesses implied in areas of absence are less than the 1 ft minimum thickness, the small implied thicknesses in areas of absence are ignored, and not corrected, in the provisional high-resolution surface models. In fact, with development of the irregular-grid model, these implied thicknesses—rather than being eliminated—are increased to 1 ft to satisfy groundwater flow-modeling requirements.

Adjustments were made to the provisional high-resolution surface model in ArcGIS after converting the interpolation results to a point-feature shapefile. Examples of these adjustments are illustrated as a plot (Figure C-5) and unrelated table (Figure C-6). The fields X (the x-coordinate), Y (the y-coordinate), and PROV (the provisional interpolated elevation value) are the

values imported from the text file holding the Surfer interpolation results. A long-integer field INDEX was added to the attribute table, as it was for all previously generated high-resolution interpolation results, and the field was populated with a unique, location-based index value using the formula $INDEX = (X \times 10000000) + Y$.

This is the same formula used for populating the INDEX field in all previously generated high-resolution interpolation results. Since the interpolations were constrained so as to give results at a consistent set of locations, the INDEX field was employed to join the attribute table to previously generated high-resolution surface models of the stratigraphically nearest-available overlying and underlying units. For example, if the subject of the data processing was a provisional high-resolution surface model of the Eau Claire Unit, the shapefile attribute table was joined to the attribute table of the high-resolution surface models of the Silurian-Devonian Carbonate Unit (the stratigraphically nearest-available high-resolution surface model of an overlying unit, since such models were not yet generated for hydrostratigraphic units between the Silurian-Devonian Carbonate Unit and the Eau Claire Unit) and the Mt. Simon Unit (the underlying unit).

Fields were added to the attribute table of the provisional high-resolution surface model to hold elevations of the underlying and overlying units from the joined tables for use as lower and upper constraints on plausible values for the provisional high-resolution surface model (LOW and UPP, respectively, in Figure C-6). The added fields were populated with elevations of the underlying and overlying units. The table join was then removed.

Three additional fields were added to the attribute table of the provisional high-resolution surface model and then populated. One was a field to hold a value calculated as the difference between the provisional high-resolution interpolation results and the final high-resolution surface elevation of the stratigraphically nearest-available underlying unit (field PROV_LOW in Figure C-6). The second was a field for a value calculated as the difference between the final high-resolution surface elevation of the stratigraphically nearest-available overlying unit and the provisional high-resolution interpolation results (field UPP_PROV in Figure C-6). The last field (FINAL in Figure C-6) was added to hold the elevations of the high-resolution surface model determined from the provisional values and the imported elevations from the high-resolution surface models of the stratigraphically nearest-available overlying and underlying units.

Records in the attribute table were selected for which provisional interpolated elevations were lower than the high-resolution surface model of the underlying surface (see records in Figure C-6 for which the field PROV_LOW is negative). Since such elevations imply that the thickness of the unit that is the subject of the data processing is negative at the selected points, an adjustment of the provisional interpolated elevation at the selected points was necessary. Thus, the elevation of the high-resolution surface model of the stratigraphically nearest-available underlying unit was employed as the elevation of the high-resolution surface model of the unit that was the subject of the data processing. In the example in Figure C-6, then, the value of the field FINAL was calculated for the selected records as the value in the field LOW. In the same way, records in the attribute table were selected for which provisional interpolated elevations were higher than the high-resolution surface model of the overlying surface (see records in Figure C-6 for which the field UPP_PROV is negative). For the selected records, the elevation of the high-resolution surface model of the stratigraphically nearest-available overlying unit was employed as the elevation of the high-resolution surface model of the unit that was the subject of the data processing. Referring to the example (Figure C-6), the value in the field FINAL was calculated for the selected records as the value in the field UPP. For all other records in the

attribute table of the provisional high-resolution surface model—those for which the provisional interpolated elevation was between the imported elevations from the high-resolution surface models of the stratigraphically nearest-available overlying and underlying units —the provisional interpolated elevation was employed as the elevation in the high-resolution surface model. In the example (Figure C-6), the field FINAL for such records was populated with the elevation in the field PROV. The high-resolution surface model consists of the x- and y-coordinates together with the adjusted interpolated elevations—that is, the data in the fields X, Y, and FINAL in the example (Figure C-6).

The adjustment process was the final step in development of each high-resolution surface model. Point features located west of the Mississippi River (the inactive portion of the regional model) were then erased from each high-resolution surface model using a polygon-shapefile delineating the portion of the regional model domain west of the Mississippi River. This step created the active-cell high-resolution surface model, which was used to develop the irregular-grid geologic model.

Table C-4. Parameters of Kriging Algorithm Having Output Grid Coincident with Regional Model Domain

<i>Gridding Method</i>	<i>Kriging</i>
Kriging Type	Point
Polynomial Drift Order	0
Kriging std. deviation grid	no
Output Grid	
Minimum x	2361500 ft
Maximum x	4269000 ft
Minimum y	2236000 ft
Maximum y	4116000 ft
x and y spacing	2500 ft
Semi-Variogram Model	
Component Type	Linear
Anisotropy Angle	0
Anisotropy Ratio	1
Variogram Slope	1
Search Parameters	
Search Ellipse Radius #1	600000 ft
Search Ellipse Radius #2	600000 ft
Search Ellipse Angle	0
Number of Search Sectors	8
Maximum Data Per Sector	8
Maximum Empty Sectors	6
Minimum Data	3
Maximum Data	64

Table C-5. Parameters of Inverse Distance Algorithm Having Output Grid Coincident with Regional Model Domain

<i>Gridding Method</i>	<i>Inverse Distance to a Power</i>
Weighting Power	1
Smoothing Factor	0
Anisotropy Ratio	1
Anisotropy Angle	0
Output Grid	
Minimum x	2361500 ft
Maximum x	4269000 ft
Minimum y	2236000 ft
Maximum y	4116000 ft
x and y spacing	2500 ft
Search Parameters	
Search Ellipse Radius #1	2280000 ft
Search Ellipse Radius #2	2280000 ft
Search Ellipse Angle	0
Number of Search Sectors	8
Maximum Data Per Sector	8
Maximum Empty Sectors	6
Minimum Data	3
Maximum Data	64

Table C-6. Cross-Validation Statistics for Interpolations of Elevation Data

Surface	Univariate Cross-Validation Statistics			Inter-Variable Correlation with Residual Z at Validation Points		
	Median Abs. Deviation of Residual Z	Mean of Residual Z	Root Mean Square of Residual Z	X	Y	Z
Top of Quaternary Unit	0.009	-0.013	1.817	-0.045	-0.020	0.002
Top of Upper Bedrock Unit (Preliminary Onshore Surface Model)	0.639	-0.267	10.426	-0.002	-0.024	-0.167
Top of Upper Bedrock Unit (Preliminary Lake Michigan Surface Model)	23.440	0.348	51.289	0.025	-0.043	-0.305
Top of Silurian-Devonian Carbonate Unit (Second Iteration)	7.338	0.034	30.729	0.011	-0.012	-0.120
Top of Silurian-Devonian Carbonate Unit (First Iteration)	8.955	0.877	31.883	-0.003	0.017	-0.137
Top of Maquoketa Unit	7.094	1.900	29.689	0.004	-0.046	-0.019
Top of Galena-Platteville Unit	15.102	0.903	46.515	-0.098	-0.054	-0.007
Top of Ancell Unit	4.217	0.164	36.201	0.019	-0.000 ¹	-0.100
Top of Prairie du Chien-Eminence Unit	6.261	-2.275	42.590	0.039	0.009	-0.115
Top of Potosi-Franconia Unit	2.967	1.169	35.794	0.004	0.031	-0.157
Top of Ironton-Galesville Unit	2.068	0.648	29.070	-0.025	0.037	-0.072
Top of Eau Claire Unit	2.028	0.702	28.089	-0.014	-0.008	-0.138
Top of Mt. Simon Unit	9.733	-4.713	74.259	-0.026	0.017	-0.100
Base of Mt. Simon Unit	27.173	0.649	113.785	-0.010	-0.024	-0.186

¹ Between 0 and -0.0005

Table C-7. High-Resolution Surface Models Used As Constraints for Adjustment of Provisional High-Resolution Surface Models

<i>Order</i>	<i>Provisional High-Resolution Surface Model</i>	<i>High-Resolution Surface Models used as Constraints</i>	
		<i>Lower Constraint</i>	<i>Upper Constraint</i>
1	Top of Quaternary Unit (Land Surface)	None	None
2	Top of Upper Bedrock Unit (Bedrock Surface)	None	Top of Quaternary Unit (Land Surface)
3	Base of Mt. Simon Unit (Precambrian Surface)	None	Top of Upper Bedrock Unit (Bedrock Surface)
4	Top of Mt. Simon Unit	Base of Mt. Simon Unit (Precambrian Surface)	Top of Upper Bedrock Unit (Bedrock Surface)
5	Top of Silurian-Devonian Carbonate Unit (First Iteration)	Top of Mt. Simon Unit	Top of Upper Bedrock Unit (Bedrock Surface)
6	Top of Eau Claire Unit	Top of Mt. Simon Unit	Top of Silurian-Devonian Carbonate Unit (First Iteration)
7	Top of Ironton-Galesville Unit	Top of Eau Claire Unit	Top of Silurian-Devonian Carbonate Unit (First Iteration)
8	Top of Potosi-Franconia Unit	Top of Ironton-Galesville Unit	Top of Silurian-Devonian Carbonate Unit (First Iteration)
9	Top of Prairie du Chien-Eminence Unit	Top of Potosi-Franconia Unit	Top of Silurian-Devonian Carbonate Unit (First Iteration)
10	Top of Ansell Unit	Top of Prairie du Chien-Eminence Unit	Top of Silurian-Devonian Carbonate Unit (First Iteration)
11	Top of Galena-Platteville Unit	Top of Ansell Unit	Top of Silurian-Devonian Carbonate Unit (First Iteration)
12	Top of Maquoketa Unit	Top of Galena-Platteville Unit	Top of Silurian-Devonian Carbonate Unit (First Iteration)
13	Top of Silurian-Devonian Carbonate Unit (Second Iteration)	Top of Maquoketa Unit	Top of Upper Bedrock Unit (Bedrock Surface)

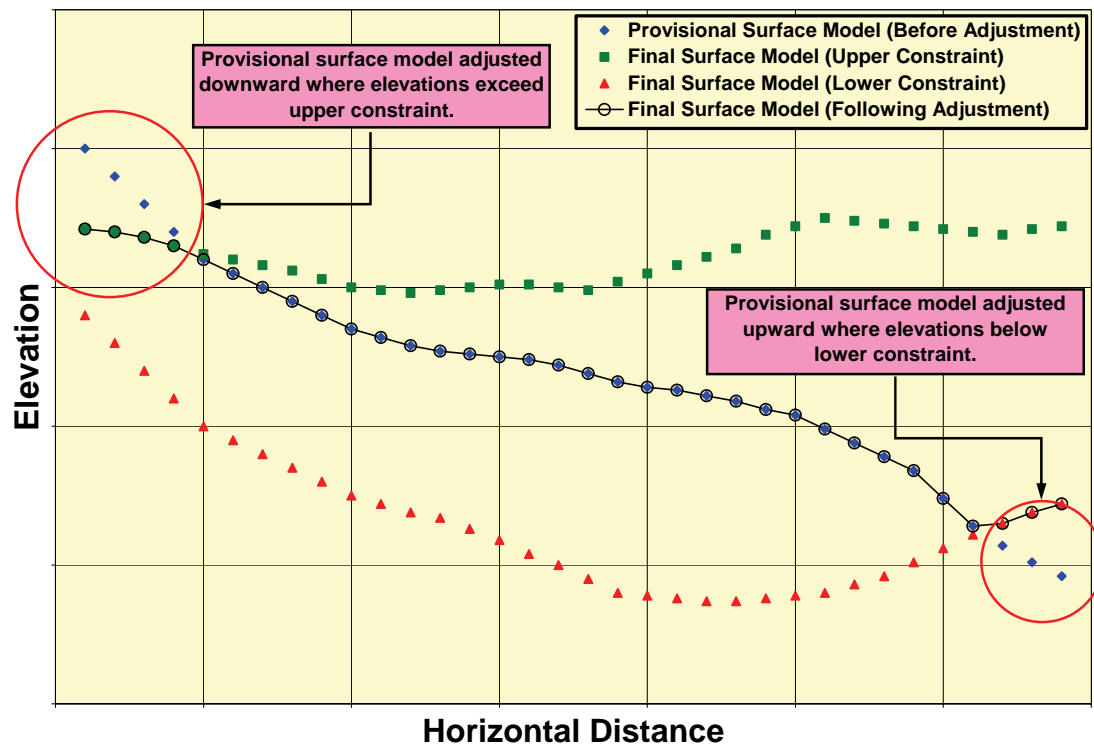


Figure C-5. Plot illustrating adjustment of provisional high-resolution surface model.

Figure C-6. Adjustment of provisional high-resolution surface model to lower (red box) and upper (green box) constraints based on previously developed high-resolution surface models of underlying and overlying units.

C.1.5. Development of High-Resolution Surface Models

C.1.5.1. Top of Quaternary Unit (Land Surface)

Development of the high-resolution model of the top of the Quaternary Unit required separate development of high-resolution surface models for the onshore area—that is, the area not occupied by Lake Michigan—and for Lake Michigan. These separate models were then combined into a single high-resolution model covering the entire area. For the onshore area, land surface elevation was estimated as the median elevation, based on USGS Digital Elevation Models (DEMs), in each 2500-by-2500 ft cell of the high-resolution grid. Since the DEM elevations represent the lake surface in the area of Lake Michigan, development of the high-resolution model of the top of the Quaternary Unit required separate construction of a model of the bottom of Lake Michigan based largely on digital Lake Michigan bathymetric mapping (National Oceanic and Atmospheric Administration Satellite and Information Service, 1996). This interpolation was conducted using a kriging algorithm designed for a rectangular area surrounding the southern part of Lake Michigan (Table C-8). Interpolation source data consisted of the digitized lake bottom elevation data and onshore land-surface elevation data obtained from DEMs. The high-resolution surface model of the top of the Quaternary Unit was completed by substituting the interpolated lake-bottom elevations for the water-surface elevations computed from the DEMs for the area of Lake Michigan.

C.1.5.2. Top of Upper Bedrock Unit (Bedrock Surface)

The second high-resolution surface model generated depicts the top of the Upper Bedrock Unit and is equivalent to a high-resolution surface model of the bedrock surface. The bedrock surface represents the surface underlying the glacial drift and—in a few major river valleys in the region—the surface underlying post-glacial alluvium. The process of developing the high-resolution surface model of the top of the Upper Bedrock Unit required development of separate preliminary high-resolution surface models of the top of the Upper Bedrock Unit in (1) the onshore part of the regional model domain (the *preliminary onshore high-resolution surface model of the top of the Upper Bedrock Unit*) and (2) the Lake Michigan part of the domain (the *preliminary Lake Michigan high-resolution surface model of the top of the Upper Bedrock Unit*). These preliminary models were then combined into a provisional high-resolution surface model of the top of the Upper Bedrock Unit, which was then adjusted to eliminate stratigraphic violations.

Several sets of source data were compiled to generate the preliminary onshore high-resolution surface model of the top of the Upper Bedrock Unit (Figure C-7). Sources include an Arc/Info coverage of bedrock-surface topography in Illinois based on Herzog et al. (1994) (Illinois Department of Natural Resources, 1996b), converted to shapefile format; polyline-feature shapefiles depicting bedrock-surface topography in Indiana (Indiana Geological Survey, personal communication, 2003) and in the seven-county southeastern Wisconsin area (Wisconsin Geological and Natural History Survey, personal communication, 2003), referenced to the Illimap projection; and a hardcopy map of bedrock-surface topography in the lower peninsula of Michigan (Western Michigan University Department of Geology, 1981), digitized for the project.

For the area of absence of the Quaternary Unit (the driftless area of southwestern Wisconsin and northwestern Illinois), source data for development of the preliminary onshore

high-resolution surface model of the top of the Upper Bedrock Unit were copied from the high-resolution surface model of the top of the Quaternary Unit using a polygon-shapefile of the driftless area described previously.

Since faulting has not affected the bedrock surface, a kriging algorithm was employed for the interpolation with parameters as specified in Table C-4. The interpolation results—by default saved in the Surfer grid format—were exported from Surfer in text format. This text file was subsequently imported to ArcGIS, where it was saved in point-shapefile format, a step marking completion of the preliminary onshore high-resolution surface model of the top of the Upper Bedrock Unit.

Fewer source data were available for developing the preliminary high-resolution Lake Michigan Upper Bedrock model (Figure C-8). Of greatest importance was a point-feature shapefile giving estimates of bedrock-surface elevation at locations in southern Lake Michigan that was provided by the Wisconsin Geological and Natural History Survey (personal communication, 2002). These data were employed in construction of a groundwater flow model covering the southeastern Wisconsin area (Feinstein et al., 2003). A second point-feature shapefile was developed from points marking the terminations at the boundary of Lake Michigan of polylines in the digital bedrock-surface maps of Illinois (Illinois Department of Natural Resources, 1996b), southeastern Wisconsin (Wisconsin Geological and Natural History Survey, personal communication, 2003), Indiana (Indiana Geological Survey, personal communication, 2003), and the hardcopy bedrock-topographic map of the lower peninsula of Michigan digitized for this project (Western Michigan University Department of Geology, 1981).

A kriging algorithm designed for a smaller output grid covering only the Lake Michigan area was employed for interpolation (Table C-8). Interpolation results were exported as a text file, which was then imported into ArcGIS and saved in point-shapefile format. The points in the resulting shapefile lying in the area outside of Lake Michigan were then erased using a polygon-shapefile of Lake Michigan, a step that marked completion of the preliminary high-resolution Lake Michigan bedrock-surface model.

The two preliminary high-resolution surface models of the top of the Upper Bedrock Unit—one of the onshore area and one of the Lake Michigan area—were then combined into a single shapefile. For the most part, the interpolated elevations along the interface between the points in the two shapefiles (that is, those points located along the Lake Michigan coast) were consistent with one another, but inconsistencies in the source data of the two interpolations resulted in significant disagreement in the interpolated elevations in the far northeastern part of Lake Michigan within the regional model domain. For this reason, a simple combination of the preliminary high-resolution onshore and Lake Michigan Upper Bedrock models would have resulted in an unlikely bedrock-surface configuration in this part of Lake Michigan. Thus, the final combination of the preliminary high-resolution surface model of the top of the Upper Bedrock Units was manually adjusted to include a small portion of the preliminary high-resolution onshore Upper Bedrock model within the area of Lake Michigan, where otherwise the preliminary high-resolution Lake Michigan Upper Bedrock model was employed (Figure C-9). To combine the two preliminary high-resolution surface models, the point features from the areas of the two models shown in Figure C-9 were selected, copied, and pasted into a new point-feature shapefile. Combination of the two preliminary high-resolution surface models of the Upper Bedrock Unit completed the provisional high-resolution surface model of the top of the Upper Bedrock Unit.

The provisional high-resolution surface model of the top of the Upper Bedrock Unit was then adjusted using the high-resolution surface model of the top of the Quaternary Unit as an upper constraint, marking completion of the high-resolution surface model of the Upper Bedrock Unit. The portion of the high-resolution surface model of the top of the Upper Bedrock Unit west of the Mississippi River was then erased to create the active-cell high-resolution surface model of the top of the Upper Bedrock Unit.

Table C-8. Parameters of Kriging Algorithm Having Output Grid Coincident with Lake Michigan Region

<i>Gridding Method</i>	<i>Kriging</i>
Kriging Type	Point
Polynomial Drift Order	0
Kriging std. deviation grid	no
Output Grid	
Minimum x	3424000 ft
Maximum x	3894000 ft
Minimum y	3128500 ft
Maximum y	4116000 ft
x and y spacing	2500 ft
Semi-Variogram Model	
Component Type	Linear
Anisotropy Angle	0
Anisotropy Ratio	1
Variogram Slope	1
Search Parameters	
Search Ellipse Radius #1	433000 ft
Search Ellipse Radius #2	433000 ft
Search Ellipse Angle	0
Number of Search Sectors	8
Maximum Data Per Sector	8
Maximum Empty Sectors	6
Minimum Data	3
Maximum Data	64

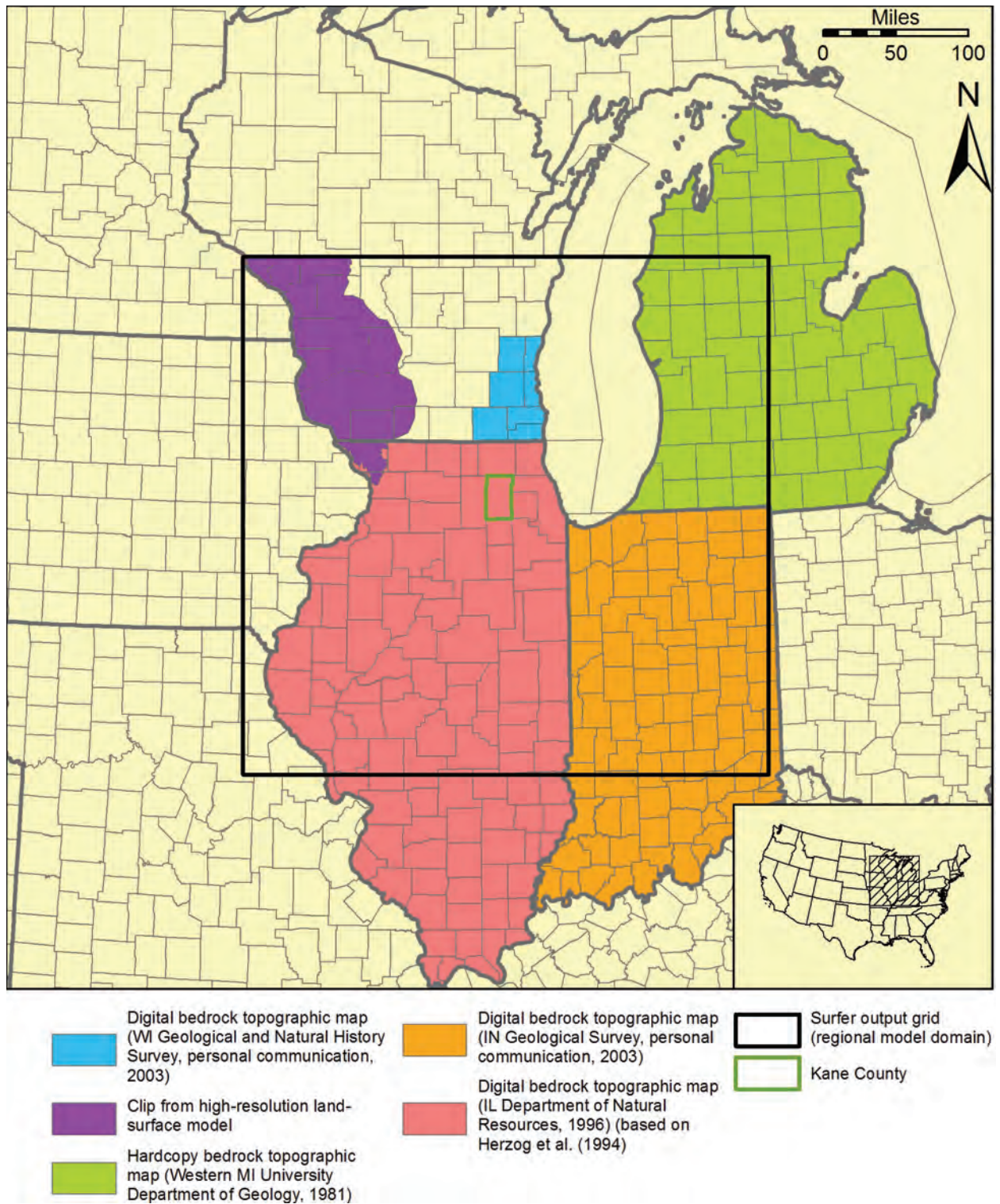


Figure C-7. Sources of data for the preliminary onshore high-resolution surface model of the top of the Upper Bedrock Unit.

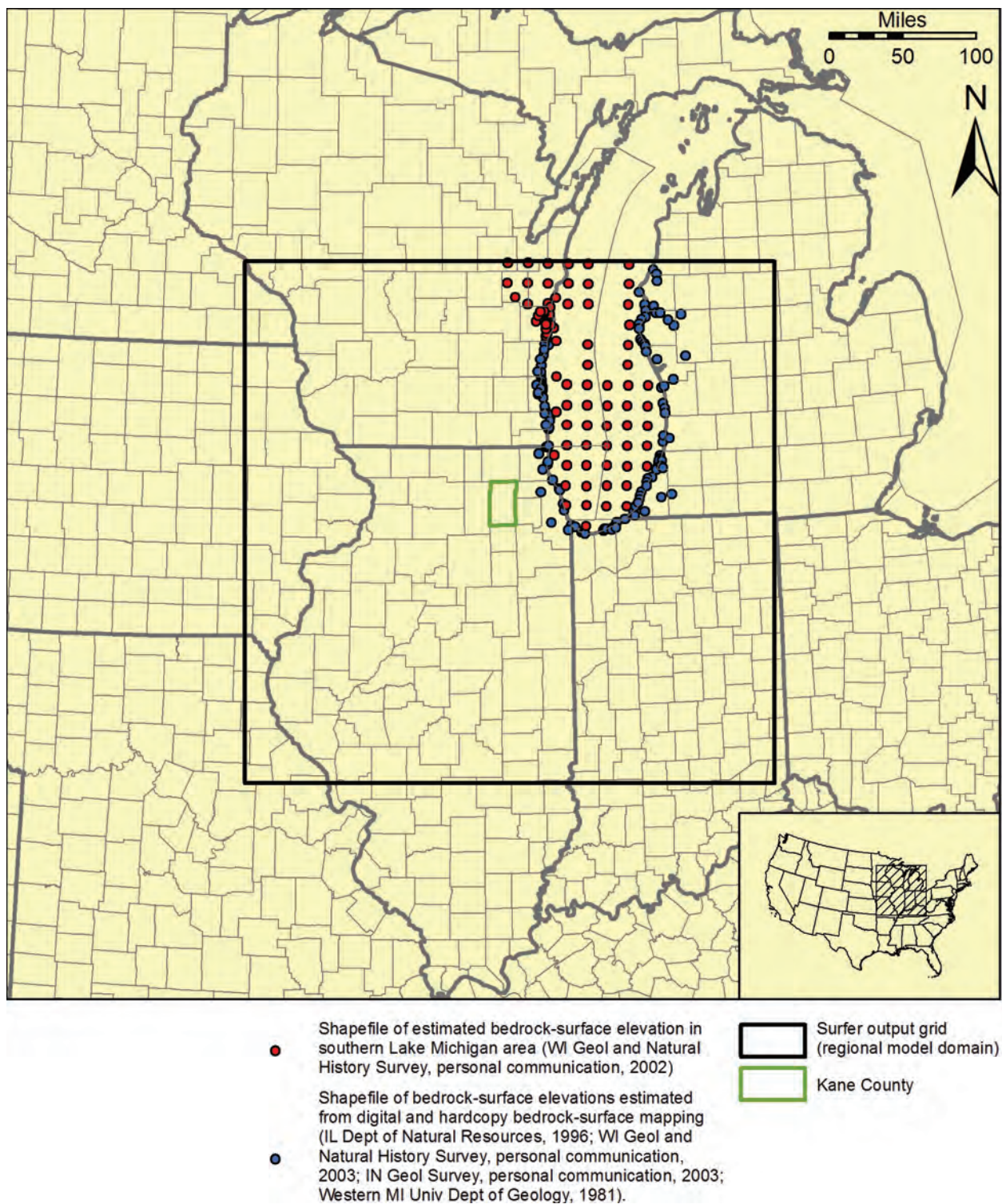


Figure C-8. Sources of data for preliminary Lake Michigan high-resolution surface model of the top of the Upper Bedrock Unit.

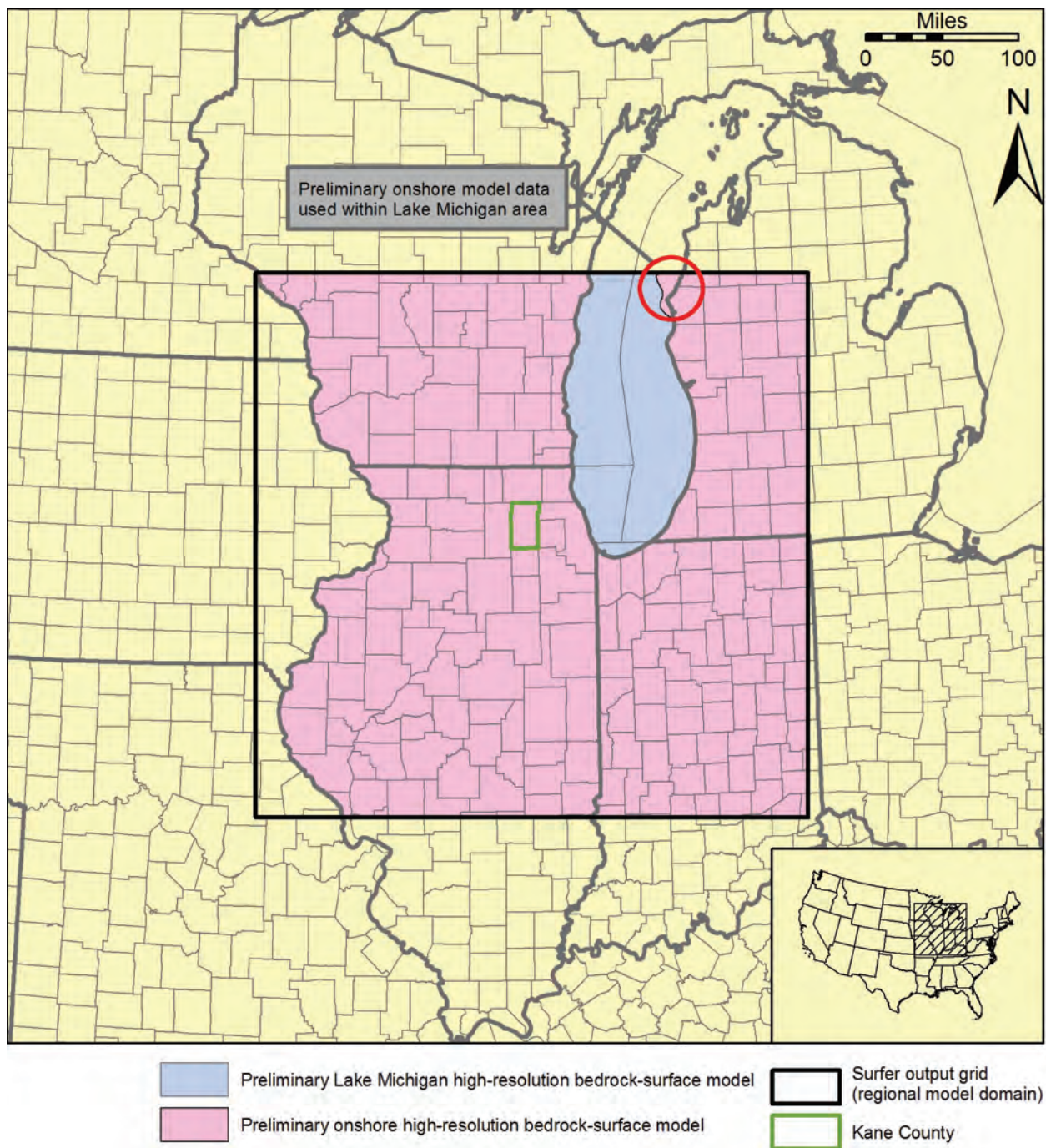


Figure C-9. Development of final high-resolution surface model of top of Upper Bedrock Unit from preliminary onshore and Lake Michigan models.

C.1.5.3. Base of Mt. Simon Unit (Precambrian Surface)

Structure-contour mapping of the Precambrian surface was digitized and employed as interpolation source data for development of the high-resolution surface model of the base of the Mt. Simon Unit for all areas except the Lower Peninsula of Michigan, most of Lake Michigan, and areas of bedrock-surface exposure of the Precambrian (Figure C-10). Structure contours digitized as polylines from the Precambrian structure-map of Visocky et al. (1985) were augmented with additional contours, positioned using professional judgment in a high-priority area encompassing the model nearfield and the Plum River Fault and Sandwich Fault Zone. The contours digitized from an unpublished structure-contour map of the Precambrian surface (USGS, Wisconsin District, personal communication, 2002) were edited to correct stratigraphic violations of digitized structure contours of overlying hydrostratigraphic units and for consistency with structure-contour maps of overlying and underlying units in the vicinity of mapped areas of absence. This mapping was not employed as the basis for the high-resolution surface model in northern Illinois, where the mapping of Visocky et al. (1985)—which is based on local studies and is presumed to be more accurate in that area—was used. The USGS mapping was employed in central Illinois, but it was edited to adjust contour positions to those along the southern border of the northern Illinois area where the data of Visocky et al. (1985) were used. Contours digitized from a structure-contour map of the Precambrian surface in Indiana (Rupp, 1991) required no editing and were not augmented.

Source data for the Michigan portion of the high-resolution surface model of the base of the Mt. Simon Unit were synthesized by effectively subtracting an isopach map of the Mt. Simon Formation from a structure-contour map of the Mt. Simon. Both maps were developed by Bricker et al. (1983). More recently published Precambrian structure-contour mapping in Michigan (Catacosinos and Daniels, 1991) was not employed as source data for the high-resolution surface model because of numerous, severe stratigraphic violations between this map and structure-contour maps of shallower horizons developed by Bricker et al. (1983) that are used extensively as source data for the high-resolution surface models of these shallower horizons. Both the Mt. Simon isopach map and structure-contour map of Bricker et al. (1983) were digitized as polyline-shapefiles. Each shapefile was then augmented with additional contours, positioned using professional judgment between the locations of the published contours. A point-shapefile was then generated from the two polyline-shapefiles containing the structure and thickness contours using an ArcGIS tool to calculate the intersections of the polylines in these shapefiles. A field was added to the attribute table of the resulting point-shapefile to represent the estimated Mt. Simon base elevation, and this field was calculated as the difference between the Mt. Simon top elevation and the Mt. Simon thickness—fields that were inherited from the parent polyline-shapefiles.

Scant geologic data is available for the area of Lake Michigan. The Precambrian structure-contour mapping of Catacosinos and Daniels (1991) was digitized and employed for a small amount of Mt. Simon base elevation data in the eastern part of Lake Michigan, but for the most part, structure contours were estimated using professional judgment for the entire area of Lake Michigan within the regional model domain. The contours were constructed to depict a simple surface, with minimal added perturbations, that completely honors the Mt. Simon base-elevation data in surrounding areas as shown in Figure C-10.

For areas of bedrock-surface exposure of the Precambrian, source data for development of the high-resolution surface model of the base of the Mt. Simon Unit were obtained from the

previously developed high-resolution surface model of the top of the Upper Bedrock Unit if they were located within polygons of a shapefile of the Precambrian bedrock-surface exposures.

Since faulting has affected the Precambrian surface, the inverse-distance algorithm (Table C-5) was employed for interpolation of the source data, with breaklines included in a .bln file developed from the shapefile containing the five fault features discussed previously (Section C.1.1.3). This provisional high-resolution surface model of the base of the Mt. Simon Unit was then adjusted using the high-resolution surface model of the top of Upper Bedrock Unit as an upper constraint. The portion of the resulting high-resolution surface model of the base of the Mt. Simon Unit west of the Mississippi River was then erased to create the active-cell high-resolution surface model of the base of the Mt. Simon Unit.

C.1.5.4. Top of Mt. Simon Unit

Structure-contour mapping of the top of the Mt. Simon Sandstone was digitized and employed as source data for development of the high-resolution surface model of the top of the Mt. Simon Unit for all areas except the northern half of Illinois, Lake Michigan, and areas of bedrock-surface exposure of the Mt. Simon Unit (Figure C-11). Structure contours digitized as polylines from the Michigan Mt. Simon structure map of Bricker et al. (1983) were augmented with contours, positioned using professional judgment between the contours appearing in the published map. Contours digitized from an unpublished structure-contour map of the Precambrian surface (USGS, Wisconsin District, personal communication, 2002) were edited to correct stratigraphic violations of digitized structure contours of overlying hydrostratigraphic units and for consistency with structure-contour maps of overlying and underlying units in the vicinity of mapped areas of absence. This mapping was not employed as the basis for the high-resolution surface model in northern Illinois, where the local Eau Claire structure-contour mapping of Visocky et al. (1985) was used in conjunction with Illinois statewide mapping of Eau Claire thickness (Willman et al., 1975) to synthesize Mt. Simon structure data. The unpublished USGS mapping was employed in central Illinois, but it was edited to adjust contour positions to those along the southern border of the northern Illinois area where the data of Visocky et al. (1985) and Willman et al. (1975) were used. Contours digitized from a structure-contour map of the Precambrian surface in Indiana (Rupp, 1991) required no editing and were not augmented.

Source data for the northern Illinois portion of the high-resolution surface model of the top of the Mt. Simon Unit were obtained by effectively subtracting an isopach map of the Eau Claire Formation (Willman et al., 1975) from a structure-contour map of the Eau Claire (Visocky et al., 1985). Visocky et al. (1985) published a structure-contour map of the top of the Elmhurst-Mt. Simon Aquifer in northern Illinois, but since this map shows the top elevation of the basal Elmhurst Member of the Eau Claire Formation, not that of the Mt. Simon Sandstone (the top of the Mt. Simon Unit of the present study), the step of subtracting a thickness map of the Eau Claire from a structure-contour map was taken to develop a more accurate Mt. Simon Sandstone structure map consistent with the definition of the *Mt. Simon Unit* employed in this study. To accomplish this, the Eau Claire structure-contour map (Visocky et al., 1985) was first digitized as a polyline-shapefile. The Eau Claire isopach map (Willman et al., 1975) was then scanned, and the scanned image was registered to the digitized Eau Claire structure-contour map. With both the digitized structure-contour map and scanned thickness map displayed on screen, a Mt. Simon structure map was constructed manually, using the approximate elevation of the top of the Mt. Simon at intersections of structure contours and isopachs as a guide. The constructed contours were then augmented with additional contours, positioned using professional judgment between the contours appearing in the published map. This augmentation process was limited to

a high-priority area encompassing the model nearfield and the Plum River Fault and Sandwich Fault Zone and was necessary to permit the interpolation algorithm to generate a geologically plausible surface from the source data.

Structure contours were estimated using professional judgment for the entire area of Lake Michigan within the regional model domain. The contours were constructed to depict a simple surface, with minimal added perturbations, that completely honors the Mt. Simon top-elevation data in surrounding areas as shown in Figure C-11.

Interpolation source data for areas of bedrock-surface exposures of the Mt. Simon Unit were generated by selecting and exporting point-features located within these exposures from the previously-developed high-resolution surface model of the top of the Upper Bedrock Unit. Similarly, interpolation source data for areas of absence of the Mt. Simon Unit were generated by selecting and exporting point-features located within these areas from the previously developed high-resolution surface model of the base of the Mt. Simon Unit.

Since faulting has affected the top of the Mt. Simon Unit, the inverse-distance algorithm (Table C-5) was employed for interpolation of the source data, with breaklines included in a .bln file developed from the shapefile containing the five fault features discussed previously (Section C.1.1.3). The provisional high-resolution surface model of the top of the Mt. Simon Unit was then adjusted using the high-resolution surface models of the top of the Upper Bedrock Unit and the base of the Mt. Simon Unit as upper and lower constraints, respectively. The portion of the resulting high-resolution surface model of the top of the Mt. Simon Unit west of the Mississippi River was then erased to create the active-cell high-resolution surface model of the top of the Mt. Simon Unit.

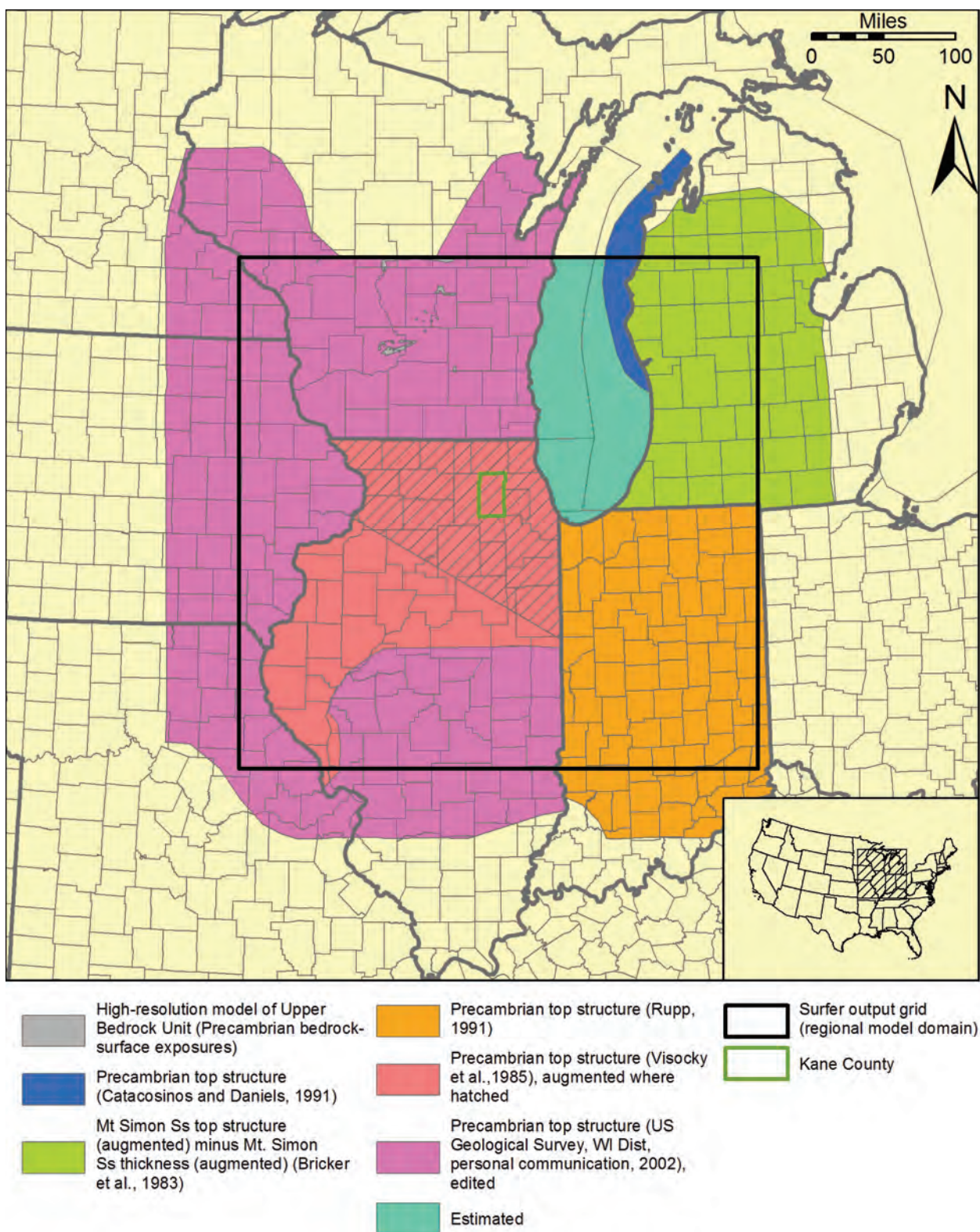


Figure C-10. Sources of data for high-resolution surface model of base of Mt. Simon Unit.

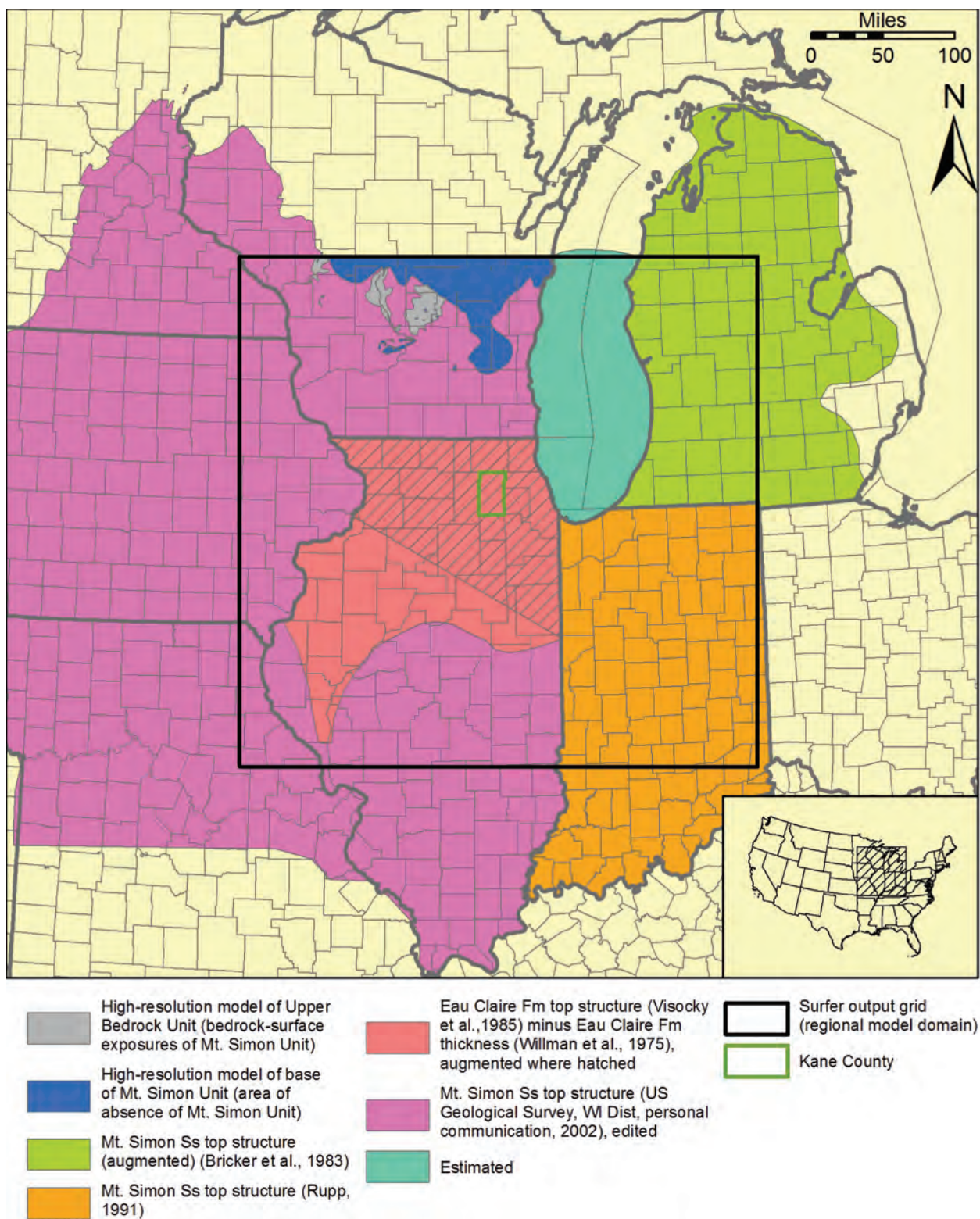


Figure C-11. Sources of data for high-resolution surface model of top of Mt. Simon Unit.

C.1.5.5. Top of Silurian-Devonian Carbonate Unit (First Iteration)

A first-iteration high-resolution surface model of the top of the Silurian-Devonian Carbonate Unit was developed for use as input to the development of the high-resolution surface models of underlying hydrostratigraphic units not yet completed (tops of the Eau Claire, Ironton-Galesville, Potosi-Franconia, Prairie du Chien-Eminence, Ancell, Galena-Platteville, and Maquoketa Units). Specifically, data from this first-iteration model of the Silurian-Devonian Carbonate Unit were used as an upper constraint in adjusting provisional high-resolution surface models of the listed underlying units. Since the Silurian-Devonian Carbonate Unit underlies the Upper Bedrock Unit, it provides a more restrictive upper constraint on plausible elevations of top of deeper units than the previously developed high-resolution surface model of the top of the Upper Bedrock Unit model and permits more accurate modeling of the tops of the deeper units. But because development of the first-iteration high-resolution surface model of the top of the Silurian-Devonian Carbonate Unit itself required use of the high-resolution surface model of the top of the Mt. Simon Unit—a unit that is stratigraphically far-removed from the Silurian-Devonian Carbonate Unit, a second-iteration high-resolution surface model of the top of the Silurian-Devonian Carbonate Unit was developed after the high-resolution surface model of the top of the Maquoketa Unit was completed. With the more restrictive constraint of the Maquoketa Unit model employed for identification of lower stratigraphic violations, rather than the model of the top of the Mt. Simon Unit, the second-iteration high-resolution surface model of the top of the Silurian-Devonian Carbonate Unit is somewhat more accurate than the first-iteration model.

Error incurred by using the first-iteration high-resolution model—and not the second-iteration model—of the top of the Silurian-Devonian Carbonate Unit as an upper constraint on plausible values of high-resolution surface models of underlying hydrostratigraphic units is insignificant. With only a single, essentially irrelevant exception, the sets of points adjusted as stratigraphic violations of the upper constraint are precisely the same for provisional high-resolution surface models of these underlying hydrostratigraphic units whether the first-iteration or second-iteration high-resolution model of the Silurian-Devonian Carbonate Unit is used as an upper constraint. The exception is the high-resolution surface model of the top of the Maquoketa Unit, for which use of the second-iteration high-resolution model as an upper constraint would have added a single point—located in the model farfield—to the set of over 69,000 points adjusted as stratigraphic violations. Thus, the first-iteration high-resolution model was not only a better tool than the high-resolution surface model of the more stratigraphically distant Upper Bedrock Unit for identifying implausibly high elevations in provisional high-resolution surface models of underlying units, but it was essentially as good a tool for this purpose as the second-iteration model.

The Silurian-Devonian Carbonate Unit is absent or exposed at the bedrock surface in a large portion of the regional model domain, and for these areas, source data for the first-iteration high-resolution model of the top of the Silurian-Devonian Carbonate Unit were obtained from previously developed high-resolution surface models of the tops of the Mt. Simon Unit and Upper Bedrock Unit, respectively (Figure C-12). Structure-contour mapping was employed elsewhere, for the most part. This mapping includes an unpublished structure-contour map of the top of the Silurian-Devonian Carbonate Unit in Illinois and areas to the west (USGS, Wisconsin District, personal communication, 2002) and published maps of the structure of the top of the Traverse Group in Michigan (Catacosinos et al., 1990) and the Muscatatuck Group in Indiana (Rupp, 1991).

Since faulting has affected the top of the Silurian-Devonian Carbonate Unit, the inverse-distance algorithm (Table C-5) was employed for interpolation of the source data, with breaklines included in a .bln file developed from the shapefile containing the five fault features discussed previously (Section C.1.1.3). The provisional first-iteration high-resolution surface model of the top of the Silurian-Devonian Carbonate Unit was then adjusted using the high-resolution surface models of tops of the Upper Bedrock Unit and Mt. Simon Unit as upper and lower constraints, respectively. Because the first-iteration high-resolution surface model of the top of the Silurian-Devonian Carbonate Unit was not employed in developing the irregular-grid model of the unit, an active-cell high-resolution surface model of the first-iteration model of the unit was not generated.

C.1.5.6. Top of Eau Claire Unit

Structure-contour mapping of the top of the Eau Claire Formation in Illinois, Wisconsin, and areas west of the Mississippi River was digitized and employed as source data for development of the high-resolution surface model of the top of the Eau Claire Unit (Figure C-13). Contours digitized from an unpublished structure-contour map of the top of the Eau Claire (USGS, Wisconsin District, personal communication, 2002) were employed in Wisconsin, a portion of central Illinois, and areas west of the Mississippi River. These contours were edited to correct stratigraphic violations of digitized structure contours of adjacent hydrostratigraphic units and for consistency with structure-contour maps of other units in the vicinity of mapped areas of absence. The unpublished USGS mapping was not employed as source data in northern Illinois, where published structure-contour mapping of the top of the Eau Claire (Visocky et al., 1985) was used. Structure contours digitized from the Eau Claire structure map of Visocky et al. (1985) were augmented with additional contours, positioned using professional judgment in a high-priority area encompassing the model nearfield and the Plum River Fault and Sandwich Fault Zone. Contours digitized from the unpublished USGS mapping showing Eau Claire structure in central Illinois were edited to adjust contour positions to those along the southern border of the northern Illinois area where the data of Visocky et al. (1985) were used.

Eau Claire top-elevation data for Michigan, Indiana, and a part of central Illinois were synthesized using isopach maps, structure-contour maps, and the previously generated high-resolution surface model of the top of the Mt. Simon Unit.

Eau Claire elevation data for Michigan were synthesized by effectively adding a digitized isopach map of the Eau Claire Formation (Bricker et al., 1983) to a digitized structure-contour map of the top of the Mt. Simon Sandstone (Bricker et al., 1983) that was augmented with additional contours, positioned using professional judgment between the locations of the published contours. This technique is discussed in reference to the generation of interpolation source data for the high-resolution surface model of the base of the Mt. Simon Unit. Although Bricker et al. (1983) published a structure-contour map of the top of the Eau Claire Formation in Michigan, this map was not employed because it includes numerous and severe stratigraphic violations of their structure-contour map of the top of the Mt. Simon Sandstone. Because the intersection points generated through the process were relatively thinly distributed across the lower peninsula of Michigan, the additional step was taken of hand-contouring a structure-contour map of the top of the Eau Claire based on the intersection points, in the form of a polyline-shapefile. This hand-contoured map honors the synthesized Eau Claire elevation data and was constructed using the structure-contour map of the top of the Mt. Simon Sandstone (Bricker et al., 1983) as a guide to the configuration of the top of the Eau Claire.

Since published structure-contour mapping of the top of the Eau Claire Formation is not available for a small portion of central Illinois within the regional model domain, and since the unpublished USGS mapping does not cover this area, Eau Claire top-elevation data were synthesized for that area by subtracting a digitized isopach map of the Ironton and Galesville Sandstones (Emrich, 1966) from a structure-contour map of the Ironton Sandstone (Emrich, 1966). This subtraction was accomplished using the same approach of calculating Eau Claire top elevation at points of intersection of polylines digitized from the structure-contour and isopach maps. Only the point-shapefile containing the intersection points was used as interpolation source data for the central Illinois area. A hand-contoured map based on the intersection points was not developed.

Eau Claire top-elevation data were also synthesized for the area of Indiana where a published Eau Claire structure-contour map is not available. To accelerate the process of synthesizing elevation data, an approach based on summation of interpolated elevation and structure data was employed for this area. An isopach map of the Eau Claire Formation (Rupp, 1991) was digitized as a polyline shapefile. An ArcGIS tool was then employed to export the vertices of the polyline-shapefile as a point-feature shapefile, and a different ArcGIS tool was used to add the x- and y-coordinates of the point features to the attribute table of the exported point-shapefile. These point data were then exported in text format (procedure Arc-k), and this file was used as input data for interpolation in Surfer of Eau Claire Formation thickness in Indiana.

A kriging algorithm was employed for the interpolation of the thickness data in Surfer (Table C-9). The output grid was designed so that interpolation results were generated for the same (x, y) coordinate pairs as all other interpolations conducted for the project, but only for those locations within the northern Indiana portion of the regional model domain. Interpolation results—a model of the thickness of the Eau Claire Formation in Indiana—were exported as a text file which was then imported into ArcGIS and saved in point-shapefile format. Cross validation statistics for the interpolation of Indiana Eau Claire thickness data are shown in Table C-10.

The attribute table of the resulting Eau Claire thickness model contained fields for the x- and y-coordinates of each point in the output grid as well as the interpolated Eau Claire thickness at the point. An additional field was added for a unique numerical index calculated from the x- and y-coordinates using the formula described previously (page C-22). Since all the interpolations were constrained so as to give results at a consistent set of locations, this index field of the Eau Claire thickness model was employed to join the attribute table of the Eau Claire thickness model to that of the previously generated high-resolution surface model of the top of the Mt. Simon Unit, which also contained the index. A field was added to the attribute table of the Eau Claire thickness model to contain the estimated Mt. Simon Unit top elevation at each point, and this field was populated with the Mt. Simon top elevations from the joined attribute table. The table join was then removed. A final field was added to the attribute table of the Eau Claire thickness model to contain an estimate of the elevation of the top of the Eau Claire Unit, and these elevations were calculated by adding the estimated top elevation of the top of the Mt. Simon Unit at each point to the estimated thickness of the Eau Claire Formation and thus generate a provisional model of the elevation of the top of the Eau Claire Unit in Indiana. These data were prepared for use as source data for interpolation of Eau Claire top elevation across the entire model domain in the same way as described previously—namely, by erasing points from buffer areas along state boundaries and by exporting the data in text format.

Structure contours were estimated using professional judgment for the entire area of Lake Michigan within the regional model domain. The contours were constructed to depict a simple surface, with minimal added perturbations, that completely honors the Eau Claire top-elevation data in surrounding areas as shown in Figure C-13.

Interpolation source data for areas of bedrock-surface exposures of the Eau Claire Unit were generated by selecting and exporting point-features located within these exposures from the previously developed high-resolution surface model of the top of the Upper Bedrock Unit. Similarly, interpolation source data for areas of absence of the Eau Claire Unit were generated by selecting and exporting point-features located within these areas from the previously developed high-resolution surface model of the top of the Mt. Simon Unit.

The inverse-distance algorithm (Table C-5) was employed for interpolation of the source data with breaklines included in a .bln file developed from the shapefile containing the five fault features discussed previously (Section C.1.1.3). The provisional high-resolution surface model of the top of the Eau Claire Unit was then adjusted using the first-iteration high-resolution surface model of the top of the Silurian-Devonian Carbonate Unit and the high-resolution surface model of the top of the Mt. Simon Unit as upper and lower constraints, respectively. The portion of the resulting high-resolution surface model of the top of the Eau Claire Unit west of the Mississippi River was then erased to create the active-cell high-resolution surface model of the top of the Eau Claire Unit.

Table C-9. Parameters of Kriging Algorithm Used for Interpolation of Eau Claire Formation Thickness Data Having Output Grid Coincident with Northern Indiana

<i>Gridding Method</i>	<i>Kriging</i>
Kriging Type	Point
Polynomial Drift Order	0
Kriging std. deviation grid	no
Output Grid	
Minimum x	3539000 ft
Maximum x	4269000 ft
Minimum y	2236000 ft
Maximum y	3203500 ft
x and y spacing	2500 ft
Semi-Variogram Model	
Component Type	Linear
Anisotropy Angle	0
Anisotropy Ratio	1
Variogram Slope	1
Search Parameters	
Search Ellipse Radius #1	1200000 ft
Search Ellipse Radius #2	1200000 ft
Search Ellipse Angle	0
Number of Search Sectors	8
Maximum Data Per Sector	8
Maximum Empty Sectors	4
Minimum Data	3
Maximum Data	64

Table C-10. Cross-Validation Statistics for Interpolations of Thickness Data

Thickness Model	Univariate Cross-Validation Statistics			Inter-Variable Correlation with Residual Z at Validation Points		
	Median Abs. Deviation of Residual Z	Mean of Residual Z	Root Mean Square of Residual Z	X	Y	Z
Maquoketa Group (Central Illinois)	0.003	0.002	0.678	-0.027	-0.049	-0.144
Utica Shale (Michigan)	0.097	-0.022	0.372	-0.020	0.042	-0.060
Ancell Group (Indiana)	0.033	0.011	0.122	0.065	0.126	-0.132
Davis Formation (Indiana)	0.119	0.006	2.320	-0.020	-0.007	-0.035
Potosi Dolomite (Indiana)	0.236	0.026	0.709	0.034	0.016	-0.060
Ironton and Galesville Sandstones (Indiana)	0.044	0.048	0.601	0.139	-0.169	-0.272
Eau Claire Formation (Indiana)	0.059	0.003	0.188	0.079	-0.007	-0.076

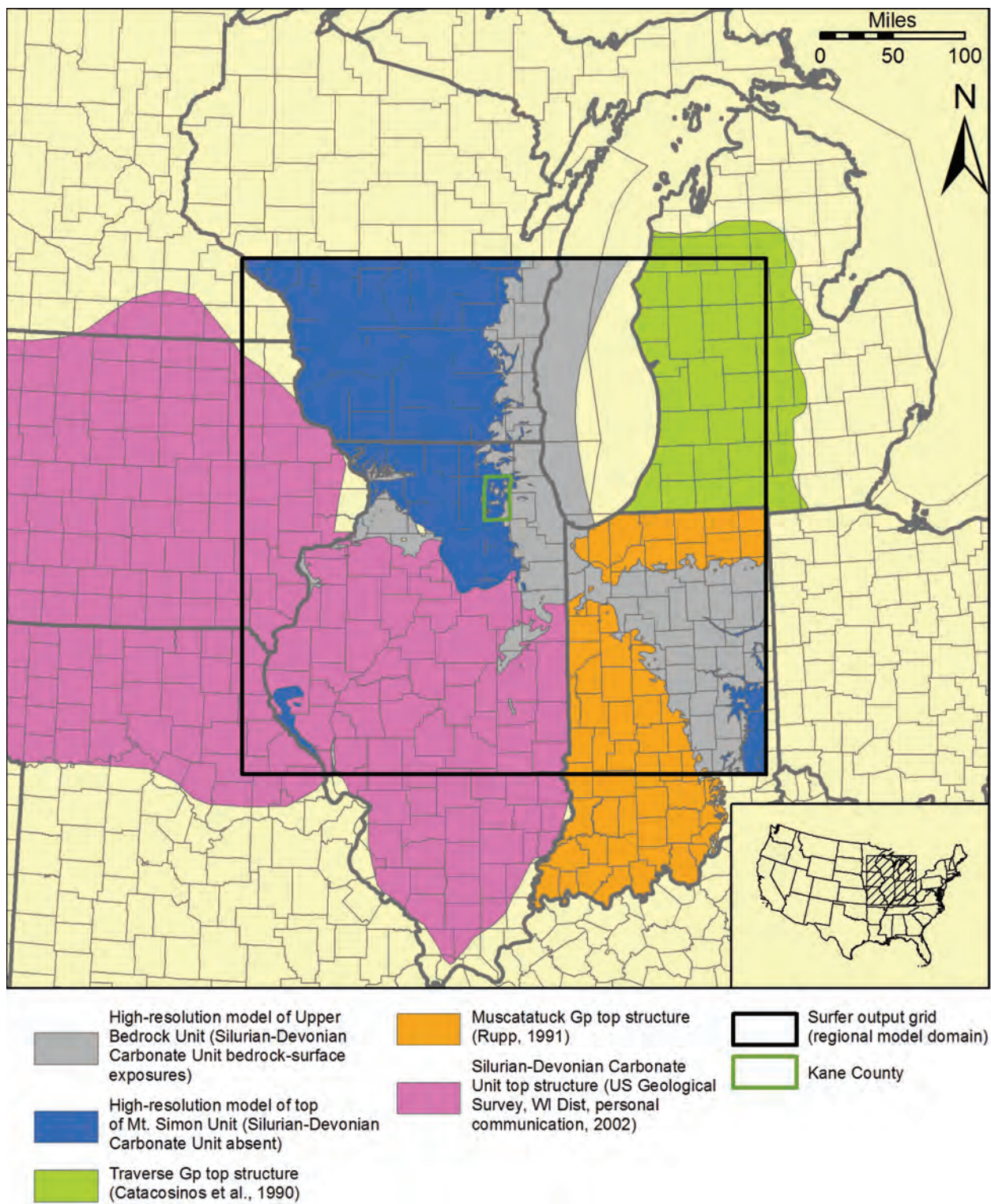


Figure C-12. Sources of data for first-iteration high-resolution surface model of top of Silurian-Devonian Carbonate Unit.

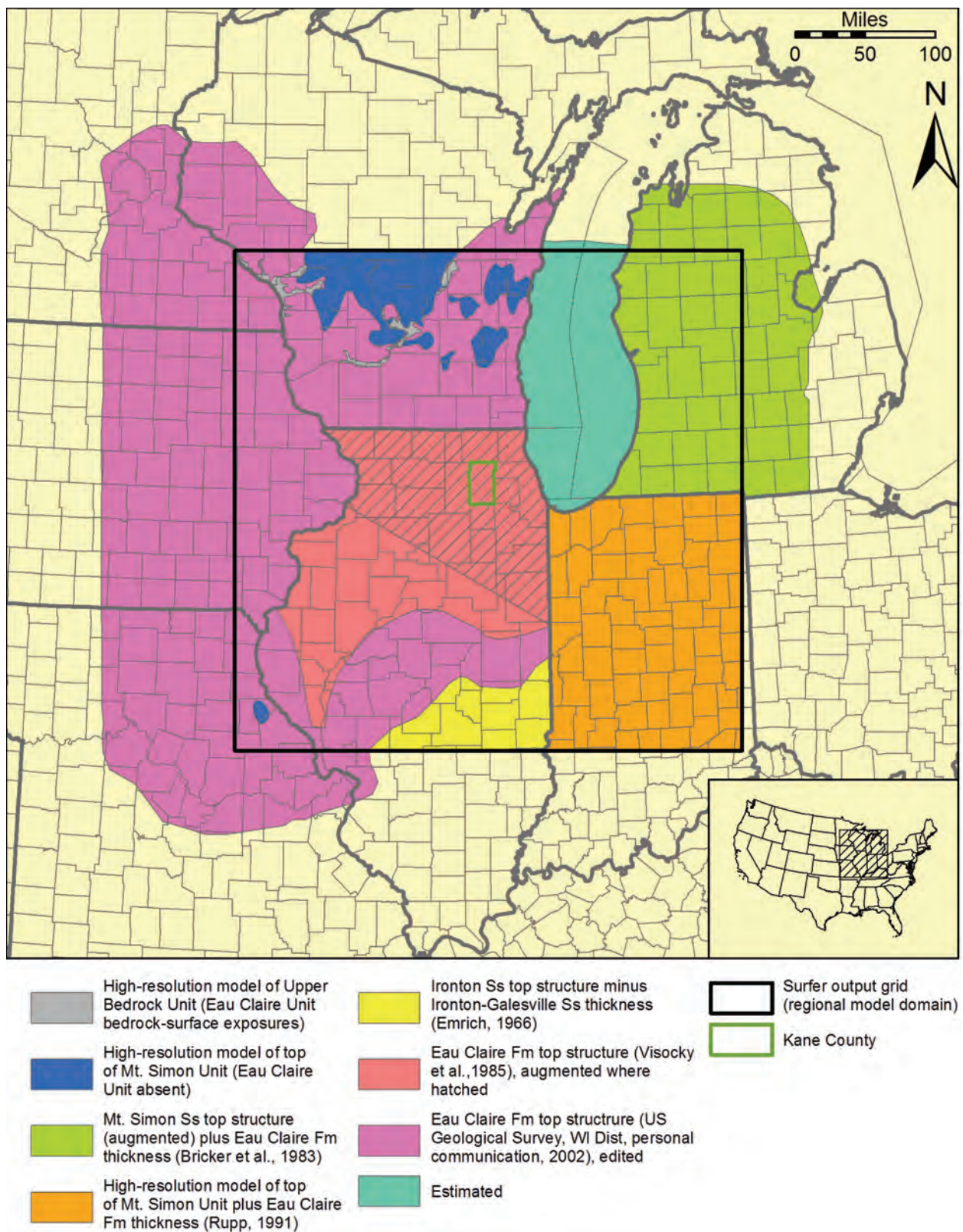


Figure C-13. Sources of data for high-resolution surface model of top of Eau Claire Unit.

C.1.5.7. Top of Ironton-Galesville Unit

Elevation data digitized from published and unpublished structure-contour mapping of the top of the Ironton-Galesville Sandstone and its equivalents were employed as source data for development of the high-resolution surface model of the top of the Ironton-Galesville Unit in much of Illinois, Wisconsin, and areas west of the Mississippi River (Figure C-14). Contours digitized from an unpublished structure-contour map of the top of the Ironton-Galesville (USGS, Wisconsin District, personal communication, 2002) were employed in Wisconsin, a portion of central Illinois, and areas west of the Mississippi River. These contours were edited to correct stratigraphic violations of digitized structure contours of adjacent hydrostratigraphic units and for consistency with structure-contour maps of other units in the vicinity of mapped areas of absence. The unpublished USGS mapping was not employed as source data in northern Illinois, where published structure-contour mapping of the top of the Ironton-Galesville (Visocky et al., 1985) was used. Structure contours digitized from the Ironton Sandstone structure map of Visocky et al. (1985) were augmented with additional contours, positioned using professional judgment in a high-priority area encompassing the model nearfield and the Plum River Fault and Sandwich Fault Zone. Contours digitized from the unpublished USGS mapping showing Ironton-Galesville structure in central Illinois were edited to adjust contour positions to those along the southern border of the northern Illinois area where the data of Visocky et al. (1985) were used. In a small portion of central Illinois not covered by the unpublished USGS mapping or the mapping of Visocky et al. (1985), elevation data were obtained by digitizing a structure-contour map of the top of the Ironton Sandstone by Emrich (1966).

Ironton-Galesville elevations in Michigan were synthesized by effectively subtracting a digitized isopach map of the Franconia Formation (Bricker et al., 1983) from a digitized structure-contour map of the top of the Franconia Formation (Bricker et al., 1983). This technique is discussed in reference to the generation of interpolation source data for the high-resolution surface model of the base of the Mt. Simon Unit. Although Bricker et al. (1983) published a structure-contour map of the top of the Ironton-Galesville in Michigan, this map was not employed because it includes numerous and severe stratigraphic violations of their structure-contour maps of the tops of the Eau Claire Formation and even the deeper Mt. Simon Sandstone. Because the intersection points generated through the process were relatively thinly-distributed across the lower peninsula of Michigan, the additional step was taken of hand-contouring a structure-contour map of the top of the Ironton-Galesville based on the intersection points, in the form of a polyline-shapefile. This hand-contoured map honors the synthesized Ironton-Galesville elevation data and was constructed using the structure-contour map of the top of the Franconia Formation (Bricker et al., 1983) as a guide to the configuration of the top of the Ironton-Galesville.

Ironton-Galesville top-elevation data were also synthesized for the area of Indiana within the regional model domain, where an Ironton-Galesville structure-contour map is not available, using an approach based on summation of interpolated thickness data and the previously generated high-resolution surface model of the Eau Claire Unit. This technique is discussed in reference to the development of interpolation source data for high-resolution surface model of the top of the Eau Claire of Indiana. The thickness model of the Ironton-Galesville employed in this process was generated by interpolation of point data generated from a digitized isopach map of the Ironton-Galesville Sandstone (Becker et al., 1978) that was augmented with additional isopachs positioned between published isopachs using professional judgment. A kriging

algorithm was employed for the interpolation (Table C-11). Cross validation statistics for the interpolation of Indiana Ironton-Galesville thickness data are shown in Table C-10.

Structure contours were estimated using professional judgment for the entire area of Lake Michigan within the regional model domain. The contours were constructed to depict a simple surface with minimal added perturbations that completely honors the Mt. Simon top-elevation data in surrounding areas as shown in Figure C-14.

Interpolation source data for areas of bedrock-surface exposure of the Ironton-Galesville Unit were generated by selecting and exporting point-features located within these exposures from the previously developed high-resolution surface model of the top of the Upper Bedrock Unit. Similarly, interpolation source data for areas of absence of the Ironton-Galesville Unit were generated by selecting and exporting point-features located within these areas from the previously developed high-resolution surface model of the top of the Eau Claire Unit.

The inverse-distance algorithm (Table C-5) was employed for interpolation of the source data with breaklines included in a .bln file developed from the shapefile containing the five fault features discussed previously (Section C.1.1.3). The provisional high-resolution surface model of the top of the Ironton-Galesville Unit was then adjusted using the first-iteration high-resolution surface model of the top of the Silurian-Devonian Carbonate Unit and the high-resolution surface model of the top of the Eau Claire Unit as upper and lower constraints, respectively. The portion of the resulting high-resolution surface model of the top of the Ironton-Galesville Unit west of the Mississippi River was then erased to create the active-cell high-resolution surface model of the top of the Ironton-Galesville Unit.

C.1.5.8. Top of Potosi-Franconia Unit

Compilation of source data for development of the high-resolution surface model of the top of the Potosi-Franconia Unit presented several challenges owing to a lack of published and unpublished structure-contour maps of the horizon. Contours digitized from an unpublished structure-contour map of the top of the Potosi-Franconia Unit (USGS, Wisconsin District, personal communication, 2002) were employed in parts of Wisconsin, a portion of central Illinois, and areas west of the Mississippi River (Figure C-15). These contours were edited to correct stratigraphic violations of digitized structure contours of adjacent hydrostratigraphic units and for consistency with structure-contour maps of other units in the vicinity of mapped areas of absence. A published structure-contour map of the bottom of the Ancell Group (Visocky et al., 1985) was employed as source data in parts of Illinois where subcrop mapping of the Tippecanoe Sequence (Willman et al., 1975) suggests that the Ancell rests on the Potosi-Franconia Unit. In other areas of the regional model domain, elevation data were synthesized using thickness data or were obtained from previously generated high-resolution surface models of other surfaces.

In parts of Illinois where the Potosi-Franconia Unit is not overlain by the Ancell Group and that were not covered by the unpublished USGS mapping with sufficient detail, elevation data were synthesized by effectively adding digitized isopach maps of the Franconia Formation and Potosi Dolomite (Willman et al., 1975) to available structure-contour mapping of the Ironton Sandstone. This technique is discussed in reference to the generation of interpolation source data for the high-resolution surface model of the base of the Mt. Simon Unit. For development of Potosi-Franconia interpolation source data in Illinois, however, the technique was applied twice. It was first applied to sum the thicknesses of the Franconia Formation and Potosi Dolomite at intersections of digitized isopachs of the two units. A hand-contoured isopach map of the combined interval, in the form of a polyline-shapefile, was then constructed based on the intersection points. The hand-contoured map of the summed thicknesses of the Franconia and

Potosi was then added to digitized structure-contour mapping of the top of the Ironton Sandstone from Visocky et al. (1985) and Emrich (1966). In much of northern Illinois, the thickness of the Potosi-Franconia Unit was added to a digitized version of the Ironton Sandstone structure-contour map of Visocky et al. (1985) that was augmented with additional contours, positioned using professional judgment in a high-priority area encompassing the model nearfield and the Plum River Fault and Sandwich Fault Zone. In a small part of central Illinois, the Potosi-Franconia thickness was added to a digitized version of the Ironton structure map of Emrich (1966). All of the intersection points estimated using Ironton structure data from Emrich (1966) and Visocky et al. (1985) and Franconia Formation and Potosi Dolomite thickness data from Willman et al. (1975) were then hand-contoured to honor the intersection points and the structure-contour map of the bottom of the Ancell Group mentioned in the preceding paragraph. A smaller contour-interval was employed in the high-priority area of northern Illinois where the Ironton structure map of Visocky et al. (1985) was augmented.

Contours digitized from the unpublished structure-contour map of the top of the Potosi-Franconia Unit (USGS, Wisconsin District, personal communication, 2002) were edited for consistency with the structure contours developed by the process discussed in the preceding paragraph.

Potosi-Franconia Unit elevation data for Michigan were synthesized by effectively adding a digitized isopach map Trempealeau Formation (Bricker et al., 1983) to a digitized structure-contour map of the top of the Franconia Formation (Bricker et al., 1983). The same technique of identification of intersections of isopachs and structure contours was employed for this addition process as discussed previously (page C-35). Although Bricker et al. (1983) published a structure-contour map of the top of the Trempealeau Formation in Michigan, this map was not employed because it includes numerous and severe stratigraphic violations of their structure-contour maps of other lithostratigraphic units. A hand-contoured structure-contour map of the top of the Potosi-Franconia Unit in Michigan was constructed, in the form of a polyline-shapefile, based on the intersection points and on structure-contour maps of the tops of the Franconia Formation and Prairie du Chien Group (Bricker et al., 1983).

It is acknowledged that the Trempealeau Formation of Michigan does not correlate directly to the Potosi Dolomite of Illinois. The Trempealeau Formation, rather, contains equivalents of both the Potosi Dolomite and the Eminence Formation of Illinois, units which cannot be distinguished in Michigan. Use of the Trempealeau Formation isopach map to define the top of the Potosi-Franconia Unit in Michigan thus has the consequence of the high-resolution surface model of the top of the Potosi-Franconia Unit being defined in Michigan by the equivalent of the Eminence Formation, a unit that is otherwise assigned to the Prairie du Chien-Eminence Unit. The resulting high-resolution surface model of the top of the Potosi-Franconia Unit does not uniformly depict the top of the Potosi Dolomite and equivalents, then. For purposes of groundwater flow modeling, this shortcoming of the geologic model is acceptable because the lithologies of the units above and below the problematic contact—equivalents of the Potosi Dolomite, Eminence Formation, and Prairie du Chien Group of Illinois—are all predominantly dolomite and are hydraulically similar.

Potosi-Franconia top-elevation data were also synthesized for the area of Indiana within the regional model domain. Thickness models of two lithostratigraphic units—the Davis Formation and the Potosi Dolomite—were added to the high-resolution surface model of the top of the Ironton-Galesville Unit to synthesize the Potosi-Franconia Unit top elevations in Indiana. The thickness models of the Davis Formation and Potosi Dolomite employed in this process

were both generated by interpolation, using a kriging algorithm (Table C-12)), of point data generated from digitized isopach maps of the Davis Formation (Rupp, 1991) and Potosi Dolomite (Droste and Patton, 1985). Cross validation statistics for the interpolation of Indiana Potosi and Davis thickness data are shown in Table C-10.

Like the Trempealeau Formation of Michigan, the Potosi Dolomite of Indiana does not correlate directly to the Potosi Dolomite of Illinois. Rather, the Potosi of Indiana contains equivalents of both the Potosi Dolomite and the Eminence Formation of Illinois, which cannot be distinguished in Indiana. Use of the Indiana Potosi Dolomite isopach map to define the top of the Potosi-Franconia Unit in Indiana thus has the consequence of the high-resolution surface model of the top of the Potosi-Franconia Unit being defined in Indiana by the equivalent of the Eminence Formation, a unit that is otherwise assigned to the Prairie du Chien-Eminence Unit. As mentioned previously in regard to use of the Trempealeau Formation isopach map in Michigan, for purposes of groundwater flow modeling, this shortcoming of the geologic model is acceptable because the lithologies of the units above and below the problematic contact—equivalents of the Potosi Dolomite, Eminence Formation, and Prairie du Chien Group of Illinois—are all predominantly dolomite and are hydraulically similar.

Interpolation source data for areas of bedrock-surface exposure of the Potosi-Franconia Unit were generated by selecting and exporting point-features located within these exposures from the previously developed high-resolution surface model of the top of the Upper Bedrock Unit. Similarly, interpolation source data for areas of absence of the Potosi-Franconia Unit were generated by selecting and exporting point-features located within these areas from the previously developed high-resolution surface model of the top of the Ironton-Galesville Unit.

Structure contours were estimated using professional judgment for the entire area of Lake Michigan within the regional model domain. The contours were constructed to depict a simple surface, with minimal added perturbations, that completely honors the Mt. Simon top-elevation data in surrounding areas as shown in Figure C-15.

The inverse-distance algorithm (Table C-5) was employed for interpolation of the source data with breaklines included in a .bln file developed from the shapefile containing the five fault features discussed previously (Section C.1.1.3). The provisional high-resolution surface model of the top of the Potosi-Franconia Unit was then adjusted using the first-iteration high-resolution surface model of the top of the Silurian-Devonian Carbonate Unit and the high-resolution surface model of the top of the Ironton-Galesville Unit as upper and lower constraints. The portion of the resulting high-resolution surface model of the top of the Potosi-Franconia Unit west of the Mississippi River was then erased to create the active-cell high-resolution surface model of the top of the Potosi-Franconia Unit.

Table C-11. Parameters of Kriging Algorithm Used for Interpolation of Ironton-Galesville Thickness Data Having Output Grid Coincident with Northern Indiana

<i>Gridding Method</i>	<i>Kriging</i>
Kriging Type	Point
Polynomial Drift Order	0
Kriging std. deviation grid	no
Output Grid	
Minimum x	3539000 ft
Maximum x	4269000 ft
Minimum y	2236000 ft
Maximum y	3203500 ft
x and y spacing	2500 ft
Semi-Variogram Model	
Component Type	Linear
Anisotropy Angle	0
Anisotropy Ratio	1
Variogram Slope	1
Search Parameters	
No Search (use all data)	

Table C-12. Parameters of Kriging Algorithm Used for Interpolation of Davis Formation, Potosi Dolomite, and Ancell Group Thickness Data Having Output Grid Coincident with Northern Indiana

<i>Gridding Method</i>	<i>Kriging</i>
Kriging Type	Point
Polynomial Drift Order	0
Kriging std. deviation grid	no
Output Grid	
Minimum x	3539000 ft
Maximum x	4269000 ft
Minimum y	2236000 ft
Maximum y	3203500 ft
x and y spacing	2500 ft
Semi-Variogram Model	
Component Type	Linear
Anisotropy Angle	0
Anisotropy Ratio	1
Variogram Slope	1
Search Parameters	
Search Ellipse Radius #1	1200000 ft
Search Ellipse Radius #2	1200000 ft
Search Ellipse Angle	0
Number of Search Sectors	8
Maximum Data Per Sector	8
Maximum Empty Sectors	6
Minimum Data	3
Maximum Data	64

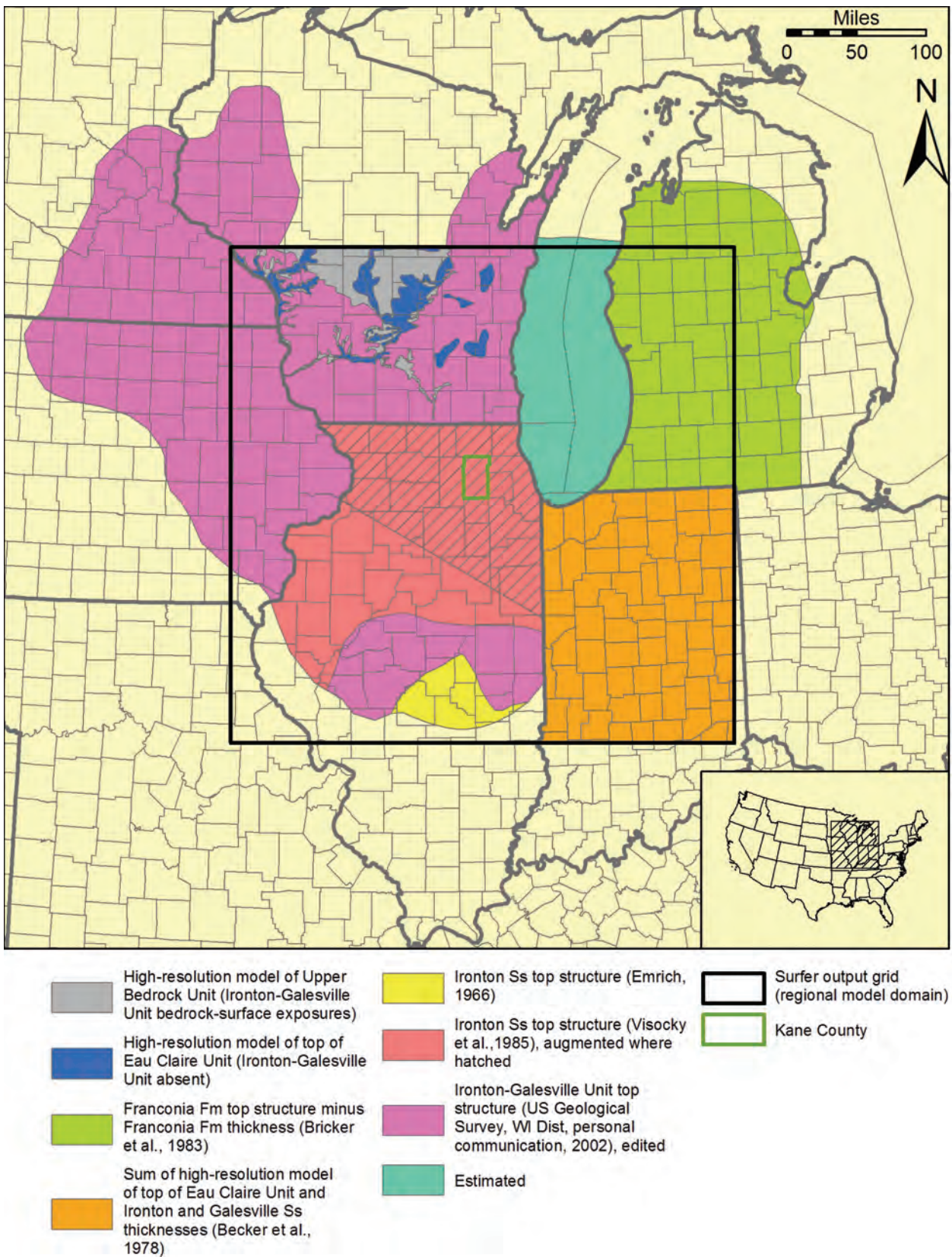


Figure C-14. Sources of data for high-resolution surface model of top of Ironton-Galesville Unit.

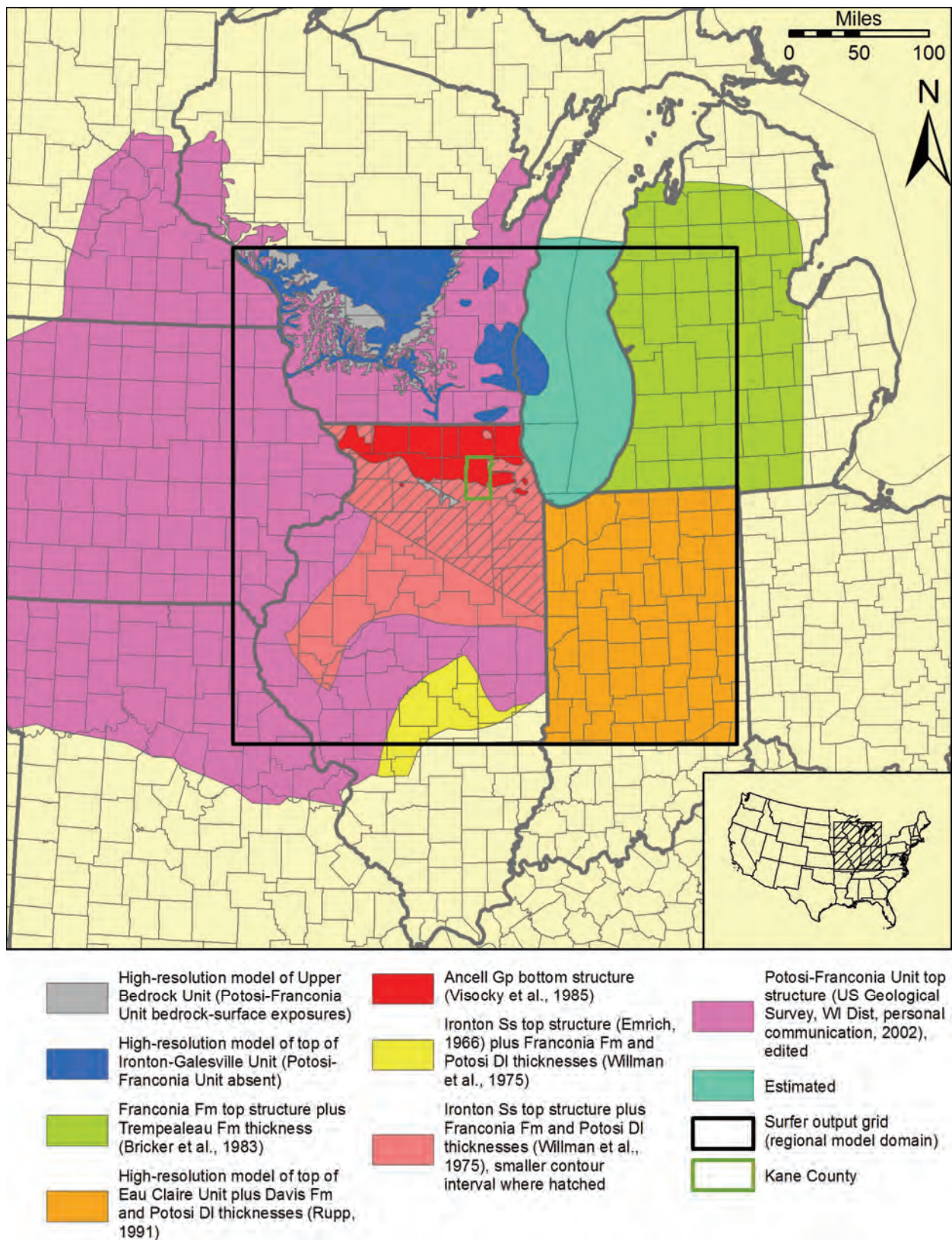


Figure C-15. Sources of data for high-resolution surface model of top of Potosi-Franconia Unit.

C.1.5.9. Top of Prairie du Chien-Eminence Unit

Elevation data digitized from published and unpublished structure-contour mapping of the top of the Prairie du Chien Group and equivalent horizons were employed as source data for development of the high-resolution surface model of the top of the Prairie du Chien-Eminence Unit in most of the regional model domain (Figure C-16). Contours digitized as a polyline-shapefile from an unpublished structure-contour map of the top of the Prairie du Chien-Eminence Unit (USGS, Wisconsin District, personal communication, 2002) were employed in portions of Wisconsin, Illinois, and Lake Michigan as well as areas west of the Mississippi River. These contours were edited to correct stratigraphic violations of digitized structure contours of adjacent hydrostratigraphic units and for consistency with structure-contour maps of other units in the vicinity of mapped areas of absence. A published structure-contour map of the bottom of the Ancell Group (Visocky et al., 1985) was digitized as a polyline-shapefile for source data in parts of Illinois covered by the map where subcrop mapping of the Tippecanoe Sequence (Willman et al., 1975) suggests that the Ancell rests on the Prairie du Chien Group. Contours digitized from the unpublished USGS mapping showing Prairie du Chien structure in central Illinois were edited to adjust contour positions to those along the southern border of the northern Illinois area where the data of Visocky et al. (1985) were used. The Prairie du Chien structure-contour map of Bricker et al. (1983) was digitized as a polyline-shapefile for source data in the lower peninsula of Michigan and adjacent areas of the Great Lakes. Finally, the Prairie du Chien structure-contour map of Rupp (1991) was digitized as a polyline-shapefile for source data in Indiana.

Interpolation source data for areas of bedrock-surface exposure of the Prairie du Chien-Eminence Unit were generated by selecting and exporting point-features located within these exposures from the previously developed high-resolution surface model of the top of the Upper Bedrock Unit. Similarly, interpolation source data for areas of absence of the Prairie du Chien-Eminence Unit were generated by selecting and exporting point-features located within these areas from the previously developed high-resolution surface model of the top of the Potosi-Franconia Unit.

Structure contours were estimated using professional judgment for part of the area of Lake Michigan within the regional model domain. The contours were constructed to depict a simple surface, with minimal added perturbations, that completely honors the Mt. Simon top-elevation data in surrounding areas as shown in Figure C-16.

The inverse-distance algorithm (Table C-5) was employed for interpolation of the source data with breaklines included in a .bln file developed from the shapefile containing the five fault features discussed previously (Section C.1.1.3). The provisional high-resolution surface model of the top of the Prairie du Chien-Eminence Unit was then adjusted using the first-iteration high-resolution surface model of the top of the Silurian-Devonian Carbonate Unit and the high-resolution surface model of the top of the Potosi-Franconia Unit as upper and lower constraints, respectively. The portion of the resulting high-resolution surface model of the top of the Prairie du Chien-Eminence Unit west of the Mississippi River was then erased to create the active-cell high-resolution surface model of the top of the Prairie du Chien-Eminence Unit.

C.1.5.10. Top of Ancell Unit

Contours digitized from an unpublished structure-contour map of the top of the Ancell Unit (USGS, Wisconsin District, personal communication, 2002) were employed as interpolation source data for the high-resolution surface model of the Ancell Unit in parts of Wisconsin, a portion of central Illinois, and areas west of the Mississippi River (Figure C-17). These contours were edited to correct stratigraphic violations of digitized structure contours of adjacent hydrostratigraphic units and for consistency with structure-contour maps of other units in the vicinity of mapped areas of absence. The unpublished USGS mapping was not employed as source data in northern Illinois, where published structure-contour mapping of the top of the Ancell Group (Visocky et al., 1985) was used. Contours digitized from the unpublished USGS mapping showing Ancell Unit structure in central Illinois were edited to adjust contour positions to those along the southern border of the northern Illinois area where the data of Visocky et al. (1985) were used.

Interpolation source data for the lower peninsula of Michigan were synthesized by effectively adding the thicknesses of the St. Peter Sandstone and Glenwood Formation, digitized as polyline-shapefiles from maps by Bricker et al. (1983), to the elevation of the top of the Prairie du Chien Group, also digitized as a polyline shapefile from a map by Bricker et al. (1983). This technique is discussed in reference to the generation of interpolation source data for the high-resolution surface model of the base of the Mt. Simon Unit. For development of Ancell interpolation source data in Michigan, however, the technique was applied twice. It was first applied to sum the thicknesses of the Glenwood Formation and St. Peter Sandstone at intersections of digitized isopachs of the two units. A hand-contoured isopach map of the combined interval was then constructed, in the form of a polyline-shapefile, based on the intersection points. The hand-contoured isopach map of the summed thicknesses of the Glenwood Formation and St. Peter Sandstone was then added to the digitized structure-contour mapping of the top of the Prairie du Chien Group. The intersection points of the isopachs and structure contours, representing the estimated elevation of the top of the Ancell Group, were then used, together with the Prairie du Chien structure map (Bricker et al., 1983), as the basis for a hand-contoured structure-contour map of the top of the Ancell Group, in the form of a polyline-shapefile. This synthesized structure contour map of the top of the Ancell Group was employed for interpolation source data for the high-resolution surface model of the top of the Ancell Unit.

Ancell Unit top-elevation data were also synthesized for the area of Indiana within the regional model domain, where an Ancell Group structure-contour map is not available, using an approach based on summation of interpolated thickness data and the previously generated high-resolution surface model of the Prairie du Chien Eminence Unit. This technique is discussed in reference to the development of interpolation source data for high-resolution surface model of the top of the Eau Claire of Indiana. The thickness model of the Ancell Group employed in this process was generated by interpolation of point data generated from a digitized isopach map of the Ancell Group (Rupp, 1991). A kriging algorithm was employed for the interpolation (Table C-12). Cross validation statistics for the interpolation of Indiana Ancell Group thickness data are shown in Table C-10.

Interpolation source data for areas of bedrock-surface exposure of the Ancell Unit were generated by selecting and exporting point-features located within these exposures from the previously-developed high-resolution surface model of the top of the Upper Bedrock Unit. Similarly, interpolation source data for areas of absence of the Ancell Unit were generated by

selecting and exporting point-features located within these areas from the previously-developed high-resolution surface model of the base of the Prairie du Chien-Eminence Unit.

Structure contours were estimated using professional judgment for part of the area of Lake Michigan within the regional model domain. The contours were constructed to depict a simple surface, with minimal added perturbations, that completely honors the Ancell Unit top-elevation data in surrounding areas as shown in Figure C-17.

The inverse-distance algorithm (Table C-5) was employed for interpolation of the source data with breaklines included in a .bln file developed from the shapefile containing the five fault features discussed previously (Section C.1.1.3). The provisional high-resolution surface model of the top of the Ancell Unit was then adjusted using the first-iteration high-resolution surface model of the top of the Silurian-Devonian Carbonate Unit and the high-resolution surface model of the top of the Prairie du Chien-Eminence Unit as upper and lower constraints, respectively. The portion of the resulting high-resolution surface model of the top of the Ancell Unit west of the Mississippi River was then erased to create the active-cell high-resolution surface model of the top of the Prairie du Chien-Eminence Unit.

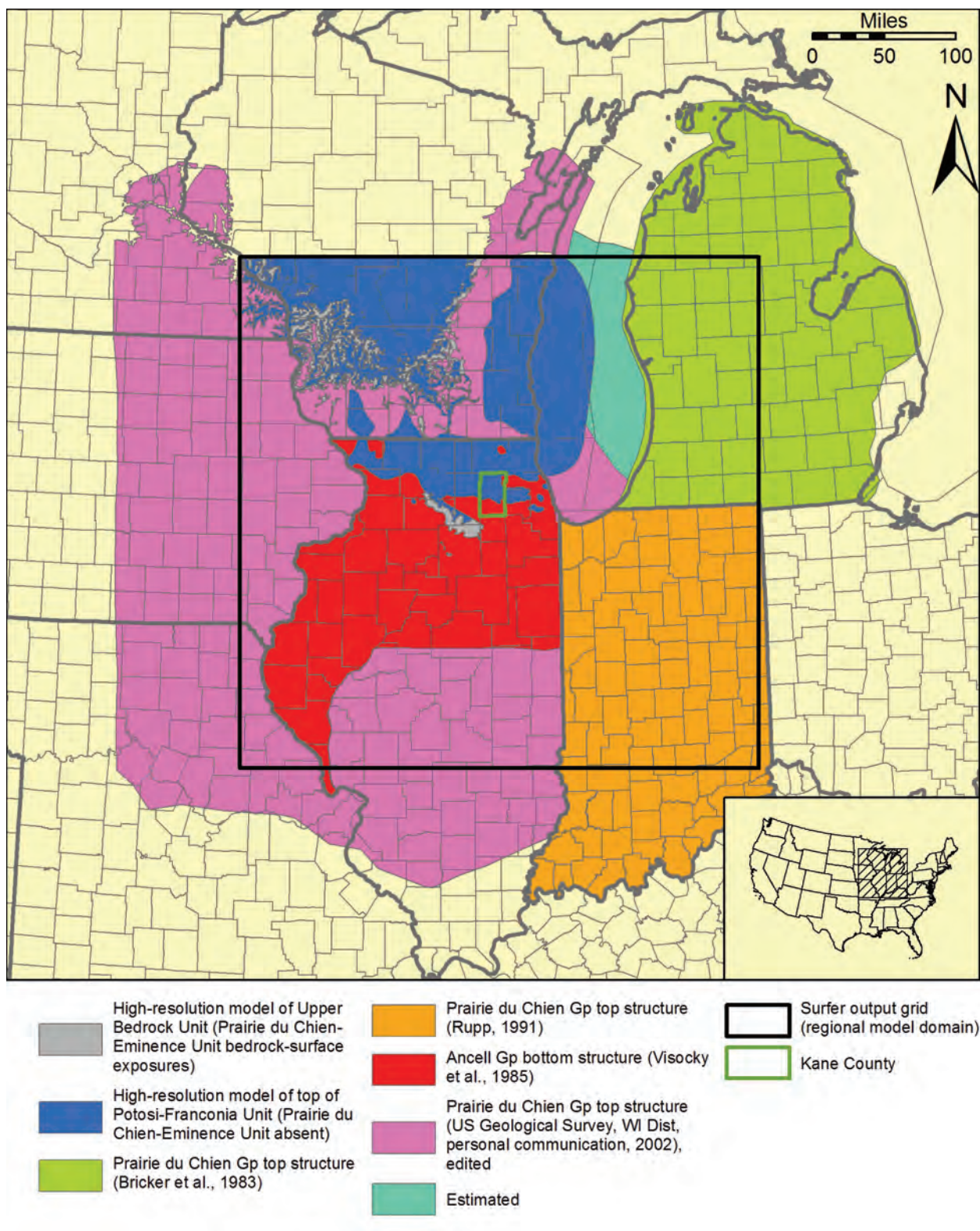


Figure C-16. Sources of data for high-resolution surface model of top of Prairie du Chien-Eminence Unit.

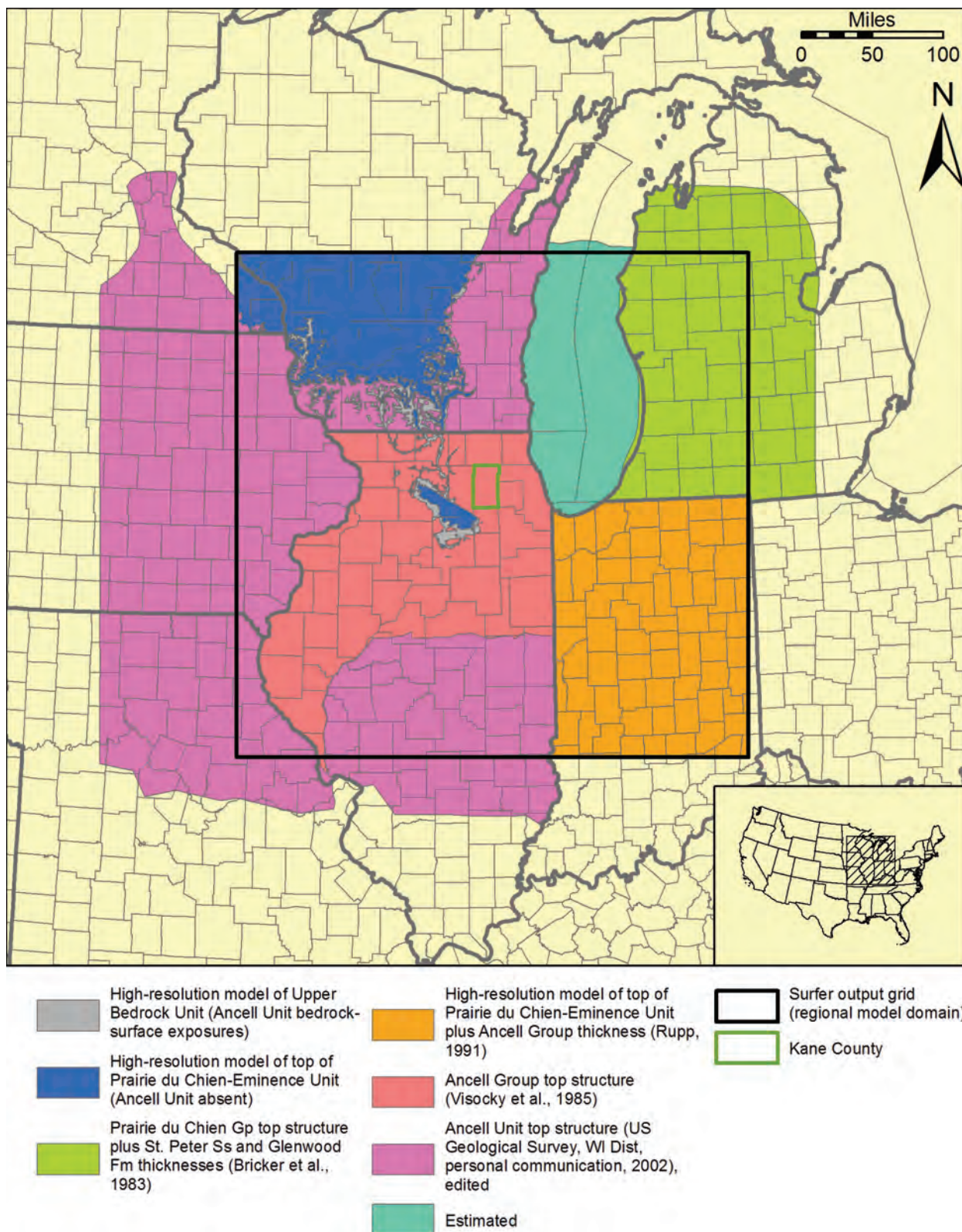


Figure C-17. Sources of data for high-resolution surface model of top of Ancell Unit.

C.1.5.11. Top of Galena-Platteville Unit

Elevation data digitized from published and unpublished structure-contour mapping of the top of the Galena Group and equivalent horizons were employed as source data for development of the high-resolution surface model of the top of the Galena-Platteville Unit in most of the regional model domain (Figure C-18). Contours digitized as a polyline-shapefile from an unpublished structure-contour map of the top of the Galena-Platteville Unit (USGS, Wisconsin District, personal communication, 2002) were employed in portions of Wisconsin, Illinois, and Lake Michigan as well as areas west of the Mississippi River. These contours were edited to correct stratigraphic violations of digitized structure contours of adjacent hydrostratigraphic units and for consistency with structure-contour maps of other units in the vicinity of mapped areas of absence. A published structure-contour map of the top of the Galena Group (Visocky et al., 1985) was digitized as a polyline-shapefile for source data in parts of Illinois covered by the map. Contours digitized from the unpublished USGS mapping showing Galena-Platteville structure in central Illinois were edited to adjust contour positions to those along the southern border of the northern Illinois area where the data of Visocky et al. (1985) were used. The Trenton Formation structure-contour map of Catocsinos et al. (1990) was digitized as a polyline-shapefile for interpolation source data in the lower peninsula of Michigan. Finally, the Trenton Group structure-contour map of Rupp (1991) was digitized as a polyline-shapefile for source data in Indiana.

Interpolation source data for areas of bedrock-surface exposure of the Galena-Platteville Unit were generated by selecting and exporting point-features located within these exposures from the previously-developed high-resolution surface model of the top of the Upper Bedrock Unit. Similarly, interpolation source data for areas of absence of the Galena-Platteville Unit were generated by selecting and exporting point-features located within these areas from the previously-developed high-resolution surface model of the top of the Ancestral Unit.

Structure contours were estimated using professional judgment for part of the area of Lake Michigan within the regional model domain. The contours were constructed to depict a simple surface, with minimal added perturbations, that completely honors the Galena-Platteville Unit top-elevation data in surrounding areas as shown in Figure C-18.

The inverse-distance algorithm (Table C-5) was employed for interpolation of the source data with breaklines included in a .bln file developed from the shapefile containing the five fault features discussed previously (Section C.1.1.3). The provisional high-resolution surface model of the top of the Galena-Platteville Unit was then adjusted using the first-iteration high-resolution surface model of the top of the Silurian-Devonian Carbonate Unit and the high-resolution surface model of the top of the Ancestral Unit as upper and lower constraints, respectively. The portion of the resulting high-resolution surface model of the top of the Galena-Platteville Unit west of the Mississippi River was then erased to create the active-cell high-resolution surface model of the top of the Galena-Platteville Unit.

C.1.5.12. Top of Maquoketa Unit

Elevation data digitized from published and unpublished structure-contour mapping of the top of the Maquoketa Group were employed as source data for development of the high-resolution surface model of the top of the Maquoketa Unit in much of the regional model domain (Figure C-19). Contours digitized as a polyline-shapefile from an unpublished structure-contour map of the top of the Maquoketa Unit (USGS, Wisconsin District, personal communication,

2002) were employed in portions of Wisconsin and Illinois as well as areas west of the Mississippi River.

These contours were edited to correct stratigraphic violations of digitized structure contours of adjacent hydrostratigraphic units and for consistency with structure-contour maps of other units in the vicinity of mapped areas of absence. A published structure-contour map of the top of the Maquoketa Group (Visocky et al., 1985) was digitized as a polyline-shapefile for source data in parts of Illinois covered by the map. Contours digitized from the unpublished USGS mapping showing Maquoketa structure in central Illinois were edited to adjust contour positions to those along the southern border of the northern Illinois area where the data of Visocky et al. (1985) were used. A Maquoketa Group structure-contour map by Rupp (1991) was digitized as a polyline-shapefile for source data in Indiana.

Maquoketa Unit top-elevation data were synthesized for the area of Michigan within the regional model domain, where a Maquoketa Group structure-contour map is not available, using an approach based on summation of interpolated thickness data and the previously generated high-resolution surface model of the Galena-Platteville Unit. This technique is discussed in reference to the development of interpolation source data for high-resolution surface model of the top of the Eau Claire of Indiana. The thickness model of the Maquoketa Group employed in this process was generated by interpolation of point data generated from a digitized isopach map of the Utica Shale (a Maquoketa Group equivalent) (Western Michigan University Department of Geology, 1981). A kriging algorithm, with a rectangular output grid covering southwestern Michigan and adjacent Lake Michigan, was employed for the interpolation (Table C-13). Cross validation statistics for the interpolation of Michigan Utica Shale thickness data are shown in Table C-10. Synthesized Maquoketa Unit elevation data for the Lake Michigan portion of the output grid—an area not covered by the Utica Shale thickness map by the Western Michigan University Department of Geology (1981) and therefore of dubious accuracy—were erased and not used as interpolation source data.

Interpolation source data for a portion of the regional model domain in central Illinois were also synthesized using the technique described on page C-42 by summing the high-resolution surface model of the Galena-Platteville Unit with a model of the thickness of the Maquoketa Group based on a polyline shapefile of the thickness of the Maquoketa Group digitized from isopach mapping by Willman et al. (1975). This part of central Illinois is not covered by the published or unpublished structure-contour mapping discussed previously. A kriging algorithm, with a rectangular output grid enclosing the part of central Illinois lacking Maquoketa elevation data, was employed for the interpolation (Table C-14). Cross validation statistics for the interpolation of central Illinois Maquoketa Group thickness data are shown in Table C-10. Synthesized Maquoketa Unit elevation data generated through this process for areas covered by the unpublished USGS Maquoketa Group structure-contour mapping were erased and not used as interpolation source data.

Interpolation source data for areas of bedrock-surface exposure of the Maquoketa Unit were generated by selecting and exporting point-features located within these exposures from the previously-developed high-resolution surface model of the top of the Upper Bedrock Unit. Similarly, interpolation source data for areas of absence of the Maquoketa Unit were generated by selecting and exporting point-features located within these areas from the previously developed high-resolution surface model of the top of the Galena-Platteville Unit.

Structure contours were estimated using professional judgment for part of the area of Lake Michigan within the regional model domain. The contours were constructed to depict a

simple surface, with minimal added perturbations, that completely honors the Maquoketa Unit top-elevation data in surrounding areas as shown in Figure C-19.

The inverse-distance algorithm (Table C-5) was employed for interpolation of the source data with breaklines included in a .bln file developed from the shapefile containing the five fault features discussed previously (Section C.1.1.3). The provisional high-resolution surface model of the top of the Maquoketa Unit was then adjusted using the first-iteration high-resolution surface model of the top of the Silurian-Devonian Carbonate Unit and the high-resolution surface model of the top of the Galena-Platteville Unit as upper and lower constraints, respectively. The portion of the resulting high-resolution surface model of the top of the Maquoketa Unit west of the Mississippi River was then erased to create the active-cell high-resolution surface model of the top of the Maquoketa Unit.

C.1.5.13. Top of Silurian-Devonian Carbonate Unit (Second Iteration)

The second-iteration model of the top of the Silurian-Devonian Carbonate Unit was developed from largely the same interpolation source data as the first-iteration model (page C-40) with two differences (Figure C-20). First, source data for areas of absence of the Silurian-Devonian Carbonate Unit were generated by selecting and exporting point-features within these areas from the previously developed high-resolution surface model of the top of the Maquoketa Unit, not the top of the Mt. Simon Unit as used for the first-iteration model. Second, interpolation source data derived from the unpublished structure-contour map of the top of the Silurian-Devonian Carbonate Unit (USGS, Wisconsin District, personal communication, 2002) and from the structure-contour map of the top of Muscatatuck Group in Indiana (Rupp, 1991) were trimmed to reduce file sizes and interpolation time. The reduction in input data was found to have no significant impact on the accuracy of the interpolation results.

The inverse-distance algorithm (Table C-5) was employed for interpolation of the source data with breaklines included in a .bln file developed from the shapefile containing the five fault features discussed previously (Section C.1.1.3). The provisional second-iteration high-resolution surface model of the top of the Silurian-Devonian Carbonate Unit was then adjusted using the high-resolution surface model of the top of the Upper Bedrock Unit and the high-resolution surface model of the top of the Maquoketa Unit as upper and lower constraints, respectively. The portion of the resulting second-iteration high-resolution surface model of the top of the Silurian-Devonian Carbonate Unit west of the Mississippi River was then erased to create the active-cell second-iteration high-resolution surface model of the top of the Silurian-Devonian Carbonate Unit.

Table C-13. Parameters of Kriging Algorithm Used for Interpolation of Utica Shale Thickness Data Having Output Grid Coincident with Southwestern Michigan Part of Regional Model Domain

<i>Gridding Method</i>	<i>Kriging</i>
Kriging Type	Point
Polynomial Drift Order	0
Kriging std. deviation grid	no
Output Grid	
Minimum x	3724000 ft
Maximum x	4269000 ft
Minimum y	3186000 ft
Maximum y	4116000 ft
x and y spacing	2500 ft
Semi-Variogram Model	
Component Type	Linear
Anisotropy Angle	0
Anisotropy Ratio	1
Variogram Slope	1
Search Parameters	
Search Ellipse Radius #1	1200000 ft
Search Ellipse Radius #2	1200000 ft
Search Ellipse Angle	0
Number of Search Sectors	8
Maximum Data Per Sector	8
Maximum Empty Sectors	6
Minimum Data	3
Maximum Data	64

Table C-14. Parameters of Kriging Algorithm Used for Interpolation of Utica Shale Thickness Data Having Output Grid Coincident with Part of the Regional Model Domain in Central Illinois

<i>Gridding Method</i>	<i>Kriging</i>
Kriging Type	Point
Polynomial Drift Order	0
Kriging std. deviation grid	no
Output Grid	
Minimum x	2579000 ft
Maximum x	3551500 ft
Minimum y	1831000 ft
Maximum y	3106000 ft
x and y spacing	2500 ft
Semi-Variogram Model	
Component Type	Linear
Anisotropy Angle	0
Anisotropy Ratio	1
Variogram Slope	1
Search Parameters	
Search Ellipse Radius #1	1700000 ft
Search Ellipse Radius #2	1700000 ft
Search Ellipse Angle	0
Number of Search Sectors	8
Maximum Data Per Sector	8
Maximum Empty Sectors	6
Minimum Data	3
Maximum Data	64

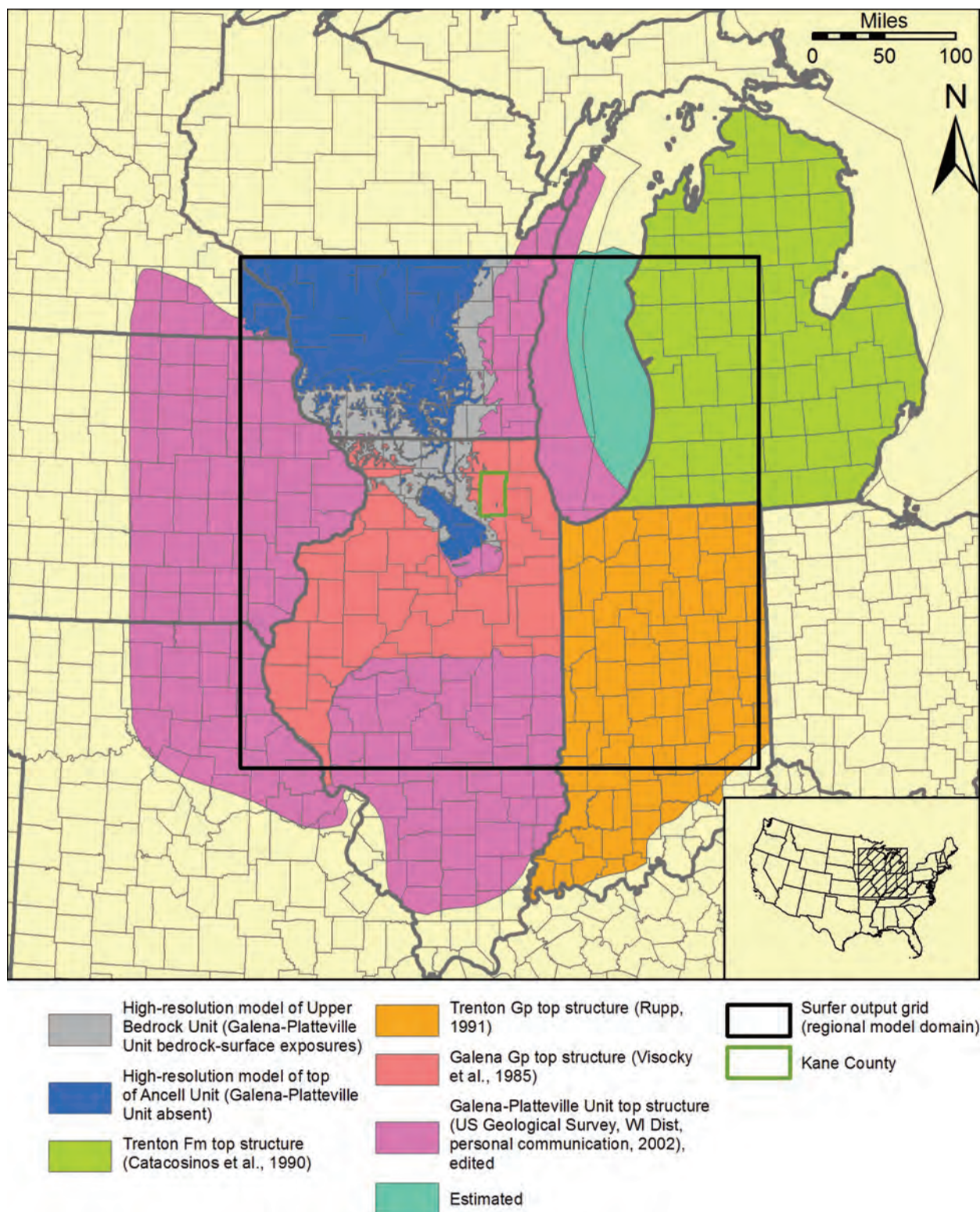


Figure C-18. Sources of data for high-resolution surface model of top of Galena-Platteville Unit.

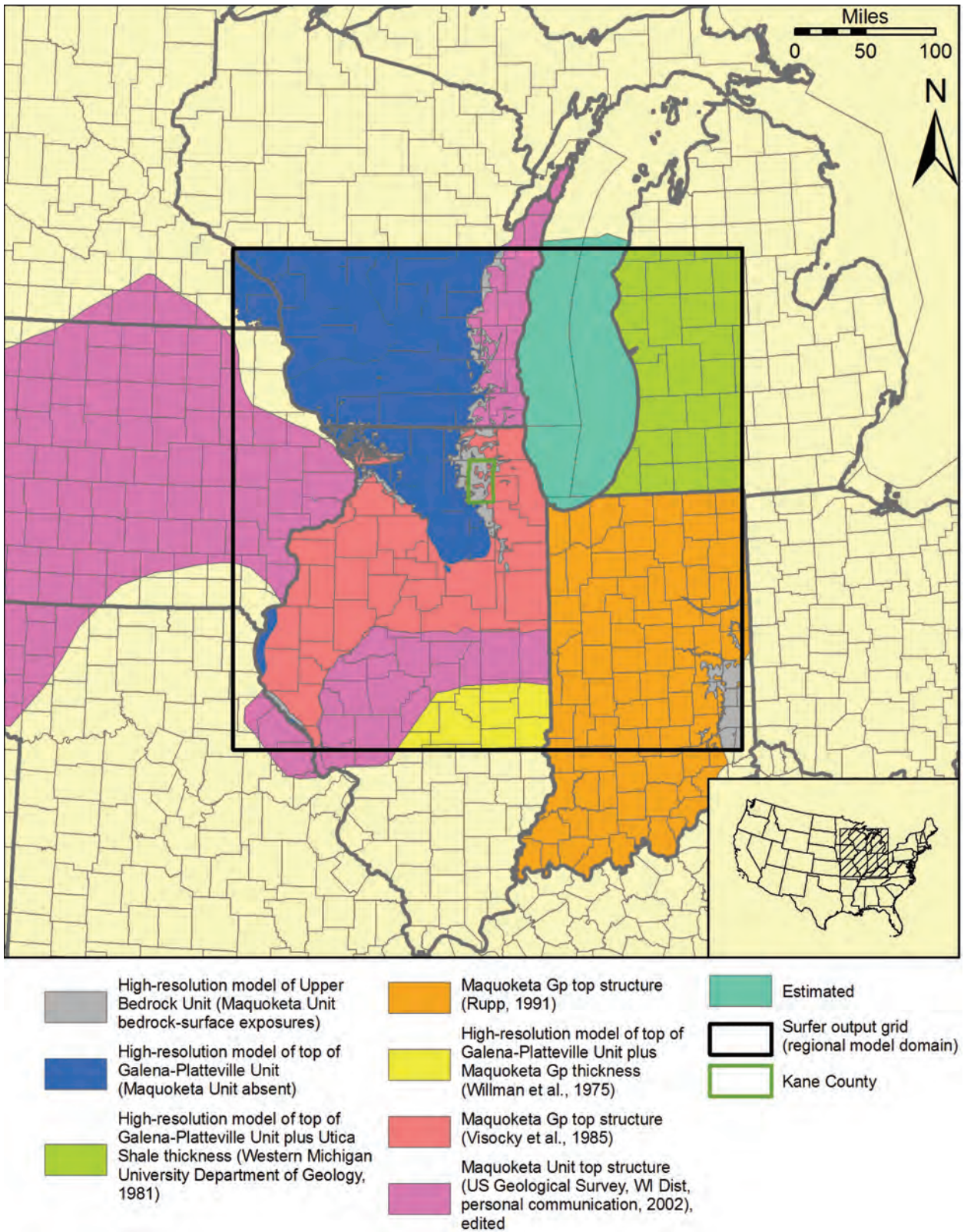


Figure C-19. Sources of data for high-resolution surface model of top of Maquoketa Unit.

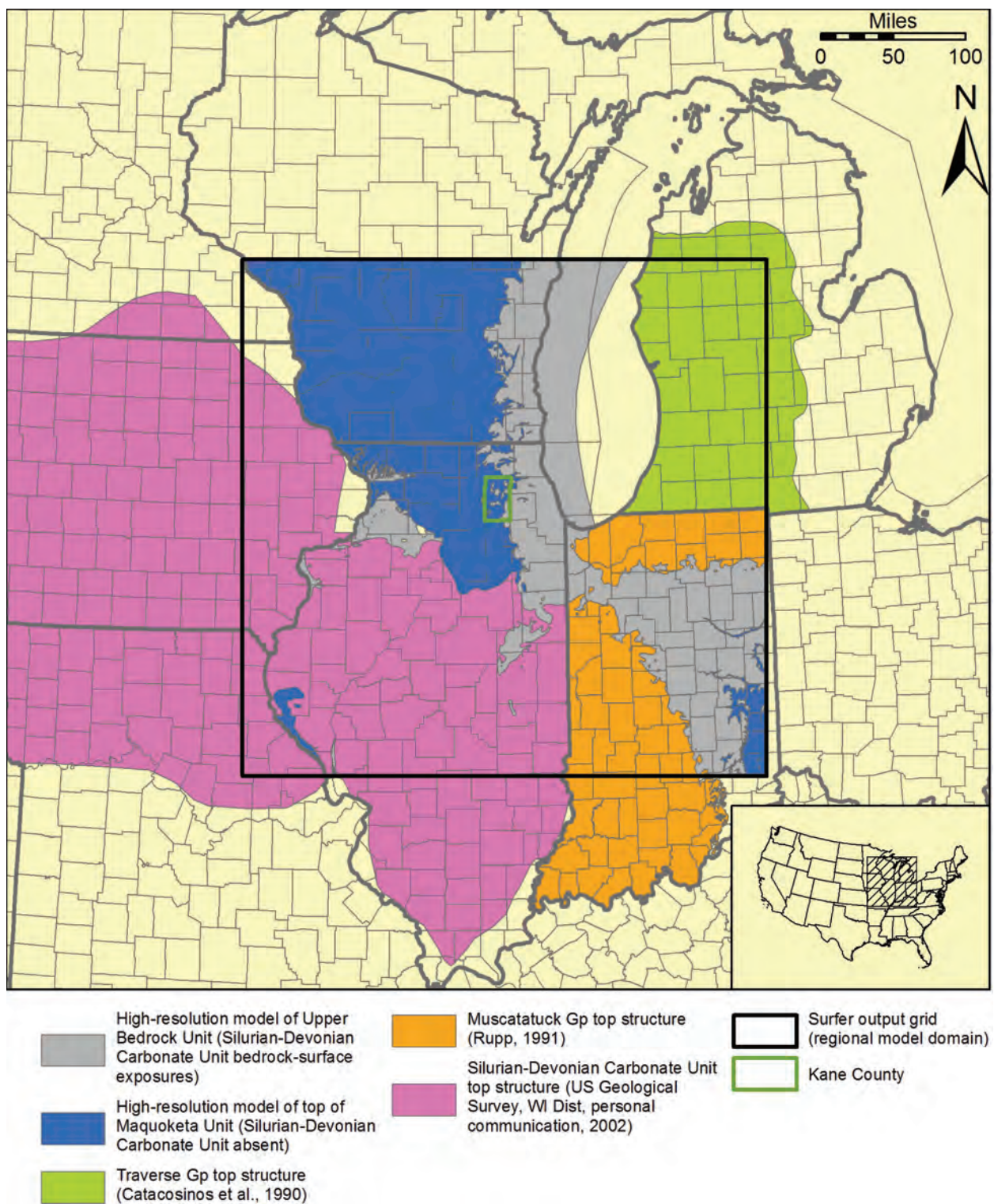


Figure C-20. Sources of data for second-iteration high-resolution surface model of top of Silurian-Devonian Carbonate Unit.

C.2. Irregular-Grid Geologic Model

An *irregular-grid geologic model* was developed from the completed high-resolution geologic model. The irregular-grid geologic model is a set of 12 *irregular-grid surface models*, each of which consists of estimates, for each active cell in the irregular finite-difference groundwater flow modeling grid, of the elevation of the top or bottom of a hydrostratigraphic unit. The 12 modeled surfaces are the tops of each of the 11 hydrostratigraphic units together with the bottom of the Mt. Simon Unit. Each irregular-grid surface model is adjusted to provide a minimum thickness of each hydrostratigraphic unit in areas of absence of the unit. These minimum thicknesses reflect the number of model layers devoted to each hydrostratigraphic unit and a 1-foot minimum thickness for each layer (Figure C-21). For example, since three model layers are devoted to the Silurian-Devonian Carbonate Unit, the minimum thickness of the Silurian-Devonian Carbonate Unit, based on a 1-foot thickness for each model layer, is 3 ft. The minimum thickness of most hydrostratigraphic units is 1 foot, since most hydrostratigraphic units are represented by only a single model layer.

Development of the irregular grid geologic model was begun using the *spatial join* utility of ArcGIS to join a polygon-shapefile of modeling grid with the active-cell high-resolution model of the top of each unit. This utility joins the attributes of two GIS layers based on the location of the features in the layers and was employed to develop a *provisional irregular-grid surface model* from each of the active-cell high-resolution surface models. The spatial-join process calculates the average elevation of the top of the unit, using elevations from the active-cell high-resolution surface model of the unit as input for each active cell in the model grid (Figure C-22). Since the active-cell high-resolution surface model includes estimated elevations at grid nodes spaced 2500 ft apart, the precise grid-cell dimensions in the model nearfield, the calculated average elevation in the model nearfield is based on a single elevation estimate. Average values calculated for larger grid cells in the model farfield are based on as many as 1024 values from the high-resolution surface model. Input data for the spatial join process was restricted to the *active-cell* high-resolution surface model to omit estimated elevations from the trans-Mississippi area, where the high-resolution model is less accurate.

The output of the spatial join process is a new polygon-shapefile with the same polygons as the modeling grid shapefile. This shapefile is referred to in this report as a *provisional irregular-grid surface model*. The attribute table of the new shapefile contains the calculated average elevation of the top of the hydrostratigraphic unit. The spatial join process was carried out 12 times to develop a provisional irregular-grid surface model of the top of each hydrostratigraphic unit as well as one of the bottom of the Mt. Simon Unit.

The average elevation of the top of each of the horizons covered by the 12 provisional irregular-grid surface models was indexed with a unique integer assigned to each cell of the modeling grid. This index was used to combine the 12 provisional irregular-grid surface models into a single Microsoft Excel (Microsoft Corporation, 2003) spreadsheet for manipulation of the average elevation data to accommodate the required minimum thickness of 1 foot per model layer. The spreadsheet contained a row for each grid cell, identified by the index value, and the average elevation of each of the 12 horizons from the provisional irregular-grid surface models of the horizons. From the elevation data, thicknesses of each of the 11 hydrostratigraphic units were calculated. Then, starting with the Quaternary Unit and working downward through the stratigraphic succession, the calculated thickness, based on the provisional irregular-grid surface modeling, was compared with the minimum thickness required to represent the unit in the regional groundwater flow model (Figure C-21). If the provisional thickness of the unit was less

than the required thickness, the bottom elevation of the unit (which is, in turn, the top elevation of the underlying unit) was recalculated as the top elevation minus the required thickness, shifting its position slightly downward. The spreadsheet rows highlighted in yellow in Figure C-23 illustrate this adjustment for a set of 20 grid cells. For cells where the provisional thickness of the Quaternary Unit was less than 3 ft, the top elevation of the Upper Bedrock Unit was recalculated as the top elevation of the Quaternary Unit minus 3 ft (1 ft for each of the three model layers representing the Quaternary Unit). Adjustment of the each unit made use of the top elevation recalculated in the adjustment of the immediately overlying unit. Thus, following on the example above, the elevation of the top of the Silurian-Devonian Carbonate Unit was recalculated as the top elevation of the Upper Bedrock Unit (after adjusting for a 3 ft minimum thickness of the Quaternary Unit) minus 1 ft.

With the completion of the adjustment, each provisional irregular-grid surface model was converted to the (final) irregular-grid surface model of the unit. Note that the provisional irregular-grid surface model of the top of the Quaternary Unit was unchanged, but all other provisional irregular-grid surface models were subject to adjustment. The set of adjusted elevations defining the geometry of the 11 hydrostratigraphic units is referred to as the irregular-grid geologic model.

C.3. Irregular-Grid Geologic Model to Geologic Framework of Regional Groundwater Flow Model

Conversion of the irregular-grid geologic model to the geologic framework of the regional model required that top elevations of individual model layers be calculated for each hydrostratigraphic unit modeled as two or more layers. For example, elevations of the top of model layers 5, 6, and 7, which represent the Silurian-Devonian Carbonate Unit, had to be calculated from the elevations of the tops of the Silurian-Devonian Carbonate Unit and the Maquoketa Unit included in the irregular-grid geologic model (Figure C-21). This arithmetic manipulation of the irregular-grid geologic model was carried out in Microsoft Excel for each hydrostratigraphic unit and each cell of the irregular model.

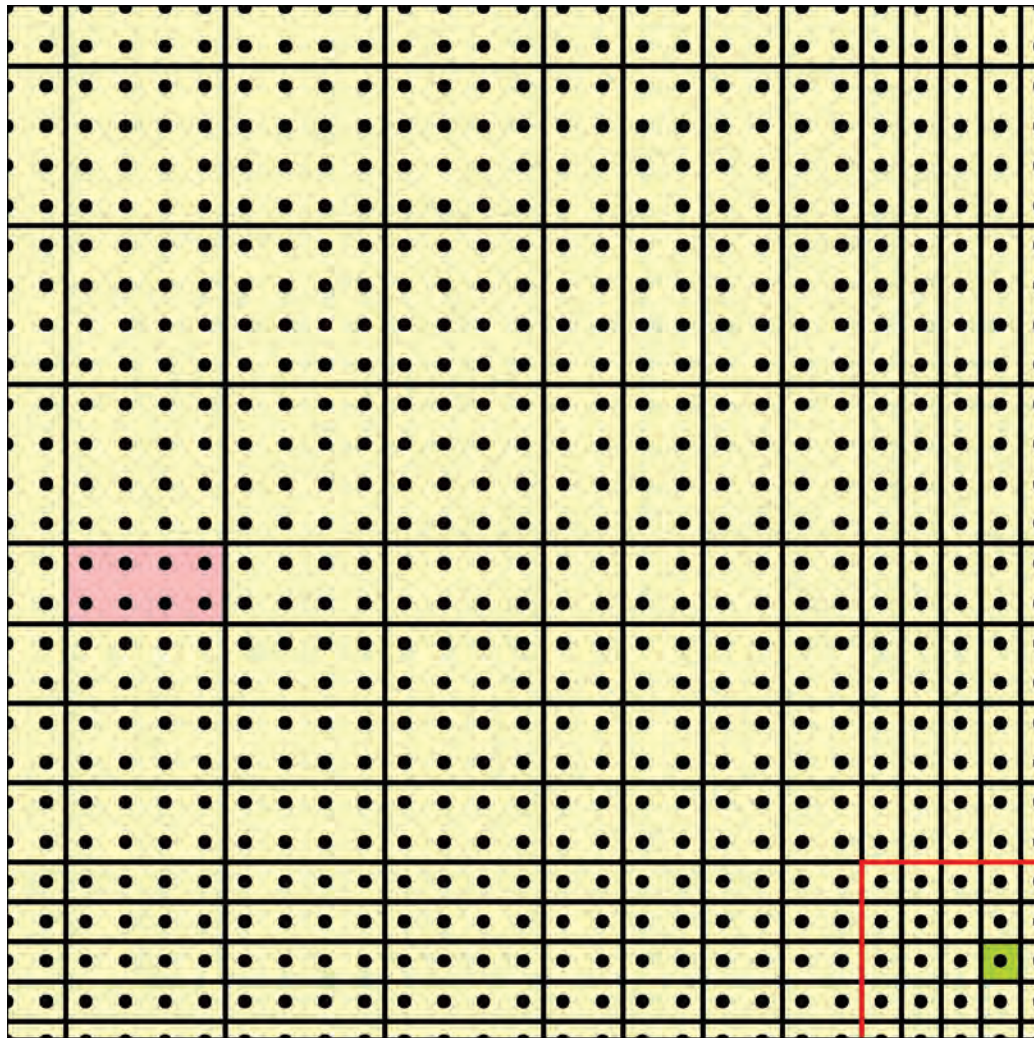
For hydrostratigraphic units represented by two or more model layers, the thickness of each individual model layer representing the unit was calculated for each cell by dividing the total thickness of the hydrostratigraphic unit, as represented in the irregular-grid geologic model, by the number of model layers devoted to the hydrostratigraphic unit (Figure C-21). Each of the model layers representing the hydrostratigraphic unit was thereby assigned an equal thickness. Thus the thickness of the three model layers representing the Silurian-Devonian Carbonate Unit in a cell was calculated as the difference in elevation between the tops of the Silurian-Devonian Carbonate Unit and the Maquoketa Unit divided by three. This layer thickness value was then employed to calculate the elevation of the tops of the model layers representing the hydrostratigraphic unit. Following on the example already begun, the elevation of the top of the model layer 6—the middle of three layers representing the Silurian-Devonian Carbonate Unit—was calculated by subtracting the layer thickness from the elevation of the top of the Silurian-Devonian Carbonate Unit. The elevation of layer 7 was calculated by multiplying the model layer thickness by 2 and subtracting the product from the elevation of the top of the Silurian-Devonian Carbonate Unit. The elevation of the top of model layer 5 is equivalent to the elevation of the top of the Silurian-Devonian Carbonate Unit.

After top elevations were assigned to all 20 layers in the regional model, the elevation data, indexed by grid cell, were exported from Microsoft Excel in text format and then imported

into Groundwater Vistas (Environmental Simulations Inc., 2005) as the geologic framework of the regional model.

HYDROSTRATIGRAPHIC UNIT	MODEL LAYER
Quaternary Unit (QT)	1
	2
	3
Upper Bedrock Unit (UB)	4
Silurian-Devonian Carbonate Unit (SD)	5
	6
	7
Maquoketa Unit (MQ)	8
	9
Galena-Platteville Unit (GP)	10
	11
Ancell Unit (AN)	12
Prairie du Chien-Eminence Unit (PE)	13
Potosi-Franconia Unit (PF)	14
Ironton-Galesville Unit (IG)	15
Eau Claire Unit (EC)	16
Mt Simon Unit (MS)	17
	18
	19
	20

Figure C-21. Relationship of hydrostratigraphic units to model layers.



- Data point, high-resolution surface model
- Finite difference cell, model nearfield: provisional irregular-grid average from spatial join based on one value from high-resolution surface model
- Finite difference cell, model farfield: provisional irregular-grid average from spatial join based on eight values from high-resolution surface model
- Regional model nearfield
- Finite-difference cell

Figure C-22. Calculation of average values for finite-difference cells through spatial-join process.

Microsoft Excel - irreg_mod_corr_for_min_m.xls									
Type a question for help:									
	A	B	C	D	E	F	G		
1	INDEX	ELEV_QUATERNARY_NOT_ADJUSTED	ELEV_UPPER_BEDROCK_NOT_ADJUSTED	THK_QUATERNARY_NOT_ADJUSTED	ELEV_QUATERNARY_ADJUSTED	ELEV_UPPER_BEDROCK_ADJUSTED	THK_QUATERNARY_ADJUSTED		
2	9721	405.1204781	395.3222029	9.79827523	405.1204781	395.3222029	9.79827523		
3	9722	397.9242902	389.5717109	8.35257929	397.9242902	389.5717109	8.35257929		
4	9723	389.5624298	383.7129609	5.84946895	389.5624298	383.7129609	5.84946895		
5	9724	380.7889519	377.6730159	3.11593599	380.7889519	377.6730159	3.11593599		
6	9725	389.9065197	388.5519966	1.3545231	389.9065197	388.5519966	1.3545231	3	
7	9726	349.7244907	349.7244907	0	349.7244907	349.7244907	0	3	
8	9727	339.3193865	339.3193865	0	339.3193865	339.3193865	0	3	
9	9728	333.6243769	331.4404289	2.18394805	333.6243769	330.6243769	3.00000000	3	
10	9729	326.9569474	313.2083291	13.74861828	326.9569474	313.2083291	13.74861828		
11	9730	318.9687135	290.056745	28.91196851	318.9687135	290.056745	28.91196851		
12	9731	308.4153324	269.2098221	39.20551032	308.4153324	269.2098221	39.20551032		
13	9732	294.7968669	245.2019751	49.59691174	294.7968669	245.2019751	49.59691174		
14	9733	279.8427484	225.0049898	54.83775854	279.8427484	225.0049898	54.83775854		
15	9734	271.8402467	214.3482231	57.49202354	271.8402467	214.3482231	57.49202354		
16	9735	263.4599315	209.1371537	54.32277783	263.4599315	209.1371537	54.32277783		
17	9736	239.3924503	205.7915945	33.60085586	239.3924503	205.7915945	33.60085586		
18	9737	271.9575099	224.3031895	47.65432039	271.9575099	224.3031895	47.65432039		
19	9738	413.6384667	298.4361583	115.2023084	413.6384667	298.4361583	115.2023084		
20	9739	559.0020744	416.8644858	142.1375886	559.0020744	416.8644858	142.1375886		
21	9740	685.3879613	452.7321493	232.655232	685.3879613	452.7321493	232.655232		
22									
23									
24									
25									
26									
27									
28									
29									
30									
31									
32									
33									
34									
35									
36									
37									
38									
39									
40									
41									
42									
43									
44									
45									
46									
47									

Figure C-23. Example of correction of provisional irregular-grid model to accommodate required minimum model layer thickness of 1 foot per model layer.

C.4. References

Becker, L.E., A.J. Hreha and T.A. Dawson. 1978. *Pre-Knox (Cambrian) Stratigraphy in Indiana*. Indiana Department of Natural Resources Geological Survey 57, Bloomington, IN.

Bricker, D.M., R.L. Milstein and J. C.R. Reszka. 1983. *Selected Studies of Cambro-Ordovician Sediments within the Michigan Basin*. Michigan Department of Natural Resources Geological Survey Division Report of Investigation 26, Lansing, MI.

Buschbach, T.C. 1964. *Cambrian and Ordovician Strata of Northeastern Illinois*. Illinois State Geological Survey Report of Investigation 218, Urbana, IL.

Cannon, W.F., T.H. Kress, D.M. Sutphin, G.B. Morey, J. Meints and R.D. Barber-Delach. 1997. Digital Geologic Map and Mineral Deposits of Minnesota, Wisconsin, and Michigan (Version 3.0) (Downloadable GIS Data). *United States Geological Survey*, <http://pubs.usgs.gov/of/1997/of97-455/> (accessed April 4, 2006).

Catacosinos, P.A. and P.A. Daniels, Jr. 1991. Stratigraphy of Middle Proterozoic to Middle Ordovician formations of the Michigan basin. In *Early sedimentary evolution of the Michigan basin*, 53-71. Edited by P.A. Catacosinos and P.A. Daniels. Geological Society of America Special Paper 256. Geological Society of America, Boulder, CO.

Catacosinos, P.A., P.A. Daniels, Jr. and W.B. Harrison, III. 1990. Structure, Stratigraphy, and Petroleum Geology of the Michigan Basin. In *Interior Cratonic Basins*, 561-601. Edited by M.W. Leighton, D.R. Kolata, D.F. Oltz and J.J. Eidel. American Association of Petroleum Geologists Memoir 51. American Association of Petroleum Geologists, Tulsa, OK.

Droste, J.B. and J.B. Patton. 1985. *Lithostratigraphy of the Sauk Sequence in Indiana*. Indiana Department of Natural Resources Geological Survey Occasional Paper 47, Bloomington, IN.

Droste, J.B. and R.H. Shaver. 1983. *Atlas of Early and Middle Paleozoic Paleogeography of the Southern Great Lakes Area*. Indiana Department of Natural Resources Geological Survey 32, Bloomington, IN.

Emrich, G.H. 1966. *Ironton and Galesville (Cambrian) Sandstones in Illinois and Adjacent Areas*. Illinois State Geological Survey Circular 403, Urbana, IL.

Environmental Simulations Inc. 2005. Groundwater Vistas Version 4.19.

Environmental Systems Research Institute. 2005. ArcGIS - Version 9.1.

Feinstein, D.T., T.T. Eaton, D.J. Hart, J.T. Krohelski and K.R. Bradbury. 2003. *Regional aquifer model for southeastern Wisconsin; Report 1: Data collection, conceptual model development, numerical model construction, and model calibration*. Wisconsin Geological and Natural History Survey administrative report prepared for Southeastern Wisconsin Regional Planning Commission.

Golden Software Inc. 2002. Surfer - Version 8.

Gray, H.H., C. Ault, S. Keller and D. Harper. 2002. BEDROCK_GEOL_MM48_IN: Bedrock Geology of Indiana (Indiana Geological Survey, 1:500,000, Polygon Shapefile). *Indiana Geological Survey*, http://igs.indiana.edu/arcims/statewide/dload_page/geology.html (accessed April 4, 2006).

Herzog, B.L., B.J. Stiff, C.H. Chenoweth, K.L. Warner, J.B. Sieverling and C. Averly. 1994. *Buried Bedrock Surface of Illinois*. Illinois State Geological Survey Illinois Map 5, Champaign, IL.

Illinois Department of Natural Resources. 1996a. Bedrock Geology, Illinois Geographic Information System, Volume I (GIS Data on CD-ROM). *Illinois Department of Natural Resources* (May 1996).

Illinois Department of Natural Resources. 1996b. Bedrock Topography, Illinois Geographic Information System, Volume I (GIS Data on CD-ROM). *Illinois Department of Natural Resources* (May 1996).

Kolata, D.R., T.C. Buschbach and J.D. Treworgy. 1978. *The Sandwich Fault Zone of Northern Illinois*. Illinois State Geological Survey Circular 505, Urbana, IL.

Microsoft Corporation. 2003. Microsoft Office Excel 2003.

National Oceanic and Atmospheric Administration Satellite and Information Service. 1996. Bathymetry of Lake Michigan. *National Oceanic and Atmospheric Administration*, <http://map.ngdc.noaa.gov/website/mgg/greatlakesbathy/viewer.htm> (accessed August 9, 2005).

Rupp, J.A. 1991. *Structure and Isopach Maps of the Paleozoic Rocks of Indiana*. Indiana Department of Natural Resources Geological Survey Special Report 48, Bloomington, IN.

Visocky, A.P., M.G. Sherrill and K. Cartwright. 1985. *Geology, Hydrology, and Water Quality of the Cambrian and Ordovician Systems in Northern Illinois*. Illinois State Geological Survey and Illinois State Water Survey Cooperative Groundwater Report 10, Champaign, IL.

Western Michigan University Department of Geology. 1981. *Hydrogeologic Atlas of Michigan prepared for United States Environmental Protection Agency, Underground Injection Control Program*. Western Michigan University, Kalamazoo, MI.

Willman, H.B., E. Atherton, T.C. Buschbach, C. Collinson, J.C. Frye, M.E. Hopkins, J.A. Lineback and J.A. Simon. 1975. *Handbook of Illinois Stratigraphy*. Illinois State Geological Survey Bulletin 95, Urbana, IL.

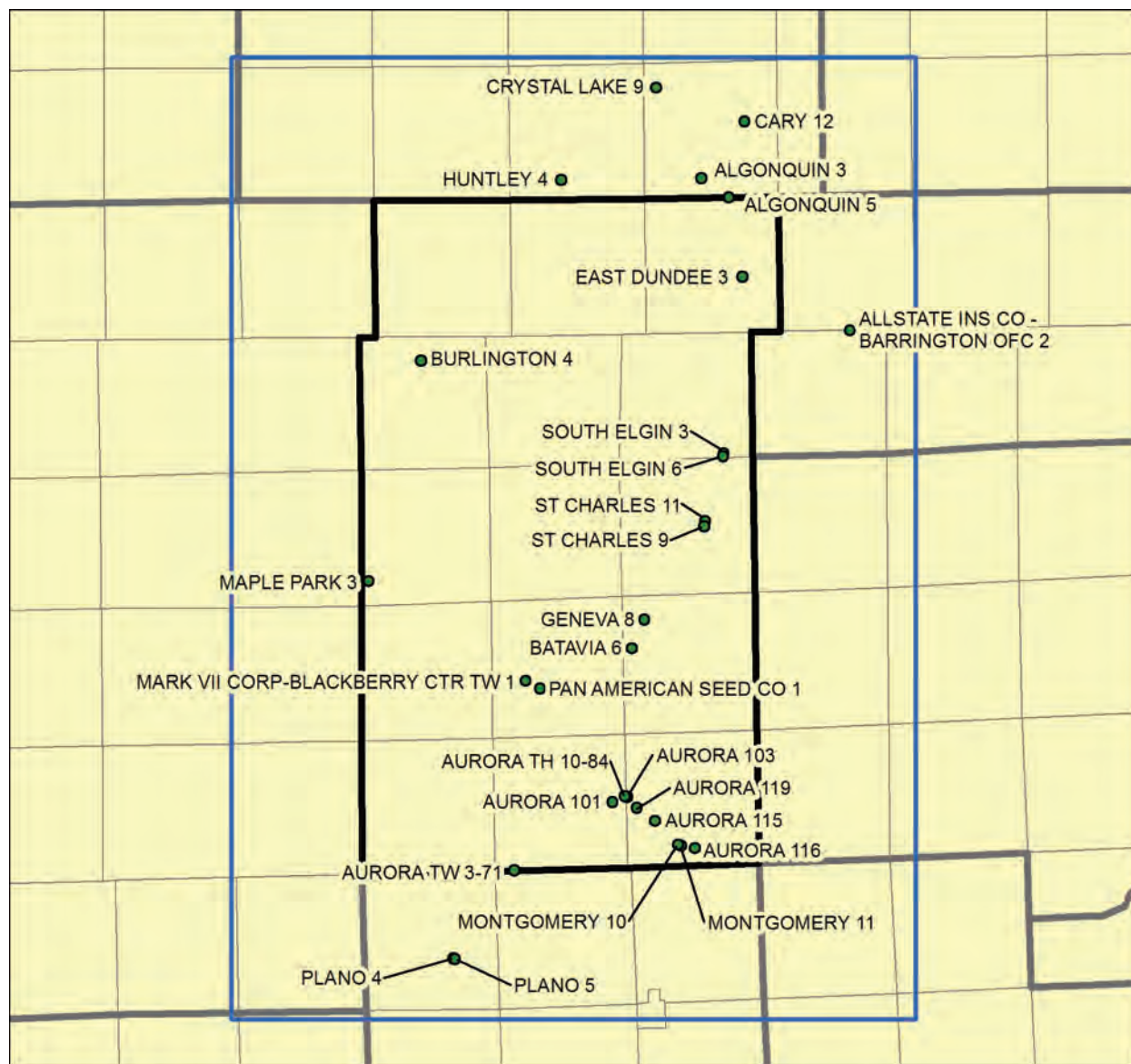
Wisconsin Geological and Natural History Survey and Wisconsin Department of Administration State Planning Office. 1976. *Glacial Deposits of Wisconsin, Sand and Gravel Resource Potential*. Wisconsin Geological and Natural History Survey Land Resources Analysis Program Map 10, Madison, WI.

Young, H.L. 1992. *Summary of Ground-Water Hydrology of the Cambrian-Ordovician Aquifer System in the Northern Midwest, United States*. United States Geological Survey Professional Paper 1405-A, Washington, DC.

Appendix D. Results of Pumping Tests of Shallow Aquifers in the Kane County Area

In a controlled pumping test, groundwater is pumped from a well at a closely monitored, constant rate, and water levels are simultaneously measured in the pumped well and, preferably, in one or more observation wells. Water levels are also measured during the recovery period after pumping has stopped. The time after the beginning or end of pumping is recorded with each water level measurement. Data obtained from controlled pumping tests may be analyzed by one or more similar graphical methods. These methods plot elapsed time since the beginning or end of pumping versus drawdown or recovery. If data are available from several observation wells, distance from the pumped well versus synchronous drawdown or recovery data can be plotted and analyzed. The plots are analyzed, frequently by comparing them to type curves developed from equations describing the relationship between the hydraulic properties of an ideal aquifer and the drawdown and recovery of water levels in the vicinity of a pumping well finished in the aquifer. Software packages automate this curve-matching process. For example, analysis of pumping test data for this project was conducted using the software package AquiferWin32 (Environmental Simulations Inc., 2001).

Locations (Figure D-1 and Figure D-2) and results (Table D-1 and Table D-2) of pumping tests of wells open to sand and gravel aquifers and the Shallow Bedrock Aquifer in the Kane County area are presented in this section. The analyzed pumping test data were obtained largely from the ISWS files and were selected on the basis of data and test quality. Test data that were selected for analysis are from tests that were generally of longer duration, characterized by a fairly constant pumping rate and by relatively frequent and precise water-level measurements. Note that estimates of hydraulic conductivity are not provided for tests of the Shallow Bedrock Aquifer (Table D-2). Hydraulic conductivity is typically calculated by dividing estimates of transmissivity (T) by aquifer thickness. It was not calculated for this study because Shallow Bedrock Aquifer thickness is not determinable from available information. Note also that more than one result is sometimes provided for a given well. Such multiple results reflect use of more than one analysis technique applied to the same data, or separate analyses of differing portions of the complete set of test data.



- Tested well
- Local model domain
- Kane County
- Township boundary

Figure D-1. Locations of pumping tests of wells open to sand and gravel aquifers in the Kane County area. See Table D-1 for analytical results.

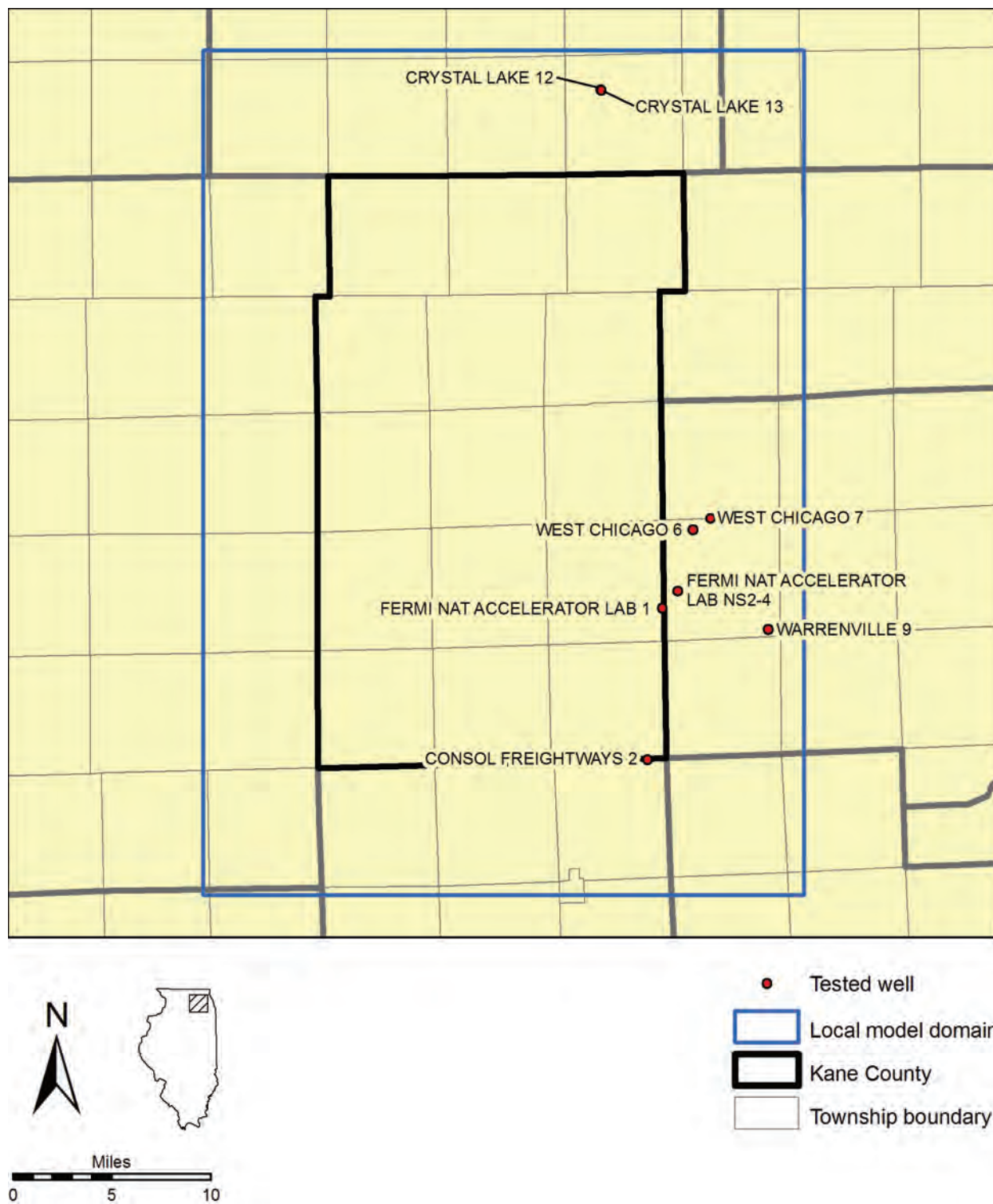


Figure D-2. Locations of pumping tests of wells open to the Shallow Bedrock Aquifer in the Kane County area. See Table D-2 for analytical results.

Table D-1. Pumping Tests of Wells Finished in Sand and Gravel Aquifers in the Kane County Area

<i>Pumped Well</i>	<i>Month/ Year</i>	<i>Tested Interval</i>	<i>Pumped Well Location</i>					<i>Analysis Well¹</i>	<i>T (ft²/d)</i>	<i>K (ft/d)</i>	<i>S</i>	<i>Analysis Method</i>
			<i>County</i>	<i>T</i>	<i>R</i>	<i>Section</i>	<i>Plot</i>					
Algonquin 5	08/1978	Ashmore Unit	McHenry	43N	8E	34	2A	PW	3672			Cooper and Jacob (1946)
Algonquin 3	04/1970	Glasford Unit (upper sand)	McHenry	43N	8E	33	4H	PW	1320	66		Cooper and Jacob (1946)
Allstate Ins Co - Barrington Ofc 2	09/1980	Yorkville Sand Unit	Cook	42N	9E	34	8A	PW	2390	70		Cooper and Jacob (1946)
Aurora 101	10/1986	Glasford Unit (lower sand)	Kane	38N	7E	24	6H	OW TH 1-86	3015	70	6.8×10^{-4}	Cooper and Jacob (1946)
								OW TH 1-86	3347	78	4.0×10^{-4}	Theis (1935)
Aurora 101	10/1987	Glasford Unit (lower sand)	Kane	38N	7E	24	6H	PW	3717	86		Cooper and Jacob (1946)
Aurora 103	07/1988	Glasford Unit (upper and lower sands)	Kane	38N	8E	18	7B	PW	4161			Cooper and Jacob (1946)
								OW West	6644			Cooper and Jacob (1946)
Aurora 115	07/1988	Glasford Unit (lower sand)	Kane	38N	8E	20	5A	PW	4646	77		Cooper and Jacob (1946)
								OW East	5524	92		Cooper and Jacob (1946)
								OW West	4626	77		Cooper and Jacob (1946)
Aurora 116	04/1988	Glasford Unit (upper sand)	Kane	38N	8E	34	8G	All OW	9388	427	5.2×10^{-4}	Theis (1935)
								All OW	9762	444	4.0×10^{-4}	Cooper and Jacob (1946)

¹ Well that is the basis for T, K, and S determination. PW: pumped well. OW: observation well.

**Table D-1. Pumping Tests of Wells Finished in Sand and Gravel Aquifers in the Kane County Area
(Continued)**

<i>Pumped Well</i>	<i>Month/ Year</i>	<i>Tested Interval</i>	<i>Pumped Well Location</i>					<i>Analysis Well¹</i>	<i>T (ft²/d)</i>	<i>K (ft/d)</i>	<i>S</i>	<i>Analysis Method</i>
			<i>County</i>	<i>T</i>	<i>R</i>	<i>Section</i>	<i>Plot</i>					
Aurora 116 (continued)	04/1988	Glasford Unit (upper sand)	Kane	38N	8E	34	8G	OW 2 (OW 9- 88)	8938	406	1.8×10^{-4}	Cooper and Jacob (1946)
								OW 2 (OW 9- 88)	7283	331	2.3×10^{-4}	Cooper and Jacob (1946)
								OW 3 (OW 10- 88)	8764	398	3.3×10^{-4}	Cooper and Jacob (1946)
								OW 3 (OW 10- 88)	8696	395	3.7×10^{-4}	Cooper and Jacob (1946)
Aurora 119	04/1989	Glasford Unit (upper and lower sands)	Kane	38N	8E	19	5E	OW 1 (TH 15- 87)	1948	32	7.0×10^{-4}	Hantush and Jacob (1955)
								OW 2 (TH 13- 87)	1831	30	2.5×10^{-4}	Hantush and Jacob (1955)
								OW 3 (TH 16- 87)	1903	31	7.8×10^{-5}	Hantush and Jacob (1955)
Aurora 101	12/1970	Glasford Unit (lower sand)	Kane	38N	7E	24	6H	PW	2880	67		Cooper and Jacob (1946)
								OW PP- 1-70	2251	52	2.5×10^{-3}	Hantush and Jacob (1955)
								OW SG- 70	3855	90	7.2×10^{-5}	Hantush and Jacob (1955)

**Table D-1. Pumping Tests of Wells Finished in Sand and Gravel Aquifers in the Kane County Area
(Continued)**

<i>Pumped Well</i>	<i>Month/ Year</i>	<i>Tested Interval</i>	<i>Pumped Well Location</i>					<i>Analysis Well¹</i>	<i>T (ft²/d)</i>	<i>K (ft/d)</i>	<i>S</i>	<i>Analysis Method</i>
			<i>County</i>	<i>T</i>	<i>R</i>	<i>Section</i>	<i>Plot</i>					
Aurora TH 10-84	12/1985	Glasford Unit (upper and lower sands)	Kane	38N	8E	18	8B	OW TH 7-84	5430	86	2.9×10^{-4}	Hantush and Jacob (1955)
								OW TH 8-84	7446	118	2.8×10^{-4}	Hantush and Jacob (1955)
								OW TH 8-84	7772	123	2.8×10^{-4}	Hantush and Jacob (1955)
								OW TH 8-84	8790	140	2.3×10^{-4}	Cooper and Jacob (1946)
Aurora TW 3-71	02/1971	Glasford Unit (upper sand)	Kane	38N	7E	31	1A	PW	6605	105		Cooper and Jacob (1946)
								OW 20B3-71 (SWS 1)	4611	77	5.5×10^{-4}	Hantush and Jacob (1955)
								OW 30B3-71 (SWS 3)	9333	156	6.6×10^{-5}	Hantush and Jacob (1955)
								OW 3-71 (SWS 2)	8877	148	8.3×10^{-5}	Hantush and Jacob (1955)
Batavia 6	12/1988	Glasford Unit (lower sand)	Kane	39N	8E	18	5G	PW	8587	296		Cooper and Jacob (1946)
								OW 2 (TH 6-88)	1075	371	3.0×10^{-4}	Hantush and Jacob (1955)
								OW 2 (TH 6-88)	9126	315	4.8×10^{-4}	Cooper and Jacob (1946)
								OW 3 (TH 7-88)	8361	288	3.1×10^{-4}	Hantush and Jacob (1955)

**Table D-1. Pumping Tests of Wells Finished in Sand and Gravel Aquifers in the Kane County Area
(Continued)**

<i>Pumped Well</i>	<i>Month/ Year</i>	<i>Tested Interval</i>	<i>Pumped Well Location</i>					<i>Analysis Well¹</i>	<i>T (ft²/d)</i>	<i>K (ft/d)</i>	<i>S</i>	<i>Analysis Method</i>
			<i>County</i>	<i>T</i>	<i>R</i>	<i>Section</i>	<i>Plot</i>					
Batavia 6 (continued)	12/1988	Glasford Unit (lower sand)	Kane	39N	8E	18	5G	OW 3 (TH 7- 88)	8922	308	2.6×10^{-4}	Cooper and Jacob (1946)
Burlington 4	12/1988	Ashmore Unit	Kane	41N	6E	09	1G	PW	1908	159		Cooper and Jacob (1946)
Cary 12	02/1993	Yorkville Sand Unit	McHenry	43N	8E	14	5C	PW	12807	366		Cooper and Jacob (1946)
Crystal Lake 9	09/1986	Glasford Unit (upper and lower sands)	McHenry	43N	8E	6	4A	PW	1972	282		Cooper and Jacob (1946)
East Dundee 3	04/1969	Ashmore Unit	Kane	42N	8E	23	6E	PW	1253	391		Cooper and Jacob (1946)
Geneva 8	06/1986	Glasford Unit (lower sand)	Kane	39N	8E	05	8A	PW	3484	850		Theis, 1935 (Recovery)
								PW	37083	904		Cooper and Jacob (1946)
								OW 2	34019	830	2.7×10^{-4}	Cooper and Jacob (1946)
								OW 2	28511	695	6.8×10^{-4}	Hantush and Jacob (1955)
								OW 3	29759	726	6.2×10^{-4}	Hantush and Jacob (1955)
								OW 4	35139	857	4.2×10^{-4}	Cooper and Jacob (1946)
								OW 4	34327	837	4.6×10^{-4}	Hantush and Jacob (1955)
								OW 5	35948	877	3.0×10^{-4}	Cooper and Jacob (1946)
								OW 5	33503	817	3.8×10^{-4}	Hantush and Jacob (1955)

**Table D-1. Pumping Tests of Wells Finished in Sand and Gravel Aquifers in the Kane County Area
(Continued)**

<i>Pumped Well</i>	<i>Month/ Year</i>	<i>Tested Interval</i>	<i>Pumped Well Location</i>					<i>Analysis Well¹</i>	<i>T (ft²/d)</i>	<i>K (ft/d)</i>	<i>S</i>	<i>Analysis Method</i>
			<i>County</i>	<i>T</i>	<i>R</i>	<i>Section</i>	<i>Plot</i>					
Huntley 4	11/1953	Batestown Sand Unit	McHenry	43N	7E	33	6H	PW	1910	83		Cooper and Jacob (1946)
Maple Park 3	05/1971	Glasford Unit (upper and lower sands)	Kane	40N	6E	30	5A	PW	110			Cooper and Jacob (1946)
Mark VII Corp- Blackberry Ctr TW 1	08/1974	Glasford Unit (upper sand)	Kane	39N	7E	20	4D	PW	8365	186	9.1×10^{-3}	Hantush and Jacob (1955)
								OW E-11	8730	194	7.0×10^{-3}	Cooper and Jacob (1946)
								OW E-11	8276	184	7.1×10^{-3}	Hantush and Jacob (1955)
								OW E-9	8726	194	1.2×10^{-2}	Cooper and Jacob (1946)
								OW E-9	8455	188	1.2×10^{-2}	Hantush and Jacob (1955)
Montgomery 10	12/1986	Glasford Unit (upper and lower sands)	Kane	38N	8E	33	4H	PW	9032	201		Cooper and Jacob (1946)
								OW 1	1995	46	1.1×10^{-4}	Hantush and Jacob (1955)
								OW 4	1904	44	3.1×10^{-4}	Hantush and Jacob (1955)
								OW 5	2766	64	8.1×10^{-5}	Hantush and Jacob (1955)
								OW SI	2461	57	1.7×10^{-4}	Hantush and Jacob (1955)
Montgomery 11	09/1987	Glasford Unit (upper and lower sands)	Kane	38N	8E	33	5H	Mont-gomery 10	4339	128	1.6×10^{-4}	Hantush and Jacob (1955)

**Table D-1. Pumping Tests of Wells Finished in Sand and Gravel Aquifers in the Kane County Area
(Continued)**

<i>Pumped Well</i>	<i>Month/ Year</i>	<i>Tested Interval</i>	<i>Pumped Well Location</i>					<i>Analysis Well¹</i>	<i>T (ft²/d)</i>	<i>K (ft/d)</i>	<i>S</i>	<i>Analysis Method</i>
			<i>County</i>	<i>T</i>	<i>R</i>	<i>Section</i>	<i>Plot</i>					
Montgomery 11 (continued)	09/1987	Glasford Unit (upper and lower sands)	Kane	38N	8E	33	5H	OW TH 1-87 DEEP	2073	61	7.0×10^{-5}	Hantush and Jacob (1955)
								OW TH 1-87 DEEP	1993	59	7.7×10^{-5}	Hantush and Jacob (1955)
								OW TH 3-87 DEEP	1894	56	3.4×10^{-4}	Hantush and Jacob (1955)
								OW TH 4-87	1246	37	4.4×10^{-5}	Hantush and Jacob (1955)
								OW TH 4-87	1712	50	4.8×10^{-5}	Hantush and Jacob (1955)
								OW TH 9-84	3636	107	2.1×10^{-4}	Hantush and Jacob (1955)
								OW TH 9-84	3692	109	1.4×10^{-4}	Hantush and Jacob (1955)
Pan American Seed Co 1	07/1985	Ashmore Unit	Kane	39N	7E	21	7A	PW	2821	134		Cooper and Jacob (1946)
Plano 4	06/1966	Glasford Unit (lower sand)	Kendall	37N	6E	23	8C	PW	1765	570		Cooper and Jacob (1946)
Plano 5	07/1966	Glasford Unit (lower sand)	Kendall	37N	6E	23	8C	PW	3121	844		Cooper and Jacob (1946)
South Elgin 3	04/1962	Ashmore Unit	Kane	41N	8E	35	3C	PW	4693	293		Cooper and Jacob (1946)
South Elgin 6	08/1987	Glasford Unit (upper sand)	Kane	41N	8E	35	3A	PW	3503	292		Cooper and Jacob (1946)
St Charles 11	11/1988	Glasford Unit (lower sand)	Kane	40N	8E	15	1C	PW	2223	2040		Cooper and Jacob (1946)

**Table D-1. Pumping Tests of Wells Finished in Sand and Gravel Aquifers in the Kane County Area
(Concluded)**

<i>Pumped Well</i>	<i>Month/ Year</i>	<i>Tested Interval</i>	<i>Pumped Well Location</i>					<i>Analysis Well¹</i>	<i>T (ft²/d)</i>	<i>K (ft/d)</i>	<i>S</i>	<i>Analysis Method</i>
			<i>County</i>	<i>T</i>	<i>R</i>	<i>Section</i>	<i>Plot</i>					
St Charles 11 (continued)	11/1988	Glasford Unit (lower sand)	Kane	40N	8E	15	1C	OW 2 (TH 4- 88)	1581	1450	1.1×10^{-2}	Cooper and Jacob (1946)
								OW 3 (TH 5- 88)	1608	1475	1.4×10^{-4}	
St Charles 9	12/1979	Glasford Unit (upper and lower sands)	Kane	40N	8E	15	2A	OW	150029	2381		Cooper and Jacob (1946)

Table D-2. Pumping Tests of Wells Finished in the Shallow Bedrock Aquifer in the Kane County Area

<i>Pumped Well</i>	<i>Month/ Year</i>	<i>Tested Interval</i>	<i>Pumped Well Location</i>					<i>Analysis Well</i>	<i>T (ft²/d)</i>	<i>S</i>	<i>Analysis Method</i>
			<i>County</i>	<i>T</i>	<i>R</i>	<i>Section</i>	<i>Plot</i>				
Consol Freightways 2	02/1973	Silurian+ Maquoketa	Kane	38N	8E	35	1A	PW	5959		Cooper and Jacob (1946)
Crystal Lake 12	12/1986	Silurian	McHenry	43N	8E	8	1C	PW	2202		Cooper and Jacob (1946)
Crystal Lake 13	02/1987	Silurian	McHenry	43N	8E	8	1C	OW (Crystal Lake 12)	2736	3.2×10 ⁻⁴	Cooper and Jacob (1946)
Warrenville 9	06/1985	Silurian+ Maquoketa	DuPage	39N	9E	36	7A	PW	4527		Cooper and Jacob (1946)
West Chicago 6	11/1980	Silurian+ Maquoketa	DuPage	39N	9E	5	4D	PW	6511		Cooper and Jacob (1946)
West Chicago 7	12/1980	Silurian+ Maquoketa	DuPage	40N	9E	33	5A	PW	1824		Cooper and Jacob (1946)
Fermi National Accelerator Laboratory 1	03/1997	Silurian+ Maquoketa	Kane	39N	8E	25	1E	OW S-1213	7985	8.5×10 ⁻⁵	Theis (1935)
Fermi National Accelerator Laboratory NS 2-4	08/1996	Silurian	DuPage	39N	9E	19	3D	All OW	53	5.4×10 ⁻⁴	Hantush and Jacob (1955)

D.1 References

Cooper, H.H., Jr. and C.E. Jacob. 1946. A generalized graphical method for evaluating formation constants and summarizing well field history. *Transactions of the American Geophysical Union* 27:526-534.

Hantush, M.S. and C.E. Jacob. 1955. Non-steady radial flow in an infinite leaky aquifer. *Transactions of the American Geophysical Union* 36:95-100.

Theis, C.V. 1935. The relation between the lowering of the piezometric surface and the rate and duration of discharge of a well using groundwater storage. In *Transactions of the American Geophysical Union 16th Annual Meeting, part 2*.

Appendix E. Analysis of Calibration Target Errors

Groundwater models are calibrated by adjusting model parameters until the simulations match observed heads and fluxes. Although an ideal model would match all observations exactly, each observation (or calibration target) has associated errors. Consequently, a calibrated model should simulate values that, on average, are centered on the calibration target value and within the range of the associated errors of the calibration target (Anderson and Woessner, 2002).

This appendix assesses the ranges of errors associated with the calibration targets, examining the greatest degree of agreement (i.e., smallest errors) that might be expected for model-simulated versus observed values. Although the regional model also includes the uppermost aquifers, the local model has greater detail and resolution for these aquifers than does the regional model. Thus, the error analyses focus on shallow targets for the local model and deep targets for the regional model.

E.1. Errors Associated with Local Head Targets

Anderson and Woessner (2002) noted that calibration targets for head in a groundwater model have several sources of error, including unmodeled temporal and spatial variability, measurement errors, etc. Under the assumption that these errors are independent, the total error variance associated with a calibration target for head is the sum of the variances of the independent errors (Larsen and Marx, 1986):

$$\sigma_H^2 = \sigma_t^2 + \sigma_m^2 + \sigma_s^2 + \sigma_K^2 + \sigma_i^2 + \sigma_n^2 + \sigma_c^2$$

where

σ_H^2 = the error variance associated with a calibration target for head

σ_t^2 = error variance for unmodeled temporal variability

σ_m^2 = variance of measurement errors

σ_s^2 = variance of scale-up errors due to vertical averaging over long piezometer intervals

σ_K^2 = variance of scale-up errors arising from unmodeled heterogeneity

σ_i^2 = variance of interpolation errors

σ_n^2 = variance of numerical errors within the solution convergence tolerance

σ_c^2 = error variance attributable to the effects of salinity.

In this study, the error variances generally are estimated using field observations. For the case of measurement and interpolation errors, only an estimate of the maximum absolute error is available. In these cases, this study will assume the errors to be normally distributed, and estimate the error variance as:

$$\sigma^2 = \left[\frac{\text{maximum absolute error}}{3} \right]^2$$

Some studies have assumed that the maximum absolute error represents two standard errors, i.e., a 95 percent confidence interval (Hill and Tiedeman, 2007). In this study, the sets of

observations are generally large (100's), which suggests that the observed maximum errors represent a higher level of confidence. This analysis therefore assumes that the range of the observations corresponds to a 99.7 percent confidence interval (equivalent to plus or minus three times the standard normal error).

Hill and Tiedeman (2007) note that calibration targets should be temporally consistent with the model simulations, that is, calibration targets should use an averaging interval for observations that is similar to that of the simulation period. Unfortunately, the wells in the local domain have insufficient records to infer a long-term average value head that would be consistent with a steady-state simulation. The errors associated with the unmodeled temporal variability are inferred from the head data collected by Locke and Meyer (2005), which included an initial measurement at each well during the inventory phase followed by the final synoptic measurement. The initial measurements were scattered over the 16 months preceding the synoptic measurement, so the differences between the initial and synoptic readings are a sample of the temporal variability of the shallow aquifers in the local model. This study uses the mean squared difference between the initial and synoptic observations to estimate the error variance due to temporal variability, yielding a value of $\sigma_i^2 = 95 \text{ ft}^2$. Mandle and Kontis (1992) noted that although water levels had declined a few tens of feet near pumping centers, there is no general long-term trend in the water levels of the shallow sand and gravel aquifers.

For measurement errors, Locke and Meyer (2005) found the maximum absolute error to be 2.4 ft for steel tape measurements. With substitution, the corresponding error variance is:

$$\sigma_m^2 = \left[\frac{2.4}{3} \right]^2 = 0.64 \text{ ft}^2$$

The scale-up error associated with vertical averaging is assumed to be negligible relative to other sources of error. This is justified by noting that the head observations of Locke and Meyer (2005) are grouped into hydrostratigraphic units that are explicitly represented by layers in the local model, limiting the impact of vertical averaging on calibration targets for head within the local model.

The scale-up error due to unmodeled heterogeneity was identified by Gelhar (1993), who suggested that a model using a homogeneous hydraulic conductivity will underestimate the actual variability of head. For an isotropic, two-dimensional hydraulic conductivity field with a multivariate lognormal distribution, Gelhar (1993) found that the unmodeled heterogeneity of hydraulic conductivity results in head variability whose variance is given by

$$\sigma_K^2 = 0.46 \sigma_{\ln K}^2 J^2 a_{\ln K}^2$$

where

$a_{\ln K}$ = range of correlation for the natural log transform of K, the hydraulic conductivity

$\sigma_{\ln K}^2$ = variance of $\ln K$

J = gradient within Kane County, measured from maps of Locke and Meyer (2005), approximately 0.003 ft/ft.

Pumping tests in Kane County indicate $\sigma_{\log K}^2 = 0.13$ (equivalent to $\sigma_{\ln K}^2 = 0.69$) within the major sand and gravel aquifers that are represented explicitly as zones within the local model. Gelhar (1993) found that the range of correlation can be estimated as 1/10 the extent of the modeled domain, which for the local model is approximately 30 miles. This makes $\alpha_{\ln K} = 30 \times 5280/10 = 1.58 \times 10^4$ ft. With substitution, the variance of scale-up errors in head due to unmodeled heterogeneity is

$$\sigma_K^2 = 0.46(0.69)(0.003^2)(1.58 \times 10^4)^2 = 7.2 \times 10^2 \text{ ft}^2$$

The interpolation error is the maximum difference in head from the model-simulated head at the center of the block to the corners of a grid block. That is, the maximum interpolation error will be the gradient times d_{\max} , the distance from the center of the node to the corner. Assuming this error is normally distributed, the interpolation error variance is:

$$\sigma_i^2 = \left(\frac{J \times d_{\max}}{3} \right)^2$$

where

J = gradient (approximately 0.003 ft/ft) within Kane County, measured from the maps of Locke and Meyer (2005)

d_{\max} = distance from the block center to the corner in the block

The local model has a grid spacing of 660 ft, so $d_{\max} = [330^2 + 330^2]^{\frac{1}{2}} = 467$ ft. With substitution, the error variance due to interpolation is:

$$\sigma_i^2 = \left[\frac{(0.003)(467)}{3} \right]^2 = 0.22 \text{ ft}^2$$

The remaining potential sources for error are believed to be small. The density of shallow groundwater changes very little, and so the errors due to unmodeled density effects are negligible. The errors due to numerical approximation should be on the order of the convergence tolerance for the numerical solution (0.01 ft or less), and are likewise negligible.

The total error variance associated with a head calibration target in the local model is found by summing the contributions of the independent errors as:

$$\begin{aligned} \sigma_H^2 &= (0.95 \times 10^2) + 0.64 + 0 + (7.2 \times 10^2) + 0.22 + 0 + 0 \\ \sigma_T^2 &= 8.2 \times 10^2 \text{ ft}^2 \end{aligned}$$

This estimate for the variance of errors associated with a calibration target for head is the expected error between the model simulated and the observed heads within the local model. That is, the standard error $\sigma_H = 29$ ft is the average error to be expected when comparing simulated heads from the local model to observed heads in the shallow aquifers.

E.2. Errors Associated with Regional Head Targets

The temporal variability of deep aquifer heads in the regional model is much less influenced than shallow aquifer heads by recharge and stream levels. Nicholas et al. (1987) noted that the temporal variability appeared to be correlated with seasonal pumping, and was as little as plus or minus 1.5 ft in locations away from pumping centers. Assuming a normal distribution, the error variance for temporal variability would then be:

$$\sigma_t^2 = \left[\frac{1.5}{3} \right]^2 = 0.25 \text{ ft}^2$$

However, temporal variability increases near pumping centers, and has been reported to have strong trends (Burch, 2002), thus unmodeled temporal variability may be much higher near pumping centers.

Observed heads in the deep aquifers generally are measured using airlines, a method that is more prone to measurement error than the steel tape method used for the shallow aquifers. Burch (2002) estimated that the maximum error of airline measurements in the deep aquifers is 10 ft. Assuming this error to be normally distributed, the variance of measurement error is estimated to be:

$$\sigma_m^2 = \left[\frac{10}{3} \right]^2 = 11 \text{ ft}^2$$

Unlike the local model, scale-up errors associated with vertical averaging in the regional model cannot be neglected because heads in the deep aquifer typically are observed in wells open to multiple hydrostratigraphic units (Burch, 2002). Nicholas et al. (1987) found that the hydraulic head in the St. Peter, Ironton-Galesville, and Elmhurst-Mt. Simon aquifers differed by approximately 60 ft (variance of $7.5 \times 10^2 \text{ ft}^2$) along a borehole located away from major water supply wells. Unfortunately, the majority of head observations in the deep aquifers are near pumping centers, where model simulations suggest that pumping induces great differences in head levels between aquifers. In such areas, the variance of model-simulated heads is $3.2 \times 10^4 \text{ ft}^2$ (see Section 3.2.1.2 for plots of model simulations of transient heads along observation wells in the deep aquifers). That is, the variance of scale-up errors due to vertical averaging could be $\sigma_s^2 = 7.5 \times 10^2 \text{ ft}^2$ away from pumping centers and model simulations suggest that it could be $\sigma_s^2 = 3.2 \times 10^4 \text{ ft}^2$ near pumping centers. This variance would be negligible for wells open to single hydrostratigraphic units that are explicitly represented as layers in the regional model.

The error due to unmodeled heterogeneity is assessed for the area of greatest resolution (northeastern Illinois), a region that is approximately 60 mi wide ($3.3 \times 10^5 \text{ ft}$). Gelhar (1993) suggests the correlation length will be approximately 1/10 the model scale, or $3.3 \times 10^4 \text{ ft}$. No region-specific estimates are available for the variance of $\ln K$, but Gelhar (1993) suggests it is approximately 1.0 for a model of this scale, and ranges from 0.36 to 2.0. Burch (2002) gives the gradient as $J = 32 \text{ ft/mi} = 0.0061 \text{ ft/ft}$. With substitution, a conservative estimate (using the low estimate of $\sigma_{\ln K}^2 = 0.36$) for the variance of scale-up error due to unmodeled heterogeneity is:

$$\sigma_K^2 = 0.46 (0.36)(0.006)^2 (3.3 \times 10^4)^2 = 6.7 \times 10^3 \text{ ft}^2$$

That is, the standard error of scale-up due to unmodeled heterogeneity is approximately 8.2×10^1 ft, based on conservative estimates of heterogeneity from studies at similar sites. An estimate using the moderate estimate of heterogeneity of $\sigma_{\ln K}^2 = 1$ yields:

$$\sigma_K^2 = 0.46 (1)(0.006)^2 (3.3 \times 10^4)^2 = 1.9 \times 10^4 \text{ ft}^2$$

The interpolation error in the regional model varies with the grid spacing; at the minimum grid spacing of 2500 ft, $d_{\max} = \left[\frac{1}{2} 2500^2 + 1250^2 \right]^{1/2} = 1.8 \times 10^3$ ft. With substitution, the error variance due to interpolation is:

$$\sigma_i^2 = \left[\frac{(0.0061)(1.8 \times 10^3)}{3} \right]^2 = 1.3 \times 10^1 \text{ ft}^2$$

The density of groundwater varies within northeastern Illinois, but Mandle and Kontis (1992) note that the effects of density do not affect groundwater flow except for deep within the Illinois and Michigan basins. For the freshwater portions of the domain emphasized in this study, the errors due to unmodeled salinity are assumed to be negligible, but this error can be large in deep, saline formations. The errors due to numerical approximation should be on the order of the convergence tolerance for the numerical solution (0.01 ft or less), and are neglected.

For wells open to single hydrostratigraphic units in the nearfield of the regional model, the total error variance associated with a head calibration target is estimated as:

$$\begin{aligned} \sigma_H^2 &= (0.25) + (1.1 \times 10^1) + (0) + (6.7 \times 10^3) + (1.3 \times 10^1) + 0 + 0 \\ \sigma_H^2 &= 6.7 \times 10^3 \text{ ft}^2 \end{aligned}$$

That is, the standard error $\sigma_H = 82$ ft is the average disagreement when comparing simulated heads from the nearfield of the regional model to heads observed in wells open to single hydrostratigraphic units that are distant from pumping.

Errors associated with calibration targets for head vary widely by location and quality within the regional model. For example, wells open to multiple aquifers near pumping centers have an estimated total error variance of:

$$\begin{aligned} \sigma_H^2 &= (0.25) + (1.1 \times 10^1) + (3.2 \times 10^4) + (6.7 \times 10^3) + (1.3 \times 10^1) + 0 + 0 \\ \sigma_H^2 &= 3.9 \times 10^4 \text{ ft}^2 \end{aligned}$$

That is, the standard error $\sigma_H = 200$ ft is the average disagreement when comparing simulated heads in the nearfield of the regional model to heads observed in wells open to multiple hydrostratigraphic units. In general, the error variance increases with grid spacing, model scale, heterogeneity, and density dependence. Estimating these errors goes beyond the available data, but the general principles outlined above indicate that calibration targets for head in the farfield of the model, with poorly defined heterogeneity, and deep in the Illinois Basin may have standard errors greater than 200 ft. These observations were assigned very low weights when calibrating the regional model.

E.3. Flux Target Errors

As noted in Section 2.3.2.2, calibration targets for flux were developed from stream gaging records and the ILSAM flow-accounting model for watersheds within the modeled domain. The flux targets represent the long-term average of total groundwater discharge, or base flow, to streams and drains within the watershed. The target values are estimated as the arithmetic average of Q_{80} and Q_{50} (Table E-1 and Table E-2).

Similar to the variance of head target errors, the error variance for flux targets might be decomposed into the independent contributing errors. However, unlike the head targets of this study, the flux targets are determined for a wide area and a long duration, similar to the areas and times simulated within the models. As a consequence, these flux targets are temporally and spatially consistent with the watershed-wide model fluxes at steady state, and this study has assumed the errors due to spatial variability, model resolution, and temporal variability to be negligible. The remaining identified sources of error are measurement errors, thus the total error variance associated with the calibration targets for long-term average flux are:

$$\sigma_Q^2 = \sigma_m^2$$

where

σ_Q^2 = the error variance associated with a calibration target for flux

σ_m^2 = variance of measurement (or simulation) errors for streamflow

Measurement errors for streamflow statistics vary depending on how the statistics were determined. For gaged stations such as those along the Fox River, the standard estimate of error for streamflow statistics is 10 percent or less, although this error can be larger for extreme values. For ungaged watersheds, errors for streamflow increase with the average permeability of the subsoil within the watershed and are proportional to the magnitude of streamflow. Within the Illinois Streamflow Assessment Model (ILSAM) in northeastern Illinois, two error rates have been inferred, one for watersheds with low permeability subsoils and another for high permeability subsoils (Knapp et al., 2007). The notable exception is Boone Creek, which may be receiving groundwater from outside its watershed and thus is less reliable, although this has not been quantified (Knapp, personal communication). Although errors in the statistics for gaged watersheds generally are less than those noted for ILSAM, extreme quantiles such as Q_{80} are thought to have slightly higher errors and thus this study will conservatively assume that the larger error variances inferred from ILSAM also apply to all flux targets in the model.

**Table E-1. Flux Targets for Calibration of Predevelopment
Steady-State Regional Model**

<i>Gage Name</i>	<i>Q₈₀ (ft³/d)</i>	<i>Q₅₀ (ft³/d)</i>	<i>Q Target (ft³/d)</i>	<i>ILSAM Error (percent)</i>	<i>Q Target Error (ft³/d)</i>
Blackberry Cr near Yorkville, IL	-1,969,920	-3,542,400	-2,756,160	12	-330,739
Ferson Cr near St Charles, IL	-578,880	-1,771,200	-1,175,040	27	-317,261
Boone Cr near McHenry, IL	-578,880	-864,000	-721,440	27	-194,789
Coon Cr at Riley, IL	-829,440	-2,505,600	-1,667,520	27	-450,230
Skokie River near Highland Park, IL	-501,120	-1,166,400	-833,760	12	-100,051
Weller Cr at Des Plaines, IL	-101,952	-293,760	-197,856	12	-23,742.7
Turtle Cr at Carvers Rock Rd near Clinton, WI	-5,184,000	-7,862,400	-6,523,200	27	-1,761,264
White River near Burlington, WI	-2,246,400	-5,097,600	-3,672,000	27	-991,440

Table E-2. Flux Targets for Calibration of Local-Scale Model

<i>Watershed</i>	<i>Q₈₀ (ft³/d)</i>	<i>Q₅₀ (ft³/d)</i>	<i>Q Target (ft³/d)</i>	<i>ILSAM Error (percent)</i>	<i>Q Target Error (ft³/d)</i>
Big Rock Cr	-362,880	-2,220,480	-1,291,680	12	-155,002
Blackberry Cr	-907,200	-2,073,600	-1,490,400	12	-178,848
Coon Cr	-829,440	-2,505,600	-1,667,520	27	-450,230
Ferson Cr	-578,880	-1,771,200	-1,175,040	27	-317,261
Mill Cr	-103,680	-561,600	-332,640	12	-39,916.8
S Br Kishwaukee River	-129,600	-725,760	-427,680	12	-51,321.6
Tyler Cr	-267,840	-915,840	-591,840	12	-71,020.8
Union Ditch No 3	-362,880	-1,702,080	-1,032,480	12	-123,898

E.4. References

Anderson, M.P. and W.W. Woessner. 2002. *Applied groundwater modeling: Simulation of flow and advective transport*. Academic Press, San Diego, CA.

Burch, S.L. 2002. *A Comparison of Potentiometric Surfaces for the Cambrian-Ordovician Aquifers of Northeastern Illinois, 1995 and 2000*. Illinois State Water Survey Data/Case Study 2002-02, Champaign, IL.

Gelhar, L.W. 1993. *Stochastic subsurface hydrology*. Prentice Hall, Englewood Cliffs, NJ.

Hill, M.C. and C.R. Tiedeman. 2007. *Effective Groundwater Model Calibration*. John Wiley and Sons, Hoboken, NJ.

Knapp, H.V., A.M. Russell, J.A. Kramer, and G.P. Rogers. 2007. *Kane County Water Resources Investigations: Surface Water Accounting for Water Supply Planning in Kane County*. Illinois State Water Survey Contract Report 2007-10, Champaign, IL.

Larsen, R.J. and M.L. Marx. 1986. *An Introduction to Mathematical Statistics and Its Applications*. Prentice-Hall, Englewood Cliffs, NJ.

Locke, R.A., II and S.C. Meyer. 2005. *Kane County Water Resources Investigations: Interim Report on Shallow Aquifer Potentiometric Surface Mapping*. Illinois State Water Survey Contract Report 2005-04, Champaign, IL.

Mandle, R.J. and A.L. Kontis. 1992. *Simulation of Regional Ground-Water Flow in the Cambrian-Ordovician Aquifer System in the Northern Midwest, United States*. United States Geological Survey Professional Paper 1405-C, Washington, DC.

Nicholas, J.R., M.G. Sherrill, and H.L. Young. 1987. *Hydrogeology of the Cambrian-Ordovician Aquifer System at a Test Well in Northeastern Illinois*. United States Geological Survey Water-Resources Investigations Open-File Report 84-4165, Urbana, IL.

Appendix F. ISWS Aquifer Code System

The ISWS characterizes the source interval of a well with a four-character aquifer code denoting the uppermost and lowermost stratigraphic unit to which the well is open (Table F-1). The first two digits of the code represent the uppermost stratigraphic unit open to the well, and the last two digits represent the lowest unit open to the well. For example, a well that is open to all units from the Galena Group (63) downward to the bottom of the Galesville Sandstone (87)—the source interval common to many wells open to the Cambrian and Ordovician aquifers of northern Illinois—is assigned the aquifer code 6387. A well that is open to the Silurian dolomite, and no other stratigraphic units, is assigned the aquifer code 5656. Since it is uncommon for the source interval of a well to be known in great lithostratigraphic detail, many assigned aquifer codes make use of two-character strings denoting unspecified lithostratigraphic units within a larger, more general unit. For example, a well that is open to a Quaternary sand-and-gravel aquifer in an unspecified stratigraphic unit is assigned the aquifer code 0101. A well that is open to an interval from the Silurian downward through an unspecified unit in the Champlainian Series is assigned the aquifer code 5660.

Table F-1. Two-Character Codes Employed in ISWS Aquifer Codes

<i>General</i>		<i>Specific</i>	
<i>Stratigraphic Unit</i>	<i>Code Range</i>	<i>Stratigraphic Unit</i>	<i>Code</i>
Quaternary System	01-14	Unspecified	01
		Cahokia Alluvium Parkland Sand	02
		Mason Group <i>Equality Formation</i>	03
		Mason Group <i>Henry Formation</i>	04
		Wedron Group	05
		Mason Group <i>Henry Formation (Ashmore Tongue)</i>	06
		Winnibago Formation	07
		Glasford Formation	09
		Pearl Formation	10
		Banner Formation (undifferentiated)	11
		Banner Formation <i>Mahomet Sand</i>	12
		Banner Formation <i>Sankoty Sand</i>	13
		Pre-Kansan	14
		Unspecified	15
Tertiary System Cretaceous System	15-19		
Pennsylvanian System	20-29	Unspecified	20
Mississippian System <i>Chesterian Series</i>	30-39	Unspecified	30
Mississippian System <i>Valmeyeran Series</i> <i>Kinderhookian Series</i>	40-49	Unspecified	40

**Table F-1. Two-Character Codes Employed in ISWS Aquifer Codes
(Continued)**

<i>General</i>		<i>Specific</i>	
<i>Stratigraphic Unit</i>	<i>Code Range</i>	<i>Stratigraphic Unit</i>	<i>Code</i>
Devonian System Silurian System	50-59	Unspecified	50
		Devonian System	51
		Silurian System	56
Ordovician System <i>Cincinnatian Series</i> <i>Champlainian Series</i>	60-69	Unspecified	60
		Maquoketa Group	61
		Galena Group	63
		Platteville Group	65
		Ancell Group	66
Ordovician System <i>Canadian Series</i>	70-79	Unspecified	70
		Prairie du Chien Group <i>Shakopee Dolomite</i>	71
		Prairie du Chien Group <i>New Richmond Sandstone</i>	73
		Prairie du Chien Group <i>Oneota Dolomite</i>	75
		Prairie du Chien Group <i>Gunter Sandstone</i>	77
Cambrian System <i>Galesville Sandstone and above</i>	80-89	Unspecified	80
		Eminence Formation Jordan Sandstone Potosi Dolomite	81
		Franconia Formation	83
		Ironton Sandstone	87
		Galesville Sandstone	

**Table F-1. Two-Character Codes Employed in ISWS Aquifer Codes
(Concluded)**

<i>General</i>		<i>Specific</i>	
<i>Stratigraphic Unit</i>	<i>Code Range</i>	<i>Stratigraphic Unit</i>	<i>Code</i>
Cambrian System <i>Eau Claire Formation</i> <i>Mt. Simon Sandstone</i>	90-99	Unspecified	90
		Eau Claire Formation	93
		<i>Proviso Siltstone Member</i> <i>Lombard Dolomite Member</i>	
		Eau Claire Formation <i>Elmhurst Sandstone Member</i> Mt. Simon Sandstone	97

Appendix G. Estimation of Future Pumping

Two forecasts of estimated future pumping from individual wells have been developed for this project and are used in analyzing the impacts of projected pumping discussed in Section 3.3. One of the forecasts assumes that modest improvements in water conservation are made in the Public Supply and Self-Supplied Commercial and Industrial water-use sectors in Illinois and, from the standpoint of preserving water availability, might be considered an optimistic forecast. These pumping conditions are referred to in this report as *low-pumping conditions*. An alternative forecast, one of *high-pumping conditions*, assumes that no such improvements in water conservation are made in the Public and Self-Supplied Commercial and Industrial sectors of Illinois. Both forecasts assume no improvements in water conservation in any water-use sectors except Public Supply and Self-Supplied Commercial and Industrial.

Both forecasts further assume existing 2000-2003 well locations and source intervals for the duration of the forecast (from 2005 through 2050). In essence, the forecasts assume that the existing 2000-2003 well network remains in service and satisfies all water demand through 2050. The authors acknowledge that maintenance of the 2000-2003 well network through 2050 and its use to satisfy all water demand through 2050 is unlikely. The modeled network is, however, representative of a probable, though conservative, future well network, wherein replacement wells are drilled in precisely the same locations and finished with precisely the same source intervals as predecessor wells taken out of service. We further acknowledge that it might be physically impossible for an existing well in the 2000-2003 network to supply the water that is forecasted to be withdrawn from it, particularly in rapidly developing counties with greatly increasing water demand. Any single forecasted well with an implausibly high forecasted withdrawal rate can, however, be considered as representing a well field, with all of the wells in the field being located in the same model cell and open to the same source interval. In the sense that well locations and source intervals do not change from those in 2002-2003, both forecasts might be considered “business-as-usual” scenarios wherein water-supply development questions are handled on a nearsighted basis, without communication or coordination among public water systems, self-supplied industries, irrigators, and other water users.

In addition to forecasted withdrawals from existing deep domestic wells, both scenarios include withdrawals from forecasted deep domestic wells that have not yet been drilled. Wells are forecasted in each cell of the regional model nearfield on the basis of 1974-2003 drilling rates of such wells as indicated by the ISWS Private Well Database, a database generally containing records of low-capacity wells supplying households and commercial facilities. The low-pumping and high-pumping estimates contain precisely the same forecasts of withdrawals from existing and projected deep domestic wells.

G.1 Forecasted Pumping from Public Wells, Self-Supplied Commercial and Industrial Wells, and Irrigation Wells

G.1.1. Illinois

G.1.1.1. Forecasted Well Locations and Source Intervals

The locations of forecasted wells in Illinois and their source intervals are based on withdrawals for the years 2000 through 2003 included in the withdrawal database compiled for this project. Most of these data were obtained from the ISWS PICS Database, an electronic database of withdrawal data compiled largely from owner-reported withdrawal measurements and estimates. These data are augmented with estimates for years of non-reporting to the ISWS by facility owners. The sources, processing, and uncertainty of these withdrawal data are discussed in detail in Appendix B). A withdrawal forecast for 2005 to 2050 was developed for wells in the withdrawal database that showed any withdrawal during the years 2000, 2001, 2002, or 2003. A total of 2007 Illinois wells satisfied this requirement.

Thus, locations and source intervals of forecasted withdrawals are identical to those of real wells used during 2000-2003, as discussed in the introduction to this appendix. Withdrawals were forecasted for wells if observed withdrawals during any one of the years 2000-2003 were nonzero to provide for the possibility that a recently used well (e.g., a well pumped during 2001, but not 2002 and 2003) would be brought back into service.

G.1.1.2. Forecasted Pumping Rates

Forecasted pumping rates are based on the water-use sector and county location of each well, on the latest pumping rate recorded in the project withdrawal database for the years 2000 through 2003, and on county-level estimates of water demand in Illinois counties developed by statistical modeling by Dziegielewski et al. (2005). The last pumping rate recorded in the withdrawal database compiled for this project for the years 2000, 2001, 2002, or 2003 was increased in proportion to the change in county-level demand for the county location of the well and the well's water-use sector. The year of the recorded withdrawal rate that was employed to develop the projected future withdrawal rate in 2005-2050 is referred to in this report as the *basis year* for the forecasted rate. Wells were assigned to one of three water-use sectors—Public Supply, Self-Supplied Commercial and Industrial, and Irrigation—based on codes already present in the ISWS PICS Database that distinguish among these water uses.

Map depictions of basis year withdrawals and projected 2025 and 2050 withdrawals from Public, Self-Supplied Commercial and Industrial, and Irrigation wells in the regional model nearfield are shown in Figure G-1 (basis year), Figure G-2 and Figure G-3 (low-pumping conditions), and Figure G-4 and Figure G-5 (high-pumping conditions).

Dziegielewski et al. (2005) used multiple regression to model Public Supply water use in 2000, 2005, 2010, 2015, 2020, and 2025 and Self-Supplied Commercial and Industrial water use in 2005, 2010, 2015, 2020, and 2025. Dziegielewski et al. (2005) recognized modest effects of water conservation as a variable explaining water use in these sectors between 1985 and 2000. They developed two separate sets of water-use estimates in the sectors for the years 2005-2025, one using a multiple-regression model

that assumes continued improvements in water conservation, and the second using a multiple-regression model that assumes improvements do not continue beyond 2000. These estimates correspond to this study's estimates of low- and high-pumping conditions described previously (page G-1). For all Illinois counties, both sets of estimates of water demand in the Public Supply and Self-Supplied Commercial and Industrial sectors were entered into a database to facilitate later data processing. In addition, estimates of observed 2000 water use in these sectors, reported by the U.S. Geological Survey (USGS) and appearing in the report by Dziegielewski et al. (2005), were entered into the database.

Water use in the Irrigation sector was estimated by Dziegielewski et al. (2005) for 2005, 2010, 2015, 2020, and 2025 using a "rainfall deficit" method. Only a single set of estimates of future irrigation water use was developed by Dziegielewski et al. (2005), and these estimates were entered into the database mentioned in the previous paragraph.

The present study employs ratios of the county-level estimates of sector water use by Dziegielewski et al. (2005) to estimate 2005-2050 water use on a well-by-well basis. These estimates are calculated from the last nonzero value of water use at the well during the basis year—2000, 2001, 2002, or 2003—as recorded in the database of groundwater withdrawals assembled for this project. This approach required that additional, provisional estimates and projections of county-level water use, by sector, be developed from the data appearing in Dziegielewski et al. (2005). Estimates were calculated for the years 2001-2003 and—on a five-year basis—projections were developed for 2030-2050. County-level water use estimates for 2001-2003 were calculated somewhat differently for the Public Supply, Self-Supplied Commercial and Industrial, and Irrigation sectors owing principally to the differing availability of estimates and data in Dziegielewski et al. (2005) for these sectors.

Figure G-6 illustrates the projection procedure for Public Supply water use in Kane County as an example of the procedure followed independently for all Illinois counties included in the project. With the exception of two counties, DuPage and Knox, estimates of 2001-2003 Public Supply water use are based on linear interpolation between the USGS reported 2000 water use and the modeled Public Supply 2005 water use. USGS reported estimates of 2000 Public Supply water use in DuPage and Knox Counties appear to be unrealistically low, probably because both of these counties import a significant proportion of water for public supply from outside the county, and these imports are not accounted for in the value reported by the USGS. Thus, projections of 2001-2003 Public Supply water use in DuPage and Knox Counties are based on linear interpolation between the modeled estimates of 2000 and 2005 Public Supply water use in those counties developed by Dziegielewski et al. (2005). Projections of 2030-2050 Public Supply water use were developed on a five-year basis by extrapolating the change in modeled water use rates between 2020 and 2025 from Dziegielewski et al. (2005) and are highly conjectural. As illustrated in Figure G-6, projections of 2001-2003 and 2030-2050 Public Supply water use were estimated for conditions of low pumping and high pumping using modeled water use estimates corresponding to these scenarios provided by Dziegielewski et al. (2005).

The projection procedure for county-level Self-Supplied Commercial and Industrial water use, shown for Kane County in Figure G-7, is similar to that used to project Public Supply water use. Self-Supplied Commercial and Industrial water use was

estimated for the years 2001-2003 by linear interpolation between the USGS reported water use in 2000 and the modeled 2005 water use in that sector developed by Dziegielewski et al. (2005). Highly speculative projections of 2030-2050 Self-Supplied Commercial and Industrial water use were developed using the change in modeled water use rates between 2020 and 2025 from Dziegielewski et al. (2005). Separate estimates of water use under low- and high-pumping conditions were developed using modeled water use estimates provided by Dziegielewski et al. (2005). In the case of Kane County, continued improvements in water conservation in the Self-Supplied Commercial and Industrial sector make the difference between increasing and decreasing water use (Figure G-7).

A similar projection procedure was employed to estimate county-level water use in the Irrigation sector in 2001-2003 and 2030-2050. Since Dziegielewski et al. (2005) did not develop separate estimates of future Irrigation water use based on whether conservation improvements continue in that sector, only a single set of projected values was generated. The projection procedure is illustrated graphically for Kane County in Figure G-8. As for the Public Supply and Self-Supplied Commercial and Industrial Irrigation water use sectors, Irrigation water use was estimated for the years 2001-2003 by linear interpolation between the USGS reported water use in 2000 and the modeled 2005 water use in that sector developed by Dziegielewski et al. (2005). Projections of 2030-2050 Irrigation water use assume the change in modeled water use rates between 2020 and 2025 from Dziegielewski et al. (2005) and are speculative.

No further efforts to generate county-level estimates of 2000-2003 sector water use were made than those based on the data provided by Dziegielewski et al. (2005), for example, consultation of either the withdrawal database developed for this project (see Appendix B) or the ISWS PICS Database (a database of water withdrawals in Illinois). The withdrawal database developed for this project is not complete enough to allow development of 2000-2003 water-use estimates, since it includes only groundwater withdrawals, not surface-water withdrawals or imports from outside a county. Moreover, the database does not even cover all groundwater withdrawals in most Illinois counties of the regional model domain. All groundwater withdrawals are included only in an accounting area covering northeastern Illinois. Estimates of sector water use could have been developed from the ISWS PICS Database, but such estimates would have required significant effort to develop and would have contributed negligibly, if at all, to the accuracy of the well-by-well projections of 2005-2050 withdrawals, which would be rough approximations of future pumping in either case. It is also noteworthy that both the USGS and Dziegielewski et al. (2005) used the ISWS PICS Database to develop their observation-based and model-based county-level estimates of sector water use.

Ratios of modeled and projected county-level sector water use in 2005-2050 to estimated county-level sector water use in 2000-2003 were calculated. These ratios were employed to project well-by-well withdrawals for all wells used in any year during 2000-2003 by multiplying the ratio by the withdrawal during the latest year of use of the well during the basis year. For example, to calculate the projected withdrawal in 2010 with improvements in conservation (low pumping conditions) for a public sector well in Kane County, which was pumped at 800 cubic feet per day (ft³/d) in 2003, the 2003 pumping rate was multiplied by the ratio of estimates of 2010 to 2003 county-level water use for the Public Supply sector in Kane County under a “conservation scenario” based in the

statistical modeling of Dziegielewski et al. (2005). Since this ratio is about 1.122, the projected 2010 withdrawal from the well in 2010 is calculated as 1.122×800 , or about 896 ft³/d. If the well was pumped at a rate of 800 ft³/d in 2001, but not in 2002 or 2003, the projected withdrawal from the well under low-pumping conditions was calculated using the ratio of estimates of 2010 to 2001 Kane County water use for the Public Supply sector in Kane County under low-pumping conditions: 1.216. Thus 2010 withdrawals are calculated as 1.216×800 , or about 973 ft³/d. If the well was used in 2000, but not in 2001-2003, projected withdrawals for the years 2005-2050 were—with the exception of two counties—calculated using the ratio of modeled (2005-2025) or projected (2030-2050) county-level sector water use to USGS-reported sector water use in 2000. In the case of Public Supply sector wells in DuPage and Knox Counties, projected withdrawals in 2005-2050 were calculated using the ratio of modeled/projected county-level sector water use in 2005-2050 to modeled Public Supply water use in 2000, as discussed on page G-3.

G.1.2. Indiana and Wisconsin

G.1.2.1. Forecasted Well Locations and Source Intervals

As described for Illinois, the locations and source intervals of forecasted wells in Indiana and Wisconsin correspond to those wells that were active during one or more years of the period 2000-2002 as indicated by the withdrawal database developed for this project (2003 is omitted because withdrawal data for 2003 were unavailable during database development). These data were obtained from the Wisconsin Geological and Natural History Survey (personal communication, 2002) and the Indiana Department of Natural Resources (personal communication, 2003). See Appendix B for details of the sources, processing, and uncertainty of these withdrawal data. If the database shows that any quantity of water was withdrawn from one of these wells in any of the years 2000, 2001, or 2002, withdrawal estimates for 2005-2050 were developed for that well based on the last year of nonzero withdrawals. A total of 771 Indiana wells and 385 Wisconsin wells satisfied this requirement.

G.1.2.2. Forecasted Pumping Rates

In a procedure closely similar to that used for Illinois withdrawal forecasting, pumping rates for Indiana and Wisconsin are forecasted on the basis of the water-use sector and county location of each well, on the latest pumping rate recorded in the project withdrawal database for the years 2000 through 2002 (the *basis year* for the projection), and on county-level estimates of water use in Indiana and Wisconsin counties developed by statistical modeling, in this case by Dziegielewski et al. (2004). The last pumping rate recorded in the project withdrawal database for the years 2000, 2001, or 2002 was increased in proportion to the change in county-level demand for the county location of the well.

Dziegielewski et al. (2004) estimated county-level water use for the Public Supply sector, and no other water use sector. For purposes of developing groundwater withdrawal forecasts for this project, the authors therefore assumed that withdrawals from all Indiana and Wisconsin wells change in proportion to county-level Public Supply water use. This assumption no doubt introduces error to the forecasted withdrawals since all of these wells do not serve the Public Supply sector. Of the 2056 Illinois wells for which

withdrawal forecasts have been developed, only 1196 (58 percent) are used for Public Supply, whereas 551 and 309 fall within the Self-Supplied Commercial and Industrial sector and Irrigation sector, respectively. Dziegielewski et al. (2004) did not develop separate county-level water use forecasts for scenarios of continuation, versus discontinuation, of improvements in water conservation, as was done for Illinois counties by Dziegielewski et al. (2005). Thus, only a single forecast of groundwater withdrawals for Indiana and Wisconsin wells was made for the present study, and this forecast was assumed to represent low- and high-pumping conditions (see p. G-1).

For all Indiana and Wisconsin counties having groundwater withdrawals represented in the project withdrawal database, county-level estimates of water use in the Public Supply sector were entered into a database to facilitate data processing. In addition, values of observed 2000 water use in the Public Supply sectors, reported by the USGS and appearing in the report by Dziegielewski et al. (2004), were entered into the database. As described previously for the Public Supply sector of Illinois (page G-3 and Figure G-6), estimates of Public Supply water use in the Indiana and Wisconsin counties were calculated for the years 2001 and 2002 and, on a five-year basis, projections were developed for the years 2030-2050. Estimates of 2001 and 2002 water use are based on linear interpolation between the USGS reported 2000 water use and the modeled Public Supply 2005 water use. Highly speculative projections of 2030-2050 Public Supply water use were developed on a five-year basis by extrapolating the change in modeled water use rates between 2020 and 2025 from Dziegielewski et al. (2004).

Ratios of modeled and projected county-level sector water use in 2005-2050 to estimated county-level sector water use in 2000-2002 were calculated. These ratios were employed to project well-by-well withdrawals for Indiana and Wisconsin wells used in any year during the period 2000-2002 by multiplying the ratio by the withdrawal during the latest year of well use in 2000-2002. An example of this calculation is described on page G-3.

G.2 Forecasted Pumping from Self-Supplied Deep Domestic Wells in Northeastern Illinois

Deep domestic wells are included in the pumping forecasts, but the wells are assumed to pump at identical rates under both low- and high-pumping conditions.

G.2.1. Forecasted Well Locations and Source Intervals

Forecasted deep domestic wells fall into two groups: (1) wells already in existence in 2003 (Figure G-9), and (2) wells that will be drilled and placed into service in 2005-2050 (Figure G-10 and Figure G-11).

Wells falling into the first group were identified to develop the database of groundwater withdrawals using the procedure discussed in Section B.2.1.4. Unless a well in this group was identified as having been sealed, the well was forecasted as being in service for the entire period 2005-2050. The specific source intervals of these wells within the deep units during 2005-2050 are unchanged from those that were characterized for the period ending in 2003 using the procedure discussed in Section B.2.1.4. Withdrawal forecasts were developed for a total of 3060 domestic wells in existence in 2003.

Wells falling into the second group, those forecasted to be drilled and placed in service during the period 2005-2050, were identified by assuming a linear growth rate of the deep domestic well population, based on 1974-2003 drilling rates, per grid cell of the regional model nearfield. Forecasted wells are located at the center of each grid cell. The open intervals of the forecasted wells are based on the subcrop belt of the well's location and on the statistical analysis of open intervals presented in Section B.2.1.4. Assumed open intervals are summarized in Table B-7. For example, predicted deep domestic wells located in the Silurian-Devonian Carbonate Unit subcrop of the Quaternary Unit are forecasted to be open to the Galena-Platteville Unit and the Ancell Unit (regional model layers 10-12). A total of 68 domestic wells were added to the withdrawal forecast for 2005, and this total rises to 2844 wells in the 2050 forecast (Figure G-12).

G.2.2. Forecasted Pumping Rates

Pumping rates for the period 2005-2050 are based on linear interpolation of estimates of per-capita self-supplied domestic water use developed at five-year increments for the period 1960-2000 by the USGS and reported by Dziegielewski et al. (2005) (Figure B-12), together with the assumption that each well supplies 3.4 people (Illinois Department of Energy and Natural Resources, 1998). Figure G-13 shows assumed pumping rates per well based on these assumptions for 2005-2050.

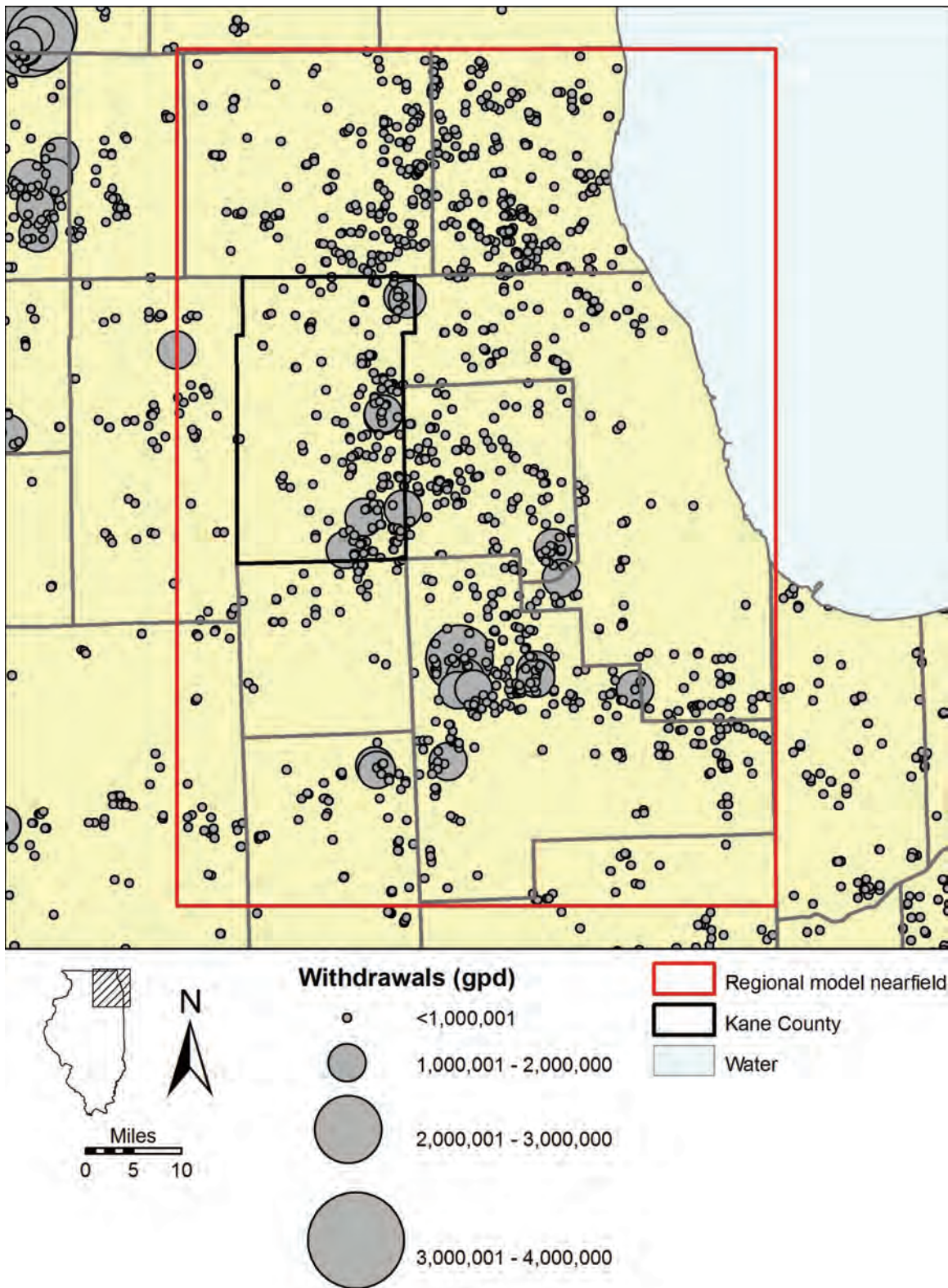


Figure G-1. Withdrawals in gallons per day (gpd) from Public Supply, Self-Supplied Commercial and Industrial, and Irrigation wells in northeastern Illinois during the basis year for projections.

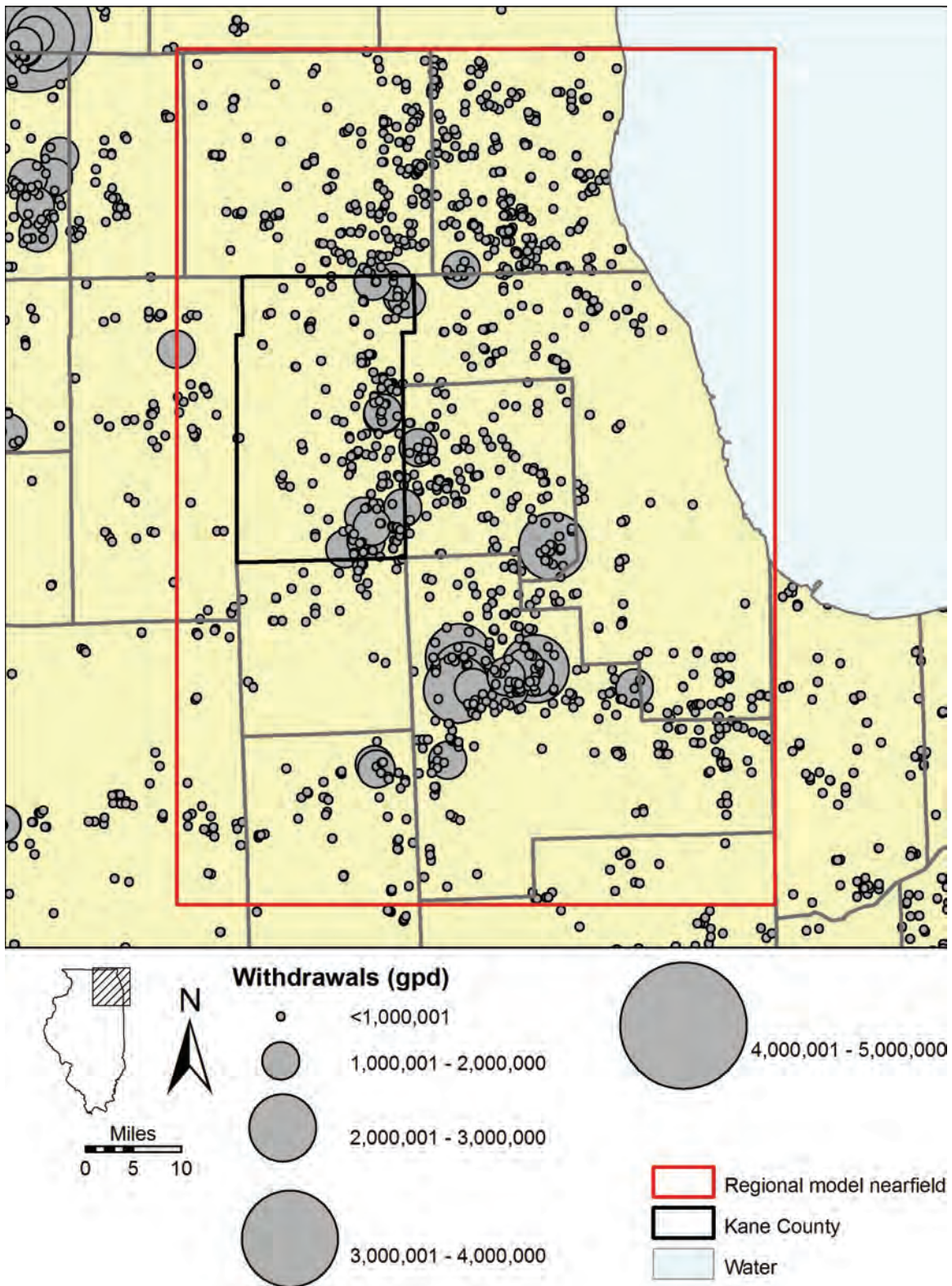


Figure G-2. Projected 2025 withdrawals from Public Supply, Self-Supplied Commercial and Industrial, and Irrigation wells in northeastern Illinois, low-pumping conditions.

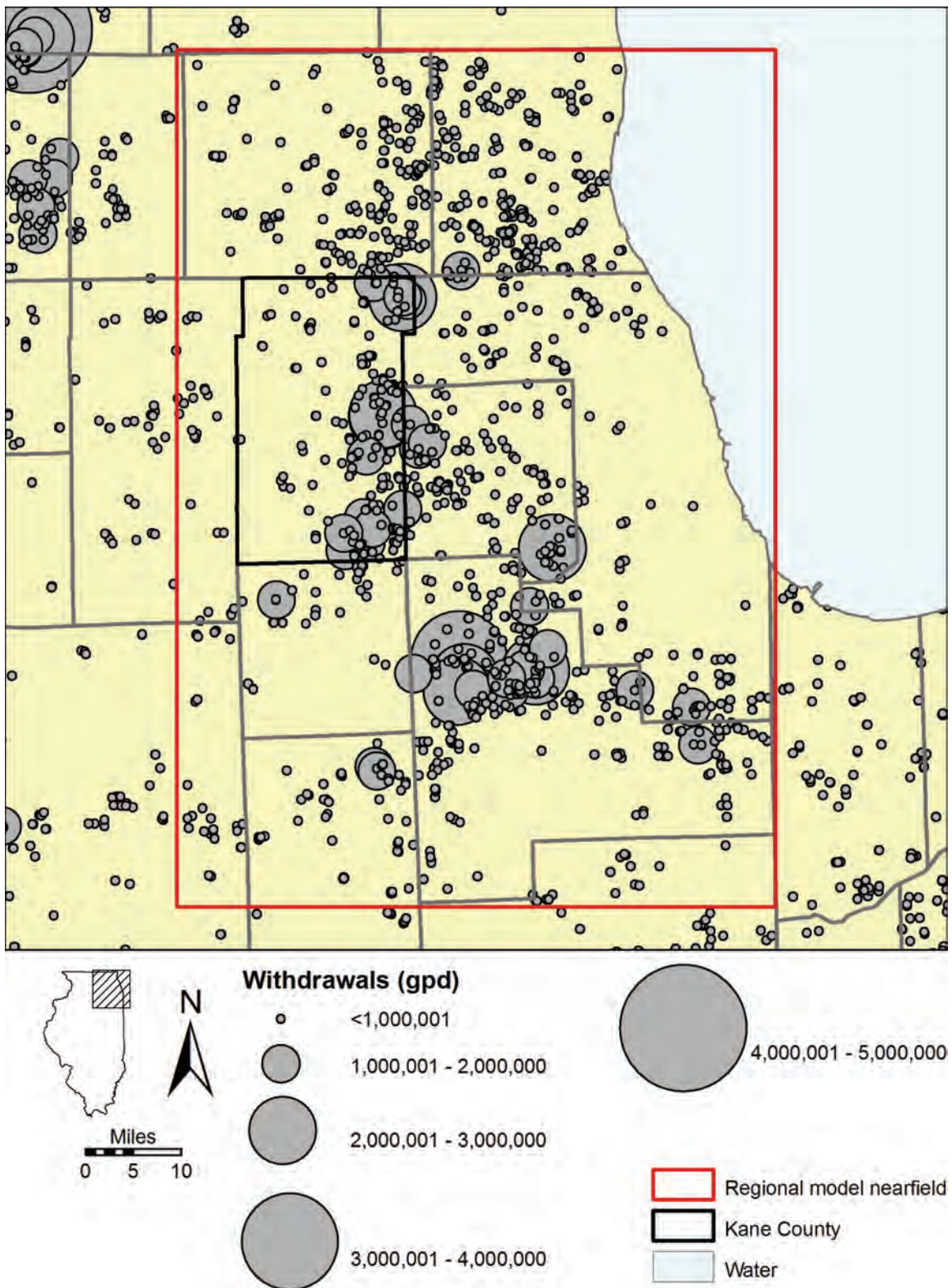


Figure G-3. Projected 2050 withdrawals from Public Supply, Self-Supplied Commercial and Industrial, and Irrigation wells in northeastern Illinois, low-pumping conditions.

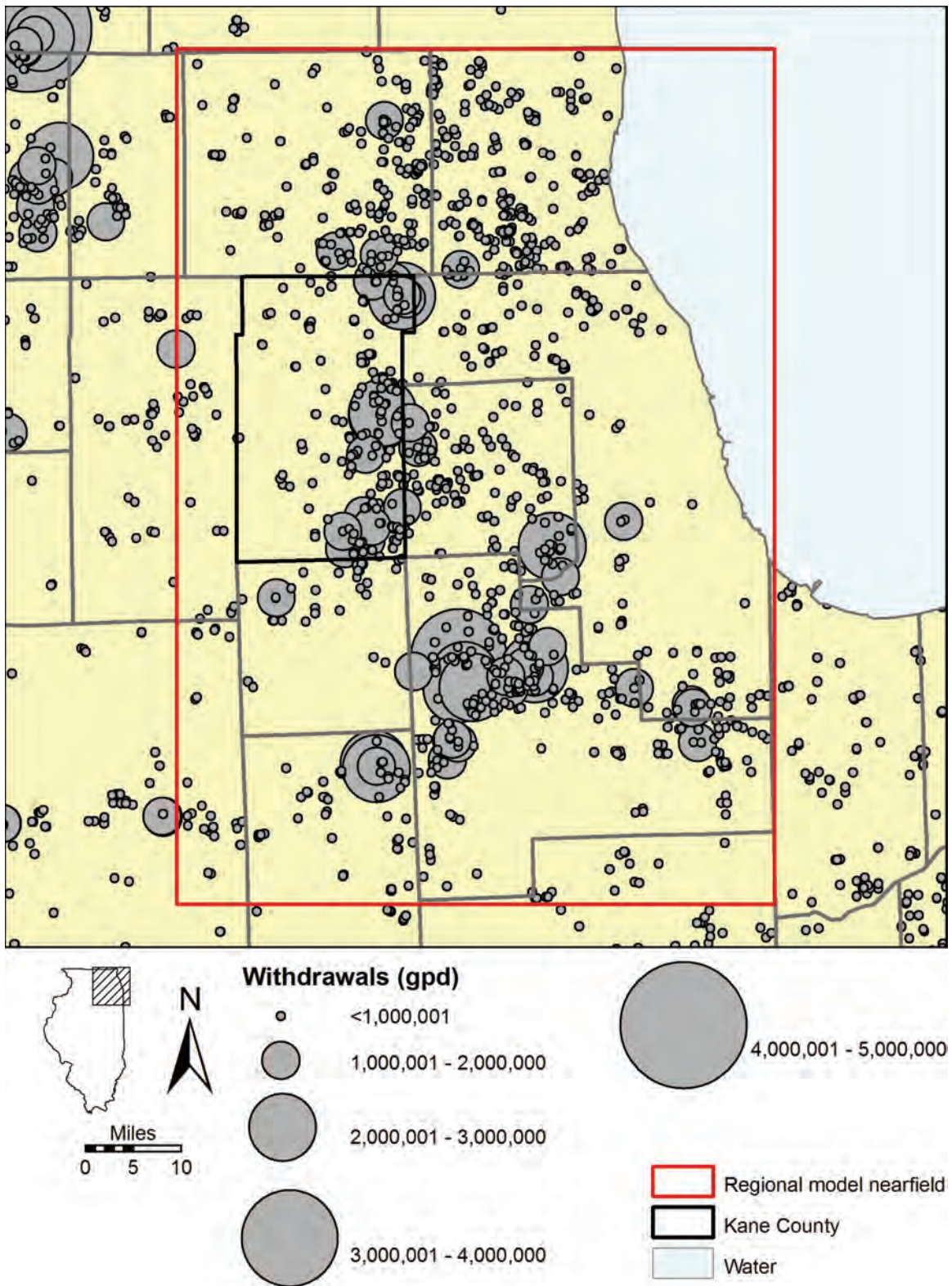


Figure G-4. Projected 2025 withdrawals from Public Supply, Self-Supplied Commercial and Industrial, and Irrigation wells in northeastern Illinois, high-pumping conditions.

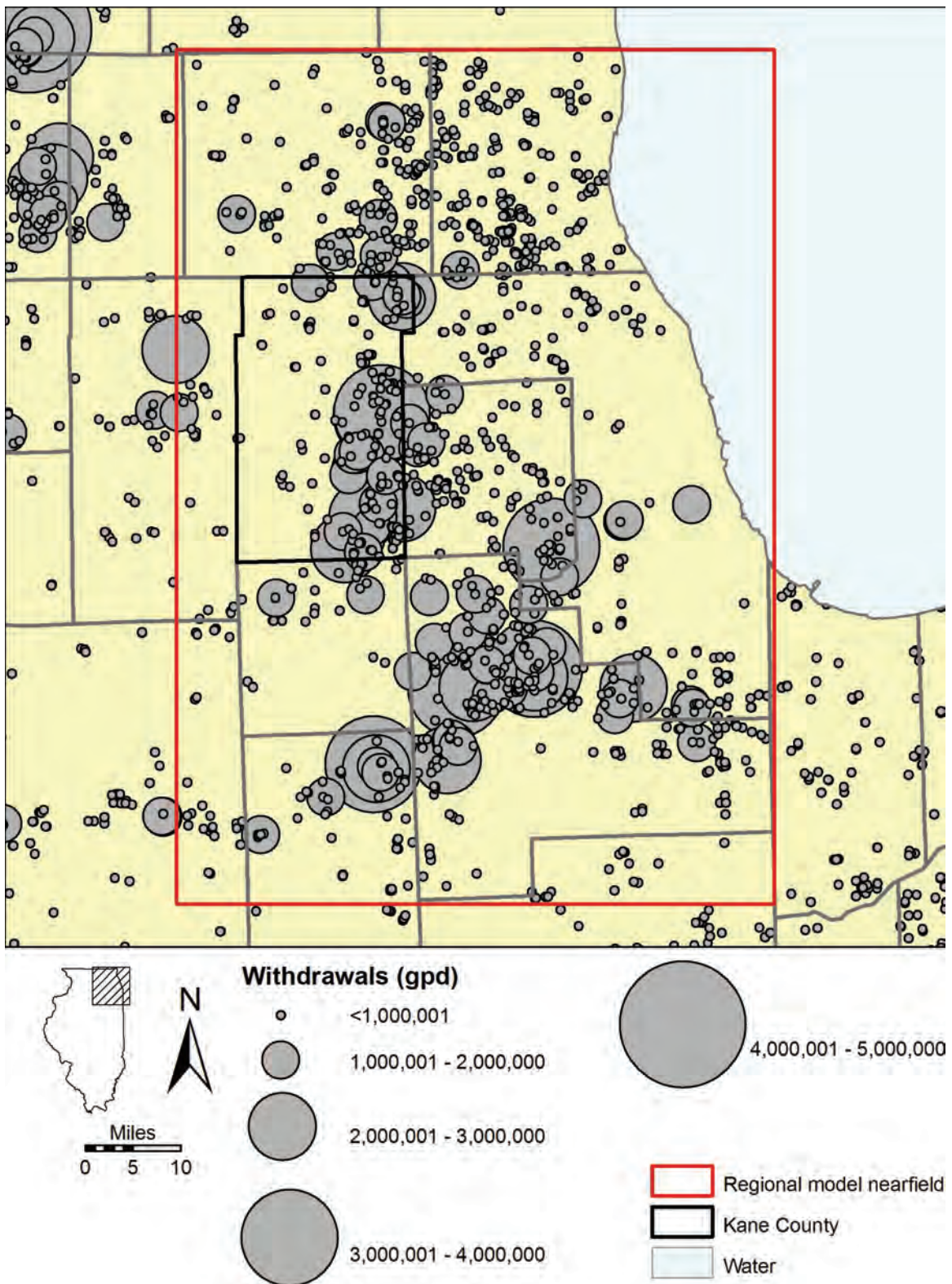


Figure G-5. Projected 2050 withdrawals from Public Supply, Self-Supplied Commercial and Industrial, and Irrigation wells in northeastern Illinois, high-pumping conditions.

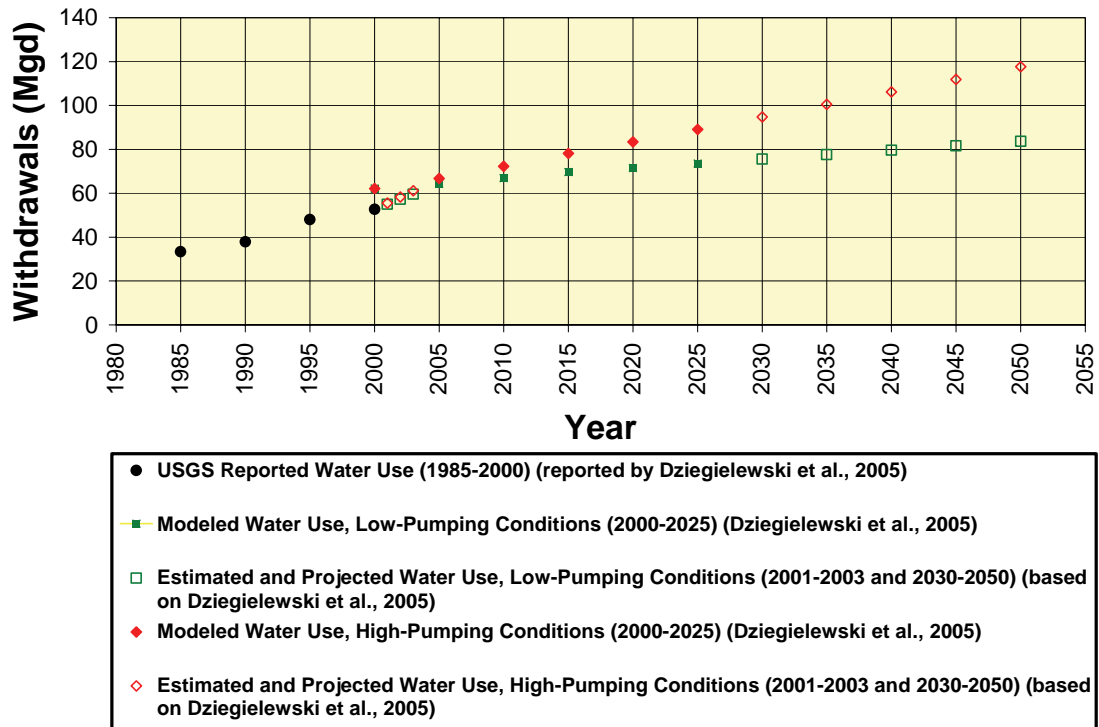


Figure G-6. Projection of Kane County water use in the Public Supply sector for the years 2001-2003 and 2030-2050 from data and estimates published by Dziegielewski et al. (2005).

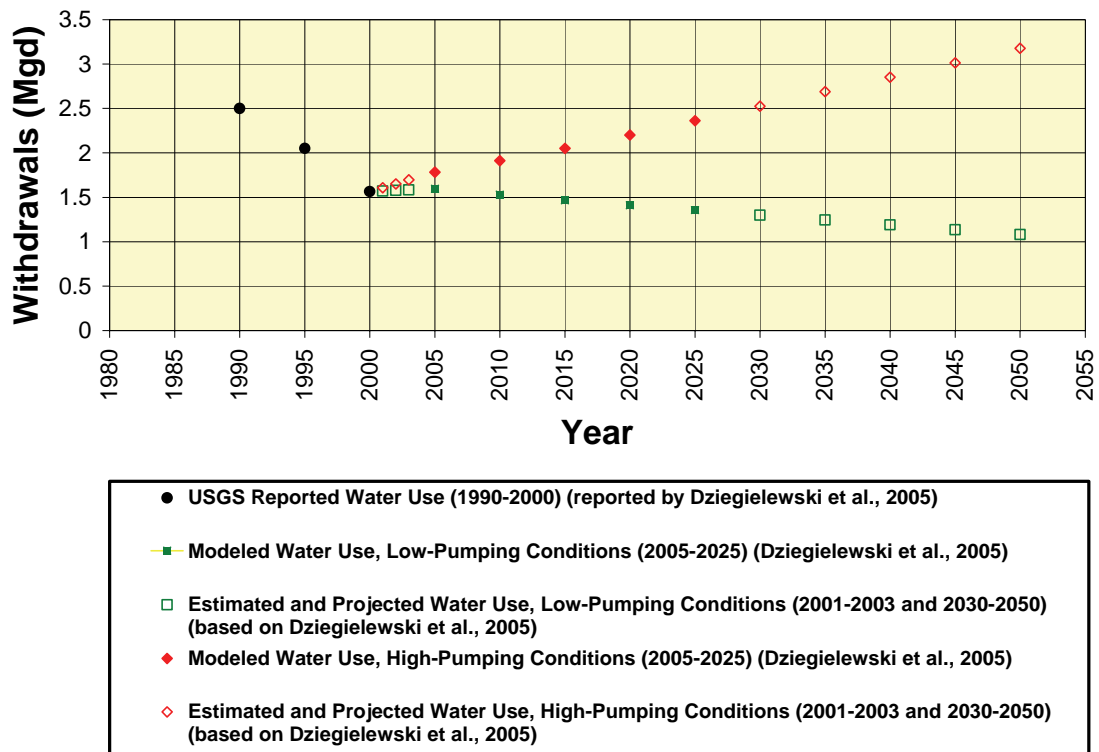


Figure G-7. Projection of Kane County water use in the Self-Supplied Commercial and Industrial sector for the years 2001-2003 and 2030-2050 from data and estimates published by Dziegielewski et al. (2005).

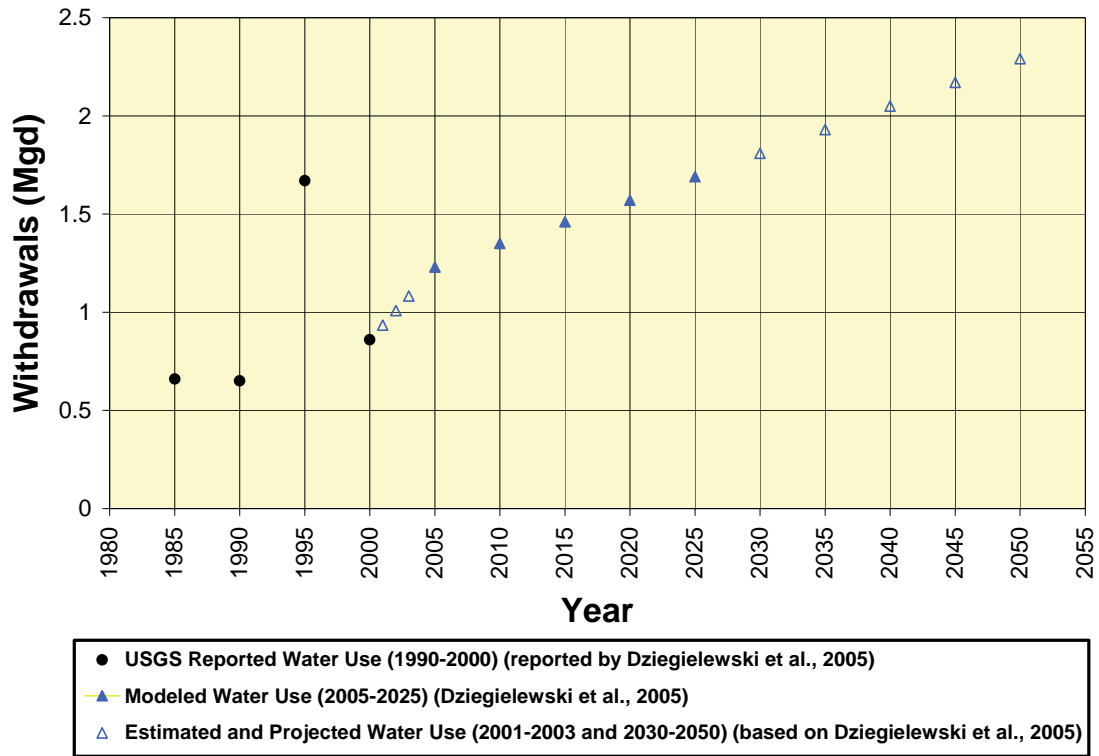


Figure G-8. Projection of Kane County water use in the Irrigation sector for the years 2001-2003 and 2030-2050 from data and estimates published by Dziegielewski et al. (2005).

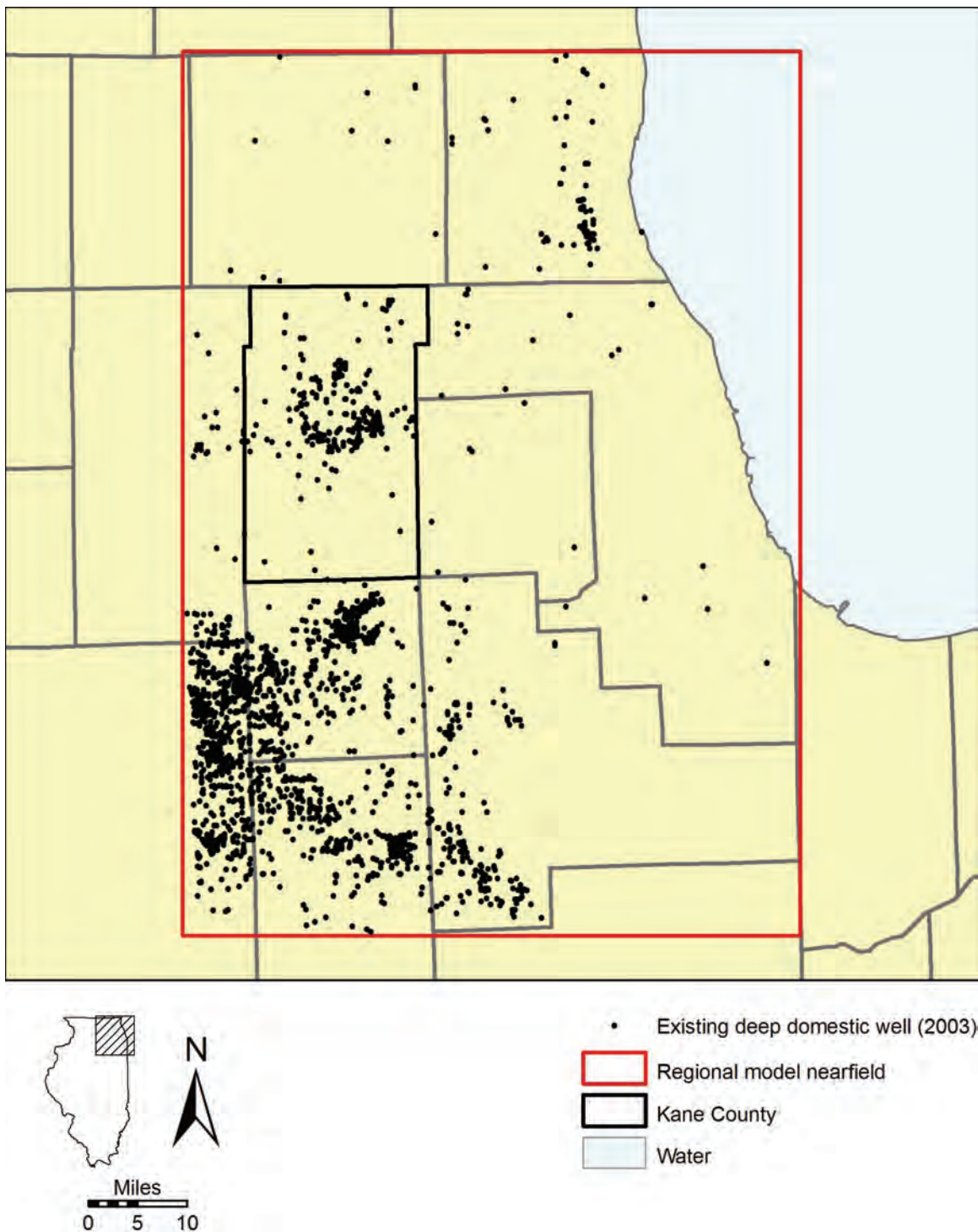


Figure G-9. Existing domestic wells open to the interval underlying the Galena-Platteville Unit for which withdrawals were projected for the period 2005-2050. See Figure G-13 for assumed withdrawal rates from these wells.

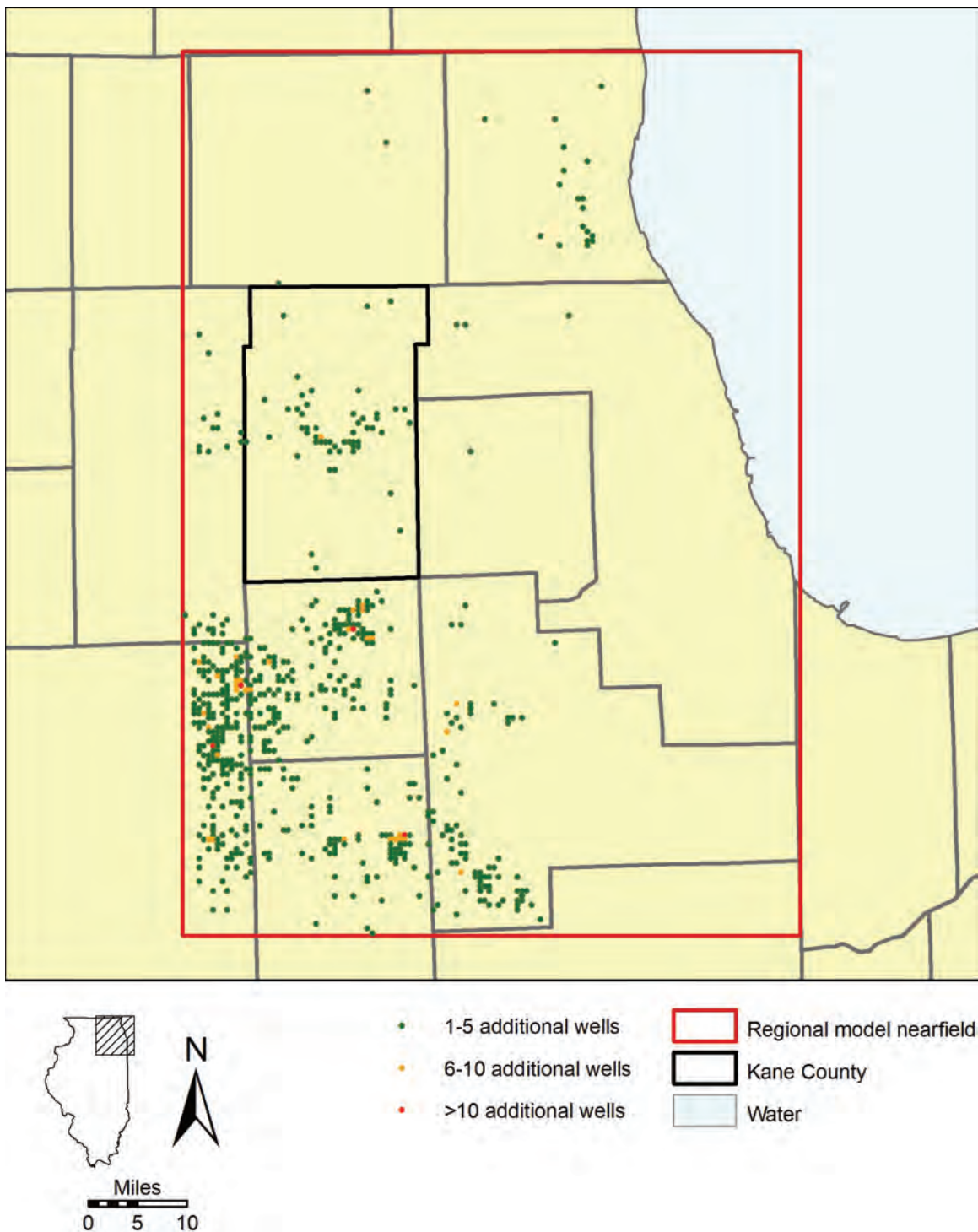


Figure G-10. Projected deep domestic wells, not existing in 2003, to be drilled and in service by 2025 and for which withdrawals were projected. See Figure G-13 for assumed withdrawal rates from these wells.

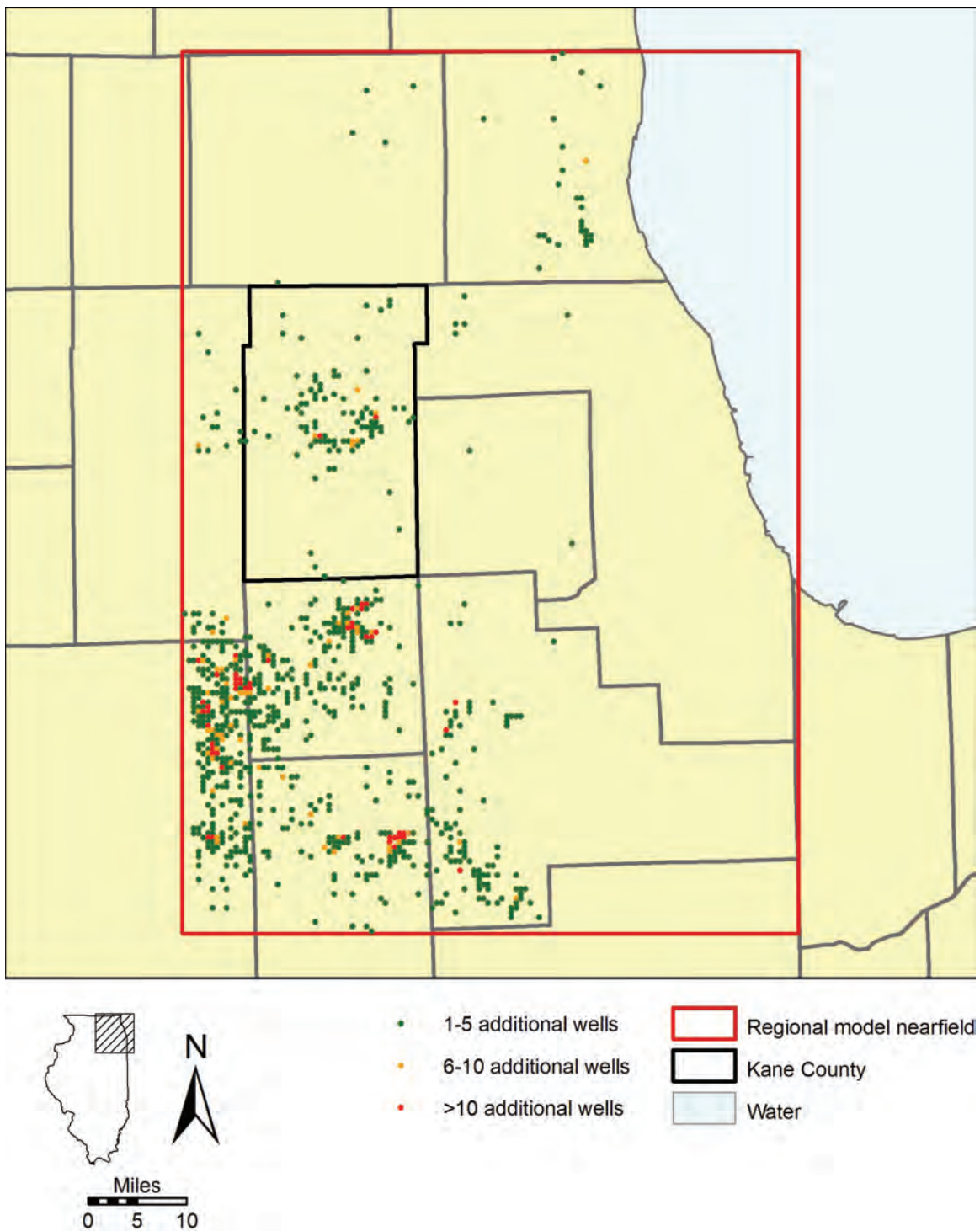


Figure G-11. Projected deep domestic wells, not existing in 2003, to be drilled and in service by 2050 and for which withdrawals were projected. See Figure G-13 for assumed withdrawal rates from these wells.

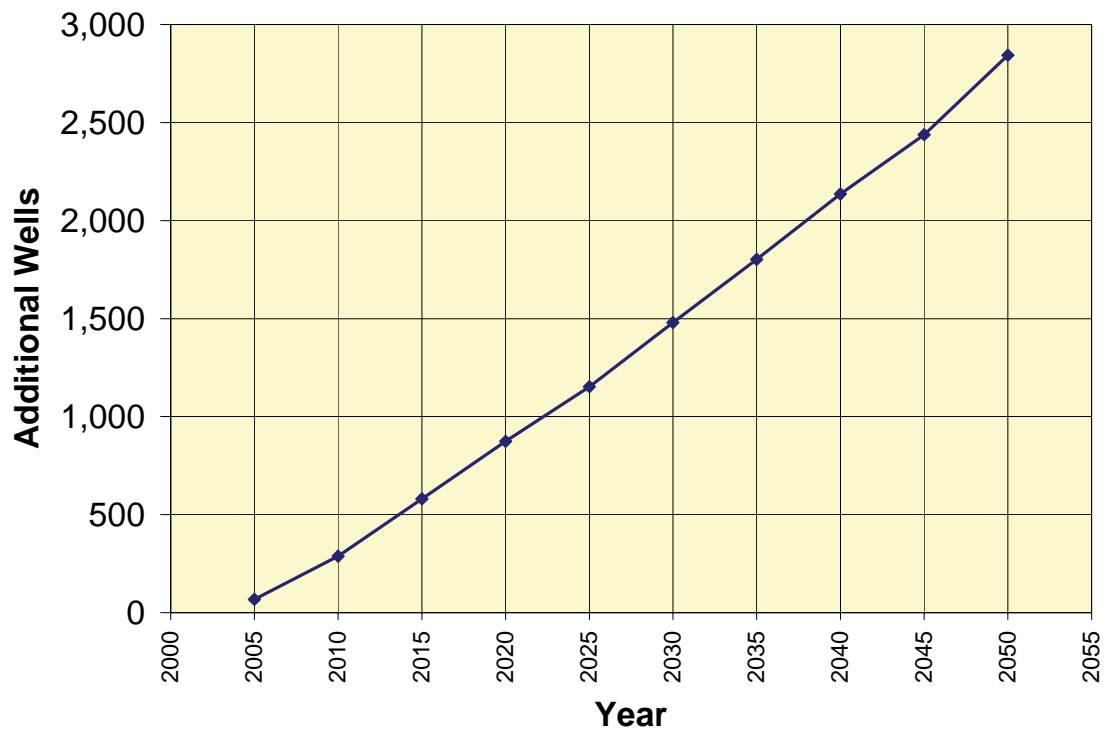


Figure G-12. Added deep domestic wells.

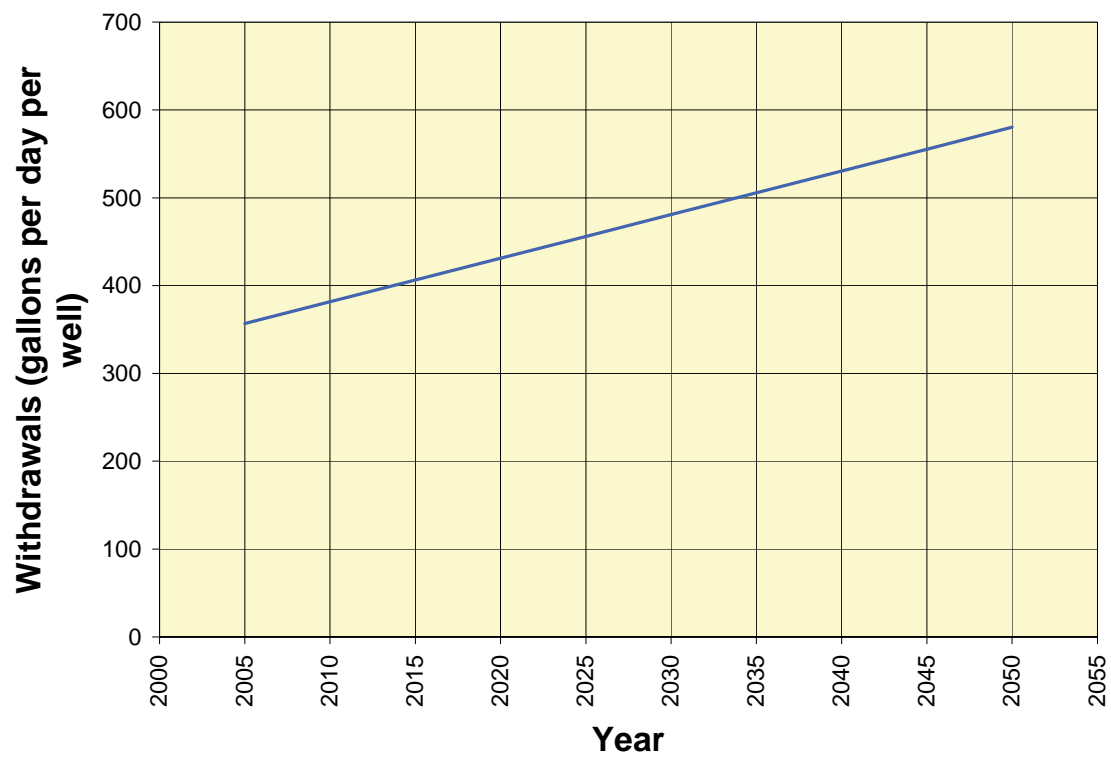


Figure G-13. Assumed withdrawal rate per well for domestic wells, 2005-2050.

G.3 References

Dziegielewski, B., T. Bik, X. Yang, H. Margono, M. Richey, and D. Sherman. 2004. *Countywide Projections of Community Water Supply Needs in the Midwest*. Department of Geography, Southern Illinois University, Carbondale, IL.

Dziegielewski, B., X. Yang, T. Bik, H. Margono, and M. Richey. 2005. *County-Level Forecasts of Water Use in Illinois: 2005-2025*. Department of Geography, Southern Illinois University, Carbondale, IL.

Illinois Department of Energy and Natural Resources. 1998. *Fox River Area Assessment. Volume 2: Water Resources*. Illinois Department of Natural Resources Critical Trends Assessment Program Document. Springfield, IL.

Appendix H. Capture Zone Delineations

Included are capture zone delineations for high-capacity public water supply wells open to the shallow aquifers in Kane County. High-capacity wells are defined in this report as wells that pumped more than 100,000 gallons per day in 2003.

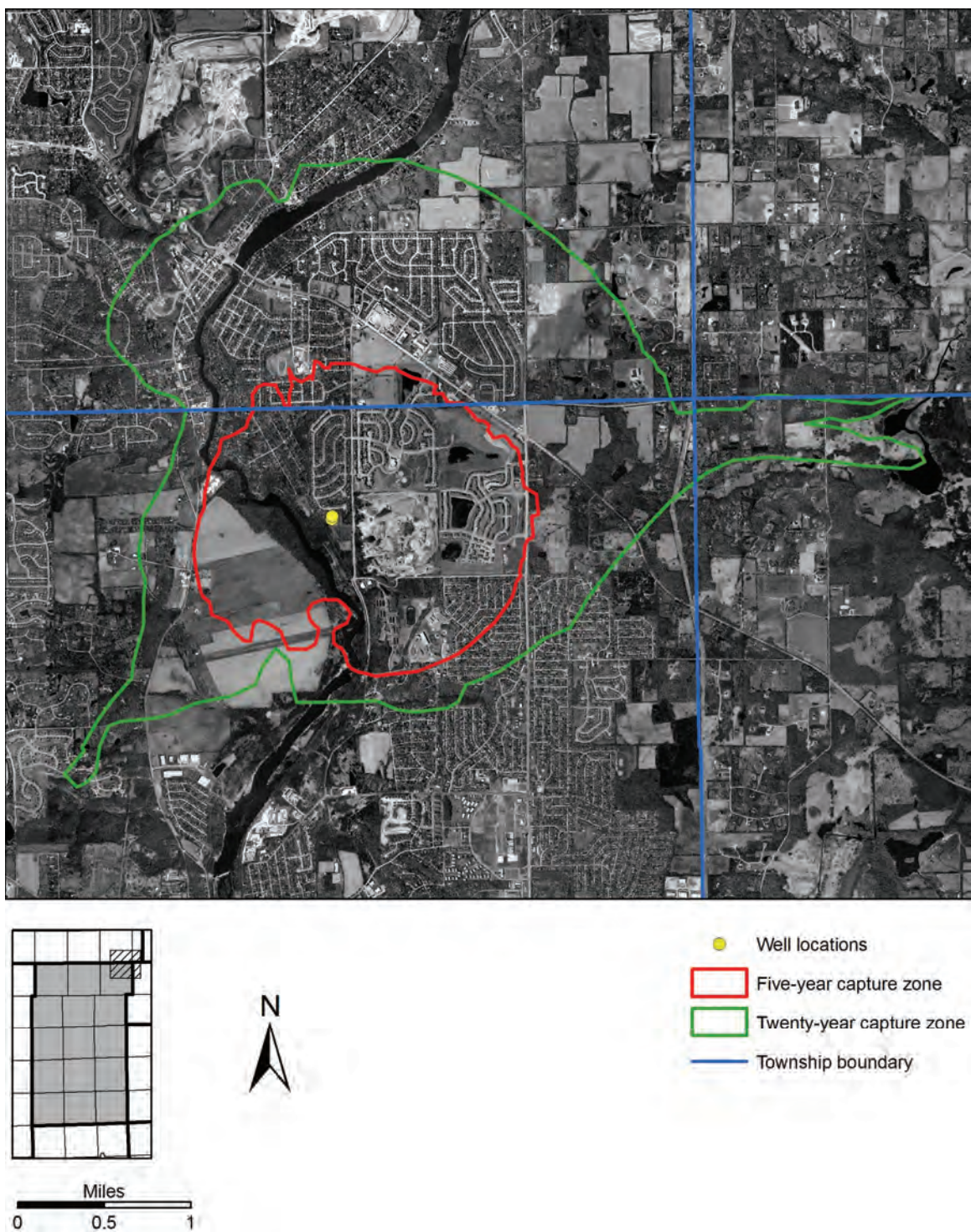


Figure H-1. Five- and twenty-year capture zones of Algonquin wells 7 and 11 superimposed on 2005 aerial photography.

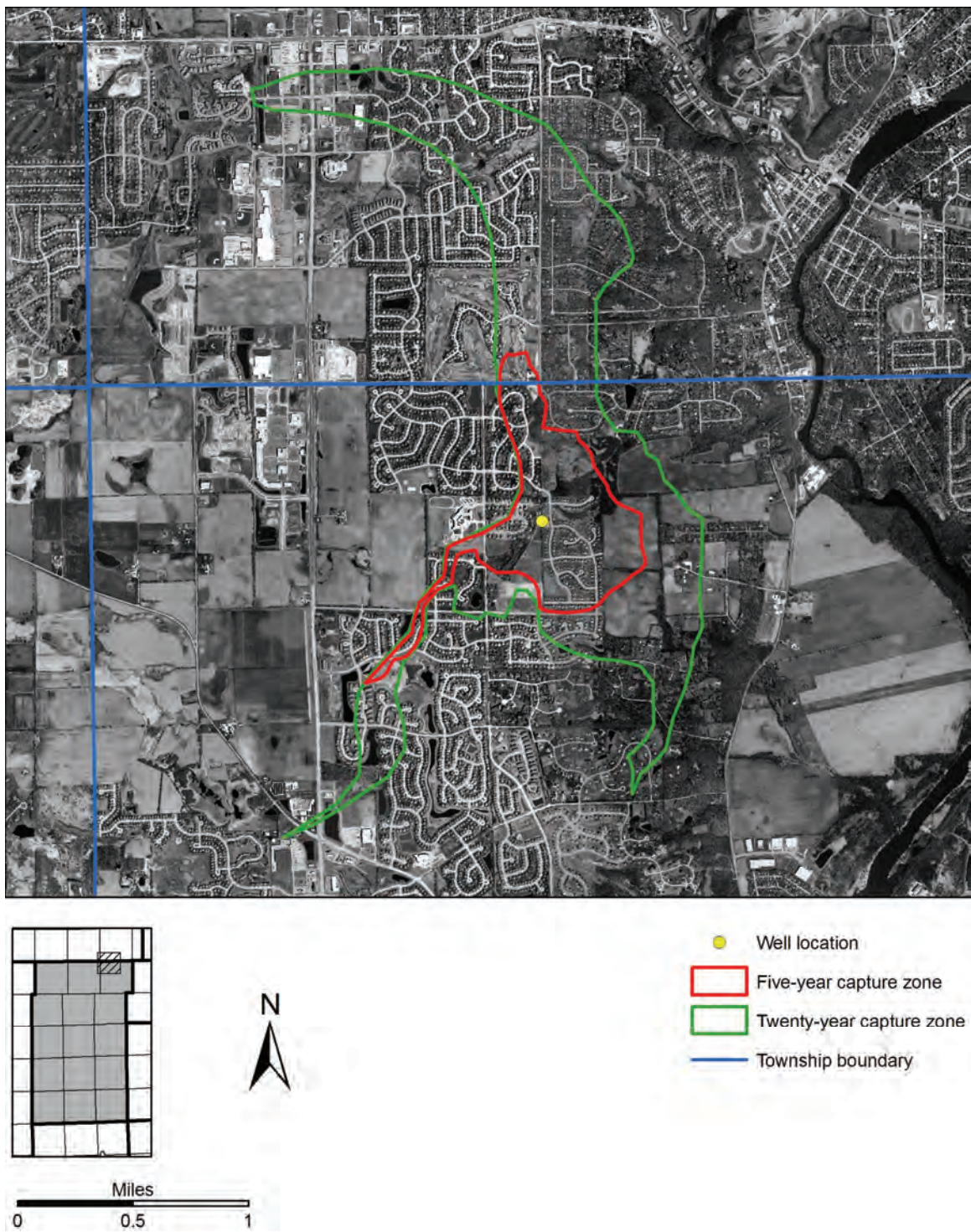


Figure H-2. Five- and twenty-year capture zones of Algonquin well 8 superimposed on 2005 aerial photography.

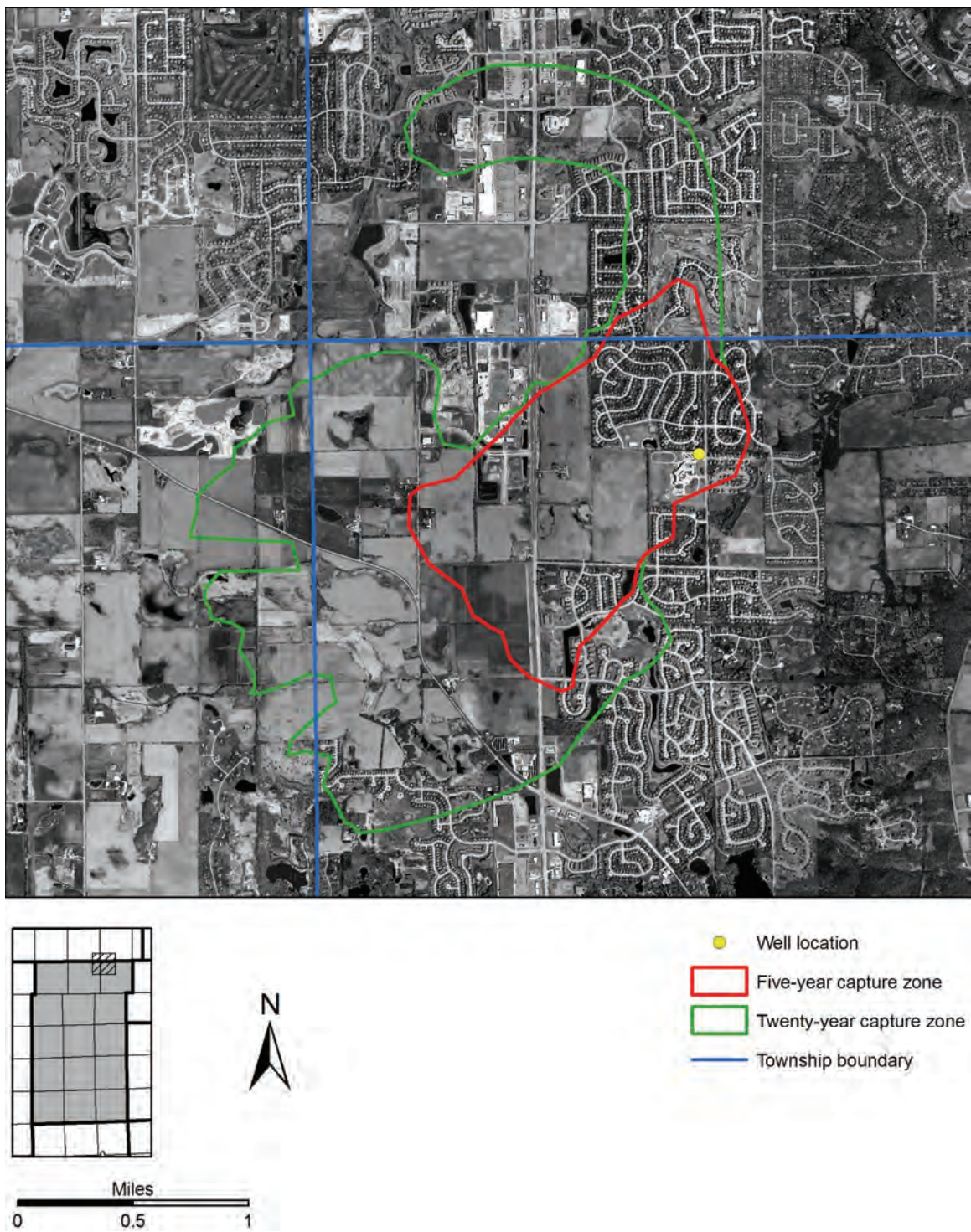


Figure H-3. Five- and twenty-year capture zones of Algonquin well 9 superimposed on 2005 aerial photography.

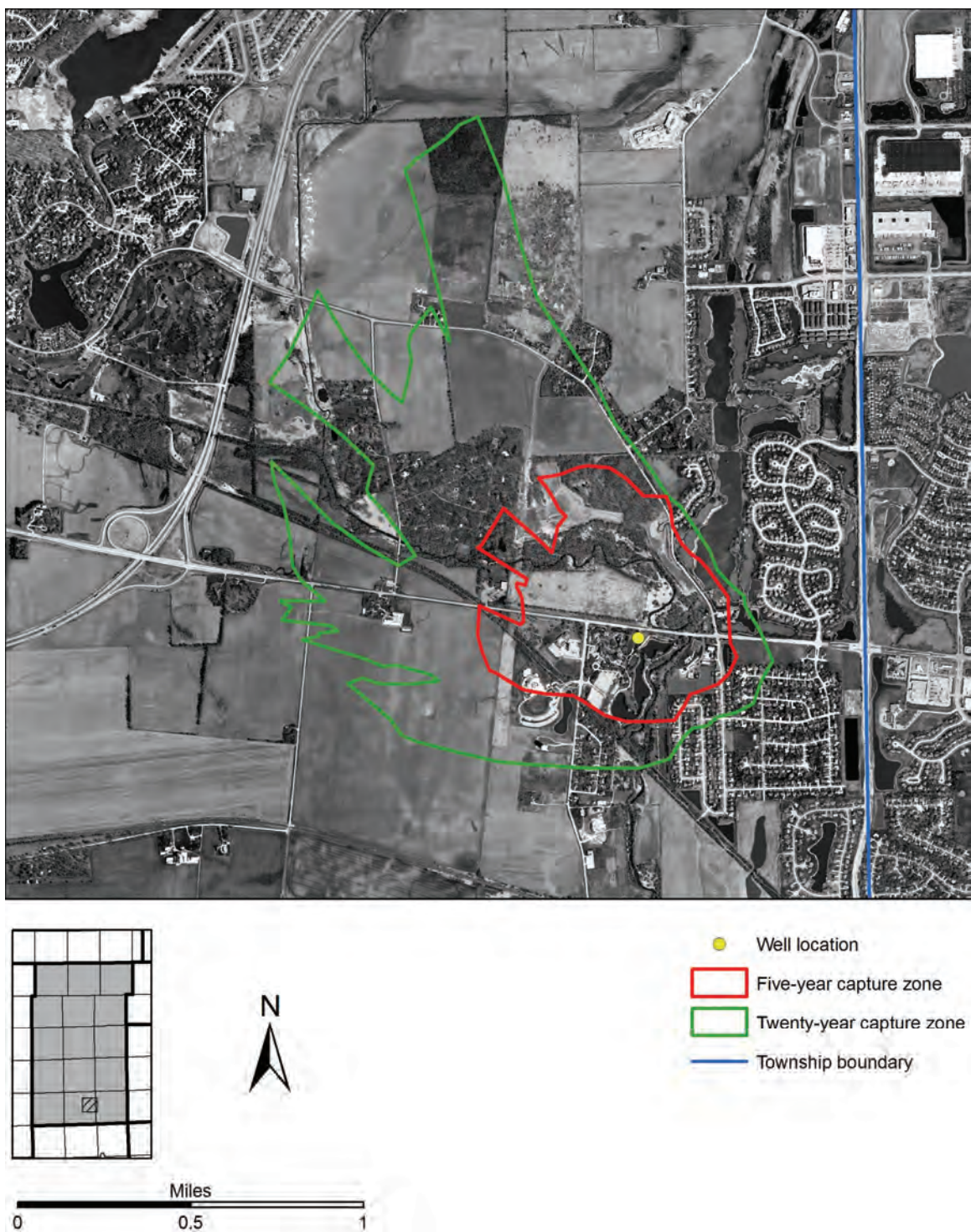


Figure H-4. Five- and twenty-year capture zones of Aurora well 101 superimposed on 2005 aerial photography.

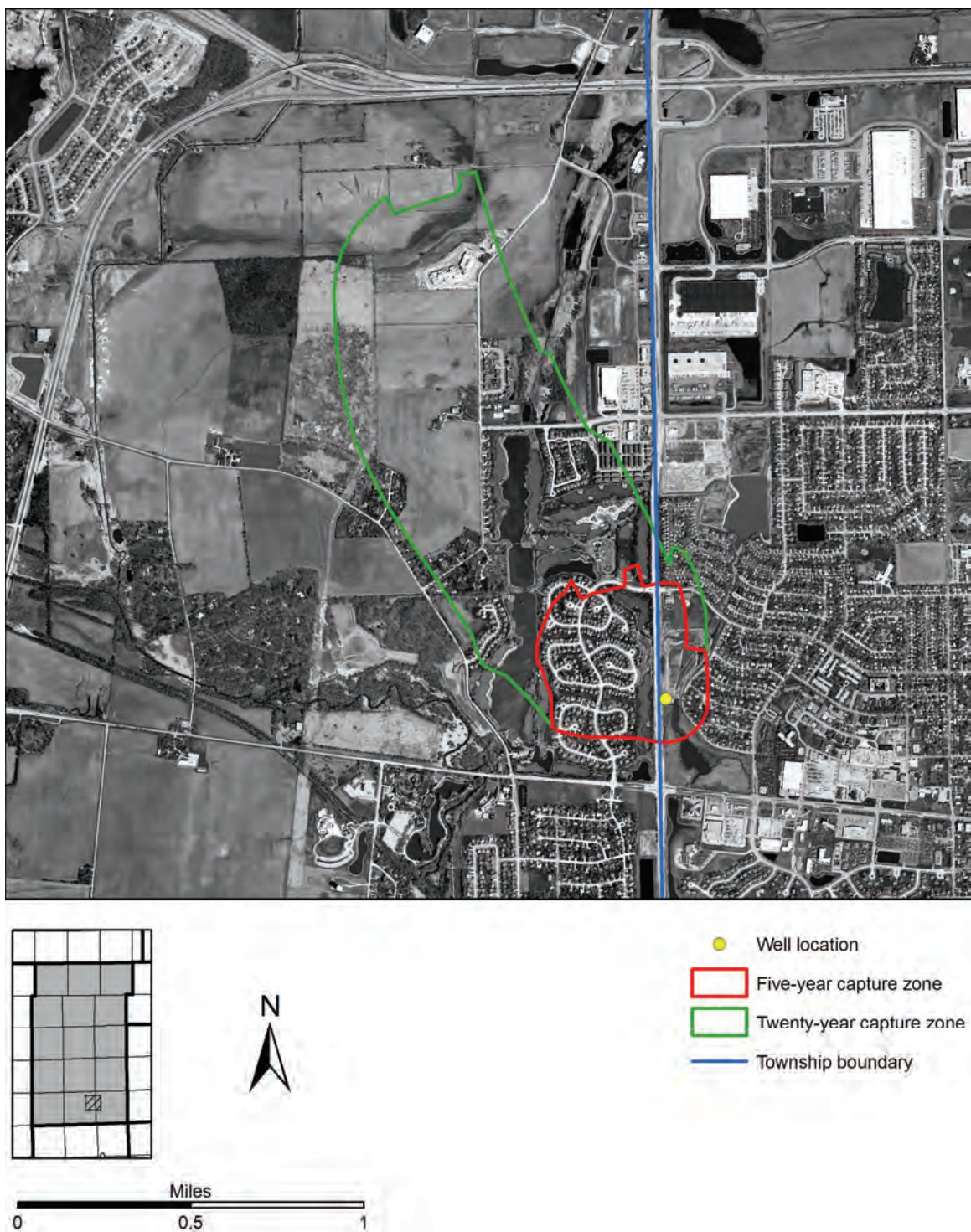


Figure H-5. Five- and twenty-year capture zones of Aurora well 103 superimposed on 2005 aerial photography.

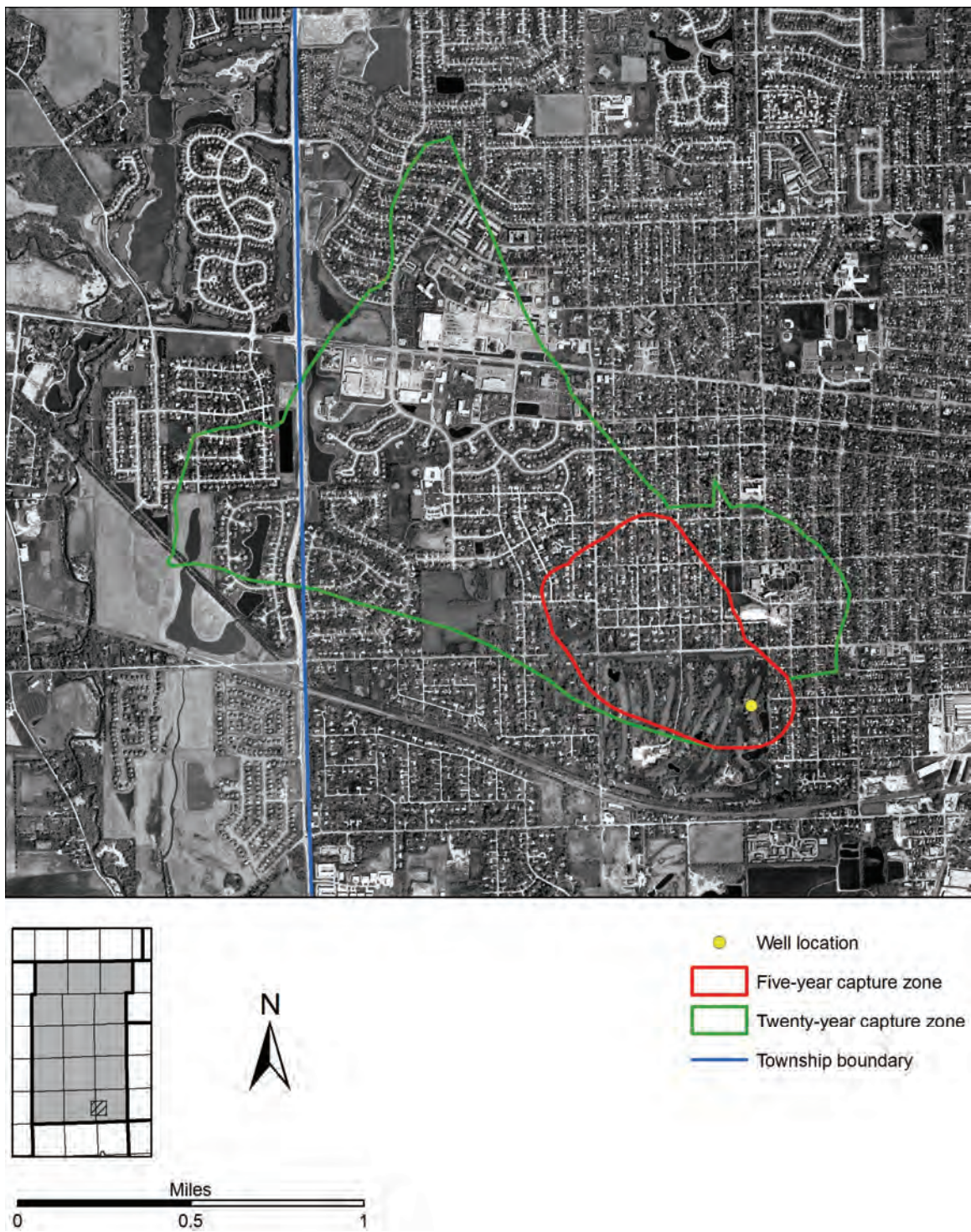


Figure H-6. Five- and twenty-year capture zones of Aurora Country Club well 6 superimposed on 2005 aerial photography.

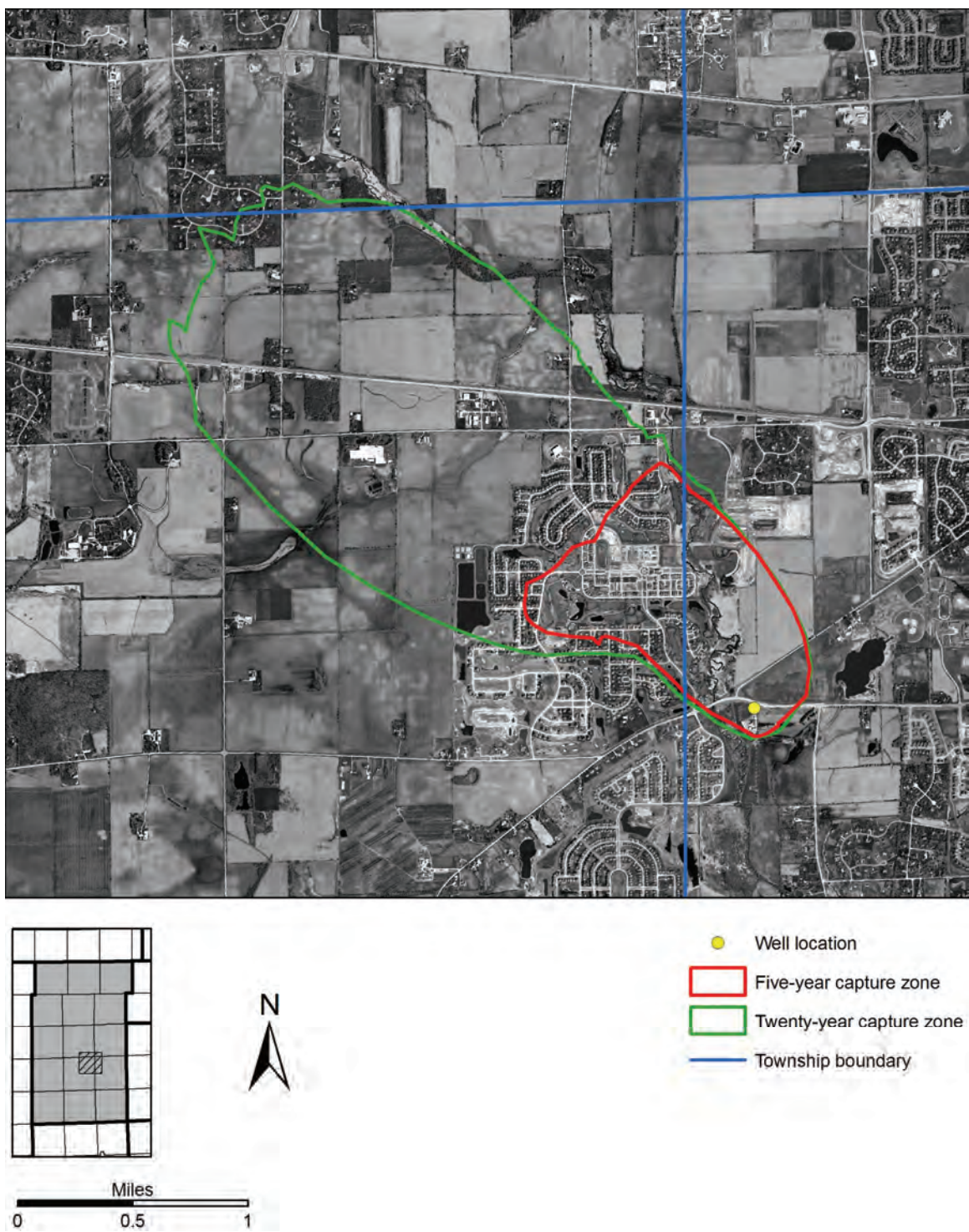


Figure H-7. Five- and twenty-year capture zones of Batavia well 6 superimposed on 2005 aerial photography.

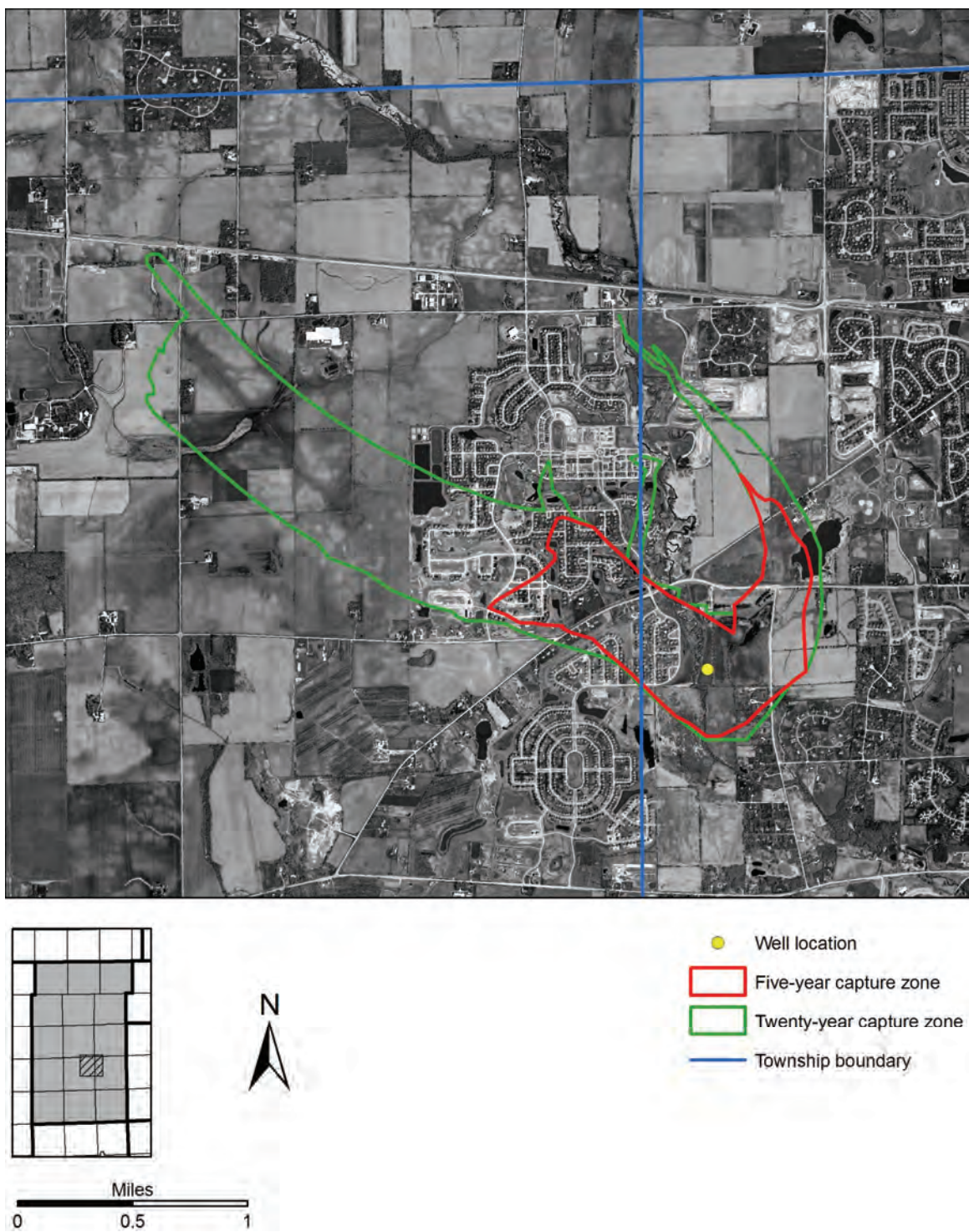


Figure H-8. Five- and twenty-year capture zones of Batavia well 7 superimposed on 2005 aerial photography.

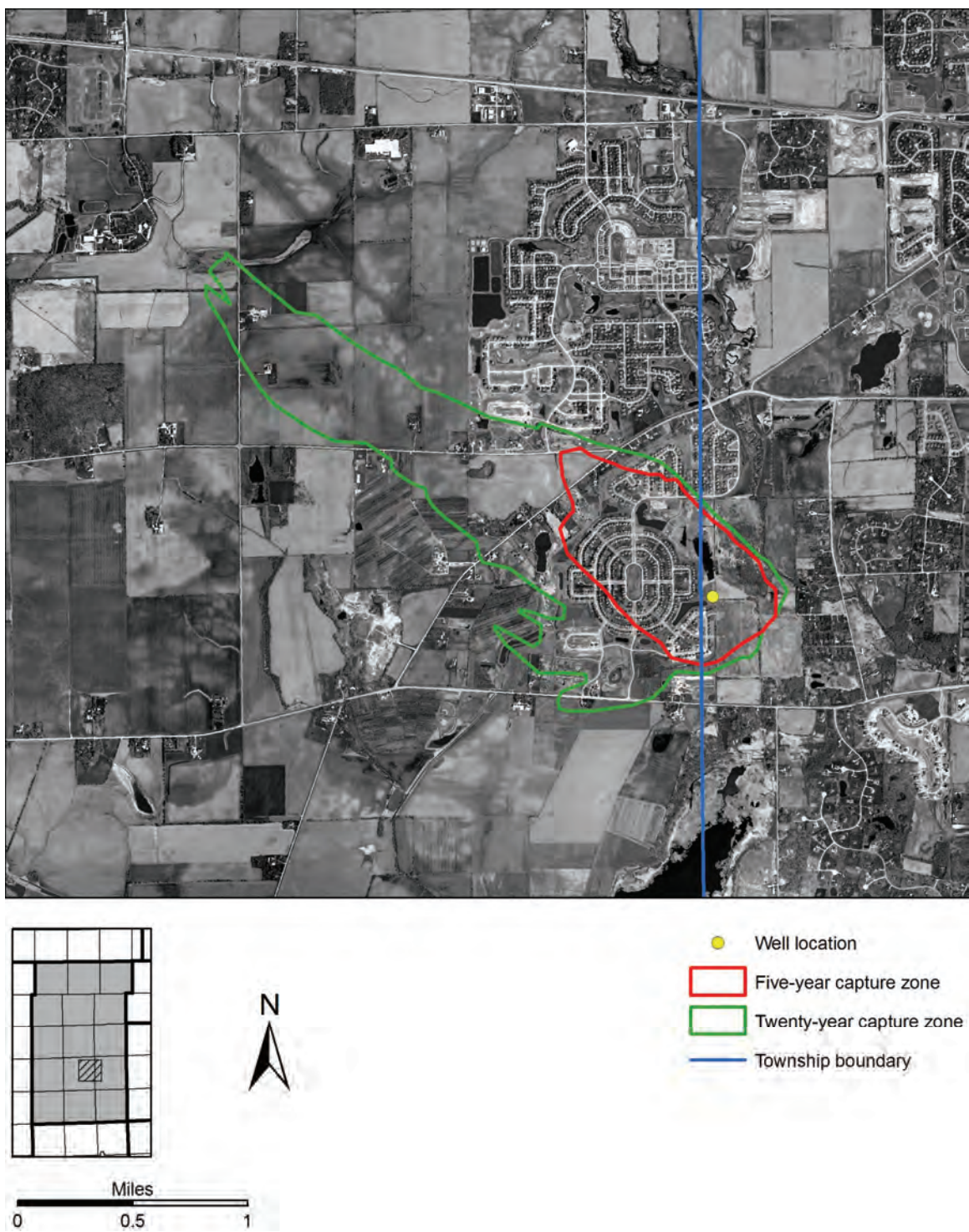


Figure H-9. Five- and twenty-year capture zones of Batavia well 8 superimposed on 2005 aerial photography.

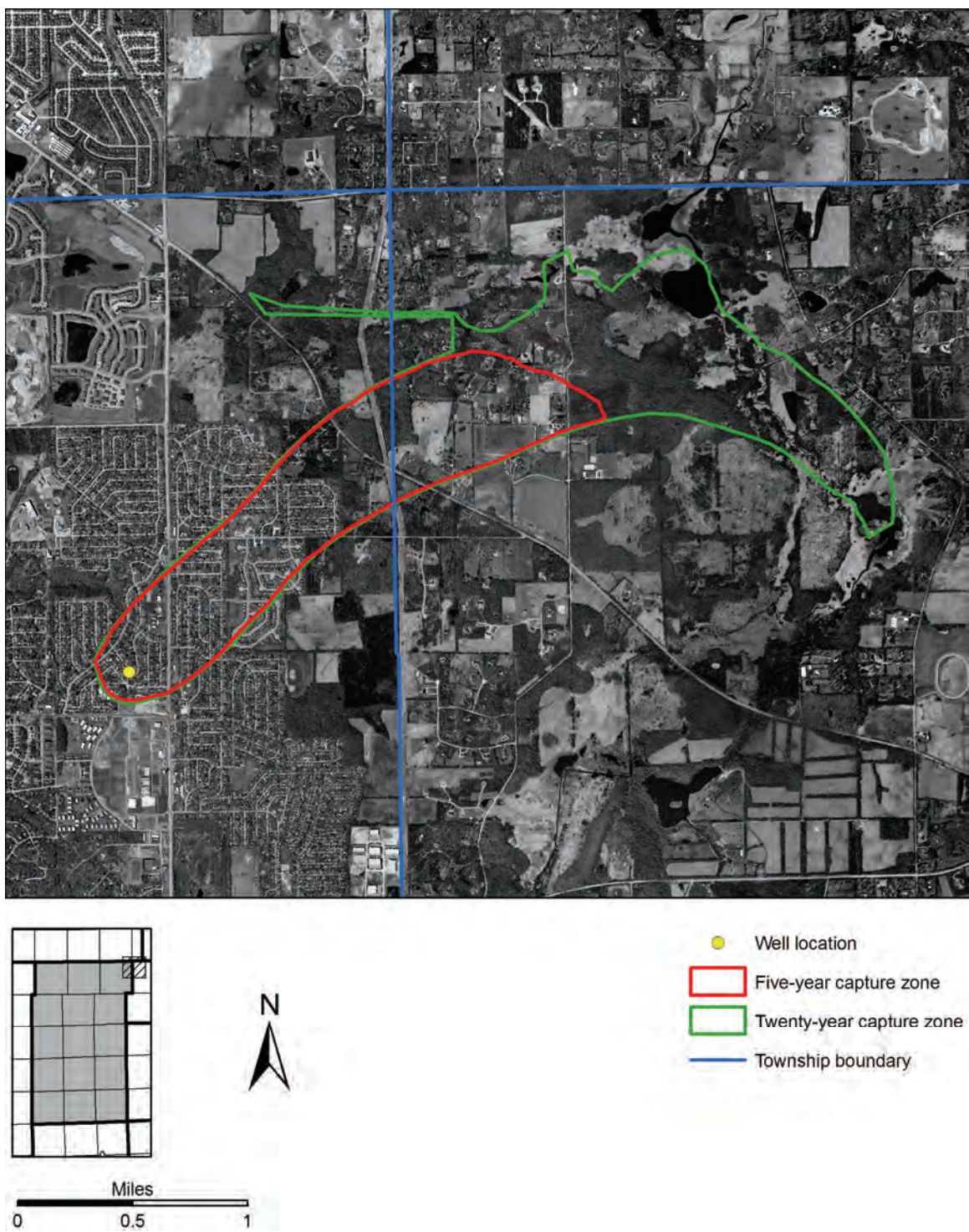


Figure H-10. Five- and twenty-year capture zones of Carpentersville well 5 superimposed on 2005 aerial photography.

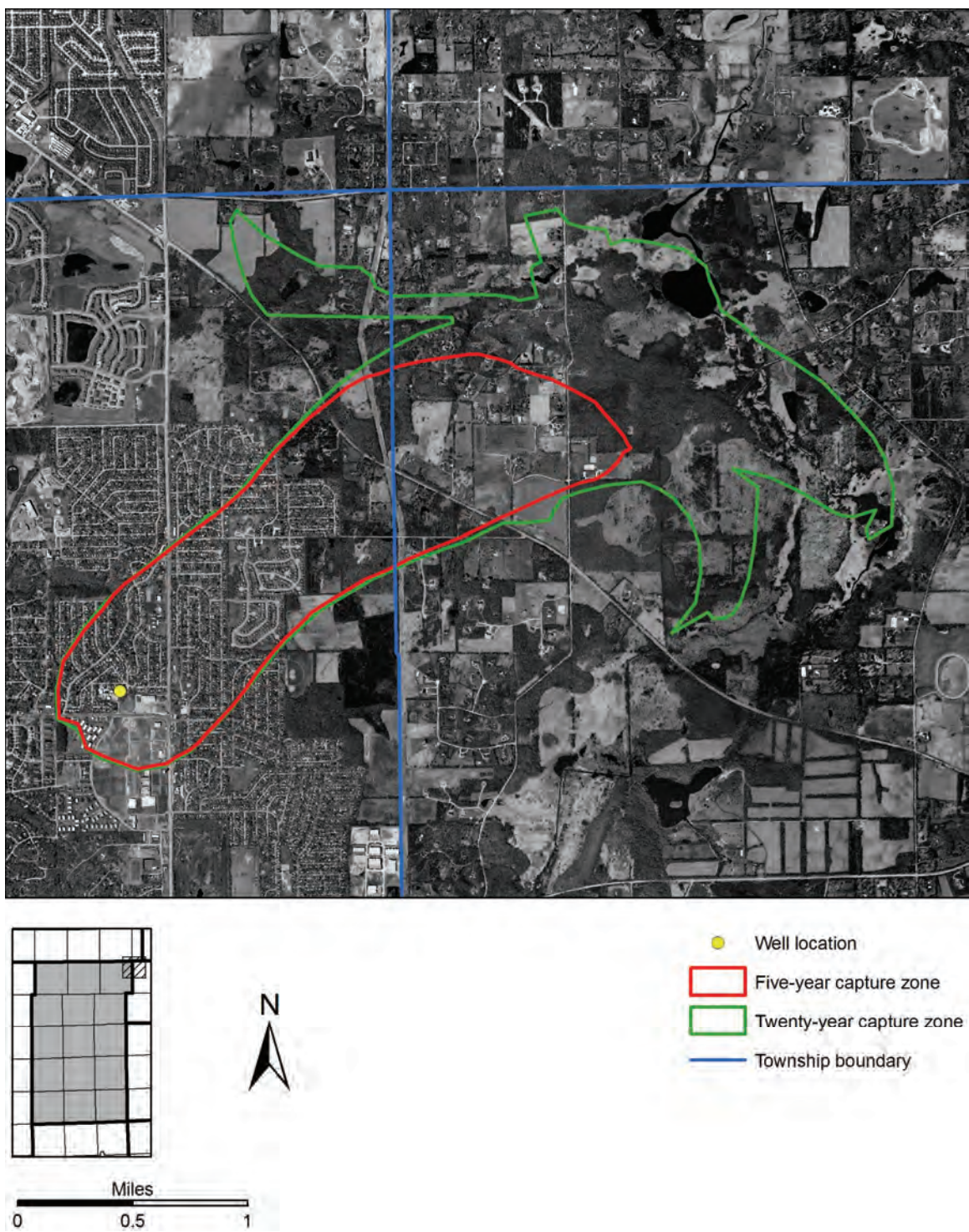


Figure H-11. Five- and twenty-year capture zones of Carpentersville well 6 superimposed on 2005 aerial photography.

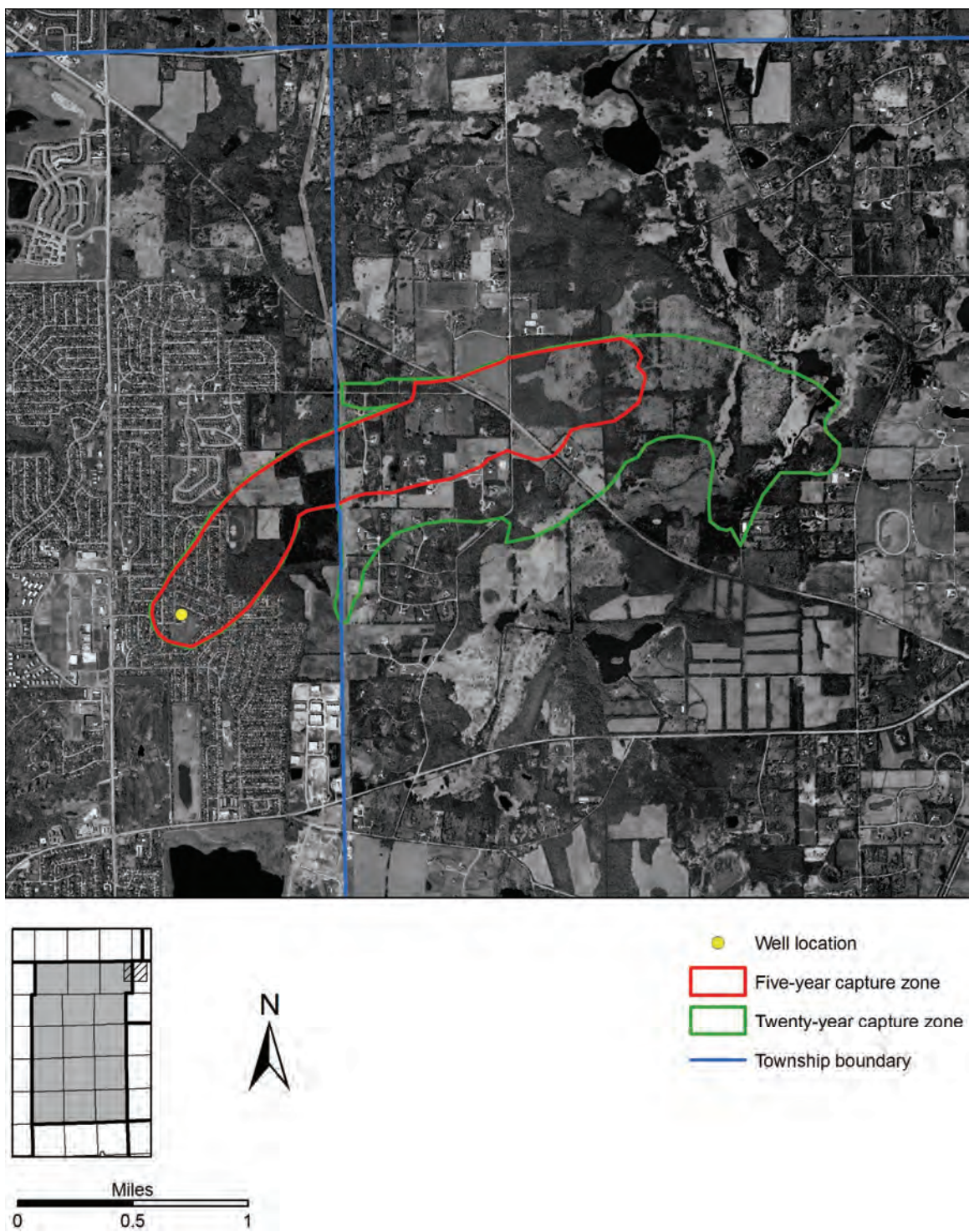


Figure H-12. Five- and twenty-year capture zones of Carpentersville well 7 superimposed on 2005 aerial photography.

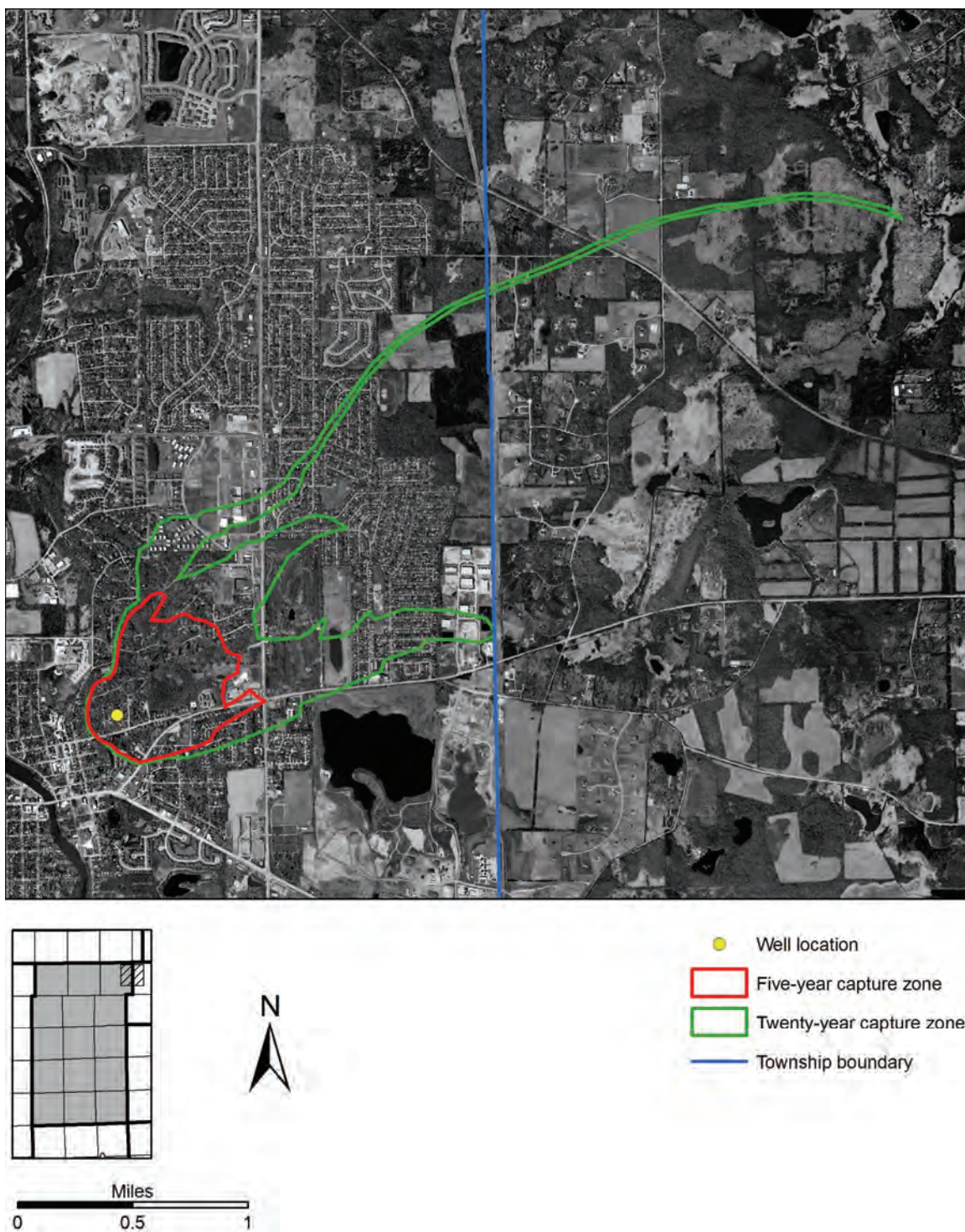


Figure H-13. Five- and twenty-year capture zones of East Dundee well 3 superimposed on 2005 aerial photography.

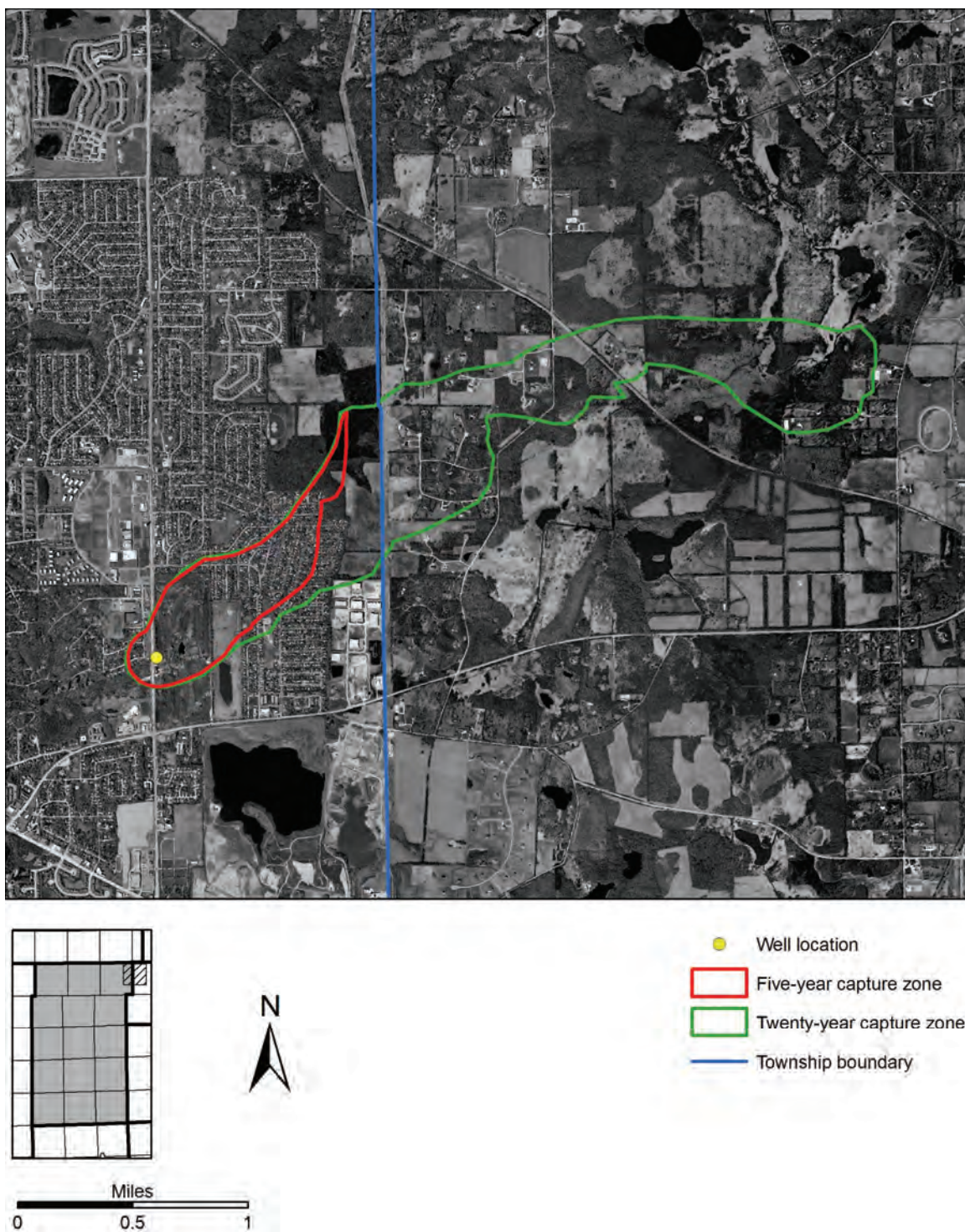


Figure H-14. Five- and twenty-year capture zones of East Dundee well 4 superimposed on 2005 aerial photography.

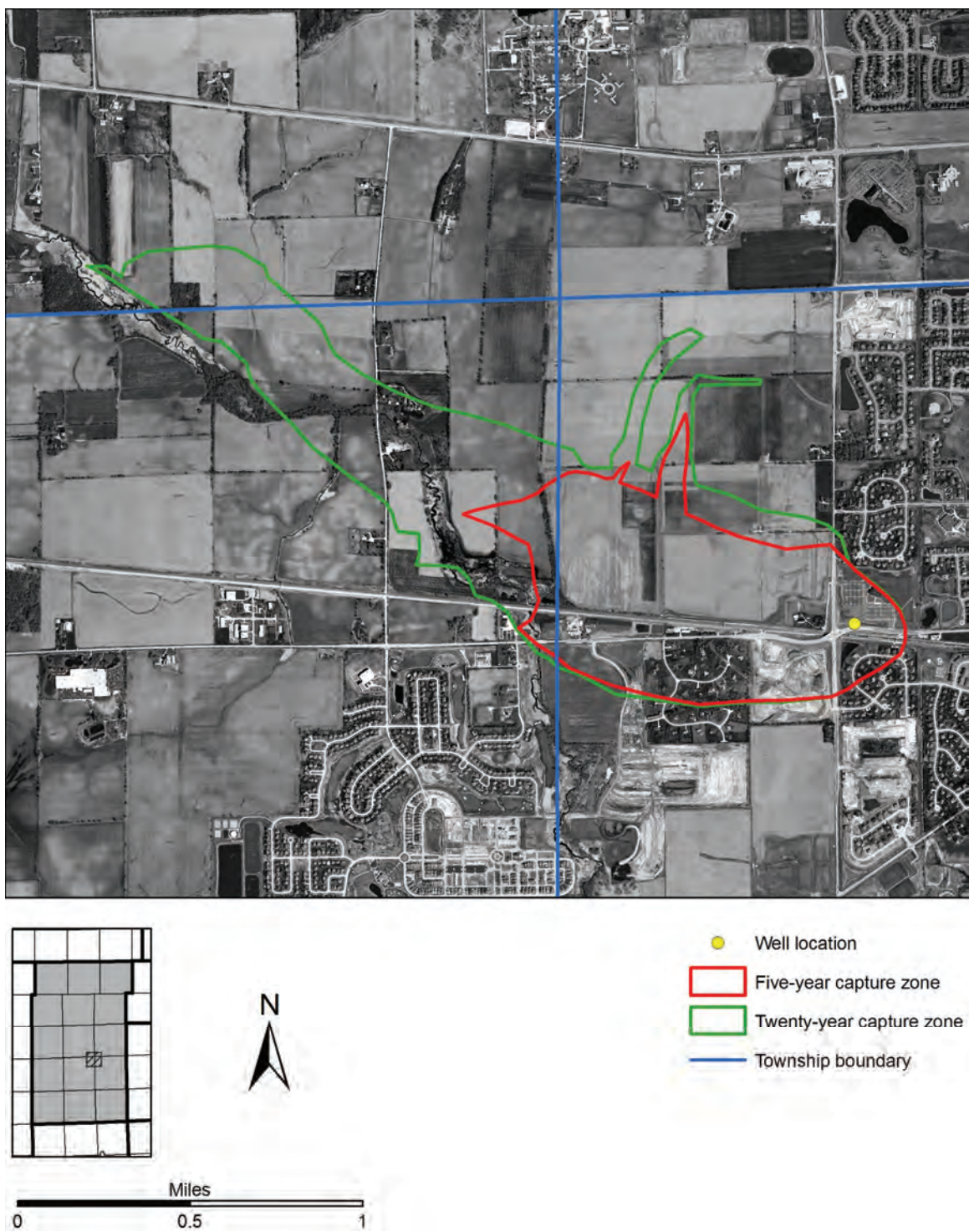


Figure H-15. Five- and twenty-year capture zones of Geneva well 8 superimposed on 2005 aerial photography.

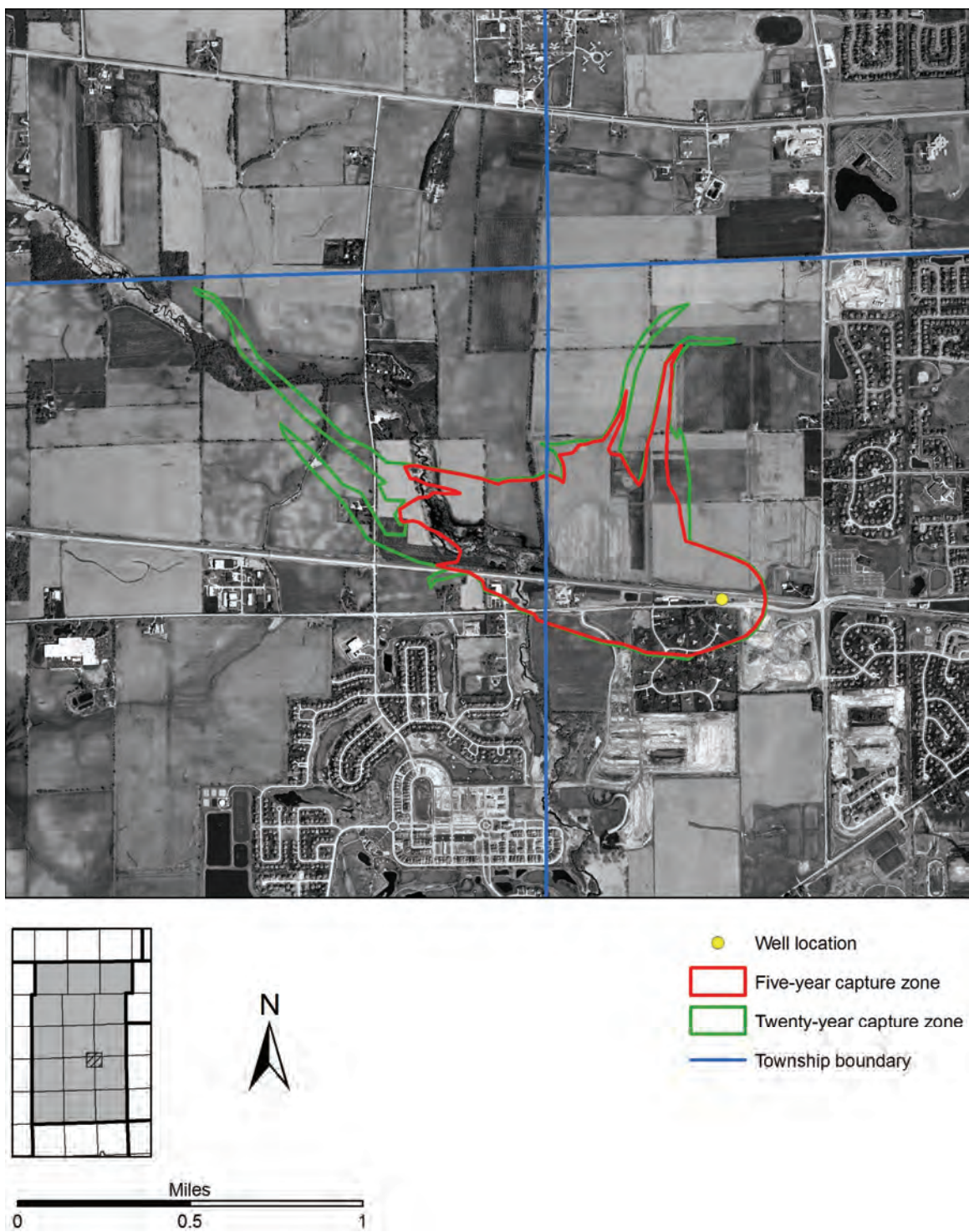


Figure H-16. Five- and twenty-year capture zones of Geneva well 9 superimposed on 2005 aerial photography.

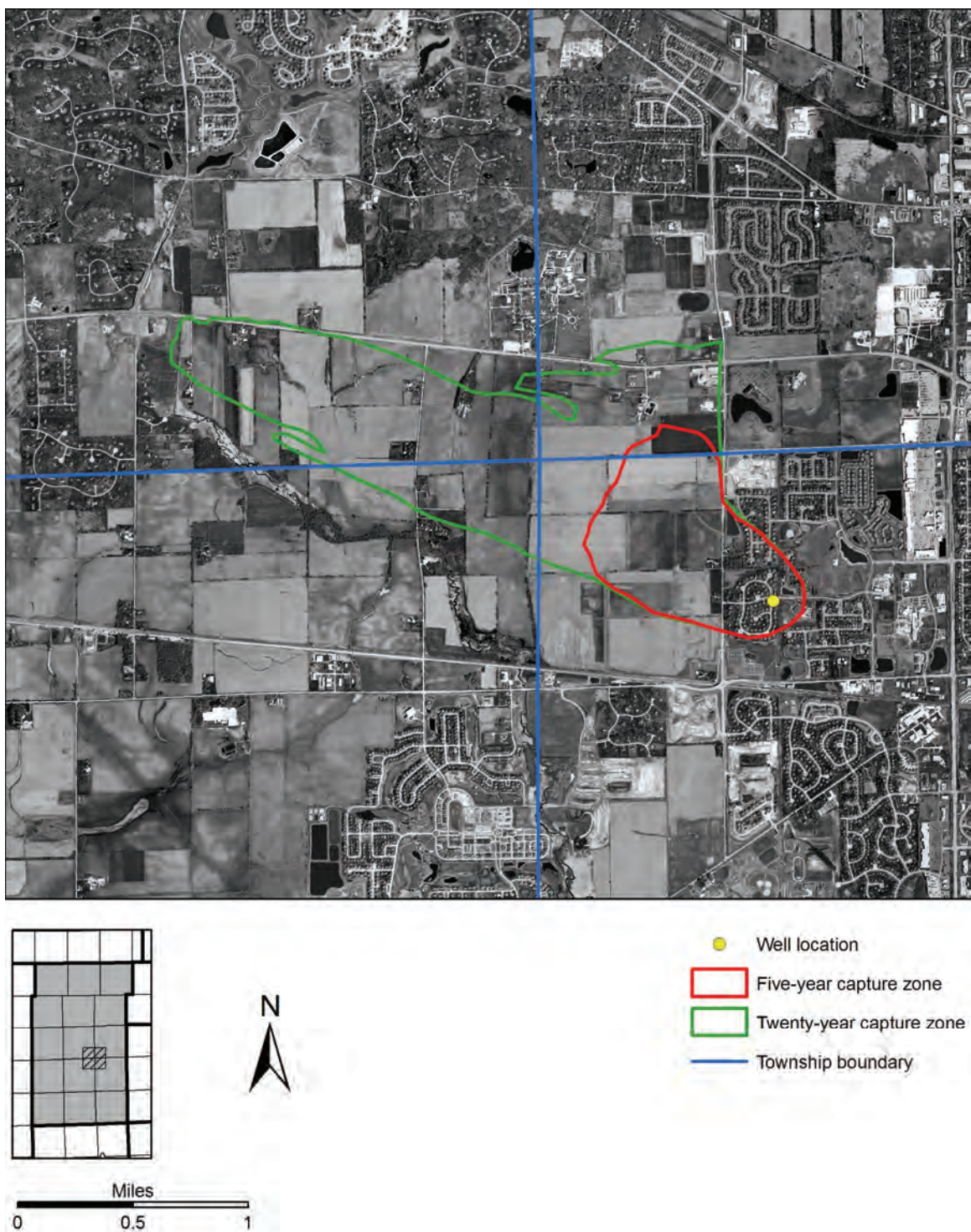


Figure H-17. Five- and twenty-year capture zones of Geneva well 10 superimposed on 2005 aerial photography.

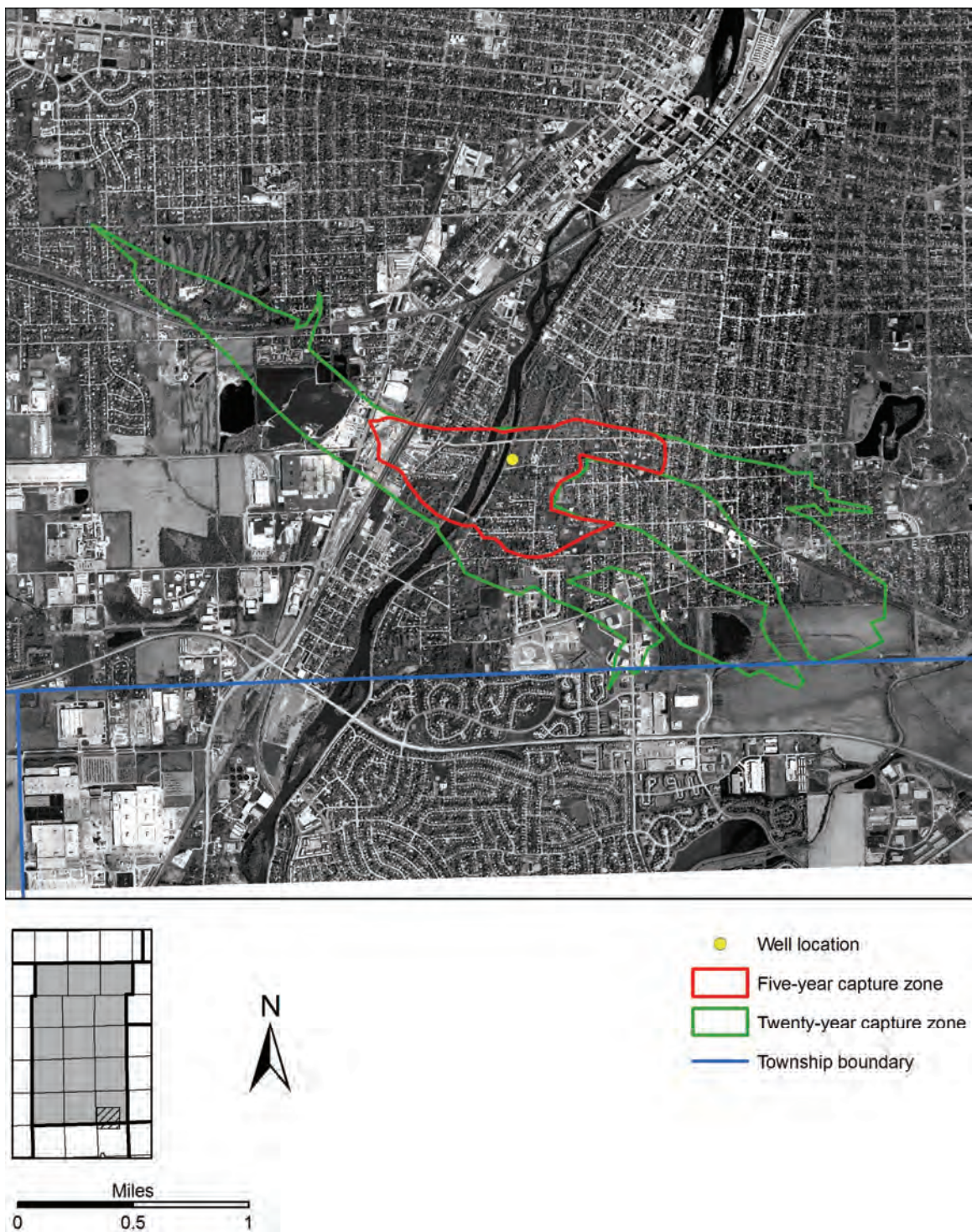


Figure H-18. Five- and twenty-year capture zones of Montgomery well 13 superimposed on 2005 aerial photography.

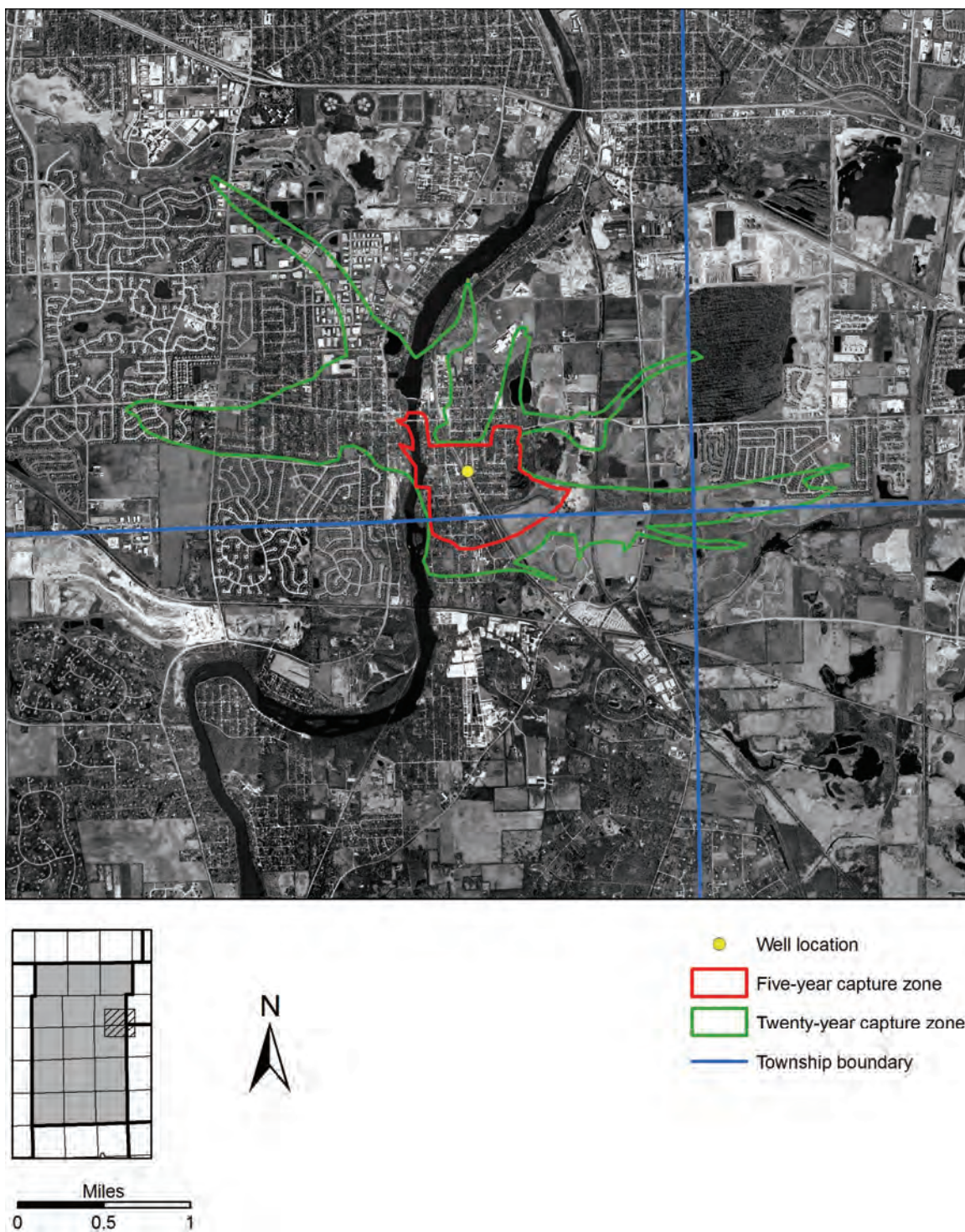


Figure H-19. Five- and twenty-year capture zones of South Elgin well 3 superimposed on 2005 aerial photography.

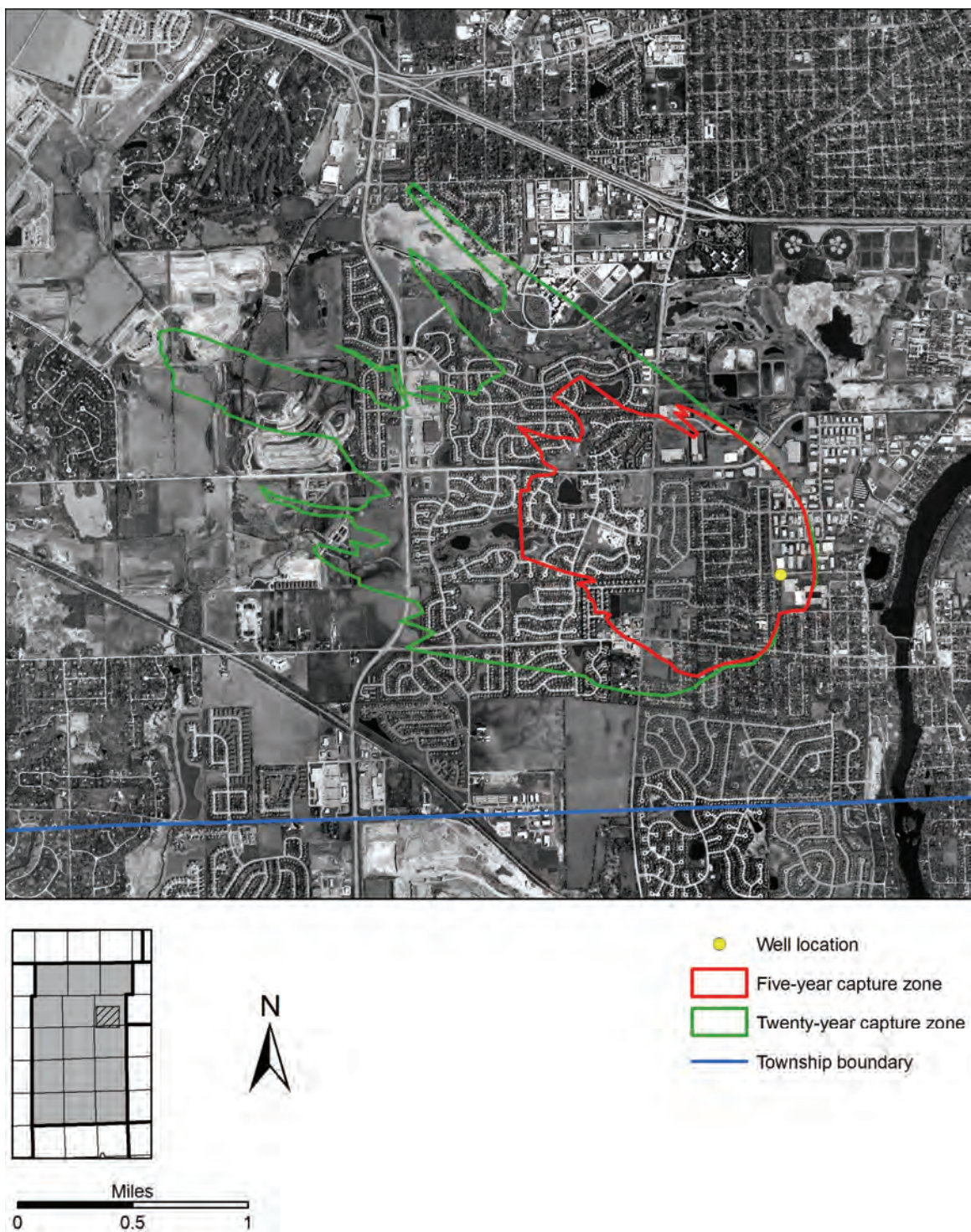


Figure H-20. Five- and twenty-year capture zones of South Elgin well 4 superimposed on 2005 aerial photography.

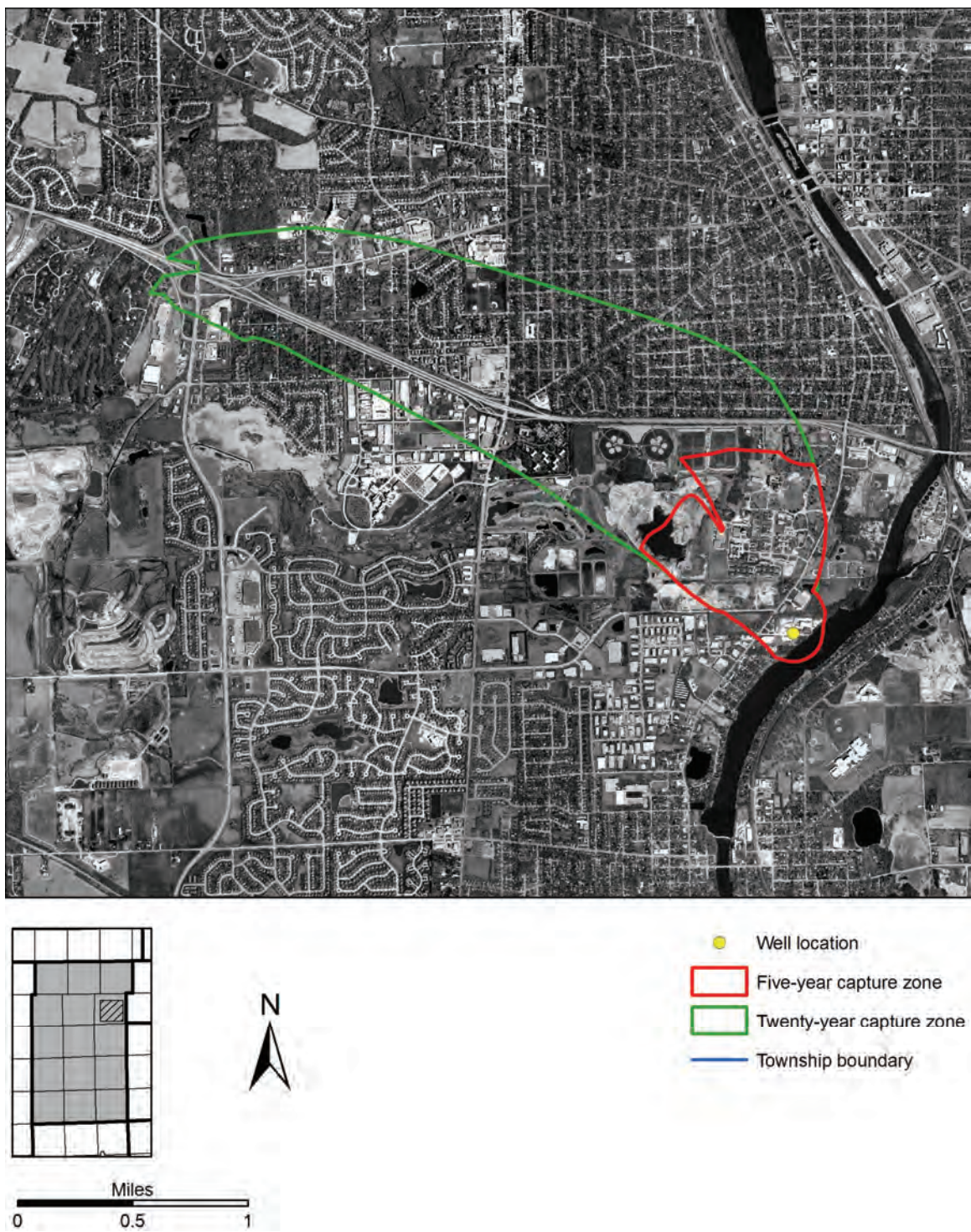


Figure H-21. Five- and twenty-year capture zones of South Elgin well 5 superimposed on 2005 aerial photography.

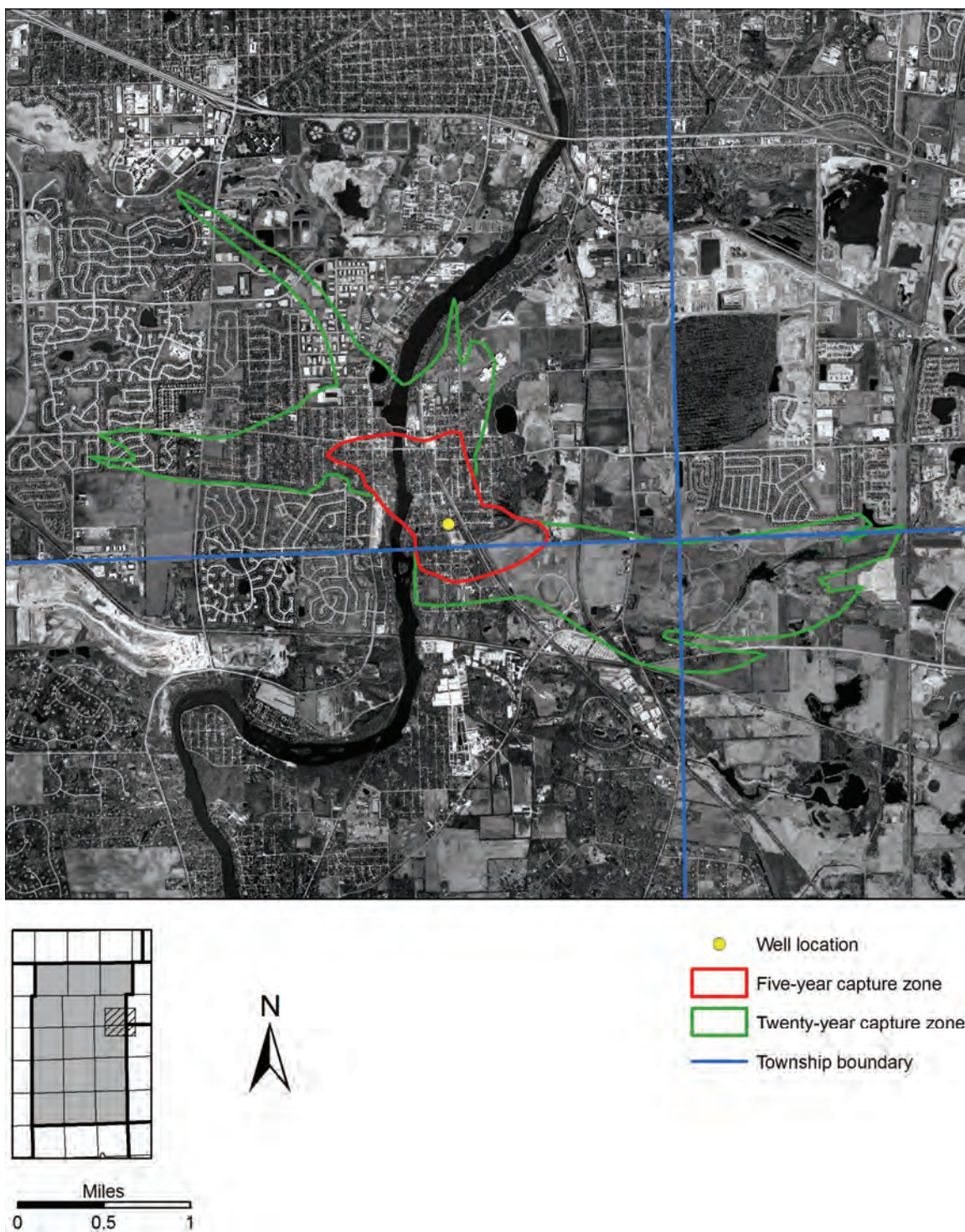


Figure H-22. Five- and twenty-year capture zones of South Elgin well 6 superimposed on 2005 aerial photography.

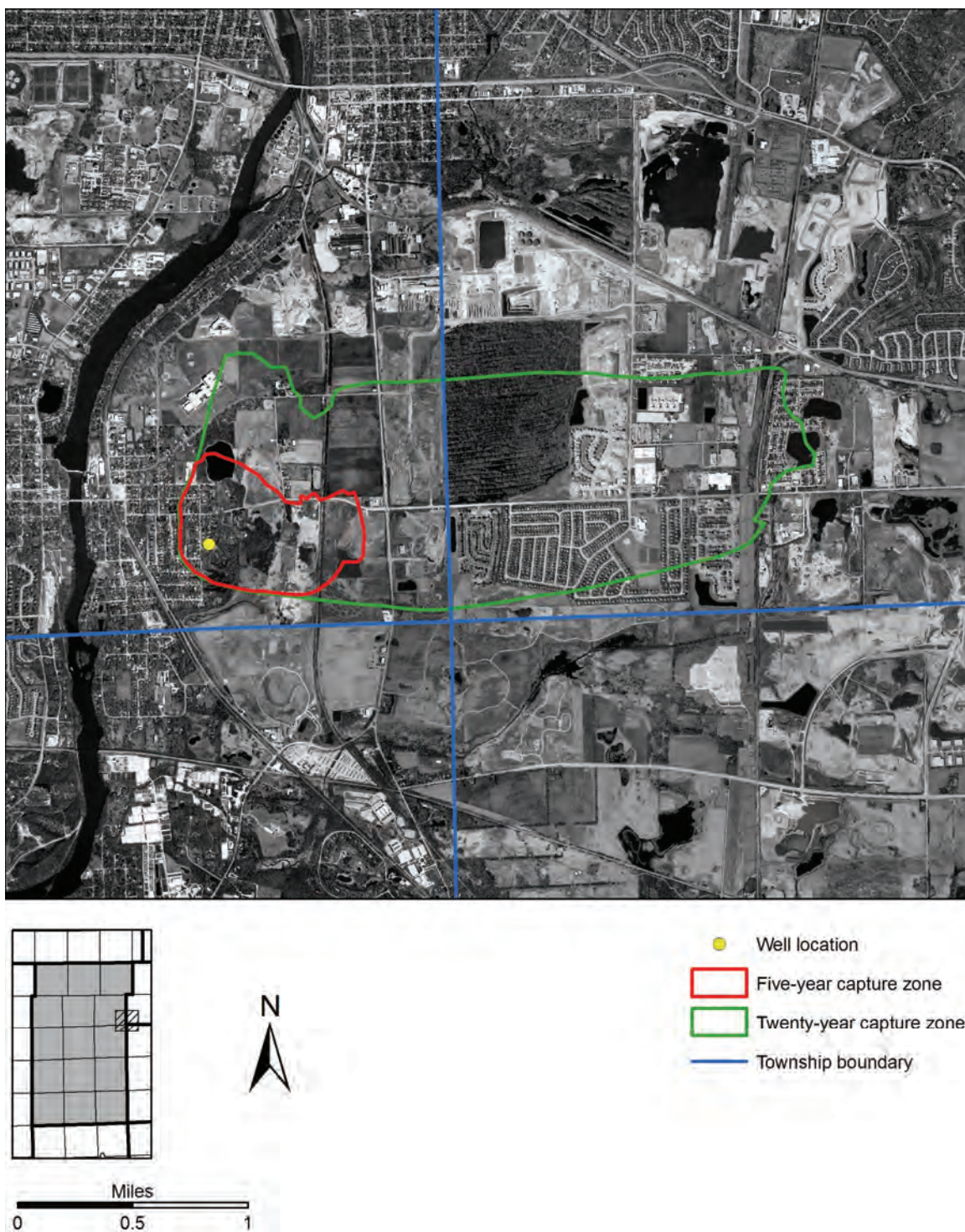


Figure H-23. Five- and twenty-year capture zones of South Elgin well 10 superimposed on 2005 aerial photography.

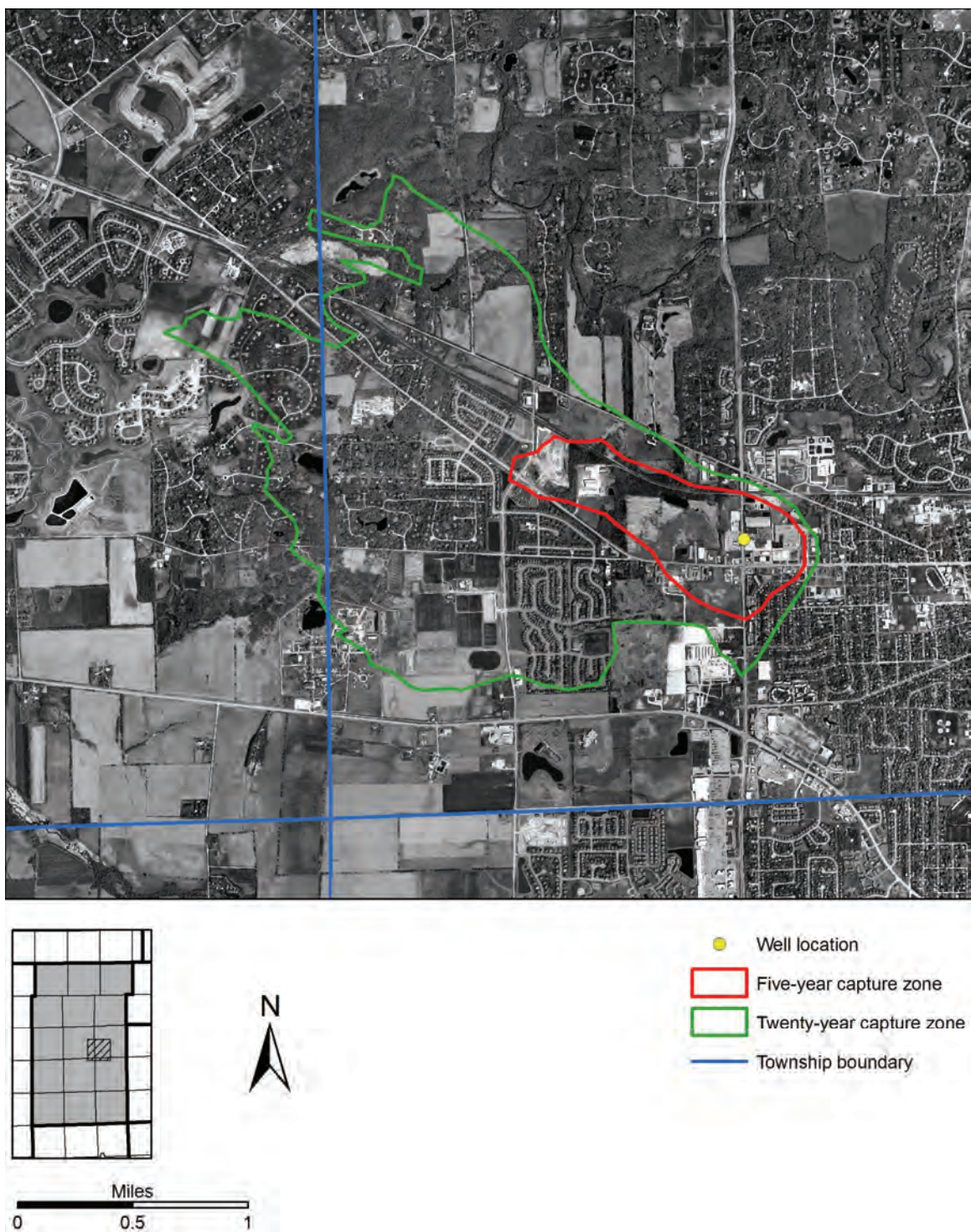


Figure H-24. Five- and twenty-year capture zones of St. Charles well 7 superimposed on 2005 aerial photography.

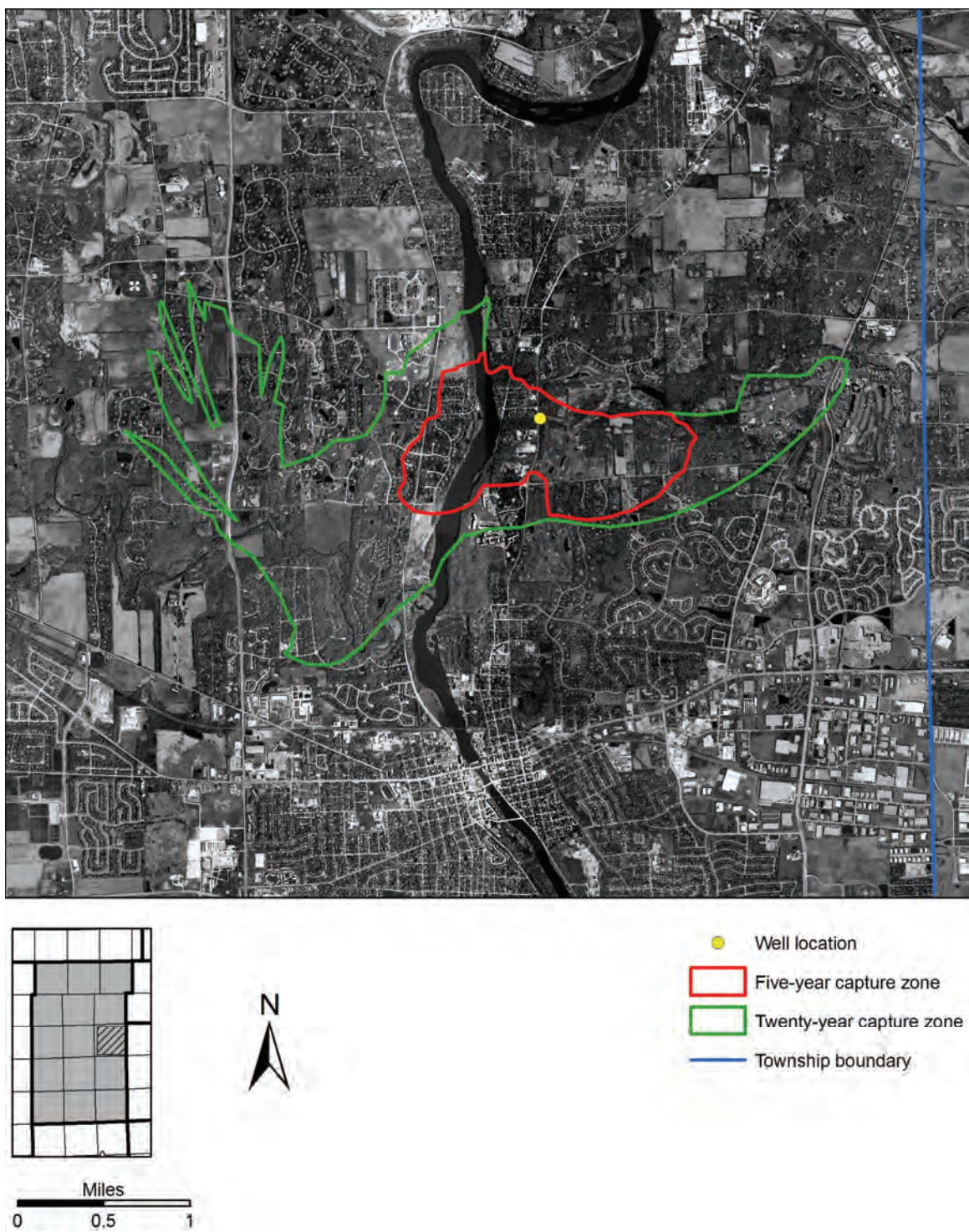


Figure H-25. Five- and twenty-year capture zones of St. Charles well 9 superimposed on 2005 aerial photography.

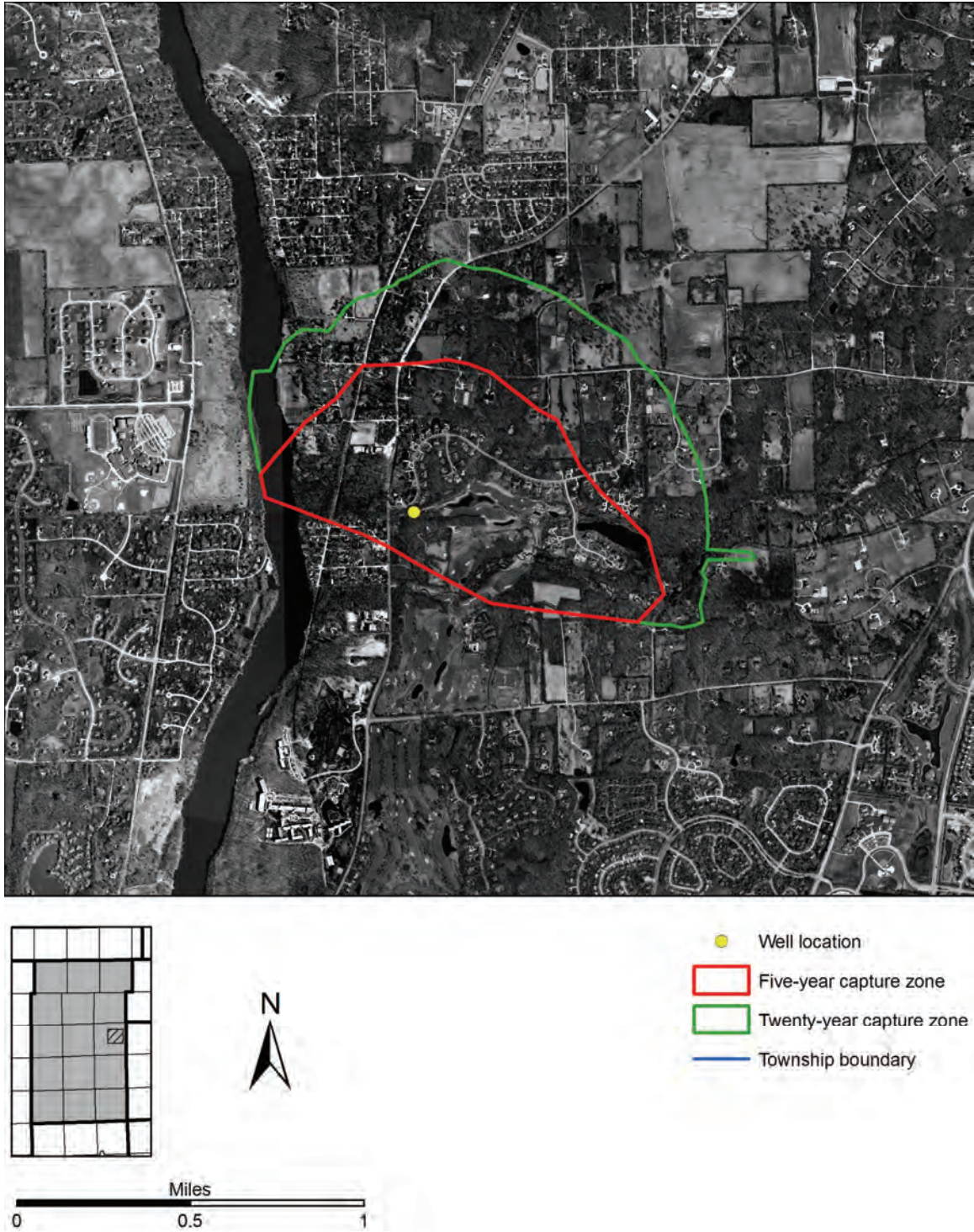


Figure H-26. Five- and twenty-year capture zones of St. Charles 11 superimposed on 2005 aerial photography.

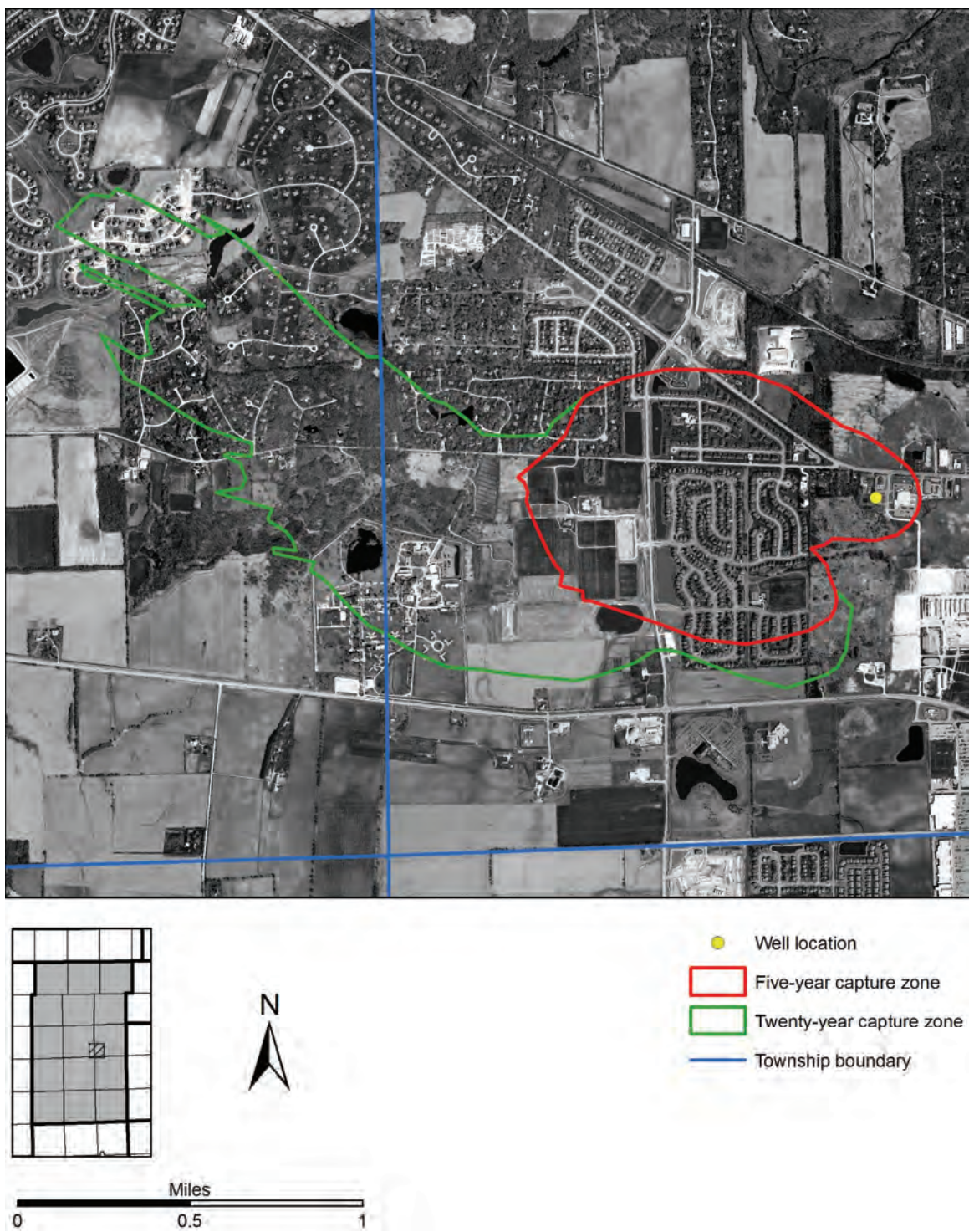


Figure H-27. Five- and twenty-year capture zones of St. Charles well 13 superimposed on 2005 aerial photography.

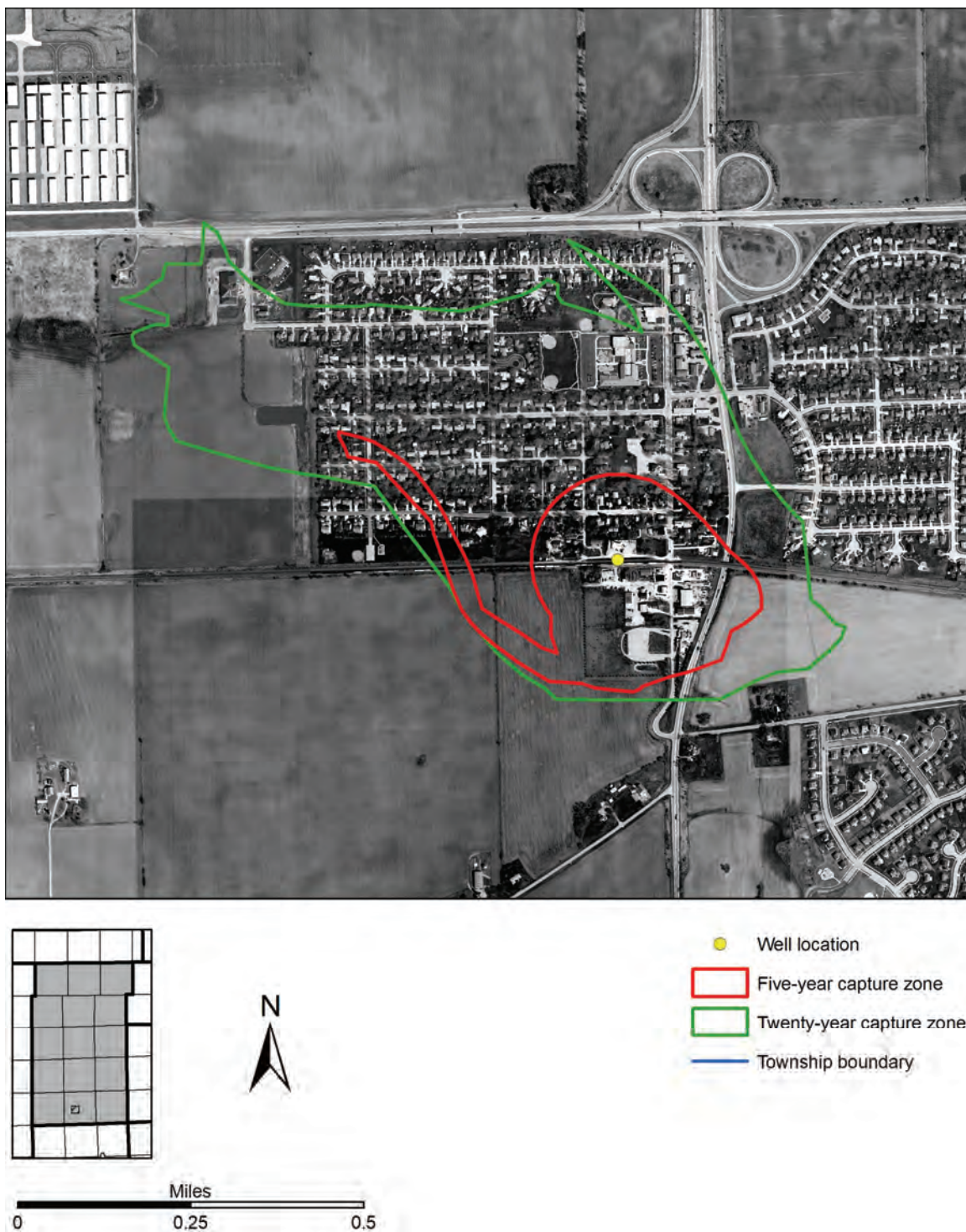


Figure H-28. Five- and twenty-year capture zones of Sugar Grove well 2 superimposed on 2005 aerial photography.



Figure H-29. Five- and twenty-year capture zones of Sugar Grove well 7 superimposed on 2005 aerial photography.

Appendix I. System of Location

Locations are described using township, range, and section numbers as established by the Northwest Ordinance of 1785. The ordinance mandated that all federal lands be surveyed into vertical strips 6 miles wide, called ranges, and horizontal strips of townships, each 6 miles wide. Ranges are numbered east or west of a principal meridian (for example, range 11 west or R11W). Township strips are numbered north or south of a base line (for example, township 5 south or T5S). Range and township strips in Kane County are surveyed relative to the Third Principal Meridian and Base Line. Range and township strips intersect to form townships, which ideally are square with sides 6 miles long and an area of 36 square miles. Townships are divided into 36 sections, each section 1 square mile in area, or 640 acres.

Subsection locations are sometimes described in this report using a coordinate system that assigns a unique number and letter to each quarter-quarter-quarter section (Figure I-1). Numbers between 1 and 8 indicate the east-west position of the location within the section, and letters between A and H indicate the north-south position. A standard section, which is 1 square mile in area, contains 64 quarter-quarter-quarter sections, each 10 acres in area. These tracts are referred to as 10-acre plots, or more simply, plots.

A complete description of location by this system includes designations for county, township, range, section, and subsection location. For example, the location of a well in Kane County, township 41 north, range 8 east, section 36 with the plot location as shown in Figure I-1 could be referenced as Kane-T41N-R8E Sec 36.4c.

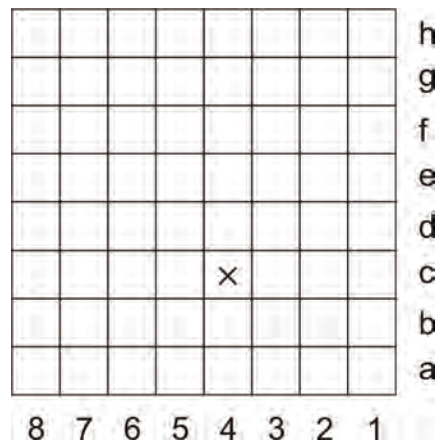


Figure I-1. Illustration of plot designation for a section.